Combination Versus Sequential Single-Agent Therapy in Metastatic Breast Cancer

David Miles, Gunter von Minckwitz and Andrew D. Seidman

Oncologist 2002;7;13-19

The Oncologist®

Errata

Combination Versus Sequential Single-Agent Therapy in Metastatic Breast Cancer

David Miles, Gunter von Minckwitz, Andrew D. Seidman

The Oncologist 2002;7:13-19

On page 15, in Table 1, the regimen identified for the *Jassem et al.* trial was erroneous. AD (doxorubicin and docetaxel) versus FAC should be AP (doxorubicin and paclitaxel) versus FAC.

Moving Forward with Capecitabine: a Glimpse of the Future

Laura Biganzoli, Miguel Martin, Chris Twelves

The Oncologist 2002;7(suppl 6):29-35

On page 31, Table 2, the legend should read "Summary of efficacy: single-agent capecitabine versus CMF as first-line treatment for metastatic breast cancer," whereas previously it read "Summary of efficacy: single-agent capecitabine versus CMF in patients with anthracycline-pretreated metastatic breast cancer." Additionally, the column headers were erroneously identified as "Capecitabine (n = 22)" and "Paclitaxel (n = 19)," respectively. The correct column headers are "Capecitabine (n = 61)" and "CMF (n = 32)," respectively.

BIOENGINEERING

Predicting therapeutic nanomedicine efficacy using a companion magnetic resonance imaging nanoparticle

Miles A. Miller,[1,2]* Suresh Gadde,[3]* Christina Pfirschke,[1] Camilla Engblom,[1] Melissa M. Sprachman,[1] Rainer H. Kohler,[1,2] Katherine S. Yang,[1] Ashley M. Laughney,[1] Gregory Wojtkiewicz,[1] Nazila Kamaly,[3] Sushma Bhonagiri,[3] Mikael J. Pittet,[1,2] Omid C. Farokhzad,[3,4†] Ralph Weissleder[1,2,5†]

Therapeutic nanoparticles (TNPs) have shown heterogeneous responses in human clinical trials, raising questions of whether imaging should be used to identify patients with a higher likelihood of NP accumulation and thus therapeutic response. Despite extensive debate about the enhanced permeability and retention (EPR) effect in tumors, it is increasingly clear that EPR is extremely variable; yet, little experimental data exist to predict the clinical utility of EPR and its influence on TNP efficacy. We hypothesized that a 30-nm magnetic NP (MNP) in clinical use could predict colocalization of TNPs by magnetic resonance imaging (MRI). To this end, we performed single-cell resolution imaging of fluorescently labeled MNPs and TNPs and studied their intratumoral distribution in mice. MNPs circulated in the tumor microvasculature and demonstrated sustained uptake into cells of the tumor microenvironment within minutes. MNPs could predictably demonstrate areas of colocalization for a model TNP, poly(D,L-lactic-*co*-glycolic acid)-*b*-polyethylene glycol (PLGA-PEG), within the tumor microenvironment with >85% accuracy and circulating within the microvasculature with >95% accuracy, despite their markedly different sizes and compositions. Computational analysis of NP transport enabled predictive modeling of TNP distribution based on imaging data and identified key parameters governing intratumoral NP accumulation and macrophage uptake. Finally, MRI accurately predicted initial treatment response and drug accumulation in a preclinical efficacy study using a paclitaxel-encapsulated NP in tumor-bearing mice. These approaches yield valuable insight into the in vivo kinetics of NP distribution and suggest that clinically relevant imaging modalities and agents can be used to select patients with high EPR for treatment with TNPs.

INTRODUCTION

Nanoscale platforms have been developed to improve drug delivery, particularly in oncology, where controlled drug release can mitigate chemotherapeutic toxicities and where structural properties of solid tumors are thought to enhance nanomedicine accumulation (*1*). Multiple factors including aberrant vascular architecture and basement membrane disruption contribute to the enhanced permeability and retention (EPR) effect, thought to facilitate accumulation of therapeutic nanoparticles (TNPs) (*2*, *3*). Several nanotherapeutics have been clinically approved for treatment of various solid cancers, including liposomal doxorubicin (Myocet), PEGylated liposomal doxorubicin (Doxil and Caelyx), NP albumin-paclitaxel (nab-paclitaxel, Abraxane), and SMANCS [poly(styrene-*co*-maleic acid)-conjugated neocarzinostatin], whereas others are undergoing clinical trials (*4*, *5*). Many such TNPs have the potential to increase efficacy by enhancing plasma and target tissue drug exposure [area under the curve (AUC)] and/or reduce toxicities by mitigating adverse effects associated with harmful solvents and high-peak drug concentrations (C_{max}) of conventional intravenous drug formulations (*5*).

There is a lack of conclusive data establishing the superior clinical impact of TNPs compared with standard treatments (*6*), and it is hypothesized that this is largely due to substantial variation in EPR from patient to patient and even across sites within individual patients (*3*). For instance, modest correlation has been observed between tumor microvasculature and highly variable tumoral accumulation of Caelyx in patients (*7*), suggesting that EPR factors may substantially contribute to clinical efficacy. Consequently, several treatment strategies aim to therapeutically augment EPR effects in patients for improving nanotherapeutic efficacy, for example, by stimulating vasodilation through heat, nitric oxide induction, and prostaglandins; by stimulating hypertension through angiotensin II; or by degrading extracellular matrix through collagenase (*6*). Whereas these approaches may potentiate EPR effects, they may also complicate the clinical development of nanotherapeutics. More recently, targeted NPs have entered human clinical trials for small interfering RNA delivery (*8*) and for small-molecule drug delivery (*9*). It is expected that these targeted TNPs may improve clinical outcome, in part by directing NP uptake more specifically to tumor cells once reaching the tumor microenvironment (*10*). Nonetheless, EPR variability continues to be a potential barrier for maximal clinical impact. Thus, one key translational challenge has been to better match patients to novel TNP therapies on the basis of physiological determinants of the EPR effect.

The U.S. Food and Drug Administration (FDA) has approved the carboxymethyl dextran–coated magnetic NP (MNP) ferumoxytol (Feraheme) for treatment of iron deficiency. Ferumoxytol and other related MNPs have been used with magnetic resonance imaging (MRI) to visualize and estimate vascular permeability, NP retention, and phagocyte

[1]Center for Systems Biology, Massachusetts General Hospital, Harvard Medical School, Boston, MA 02114, USA. [2]Department of Radiology, Massachusetts General Hospital, Harvard Medical School, Boston, MA 02114, USA. [3]Laboratory of Nanomedicine and Biomaterials, Department of Anesthesiology, Brigham and Women's Hospital, Harvard Medical School, Boston, MA 02115, USA. [4]King Abdulaziz University, Jeddah, Saudi Arabia. [5]Department of Systems Biology, Harvard Medical School, Boston, MA 02115, USA.
*These authors contributed equally to this work.
†Corresponding author. E-mail: rweissleder@mgh.harvard.edu (R.W.); ofarokhzad@bwh.harvard.edu (O.C.F.)

infiltration in both cancer (*11*, *12*) and inflammation (*13*). Consequently, ferumoxytol has potential as a quantifier of EPR and thus a means of patient stratification. Despite clinical introduction several years ago and several studies for different indications (*11*, *14*), relatively little is known regarding how these MNPs distribute in different tumor compartments and cell types, how distribution is related to EPR effects, how MNP distribution correlates with TNP distribution, and whether MNP imaging can be used to stratify patients according to preferable tumor uptake of TNPs.

The goal of this study was to understand TNP distribution in vivo and determine whether MNPs can be used as companion particles for predicting therapeutic efficacy. We used high-resolution microscopic imaging in live tumor-bearing mice, which allows single-cell quantification of NP uptake in specific cell populations (tumor versus host) at a resolution superior to MRI (*15*, *16*). Results from these in vivo imaging studies as well as prospective MRI in mice demonstrate the feasibility of using MNPs as surrogate markers of intratumoral nanomedicine transport, particularly by labeling NP circulation in the tumor microvasculature and accumulation in macrophages within the tumor mass. We validate these findings in various orthotopic and syngeneic cancer models and further provide a computational framework to parse measurements for predictive modeling of TNP transport and single-cell uptake in vivo.

RESULTS

Magnetic and therapeutic NPs exhibit related intratumoral pharmacokinetics

Using intravital imaging, we first studied the intratumoral pharmacokinetics (PK) of ferumoxytol to see if this MNP behaved similarly to a model TNP (*9*, *17*, *18*). Poly(D,L-lactic-*co*-glycolic acid)-*b*-poly(ethylene glycol) (PLGA-PEG) polymeric TNPs are an attractive drug delivery platform for several reasons, including controlled drug release, tunable physical properties, extended plasma half-lives ($t_{1/2}$), safety, and biodegradability. A fluorescent version of a model PLGA-PEG polymeric NP (λ_{ex} = 488 nm) (fig. S1) was co-injected with the MNP ferumoxytol-VT680XL (λ_{ex} = 630 nm) (Fig. 1A), and both NPs were simultaneously tracked in subcutaneous HT1080 human fibrosarcoma xenografts in nude mice (Fig. 1B and fig. S2, A and B). MNPs distributed throughout the entire tumor microcirculation with an initial $t_{1/2\ plasma,\ tumor}$ of 70 min (Fig. 1C), which is consistent with ear imaging measurements in non–tumor-bearing mice (initial $t_{1/2\ plasma,\ ear}$ = 71 min; fig. S3, A and B) and previous studies in non–tumor-bearing rats (initial $t_{1/2\ plasma}$ = 67 min) (*19*) and which would scale to a terminal $t_{1/2\ plasma}$ of 10 to 14 hours in humans by allometric predictions (*11*). The TNPs exhibited similar initial plasma half-lives in both the tumor microvasculature (Fig. 1C; initial $t_{1/2\ plasma,\ tumor}$ = 55 min) and ear vasculature in healthy animals (initial $t_{1/2\ plasma,\ ear}$ = 56 min; fig. S3, A and B), with initial kinetics approximately in the range of other clinically relevant polymeric and liposomal formulations (*9*, *17*) such as PEGylated liposomal doxorubicin [initial $t_{1/2\ plasma}$ of 0.8 to 2.2 hours in rats (*20*, *21*) and an initial $t_{1/2\ plasma}$ of 5.2 hours in humans for Doxil at 20 mg/m^2 (*22*)].

Pixel-by-pixel correlation showed colocalization between MNPs and TNPs, particularly at early time points when the NPs were mostly confined to circulating in the tumor microvasculature, with MNPs successfully labeling >95% of the vasculature accessible to TNPs (Fig. 1B). Single-injection control experiments for each NP confirmed no fluorescence bleed-through (fig. S2, C and D) and demonstrated that MNP injection at the imaging dose does not affect tumor accumulation of subsequently injected TNPs (fig. S3, C and D).

Once reaching the tumor microvasculature, MNPs accumulated rapidly (within minutes) in perivascular host cells that closely neighbored or extended cytoplasmic processes to tumor capillaries (Fig. 1, D and E). Phagocytic perivascular macrophages influence vessel permeability and cancer intravasation during metastasis; thus, to further study these cells in the context of EPR effects, we imaged several metastases of human ovarian cancer after NP administration. MNPs again accumulated within minutes in the metastases (fig. S4). Polymeric TNPs were also taken up by perivascular host cells within the tumor, albeit at a lower level and more slowly (Fig. 1, E and F, and fig. S4). We also imaged MNP distribution in tumor-associated host cells in fractalkine *Cx3cr1*$^{GFP/+}$ reporter mice, which have green fluorescent protein (GFP)–positive macrophages. MNPs accumulated exclusively within these GFP$^+$ host leukocytes (fig. S5, A and B). Global expression of membrane-targeted tdTomato in all host cells of the *Cx3cr1*$^{GFP/+}$ mice enabled simultaneous visualization of endothelium near tumor xenografts, revealing MNP uptake, especially in host leukocytes adjacent to tumor microvasculature (fig. S5, C and D).

Although the initial plasma kinetic time scale was about 1 hour for both MNPs and TNPs, extended circulating NP half-life and the EPR effect drove gradual accumulation in tumor tissue over the course of 24 hours (fig. S6, A to C). TNP accumulation in tumor cells increased by nearly 20-fold from 3 to 24 hours after administration (fig. S6C), despite the fact that plasma levels had significantly declined by this time (Fig. 1C). An increase in TNP accumulation was also seen in host cells (fig. S6C). These results underscore that intratumoral NP accumulation through EPR effects continued over the course of 24 hours, despite a faster initial phase of plasma clearance.

NPs colocalize with tumor cells at a macroscopic but not single-cell level

Low-magnification tumor imaging showed substantial accumulation and colocalization between NPs and the bulk tumor mass 24 hours after treatment (Fig. 2A), which likely explains MRI observations of enhanced MNP accumulation in various cancers (*2*, *6*, *14*). At the cellular level, although host cells within the tumor microenvironment substantially accumulated both NPs (Fig. 2A), tumor cell uptake was considerably lower and slower (Fig. 1F): 3 hours after injection, >90% of both NPs were associated with host cells rather than tumor cells (fig. S6C). Although MNPs underestimate the amount of TNPs taken up by tumor cells, they do label host cells, such as leukocytes, that accumulate TNPs with >85% accuracy (fig. S6C). An orthotopic model of disseminated metastatic ovarian cancer showed similar patterns of colocalization and predominant accumulation in host rather than tumor cells (fig. S6, D and E). MNPs also colocalized with a model phosphatidylcholine/cholesterol liposomal formulation (mean diameter ± SEM, 171 ± 15 nm; n = 9) in tumor-associated host cells (fig. S7A). There was no significant difference in spatial colocalization according to pixel-by-pixel correlation when using five alternative fluorophores (fig. S7B).

We next computationally modeled how our high-resolution microscopy results would apply to more clinically relevant imaging modalities, such as MRI, which has substantially lower spatial resolution. We decreased the microscopy resolution by down-sampling and then calculated the correlation between MNP and TNP fluorescence intensities as they varied from pixel to pixel. Although MNPs and TNPs

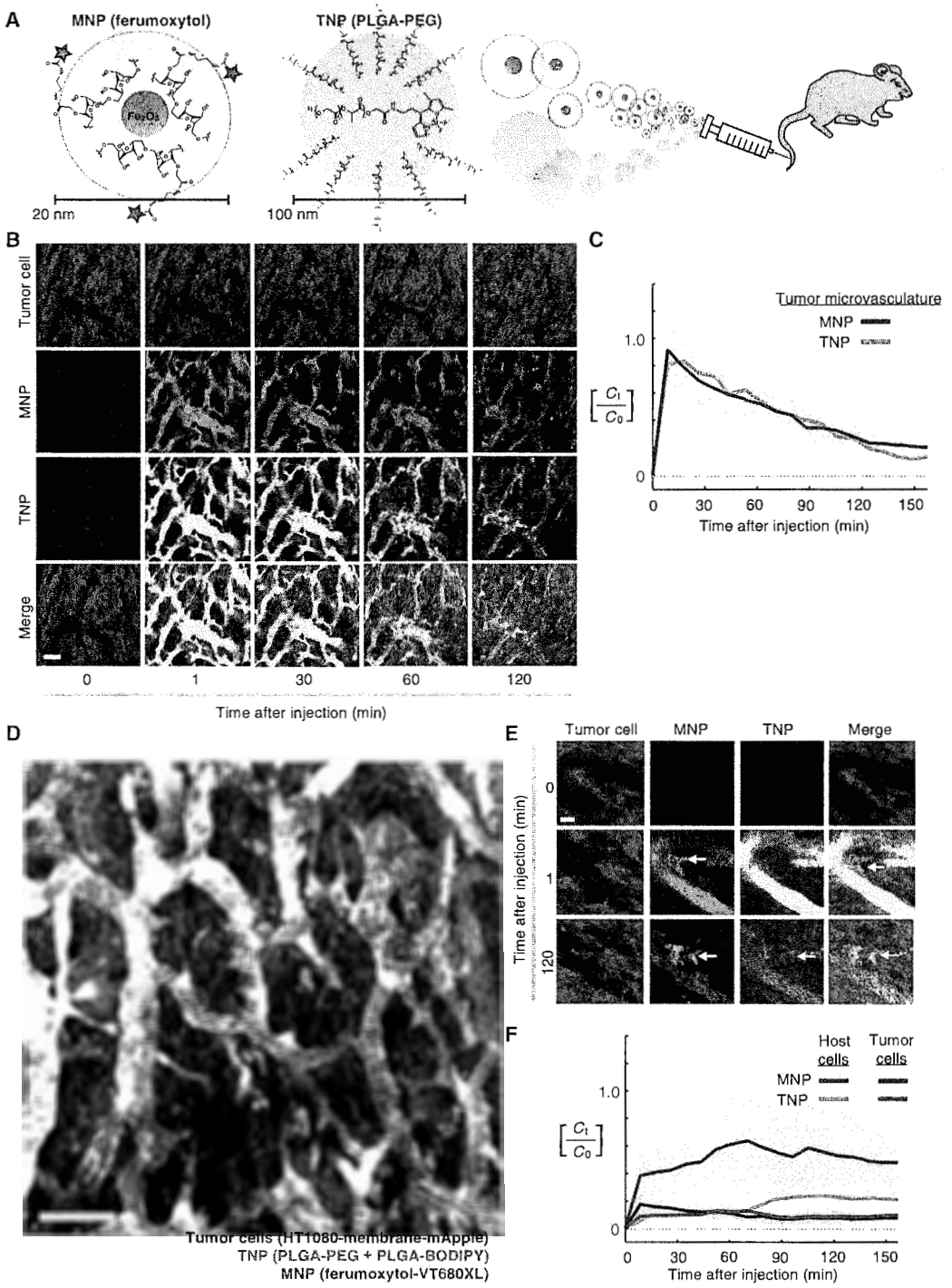

Fig. 1. High-resolution intravital imaging of ferumoxytol and polymeric NPs show similar intratumoral behavior. (**A**) Fluorescently labeled ferumoxytol (MNP) and PLGA-PEG (TNP) were co-injected intravenously into mice for real-time imaging. (**B**) Time-course measurement of intratumoral MNP and TNP distribution within a live xenograft mouse model of fibrosarcoma transgenically expresses membrane-localized red fluorescent protein/mApple (HT1080-membrane-mApple). Scale bar, 50 μm. (**C**) PK and tumor tissue uptake were quantified for MNPs and TNPs, normalized to concentration (C_t) as a fraction of initial vascular concentration (C_0). Data are means (thick lines) ± SD (shading; $n \geq 7$ tumor areas across $n = 3$ animals). (**D**) In the same tumor model as in (B) and (C), contrast-enhanced images show perivascular host cells (green) 10 min after NP injection, distinguishable by cellular morphology, perivascular location, lack of tumor-specific mApple, and MNP accumulation but lack of TNP uptake at early time points. Scale bar, 50 μm. (**E**) Zoomed-in MNP/TNP distribution within a perivascular host cell (arrows). Note the accumulation kinetics within minutes. Scale bar, 14 μm. (**F**) Perivascular host cells take up MNP more rapidly than TNP. Data are means (thick lines) ± SD (shading; $n = 3$ tumors; $n > 50$ cells).

exhibited modest high-resolution correlation ($\rho = 0.2$) 24 hours after injection, correlation increased nearly threefold ($\rho = 0.55$) at spatial resolutions typical of clinical MRI (Fig. 2C). This trend was not evident when comparing MNPs to the spatial distribution of free docetaxel, which was not encapsulated in an NP, demonstrating that increased MNP/TNP colocalization at lower spatial resolution is not simply an artifact of all injected compounds (Fig. 2, B and C). Overall, these data show that EPR effects, largely influenced by NP uptake in host cells, contribute to selective MNP and TNP accumulation within the bulk tumor mass, and suggest that imaging MNPs at a lower MRI resolution will still be able to predict TNP accumulation.

MNPs and TNPs are primarily taken up by tumor-associated macrophages

We next used flow cytometry and histology to quantitatively map NP distribution to immunologically defined cell populations within the bulk tumor mass. To better understand tumor interactions with the immune system, we used a syngeneic immunocompetent model of non–small cell lung cancer based on the subcutaneous implantation of *Kras* mutant $p53^{-/-}$ (KP) cells derived from autochthonous lung tumors in a genetically engineered mouse model (*23*). Leukocytes ($CD45^+$ cells) comprised about one-third of all cells in the tumor (Fig. 3A). Similar to our observations in xenograft models of fibrosarcoma (Fig. 1 and fig. S6, B and C) and ovarian cancer (fig. S6D), host phagocytes (macrophages and neutrophils) accumulated more MNPs and TNPs than did tumor cells (Fig. 3, B to F). Although phagocytosis of tumor cells by host macrophages may complicate both flow cytometric and imaging analyses, imaging data suggest that this population represents <5% of all cells analyzed and therefore has minimal impact on the median-based statistics calculated here. $CD45^-$ host cell populations, which include endothelial cells and tumor-associated fibroblasts, did not accumulate substantial levels of any NPs (Fig. 3B), consistent with a report that fibroblasts limit rather than enhance intratumoral NP accumulation (*24*).

NP spatiotemporal mapping quantifies EPR effects

Computational modeling was used to quantify the observed kinetic processes involved in intratumoral NP accumulation and retention; to compare differences among NPs; to predict in vivo behavior in different tumor models; and to rank the relative contributions of individual parameters, such as vessel permeability, macrophage content, cellular uptake rates, and interstitial diffusion. We used an approach based on

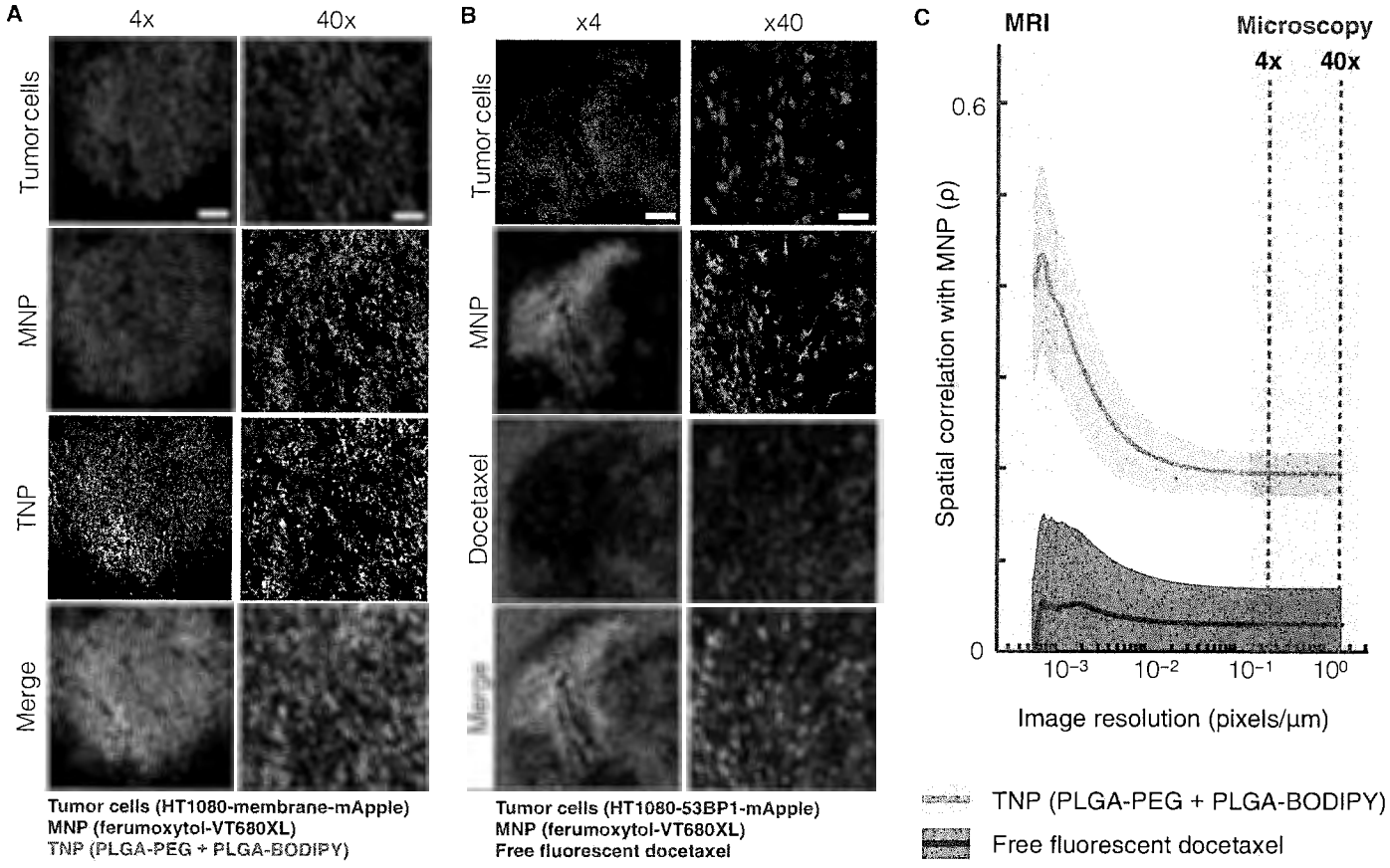

Fig. 2. Multiscale spatial colocalization between MNP and TNP. (**A** and **B**) NP tumor uptake in a live xenograft model, 24 hours after injection with MNP. For low (×4) and high (×40) magnification, scale bar denotes 500 and 50 μm, respectively. Intravenous co-injection with either TNP (A) or a free, unencapsulated fluorescent derivative of docetaxel (B) was imaged after vascular clearance. (**C**) MNP and TNP colocalization improves at lower spatial resolution, but MNP and docetaxel colocalization does not. Microscopy images (A and B) were computationally down-sampled to reduce spatial resolution, and pixel-by-pixel Pearson's correlations (ρ) between MNP/TNP and MNP/docetaxel intensities were calculated across a range of pixel resolutions. Data are means (thick lines) ± SE ($n = 3$ animals and >400 images).

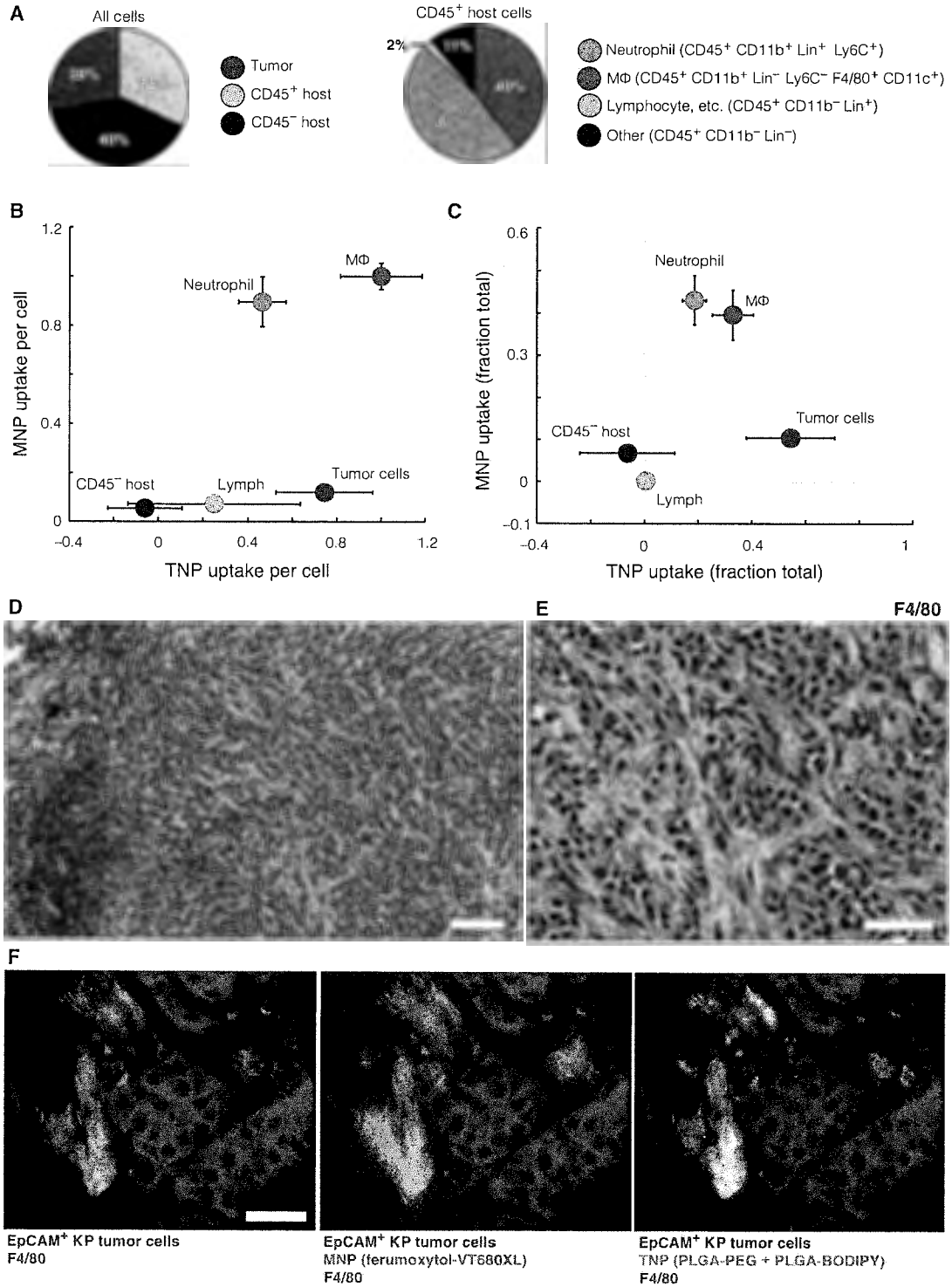

Fig. 3. MNP and TNP colocalize to tumor-associated macrophages in a syngeneic cancer model. (**A** and **B**) Flow cytometric analysis of intratumoral cellular composition (A) and single-cell NP distribution (B) in KP subcutaneous xenografts cotreated with TNP and MNP for 24 hours. Cellular NP uptake was quantified by fluorescence intensity after subtracting the autofluorescence of each population and normalized to the highest average NP uptake (macrophage). (**C**) Cumulative NP uptake across total cell populations within the bulk tumor mass, normalized such that NP uptake across all cell populations, weighted by their relative frequency, sums to 1. Data are means ± SEM (n = 12). (**D** and **E**) KP xenografts were excised 24 hours after MNP and TNP cotreatment, stained with hematoxylin and F4/80 (brown), and imaged at ×10 (D) and ×40 (E) magnification. Scale bars, 100 μm (D); 50 μm (E). (**F**) Adjacent tumor sections were immunostained for EpCAM to label tumor cells and for F4/80 to label macrophages.

finite-element analysis that incorporated spatial NP diffusion and heterogeneous NP uptake at the single-cell level (Fig. 4A). Reaction/diffusion parameters were computationally inferred for each type of NP (table S1), and comparison of these parameter sets for each NP allowed for the derivation of a quantitative normalization factor that corrected for differences in their kinetics.

Nonlinear PK correction, when applied to MNP images, improved the spatial correlation between MNPs and TNPs by ~300% and thus greatly increased the accuracy of MNPs in predicting intratumoral TNP levels (Fig. 4B). The upper accuracy limit for the computational framework was determined by measuring how well the model fit the original training image data set (Fig. 4B, green and yellow bars); encouragingly, the nonlinear PK correction enabled the spatial correlation between MNPs and TNPs to reach this limit. Thus, although MNP and TNP kinetics differed, they overlapped in spatial distribution, particularly among host phagocytes.

To assess the relative importance of different EPR factors in intratumoral NP accumulation, we performed a parametric sensitivity analysis for each NP type by locally adjusting individual modeling parameters (±25%), simulating NP behavior with the new parameter sets, and recording the resulting impact on bulk tumor NP accumulation (including tumor cells and host phagocytes but excluding vasculature) at 2 hours after injection. This analysis revealed that extracellular volume fraction in the tissue, ε, and systemic plasma half-life of the NPs, $t_{1/2\ plasma}$, were the two most important factors governing tumor uptake 2 hours after injection (Fig. 4C), suggesting that cellular uptake was limited at this early time point.

Because MNPs and TNPs have multiple distinct parameters that interact with each other, local changes in reaction rates can affect accumulation

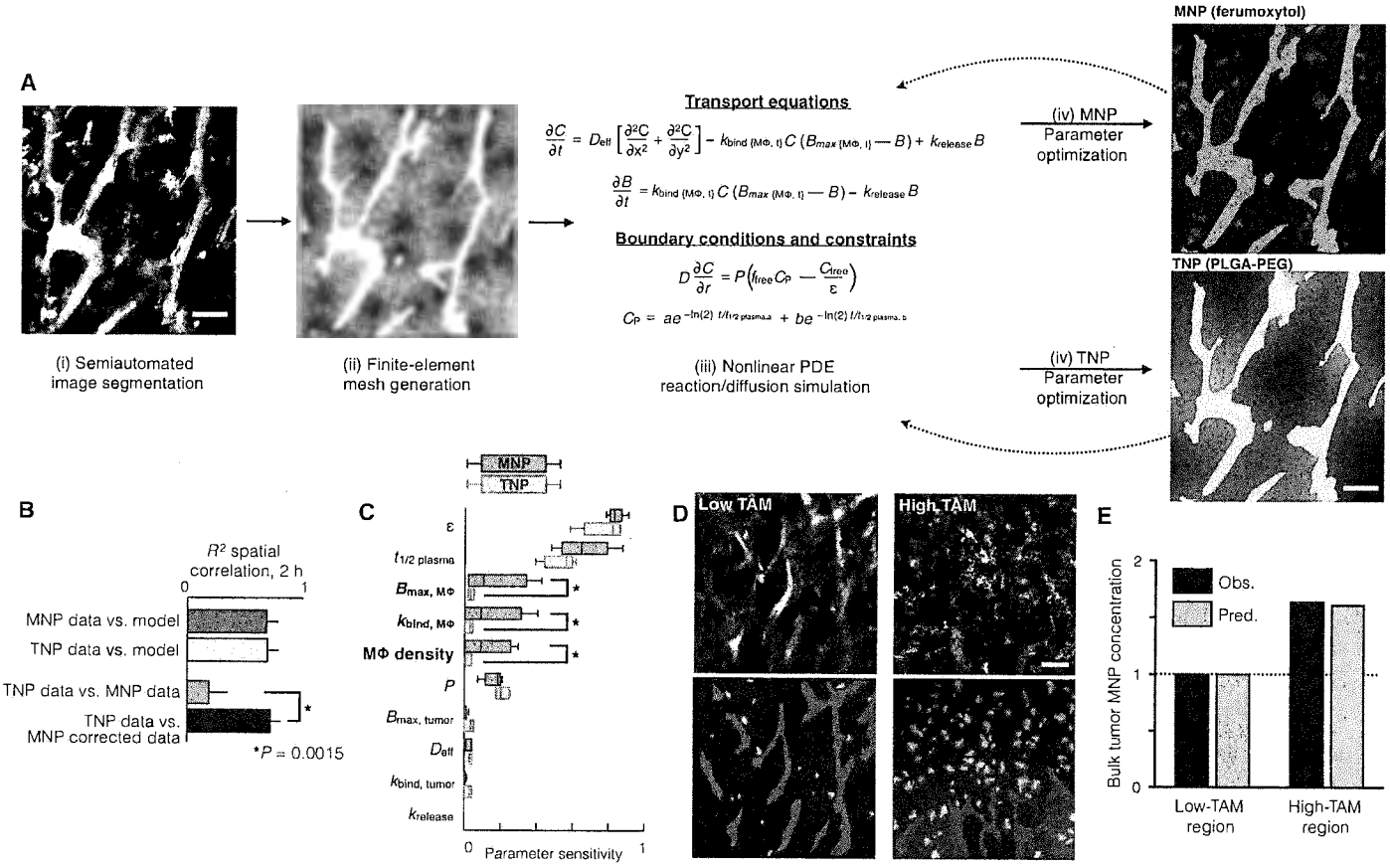

Fig. 4. Quantitative finite-element analysis describes single-cell reaction-diffusion processes of the EPR effect. (**A**) Overview of computational modeling and optimization. (i) In HT1080 xenografts, automated morphological criteria identify vessels (green/red masking), and early MNP accumulation (white) identifies macrophage (as in Fig. 1D), which were computationally segmented with manual optimization. (ii) The finite-element mesh was generated on the basis of image segmentation. (iii) Change in concentration over time of free NP (dC/dt) and bound NP (dB/dt), along with boundary conditions describing NP flux across vessel walls [$D(dC/dr)$], and vessel NP concentrations over time (C_P) were integrated across the finite-element mesh. (iv) Parameters were iteratively optimized by fitting model results to time-lapse imaging data. PDE, partial differential equation. (**B**) Model-fitting validation (green and yellow bars) and spatial correlation between MNPs and TNPs, with and without nonlinear PK correction based on finite-element modeling (gray and black bars). Correlation data are means ± SEM ($n > 200$ regions; P value determined by permutation test). (**C**) Parametric sensitivity analysis showing modeling parameters that most sensitively influence total NP accumulation within the bulk tumor at 2 hours after injection. B_{max}, maximum NP cellular uptake; k_{bind}, NP uptake rate; P, vessel permeability. Data are medians ± interquartile range (IQR) ($n = 5$; *$P = 0.01$, pooled two-tailed t test). (**D**) Example images and corresponding modeling show heterogeneous MNP accumulation in tumor regions with few ($n = 18$; left) and many ($n = 98$; right) phagocytes. Scale bars, 50 μm. (**E**) Finite-element modeling predicted increased MNP accumulation in the high-TAM tumor region (D), measured as average MNP concentration in tumor tissue outside of vessels.

of each type of NP differently. MNPs were highly sensitive to macrophage uptake capacity ($B_{max,,M\Phi}$), kinetics ($k_{bind,,M\Phi}$), and density (macrophages per tumor tissue area), whereas TNPs were not, largely because MNP uptake far outstripped TNP uptake at the early time point of 2 hours (Fig. 4C). Macrophage density has been previously reported as varying widely across tumor types and patients, often correlating with clinical outcome (*25*). There was heterogeneity in macrophage density even within different regions of single tumors [Fig. 4D, top images; coefficient of variation (CV), 100% across 6 tumors]. We independently tested the computational model on such heterogeneous regions and accurately captured the significant effects of variable macrophage density on NP accumulation (Fig. 4, D and E).

MRI before treatment predicts extent of tumor cell DNA damage after TNP administration

To test whether MNP MRI would help to select animals for preclinical trials, we performed several prospective experiments to mimic a clinical scenario. A cohort of mice bearing subcutaneous human fibrosarcoma (HT1080) tumors was imaged by MRI before and after intravenous administration of ferumoxytol MNP to measure total tumor accumulation. MRI at 1 hour after ferumoxytol administration was used to assess tumor microvascularization accessible to circulating TNPs, and MRI at 24 hours labeled cellular uptake within the bulk tumor mass. Change in average T2 mapping of the tumor region (ΔT2) between 1 and 24 hours indicated highly heterogeneous MNP accumulation across the cohort (CV, 750%). We used this metric to stratify mice into "low," "medium," and "high" MNP categories (Fig. 5, A and B).

Paclitaxel-loaded TNPs (fig. S8, A to C) were then administered, with a paclitaxel dose of 3 mg/kg, and tumors were analyzed for subsequent treatment responses (Fig. 5C). The different imaging groups had vastly different therapeutic responses, measured by cell cycle distribution and DNA damage (Fig. 5, D to F). Compared to tumors with medium MNP uptake, we found that high-MNP tumors contained substantially more cells with abnormally low DNA content ("sub-G_1" population) and elevated DNA damage response, as measured by γH2A.X staining (Fig. 5, D and E). These sub-G_1 cells were mostly viable, with only 2 to 10% (IQR over all tumors) of the sub-G_1 cells being apoptotic (Fig. 5F), and have been implicated as a key feature in paclitaxel action (*26*). There was no significant difference in apoptosis between low-MNP and high-MNP tumors ($P = 0.3$, one-way analysis of variance). In contrast, low-MNP tumors exhibited substantially lower levels of DNA damage response compared to the medium-MNP tumors (Fig. 5, D and E). These data indicate that MRI can preliminarily stratify tumors by response to TNP treatment.

MNP distribution predicts disease progression and TNP accumulation

MNP MRI could be used to predict longitudinal disease progression after TNP treatment. A total of 33 subcutaneous HT1080 tumors were imaged before and after ferumoxytol administration to quantify MNP uptake. To induce greater heterogeneity of tumoral MNP concentration (similar to what is observed clinically), half of the cohort was pretreated with systemic liposomal clodronate to reduce tumor-associated macrophages (TAMs) before NP administration and MRI. As done in a previous experiment in Fig. 5, MRI of MNP uptake was quantified by calculating ΔT2 between 1 and 24 hours after administration of MNP. Tumors were stratified into low-, medium-, and high-MNP groups; paclitaxel-encapsulated TNPs (3 mg/kg) were administered intravenously immediately after MNP MRI; and tumor sizes were measured daily until excised for further analysis. MNP accumulation predicted tumor growth after TNP treatment: the low-MNP tumors grew twofold faster than the medium-MNP tumors, whereas the high-MNP tumors did not increase in size (Fig. 6A).

We next investigated the degree to which MNPs predict accumulation of the TNP chemotherapeutic payload itself. For these experiments, we used a syngeneic, orthotopic model of invasive breast cancer consisting of 4T1 mouse mammary carcinoma cells implanted into the mammary fat pads of immunocompetent BALB/c mice. To quantitatively and sensitively detect drug accumulation within tumors, we loaded TNPs with a fluorescent docetaxel derivative (fig. S8D). MNPs and docetaxel-encapsulated TNPs were administered intravenously, and 20 hours later, tumors were excised and analyzed for TNP accumulation. Tumor MNP levels correlated significantly with accumulation of the TNP therapeutic payload, such that high-MNP tumors exhibited about 25-fold higher levels of docetaxel compared to low-MNP tumors (Fig. 6B).

Using the same 4T1 tumor model, we performed a control experiment to determine how effectively MNPs predict tumoral accumulation of free docetaxel. For this control, we used a silicon-rhodamine fluorophore to generate a spectrally distinguishable fluorescent docetaxel derivative that exhibits similar PK properties as the BODIPY-labeled drug (fig. S8E). After MNP and unencapsulated solvent-based docetaxel injection, tumors were excised and analyzed for drug and MNP uptake. Although MNPs somewhat predicted the accumulation of unencapsulated solvent-based docetaxel, the difference between the low-MNP and high-MNP tumors was more modest (2.8-fold) (Fig. 6C) compared to when docetaxel was encapsulated in TNPs (Fig. 6B).

As another control experiment, we investigated whether intratumoral TNP could be accurately stratified by accumulation of an antibody targeting epidermal growth factor receptor (EGFR), which has been used for imaging tumor burden, selecting treatments, and monitoring response in patients with EGFR-overexpressing cancers, including those receiving docetaxel and other chemotherapeutics (*27*). With the EGFR-expressing 4T1 tumor model (*28*), we stratified excised tumors into low, medium, and high antibody groups. Although the anti-EGFR antibody could predict docetaxel TNP accumulation for high versus low and high versus medium groups, the difference between low and high was modest (3.3-fold) (Fig. 6D). The greater order of magnitude of effect for correlation between MNPs and TNPs suggests that NP-specific EPR factors play a dominant role in governing heterogeneous TNP tumor accumulation. The poor correlation between antibody labeling (EGFR expression) and TNP accumulation imply that the anti-EGFR antibody is a poor predictor of tumor response to TNP treatment. Together, these results demonstrate that MNPs are effective predictors of TNP payload accumulation within tumors and, in turn, therapeutic efficacy.

DISCUSSION

TNPs distribute differently across tumors in different patients. A central question in nanomedicine is whether imaging could be used to identify patients with higher predisposition to TNP accumulation and, in turn, efficacy (*5*, *9*). Answering this question could aid in the decision of whether to actively target TNPs or to let them accumulate "passively" within a tumor (*3*). These issues are at the core of understanding how to best exploit EPR effects (*6*) for clinical applications, how to design better TNPs, and how to alter key physiologic parameters to maximize distributions to and within tumors.

We hypothesized that an FDA-approved carboxymethyl dextran–coated MNP (ferumoxytol) can be used to predict TNP behavior by measuring its intratumoral distribution and kinetics across different tumor compartments. To define these compartments, we relied on intravital imaging capable of resolving intracellular details (*15*). Our study uncovered several findings, paving the way for companion particles in predictive nanomedicine. MNPs and TNPs, despite being of different sizes and composition, colocalized to a high degree, especially in the circulating vascular phase, at the macroscopic level (that is, resolutions used in MRI), and in phagocytic host cells. MNP accumulation within the bulk tumor was significantly influenced by host phagocyte content and surprisingly rapid peritumoral host cell uptake within minutes. For both

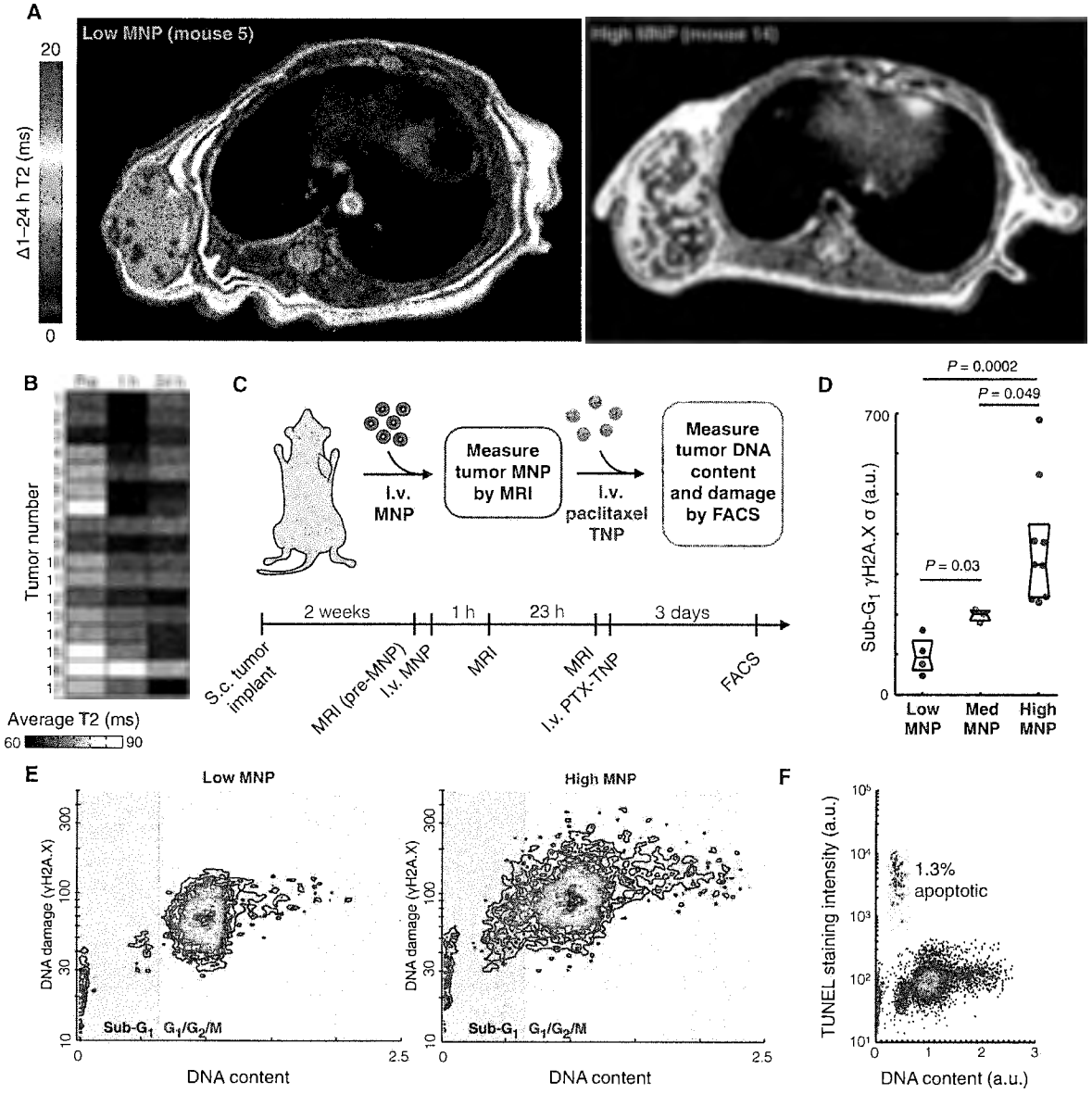

Fig. 5. MRI quantifies heterogeneous MNP accumulation and predicts initial TNP response. (**A**) Representative cross-sectional T2 images of HT1080 tumors accumulating low and high intratumoral MNP, with pseudocolor overlays indicating ΔT2 within the tumor region. (**B**) Heat map shows T2 mapping averaged over the entire area of each tumor, which stratified a subset of tumors as low, medium, or high MNP. (**C**) Experimental design for using MNP MRI to predict paclitaxel (PTX)–loaded TNP response in HT1080 xenografts. s.c., subcutaneous; i.v., intravenous. (**D**) Fluorescence-activated cell sorting (FACS) analysis shows drug response in tumors exhibiting either low, medium, or high MNP uptake, as determined by MRI. Tumors with high MNP showed greater populations with abnormally low DNA content (sub-G_1 cells) and elevated heterogeneous levels of DNA damage response, determined by deviation (σ) in γH2A.X staining across the population. Data are medians ± IQR (two-tailed *t* test). a.u., arbitrary units. (**E**) Representative FACS data for DNA content (using a DNA-intercalating dye) and DNA damage response (using γH2A.X immunostaining) in low-MNP and high-MNP tumors. (**F**) Representative FACS data for DNA content (using a DNA-intercalating dye) and apoptosis (TUNEL staining) in tumor cells from a high-MNP tumor. Contour lines and colors (E and F) denote single-cell distribution density.

NPs, tumor cell uptake was much slower than expected but was greater for TNPs than MNPs despite the larger size of the TNP. For translation to a therapeutic setting, the heterogeneity of intratumoral TNP accumulation could be predicted and measured by MRI and correlated with responsiveness to TNP treatment. In contrast, intratumoral MNP only modestly correlated with soluble therapeutic accumulation, and a common tumor-targeting antibody (anti-EGFR) performed poorly in predicting TNP accumulation. Thus, MNP imaging effectively captured EPR factors that concordantly governed both NPs yet did not equally extend to solvent-based formulations or antibodies.

Understanding individual EPR factors is essential for predicting and eventually tailoring NP behavior. EPR effects of vascular permeability have been studied extensively in the past (*2*, *3*, *24*, *29*); however, these studies have been limited by spatiotemporal resolution and do not sufficiently account for heterogeneous behavior at the single-cell level, particularly in TAMs. We not only studied the multiple EPR factors but also used high-resolution time-lapse microscopy to reveal their highly dynamic character. Vascularization and permeability drove PK at early time points ($t < t_{1/2\ plasma}$) for both NPs, and rapid cellular uptake contributed to early EPR effects for MNPs, particularly in perivascular regions where capillary-associated phagocytes accumulated MNPs within minutes. TNP uptake was minimal at this early stage. In contrast, after 24 hours ($t >> t_{1/2\ plasma}$), EPR effects were dominated by cellular NP uptake, particularly in TAMs.

TNPs are typically engineered to release chemotherapeutic payloads at prescribed and tunable rates. The relative therapeutic importance of tumor vascularity, vessel permeability, interstitial fluid content and pressure, extracellular matrix, and phagocyte infiltration will ultimately depend on TNP physicochemical properties including size, shape, payload release kinetics, and transport properties of the released drug. When keeping the TNP physicochemical properties constant, as done in our study, both slow and rapid payload release will influence intratumoral distribution: cellular NP uptake will dominate in the former, whereas vascular permeability and extracellular volume fraction will dominate in the latter. Although we did not extensively investigate different TNP formulations, our study lays the groundwork for understanding how heterogeneous cell populations and the EPR within the tumor microenvironment affect drug delivery, and demonstrates that MNPs may be used to predict the behavior of NPs with differing physicochemical properties.

We used computational modeling to provide a framework for quantifying and comparing physiological effects that govern tumoral NP accumulation. This work extends previous modeling of drug transport (*15*) to nanotherapeutics, which required the explicit modeling of NP uptake at single-cell resolution. The largest differences in NP behavior were all related to heterogeneous cellular NP uptake. For macrophages, the MNP uptake rate was about sixfold faster than for TNP, and maximum uptake levels were threefold higher, which is not surprising considering the differences in surface modifications between MNPs and TNPs. Future studies should extend this approach to better capture three-dimensional behavior; link NP kinetics with drug payload release and cellular response; more closely examine differences in tumoral penetration between MNPs and TNPs; and address additional heterogeneity in parameters related to interstitial pressure, convection, diffusion through fibrotic tissue, and pH.

Several of our findings have direct implications for the effective design of nanotherapeutic clinical trials. Heterogeneous tumor vascularization is a recognized clinical feature that can be detected using various angiography modalities and that can affect both drug delivery (*29*) and overall survival (*30*). Immediate MNP MRI showed the tumor vasculature accessible to TNPs, which will be especially important in the context of therapeutics that affect vascular structure, such as targeted antiangiogenics, vascular dilators, and hyperthermic induction. MNP imaging after 24 hours revealed peritumoral cell populations that accumulated high levels of TNPs. Macrophage content represents a critical yet highly variable component of the overall EPR effect. Recent work has highlighted the extensive heterogeneity of phagocyte populations within tumors and its significant effects on drug response and clinical outcome (*25*). Moreover, several therapeutics directly target TAMs, for instance, by blocking colony-stimulating factor 1 receptor; therefore,

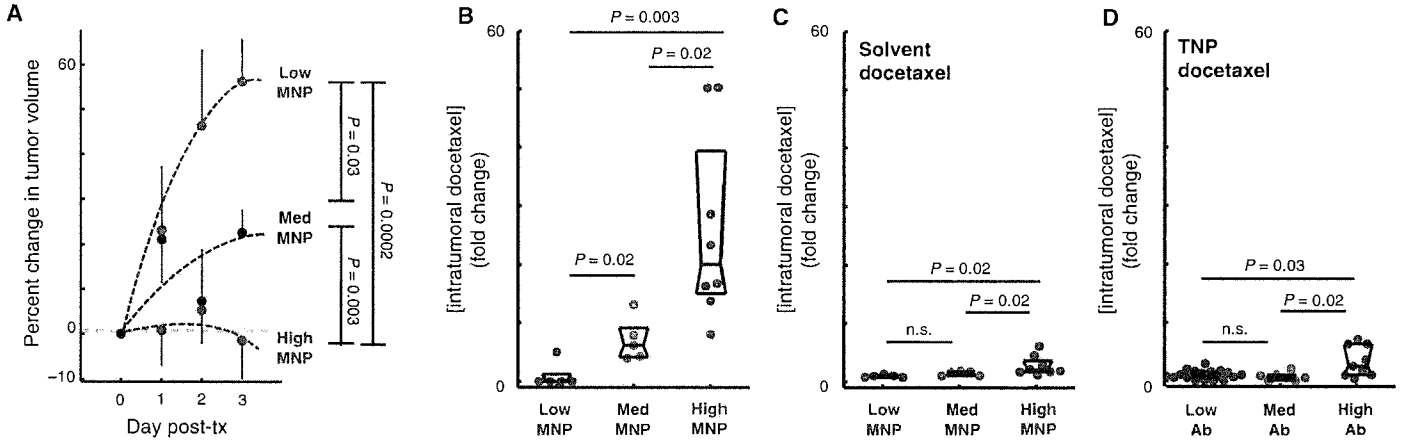

Fig. 6. MNP predicts longitudinal TNP response and accumulation of TNP payload. (**A**) Tumor progression in HT1080 tumors ranked according to low, medium, and high MNP as measured by MNP MRI. Data are means ± SEM (total $n = 33$). (**B**) In orthotopic 4T1 breast cancer tumors, MNP prediction of TNP-encapsulated docetaxel, as determined by fluorescence of excised tumors 1 day after MNP/TNP injection. (**C**) MNP prediction of unencapsulated solvent-docetaxel accumulation as determined by fluorometry, using the same tumor model as in (B). (**D**) EGFR expression–based prediction of TNP-encapsulated docetaxel accumulation, using the same tumor model as in (B). TNP-docetaxel was co-injected with fluorescent tumor-targeting (α-EGFR) antibody, which stratified tumors into low, medium, or high expression groups. In all graphs, data are medians ± IQR. *P* values were determined by two-tailed *t* tests. n.s., not significant.

assessing phagocyte content will be especially important for selecting patients to receive these drugs and to monitor their response.

To progress clinically, more human-representative disease models, such as patient-derived xenografts, genetically engineered autochthonous mouse models, and larger animals, should be used to study EPR effects in metastatic lesions, to examine the correlation between MNP uptake and long-term efficacy, and to see if MNPs can indicate which cancer types may be more responsive to nano-based drug delivery. Ultimately, we have provided a high-resolution description of dynamic EPR effects governing nanomedicine transport and demonstrated the potential of MNPs and imaging to predict TNP efficacy in the clinic—a major stepping stone toward translation of new nanomedicine and for eventually selecting patients for nanotherapeutic trials.

MATERIALS AND METHODS

Study design

The hypothesis was that MNP would predict accumulation and efficacy of TNP in tumors. Imaging studies and drug accumulation measurements were designed to measure the kinetics and colocalization between MNP and TNP within tumor tissue; tumor caliper measurements, along with flow cytometry measurement of DNA damage, cell cycle, and apoptosis were designed to assess the correlation between MNP accumulation and drug response efficacy. All experiments were performed with at least two independent replicates (specified in figure legends). Data collection methods were predetermined for all experiments, and animals were assigned randomly to treatment groups. No outliers were excluded. Cohort sizes in the experiments using the 4T1 model (Fig. 6) were informed by a power analysis based on MRI data in the HT1080 model (Fig. 5), using the measured intragroup heterogeneity in MNP uptake (CV, 60%), an intergroup difference of 80% between low- and high-MNP groups, and an objective power ($1 - \beta$) of 0.95 calculated with available software (*31*). Researchers were blinded to groups for MNP and anti-EGFR antibody uptake during nonimaging experiments in Figs. 5 and 6, including caliper measurement, because prespecified stratification procedures were not performed until after all data had been collected.

TNP synthesis

All polymeric TNPs were synthesized by nanoprecipitation, were characterized by size and surface charge using dynamic light scattering (Malvern Zetasizer), and were freshly prepared before each experiment. Synthesis details are given in Supplementary Methods.

Animal and cell models

All animal research was performed in accordance with the guidelines from the Institutional Subcommittee on Research Animal Care. All experiments were performed using female mice that were 5 to 7 weeks old at the start of the experiment. For experiments with human HT1080 tumors, 2×10^6 cells were subcutaneously implanted into nu/nu mice; 2 to 3 weeks later (once tumors reached about 8 mm in diameter), imaging experiments were initiated. For 4T1 tumors, 0.5 million cells were implanted into the mammary fat pads of BALB/c mice; about 10 days later, imaging and therapeutic agents were intravenously injected, and tumors were excised for analysis the following day. For ovarian cancer imaging, 10^7 A2780CP cells were injected intraperitoneally into nu/nu mice, and experiments were performed about 6 weeks later with evident ascites or tumor masses. For imaging experiments using KP1.9 cells, 10^6 cells were subcutaneously implanted into C57Bl/6 background animals (all JAX), including *Cx3cr1*$^{GFP/+}$ and *Cx3cr1*$^{GFP/+}$ *R26*$^{mT\text{-}mG/+}$ dual-reporter mice, both containing GFP$^+$ monocytes, macrophages, and dendritic cells. The mouse and human cell lines HT1080, A2780CP, 4T1, and KP1.9 are described in Supplementary Methods.

Intravital microscopic imaging

Intravital microscopy was performed on an Olympus FV1000 confocal multiphoton imaging system using a XLUMPLFLN 20× water immersion objective (numerical aperture, 1.0; Olympus America) with 2× digital zoom. Images were scanned sequentially using 405-, 473-, 559-, and 635-nm diode lasers with a DM405/473/559/635-nm dichroic beam splitter; emitted light was collected using combinations of beam splitters (SDM473, SDM560, and/or SDM 640) and emission filters BA430-455, BA490-540, BA575-620, and BA655-755 (all Olympus America).

Dorsal window chamber imaging was performed following previously described procedures (*16*); briefly, 2 million HT1080-membrane-mApple cells in 50 μl of phosphate-buffered saline (PBS) were injected under the fascia of nu/nu mice (Cox7, Massachusetts General Hospital) 30 min after surgical chamber implantation and were imaged 2 weeks later.

Magnetic resonance imaging

Mice were anesthetized by isoflurane inhalation and placed in a birdcage radio frequency coil with an inner diameter of 38 mm. Mice were scanned for a baseline T2 value before MNP injection, using a 4.7-T MRI system (PharmaScan, Bruker BioSpin). Without removal of the mouse from the coil, mice were scanned after intravenous MNP injection (20 mg Fe/kg body weight), and a third scan was performed 24 hours later. T2 values were calculated by fitting of a standard exponential relaxation model to the data averaged over the tumor region of interest on each slice, using Osirix software. The quantitative probe accumulation was calculated as follows: $[\ln (T2_{1h\ post\text{-}MNP}/T2_{24h\ post\text{-}MNP})]$, where $T2_{1h\ post\text{-}MNP}$ indicates the T2 value 1 hour after MNP injection (vascular phase) and $T2_{24h\ post\text{-}MNP}$ indicates the T2 value 24 hours after MNP injection (cell accumulation phase).

Computational image analysis

Intravital microscopy images were analyzed using either MATLAB (MathWorks) or ImageJ and were preprocessed using background subtraction based on data acquired immediately before NP injection. Vascular half-life calculations, finite-element analysis, and other details are described in Supplementary Methods.

MNP prediction of drug uptake, response, and progression

Three-week-old subcutaneous HT1080 tumors were imaged before and 1 and 24 hours after intravenous ferumoxytol injection, once tumors reached an average diameter of 8 mm. To generate heterogeneity in EPR effects (Fig. 6A), tumors were evenly split into two groups of equally distributed tumor sizes, receiving either clodronate liposomes (5 mg/ml) or PBS liposomes as a vehicle control, with 150 μl administered intraperitoneally 3 days before imaging and 100 μl administered intravenously 24 hours before imaging (ClodLip BV). Tumoral MNP uptake was quantified as $[T2_{1h\ post\text{-}MNP} - T2_{24h\ post\text{-}MNP}]$ and weighted by MNP plasma half-life for each treatment group to control for residual MNP in circulation (*32*). To measure tumor volume ($V = 4/3\pi r^3$), caliper measurements were performed by two blinded researchers. Results were categorized into three groups defined by boundaries that maximized

the statistical significance in differential drug response and tumor progression as measured by DNA damage response or tumor volume, respectively. Magnetic resonance images (Fig. 5A) were selected on the basis of their representativeness for each group and also for tumors being of roughly equal anatomical position and size. For correlation analysis between tumor uptake of MNPs, TNP, free drug, and EGFR-targeting antibody, we used the orthotopic 4T1 breast cancer syngeneic mouse model, as described in Supplementary Methods.

Statistical analysis

Statistical analyses were performed using GraphPad Prism, MATLAB, and Microsoft Excel. Measurement uncertainties throughout are denoted by error bars and shading as indicated in figure legends. All statistical tests were two-tailed with testing level thresholds of $\alpha = 0.05$. As a predefined procedure, stratifications by MNP or antibody uptake (Figs. 5 and 6) were performed using thresholds that maximized the statistical difference (using t tests) in drug response, tumor progression, or docetaxel uptake.

SUPPLEMENTARY MATERIALS

www.sciencetranslationalmedicine.org/cgi/content/full/7/314/314ra183/DC1
Methods
Fig. S1. Fluorescent NP synthesis and characterization.
Fig. S2. Imaging single-cell kinetics of MNP distribution with no TNP/MNP fluorescence spectral bleed-through.
Fig. S3. MNP matches TNP plasma kinetics and does not influence TNP uptake.
Fig. S4. MNP and TNP uptake by perivascular host cells in ovarian cancer.
Fig. S5. MNP uptake in tumor-associated $Cx3cr1^+$ host cells.
Fig. S6. Imaging cytometric analysis of single-cell NP distribution kinetics.
Fig. S7. MNPs colocalize with liposomes in tumor-associated cells.
Fig. S8. Characterization of paclitaxel-loaded TNP and fluorescent derivatives.
Table S1. Optimized finite-element method modeling parameters and reference values.
References (*33*–*38*)

REFERENCES AND NOTES

1. E. K. Chow, D. Ho, Cancer nanomedicine: From drug delivery to imaging. *Sci. Transl. Med.* **5**, 216rv4 (2013).
2. H. Maeda, H. Nakamura, J. Fang, The EPR effect for macromolecular drug delivery to solid tumors: Improvement of tumor uptake, lowering of systemic toxicity, and distinct tumor imaging in vivo. *Adv. Drug Deliv. Rev.* **65**, 71–79 (2013).
3. N. Bertrand, J. Wu, X. Xu, N. Kamaly, O. C. Farokhzad, Cancer nanotechnology: The impact of passive and active targeting in the era of modern cancer biology. *Adv. Drug Deliv. Rev.* **66**, 2–25 (2014).
4. J. C. Kraft, J. P. Freeling, Z. Wang, R. J. Ho, Emerging research and clinical development trends of liposome and lipid nanoparticle drug delivery systems. *J. Pharm. Sci.* **103**, 29–52 (2014).
5. N. Kamaly, Z. Xiao, P. M. Valencia, A. F. Radovic-Moreno, O. C. Farokhzad, Targeted polymeric therapeutic nanoparticles: Design, development and clinical translation. *Chem. Soc. Rev.* **41**, 2971–3010 (2012).
6. U. Prabhakar, H. Maeda, R. K. Jain, E. M. Sevick-Muraca, W. Zamboni, O. C. Farokhzad, S. T. Barry, A. Gabizon, P. Grodzinski, D. C. Blakey, Challenges and key considerations of the enhanced permeability and retention effect for nanomedicine drug delivery in oncology. *Cancer Res.* **73**, 2412–2417 (2013).
7. M. I. Koukourakis, S. Koukouraki, A. Giatromanolaki, S. C. Archimandritis, J. Skarlatos, K. Beroukas, J. G. Bizakis, G. Retalis, N. Karkavitsas, E. S. Helidonis, Liposomal doxorubicin and conventionally fractionated radiotherapy in the treatment of locally advanced non-small-cell lung cancer and head and neck cancer. *J. Clin. Oncol.* **17**, 3512–3521 (1999).
8. M. E. Davis, J. E. Zuckerman, C. H. Choi, D. Seligson, A. Tolcher, C. A. Alabi, Y. Yen, J. D. Heidel, A. Ribas, Evidence of RNAi in humans from systemically administered siRNA via targeted nanoparticles. *Nature* **464**, 1067–1070 (2010).
9. J. Hrkach, D. Von Hoff, M. Mukkaram Ali, E. Andrianova, J. Auer, T. Campbell, D. De Witt, M. Figa, M. Figueiredo, A. Horhota, S. Low, K. McDonnell, E. Peeke, B. Retnarajan, A. Sabnis, E. Schnipper, J. J. Song, Y. H. Song, J. Summa, D. Tompsett, G. Troiano, T. Van Geen Hoven, J. Wright, P. LoRusso, P. W. Kantoff, N. H. Bander, C. Sweeney, O. C. Farokhzad, R. Langer, S. Zale, Preclinical development and clinical translation of a PSMA-targeted docetaxel nanoparticle with a differentiated pharmacological profile. *Sci. Transl. Med.* **4**, 128ra39 (2012).
10. D. B. Kirpotin, D. C. Drummond, Y. Shao, M. R. Shalaby, K. Hong, U. B. Nielsen, J. D. Marks, C. C. Benz, J. W. Park, Antibody targeting of long-circulating lipidic nanoparticles does not increase tumor localization but does increase internalization in animal models. *Cancer Res.* **66**, 6732–6740 (2006).
11. M. Harisinghani, R. W. Ross, A. R. Guimaraes, R. Weissleder, Utility of a new bolus-injectable nanoparticle for clinical cancer staging. *Neoplasia* **9**, 1160–1165 (2007).
12. Y. Tang, M. Kim, D. Carrasco, A. L. Kung, L. Chin, R. Weissleder, In vivo assessment of RAS-dependent maintenance of tumor angiogenesis by real-time magnetic resonance imaging. *Cancer Res.* **65**, 8324–8330 (2005).
13. R. Weissleder, M. Nahrendorf, M. J. Pittet, Imaging macrophages with nanoparticles. *Nat. Mater.* **13**, 125–138 (2014).
14. M. R. Bashir, L. Bhatti, D. Marin, R. C. Nelson, Emerging applications for ferumoxytol as a contrast agent in MRI. *J. Magn. Reson. Imaging* **41**, 884–898 (2015).
15. G. M. Thurber, K. S. Yang, T. Reiner, R. H. Kohler, P. Sorger, T. Mitchison, R. Weissleder, Single-cell and subcellular pharmacokinetic imaging allows insight into drug action in vivo. *Nat. Commun.* **4**, 1504 (2013).
16. M. A. Miller, B. Askevold, K. S. Yang, R. H. Kohler, R. Weissleder, Platinum compounds for high-resolution in vivo cancer imaging. *ChemMedChem* **9**, 1131–1135 (2014).
17. S. Dhar, N. Kolishetti, S. J. Lippard, O. C. Farokhzad, Targeted delivery of a cisplatin prodrug for safer and more effective prostate cancer therapy in vivo. *Proc. Natl. Acad. Sci. U.S.A.* **108**, 1850–1855 (2011).
18. O. C. Farokhzad, J. Cheng, B. A. Teply, I. Sherifi, S. Jon, P. W. Kantoff, J. P. Richie, R. Langer, Targeted nanoparticle-aptamer bioconjugates for cancer chemotherapy in vivo. *Proc. Natl. Acad. Sci. U.S.A.* **103**, 6315–6320 (2006).
19. G. H. Simon, J. von Vopelius-Feldt, Y. Fu, J. Schlegel, G. Pinotek, M. F. Wendland, M. H. Chen, H. E. Daldrup-Link, Ultrasmall supraparamagnetic iron oxide-enhanced magnetic resonance imaging of antigen-induced arthritis: A comparative study between SHU 555 C, ferumoxtran-10, and ferumoxytol. *Invest. Radiol.* **41**, 45–51 (2006).
20. A. Bao, B. Goins, R. Klipper, G. Negrete, W. T. Phillips, Direct ^{99m}Tc labeling of pegylated liposomal doxorubicin (Doxil) for pharmacokinetic and non-invasive imaging studies. *J. Pharmacol. Exp. Ther.* **308**, 419–425 (2004).
21. A. Soundararajan, A. Bao, W. T. Phillips, R. Perez III, B. A. Goins, ^{186}Re-liposomal doxorubicin (Doxil): In vitro stability, pharmacokinetics, imaging and biodistribution in a head and neck squamous cell carcinoma xenograft model. *Nucl. Med. Biol.* **36**, 515–524 (2009).
22. *Doxil (Package Insert)* (Janssen Products, LP, Horsham, PA, 2015).
23. M. DuPage, A. L. Dooley, T. Jacks, Conditional mouse lung cancer models using adenoviral or lentiviral delivery of Cre recombinase. *Nat. Protoc.* **4**, 1064–1072 (2009).
24. H. Cabral, Y. Matsumoto, K. Mizuno, Q. Chen, M. Murakami, M. Kimura, Y. Terada, M. R. Kano, K. Miyazono, M. Uesaka, N. Nishiyama, K. Kataoka, Accumulation of sub-100 nm polymeric micelles in poorly permeable tumours depends on size. *Nat. Nanotechnol.* **6**, 815–823 (2011).
25. Q. W. Zhang, L. Liu, C. Y. Gong, H. S. Shi, Y. H. Zeng, X. Z. Wang, Y. W. Zhao, Y. Q. Wei, Prognostic significance of tumor-associated macrophages in solid tumor: A meta-analysis of the literature. *PLOS One* **7**, e50946 (2012).
26. Z. N. Demidenko, S. Kalurupalle, C. Hanko, C.-u. Lim, E. Broude, M. V. Blagosklonny, Mechanism of G1-like arrest by low concentrations of paclitaxel: Next cell cycle p53-dependent arrest with sub G1 DNA content mediated by prolonged mitosis. *Oncogene* **27**, 4402–4410 (2008).
27. V. Tolmachev, S. Stone-Elander, A. Orlova, Radiolabelled receptor-tyrosine-kinase targeting drugs for patient stratification and monitoring of therapy response: Prospects and pitfalls. *Lancet Oncol.* **11**, 992–1000 (2010).
28. S. Rao, A.-L. Larroque-Lombard, L. Peyrard, C. Thauvin, Z. Rachid, C. Williams, B. J. Jean-Claude, Target modulation by a kinase inhibitor engineered to induce a tandem blockade of the epidermal growth factor receptor (EGFR) and c-Src: The concept of type III combi-targeting. *PLOS One* **10**, e0117215 (2015).
29. V. P. Chauhan, T. Stylianopoulos, J. D. Martin, Z. Popovic, O. Chen, W. S. Kamoun, M. G. Bawendi, D. Fukumura, R. K. Jain, Normalization of tumour blood vessels improves the delivery of nanomedicines in a size-dependent manner. *Nat. Nanotechnol.* **7**, 383–388 (2012).
30. M. A. Goscinski, J. M. Nesland, K. E. Giercksky, H. P. Dhakal, Primary tumor vascularity in esophagus cancer. CD34 and HIF1-α expression correlate with tumor progression. *Histol. Histopathol.* **28**, 1361–1368 (2013).
31. R. V. Lenth, Statistical power calculations. *J. Anim. Sci.* **85**, E24–E29 (2007).
32. S. W. Jones, R. A. Roberts, G. R. Robbins, J. L. Perry, M. P. Kai, K. Chen, T. Bo, M. E. Napier, J. P. Ting, J. M. Desimone, J. E. Bear, Nanoparticle clearance is governed by Th1/Th2 immunity and strain background. *J. Clin. Invest.* **123**, 3061–3073 (2013).
33. G. Lukinavičius, L. Reymond, E. D'Este, A. Masharina, F. Göttfert, H. Ta, A. Güther, M. Fournier, S. Rizzo, H. Waldmann, C. Blaukopf, C. Sommer, D. W. Gerlich, H. D. Arndt, S. W. Hell, K. Johnsson,

Fluorogenic probes for live-cell imaging of the cytoskeleton. *Nat. Methods* **11**, 731–733 (2014).
34. A. M. Courtis, S. A. Santos, Y. Guan, J. A. Hendricks, B. Ghosh, D. M. Szantai-Kis, S. A. Reis, J. V. Shah, R. Mazitschek, Monoalkoxy BODIPYs–a fluorophore class for bioimaging. *Bioconjug. Chem.* **25**, 1043–1051 (2014).
35. E. van der Pol, F. A. Coumans, A. E. Grootemaat, C. Gardiner, I. L. Sargent, P. Harrison, A. Sturk, T. G. van Leeuwen, R. Nieuwland, Particle size distribution of exosomes and microvesicles determined by transmission electron microscopy, flow cytometry, nanoparticle tracking analysis, and resistive pulse sensing. *J. Thromb. Haemost.* **12**, 1182–1192 (2014).
36. E. A. Mun, C. Hannell, S. E. Rogers, P. Hole, A. C. Williams, V. V. Khutoryanskiy, On the role of specific interactions in the diffusion of nanoparticles in aqueous polymer solutions. *Langmuir* **30**, 308–317 (2014).
37. M. R. Dreher, W. Liu, C. R. Michelich, M. W. Dewhirst, F. Yuan, A. Chilkoti, Tumor vascular permeability, accumulation, and penetration of macromolecular drug carriers. *J. Natl. Cancer Inst.* **98**, 335–344 (2006).
38. D. Vincensini, V. Dedieu, P. A. Eliat, C. Vincent, C. Bailly, J. de Certaines, F. Joffre, Magnetic resonance imaging measurements of vascular permeability and extracellular volume fraction of breast tumors by dynamic Gd-DTPA-enhanced relaxometry. *Magn. Reson. Imaging* **25**, 293–302 (2007).

Acknowledgments: We thank A. Zaltsman, D. Pirovich, M. Sebas, O. Kister, N. Sergeyev, K. King, and Y. Iwamoto for technical assistance; S. Lippard and Y. Zheng for helpful discussions. **Funding:** This work was supported in part by the NIH (R01CA164448, U54-CA151884, SP50CA086355, and HL084312), DoD (PC140318), and the David H. Koch–Prostate Cancer Foundation Award in Nanotherapeutics. M.A.M. was supported by T32 CA 79443. C.P. is in part supported by Deutsche Forschungsgemeinschaft (DFG) PF809/1-1. **Author contributions:** M.A.M., S.G., O.C.F., and R.W. developed the concept; M.A.M., S.G., C.P., M.J.P., O.C.F., and R.W. designed the experiments; M.A.M., S.G., N.K., and S.B. synthesized and characterized PLGA-PEG NPs; M.A.M. synthesized and characterized MNP, docetaxel-TNP, and antibody-dye conjugate; M.A.M., C.P., and C.E. performed FACS experiments; M.A.M. and R.H.K. performed intravital imaging experiments; M.A.M., G.W., O.C.F., and R.W. designed or performed therapeutic MRI experiments; M.M.S. designed and synthesized docetaxel-dye conjugates; M.A.M., A.M.L., and K.S.Y. generated the cell lines; M.A.M., S.G., O.C.F., and R.W. wrote the paper; all authors analyzed the results and edited the manuscript. **Competing interests:** In compliance with institutional guidelines, O.C.F. discloses his financial interest in BIND Therapeutics, Selecta Biosciences, and Blend Therapeutics, which develop NP medical technologies but did not support this study. The other authors declare that they have no competing interests. **Data and materials availability:** All cell lines were obtained through material transfer agreements. Requests for collaboration involving materials used in this research will be fulfilled provided that a written agreement is executed in advance between Brigham and Women's Hospital or Massachusetts General Hospital and the requesting parties.

Submitted 26 May 2015
Accepted 15 September 2015
Published 18 November 2015
10.1126/scitranslmed.aac6522

Citation: M. A. Miller, S. Gadde, C. Pfirschke, C. Engblom, M. M. Sprachman, R. H. Kohler, K. S. Yang, A. M. Laughney, G. Wojtkiewicz, N. Kamaly, S. Bhonagiri, M. J. Pittet, O. C. Farokhzad, R. Weissleder, Predicting therapeutic nanomedicine efficacy using a companion magnetic resonance imaging nanoparticle. *Sci. Transl. Med.* **7**, 314ra183 (2015).

Science Translational Medicine
AAAS

Predicting therapeutic nanomedicine efficacy using a companion magnetic resonance imaging nanoparticle

Miles A. Miller, Suresh Gadde, Christina Pfirschke, Camilla Engblom, Melissa M. Sprachman, Rainer H. Kohler, Katherine S. Yang, Ashley M. Laughney, Gregory Wojtkiewicz, Nazila Kamaly, Sushma Bhonagiri, Mikael J. Pittet, Omid C. Farokhzad and Ralph Weissleder (November 18, 2015)

Science Translational Medicine 7 (314), 314ra183. [doi: 10.1126/scitranslmed.aac6522]

Editor's Summary

Particle prediction

One particle, it seems, can predict the behavior of another. Thankfully, this is not the beginning of a lesson on quantum physics; instead, it is the basis for potentially designing targeted clinical trials in nanomedicine, by knowing if a tumor is likely to respond to a particular therapeutic nanoparticle. Miller *et al.* hypothesized that if a tumor readily takes up magnetic nanoparticles (MNP), it will also accumulate other nanoparticles carrying a deadly payload. The authors injected MNPs and a fluorescent version of the therapeutic nanoparticles into mice and followed their biodistribution using imaging. Both types of nanoparticles had similar pharmacokinetics and uptake in tumor-associated host cells owing to the enhanced permeability and retention effect. In mice with human tumors, Miller and colleagues found that the tumors with high MNP uptake were significantly more responsive than those with medium or low uptake to nanoparticles delivering chemotherapeutics. Thus, MNPs can be used as companion imaging agents during nanomedicine trials to predict the therapeutic effect of their nanosized counterparts.

Science Translational Medicine
AAAS

www.sciencetranslationalmedicine.org/cgi/content/full/7/314/314ra183/DC1

Supplementary Materials for

Predicting therapeutic nanomedicine efficacy using a companion magnetic resonance imaging nanoparticle

Miles A. Miller, Suresh Gadde, Christina Pfirschke, Camilla Engblom, Melissa M. Sprachman, Rainer H. Kohler, Katherine S. Yang, Ashley M. Laughney, Gregory Wojtkiewicz, Nazila Kamaly, Sushma Bhonagiri, Mikael J. Pittet, Omid C. Farokhzad,* Ralph Weissleder*

*Corresponding author. E-mail: rweissleder@mgh.harvard.edu (R.W.); ofarokhzad@bwh.harvard.edu (O.C.F)

Published 18 November 2015, *Sci. Transl. Med.* 7, 314ra183 (2015)
DOI: 10.1126/scitranslmed.aac6522

The PDF file includes:

SUPPLEMENTARY METHODS

General synthesis materials

Moisture-sensitive reactions were performed under an atmosphere of nitrogen or argon. ^{1}H NMR spectra were referenced to residual DMSO (^{1}H, 2.50) of $CHCl_3$ (^{1}H, 7.26) (and chemical shifts (δ) are reported in ppm using the following convention: chemical shift, (multiplicity (s = singlet, d = doublet, t = triplet, q = quartet, m = multiplet, b =broad), coupling constants, and integration). A Biotage Isolera Four system was used for performing separations by automated chromatography, and reverse-phase chromatography was accomplished using C_{18} cartridges purchased from Fisher Scientific (KP-C_{18}-HS). High performance liquid chromatography-mass spectroscopy (HPLC-MS) data were obtained using a Waters instrument equipped with a Waters 2424 ELS Detector, Waters 2998 UV-Vis diode array detector. For analytical separations, a Waters XTerra C_{18} 5-μm column was used (eluents 0.1% formic acid (v/ v) in water and MeCN; gradient: 0–1.5 min, 5–100% then 1.5–2.0 min 100%.

N,*N*'-Diisopropylcarbodiimide (DIC), *N*-(3-dimethylaminopropyl)-*N'*-ethylcarbodiimide hydrochloride (EDC), *N*-hydroxysuccinimide (NHS), *N*,*N*-diisopropylethylamine (DIEA), 4-dimethylaminopyridine (DMAP), dichloromethane (CH_2Cl_2), and dimethylformamide (DMF) were purchased from Sigma-Aldrich, 50:50 poly(D,L-lactide-*co*-glycolide) polymer with carboxylic acid terminated group (PLGA-COOH, inherent viscosity 0.15-0.25) was purchased from Lactel Absorbable Polymers. The dialysis membrane was purchased from Spectrum Labs (1 kDa MWCO, Spectra/Por membrane dialysis).

PLGA-PEG synthesis

For PLGA-PEG synthesis, 250 mg of PLGA-COOH and 5.75 mg of EDC were dissolved in 2-4 ml of CH_2Cl_2 and stirred at room temperature (RT) for 10 min. 3.45 mg of NHS was then added to the mixture and continued stirring for 1 h. The solution was then added drop-wise to methanol to precipitate PLGA-NHS. The PLGA-NHS was collected, redissolved in CH_2Cl_2, and precipitated in methanol once more. The resultant PLGA-NHS was dried under vacuum for 60 min. and then dissolved in 1 ml of CH_2Cl_2, to which 20 mg of NH2-PEG-COOH and 12.5 ml of DIEA were added and stirred overnight at RT. The reaction mixture was precipitated by adding dropwise to cold diethyl ether/methanol to obtain PLGA-PEG copolymer. The copolymer was redissolved in CH_2Cl_2 and precipitated again in cold diethyl ether/methanol; this step was repeated 3 times. The precipitate was collected and dried vacuum to obtain PLGA-PEG copolymer. ^{1}H NMR (400 MHz, CDCl3): δ (in ppm) 5.1-5.3 (m, (-OCH(CH3)CO)), 4.6-4.9 (m, (-OCH2COO-)), 3.62(s, -OCH2CH2O-), 1.51-1.64 (m, (-OCH(CH3)CO-).

PLGA-BODIPY synthesis

The PLGA-BODIPY conjugate was synthesized by reacting the terminal carboxylic group of PLGA with the amine group of 8-(4,4-difluoro-5,7-dimethyl-4-bora-3a,4a-diaza-s-indacene)ethylamine (amino-BODIPY). PLGA-COOH polymer (245 mg) was added to DMF (3 ml) and stirred until the polymer completely dissolved. To this solution, DIC (11 µl, 0.073 mmol) and amino-BODIPY (10 mg, 0.037 mmol) were added and stirred at RT for 15 min. Then DMAP (6.7 mg, 0.055 mmol) was added to the reaction mixture and stirred for 24 h in the dark. The reaction mixture was concentrated to 500 µl under reduced pressure and added dropwise to ice-cold methanol, producing a yellow precipitate of PLGA-BODIPY. The precipitate was collected and purified by dissolving in CH_2Cl_2 (500 µl) and then re-precipitated in ice-cold methanol, and this process was repeated two more times. The precipitate was

then dissolved in 1 ml of CH_2Cl_2 and dialyzed for ~4 h, and the resulting CH_2Cl_2 solution was evaporated and dried under vacuum to obtain purified PLGA-BODIPY conjugate. The conjugate was characterized by ^1H NMR. ^1H NMR (400 MHz, $CDCl_3$): δ (in ppm) 5.1-5.3 (m, (-OCH(CH3)CO)), 4.55-4.9 (m, (-OCH2COO-)), 1.51-1.64 (m, (-OCH(CH3)CO-), 7.60, 6.44, 6.19 (BODIPY).

Dye-conjugated liposome synthesis

PBS-loaded liposomes composed of phosphatidylcholine (Lipoid EPC; Lipoid GmbH) and cholesterol (Sigma) were purchased from N. van Rooijen (Vrije Universiteit, The Netherlands). Liposomes were labeled with either DiO (max $\lambda_{ex}/\lambda_{em}$ = 484/501 nm) or DiD (max $\lambda_{ex}/\lambda_{em}$ = 644/665 nm) using Vybrant labeling solution (Molecular Probes) according to manufacturer's guidelines, and purified by repeat (5x) washing, centrifugation pelleting, and filtration through 0.45 μm cellulose acetate filter (Cole-Parmer) as prescribed by the manufacturer.

Dye-conjugated antibody synthesis

Affinity-purified goat IgG targeting murine EGFR (AF1280; R&D Systems) was labeled with Alexa405 (max $\lambda_{ex}/\lambda_{em}$ = 401/421 nm) using the succinimidyl ester dye conjugate and following manufacturer guidelines (Life Technologies) in DMSO solvent. Unreacted dye was removed by repeated (5x) washing and centrifugation using 30 kDa MWCO centrifugal filters (Amicon; Millipore).

PLGA-BODIPY nanoparticle synthesis

PLGA-BODIPY NPs were prepared by nanoprecipitation. Briefly, PLGA-PEG and PLGA-BODIPY were dissolved in acetone at a concentration of 10 mg/ml. The acetone solutions were mixed together at desired ratios (20:1; v/v) and added dropwise to nuclease-free H_2O while maintaining a ratio of 10:1

H_2O to organic solvent. NPs were stirred overnight and filtered through sterile 0.45-μm syringe filters (regenerated cellulose, 17 mm, Cole Palmer). The NPs were concentrated by centrifugation using Amicon Ultra-15 centrifugal filter units (MWCO 100 or 50 kDa). The concentrated NPs were washed twice with de-ionized H_2O and re-suspended in 1 ml of nuclease-free H_2O. NPs were diluted 20X in water and subjected to size and surface charge measurements using dynamic light scattering (Malvern Zetasizer). BODIPY concentration was determined by a microplate fluorimeter after diluting NPs in DMF and using pure amino-BODIPY for a standard curve. Transmission electron microscopy (TEM) experiments were performed on a TecnaiTM G2 Spirit BioTWIN electron microscope equipped with an AMT 2k CCD camera and low-dose software (80 kV, direct magnification 98,000x). The TEM sample was prepared by depositing 10 μl of NPs (1.0 mg/ml) onto a carbon-coated copper grid. The excess solution was blotted, and the grids were immersed in a solution of 0.75% uranyl formate stain. The stain was blotted, and dried grids were used for imaging within one hour of the preparation of NPs.

Dye-conjugated ferumoxytol nanoparticle (MNP) synthesis

Ferumoxytol (AMAG Pharmaceuticals) was dialyzed against H_2O overnight. One gram of EDC-HCl (*N*-(3-dimethylaminopropyl)-*N*-ethylcarbodiimide hydrochloride) was added to 9 ml of dialyzed ferumoxytol (6 mg/ml Fe) and then added to 3 ml of 2-M ethylenediamine dihydrochloride (EDA-HCl). Reaction was incubated overnight at RT, pH 6.5. Aminated ferumoxytol was then dialyzed against a pH 8 solution of 0.02-M sodium citrate and 0.15-M NaCl, then 1.4 ml of 21 mg/ml was added to 1 ml of 0.2-M HEPES, pH 7.75, and 0.5 ml of 10 mg/ml VivoTag 680 XL (VT680XL; Perkin Elmer; max $\lambda_{ex}/\lambda_{em}$ = 665/688 nm), VivoTag S 750 (VT750; Perkin Elmer; max $\lambda_{ex}/\lambda_{em}$ = 750/775 nm), Pacific Blue (Life Technologies; max $\lambda_{ex}/\lambda_{em}$ = 415/451 nm), or Alexa568 (A568; Life Technologies; max $\lambda_{ex}/\lambda_{em}$ = 578/603 nm) in DMF. The reaction was incubated at RT overnight in the dark, and free dye was then

removed by chromatography (PD-10 desalting columns; GE Healthcare) equilibrated with a pH 8 solution of 20 mM Na-citrate and 0.15 M NaCl. Using a plate fluorimeter, conjugation was determined to be roughly 3 dye molecules per ferumoxytol nanoparticle, with a final dye concentration of roughly 5 mM.

Synthesis of fluorescent docetaxel derivatives

The silicon-rhodamine (SiR) docetaxel derivative was synthesized according to (*33*). Fluorophore **1** (fig. S8D) was synthesized according to (*34*).

6-(3-(5-Fluoro-5-(2-hydroxyethoxy)-1,3,7,9-tetramethyl-5H-4λ⁴,5λ⁴-dipyrrolo(1,2-c2',1'-f, 1,3,2)diazaborinin-10-yl)propanamido)hexanoic acid **3** (fig. S8D). A solution of **1** (20.0 mg, 0.0435 mmol) in anhydrous DMF (435 µl) was treated with *i*-Pr_2EtN (15 µl, 0.087 mmol) and 6-aminohexanoic acid **2** (8.6 mg, 0.065 mmol). The solution was stirred for 30 min at RT and then loaded onto a Biotage SiO_2 column. Purification (Biotage 10 g SiO_2 column, 0-10% MeOH/CH_2Cl_2) afforded **3** (17 mg, 82%) as an orange solid: ^{1}H NMR (400 MHz, DMSO-d_6) δ 7.96 (bs, 1 H), 6.19 (s, 2 H), 3.25 (t, J = 6.1 Hz, 2 H), 3.20-3.16 (m, 2 H), 3.07, 3.04 (AB, J = 6.6 Hz, 2 H), 2.97 (dt, J = 13.1, 6.6 Hz, 1 H), 2.75-2.72 (m, 2 H), 2.69 (s, 6 H), 2.44 (s, 3 H), 2.41 (s, 3 H), 2.38-2.24 (m, 2 H), 2.16 (t, J = 7.3 Hz, 2 H), 1.52-1.44 (m, 2 H), 1.41-1.36 (m, 2 H), 1.29-1.23 (m, 2 H); 13 C NMR (100 MHz, DMSO-d6) δ 174.3, 169.8, 153,5, 139.8, 131.3, 121.5, 62.9, 61.6, 47.6, 36.6, 28.7, 26.0, 24.3, 23.8, 20.7, 16.9, 16.0, 14.2; LC-MS (ESI) calc for $C_{24}H_{35}BFN_3NaO_5$ (*M+Na*)+ 498.26, found 498.34.

Docetaxel conjugate **5** (fig. S8D). A solution of **3** (17 mg, 0.036 mmol) in DMF (360 µl) was treated with *i*-Pr_2EtN (130 µl, 0.75 mmol) and TSTU (*N,N,N',N'*-tetramethyl-*O*-(*N*-succinimidyl)uronium tetrafluoroborate; 14 mg, 0.047 mmol) and incubated at RT for 10 min. To this solution was added docetaxel formate salt **4** (see below) (568 µl, 0.0568 mmol, c = 100 mM in DMF),

and the solution was incubated for 3 h at RT. The solution was loaded directly onto a Biotage C18 column. Purification by chromatography (Biotage, 25 g C18, 10% MeCN/H_2O to 70% MeCN/H_2O; product elutes at ca. 45-55% MeCN/H_2O) afforded **5** (20.9 mg, 50%) as an orange solid: ^{1}H NMR (400 MHz, DMSO-d_6) δ 8.38 (d, J = 8.9 Hz, 1 H), 8.02-7.93 (m, 2 H), 7.70-7.65 (m, 2 H), 7.38-7.30 (m, 4 H), 7.22-7.19 (m, 1 H), 6.19 (s, 2 H), 5.97-5.89 (m, 1 H), 5.42 (d, J = 7.0 Hz, 1 H), 5.27 (dd, J = 9.3, 6.2 Hz, 1 H), 5.22 (bs, 1 H), 5.10-5.09 (m, 1 H), 5.01 (d, J = 7.2 Hz, 1 H), 4.94 (d, J = 2.2 Hz, 1 H), 4.91 (d, J = 8.6 Hz, 1 H), 4.43-4.38 (m, 2 H), 4.32 (t, J = 5.7 Hz, 1 H), 4.08-3.99 (m, 3 H), 3.68 (d, J = 7.0 Hz, 1 H), 3.25 (dd, J = 11.7, 5.8 Hz, integration obscured by water peak), 3.18-3.14 (m, 4 H), 3.05-2.99 (m, 2 H), 2.96 (dt, J = 13.2, 6.6 Hz, 1 H), 2.74 (t, J = 6.0 Hz, 2 H), 2.43 (s, 6 H), 2.41 (s, 6 H), 2.33-2.32 (m, 2 H), 2.24 (s, 3 H), 2.20-2.14 (m, 2 H), 1.77-1.72 (m, 4 H), 1.53 (s, 3 H), 1.50-1.46 (m, 2 H), 1.40-1.32 (m, 3 H), 1.24-1.19 (m, 3 H), 0.95 (s, 3 H), 0.93 (s, 3 H); LC-MS (ESI) calc for $C_{62}H_{78}BFN_4NaO_{16}$ $(M+Na)+$ 1187.54, found 1187.66.

Docetaxel formate salt **4** (fig. S8D) was prepared as described previously (*33*) and stored as 100-mM aliquots in DMF.

Paclitaxel-loaded TNP synthesis

As with PLGA-BODIPY nanoparticle synthesis, TNP-encapsulated paclitaxel and docetaxel—BODIPY were prepared by nano-precipitation. Briefly, the following reagents were dissolved in 50:50 v/v DMF:ACN at the indicated concentrations: $PLGA_{30\text{-}60kDa}$ (0.17 mg/ml; lactide:glycolide (50:50); Sigma), paclitaxel (0.08 mg/ml; LC Labs) or docetaxel-BODIPY (0.08 mg/ml), and $PLGA_{7\text{-}17kDa}$-PEG_{5kDa} (0.83 mg/ml; lactide:glycolide (75:25); Advanced Polymer Materials, Inc). The resulting solution was then mixed and added drop-wise to nuclease-free H_2O while maintaining a ratio of 20:1 H_2O to organic solvent. TNPs were stirred overnight and filtered through sterile 0.45 μm syringe filters

(regenerated cellulose, 17 mm, Cole Palmer). The TNPs were concentrated by centrifugation using centrifugal filter units (Amicon; Millipore; MWCO 100 kDa). The concentrated TNPs were washed twice with de-ionized H_2O and re-suspended in 1 ml of nuclease-free H_2O. TNPs were diluted 10 times in H_2O and characterized by size and surface charge using dynamic light scattering (DLS; Malvern Zetasizer). The paclitaxel loading concentrations were determined by LC/MS and using a 9-point standard curve generated from purified paclitaxel ($R^2 > 99.5\%$). Docetaxel-BODIPY loading concentrations were determined by absorbance at 488 nm (NanoDrop; Thermo) and a 5-point standard curve ($R^2 > 99.9\%$). To characterize payload release, paclitaxel-NPs were incubated in PBS at 37°C, filtered using 100 kDa MWCO centrifugal filters (Amicon; Millipore) at the indicated time-points and resuspended in fresh PBS. Filtrate was frozen for later analysis by LC/MS. Both the paclitaxel-TNPs and the filtrate were analyzed at the terminal time-point to quantify the remaining unreleased paclitaxel.

Animal and cell models

HT1080 (ATCC) and A2780CP (Sigma) were routinely cultured according to the manufacturer's guidelines. The murine lung adenocarcinoma cell line KP1.9 was generated from lung tumor cells of *Kras*$^{LSL\text{-}G12D/+}$;*p53*$^{fl/fl}$ mice (C57/Bl6 background). These mice develop lung adenocarcinoma after infection with an adenovirus expressing Cre recombinase by intratracheal instillation as described previously (*21*). KP1.9 cells were maintained in Iscove's DMEM media supplemented with 10% fetal bovine serum (FBS) and 5% penicillin/streptomycin.

Apple fluorescent protein was subcloned into the pLVX-mApple vector using AfeI and NotI restriction enzymes. A XhoI site was inserted in the 5' end of the pLVX-mApple multiple cloning site using QuikChange site-directed mutagenesis (Agilent). The membrane-targeting sequence from pDsRed-Monomer-Mem (Clontech) was PCR-amplified for In-Fusion cloning to make pLVX-Mem-mApple. The PCR product was ligated into pLVX-Apple after AfeI and XhoI digestion, and then

sequenced in its entirety. The vector was transfected into 293T packaging cells using the Lenti-X HTX Packaging System (Clontech) to produce lentiviral particles for transduction into HT1080 and A2780CP cells. Mem-mApple-expressing cells were selected in 3 μg/ml puromycin, and clones were screened for fluorescent expression by microscopy over multiple passages.

Cx3cr1$^{GFP/+}$ animals were generated by crossing *Cx3cr1*$^{GFP/GFP}$ mice with C57BL/6J, and the *Cx3cr1*$^{GFP/+}$ mice have a *Cx3cr1* allele replaced with *eGFP* and can be used to track monocytes, macrophages, and dendritic cells. For dual reporter mice, *Cx3cr1*$^{GFP/GFP}$ animals were crossed with *R26*$^{mT\text{-}mG/mT\text{-}mG}$ animals that ubiquitously express membrane-anchored tdTomato. The resulting *Cx3cr1*$^{GFP/+}$ *R26*$^{mT\text{-}mG/+}$ animals can be used to visualize GFP+ tdTomato+ macrophages, monocytes, and dendritic cells, as well as tdTomato+ stroma and endothelium.

Histology

Subcutaneous tumors (KP1.9 cells) were harvested from C57/Bl6 mice 3 weeks post-implantation and 24 h post-treatment with MNPs and TNPs, just as performed for the flow-cytometry experiments in the KP model (Fig. 3). Excised tumors were embedded in O.C.T. compound (Sakura Finetek). Fresh-frozen 6-μm thick sections were prepared and stained with anti-mouse F4/80 antibody (clone: BM8, eBioscience). For immunohistochemistry, a biotinylated anti-rat IgG antibody was applied, and VECTASTAIN ABC kit (Vector Laboratories Inc.) along with a 3-amino-9-ethylcarbazole substrate (Dako) were used for color development. The sections were counterstained with Harris hematoxylin solution (Sigma-Aldrich) and scanned by using Nanozoomer 2.0RS (Hamamatsu, Japan). For immunofluorescence, anti-rat IgG-Alexa Fluor 405 (Abcam) as a secondary antibody and anti-mouse CD326 (EpCAM)-PE antibody (clone: G8.8, eBioscience) were used, and the images were captured

using BX63 (Olympus) equipped with ANDOR Neo sCMOS Monochrome Camera (Andor Technology Ltd.).

Intravital imaging

Dextran pacific blue (λ_{ex} = 405 nm) was injected to initially locate tumor vasculature; for synthesis, 500 kDa amino-dextran (Life Technologies) was conjugated to Pacific-Blue succinimidyl ester (Life Technologies) according to manufacturer's instructions, quenched with Tris buffer, and free dye was removed by repeat (5x) washing in H_2O using Amicon-Ultra 100 kDa MWCO spin-filters (Millipore).

Terminal orthotopic imaging was performed by surgically opening the peritoneal cavity of nu/nu mice approximately 6 weeks following intraperitoneal injection of 10 million A2780CP-membrane-mApple cells. For ear vasculature measurements, naïve *nu/nu* mice were imaged using an Olympus IV110 laser-scanning microscope. Liposomes and ferumoxytol-VT750 were also imaged with the IV110, using sequential scanning with 488-nm, 561-nm, 633-nm, and 748-nm lasers and a 20x objective (all Olympus America). Terminal imaging of subcutaneous tumors was performed by immediately imaging following animal sacrifice, tumor excision, and suspension in PBS using FV1000 and IV110 confocal microscopes.

MR imaging

The imaging protocol included multiple-slice and multiple-echo spin-echo sequences with 16 different echo times: 8.68, 17.36, 26.04, 34.72, 43.40, 52.08, 60.76, 69.44, 78.12, 86.80, 95.48,104.16, 112.84, 121.52, 130.20, and 138.88 ms. Other parameters included the following: repetition time, 2325 ms; field of view, 4 cm × 4 cm; matrix size, 128 × 128; slice thickness, 1 mm (interleaved); number of excitations, 8. To cover the entire abdominal region, 16 sequential coronal images were obtained. Entire tumors were manually segmented in both the 1 h and 24 h post injection scans using Osirix. Segmented

tumors were then fused and subtracted using a normalized mutual information algorithm in Amira software. The 2D slices of the Δ(1h-24h) overlaid on a T2 image of the mouse prior to injection were performed in Osirix.

Flow cytometry

Subcutaneous tumors (KP1.9 cells) were harvested from C57/Bl6 mice 3 weeks post-implantation, cut into small pieces, and incubated in RPMI 1640 media containing 0.2mg/ml collagenase type I (Worthington Biochemical Corporation) for 30 min at 37°C while shaking (600 rpm). Digested tumors were filtered through a 40 μm cell strainer (BD Falcon). The resulting single-cell suspensions were washed and resuspended in PBS with 0.5% BSA and 2 mM EDTA and incubated for 15 min at 4°C with Fc blocking reagent (TruStain fcX anti-mouse CD16/32; clone 93; Biolegend). Cell labeling was performed with appropriate antibodies as indicated below for 45 min at 4°C. The following cell types were identified by flow cytometry (LSRII, BD Biosciences) depending on cell marker expression: tumor cells ($CD45^-EpCAM^+$), MF ($CD45^+CD11b^+Ly6C^-Lin^-CD11c^+F4/80^+$), neutrophils ($CD45^+CD11b^+Ly6C^+Lin^+$) and lymphocyte-like cells ($CD45^+CD11b^-Lin^+$). The following anti-mouse antibodies were used from eBioscience: EpCAM (clone G8.8); from Biolegend: CD45 (clone 30-F11), F4/80 (clone BM8), CD11c (clone N418), Ly6C (clone HK1.4) and from BD Biosciences: CD11b (clone M1/70). The lineage (Lin) antibody mix contained the following antibodies (all purchased from BD Biosciences): anti-CD90.2 (clone 53-2.1), anti-B220 (clone RA3-6B2), anti-NK1.1 (clone PK136), anti-CD49b (clone DX5), anti-Ter119 (cloneTER-119) and anti-Ly6G (clone 1A8). To exclude dead cells, 7-aminoactinomycin D (7-AAD, Sigma-Aldrich) was used.

Data were analyzed using FlowJo v.8.8.7 (Tree Star, Inc.) and MATLAB. VT680 and BODIPY-

FL fluorescence were directly assessed using the LSRII flow cytometer. For each tumor, NP uptake was quantified by median fluorescence intensity for each cell population, after subtraction of the median fluorescence intensity for the same cell population in the vehicle-injected (control) tumors. Relative NP uptake per cell was then normalized to the maximum average NP uptake among all cell populations. For both TNP and MNP, this was the MΦ population.

For quantification of DNA content and DNA damage response, $2x10^6$ HT1080 cells were suspended in 50 µl PBS and injected subcutaneously in *nu/nu* mice (Cox7, MGH). Following the timeline outlined in Fig. 5C, tumors were excised and processed for flow cytometry as described above but with several alterations. Dead cells were excluded using LIVE/DEAD fixable violet dead cell stain (Life Technologies). HT1080 tumor cells were identified by hCD29 (clone MAR4; BD), and cells were then fixed in 70% ethanol overnight at -20°C, rinsed, and permeabilized in 0.1% Triton-X-100. Cells were blocked for 1h in Odyssey Blocking Buffer (Li-Cor). Apoptosis was measured using the In Situ Direct DNA Fragmentation (TUNEL) Assay Kit (Abcam) according to manufacturer's guidelines. γH2A.X (clone 20E3; Cell Signaling Technology) and TUNEL staining were used in conjunction with FxCycle Far Red DNA counterstain (Life Technologies). Cells were treated with 100 µg/ml RNaseA (Thermo) and rinsed before analysis. Sub-G1 and G1 populations were manually gated in FloJo based on DNA content, and γH2A.X staining and standard deviation (σ) were calculated for individual populations.

Computational image analysis

For vascular half-life calculations, fluorescence time-lapse values from multiple vessels across multiple animals were recorded, averaged, and fit to an exponential decay model. Initial vascular concentrations of NPs (C_0; Fig. 1) were based on confocal fluorescence measurements and inferred from the

exponential decay model described above, extrapolated to t = 0 minutes post-injection. Single-cell segmentation for image cytometry analysis was performed using a custom CellProfiler (CellProfiler.org) pipeline. Briefly, fluorescence channels were merged, cells were identified based on intensity and morphology criteria, and accuracy was validated by visual inspection.

Finite element analysis used a previously described framework, including mesh generation, governing equations, boundary conditions, and initial conditions (*15*), but with explicit modeling of heterogeneous phagocyte activity. Bound drug obeyed a no-flux boundary condition. NP uptake reactions (binding and release) were modeled by mass-action kinetics integrated at each time-step, and PDEs were integrated using the parabolic solver in the Matlab PDE toolbox. The optimization cost function was calculated as a sum of squared residuals in NP concentration at each time-point and each point in the FEM. For the addition of phagocyte modeling, images acquired immediately after NP injection were first segmented using CellProfiler to define vascular structure and host phagocyte location, and segmentation results were then manually optimized. Host phagocyte location followed the same governing-rate equations (Fig. 4A) but were modeled according to distinct parameters (table S1). Nonspecific NP binding was assumed negligible. Reaction parameters were initially estimated based on a mix of previously published results and the intravital imaging data presented here (table S1). For each type of NP, rates were then simultaneously and globally optimized using a simulated-annealing algorithm (Matlab) to maximize the fit between the model predictions and the time-lapse images during the first 2 h after NP injection.

The inherently stochastic simulated annealing algorithm was performed with 100 optimization generations (1000 additional optimization generations only modestly improved the model fit with <1% improvement, so 100 was deemed sufficient), and this optimization was repeated across 10 independent optimization runs. Optimal parameter sets were averaged across these independent runs (table S1). This

analysis yielded two sets of optimized modeling parameters, one describing ferumoxytol (MNP) and one describing PLGA-PEG (TNP) (Fig. 4A, right; table S1). To calculate spatial correlation for MNP and TNP model fits (Fig. 4B), images were manually segmented into individual cells and vessels, integrated intensity values were measured for each segmented object, and results were then correlated across >200 objects between the computational model and the image data. MNP and TNP co-mapping was performed by first calculating a ratio of computationally modeled TNP/MNP values across individually segmented cells and vessels. This ratio was then multiplied by the MNP images to yield "MNP-corrected data."

Parametric sensitivity analysis was performed to assess how changes in model parameters (rate constants, macrophage density, etc.) affected total NP accumulation within the bulk tumor mass after 2 h (Fig. 4C). For this analysis, parameters were individually adjusted by ± 25%, and total simulated NP accumulation at 2 h was then recorded. Macrophage density was adjusted by reverting segmented macrophage regions into tumor-cell regions. The change in NP accumulation as a function of the change in rate constant k was then calculated for each parameter, as a fraction of baseline NP accumulation predictions: $(d(NP)/dk)*(k/(NP0))$. This procedure of parameter adjustment and simulation analysis was performed across the multiple optimized parameter sets from the independent simulated annealing optimizations, allowing for calculation of average parametric uncertainties and corresponding standard error measurements.

To adjust image resolution, 4x, 10x, and 40x microscopy images were randomly and iteratively cropped and then automatically down-sampled using Matlab. Correlation between MNP and TNP intensities were then calculated across all down-sampled pixels for each image, and correlation values were then averaged across all images. This process was performed for resolution downsampling factors from 1x to 340x at intervals of 0.1, results were smoothed using robust weighted linear least squares

local regression (thick line in plot), and error (shaded area in the plot) was calculated from the square root of the smoothed squared fit residuals. Results were relatively independent of image resizing method (nearest neighbor shown; bilinear and bicubic also tested).

MNP prediction of drug uptake

For correlation between tumoral uptake of MNPs, TNP, free drug, and EGFR-targeting antibody, we used the orthotopic 4T1 breast cancer syngeneic mouse model. Once tumors reached roughly 8 mm in diameter, animals were co-injected with combinations of one or more of the following: 1 mg/kg TNP-encapsulated TXT-BODIPY; 1 mg/kg un-encapsulated TXT-SiR; ferumoxytol-VT750XL (750 μg Fe); and/or 10 μg anti-EGFR Ab-Alexa405. NPs and Ab's were injected i.v. 20 h before imaging, and un-encapsulated drug was injected 5h before imaging; injections were staggered to account for differences in plasma clearance. Following injection, tumors were excised, mechanically homogenized in cold PBS, and lysed using 1% Triton X-100, 150 mM NaCl, 50 mM Tris pH 8.0, and cOmplete protease inhibitor cocktail (Roche). Tumor lysate was then strained through 50-μm nylon mesh, spun at 16,000 x g for 10 min to remove insoluble material, and immediately analyzed using a fluorescence plate-reader (Tecan). Measurements were normalized to protein concentration as determined by the micro-BCA assay (Pierce); samples below the minimum protein concentration determined by sensitivity of a standard curve (R^2>99.9%; provided by manufacturer) were excluded. Background fluorescence from no-injection control tumors was subtracted, and values were reported as a fraction of the average "low MNP/low Ab" group.

SUPPLEMENTARY FIGURES

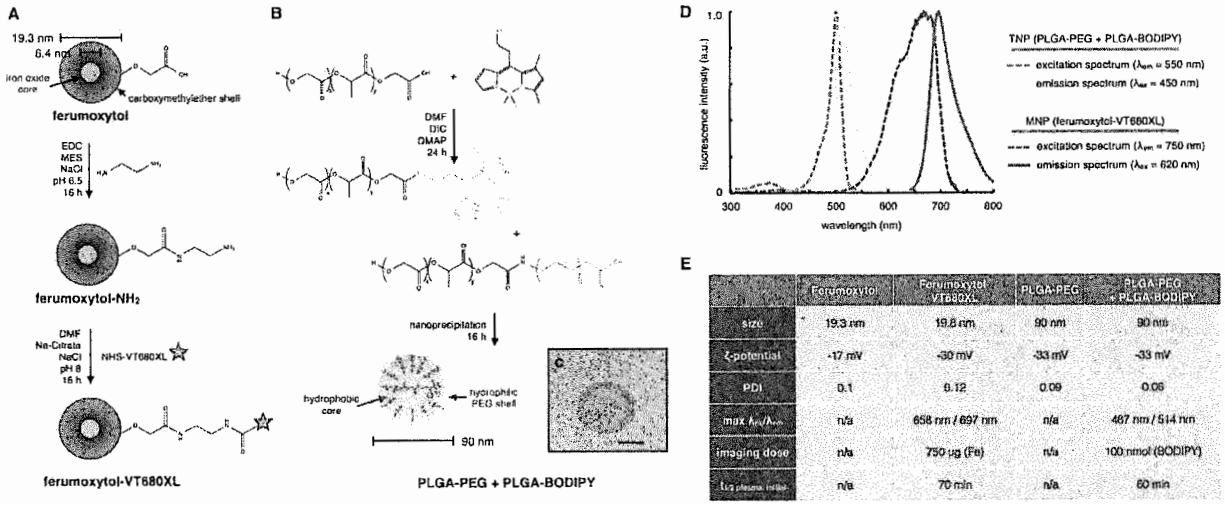

	Ferumoxytol	Ferumoxytol-VT680XL	PLGA-PEG	PLGA-PEG + PLGA-BODIPY
size	19.3 nm	19.8 nm	90 nm	90 nm
ζ-potential	-17 mV	-30 mV	-33 mV	-33 mV
PDI	0.1	0.12	0.09	0.06
max $\lambda_{ex}/\lambda_{em}$	n/a	658 nm / 697 nm	n/a	467 nm / 514 nm
imaging dose	n/a	750 µg (Fe)	n/a	100 nmol (BODIPY)
$t_{1/2}$ plasma half-life	n/a	70 min	n/a	60 min

Figure S1. Fluorescent NP synthesis and characterization. (**A**) VT680XL conjugation to MNP (ferumoxytol). (**B**) TNP (PLGA-PEG nanoparticle) doping with PLGA-BODIPY. (**C**) Transmission electron microscopy of a TNP described in (B). Note transmission electron microscopy preparation reduces NP size (*35*). Scale bar, 20 nm. (**D**) Fluorescent excitation (ex) and emission (em) spectra, measured at 30 µM dye equivalents in phosphate-buffered saline. The legend lists the excitation and emission wavelengths used in measuring the emission and excitation spectra, respectively. (**E**) NP properties.

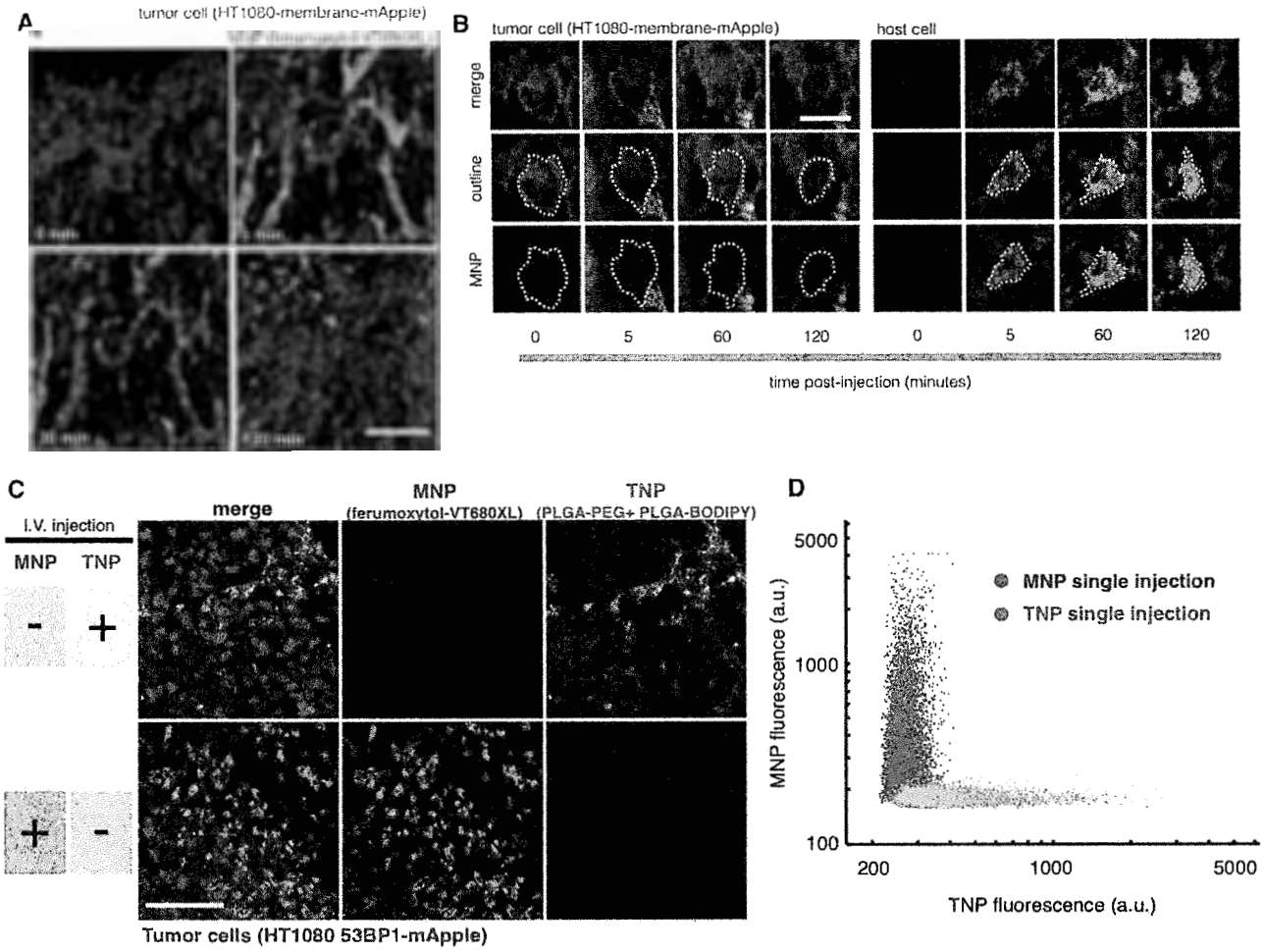

Figure S2. Imaging single-cell kinetics of MNP distribution with no TNP/MNP fluorescence spectral bleed-through. (**A**) Time-course measurement of the single-cell distribution of MNP ferumoxytol (green) to tumor cells (expressing membrane-localized RFP/mApple) and host cells within a live xenograft mouse model and the dorsal window chamber. Scale bar, 100 μm. (**B**) Zoomed-in images demonstrate real-time single-cell tracking. Scale bar, 25 μm. (**C**) Single-injection controls for intravital imaging of NP uptake within subcutaneous HT1080 tumors expressing a nuclear-localized fluorescent protein (53BP1-mApple). Animals received either MNP or TNP injection, and 5 h later tumors were excised and imaged using acquisition setup in Figs. 1 and 2. Scale bar, 100 μm. (**D**) Quantification of images in (C), demonstrating no major bleed-through or spectral overlap in the fluorescence imaging of MNPs and TNPs.

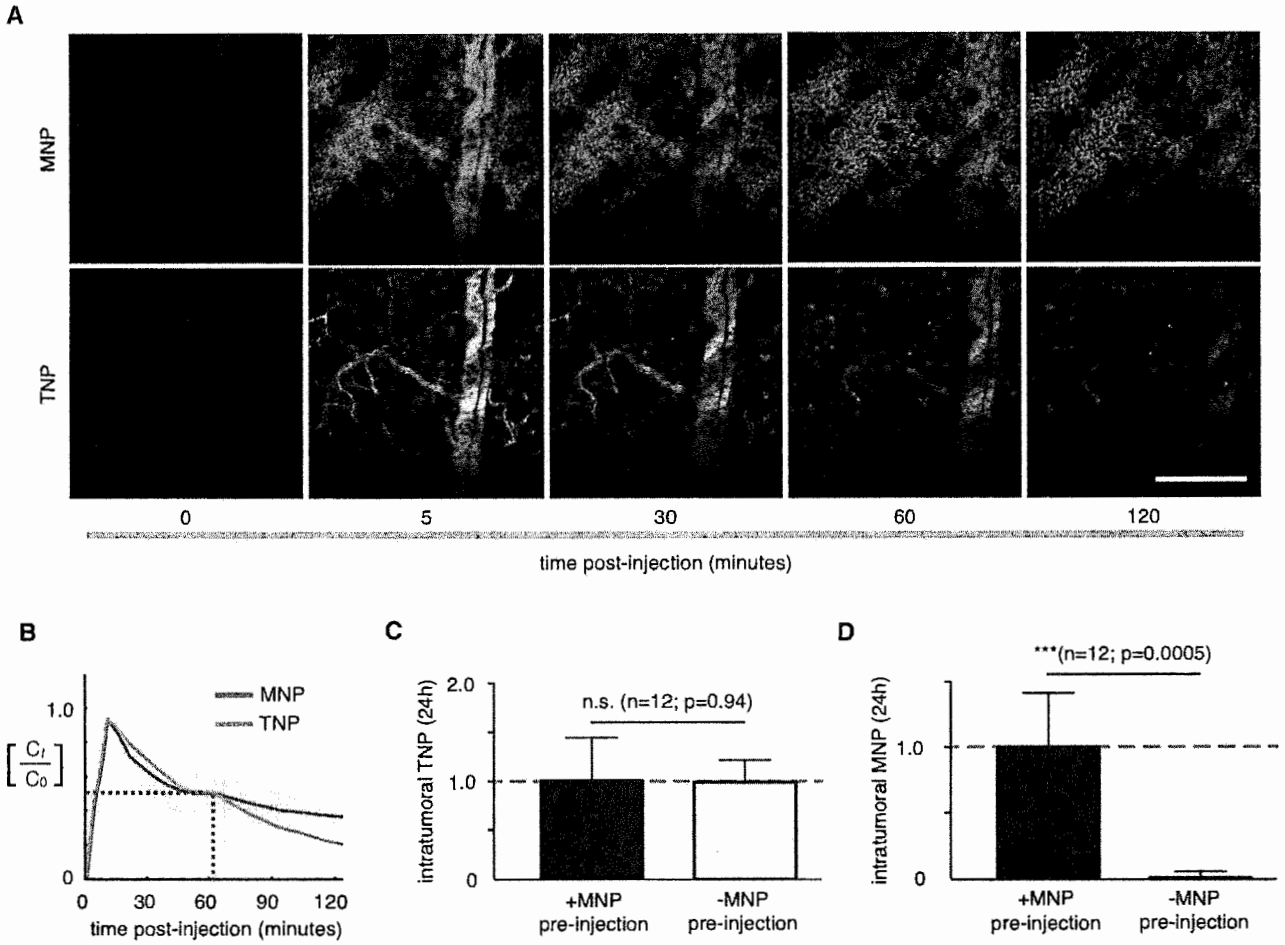

Figure S3. MNP matches TNP plasma kinetics and does not influence TNP uptake. (**A** and **B**) Ear vasculature was imaged in naive *nu/nu* mice immediately following i.v. NP administration (A), and quantified across $n \geq 4$ vessels and $n = 3$ animals after normalizing the time-dependent concentration (C_t) to fraction of initial vascular concentration (C_0), which was determined by fitting kinetics to a model of exponential decay (B). Data are means (lines) ± SD (shading). Scale bar, 500 μm. (**C** and **D**) NP accumulation in HT1080 tumors, 24 h after TNP injection (C) and 48 h after MNP (D) or saline injection. On day 3, tumors were excised and analyzed for NP uptake by fluorescence imaging. Data are means ± SD, normalized to the average tumor fluorescence in the MNP pre-injected group. *P* values determined by two-tailed t-test.

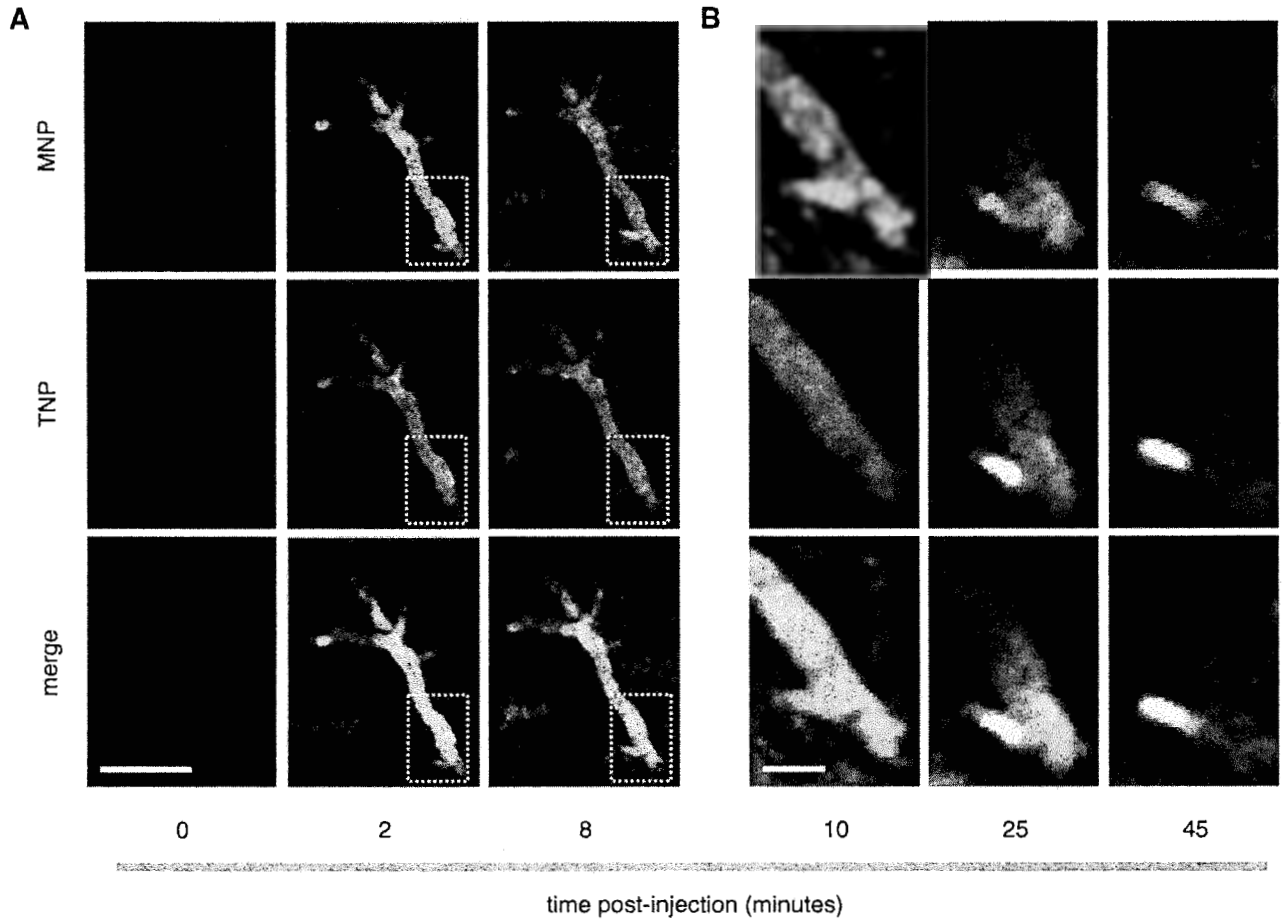

Figure S4. MNP and TNP uptake by perivascular host cells in ovarian cancer. (**A**) Representative time-lapse image showing NP labeling of circulation within tumor microvasculature and rapid NP uptake in vivo in an orthotopic human metastatic ovarian tumors. A2780CP ovarian cancer cells were injected intraperitoneally, and 6 weeks later a tumor on the surface of the intestine was imaged during i.v. NP administration. Scale bar, 200 μm. (**B**) Magnified images corresponding to the white dashed boxes in (A). Scale bar, 40 μm.

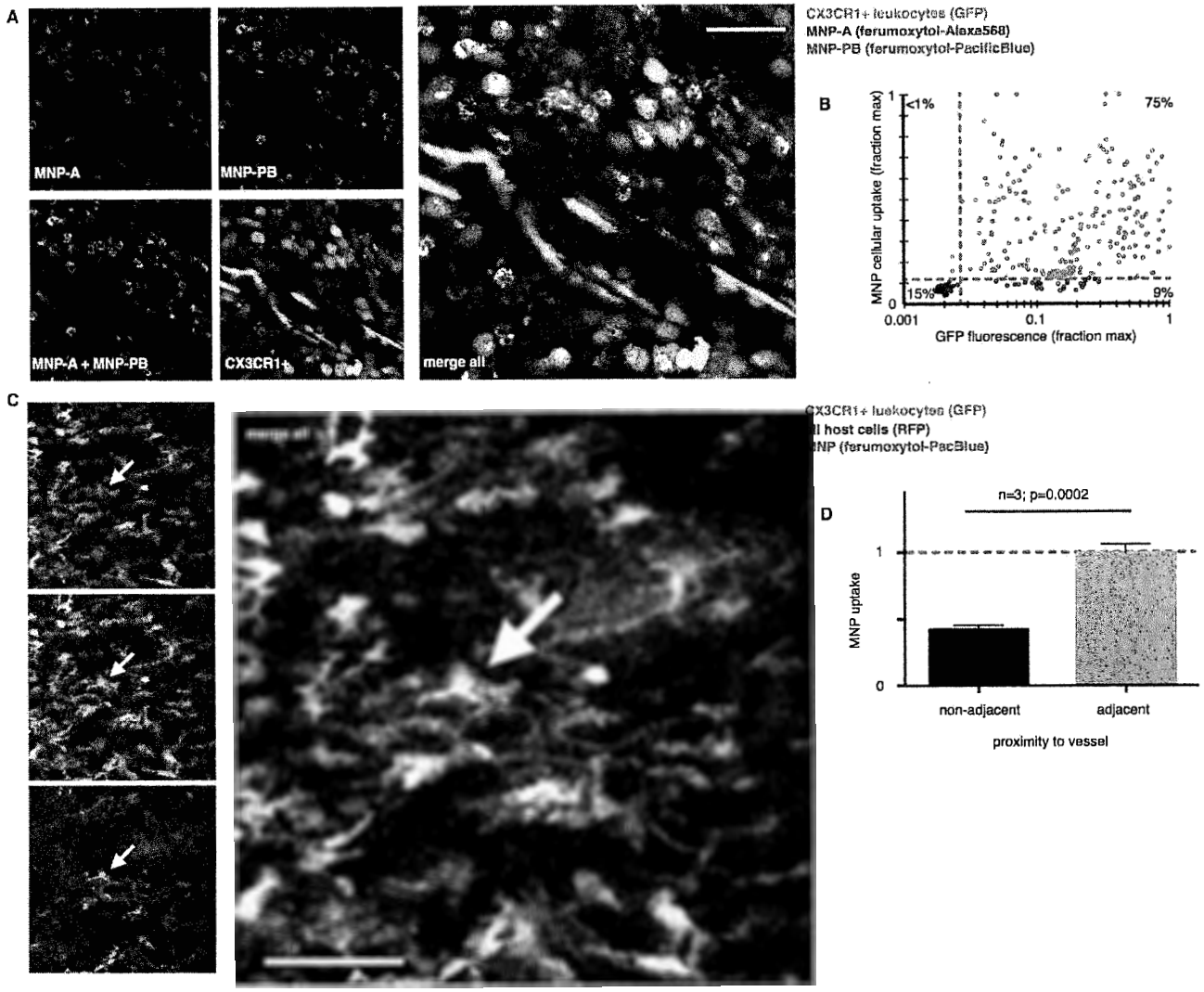

Figure S5. MNP uptake in tumor-associated Cx3cr1^{+} host cells. *Kras* mutant *p53*$^{-/-}$ (KP) cells derived from autochthonous lung tumors were subcutaneously implanted into fractalkine *Cx3cr1*$^{GFP/+}$ reporter mice in a C57Bl/6J background, for directly visualizing host leukocytes, including GFP+ monocytes, dendritic cells, and TAMs. Two different fluorophore-conjugated ferumoxytol formulations were injected to control for fluorophore-induced bias (which was minimal given the strong co-localization between the two MNPs), and tumors along with stromal regions adjacent to tumors were confocally imaged the following day. (**A** and **B**) GFP and MNP fluorescence intensities were quantified for single-cells based on the images in (A), showing that all cells accumulating significant MNP were also GFP^{+} (n = 3 animals, n = 300 cells). Scale bar, 50 μm. (**C**) Tumor-adjacent stroma was imaged 24 h post-injection of MNP in *Cx3cr1*$^{GFP/+}$ reporter mice also ubiquitously expressing membrane-anchored tdTomato in all host cells including endothelium. Arrow indicates a perivascular GFP^{+} host leukocyte that has taken up MNPs. Scale bar, 50 μm. (**D**) MNP accumulation in perivascular (adjacent) GFP+ host cells compared with cells not adjacent to the tumor microvasculature. Data are means ± SEM (n > 200 cells across 3 tumors). P value determined by two-tailed t-test.

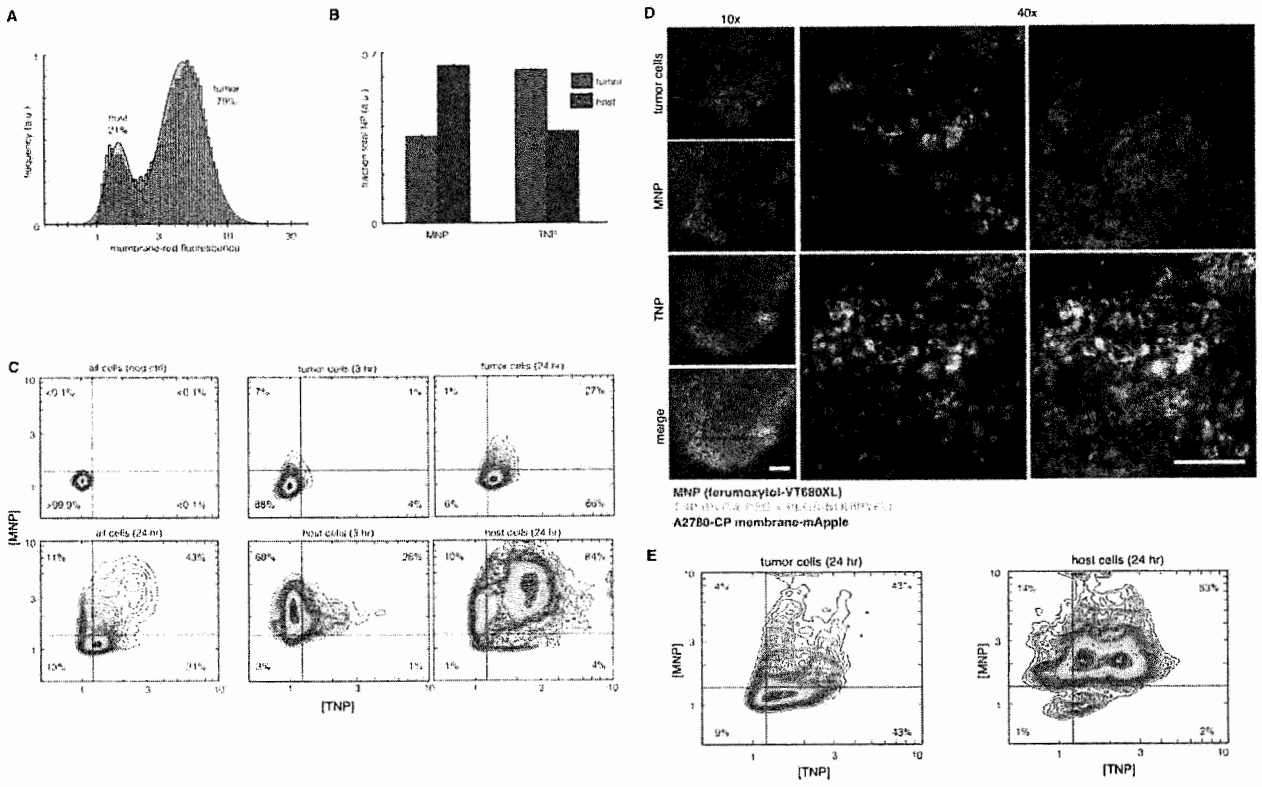

Figure S6. Imaging cytometric analysis of single-cell NP distribution kinetics. (**A**) Single-cell distribution of the tumor cell–specific fluorescent reporter (membrane-red) from image segmentation analysis describes the relative levels of host vs. tumor cells within the bulk tumor mass. (**B**) Following single-cell image segmentation, all identified cells were quantified according to TNP and MNP fluorescence. Fluorescence signals were then integrated over all tumor- and host- cell populations corresponding to (A). (**C**) NP fluorescence shown as contour plots where lines and color indicate single-cell distribution density. Data were generated from $n = 3$ animals and >400 images. (**D**) Representative image showing intratumoral NP accumulation in vivo in an orthotopic mouse model of human metastatic ovarian cancer. A2780CP cells were injected i.p., and 6 weeks later a tumor on the lining of the peritoneum was imaged 24 h after NP administration. Scale bars, 100 and 50 μm for 10x and 40x images, respectively. (**E**) Following single-cell image segmentation, all identified cells were quantified according to PLGA-PEG nanoparticle (TNP) and ferumoxytol (MNP) fluorescence intensities, shown as contour plots where lines and color indicate single-cell distribution density. Data in (D and E) are averages of >500 cells, from >30 tumor areas in $n = 2$ animals.

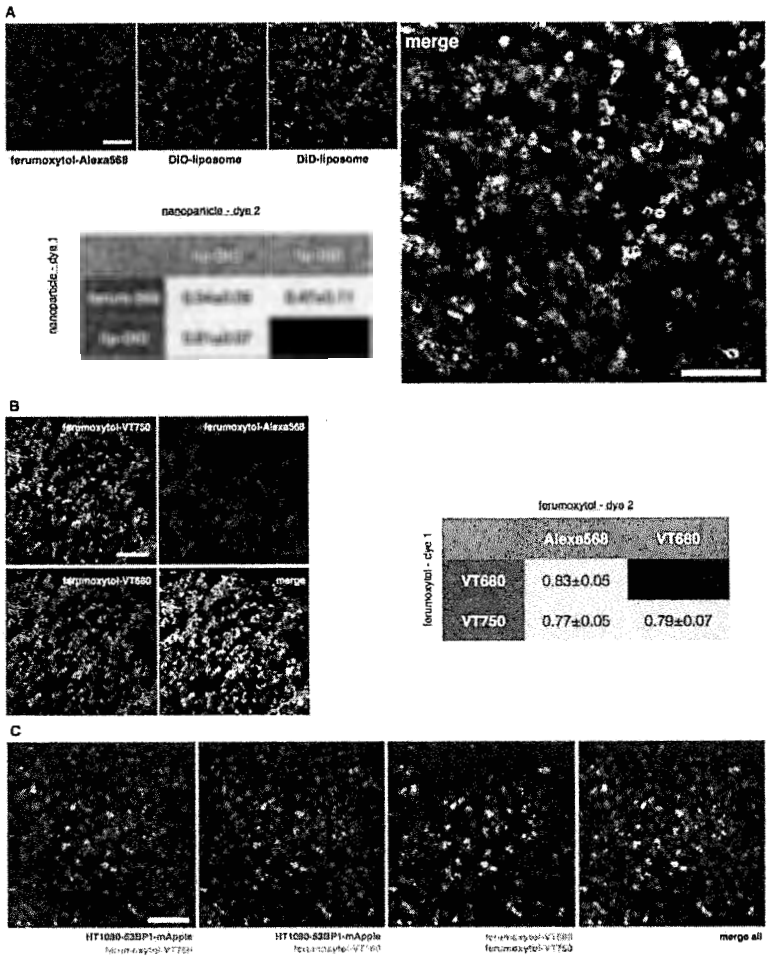

Figure S7. MNPs colocalize with liposomes in tumor-associated cells. (**A**) Dye-labeled ferumoxytol (MNP) and phosphatidylcholine:cholesterol liposomes (model TNP) were intravenously co-injected into HT1080 53BP1-mApple xenografted mice. Twenty-four h later, tumors were excised and immediately imaged by fluorescence confocal microscopy. Example images from individual fluorescent channels (left) correspond to the merged image, showing host cells accumulating both ferumoxytol and liposome in stromal regions adjacent to the tumor. Pearson's correlation coefficient was calculated by comparing fluorescence intensities as they varied across pixels (± SEM; $n = 4$), and results did not depend on the fluorophores used in the correlation measurement ($P > 0.05$, two-tailed t-test). (**B**) Three separate batches of ferumoxytol were labeled with three distinct fluorophores and were subsequently co-injected i.v. into HT1080 53BP1-mApple xenografted mice. Tumors were excised 24 h later and immediately imaged by fluorescence confocal microscopy. Example images from individual fluorescent channels show host cells accumulating substantial amounts of all ferumoxytol-dye conjugates in stromal regions adjacent to the tumor. Pearson's correlation coefficient was calculated from fluorescence intensity variation across pixels (± SEM, $n = 4$), and results did not depend on the fluorophores used in the correlation measurement ($P > 0.05$; two-tailed t-test). (**C**) Two different ferumoxytol dye conjugates (VT750 and VT680) were intravenously co-injected into tumor-bearing mice, as above. Excised tumors were imaged, revealing that both dye-conjugated MNPs strongly co-localize in tumor-associated host phagocytes rather than tumor cells.

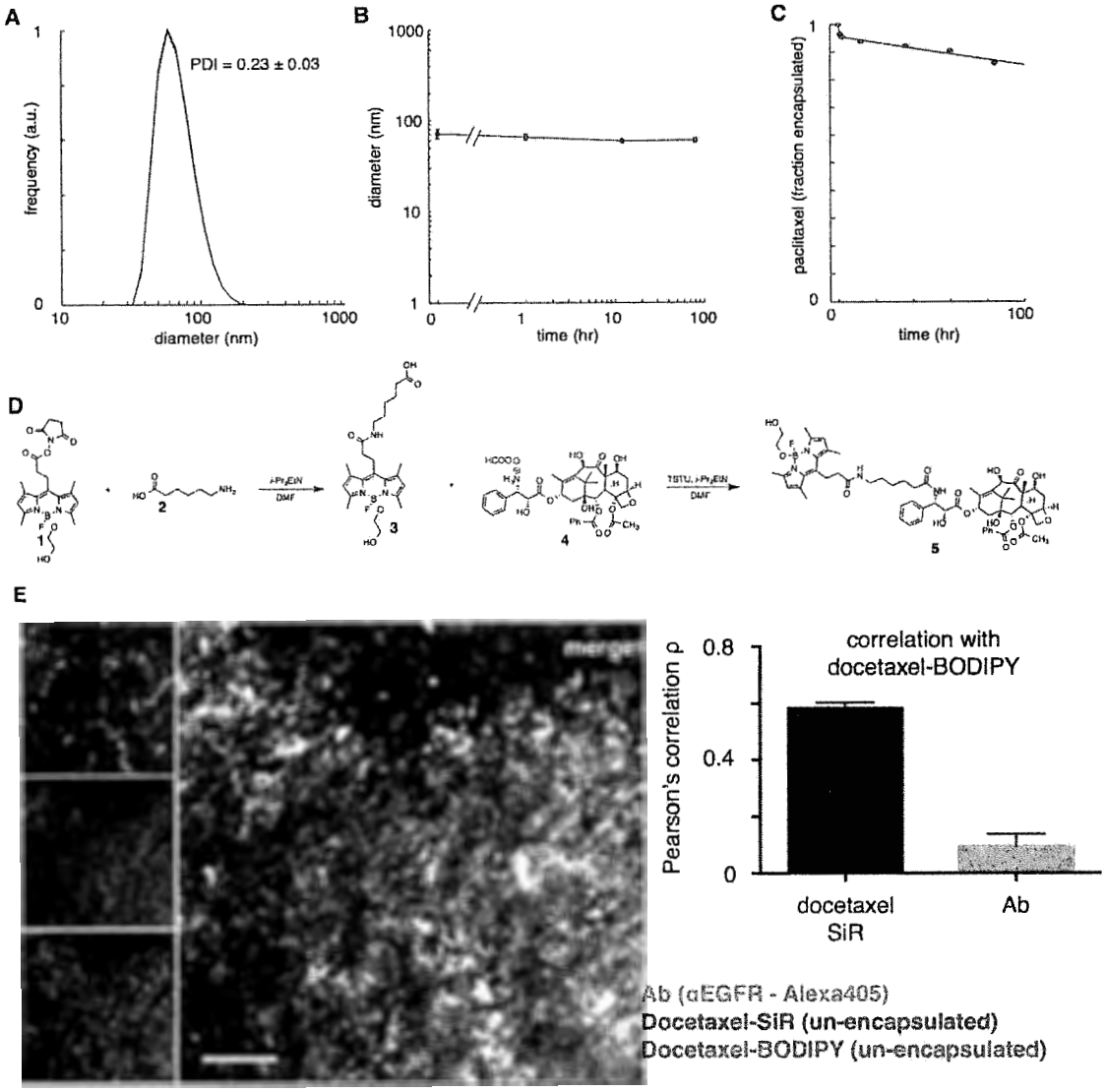

Figure S8. Characterization of paclitaxel-loaded TNP and fluorescent derivatives. (A) Size distribution of paclitaxel-TNP, as measured by DLS (thick line and blue shading, along with PDI, are means ± SD; $n \geq 3$). **(B)** Stability of paclitaxel-TNP in 37°C PBS, measured by DLS. Data are means ± SD ($n \geq 3$). **(C)** Paclitaxel release from TNP vehicle over time in 37°C PBS. Data are means ± SD ($n = 2$). **(D)** Synthetic scheme reaction scheme for docetaxel labeled with a fluorescent BODIPY derivative (compound **5**). **(E)** Structure of the silicon-rhodamine (SiR) fluorophore-labeled docetaxel derivative. **(F)** BODIPY and SiR docetaxel co-localize *in vivo*. Un-encapsulated fluorescent docetaxel derivatives were co-injected along with fluorescent tumor-targeting antibody into BALB/c mice bearing orthotopic 4T1 tumors. Five hours after injection, tumors were excised and immediately imaged. Scale bar, 50 μm. From these images, pixel-by-pixel Pearson's correlation was calculated to measure co-localization between docetaxel-BODIPY and either docetaxel-SiR or anti-EGFR antibody (± SEM, $n = 3$).

SUPPLEMENTARY TABLE

Table S1. Optimized finite-element modeling parameters and reference values. Reference parameter values were used to initialize the global parameter optimization algorithm when available. Other parameters were initialized by estimating individual values directly from intravital imaging data. All parameters were simultaneously and globally optimized using a simulated annealing algorithm (Matlab); the optimization was iteratively repeated, and median parameter values are reported (± SE) for MNP. For TNP, SE was zero (stochastic optimizations converged more consistently), and range was reported instead.

Model parameter	MNP (median ± SE)	TNP (median ± range)	Parameter description and reference value (if available)
D_{eff} ($\mu m^2/s$)	2.75 ± 0.008	3.4 ± 0.8	Effective NP diffusion D_{eff} = 5 $\mu m^2/s$ (*36*)
P ($\mu m/s$)	0.005 ± $1x10^{-6}$	0.005 ± $5x10^{-5}$	Vessel permeability P = 0.003 $\mu m/s$ (*37*)
$B_{max,t}$ (μM)	0.006 ± 0.02	0.05 ± 0.09	Max NP uptake in tumor cells
$B_{max,M\phi}$ (μM)	1 ± 0.002	0.5 ± 0.2	Max NP uptake in macrophage
ε	0.39 ± 0.01	0.4 ± 0.003	Extracellular volume fraction ε = 0.3–0.5 (*38*)
$k_{bind,t}$ ($\mu M^{-1} s^{-1}$)	$3x10^{-7}$ ± $6x10^{-7}$	0.0005 ± 0.0001	NP uptake rate in tumor cells
$k_{bind,M\phi}$ ($\mu M^{-1} s^{-1}$)	0.006 ± 0.002	0.001 ± 0.0001	NP uptake rate in macrophage
$k_{release}$ (s^{-1})	$3x10^{-17}$ ± $1x10^{-16}$	$7x10^{-9}$ ± $7x10^{-9}$	NP rate of release from cells

nature COMMUNICATIONS

ARTICLE

Received 29 Dec 2014 | Accepted 22 Sep 2015 | Published 27 Oct 2015

DOI: 10.1038/ncomms9692 OPEN

Tumour-associated macrophages act as a slow-release reservoir of nano-therapeutic Pt(IV) pro-drug

Miles A. Miller[1], Yao-Rong Zheng[2], Suresh Gadde[3,†], Christina Pfirschke[1], Harshal Zope[3], Camilla Engblom[1], Rainer H. Kohler[1], Yoshiko Iwamoto[1], Katherine S. Yang[1], Bjorn Askevold[1], Nagesh Kolishetti[3], Mikael Pittet[1], Stephen J. Lippard[2], Omid C. Farokhzad[3,4] & Ralph Weissleder[1,5]

Therapeutic nanoparticles (TNPs) aim to deliver drugs more safely and effectively to cancers, yet clinical results have been unpredictable owing to limited *in vivo* understanding. Here we use single-cell imaging of intratumoral TNP pharmacokinetics and pharmacodynamics to better comprehend their heterogeneous behaviour. Model TNPs comprising a fluorescent platinum(IV) pro-drug and a clinically tested polymer platform (PLGA-*b*-PEG) promote long drug circulation and alter accumulation by directing cellular uptake toward tumour-associated macrophages (TAMs). Simultaneous imaging of TNP vehicle, its drug payload and single-cell DNA damage response reveals that TAMs serve as a local drug depot that accumulates significant vehicle from which DNA-damaging Pt payload gradually releases to neighbouring tumour cells. Correspondingly, TAM depletion reduces intratumoral TNP accumulation and efficacy. Thus, nanotherapeutics co-opt TAMs for drug delivery, which has implications for TNP design and for selecting patients into trials.

[1] Center for Systems Biology, Massachusetts General Hospital (MGH), Harvard Medical School, 185 Cambridge Street, Boston, Massachusetts 02114, USA. [2] Department of Chemistry, Massachusetts Institute of Technology (MIT), 77 Massachusetts Avenue, Cambridge, Massachusetts 02139, USA. [3] Laboratory of Nanomedicine and Biomaterials, Department of Anesthesiology, Brigham and Women's Hospital (BWH), Harvard Medical School, 75 Francis Street, Boston, Massachusetts 02115, USA. [4] King Abdulaziz University, Jeddah, Saudi Arabia. [5] Department of Systems Biology, Harvard Medical School, 200 Longwood Avenue, Boston, Massachusetts 02115, USA. † Present address: Department of Biochemistry, Microbiology and Immunology, University of Ottawa, 451 Smyth Road, Ottawa, Canada K1H 8M5. Correspondence and requests for materials should be addressed to R.W. (email: rweissleder@mgh.harvard.edu).

Approximately half of all cancer patients who receive chemotherapy are treated with one of three clinically approved platinum (Pt) drugs—cisplatin, carboplatin, and oxaliplatin[1]. These Pt compounds are first-line agents in ovarian, lung, head and neck and testicular cancers, among others, and development of combination therapies using Pt compounds is an active area of research[2]. Unfortunately, most cancers either exhibit intrinsic Pt resistance or ultimately develop resistance to treatment through mechanisms including reduced drug uptake, altered cellular metabolism, increased DNA repair, chemoprotective niche formation and/or activation of oncogenic and anti-apoptotic pathways[3]. Dose escalation and combination drug regimens help overcome resistance. However, Pt-related toxic side-effects including neurotoxicity and nephrotoxicity limit some of these approaches, indicating the need for new strategies.

To circumvent these problems, specialized drug-delivery mechanisms such as nanoparticles (NPs) have been introduced to enhance local drug accumulation in tumours while simultaneously mitigating systemic toxicities[4,5]. Non-encapsulated Pt compounds in particular are often plagued by poor pharmacokinetic (PK) properties. They generally must be intravenously administered over a prolonged period (sometimes over 24 h) because promiscuous Pt reactivity causes side effects and the covalent binding to plasma proteins such as albumin consequently neutralizes its activity. Recent work has demonstrated the possibility of using NPs to encapsulate Pt pro-drugs, thereby (i) extending the circulating half-life of the unreacted Pt compound and enabling controlled drug release[6]; (ii) facilitating precisely engineered Pt-based combination therapies through co-encapsulation with additional drugs[7,8] (or small interfering RNA treatments[9]); (iii) enabling the administration of more lipophilic and newer-generation Pt compounds[10] and (iv) modifying tissue distribution and enhancing intratumoral accumulation[6,9]. The last is thought to occur through enhanced permeability and retention (EPR) effects and has been termed 'passive NP targeting'[11]. In theory, enhanced permeability of the abnormal tumour microvasculature (TMV) should allow therapeutic nanoparticles (TNPs) to enter the tumour interstitial space, whereas suppressed lymphatic filtration and increased cellular uptake should allow them to stay there[12]. Although TNPs of Pt-based anticancer agents have advanced to clinical trials[13,14], results have been mixed, presumably due to heterogeneous EPR effects in different tumours combined with limited experimental data from patients on the effectiveness of this mechanism as related to enhanced drug accumulation[15]. Furthermore, the inter-related *in vivo* PK and pharmacodynamics (PD) of TNPs are more difficult to understand than those of the unencapsulated drug. TNP drug delivery is inherently a multi-step process, defined by PK of the TNP vehicle, drug release dynamics that may change depending on the *in vivo* environmental context, and PK of the Pt payload itself. Little experimental evidence exists that describes how this multi-step drug delivery sequence performs *in vivo* and within tumours, despite its critical importance to overall therapeutic outcome. This lack of understanding clearly represents a bottleneck in the design and development of more efficacious therapies.

Here we use high-resolution microscopic imaging in live tumour-bearing mice to test the hypothesis that therapeutic nano-encapsulation not only affects traditional bulk PK properties, but also significantly influences heterogeneous drug uptake and response at the single-cell level within tumours[16,17]. We engineer a platform that for the first time allows simultaneous imaging of both a ~100-nm TNP vehicle as well as its Pt payload, in addition to monitoring DNA damage at the single-cell level in real time. As expected, our results show that nano-encapsulated Pt exhibits a longer circulating half-life than traditional unencapsulated Pt compounds. However, we quite unexpectedly find that TNPs accumulate at high levels within tumour-associated macrophages (TAMs), and that TAMs serve as 'cellular drug reservoirs'. Indeed, TAMs release the Pt payload into neighbouring tumour cells over time. Depletion of macrophages significantly decreases intratumoral Pt accumulation and correspondingly increases tumour growth. Overall, this work establishes a paradigm for NP drug delivery based on the principle that TAMs can sequester TNP payload and gradually release it into the surrounding tissue, thereby serving as 'drug depots.'

Results

Dual imaging shows congruent vehicle and payload kinetics. For clinical applicability and generalizability, TNPs in this study were designed to incorporate desirable properties of previously described polymeric nano-formulations that have entered clinical trials[5], especially those of materials that have received Food and Drug Adminstration approval. TNPs were formulated by combining three compounds (compounds **1–3**, Fig. 1a) via nano-precipitation, using spectrally complementary derivatives of BODIPYs as ideal fluorophores for efficient nano-encapsulation that convey lipophilicity and robust *in vivo* imaging arising from *in vivo* structural stability, environmentally robust fluorescence, high brightness and high photostability[16,18–20]. Compound **3** (poly(D,L-lactic-*co*-glycolic acid)-*b*-poly(ethylene glycol); PLGA-*b*-PEG) self-assembles to form the hydrophobic PLGA core of the NP and hydrophilic PEG outer shell. For the cytotoxic payload, we used a novel Pt(IV) pro-drug (*c,c,t*-$Pt(NH_3)_2Cl_2$-(hexadecylcarbamate)[4-((2-(4,4-difluoro-1,3,5,7-tetramethyl-4-dora-3a,4a-diaza-s-Indacene)ethyl)amino)-4-oxobutanoate]) with a C_{16} aliphatic carbon chain and a BODIPY ($\lambda_{ex} = 498$ nm, $\lambda_{em} = 543$ nm; Supplementary Fig. 1a) as the two lipophilic ligands axially coordinated to the Pt(IV) centre. NPs were similar in size (135 ± 1 nm; standard error of the mean (s.e.m.), across $n = 12$; Supplementary Fig. 1b-c), polydispersity (PDI $= 0.18 \pm 0.01$; s.e.m. across $n = 12$) and drug release rates ($t_{1/2\ release} = 15$ h; $n = 2$; Supplementary Fig. 1d) compared with previously published Pt(IV) nano-formulations[6,9], and were stable in physiological saline (Supplementary Fig. 1e). Free carboxylic acid terminal groups on the PEG gave TNPs a slight negative charge (zeta-potential $= -23 \pm 1.4$ mV; s.e.m. across $n = 4$), which has been shown in some cases to benefit tumoral accumulation[21–24] and mirrors TNPs in the clinic[5]. C_{16}-Pt(IV) remains relatively stable in whole blood[25]. However, upon reduction to the active Pt(II) compound cisplatin, dissociated BODIPY increases fluorescence by sevenfold owing to loss of quenching by Pt(IV) (Supplementary Fig. 1f-g). BODIPY fluorescence thus serves as an effective indicator of both pro-drug delivery and activation. Overall, these properties enable clearly distinguishable imaging of both the TNP vehicle and its payload, in a stable and clinically relevant nano-formulation platform.

We performed a series of *in vitro* experiments to characterize TNP behaviour in tumour cell culture (Supplementary Fig. 2a). Co-localization studies with fluorescent compartmentally localized proteins showed that the TNP vehicle moved from early to late endosomes over the course of 24 h (Supplementary Fig. 2b). Compared with the TNP vehicle, the TNP payload exhibited more diffuse intracellular localization, and co-localization peaked in the late endosome 24 h post treatment (Supplementary Fig. 2c). Payload fluorescence increased over time owing to Pt reduction and BODIPY de-quenching (Supplementary Fig. 2d). Dose–response TNP treatment indicated that intracellular fluorescence correlates well with overall Pt uptake ($R^2 > 0.99$) and resulting

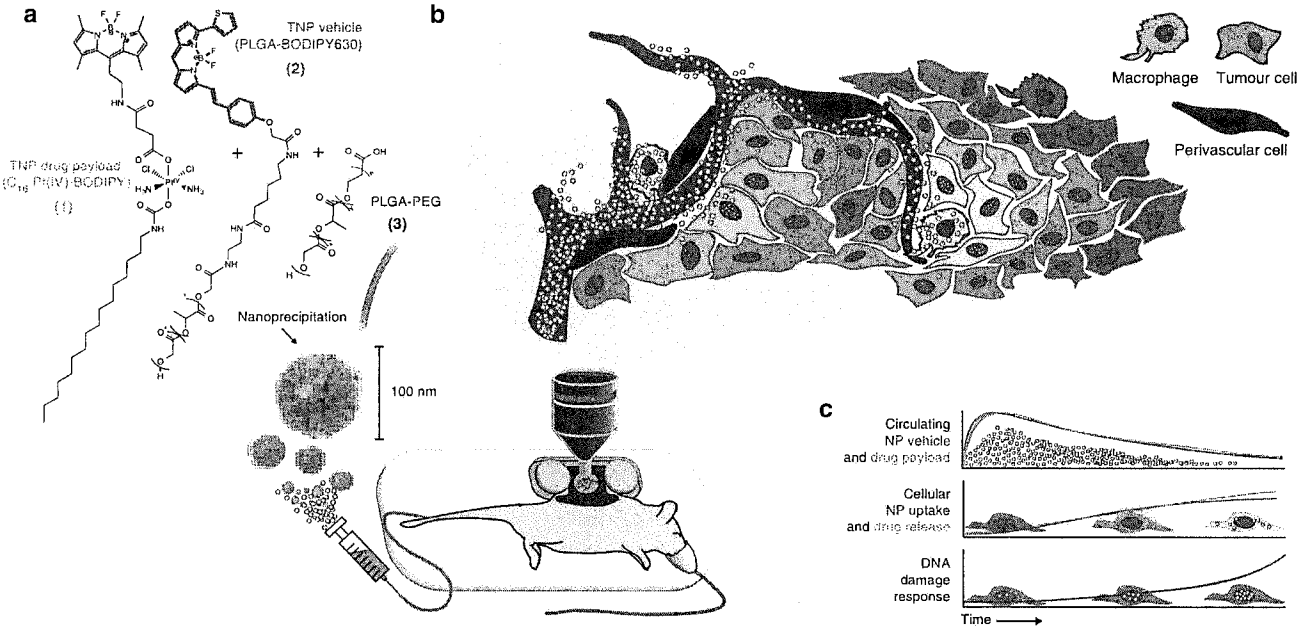

Figure 1 | Overview schematic of intravital nanoparticle imaging for pharmacokinetic and pharmacodynamic analysis. Nanoparticles (**a**) were injected by tail-vein catheter and imaged in real time within the tumour using a dorsal window chamber (**b**). Imaging results enable simultaneous monitoring of circulating pharmacokinetics within the TMV (**c**, top); single-cell uptake of the nanoparticle vehicle and its drug payload (**c**, middle); and DNA damage response in tumour cells, monitored by 53BP1 puncta formation (**c**, bottom).

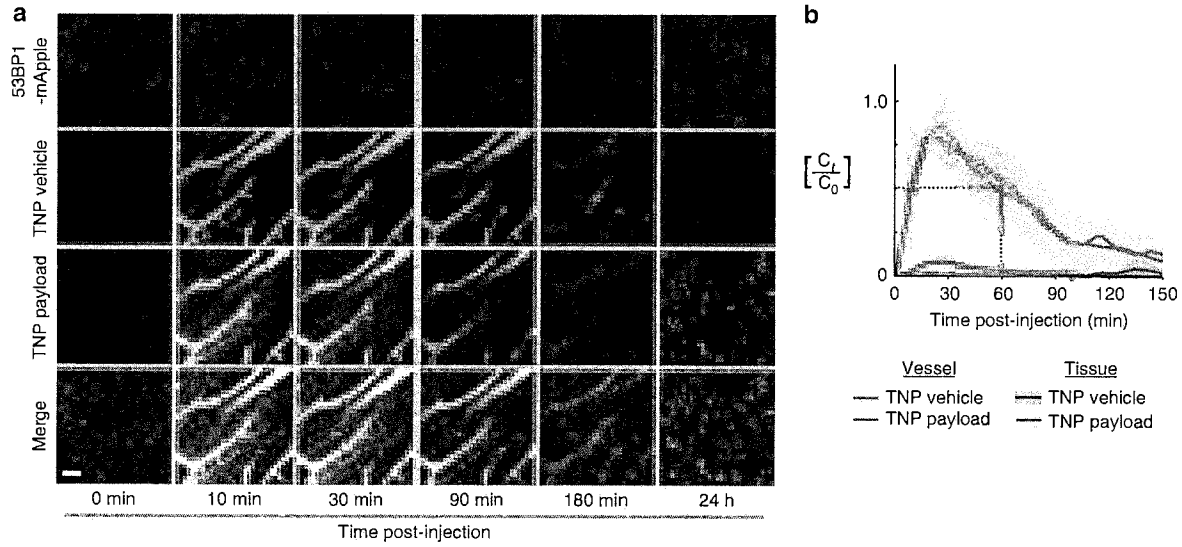

Figure 2 | Pharmacokinetic analysis of nanoparticle shows extended microvasculature half-life and heterogeneous tissue accumulation. (**a**) Nanoparticle concentrations are monitored (**a**) and quantified (**b**) using time-lapse confocal fluorescence microscopy in the dorsal window chamber model. Nanoencapsulation extends the TMV half-life to 55 min, a >5-fold increase compared with unencapsulated Pt(II) compounds in the same animal model[29]. Scale bar, 50 μm. Thick lines and shading denote means ± s.e.m. ($n = 6$).

DNA damage (Supplementary Fig. 3), thereby validating the use of fluorescence as a surrogate marker of cellular payload content. Together, these results provide evidence that, over the course of 24 h, TNPs accumulate in endosomes and lysosomal compartments, where the Pt pro-drug is activated through reduction to form cisplatin.

TNPs exhibit long TMV half-life and perivascular cell uptake. We first used time-lapse intravital imaging to characterize PK within a xenograft tumour model often used for intravital studies (Fig. 1)[16,26–28]. Tumours were generated from subcutaneously implanted HT1080 cells expressing a fluorescently tagged DNA damage response protein, 53BP1, which localizes to the nucleus[29,30]. TNPs reached the TMV within 10–15 min of intravenous injection, and at early time points ($t < 30$ min) the vehicle and its payload exhibited strong co-localization within vessels (Fig. 2a; intravascular Pearson's correlation $\rho = 0.8 \pm 0.02$, s.e.m. across $n = 4$; Mander's M1 and M2 > 0.95). Both the vehicle and its payload showed initial vascular PK similar to each

other (Fig. 2b; $t_{1/2\ vehicle} = 55 \pm 5$ min; $t_{1/2\ payload} = 61 \pm 6$ min; s.e.m. across $n = 6$), to previous studies using similar nano-formulations entering the clinic[5,6,31], and to clinical NP formulations such as PEGylated liposomal doxorubicin (DOXIL; $t_{1/2\ initial} < 5.2$ h in humans and 2 h in rats[32,33]). Immediately as the TNPs reached the TMV, roughly 10% of the payload diffused into the surrounding tumour tissue. Such an initial burst of drug release was also observed *in vitro* (Supplementary Fig. 1d) and with similar previously described nano-formulations[34,35], characterized by significantly faster release kinetics at initial phases followed by a later phase of slower release. Notably, PK imaging of BODIPY-labelled Pt compounds that were not nano-encapsulated revealed much more rapid vascular PK ($t_{1/2\ unencapsulated} = 10 \pm 5$ min[29]). Therefore, despite an initial burst of Pt release seen both *in vitro* (Supplementary Fig. 1d) and *in vivo* (Fig. 2), nano-encapsulation conferred a relatively long circulation half-life.

Over the course of several hours, TNPs moved from the TMV ($t < 1$ h) specifically to peritumoral host cells (1–3 h) adjacent to or even extending processes into the TMV. Uptake of TNPs by tumour cells themselves occurred more gradually and to a lesser degree compared with these perivascular host cells. By 24 h, TNPs were undetectable in vessels and had accumulated primarily in a heterogeneous mix of tumour cells and host cells, with host-cell uptake characterized by high local accumulation within cell-sized (7 ± 1 μm; s.e.m. across $n = 4$ tumours) diameters. At 24 h post-injection, the TNP payload also co-localized with the TNP vehicle in these host cells (Pearson's correlation within tumour tissue: $\rho = 0.7 \pm 0.08$; Mander's M1 and M2 $> 0.6 \pm 0.05$; s.e.m. across $n = 4$). Compared with the TNP vehicle, however, the payload accumulated more diffusely throughout the bulk tumour tissue, suggesting some payload release from the TNP vehicle (Supplementary Fig. 4a). We quantified these observations by measuring the coefficient of variation (CV) across cells within the tumour tissue (Supplementary Fig. 4b). The payloads exhibited $> 40\%$ decrease in CV compared with the TNP vehicle, indicating more homogeneous distribution. In contrast to TNPs, naked BODIPY-labelled Pt that was injected in the absence of an encapsulating NP vehicle showed a substantially more homogeneous distribution within tumour tissue, with little preferential accumulation in any particular cell type (Supplementary Fig. 4; 60% reduction in CV). In summary, these data show that (i) nano-encapsulation enables a relatively long circulating half-life of the Pt(IV) pro-drug; (ii) nano-encapsulation influences spatial distribution within the bulk tumour tissue and (iii) TNPs primarily accumulate in perivascular host cells and, to a lesser extent, tumour cells.

TNPs cause mitotic arrest and localized DNA damage. In addition to PK analysis, high-resolution intravital imaging allowed for simultaneous monitoring of the cellular response to TNPs at the molecular level. Fluorescently tagged 53BP1 is a key member of the non-homologous end-joining pathway that forms visible puncta at sites of DNA double-strand breaks[29,36]. Based on the hypothesis that treatment with a cisplatin pro-drug would lead to increased DNA damage in tumour cells, we imaged 53BP1 puncta in response to TNP and quantitated the DNA damage response across populations of individual tumour cells at various time points (Fig. 3a). The results show a dose- and time-dependent increase in the fraction of tumour cells exhibiting high levels of DNA damage (Fig. 3b). We next tested whether there was an observable relationship between local payload accumulation and resulting single-cell DNA damage response. We used automated three-dimensional (3D) segmentation software to quantify TNP vehicle and payload accumulation within individual tumour nuclei, and correlated this information with DNA damage response in those cells. The results showed that cells exhibiting high levels of DNA damage also had a roughly 300% higher local payload concentration (Fig. 3c). Compared to TNP payload, local concentration of TNP vehicle also correlated with DNA damage, but to a lesser degree (Fig. 3c). DNA damage elicited by Pt treatment generally induces mitotic arrest *in vitro*[25], but it has been difficult to directly observe this response *in vivo*, where anti-mitotics often behave much differently[26]. To determine TNP effects on cell growth, we used time-lapse intravital imaging to track individual tumour cells and mitotic events over the first 3 h following TNP injection in the HT1080 model (Supplementary Fig. 5) and found that TNP indeed caused a substantial reduction in tumour cell division (Fig. 3d). To test generalizability in another tumour model, we next examined local drug accumulation and DNA damage in an orthotopic model of disseminated ovarian cancer (OVCA)[37]. Human A2780CP OVCA cells were intraperitoneally injected in nu/nu mice, and 6 weeks later (once palpable tumours and/or ascites had developed), animals received TNP treatment. The following day, tumours were excised and imaged for TNP accumulation and DNA damage. Imaging shows similar TNP localization patterns as observed with the HT1080 model (Fig. 4a). We also found similar statistically significant correlation between local TNP payload levels and tumour cell DNA damage (Fig. 4b). Taken together, these results demonstrate that TNPs elicit substantial DNA damage response activity and corresponding growth arrest *in vivo*. In both the subcutaneous and orthotopic OVCA tumour models, the correlation between local drug accumulation and DNA damage response implies that NP-mediated drug delivery plays a significant role in governing such PD.

Identification of cell populations with drug in steady state. We next performed a combination of intravital imaging, flow cytometry and histology studies to determine in which immunologically defined cell populations the TNP vehicle and its payload accumulated within the bulk tumour mass at 24 h, after TNPs had largely cleared the circulation. With the same HT1080 xenograft model used in the previous imaging experiments, we labelled TAMs with a fluorescent dextran-coated NP[16] and found significant TNP uptake in TAM-rich regions of the bulk tumour mass (Fig. 5a). For more detailed immunological examination, we next performed flow cytometry analysis of HT1080 tumours. Results show that tumour cells made up 61% of the bulk tumour; 31% of the cells within the bulk tumour were $CD45^-$ host cells (erythrocytes, tumour associated fibroblasts, endothelium and others); and the remaining 8% were $CD45^+$ leukocytes (Fig. 5b). TAMs made up the largest population of leukocytes within the bulk tumour and also accumulated the highest levels of both TNP vehicle and payload on a per-cell basis (Fig. 5c). Because tumour cells far outnumbered TAMs in the HT1080 xenograft model, the majority of TNP vehicle and payload within the bulk tumour still resided in tumour cells themselves (Fig. 5d). Nonetheless, even though TAMs comprised only 4% of cells within the total tumour mass, they accumulated more than 40% of the total injected TNPs relative to tumour cells, and 30% of the total TNP overall.

To directly visualize genetically defined tumour-associated host leukocytes, we imaged TNP vehicle uptake in tumour-bearing fractalkine $Cx3cr1^{GFP/+}$ reporter mice, which are known to contain GFP^+ macrophages[38]. In this model, *KRAS* mutant $p53^{-/-}$ (KP) cells derived from autochthonous lung tumours[39] were subcutaneously implanted into immunocompetent $Cx3cr1^{GFP/+}$ reporter mice, and TNP vehicle (without the green fluorescent payload) was intravenously administered. The vast majority of TNP vehicle accumulated within these GFP^+ host leukocytes, especially near TMV (Fig. 6a,b). Using the above described KP lung cancer and intraperitoneal OVCA xenografts,

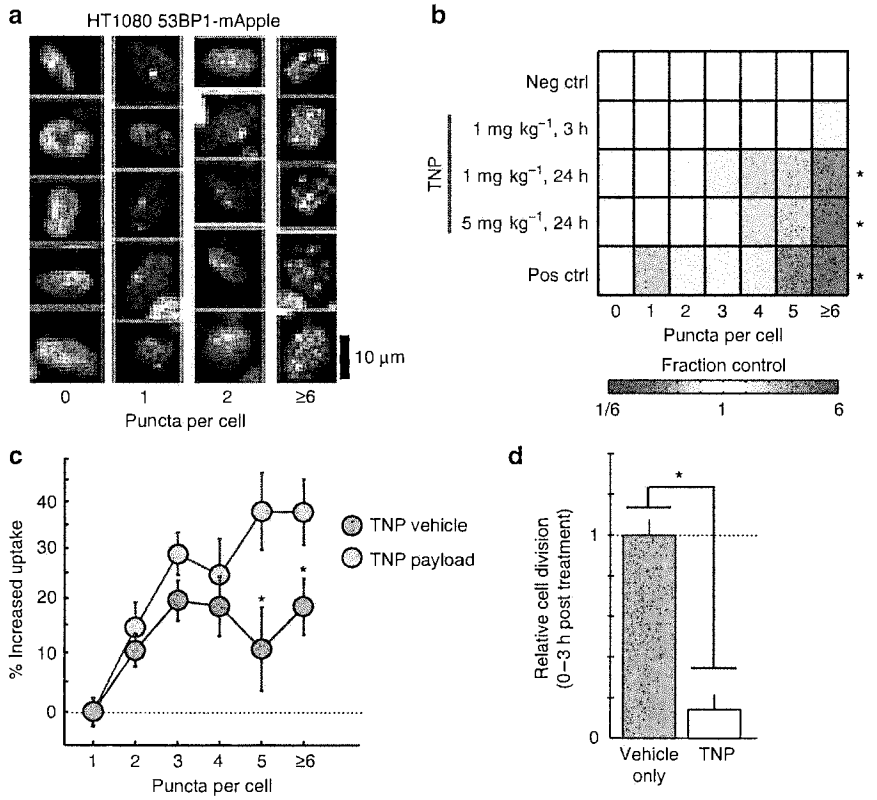

Figure 3 | TNP causes mitotic arrest and DNA damage in a spatially defined dose-dependent manner. (**a**) Example images of 53BP1 puncta, 24 h post treatment with 1 mg kg^{-1} TNP, scale bar, 10 μm. (**b**) TNP treatment increases the fraction of cells exhibiting many 53BP1 puncta, measured across $n \geq 3$ animals and $n > 2{,}000$ cells (*$P < 0.01$, two-tailed t-test). Positive control (Pos. ctrl): 24 h supra-therapeutic cisplatin, 9 mg kg^{-1}. (**c**) Heterogeneous local TNP vehicle and payload accumulation within 5 μm of single-cell nuclei correlate with corresponding DNA damage response in those cells (one-way analysis of variance; $n > 6{,}000$ cells across $n = 5$ animals; $P < 10^{-21}$ for both vehicle and payload); the local TNP payload correlates better with response compared with TNP vehicle (*$P < 0.05$; two-tailed t-test). (**d**) Cell division events were quantified from time-lapse movies across $n > 1{,}000$ cells (*$P = 0.001$; two-tailed t-test; $n = 3$ animals). All dosages in mg of Pt. Data are means ± s.e.m. Neg ctrl, negative control.

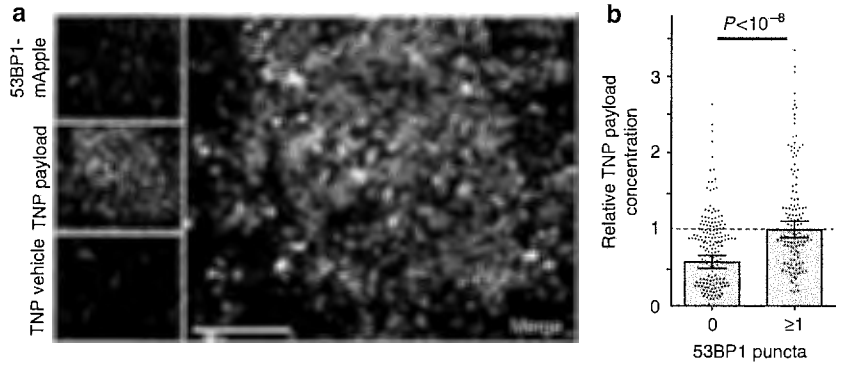

Figure 4 | Local TNP payload accumulation correlates with DNA damage in OVCA. (**a**) Single-cell DNA damage response correlates with local TNP payload levels in a model of disseminated metastatic OVCA. A2780CP OVCA cells were injected intraperitoneally; 6 weeks later, TNP was i.v. injected, and the following day intraperitoneal lesions were excised and imaged for DNA damage response (using 53BP1 puncta) and TNP uptake. Scale bar, 50 μm. (**b**) OVCA cells exhibiting detectable DNA damage by 53BP1-puncta have higher TNP payload levels, compared with those without (two-tailed t-test; s.e.m. across $n = 3$ animals).

we confirmed by histology that high levels of TNP vehicle accumulate in F4/80^{+} host phagocytes in these disease models as well (Fig. 6c and Supplementary Fig. 6). These analyses ultimately corroborate results from the intravital imaging data showing uptake of TNPs in tumour cells but also host cells, which are confirmed here as TAMs.

TNP payload spatially redistributes from TAMs to tumour cells. Based on intravital imaging evidence showing that the Pt(IV)-payload was more diffusely distributed within tumour tissue compared with its TNP vehicle (Supplementary Fig. 4), we next quantified the extent of payload redistribution and its effect on drug response. Using flow-cytometry data, we confirmed that

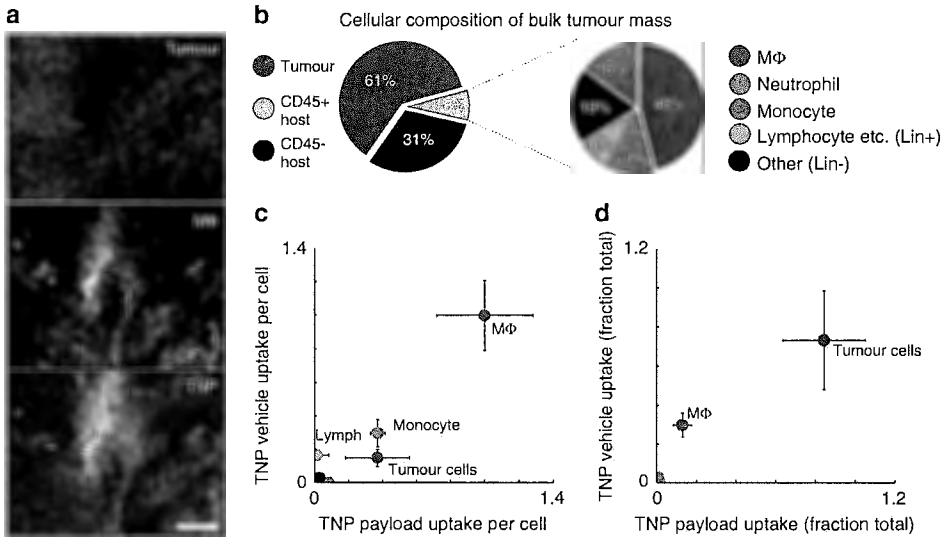

Figure 5 | TNPs primarily accumulate in tumour cells and tumour-associated macrophages in steady state. (**a**) Intravital imaging of subcutaneous HT1080-53BP1-mApple tumours 24 h post injection with TNP (payload shown in yellow). TAMs (white) were labelled by dextran-coated nanoparticles injected 24 h prior. Scale bar, 100 μm. (**b**) Single-cell suspensions of the bulk tumour mass were immunostained and gated into various cell-populations, quantified here as fractions of the total number of cells analysed. (**c**) Macrophages accumulate the most TNP per cell. Using flow cytometry, uptake of both the TNP vehicle and its payload were quantified by fluorescence for each of the cell populations shown in **b**, 24 h post injection. $CD45^-$ host cells, neutrophils and 'other' $CD45^+$ leukocytes did not accumulate significant TNP vehicle or payload. Fluorescence values normalized to the average macrophage values, after subtracting background autofluorescence of each cell population measured from control-treated tumours. (**d**) Most TNP accumulates in tumour cells and macrophages within the bulk tumour mass. TNP uptake measurements from **c** were weighted against the relative prevalence of each cell population in **b** to calculate the total fraction of TNP uptake within each cell population. For **b**–**d**, error bars denote standard error ($n \geq 4$).

tumour cells exhibited more than twice the amount of payload accumulation as a ratio of vehicle accumulation, compared with TAMs (Fig. 7a), thereby suggesting that payload may transfer from TAMs to tumour cells. We hypothesized that local payload release from TAMs into neighbouring tumour cells would lead to elevated payload concentration in these tumour cells, which would in turn enhance DNA damage. By histology we also measured greater than threefold elevated payload concentrations within roughly one cell-length (15 μm) of TAMs (Fig. 7b,c), and analysis of intravital imaging data provided further evidence that relevant payload concentration gradients occur over length-scales of <25 μm (Supplementary Fig. 7a). One explanation for these observations is that TAMs induce neighbouring tumour cells to take up more TNP directly; however, the TNP vehicle itself was not similarly elevated in the same neighbouring region (Fig. 7c). Tumour cells within the same phagocyte-neighbouring region also exhibited higher DNA damage on average, as determined by histology (Fig. 7d) and supported by corroborating intravital imaging analysis (Supplementary Fig. 7b). These analyses cumulatively show local payload redistribution from TAMs to neighbouring tumour cells exhibiting elevated DNA damage.

We next performed a series of *in vitro* experiments to directly test whether macrophages could release functional, DNA-damaging TNP payload into their surrounding environment. Similar to *in vivo* observations, we found that *in vitro* macrophages accumulated TNPs more rapidly and to a greater degree than tumour cells (Supplementary Fig. 8a). Once taken up by macrophages, Pt-payload was released at high levels into the extracellular supernatant. In fact, over the course of 24 h, more Pt was found in the supernatant than in the macrophages themselves (Supplementary Fig. 8b,c). The Pt-containing macrophage supernatant was both DNA damaging (Supplementary Fig. 8d) and cytotoxic (Supplementary Fig. 8e). In contrast, supernatant from macrophages treated with unencapsulated cisplatin at concentrations ranging from 1 to 300 μM was not cytotoxic to tumour cells (Supplementary Fig. 8e). For supernatant from TNP-treated macrophages, filtration with molecular-weight cut-off filters (3 and 100 kDa) did not reduce its potency, which indicated that cytotoxic effects were independent of macrophage-derived cytokines or other signalling proteins (Supplementary Fig. 8f). In addition, Pt-containing macrophage supernatant exhibited 50% inhibitory effect on tumour cell viability/cytotoxicity at Pt concentrations of 1.5 ± 0.5 μM (s.e.m. across $n = 3$) within the macrophage supernatant (Supplementary Fig. 7e), which is comparable to the potency of the Pt-payload when TNP was directly applied to tumour cells ($IC_{50} = 1.7 \pm 0.02$ μM; s.e.m. across $n = 2$; Supplementary Table 1). Taken together, these combined *in vitro* and *in vivo* data further confirmed that TAMs can serve as drug depots that accumulate high levels of TNPs and then release their DNA-damaging cytotoxic payload to the surrounding tumour tissue.

TAM depletion reduces TNP accumulation and efficacy. Finally, we tested whether TAM depletion would reduce the therapeutic efficacy of TNP in cancers. Macrophages were systemically depleted by pre-treatment with clodronate liposomes (clod-lip)[40] before TNP injection. In this tumour model, macrophage depletion itself had no detectable impact on tumour growth ($P = 0.2$; two-tailed two-way analysis of variance; $n = 38$ mice). However, it substantially reduced the degree to which TNP treatment was able to slow tumour growth (Fig. 8a). Direct measurement of intratumoral TNP accumulation confirmed that macrophages play a key role in mediating drug delivery: macrophage-depleted tumours exhibited both lower total intratumoral Pt (Fig. 8b) and a lower concentration of Pt (Fig. 8c) compared with macrophage-containing tumours, 24 h post administration of TNP, at which time no TNP remained circulating in the TMV of any tumour. The 24% decrease in Pt

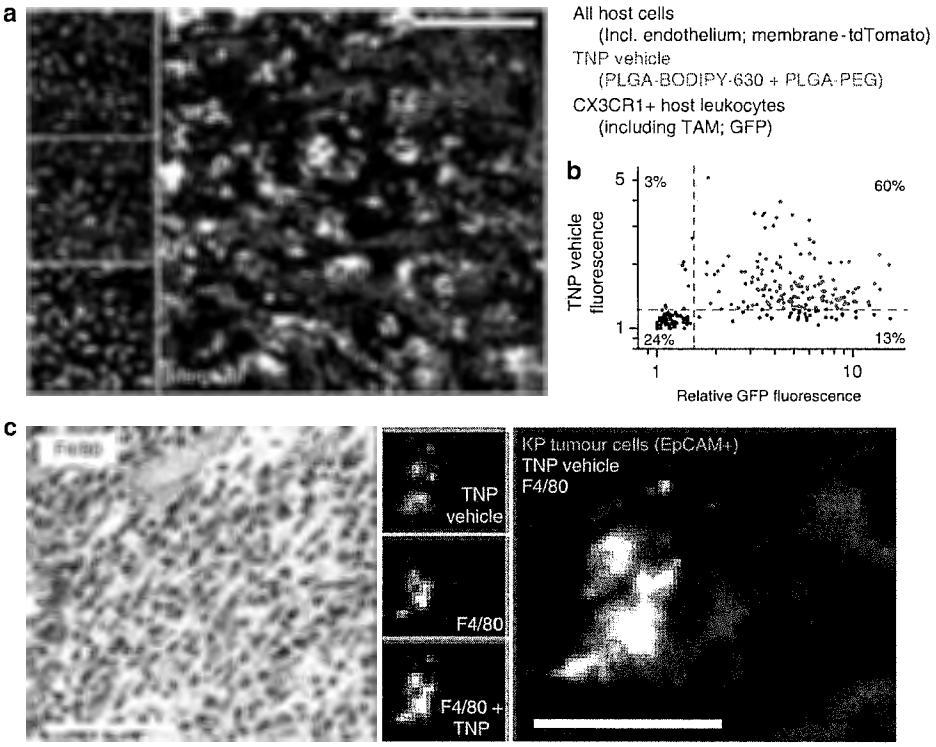

Figure 6 | Tumour-associated CX3CR1$^+$ and F4/80$^+$ host phagocytes accumulate TNP vehicle in a syngeneic model of lung cancer. *Kras* mutant *p53*$^{-/-}$ (KP) lung cancer cells were subcutaneously implanted into *Cx3cr1*$^{GFP/+}$ reporter mice for directly visualizing GFP$^+$ monocytes, dendritic cells and TAMs. Tumour-adjacent stromal regions were imaged 24 h following i.v. injection with TNP vehicle. Reporter mice expressed membrane-anchored tdTomato in all host cells, most visibly here with endothelium. Scale bar, 50 μm. (**b**) Fluorescence intensities of GFP and TNP vehicle were quantified across single-cells based on **a**, showing most stromal cells that accumulate TNP vehicle were also GFP$^+$ ($n=4$ animals, $n=250$ cells). (**c**) Histological analysis of F4/80$^+$ host phagocytes, 24 h post injection with TNP vehicle. Immunohistochemistry (left) shows tumours stained with haematoxylin and F4/80 (brown; scale bar, 100 μm), and corresponds with immunofluorescence (right) showing F4/80$^+$ host phagocytes, EpCAM$^+$ KP tumour cells, and local accumulation of TNP vehicle (scale bar, 25 μm). F4/80 labels a subset of GFP$^+$ cells in *Cx3cr1*$^{GFP/+}$ reporter mice[38] (namely, macrophages).

concentration (from 5 to 3.8 μM; Fig. 8c after converting to molarity) correlates well with the flow cytometry-based estimate that TAMs accumulate 30% of the total intratumoral TNP. It also correlates with the observation that unencapsulated Pt exhibits 37% lower intratumoral accumulation than nano-encapsulated Pt (Supplementary Table 1)[9]. This decrease disproportionately impacted TNP effects on tumour growth, probably because intratumoral Pt concentrations were near the threshold at which HT1080 tumour cells respond (*in vitro* $IC_{50}=3.7\pm0.1$ μM for unencapsulated Pt(IV) payload; s.e.m. across $n=2$). TNP clearance kinetics, TMV leakiness and other EPR factors all may influence drug accumulation within the tumour; nonetheless, the experiments here show that all things being equal, macrophage uptake substantially contributes both to the delivery of TNP to the tumour and, consequently, to the therapeutic impact on tumour growth.

Liver TNP uptake is well tolerated and blocks metastasis. Given our evidence for TAMs in mediating TNP delivery, we next investigated TNP effects in the liver, which is a prominent site of the mononuclear phagocyte system and is known to accumulate NPs[6]. Despite substantial liver accumulation (Supplementary Fig. 9a), TNPs did not significantly impact animal body weight (Supplementary Fig. 9b) and did not cause changes outside of the normal range in blood markers of renal or liver toxicity at the therapeutic dose (Supplementary Fig. 9c). Within the bone marrow, another important site of the mononuclear phagocyte system, TNP payload concentrations were much lower (Supplementary Fig. 9d,e). Although clinically relevant doses of un-encapsulated cisplatin caused a significant reduction in the number of nucleated cells in the bone marrow, TNP effects were not statistically significant (Supplementary Fig. 9f,g). Overall, these results demonstrate a positive safety profile despite liver accumulation.

We next tested whether TNP treatment could block the development of liver micro-metastases in a model of haematogenous breast cancer dissemination. 4T1 murine breast cancer cells were intravenously injected into immunocompetent balb/c mice, thus forming tumours in the liver, lung and other organs. To primarily deliver TNPs to host phagocytes rather than tumour cells, we pre-treated naive mice with TNPs, waited 6 h for a majority of the drug to clear circulation, and then injected a single-cell suspension of 4T1 cells. Two weeks later, livers were excised and analysed by histology for tumour burden. Results show that pre-treatment with TNPs reduced the development of micro-metastases by over 65%, and repeated TNP doses caused a slightly greater reduction of 80% (Fig. 9). No treatment impacted tumour burden in the lung (two-tailed *t*-test; $n\geq5$). Taken together, these results demonstrate that TNPs can safely accumulate in host cells of the liver, thus allowing TNP payload to block the development of local metastases from haematogenously disseminated cancer cells.

Discussion

This work presents a new paradigm for employing TAMs as 'drug depots' for local delivery of nanotherapeutics to neighbouring

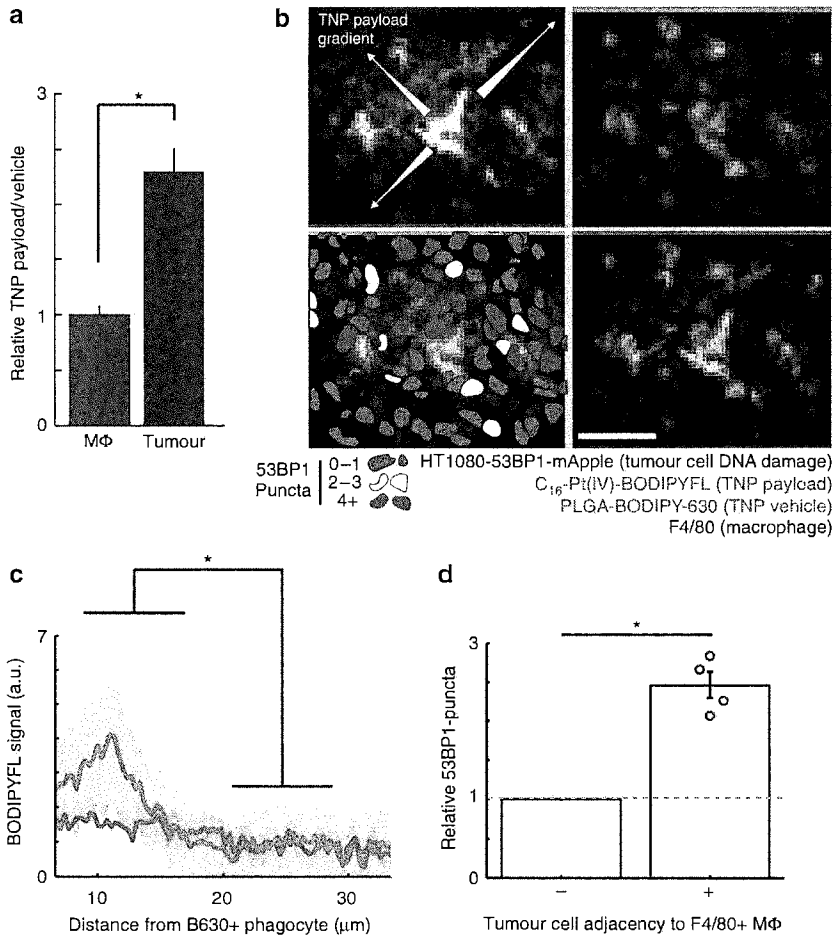

Figure 7 | DNA-damaging TNP payload redistributes from TAMs to neighbouring tumour cells. (**a**) Compared with TAMs, tumour cells exhibit elevated TNP payload as a fraction of TNP vehicle (measured by flow-cytometry), suggesting payload redistribution (*$P = 0.005$; two-tailed t-test; $n \geq 4$ per group). (**b**) Example immunofluorescence showing TNP vehicle uptake by F4/80$^+$ macrophages and payload diffusion into surrounding tumour tissue. In lower left panel, red pseudo-colour indicates tumour cells with high levels of 53BP1 puncta. Of note, these cells are also adjacent to F4/80$^+$ macrophages and contain elevated TNP payload. Scale bar, 50 μm. (**c**) By histological analysis, TNP payload but not vehicle is present at elevated levels within a 15-μm range of host phagocytes (*$P = 0.047$, two-tailed t-test; $n = 3$ animals). (**d**) By histological analysis, tumour cells immediately adjacent to F4/80$^+$ macrophages exhibit elevated DNA damage response, compared with average DNA damage response seen in non-adjacent tumour cells for each of four animals shown by individual data points (*$P = 0.007$; matched two-tailed t-test).

tumour cells. Key to the development of this model was new technology for the *in vivo* visualization of multi-step drug delivery and the corresponding single-cell PD response at high spatio-temporal resolution. With this approach we demonstrated that nano-encapsulation allows for long circulating drug half-life and guides the delivery of drugs to TAMs, from which their functional cytotoxic payloads locally transfer to and damage neighbouring tumour cells. This paradigm most likely extends to other nano-encapsulated therapeutics and non-cancer disease indications in which macrophages accumulate near the target tissue. The clinically tested TNP platform used here[14] can encapsulate other therapeutics including paclitaxel, doxorubicin and irinotecan, which exhibit release rates similar to the Pt(IV) payload[5–7]. Of relevance is that local macrophage accumulation occurs in multiple diseases including type 1 diabetes[41], rheumatoid arthritis[42], endometriosis[43] and cardiovascular diseases such as atherosclerosis and myocardial infarction[44,45]. The imaging approach we describe may thus apply to these other pathologies, especially where intravital microscopy has already been successfully used[46]. Although macrophages themselves are often pharmacological targets[47], concomitant drug delivery to surrounding tissue may be advantageous[48]. Overall, the drug delivery paradigm presented here, along with the complementary imaging technology, portend broad applicability to other TNP strategies and disease indications.

TAMs have been extensively studied and targeted for their roles in disease development, progression and therapeutic response[48,49]. Nonetheless, TAMs have received less consideration in the context of novel nanotherapeutics entering the clinic. Because of their secretion of growth factors, cytokines and proteases, TAMs have been implicated in supporting disease progression by enhancing angiogenesis, metastasis and cancer stem cell niche formation, all while suppressing anti-cancer immune responses. In multiple indications, high TAM accumulation at tumour sites correlates with poor prognosis[50,51]. Although TAM-mediated tumour neo-vascularization can increase vascular leakage and corresponding therapeutic delivery[52], TAMs also provide chemoprotective cues to tumour cells, and TAM infiltration following chemotherapy correlates with poor treatment response[52,53]. For these reasons, therapeutic TAM killing or TAM re-polarization into an anti-cancer phenotype represents an active area of development, for

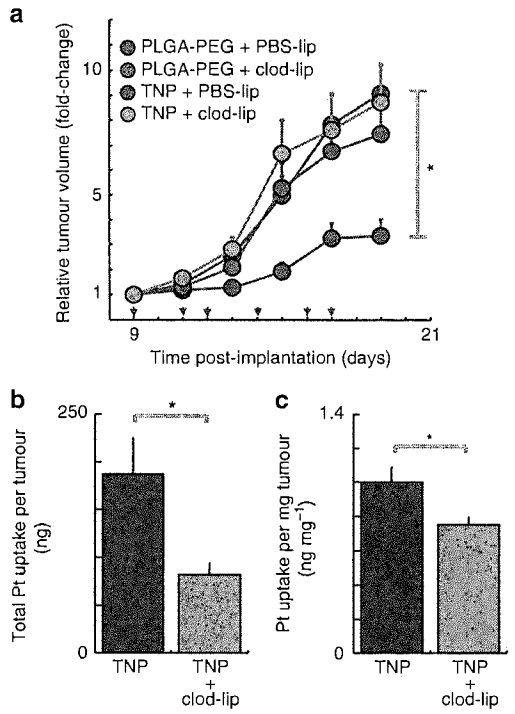

Figure 8 | Macrophage depletion reduces intratumoral accumulation and efficacy of TNP. (**a**) TNP reduces tumour growth in a macrophage-dependent manner. Animals were treated with TNP (green arrows) and clodronate liposomes (clod-lip; red arrows) to systemically deplete macrophages. Drug-free PLGA-PEG polymeric NPs and phosphate buffered saline liposomes (PBS-lip) were used as vehicle controls. TNP significantly reduced tumour growth ($P=0.039$), whereas clod-lip did not ($P=0.21$); however, clod-lip significantly reduced the impact of TNP ($P=0.039$ interaction term; all P-values used the two-tailed two-way analysis of variance, total $n=38$ animals). (**b**,**c**) Macrophage depletion using liposomal clodronate reduced the total amount (**b**) and concentration (**c**) of intratumoral Pt, measured using AAS ($P=0.02$ and $P=0.03$, respectively, two-tailed t-test; total $n=22$).

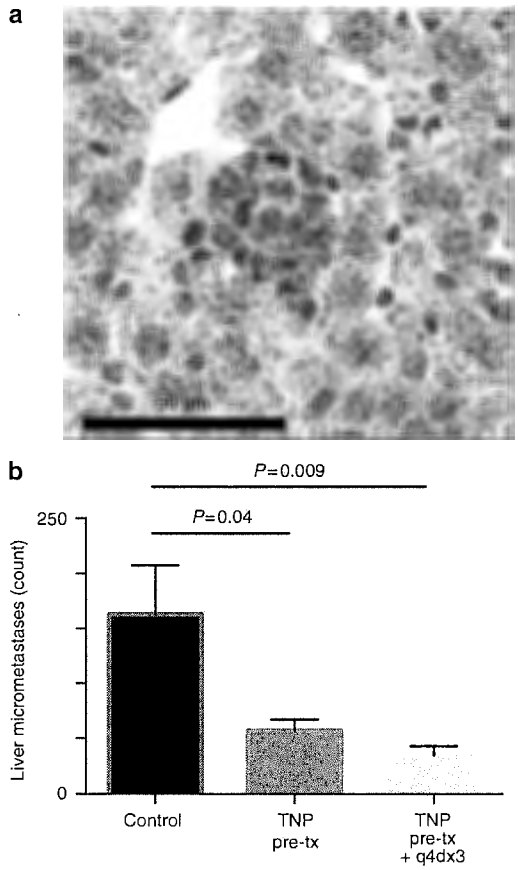

Figure 9 | TNP delivery to the liver blocks development of micro-metastases. (**a**) Representative liver micro-metastasis, 2 weeks after i.v. injection of 4T1 breast cancer cells (haematoxylin and eosin staining of FFPE tissue section). (**b**) TNP reduces liver micro-metastasis development in the 4T1 model of haematogenous metastasis (two-tailed t-test; shown as mean ± s.e.m.; $n \geq 5$). To initially deliver TNPs to host phagocytes (rather than tumour cells), TNPs were i.v. administered (1 mg kg^{-1}) 6 h before i.v. injection of 4T1 cancer cells, such that TNP largely cleared the circulation at the time of cancer cell administration. One-third of the cohort received subsequent TNP treatments as indicated.

example, by targeting colony-stimulating factor 1 receptor (CSF1R)[54–56]. In several examples, blocking leukocyte infiltration via CSF1R inhibition or chemokine receptor type 2 ablation enhances response to chemotherapeutics including cisplatin[52]. However, very little experimental data describes how TAM depletion affects the response to nanotherapeutic formulations, and evidence presented here suggests that complete TAM elimination would be undesirable in such contexts.

In contrast to previous reports that focus chiefly on traditional unencapsulated cytotoxic therapies, we show here that TAMs are critical mediators of drug action for nano-encapsulated therapeutics. TAMs and other leukocytes are implicated in taking up a wide range of clinically relevant nanotherapeutics, including liposomal[57], polymeric[58] and albumin-binding[59] formulations. Nonetheless, in the past, imaging capabilities have generally not allowed detailed insight into the kinetics of drug uptake, payload redistribution and corresponding PD responses at the single-cell or subcellular level to be determined for these compounds[57,60]. Compared with polymeric NPs such as those used here, liposomal formulations generally are associated with slower payload release and decreased payload bioavailability, and there is little evidence that doxorubicin is released from TAMs after they have taken up liposomes[57,61]. In fact, previous failures to develop liposomal cisplatin have been attributed to insufficiently fast drug release[13]. By contrast, polymeric nano-formulations can be designed to release payloads at prescribed rates[5] and even at programmed environmental (for example, pH) conditions[62]. Here, TNPs were engineered to release their payload over a slightly longer time scale (50% drug release at 15 h; Supplementary Fig. 1d) relative to the observed PKs of cellular uptake (TAM uptake observable at 1 h and gradually increases by 24 h), and therefore were ideally suited for TAM-mediated drug delivery as described herein. Overall, this work builds on previous studies that implicate macrophages in TNP uptake; however, through engineered drug release and fluorescence imaging strategies, we demonstrate how the TNP payload can redistribute to neighbouring tumour cells at the site of local TAM accumulation in a therapeutically beneficial manner.

The results presented have implications for future development and clinical use of TNPs. Given that TNPs accumulate in TAMs at high levels, it follows that one criterion for selecting patients into TNP trials may be the degree of peritumoral TAM content, which can be assessed by magnetic resonance imaging using clinically approved NP contrast agents such as ferumoxytol (Feraheme)[63] or experimental theranostics including drug-conjugated ferumoxytol derivatives[64,65]. TAM content is

especially important in the context of therapies that either increase or decrease infiltration of macrophages to tumours. For instance, doxorubicin[52] and CD40 agonist antibodies[66] enhance macrophage infiltration, whereas CSF1R inhibitors[56] and the clinically approved trabectedin[67] decrease TAM accumulation. The paradigm of TAM-mediated drug delivery presented offers a compelling case for consideration of competing drug effects on TAM recruitment, and highlights the potential use of TNP vehicles for more efficient (via improved kinetics and/or targeting subsets) targeting of both TAMs and their neighbouring tumour cells.

Methods

C_{16}-Pt(IV)-BODIPY synthesis. A 0.2-ml N,N-Dimethylformamide (DMF) solution of *cis,cis,trans*-[$Pt(NH_3)_2Cl_2(O_2CCH_2CH_2COOH)(OCONH(CH_2)_{15}CH_3)$] (15 mg, 21 μmol) and 1-[Bis(dimethylamino)methylene]-1H-1,2,3-triazolo[4,5-b]pyridinium 3-oxid hexafluorophosphate (HATU) (8 mg, 21 μmol) was stirred at room temperature (RT) for 15 min. To the clear solution was added a 0.4 ml DMF suspension of the amino BODIPY (4,4-difluoro-5,7-di- methyl-4-bora-3a,4a-daiza-s-indacene; 6 mg, 21 μmol), and the orange suspension was stirred at RT for 30 min. Finally, a 4 μl portion of N,N-Diisopropylethylamine (DIPEA) was added to the mixture and the resulting orange solution was stirred at RT for 5 h. A 5-ml volume of saturated aqueous NaCl was added to the reaction mixture and a red precipitate was obtained. The precipitate was washed with 3 × 3 ml water. The resulting orange solid was dried in the vacuum overnight and the product was isolated by silica chromatography (acetone, $R_f = 0.5$). Yield: 7 mg (30%). ^{1}H NMR (400 MHz, acetone-d_6): δ: 7.73 (s, 1H, $NHCH_2CH_2$-BODIPY), 6.54 (m, 6H, NH3), 6.18 (s, 1H, BODIPY), 5.80 (s, 1H, $NH_{carbamate}$), 3.42 (m, 2H, $NHCH_2CH_2$-BODIPY), 3.29 (m, 2H, $NHCH_2CH_2$-BODIPY), 3.01 (m, 2H, $CH_2(CH_2)_{14}CH_3$), 2.45 (s, 6H, BODIPY), 2.21 (m, 10H, BODIPY, succinate), 1.20 (m, 28H, $CH_2(CH_2)_{14}CH_3$), 0.8(t, 3H, $CH_2(CH_2)_{14}CH_3$). ^{13}C NMR (100 MHz, DMSO-d_6): δ: 180.4, 172.1, 164.4, 153.9, 143.0, 142.0, 131.5, 122.3, 41.5, 40.9, 31.9, 31.8, 30.3, 29.5, 29.4, 29.2, 29.1, 22.6, 16.5, 14.6, 14.4. ^{195}Pt NMR (86 MHz, DMSO-d_6): δ: 1,240.1. High resolution electrospray ionization mass spectrometry (HR-ESI-MS) (positive mode) for $C_{36}H_{63}BCl_2F_2N_6O_5Pt$: m/z $[M-H]^+$ calculated: 975.4020; observed: 975.4001.

Polymer materials. Unless otherwise stated, all chemical reagents were purchased from Sigma-Aldrich. PLGA(55:45 lactide/glycolide)$_{35.2kDa}$-$PEG_{3.5\,kDa}$ was purchased from Advanced Polymer Materials, Inc. (Cat. #13-01-CX-55/45-35.2k/3.5k; lot 14-02-169). From the vender, gel permeation chromatography indicated $M_n = 38.8$ kDa, $M_w = 58.8$ kDa and PI = 1.52. PEG weight fraction (8.7% ± 0.3%) and molecular weight were confirmed by ^{1}H NMR peak integration values, which were also used to calculate the lactide/glycolide ratio. ^{1}H NMR in $CDCl_3$: δ (in p.p.m.) 5.12–5.28 (m, (-OC**H**(CH_3)CO)), 4.66–4.9 (m, (-O**CH_2**COO-)), 3.64 (s, -O**CH_2**CH_2O-), 1.52–1.62 (m, (-OCH(**CH_3**)CO-). Differential scanning calorimetry was performed (Q10; TA Instruments), heating from −60 °C to 100 °C at 10 °C min^{-1}, with no apparent crystallization or melting temperature (Tm); glass temperature (Tg) was observed at 39.5 °C. BODIPY-630-NH_2 (Life Technologies; 2.8 mg, 0.0046 mmol) was conjugated to PLGA(50:50 lactide:glycolide)$_{30-60\,kDa}$ (100 mg, ca 0.0023 mmol; Sigma) using previously published procedures[27], by stirring at RT under Ar for 10 min, adding 1-Ethyl-3-(3-dimethylaminopropyl)carbodiimide (EDCI) (4.4 mg, 0.023 mmol) and 4-Dimethylaminopyridine (DMAP) (2.8 mg, 0.023 mmol) in CH_2Cl_2 (0.5 ml), and stirring overnight. Polymer was precipitated in cold 1:1 MeOH/Et_2O, centrifuged (2,700*g*, 10 min) and repeatedly washed in minimal CH_2Cl_2, followed by MeOH/Et_2O precipitation and centrifugation. The resulting blue precipitate was dried under vacuum.

NP synthesis and characterization. TNPs were prepared by nano-precipitation. Briefly, the following reagents were dissolved in 50:50 (v/v) DMF/acetonitrile (ACN) at the indicated concentrations: PLGA-BODIPY-630 (0.17 mg ml^{-1}), C_{16}-Pt(IV)-BODIPY (0.17 mg ml^{-1}) and PLGA-PEG (0.83 mg ml^{-1}). The resulting solution was then mixed and added drop-wise to nuclease-free H_2O while maintaining a ratio of 20:1 H_2O to organic solvent. TNPs were stirred overnight and filtered through sterile 0.45 μm syringe filters (regenerated cellulose, 17 mm, Cole Palmer). The TNPs were concentrated by centrifugation using centrifugal filter units (Amicon; Millipore; molecular weight cut-off, MWCO = 100 kDa). The concentrated TNPs were washed twice with de-ionized H_2O and re-suspended in 1 ml of nuclease-free H_2O. TNPs were diluted ten times in H_2O and characterized by size using dynamic light scattering (DLS; Malvern Zetasizer). Zeta-potential was also measured by DLS in dI-H_2O (−25 ± 2.5 mV) and PBS, pH 7.4 (−23 ± 1.4 mV). Although the buffered solution produced a slightly higher zeta-potential, measurements were not statistically different from each other (two-tailed *t*-test; $\alpha = 0.05$). The Pt concentration was determined by graphite furnace flameless atomic absorption spectroscopy (AAS). BODIPY-630 concentration was determined by a microplate fluorimeter after diluting TNPs in DMF and using pure BODIPY-630 for a standard curve. Transmission electron microscopy (TEM) experiments were performed on a JEOL 1011 electron microscope (JEOL). The TEM sample was prepared by depositing 10 μl of TNPs (5 mg ml^{-1}) onto a carbon-coated copper grid. The excess solution was blotted, and the grids were immersed in a solution of phosphotungstic acid stain. The stain was blotted, and the dried grids were immediately used for imaging. To characterize payload release from TNPs (Supplementary Fig. 1d), they were incubated in PBS at 37 °C, filtered using 100 kDa MWCO centrifugal filters (Amicon; Millipore) at the indicated time points and resuspended in fresh PBS. Filtrate was frozen for later analysis by AAS. After 72 h, both the TNPs and the filtrate were analysed by AAS to quantify the remaining Pt. Based on the above procedure, <5% of total PLGA-BODIPY-630 was released from TNPs over the course of 48 h.

Animal models. All animal research was performed in accordance with guidelines from the Institutional Subcommittee on Research Animal Care (Massachusetts General Hospital). All experiments were performed using female mice that were 5- to 7-week old at the start of the experiment. For experiments with HT1080 tumours, 2 million cells in PBS were subcutaneously implanted into nu/nu mice; roughly 2–3 weeks later (once tumours reached ~8 mm diameter), imaging experiments were initiated. For the experimental model of haematogenous metastatic dissemination, 0.25 million 4T1 breast cancer cells suspended in PBS were intravenously (i.v.) injected into balb/c mice; roughly 2 weeks later tumours were excised for histological quantification of liver and lung tumour burden in formalin-fixed paraffin-embedded (FFPE), haematoxylin and eosin-stained sections. For intraperitoneal OVCA imaging, 10 million A2780CP cells suspended in PBS were intraperitoneally injected into nu/nu mice. TNP injection and imaging were performed once ascites or tumour masses became evident (roughly 6 weeks later). For histology and imaging experiments using KP cells, 1 million cells were subcutaneously implanted into C57Bl/6 background animals (all JAX), including $Cx3cr1^{GFP/+}R26^{mT-mG/+}$ dual-reporter mice. For dual reporter mice generation, $Cx3cr1^{GFP/GFP}$ animals were crossed with $R26^{mT-mG/mT-mG}$ animals that ubiquitously express membrane-anchored tdTomato[68]. The resulting $Cx3cr1^{GFP/+}$ $R26^{mT-mG/+}$ animals can be used to visualize GFP^+ $tdTomato^+$ macrophages, monocytes and dendritic cells, as well as $tdTomato^+$ stroma and endothelium.

Cell lines. With some exceptions, cell lines were obtained from American Type Culture Collection and routinely cultured according to the manufacturer's guidelines. OVCA-429 were a kind gift from Dr Michael Birrer (MGH), and A2780CP were from Sigma. The murine lung adenocarcinoma cell line KP1.9 was generated from lung tumour cells of $Kras^{LSL-G12D/+}$;$p53^{fl/fl}$ mice (C57/Bl6 background), which develop lung adenocarcinoma after infection with an adenovirus expressing Cre recombinase by intratracheal administration[39]. KP cells were maintained in Iscove's DMEM media supplemented with 10% fetal bovine serum and 5% penicillin/streptomycin. All cell lines were routinely tested for contamination using mouse antibody production testing (VRL Laboratories) and assaying for mycoplasma (VRL Laboratories; Lonza MycoAlert). The fluorescent protein mApple was subcloned into the pLVX vector using restriction enzymes *Afe*I and *Not*I. We inserted a *Xho*I site at in the 5′ end of the pLVX-mApple multiple cloning site using QuikChange site-directed mutagenesis (Agilent). The pDsRed-Monomer-Mem membrane targeting sequence (Clontech) was PCR amplified for In-Fusion cloning to construct pLVX-Mem-mApple. PCR product was then ligated into pLVX-Apple after *Afe*I and *Xho*I digestion, and fully sequenced. Lentiviral particles were produced using Lenti-X HTX Packaging System (Clontech) for transduction into HT1080 and A2780CP cells, which were then selected using 3 μg ml^{-1} puromycin. HT1080–53BP1-mApple and A2780CP-53BP1-mApple were developed as previously described[29].

Intravital microscopic imaging. TNPs were injected at the indicated dose (1 mg kg^{-1} unless otherwise stated) via tail-vein catheter immediately after mixing to a final 1 × PBS solution, at a final volume of 100 μl. Intravital microscopy was performed on an Olympus FV1000 multiphoton imaging system using a XLUMPLFLN × 20 water immersion objective (numerical aperture = 1.0; Olympus America). Images were scanned sequentially using 405-, 473-, 559- and 633-nm diode lasers in combination with a DM405/488/559/635-nm dichroic beam splitter. Emitted light was then separated and collected using appropriate combinations of beam splitters (SDM473, SDM560 and/or SDM 640) and emission filters BA490–540, BA575–620, BA575–675 and/or BA655–755 (all Olympus America). Dextran pacific blue ($\lambda_{ex} = 405$ nm) was injected to initially image TMV as previously described[29]. Briefly, 500-kDa amino-dextran (Thermo) was labelled with Pacific Blue succinimidyl ester (Thermo), purified using 30 kDa MWCO centrifugal filtration (Amicon), and 250 μg i.v. injected 10 min before imaging. Dorsal window chamber imaging was performed following previously described procedures[29,69,70]. Briefly, 2 million HT1080–53BP1-mApple cells were suspended in 50 μl PBS and injected under the fascia of nu/nu mice (Cox7, MGH) 30 min following surgical chamber implantation, and imaged 2 weeks later.

Histology. Excised tumours were embedded in optimal cutting temperature (OCT) compound, flash-frozen, sectioned using a Leica CM1900 Rapid Sectioning Cryostat (Leica), stained using anti-mouse F4/80 antigen eFluor 450 (clone BM8;

eBioscience), and imaged using an upright Olympus BX63 microscope and a ×100 oil-immersion objective. For immunohistochemistry, a biotinylated anti-rat IgG antibody was applied, and VECTASTAIN ABC kit (Vector Laboratories Inc.) along with a 3-amino-9-ethylcarbazole substrate (Dako) were used for colour development. The sections were counterstained with Harris haematoxylin solution (Sigma-Aldrich) and scanned by using Nanozoomer 2.0RS (Hamamatsu). For immunofluorescence, anti-rat IgG-Alexa Fluor 405 (Abcam) as a secondary antibody and anti-mouse CD326 (EpCAM)-PE antibody (clone: G8.8, eBioscience) were used.

***In vitro* NP characterization.** For cytotoxicity assays (Supplementary Table 1), 5,000 cells per well were plated in 96-well plates, treated the next day with Pt-compound or the appropriate buffer control (DMF or drug-free PLGA-PEG NPs, as appropriate), and assessed for viability 72 h later using PrestoBlue (Life Technologies) following the manufacturer's protocol. IC_{50} values for each compound were calculated by interpolating from an 11-point dose–response curve.

For live-cell *in vitro* microscopy of TNP uptake (Supplementary Fig. 2a), HT1080–53BP1-mApple cells were seeded on an optical-bottom 96-well plate (Ibidi; Applied Biophysics), treated the following day with 1 μM TNP for 24 h, washed in warm medium, and immediately imaged on a DeltaVision (Applied Precision) modified Olympus BX63 microscopy system with an environmental chamber. Dose–response analysis of TNP uptake (Supplementary Fig. 3) followed the same protocol. Corresponding measurements of intracellular Pt uptake (Supplementary Fig. 3d) were performed by treating 80% confluent cells in six-well plates for 24 h with TNP, rinsing with PBS, trypsinizing, centrifuging the cell pellet for 300*g* for 5 min, re-suspending the pellet in 50 μl fresh PBS, and freezing it for subsequent AAS analysis.

CellLight BacMam (Life Technologies) fluorescent protein-signal peptide fusions, delivered using baculovirus, were used for subcellular compartment co-localization experiments (Supplementary Fig. 2b). Briefly, 10,000 HT1080 cells were treated overnight with 20 μl CellLight reagent in 12-well dishes, plated the next day on collagen-I-coated glass coverslips in six-well dishes, and the following day were treated with 0.5 μM TNP for either 3 or 24 h. Following treatment, cells were counterstained with Hoechst 33342 and immediately imaged. Collagen-coating was performed by treating coverslips with 100 μg ml^{-1} rat-tail collagen-I (BD Biosciences) overnight and then rinsing with PBS.

To analyse de-quenching of the C_{16}-Pt(IV)-BODIPY compound (Supplementary Fig. 2d), TNPs were added at 1 μM to full serum medium (DMEM + 10% fetal bovine serum + 1% penicillin/streptomycin) in the presence or absence of 90% confluent HT1080 in 96-well plates. Fluorescence was monitored by a Tecan Safire 2 fluorescence plate reader. For monitoring TNP uptake kinetics (Supplementary Fig. 8a), equal numbers of RAW 264.7 macrophages or HT1080 cells were plated in 96-well plates and incubated with 1 μM TNP. At the indicated time points, medium was temporarily transferred to empty wells and replaced with fresh media on cells. Cells were then immediately measured using a plate reader for BODIPY-630 fluorescence, and the TNP-containing media were replaced onto the cells again.

To analyse Pt uptake and release into supernatant by macrophages (Supplementary Fig. 8c), confluent 10 cm tissue-culture dishes of RAW macrophages were treated with 62 μM TNP for 24 h, rinsed in PBS, treated with fresh media, incubated for another 24 h and then analysed for Pt content by AAS. The supernatant was clarified by centrifugation (300*g* for 5 min) before AAS analysis. Cells were harvested by trypsinization, centrifugation (300*g* for 5 min), resuspension of the cell pellet in 50 μl PBS and freezing for subsequent AAS analysis.

To analyse whether the Pt-containing macrophage supernatant could invoke a DNA damage response in tumour cells (Supplementary Fig. 8d), RAW macrophages were treated for 6 h with 15 μM TNP, then rinsed and incubated in fresh media. After 24 h, media were clarified by centrifugation (300*g* for 5 min), transferred to HT1080–53BP1-mApple cells plated on optical-bottom 96-well plates (Ibidi; Applied Biophysics), and incubated overnight. The following day cells were rinsed and immediately imaged.

To analyse whether Pt-containing macrophage supernatant cause cytotoxic effects on tumour cells (Supplementary Fig. 8e), RAW macrophages were treated for 24 h with either TNP or unencapsulated C_{16}-Pt(IV)-BODIPY (the latter to achieve high Pt concentrations), then rinsed and incubated in fresh media. After 24 h, media were clarified by centrifugation (300*g* for 5 min), then transferred to 5000 HT1080 cells per well of a 96-well plate. After 72 h, the cell count was determined by the PrestoBlue assay (Life Technologies).

To analyse whether the above cytotoxic effects depend on proteins in the Pt-containing macrophage supernatant (Supplementary Fig. 8f), RAW macrophages were treated for 16 h with 60 μM TNP, then rinsed and incubated in fresh media. After an additional 16 h, media were clarified by centrifugation (300*g* for 5 min), filtered using MWCO centrifugal filters (Amicon; Millipore), and transferred to 5000 HT1080 cells per well of a 96-well plate. After an additional 72 h, the cell count was determined by the PrestoBlue assay (Life Technologies).

Tumour growth. Subcutaneous tumours were implanted in 7-week-old female nu/nu mice (Cox7, MGH), injected in four quadrant animal flanks as 1 million HT1080 cells suspended in 50 μl PBS. Nine days later, animals were ranked and sorted into groups of four based on tumour size. According to predefined protocol guidelines, mice were killed when tumour burden reached more than 1 cm in diameter, or 2 cm in diameter if only one tumour was present. Tumour volumes were measured two to three times per week, estimated using the spherical tumour volume formula $V = {}^4/_3\,\pi r^3$, where r is averaged from four caliper measurements performed by two blinded researchers. Each size-group was randomly distributed to the four treatment-groups such that final treatment-groups exhibited roughly equal distribution in tumour size, with 9–10 mice per group. Groups received 150 μl of clodronate liposomes (clod-lip) or PBS liposomes as a vehicle control, intraperitoneally, on the indicated days (Fig. 8a). Liposomes were from ClodLip BV (Haarlem), with clodronate at a concentration of 5 mg ml^{-1}. As separate intravenous injections on indicated days (Fig. 8a), groups received 1 mg kg^{-1} Pt of either TNP or the TNP without Pt(IV) as a vehicle control. TNPs for this experiment were formulated as described above, using $PLGA_{8kDa}$-PEG_{5kDa} and non-fluorescent $PLGA_{30\text{–}60kDa}$ rather than $PLGA_{30\text{–}60kDa}$-BODIPY-630. TNP formulations were made fresh before each injection, and batches were tested for size and monodispersity by DLS and TEM. Pt loading was measured by AAS, and appropriate drug release was measured as previously described. At 19 days post implantation, tumours were excised, rinsed in PBS and processed for histology by freezing in OCT compound, or alternatively processed for AAS analysis by blotting tissue to remove excess water and freezing. One of thirty-eight animals was prematurely killed owing to biting and cachexia.

Flow cytometry. Subcutaneous tumours (HT1080 cells) were harvested from nu/nu mice 3 weeks post implantation, cut into small pieces and incubated in RPMI 1640 medium containing 0.2 mg ml^{-1} collagenase type I (Worthington Biochemical Corporation) for 1 h at 37 °C while shaking (250 r.p.m.). Digested tumours were filtered through a 70-μm cell strainer (BD Falcon). The resulting single-cell suspensions were washed and resuspended in PBS with 0.5% BSA and 2 mM EDTA. Cell labelling was performed with appropriate antibodies as indicated below for 45 min at 4 °C. The following cell types were identified by flow cytometry (LSRII, BD Biosciences) depending on cell marker expression: tumour cells ($hCD29^+$), macrophages ($CD45^+CD11b^+Ly6C^-Lin^-CD11c^+F4/80^+$), neutrophils ($CD45^+CD11b^+Ly6C^+Lin^+$) and lymphocyte-like cells ($CD45^+Lin^+CD11b^-Ly6G^-$). The anti-human CD29 antibody (clone MAR4) was from BD, and the following anti-mouse antibodies used were from BioLegend: CD45 (clone 30-F11), F4/80 (clone BM8), CD11c (clone N418), Ly6C (clone HK1.4). CD11b (clone M1/70) was from BD Biosciences, along with all antibodies used in the lineage (Lin) mixture: anti-CD90.2 (clone 53–2.1), anti-B220 (clone RA3–6B2), anti-NK1.1 (clone PK136), anti-CD49b (clone DX5), anti-Ter119 (cloneTER-119) and anti-Ly6G (clone 1A8). To exclude dead cells, 7-aminoactinomycin D (Sigma-Aldrich) was used. Data were analysed using FlowJo v.8.8.7 (Tree Star, Inc.) and MATLAB. BODIPY-630 and amino-BODIPY fluorescence was assessed by using an LSRII flow cytometer and the mean fluorescence intensity (MFI) of the different cell populations was determined. Background autofluorescence for each immunologically defined cell population was measured from control-treated animals that were injected with non-fluorescent PLGA-PEG vehicle; this value was subtracted from the data for the fluorescent TNP-treated animals.

Computational image analysis. Intravital microscopy images were analysed using either Matlab (Mathworks) or ImageJ and were pre-processed using background subtraction based on data acquired immediately before TNP injection. For vascular half-life calculations, fluorescence time-lapse values from multiple vessels across multiple animals were recorded, averaged and fit to an exponential decay model using nonlinear regression in MATLAB. Single-cell 3D segmentation for image cytometry analysis was performed using a custom MATLAB pipeline. Briefly, a previously described 3D nuclear-segmentation algorithm was modified to measure the MFI of TNP vehicle and its payload within a given radius of each nucleus. These measurements were then correlated with observed 53BP1-puncta in each individual nucleus, validated by eye (Fig. 3c). Throughout the manuscript, data falling >2 standard deviations from the mean were excluded as outliers from the statistical calculations. For calculation of spatial heterogeneity, measured by the CV (Supplementary Fig. 4), cell-sized regions of interest within images were quantified for MFI. CV for TNP and unencapsulated Pt (CP-11 (ref. 29)) were measured >20 half-lives post injection as an approximation of steady-state tissue distribution (5 and 24 h, respectively).

Liver and BM analysis. Pt concentrations in the liver and bone marrow were determined by AAS and fluorescence imaging. Briefly, naive female nu/nu mice 8-week old were i.v. injected with TNP at a dose of 1 mg kg^{-1} Pt. 24 h later, animals were perfused with PBS by intracardiac injection before dissection. For fluorescence quantification of TNP payload, livers were excised and frozen in OCT compound for later sectioning. Femoral BM was flushed using PBS and smeared on a glass slide for immediate imaging. Un-injected control animals were used to measure background signal for each organ, which was baseline-subtracted in the quantification. For AAS analysis of Pt content, livers were excised, patted dry and frozen. BM was flushed using PBS, centrifuged at 16,000*g* to pellet cells and frozen. Tissue was then dissolved in 70% nitric acid and analysed as with the HT1080 tumours (Fig. 8). For quantification of BM cellularity, femurs were excised 24 h

post injection with TNP, formalin-fixed overnight, decalcified in EDTA and processed for FFPE sectioning. Immunohistochemistry was performed for apoptosis analysis by terminal deoxynucleotidyl transferase dUTP nick-end labelling, using Apoptag Peroxidase In Situ Apoptosis Detection Kit (Millipore), counterstaining with Harris haematoxylin solution (Sigma-Aldrich), and scanning with a Nanozoomer 2.0RS (Hamamatsu).

Metastasis burden in the lung and liver was quantified by morphological assessment in haematoxylin and eosin-stained liver FFPE sections that had been imaged using Nanozoomer 2.0RS, with organ excision at time of animal euthanasia according to the institutional guidelines (body condition score of 2) or 20 days post cancer injection, whichever came first. No statistically significant difference was observed in animal survival, body weight loss or lung tumour burden across the groups. One mouse from the group receiving repeated TNP dosing was excluded from analysis since no lung tumours (and very few liver tumours) were found by histology, presumably due to failed initial intravenous injection.

Clinical chemistry measurements in Swiss albino mice were performed using previously described TNP and methods[6]. Graphically re-plotted here for context (Supplementary Fig. 9a), bio-distribution of Pt in male rats was measured as described previously[6].

References

1. Kelland, L. The resurgence of platinum-based cancer chemotherapy. *Nat. Rev. Cancer* **7**, 573–584 (2007).
2. O'Shaughnessy, J. *et al.* Phase III study of iniparib plus gemcitabine and carboplatin versus gemcitabine and carboplatin in patients with metastatic triple-negative breast cancer. *J. Clin. Oncol.* **32**, 3840–3847 (2014).
3. Cooke, S. L. & Brenton, J. D. Evolution of platinum resistance in high-grade serous ovarian cancer. *Lancet Oncol.* **12**, 1169–1174 (2011).
4. Bertrand, N., Wu, J., Xu, X., Kamaly, N. & Farokhzad, O. C. Cancer nanotechnology: the impact of passive and active targeting in the era of modern cancer biology. *Adv. Drug Deliv. Rev.* **66**, 2–25 (2014).
5. Hrkach, J. *et al.* Preclinical development and clinical translation of a PSMA-targeted docetaxel nanoparticle with a differentiated pharmacological profile. *Sci. Transl. Med.* **4**, 128ra39 (2012).
6. Dhar, S., Kolishetti, N., Lippard, S. J. & Farokhzad, O. C. Targeted delivery of a cisplatin prodrug for safer and more effective prostate cancer therapy *in vivo*. *Proc. Natl Acad. Sci. USA* **108**, 1850–1855 (2011).
7. Valencia, P. M. *et al.* Synergistic cytotoxicity of irinotecan and cisplatin in dual-drug targeted polymeric nanoparticles. *Nanomedicine (Lond.)* **8**, 687–698 (2013).
8. Gadde, S. Multi-drug delivery nanocarriers for combination therapy. *Med. Chem. Commun.* doi: 10.1039/C5MD00365B (2015).
9. Xu, X. *et al.* Enhancing tumor cell response to chemotherapy through nanoparticle-mediated codelivery of siRNA and cisplatin prodrug. *Proc. Natl Acad. Sci. USA* **110**, 18638–18643 (2013).
10. Johnstone, T. C. *et al.* Nanoparticle encapsulation of mitaplatin and the effect thereof on *in vivo* properties. *ACS Nano* **7**, 5675–5683 (2013).
11. Prabhakar, U. *et al.* Challenges and key considerations of the enhanced permeability and retention effect for nanomedicine drug delivery in oncology. *Cancer Res.* **73**, 2412–2417 (2013).
12. Maeda, H., Nakamura, H. & Fang, J. The EPR effect for macromolecular drug delivery to solid tumors: Improvement of tumor uptake, lowering of systemic toxicity, and distinct tumor imaging *in vivo*. *Adv. Drug Deliv. Rev.* **65**, 71–79 (2013).
13. Harrington, K. J. *et al.* Phase I-II study of pegylated liposomal cisplatin (SPI-077) in patients with inoperable head and neck cancer. *Ann. Oncol.* **12**, 493–496 (2001).
14. Wright, J. Nanotechnology: deliver on a promise. *Nature* **509**, S58–S59 (2014).
15. Caron, W. P., Song, G., Kumar, P., Rawal, S. & Zamboni, W. C. Interpatient pharmacokinetic and pharmacodynamic variability of carrier-mediated anticancer agents. *Clin. Pharmacol. Ther.* **91**, 802–812 (2012).
16. Thurber, G. M. *et al.* Single-cell and subcellular pharmacokinetic imaging allows insight into drug action in vivo. *Nat. Commun.* **4**, 1504 (2013).
17. Yamamoto, N. *et al.* Cellular dynamics visualized in live cells in vitro and in vivo by differential dual-color nuclear-cytoplasmic fluorescent-protein expression. *Cancer Res.* **64**, 4251–4256 (2004).
18. Hinkeldey, B., Schmitt, A. & Jung, G. Comparative photostability studies of BODIPY and fluorescein dyes by using fluorescence correlation spectroscopy. *ChemPhysChem* **9**, 2019–2027 (2008).
19. Karolin, J., Johansson, L. B.-A., Strandberg, L. & Ny, T. Fluorescence and absorption spectroscopic properties of dipyrromethene boron difluoride (BODIPY) derivatives in liquids, lipid membranes, and proteins. *J. Am. Chem. Soc.* **116**, 7801–7806 (1994).
20. Ulrich, G., Ziessel, R. & Harriman, A. The chemistry of fluorescent bodipy dyes: versatility unsurpassed. *Angew Chem. Int. Ed. Engl.* **47**, 1184–1201 (2008).
21. Xiao, K. *et al.* The effect of surface charge on in vivo biodistribution of PEG-oligocholic acid based micellar nanoparticles. *Biomaterials* **32**, 3435–3446 (2011).
22. He, C., Hu, Y., Yin, L., Tang, C. & Yin, C. Effects of particle size and surface charge on cellular uptake and biodistribution of polymeric nanoparticles. *Biomaterials* **31**, 3657–3666 (2010).
23. Yamamoto, Y., Nagasaki, Y., Kato, Y., Sugiyama, Y. & Kataoka, K. Long-circulating poly(ethylene glycol)-poly(D,L-lactide) block copolymer micelles with modulated surface charge. *J. Control Release* **77**, 27–38 (2001).
24. Kommareddy, S. & Amiji, M. Biodistribution and pharmacokinetic analysis of long-circulating thiolated gelatin nanoparticles following systemic administration in breast cancer-bearing mice. *J. Pharm. Sci.* **96**, 397–407 (2007).
25. Zheng, Y. R. *et al.* Pt(IV) prodrugs designed to bind non-covalently to human serum albumin for drug delivery. *J. Am. Chem. Soc.* **136**, 8790–8798 (2014).
26. Orth, J. D. *et al.* Analysis of mitosis and antimitotic drug responses in tumors by in vivo microscopy and single-cell pharmacodynamics. *Cancer Res.* **71**, 4608–4616 (2011).
27. Laughney, A. M. *et al.* Single-cell pharmacokinetic imaging reveals a therapeutic strategy to overcome drug resistance to the microtubule inhibitor eribulin. *Sci. Transl. Med* **6**, 261ra152 (2014).
28. Yang, M., Jiang, P. & Hoffman, R. M. Whole-body subcellular multicolor imaging of tumor-host interaction and drug response in real time. *Cancer Res.* **67**, 5195–5200 (2007).
29. Miller, M. A., Askevold, B., Yang, K. S., Kohler, R. H. & Weissleder, R. Platinum compounds for high-resolution in vivo cancer imaging. *ChemMedChem* **9**, 1131–1135 (2014).
30. Miwa, S. *et al.* Imaging UVC-induced DNA damage response in models of minimal cancer. *J. Cell Biochem.* **114**, 2493–2499 (2013).
31. Beletsi, A., Panagi, Z. & Avgoustakis, K. Biodistribution properties of nanoparticles based on mixtures of PLGA with PLGA-PEG diblock copolymers. *Int. J. Pharm.* **298**, 233–241 (2005).
32. Doxil (package insert)Horsham, P. A. Janssen Products, LP (2015).
33. Gabizon, A., Shmeeda, H. & Barenholz, Y. Pharmacokinetics of pegylated liposomal doxorubicin: review of animal and human studies. *Clin. Pharmacokinet.* **42**, 419–436 (2003).
34. Kolishetti, N. *et al.* Engineering of self-assembled nanoparticle platform for precisely controlled combination drug therapy. *Proc. Natl Acad. Sci. USA* **107**, 17939–17944 (2010).
35. Dhar, S., Gu, F. X., Langer, R., Farokhzad, O. C. & Lippard, S. J. Targeted delivery of cisplatin to prostate cancer cells by aptamer functionalized Pt(IV) prodrug-PLGA-PEG nanoparticles. *Proc. Natl Acad. Sci. USA* **105**, 17356–17361 (2008).
36. Karanam, K., Kafri, R., Loewer, A. & Lahav, G. Quantitative live cell imaging reveals a gradual shift between DNA repair mechanisms and a maximal use of HR in mid S phase. *Mol. Cell* **47**, 320–329 (2012).
37. Shaw, T. J., Senterman, M. K., Dawson, K., Crane, C. A. & Vanderhyden, B. C. Characterization of intraperitoneal, orthotopic, and metastatic xenograft models of human ovarian cancer. *Mol. Ther.* **10**, 1032–1042 (2004).
38. Ginhoux, F. *et al.* Fate mapping analysis reveals that adult microglia derive from primitive macrophages. *Science* **330**, 841–845 (2010).
39. DuPage, M., Dooley, A. L. & Jacks, T. Conditional mouse lung cancer models using adenoviral or lentiviral delivery of Cre recombinase. *Nat. Protoc.* **4**, 1064–1072 (2009).
40. Zeisberger, S. M. *et al.* Clodronate-liposome-mediated depletion of tumour-associated macrophages: a new and highly effective antiangiogenic therapy approach. *Br. J. Cancer* **95**, 272–281 (2006).
41. Denis, M. C., Mahmood, U., Benoist, C., Mathis, D. & Weissleder, R. Imaging inflammation of the pancreatic islets in type 1 diabetes. *Proc. Natl Acad. Sci. USA* **101**, 12634–12639 (2004).
42. McInnes, I. B. & Schett, G. The pathogenesis of rheumatoid arthritis. *N. Engl. J. Med.* **365**, 2205–2219 (2011).
43. Beste, M. T. *et al.* Molecular network analysis of endometriosis reveals a role for c-Jun-regulated macrophage activation. *Sci. Transl. Med.* **6**, 222ra16 (2014).
44. Moore, K. J. & Tabas, I. Macrophages in the pathogenesis of atherosclerosis. *Cell* **145**, 341–355 (2011).
45. Frantz, S. & Nahrendorf, M. Cardiac macrophages and their role in ischaemic heart disease. *Cardiovasc. Res.* **102**, 240–248 (2014).
46. Weissleder, R., Nahrendorf, M. & Pittet, M. J. Imaging macrophages with nanoparticles. *Nature Mater.* **13**, 125–138 (2014).
47. Aouadi, M. *et al.* Orally delivered siRNA targeting macrophage Map4k4 suppresses systemic inflammation. *Nature* **458**, 1180–1184 (2009).
48. De Palma, M. & Lewis, C. E. Macrophage regulation of tumor responses to anticancer therapies. *Cancer Cell* **23**, 277–286 (2013).
49. Cortez-Retamozo, V. *et al.* Origins of tumor-associated macrophages and neutrophils. *Proc. Natl Acad. Sci. USA* **109**, 2491–2496 (2012).
50. Steidl, C. *et al.* Tumor-associated macrophages and survival in classic Hodgkin's lymphoma. *N. Engl. J. Med.* **362**, 875–885 (2010).
51. Zhang, Q. W. *et al.* Prognostic significance of tumor-associated macrophages in solid tumor: a meta-analysis of the literature. *PLoS ONE* **7**, e50946 (2012).

52. Nakasone, E. S. *et al.* Imaging tumor-stroma interactions during chemotherapy reveals contributions of the microenvironment to resistance. *Cancer Cell* **21,** 488–503 (2012).
53. Zhang, W. *et al.* Depletion of tumor-associated macrophages enhances the effect of sorafenib in metastatic liver cancer models by antimetastatic and antiangiogenic effects. *Clin. Cancer Res.* **16,** 3420–3430 (2010).
54. Pyonteck, S. M. *et al.* CSF-1R inhibition alters macrophage polarization and blocks glioma progression. *Nature Med.* **19,** 1264–1272 (2013).
55. Zhu, Y. *et al.* CSF1/CSF1R blockade reprograms tumor-infiltrating macrophages and improves response to T-cell checkpoint immunotherapy in pancreatic cancer models. *Cancer Res.* **74,** 5057–5069 (2014).
56. Ries, C. H. *et al.* Targeting tumor-associated macrophages with anti-CSF-1R antibody reveals a strategy for cancer therapy. *Cancer Cell* **25,** 846–859 (2014).
57. Mayer, L. D., Dougherty, G., Harasym, T. O. & Bally, M. B. The role of tumor-associated macrophages in the delivery of liposomal doxorubicin to solid murine fibrosarcoma tumors. *J. Pharmacol. Exp. Ther.* **280,** 1406–1414 (1997).
58. Hirota, K. *et al.* Optimum conditions for efficient phagocytosis of rifampicin-loaded PLGA microspheres by alveolar macrophages. *J. Control. Release* **119,** 69–76 (2007).
59. Liu, H. *et al.* Structure-based programming of lymph-node targeting in molecular vaccines. *Nature* **507,** 519–522 (2014).
60. Kirpotin, D. B. *et al.* Antibody targeting of long-circulating lipidic nanoparticles does not increase tumor localization but does increase internalization in animal models. *Cancer Res.* **66,** 6732–6740 (2006).
61. Venkatraman, S. S., Ma, L. L., Natarajan, J. V. & Chattopadhyay, S. Polymer- and liposome-based nanoparticles in targeted drug delivery. *Front. Biosci. (Schol. Ed)* **2,** 801–814 (2010).
62. She, W. *et al.* The potential of self-assembled, pH-responsive nanoparticles of mPEGylated peptide dendron-doxorubicin conjugates for cancer therapy. *Biomaterials* **34,** 1613–1623 (2013).
63. Harisinghani, M., Ross, R. W., Guimaraes, A. R. & Weissleder, R. Utility of a new bolus-injectable nanoparticle for clinical cancer staging. *Neoplasia* **9,** 1160–1165 (2007).
64. Ansari, C. *et al.* Development of novel tumor-targeted theranostic nanoparticles activated by membrane-type matrix metalloproteinases for combined cancer magnetic resonance imaging and therapy. *Small* **10,** 417 (2014).
65. Kaittanis, C. *et al.* Environment-responsive nanophores for therapy and treatment monitoring via molecular MRI quenching. *Nat. Commun.* **5,** 3384 (2014).
66. Beatty, G. L. *et al.* CD40 agonists alter tumor stroma and show efficacy against pancreatic carcinoma in mice and humans. *Science* **331,** 1612–1616 (2011).
67. Germano, G. *et al.* Role of macrophage targeting in the antitumor activity of trabectedin. *Cancer Cell* **23,** 249–262 (2013).
68. Muzumdar, M. D., Tasic, B., Miyamichi, K., Li, L. & Luo, L. A global double-fluorescent Cre reporter mouse. *Genesis* **45,** 593–605 (2007).
69. Alieva, M., Ritsma, L., Giedt, R. J., Weissleder, R. & van Rheenen, J. Imaging windows for long-term intravital imaging. *IntraVital* **3,** e29917 (2014).
70. Turetsky, A., Kim, E., Kohler, R. H., Miller, M. A. & Weissleder, R. Single cell imaging of Bruton's tyrosine kinase using an irreversible inhibitor. *Sci. Rep.* **4,** 4782 (2014).

Acknowledgements

This work was supported in part by the US National Institutes of Health (NIH) grants RO1-CA164448, P50-CA086355, PO1-CA139980, U54-CA151884 (to R.W.) and RO1-CA034992 from the National Cancer Institute (to SJL), along with the David Koch-PCF Program in Nanotherapeutics (to O.C.F.). C.P. is supported by the Deutsche Forschungsgemeinschaft (DFG) PF809/1-1. We thank Dr Kevin King, Dr Julia Kalow, Dr Basit Yameen, Alex Zaltsman, Matthew Sebas, Greg Wojtkiewicz, David Pirovich and Olivier Kister for technical assistance, and Dr Melissa Sprachman for helpful discussions.

Author contributions

M.A.M., Y.-R.Z., S.G., C.P., H.Z., C.E., M.P., S.J.L., O.C.F. and R.W. developed the concepts and designed the experiments; M.A.M., S.G. and H.Z. synthesized and characterized TNPs; Y.-R.Z. and B.A. synthesized and characterized C_{16}-Pt(IV)-BODIPY; M.A.M., C.P. and C.E. performed and analysed the FACS experiments; M.A.M. and R.H.K. performed imaging experiments; M.A.M. and K.S.Y. generated the cell lines; M.A.M. developed and performed the image processing; M.A.M. and Y.I. performed and analysed the histology; M.A.M. and Y.-R.Z. performed and analysed the AAS experiments; M.A.M. performed all tissue culture experiments; M.A.M. and R.W. wrote the paper; all authors analysed results, wrote the methods section and edited the manuscript.

Additional information

Supplementary Information accompanies this paper at http://www.nature.com/naturecommunications

Competing financial interests: O.C.F. has a financial interest in BIND Therapeutics, Blend Therapeutics and Selecta Biosciences, biotechnology companies developing nanoparticle technologies for medical applications. S.J.L. discloses a financial interest in Blend Therapeutics. The remaining authors declare no competing financial interests.

Reprints and permission information is available online at http://npg.nature.com/reprintsandpermissions/

How to cite this article: Miller, M. A. *et al.* Tumour-associated macrophages act as a slow-release reservoir of nano-therapeutic Pt(IV) pro-drug. *Nat. Commun.* 6:8692 doi: 10.1038/ncomms9692 (2015).

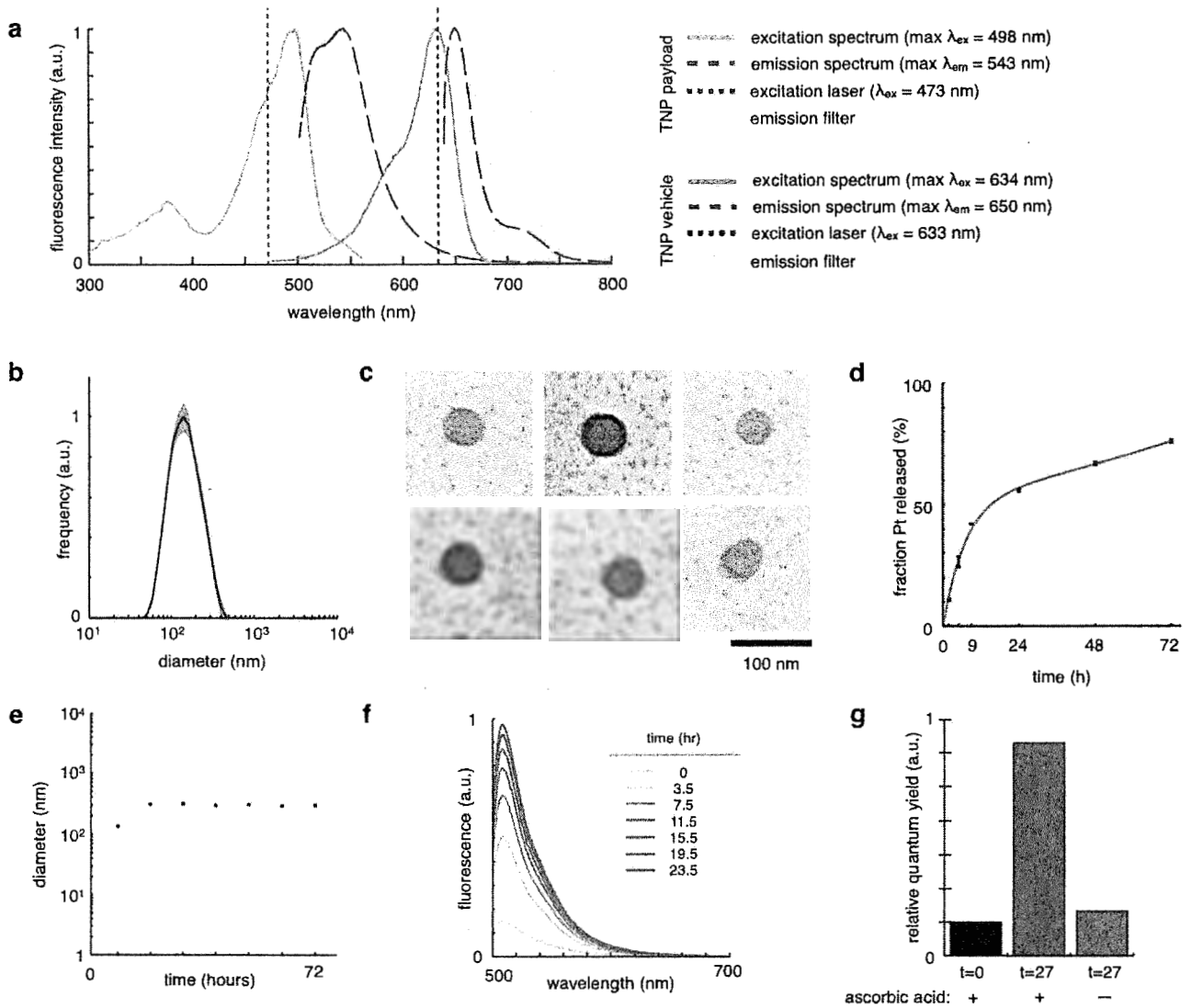

Supplementary Figure 1: TNP physicochemical characterization. (a) Excitation and emission spectra of the TNP vehicle and payload. (b) Dynamic light scattering (DLS) measurements of TNP diameter (line and shaded area denote mean ± S.E.M.; n=12). (c) Transmission electron microscopy (TEM) of TNP. (d) Kinetics of Pt-payload release from TNP into PBS at 37°C, measured by AAS (data are means ± S.E.M.; n=2). (e) Average TNP diameter as a function of incubation time in PBS at 37°C, measured by DLS (data are means ± S.E.M.; n=2). (f) Fluorescence turn-on upon Pt-reduction by incubation with 300 μM ascorbic acid in PBS. (g) Quantification of data in ***f***, showing 6.3-fold fluorescence turn-on after 24 hr ascorbic acid incubation.

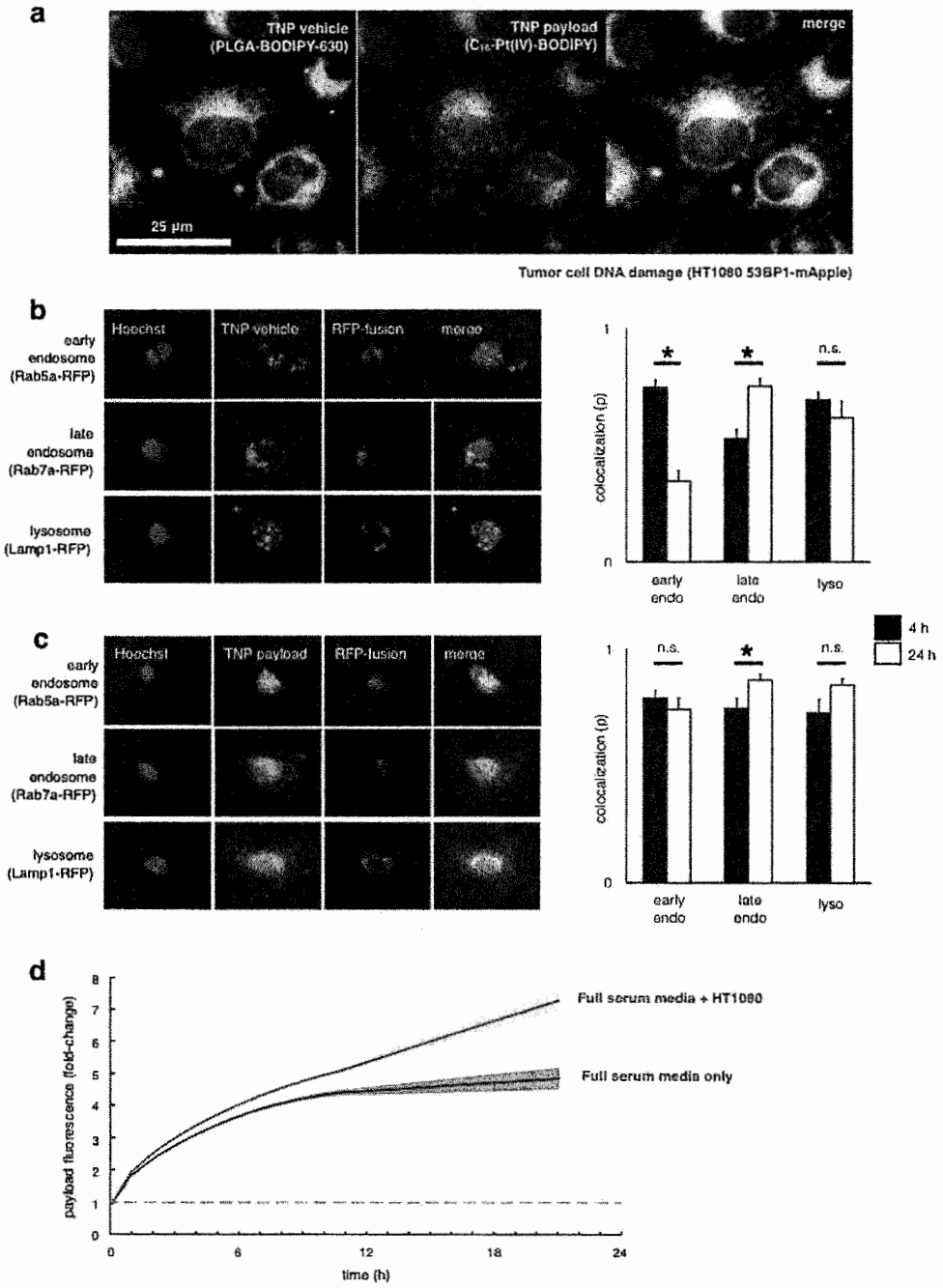

Supplementary Figure 2: Characterization of cellular TNP uptake. (a) Intracellular uptake of TNP after 24 hr incubation at 1 μM in live cells. (b-c) Co-localization analysis of TNP vehicle (b) and payload (c) with fluorescent proteins localized to endosomal and lysosomal compartments. Correlation was quantified over n=3 replicate plates, *p<0.05, two-sided t-test (means ± S.E.M.). (d) Payload fluorescence increases over time as it reduces from Pt(IV) to Pt(II). Lines and shaded area denote means ± S.E.M. (n=12).

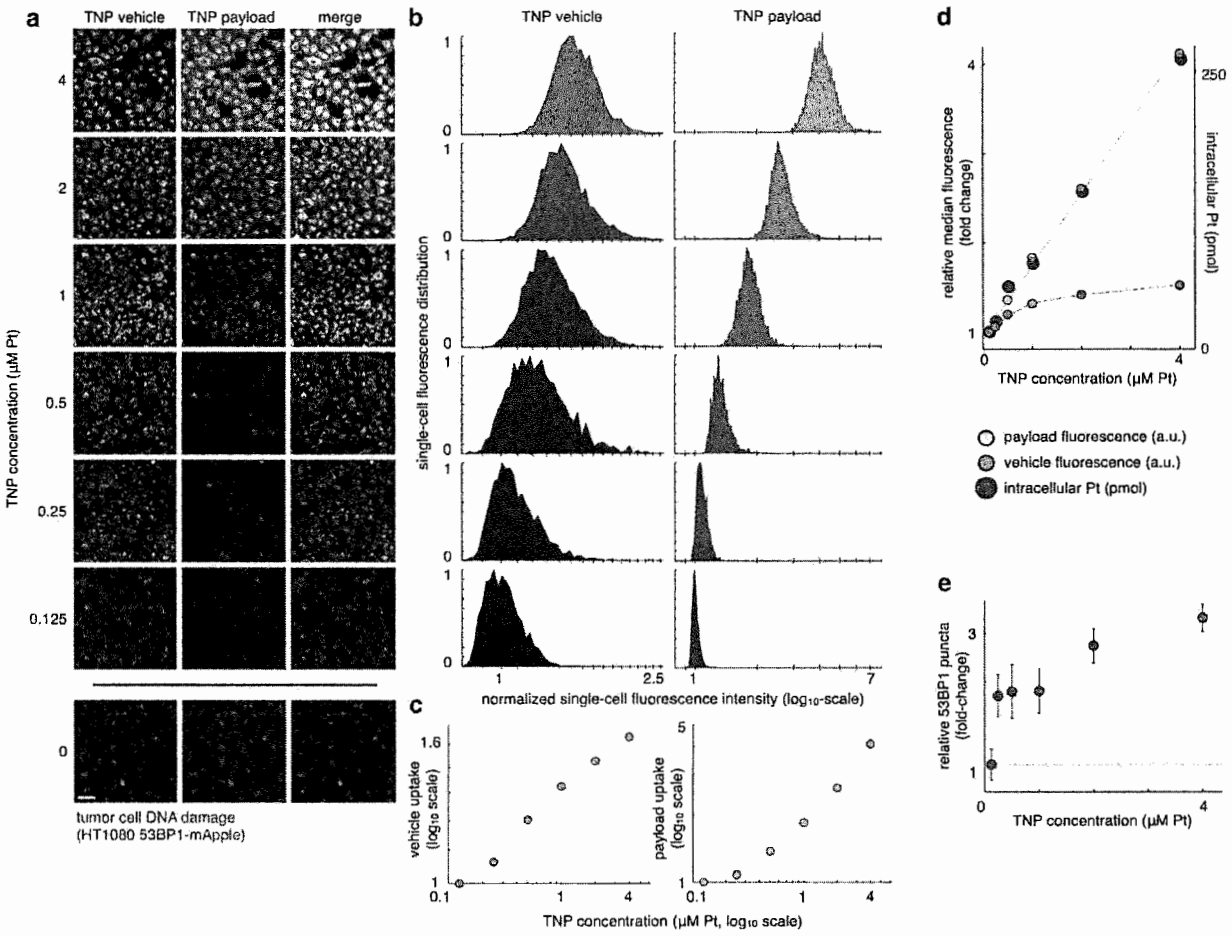

Supplementary Figure 3: TNP imaging calibration curves. (a) Images of TNP uptake were taken 24 hr following incubation. Scale bar = 50μm. (b) Single-cell TNP uptake was quantified after background-subtraction and normalization to the lowest concentration median (n > 16 replicate images). Plots correspond by row to sample images in ***a***. (c) Log-log plot of TNP fluorescence as a function of dose, corresponding to ***b***. Note the difference in slopes between vehicle and payload. (d) Linear plot of TNP fluorescence (left axis) as a function of dose (bottom axis) and intracellular Pt content, measured by AAS (right axis; n=3). The linear relationship between payload fluorescence and intracellular Pt content (R^2>0.99) supports their interconversion. (e) Relative DNA damage, measured by the fraction of cells exhibiting high (>5) 53BP1 puncta, and normalized to the untreated control, corresponding to dataset in ***a*** (means ± S.E.M.; n=3).

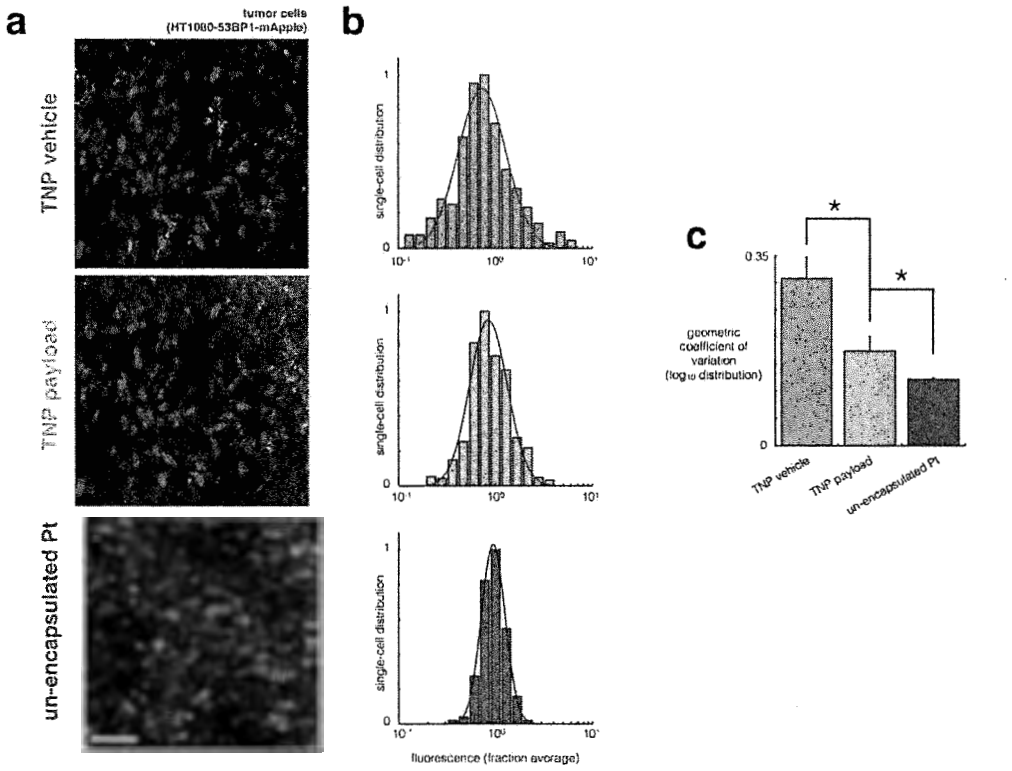

Supplementary Figure 4: TNP exhibits spatially heterogeneous accumulation within bulk tumor tissue. (a) Example images showing intratumoral distribution of TNP and unencapsulated BODIPY-labeled Pt(II), measured approximately 20 plasma half-lives post-injection. Scale bar = 50μm. (b) Distribution of fluorescence concentrations measured across single cells, mean-centered and log-transformed (n>200 cells / group across n=6 animals), corresponding to ***a***. Note the wider distribution for TNP vehicle. By comparison, the unencapsulated Pt(II) compound (CP-11) [1] exhibits more homogeneous accumulation. (c) Quantification of variance in ***b*** (*$p<0.05$, two-sided t-test; data are means ± S.E.M.; $n\geq2$).

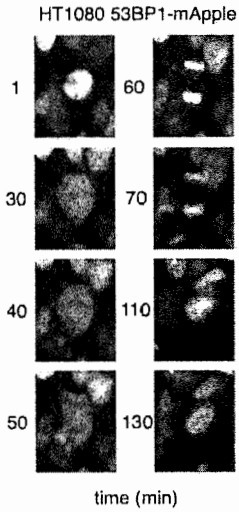

Supplementary Figure 5: Intravital imaging supports the real-time tracking of cell division events. In HT1080 xenografts, time-lapse confocal fluorescence microscopy allowed for the tracking of individual tumor cells over the course of 3 hr following injection of either TNP or the vehicle control. Cell division could then be identified in real time, shown here by example time-lapse images of an actively dividing cell monitored in the absence of TNP treatment.

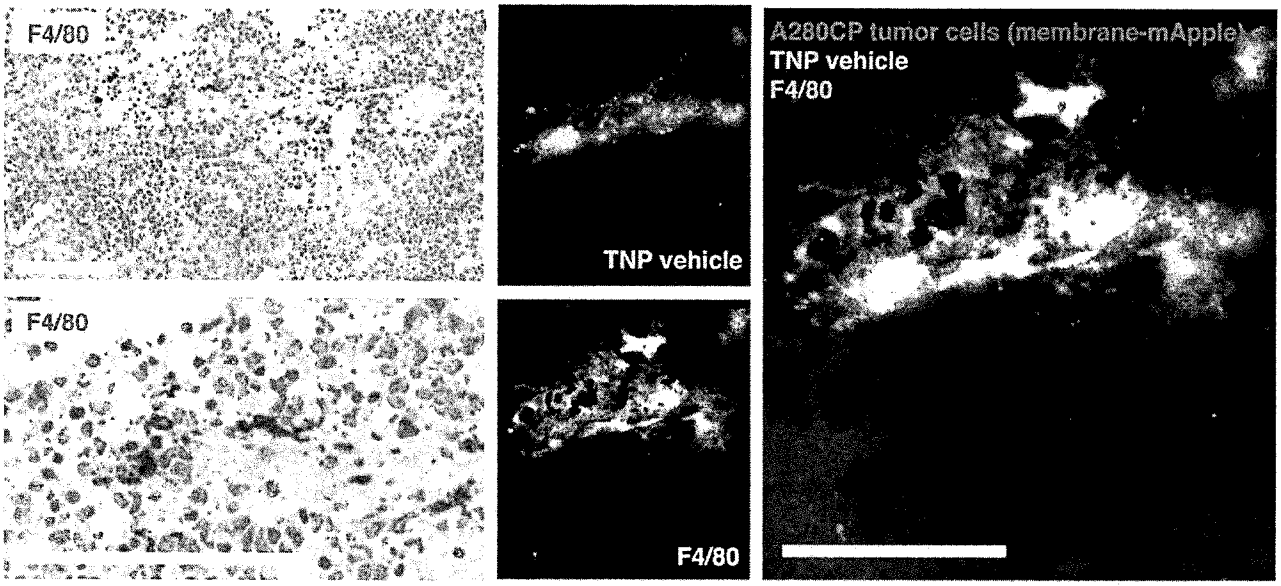

Supplementary Figure 6: TNP vehicle uptake in OVCA-associated F4/80+ host phagocytes. *Left:* 10x (top) and 40x (bottom) magnification images of immunohistochemistry, showing A2780CP tumors stained with hematoxylin and F4/80 (brown). Scale bar = 100μm. Immunohistochemistry corresponds with immunofluorescence (*middle/right)* of host phagocytes (stained for F4/80), tumor cells, and local accumulation of fluorescent TNP vehicle. Scale bar = 25 μm. OVCA cells (A2780CP) expressed membrane-tagged fluorescent protein (mApple). This representative histology provides further evidence that TNP vehicle is taken up by host phagocytes. F4/80 is one of several immunological markers used to identify TAMs as done here with flow cytometry (Fig. 5), which also shows significant TAM uptake of TNP vehicle.

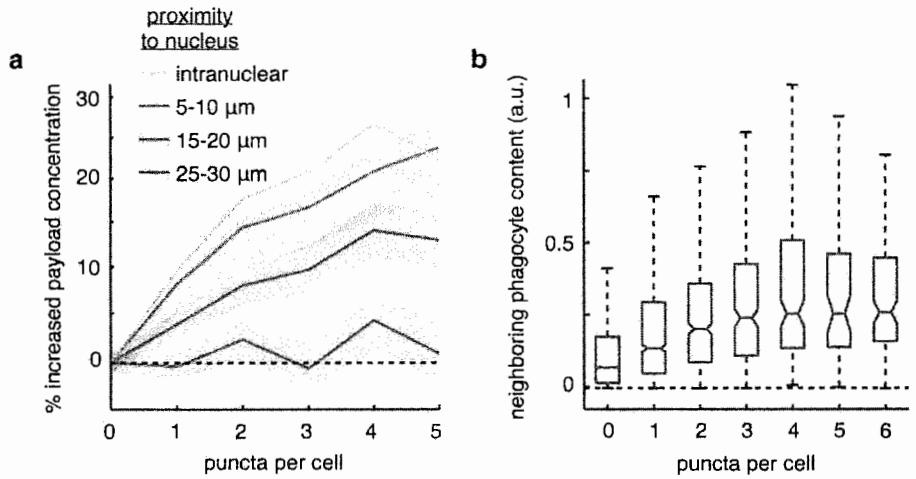

Supplementary Figure 7: Automated intravital imaging analysis shows that local phagocyte populations correlate with local TNP accumulation and tumor-cell DNA damage. (a) In HT1080 tumors, correlation between DNA damage and payload concentration significantly diminishes beyond 25 µm from cell nuclei (n>6000 cells; n=5 animals). Intravital images 3 hr after TNP injection were analyzed for single-cell DNA damage response (using 53BP1 puncta); automated image segmentation then computed correlation between DNA damage and corresponding local levels of payload fluorescence. Lines and shading denote means ± S.E.M. (b) Levels of single-cell DNA damage response correlate with the local accumulation of phagocytes that accumulate significant TNP-vehicle within 15 µm of each tumor cell nucleus (n>6000 cells; n=5 animals). Plots show boxes (25^{th} and 75^{th} quartiles), whiskers (10^{th} and 90^{th} percentiles), and medians (center line).

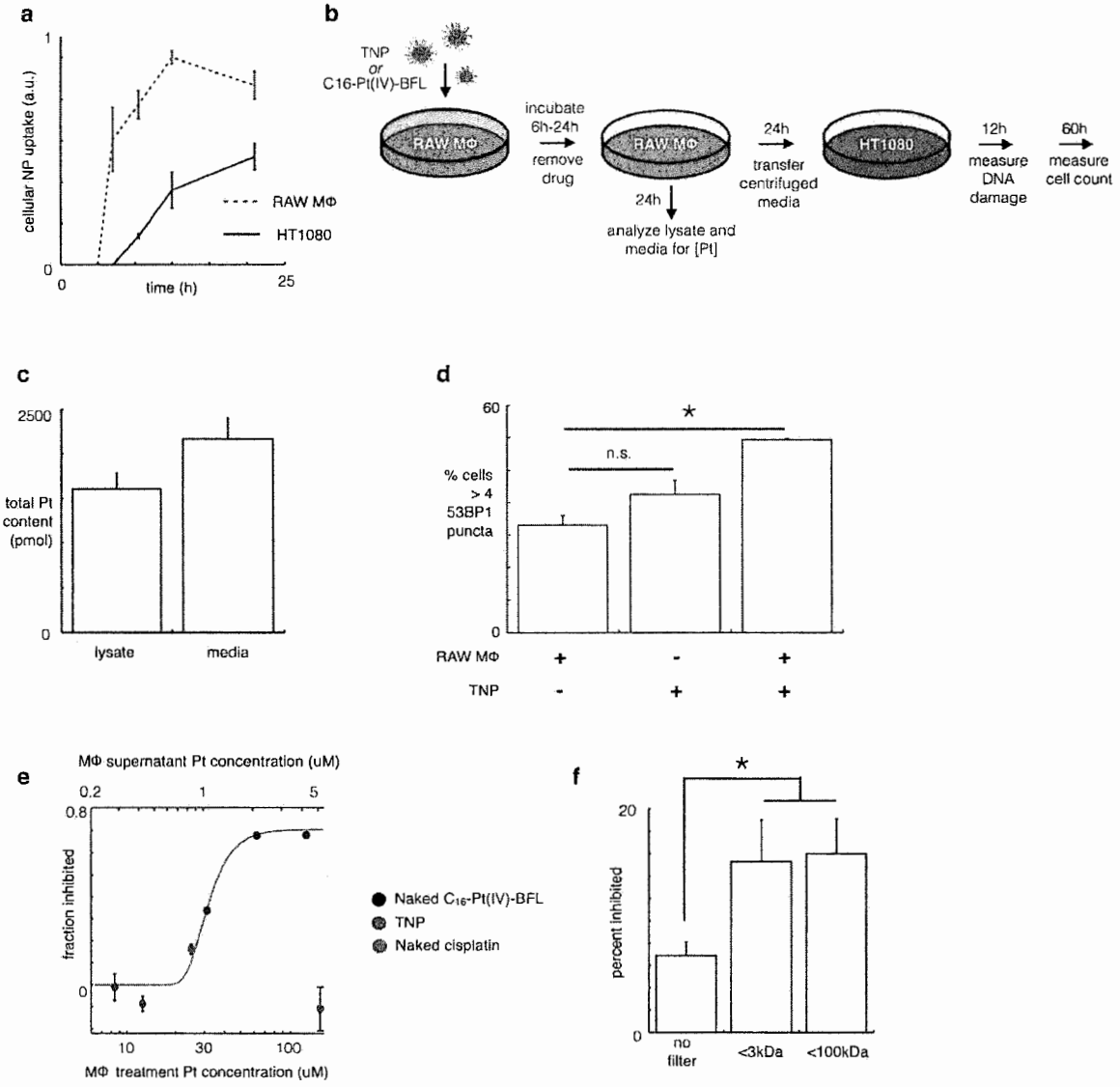

Supplementary Figure 8: TNP uptake in macrophages leads to increased Pt payload concentration in cell supernatant, which exhibits cytotoxic and DNA damaging capability. (a) Macrophages take up TNPs more rapidly and to a higher degree than tumor cells, as quantified by fluorescence and normalized to cell count (means ± S.E.M.; n=4). (b) Schematic of conditioned-medium experiments involving treatment of macrophages with TNPs, followed by analysis or transfer of conditioned medium to tumor cells. (c) Macrophages treated with TNP for 24 hr and then incubated in fresh medium for 24 hr ultimately release a substantial amount of Pt into the supernatant, as measured by AAS (means ± S.E.M.; n=3). (d-e) Transfer of Pt-containing conditioned medium from macrophages to tumor cells elicits an increase in DNA damage response after 24 hr (d) and reduces the number of live tumor cells after 72 hr (e) (means ± S.E.M.; n=3). (f) Size-exclusion filtration with either a 3 kDa or 100 kDa molecular weight cut-off filter does not reduce the cytotoxic impact of conditioned Pt-containing macrophage medium upon transfer to tumor cells, but rather increases it (p=0.005, two-tailed t-test, n = 5).

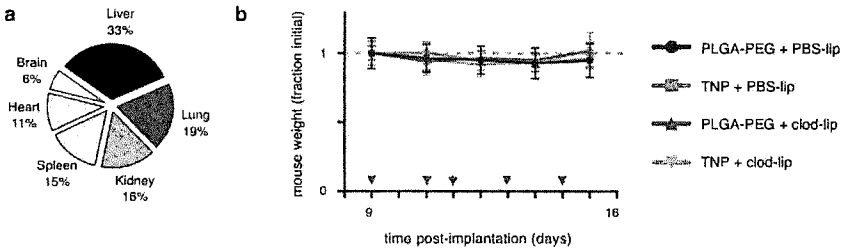

c

Cisplatin

Pt dose (mg/kg)	Blood Urea Nitrogen BUN (mg/dL)	Globulin GLOB (g/dL)	Aspartate Amino Transferase AST (U/L)	Cholesterol CH (mg/dL)	Creatinine CRT (mg/dL)
0	18	2	88.3	154.7	<0.2
1	21	2	83	138.3	<0.2
3	32	1.7	105	149	n.a.
5	20	1.8	51	133.7	<0.2

TNP

Pt dose (mg/kg)	Blood Urea Nitrogen BUN (mg/dL)	Globulin GLOB (g/dL)	Aspartate Amino Transferase AST (U/L)	Cholesterol CH (mg/dL)	Creatinine CRT (mg/dL)
0	18	2	88.3	154.7	<0.2
1	20.3	2.1	100	140.3	<0.2
3	21.5	2	140	136.7	<0.2
5	17.3	1.8	147	127.3	<0.2

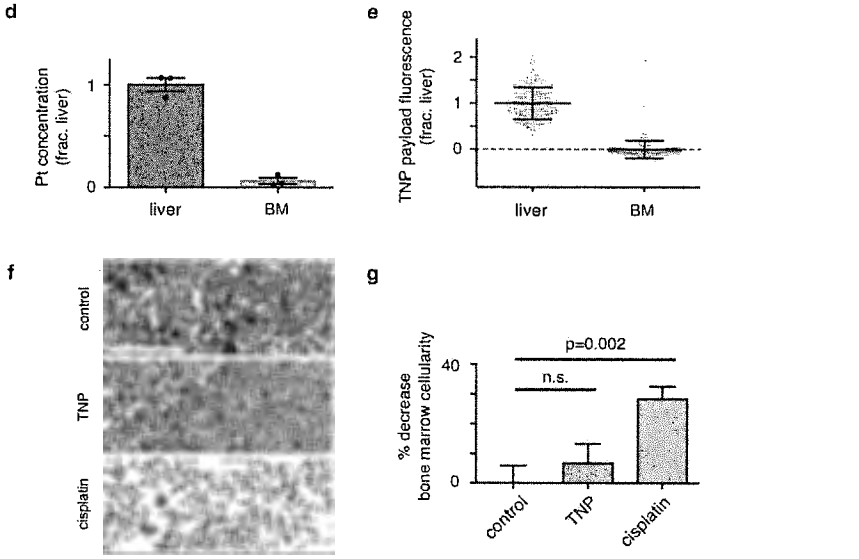

Supplementary Figure 9: TNP safely accumulates in the liver. (a) Pt accumulates most in the liver, 24 hr following i.v. TNP administration in male rats, measured by AAS (modified from Dhar et al.[2]). (b) TNP administration does not significantly impact mouse body weight, corresponding to treatment conditions in Fig. 8a (1 mg kg^{-1} Pt dose). Animals were treated with TNP (green arrow) and clodronate liposomes (red arrows) to systemically deplete macrophages (means ± S.E.M.; n≥9). (c) Therapeutic TNP doses do not significantly impact clinical chemistry measurements in Swiss albino mice (n=3). (d-e) TNP payload accumulation in the bone marrow (BM) is much less than with liver, measured by AAS (d) and C_{16}-Pt^{IV}-BODIPY fluorescence (e) (means ± S.E.M.; n=3). (f-g) Clinically equivalent i.v. dose of non-encapsulated cisplatin (7 mg kg^{-1}; [3]) causes significant loss of nucleated BM cell density, but while TNP does not. >10 fields of view (f) were quantified across n≥2 animals per group using automated CellProfiler analysis, quantified in *g* (*two-tailed t-test). TUNEL staining (brown) was also performed, but no statistically significant differences were observed across the 3 groups (n≥2). Scale bar = 100 μm.

	Un-encapsulated Pt	Nano-encapsulated Pt
HT1080 IC_{50} (μM)	1.7 ± 0.1	1.7 ± 0.02 (TNP) 3.7 ± 0.1 (un-encapsulated payload)
OVCA429 IC_{50} (μM)	15 ± 1	1.3 ± 0.1
SKOV3 IC_{50} (μM)	3 ± 0.3	1.5 ± 0.3
MDAMB231 IC_{50} (μM)	21.5 ± 1	5.2 ± 0.2
PACA02 IC_{50} (μM)	5.3 ± 0.3	1.2 ± 0.01
PANC1 IC_{50} (μM)	5.2 ± 0.5	8.7 ± 1.9
PANC02 IC_{50} (μM)	9.1 ± 0.8	8.1 ± 1
Circulation half-life (min)	10 ± 5 (depending on Pt derivative) [Miller et al., 2014][1]	55 ± 5 (payload) 61 ± 6 (vehicle)
Tissue heterogeneity (CV of cellular uptake)	12%	17% (payload) 31% (vehicle)
Relative tumor uptake	63% [Xu et al., 2013][4]	100% [Xu et al., 2013][4]
Size (nm)	n/a	135 ± 0.9
PDI	n/a	0.18 ± 0.01
Zeta potential (mV)	n/a	-23 ± 1.4
Loading efficiency	n/a	9.1%
Encapsulation efficiency	n/a	73%
Ex/Em wavelengths (nm)	n/a	498/543 (payload) 634/650 (vehicle)

Supplementary Table 1: Characterization of Pt compounds. IC_{50} measured by cell count 72 hr after drug treatment. IC_{50} of unencapsulated Pt (left column) corresponds to cisplatin. Initial circulation half-life and tissue heterogeneity were measured by time-lapse fluorescence imaging in live animals. Reported tumor uptake measured by Pt content within bulk tumor using AAS. Size, poly-dispersity index (PDI), and zeta potential all measured by dynamic light scattering (DLS). For all values, n≥2 ± standard error.

Supplementary References:

1. Miller, M. A., Askevold, B., Yang, K. S., Kohler, R. H. & Weissleder, R. Platinum compounds for high-resolution in vivo cancer imaging. *ChemMedChem* **9**, 1131-1135 (2014).
2. Dhar, S., Kolishetti, N., Lippard, S. J. & Farokhzad, O. C. Targeted delivery of a cisplatin prodrug for safer and more effective prostate cancer therapy in vivo. *Proc Natl Acad Sci U S A* **108**, 1850-1855 (2011).
3. Nakagawa, T. et al. Expression of copper-transporting P-type adenosine triphosphatase (ATP7B) correlates with cisplatin resistance in human non-small cell lung cancer xenografts. *Oncol Rep* **20**, 265-270 (2008).
4. Xu, X. et al. Enhancing tumor cell response to chemotherapy through nanoparticle-mediated codelivery of siRNA and cisplatin prodrug. *Proc Natl Acad Sci U S A* **110**, 18638-18643 (2013).

Pharmaceutical Research (2018) 35: 31
https://doi.org/10.1007/s11095-017-2278-0

RESEARCH PAPER

Liposomal Irinotecan Accumulates in Metastatic Lesions, Crosses the Blood-Tumor Barrier (BTB), and Prolongs Survival in an Experimental Model of Brain Metastases of Triple Negative Breast Cancer

Afroz S. Mohammad[1] · Jessica I. Griffith[1] · Chris E. Adkins[1] · Neal Shah[1] · Emily Sechrest[1] · Emma L. Dolan[1] · Tori B. Terrell-Hall[1] · Bart S. Hendriks[2] · Helen Lee[2] · Paul R. Lockman[1]

Received: 18 August 2017 / Accepted: 6 October 2017 / Published online: 9 January 2018

ABSTRACT

Purpose The blood-tumor barrier (BTB) limits irinotecan distribution in tumors of the central nervous system. However, given that the BTB has increased passive permeability we hypothesize that liposomal irinotecan would improve local exposure of irinotecan and its active metabolite SN-38 in brain metastases relative to conventional irinotecan due to enhanced-permeation and retention (EPR) effect.

Methods Female nude mice were intracardially or intracranially implanted with human brain seeking breast cancer cells (brain metastases of breast cancer model). Mice were administered vehicle, non-liposomal irinotecan (50 mg/kg), liposomal irinotecan (10 mg/kg and 50 mg/kg) intravenously starting on day 21. Drug accumulation, tumor burden, and survival were evaluated.

Results Liposomal irinotecan showed prolonged plasma drug exposure with mean residence time (MRT) of 17.7 ± 3.8 h for SN-38, whereas MRT was 3.67 ± 1.2 for non-liposomal irinotecan. Further, liposomal irinotecan accumulated in metastatic lesions and demonstrated prolonged exposure of SN-38 compared to non-liposomal irinotecan. Liposomal irinotecan achieved AUC values of 6883 ± 4149 ng-h/g for SN-38, whereas non-liposomal irinotecan showed significantly lower AUC values of 982 ± 256 ng-h/g for SN-38. Median survival for liposomal irinotecan was 50 days, increased from 37 days ($p<0.05$) for vehicle.

Conclusions Liposomal irinotecan accumulates in brain metastases, acts as depot for sustained release of irinotecan and SN-38, which results in prolonged survival in preclinical model of breast cancer brain metastasis.

KEY WORDS chemotherapy · enhanced permeation and retention · nanoparticles · permeability · pharmacokinetics

ABBREVIATIONS

AUC	Area under the curve
BBB	Blood-brain barrier
BTB	Blood-tumor barrier
Cl	Clearance
CNS	Central nervous system
DAPI	4',6-diamidino-2-phenylindole
DiI5	Carbocyanine tracer DiIC18 (5)-DS
EPR	Enhanced permeation and retention
ER	Estrogen receptor
HER2	Human epidermal growth factor receptor 2
IRN-50	Non-liposomal Irinotecan (50 mg/kg)
MRT	Mean residence time
nal-IRI-10	Nano-liposomal Irinotecan (10 mg/kg, Irinotecan equivalent)
nal-IRI-50	Nano-liposomal (50 mg/kg, Irinotecan equivalent)
P-gp	P-glycoprotein (ABCB1)
PK	Pharmacokinetics
PR	Progesterone receptor
SRS	Stereotaxic radiosurgery
TNBC	Triple negative breast cancer
Vd	Apparent volume of distribution
WBRT	Whole brain radiotherapy

✉ Paul R. Lockman
prlockman@hsc.wvu.edu

[1] School of Pharmacy, Department of Pharmaceutical Sciences, West Virginia University Health Sciences Center, 1 Medical Center Drive, Morgantown, West Virginia 26506-9050, USA

[2] Merrimack Pharmaceuticals, Cambridge, Massachusetts 02139, USA

INTRODUCTION

More than 230,000 women are diagnosed with breast cancer every year (1). Of this general population of women with breast cancer, 6% present with distant metastases at the time of diagnosis, and 10-15% will develop brain metastases at some period during their lifetime. After diagnosis of a brain metastasis, survival is approximately 3-25 months depending on breast cancer subtype, total body burden, and treatment regimen (2,3). Brain metastases are common in human epidermal growth factor receptor 2 overexpressing (HER2+) cancers and triple negative breast cancer (4–6). While the HER2 receptor can be targeted to treat primary breast cancer, unfortunately these therapies (e.g., trastuzumab and lapatinib) have limited distribution to HER2+ brain metastases and accordingly have poor efficacy (6–8). There are no such targeted therapies for the treatment of basal-like triple negative breast cancer (TNBC). Triple negative breast cancer is characterized by the absence of the oncogenic overexpression of HER2, estrogen receptors (ER) and progesterone receptors (PR). Of significance is the fact that brain metastases are a major sequelae of TNBC, as one study found that as many as 36% of women with TNBC will develop metastatic CNS lesions over their lifetime (9).

A major impediment in effectively treating brain metastases of breast cancer is the distribution of chemotherapeutics past the blood-brain barrier (BBB). The BBB, which remains intact to a large degree in metastatic brain lesions of breast cancer (blood-tumor barrier; BTB), significantly limits the passive permeation of drugs from blood to tumor (10,11) and continues to actively extrude and limit lesion accumulation of substrates subject to drug-resistance efflux transporters. For example, paclitaxel, which is used in treating breast cancer, is unable to permeate the BTB at rates to achieve a therapeutically relevant concentration (10,12,13). Approaches to treatment of brain metastases include stereotactic radiosurgery (SRS) or whole brain radiation therapy (WBRT) in combination with systemic therapy, though these therapies are largely palliative and may result in neurocognitive degeneration (14,15).

Nanoparticles and other polymeric drug formulations have shown promise for the delivery of chemotherapeutics, primarily through extravasation across the BTB (11,16,17). This strategy has been particularly effective in fast-growing, aggressive metastases, which produce more growth factors associated with angiogenesis and have a resultant vasculature that is more permeable than BBB (18). In addition, nanoparticles have prolonged residence times within lesions due to increased circulation half-life, while small molecules leave the tumor interstitial space much faster. Consequently, the increased residence time of the nanoparticles results in significantly greater total drug exposure (area under the curve) (19). Improvements in pharmacokinetics and reduced toxicity are evident with nano-liposome encapsulated anticancer agents such as vinorelbine, docetaxel and doxorubicin (20,21).

Recently, Nobel et al. demonstrated that a liposomal nanoparticle increased concentration of irinotecan by 3.1-fold in glioblastoma xenograft tumors compared to non-liposomal irinotecan (22). The 3-fold increase in C_{max} was mirrored by similar increases observed for the active metabolite of irinotecan, SN-38, in the tumor (22). The liposomes preferentially accumulated in tumor tissues, with a 35-fold increase in irinotecan concentration from normal brain concentration, whereas non-liposomal irinotecan showed 9.5 fold increase in irinotecan concentration in tumor tissue compared to normal brain (22). Consistent with previous work showing nanoparticles increase total tumor exposure (area under the curve), the 3.1-fold increased peak concentrations were reached at 12 h in comparison to 15 min with non-liposomal irinotecan (22).

In the clinical setting, delivery of liposomes to brain lesions was previously observed with multiple methods. Detectable and variable uptake of ^{111}In labelled non-PEGylated liposomes at 72 h was observed in brain tumors across multiple patients with malignant glioma using single photon emission tomography(23). In another study, delivery of ^{99m}Tc labelled liposomal doxorubicin to glioblastomas and metastatic brain tumors of various origin was also observed using planar and SPECT scintigraphy (24). Most recently, delivery of ^{64}Cu labelled HER2-targeted liposomal doxorubicin was noted by PET/CT in breast cancer brain metastases (25). These studies highlight the potential for liposomes to enable drug delivery to brain metastases.

We hypothesize that liposomal irinotecan (nal-IRI, irinotecan liposome injection) will effectively deliver irinotecan and SN-38 resulting in efficacy and prolonged survival in a preclinical model of brain metastases of TNBC. nal-IRI, in combination with 5-fluorouracil and leucovorin, has recently been approved in the US and EU for the treatment of patients with advanced metastatic pancreatic adenocarcinoma after disease progression following gemcitabine-based therapy.

MATERIALS AND METHODS

Chemicals

Irinotecan HCl, nal-IRI were supplied by Merrimack Pharmaceuticals (Cambridge, US), which were prepared as reported by Noble et al. and Kalra et al. (22,26). Fluorescently-labeled liposomal irinotecan (DiI5-liposomal irinotecan) was also provided by Merrimack Pharmaceuticals, which was prepared following previously reported methods (27). The lipid mixture of nal-IRI consisting of distearoylphosphatidylcholine, cholesterol, and

polyethyleneglycol-distearoylphosphatidyl-ethanolamine at the molar ration of 3:2:0.015(22). Irinotecan HCl was in the liposomes at a ratio of 750 g irinotecan HCl / mol phospholipid (22). Carbocyanine tracer DiIC18 (5)-DS (D12730; Life Technologies) was incorporated into the lipid bilayer of the liposome prior to drug loading. All other chemicals were analytical grade purchased from Sigma-Aldrich (St. Louis, MO).

Animals

Female athymic nude mice (Charles River Laboratories, Kingston, NY) were used for all experiments in the study. Mice were 6-8 weeks of age and weighed 22-28 g before injecting with cancer cells and were housed under 12-hour light/dark conditions with food and water *ad libitum*, and mice were acclimated for 1 week prior to use. All animal work was approved by West Virginia University Institutional Animal care and Use Committee (IACUC protocols 13-1207). All animal experiments were performed according to the principles of the *Guide for the Care and use of Laboratory animals*.

Cell Culture

Brain-seeking human triple negative breast cancer cells, transfected to express firefly luciferase (MDA-MB-231Br-Luc), were cultured in Dulbecco's Modified Eagle's Medium (DMEM) with 10% fetal bovine serum (FBS). MDA-MB-231Br-Luc cells were kindly provided by Dr. Patricia Steeg, of the National Institute of Health Center for Cancer Research. All cell work was performed under aseptic conditions, and cells were cultured at 37°C with 5% CO_2.

Pharmacokinetic Study of Irinotecan and Liposomal Irinotecan in Brain Tumors

MDA-MB-231Br-Luc cells (5×10^5) cells were injected intracranially as described previously (28). Tumors were allowed to grow until neurological symptoms developed, and the animals were intravenously administered Non-liposomal irinotecan (50 mg/kg, IRN-50), and two different doses of liposomal irinotecan, 10 mg/kg (nal-IRI-10) and 50 mg/kg (nal-IRI-50). Non-liposomal irinotecan-treated animals (n=5/time point) were sacrificed at 0.083, 0.5, 1, 2, 6, 12 and 24 h after administration, and liposomal irinotecan treated animals (n=5/time point) were sacrificed at 0.5, 2, 6, 24, 72, 48 and 168 h after administration. The animals were anesthetized (ketamine/xylazine; 100 mg/kg and 8 mg/kg respectively) and sacrificed by decapitation to collect blood, tumor, and normal brain tissue samples. Irinotecan and SN-38 concentrations in normal brain and brain tumor samples were analyzed by liquid chromatography-tandem mass spectrometry (LC/MS) at Roswell Park Cancer Institute's Bioanalytics, Metabolomics & Pharmacokinetics (BMPK) Facility. Metabolite levels in plasma samples were measured using high performance liquid chromatography (HPLC) methods reported previously (26). The limit of quantification for irinotecan was 25 ng/ml and for its active metabolite SN-38 was 2 ng/ml. A non-compartmental analysis was used to study plasma pharmacokinetic parameters for irinotecan and its active metabolite SN-38 from liposomal formulation and compared to non-liposomal formulation The calculated parameters include area under the curve (AUC) and area under the first moment curve (AUMC) using linear trapezoid method; mean residence time (MRT), where MRT = AUMC/AUC; clearance (Cl), where Cl= Dose/AUC; volume of distribution (Vd), where Vd= MRT × Cl. The data are presented as mean ± SD.

Survival of Animals with Brain Metastases After Treatment

MDA-MB-231Br-Luc cells (1.75×10^5) cells were injected intracardially into the left ventricle and allowed to develop into CNS metastases for 21 days. The presence of metastases was confirmed by bioluminescence imaging (BLI) using the IVIS Lumina *in vivo* imaging system (PerkinElmer, Waltham, MA) after 15 min intraperitoneal administration of D-luciferin potassium salt (150 mg/kg; PerkinElmer). Animals were then randomized into treatment groups (Saline, n=10), IRN-50 (n=10), nal-IRI-10 (n=10), and nal-IRI-50 (n=10). Drugs were administered intravenously via tail vein injection. Treatments were repeated once weekly, and BLI data was gathered twice weekly to quantify tumor burden and progression in different groups, similar to our previous work (16). Once animals developed neurological symptoms, they were sacrificed under anesthesia.

Uptake and Accumulation of Liposomal Irinotecan Formulation

Animals from the liposomal irinotecan group were administered with DiI5-labelled liposomes intravenously. After 24 h, animals were sacrificed under anesthesia as described above. The brain was immediately harvested, frozen in 2-methylbutane at -50°C, and sectioned into 20 μm thick sections (Leica CM3050 S cryostat). The sections were imaged with an Olympus MVX10 microscope with a 2x objective (NA=0.5) using the Cy5 channel. The same sections were then stained with cresyl violet and compared to fluorescent images to confirm the accumulation of DiI-5 labeled liposomes within the metastatic tumors. Sections were also stained for cytokeratin and DAPI, a fluorescent stain that binds to DNA to visualize the accumulation of liposomes within the cancer cell using Nikon N-Storm super-resolution microscope system.

Data Analysis

Differences among treatment groups in the survival study were compared by log-rank test (GraphPad® Prism 6.0, San Diego, CA) and were considered statistically significant at $p<0.05$. Living Image V4.0 software (PerkinElmer, Waltham, MA) was used to quantify tumor burden in different groups.

RESULTS

Liposomal Irinotecan Increased Plasma Half-Life and Total Exposure of Both Irinotecan and its Active Metabolite SN-38

Initially, we set out to study the plasma concentration time profile of irinotecan and its active metabolite, SN-38, after the administration of IRN-50, nal-IRI-10, and nal-IRI-50. We observed the plasma half-life of irinotecan increased in liposomal formulations, nal-IRI-10 and nal-IRI-50 with half-lives of 12.7 ± 0. 5 h and 10.9 ± 0.3 h respectively, when compared to that of IRN-50 with a half-life of 3.3 ± 0.1 h. Plasma half-life of SN-38 was also increased for nal-IRI with 21 ± 2.9 h in nal-IRI-10 group and 18 ± 1.3 h in nal-IRI-50 group when compared to that of IRN-50 with a half-life of 3.17 ± 0.43 h (Table I). We also observed that the mean residence time (MRT) for liposomal formulation increased with 4.5 ± 0.4 h for nal-IRI-10 and 7.3 ± 2.6 h for nal-IRI-50, whereas IRI-50 showed MRT of 2 ± 0.5 h for plasma irinotecan. We found similar trend for its active metabolite SN-38 with MRT of 16.7 ± 8.3 h and 17.7 ± 3.8 h for nal-IRI-10 and nal-IRI-50 respectively, while MRT for IRI-50 was 3.67 ± 1.2 (Table I). Clearance (Cl) of irinotecan for IRI-50 was 85.7 ± 22.8 ml/h with apparent volume of distribution (Vd) 178.6 ± 64.7, whereas for liposomal irinotecan clearance and volume of distribution significantly decreased with values 0.6 ± 0.2 ml/h and 2.9 ± 0.5 ml respectively for nal-IRI-10 and clearance value of 0.3 ± 0.1 ml/h and volume of distribution of 2.2 ± 1.1 ml for nal-IRI-50. We have seen the similar trend for plasma SN-38 clearance and volume of distribution values, for liposomal irinotecan both clearance and volume of distribution values were significantly lower than that of IRI-150 values (Table I).

We also observed the area under the curve (AUC) significantly increased with nal-IRI, 3.20± 0.94 ng-hr/ml $\times 10^5$ for nal-IRI-10 and 45.05 ± 5.52 ng-hr/ml $\times 10^5$ for nal-IRI-50 compared with IRN-50, which had an AUC of 0.15 ± 0.02 ng-hr/ml $\times 10^5$ (Fig. 1b). With the increase in AUC for free irinotecan from nal-IRI formulations, we also observed significant increase in AUC for the active metabolite SN-38 from the liposomal formulations with 2.56 ±0.63 ng-hr/ml $\times 10^3$ for nal-IRI-10 and 9.66 ± 0.44 ng-hr/ml $\times 10^3$ for nal-IRI-50, compared to the AUC for IRN-50 at 0.55 ± 0.08 ng-hr/ml $\times 10^3$ (Fig. 1d). These results confirm the increased plasma exposure of irinotecan and its active metabolite SN-38 from nal-IRI-10 and nal-IRI-50 formulations when compared to IRN-50 (Fig. 1).

Dil-5 Labelled Liposomes Cross the BTB and Accumulate in Brain Metastases

To understand tumor localization of nal-IRI, we studied the spatial distribution of the liposomal formulation incorporated with a fluorescent dye (Dil-5). After confirmation of the presence of metastatic lesions by BLI (Fig. 2a), Dil5-labelled liposomes were administered and allowed to circulate for 24 hr, at which time brain tissue was harvested and sectioned to allow for microscopic distribution visualization (Fig. 2b). Brain sections corresponding to regions 1, 2, 3 and 4, as shown in Fig. 2b, were also imaged for visualization of Dil-5 liposomes (Fig. 2D1-D4). The same sections were stained with cresyl violet and imaged for histopathologic visualization of lesions (Fig. 2 C1-C4). Cresyl violet images (Fig. 2 C1-C4) and their corresponding fluorescent images (Fig. 2 D1-D4) show that there is localization of Dil-5 liposomes within metastatic

Table I Plasma Pharmacokinetics of Non-Liposomal Irinotecan and Liposomal Irinotecan

Treatment	$AUC_{0-\alpha}$ (ng-hr/mL) $\times 10^5$	$t_{1/2}$ (h)	MRT (h)	Cl (ml/h)	Vd (ml)
Plasma Irinotecan					
IRI-50	0.2 ± 0.02	3.3 ± 0.1	2 ± 0.5	85.7 ± 22.8	178.6 ± 64.7
nal-IRI-10	3.2± 0.9	12.7 ± 0.5	4.5 ± 0.4	0.6 ± 0.2	2.9 ± 0.5
nal-IRI-50	45 ± 5.5	10.9 ± 0.3	7.3 ± 2.6	0.3 ± 0.1	2.2 ± 1.1
Treatment	$AUC_{0-\alpha}$ (ng-hr/mL) $\times 10^3$	$t_{1/2}$ (h)	MRT (h)	Cl (ml/h)	Vd (ml)
Plasma SN-38					
IRI-50	0.6 ± 0.08	4.32 ± 3.2	3.67 ± 1.2	2472 ± 881	7845.6 ± 2023
nal-IRI-10	2.6 ±0.6	21 ± 2.9	16.7 ± 8.3	80.9 ± 13.5	1327.5 ± 678
nal-IRI-50	9.7 ± 0.4	18 ± 1.3	17.7 ± 3.8	130.2 ±11.9	1990.3 ± 329

$AUC_{0-\alpha}$ Area under the time-concentration cure, *Cl* Clearance, *MRT* Mean residence time, *$t_{1/2}$* plasma half-life of the drug, *Vd* Apparent volume of distribution

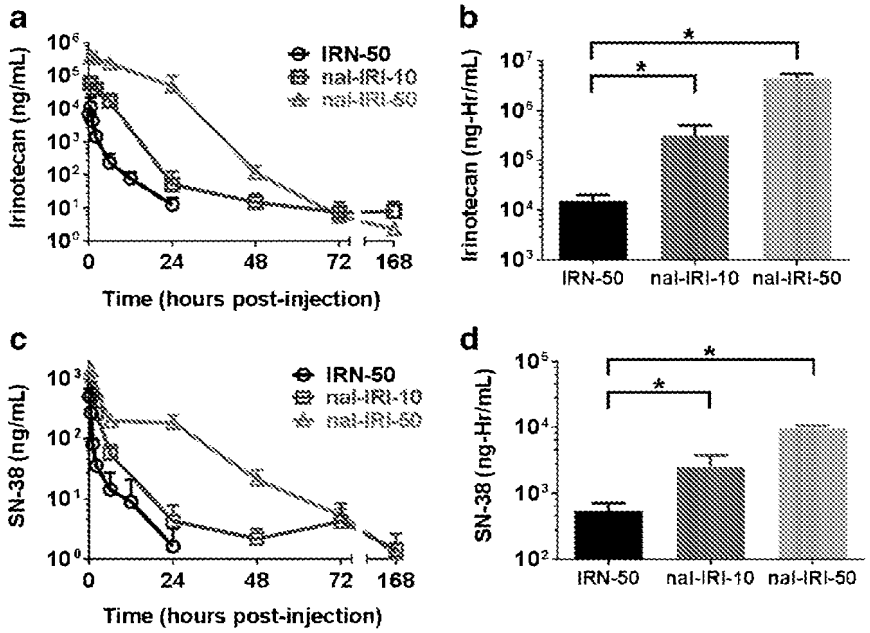

Fig. 1 (**a** and **c**) Plasma concentration-time profile of irinotecan and its active metabolite SN-38 after IV bolus administration of IRN-50, nal-IRI-10 and nal-IRI -50. Irinotecan and SN-38 essentially cleared from circulation within 24 hr from IRN-50, whereas in nal-IRI-10 and nal-IRI -50 formulations, we observed a prolonged exposure of both irinotecan and SN-38 until 168 hr. (**b** and **d**) Plasma drug exposure of irinotecan and SN-38 expressed by area under the curve (AUC) after IV bolus administration of IRN-50, nal-IRI -10 and nal-IRI -50. Both Irinotecan and SN-38 AUCs for nal-IRI -10 and nal-IRI -50 were significantly higher than that of IRN-50 ($p<0.05$). Data represents mean ± SD for n=4 animals per time point.

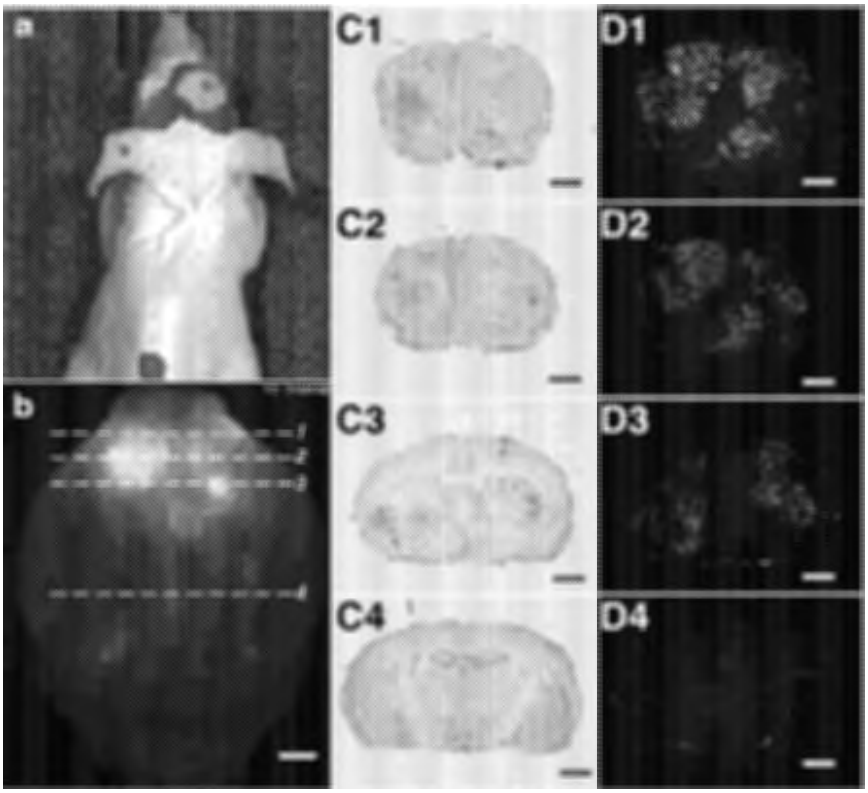

Fig. 2 DiI5-labelled liposomes accumulates in metastatic lesions in preclinical brain metastases of breast cancer model after 24 hr intravenous administration. (**a**) Image showing MDA-MB-231Br-Luc brain metastases BLI signal before administration of DiI5-labelled liposomes. (**b**) Image showing accumulation of fluorescent liposomes in brain after 24 hr circulation. The numbered dashed lines 1, 2, 3 and 4 corresponds to the numbered coronal sections (C and D panels). (**c**) Brain metastases localization and identification of coronal sections based on cresyl violet staining. (C1= Bregma 2.24 mm; C2=1.54 mm; C3= 0.5 mm; C4= -0.7 mm). (**d**) DiI5 Florescence shows the accumulation of liposomes in the corresponding brain tumors. (D1= Bregma 2.24 mm; D2=1.54 mm; D3= 0.5 mm; D4= -0.7 mm). Scale bars = 1 mm.

lesions (i.e. cresyl violet positive regions). We also confirmed normal brain tissue (i.e. brain regions devoid of any metastases) has undetectable amounts of Dil-5 labelled liposomes (Fig. 2 C4 and 2D4). The sections were then stained for cytokeratin and DAPI for high-resolution visualization within the metastatic lesions using Nikon N-Storm super-resolution microscope system (Fig. 3). We found that the Dil5 labelled liposomes not only crossed the BTB, but also localized within the cancer cells in the perinuclear regions, as shown in Fig. 3.

Liposomal Irinotecan Acts as Reservoir and Increase the Exposure of Irinotecan and SN-38 in Brain Tumors

After confirming preferential accumulation of Dil-5 labelled liposomes in brain tumors, we set out to assess the concentrations of irinotecan, and its active metabolite, SN-38, in metastatic lesions and normal brain tissue after the administration of liposomal formulations and conventional irinotecan. After the administration of IRN-50, irinotecan and SN-38 concentrations in brain tumors peaked at 0.5 to 2 h post-administration (Fig. 4a and c). Both irinotecan and SN-38 were cleared rapidly after 6 h with tumor-to-plasma ratios ranged from 3.0 to 10 for irinotecan and 0.62-5.1 for SN-38 (Fig 4a and c). After administration of nal-IRI-50, irinotecan and SN-38 concentrations continue to accumulate in brain tumors over 168 h with tumor-to-plasma ratios of 0.05-90 and 0.59-39 for irinotecan and SN-38, respectively. Tumor SN-38 concentration in mice treated with nal-IRI-50 at 168 h was found to be 50 ± 30 ng/g, whereas SN-38 concentration in non-liposomal irinotecan treated group was undetectable (<10 ng/g) at 12 h post-administration (Fig. 4c). The AUC of both irinotecan and SN-38 from nal-IRI-50 in brain tumors was found to be significantly higher than that of IRN-50 (Fig. 4b and d). These results suggest that nal-IRI prolonged drug exposure in brain tumors compared to conventional irinotecan.

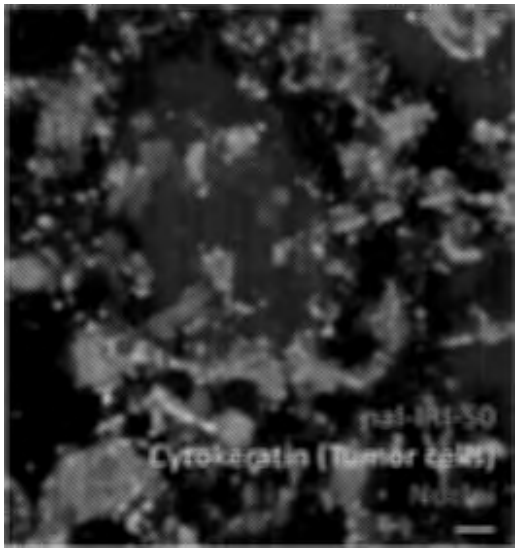

Fig. 3 Dil5-labelled liposomes accumulate in metastatic lesions in preclinical brain metastases of breast cancer model 24 hr after intravenous administration. Mouse brain tissue sections were stained for DAPI (blue) and cytokeratin (green) after 24 hr circulation of Dil5-labelled liposomes. DAPI highlights the nucleus and cytokeratin highlights MDA-MB-231Br-Luc brain metastases. We observed Dil5-labelled liposomes (red) accumulated in the MDA-MB-231Br-Luc cancer cell (green) around the nucleus (blue). Images were acquired from Nikon N-Storm super-resolution microscope system. Scale bar = 1 μm.

Liposomal Irinotecan Reduces Tumor Burden and Prolongs Survival in Animals with Brain Metastases of Breast Cancer

Lastly, we set out to determine if the increased accumulation of Dil5-liposomal irinotecan and prolonged drug exposure would result in increased median survival in our experimental model. To evaluate this, mice injected with TNBC cells intracardially for metastases development; after 21 days, mice were randomized to receive different therapeutic treatment regimens (Saline, IRN-50, nal-IRI-10 and nal-IRI-50). We observed that progression of tumor burden in liposomal irinotecan-treated groups (nal-IRI-10 and nal-IRI-50) was significantly lowered when compared to vehicle and IRN-50 groups (Fig. 5a and b). We also noted that liposomal irinotecan formulations significantly improved survival when compared to both the vehicle group and conventional irinotecan group (Fig. 6). The median survival for liposomal irinotecan groups were 48 and 50 days for nal-IRI-10 and nal-IRI-50 respectively, while for vehicle and non-liposomal irinotecan (50 mg/kg) group's median survival were 37 and 35 days, respectively (Fig.6).

DISCUSSION

The results of this study show that nal-IRI penetrates the BTB and accumulates within metastases in a preclinical model of MDA-MB-231Br-Luc brain metastases. Upon accumulation in metastatic tumors, the liposomes appear to act as reservoir for the release of irinotecan. The local release of irinotecan improved free drug exposure to tumor and presumably delayed the progression of tumor burden, which ultimately corresponded to significant prolonged survival.

In general, nanoparticles with sizes ranging from 80 to 200 nm are expected to have optimal tumor distribution and accumulation due to enhanced permeation and retention (EPR) through the leaky vasculature of tumors (18,29,30). It has been posited, based upon liver and renal clearance of nanoparticles, that ideal size of liposomes for maximum distribution and to maintain prolonged plasma residence times is approximately 100 nm (31). The liposomal irinotecan formulation described in this study were between 100-110 nm (22). Once liposomes accumulate in tumors due to EPR effect, the

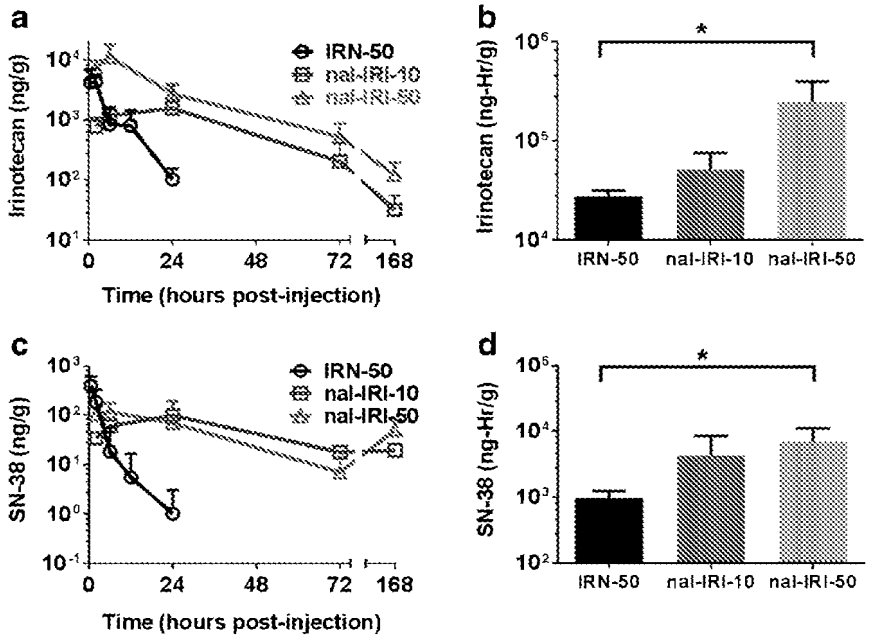

Fig. 4 (**a** and **c**) Brain tumor concentration-time profiles of irinotecan and active metabolite SN-38 after IV bolus administration of IRN-50, nal-IRI -10 and nal-IRI -50. Irinotecan and SN-38 nearly cleared from circulation within 24 hr from IRN-50, whereas in nal-IRI -10 and nal-IRI -50 formulations, we observed a prolonged exposure of both irinotecan and SN-38 until 168 hr. (**b** and **d**) Brain tumor exposure of irinotecan and SN-38 expressed by area under the curve (AUC) after IV bolus administration of IRN-50, nal-IRI -10 and nal-IRI -50. Both Irinotecan and SN-38 AUCs for nal-IRI -50 were significantly higher than that of IRN-50 ($p<0.05$). Data represents mean ± SD for n=4 animals per time point.

clearance from the tumor is limited because of its size and impaired lymphatic system, which results in prolonged drug exposure (32,33). On the other hand, non-liposomal irinotecan is rapidly cleared from the tumor due to its smaller size, leading to sub-therapeutic drug levels in tumor between the cycles of treatment. The accumulation of Dil-5 labelled liposomes in brain metastases, and the increased concentrations of drug payload over a period of time align with previous observations of passive targeting in tumors with nanoparticles like liposomes (34,35). These observations support that liposomal irinotecan

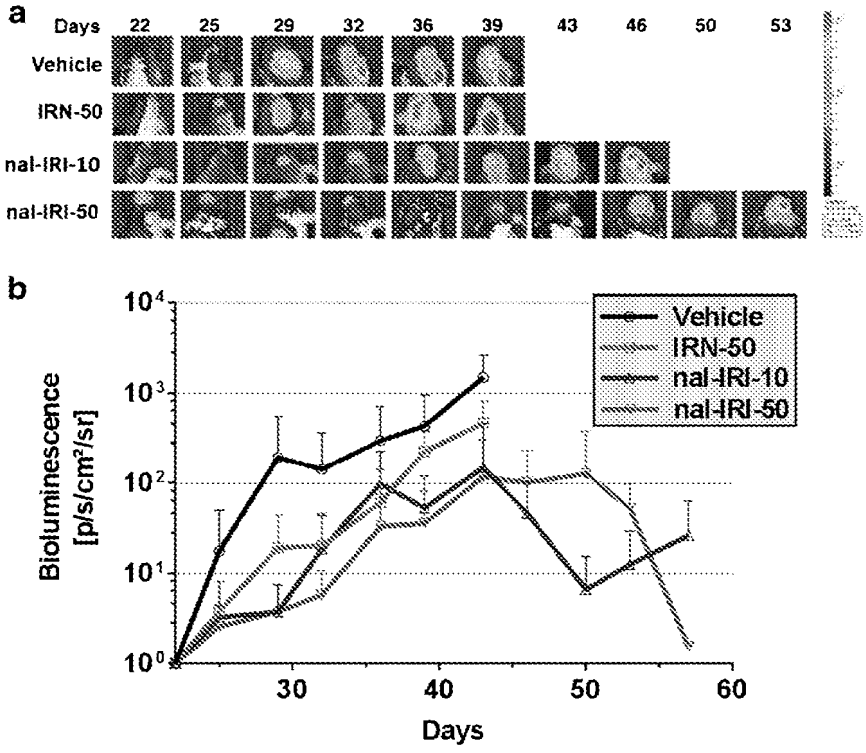

Fig. 5 (**a**) *In vivo* optical imagining (IVIS Lumina) was used to confirm and monitor the metastatic tumor growth after intracardiac injection. Increase in BLI signal in brain reflects the pattern of metastatic tumor growth in different treatment groups. Images acquired are of same animal sequentially over time. (**b**) Mean BLI signal *versus* time in mice exhibiting brain metastases. Treatment was initiated on day 21. Each data point represents mean ± SD. Tumor burden in groups treated with liposomal irinotecan were significantly lower ($P<0.05$).

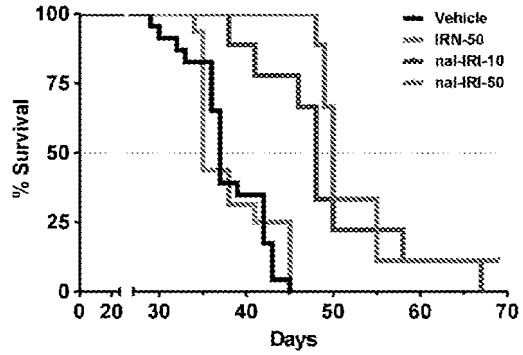

Fig. 6 Kaplan-Meier Survival Plot of mice bearing metastatic brain tumors from human triple negative breast cancer. The mice were treated weekly via IV bolus with vehicle (n=23), IRN-50 (n = 16), nal-IRI -10 (n=8) and nal-IRI -50 (n=9) starting 21 days after intracardiac injection of MDA-MB-231Br-Luc cancer cells. The median survival time was 37 days for vehicle, 35 days for IRN-50, 48 and 50 days for nal-IRI -10 and nal-IRI -50 respectively. The median survival for liposomal irinotecan groups (nal-IRI -10 and nal-IRI -50) significantly increased ($P < 0.05$) when compared to vehicle group. The groups were compared to vehicle by Log-rank statistical analysis.

accumulates in brain metastases via the EPR effect, similar to that reported for other solid tumor types (26). This maintenance of prolonged SN-38 cytotoxic concentrations and high tumor-to-normal tissue ratio are likely responsible for the prolonged survival observed in our animal model.

Further mechanistic possibilities for the increased drug uptake and accumulation from liposomal irinotecan is that it may avoid efflux by multidrug resistant proteins like P-gp and BCRP (12,36–38). The uptake of conventional anticancer agents is limited by multidrug resistant protein present on membranes of cancer cells (38). In addition to efflux mechanisms on cancer cells, the BBB and BTB also express variety of multidrug resistant proteins, which further limits the uptake of chemotherapy (39). Uptake of conventional irinotecan is also restricted by P-gp efflux (12,38,40), but we hypothesize that the liposomal irinotecan formulation bypasses multidrug resistant proteins both at the BBB/BTB and the efflux proteins associated with cancer cells (41,42).

Irinotecan is a widely used chemotherapeutic agent, upon administration it is converted to its active metabolite SN-38, which is a potent topoisomerase I inhibitor (16). Irinotecan is mostly converted to SN-38 in liver, whereas, liposomal irinotecan formulation leads to local conversion of irinotecan to SN-38 upon accumulation in the tumor (43). We observed that clearance rates for both irinotecan and its active metabolite SN-38 was significantly lower in liposomal irinotecan groups when compared to non-liposomal irinotecan group and this lower clearance rates for liposomes are responsible for prolonged plasma halves and mean residence times for both irinotecan and SN-38 with liposomal irinotecan formulation. The rate of clearance for liposomes are determined by both drug release and also uptake of liposomes by mononuclear phagocyte system (MPS) (44,45). The liposomes used for this study are "PEGylated" with approximately one polyethyleneglycol (PEG) molecule for 200 phospholipid molecules and PEGylated liposomes have long circulation time (46,47). This increase in circulation time also accounts for the decrease in volume of distribution of both irinotecan and SN-38 from liposomal formulations when compared to non-liposomal irinotecan formulation (Table I).

In addition to preferential accumulation of liposomal irinotecan in metastatic lesions, we observed that the progression of tumor burden was delayed in liposomal irinotecan groups, which correlated with prolonged survival. The median survival of the vehicle group was found to be 37 days (16,48). Treatment with conventional irinotecan (50 mg/kg) showed no improvement in survival (median survival of 35 days). However, liposomal irinotecan-treated groups significantly prolonged median survival to 50 days in 50 mg/kg group and 48 days in 10 mg/kg group (Fig.6). We hypothesize that after accumulation of liposomal irinotecan formulation in brain tumors, they act as reservoir for the release of irinotecan as described in other previous studies (49,50). The prolonged release of the chemotherapy from the liposomes provides sustained tumor drug concentration, as shown in the pharmacokinetic results. Maintenance of the irinotecan concentration in between cycles of treatments in liposomal irinotecan groups may be responsible for the prolonged survival when compared to vehicle and conventional irinotecan groups. We have demonstrated that nal-IRI permeates the BTB and accumulates in metastatic brain tumors due to the EPR effect, prolonged systemic circulation, and potentially bypassing the efflux mechanisms. We also observed accumulation of liposomes in lesions with sustained release of irinotecan. We believe this is responsible for the increase in survival in liposomal irinotecan groups compared to non-liposomal irinotecan group. Clinically, the chemotherapy used for the management of brain metastases of breast cancer are conventional cytotoxic agents such as cyclophosphamide, fluorouracil, methotrexate, and doxorubicin based upon their increased permeability through tumor vasculature (51,52). Collectively, results presented herein support the on-going clinical study of nal-IRI in patients with breast cancer brain metastases (NCT01770353) and indicates its potential for treatment of brain metastases of breast cancer.

CONCLUSIONS

In summary, we demonstrated efficacy of liposomal irinotecan in a preclinical model of a metastatic brain tumors. We observed the preferential uptake and accumulation of liposomal irinotecan into the brain tumors, followed by sustained concentration of irinotecan and its active metabolite SN-38 in plasma and tumor, ultimately correlating with increased survival.

ACKNOWLEDGMENTS AND DISCLOSURES. This research was supported by Merrimack Pharmaceuticals, Inc., and a grant from the National Cancer Institute (R01CA166067-01A1). Publication support was received from Ipsen Biopharmaceuticals, Inc. Additional support for this research was provided through the National Institute of General Medical Sciences of the National Institutes of Health (CTSI Award: U54GM104942, and the CoBRE P30 GM103488).

REFERENCES

1. Society AC. Breast cancer facts & figures 2015–2016. 2015.
2. Sperduto PW, Kased N, Roberge D, Xu Z, Shanley R, Luo X, et al. Summary report on the graded prognostic assessment: an accurate and facile diagnosis-specific tool to estimate survival for patients with brain metastases. J Clin Oncol. 2012;30(4):419–25.
3. Siegel RL, Miller KD, Jemal A. Cancer statistics, 2015. CA Cancer J Clin. 2015;65(1):5–29.
4. H. Nitta BD Kelly, C. Alfred, S. Jewell, P. Banks, E. Dennis, T.M. Grogan. The assessment of HER2 status in breast cancer: the past, the present, and the future. Pathol Int. 2016.
5. Bachelot T, Romieu G, Campone M, Dieras V, Cropet C, Dalenc F, et al. Lapatinib plus capecitabine in patients with previously untreated brain metastases from HER2-positive metastatic breast cancer (LANDSCAPE): a single-group phase 2 study. Lancet Oncol. 2013;14(1):64–71.
6. Bohn KA, Adkins CE, Mittapalli RK, Terrell-Hall TB, Mohammad AS, Shah N, et al. Semi-automated rapid quantification of brain vessel density utilizing fluorescent microscopy. J Neurosci Methods. 2016.
7. Morikawa A, Peereboom DM, Thorsheim HR, Samala R, Balyan R, Murphy CG, et al. Capecitabine and lapatinib uptake in surgically resected brain metastases from metastatic breast cancer patients: a prospective study. Neuro-Oncology. 2015;17(2):289–95.
8. Taskar KS, Rudraraju V, Mittapalli RK, Samala R, Thorsheim HR, Lockman J, et al. Lapatinib distribution in HER2 overexpressing experimental brain metastases of breast cancer. Pharm Res. 2012;29(3):770–81.
9. Lin NU, Vanderplas A, Hughes ME, Theriault RL, Edge SB, Wong YN, et al. Clinicopathologic features, patterns of recurrence, and survival among women with triple-negative breast cancer in the National Comprehensive Cancer Network. Cancer. 2012;118(22):5463–72.
10. Lockman PR, Mittapalli RK, Taskar KS, Rudraraju V, Gril B, Bohn KA, et al. Heterogeneous blood-tumor barrier permeability determines drug efficacy in experimental brain metastases of breast cancer. Clin Cancer Res Off J Am Assoc Cancer Res. 2010;16(23):5664–78.
11. Mittapalli RK, Adkins CE, Bohn KA, Mohammad AS, Lockman JA, Lockman PR. Quantitative fluorescence microscopy measures vascular pore size in primary and metastatic brain tumors. Cancer Res. 2017;77(2):238–46.
12. Adkins CE, Mittapalli RK, Manda VK, Nounou MI, Mohammad AS, Terrell TB, et al. P-glycoprotein mediated efflux limits substrate and drug uptake in a preclinical brain metastases of breast cancer model. Front Pharmacol. 2013;4:136.
13. Geldenhuys WJ, Mohammad AS, Adkins CE, Lockman PR. Molecular determinants of blood-brain barrier permeation. Ther Deliv. 2015;6(8):961–71.
14. Halasz LM, Uno H, Hughes M, D'Amico T, Dexter EU, Edge SB, et al. Comparative effectiveness of stereotactic radiosurgery versus whole-brain radiation therapy for patients with brain metastases from breast or non-small cell lung cancer. Cancer. 2016;122(13):2091–100.
15. El-Habashy SE, Nazief AM, Adkins CE, Wen MM, El-Kamel AH, Hamdan AM, et al. Novel treatment strategies for brain tumors and metastases. Pharm Pat Anal. 2014;3(3):279–96.
16. Adkins CE, Nounou MI, Hye T, Mohammad AS, Terrell-Hall T, Mohan NK, et al. NKTR-102 Efficacy versus irinotecan in a mouse model of brain metastases of breast cancer. BMC Cancer. 2015;15:685.
17. Mittapalli RK, Liu X, Adkins CE, Nounou MI, Bohn KA, Terrell TB, et al. Paclitaxel-hyaluronic nanoconjugates prolong overall survival in a preclinical brain metastases of breast cancer model. Mol Cancer Ther. 2013;12(11):2389–99.
18. Greish K. Enhanced permeability and retention (EPR) effect for anticancer nanomedicine drug targeting. Methods Mol Biol. 2010;624:25–37.
19. Sambade M, Deal A, Schorzman A, Luft JC, Bowerman C, Chu K, et al. Efficacy and pharmacokinetics of a modified acid-labile docetaxel-PRINT((R)) nanoparticle formulation against non-small-cell lung cancer brain metastases. Nanomedicine (Lond). 2016;11(15):1947–55.
20. Drummond DC, Noble CO, Guo Z, Hayes ME, Park JW, Ou CJ, et al. Improved pharmacokinetics and efficacy of a highly stable nanoliposomal vinorelbine. J Pharmacol Exp Ther. 2009;328(1):321–30.
21. Maeda H, Nakamura H, Fang J. The EPR effect for macromolecular drug delivery to solid tumors: Improvement of tumor uptake, lowering of systemic toxicity, and distinct tumor imaging in vivo. Adv Drug Deliv Rev. 2013;65(1):71–9.
22. Noble CO, Krauze MT, Drummond DC, Forsayeth J, Hayes ME, Beyer J, et al. Pharmacokinetics, tumor accumulation and antitumor activity of nanoliposomal irinotecan following systemic treatment of intracranial tumors. Nanomedicine (Lond). 2014;9(14):2099–108.
23. Khalifa A, Dodds D, Rampling R, Paterson J, Murray T. Liposomal distribution in malignant glioma: possibilities for therapy. Nucl Med Commun. 1997;18(1):17–23.
24. Koukourakis MI, Koukouraki S, Fezoulidis I, Kelekis N, Kyrias G, Archimandritis S, et al. High intratumoural accumulation of stealth liposomal doxorubicin (Caelyx) in glioblastomas and in metastatic brain tumours. Br J Cancer. 2000;83(10):1281–6.
25. Lee H, Shields AF, Siegel BA, Miller KD, Krop I, Ma CX, et al. 64Cu-MM-302 positron emission tomography quantifies variability of enhanced permeability and retention of nanoparticles in relation to treatment response in patients with metastatic breast cancer. Clin Cancer Res Off J Am Assoc Cancer Res. 2017.
26. Kalra AV, Kim J, Klinz SG, Paz N, Cain J, Drummond DC, et al. Preclinical activity of nanoliposomal irinotecan is governed by tumor deposition and intratumor prodrug conversion. Cancer Res. 2014;74(23):7003–13.
27. Espelin CW, Leonard SC, Geretti E, Wickham TJ, Hendriks BS. Dual HER2 targeting with trastuzumab and liposomal-encapsulated doxorubicin (MM-302) demonstrates synergistic antitumor activity in breast and gastric cancer. Cancer Res. 2016;76(6):1517–27.
28. Adkins CE, Nounou MI, Mittapalli RK, Terrell-Hall TB, Mohammad AS, Jagannathan R, et al. A novel preclinical method to quantitatively evaluate early-stage metastatic events at the murine blood–brain barrier. Cancer Prev Res. 2015;8(1):68–76.
29. Yuan F, Dellian M, Fukumura D, Leunig M, Berk DA, Torchilin VP, et al. Vascular permeability in a human tumor xenograft: molecular size dependence and cutoff size. Cancer Res. 1995;55(17):3752–6.

30. Raza K, Shareef MA, Singal P, Sharma G, Negi P, Katare OP. Lipid-based capsaicin-loaded nano-colloidal biocompatible topical carriers with enhanced analgesic potential and decreased dermal irritation. J Liposome Res. 2014;24(4):290–6.
31. Drummond DC, Meyer O, Hong K, Kirpotin DB, Papahadjopoulos D. Optimizing liposomes for delivery of chemotherapeutic agents to solid tumors. Pharmacol Rev. 1999;51(4):691–743.
32. Iwai K, Maeda H, Konno T. Use of oily contrast medium for selective drug targeting to tumor: enhanced therapeutic effect and X-ray image. Cancer Res. 1984;44(5):2115–21.
33. Abrams HL. The response of neoplastic renal vessels to epinephrine in man. Radiology. 1964;82:217–24.
34. Jain RK, Stylianopoulos T. Delivering nanomedicine to solid tumors. Nat Rev Clin Oncol. 2010;7(11):653–64.
35. Liu J, Yu M, Zhou C, Yang S, Ning X, Zheng J. Passive tumor targeting of renal-clearable luminescent gold nanoparticles: long tumor retention and fast normal tissue clearance. J Am Chem Soc. 2013;135(13):4978–81.
36. Michieli M, Damiani D, Ermacora A, Masolini P, Michelutti A, Michelutti T, et al. Liposome-encapsulated daunorubicin for PGP-related multidrug resistance. Br J Haematol. 1999;106(1):92–9.
37. Lo YL, Tu WC. Co-encapsulation of chrysophsin-1 and epirubicin in PEGylated liposomes circumvents multidrug resistance in HeLa cells. Chem Biol Interact. 2015;242:13–23.
38. Bansal T, Mishra G, Jaggi M, Khar RK, Talegaonkar S. Effect of P-glycoprotein inhibitor, verapamil, on oral bioavailability and pharmacokinetics of irinotecan in rats. Eur J Pharm Sci Off J Eur Fed Pharm Sci. 2009;36(4-5):580–90.
39. Mittapalli RK, Chung AH, Parrish KE, Crabtree D, Halvorson KG, Hu G, et al. ABCG2 and ABCB1 limit the efficacy of dasatinib in a PDGF-B-driven brainstem glioma model. Mol Cancer Ther. 2016;15(5):819–29.
40. Mittapalli RK, Manda VK, Bohn KA, Adkins CE, Lockman PR. Quantitative fluorescence microscopy provides high resolution imaging of passive diffusion and P-gp mediated efflux at the in vivo blood-brain barrier. J Neurosci Methods. 2013;219(1):188–95.
41. Ma P, Mumper RJ. Anthracycline nano-delivery systems to overcome multiple drug resistance: a comprehensive review. Nano Today. 2013;8(3):313–31.
42. Zhao YZ, Dai DD, Lu CT, Chen LJ, Lin M, Shen XT, et al. Epirubicin loaded with propylene glycol liposomes significantly overcomes multidrug resistance in breast cancer. Cancer Lett. 2013;330(1):74–83.
43. Wang X, Rao Z, Qin H, Zhang G, Ma Y, Jin Y, et al. Effect of hesperidin on the pharmacokinetics of CPT-11 and its active metabolite SN-38 by regulating hepatic Mrp2 in rats. Biopharm Drug Dispos. 2016;37(7):421–32.
44. Patel HM, Moghimi SM. Serum-mediated recognition of liposomes by phagocytic cells of the reticuloendothelial system - The concept of tissue specificity. Adv Drug Deliv Rev. 1998;32(1-2):45–60.
45. Patel HM. Serum opsonins and liposomes: their interaction and opsonophagocytosis. Crit Rev Ther Drug Carrier Syst. 1992;9(1):39–90.
46. Gabizon A, Catane R, Uziely B, Kaufman B, Safra T, Cohen R, et al. Prolonged circulation time and enhanced accumulation in malignant exudates of doxorubicin encapsulated in polyethyleneglycol coated liposomes. Cancer Res. 1994;54(4):987–92.
47. Bayever E, Fitzgerald JB, Kim J, Klinz S. Treatment of breast cancer with liposomal irinotecan. Google Patents; 2016.
48. Adkins CE, Mohammad AS, Terrell-Hall TB, Dolan EL, Shah N, Sechrest E, et al. Characterization of passive permeability at the blood-tumor barrier in five preclinical models of brain metastases of breast cancer. Clin Exp Metastasis. 2016;33(4):373–83.
49. Liu D, Yang P, Hu D, Liu F. Minocycline hydrochloride liposome controlled-release gel improves rat experimental periodontitis. Hua xi kou qiang yi xue za zhi = Huaxi kouqiang yixue zazhi = West China Journal of Stomatology. 2013;31(6):592–6.
50. Ostrowski AD, Lin BF, Tirrell MV, Ford PC. Liposome encapsulation of a photochemical NO precursor for controlled nitric oxide release and simultaneous fluorescence imaging. Mol Pharm. 2012;9(10):2950–5.
51. Lin NU, Bellon JR, Winer EP. CNS metastases in breast cancer. J Clin Oncol Off J Am Soc Clin Oncol. 2004;22(17):3608–17.
52. Boogerd W, Dalesio O, Bais EM, van der Sande JJ. Response of brain metastases from breast cancer to systemic chemotherapy. Cancer. 1992;69(4):972–80.

Breast Cancer Res Treat (2011) 130:635–644
DOI 10.1007/s10549-011-1646-4

EPIDEMIOLOGY

Elevated PCNA+ tumor-associated macrophages in breast cancer are associated with early recurrence and non-Caucasian ethnicity

Rita A. Mukhtar · Amy P. Moore · Onouwem Nseyo · Frederick L. Baehner · Alfred Au · Dan H. Moore · Patrick Twomey · Michael J. Campbell · Laura J. Esserman

Received: 29 November 2010 / Accepted: 18 June 2011 / Published online: 30 June 2011

Abstract African American and Hispanic women develop more triple negative breast cancer at younger ages than Caucasian women. The frequently observed association between race and socioeconomic status (SES) has confounded our understanding of the outcomes disparities seen in these groups. Given the association between inflammatory cells and high-grade, triple negative tumors, we sought to investigate whether differences in the presence of these cells varies by race. We evaluated breast tumor specimens for the presence PCNA+ tumor-associated macrophages (TAMs) in consecutive cases from a county hospital serving primarily un- or under-insured patients. All patients in this cohort had elevated PCNA + TAM levels. Higher PCNA + TAM counts were associated with hormone receptor (HR) negative tumors and non-Caucasian ethnicity. Hispanic women specifically had significantly higher PCNA + TAM counts than Caucasian patients and shorter disease-free survival. These findings implicate immune function in the development of aggressive breast cancer and suggest a possible link between SES and the inflammatory response.

Keywords Tumor-associated macrophage · Breast cancer · Prognosis · Outcomes disparities

Presented in part at the American Society of Clinical Oncology Annual Meeting, Chicago, IL, June 2010.

R. A. Mukhtar · A. P. Moore · O. Nseyo · F. L. Baehner · A. Au · D. H. Moore · P. Twomey · M. J. Campbell · L. J. Esserman (✉)
University of California, San Francisco, San Francisco, CA, USA
e-mail: Laura.esserman@ucsfmedctr.org

Introduction

Breast cancer remains the most common malignancy affecting women in the United States [1]. Despite improvements in screening and treatment, African American and Hispanic women bear a disproportionate burden of aggressive breast cancer with poor outcomes [2–4]. Traditionally, such outcomes disparities have been attributed to lower socioeconomic status (SES) and an associated decrease in access to care. However, even when patients have similar access to care, investigators note disparities between racial groups [2, 3, 5, 6].

Increasing evidence suggests that the breast tumors affecting African American and Latina women are biologically more aggressive [7]. In African American women, the likelihood of developing disease at younger ages and having poor outcomes is higher than in Caucasian women [1, 8, 9]. Studies show an increased incidence of triple negative and basal-like breast cancers in African Americans compared to Caucasians [7, 10–15].

Latina patients also have an elevated incidence of triple negative disease, with biological differences in tumors contributing to poor outcomes [4]. A family history of breast cancer confers a higher risk of developing estrogen receptor (ER) negative disease in Hispanic women compared to Caucasian women, suggesting a possible difference in breast cancer subtypes [16].

Thus, outcomes disparities in African American and Hispanic breast cancer patients may reflect a susceptibility to specific tumor types and warrants investigation into host response and tumor biology. There is increasing interest in the role of the immune response in breast tumors, with evidence implicating the overall immune environment in either promoting or inhibiting tumor growth and spread [17–21]. The inflammatory response to tumors includes the

recruitment of innate immune effector cells termed tumor-associated macrophages (TAMs) [22].

Once thought to be a part of the host response to tumors, TAMs are now known to contribute to tumor growth by producing angiogenic factors, stromal breakdown factors, and suppressing adaptive immunity [23–27]. TAMs have a spectrum of activation states, often dichotomized as the M1, or anti-tumoral, classic activation state, and the M2, or pro-tumoral, alternative activation state [28]. Recent work suggests that these two states represent the extremes on a continuum and that macrophage populations can contain considerable heterogeneity [17, 29]. Tumor cells themselves produce factors (e.g., colony stimulating factor-1, or M-CSF, and CCL2, or MCP-1) that recruit macrophages and promote them to take on a pro-tumoral phenotype [23, 30–33].

We previously identified a subpopulation of TAMs expressing proliferating cellular nuclear antigen (PCNA) that are associated with high-grade, HR negative breast cancer with increased risk of recurrence [34]. Since African American and Hispanic women have an unexplained higher incidence of high-risk breast cancer, we hypothesized that their tumors would have higher levels of PCNA + TAMs as well. The identification of high levels of this macrophage population would potentially give insight into the biology of aggressive breast cancers in these groups of women (Fig. 1).

Materials and methods

Patients

Tumors evaluated in this study came from patients treated at Highland Hospital in Oakland, CA, Alameda County's major source of acute care for the medically indigent and uninsured. We searched the pathology archives between the years 1996 and 2001, identifying 96 consecutive invasive breast cancer cases. Four patients with stage 4 disease and four patients who had neoadjuvant treatment were excluded, leaving 88 cases. Available tumor tissue was reviewed, and 18 cases were found inadequate for staining due to either lack of invasive tumor in the specimen or poor fixation, leaving 70 cases for analysis (Fig. 2). We reviewed medical records to determine tumor grade, histological type, HR and Her-2 *neu* status, as well as patient age, self-reported race, clinical stage at presentation, follow-up time, and the presence of recurrence or death. We also utilized the Social Security Death Index and county death records to identify and confirm deaths. All patients underwent surgical treatment for breast cancer, and adjuvant treatment was given at the discretion of the treating physicians. This study was approved by the institutional review boards at UCSF and Alameda County Medical Center (study approval numbers H41781-27112-05 and IRB07-12113A, respectively).

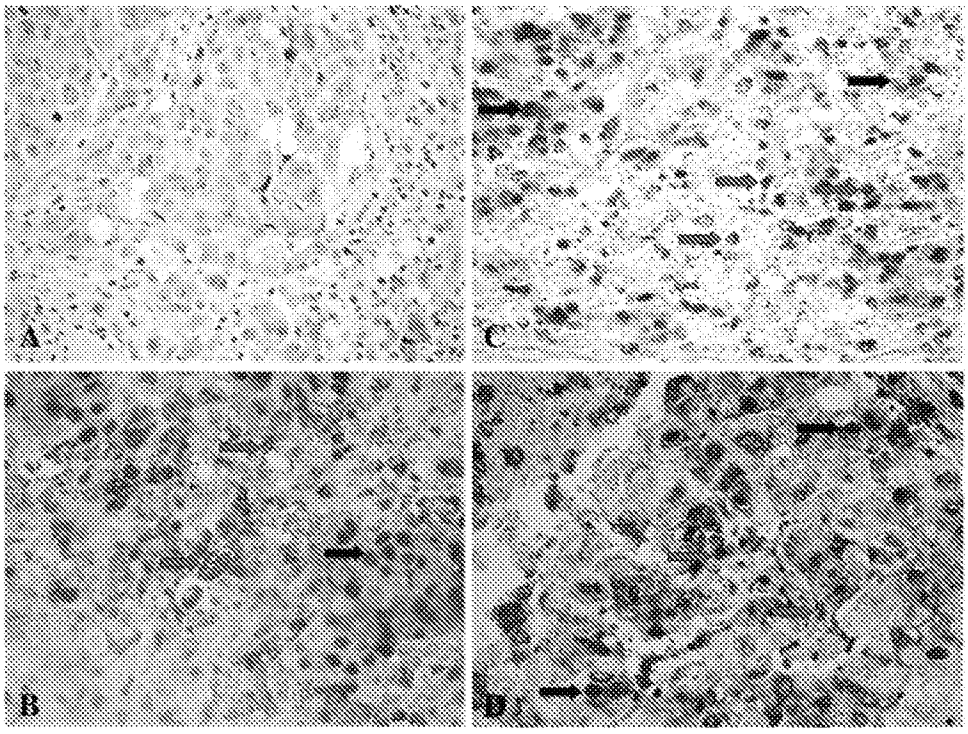

Fig. 1 **a** Hematoxylin and eosin (H&E) stain of a poorly differentiated ductal carcinoma, NOS, and associated mononuclear inflammatory cells (×400). **b–d** Examples of poorly differentiated ductal carcinomas characterized by large cells showing blue nuclear PCNA staining (*black arrows*) and infiltrating macrophages with foamy cytoplasm showing both brown cytoplasmic CD68 staining and blue nuclear PCNA staining (*red arrows*), characteristic both morphologically and immunophenotypically of PCNA positive tumor-associated macrophages (TAMs) (×400)

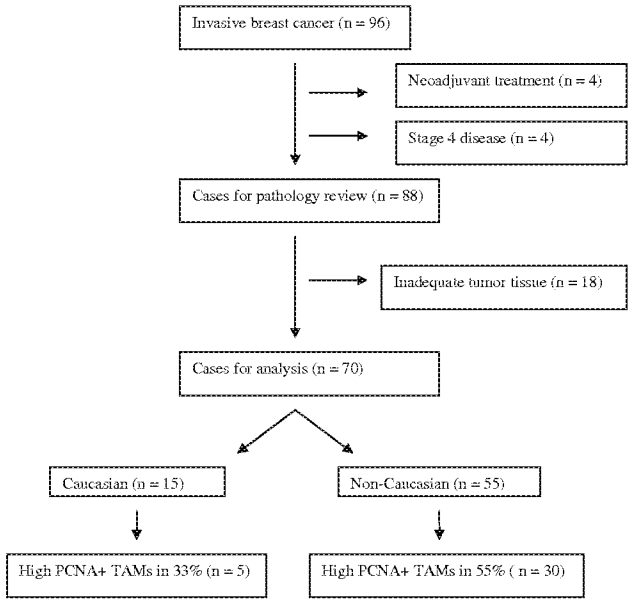

Fig. 2 Flow diagram of subjects included and excluded from analysis

Assay methods

Formalin-fixed, paraffin-embedded tumor blocks were cut into 5 μm sections, and immunohistochemistry was performed using a standard streptavidin–biotin peroxidase method. Sections were deparaffinized in xylene and rehydrated using graded ethanol. Antigen retrieval was performed using microwave-heated 10-mM citrate buffer for 10 min. Sections were double stained for CD68, a pan-macrophage marker, and PCNA, a protein required for DNA synthesis and repair. Double staining for CD68/PCNA was performed using dual endogenous enzyme block (Dako) for 10 min and incubation with anti-CD68 mouse monoclonal antibody (Dako M0876, 1:50 dilution) for 30 min, followed by a second incubation with anti-PCNA mouse monoclonal antibody (Dako M0879, 1:500 dilution) overnight at 4°C. For anti-CD68, DAB plus (Dako K1395) was used as a substrate and for anti-PCNA, BCIP/NPT substrate (Dako K0598) was used. The slides were counterstained with periodic acid Schiff reagent (American Master Tech Scientific KTPAS) for 10 min at room temperature. For use as a positive control and to control lot-to-lot variability across clinical studies, a control tissue microarray (TMA), comprised 1.0 mm breast tumor cores, was stained with all IHC staining runs and assessed to assure for batch to batch consistency [35].

Two pathologists independently evaluated the immunostains without knowledge of clinical characteristics. Cells staining doubly positive for CD68 and PCNA were considered to be PCNA + TAMs. PCNA + TAMs were counted in each of the three representative high power fields (hpf), and the mean number was used for the final PCNA + TAM count.

Study design

All invasive breast cancer cases in the pathology archives during the period 1996–2001 were evaluated for inclusion in this retrospective analysis of PCNA + TAM levels. Median follow-up time was 10.34 years. Our primary endpoint was the number of PCNA + TAMs present in tumor tissue in different ethnic groups. Secondary endpoints included HR status, grade, recurrence-free survival, and overall survival. Based on a previous report of African American patients having nearly 30% more TAMs than Caucasian patients [36], we wanted to identify a 30% difference in PCNA + TAM levels between African American/Hispanic patients and Caucasian patients. Having 49 patients in each group provides 80% power to identify a difference of 30%. Based on the ethnic diversity of Highland Hospital, we aimed to identify ~100 patients for analysis, with the assumption that half would be either African American or Hispanic. The study is reported according to the recommended REMARK guidelines for prognostic studies [37].

Statistical analysis

Statistical analyses were performed using version 11 of Stata (Stata Corporation, College Station, TX). PCNA + TAM counts were analyzed continuously and dichotomized as "high" or "low" using both a previously defined cutpoint of greater or equal to 5 PCNA + TAMs/hpf [34] as well as using median PCNA + TAM count as a cutpoint. We used the χ^2, Fisher's exact, and Student's t test to compare categorical and continuous outcomes, the Mann–Whitney test for non-normally distributed variables, and linear regression models for continuous outcomes. Survival and recurrence data were analyzed using the Kaplan–Meier method with the log-rank test, and Cox proportional hazards models. Subjects with missing data were excluded from relevant analyses. All reported P values are two sided.

Results

Patient characteristics

The cohort of 70 women ranged in age from 30 to 74 years, with a mean age of 50 years. The group was ethnically diverse, with 42% African American, 19% Asian, 21% Caucasian, and 17% Hispanic patients. 77% of patients presented with stage 1 or 2 cancers, and mean follow-up time was 10.1 years (Table 1).

Tumor characteristics

The majority of tumors (76%) were grade 3, and 33% were HR negative [lacking both ER and progesterone receptor (PR)]. Histologically, 83% of tumors were invasive ductal, 7% were invasive lobular, 6% were mucinous, 3% were mixed ducto-lobular, and 1% were medullary carcinomas. Of the 70 tumors evaluated, 8 were missing grade, 5 were missing Her-2 status, and 2 were missing ER and PR status (Table 2).

PCNA + TAMs and tumor histology

Using our previously established cut-point of 5 or more PCNA + TAMs/hpf, every patient in this cohort had high PCNA + TAM counts [34]. Median PCNA + TAM count was 38.5/hpf. For purposes of analysis, we analyzed PCNA + TAMs continuously and as a dichotomous variable, comparing those with higher than median counts to those with lower than median counts in this group. Higher PCNA + TAM counts were associated with HR negativity ($P = 0.001$) and were more common among higher grade tumors, 0 of 3 grade 1 tumors (0%) had high PCNA + TAM counts, while 30 of 59 higher grade tumors (51%) had high PCNA + TAM counts ($P = 0.086$, Table 2).

PCNA + TAMs and race

Higher than median PCNA + TAMs were present in 33% of Caucasian women, 52% of African American women, 46% of Asian women, and 75% of Hispanic women (Fig. 3). There was no overall difference in mean PCNA + TAM count when comparing all races individually, however, non-Caucasian patients had significantly higher PCNA + TAM counts than Caucasian patients (45 vs. 32 PCNA + TAMs/hpf, $P = 0.04$), which persisted even when controlling for HR status, grade, and age ($P = 0.042$, 95% CI 0.5–25.3). This difference was most marked in Hispanic patients compared to Caucasian patients, where pairwise analysis showed a mean of 54 PCNA + TAMs/hpf in Hispanic patients compared to a mean of 31/hpf in Caucasian patients ($P = 0.03$, Fig. 4). There was no association between race and the following factors: age, clinical stage at presentation, tumor grade, or HR status.

PCNA + TAMs and outcomes

Non-Caucasian subjects had both significantly higher PCNA + TAM counts than Caucasian subjects and significantly shorter recurrence-free survival ($P = 0.02$, Fig. 4). This was also seen in the Hispanic subset of patients ($P = 0.02$, Fig. 5). Patients who had early recurrences (within 5 years of diagnosis) were more likely to have high PCNA + TAM levels compared to those with no or late recurrences (hazard ratio for early recurrence = 2.3, $P = 0.037$, Table 3). This increased risk persisted when grade was added to the model, but the effect of high PCNA + TAMs was decreased with the addition of HR status. Similarly, high PCNA + TAMs were significantly more common among subjects who died than those who survived (hazard ratio 2.44, $P = 0.021$), although this was

Table 1 Patient characteristics overall and by PCNA + TAM count

Patient characteristics	Overall *n* (%)	Low PCNA + TAMs *n* (%)	High PCNA + TAMs *n* (%)	*P* value
Subjects	70	35 (50)	35 (50)	
Mean age (years)	50, range 30–74	50.5	51.6	0.65
Race				
African American	29 (42)	14 (40)	15 (43)	0.22
Caucasian	15 (21)	10 (29)	5 (14)	
Asian	13 (19)	7 (20)	6 (17)	
Hispanic	12 (17)	3 (9)	9 (26)	
Other	1 (1)	1 (3)	0 (0)	
Clinical stage at presentation				0.89
1	18 (26)	10 (29)	8 (24)	
2	35 (51)	17 (49)	18 (53)	
3	16 (23)	8 (23)	8 (24)	
Mean follow-up time (years)	7.3, range 0.5–13	8.2	6.4	0.05
Recurrences	30 (43)	12 (34)	18 (51)	0.15
Deaths	30 (43)	10 (29)	20 (57)	0.02

Table 2 Tumor characteristics overall and by PCNA + TAM count

Tumor characteristics	Overall *n* (%)	Low PCNA + TAMs *n* (%)	High PCNA + TAMs *n* (%)	*P* value
Grade				0.18
1	3 (5)	3 (9)	0 (0)	
2	12 (19)	7 (22)	5 (17)	
3	47 (76)	22 (69)	25 (83)	
Histology				0.042
Invasive ductal carcinoma	58 (83)	28 (80)	30 (86)	
Mucinous	4 (6)	4 (11)	0 (0)	
Invasive lobular carcinoma	5 (7)	3 (9)	2 (6)	
Invasive ducto-lobular carcinoma	2 (3)	0 (0)	2 (6)	
Medullary	1 (1)	0 (0)	1 (3)	
Hormone receptor positive	47 (67)	30 (86)	17 (49)	0.001
Her 2 neu amplified	20 (31)	9 (26)	11 (37)	0.34

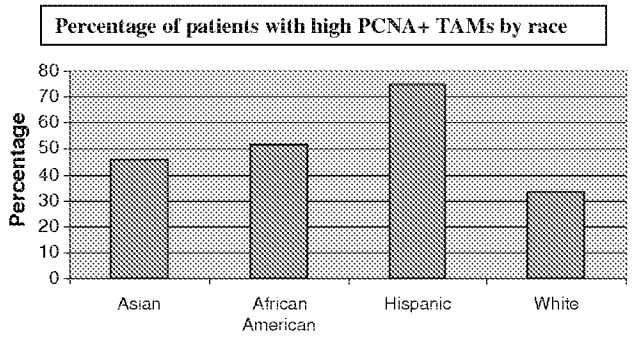

Fig. 3 PCNA + TAM levels were elevated in the entire cohort, but were highest in the non-Caucasian subjects

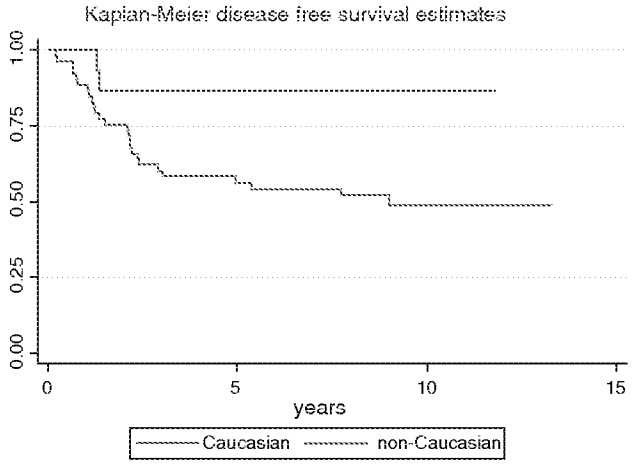

Fig. 4 Recurrence-free survival was significantly shorter in Caucasian versus non-Caucasian subjects ($P = 0.02$)

mitigated by controlling for HR status (hazard ratio = 1.99, $P = 0.097$, 95% CI 0.9–4.5). Patients with high PCNA + TAMs had significantly shorter overall survival than those with low PCNA + TAMs ($P < 0.02$, Fig. 6).

PCNA + TAMs and adjuvant treatment

71% of patients received adjuvant chemotherapy. Of note, the use of chemotherapy did not differ by race and was not significantly associated with PCNA + TAM counts or outcomes. High PCNA + TAM counts were still associated with decreased overall survival (HR = 2.4, $P = 0.03$, 95% CI 1.1–5.5), as well as with increased risk of early recurrence (HR = 2.3, $P < 0.05$, 95% CI 1.01–5.2), even when adjusting for chemotherapy administration.

The use of tamoxifen was only available on 27 patients (39%), with 8 of these subjects receiving tamoxifen. As would be expected, tamoxifen usage was strongly associated with ER positivity ($P < 0.001$). In this small group, tamoxifen usage was not associated with recurrence or overall survival.

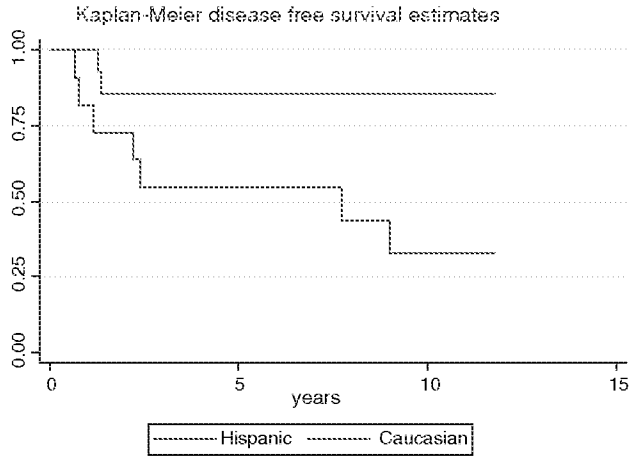

Fig. 5 Recurrence-free survival was significantly shorter in Hispanic subjects compared to Caucasian subjects ($P = 0.02$)

Table 3 Cox proportional hazards models showing the hazard ratio for early recurrence in those with high PCNA + TAMs, adjusted for grade and HR positivity

Cox model	Predictor	Hazard ratio	*P* value	95% Confidence interval
1	High PCNA + TAMs	2.3	0.037	1.05–4.9
2	High PCNA + TAMs	2.4	0.04	1.04–5.4
	Low grade (1 or 2)	0.7	0.5	0.27–2
3	High PCNA + TAMs	1.97	0.15	0.8–4.9
	Low grade (1 or 2)	0.67	0.49	0.2–2.1
	HR positivity	0.76	0.56	0.3–1.9

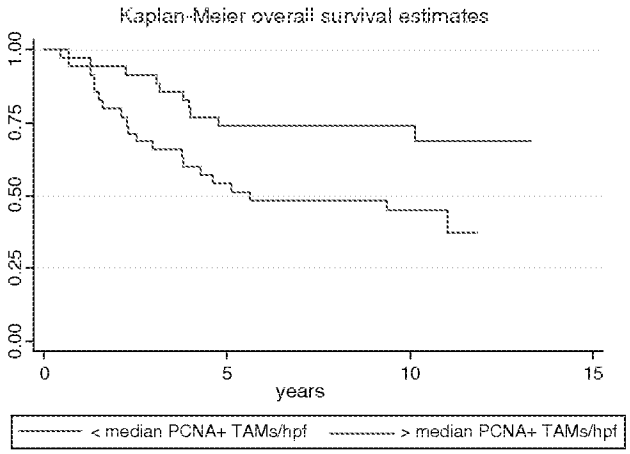

Fig. 6 Overall survival was significantly shorter in subjects with high PCNA + TAM levels compared to those with lower PCNA + TAM levels ($P < 0.02$)

Discussion

In this cohort of breast cancer patients from a public safety-net hospital treating un- or under-insured patients, all patients had high PCNA + TAM counts based on our previously established cut-point. However, we again observed an association between the highest PCNA + TAM levels and HR negative tumors with increased risk of recurrence. Interestingly, this patient population had a high incidence of grade 3 disease, which likely contributes to the overall high PCNA + TAM counts. Hispanic patients had both the highest levels and the shortest time to recurrence. The association between PCNA + TAM levels and high-grade disease with early recurrence underscores the importance of the inflammatory response in contributing to high grade, HR negative breast cancer biology.

The inflammatory response to tumors includes the recruitment of TAMs [22]. These normal immune effector cells have various phenotypic states, described as the classically activated M1 state, the alternatively activated M2 state [28], or the three types known as classical, wound healing, and regulatory. TAMs possess characteristics of the M2 state [22] and the wound healing/regulatory states [29]. In animal models, TAMs promote tumor growth and metastases [38, 39]. While we hypothesize that these PCNA + TAMs are polarized toward the M2 phenotype, this cannot be determined without assessing for specific M2 markers, something we are undertaking in future studies. Interestingly, in a different patient cohort with tumor gene expression data available, we found that subjects with high levels of PCNA + TAMs express high levels of both M1- and M2-related genes (unpublished data), perhaps fitting with the complexity noted in macrophage populations.

Previous studies have found associations between total TAMs and breast cancer with poor prognostic features [40–44], and one study found higher levels of TAMs in breast cancer patients of African American race [36]. Of note, this ethnically diverse patient population had strikingly high PCNA + TAM levels overall compared to previously studied groups. In a cohort of patients treated at the University of California, San Francisco, the mean PCNA + TAM count among the grade 3 cases was 10/hpf, compared to the mean of 42/hpf found in the current cohort. The explanation for this difference is unclear, but given that this cohort comes from a county hospital that provides care to un- or under-insured patients, it raises questions about how SES and environmental factors may influence the host inflammatory response to breast cancer. To control for sources of preanalytic variability that could lead to assay drift we used a tissue micro array (TMA) of breast carcinomas both as a positive control and to control for any potential lot to lot variability. Sections from this TMA were stained in parallel with all IHC staining runs and assessed to assure consistency. No drift in staining pattern or intensity was observed either within this study or across studies.

We did not observe an association between race and HR negative, high-grade cancers. This could reflect racial admixture, inaccuracies in racial designation, low SES overall, small sample size, or, could be due to the unusually high rate of HR negative, high grade cancer in the entire cohort. Nearly 75% of tumors in this patient population

were grade 3, compared to the 30% incidence of grade 3 tumors reported in a large, nation-wide screening study [45]. Similarly, 33% of tumors in this cohort were HR negative, with Asian and Hispanic patients having higher rates of HR negative tumors than previously reported [46]. The rate of HR negative breast cancer has been reported to increase with low SES [47–49].

Given the association between PCNA + macrophages and a variety of disease states, such as viral infection and kidney disease, differences in the prevalence of these diseases between ethnic groups could potentially contribute to overall differences in immune function and breast cancer risk. Information on co-morbid medical diseases was not available in this study, but this should be investigated in future work.

There may be differences in the normal basal levels of circulating monocytes by ethnicity, although existing data are inconsistent. Two studies found that African Americans had lower white blood cell counts than Caucasians, but that this was due to decreased granulocytes. Monocytes were decreased in African American men, but similar between African American and Caucasian women [50, 51]. Another study found that African American subjects had higher monocyte levels and that Asian subjects had lower monocyte levels [52]. As our current study was retrospective, peripheral blood monocyte levels were not available. In future work, it would be prudent to obtain peripheral blood leukocytes and review the complete blood count with differential to determine whether changes in routine counts vary with tumor types and TAM levels. This would be of interest, particularly since differences in basal circulating monocyte levels in healthy subjects suggests a potential underlying difference in immune function.

Future work will also include measuring serum cytokines/chemokines and correlating their levels with TAMs. In a separate patient cohort with tumor gene expression available, CCL2 expression levels correlate with PCNA + TAM levels (unpublished data). CCL2 is known to recruit monocytes, memory T cells, and dendritic cells to sites of inflammation, and polarizes TAMs toward the M2 phenotype [53, 54].

While we expected to find higher PCNA + TAM levels in African American and Hispanic patients, we did not necessarily expect that levels would be elevated in all non-Caucasian patients. This finding likely reflects the diversity in breast cancers found in Asian American patients. Many non-Caucasian groups, including Asian Americans, have been noted to have worse cancer outcomes than Caucasians [55]. Among Asian Americans, recent work has identified differences in proportions of breast cancer subtypes compared to Caucasian women, with a higher incidence of Her-2 *neu* positive disease among Asian Americans [56]. Additionally, immigrant status among Asian Americans affects breast cancer outcomes [57]. This, combined with ethnic diversity among patients categorized as Asian American likely contribute to conflicting reports on breast cancer disparities in this group [58]. Another factor to consider is inaccuracy in self-reported race, as genetic ancestry can differ from self-perceived race [59, 60].

Of note, we previously designated PCNA + TAMs as proliferating macrophages, or "promacs." However, the presence of PCNA in these cells does not in and of itself confirm proliferation. Expressed during the G1 and S phases of the cell cycle, PCNA is required for DNA synthesis and mismatch repair [61]. Levels are particularly high in proliferating cells [62]; however, tissue macrophages are thought to be terminally differentiated cells that do not proliferate [63–65]. Review of recent work suggests that monocytes that have recently migrated into the tissue may retain the ability to proliferate prior to differentiating into resident tissue macrophages.

In a study of simian immunodeficiency virus, PCNA + perivascular macrophages did not incorporate 5-bromo-2′-deoxyuridine (BrdU) or express other proliferation markers, suggesting the absence of proliferation [66]. However, in a rat model of glomerulonephritis, PCNA + tissue macrophages were found to incorporate BrdU, suggesting the presence of proliferation. These proliferating tissue macrophages expressed monocyte markers, while more differentiated resident tissue macrophages did not proliferate [67]. These findings suggest that while recently extravasated monocytes may retain the capacity to proliferate in the tissue, resident macrophages do not [68]. Aziz et al. recently found that myelomonocytic progenitors proliferate in response to M-CSF while differentiated macrophages do not, likely due to the presence of transcription factors MafB and c-Maf [69].

TAMs expressing PCNA could then be resident tissue macrophages undergoing DNA repair but not proliferation, recently extravasated undifferentiated tissue macrophages undergoing proliferation, or resident tissue macrophages that have lost MafB/c-Maf, allowing them to proliferate. Distinguishing between these scenarios will require examining these PCNA+ cells for more specific proliferation markers and transcription factors.

This study's limitations include lack of SES by individual patients, the self-reporting of race into pre-determined categories [59], and the size of the cohort. While we were unable to assess mammography usage in this population, results from prior studies suggest that it would be unlikely to significantly change the results [70, 71]. Early detection may not be as useful for high grade, rapidly growing tumors, of which there are an excess in African American and Hispanic women due to the association between young age and high-risk tumors. While screening rates are often lower in low SES populations, this does not

wholly account for the high grade nature of the tumors seen in these populations. High grade, locally advanced tumors are more likely to present between screenings as interval cancers [72]. While this is a relatively small study, it provides characterization of serial patients seen at a public safety-net hospital, who have a strikingly high proportion of cases with elevated PCNA + TAMs.

Studying PCNA + TAMs in breast cancer could ultimately serve to identify patients who would benefit from targeted therapy. Methods of changing TAM phenotype from pro-tumoral to anti-tumoral have been described [21, 73], and anti-macrophage agents are currently in development [23, 32]. Future directions include specifically studying the relationship between SES and the inflammatory response to breast cancer, as these early findings suggest that there may be a link between the two, and a potential interaction between race and SES in the development of aggressive breast cancer.

Conclusions

Elevated PCNA + TAMs are associated with poor prognostic features such as HR negativity and high-tumor grade. Non-Caucasian women had significantly higher PCNA + TAM levels than Caucasian women and had shorter disease-free survival. These results and the overall frequent finding of high-grade disease and elevated PCNA + TAM levels in this low SES patient population warrant further investigation and potentially implicate altered immune function in the pathogenesis of high-risk breast cancers in the setting of outcomes disparities.

Acknowledgments We thank Doris Rivas for contributing to data collection. This work was supported by the California Breast Cancer Research Program (Post-doctoral fellowship 15FB-0108).

Conflict of interest None of the authors have any conflicts of interest to report for this manuscript.

References

1. Jemal A, Siegel R, Xu J, Ward E (2010) Cancer statistics, 2010. CA Cancer J Clin. doi:10.3322/caac.20073
2. Zaloznik AJ (1995) Breast cancer stage at diagnosis: Caucasians versus Afro-Americans. Breast Cancer Res Treat 34(3):195–198
3. Zaloznik AJ (1997) Breast cancer stage at diagnosis: Caucasians versus Hispanics. Breast Cancer Res Treat 42(2):121–124
4. Patel TA, Colon-Otero G, Bueno Hume C, Copland JA III, Perez EA (2010) Breast cancer in Latinas: gene expression, differential response to treatments, and differential toxicities in Latinas compared with other population groups. Oncologist 15(5): 466–475. doi:10.1634/theoncologist.2010-0004
5. Albain KS, Unger JM, Crowley JJ, Coltman CA Jr, Hershman DL (2009) Racial disparities in cancer survival among randomized clinical trials patients of the Southwest Oncology Group. J Natl Cancer Inst 101(14):984–992. doi:10.1093/jnci/djp175
6. Newman LA, Griffith KA, Jatoi I, Simon MS, Crowe JP, Colditz GA (2006) Meta-analysis of survival in African American and white American patients with breast cancer: ethnicity compared with socioeconomic status. J Clin Oncol 24(9):1342–1349. doi: 10.1200/JCO.2005.03.3472
7. Dunn BK, Agurs-Collins T, Browne D, Lubet R, Johnson KA (2010) Health disparities in breast cancer: biology meets socioeconomic status. Breast Cancer Res Treat 121(2):281–292. doi: 10.1007/s10549-010-0827-x
8. Baquet CR, Mishra SI, Commiskey P, Ellison GL, DeShields M (2008) Breast cancer epidemiology in blacks and whites: disparities in incidence, mortality, survival rates and histology. J Natl Med Assoc 100(5):480–488
9. Anderson WF, Rosenberg PS, Menashe I, Mitani A, Pfeiffer RM (2008) Age-related crossover in breast cancer incidence rates between black and white ethnic groups. J Natl Cancer Inst 100(24):1804–1814. doi:10.1093/jnci/djn411
10. Carey LA, Perou CM, Livasy CA, Dressler LG, Cowan D, Conway K, Karaca G, Troester MA, Tse CK, Edmiston S, Deming SL, Geradts J, Cheang MC, Nielsen TO, Moorman PG, Earp HS, Millikan RC (2006) Race, breast cancer subtypes, and survival in the Carolina Breast Cancer Study. JAMA 295(21):2492–2502. doi:10.1001/jama.295.21.2492
11. Morris GJ, Naidu S, Topham AK, Guiles F, Xu Y, McCue P, Schwartz GF, Park PK, Rosenberg AL, Brill K, Mitchell EP (2007) Differences in breast carcinoma characteristics in newly diagnosed African-American and Caucasian patients: a single-institution compilation compared with the National Cancer Institute's Surveillance, Epidemiology, and End Results database. Cancer 110(4):876–884. doi:10.1002/cncr.22836
12. Stark A, Kapke A, Schultz D, Brown R, Linden M, Raju U (2008) Advanced stages and poorly differentiated grade are associated with an increased risk of HER2/neu positive breast carcinoma only in White women: findings from a prospective cohort study of African-American and White-American women. Breast Cancer Res Treat 107(3):405–414. doi:10.1007/s10549-007-9560-5
13. Lund MJ, Butler EN, Bumpers HL, Okoli J, Rizzo M, Hatchett N, Green VL, Brawley OW, Oprea-Ilies GM, Gabram SG (2008) High prevalence of triple-negative tumors in an urban cancer center. Cancer 113(3):608–615. doi:10.1002/cncr.23569
14. Moran MS, Yang Q, Harris LN, Jones B, Tuck DP, Haffty BG (2008) Long-term outcomes and clinicopathologic differences of African-American versus white patients treated with breast conservation therapy for early-stage breast cancer. Cancer 113(9):2565–2574. doi:10.1002/cncr.23881
15. Chlebowski RT, Chen Z, Anderson GL, Rohan T, Aragaki A, Lane D, Dolan NC, Paskett ED, McTiernan A, Hubbell FA, Adams-Campbell LL, Prentice R (2005) Ethnicity and breast cancer: factors influencing differences in incidence and outcome. J Natl Cancer Inst 97(6):439–448. doi:10.1093/jnci/dji064
16. Hines LM, Risendal B, Slattery ML, Baumgartner KB, Giuliano AR, Byers T (2008) Differences in estrogen receptor subtype according to family history of breast cancer among Hispanic, but not non-Hispanic White women. Cancer Epidemiol Biomarkers Prev 17(10):2700–2706. doi:10.1158/1055-9965.EPI-08-0504
17. Sica A, Larghi P, Mancino A, Rubino L, Porta C, Totaro MG, Rimoldi M, Biswas SK, Allavena P, Mantovani A (2008) Macrophage polarization in tumour progression. Semin Cancer Biol 18(5):349–355. doi:10.1016/j.semcancer.2008.03.004
18. Porta C, Larghi P, Rimoldi M, Totaro MG, Allavena P, Mantovani A, Sica A (2009) Cellular and molecular pathways linking inflammation and cancer. Immunobiology 214(9–10):761–777. doi:10.1016/j.imbio.2009.06.014

19. Hansen BD, Schmidt H, von der Maase H, Sjoegren P, Agger R, Hokland M (2006) Tumour-associated macrophages are related to progression in patients with metastatic melanoma following interleukin-2 based immunotherapy. Acta Oncol 45(4):400–405. doi:10.1080/02841860500471798
20. Steidl C, Lee T, Shah SP, Farinha P, Han G, Nayar T, Delaney A, Jones SJ, Iqbal J, Weisenburger DD, Bast MA, Rosenwald A, Muller-Hermelink HK, Rimsza LM, Campo E, Delabie J, Braziel RM, Cook JR, Tubbs RR, Jaffe ES, Lenz G, Connors JM, Staudt LM, Chan WC, Gascoyne RD (2010) Tumor-associated macrophages and survival in classic Hodgkin's lymphoma. N Engl J Med 362(10):875–885. doi:10.1056/NEJMoa0905680
21. Solinas G, Germano G, Mantovani A, Allavena P (2009) Tumor-associated macrophages (TAM) as major players of the cancer-related inflammation. J Leukoc Biol 86(5):1065–1073. doi:10.1189/jlb.0609385
22. Siveen KS, Kuttan G (2009) Role of macrophages in tumour progression. Immunol Lett 123(2):97–102. doi:10.1016/j.imlet.2009.02.011
23. Allavena P, Sica A, Solinas G, Porta C, Mantovani A (2008) The inflammatory micro-environment in tumor progression: the role of tumor-associated macrophages. Crit Rev Oncol Hematol 66(1):1–9. doi:10.1016/j.critrevonc.2007.07.004
24. Mantovani A, Sica A, Locati M (2005) Macrophage polarization comes of age. Immunity 23(4):344–346. doi:10.1016/j.immuni.2005.10.001
25. Mantovani A, Allavena P, Sica A, Balkwill F (2008) Cancer-related inflammation. Nature 454(7203):436–444. doi:10.1038/nature07205
26. Talmadge JE, Donkor M, Scholar E (2007) Inflammatory cell infiltration of tumors: Jekyll or Hyde. Cancer Metastasis Rev 26(3–4):373–400. doi:10.1007/s10555-007-9072-0
27. Zhu X, Mulcahy LA, Mohammed RA, Lee AH, Franks HA, Kilpatrick L, Yilmazer A, Paish EC, Ellis IO, Patel PM, Jackson AM (2008) IL-17 expression by breast-cancer-associated macrophages: IL-17 promotes invasiveness of breast cancer cell lines. Breast Cancer Res 10(6):R95. doi:10.1186/bcr2195
28. Van Ginderachter JA, Movahedi K, Hassanzadeh Ghassabeh G, Meerschaut S, Beschin A, Raes G, De Baetselier P (2006) Classical and alternative activation of mononuclear phagocytes: picking the best of both worlds for tumor promotion. Immunobiology 211(6–8):487–501. doi:10.1016/j.imbio.2006.06.002
29. Mosser DM, Edwards JP (2008) Exploring the full spectrum of macrophage activation. Nat Rev Immunol 8(12):958–969. doi:10.1038/nri2448
30. Balkwill F, Mantovani A (2010) Cancer and inflammation: implications for pharmacology and therapeutics. Clin Pharmacol Ther 87(4):401–406. doi:10.1038/clpt.2009.312
31. Patsialou A, Wyckoff J, Wang Y, Goswami S, Stanley ER, Condeelis JS (2009) Invasion of human breast cancer cells in vivo requires both paracrine and autocrine loops involving the colony-stimulating factor-1 receptor. Cancer Res 69(24):9498–9506. doi:10.1158/0008-5472.CAN-09-1868
32. Sica A, Schioppa T, Mantovani A, Allavena P (2006) Tumour-associated macrophages are a distinct M2 polarised population promoting tumour progression: potential targets of anti-cancer therapy. Eur J Cancer 42(6):717–727. doi:10.1016/j.ejca.2006.01.003
33. Fujimoto H, Sangai T, Ishii G, Ikehara A, Nagashima T, Miyazaki M, Ochiai A (2009) Stromal MCP-1 in mammary tumors induces tumor-associated macrophage infiltration and contributes to tumor progression. Int J Cancer 125(6):1276–1284. doi:10.1002/ijc.24378
34. Campbell MJ, Tonlaar NY, Garwood ER, Huo D, Moore DH, Khramtsov AI, Au A, Baehner F, Chen Y, Malaka DO, Lin A, Adeyanju OO, Li S, Gong C, McGrath M, Olopade OI, Esserman LJ (2010) Proliferating macrophages associated with high grade, HR negative breast cancer and poor clinical outcome. Breast Cancer Res Treat. doi:10.1007/s10549-010-1154-y
35. Yaziji H, Taylor CR, Goldstein NS, Dabbs DJ, Hammond EH, Hewlett B, Floyd AD, Barry TS, Martin AW, Badve S, Baehner F, Cartun RW, Eisen RN, Swanson PE, Hewitt SM, Vyberg M, Hicks DG (2008) Consensus recommendations on estrogen receptor testing in breast cancer by immunohistochemistry. Appl Immunohistochem Mol Morphol 16(6):513–520. doi:10.1097/PAI.0b013e31818a9d3a
36. Martin DN, Boersma BJ, Yi M, Reimers M, Howe TM, Yfantis HG, Tsai YC, Williams EH, Lee DH, Stephens RM, Weissman AM, Ambs S (2009) Differences in the tumor microenvironment between African-American and European-American breast cancer patients. PLoS One 4(2):e4531. doi:10.1371/journal.pone.0004531
37. McShane LM, Altman DG, Sauerbrei W, Taube SE, Gion M, Clark GM (2005) Reporting recommendations for tumor marker prognostic studies. J Clin Oncol 23(36):9067–9072. doi:10.1200/JCO.2004.01.0454
38. Qian B, Deng Y, Im JH, Muschel RJ, Zou Y, Li J, Lang RA, Pollard JW (2009) A distinct macrophage population mediates metastatic breast cancer cell extravasation, establishment and growth. PLoS One 4(8):e6562. doi:10.1371/journal.pone.0006562
39. Galmbacher K, Heisig M, Hotz C, Wischhusen J, Galmiche A, Bergmann B, Gentschev I, Goebel W, Rapp UR, Fensterle J (2010) Shigella mediated depletion of macrophages in a murine breast cancer model is associated with tumor regression. PLoS One 5(3):e9572. doi:10.1371/journal.pone.0009572
40. Steele RJ, Eremin O, Brown M, Hawkins RA (1984) A high macrophage content in human breast cancer is not associated with favourable prognostic factors. Br J Surg 71(6):456–458
41. Volodko NRA, Rudas M, Jakesz R (1998) Tumour-associated macrophages in breast cancer and their prognostic correlations. The Breast 7(2):99–105
42. Leek RD, Hunt NC, Landers RJ, Lewis CE, Royds JA, Harris AL (2000) Macrophage infiltration is associated with VEGF and EGFR expression in breast cancer. J Pathol 190(4):430–436. doi:10.1002/(SICI)1096-9896(200003)190:4<430::AID-PATH538>3.0.CO;2-6
43. Leek RD, Landers RJ, Harris AL, Lewis CE (1999) Necrosis correlates with high vascular density and focal macrophage infiltration in invasive carcinoma of the breast. Br J Cancer 79(5–6):991–995. doi:10.1038/sj.bjc.6690158
44. Leek RD, Lewis CE, Whitehouse R, Greenall M, Clarke J, Harris AL (1996) Association of macrophage infiltration with angiogenesis and prognosis in invasive breast carcinoma. Cancer Res 56(20):4625–4629
45. Smith-Bindman R, Miglioretti DL, Lurie N, Abraham L, Barbash RB, Strzelczyk J, Dignan M, Barlow WE, Beasley CM, Kerlikowske K (2006) Does utilization of screening mammography explain racial and ethnic differences in breast cancer? Ann Intern Med 144(8):541–553
46. Setiawan VW, Monroe KR, Wilkens LR, Kolonel LN, Pike MC, Henderson BE (2009) Breast cancer risk factors defined by estrogen and progesterone receptor status: the multiethnic cohort study. Am J Epidemiol 169(10):1251–1259. doi:10.1093/aje/kwp036
47. Bauer KR, Brown M, Cress RD, Parise CA, Caggiano V (2007) Descriptive analysis of estrogen receptor (ER)-negative, progesterone receptor (PR)-negative, and HER2-negative invasive breast cancer, the so-called triple-negative phenotype: a population-based study from the California cancer Registry. Cancer 109(9):1721–1728. doi:10.1002/cncr.22618
48. Gordon NH (1995) Association of education and income with estrogen receptor status in primary breast cancer. Am J Epidemiol 142(8):796–803

49. Thomson CS, Hole DJ, Twelves CJ, Brewster DH, Black RJ (2001) Prognostic factors in women with breast cancer: distribution by socioeconomic status and effect on differences in survival. J Epidemiol Community Health 55(5):308–315
50. Tollerud DJ, Clark JW, Brown LM, Neuland CY, Pankiw-Trost LK, Blattner WA, Hoover RN (1989) The influence of age, race, and gender on peripheral blood mononuclear-cell subsets in healthy nonsmokers. J Clin Immunol 9(3):214–222
51. Bain BJ (1996) Ethnic and sex differences in the total and differential white cell count and platelet count. J Clin Pathol 49(8):664–666
52. Saxena S, Wong ET (1990) Heterogeneity of common hematologic parameters among racial, ethnic, and gender subgroups. Arch Pathol Lab Med 114(7):715–719
53. Soria G, Ben-Baruch A (2008) The inflammatory chemokines CCL2 and CCL5 in breast cancer. Cancer Lett 267(2):271–285. doi:10.1016/j.canlet.2008.03.018
54. Watkins SK, Li B, Richardson KS, Head K, Egilmez NK, Zeng Q, Suttles J, Stout RD (2009) Rapid release of cytoplasmic IL-15 from tumor-associated macrophages is an initial and critical event in IL-12-initiated tumor regression. Eur J Immunol 39(8): 2126–2135. doi:10.1002/eji.200839010
55. Ward E, Jemal A, Cokkinides V, Singh GK, Cardinez C, Ghafoor A, Thun M (2004) Cancer disparities by race/ethnicity and socioeconomic status. CA Cancer J Clin 54(2):78–93
56. Telli ML, Chang ET, Kurian AW, Keegan TH, McClure LA, Lichtensztajn D, Ford JM, Gomez SL (2010) Asian ethnicity and breast cancer subtypes: a study from the California Cancer Registry. Breast Cancer Res Treat. doi:10.1007/s10549-010-1173-8
57. Fong M, Henson DE, Devesa SS, Anderson WF (2006) Inter- and intra-ethnic differences for female breast carcinoma incidence in the continental United States and in the state of Hawaii. Breast Cancer Res Treat 97(1):57–65. doi:10.1007/s10549-005-9088-5
58. Kakarala M, Rozek L, Cote M, Liyanage S, Brenner DE (2010) Breast cancer histology and receptor status characterization in Asian Indian and Pakistani women in the U.S.—a SEER analysis. BMC Cancer 10:191. doi:10.1186/1471-2407-10-191
59. Zakharia F, Basu A, Absher D, Assimes TL, Go AS, Hlatky MA, Iribarren C, Knowles JW, Li J, Narasimhan B, Sidney S, Southwick A, Myers RM, Quertermous T, Risch N, Tang H (2009) Characterizing the admixed African ancestry of African Americans. Genome Biol 10(12):R141. doi:10.1186/gb-2009-10-12-r141
60. Root M (2003) The use of race in medicine as a proxy for genetic differences. Philos Sci 70(5):1173–1183
61. Moldovan GL, Pfander B, Jentsch S (2007) PCNA, the maestro of the replication fork. Cell 129(4):665–679. doi:10.1016/j.cell.2007.05.003
62. Wang SC, Nakajima Y, Yu YL, Xia W, Chen CT, Yang CC, McIntush EW, Li LY, Hawke DH, Kobayashi R, Hung MC (2006) Tyrosine phosphorylation controls PCNA function through protein stability. Nat Cell Biol 8(12):1359–1368. doi:10.1038/ncb1501
63. Lewis CE, Pollard JW (2006) Distinct role of macrophages in different tumor microenvironments. Cancer Res 66(2):605–612. doi:10.1158/0008-5472.CAN-05-4005
64. Griffiths L, Binley K, Iqball S, Kan O, Maxwell P, Ratcliffe P, Lewis C, Harris A, Kingsman S, Naylor S (2000) The macrophage—a novel system to deliver gene therapy to pathological hypoxia. Gene Ther 7(3):255–262. doi:10.1038/sj.gt.3301058
65. Burdo TH, Soulas C, Orzechowski K, Button J, Krishnan A, Sugimoto C, Alvarez X, Kuroda MJ, Williams KC (2010) Increased monocyte turnover from bone marrow correlates with severity of SIV encephalitis and CD163 levels in plasma. PLoS Pathog 6(4):e1000842. doi:10.1371/journal.ppat.1000842
66. Williams K, Schwartz A, Corey S, Orandle M, Kennedy W, Thompson B, Alvarez X, Brown C, Gartner S, Lackner A (2002) Proliferating cellular nuclear antigen expression as a marker of perivascular macrophages in simian immunodeficiency virus encephalitis. Am J Pathol 161(2):575–585. doi:10.1016/S0002-9440(10)64213-7
67. Lan HY, Nikolic-Paterson DJ, Mu W, Atkins RC (1995) Local macrophage proliferation in the progression of glomerular and tubulointerstitial injury in rat anti-GBM glomerulonephritis. Kidney Int 48(3):753–760
68. Dijkstra CD, Dopp EA, Joling P, Kraal G (1985) The heterogeneity of mononuclear phagocytes in lymphoid organs: distinct macrophage subpopulations in the rat recognized by monoclonal antibodies ED1, ED2 and ED3. Immunology 54(3):589–599
69. Aziz A, Soucie E, Sarrazin S, Sieweke MH (2009) MafB/c-Maf deficiency enables self-renewal of differentiated functional macrophages. Science 326(5954):867–871. doi:10.1126/science.1176056
70. Watlington AT, Byers T, Mouchawar J, Sauaia A, Ellis J (2007) Does having insurance affect differences in clinical presentation between Hispanic and non-Hispanic white women with breast cancer? Cancer 109(10):2093–2099. doi:10.1002/cncr.22640
71. Wojcik BE, Spinks MK, Stein CR (2003) Effects of screening mammography on the comparative survival rates of African American, white, and Hispanic beneficiaries of a comprehensive health care system. Breast J 9(3):175–183
72. Rayson D, Payne JI, Abdolell M, Barnes PJ, MacIntosh RF, Foley T, Younis T, Burns A, Caines J (2011) Comparison of clinical-pathologic characteristics and outcomes of true interval and screen-detected invasive breast cancer among participants of a Canadian breast screening program: a nested case-control study. Clin Breast Cancer 11(1):27–32. doi:10.3816/CBC.2011.n.005
73. Eubank TD, Roberts RD, Khan M, Curry JM, Nuovo GJ, Kuppusamy P, Marsh CB (2009) Granulocyte macrophage colony-stimulating factor inhibits breast cancer growth and metastasis by invoking an anti-angiogenic program in tumor-educated macrophages. Cancer Res 69(5):2133–2140. doi:10.1158/0008-5472.CAN-08-1405

Published in final edited form as:
DNA Repair (Amst). 2014 September ; 21: 177–182. doi:10.1016/j.dnarep.2014.03.006.

Identification of novel PARP inhibitors using a cell-based TDP1 inhibitory assay in a quantitative high-throughput screening platform

Junko Murai[1,#], **Christophe Marchand**[1,#], **Sampada A. Shahane**[2], **Hongmao Sun**[2], **Ruili Huang**[2], **Yiping Zhang**[3], **Adel Chergui**[1], **Jiuping Ji**[3], **James H. Doroshow**[1,3], **Ajit Jadhav**[2], **Shunichi Takeda**[4], **Menghang Xia**[2], and **Yves Pommier**[1,*]

[1]Developmental Therapeutics Branch, Laboratory of Molecular Pharmacology, Center for Cancer Research, National Cancer Institute, National Institutes of Health, Bethesda, MD, 20892

[2]National Center for Advancing Translational Sciences (NCATS), National Institutes of Health, Bethesda, MD, 20892

[3]National Clinical Target Validation Laboratory, National Cancer Institute, National Institutes of Health, Bethesda, MD, 20892

[4]Department of Radiation Genetics, Graduate School of Medicine, Kyoto University, Yoshidakonoe, Sakyo-ku, Kyoto, Japan 606-8501

Abstract

Anti-cancer topoisomerase I (Top1) inhibitors (camptothecin and its clinical derivatives irinotecan and topotecan, and the indenoisoquinolines) induce lethal DNA lesions by stabilizing Top1-DNA cleavage complex (Top1cc). These lesions are repaired by parallel repair pathways including the tyrosyl-DNA phosphodiesterase 1 (TDP1)-related pathway and homologous recombination. As TDP1-deficient cells in vertebrates are hypersensitive to Top1 inhibitors, small molecules inhibiting TDP1 should augment the cytotoxicity of Top1 inhibitors. We developed a cell-based high-throughput screening assay for the discovery of inhibitors for human TDP1 using a TDP1-deficient chicken DT40 cell line (*TDP1*-/-) complemented with human TDP1 (*hTDP1*). Any compounds showing a synergistic effect with the Top1 inhibitor camptothecin (CPT) in hTDP1 cells should either be a TDP1 inhibitor or an inhibitor of alternate repair pathways for Top1cc. We screened the 400,000-compound Small Molecule Library Repository (SMLR, NIH Molecular Libraries) against hTDP1 cells in the absence or presence of CPT. After confirmation in a secondary screen using both hTDP1 and TDP1-/- cells in the absence or presence of CPT, five compounds were confirmed as potential TDP1 pathway inhibitors. All five compounds showed

*Correspondence: Yves Pommier, M.D., Ph.D., Developmental Therapeutics Branch, Laboratory of Molecular Pharmacology, Center for Cancer Research, National Cancer Institute, National Institutes of Health, Bethesda, MD, 20892, Phone: +1-301-496-5944, pommier@nih.gov.
#These authors contributed equally.

The authors declare no conflict of interest.

synergistic effect with CPT in hTDP1 cells, but not in *TDP1-/-* cells, indicating that the compounds inhibited a TDP1-related repair pathway. Yet, *in vitro* gel-based assay revealed that the five compounds did not inhibit TDP1 catalytic activity directly. We tested the compounds for their ability to inhibit poly(ADP-ribose)polymerase (PARP) because PARP inhibitors are known to potentiate the cytotoxicity of CPT by inhibiting the recruitment of TDP1 to Top1cc. Accordingly, we found that the five compounds inhibit PARP activity by ELISA and Western blotting. We identified the most potent compound (Cpd1) that offers characteristic close to veliparib, a leading clinical PARP inhibitor. Cpd1 may represent a new scaffold for the development of PARP inhibitors.

Keywords

TDP1; PARP; topoisomerases; drug discovery; combination therapy

1. Introduction

Tyrosyl-DNA phosphodiesterase 1 (TDP1) is a DNA repair enzyme (for review see [1, 2]) that removes topoisomerase I (Top1) cleavage complexes (Top1 cc) resulting from the trapping of Top1 on DNA. Reversible Top1 cc are generated during replication and transcription to relax DNA supercoiling. However, they can also be trapped by DNA lesions including abasic sites, oxidized bases and carcinogenic adducts [3-5]. Anticancer Top1 inhibitors such as topotecan, irinotecan and non-camptothecin indenoisoquinolines stabilize Top1cc and cause lethal DNA double-strand ends when Top1cc are collided by replication forks [6-10] and transcription complexes [11-14]. TDP1 repairs Top1cc by excising the covalent bond between the catalytic tyrosine residue of Top1 linked and the DNA 3'-phosphate group [15-17]. TDP1 can also remove a wide variety of 3'-DNA blocking lesions including 3'-phosphoglycolates [18, 19], 3'-deoxyribose phosphate [20, 21] and chain-terminating nucleotides [22]. In addition, TDP1 plays a role in the backup of the topoisomerase II (Top2) cleavage complexes repair pathway [23, 24]. TDP1 is part of the XRCC1 complex that interacts with poly(ADP-ribose)polymerase 1 (PARP1) in the repair of Top1cc [25-27]. PARP1 poly-ADP-ribosylates TDP1, which enhances TDP1 stability and its recruitment to DNA damage sites [25]. Hence, PARP1 is emerging as a key component driving the repair of Top1cc by TDP1, which, at least in part [28, 29], accounts for the synergistic effect of PARP inhibitors with Top1 inhibitors.

The rationale for developing TDP1 inhibitors is rooted in the hypersensitivity of TDP1-deficient cells to Top1 inhibitors [12, 13, 30], to monofunctional alkylating agents including temozolomide [31, 32] and to chain terminating nucleosides [22]. Therefore, TDP1 inhibitors should exhibit synergistic activity when administered in combination with Top1 inhibitors, temozolomide, and chain terminators. Furthermore, cancer cells are very often deficient in alternative DNA repair and/or checkpoint pathways [33]. For example, deficiency in XPF-ERCC1, which belong to the exonuclease pathway for Top1cc repair, selectively sensitizes cancer cells to the combination of PARP and Top1 inhibitors [27]. It is also possible that deficiency in BRCA1, a key player of homologous recombination (HR) might sensitize familial breast and ovarian cancers to combination therapy with Top1

inhibitors and TDP1 inhibitors, in addition to the established activity of PARP inhibitors in BRCA-deficient tumors [34, 35]. This is because both the HR and TDP1 pathways act in parallel (synthetic lethality paradigm) for the repair of Top1-induced lesions. Still, there is currently no TDP1 inhibitor with desirable properties for drug development [for review see [36]]. In this study, we developed a cell-based high throughput-screening method for TDP1 pathway inhibitors, screened 400,000-compounds, and report small molecules that potentiate the cytotoxicity of CPT, and which all turn out to be PARP inhibitors.

2. Material and Methods

2.1. Cell lines and Drugs

DT40 cells were cultured with RPMI 1640 medium (GIBCO 11875-093) supplemented with 10% fetal calf serum (Gemini Bio-Products 100-106), 1% chicken serum (Invitrogen 16110082), and 50 μM β-mercaptoethanol at 37°C. TDP1-deficient (*TDP1-/-*) cells, and *TDP1-/-* cells complemented with human *TDP1* (hTDP1) in chicken DT40 B cell line have previously been reported and described here [23]. Wild-type, PARP1-deficient (*PARP1-/-*), and BRCA2-trancate mutant (*BRCA2tr/-*) DT40 cells were obtained from Dr. Takeda, Laboratory of Radiation Genetics, Graduate School of Medicine, Kyoto University (Kyoto, Japan), and described before [37, 38]. CPT and veliparib were obtained from the Drug Synthesis and Chemistry Branch, Developmental Therapeutics Program, DCTD, NCI. Tetra-n-octylammonium bromide was obtained from Sigma-Aldrich (St. Louis, MO).

2.2. Primary high-throughput screening assay

Conditions and details for our cell-based high-throughput screening assay can be found on PubChem under the AID# 686978 and 686979 (https://pubchem.ncbi.nlm.nih.gov/assay/assay.cgi?aid=686981&loc=ea_ras). Briefly, DT40 hTDP1 cells cultured without or with 20 nM CPT were dispensed at 400 cells in 5 μl per well in 1536-well white wall/solid bottom assay plates (Greiner Bio-One North America, NC) using a Multidrop Combi 8 channel dispenser (Thermo Fisher, Waltham, MA). Compounds at various concentrations were transferred in a volume of 23 nl to the assay plates using a pintool station (Kalypsys, San Diego, CA). Assay plates were then incubated at 37°C for 48 h, followed by addition of 3 μl/well of CellTiter-Glo reagent (cell viability assay, Promega, Madison, WI) for measurement of intracellular ATP level. After 30 min incubation at room temperature in the dark, the luminescence intensity of the plates was measured using a ViewLux plate reader (PerkinElmer, Shelton, CT).

2.3. Secondary screening assay

Drug cellular sensitivity was measured as previously described [39]. Briefly, cells were continuously exposed to various drug concentrations for 72 h in triplicate. DT40 cells were seeded at 200 cells per well into 384-well white plate (PerkinElmer) in 40 μl of medium. Cell viability was determined at 72 h by adding 20 μl of ATPlite solution (ATPlite 1-step kit, PerkinElmer). After 5 min incubation, luminescence was measured on an EnVision Plate Reader (PerkinElmer). The ATP level in untreated cells was defined as 100% percent and viability of treated cells was defined as (ATP level of treated cell/ ATP level of untreated cells) ×100.

2.4. PAR ELISA assay

Poly-ADP-ribosylation was measured by the previously reported PAR enzyme-linked immunosorbent assay (ELISA) [40, 41]. Detailed procedure can be viewed at http://dctd.cancer.gov/ResearchResources/biomarkers/PolyAdenosylRibose.htm.

2.5. PAR immunoblotting assay

Poly-ADP-ribosylation was also measured by immunoblotting. Briefly, five million DT40 cells in 10 ml medium were treated without or with drug for 30 min Cells were collected and lysed with CelLytic™M lysis reagent (C2978, Sigma-Aldrich, St Louis, MO). After thorough mixing and incubation at 4°C for 30 min, lysates were centrifuged at 20,000 g (~15,000 rpm) at 4°C for 10 min, and supernatants were collected. Immunoblotting was carried out using standard procedures. Rabbit polyclonal anti-PAR polymer antibody (#4336-BPC-100) was from Trevigen (Gaithersburg, MD). Secondary antibodies were horseradish peroxidase (HRP)-conjugated antibodies to rabbit IgG (GE Healthcare, Pittsburgh, PA).

2.6. Gel-based TDP1 inhibition assay

TDP1 gel-based assays were performed as described [31]. Briefly, a 5'-[^{32}P]-labeled single-stranded 14 nt DNA oligonucleotide containing a 3'-phosphotyrosine (N14Y) was incubated with 5 pM recombinant human TDP1 in the absence or presence of inhibitor for 15 min at room temperature in a buffer containing 50 mM Tris HCl, pH 7.5, 80 mM KCl, 2 mM EDTA, 1 mM DTT, 40 μg/ml BSA and 0.01% Tween-20. Reactions were terminated by the addition of 1 volume of gel loading buffer [99.5% (v/v) formamide, 5 mM EDTA, 0.01% (w/v) xylene cyanol, and 0.01% (w/v) bromophenol blue]. Samples were subjected to a 16% denaturing PAGE and gels were exposed after drying to a PhosphorImager screen (GE Healthcare). Gel images were scanned using a Typhoon 8600 (GE Healthcare).

3. Results and discussion

3.1. Screening strategy and experimental design

A cell-based assay was developed in a quantitative high throughput-screening (qHTS) format to discover novel TDP1 pathway inhibitors capable of synergizing with CPT. We used chicken DT40 B lymphoma cells that are widely used for reverse genetic studies [42]. DT40 cells have several advantages for drug screening, including efficient gene targeting, a stable phenotype, rapid proliferation, and easy handling [23, 39]. These advantages are suitable for qHTS implementation, which requires fast inhibition of growth within 48 h. Our overall screening strategy is summarized in Figure 1. The first assay (primary qHTS screen, Fig. 1 upper panel) consisted in a 1536-well plate format robotic cell-based high throughput-screening (HTS) assay measuring viability of *hTDP1* cells (*TDP1-/-* cells complemented with human TDP1) exposed to a range of concentrations for each compound of the library in the absence or presence of CPT. Since *hTDP1* cells are much more tolerant to CPT compared to *TDP1-/-* cells [23], TDP1 inhibitors were therefore expected to show a synergistic effect in the presence of CPT and to reduce cell viability to levels similar to *TDP1-/-* cells (Fig. 1A). This hypersensitivity should not be observed in the absence of CPT. Compounds identified in the primary qHTS screen for their synergistic effect in the presence

of CPT were then characterized in a cell-based assay secondary screen (Fig. 1B). In this secondary cell viability assay, both *hTDP* and *TDP1-/-* cells were exposed to the compound of interest in the absence or presence of CPT. Inhibitors of the TDP1 pathway are supposed to maintain their synergistic effect with CPT in *hTDP1* cells but not in *TDP1-/-* cells (Fig. 1B).

Because we recently demonstrated that PARP1 appears to drive the TDP1-related repair pathway [25, 27], we used veliparib (ABT-888) as a positive control in the screening assay. Tetra-n-octylammonium bromide, a highly cytotoxic compound, was used as a non-specific control (Supplemental Figure S1). Veliparib showed average IC_{50} values (Inhibitory concentration 50%) of 20.4 μM for untreated cells (No CPT) and 0.064 μM for the cells treated with 20 nM CPT, resulting in a 438-fold increase in potency, which recapitulates our recent data [25]. On the other hand, tetra-n-octylammonium bromide as a non-specific control showed average IC_{50} values of 1.3 and 2.4 μM for untreated cells and cells treated with 20 nM CPT, respectively.

3.3. Primary Screen

The 400,000-compound Small Molecule Library Repository (NIH Molecular Libraries) was screened on the robotic platform of the NIH Chemical Genomics Center (NCGC, now is part of the National Center for Advancing Translational Sciences, NCATS). The entire results were deposited into PubChem (https://pubchem.ncbi.nlm.nih.gov/assay/assay.cgi?aid=686981&loc=ea_ras) under AID# 686978 and AID# 686979. Both Pubchem sites list the most cytotoxic compounds identified in the absence (AID# 686978) and in the presence (AID# 686979) of CPT and do not report the positive hits selected for confirmation and characterization. Positive hits were selected based on their IC_{50} value and inhibition curve quality (curve class) [43]. Compounds showing more than 2-fold decreased in IC_{50} value for the 20 nM CPT-treated cells (CPT20) compared to untreated cells were selected as positive hits. Compounds that exhibited a class 4 curve (non responsive class) in the absence of CPT and a curve in the presence of CPT categorized as class 1, 2 or 3 (responsive class with various degrees), were selected as primary hits because some compounds may only exhibit their cytotoxicity when combined with CPT. Compounds meeting the above criterions but showing an IC_{50} value greater than 20 μM in the presence of CPT were not retained based on their lack of potency. Based on these criterions, 500 best compounds were selected and retested in quadruplicate using the primary qHTS assay in the absence and the presence of CPT using *hTDP1* cells (See Fig. 1B). Five positive hits were selected for further characterization and the mean of their IC_{50} values in the absence or presence of CPT are reported in Table 1.

3.3. Secondary Screen

The five selected compounds from the primary screen were tested in the secondary screen (Fig. 1B) in the absence and the presence of CPT in *hTDP1* and *TDP1-/-* cells (15 and 20 nM CPT for *hTDP1* cells and 5 and 10 nM CPT for *TDP1-/-* cells). The cell viability curves for the five compounds are presented in Table 1, Figure 2A and Supplemental Figure S2. Cpd1 showed the greatest potentiating effect in the presence of CPT in *hTDP* cells (Fig. 2A) without showing any apparent potentiating effect with CPT in *TDP1-/-* cells, which, as

expected were exquisitely hypersensitive to CPT compared to the *hTDP1* cells [23, 39] (Fig. 2B). The synergistic effect observed in *hTDP1* cells for MLS002706582 (Cpd1) is very similar that for veliparib (Fig. 2C) with IC_{50} values of 150 nM and 6 nM for Cpd1 and veliparib, respectively (Table 1). Cpd1 also behaves similarly to veliparib regarding its lack of synergistic effect with CPT in *TDP1-/-* cells (Fig. 2D). All five compounds were not cytotoxic as single agents at concentrations below 25 μM (Table 1) but in the presence of CPT, Cpd1 exhibited a 166-fold potentiation of cytotoxicity (466-fold for veliparib). These results suggested that Cpd1 was either a direct inhibitor of TDP1 or a TDP1 repair pathway inhibitor (acting indirectly on TDP1 in cells).

3.4. TDP1 catalytic inhibition

To determine whether the five selected compounds from both the primary and secondary screens were direct TDP1 inhibitors, we ran them against recombinant TDP1 in our gel-based biochemical assays [23, 26]. When tested in comparison with a published TDP1 inhibitor [44, 45], none of the five compounds could inhibit efficiently recombinant TDP1 (Supplemental Figure S3). Although, we found a weak TDP1 inhibition for Cpd5 at a dose above 300 μM, these results suggested that the five compounds did not directly target TDP1.

3.5. PARP catalytic inhibition

Because these five compounds contained nicotinamide mimicking moieties (see structures in Table 1) and behave like veliparib (see Fig. 2), we next evaluated their potency as PARP inhibitors. All five compounds inhibited PARP. Moreover, Cpd1 showed PARP catalytic inhibition comparable to veliparib in ELISA assay [40, 41] (Fig. 2E) with sub-nanomolar IC_{50} values for both compounds (Table 1). These results were confirmed by immunoblotting assay [37]. Thus, all five compounds derived from the cell-based TDP1 screen turned out to be PARP inhibitors (Fig. 2F).

3.6. Hypersensitivity of BRCA2-deficient cells

Because PARP inhibitors are known to be selectively cytotoxic to homologous recombination-deficient cells [34, 35], MLS002706582 (Cpd1) was tested for its cytotoxic effect in *BRCA2tr/-* cells (homologous recombination-deficient cells) in comparison to *PARP1-/-* and *hTDP1* cells. Cpd1, similar to veliparib [37], was selectively cytotoxic to *BRCA2tr/-* cells but not to *PARP1-/-* and *hTDP1* cells (Fig. 2G).

4. Conclusions

Altogether, our results demonstrate that screening of the 400,000-compound Small Molecule Library Repository (NIH Molecular Libraries) allowed the identification of five compounds as inhibitors of the TDP1-related DNA repair pathway. These compounds do not inhibit TDP1 directly but act indirectly on the TDP1 pathway by inhibiting PARP1. These finding are in agreement with recent mechanism-based molecular studies showing that PARP is critical to stabilize and recruit TDP1 to Top1-induced DNA lesions [25]. Among the five compounds identified, one of them, Cpd1 offers characteristic close to veliparib and may represent a new scaffold for the development of PARP inhibitors.

Supplementary Material

Refer to Web version on PubMed Central for supplementary material.

Acknowledgments

This study was supported in part by the Intramural Research Program of the Center for Cancer Research, National Cancer Institute, NIH (Z01 BC 006150) and by the NIH R03 Grant MH095538-01A1 (YP).

References

1. Dexheimer TS, Antony S, Marchand C, Pommier Y. Tyrosyl-DNA phosphodiesterase as a target for anticancer therapy. Anticancer Agents Med Chem. 2008; 8:381–389. [PubMed: 18473723]
2. El-Khamisy SF. To live or to die: a matter of processing damaged DNA termini in neurons. Embo Mol Med. 2011; 3:78–88. [PubMed: 21246735]
3. Dexheimer TS, Kozekova A, Rizzo CJ, Stone MP, Pommier Y. The modulation of topoisomerase I-mediated DNA cleavage and the induction of DNA-topoisomerase I crosslinks by crotonaldehyde-derived DNA adducts. Nucleic Acids Res. 2008; 36:4128–4136. [PubMed: 18550580]
4. Pommier Y, Kohlhagen G, Pourquier P, Sayer JM, Kroth H, Jerina DM. Benzo[a]pyrene epoxide adducts in DNA are potent inhibitors of a normal topoisomerase I cleavage site and powerful inducers of other topoisomerase I cleavages. Proc Natl Acad Sci U S A. 2000; 97:2040–2045. [PubMed: 10688881]
5. Pourquier P, Pommier Y. Topoisomerase I-mediated DNA damage. Adv Cancer Res. 2001; 80:189–216. [PubMed: 11034544]
6. Pommier Y. DNA topoisomerase I inhibitors: chemistry, biology, and interfacial inhibition. Chem Rev. 2009; 109:2894–2902. [PubMed: 19476377]
7. Pommier Y. Drugging topoisomerases: lessons and challenges. ACS Chem Biol. 2013; 8:82–95. [PubMed: 23259582]
8. Hsiang Y-H, Lihou MG, Liu LF. Arrest of DNA replication by drug-stabilized topoisomerase I-DNA cleavable complexes as a mechanism of cell killing by camptothecin. Cancer Res. 1989; 49:5077–5082. [PubMed: 2548710]
9. Holm C, Covey JM, Kerrigan D, Pommier Y. Differential requirement of DNA replication for the cytotoxicity of DNA topoisomerase I and II inhibitors in Chinese hamster DC3F cells. Cancer Res. 1989; 49:6365–6368. [PubMed: 2553254]
10. Strumberg D, Pilon AA, Smith M, Hickey R, Malkas L, Pommier Y. Conversion of topoisomerase I cleavage complexes on the leading strand of ribosomal DNA into 5'-phosphorylated DNA double-strand breaks by replication runoff. Mol Cell Biol. 2000; 20:3977–3987. [PubMed: 10805740]
11. El-Khamisy SF, Katyal S, Patel P, Ju L, McKinnon PJ, Caldecott KW. Synergistic decrease of DNA single-strand break repair rates in mouse neural cells lacking both Tdp1 and aprataxin. DNA Repair (Amst). 2009; 8:760–766. [PubMed: 19303373]
12. El-Khamisy SF, Saifi GM, Weinfeld M, Johansson F, Helleday T, Lupski JR, Caldecott KW. Defective DNA single-strand break repair in spinocerebellar ataxia with axonal neuropathy-1. Nature. 2005; 434:108–113. [PubMed: 15744309]
13. Miao ZH, Agama K, Sordet O, Povirk L, Kohn KW, Pommier Y. Hereditary ataxia SCAN1 cells are defective for the repair of transcription-dependent topoisomerase I cleavage complexes. DNA Repair (Amst). 2006; 5:1489–1494. [PubMed: 16935573]
14. Sordet O, Redon CE, Guirouilh-Barbat J, Smith S, Solier S, Douarre C, Conti C, Nakamura AJ, Das BB, Nicolas E, Kohn KW, Bonner WM, Pommier Y. Ataxia telangiectasia mutated activation by transcription- and topoisomerase I-induced DNA double-strand breaks. EMBO Rep. 2009; 10:887–893. [PubMed: 19557000]
15. Davies DR, Interthal H, Champoux JJ, Hol WGJ. Crystal structure of a transition state mimic for Tdp1 assembled from vanadate, DNA, and a topoisomerase I-derived peptide. Chem Biol. 2003; 10:139–147. [PubMed: 12618186]

16. Interthal H, Pouliot JJ, Champoux JJ. The tyrosyl-DNA phosphodiesterase Tdp1 is a member of the phospholipase D superfamily. Proc Natl Acad Sci U S A. 2001; 98:12009–12014. [PubMed: 11572945]

17. Yang SW, Burgin AB Jr, Huizenga BN, Robertson CA, Yao KC, Nash HA. A eukaryotic enzyme that can disjoin dead-end covalent complexes between DNA and type I topoisomerases. Proc Natl Acad Sci U S A. 1996; 93:11534–11539. [PubMed: 8876170]

18. El-Khamisy SF, Hartsuiker E, Caldecott KW. TDP1 facilitates repair of ionizing radiation-induced DNA single-strand breaks. DNA Repair (Amst). 2007; 6:1485–1495. [PubMed: 17600775]

19. Zhou T, Akopiants K, Mohapatra S, Lin PS, Valerie K, Ramsden DA, Lees-Miller SP, Povirk LF. Tyrosyl-DNA phosphodiesterase and the repair of 3'-phosphoglycolate-terminated DNA double-strand breaks. DNA Repair (Amst). 2009; 8:901–911. [PubMed: 19505854]

20. Dexheimer TS, Stephen AG, Fivash MJ, Fisher RJ, Pommier Y. The DNA binding and 3'-end preferential activity of human tyrosyl-DNA phosphodiesterase. Nucleic Acids Res. 2010; 38:2444–2452. [PubMed: 20097655]

21. Interthal H, Chen HJ, Champoux JJ. Human Tdp1 cleaves a broad spectrum of substrates, including phosphoamide linkages. J Biol Chem. 2005; 280:36518–36528. [PubMed: 16141202]

22. Huang SY, Murai J, Dalla Rosa I, Dexheimer TS, Naumova A, Gmeiner WH, Pommier Y. TDP1 repairs nuclear and mitochondrial DNA damage induced by chain-terminating anticancer and antiviral nucleoside analogs. Nucleic Acids Research. 2013; 41:7793–7803. [PubMed: 23775789]

23. Murai J, Huang SY, Das BB, Dexheimer TS, Takeda S, Pommier Y. Tyrosyl-DNA phosphodiesterase 1 (TDP1) repairs DNA damage induced by topoisomerases I and II and base alkylation in vertebrate cells. The Journal of biological chemistry. 2012; 287:12848–12857. [PubMed: 22375014]

24. Nitiss KC, Malik M, He X, White SW, Nitiss JL. Tyrosyl-DNA phosphodiesterase (Tdp1) participates in the repair of Top2-mediated DNA damage. Proc Natl Acad Sci U S A. 2006; 103:8953–8958. [PubMed: 16751265]

25. Das B, Huang SN, Murai J, Rehman I, Amé J-C, Sengupta S, Das SK, Majumdar P, Zhang H, Biard D, Majumder HK, Schreiber V, Pommier Y. PARP1-TDP1 coupling for the repair of topoisomerase I-induced DNA damage. Nucl Acids Res. 2014 In press.

26. Plo I, Liao ZY, Barcelo JM, Kohlhagen G, Caldecott KW, Weinfeld M, Pommier Y. Association of XRCC1 and tyrosyl DNA phosphodiesterase (Tdp1) for the repair of topoisomerase I-mediated DNA lesions. DNA Repair (Amst). 2003; 2:1087–1100. [PubMed: 13679147]

27. Zhang YW, Regairaz M, Seiler JA, Agama KK, Doroshow JH, Pommier Y. Poly(ADP-ribose) polymerase and XPF-ERCC1 participate in distinct pathways for the repair of topoisomerase I-induced DNA damage in mammalian cells. Nucleic Acids Res. 2011

28. Berti M, Chaudhuri AR, Thangavel S, Gomathinayagam S, Kenig S, Vujanovic M, Odreman F, Glatter T, Graziano S, Mendoza-Maldonado R, Marino F, Lucic B, Biasin V, Gstaiger M, Aebersold R, Sidorova JM, Monnat RJ Jr, Lopes M, Vindigni A. Human RECQ1 promotes restart of replication forks reversed by DNA topoisomerase I inhibition. Nat Struct Mol Biol. 2013; 20:347–354. [PubMed: 23396353]

29. Ray Chaudhuri A, Hashimoto Y, Herrador R, Neelsen KJ, Fachinetti D, Bermejo R, Cocito A, Costanzo V, Lopes M. Topoisomerase I poisoning results in PARP-mediated replication fork reversal. Nat Struct Mol Biol. 2012

30. Katyal S, el-Khamisy SF, Russell HR, Li Y, Ju L, Caldecott KW, McKinnon PJ. TDP1 facilitates chromosomal single-strand break repair in neurons and is neuroprotective in vivo. EMBO J. 2007; 26:4720–4731. [PubMed: 17914460]

31. Marchand C, Lea WA, Jadhav A, Dexheimer TS, Austin CP, Inglese J, Pommier Y, Simeonov A. Identification of phosphotyrosine mimetic inhibitors of human tyrosyl-DNA phosphodiesterase I by a novel AlphaScreen high-throughput assay. Mol Cancer Ther. 2009; 8:240–248. [PubMed: 19139134]

32. Alagoz M, Wells OS, El-Khamisy SF. TDP1 deficiency sensitizes human cells to base damage via distinct topoisomerase I and PARP mechanisms with potential applications for cancer therapy. Nucleic Acids Res. 2014 In press.

33. Curtin NJ. DNA repair dysregulation from cancer driver to therapeutic target. Nature reviews Cancer. 2012; 12:801–817.

34. Bryant HE, Schultz N, Thomas HD, Parker KM, Flower D, Lopez E, Kyle S, Meuth M, Curtin NJ, Helleday T. Specific killing of BRCA2-deficient tumours with inhibitors of poly(ADP-ribose) polymerase. Nature. 2005; 434:913–917. [PubMed: 15829966]

35. Farmer H, McCabe N, Lord CJ, Tutt AN, Johnson DA, Richardson TB, Santarosa M, Dillon KJ, Hickson I, Knights C, Martin NM, Jackson SP, Smith GC, Ashworth A. Targeting the DNA repair defect in BRCA mutant cells as a therapeutic strategy. Nature. 2005; 434:917–921. [PubMed: 15829967]

36. Huang SY, Pommier Y, Marchand C. Tyrosyl-DNA Phosphodiesterase 1 (Tdp1) inhibitors. Expert Opin Ther Pat. 2011; 21:1285–1292. [PubMed: 21843105]

37. Murai J, Huang SY, Das BB, Renaud A, Zhang Y, Doroshow JH, Ji J, Takeda S, Pommier Y. Trapping of PARP1 and PARP2 by Clinical PARP Inhibitors. Cancer research. 2012; 72:5588–5599. [PubMed: 23118055]

38. Murai J, Huang SY, Renaud A, Zhang Y, Ji J, Takeda S, Morris J, Teicher B, Doroshow JH, Pommier Y. Stereospecific PARP Trapping by BMN 673 and Comparison with Olaparib and Rucaparib. Mol Cancer Ther. 2014; 13:433–443. [PubMed: 24356813]

39. Maede Y, Shimizu H, Fukushima T, Kogame T, Nakamura T, Miki T, Takeda S, Pommier Y, Murai J. Differential and Common DNA Repair Pathways for Topoisomerase I- and II-Targeted Drugs in a Genetic DT40 Repair Cell Screen Panel. Mol Cancer Ther. 2014; 13:214–220. [PubMed: 24130054]

40. Ji J, Kinders RJ, Zhang Y, Rubinstein L, Kummar S, Parchment RE, Tomaszewski JE, Doroshow JH. Modeling pharmacodynamic response to the poly(ADP-Ribose) polymerase inhibitor ABT-888 in human peripheral blood mononuclear cells. PloS one. 2011; 6:e26152. [PubMed: 22028822]

41. Kummar S, Kinders R, Gutierrez ME, Rubinstein L, Parchment RE, Phillips LR, Ji J, Monks A, Low JA, Chen A, Murgo AJ, Collins J, Steinberg SM, Eliopoulos H, Giranda VL, Gordon G, Helman L, Wiltrout R, Tomaszewski JE, Doroshow JH. Phase 0 clinical trial of the poly (ADP-ribose) polymerase inhibitor ABT-888 in patients with advanced malignancies. J Clin Oncol. 2009; 27:2705–2711. [PubMed: 19364967]

42. Buerstedde JM, Takeda S. Increased ratio of targeted to random integration after transfection of chicken B cell lines. Cell. 1991; 67:179–188. [PubMed: 1913816]

43. Inglese J, Auld DS, Jadhav A, Johnson RL, Simeonov A, Yasgar A, Zheng W, Austin CP. Quantitative high-throughput screening: a titration-based approach that efficiently identifies biological activities in large chemical libraries. Proc Natl Acad Sci U S A. 2006; 103:11473–11478. [PubMed: 16864780]

44. Conda-Sheridan M, Reddy PV, Morrell A, Cobb BT, Marchand C, Agama K, Chergui A, Renaud A, Stephen AG, Bindu LK, Pommier Y, Cushman M. Synthesis and Biological Evaluation of Indenoisoquinolines That Inhibit Both Tyrosyl-DNA Phosphodiesterase I (Tdp1) and Topoisomerase I (Top1). J Med Chem. 2013; 56:182–200. [PubMed: 23259865]

45. Nguyen TX, Morrell A, Conda-Sheridan M, Marchand C, Agama K, Bermingam A, Stephen AG, Chergui A, Naumova A, Fisher R, O'Keefe BR, Pommier Y, Cushman M. Synthesis and Biological Evaluation of the First Dual Tyrosyl-DNA Phosphodiesterase I (Tdp1)-Topoisomerase I (Top1) Inhibitors. J Med Chem. 2012; 55:4457–4478. [PubMed: 22536944]

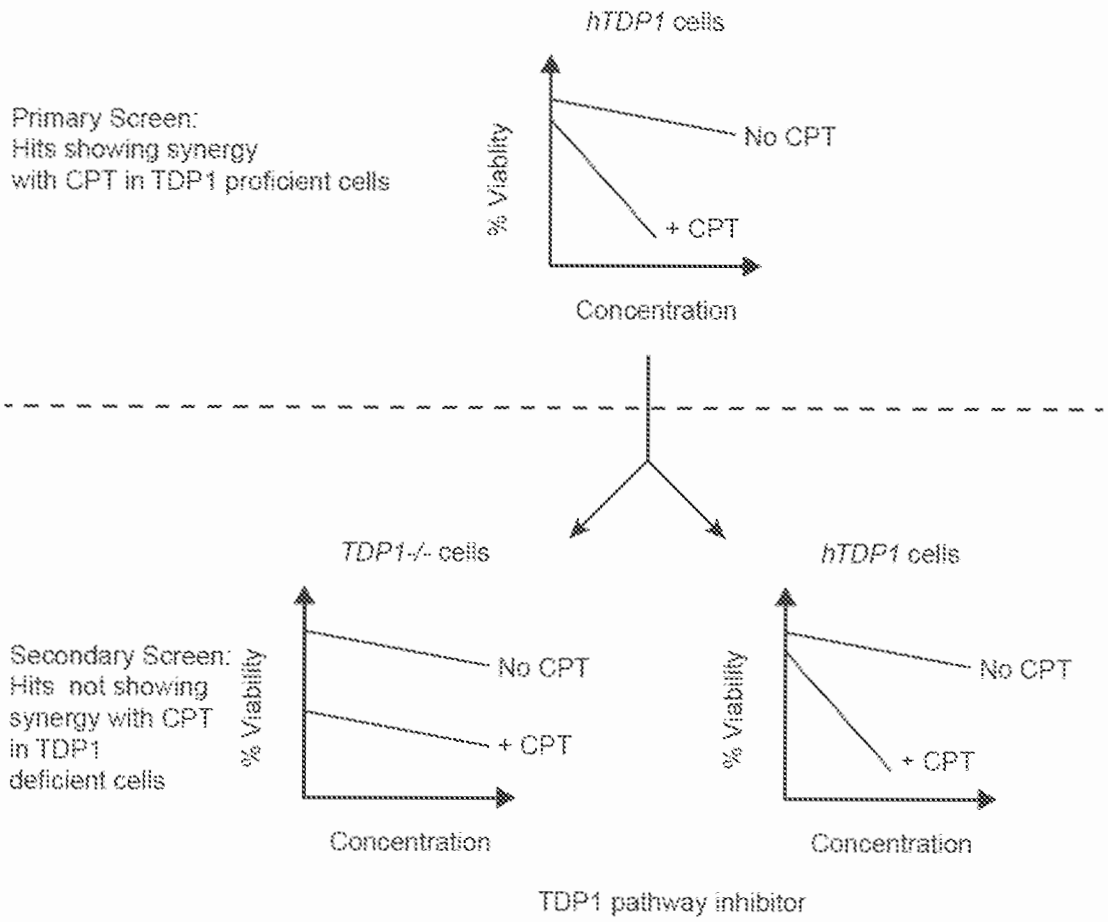

Figure 1.

Screening strategy. **A**: A quantitative robotic high throughput screening (qHTS) assay was run as a primary screen using DT40 chicken B lymphoma cells genetically modified to express human TDP1 (*hTDP1*) in a knockout background for the chicken TDP1 gene (*TDP1-/-*) [23]. The compound library was the NIH Roadmap Molecular Libraries 400,000 compound repository. Positive hits were selected based on cellular hypersensitivity in the presence of the Top1 inhibitor camptothecin (CPT). **B**: Positive hits identified during the HTS assay were confirmed in a secondary screen against both *hTDP1* and *TDP1-/-* cells. Inhibitors of the TDP1 pathway were selected for further characterization based on supra-additive cytotoxicity in the presence of CPT in *hTDP1* cells but not in *TDP1-/-* cells.

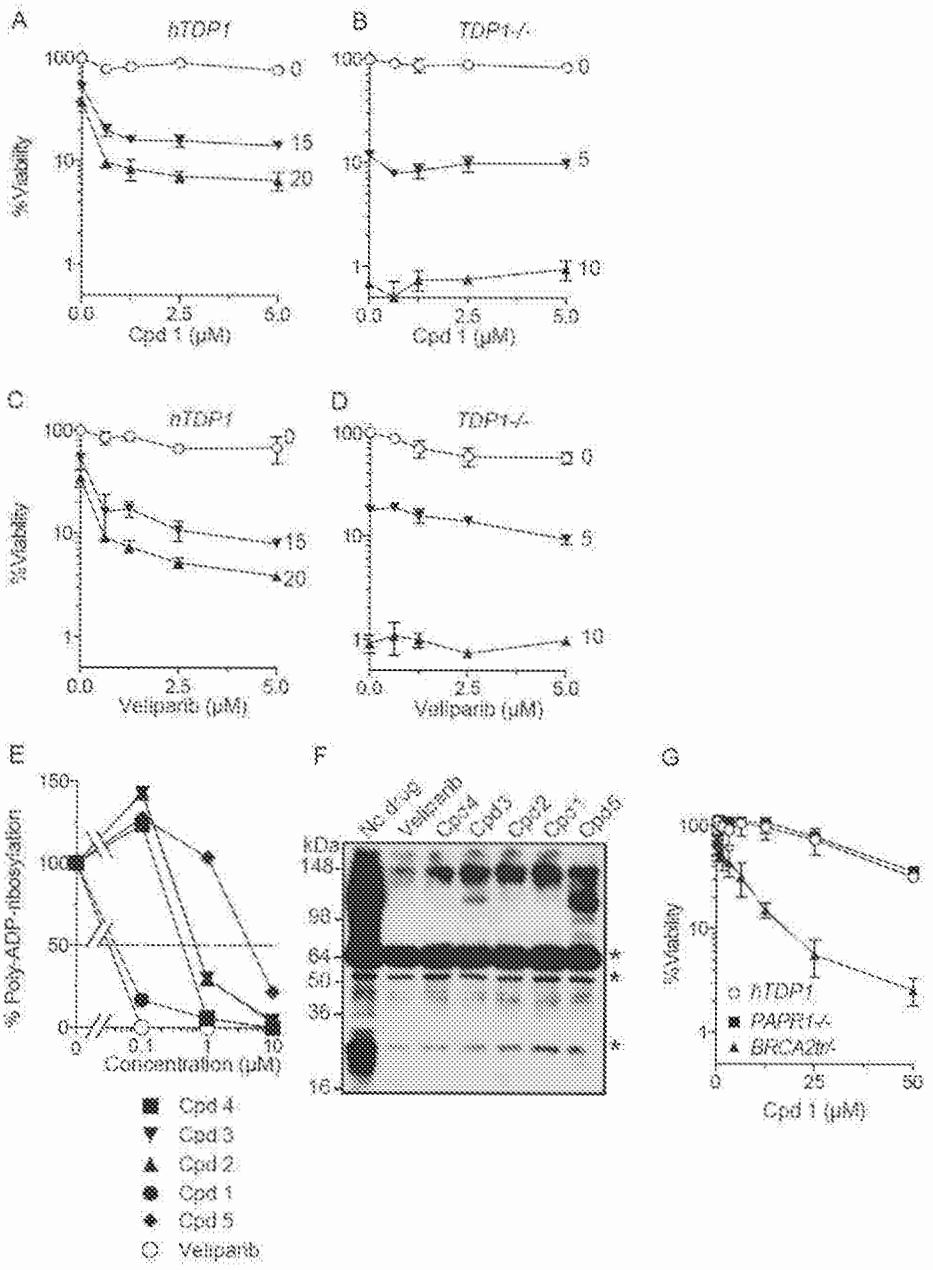

Figure 2.

Inhibition of PARP1 by compound 1 (**Cpd1**). **A** & **B**: Cellular viability in the presence of **Cpd1** and various concentrations of CPT (indicated beside each curve in nanomolar unit) in *hTDP1* (**A**) and *TDP1-/-* cells (**B**). **C** & **D**: Cellular viability curves in the presence of veliparib and various concentrations of CPT (indicated beside each curve in nanomolar unit) in *hTDP1* (**C**) and *TDP1-/-* cells (**D**). **E** & **F**: Inhibition of PARP1 by compounds **1-5** in comparison to the PARP inhibitor veliparib measured by ELISA (**E**) and by Western blotting (**F**). Asterisks in (F) indicate non-specific bands. **G: Cpd1**-dependent viability curves in *PARP1-/-*, *BRCA2fr/-* and *hTDP1* cells.

Table 1

Cpd	Name	Structure	IC_{50} (μM)			
			HTS			
			MO CPT	CPT	Poly (ADP-ribose) lation	
1	MLS002706582		25.42 ± 6.07	0.15 ± 0.18		<0.02
2	NCGC00345095		25.72 ± 2.90	1.45 ± 0.62		0.68
3	MLS000532049		>42	3.96 ± 0.48		0.68
4	NCGC00119675		>42	5.19 ± 1.03		0.42
5	MLS003171605		>42	11.67 ± 2.65		4.6

Cpd	Name	Structure	IC_{50} (μM)			
			BTS			
			NO CPT	CPT	Poly (ADP-ribose) lation	
	Veliparib		28.42 ± 8.58	0.06 ± 0.06	<0.02	

1521-0103/349/3/408–416$25.00
THE JOURNAL OF PHARMACOLOGY AND EXPERIMENTAL THERAPEUTICS

http://dx.doi.org/10.1124/jpet.113.210146
J Pharmacol Exp Ther 349:408–416, June 2014

The Journal of PHARMACOLOGY And Experimental Therapeutics

Rationale for Poly(ADP-ribose) Polymerase (PARP) Inhibitors in Combination Therapy with Camptothecins or Temozolomide Based on PARP Trapping versus Catalytic Inhibition[S]

Junko Murai, Yiping Zhang, Joel Morris, Jiuping Ji, Shunichi Takeda, James H. Doroshow, and Yves Pommier

Developmental Therapeutics Branch, Laboratory of Molecular Pharmacology, Center for Cancer Research (Ju.M., J.H.D., Y.P.), National Clinical Target Validation Laboratory (Y.Z., J.J.), and Division of Cancer Treatment and Diagnosis (Jo.M., J.H.D.), National Cancer Institute, National Institutes of Health, Bethesda, Maryland; and Department of Radiation Genetics, Graduate School of Medicine, Kyoto University, Yoshidakonoe, Sakyo-ku, Kyoto, Japan (Ju.M., S.T.)

Received September 30, 2013; accepted March 10, 2014

ABSTRACT

We recently showed that poly(ADP-ribose) polymerase (PARP) inhibitors exert their cytotoxicity primarily by trapping PARP-DNA complexes in addition to their NAD^+-competitive catalytic inhibitory mechanism. PARP trapping is drug-specific, with olaparib exhibiting a greater ability than veliparib, whereas both compounds are potent catalytic PARP inhibitors. Here, we evaluated the combination of olaparib or veliparib with therapeutically relevant DNA-targeted drugs, including the topoisomerase I inhibitor camptothecin, the alkylating agent temozolomide, the cross-linking agent cisplatin, and the topoisomerase II inhibitor etoposide at the cellular and molecular levels. We determined PARP-DNA trapping and catalytic PARP inhibition in genetically modified chicken lymphoma DT40, human prostate DU145, and glioblastoma SF295 cancer cells. For camptothecin, both PARP inhibitors showed highly synergistic effects due to catalytic PARP inhibition, indicating the value of combining either veliparib or olaparib with topoisomerase I inhibitors. On the other hand, for temozolomide, PARP trapping was critical in addition to catalytic inhibition, consistent with the fact that olaparib was more effective than veliparib in combination with temozolomide. For cisplatin and etoposide, olaparib only showed no or a weak combination effect, which is consistent with the lack of involvement of PARP in the repair of cisplatin- and etoposide-induced lesions. Hence, we conclude that catalytic PARP inhibitors are highly effective in combination with camptothecins, whereas PARP inhibitors capable of PARP trapping are more effective with temozolomide. Our study provides insights in combination treatment rationales for different PARP inhibitors.

Introduction

Since the discovery of the synthetic lethality of poly(ADP-ribose) polymerase (PARP) inhibitors in BRCA-deficient cells (Bryant et al., 2005; Farmer et al., 2005; McCabe et al., 2006; Helleday, 2011; Lord and Ashworth, 2012), the mechanism by which PARP inhibitors exert their cytotoxicity has been dominantly interpreted by an accumulation of unrepaired single-strand breaks (SSBs) resulting from catalytic PARP inhibition. This interpretation has recently been revisited after the demonstration that PARP inhibitors also trap PARP1- and PARP2-DNA complexes at DNA damage sites that arise spontaneously and/or are produced by the classic alkylating agent, methyl methanesulfonate (MMS) (Murai et al., 2012b). The fact that PARP1-depleted cells become tolerant to PARP inhibitors also supports the cytotoxic mechanisms of PARP trapping (Liu et al., 2009; Pettitt et al., 2013). PARP trapping is not merely interpreted as resulting from catalytic PARP inhibition, which prevents dissociation of PARP from DNA and is required for repair completion (Satoh and Lindahl, 1992). Indeed, BMN 673 (see Murai et al., 2014), olaparib (AZD-2281), and niraparib (MK-4827) are much more effective than veliparib (ABT-888) for PARP trapping at concentrations where BMN 673, olaparib, niraparib, and veliparib fully inhibit PARylation (Murai et al., 2012b, 2014). Based on the fact that olaparib and niraparib are much more cytotoxic than veliparib as single agents, it is plausible that PARP trapping is more cytotoxic than unrepaired SSBs caused by the absence of PARylation (Murai et al., 2012b, 2014). Chemical differences in drug structures may cause different allosteric effects between the PARP catalytic and DNA-binding domains, and we have proposed to classify PARP inhibitors based on their dual molecular mechanisms of action:

J.M. is a recipient of fellowships from the John Mung program (Kyoto University) and the Kyoto University Foundation. This work was supported by the Intramural Research Program of the National Institutes of Health [National Cancer Institute]; and the Center for Cancer Research [Grant Z01 BC 006150]. J.M. was supported by Japan Society for the Promotion of Science KAKENHI program [Grant 25740016]. J.J. was supported by the National Institutes of Health National Cancer Institute [Contract no. HHSN261200800001E].
dx.doi.org/10.1124/jpet.113.210146.
[S] This article has supplemental material available at jpet.aspetjournals.org.

ABBREVIATIONS: ABT-888, veliparib; AZD-2281, olaparib; CI, combination index; dRP, deoxyribose phosphate; Fa, fraction affected; MK-4827, niraparib; MMS, methyl methanesulfonate; PAR, poly(ADP-ribose); PARP, poly(ADP-ribose) polymerase; PCNA, proliferating cell nuclear antigen; SSB, single-strand break.

catalytic inhibition and trapping of PARP (Murai et al., 2012b, 2014; Fojo and Bates, 2013).

Combinations of different PARP inhibitors with a broad spectrum of genotoxic drugs are in clinical trials. These combinations include alkylating agents (temozolomide), topoisomerase I inhibitors (the camptothecin derivatives topotecan and irinotecan), topoisomerase II inhibitors (etoposide), and cross-linking agents (cisplatin) (Rouleau et al., 2010; Kummar et al., 2012; Curtin and Szabo, 2013). However, based on the fact that not all PARP inhibitors act similarly (Murai et al., 2012b, 2014; Fojo and Bates, 2013), it is critical to rationalize the most relevant combinations by choosing which PARP inhibitor and which chemotherapeutic agent act most effectively. It is also important to elucidate which combinations induce PARP trapping. Under such circumstances, highly potent PARP-trapping drugs should be more effective than simple catalytic PARP inhibitors (olaparib > veliparib). On the other hand, if the synergistic effect is caused by catalytic PARP inhibition, veliparib should be comparable to olaparib.

In this study, we compared olaparib and veliparib in combination with four drugs from different therapeutically relevant classes (temozolomide, camptothecin, cisplatin, and etoposide) to evaluate the potential and rationale for each combination. To determine whether potentiation was related to PARP catalytic inhibition or trapping, we used genetically modified chicken lymphoma DT40 cells (Buerstedde and Takeda, 1991; Maede et al., 2014), as well as human cancer cell lines, and measured olaparib- and veliparib-induced PARP-DNA complexes (PARP trapping). We chose human prostate cancer cells (DU145) and human glioblastoma cells (SF295) from the NCI60 cell line panel because, in our previous studies, these cell lines showed differential responses to veliparib and olaparib with respect to drug sensitivity and PARP trapping (Murai et al., 2012b, 2014).

Materials and Methods

Cell Lines and Drugs. DT40 cell lines were obtained from the Laboratory of Radiation Genetics Graduate School of Medicine at Kyoto University (Kyoto, Japan). Human prostate cancer cells (DU145; sex: male) and human glioblastoma cells (SF295; sex: female) were obtained from the National Cancer Institute Developmental Therapeutics Program (Frederick, MD). Olaparib, veliparib, and camptothecin were obtained from the Drug Synthesis and Chemistry Branch, Developmental Therapeutics Program, and Division of Cancer Treatment and Diagnosis, National Cancer Institute (Bethesda, MD). Temozolomide (T2577) and cisplatin (P4394) were purchased from Sigma-Aldrich (St. Louis, MO). Drug stock solutions were made in dimethylsulfoxide at 10 mM for olaparib and veliparib, 10 μM for camptothecin, 100 mM for temozolomide and in 0.75 M NaCl (pH 5) at 5 mM for cisplatin. Drug stock solutions were stored at −20°C in the dark and diluted in culture medium immediately before use. MMS (10%) was prepared fresh from 99% MMS (129925; Sigma-Aldrich) in phosphate-buffered saline, and diluted in culture medium immediately.

Immunoblotting. Ten million DT40 cells with 10 ml of medium in a 15-ml tube or semiconfluent human cells with 5 ml of medium in a six-well dish were treated as indicated for 30 minutes or 4 hours, respectively, and then cells were collected. To prepare subcellular chromatin fractions, we used a Subcellular Protein Fractionation Kit from Thermo Fisher Scientific (Rockford, IL) following the manufacturer's instructions. Immunoblotting was carried out using standard procedures (Murai et al., 2012b). Densitometric analyses of immunoblots were carried out using ImageJ software (National Institutes of Health). Each band blotted against PARP1 or histone H3 was selected with the rectangular selection tool, measured the intensity (area × mean), and the intensity of background was subtracted from the intensity of each band. The intensity of the PARP1 band was divided by the intensity of the corresponding histone H3.

Antibodies. Rabbit polyclonal anti-PARP1 antibody (sc-7150) and mouse monoclonal anti–proliferating cell nuclear antigen (anti–PCNA) antibody (sc-56) were from Santa Cruz Biotechnology (Santa Cruz, CA). Rabbit polyclonal anti–histone H3 antibody (07-690) was from Upstate Biotechnology (Lake Placid, NY). Rabbit polyclonal anti–poly (ADP-ribose) (PAR) polymer antibody (336-BPC-100) was from Trevigen (Gaithersburg, MD). Secondary antibodies were horseradish peroxidase–conjugated antibodies to rabbit or mouse IgG (GE Healthcare, Chalfont St. Giles, Buckinghamshire, UK).

Immunoassay for PAR Substrate. The validated chemiluminescent immunoassay for PAR using commercially available reagents was performed (for detailed laboratory procedures, go to http://dctd.cancer.gov/ResearchResources/biomarkers/PolyAdenosylRibose.htm).

Measurement of Cellular Sensitivity to Drug Treatment. Cells were continuously exposed in triplicate to the indicated drug concentrations for 72 hours. For DT40 cells, 200 cells were seeded into 384-well white plates (PerkinElmer Life and Analytical Sciences, Waltham, MA) in 40 μl of medium per well (Murai et al., 2012a; Maede et al., 2014). For human cells, 1500 DU145 cells or 500 SF295 cells were seeded in 96-well white plates (PerkinElmer Life and Analytical Sciences) in 100 μl of medium per well. Cell viability was determined using the ATPlite 1-step kit (PerkinElmer Life and Analytical Sciences). In brief, 20 or 50 μl of ATPlite solution for 384-well or 96-well plates, respectively, was added to each well. After 5 minutes, luminescence was measured by EnVision 2104 Multilabel Reader (PerkinElmer Life and Analytical Sciences). The ATP concentration in untreated cells was defined as 100%. Viability (percentage) of treated cells was defined as (ATP concentration in treated cells/ATP concentration in untreated cells) × 100.

Flow Cytometric Analysis of Cell Cycle Progression. Cells were pulse labeled with 50 μM bromodeoxyuridine during the last 20 minutes of drug treatment. Cells were harvested, fixed in 70% ethanol, and stored at −20C° for 10 minutes. Cells were incubated for 30 minutes at room temperature in 2 N HCl–0.5% Triton X-100 to allow DNA denaturation. The cells were washed twice with phosphate-buffered saline containing 0.5% Tween 20 and 0.5% bovine serum albumin. Cells were incubated for 1 hour at room temperature with a fluorescein isothiocyanate–conjugated anti-bromodeoxyuridine antibody (BD Biosciences, Franklin Lakes, NJ) and treated with 0.5 mg/ml RNase A and 5 μg/ml propidium idodide. Samples were analyzed with a flow cytometer (FACScan; BD Biosciences) using the CellQuest software (BD Biosciences).

Analysis of Combination Effects. The synergism analysis for the combination effects was conducted using the Chou-Talalay method (Chou, 2010). The combination index (CI) of each combination treatment was calculated using CalcuSyn software (Biosoft, Inc., Cambridge, UK), and CI 0.3–0.7, CI 0.1–0.3, and CI < 0.1 were defined as synergism, strong synergism, and very strong synergism, respectively (Chou, 2006).

Statistical Analyses. Results are presented as means ± S.D. ($n \geq 3$) or as means ($n = 2$). Differences between samples were assessed using the unpaired t test. All analyses were conducted with Prism 5.0 (GraphPad Software, La Jolla, CA). P values were two-sided and considered statistically significant when $P < 0.05$.

Results

Olaparib Potentiates Temozolomide Better than Veliparib. Temozolomide is a commonly used anticancer drug, which, similar to MMS, induces base damage resulting in abasic sites and single-strand breaks. Synergy between temozolomide and PARP inhibitors has been reported by independent studies

(Boulton et al., 1995; Horton and Wilson, 2013; Kedar et al., 2012). To compare olaparib and veliparib, we exposed wild-type and PARP1-deficient (*PARP1*$^{-/-}$) DT40 cells to temozolomide with or without the PARP inhibitors (Fig. 1, A and B). Note that *PARP1*$^{-/-}$ DT40 cells are equivalent to PARP1 and PARP2 dual-knockout cells because of genetic lack of PARP2 in avian cells (Hochegger et al., 2006; Murai et al., 2012b). Consistent with the widely accepted concept that PARP1 is necessary for SSB repair, we found that *PARP1*$^{-/-}$ cells were hypersensitive to temozolomide (compare upper and lower panels of either Fig. 1, A or B). The addition of 10 μM olaparib or veliparib had no impact on *PARP1*$^{-/-}$ cells, confirming a lack of off-target effect of either drug (Murai et al., 2012b). Olaparib synergistically sensitized wild-type cells in a concentration-dependent manner, with a low combination index (CI < 0.3; Supplemental Table 1) at several points, and the sensitization with 0.1 μM olaparib went beyond that of *PARP1*$^{-/-}$ cells (compare the panels of Fig. 1A). Veliparib also synergized the cytotoxicity of temozolomide with a low CI (<0.3; Supplemental Table 1), but at a higher concentration than olaparib. Moreover, a high concentration of veliparib (10 μM; >100-fold higher than olaparib) was required to go beyond the sensitivity of *PARP1*$^{-/-}$ cells.

To further document the marked difference between olaparib and veliparib in the cell viability assays, we examined cell cycle after drug treatments (Fig. 1, C–F). Whereas 1 μM olaparib or veliparib or 100 μM temozolomide alone had no significant impact, the combination of temozolomide with olaparib induced substantial G2-M accumulation in wild-type cells (Fig. 1, C and D; Supplemental Table 2). Temozolomide with veliparib (Fig. 1, C and D) and temozolomide in *PARP1*$^{-/-}$ cells (Fig. 1, E and F)

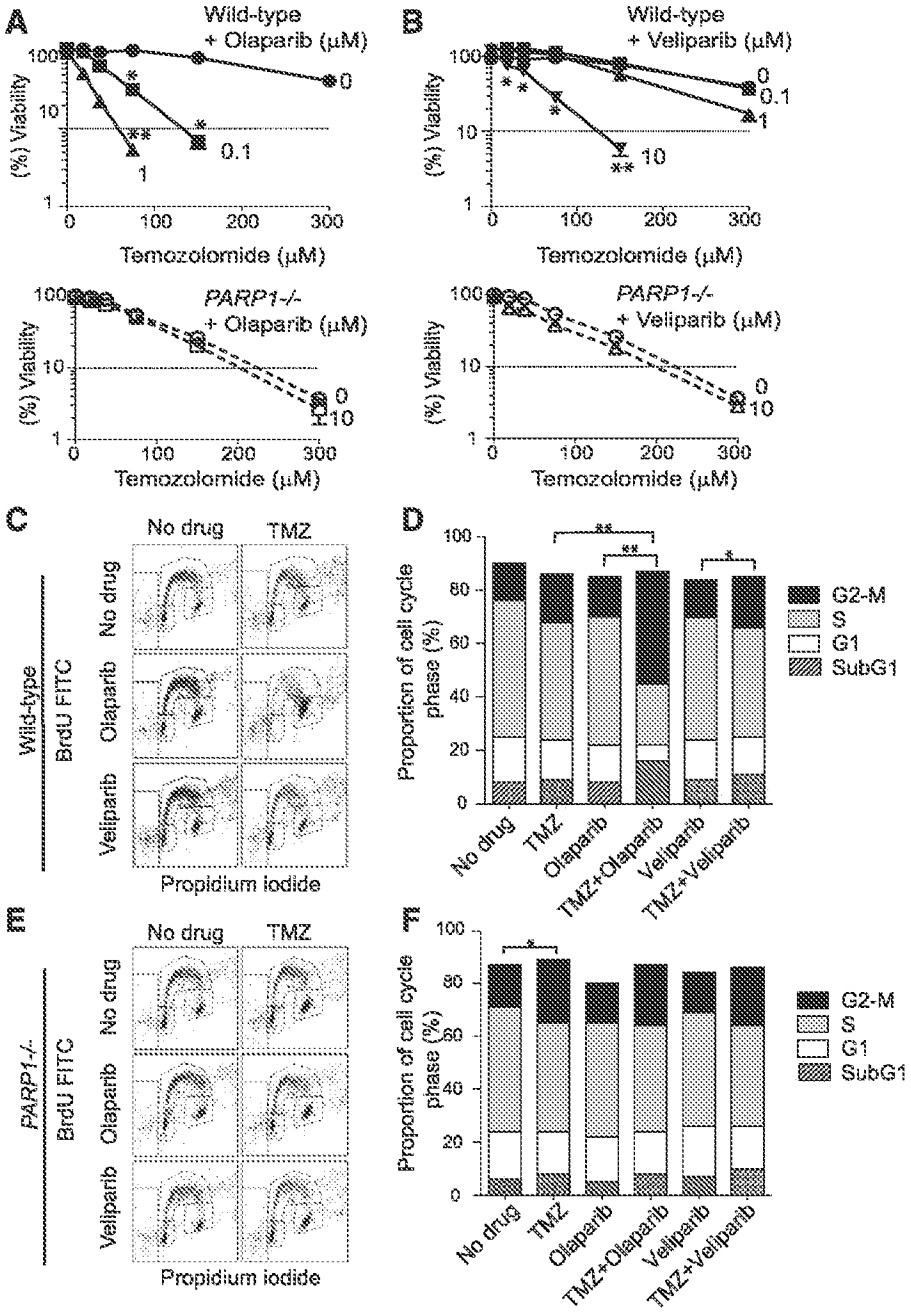

Fig. 1. Olaparib augments the cytotoxicity of temozolomide better than veliparib and PARP deficiency. (A and B) Viability curves of the indicated cell lines after continuous treatment for 72 hours with the indicated drugs. Cellular ATP concentration was used to measure cell viability. The viability of untreated cells was set as 100%. Error bars represent the S.D. (n = 3). *CI = 0.1–0.3 and **CI < 0.1 are indicated as strong and very strong synergy between the two treatments, respectively (see Fig. 6 and Supplemental Table 1). Viability curves of wild-type (upper panels) and *PARP1*$^{-/-}$ cells (lower panels) treated with temozolomide alone or with the indicated concentrations of olaparib (A) or veliparib (B). The concentrations of PARP inhibitors are shown beside each curve in micromolar units. (C–F) Cell cycle analyses of wild-type (C and D) and *PARP1*$^{-/-}$ cells (E and F) 12 hours after the indicated drug treatments [temozolomide (TMZ; 100 μM), olaparib (1 μM), and veliparib (1 μM)]. Representative data are shown from independent experiments with consistent results experiments (C and E). Percentages of cells in the sub-G1, G1, S, and G2-M phases are shown (D and F). Total counts within the outer frame of (C) or (E) are set as 100%. Results are the average of three independent experiments. Statistical analyses were performed for the G2-M population. *P < 0.05; **P < 0.01. Data of average and S.D. for all phases are shown in Supplemental Table 2. BrdU, bromodeoxyuridine; FITC, fluorescein isothiocyanate.

also induced significant G2-M accumulation. However, these effects were not as pronounced as for temozolomide with olaparib. Together, these results suggest that the combination of temozolomide with olaparib (≥0.1 μM) or veliparib (≥10 μM) induces additional cytotoxicity to PARP catalytic inhibition.

Olaparib and Veliparib Potentiate Camptothecin Comparably. Synergism between camptothecin and PARP inhibitors is well established (Smith et al., 2005; Daniel et al., 2009; Rouleau et al., 2010; Zhang et al., 2011; Brenner et al., 2012). As expected, *PARP1*$^{-/-}$ cells were hypersensitive to camptothecin (Hochegger et al., 2006) (Fig. 2, A and B, bottom panels), indicating the involvement of PARP1 in the repair of camptothecin-induced lesions. The combination of camptothecin with veliparib or olaparib synergistically sensitized wild-type DT40 cells with low CI (<0.3; Supplemental Table 1) at several points (upper panels of Fig. 2, A and B). Olaparib was more potent than veliparib. However, its concentration-dependent effect was not as pronounced as for the combination of temozolomide and PARP inhibitors (compare Fig. 2, A and B with Fig. 1, A and B). Furthermore, the sensitivity curves of both combinations never went beyond those of *PARP1*$^{-/-}$ cells (Fig. 2, A and B). Cell cycle analyses showed that the combination of 20 nM camptothecin with 1 μM olaparib or veliparib induced substantial G2-M accumulation (Fig. 2, C and D; Supplemental Table 2). Notably, this pattern was similar to that of *PARP1*$^{-/-}$ cells treated with 20 nM camptothecin (Fig. 2, E and F), suggesting that catalytic PARP inhibition causes the synergistic effect in the case of camptothecin.

We also examined the different synergistic patterns in human prostate DU145 and glioblastoma SF295 cell lines. We

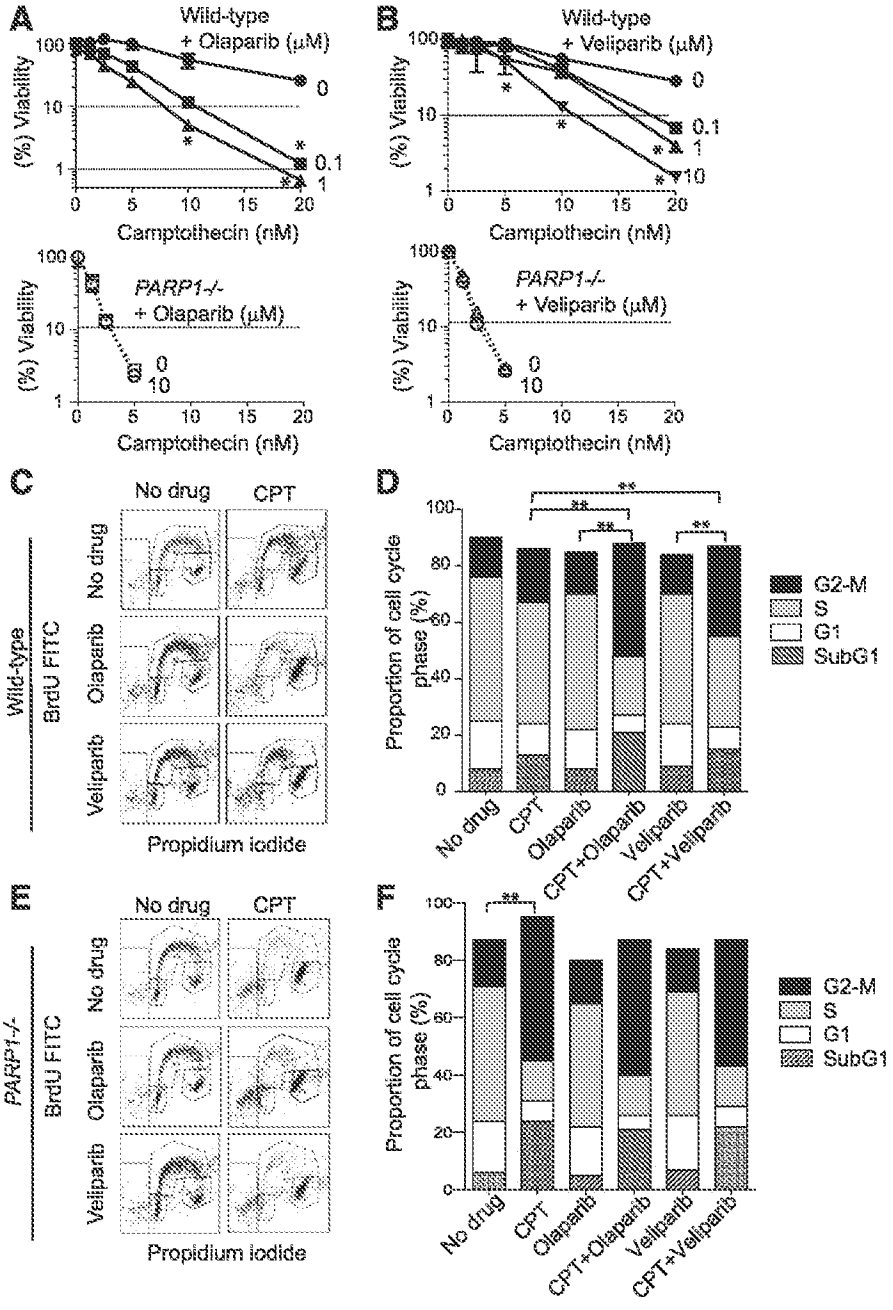

Fig. 2. Olaparib and veliparib augment the cytotoxicity of camptothecin (CPT) comparably. (A and B) Viability curves are shown as in Fig. 1A. *CI 0.1–0.3 and **CI < 0.1 are described as strong and very strong synergy between the two treatments, respectively. (C–F) Cell cycle analyses of wild-type (C and D) and *PARP1*$^{-/-}$ cells (E and F) 12 hours after the indicated drug treatments [CPT (20 nM), olaparib (1 μM), and veliparib (1 μM)]. Representative data are shown from multiple experiments (C and E). Percentages of cells in the sub-G1, G1, S, and G2-M phases are shown (D and F). Total counts within the outer frame of (C) or (E) are set as 100%. Results are the average of three independent experiments. Statistical analyses were performed for the G2-M population. *$P < 0.05$; **$P < 0.01$. Data of average and S.D. for all phases are shown in Supplemental Table 2. BrdU, bromodeoxyuridine; FITC, fluorescein isothiocyanate.

compared the effect of olaparib and veliparib at 1 μM, where PAR levels are indistinguishably low (Supplemental Fig. 1, right) and viability is not affected (see the starting points at the y-axis of each curve; Fig. 3). The synergistic effect was markedly greater for olaparib with temozolomide than for veliparib with temozolomide in both cells (Fig. 3A). For camptothecin, olaparib was still more potent than veliparib in DU145, but the difference was not as pronounced as for temozolomide (Fig. 3B, top panel). Furthermore, olaparib and veliparib were comparably potent for camptothecin in SF295 cells (Fig. 3B, bottom panel). These results are consistent to those obtained with DT40 cells (Figs. 1 and 2).

PARP Trapping by Temozolomide but Not Camptothecin in Combination with PARP Inhibitors. We examined PARP-DNA complexes by Western blotting under different conditions (Fig. 4). Ten micromolar veliparib with temozolomide induced PARP-DNA complexes less efficiently than 1 μM olaparib in DT40 and DU145 cells (Fig. 4A, compare lanes 5 versus 8, and 13 versus 16), suggesting that a 10-fold higher concentration of veliparib than olaparib is not enough to induce the same amount of PARP-DNA complexes induced by olaparib (Fig. 4B). On the other hand, PAR levels were quite low under conditions where the differential PARP-DNA complexes were detected (Fig. 4A, lanes 5–8 and 13–16). We also confirmed that PAR levels at 1 μM olaparib and 1 μM veliparib were 1.5 and 6.6%, respectively, for DT40 cells, and 7.4 and 8.1%, respectively, for DU145 cells (Supplemental Fig. 1). Thus, olaparib and veliparib had similar PARP catalytic inhibition potencies at $\geq$1 μM. These results suggest that PARP inhibitors synergize temozolomide primarily by trapping PARP rather than by inhibiting the catalytic activity of PARP. Therefore, we conclude that highly potent PARP-trapping agents potentiate temozolomide more efficiently than simple catalytic PARP inhibitors, and that olaparib is superior to veliparib in combination with temozolomide.

We also checked PARP trapping by the olaparib-camptothecin combination, and found that olaparib did not produce detectable PARP-DNA complexes in combination with camptothecin (Fig. 4C, lanes 5–7 and 12–13). These results indicate that the synergistic effect of camptothecin with PARP inhibitors is due to catalytic PARP inhibition rather than PARP trapping (Das et al., 2014). Therefore, we conclude that catalytic PARP inhibition is critical to potentiate camptothecin, and that veliparib and olaparib are both potent in combination with camptothecins.

Neither PARP Inactivation nor PARP Trapping Appears Relevant for the Combination of Olaparib with Cisplatin or Etoposide. Next, we examined whether PARP inactivation or trapping affected the cytotoxicity of cisplatin or etoposide (Fig. 5). Whereas *PARP1*$^{-/-}$ DT40 cells were hypersensitive to temozolomide and camptothecin (Figs. 1A and 2A), *PARP1*$^{-/-}$ cells were not sensitive to cisplatin or etoposide compared with wild-type cells (Fig. 5, A and C, top panels), indicating that PARP1 is not involved in the repair of cisplatin- and etoposide-induced lesions in cellular models. Addition of olaparib in wild-type DT40 cells reduced the viability in a concentration-dependent manner (Fig. 5, A and C, bottom panels). However, the curves were almost parallel, indicating that olaparib added its own cytotoxicity to that of cisplatin or etoposide. Furthermore, the CI of each point was never below 0.3 (Supplemental Table 1), indicating a lack of strong synergy observed with temozolomide and camptothecin. Olaparib did not potentiate the activity of cisplatin and etoposide in DU145 cells (Fig. 5, B and D) to the extent observed for temozolomide and camptothecin (see Fig. 3). Furthermore, the combination of cisplatin and olaparib did not induce detectable PARP-DNA complexes (Supplemental Fig. 2). Hence, the rationale for combining PARP inhibitors with cisplatin or etoposide is based on neither PARP-DNA trapping nor PARP catalytic inhibition.

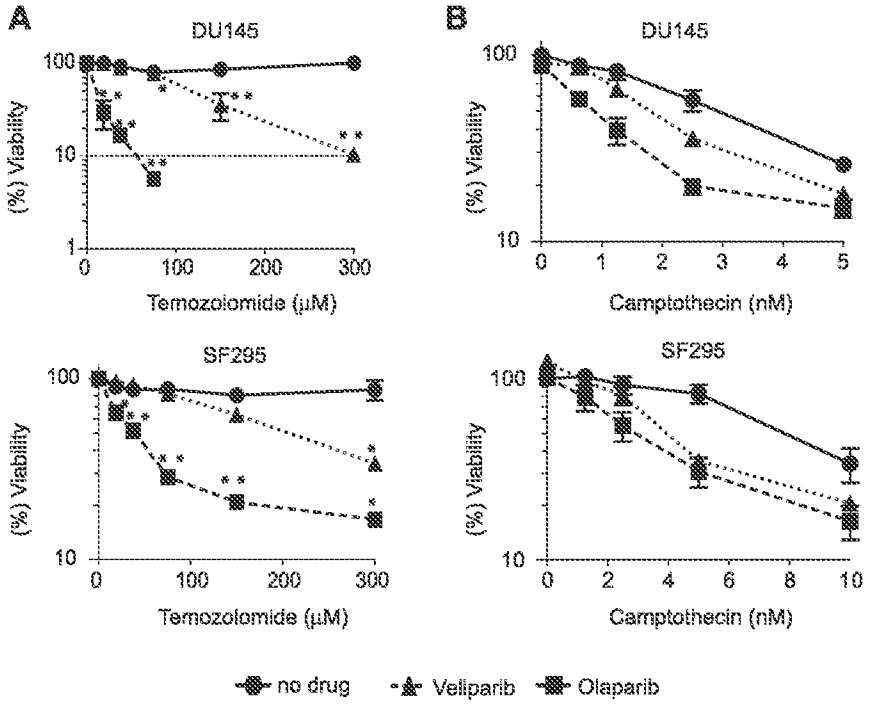

Fig. 3. Differential effect of olaparib and veliparib with temozolomide (A) or camptothecin (B) in human cell lines. Viability curves of human prostate cancer DU145 cells (top panels) and human glioblastoma SF295 cells (bottom panels) after continuous treatment for 72 hours with the indicated drug treatments [olaparib (1 μM) and veliparib (1 μM)]. Viability curves are shown as in Fig. 1A. *CI = 0.1–0.3 and **CI < 0.1 are described as strong and very strong synergy between the two treatments, respectively.

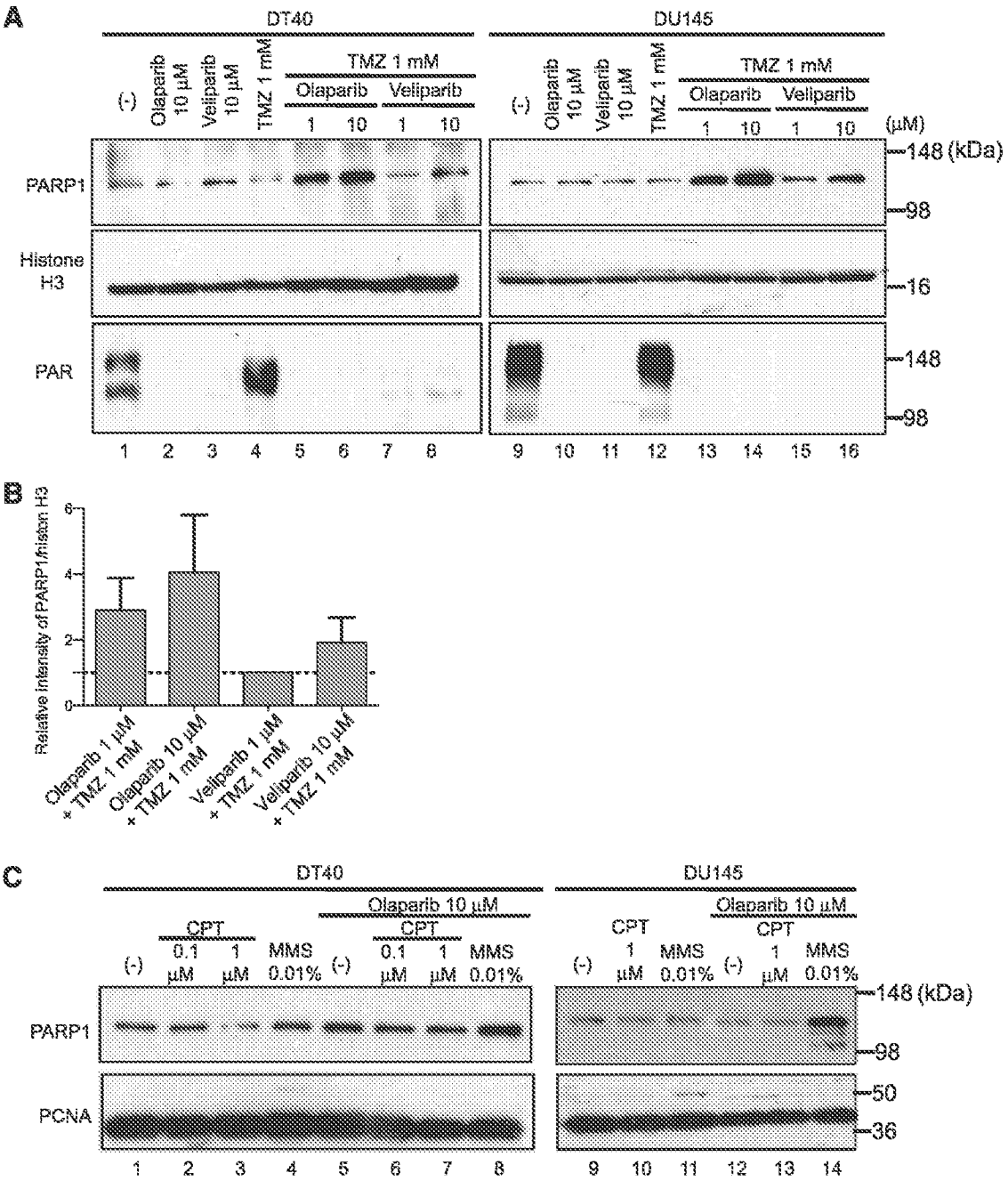

Fig. 4. PARP inhibitors induce PARP-DNA complexes with temozolomide (TMZ) but not with camptothecin (CPT). Western blot of chromatin-bound fractions against anti-PARP1, anti–histone H3, and anti-PAR antibodies (A). Western blot of chromatin-bound fractions against anti-PARP1 and anti-PCNA antibodies (C). Samples were prepared from wild-type DT40 cells (left) and DU145 cells (right) treated for 30 minutes and 4 hours, respectively, with the indicated drugs. Controls without drug are shown in lanes 1 and 9. Histone H3 (A) and PCNA (C) were used as positive markers for loading control. The blots are representatives of multiple experiments. (B) Quantification of PARP-DNA complexes after the indicated treatments. Signal intensity was quantified using ImageJ software (National Institutes of Health) from four independent Western blot analyses (two blots of wild-type DT40 and two blots of DU145 cells). The intensity of the PARP1 blot divided by the intensity of the corresponding histone H3 blot was measured for each treatment, and normalized to the sample of 1 μM veliparib + 1 mM TMZ treatment. Means ± S.D. (n = 4) are shown.

Finally, to compare the drug combination results better, we prepared fraction-affected (Fa)–CI plots from the wild-type DT40 data with olaparib and/or veliparib (Fig. 6) (Chou, 2010). In these plots, we fixed the concentration of PARP inhibitors at 1 μM, because this concentration was common to all the combination studies, and because 1 μM of either olaparib or veliparib reduced PAR levels below 10%. Full information for CI is shown in Supplemental Table 1. Fa = 1.0 means 100% reduction of viability, and the CI at the highest Fa is the most meaningful for combination therapy. At the highest Fa, the combination of temozolomide with olaparib showed the lowest CI (CI = 0.046), followed by camptothecin with olaparib (CI = 0.211), camptothecin with veliparib (CI = 0.296), temozolomide with veliparib (CI = 0.357), etoposide with olaparib (CI = 0.536), and cisplatin with olaparib (CI = 0.562). All together, the combination demonstrates the highest synergisms are demonstrated for combinations of olaparib with temozolomide and for veliparib or olaparib with camptothecin.

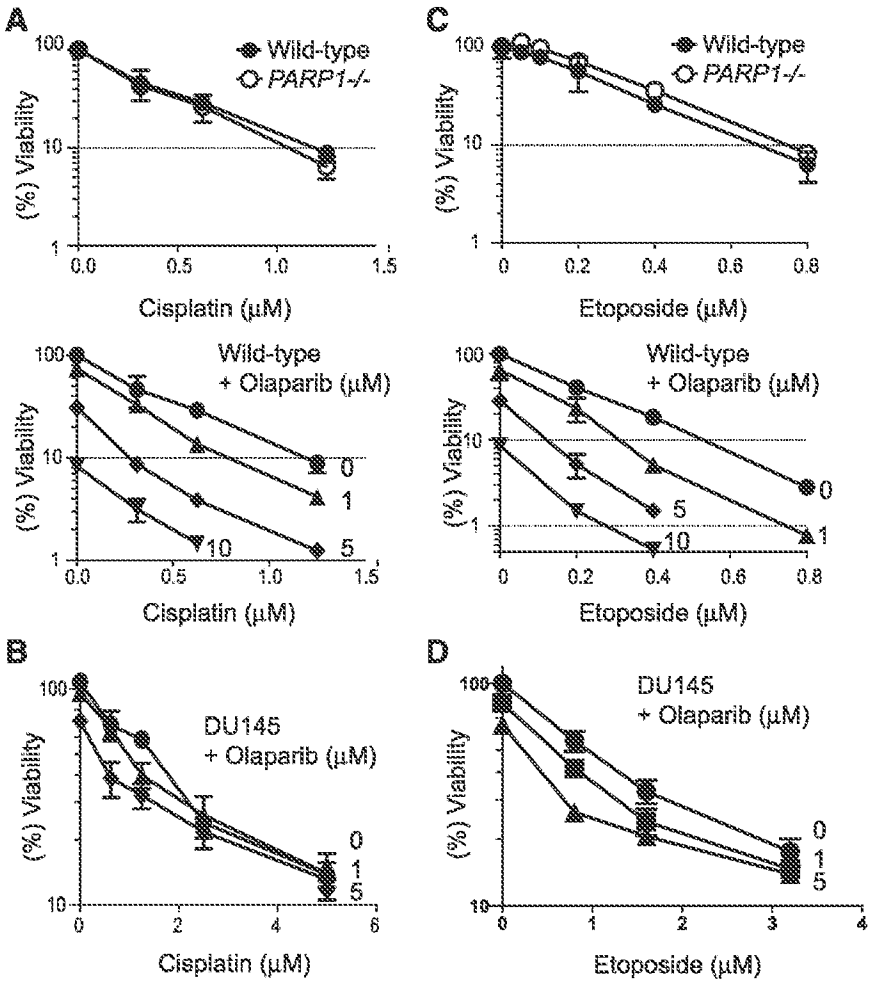

Fig. 5. PARP1 is not involved in the repair of cisplatin- and etoposide-induced lesions. Viability curves are shown as in Fig. 1A. (A and C) Viability curves of wild-type and *PARP1*$^{-/-}$ DT40 cells treated with cisplatin (left) or etoposide (right) (top panels). (Bottom panels) Viability curves of wild-type DT40 cells in combinations with the indicated concentrations of olaparib (micromolar units beside curves) with cisplatin (left) or etoposide (right). (B and D) Viability curves of human prostate cancer DU145 cells in combination with the indicated concentrations of olaparib (micromolar units beside curves) with cisplatin (left) or etoposide (right).

Discussion

Although combining PARP inhibitors with a wide range of drugs is actively being pursued, it is critical to elucidate whether different PARP inhibitors should be considered equal and how such combinations work because some PARP inhibitors selectively induce PARP-DNA trapping in addition to catalytic PARP inhibition (Murai et al., 2012b, 2014). Our study demonstrates marked differences among combinations of four established chemotherapeutic agent classes (temozolomide, camptothecin, cisplatin, and etoposide) with two PARP inhibitors in advanced clinical development, olaparib and veliparib, which differ by their PARP-trapping efficiencies (Murai et al., 2012b; present study).

Temozolomide induces base damage (Newlands et al., 1997), generating abasic sites that are cleaved by apurinic/apyrimidinic endonuclease 1, producing a 1-nucleotide gap with 3′-OH and 5′-deoxyribose phosphate (5′-dRP) groups at the ends of the breaks (Hazra et al., 2007). Camptothecins also induce single-strand breaks, but their 3′-DNA ends are covalently attached to topoisomerase I, whereas the 5′-DNA ends bear a sugar hydroxyl (Pommier, 2012, 2013). The binding of PARP1 depends on the DNA substrate (Horton and Wilson, 2013). PARP1 preferentially binds directly to base excision repair–intermediates with a 5′-dRP rather than to 5′-phosphate ends (Cistulli et al., 2004). This can explain the formation of PARP-DNA complexes at SSBs induced by temozolomide and suggests that combining temozolomide with a potent PARP-trapping agent, such as olaparib, is more rational than combining it with a potent catalytic inhibitor with lower PARP-trapping potency, such as veliparib (Table 1).

On the other hand, in the case of camptothecin, the absence of 5′-dRP ends and the steric hindrance of the breaks by the covalently bound topoisomerase I at the 3′ ends of the broken DNA (Pommier, 2012, 2013) probably explain the lack of detectable PARP-DNA complexes (Fig. 4). However, PARP is critical for the repair of topoisomerase I cleavage complexes (Smith et al., 2005; Zhang et al., 2011; Brenner et al., 2012). PARylation, which can be readily detected in camptothecin-treated cells (Zhang et al., 2011; Brenner et al., 2012), can reverse topoisomerase I cleavage complexes (Malanga and Althaus, 2004), limit replication fork collisions (Ray Chaudhuri et al., 2012; Berti et al., 2013), and facilitate homologous recombination at replication forks stalled by topoisomerase I cleavage complexes (Sugimura et al., 2008). PARP also repairs transcription-mediated DNA damage by topoisomerase I cleavage complexes by acting in the same pathway as tyrosyl-DNA phosphodiesterase 1, a critical repair enzyme that removes topoisomerase I–DNA covalent complexes (Zhang et al., 2011). We recently revealed the coupling of tyrosyl-DNA phosphodiesterase 1 and PARP1 for the repair of topoisomerase I–DNA covalent complexes (Das et al., 2014). Considering that PARP-DNA complexes are undetectable even at high concentrations of camptothecin (1 μM), and that

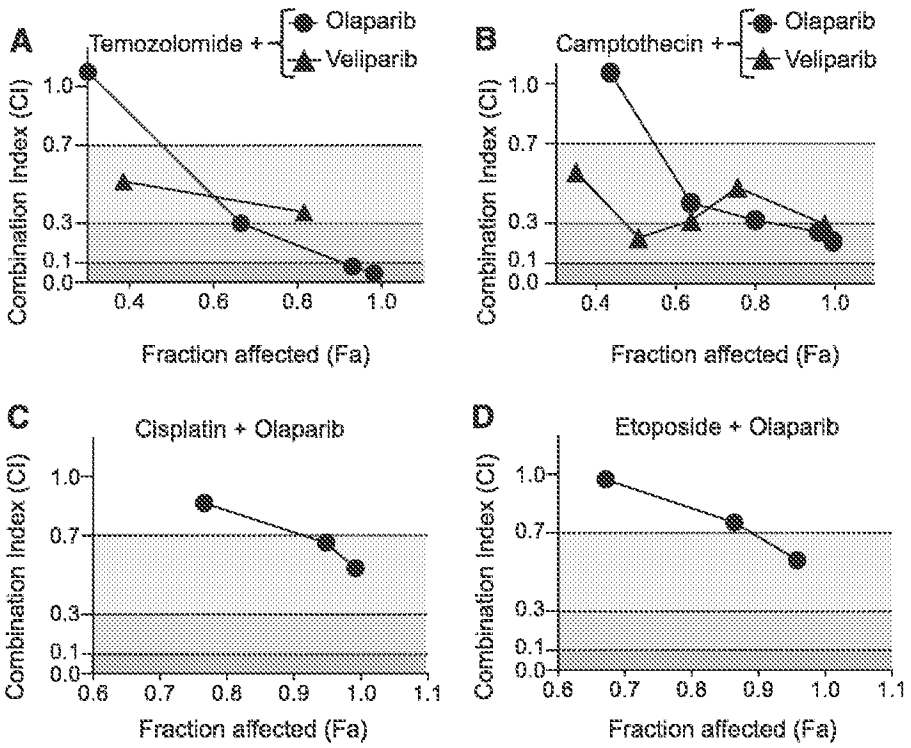

Fig. 6. Quantitative analyses of synergistic effects in the different combinations. (A) Fa-CI plots obtained from the data of Fig. 1 (A and B) for temozolomide in combination with 1 μM olaparib or 1 μM veliparib. (B) Fa-CI plots obtained from the data of Fig. 2 (A and B) for camptothecin in combination with 1 μM olaparib or 1 μM veliparib. (C and D) Fa-CI plots obtained from the data of Fig. 5A (bottom panel) for cisplatin (C) and Fig. 5C (bottom panel) for etoposide (D) in combination with 1 μM olaparib. (A–D) Shading reflects the level of synergism. CI between 0.3 and 0.7, CI between 0.1 and 0.3, and CI less than 0.1 indicate synergy, strong synergy, and very strong synergy, respectively. All data for CI are shown in Supplemental Table 1.

the combination of olaparib or veliparib never exceeds the hypersensitivity of *PARP1*$^{-/-}$ cells, we conclude that the contribution, if any, of PARP-DNA complexes is minimal in the case of camptothecin. Ten micromolar veliparib, which reduces PAR levels to 1% (Supplemental Fig. 1), still was not enough to reach the hypersensitivity of PARP1$^{-/-}$ cells (Fig. 2B). The greater sensitivity of the PARP1$^{-/-}$ cell compared with the drug-treated wild-type cells could be due to the low-level residual PARylation, which might be sufficient to counter DNA damage. Nevertheless, since catalytic PARP inhibition explains the potentiation of camptothecins, highly potent PARP catalytic inhibitors devoid of cytotoxic effects, such as veliparib, can be viewed as a rational combination with camptothecins (Table 1). Indeed, recent publications show synergy between topoisomerase I inhibitors and veliparib in chemo-resistant colon cancer cell lines (in vitro and/or in vivo studies) (Zhang et al., 2011; Davidson et al., 2013; Shelton et al., 2013).

Enhanced effects of PARP inhibitors with cisplatin have been reported (Rottenberg et al., 2008; Hastak et al., 2010; Chuang et al., 2012). However, the synergistic effects in these studies are relatively weak compared with those in the reports dealing with temozolomide (Brenner et al., 2012; Kedar et al., 2012; Horton and Wilson, 2013) and camptothecin (Smith et al., 2005; Daniel et al., 2009; Zhang et al., 2011). The weaker synergistic effect of PARP inhibitors with cisplatin than with temozolomide or camptothecin would be caused by the lack of involvement of PARP in cisplatin sensitivity (Fig. 5A, top panel). The same holds true for the topoisomerase II–targeted drug etoposide. Accordingly, drug-induced topoisomerase II–DNA complexes fail to activate PARP (Zwelling et al., 1982). The lack of synergy between etoposide and PARP inhibitors has also been previously reported (Bowman et al., 2001).

In summary, we propose that combination strategies with PARP inhibitors and the choice of PARP inhibitor should be

TABLE 1
Summary of the differential effects of the PARP inhibitors, olaparib and veliparib, in combination with temozolomide or camptothecin

	Temozolomide	Camptothecin
Trapping of PARP-DNA complex	++[a]	No[a]
PARylation inhibition	++[b]	++[b]
	BER inhibition	=> TDP1 inactivation
		=> Persistent Top1cc
		=> Replication fork stalling
Combination index[c]	Olaparib > > Veliparib	Veliparib ≈ Olaparib

BER, base excision repair; TDP1, tyrosyl-DNA phosphodiesterase 1; Top1cc, topoisomerase I cleavage complex.
[a]Temozolomide in combination with PARP inhibitors (olaparib > > veliparib) induces the trapping of cytotoxic PARP-DNA complexes, whereas camptothecin does not induce detectable PARP-DNA complexes (see Fig. 3).
[b]The effect of PARylation inhibiton for temozolomide and camptothecin is functionally different (see *Discussion*), and both olaparib and veliparib effectively inhibit PARylation.
[c]Fa-CI plots (see Fig. 6) revealed that olaparib is more effective than veliparib for temozolomide, whereas veliparib is at least as effective as olaparib.

based not only on whether PARP is involved in the repair of the DNA lesions produced by the agent with which the PARP inhibitor will be combined but also on whether the lesions produced by the combination trap PARP-DNA complexes. Accordingly, PARP inhibitors that most efficiently trap PARP-DNA complexes, such as olaparib, niraparib, and BMN 673 (Murai et al., 2012b, 2014), would be preferable to veliparib in the case of temozolomide combinations. On the other hand, veliparib should remain a valuable agent in combination with camptothecins, as synergism for topoisomerase I inhibitors involves catalytic inhibition but not PARP trapping (Das et al., 2014). Table 1 summarizes these differences.

Acknowledgments

The authors thank Dr. Yasushi Okuno (Kyoto University, Japan) and Dr. Masahiko Nakatsui (Kobe University, Japan) for advising on combination effect analyses.

Authorship Contributions

Participated in research design: Murai, Ji, Pommier.

Conducted experiments: Murai, Zhang, Ji.

Contributed new reagents or analytic tools: Zhang, Ji, Morris, Takeda, Doroshow.

Performed data analysis: Murai, Zhang, Ji, Pommier.

Wrote or contributed to the writing of the manuscript: Murai, Pommier.

References

Berti M, Ray Chaudhuri A, Thangavel S, Gomathinayagam S, Kenig S, Vujanovic M, Odreman F, Glatter T, Graziano S, and Mendoza-Maldonado R, et al. (2013) Human RECQ1 promotes restart of replication forks reversed by DNA topoisomerase I inhibition. *Nat Struct Mol Biol* **20**:347–354.

Boulton S, Pemberton LC, Porteous JK, Curtin NJ, Griffin RJ, Golding BT, and Durkacz BW (1995) Potentiation of temozolomide-induced cytotoxicity: a comparative study of the biological effects of poly(ADP-ribose) polymerase inhibitors. *Br J Cancer* **72**:849–856.

Bowman KJ, Newell DR, Calvert AH, and Curtin NJ (2001) Differential effects of the poly (ADP-ribose) polymerase (PARP) inhibitor NU1025 on topoisomerase I and II inhibitor cytotoxicity in L1210 cells in vitro. *Br J Cancer* **84**:106–112.

Brenner JC, Feng FY, Han S, Patel S, Goyal SV, Bou-Maroun LM, Liu M, Lonigro R, Prensner JR, and Tomlins SA, et al. (2012) PARP-1 inhibition as a targeted strategy to treat Ewing's sarcoma. *Cancer Res* **72**:1608–1613.

Bryant HE, Schultz N, Thomas HD, Parker KM, Flower D, Lopez E, Kyle S, Meuth M, Curtin NJ, and Helleday T (2005) Specific killing of BRCA2-deficient tumours with inhibitors of poly(ADP-ribose) polymerase. *Nature* **434**:913–917.

Buerstedde JM and Takeda S (1991) Increased ratio of targeted to random integration after transfection of chicken B cell lines. *Cell* **67**:179–188.

Chou TC (2006) Theoretical basis, experimental design, and computerized simulation of synergism and antagonism in drug combination studies. *Pharmacol Rev* **58**: 621–681.

Chou TC (2010) Drug combination studies and their synergy quantification using the Chou-Talalay method. *Cancer Res* **70**:440–446.

Chuang HC, Kapuriya N, Kulp SK, Chen CS, and Shapiro CL (2012) Differential anti-proliferative activities of poly(ADP-ribose) polymerase (PARP) inhibitors in triple-negative breast cancer cells. *Breast Cancer Res Treat* **134**:649–659.

Cistulli C, Lavrik OI, Prasad R, Hou E, and Wilson SH (2004) AP endonuclease and poly(ADP-ribose) polymerase-1 interact with the same base excision repair intermediate. *DNA Repair (Amst)* **3**:581–591.

Curtin NJ and Szabo C (2013) Therapeutic applications of PARP inhibitors: anticancer therapy and beyond. *Mol Aspects Med* **34**:1217–1256.

Daniel RA, Rozanska AL, Thomas HD, Mulligan EA, Drew Y, Castelbuono DJ, Hostomsky Z, Plummer ER, Boddy AV, and Tweddle DA, et al. (2009) Inhibition of poly(ADP-ribose) polymerase-1 enhances temozolomide and topotecan activity against childhood neuroblastoma. *Clin Cancer Res* **15**:1241–1249.

Das BB, Huang SY, Murai J, Rehman I, Amé J-C, Sengnpta S, Das SK, Majumdar P, Zhang H, and Biard D, et al. (2014) PARP1-TDP1 coupling for the repair of topoisomerase I-induced DNA damage. *Nucleic Acids Res* doi: 10.1093/nar/gku088.

Davidson D, Wang Y, Aloyz R, and Panasci L (2013) The PARP inhibitor ABT-888 synergizes irinotecan treatment of colon cancer cell lines. *Invest New Drugs* **31**: 461–468.

Farmer H, McCabe N, Lord CJ, Tutt AN, Johnson DA, Richardson TB, Santarosa M, Dillon KJ, Hickson I, and Knights C, et al. (2005) Targeting the DNA repair defect in BRCA mutant cells as a therapeutic strategy. *Nature* **434**:917–921.

Fojo T and Bates S (2013) Mechanisms of resistance to PARP inhibitors–three and counting. *Cancer Discov* **3**:20–23.

Hastak K, Alli E, and Ford JM (2010) Synergistic chemosensitivity of triple-negative breast cancer cell lines to poly(ADP-Ribose) polymerase inhibition, gemcitabine, and cisplatin. *Cancer Res* **70**:7970–7980.

Hazra TK, Das A, Das S, Choudhury S, Kow YW, and Roy R (2007) Oxidative DNA damage repair in mammalian cells: a new perspective. *DNA Repair (Amst)* **6**:470–480.

Helleday T (2011) The underlying mechanism for the PARP and BRCA synthetic lethality: clearing up the misunderstandings. *Mol Oncol* **5**:387–393.

Hochegger H, Dejsuphong D, Fukushima T, Morrison C, Sonoda E, Schreiber V, Zhao GY, Saberi A, Masutani M, and Adachi N, et al. (2006) Parp-1 protects homologous recombination from interference by Ku and Ligase IV in vertebrate cells. *EMBO J* **25**:1305–1314.

Horton JK and Wilson SH (2013) Predicting enhanced cell killing through PARP inhibition. *Mol Cancer Res* **11**:13–18.

Kedar PS, Stefanick DF, Horton JK, and Wilson SH (2012) Increased PARP-1 association with DNA in alkylation damaged, PARP-inhibited mouse fibroblasts. *Mol Cancer Res* **10**:360–368.

Kummar S, Chen A, Parchment RE, Kinders RJ, Ji J, Tomaszewski JE, and Doroshow JH (2012) Advances in using PARP inhibitors to treat cancer. *BMC Med* **10**:25.

Liu X, Han EK, Anderson M, Shi Y, Semizarov D, Wang G, McGonigal T, Roberts L, Lasko L, and Palma J, et al. (2009) Acquired resistance to combination treatment with temozolomide and ABT-888 is mediated by both base excision repair and homologous recombination DNA repair pathways. *Mol Cancer Res* **7**:1686–1692.

Lord CJ and Ashworth A (2012) The DNA damage response and cancer therapy. *Nature* **481**:287–294.

Maede Y, Shimizu H, Fukushima T, Kogame T, Nakamura T, Miki T, Takeda S, Pommier Y, and Murai J (2014) Differential and common DNA repair pathways for topoisomerase I- and II-targeted drugs in a genetic DT40 repair cell screen panel. *Mol Cancer Ther* **13**:214–220.

Malanga M and Althaus FR (2004) Poly(ADP-ribose) reactivates stalled DNA topoisomerase I and Induces DNA strand break resealing. *J Biol Chem* **279**:5244–5248.

McCabe N, Turner NC, Lord CJ, Kluzek K, Bialkowska A, Swift S, Giavara S, O'Connor MJ, Tutt AN, and Zdzienicka MZ, et al. (2006) Deficiency in the repair of DNA damage by homologous recombination and sensitivity to poly(ADP-ribose) polymerase inhibition. *Cancer Res* **66**:8109–8115.

Murai J, Huang SY, Das BB, Dexheimer TS, Takeda S, and Pommier Y (2012a) Tyrosyl-DNA phosphodiesterase 1 (TDP1) repairs DNA damage induced by topoisomerases I and II and base alkylation in vertebrate cells. *J Biol Chem* **287**: 12848–12857.

Murai J, Huang SY, Das BB, Renaud A, Zhang Y, Doroshow JH, Ji J, Takeda S, and Pommier Y (2012b) Trapping of PARP1 and PARP2 by Clinical PARP Inhibitors. *Cancer Res* **72**:5588–5599.

Murai J, Huang SY, Renaud A, Zhang Y, Ji J, Takeda S, Morris J, Teicher B, Doroshow JH, and Pommier Y (2014) Stereospecific PARP Trapping by BMN 673 and Comparison with Olaparib and Rucaparib. *Mol Cancer Ther* **13**:433–443.

Newlands ES, Stevens MF, Wedge SR, Wheelhouse RT, and Brock C (1997) Temozolomide: a review of its discovery, chemical properties, pre-clinical development and clinical trials. *Cancer Treat Rev* **23**:35–61.

Pettitt SJ, Rehman FL, Bajrami I, Brough R, Wallberg F, Kozarewa I, Fenwick K, Assiotis I, Chen L, and Campbell J, et al. (2013) A genetic screen using the PiggyBac transposon in haploid cells identifies Parp1 as a mediator of olaparib toxicity. *PLoS ONE* **8**:e61520.

Pommier Y (2012) *DNA Topoisomerases and Cancer*, Springer & Humana Press, New York, Dordrecht, Heidelberg, London.

Pommier Y (2013) Drugging topoisomerases: lessons and challenges. *ACS Chem Biol* **8**:82–95.

Ray Chaudhuri A, Hashimoto Y, Herrador R, Neelsen KJ, Fachinetti D, Bermejo R, Cocito A, Costanzo V, and Lopes M (2012) Topoisomerase I poisoning results in PARP-mediated replication fork reversal. *Nat Struct Mol Biol* **19**:417–423.

Rottenberg S, Jaspers JE, Kersbergen A, van der Burg E, Nygren AO, Zander SA, Derksen PW, de Bruin M, Zevenhoven J, and Lau A, et al. (2008) High sensitivity of BRCA1-deficient mammary tumors to the PARP inhibitor AZD2281 alone and in combination with platinum drugs. *Proc Natl Acad Sci USA* **105**:17079–17084.

Rouleau M, Patel A, Hendzel MJ, Kaufmann SH, and Poirier GG (2010) PARP inhibition: PARP1 and beyond. *Nat Rev Cancer* **10**:293–301.

Satoh MS and Lindahl T (1992) Role of poly(ADP-ribose) formation in DNA repair. *Nature* **356**:356–358.

Shelton JW, Waxweiler TV, Landry J, Gao H, Xu Y, Wang L, El-Rayes B, and Shu HK (2013) In vitro and in vivo enhancement of chemoradiation using the oral PARP inhibitor ABT-888 in colorectal cancer cells. *Int J Radiat Oncol Biol Phys* **86**: 469–476.

Smith LM, Willmore E, Austin CA, and Curtin NJ (2005) The novel poly(ADP-Ribose) polymerase inhibitor, AG14361, sensitizes cells to topoisomerase I poisons by increasing the persistence of DNA strand breaks. *Clin Cancer Res* **11**:8449–8457.

Sugimura K, Takebayashi S, Tagnchi H, Takeda S, and Okumura K (2008) PARP-1 ensures regnlation of replication fork progression by homologous recombination on damaged DNA. *J Cell Biol* **183**:1203–1212.

Zhang YW, Regairaz M, Seiler JA, Agama KK, Doroshow JH, and Pommier Y (2011) Poly(ADP-ribose) polymerase and XPF-ERCC1 participate in distinct pathways for the repair of topoisomerase I-induced DNA damage in mammalian cells. *Nucleic Acids Res* **39**:3607–3620.

Zwelling LA, Kerrigan D, Pommier Y, Michaels S, Steren A, and Kohn KW (1982) Formation and resealing of intercalator-induced DNA strand breaks in permeabilized L1210 cells without the stimulated synthesis of poly(ADP-ribose). *J Biol Chem* **257**:8957–8963.

Address correspondence to: Yves Pommier, Developmental Therapeutics Branch, Laboratory of Molecular Pharmacology, Center for Cancer Research, National Cancer Institute, 37 Convent Drive, Building 37, Room 5068, National Institutes of Health, Bethesda, MD 20892-4255. E-mail: pommier@nih.gov

Novel Nanoliposomal CPT-11 Infused by Convection-Enhanced Delivery in Intracranial Tumors: Pharmacology and Efficacy

Charles O. Noble,[1] Michal T. Krauze,[2] Daryl C. Drummond,[3] Yoji Yamashita,[2] Ryuta Saito,[2] Mitchel S. Berger,[2] Dmitri B. Kirpotin,[3] Krystof S. Bankiewicz,[2] and John W. Park[1]

[1]Division of Hematology/Oncology and [2]Department of Neurological Surgery, Brain Tumor Research Center, University of California at San Francisco, San Francisco, California and [3]Hermes Biosciences, Inc., South San Francisco, California

Abstract

We hypothesized that combining convection-enhanced delivery (CED) with a novel, highly stable nanoparticle/liposome containing CPT-11 (nanoliposomal CPT-11) would provide a dual drug delivery strategy for brain tumor treatment. Following CED in rat brains, tissue retention of nanoliposomal CPT-11 was greatly prolouged, with >20% injected dose remaining at 12 days for all doses. Tissue residence was dose dependent, with doses of 60 μg (3 mg/mL), 0.8 mg (40 mg/mL), and 1.6 mg (80 mg/mL) resulting in tissue half-life ($t_{1/2}$) of 6.7, 10.7, and 19.7 days, respectively. In contrast, CED of free CPT-11 resulted in rapid drug clearance (tissue $t_{1/2}$ = 0.3 day). At equivalent CED doses, nanoliposomal CPT-11 increased area under the time-concentration curve by 25-fold and tissue $t_{1/2}$ by 22-fold over free CPT-11; CED in intracranial U87 glioma xenografts showed even longer tumor retention (tissue $t_{1/2}$ = 43 days). Plasma levels were undetectable following CED of nanoliposomal CPT-11. Importantly, prolonged exposure to nanoliposomal CPT-11 resulted in no measurable central nervous system (CNS) toxicity at any dose tested (0.06-1.6 mg/rat), whereas CED of free CPT-11 induced severe CNS toxicity at 0.4 mg/rat. In the intracranial U87 glioma xenograft model, a single CED infusion of nanoliposomal CPT-11 at 1.6 mg resulted in significantly improved median survival (>100 days) compared with CED of control liposomes (19.5 days; $P = 4.9 \times 10^{-5}$) or free drug (28.5 days; $P = 0.011$). We conclude that CED of nanoliposomal CPT-11 greatly prolonged tissue residence while also substantially reducing toxicity, resulting in a highly effective treatment strategy in preclinical brain tumor models. (Cancer Res 2006; 66(5): 2801-6)

Introduction

Outcomes for brain tumor patients, particularly those with high-grade gliomas, remain suboptimal and highlight the need for novel therapeutic approaches. Because restricted access is one of the hallmarks of these tumors, strategies for improving drug delivery have attracted much interest. These strategies include regional administration approaches within the central nervous system (CNS) as well as particle-based carriers of drugs.

Convection-enhanced delivery (CED) is a local-regional drug delivery technique that uses a pressure-driven bulk-flow process to distribute agents, including macromolecules, to clinically relevant volumes of solid tissues (1, 2). CED can be used to circumvent the blood-brain barrier, which is a considerable obstacle for many systemically applied drugs (3, 4). CED represents a promising approach to treat various CNS diseases, including brain tumors, which cannot be controlled by local treatment and are poorly responsive to systemic treatment. Compared with routes of administration dependent on diffusion from the injection/implantation site, CED shows a greater volume of distribution and is designed to direct a drug to specific target volumes (5–8).

Liposomes are nano- or microscale carriers typically consisting of a phospholipid membrane shell surrounding a hollow core that can be used to encapsulate small molecules. Liposomal anthracyclines represent the first successful examples of nanoparticle-based anticancer treatment, including marketed agents pegylated liposomal doxorubicin (Doxil, Alza Pharmaceuticals, Inc., Mountain View, CA; Caelyx, Schering-Plough, Inc., Kenilworth, NJ) and liposomal daunorubicin (Daunoxome, Gilead, Inc., Foster City, CA; refs. 9–14). To encapsulate other drugs, we have recently developed a novel intraliposomal drug loading and stabilization technology: poly(anionic) polyols were used to generate new liposomal drugs with unusual drug stability and favorable preclinical pharmacokinetics (15–17). One of these new agents, nanoparticle/liposome containing CPT-11 (nanoliposomal CPT-11; refs. 18–20), encapsulates the camptothecin derivative and topoisomerase I inhibitor CPT-11/irinotecan (Camptosar, Pfizer, New York, NY). Although highly active against many cancer types, CPT-11 displays complex pharmacology characterized by diverse biochemical transformations and potential toxicities (21, 22). In particular, CPT-11 requires conversion to SN-38 for optimal activity yet must avoid inactivation via simple hydrolysis of the requisite lactone configuration to an inactive carboxylate. Furthermore, hepatic conversion to SN-38 leads to biliary excretion of this potent metabolite and resulting gastrointestinal toxicity. In principle, the pharmacologic profile of CPT-11 can be improved by tumor-directed drug delivery, including liposomal encapsulation.

We hypothesized that a combined drug delivery approach featuring nanoliposomal CPT-11 given by CED is feasible and therapeutically advantageous. In previous studies, we showed that CED can be used to achieve extensive distribution of liposomes in rodent brains, orthotopic brain tumor xenografts (23, 24), and monkey brains (25–27). We now report the pharmacology and efficacy of a novel nanoparticle/liposome-based drug given by CED in preclinical brain tumor models.

Materials and Methods

Nanoparticle/liposome constructs. Lipids included 1,2-distearoyl-*sn*-glycero-3-phosphocholine (DSPC), 1,2-distearoyl-*sn*-glycero-3-phosphoethanolamine-*N*-[methoxy(polyethylene glycol)-2000] (PEG-DSPE; Avanti Polar Lipids, Inc., Alabaster, AL), and cholesterol (Calbiochem, San Diego, CA). Small unilamellar liposomes were composed of DSPC, cholesterol, and

Note: C.O. Noble and M.T. Krauze contributed equally to this work.

Requests for reprints: John W. Park, University of California San Francisco, Division of Hematology-Oncology, 1600 Divisidaro Street 2nd Floor, San Francisco, CA 94115. Phone: 415-502-3844; Fax: 415-353-9571; E-mail: jpark@cc.ucsf.edu.

doi:10.1158/0008-5472.CAN-05-3535

PEG-DSPE at a molar ratio of 3:2:0.015. Liposomes were prepared by dissolving all lipids in chloroform/methanol (9:1, v/v) and removing solvent by rotary evaporation to form a dried lipid foam. After hydration, the lipid suspension was briefly vacuumized on a rotary evaporator to remove any trace of organic solvents. Unilamellar liposomes were formed by extrusion at 60°C using gas-pressure thermostatted barrel extruder (Lipex Biomembranes, Vancouver, British Columbia, Canada) through polycarbonate membranes (Whatman Nucleopore, Clifton, NJ) having a pore size of 200 nm (6 times) and 100 nm (12 times) and yielding a final diameter of 96 to 101 nm as determined by light scattering (N4Plus particle size analyzer, Beckman Coulter, Fullerton, CA). *N,N'*-bis-octadecyl-4,4,4',4'-tetramethylindacarbocyanin iodide [$DiIC_{18}(3)$; Molecular Probes, Inc., Eugene, OR] was included for fluorescent labeling.

Drug loading. To prepare triethylammonium sucrose octasulfate (TEA-SOS) as a drug-trapping agent, 0.3 mol/L sodium sucrose octasulfate (Toronto Research Chemicals, Inc., North York, Ontario, Canada) was applied to a column containing Dowex 50W-8X-200 cation exchange resin (equilibrated with 3 mol/L HCl) to convert the sodium salt of sucrose octasulfate to free acid form. Sucrose octasulfuric acid was eluted from the column with double-distilled water using an inline conductivity detector. The solution was then neutralized with neat triethylamine and diluted to a concentration corresponding to 0.65 mol/L triethylammonium with an osmolality of 480 to 530 mmol/kg (pH 5.5-6.0). Residual sodium was determined by potentiometry using a sodium-sensitive glass electrode. For TEA-SOS-containing liposomes, dried lipids were hydrated in 81 mmol/L aqueous TEA-SOS solution (0.65 mol/L triethylamine) at 60°C, and the hydrated lipid suspension was subjected to eight cycles of freezing (−80°C) and thawing (60°C). Extraliposomal TEA-SOS was removed by size exclusion chromatography on Sepharose CL-4B.

CPT-11 (a kind gift of PharmaEngine, Inc., Taipei, Taiwan) was loaded into TEA-SOS-containing liposomes by addition of a 15 mg/mL solution of CPT-11/HCl to a final drug-to-lipid ratio of 500 g CPT-11/mol phospholipid (for 0.06-0.8 mg/rat dose levels) or 800 g CPT-11/mol phospholipid (for 1.6 mg/rat dose level), with incubation of the drug-liposome mixture at 60°C (pH 6.0) for 45 minutes followed by quenching on ice for 15 minutes. Unencapsulated CPT-11 was removed by Sephadex G75 size exclusion chromatography, and the drug-loaded liposomes were stored at 4°C until use. The resulting nanoliposomal CPT-11 was concentrated on a stirred cell concentrator containing a regenerated cellulose 1×10^5 NMWL membrane (Amicon, Millipore Corp., Billerica, MA) and sterilized by passage through 0.2-μm PES syringe filter. CPT-11 concentration was determined by measuring absorbance at 375 nm of a solubilized sample. Briefly, 0.1 mL of an aqueous portion of the sample containing nanoliposomal CPT-11 or standards was added to 0.9 mL of a solution containing 72 vol % methanol, 18 vol % of 0.1 mol/L phosphoric acid, and 10 vol % chloroform. Phospholipid was measured using blue phosphomolybdate-based spectrophotometric assay (28).

Animal models. Toxicity studies used healthy male Sprague-Dawley rats weighing ~250 g (Charles-River Laboratories, Wilmington, MA). For xenograft studies, congenitally athymic, male, nude rats (*rnu/rnu*, homozygous) weighing ~150 to 200 g (National Cancer Institute Animal Production Program, Frederick, MD) were housed under aseptic conditions, which included filtered air and sterilized food, water, bedding, and cages. For the intracranial xenograft tumor model, U87 glioblastoma cells (Brain Tumor Research Center Tissue Bank, University of California at San Francisco, San Francisco, CA) were harvested by trypsinization, washed once with HBSS without Ca^{2+} and Mg^{2+}, and resuspended in HBSS for implantation. Cells (5×10^5) in 10 μL HBSS were implanted into the striatal region of athymic rat brains as follows: under deep isoflurane anesthesia, rats were placed in a small-animal stereotaxic frame (David Kopf Instrument, Tujunga, CA). A sagittal incision was made to expose the cranium and followed by a burr hole in the skull at 0.5 mm anterior and 3 mm lateral from the bregma using a small dental drill. Cell suspension (5 μL) was injected over 2 minutes at a depth of 4.5 mm from the brain surface; after a 2-minute wait, another 5 μL were injected over 2 minutes at a depth of 4 mm, and after a final 2-minute wait, the needle was removed and the wound was sutured.

Convection-enhanced delivery. CED of free CPT-11 or nanoliposomal CPT-11 was done using a volume of 20 μL as described (24, 29). Briefly, the infusion system consisted of a fused-silica needle cannula that was connected to a loading line (containing the therapeutic agent) and an olive oil infusion line. A 1-mL syringe (filled with oil) mounted onto a microinfusion pump (BeeHive, Bioanalytical Systems, West Lafayette, IN) regulated the flow of fluid through the system. Based on chosen coordinates, needle cannula was mounted onto stereotactic holders and guided to targeted region of the brain through burr holes made in the skull. The following ascending infusion rates were applied to achieve the 20-μL total infusion volume: 0.2 μL/min (15 minutes) + 0.5 μL/min (10 minutes) + 0.8 μL/min (15 minutes).

Tissue pharmacokinetics. Rats were given a single 20-μL infusion by CED of free or nanoliposomal CPT-11, and the animal was sacrificed at prescribed times. The appropriate brain hemisphere was perfused with PBS, surgically removed, and frozen. Either the tissue was ground under liquid nitrogen or water was added to the tissue at a 50% (w/w) ratio, and the tissue was homogenized using a mechanical homogenizer in an ice bath. The homogenates (0.1 mL) were extracted as the lactone form of CPT-11 and SN-38 with 0.4 mL of an acidic methanol solution (20% 0.1 mol/L phosphoric acid/80% methanol) by vortexing for 10 seconds twice and centrifugation at 13,000 rpm for 10 minutes, and the supernatants were transferred to autosampler vials for high-pressure liquid chromatography (HPLC) analysis. Blank homogenates were added to CPT-11 and SN-38 to estimate extraction efficiency. Analysis was conducted on a Dionex HPLC system using a C_{18} reverse-phase silica column preceded by a Supelco C_{18} guard column. A sample injection volume of 50 μL was used, and the column was eluted isocratically at a flow rate of 1.0 mL/min with a mobile phase consisting of 3% by volume of aqueous (pH 5.5) triethylammonium acetate and acetonitrile (73:27). CPT-11 and SN-38 were typically eluted in 5.1 and 9.8 minutes, respectively, and both were detected by fluorescence at 420 nm (365 nm excitation).

Tissue pharmacokinetics was fit to a monoexponential decay equation using the trend analysis of Microsoft Excel (Microsoft Corp., Redmond, WA). Pharmacokinetic variables, including tissue half-life ($t_{1/2}$), clearance, mean residence time in brain or brain tumor tissue, and area under the time-concentration curve (AUC_∞), were all determined by noncompartmental pharmacokinetics data analysis using PK Solutions 2.0 software (Summit Research Services, Montrose, CO).

Therapy studies. To evaluate toxicity, healthy rats received a single infusion of free or nanoliposomal CPT-11 via CED. Rats were monitored daily for survival, weekly weights, and general health (alertness, grooming, feeding, excreta, skin, fur, mucous membrane conditions, ambulation, breathing, and posture). Rats were euthanized 60 days after CED treatments, and their brains were removed, fixed in 10% buffered formalin phosphate and then in 30% sucrose, and cut into sections (25 μm) for H&E staining.

To evaluate survival, rats were randomly assigned to five groups (n = 8 rats per group) and U87 tumor cells were implanted into each rat brain. Five days after tumor implantation, a single CED infusion of 20 μL was done using different treatment conditions as described in the text. Rats were evaluated for clinical and tissue toxicity as described above.

Results

Construction of nanoliposomal CPT-11 for brain tumor treatment. CPT-11 was encapsulated in small unilamellar phospholipid vesicles at extremely high concentrations not previously attainable using intraliposomal sucrose octasulfate for high capacity binding to CPT-11, combined with effective transmembrane exchange of intraliposomal triethylammonium for the drug cation (15, 16). Drug loading efficiencies were 86% to 101% of added drug. Constructs were 96 to 101 nm in diameter and achieved drug-to-lipid ratios of 691 to 812 g CPT-11/mol phospholipid, corresponding to payloads of 0.9×10^5 to 1.0×10^5 drug molecules per nanoparticle based on 8×10^5 phospholipids/nanoparticle. The resulting nanoparticle/liposome construct

(termed nanoliposomal CPT-11 to indicate a lipid bilayer-based nanoparticle encapsulating a stably entrapped nanoscale drug complex) could be concentrated without aggregation or precipitation up to 80 mg CPT-11/mL in aqueous solution, which is ~4-fold greater than the solubility of CPT-11 as a free drug. Nanoliposomal CPT-11 showed excellent storage stability at 4°C; at 6 months, no particle size change and only 0.3% drug leakage were detected.

Tissue pharmacokinetics of nanoliposomal CPT-11 following CED in normal adult rat brains or intracranial U87 tumor xenografts. Free CPT-11 or nanoliposomal CPT-11 were given via single CED treatment into the brains of normal adult Sprague-Dawley rats, and tissue levels were determined at varying times after infusion by HPLC. Tissue retention of nanoliposomal CPT-11 was dose dependent, with doses of 60 μg (3 mg/mL), 0.8 mg (40 mg/mL), and 1.6 mg (80 mg/mL) resulting in brain tissue $t_{1/2}$s of 6.7, 10.7, and 19.7 days, respectively (Table 1). Tissue concentration versus dose was not a linear function, as even low doses (60 μg) of nanoliposomal CPT-11 resulted in substantial levels of drug: >20% injected dose (ID) remained at 12 days after infusion. In contrast, CED of free CPT-11 at the equivalent dose, which was also its highest tolerable dose tested, was cleared from the brain within 1 day (Fig. 1). Hence, at equivalent doses of nanoliposomal and free CPT-11, the AUC_∞ was increased by 25-fold for nanoliposomal CPT-11, and the tissue $t_{1/2}$ was improved from 0.3 day for free CPT-11 to 6.7 days (22-fold) for the liposomal drug. Because nanoliposomal CPT-11 could be infused at much higher doses than free CPT-11 due to its reduced toxicity (shown in the next section), nanoliposomal CPT-11 at its highest tested dose improved the AUC_∞ by 1,636-fold and tissue $t_{1/2}$ by 66-fold over that of free CPT-11 at its highest tolerable dose.

Systemic levels of CPT-11 following CED of nanoliposomal CPT-11 were measured concurrently in the plasma of healthy rats receiving 1.6 mg nanoliposomal CPT-11 (Fig. 1). Plasma CPT-11 levels were not detectable in any sample, indicating that CED abrogated significant systemic exposure.

Drug delivery to tumor tissue was evaluated in an orthotopic U87 tumor xenograft model in athymic rats, in which U87 glioma cells were implanted intracranially and allowed to grow for 10 days before treatment. In comparison with normal brain tissue, drug clearance from U87 tumors was significantly slower (Fig. 2*A*; Table 1). The tissue $t_{1/2}$ of drug (Table 1) was extended by ~4-fold (10.7 versus 43.0 days) when nanoliposomal CPT-11 was infused in the tumor xenograft model compared with normal rat brain tissue.

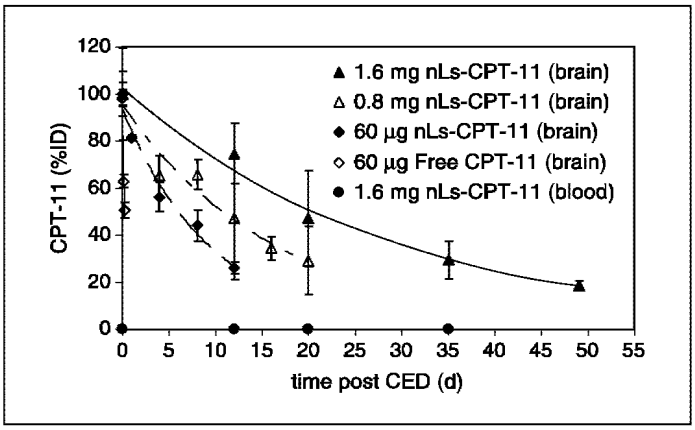

Figure 1. Tissue pharmacokinetics of free CPT-11 and nanoliposomal (nLs) CPT-11 in the normal adult rat brain and blood following single CED infusion. All values are %ID versus time after CED of 20-μL infusate. Drug concentrations were determined by HPLC assay for CPT-11/HCl. CPT-11 concentrations in blood were all below the detection limit of 1 ng/mL (~0.03%ID).

Tumor penetration of free CPT-11 given systemically (tail vein injection) in rats with intracranial U87 tumors was examined by measuring the drug in tumor tissue and plasma (Fig. 2*B*). Fifteen minutes after i.v. injection of free CPT-11 at its established maximum tolerated doses of 100 mg/kg (29.3 mg; ref. 30), drug levels in tumor were 2.7 μg/g (0.009% ID/g tissue), and at 5 hours, this had declined to 1.7 μg/g. These miniscule concentrations were much lower than the 46.2 μg/g tissue achieved 15 minutes after CED of free CPT-11 (17-fold) and, even more so, the 921 μg/g tissue after CED of 1.6 mg nanoliposomal CPT-11 (341-fold).

SN-38, the highly active metabolite of CPT-11, was also assayed in tissue and plasma samples but was undetectable in all samples. Using several different extraction methods for the detection of SN-38 by HPLC analysis (31–33), a detection limit of 1 ng/mL was established with spiked tissue recovery of >95% using an acidic methanol extraction.

Host toxicity of CED of free CPT-11 and nanoliposomal CPT-11 in rodent CNS. Free CPT-11 (60 μg or 0.4 mg) or nanoliposomal CPT-11 (0.06, 0.4, 0.8, and 1.6 mg) were given via a single 20-μL CED infusion into normal adult rat brains (Fig. 3). After sacrifice at 42 days after treatment, histologic evidence of neurotoxic injury was scored on a scale of 0 to 3+. In animals receiving CED of free CPT-11 at 60 μg, brain tissue contained evidence of minor trauma at the

Table 1. Tissue pharmacokinetics of CPT-11 formulations given by CED

Brain				
	$t_{1/2}$ (d)	AUC_∞ (μg d/g)	Clearance (g/d)	Mean residence time (d)
60 μg free CPT-11	0.3	16.4	3.6	0.4
60 μg nanoliposomal CPT-11	6.7	417	0.14	9.6
0.8 mg nanoliposomal CPT-11	10.7	13,723	0.058	15.4
1.6 mg nanoliposomal CPT-11	19.7	26,823	0.06	28.5
U87 Tumor				
	$t_{1/2}$ (d)	AUC_∞ (μg d/g)	Clearance (g/d)	Mean residence time (d)
0.8 mg nanoliposomal CPT-11	43.0	40,315	0.02	62.0

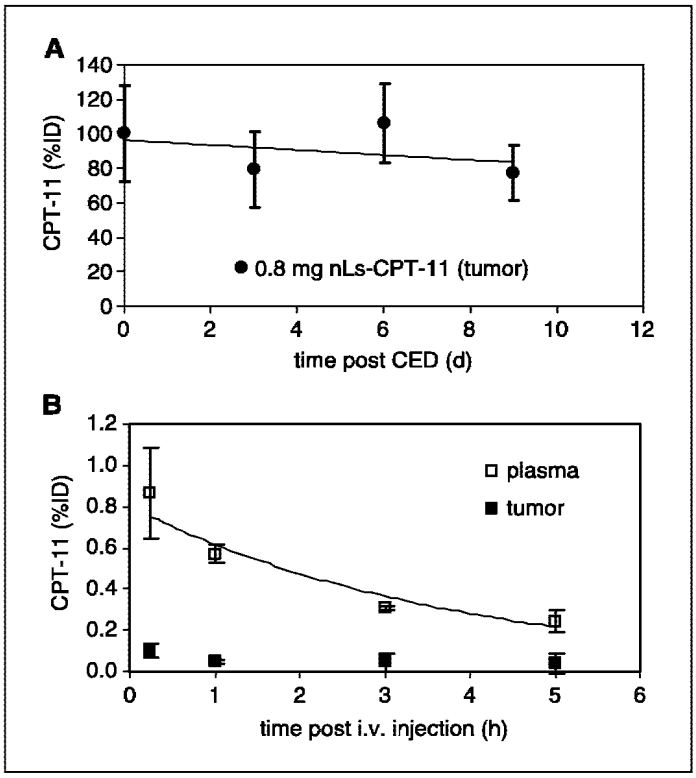

Figure 2. Tumor tissue pharmacokinetics of free CPT-11 and nanoliposomal CPT-11 in intracranial U87 tumor xenografts. Tumors were implanted and allowed to grow for 10 days before CED or i.v. treatment. *A*, nanoliposomal CPT-11, single CED treatment at 0.8 mg (20 μL). *B*, free CPT-11, following bolus i.v. injection at 100 mg/kg. Two to four rats per time point.

site of the infusion cannula (arrows) in the striatum but otherwise no apparent tissue toxicity (score = 0; Fig. 3*A*). However, all animals that received free CPT-11 at 0.4 mg/rat were observed to have extensive tissue necrosis within the CNS (score = 3+; Fig. 3*B*). In contrast, animals receiving nanoliposomal CPT-11 at all doses tested showed no evidence of CNS toxicity (score = 0 for all animals), and the only finding was minor trauma at the infusion cannula site (Fig. 3*C*).

No systemic toxicities, including weight loss or diarrhea, were observed following CED of any of the treatments (Fig. 3*D*). Furthermore, no gross neurologic or behavioral changes were noted after treatment. Indeed, no dose-limiting toxicities for nanoliposomal CPT-11 were identified up to 1.6 mg/rat, which represented the highest feasible dose. Higher doses were precluded by formulation viscosity at concentrations >80 mg/mL, although this was 4-fold greater than the solubility of free CPT-11. Taken together, these data indicated that nanoliposomal CPT-11 greatly extended the tissue tolerance and maximum tolerated doses of the drug; whereas the highest tolerable dose of free CPT-11 was 60 μg/rat, that for nanoliposomal CPT-11 was at least 1.6 mg/rat.

Efficacy of CED of free CPT-11 and nanoliposomal CPT-11. The antitumor efficacy of nanoliposomal CPT-11 (0.06, 0.8, and 1.6 mg/rat) and free CPT-11 (at the highest tolerable dose tested, 0.06 mg/rat) was evaluated following single CED infusion in the intracranial U87 tumor xenograft model. The control group received a CED infusion of "empty" liposomes of the same lipid composition as nanoliposomal CPT-11 but without any encapsulated drug and labeled with the lipophilic fluorescent marker, $DiIC_{18}$(3). As shown in Fig. 4, all animals in the control group expired due to tumor progression by day 22, and mean survival was only 20 days (median, 19.5 days). Treatment with free CPT-11 showed a slight improvement in survival, although all animals still expired by day 30 and mean survival was 28 days (median, 28.5 days). At the equivalent dose of 0.06 mg/rat, treatment with nanoliposomal CPT-11 resulted in mean survival of 36 days (median, 30 days) and one of eight rats surviving beyond 100 days; this suggested a trend toward superiority for nanoliposomal CPT-11 over free drug ($P = 0.09$, pairwise comparison). Treatment with nanoliposomal CPT-11 at 0.8 mg/rat resulted in 50% of the animals surviving beyond day 100 and mean survival of 71 days (median, 78 days). Animals treated with nanoliposomal CPT-11 at 1.6 mg/rat showed excellent survival, with five of eight rats surviving beyond day 100 and mean survival of 83 days (median, >100 days). Overall, CED infusion of nanoliposomal CPT-11 produced greatly enhanced survival compared with CED of free CPT-11 (hazard ratio = 0.39; $P = 0.01$). The improved survival associated with nanoliposomal CPT-11 treatment was dose dependent, with risk of death versus control of 90%, 24%, and 5.8% for the animals receiving the 0.06, 0.8, and 1.6 mg/rat treatments, respectively ($P < 0.001$, Cox proportional hazards model).

Histopathologic evaluation of brain tissue was done in all animals at death or after study sacrifice. Animals showing clinical signs of tumor progression were euthanized. Of the 10 animals surviving to study end at day 100, which only occurred within the groups receiving nanoliposomal CPT-11 at 0.06, 0.4, 0.8, and 1.6 mg/

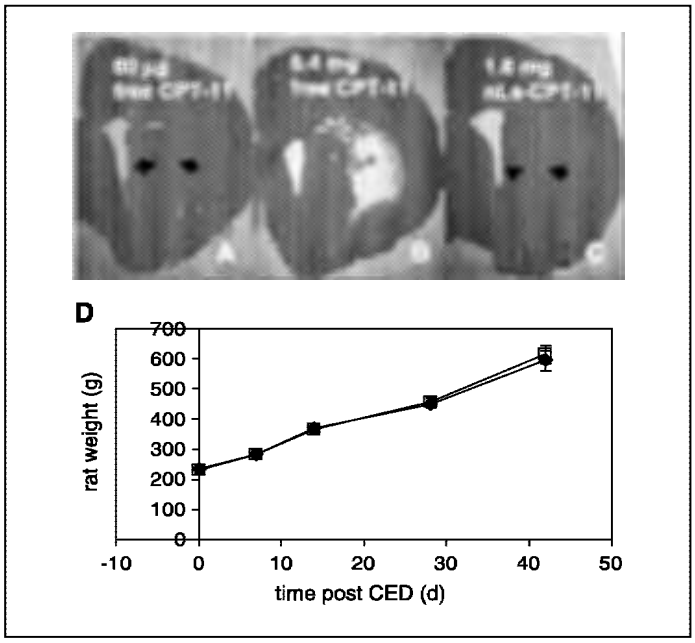

Figure 3. Tissue toxicity of free CPT-11 and nanoliposomal CPT-11 in the normal adult rat brain following CED. *A*, rats (four per group) treated with a single CED infusion of free CPT-11 at 60 μg (3 mg/mL) using an infusion volume of 20 μL. *B*, rats (four per group) treated with a single CED infusion of free CPT-11 at 0.4 mg (20 mg/mL) using an infusion volume of 20 μL. *C*, rats (four per group) treated with a single CED infusion of nanoliposomal CPT-11 at 1.6 mg (80 mg/mL) using an infusion volume of 20 μL. Six weeks after CED, animals were sacrificed and brains were processed for histopathology. Representative H&E sections from each group. Extensive tissue injury was observed in all animals treated with 0.4 mg free CPT-11. *Arrows*, rats in other treatment groups showed only focal traumatic injury at the site of the infusion cannula. *D*, serial weight measurements in control rats (□) and rats given 1.6 mg nanoliposomal CPT-11 by CED (♦). *Bars*, SD.

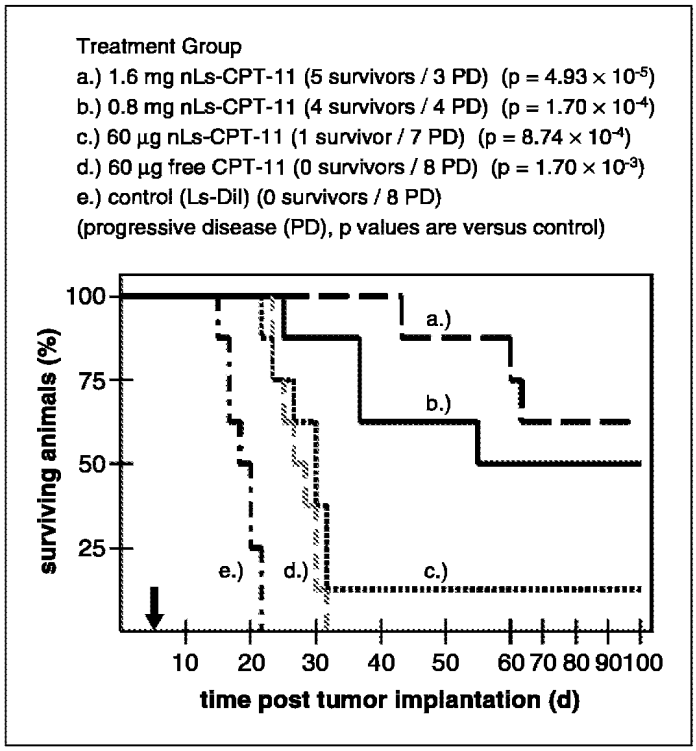

Figure 4. Treatment of rats bearing orthotopic U87 tumors with single CED infusion of free or nanoliposomal CPT-11. Five days after tumor implantation within the brain (*arrow*), rats were treated with nanoliposomal CPT-11 at 1.6 mg (80 mg/mL; *a*), nanoliposomal CPT-11 at 0.8 mg (40 mg/mL; *b*), nanoliposomal CPT-11 at 60 μg (3 mg/mL; *c*), free CPT-11 at 60 μg (3 mg/mL; *d*), and liposomal $DiIC_{18}(3)$ without encapsulated drug (empty liposomes; *e*). Eight animals per group. Median survival for each group was >100 days (*a*), 78 days (*b*), 30 days (*c*), 28.5 days (*d*), and 19.5 days (*e*).

rat, only 1 rat (0.8 mg/rat) showed histologic evidence of residual brain tumor; complete pathologic responses were noted in the 9 other survivors (Fig. 5*A* and *B*). In all cases of animal death, tumor progression was observed in the brains of the rats (Fig. 5*C* and *D*).

Discussion

We reported previously that liposomes in the range of 40 to 100 nm can be efficiently infused by CED into large volumes within the brains of rodents (23, 24) and primates (25, 26), indicating the feasibility of this approach as a drug delivery strategy. We now describe, to our knowledge, the first such example of a liposome- or nanoparticle-based drug given via CED for brain tumor treatment in preclinical models. These results indicated that combining the novel agent nanoliposomal CPT-11, which features highly efficient and stable encapsulation of CPT-11 in lipidic nanoparticles, with CED provided significant anticancer activity with a large therapeutic index against brain tumors.

These studies confirmed the difficulties associated with systemic chemotherapy for brain tumor treatment. I.v. administration of free CPT-11, a drug that seems promising against brain tumors (34), resulted in very low drug concentrations within the rat CNS due to rapid systemic clearance within hours as well as limited blood-brain barrier penetration. The problem of low therapeutic levels is compounded by the considerable systemic toxicities of this drug in its free form (35). CED is designed to provide high local-regional drug levels while reducing systemic exposure, and this was evidenced in these studies. In human brain tumors, disruption of the tumor-blood barrier could increase systemic access of this agent following CED; however, animals receiving CED of nanoliposomal CPT-11 at the highest dose tested (1.6 mg/rat, 80 mg/mL CPT-11/HCl) showed undetectable drug levels in plasma. Furthermore, this CED dose amounted to ~18-fold less total drug than an i.v. injection of free CPT-11 at 100 mg/kg (29.3 mg CPT-11/HCl). Finally, the slow and sustained release of drug from nanoliposomal CPT-11 provides an additional safety margin upon any systemic exposure.

Compared with systemic therapy, CED of free CPT-11 yielded much higher drug levels in brain tissue (17-fold) and even greater drug concentrations when CED was combined with nanoliposomal CPT-11 (341-fold). Furthermore, whereas CED of free CPT-11 was cleared from the brain quickly (<1 day), nanoliposomal CPT-11 was retained for many days in a dose-dependent manner; a single CED administration at 1.6 mg/rat was detectable over weeks (>49 days). Encapsulation of CPT-11 in these nanoliposome constructs resulted in at least 196-fold prolongation of residence time in normal tissue.

It is striking that greatly prolonged tissue retention of nanoliposomal CPT was associated with a substantial decrease in CNS toxicity compared with free drug and indeed was well tolerated up to the highest dose tested, 1.6 mg/rat. Since significant CNS toxicity was observed with free CPT-11 at 0.4 mg/rat, encapsulation in the nanoliposome construct increased tissue tolerance by

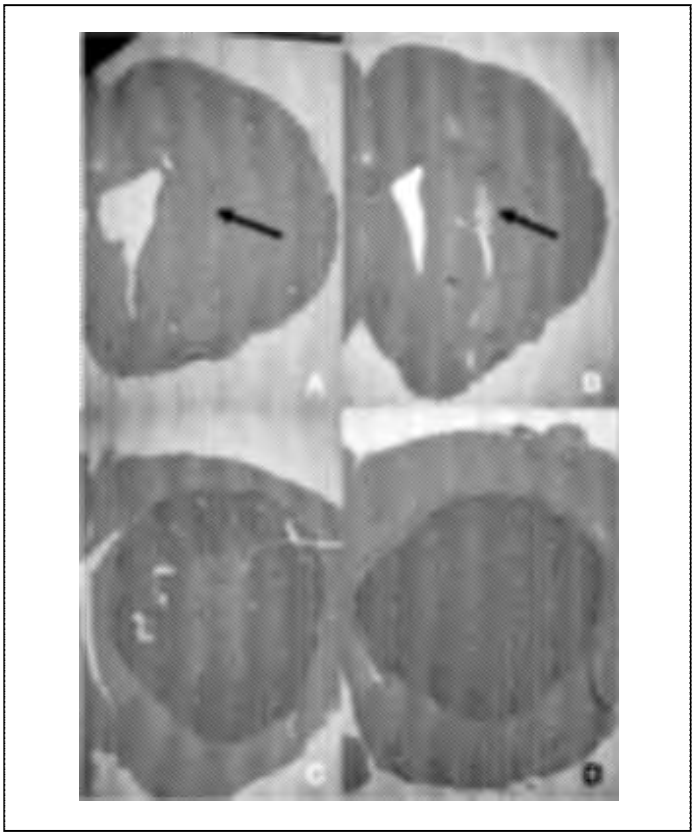

Figure 5. Representative brain sections from each experimental group in the therapy study. *A*, 1.6 mg nanoliposomal CPT-11 (obtained from a survivor and showing no residual tumor). *B*, 0.8 mg nanoliposomal CPT-11 (obtained from a survivor and show no residual tumor). *C*, 60 μg free CPT-11 (showing a typical tumor found in nonsurviving animals, in which tumor progression led to death). *D*, liposomal $DiIC_{18}(3)$ (empty liposomes; showing a typical tumor found in nonsurviving animals, in which tumor progression led to death). *Arrows*, scar from the cannula used for tumor implantation and CED.

>4-fold. This protective effect may be due to lower acute tissue exposure associated with particle encapsulation and its attendant slow rate of drug release.

Although equivalent CED doses of free CPT-11 and nanoliposomal CPT-11 indicated a slight but nonsignificant survival benefit for the latter, the treatment advantage provided by the nanoliposome construct was largely attributable to its much wider therapeutic index, enabling significantly higher doses with no added toxicity. It is possible that other mechanisms of delivery may also have contributed to the observed anticancer efficacy. Following initial distribution within brain tissue by CED, liposomes provided sustained drug levels for a prolonged period, resulting in continuous tumor exposure and a metronomic chemotherapy effect.

Nanoliposomal CPT-11 is a novel lipidic nanoparticle carrier that may be particularly well suited for brain tumor treatment. CPT-11 is very active against brain tumor cells (36, 37) and is being evaluated in clinical trials despite its pharmacologic limitations (19, 38). Using a sucrose octasulfate-based method for intraliposomal loading and stabilization, nanoliposomal CPT-11 provided clearly superior drug delivery and efficacy in conjunction with CED infusion. The highly concentrated dose of CPT-11 achieved (up to 1.6 mg/rat) was a direct result of the extremely high drug-to-lipid ratio ($\sim$800 g CPT-11/mol phospholipid, 1×10^5 CPT-11 molecules per liposome particle) attainable using this drug loading technology. This system can also, in principle, be used to deliver other drugs and/or diagnostic agents. For example, we have reported previously that similar liposomes loaded with gadolinium chelates can be readily visualized by real-time magnetic resonance imaging in the rodent (24) and monkey (25) CNS.

We conclude that nanoliposomal CPT-11 can be infused by CED into the CNS, resulting in substantial improvement in pharmacologic profile and therapeutic index. The strategy of combining a novel nanoparticle chemotherapeutic with CED may circumvent the drug delivery barriers posed by brain tumors.

Acknowledgments

Received 10/3/2005; revised 12/5/2005; accepted 12/12/2005.

Grant support: National Cancer Institute Specialized Programs of Research Excellence in Brain Tumors grant P50-CA097257 and Accelerated Brain Cancer Cure; New Investigator Award from California's Breast Cancer Research Program of the University of California grant 7KB-0066 (D.C. Drummond).

The costs of publication of this article were defrayed in part by the payment of page charges. This article must therefore be hereby marked *advertisement* in accordance with 18 U.S.C. Section 1734 solely to indicate this fact.

We thank Dr. Dan Moore (University of California at San Francisco) for expert biostatistical assistance.

References

1. Bobo RH, Laske DW, Akbasak A, Morrison PF, Dedrick RL, Oldfield EH. Convection-enhanced delivery of macromolecules in the brain. Proc Natl Acad Sci U S A 1994;91:2076–80.
2. Morrison PF, Chen MY, Chadwick RS, Lonser RR, Oldfield EH. Focal delivery during direct infusion to brain: role of flow rate, catheter diameter, and tissue mechanics. Am J Physiol Regul Integr Comp Physiol 1999;277:R1218–29.
3. Pardridge WM. Drug and gene targeting to the brain with molecular Trojan horses. Nat Rev Drug Discov 2002;1:131–9.
4. Pardridge WM. Blood-brain barrier drug targeting: the future of brain drug development. Mol Interv 2003;3:90–105.
5. Kunwar S. Convection-enhanced delivery of IL13-38QQR for treatment of recurrent malignant glioma: presentation of interim findings from ongoing phase 1 studies. Acta Neurochir Suppl 2003;88:105–11.
6. Lidar Z, Mardor Y, Jonas T, et al. Convection-enhanced delivery of paclitaxel for the treatment of recurrent malignant glioma: a phase I/II clinical study. J Neurosurg 2004;100:472–9.
7. Mardor Y, Roth Y, Lidar Z, et al. Monitoring response to convection-enhanced Taxol delivery in brain tumor patients using diffusion-weighted magnetic resonance imaging. Cancer Res 2001;61:4971–3.
8. Poepperl G, Goldbrunner R, Gildehaus FJ, Tanner P, Tatsch K. F-18 FET PET for monitoring the effects of convection-enhanced delivery of paclitaxel in patients with recurrent glioblastoma. Eur J Nucl Med Mol Imaging 2005;32:1018–25.
9. Gabizon A, Isacson R, Libson E, et al. Clinical studies of liposome-encapsulated doxorubicin. Acta Oncol 1994; 33:779–86.
10. Zucchetti M, Boiardi A, Silvani A, Parisi I, Piccolrovazzi S, D'Incalci M. Distribution of daunorubicin and daunorubicinol in human glioma tumors after administration of liposomal daunorubicin. Cancer Chemother Pharmacol 1999;44:173–6.
11. Thigpen JT, Aghajanian CA, Alberts DS, et al. Role of pegylated liposomal doxorubicin in ovarian cancer. Gynecol Oncol 2005;96:10–8.
12. Zamboni WC, Ramalingam S, Friedland DM, et al. Phase I and pharmacokinetic (PK) study of STEALTH® liposomal CKD-602 (S-CKD602) in patients with advanced solid tumors. American Society of Clinical Oncology Annual Meeting; 2005; Orlando, FL. p. 2069.
13. Seiden MV, Muggia F, Astrow A, et al. A phase II study of liposomal lurtotecan (OSI-211) in patients with topotecan resistant ovarian cancer. Gynecol Oncol 2004;93:229–32.
14. Gelmon KA, Tolcher A, Diab AR, et al. Phase I study of liposomal vincristine. J Clin Oncol 1999;17:697–705.
15. Drummond DC, Noble CO, Mamot C, et al. Development of novel liposomal and receptor tyrosine kinase-targeted immunoliposomal vinorelbine formulations with improved drug retention [abstract]. Proc Am Assoc Cancer Res 2005;56:4394.
16. Drummond DC, Noble CO, Guo Z, et al. Development of a highly active nanoliposomal irinotecan using a novel intraliposomal stabilization strategy. Cancer Res. In press 2006.
17. Drummond DC, Marx C, Guo Z, et al. Enhanced pharmacodynamic and antitumor properties of a histone deacetylase inhibitor encapsulated in liposomes or ErbB2-targeted immunoliposomes. Clin Cancer Res 2005;11:3392–401.
18. Gilbert MR, Supko JG, Batchelor T, et al. Phase I clinical and pharmacokinetic study of irinotecan in adults with recurrent malignant glioma. Clin Cancer Res 2003;9:2940–9.
19. Friedman HS, Petros WP, Friedman AH, et al. Irinotecan therapy in adults with recurrent or progressive malignant glioma. J Clin Oncol 1999;17:1516–25.
20. Chou R, Chen A, Lau D. Complete response of brain metastases to irinotecan-based chemotherapy. J Clin Neurosci 2005;12:242–5.
21. Mathijssen RHJ, van Alphen RJ, Verweij J, et al. Clinical pharmacokinetics and metabolism of irinotecan (CPT-11). Clin Cancer Res 2001;7:2182–94.
22. Lokiec F, duSorbier BM, Sanderink GJ. Irinotecan (CPT-11) metabolites in human bile and urine. Clin Cancer Res 1996;2:1943–9.
23. Mamot C, Nguyen JB, Pourdehnad M, et al. Extensive distribution of liposomes in rodent brains and brain tumors following convection-enhanced delivery. J Neurooncol 2004;68:1–9.
24. Saito R, Bringas JR, McKnight TR, et al. Distribution of liposomes into brain and rat brain tumor models by convection-enhanced delivery monitored with magnetic resonance imaging. Cancer Res 2004;64:2572–9.
25. Saito R, Krauze MT, Bringas J, et al. Gadolinium-loaded liposomes allow for real-time magnetic resonance imaging of convection-enhanced delivery in the primate brain. Exp Neurol 2005;196:381–9.
26. Krauze MT, McKnight TR, Yamashita Y, et al. Real-time visualization and characterization of liposomal delivery into the monkey brain by magnetic resonance imaging. Brain Res Prot 2005;16:20–6.
27. Krauze MT, Saito R, Noble C, et al. Effects of the perivascular space on convection-enhanced delivery of liposomes in primate putamen. Exp Neurol 2005;196: 104–11.
28. Bartlett GR. Phosphorous assay in column chromatography. J Biol Chem 1959;234:466–8.
29. Bankiewicz KS, Eberling JL, Kohutnicka M, et al. Convection-enhanced delivery of AAV vector in parkinsonian monkeys; *in vivo* detection of gene expression and restoration of dopaminergic function using prodrug approach. Exp Neurol 2000;164:2–14.
30. Cao SS, Rustum YM. Synergistic antitumor activity of irinotecan in combination with 5-fluorouracil in rats bearing advanced colorectal cancer: role of drug sequence and dose. Cancer Res 2000;60:3717–21.
31. Escoriaza J, Aldaz A, Castellanos C, Calvo E, Giraldez J. Simple and rapid determination of irinotecan and its metabolite SN-38 in plasma by high-performance liquid chromatography: application to clinical pharmacokinetic studies. J Chromatogr B 2000;740:159–68.
32. Warner DL, Burke TG. Simple and versatile high-performance liquid chromatographic method for the simultaneous quantitation of the lactone and carboxylate forms of camptothecin anticancer drugs. J Chromatogr B 1997;691:161–71.
33. Zufia L, Aldaz A, Giraldez J. Separation methods for camptothecin and related compounds. J Chromatogr B 2001;764:141–59.
34. Friedman HS, Keir ST, Houghton PJ. The emerging role of irinotecan (CPT-11) in the treatment of malignant glioma in grain tumors. Cancer 2003;97:2359–62.
35. Rothenberg ML, Meropol NJ, Poplin EA, Van Cutsem E, Wadler S. Mortality associated with irinotecan plus bolus fluorouracil/leucovorin: summary findings of an independent panel. J Clin Oncol 2001;19:3801–7.
36. Chen TC, Su S, Fry D, Liebes L. Combination therapy with irinotecan and protein kinase C inhibitors in malignant glioma. Cancer 2003;97:2363–73.
37. Nakatsu S, Kondo S, Kondo Y, et al. Induction of apoptosis in multi-drug resistant (MDR) human glioblastoma cells by SN-38, a metabolite of the camptothecin derivative CPT-11. Cancer Chemother Pharmacol 1997;39:417–23.
38. Reardon DA, Friedman HS, Powell JBJ, Gilbert M, Yung WK. Irinotecan: promising activity in the treatment of malignant glioma. Oncology 2003;17:9–14.

Research Article

Nanomedicine

Pharmacokinetics, tumor accumulation and antitumor activity of nanoliposomal irinotecan following systemic treatment of intracranial tumors

Aim: We sought to evaluate nanoliposomal irinotecan as an intravenous treatment in an orthotopic brain tumor model. **Materials & methods:** Nanoliposomal irinotecan was administered intravenously in the intracranial U87MG brain tumor model in mice, and irinotecan and SN-38 levels were analyzed in malignant and normal tissues. Therapy studies were performed in comparison to free irinotecan and control treatments. **Results:** Tissue analysis demonstrated favorable properties for nanoliposomal irinotecan, including a 10.9-fold increase in tumor AUC for drug compared with free irinotecan and 35-fold selectivity for tumor versus normal tissue exposure. As a therapy for orthotopic brain tumors, nanoliposomal irinotecan showed a mean survival time of 54.2 versus 29.5 days for free irinotecan. A total of 33% of the animals receiving nanoliposomal irinotecan showed no residual tumor by study end compared with no survivors in the other groups. **Conclusion:** Nanoliposomal irinotecan administered systemically provides significant pharmacologic advantages and may be an efficacious therapy for brain tumors.

Original submitted 1 March 2013; Revised submitted 10 October 2013

Keywords: drug delivery • glioma • irinotecan • liposome • nanoliposome • nanoparticle

Charles O Noble*[,1,2], Michal T Krauze*[,3], Daryl C Drummond[2], John Forsayeth[3], Mark E Hayes[2], Janine Beyer[3], Piotr Hadaczek[3], Mitchel S Berger[3], Dmitri B Kirpotin[2], Krystof S Bankiewicz[3] & John W Park*[,1]

[1]Division of Hematology–Oncology, University of California San Francisco, San Francisco, CA 94115, USA
[2]Merrimack Pharmaceuticals, Cambridge, MA 02139, USA
[3]Department of Neurological Surgery, Brain Tumor Research Center, University of California San Francisco, San Francisco, CA, USA
*Author for correspondence:
Tel.: +1 415 502 3844
Fax: +1 415 353 9592
jpark@cc.ucsf.edu
[†]Authors contributed equally

Despite progress in brain tumor research, treatment options for malignant glioma patients remain limited [1–3]. Chemotherapy has proven particularly challenging, at least in part due to the blood–brain barrier (BBB) and its associated low permeability to a wide variety of drugs [4,5]. New approaches have been sought to improve drug delivery to brain tumors.

Liposomes can be used to package and deliver anticancer compounds [6,7], and examples include currently approved agents liposomal daunorubicin (DaunoXome®, Gilead Inc., CA, USA), PEGylated liposomal doxorubicin (Doxil®, Alza Pharmaceuticals Inc., CA, USA; Caelyx®, Schering-Plough Inc., NJ, USA) [8–13] and liposomal vincristine (Marqibo®, Talon Therapeutics, CA, USA) [14–16]. Our previous work has demonstrated the promise of polyanionic polyols in stabilizing certain difficult to formulate small molecule chemotherapeutics in liposomes [17–20]. One of the resulting agents is a nanoliposomal formulation of the topoisomerase I inhibitor irinotecan [18,21–23]. Irinotecan, a widely used cancer chemotherapeutic, displays antitumor activity against a number of different cancer types, including malignant gliomas [24]; however, its utility has been limited by its complex metabolic profile. Irinotecan is mainly a prodrug, dependent upon conversion to SN-38 by carboxylesterases for optimal anticancer activity [25]. Furthermore, clearance of SN-38 is dependent on glucuronidation to SN-38G by glucuronidase [26,27]. Both of these enzymatic conversions are highly variable from patient to patient [28,29]. For these reasons, it is an attractive case for drug delivery, which can, in principle, protect the compound from premature metabolism until chaperoned to

Future Medicine part of fsg

tumor tissue. Previously, delivery of irinotecan via our nanoliposomal formulation has shown both increased efficacy and reduced host toxicity in various preclinical cancer models [18,21,30].

Brain tumor treatment involves additional complexities for nanocarrier-mediated drug delivery. These include limited penetration into the brain parenchyma due to the BBB, as well as assuring acceptable safety of carrier and drug within the CNS [31,32]. Nanoparticles can benefit from the enhanced permeability and retention effect, where they selectively extravasate via fenestrations in rapidly growing tumor vasculature [33–35]. This selectivity appears to persist in preclinical brain tumor models despite the BBB, at least for some nanoparticle types such as certain liposomes [36–39], and including unique liposome formulations of irinotecan from those described by us [40,41].

Here, we demonstrate that nanoliposomal irinotecan can be administered systemically in an orthotopic brain tumor model and that this delivery strategy is associated with significant therapeutic advantages over the free drug. We report the tissue pharmacokinetics, antitumor efficacy and host toxicity of this treatment.

Materials & methods

Materials

Distearoylphosphatidylcholine and poly(ethylene) glycol-derivatized distearoylphosphatidylethanolamine were purchased from Avanti Polar Lipids (AL, USA). Cholesterol was obtained from Calbiochem (CA, USA). Irinotecan was purchased from Scinopharm (Shan-Hua, Taiwan). Sucrose octasulfate (sodium salt) was obtained from Formosa Laboratories (Taoyuan, Taiwan). Sephadex® G-75 size exclusion resin, Dowex® 50W-8X 200 cation exchange resin, Amberlite® IRA910 anion exchange resin and triethylamine were all obtained from Sigma-Aldrich (MO, USA).

Nanoliposomal irinotecan formulation

The nanoliposomal irinotecan formulation is composed of lipid mixture consisting of distearoylphosphatidylcholine, Chol and poly(ethylene) glycol-distearoylphosphatidylethanolamine at a molar ratio of 3:2:0.015. The lipids were dissolved in chloroform:methanol (9:1 vol:vol), and the solvent was removed by rotary evaporation to produce a dried lipid foam, which was further dried under vacuum for 12 h. The lipids were then resuspended in ethanol at 60°C. An aqueous solution of 0.65 M triethylammonium sucrose octasulfate (TEA_8SOS) was prepared by cation exchange chromatography, as previously described [17]. Liposomes were formed by injection of the aqueous TEA_8SOS solution into the ethanolic lipid solution (both solutions at 60°C) to a final concentration of 10% ethanol and 50–60 mM phospholipid. The liposomes were sized by extrusion through polycarbonate membranes (Whatman Nucleopore, NJ, USA) with an average pore size of 100 nm. The resulting liposomes had an average size ranging from 102 to 113 nm in diameter, depending on the batch. The liposome size (dynamic light scattering) was determined using a Coulter N4 Plus particle size analyzer (Beckman Coulter, CA, USA). The term 'nanoliposome' is used here to indicate liposome-based nanoparticles of approximately 100 nm diameter, rather than the so-called conventional or other liposomes of greater diameter. Unencapsulated TEA_8SOS was removed using an ion exchange column consisting of Amberlite IRA910 anion exchange resin eluted with water, followed by size exclusion chromatography with Sephadex G-75 eluted with water. Concentrated stocks of dextrose and 4-(2-hydroxyethyl)-1-piperazineethanesulfonic acid (HEPES) were added to the liposome solution to give a final concentration of 5 mM HEPES and 5% dextrose. The pH of the liposome solution was adjusted to pH 6.5 with 1 N NaOH and 1 N HCl.

Irinotecan was dissolved in water and a 40% dextrose stock was added to a final concentration of 5% dextrose and 15 mg/ml irinotecan·HCl. Drug was added at a ratio of 750 g irinotecan·HCl/mol phospholipid and loading was facilitated by adjusting the pH to 6.2, initiated by incubating for 30 min at 60°C, followed by quenching on ice for 15 min. Unencapsulated irinotecan was removed by Sephadex G-75 size exclusion chromatography, eluting with HEPES-buffered saline (5 mM HEPES, 145 mM NaCl, pH 6.5). The irinotecan and SN-38 were quantitated by HPLC using a modification of the method by Warner and Burke [42], using a HPLC system (Dionex, CA, USA) with a C_{18} reverse-phase silica column (Supelco® C18 column; Sigma-Aldrich; 250 × 4 mm, particle size of 5 µm) preceded by a Supelco C18 guard column. The mobile phase consisted of 0.21 M diethylammonium acetate pH 5.5 (73%) and acetonitrile (27%), with isocratic elution at a flow rate of 1.0 ml/min. Nanoliposome samples were detected by absorbance at 375 nm. Tissue samples were detected by fluorescence detection, with an excitation at 370 nm and emission at 535 nm. The observed retention times for irinotecan and SN-38 were 6.1 and 8.0 min, respectively. The phospholipid concentration in the nanoliposomal irinotecan was quantitated spectrophotometrically using a standard phosphate assay [43]. The final nanoliposomal irinotecan formulations used in this work had a drug-to-lipid ratio ranging from 684 to 743 g irinotecan·HCl/mol phospholipid. Stability studies indicated that storage at 4°C for 6 months results in no detectable drug leak-

age and no detectable aggregation as determined by change in size.

Intracranial tumor model

An established glioblastoma multiforme cell line, U87MG, was obtained from the Brain Tumor Research Center Tissue Bank at the University of California, San Francisco (USA). Cells were maintained as monolayers in a complete medium consisting of Eagle's minimal essential medium supplemented with 10% fetal calf serum, nonessential amino acids, 0.1 mg/ml streptomycin sulfate and 100 U/ml penicillin G. Cells were cultured at 37°C in a humidified atmosphere containing 95% air and 5% CO_2. All tumor-bearing animals were congenitally athymic, male, nude rats (rnu/rnu, homozygous), weighing approximately 250–290 g, and were purchased from the National Cancer Institute (MD, USA). The rats were housed under aseptic conditions, which included filtered air and sterilized food, water, bedding and cages. All protocols used in the animal studies were approved by the University of California, San Francisco Institutional Animal Care and Use Committee.

For the intracranial xenograft tumor model, cells were harvested by trypsinization, washed once with Hanks' balanced salt solution without Ca^{2+} and Mg^{2+}, and resuspended in Hanks' balanced salt solution for implantation. A cell suspension containing 5×10^5 cells/10 µl in Hanks' balanced salt solution was used for implantation into the striatal region of athymic rat brains. Under deep isofluorane anesthesia, rats were placed in a small-animal stereotaxic frame (David Kopf Instruments, CA, USA). A sagittal incision was made through the skin to expose the cranium, and a burr hole was made in the skull at 0.5 mm anterior and 3 mm lateral from the bregma using a small dental drill. At a depth of 4.5 mm from the brain surface, 5 µl of cell suspension was injected; 2 min later, another 5 µl was injected at a depth of 4 mm, and after a final 2-min period, the needle was removed and the wound was sutured.

Tissue pharmacokinetics

Rats were treated intravenously with a single bolus injection of free or nanoliposomal irinotecan and animals were sacrificed at prescribed time points. The brain was perfused with phosphate-buffered saline, surgically removed and the tumor mass separated from the surrounding striatum. The tissues were frozen and stored at -80°C until further processing. The tissues were ground under liquid nitrogen, then water was added at a 20% wt/wt ratio. The homogenates (30 µl) were extracted as the lactone form of irinotecan and SN-38 with 0.37 ml of an acidic methanol solution (20% [0.83 M perchloric acid]/ 80% methanol) by vortexing for 10 s (twice), centrifuged at 13,000 rpm for 10 min and the supernatants transferred to autosampler vials for HPLC analysis. Blank homogenates were spiked with irinotecan and SN-38 to estimate extraction efficiency. HPLC analysis was conducted as described above. Pharmacokinetic parameters including the tissue half-lifes of the drug, clearance, the mean residence time in the tumor and the area under the concentration versus time curve were all determined by noncompartmental pharmacokinetics data analysis using PK Solutions 2.0 software (Summit Research Services, CO, USA).

Survival study using the U87 intracranial xenograft model

A total of 36 rats (rnu/rnu, homozygous), implanted with U87MG tumor cells, were randomly divided into three groups (each group n = 12):

- Saline control
- 50 mg/kg/dose free irinotecan
- 50 mg/kg/dose nanoliposomal irinotecan

At 5 days after tumor cell implantation, each group was given four treatments on a schedule of two treatments per week. Rats were monitored daily for survival and general health of the animals (e.g., alertness, grooming, feeding, excreta, skin, fur, mucous membrane conditions, ambulation, breathing and posture). Animals were weighed every 3 days. Kaplan–Meier survival plots were generated from the data. At the end of the study (day 100 post-tumor implantation), the surviving animals were euthanized and necropsied, as were the animals that expired prior to the study end. Brains were excised at the time of necropsy and fixed in 10% buffered formalin phosphate, then 30% sucrose, cut into sections that were 25 µm in thickness and stained with hematoxylin and eosin for histopathological examination. Statistical analysis was performed using a log-rank test with SigmaStat 3.1 software (SigmaStat, CA, USA).

Results

Tumor tissue pharmacokinetics of free & nanoliposomal irinotecan

Pharmacokinetics of the liposome carrier itself were not measured here as the liposome was not labeled. However, we and others have extensively described the PK profile of this carrier system in other reports [18,19,44]. Tumor tissue levels of irinotecan following intravenous (iv.) administration of either free versus nanoliposomal irinotecan were evaluated in the rat intracranial

U87 tumor xenograft model. A single iv. injection of 50 mg/kg of free irinotecan yielded an initial peak (time of maximum concentration at 15 min) in drug concentration followed by rapid decay. Maximum tissue concentration (C_{max}) was 10.2 µg/g for free irinotecan. Nanoliposomal irinotecan given at the same irinotecan dose resulted in a C_{max} of 31.9 µg irinotecan/g, a 3.1-fold higher tissue level than with free drug. Importantly, nanoliposomal irinotecan was associated with markedly prolonged tumor accumulation/retention with a time of maximum concentration at 12 h (Figure 1A). Nanoliposomal irinotecan resulted in tumor AUC for drug of 520.6 µg·h/g compared with AUC following free irinotecan of 47.6 µg·h/g, a 10.9-fold increase (Table 1).

We also analyzed SN-38 levels within the CNS post-treatment. Nanoliposome delivery was again associated with increased tumor accumulation of SN-38 compared with free drug administration (Figure 1C). Maximum SN-38 concentration (C_{max}) following nanoliposomal irinotecan treatment was 95.6 ng SN-38/g, compared with C_{max} of 30.3 ng SN-38/g following free irinotecan treatment, which represented an increase of 3.2-fold. The tumor AUC for SN-38 was 1125 ng·h/g following administration of nanoliposomal irinotecan, compared with an AUC of 640 ng·h/g following free irinotecan – an increase of 1.8-fold. It is notable that nanoliposome delivery showed parallel tissue pharmacokinetics for irinotecan and SN-38 (Figure 1A vs Figure 1C), and also improved tumor C_{max} of both irinotecan and SN-38 to the same approximate threefold extent. These results are consistent with nanoparticle-mediated delivery of precursor irinotecan to brain tumors followed by *in situ* conversion to SN-38 as the predominant mechanism for increased SN-38 levels. Furthermore, nanoliposomal delivery increased tumor AUC by 10.9-fold for irinotecan but only by 1.8-fold for SN-38, also suggesting no appreciable contribution to CNS levels from any peripheral conversion of SN-38.

Nonmalignant striatal tissue surrounding the tumor was also harvested and analyzed for irinotecan (Figure 1B). AUC for irinotecan within normal striatum following treatment with free irinotecan was 5.2 µg·h/g; since AUC within tumor tissue was 47.6 µg·h/g, free irinotecan treatment was associated with a 9.2-fold selectivity for tumor versus normal tissue exposure. Following nanoliposomal irinotecan treatment, AUC within normal striatum was 14.8 µg·h/g; since the AUC within tumor tissue was 520.6 µg·h/g, treatment with nanoliposomal irinotecan yielded 35-fold selectivity for tumor versus normal tissue exposure. SN-38 was undetectable in striatal tissue following either free or nanoliposomal irinotecan treatment (limit of detection = 0.1 ng/g for this fluorescence-based HPLC method).

Therapeutic efficacy of nanoliposomal irinotecan

The therapeutic efficacy of systemically administered nanoliposomal irinotecan was evaluated in comparison with free irinotecan and saline control in the rat U87 glioblastoma intracranial tumor model (Figure 2). This animal model features rapid intracranial tumor growth, allowing a survival end point rather than surrogates or biomarkers such as apoptosis or even tumor size. Tumors were allowed to become established in the brain and then treatments were administered as four iv. doses on days 5, 8, 11 and 14. Both free and nanoliposomal irinotecan were administered at 50 mg irinotecan/kg per dose. The dose and schedule selected is near the maximum tolerated dose, based on prior studies in mice and rats (data not shown). In the saline control group, all animals (n = 12) showed rapid onset of neurologic deterioration due to tumor growth, and had to be euthanized at 19–22 days post-tumor implantation (mean survival = 20.8 ± 0.9 days). In the free irinotecan group, animals showed improved survival compared with the control group (mean survival = 29.5 ± 1.38 days), which was statistically significantly superior (Kaplan–Meier analysis, $p < 0.001$, log-rank test). Nevertheless, all animals (n = 12) had to be euthanized by 27–32 days after tumor cell implantation per protocol due to severe neurologic dysfunction. By contrast, the nanoliposomal irinotecan treatment group displayed prolonged survival (mean survival = 54.2 ± 19.2 days); the Kaplan–Meier analysis confirmed a significant survival advantage for nanoliposomal irinotecan over free irinotecan ($p < 0.001$, log-rank test) (Figure 2).

Of the 12 rats in the nanoliposomal irinotecan group, eight had to be euthanized 26–35 days after tumor implantation; the remaining four rats lived until termination of the study on day 100 with apparent cures. The apparent cure rate of 33% associated with nanoliposomal irinotecan treatment was significantly superior to the 0% apparent cures in the control and free irinotecan groups ($p = 0.008$, Fisher's test).

Histopathologic evaluation of antitumor activity

Brains and brain tumors in the treated animals were analyzed postmortem. All animals from the control group (n = 12) and the free irinotecan group (n = 12), as well as those animals in the nanoliposomal irinotecan group that were euthanized prior to study termination (n = 8 out of 12), showed evidence of large intracranial U87 tumors (Figures 3A & 3B), consistent with tumor progression as the cause of death. All of the four surviving animals in the nanoliposomal irinotecan group showed no histological evidence of tumor (Figure 3C), and demonstrated scarring

responses consistent with post-treatment effect in the striatum (arrow).

Host toxicity

The animals used in the determination of antitumor efficacy were also monitored for signs of toxicity during the course of treatment. Animals receiving nanoliposomal irinotecan lost on average 8.8% (27 g) of their initial bodyweight over the treatment protocol ending on day 14, but showed rapid regain of weight immediately after the treatment protocol was finished. Blank nanoliposomes without drug were not evaluated here. Detailed toxicology studies of nanoliposomes having no drug but containing the same TEA_8SOS trapping agent used here have been previously reported [19]. These studies showed no adverse effects up to 583 umol phopholipid/kg, which is eightfold higher than the dose used here. Animals receiving free irinotecan showed slight weight gain (mean = 0.66 g, 0.3% of initial bodyweight) over the treatment protocol. Control animals that received normal saline injections also showed weight gain (mean = 22 g, 8.1% of initial bodyweight) during the treatment protocol. Weight loss was not generally observed in the control and free drug groups, presumably because rapid intracranial tumor growth caused death prior to cachexia or other systemic effects of tumor progression. All animals were observed to have short-term diarrhea after tail-vein injections of irinotecan and nanoliposomal irinotecan, which resolved within 1 day. Animals were inspected routinely as mandated by the Institutional Animal Care and Use Committee-approved protocol. Except for short-term diarrhea and weight loss, there were no observed changes in general health for the mice in any treatment group.

Discussion

Poor outcomes for patients afflicted with malignant brain tumors warrant the development of new and improved approaches for drug treatment. Certain liposome-based drugs can substantially increase circulation time of the delivered drug, potentially resulting in increased tumor accumulation and improved antitumor activity [6]; and this delivery advantage has been proposed to be applicable to intracranial tumors [32]. Here, we hypothesized that systemic administration of nanoliposomal irinotecan may provide significant advantages over free irinotecan in the treatment of orthotopic brain tumor xenografts in rats.

Tissue pharmacokinetic analysis revealed that nanoliposomal irinotecan treatment resulted in considerably greater brain tumor exposure than that associated with free drug treatment. We previously reported a large advantage in circulation time for nanoliposomal irinotecan versus free irinotecan [18],

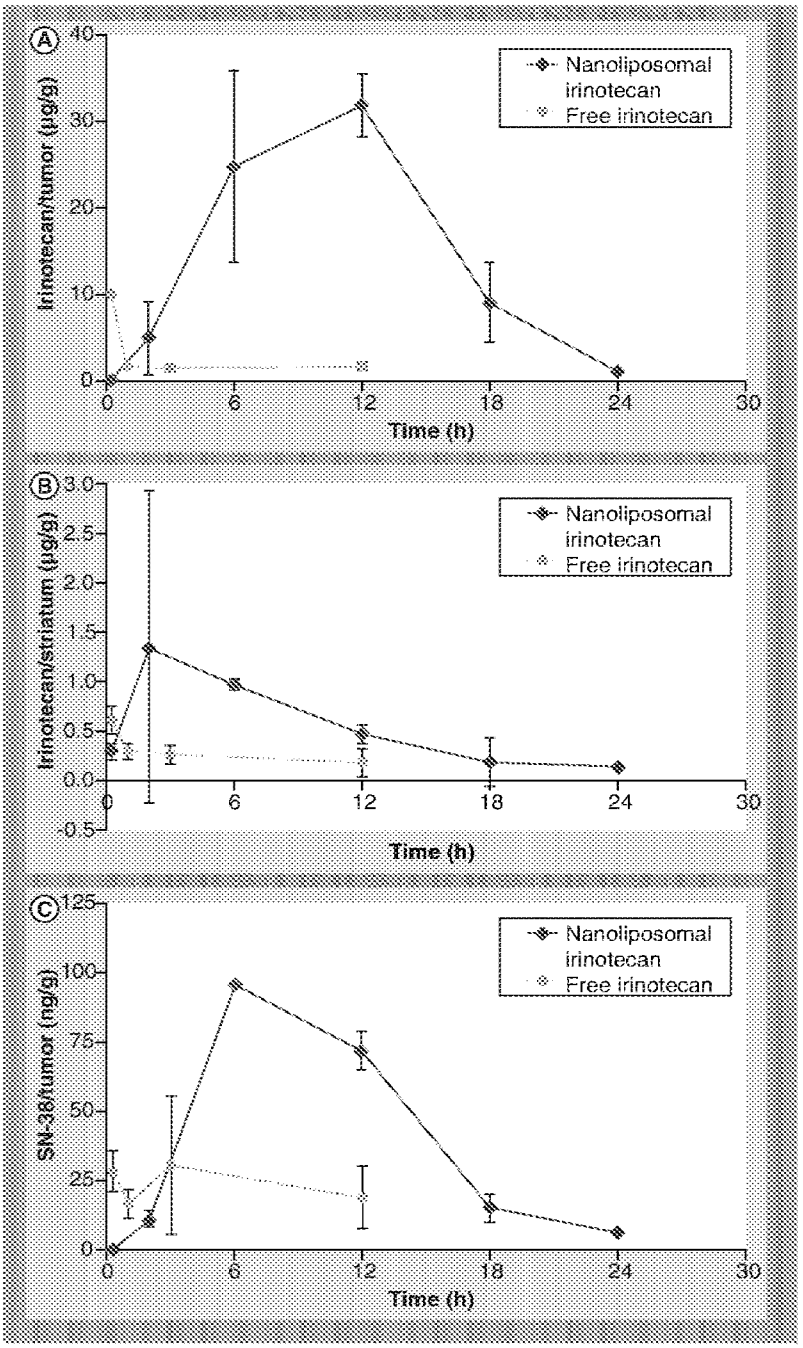

Figure 1. Tissue pharmacokinetics in normal brain and brain tumor following free or nanoliposomal irinotecan treatment. Animals bearing intracranial U87 tumors were treated with a single bolus intravenous injection of free irinotecan or nanoliposomal irinotecan at a dose of 50 mg/kg. Tumors were allowed to grow for 10 days before treatment. At the indicated times, the brains were removed and the tumor and surrounding striatum were isolated. Results from tissue analysis are shown for free irinotecan and nanoliposomal irinotecan in the **(A)** tumor and **(B)** striatum. **(C)** Tumor concentrations of SN-38, the active metabolite of irinotecan, are given for animals receiving each treatment. The error bars represent standard deviation.

Table 1. Tissue pharmacokinetics of free irinotecan and nanoliposomal irinotecan.

Tissue and analyte	Administered formulation	$t_{1/2}$ (h)	C_{max}	AUC_0	CL (g/h)	MRT (h)
Tumor irinotecan	Free irinotecan	9.3	10.2 µg/g	47.6 µg·h/g	315	15.1
Tumor irinotecan	nLs irinotecan	2.5	31.9 µg/g	520.6 µg·h/g	28.8	8.2
Striatum irinotecan	Free irinotecan	8.9	0.60 µg/g	5.2 µg·h/g	2900	13.4
Striatum irinotecan	nLs irinotecan	6.2	1.34 µg/g	14.8 µg·h/g	1017	9.5
Tumor SN-38	Free irinotecan	12.9	30.3 ng/g	641 ng·h/g	23.4	19.1
Tumor SN-38	nLs irinotecan	4.3	95.6 ng/g	1125 ng·h/g	13.3	10.2

AUC_0: Area under the time–concentration curve; CL: Tissue clearance; C_{max}: Maximum concentration measured; MRT: Mean residence time; nLs: Nanoliposomal; $t_{1/2}$: Tissue half-life of the drug.

which presumably provided the driving force for enhanced brain tumor penetration. The peak concentration of irinotecan in brain tumor tissue was improved by threefold via nanoliposome delivery compared with free drug, while tumor AUC was improved by 10.9-fold. A significant portion of the tumor AUC for free irinotecan is contributed by the later elimination phase time points of the exponential curve, where the clearance rate is slow, thus the tumor tissue half-life for free irinotecan is longer than that of nanoliposomal irinotecan, which has more of a Gaussian shape tumor accumulation profile. The tumor C_{max} for the nanoliposomal irinotecan is not reached until 12 h.

The selectivity of nanoliposomal irinotecan for tumor versus normal tissue within the brain was also pronounced as compared with free drug. Because of the BBB, free irinotecan was restricted in reaching normal brain tissue, and showed 9.2-fold greater uptake in brain tumors. Nanoliposomal irinotecan demonstrated a striking 35-fold selectivity for brain tumors versus normal striatal tissue. This result suggests that properties of brain tumor vessels can be particularly exploited via nanoliposomal delivery to enhance drug concentrations within brain tumors while simultaneously minimizing exposure within normal brain tissue.

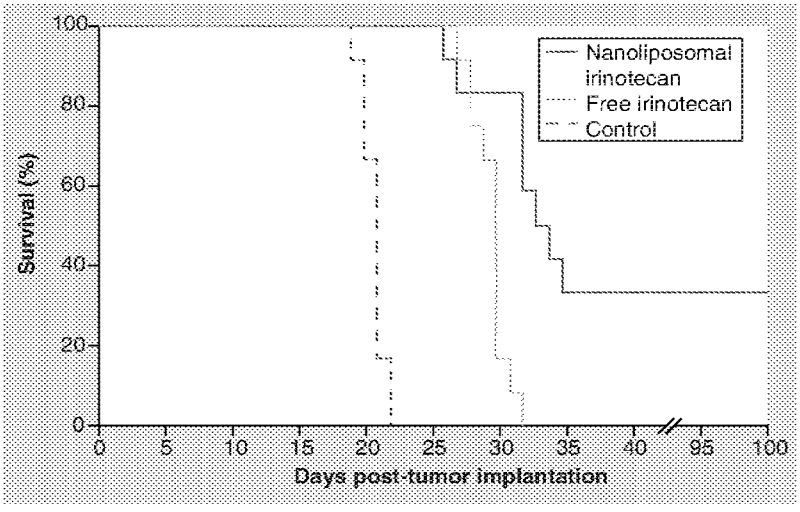

Figure 2. Kaplan–Meier survival curves for of an orthotopic U87MG glioma rat model treated with free irinotecan and nanoliposomal irinotecan. A total of 12 animals were used for each group and tumors were allowed to grow for 5 days before treatment, with control (drug-free liposomes), 50 mg/kg free irinotecan (Camptosar®; Pfizer, NY, USA) or 50 mg/kg nanoliposomal irinotecan. Each formulation was administered twice weekly for a total of four treatments. Animals were euthanized upon development of neurological symptoms associated with tumor progression.

Irinotecan is mainly a prodrug that is enzymatically activated to metabolite SN-38 by carboxylesterases [45], in particular human carboxylesterase-2 [46], either directly or after CYP450 3A-mediated oxidation to 7-ethyl-10-[4-(1-piperidino)-1-amino] carbonyl-oxycamptothecin. Free irinotecan is subject to carboxylesterase action within liver and intestinal tissues [47], which is believed to be a major source of SN-38 eventually reaching tumors. However, our data indicate that nanoliposomal delivery of irinotecan produced very high concentrations and prolonged exposure of irinotecan within brain tumors, which was consequently associated with increased intratumoral SN-38 levels as well. Although we cannot formally exclude the possibility that some peripheral conversion of irinotecan to SN-38 may have contributed to the SN-38 measured within the rodent brain tumors, SN-38 is a short-lived metabolite (tissue half-life of 7 min) [48], and accumulation within brain tumors following hepatic conversion is unlikely to have been significant. Finally, nanoliposomal irinotecan treatment produced parallel tumor tissue pharmacokinetic profiles for both irinotecan and SN-38, and no evidence for additional SN-38 arising elsewhere.

Our results suggest a mechanism of delivery in which nanoliposomal irinotecan accumulates progressively to high levels within brain tumors by exploiting permissive tumor vessel properties, followed by intratumoral conversion to SN-38. Within tumor tissue, irinotecan may slowly leak from the liposome and be converted to SN-38 by endogenous tumor carboxylesterases [49]. Conversion of irinotecan to SN-38 has been observed in U87MG cells *in vitro* and *in vivo* [50,51]. Alternatively, intact particles could

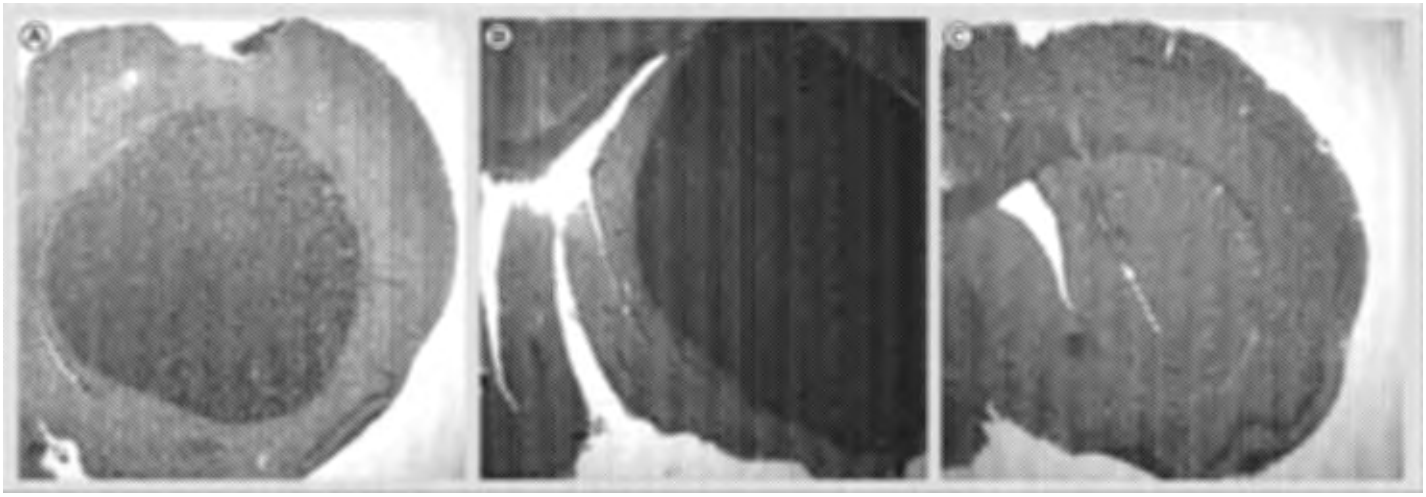

Figure 3. Histological evaluation of brains from animals used in the efficacy study. All animals were examined at death or at the study end. Hematoxylin and eosin sections of rodent striatum from groups receiving **(A)** control and **(B)** free irinotecan showing large intracranial tumor size at the time of euthanasia are representative of all animals euthanized prior to study termination at day 100. **(C)** Hematoxylin and eosin section from a surviving animal receiving nanoliposomal irinotecan, which is representative of all four animals surviving tumor-free until the end of the projected survival study showing no evidence of tumor cells and only a scar remaining (arrow).

be phagocytosed by tumor-associated macrophages, which have high carboxylesterase activity [18,52].

Treatment of intracranial U87MG xenografts demonstrated that these delivery advantages of nanoliposomal irinotecan produced superior antitumor efficacy compared with free irinotecan. Although this study of 12 rats per group was somewhat limited in scope, the approach of using nanoliposomal irinotecan rather than the free drug was associated with improvements in both median survival and cure end points. These included a significant survival advantage ($p < 0.001$) versus free irinotecan, as well as apparent cures in 33% of animals.

The nanoliposomal irinotecan agent may be useful in other anticancer applications. Our laboratory and others have previously reported the use of convection-enhanced delivery (CED) for extensive nanoparticle distribution in the CNS [53,54]. CED is a technique for local delivery to the brain using a bulk convective flow to push material away from the infusion site into the surrounding brain tissue. CED can be used to effectively distribute small molecules or nanoscale material, such as macromolecules and liposomes [53–55]. Nanoliposomal irinotecan can be infused via CED in intracranial tumors and this approach is significantly more efficacious than CED of free irinotecan [21,56]. However, since CED is invasive and can be unavailable or infeasible for some patients, it was of interest to evaluate this novel agent as an intravenous treatment. In addition, liposomal drugs such as this can be converted to targeted immunoliposome versions via incorporation of antibody fragments onto the membrane surface [57–60].

Conclusion

We conclude that iv. nanoliposomal irinotecan treatment is associated with greater intracranial tumor tissue accumulation for irinotecan and SN-38 than associated with free drug, which translated into significant therapeutic advantage in preclinical studies. Systemic nanoliposomal irinotecan (MM-398; Merrimack Pharmaceuticals, MA, USA; irinotecan sucrosofate) is currently being evaluated in a Phase I clinical trial in patients with recurrent high-grade gliomas.

Financial & competing interests disclosure

This work was supported by grants from the NIH, the National Cancer Institute Specialized Programs of Research Excellence in Brain Tumors grant P50-CA097257 and Accelerated Brain Cancer Cure. CO Noble, ME Hayes, DC Drummond and DB Kirpotin are equity holders of Merrimack Pharmaceuticals (MA, USA). JW Park is an advisor and equity holder of Merrimack Pharmaceuticals. The authors have no other relevant affiliations or financial involvement with any organization or entity with a financial interest in or financial conflict with the subject matter or materials discussed in the manuscript apart from those disclosed.

No writing assistance was utilized in the production of this manuscript.

Ethical conduct of research

The authors state that they have obtained appropriate institutional review board approval or have followed the principles outlined in the Declaration of Helsinki for all human or animal experimental investigations.

Executive summary

Background

- We evaluated the pharmacologic and therapeutic properties of nanoliposomal irinotecan, a novel liposome-based nanoparticle formulation of irinotecan, following intravenous administration in an orthotopic brain tumor model.

Results

- Nanoliposomal irinotecan resulted in maximum tissue concentration (C_{max}) of 31.9 µg irinotecan/g, a 3.1-fold higher tissue level than with free drug.
- Nanoliposomal irinotecan was associated with markedly prolonged tumor accumulation/retention. Its tumor AUC for drug was 520.6 µg·h/g compared with an AUC following free irinotecan of 47.6 µg·h/g – a 10.9-fold increase.
- Maximum SN-38 concentration (C_{max}) following nanoliposomal irinotecan treatment was 95.6 ng SN-38/g, compared with C_{max} of 30.3 g SN-38/g following free irinotecan treatment – an increase of 3.2-fold. Tumor AUC for SN-38 was 1125 ng·h/g following administration of nanoliposomal irinotecan compared with an AUC of 640 ng·h/g following free irinotecan – an increase of 1.8-fold.
- Tissue pharmacokinetic analysis of irinotecan and SN-38 levels suggested that nanoparticle-mediated delivery of precursor irinotecan to brain tumors, followed by *in situ* conversion to SN-38, was the predominant mechanism for increased SN-38 levels.
- Following nanoliposomal irinotecan treatment, AUC within normal striatum was 14.8 µg·h/g, representing a 35-fold selectivity for tumor versus normal tissue exposure.
- As a therapy for orthotopic brain tumors, nanoliposomal irinotecan showed a mean survival time of 54.2 versus 29.5 days for free irinotecan ($p < 0.001$, log-rank test).
- The apparent cure rate of 33% associated with nanoliposomal irinotecan treatment was significantly superior to the 0% apparent cures in the control and free irinotecan groups ($p = 0.008$, Fisher's test).

Discussion

- Nanoliposomal irinotecan shows promise as systemic treatment for brain tumors.

References

Papers of special note have been highlighted as:
• of interest; •• of considerable interest

1 Fisher PG, Buffler PA. Malignant gliomas in 2005: where to GO from here? *JAMA* 293(5), 615–617 (2005).

2 Reardon DA, Friedman HS, Powell JBJ, Gilbert M, Yung WK. Irinotecan: promising activity in the treatment of malignant glioma. *Oncology* 17(5 Suppl. 5), 9–14 (2003).

3 Surawicz TS, Davis F, Freels S, Laws ER Jr, Menck HR. Brain tumor survival: results from the National Cancer Data Base. *J. Neurooncol.* 40(2), 151–160 (1998).

4 Reese TS, Karnovsky MJ. Fine structural localization of a blood–brain barrier to exogenous peroxidase. *J. Cell Biol.* 34(1), 207–217 (1967).

5 Pardridge WM. Molecular biology of the blood–brain barrier. *Mol. Biotech.* 30(1), 57–69 (2005).

6 Drummond DC, Meyer O, Hong KL, Kirpotin DB, Papahadjopoulos D. Optimizing liposomes for delivery of chemotherapeutic agents to solid tumors. *Pharmacol. Rev.* 51(4), 691–743 (1999).

• Comprehensive review on liposome therapeutics.

7 Allen TM, Cullis PR. Liposomal drug delivery systems: from concept to clinical applications. *Adv. Drug Deliv. Rev.* 65(1), 36–48 (2013).

8 Gibson JM, Alzghari S, Ahn C, Trantham H, La-Beck NM. The role of PEGylated liposomal doxorubicin in ovarian cancer: a meta-analysis of randomized clinical trials. *Oncologist* 18(9), 1022–1031 (2013).

9 Gabizon A, Isacson R, Libson E *et al.* Clinical studies of liposome-encapsulated doxorubicin. *Acta Oncol.* 33, 779–786 (1994).

10 Thigpen JT, Aghajanian CA, Alberts DS *et al.* Role of PEGylated liposomal doxorubicin in ovarian cancer. *Gynecol. Oncol.* 96(1), 10–18 (2005).

11 Rose PG. PEGylated liposomal doxorubicin: optimizing the dosing schedule in ovarian cancer. *Oncologist* 10(3), 205–214 (2005).

12 Rifkin RM, Gregory SA, Mohrbacher A, Hussein MA. PEGylated liposomal doxorubicin, vincristine, and dexamethasone provide significant reduction in toxicity compared with doxorubicin, vincristine, and dexamethasone in patients with newly diagnosed multiple myeloma: a Phase III multicenter randomized trial. *Cancer* 106(4), 848–858 (2006).

13 Al-Batran SE, Bischoff J, von Minckwitz G *et al.* The clinical benefit of PEGylated liposomal doxorubicin in patients with metastatic breast cancer previously treated with conventional anthracyclines: a multicentre Phase II trial. *Br. J. Cancer* 94(11), 1615–1620 (2006).

14 Rodriguez MA, Pytlik R, Kozak T *et al.* Vincristine sulfate liposomes injection (Marqibo) in heavily pretreated patients with refractory aggressive non-Hodgkin lymphoma: report of the pivotal Phase 2 study. *Cancer* 115(15), 3475–3482 (2009).

15 Webb MS, Harasym TO, Masin D, Bally MB, Mayer LD. Sphingomyelin–cholesterol liposomes significantly enhance the pharmacokinetic and therapeutic properties of vincristine in murine and human tumour models. *Br. J. Cancer* 72(4), 896–904 (1995).

16 Webb MS, Logan P, Kanter PM *et al.* Preclinical pharmacology, toxicology and efficacy of sphingomyelin/cholesterol liposomal vincristine for therapeutic treatment of cancer. *Cancer Chemother. Pharmacol.* 42(6), 461–470 (1998).

17 Drummond DC, Marx C, Guo Z *et al.* Enhanced pharmacodynamic and antitumor properties of a histone deacetylase inhibitor encapsulated in liposomes or ErbB2-targeted immunoliposomes. *Clin. Cancer Res.* 11(9), 3392–3401 (2005).

18 Drummond DC, Noble CO, Guo Z *et al.* Development of a highly active nanoliposomal irinotecan using a novel intraliposomal stabilization strategy. *Cancer Res.* 66(6), 3271–3277 (2006).

19 Drummond DC, Noble CO, Guo Z *et al.* Improved pharmacokinetics and efficacy of a highly stable nanoliposomal vinorelbine. *J. Pharmacol. Exp. Ther.* 328(1), 321–330 (2009).

20 Noble CO, Guo Z, Hayes ME *et al.* Characterization of highly stable liposomal and immunoliposomal formulations of vincristine and vinblastine. *Cancer Chemother. Pharmacol.* 64(4), 741–751 (2009).

21 Noble CO, Krauze MT, Drummond DC *et al.* Novel nanoliposomal CPT-11 infused by convection-enhanced delivery in intracranial tumors: pharmacology and efficacy. *Cancer Res.* 66(5), 2801–2806 (2006).

22 Ko AH, Tempero MA, Shan YS *et al.* A multinational Phase 2 study of nanoliposomal irinotecan sucrosofate (PEP02, MM-398) for patients with gemcitabine-refractory metastatic pancreatic cancer. *Br. J. Cancer* 109(4), 920–925 (2013).

• **Describes use of nanoliposomal irinotecan in the clinic setting.**

23 Roy AC, Park SR, Cunningham D *et al.* A randomized Phase II study of PEP02 (MM-398), irinotecan or docetaxel as a second-line therapy in patients with locally advanced or metastatic gastric or gastro-oesophageal junction adenocarcinoma. *Ann. Oncol.* 24(6), 1567–1573 (2013).

24 Prados MD, Yung WK, Jaeckle KA *et al.* Phase 1 trial of irinotecan (CPT-11) in patients with recurrent malignant glioma: a North American Brain Tumor Consortium study. *Neuro Oncol.* 6(1), 44–54 (2004).

25 Kaneda N, Nagata H, Furuta T, Yokokura T. Metabolism and pharmacokinetics of the camptothecin analogue CPT-11 in the mouse. *Cancer Res.* 50(6), 1715–1720 (1990).

•• **Describes conversion of CPT-11 to more active SN-38.**

26 Garcia-Carbonero R, Supko JG. Current perspectives on the clinical experience, pharmacology, and continued development of the camptothecins. *Clin. Cancer Res.* 8(3), 641–661 (2002).

27 Mathijssen RHJ, van Alphen RJ, Verweij J *et al.* Clinical pharmacokinetics and metabolism of irinotecan (CPT-11). *Clin. Cancer Res.* 7(8), 2182–2194 (2001).

28 Rivory LP, Chatelut E, Canal P, Mathieu-Boue A, Robert J. Kinetics of the *in vivo* interconversion of the carboxylate and lactone forms of irinotecan (CPT-11) and of its metabolite SN-38 in patients. *Cancer Res.* 54(24), 6330–6333 (1994).

29 Cecchin E, Corona G, Masier S *et al.* Carboxylesterase isoform 2 mRNA expression in peripheral blood mononuclear cells is a predictive marker of the irinotecan to SN38 activation step in colorectal cancer patients. *Clin. Cancer Res.* 11(19 Pt 1), 6901–6907 (2005).

30 Krauze MT, Noble CO, Kawaguchi T *et al.* Convection-enhanced delivery of nanoliposomal CPT-11 (irinotecan) and PEGylated liposomal doxorubicin (Doxil) in rodent intracranial brain tumor xenografts. *Neuro Oncol.* 9(4), 393–403 (2007).

31 Pardridge WM. Blood–brain barrier drug targeting: the future of brain drug development. *Mol. Interv.* 3(2), 90–105, 151 (2003).

32 Huynh GH, Deen DF, Szoka FC Jr. Barriers to carrier mediated drug and gene delivery to brain tumors. *J. Control. Release* 110(2), 236–259 (2006).

33 Huang SK, Martin FJ, Jay G *et al.* Extravasation and transcytosis of liposomes in Kaposi's sarcoma-like dermal lesions of transgenic mice bearing the HIV *Tat* gene. *Am. J. Path.* 143, 10–14 (1993).

34 Stapleton S, Allen C, Pintilie M, Jaffray DA. Tumor perfusion imaging predicts the intra-tumoral accumulation of liposomes. *J. Control. Release* 172(1), 351–357 (2013).

35 Torchilin VP. Passive and active drug targeting: drug delivery to tumors as an example. *Handb. Exp. Pharmacol.* (197), 3–53 (2010).

36 Hobbs SK, Monsky WL, Yuan F *et al.* Regulation of transport pathways in tumor vessels: role of tumor type and microenvironment. *Proc. Natl Acad. Sci. USA* 95(8), 4607–4612 (1998).

• **Detailed assessment of the effect of nanoparticle size on tumor accumulation.**

37 Pluen A, Boucher Y, Ramanujan S *et al.* Role of tumor–host interactions in interstitial diffusion of macromolecules: cranial vs. subcutaneous tumors. *Proc. Natl Acad. Sci. USA* 98(8), 4628–4633 (2001).

38 Siegal T, Horowitz A, Gabizon A. Doxorubicin encapsulated in sterically stabilized liposomes for the treatment of a brain–tumor model – biodistribution and therapeutic efficacy. *J. Neurosurg.* 83(6), 1029–1037 (1995).

•• **Uptake of liposomal therapeutic in brain tumor model is demonstrated.**

39 Arnold RD, Mager DE, Slack JE, Straubinger RM. Effect of repetitive administration of doxorubicin-containing liposomes on plasma pharmacokinetics and drug biodistribution in a rat brain tumor model. *Clin. Cancer Res.* 11(24 Pt 1), 8856–8865 (2005).

40 Verreault M, Strutt D, Masin D *et al.* Irinophore C, a lipid-based nanoparticulate formulation of irinotecan, is more effective than free irinotecan when used to treat an orthotopic glioblastoma model. *J. Control. Release* 158(1), 34–43 (2012).

41 Verreault M, Strutt D, Masin D *et al.* Vascular normalization in orthotopic glioblastoma following intravenous treatment with lipid-based nanoparticulate formulations of irinotecan (Irinophore C), doxorubicin

(Caelyx(R)) or vincristine. *BMC Cancer* 11(124), 124 (2011).

42 Warner DL, Burke TG. Simple and versatile high-performance liquid chromatographic method for the simultaneous quantitation of the lactone and carboxylate forms of camptothecin anticancer drugs. *J. Chromatogr. B Biomed. Sci. Appl.* 691(1), 161–171 (1997).

43 Bartlett GR. Phosphorus assay in column chromatography. *J. Biol. Chem.* 234(3), 466–468 (1959).

44 Messerer CL, Ramsay EC, Waterhouse D *et al.* Liposomal irinotecan: formulation development and therapeutic assessment in murine xenograft models of colorectal cancer. *Clin. Cancer Res.* 10(19), 6638–6649 (2004).

45 Rivory LP, Bowles MR, Robert J, Pond SM. Conversion of irinotecan (CPT-11) to its active metabolite, 7-ethyl-10-hydroxycamptothecin (SN-38), by human liver carboxylesterase. *Biochem. Biopharmacol.* 52(7), 1103–1111 (1996).

46 Humerickhouse R, Lohrbach K, Li L, Bornson WF, Dolan ME. Characterization of CPT-11 hydrolysis by human liver carboxylesterase isoforms hCE-1 and hCE-2. *Cancer Res.* 60(5), 1189–1192 (2000).

47 Hennebelle I, Terret C, Chatelut E *et al.* Characterization of CPT-11 converting carboxylesterase activity in colon tumor and normal tissues: comparison with p-nitrophenylacetate converting carboxylesterase activity. *Anticancer Drugs* 11(6), 465–470 (2000).

48 Atsumi R, Okazaki O, Hakusui H. Metabolism of irinotecan to SN-38 in a tissue-isolated tumor model. *Biol. Pharm. Bull.* 18(7), 1024–1026 (1995).

49 Guichart S, Terret C, Hennebelle I *et al.* CPT-11 converting carboxylesterase and topoisomerase I activities in tumour and normal colon and liver tissues. *Br. J. Cancer* 80(3/4), 364–370 (1999).

50 Chen TC, Su S, Fry D, Liebes L. Combination therapy with irinotecan and protein kinase C inhibitors in malignant glioma. *Cancer* 97(9), 2363–2373 (2003).

51 Wang W, Ghandi A, Liebes L *et al.* Effective conversion of irinotecan to SN-38 after intratumoral drug delivery to an intracranial murine glioma model *in vivo*. Laboratory investigation. *J. Neurosurg.* 114(3), 689–694 (2007).

52 Needham LA, Davidson AH, Bawden LJ *et al.* Drug targeting to monocytes and macrophages using esterase-sensitive chemical motifs. *J. Pharmacol. Exp. Ther.* 339(1), 132–142 (2011).

53 Saito R, Krauze MT, Bringas J *et al.* Gadolinium-loaded liposomes allow for real-time magnetic resonance imaging of convection-enhanced delivery in the primate brain. *Exp. Neurol.* 196(2), 381–389 (2005).

54 MacKay JA, Deen DF, Szoka FC. Distribution in brain of liposomes after convection enhanced delivery; modulation by particle charge, particle diameter, and presence of steric coating. *Brain Res.* 1035(2), 139–153 (2005).

55 Bobo RH, Laske DW, Akbasak A *et al.* Convection-enhanced delivery of macromolecules in the brain. *Proc. Natl Acad. Sci. USA* 91(6), 2076–2080 (1994).

56 Chen PY, Ozawa T, Drummond DC *et al.* Comparing routes of delivery for nanoliposomal irinotecan shows superior anti-tumor activity of local administration in treating intracranial glioblastoma xenografts. *Neuro Oncol.* 15(2), 189–197 (2013).

57 Gupta B, Torchilin VP. Monoclonal antibody 2C5-modified doxorubicin-loaded liposomes with significantly enhanced therapeutic activity against intracranial human brain U-87 MG tumor xenografts in nude mice. *Cancer Immunol. Immunother.* 56(8), 1215–1223 (2007).

- **Demonstrates a case where antibody targeting improves the efficacy of a liposomal therapeutic in an intracranial brain tumor model.**

58 Mamot C, Drummond DC, Noble CO *et al.* Epidermal growth factor receptor-targeted immunoliposomes significantly enhance the efficacy of multiple anticancer drugs *in vivo*. *Cancer Res.* 65(24), 11631–11638 (2005).

59 Nellis DF, Ekstrom DL, Kirpotin DB *et al.* Preclinical manufacture of an anti-HER2 scFv-PEG-DSPE, liposome-inserting conjugate. 1. Gram-scale production and purification. *Biotechnol. Prog.* 21(1), 205–220 (2005).

60 Nellis DF, Giardina SL, Janini GM *et al.* Preclinical manufacture of anti-HER2 liposome-inserting, scFv-PEG-Lipid conjugate. 2. Conjugate micelle identity, purity, stability, and potency analysis. *Biotechnol. Prog.* 21(1), 221–232 (2005).

VOLUME 24 · NUMBER 34 · DECEMBER 1 2006

JOURNAL OF CLINICAL ONCOLOGY

ORIGINAL REPORT

Phase III Trial Comparing Supportive Care Alone With Supportive Care With Oral Topotecan in Patients With Relapsed Small-Cell Lung Cancer

Mary E.R. O'Brien, Tudor-Eliade Ciuleanu, Hristo Tsekov, Yaroslav Shparyk, Branka Čučeviá, Gabor Juhasz, Nicholas Thatcher, Graham A. Ross, Graham C. Dane, and Theresa Crofts

From the Royal Marsden Hospital, Sutton; Christie Hospital, Manchester; GlaxoSmithKline, Harlow, United Kingdom; Institutul Oncologic, Cluj-Napoca, Romania; Active Treatment Hospital, Varna, Bulgaria; Lviv State Oncology, Lviv, Ukraine; Klinika za plućne bolesti Jordanovac, Zagreb, Croatia; and Margit Kórnáz, Csorna, Hungary.

Submitted March 28, 2006; accepted September 25, 2006.

Supported by GlaxoSmithKline, Middlesex, United Kingdom.

Presented in part at the International Association for the Study of Lung Cancer's 11th World Conference on Lung Cancer, Barcelona, Spain, July 3-6, 2005.

The trial was designed by the sponsor (G.S.K.) who held and analyzed the data. The contents of this article were reviewed and approved by all authors.

Authors' disclosures of potential conflicts of interest and author contributions are found at the end of this article.

Address reprint requests to Mary O'Brien, MD, FRCP, Royal Marsden Hospital, National Health System Trust, Sutton Surrey, SM2 5 PT, England; e-mail: mary.o'brien@rmh.nhs.uk.

0732-183X/06/2434-5441/$20.00

DOI: 10.1200/JCO.2006.06.5821

ABSTRACT

Purpose
For patients with small-cell lung cancer (SCLC), further chemotherapy is routinely considered at relapse after first-line therapy. However, proof of clinical benefit has not been documented.

Patients and Methods
This study randomly assigned patients with relapsed SCLC not considered as candidates for standard intravenous therapy to best supportive care (BSC) alone (n = 70) or oral topotecan (2.3 mg/m^2/d, days 1 through 5, every 21 days) plus BSC (topotecan; n = 71).

Results
In the intent-to-treat population, survival (primary end point) was prolonged in the topotecan group (log-rank P = .0104). Median survival with BSC was 13.9 weeks (95% CI, 11.1 to 18.6) and with topotecan, 25.9 weeks (95% CI, 18.3 to 31.6). Statistical significance for survival was maintained in a subgroup of patients with a short treatment-free interval (≤ 60 days). Response to topotecan was 7% partial and 44% stable disease. Patients on topotecan had slower quality of life deterioration and greater symptom control. Principal toxicities with topotecan were hematological: grade 4 neutropenia, 33%; grade 4 thrombocytopenia, 7%; and grade 3/4 anemia, 25%. Comparing topotecan with BSC, infection ≥ grade 2 was 14% versus 12% and sepsis 4% versus 1%; other grade 3/4 events included vomiting 3% versus 0, diarrhea 6% versus 0, dyspnea 3% versus 9%, and pain 3% versus 6%. Toxic deaths occurred in four patients (6%) in the topotecan arm. All cause mortality within 30 days of random assignment was 13% on BSC and 7% on topotecan.

Conclusion
Chemotherapy with oral topotecan is associated with prolongation of survival and quality of life benefit in patients with relapsed SCLC.

J Clin Oncol 24:5441-5447. © 2006 by American Society of Clinical Oncology

INTRODUCTION

The majority of patients with small-cell lung cancer (SCLC) who are treated with standard chemotherapy experience relapse within 1 year of treatment. At relapse, patients are routinely considered for further chemotherapy, and there is evidence that this is associated with symptom improvement in patients who have a relatively long treatment-free interval (TFI) after first-line therapy (considered sensitive disease).[1,2] Patients with short TFI (or resistant SCLC) are less likely to achieve objective tumor response than patients with sensitive SCLC,[3] and for them the risks versus benefits of chemotherapy at relapse are ill defined.

Topotecan (Hycamtin; GlaxoSmithKline, Research Triangle Park, NC) inhibits the cut-and-repair nuclear enzyme topoisomerase I. The intravenous formulation is active against relapsed ovarian cancer and SCLC.[4-8] An oral formulation of topotecan has similar efficacy to the intravenous formulation in patients with relapsed SCLC.[9-11] In a phase III study of patients with relapsed sensitive SCLC, response rates with oral and intravenous topotecan were 18.3% and 21.9%, respectively.[11]

In order to define the actual risk and benefit associated with chemotherapy at relapse with SCLC, a randomized study was conducted. Patients unsuitable for standard intravenous chemotherapy received either oral topotecan plus best supportive care (topotecan) or best supportive care alone (BSC) and were evaluated for survival, quality of life (QOL), and adverse experiences.

PATIENTS AND METHODS

Patient Selection

Patients were randomly assigned 1:1 using a centralized automated registration and randomization system (JhoyLink, Paris, France),[12] stratified by sex, performance status (PS 0/1 or 2), TFI (≤ 60 days or > 60 days), and presence of liver metastases.

Because of the possibility of being randomly assigned to BSC alone, only patients considered unsuitable for further intravenous chemotherapy were recruited. Unsuitability was based on local policy concerning the unproven risk and benefit in patients with resistant (short TFI) SCLC and assessed on an individual basis by the attending oncologist. Initially excluded from the protocol were patients who had a TFI of longer than 90 days for whom treatment with BSC alone was not acceptable. However, as the study progressed, it became apparent that some patients with sensitive SCLC refuse further chemotherapy because of the risk of toxicity or become unsuitable for standard chemotherapy because of comorbidities. The protocol was therefore amended to allow the inclusion of such patients. As the population was stratified at random assignment, the final study population is comprised of two predefined subsets according to TFI. A minimum of 45 days was required after initial chemotherapy to ensure bone marrow recovery.

Other eligibility criteria included extensive or limited SCLC, one prior chemotherapy regimen, age ≥ 18 years, PS (Eastern Cooperative Oncology Group scale) of 0, 1, or 2, hemoglobin ≥ 9.0 g/dL, WBC count ≥ 3,500/mm^3, platelets ≥ 100,000/mm^3, neutrophils ≥ 1,500/mm^3, calculated creatinine clearance ≥ 60 mL/min, serum bilirubin ≤ 2.0 mg/dL AST and ALT and alkaline phosphatase ≤ five times upper limit of normal with liver metastases or ≤ two times without, at least 24 hours since last radiotherapy, and at least 3 months since last immunotherapy.

Exclusion criteria were symptomatic CNS metastases, concomitant or previous malignancies within the last 5 years (except SCLC and adequately treated nonmelanoma skin cancer, cervical carcinoma in situ, or localized low-grade prostate cancer), infection, severe comorbidities, gastrointestinal conditions or drugs affecting gastrointestinal absorption, prior topotecan therapy, or hypersensitivity or other contraindication to the study drugs.

The protocol was approved by the institutional review board/ethics committee at each site, and each patient provided written informed consent.

Interventions

All patients had equal access to supportive care measures including analgesics, antibiotics, corticosteroids, appetite stimulants, antidepressants, RBC transfusions, deep relaxation therapy, and palliative radiotherapy or surgical procedures. All therapies with potential systemic antitumor effect (including immunotherapies) were excluded. Topotecan hydrochloride was supplied in capsules containing the equivalent to 0.25 mg or 1.00 mg of the anhydrous free base (GlaxoSmithKline, Middlesex, United Kingdom) and was dosed 2.3 mg/m^2/d on days 1 through 5 every 21 days according to marrow recovery. Compliance was documented by returned capsule count. At least four treatment cycles were recommended, depending on tolerability and response, in order to ensure that patients received optimal benefit from topotecan.

Dose Delays and Modifications

Topotecan therapy was delayed if the following parameters were not met: hemoglobin more than 9.0 g/dL, neutrophils more than 1,000/mm^3, platelets more than 100,000/mm^3, or recovery from other clinically significant nonhematologic toxicity.

To ensure optimal topotecan exposure, individual dose adjustments were prescribed in the protocol. The topotecan dose was reduced by 0.4 mg/m^2/d for neutrophils less than 500/mm^3 associated with fever/infection or lasting ≥ 7 days, neutrophils 500 to 900/mm^3 lasting beyond day 21, platelets less than 25,000/mm^3, or grade 3/4 nonhematologic toxicity excluding grade 3 nausea and grade 3/4 vomiting. The minimum topotecan dose was 1.5 mg/m^2/d; delays of more than 2 weeks at this dose resulted in withdrawal. Conversely, topotecan dose increases in increments of 0.4 mg/m^2 were permitted up to a maximum dose of 3.1 mg/m^2/d if no toxicity higher than grade 2 occurred during the previous course.

Assessments

Baseline evaluations included medical history and examination, documented evidence of progressive disease, symptom assessment questionnaire (Patient Self Assessment [PSA]) and QOL evaluation. The PSA resembles the approach used in the well-validated and referenced Lung Cancer Symptom Scale,[13] evaluating the degree to which patients experienced nine common and clinically relevant symptoms using a Likert scale for severity (from 1 [not at all] to 4 [very much]). The EuroQol-5 Dimensions Health Questionnaire (EQ-5D), is an evaluation of five health status dimensions: mobility, self-care, usual activities, pain/discomfort, and anxiety/depression. The evaluation is a rating from 1 (no problem) to 3 (an extreme problem), and a visual analog scale ranging from 0 (worst imaginable) to 100 (best imaginable health state).[14,15]

Patients on both study arms were evaluated at similar intervals: before each course of topotecan or approximately every 21 days for patients on the BSC arm. At each visit, the patient was interviewed and examined and completed the PSA and EQ-5D. PS was recorded and palliative measures documented. In the topotecan arm, toxicity (according to National Cancer Institute Common Toxicity Criteria) was evaluated and blood counts were obtained. During treatment, blood counts were obtained on day 8 and blood chemistries on day 15. Hematologic and biochemical toxicities were assessed from laboratory values; all other toxicities were from investigator-reported adverse events. Radiographic disease assessment was only required in the topotecan arm after three courses and thereafter only to confirm response or progressive disease. Response was assessed according to WHO criteria. Independent review of responses was not conducted. Poststudy follow-up occurred at least every 2 months for the full duration of survival.

The primary end point was overall survival (all cause mortality). Secondary end points were response rate, time to disease progression (TTP), patient symptom assessment, QOL evaluation, and safety.

Statistical Methods

Efficacy assessments were based on all randomly assigned patients, the intent-to-treat population. Safety and QOL assessments were based on all patients who received at least one postrandom assignment evaluation on the BSC arm or one dose of topotecan.

This trial was designed to detect a 66.7% difference in median survival. The expected survival in the BSC arm was 12 weeks. The estimated median survival in the BSC plus oral topotecan arm was 20 weeks. Although initial sample size calculations determined that 220 patients (110 per arm) were needed to assess a survival benefit for topotecan with 90% power and a significance level of .05, recruitment was slower than expected. A formal protocol amendment was implemented to terminate the study once 125 deaths had been reported, thus providing 80% power to assess a survival benefit for topotecan at a .05 significance level. This point was reached when 141 patients had been recruited. No interim analyses were conducted.

Overall survival was analyzed using the Kaplan-Meier method and compared using the log-rank test. Analyses of all secondary end points were descriptive; no adjustments were made for multiplicity. For the topotecan group, response rates were summarized along with a binomial 95% CI and TTP was summarized by Kaplan-Meier estimates. All P values are two sided.

For the PSA, a generalized estimating equations model using PROC GENMOD version 8.1 (SAS Institute, Cary, NC) was fitted to longitudinal symptom data across visits to estimate the treatment effect on each of the symptoms (response was categorized as favorable or unfavorable). A logit link function along with exchangeable correlation structure was used for fitting the model. The rate of change in EQ-5D score in each arm was evaluated with a longitudinal analysis using a mixed model with change from baseline in score as response. Visual analog scale results were summarized using descriptive statistics.

RESULTS

Patients

Patients were recruited from 40 centers in Europe, Canada, and Russia. Between November, 2000, and March, 2004, a total of 141

patients were randomly assigned: 70 to BSC and 71 to topotecan. Patient demographics were well matched between arms, particularly with respect to the major prognostic variables of PS and sex (Table 1). The median TFI after first-line therapy was 90 days on BSC and 84 days on topotecan. The most commonly received first-line chemotherapeutic agents were cisplatin or carboplatin (77% of patients in the BSC group and 80% in the topotecan group) and etoposide (74% in the BSC group and 76% in the topotecan group), consistent with current guidelines.[16-18]

Median time on study was 7.8 weeks in the BSC group and 12.3 weeks in the topotecan group. In total, 141 patients were evaluated for efficacy. More patients in the topotecan group completed the study (70% v 53%; Table 2). Three patients in the BSC arm had no post-baseline evaluations (lost to follow-up [one patient], death from disease progression [one patient], and withdrawal to begin chemotherapy [one patient]) and one patient in the topotecan arm did not receive treatment (infection-related death). Thus 67 patients in the BSC arm and 70 patients in the topotecan arm were evaluated for toxicity and QOL.

Table 1. Baseline Characteristics of Randomly Assigned Patients

Characteristic	BSC (n = 70) No. of Patients	%	Topotecan (n = 71) No. of Patients	%
Sex				
Male	51	73	52	73
Female	19	27	19	27
Age, years				
Mean	58.6		59.8	
SD	8.2		9.0	
Range	43-79		37-76	
Performance status				
0	6	9	8	11
1	41	59	44	62
2	23	33	19	27
Disease stage				
Limited	27	39	23	32
Extensive	43	61	48	68
Maximum lesion diameter, cm				
< 2	2	3	7	10
2- < 5	25	36	34	48
5-10	32	46	19	27
> 10	5	7	2	3
Not measurable	6	9	9	13
Prior cancer therapy*				
Any prior therapy	48	69	46	65
Radiotherapy	34	49	38	54
Surgery	20	29	18	25
Immunotherapy	4	6	0	
Liver metastases				
No	56	80	51	72
Yes	14	20	20	28
Treatment-free interval, days†				
≤ 60	20	29	22	31
> 60	50	71	49	69
≤ 90	35	50	41	58
> 90	35	50	30	42
Median	90		84	
Range	14 to 1,409		34-1,996	

Abbreviations: BSC, best supportive care; SD, standard deviation.
*Excludes chemotherapy.
†Defined as time to progression since completion of first-line chemotherapy.

Table 2. Reasons for Study Conclusion

Reason	BSC (n = 70) No. of Patients	%	Topotecan (n = 71) No. of Patients	%
Completed study	37	53	50	70
Reason for withdrawal				
Adverse event	9	13	13	18
Protocol violation	7	10	0	
Lost to follow-up	4	6	2	3
Other	13*	19	5†	7
Ongoing	0		1	1
Total withdrawn	33	47	21	30

Abbreviation: BSC, best supportive care.
*Patient choice (6), death (2), progressive disease (2); patient moved (1), patient received terminal care at home (1), patient started second-line chemotherapy (1).
†Patient choice (4), lack of compliance (1).

Delivered Chemotherapy

A total of 278 topotecan courses were administered (median, 4; range, 1 to 10). Sixty-nine patients (99%) took ≥ 90% of their prescribed capsules. Patients in the BSC group were observed for the equivalent of a median of three courses (range, 1 to 13).

Topotecan dose reduction occurred in 16 courses (8%) primarily due to hematologic toxicity (13 courses, 6%). Dose delays occurred in 41 topotecan courses (20%) most commonly for hematologic toxicity (25 courses, 12%). Dose escalation of topotecan occurred in 39 courses (14%). The median topotecan dose intensity achieved was 3.77 mg/m^2/wk representing 98% of the scheduled dose.

Some patients who were randomly assigned to receive BSC alone withdrew consent and elected to receive standard intravenous chemotherapy. In all, 13 patients in each arm (18.3% on BSC and 18.6% on topotecan) received poststudy chemotherapy either alone or in combination with other therapy such as radiotherapy and surgery. In addition, poststudy radiotherapy alone was received by seven patients

Table 3. Palliative Care Measures

Therapy	Patients: BSC (n = 67) No.	%	Topotecan (n = 70) No.	%
Any medication	55	82	42	60
Pain medication	46	69	33	47
Radiotherapy	17	25	10	14
Transfusions	7	10	23	33
Other procedures	9	13	6	9

NOTE. For all patients who had at least one post–random assignment evaluation in the BSC alone group or one dose of study medication in the topotecan group.
Abbreviation: BSC, best supportive care.

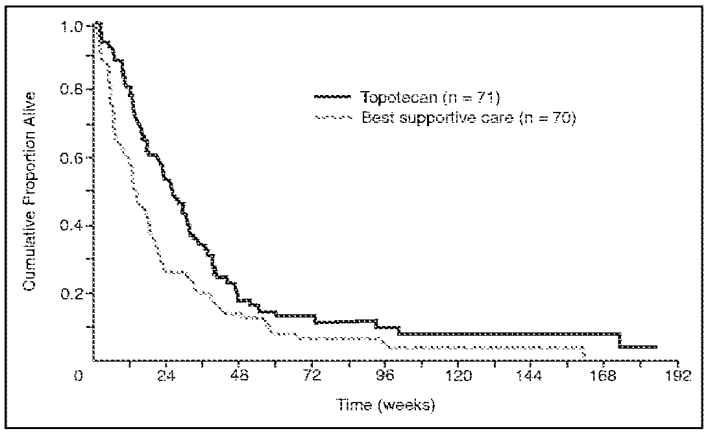

Fig 1. Kaplan-Meier estimates for overall survival in the intent-to-treat population (log-rank $P = .01$). The unadjusted hazard ratio for overall survival was 0.64 (95% CI, 0.45 to 0.90) for topotecan relative to best supportive care alone. Adjusted for stratification factors, the hazard ratio was 0.61 (95% CI, 0.43 to 0.87).

(10%) in the topotecan arm and one patient (1%) in the BSC arm. Crossover to topotecan was not allowed by protocol.

Supportive Care

Palliative medications and radiotherapy were used more frequently in the BSC group, while transfusions were used more frequently in the topotecan group (Table 3).

Efficacy

Overall survival was significantly longer in the topotecan group (Fig 1; log-rank $P = .01$). The median survival times were 13.9 weeks (95% CI, 11.1 to 18.6) in the BSC arm and 25.9 weeks (95% CI, 18.3 to 31.6) in the topotecan arm. Six-month survival rates were 26% in the BSC group and 49% in the topotecan group.

Prolongation of survival in the topotecan group was preserved when analyzed according to sex, TFI from prior therapy ($\leq$ 60 days or $>$ 60 days), PS (0/1 or 2), and presence of liver metastases (Fig 2). Even for the group of patients considered least likely to benefit from therapy (those with TFI of $\leq$ 60 days), the median survival on BSC was 13.2 weeks (95% CI, 7.0 to 21.0), and on topotecan 23.3 weeks (95% CI, 10.7 to 30.9). For patients with a PS 2, the median survival on BSC was 7.7 weeks (95% CI, 5.3 to 13.1) and on topotecan 20.9 weeks (95% CI, 13.4 to 26.9). These data are presented graphically in Figure 2. The 95% CIs for the hazard ratios indicate a survival trend favoring topotecan in all subgroups.

Fifty-nine subjects (83%) in the topotecan arm experienced progression. The median TTP in the topotecan arm was 16.3 weeks (95% CI, 12.9 to 20.0).

The overall response rate to topotecan was 7% and a further 44% of patients achieved stabilization of disease, which was confirmed after no less than 56 days (Table 4). Reponses according to the prospectively defined stratification of TFI $\leq$ 60 days versus more than 60 days, as well as according to TFI $\leq$ 90 days versus more than 90 days are presented in Table 4.

QOL

Overall, measures of QOL favored the topotecan group. Baseline EQ-5D questionnaires were completed by 68 patients (96%) in the topotecan group and 65 patients (93%) in the BSC group. At least one postbaseline EQ-5D questionnaire was completed by 63 patients (89%) in the topotecan group and 49 patients (70%) in the BSC group. For all patients with data, the rate of deterioration per 3-month interval in EQ-5D scores was -0.20 (95% CI, -0.27 to -0.12) on BSC compared with -0.05 (95% CI, -0.11 to 0.02) on topotecan. The difference in rate of change was $+0.15$ (95% CI, 0.05 to 0.25) indicating that the EQ-5D score worsened significantly faster in the BSC arm. Odds ratios of individual symptoms evaluated by the PSA indicate a greater likelihood of achieving symptom improvement on topotecan for every symptom (Table 5). For shortness of breath, sleep interference, and fatigue, the odds ratio CIs indicate statistical superiority at the .05 significance level in favor of topotecan.

Toxicity

In the topotecan group, grade 3/4 neutropenia, grade 3/4 thrombocytopenia, and grade 3/4 anemia occurred in 61%, 38%, and 25% of

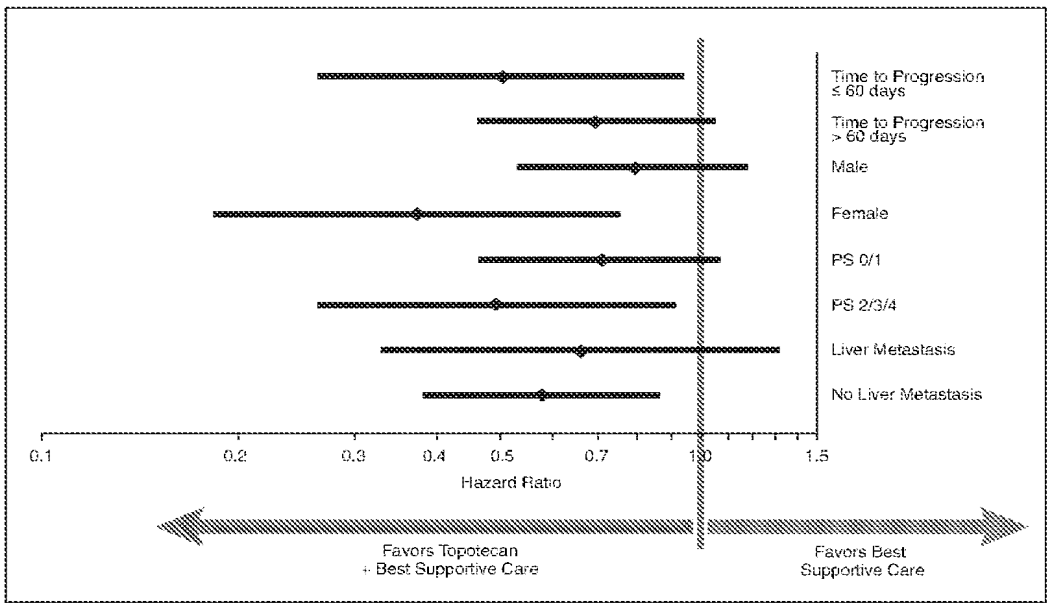

Fig 2. Subgroup analysis of survival according to the stratification factors of sex, performance status (PS), time to progression from prior therapy, and presence of liver metastases.

Table 4. Response in the Oral Topotecan Group According to Length of Treatment-Free Interval

	Topotecan		Treatment-Free Interval							
	All (N = 71)		≤ 60 Days (n = 22)		> 60 Days (n = 49)		≤ 90 Days (n = 41)		> 90 Days (n = 30)	
Best Response	No.	%	No.	%	No.	%	No.	%	No.	%
CR	0		0		0		0		0	
PR	5	7	4	18	1	2	4	10	1	3
Total responses (CR + PR)	5	7	4	18	1	2	4	10	1	3
95% CI	2.33 to 15.67		5.2 to 40.3		0.05 to 10.9		2.7 to 23.1		0.08 to 17.2	
Stable disease	31	44	7	32	24	49	17	42	14	47
Progressive disease	24	34	7	32	17	35	12	29	12	40
Response not assessed	11	16	4	18	7	14	8	20	3	10

Abbreviations: CR, complete response; PR, partial response.

patients, respectively. Febrile neutropenia occurred in 3%. Among all patients on BSC, nonsepsis infection ≥ grade 2 occurred in eight patients (12%) in the BSC arm and 10 patients (14%) in the topotecan arm. Sepsis occurred in three patients (4%) in the topotecan group and one patient (1%) in the BSC group. In the topotecan arm, two patients (3%) received granulocyte colony-stimulating factor or granulocyte-macrophage colony-stimulating factor and two patients (3%) received erythropoietin.

The most commonly occurring grade 3/4 nonhematologic toxicities were diarrhea (6%), fatigue (4%), vomiting (3%), and dyspnea (3%) in the topotecan group and dyspnea (9%), fatigue (4%), and cough (2%) in the BSC group. Toxic deaths occurred in four patients (6%) in the topotecan arm with three due to hematologic toxicity. Of these three deaths, one was attributed to severe cytopenia and infection, one to neutropenia and pneumonia, and one to neutropenia and thrombocytopenia. All cause mortality within 30 days of random assignment was 7% in the topotecan arm (five patients: progressive disease, one; drug toxicity, three; other reason, one) and 13% in the BSC arm (nine patients, all due to progressive disease). Patients on BSC were at greater risk of death compared with patients on topotecan at all stages of the study.

DISCUSSION

This study has successfully quantified the clinical benefit associated with active chemotherapy in patients with relapsed SCLC. Treatment with oral topotecan prolonged survival and improved QOL compared with BSC alone and the improvements can be considered clinically and statistically significant. In patients with sensitive SCLC, the study confirms the previous observation of survival benefit and symptom palliation associated with active chemotherapy. More importantly, the treatment dilemma concerning patients with short TFI or PS 2 is also resolved. This study suggests that with oral topotecan the benefits of therapy outweigh the risks in all patient groups and therefore all subgroups of patients with relapsed SCLC (sensitive or resistant) should now be considered for this treatment.

Two randomized studies have shown that similar clinical activity is achieved with either oral or intravenous topotecan in SCLC.[9,10] In a different setting, a survey of patients showed that patients prefer oral over intravenous chemotherapy in the palliative setting if clinical activity is not compromised.[19] Thus, physicians treating patients with

Table 5. Patient Symptom Assessment

Symptom	Odds Ratio†	95% CI	No. of Patients With Data*	
			BSC	Topotecan
Shortness of breath	2.18‡	1.09 to 4.38‡	48	61
Cough	1.35	0.68 to 2.66	47	61
Chest pain	2.07	1.00 to 4.28	48	61
Coughing up blood	1.95	0.46 to 8.27	47	61
Loss of appetite	1.02	0.57 to 1.84	47	61
Interference with sleep	2.16‡	1.15 to 4.06‡	48	61
Hoarseness	1.35	0.63 to 2.87	48	60
Fatigue	2.29‡	1.25 to 4.19‡	48	61
Interference with daily activities	1.70	0.95 to 3.03	48	61

Abbreviation: BSC, best supportive care.
*Baseline questionnaires were completed by 67 patients in the BSC arm and 70 patients in the topotecan arm. The numbers of patients with sufficient data to be included in the analysis are listed.
†Topotecan relative to BSC (odds ratio > 1 indicates greater likelihood of symptom improvement on topotecan).
‡The odds ratio and 95% CIs indicate statistical superiority at the .05 significance level in favor of topotecan.

recurrent SCLC would have an effective oral option when patients identify this preference.

With the median survival of the treated group at 25.9 weeks and the fact that around 50% of these patients in both arms had a good PS of 0 to 1 at study entry, and 42% and 59%, respectively, of patients had a TFI longer than 90 days, one could argue that this was a group of patients who should have been offered standard intravenous chemotherapy. We did not collect data on specific comorbidities or the reasons why individual patients were not offered standard intravenous chemotherapy by their oncologists. However, one recent study suggests that our study was indeed a real clinical situation. Sundstrom et al[20] randomly assigned and treated patients at diagnosis with either etoposide and cisplatin or cyclophosphamide, epirubicin, and vincristine; at relapse patients received the alternate, crossover regimen. Of 286 patients randomly assigned initially, only 120 were suitable for second-line therapy; the remaining 166 patients received BSC. In the group offered BSC alone, 38% had a PS of 0 to 1 and 43% had a TFI longer than 3 months—very similar to our trial group. The median survival in the crossover arms were 3.9 and 4.5 months, respectively, for etoposide and cisplatin and cyclophosphamide, epirubicin, and vincristine.[20]

Other important clinical issues have been addressed. The number of patients deriving benefit from oral topotecan exceeds the 7% who achieved a partial response. This response rate is lower than that reported in previous studies with patients selected on their sensitivity to previous treatments. This corroborates previous suggestions that stabilization of disease as measured by WHO criteria is associated with clinical benefit,[21] though we accept that the data on symptom control in both arms is less reliable than if a placebo had been included. The natural course of untreated SCLC has been defined, and this study will provide the benchmark against which future treatment strategies in this indication can be judged.

REFERENCES

1. Spiro SG, Souhami RL, Geddes DM, et al: Duration of chemotherapy in small cell lung cancer: A cancer research campaign trial. Br J Cancer 59: 578-583, 1989

2. von Pawel J, Depierre A, Hans K, et al: Topotecan (Hycamtin™) in small cell lung cancer (SCLC) after failure of first line therapy: Multicentre phase II study. Eur J Cancer 33:S229, 1997 (suppl 8; abstr 1038)

3. Giaccone G: Identification of new drugs in pretreated patients with small cell lung cancer. Eur J Cancer 25:411-413, 1989

4. ten Bokkel Huinink W, Gore M, Carmichael J, et al: Topotecan vs paclitaxel in relapsed ovarian cancer. J Clin Oncol 15:2183-2193, 1997

5. Ardizzoni A, Hansen H, Dombernowsky P, et al: Topotecan, a new active drug in the second-line treatment of small-cell lung cancer: A phase II study in patients with refractory and sensitive disease. J Clin Oncol 15:2090-2096, 1997

6. Depierre A, von Pawel J, Hans K, et al: Evaluation of topotecan (Hycamtin™) in relapsed small cell lung cancer (SCLC): A multicentre phase II study. Lung Cancer 18:35, 1997 (suppl 1; abstr 126)

7. Eckardt J, Gralla R, Palmer MC, et al: Topotecan (T) as second-line therapy in patients (Pts) with small cell lung cancer (SCLC): A phase II study. Ann Oncol 7:107, 1996 (suppl 5; abstr 513P)

8. von Pawel J, Schiller JH, Shepherd FA, et al: Topotecan versus cyclophosphamide, doxorubicin, and vincristine for the treatment of recurrent small-cell lung cancer. J Clin Oncol 17:658-667, 1999

9. von Pawel J, Gatzemeier U, Pujol JL, et al: A phase II comparator study of oral versus intravenous topotecan in patients with chemosensitive small cell lung cancer. J Clin Oncol 19:1743-1749, 2001

10. Eckardt JR, Von Pawel J, Hainsworth JD, et al: Single agent oral topotecan (PO) versus intravenous topotecan (IV) in patients (pts) with chemosensitive small cell lung cancer (SCLC): An international phase III study. Proc Am Soc Clin Oncol 22:619, 2003 (abstr 2488)

11. Gralla RJ, Eckardt J, von Pawel J, et al: Quality of life with single agent oral topotecan vs intravenous topotecan in patients with chemosensitive small cell lung cancer (SCLC): An international phase III study. Lung Cancer 41:S237, 2003 (suppl 2; abstr P-578)

12. Freedman LS, White SJ: On the use of Pocock and Simon's method for balancing treatment numbers over prognostic factors in the controlled clinical trial. Biometrics 32:691-694, 1976

13. Hollen PJ, Gralla RJ, Kris MG, et al: Quality of life assessment in individuals with lung cancer: Testing the Lung Cancer Symptom Scale (LCSS). Eur J Cancer 29A:S51-S58, 1993 (suppl 1)

14. Brooks R: EuroQol: The current state of play. Health Policy 37:53-72, 1996

15. The EuroQol Group: EuroQol: A new facility for the measurement of health-related quality of life. Health Policy 16:199-208, 1990

16. Bunn P, Cullen M, Fukuoka M, et al: Chemotherapy in small cell lung cancer: A consensus report. Lung Cancer 5:127-134, 1989

17. Small cell lung cancer: START – State of the Art Oncology in Europe. American Italian Cancer Foundation, NY, Instituto Nazionale per lo Studio e la Cura dei Tumori, Milan, Italy, 2002

18. National Comprehensive Cancer Network: Clinical practice guidelines in oncology: Small cell lung cancer, Version 1.2006, 2006. http://www.nccn.org/professionals/physician_gls/PDF/sclc.pdf

19. Liu G, Franssen E, Fitch MI, et al: Patient preferences for oral versus intravenous palliative chemotherapy. J Clin Oncol 15:110-115, 1997

20. Sundstrøm S, Bremnes RM, Kaasa S, et al: Second-line chemotherapy in recurrent small cell lung cancer: Results from a crossover schedule after primary treatment with cisplatin and etoposide (EP-regimen) or cyclophosphamide, epirubicin, and vincristin (CEV-regimen). Lung Cancer 48:251-261, 2005

21. Cesano A, Lane SR, Poulin R, et al: Stabilization of disease as a useful predictor of survival following second-line chemotherapy in small cell lung cancer and ovarian cancer patients. Int J Oncol 15:1233-1238, 1999

Authors' Disclosures of Potential Conflicts of Interest

Although all authors completed the disclosure declaration, the following authors or their immediate family members indicated a financial interest. No conflict exists for drugs or devices used in a study if they are not being evaluated as part of the investigation. For a detailed description of the disclosure categories, or for more information about ASCO's conflict of interest policy, please refer to the Author Disclosure Declaration and the Disclosures of Potential Conflicts of Interest section in Information for Contributors.

Authors	Employment	Leadership	Consultant	Stock	Honoraria	Research Funds	Testimony	Other
Mary E.R. O'Brien			GlaxoSmithKline		GlaxoSmithKline			
Tudor-Eliade Ciuleanu						GlaxoSmithKline		
Yaroslav Shparyk						GlaxoSmithKline		
Branka Čučević						GlaxoSmithKline		GlaxoSmith-Kline
Nicholas Thatcher			GlaxoSmithKline		GlaxoSmithKline			
Graham A. Ross	GlaxoSmithKline			GlaxoSmithKline				
Graham C. Dane	GlaxoSmithKline			GlaxoSmithKline				
Theresa Crofts	GlaxoSmithKline			GlaxoSmithKline				

Author Contributions

Conception and design: Mary E.R. O'Brien, Graham A. Ross, Graham C. Dane, Theresa Crofts
Financial support: Graham A. Ross, Graham C. Dane
Administrative support: Graham A. Ross, Graham C. Dane
Provision of study materials or patients: Mary E.R. O'Brien, Tudor-Eliade Ciuleanu, Yaroslav Shparyk, Branka Čučević, Gabor Juhasz, Nicholas Thatcher, Graham A. Ross, Graham C. Dane
Collection and assembly of data: Tudor-Eliade Ciuleanu, Yaroslav Shparyk, Graham A. Ross, Graham C. Dane
Data analysis and interpretation: Mary E.R. O'Brien, Hristo B. Tsekov, Nicholas Thatcher, Graham A. Ross, Graham C. Dane, Theresa Crofts
Manuscript writing: Mary E.R. O'Brien, Nicholas Thatcher, Graham A. Ross, Theresa Crofts
Final approval of manuscript: Mary E.R. O'Brien, Tudor-Eliade Ciuleanu, Branka Čučević, Gabor Juhasz, Nicholas Thatcher, Graham A. Ross
Other: Graham A. Ross [Medical monitoring of data during study conduct]

A Systematic Analysis of Efficacy of Second-Line Chemotherapy in Sensitive and Refractory Small-Cell Lung Cancer

Taofeek K. Owonikoko, MD,† Madhusmita Behera, MS,* Zhengjia Chen, PhD,† Chandar Bhimani, MD,* Walter J. Curran, MD,‡ Fadlo R. Khuri, MD,* and Suresh S. Ramalingam, MD**

Introduction: Small-cell lung cancer (SCLC) patients unresponsive or relapsing within 90 days after frontline chemotherapy have poor prognosis and are treated with regimens different from the first-line regimen. Potential differences in the efficacy of second-line therapy for refractory and sensitive SCLC have not been well studied.

Methods: Studies that enrolled sensitive and refractory (relapse < 90 days or > 90 days) SCLC patients for second-line therapy were identified using electronic databases (MEDLINE, EMBASE, and Cochrane library), and meeting abstracts databases. A systematic analysis was conducted using Comprehensive Meta Analysis (version 2.2.048) software to calculate the odds ratio of response and 95% confidence interval. Median overall survival time for sensitive and resistant SCLC patients was compared by two-sided Student's *t* test. We tested for significant heterogeneity by Cochran's chi-square test and I-square index.

Results: Twenty-one studies published between 1984 and 2011 were eligible for this analysis with a total of 1692 patients enrolled; 912 with sensitive and 780 with refractory SCLC. The overall response rate was 17.9% with a higher response rate of 27.7% (range, 0%–77%) for sensitive SCLC versus 14.8% (range, 0%–70%) for refractory patients; p=0.0001. Pooled overall odds ratio of response was 2.235 (95% confidence interval: 1.518–3.291; p=0.001) favoring patients with sensitive disease. Median overall survival time was 6.7 months with a weighted survival of 7.7 and 5.4 months for sensitive and refractory SCLC, respectively (p = 0.0035).

Conclusions: Refractory SCLC patients derive modest clinical benefit from second-line chemotherapy. However, response and survival outcomes are superior with chemosensitive disease.

Key Words: Small-cell lung cancer, Chemotherapy, Sensitive, Resistant, Refractory.

(*J Thorac Oncol* 2012;7: 866–872)

*Department of Hematology and Medical Oncology, †Department of Biostatistics and Bioinformatics, and ‡Department of Radiation Oncology, Emory University School of Medicine, Atlanta, Georgia.

Disclosure: The authors declare no conflict of interest.

Address for correspondence: Taofeek K. Owonikoko, MD, PhD, Department of Hematology & Medical Oncology, Emory University School of Medicine and Winship Cancer Institute, 1365 Clifton Road, NE Room C3080, Atlanta, GA 30322. Email: towonik@emory.edu

ISSN: 1556-0864/12/866-872

Approximately 30,000 new patients are diagnosed with small-cell lung cancer (SCLC) in the United States on an annual basis.[1,2] Majority of these patients have extensive stage of the disease, which is incurable with currently available treatment options. The efficacy of platinum-based chemotherapy for frontline therapy has been established in randomized clinical trials[3–7] with objective responses in approximately 70% of patients with limited-stage SCLC and in 50% of patients with extensive-stage disease.[5,8–10] Despite this high initial response, the majority of SCLC patients require salvage therapy for disease progression within several months after frontline therapy. Although various chemotherapeutic agents have been evaluated either singly or in combination for progressive SCLC after disease progression, topotecan is the only approved second-line therapy for SCLC in the U.S. population.[11,12]

The quality and duration of response to frontline therapy strongly predict the survival outcome in SCLC. Patients with durable response lasting more than 3 months are considered sensitive to the platinum-based frontline therapy. Refractory patients do not achieve any objective response whereas resistant disease is characterized by initial response followed by very early disease recurrence usually within 90 days of completing frontline therapy.[12–14] Patients with chemosensitive disease and durable response lasting more than 6 months are treated with the original frontline regimen at the time of progression whereas patients with resistant or refractory disease are considered for treatment options different from the frontline regimen. Whether this treatment paradigm results in better outcome for patients with resistant/refractory SCLC is an area that has not been well studied.[14,15] This systematic analysis is the first major attempt to bridge this knowledge gap by using data pooled from published results of clinical studies that enrolled sensitive- and resistant/refractory-SCLC patients to assess the clinical efficacy of systemic chemotherapy in the second-line setting.

MATERIALS AND METHODS

Study Eligibility

Prospective clinical trials that enrolled patients with both sensitive and resistant/refractory SCLC for the evaluation of second-line chemotherapy regimens were included in this analysis. In addition, qualifying studies must have enrolled minimum of 10 patients and reported on the clinical

outcome (overall survival [OS] or response rate [RR]) for both subgroups of patients. Studies published in a language other than English were excluded.

Literature Search Strategy

We identified eligible clinical trials using the main computerized databases of published biomedical literature (MEDLINE, EMBASE, and Cochrane Library). We used the search terms "small cell lung cancer AND clinical trial" along with the following limit terms: humans, clinical trial, English, and cancer, all adult: 19+ years for the MEDLINE search. Conference proceedings of the annual meetings of the American Society of Clinical Oncology and the International Association for the Study of Lung Cancer were also searched for relevant abstracts. The retrieved studies were reviewed independently by two of the authors (T.K.O. and M.B.). Final determination of study eligibility was made by the concurrence of both investigators at a follow-up consensus meeting.

Data Extraction and Synthesis

Pertinent extracted data included patient demographics, number and distribution of enrolled patients, specific therapy and clinical outcome of RR, and survival OS. The RR data was pooled for the two patient subgroups to generate a weighted overall RR for sensitive and resistant/refractory SCLC. We also calculated a weighted mean survival time for the sensitive and resistant/refractory patient groups as the product of the median survival time and number of patients.

Statistical Approach

Analysis of the extracted data was conducted using Comprehensive Meta Analysis (Version 2.2.048) software. Using a random-effect model, the likelihood of response to second-line treatment based on patients' response to frontline chemotherapy (sensitive versus resistant/refractory) was calculated as odds ratio (OR) along with 95% confidence interval. Statistical difference in the weighted mean RR and OS for sensitive and resistant/refractory SCLC patients was assessed by a two-sided *t*-test.

Sensitivity Testing

We conducted an initial analysis for the OR of response between sensitive and resistant/refractory population using the random effect model. A repeat analysis using a fixed effect model was performed to validate the initial results. Significant heterogeneity among the studies employed for this analysis was formally assessed by Cochran's chi-square test and the I-square index where a p value < 0.1 by chi-square test and I^2 value < 0.25 indicate a low degree of heterogeneity.[16] Finally, sensitivity analyses were conducted to exclude potential confounding of the results by an individual study or a group of studies by repeating the analysis after excluding each study in turn (leave-one-out model); by excluding studies of single agent and combination regimen; after excluding studies that evaluated topotecan and after excluding large studies that enrolled more than 50 patients.

RESULTS

Study and Patient Demographics

Starting with 1141 studies, 53 studies published between 1984 and 2011 were identified as potentially eligible for this analysis. Based on the predefined eligibility criteria, we selected 21 studies that met the qualitative and quantitative requirements of the systematic analysis. A consort diagram of the stepwise identification of eligible studies is detailed in Figure 1. A total of 1692 patients were enrolled across the selected trials. Response data was available for 1055 patients across 20 studies; 570 (54.0%) with chemosensitive disease and 485 (45.9%) with resistant/refractory SCLC. Survival data from 1219 patients from 11 different studies was also analyzed; 678 (56%) and 541 (44%) with sensitive and resistant/refractory SCLC respectively. Details of patient demographics and study designs are included in Table 1.

Tumor Response

The overall RR of relapsed SCLC patients to second line treatment was 17.9% with 27.7% in patients with sensitive

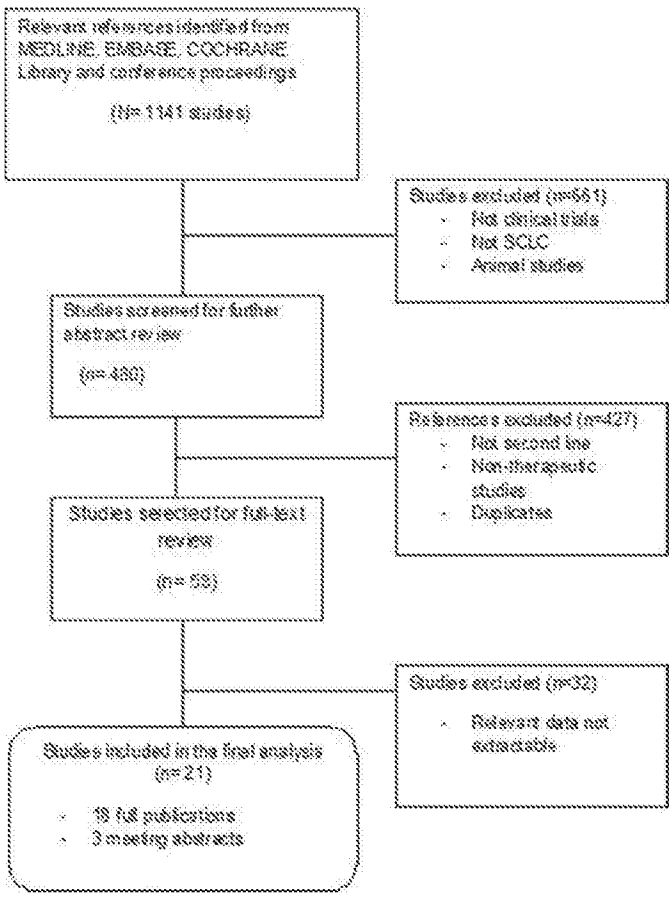

FIGURE 1. Consort diagram detailing search strategy and study selection for this systematic analysis.

TABLE 1. Study characteristics and clinical outcome of patients with sensitive or refractory small-cell lung cancer after treatment with a second-line chemotherapy

Study	Total (Sensitive/ Refractory)	PS (0/1/2)	Study Design	Therapy	RR (%)		OS (months)	
					Sensitive	Refractory	Sensitive	Refractory
Eckardt et al.[17]	77 (6/71)	9/51/17	Phase II single arm	Picoplatin	17	8	NR	NR
Jalal et al.[18]	43 (20/23)	14/18/11	Single arm phase II	Pemetrexed	5	4	4.4	2.7
Gronberg et al.[19]	34 (25/9)	5/18/11	Multicenter phase II	Pemetrexed	0	11	5.7	3.8
Rocha-Lima et al.[20]	71 (35/36)	19/41/11	Phase II single arm	Irinotecan Gemcitabine	31	11	7.1	3.5
Ardizzoni et al.[21]	110 (68/42)	17/75/18	Multicenter single arm phase II	Topotecan + Cisplatin	29	24	NR	NR
Naka et al.[22]	29 (16/13)	0/16/13	Single arm phase II	Irinotecan + Carboplatin	38	23	6.1	5.7
Seutter et al.[23]	45 (29/16)	NR	Randomized phase II	Cisplatin-etoposide/ carboplatin	49	19	7.7	7.4
Kosmas et al.[24]	33 (13/20)	NR	Single arm phase II	Paclitaxel, Ifosfamide and Cisplatin	77	70	NR	NR
Sonpavde et al.[25]	46 (32/14)	NR	Single arm phase II	Doxorubicin + Paclitaxel	53	14	NR	NR
Ardizzoni et al.[26]	92 (45/47)	NR	Single arm phase II	Topotecan	37.5	6.4	6.9	4.7
Schuette et al.[27]	35 (20/15)	9/21/5	Single arm phase II	Gemcitabine + Irinotecan	10	26	4.5	4.5
Ichiki et al.[28]	34 (24/10)	7/16/11	Single arm phase II	Irinotecan + Ifosfamide	62.5	30	NR	NR
Hensing et al.[29]	37 (20/17)	NR	Single arm phase II	BBR 3464 (Triplatin)	NR	NR	6.8	2.5
Domine et al.[30]	20 (10/10)	NR	Multicenter phase II	Gemcitabine + Paclitaxel	60	50	NR	NR
Dongiovanni et al.[31]	31 (21/10)	3/20/8	Single institution phase	Gemcitabine + Paclitaxel	28.6	20	NR	NR
Hoang et al.[32]	27 (15/12)	25/0/2	Single arm phase II	Gemcitabine	NR	NR	8.8	4.2
Hainsworth et al.[33]	29 (12/17)	NR	Single arm phase II	Gemcitabine and Vinorelbine	25	0	NR	NR
Sessa et al.[34]	66 (37/29)	15/39/12	Single arm phase II	GI147211 (Camptothecin)	21.6	10.3	NR	NR
Huber et al.[35]	169 (111/58)	34/92/37	Multicenter single arm phase II	Topotecan	17.2	8.6	5.04	5.33
Von Pawel et al.[36]	Amrubicin (225/199)	NR	Multicenter phase III trial	Amrubicin	NR	NR	9.2	6.2
	Topotecan (117/96)			Topotecan	NR	NR	9.9	5.7
Vigano et al.[37]	27	NA	Single arm phase II	NGR-hTNF + Doxorubicin	27	19	NR	NR
Overall	1692 (901/764)	157/407/156			27.7	14.8	7.73	5.45

PS, performance status using Eastern Cooperative Oncology Group scale;RR, response rate; OS, overall survival; NR, not reported; NA, not adequate; SCLC, small-cell lung cancer.

disease (range: 0%–77%) and 14.8% (range: 0%–70%) for resistant/refractory patients; $p < 0.0001$. The overall OR of response was 2.235 (95% confidence interval: 1.518–3.291; $p < 0.0001$) in favor of patients with sensitive disease (Fig. 2).

Survival

The weighted average of the overall median survival time following second line therapy was 6.7 months with a weighted average of 7.73 months (range: 2.7–8.7) for sensitive SCLC and 5.45 months (range: 4.4–9.9) for resistant/refractory disease ($p < 0.0035$).

Sensitivity Testing

The test of heterogeneity using I-square test was 9.029% (p=0.347) indicating a low degree of heterogeneity. The overall trends from the initial results remained unchanged after repeat analyses using the fixed-effect model (OR 2.227; 1.550–3.198; Fig. 3) and after excluding studies with large sample size (OR 1.926; 1.093–3.393; Fig. 4), studies of topotecan (2.170; 1.378–3.418; Fig. 5), studies of combination regimens (2.480; 1.060–5.802; Fig. 6), or studies of single-agent treatment (2.040; 1.318–3.158; Fig. 7), and following the leave-one-out analyses (Table 2).

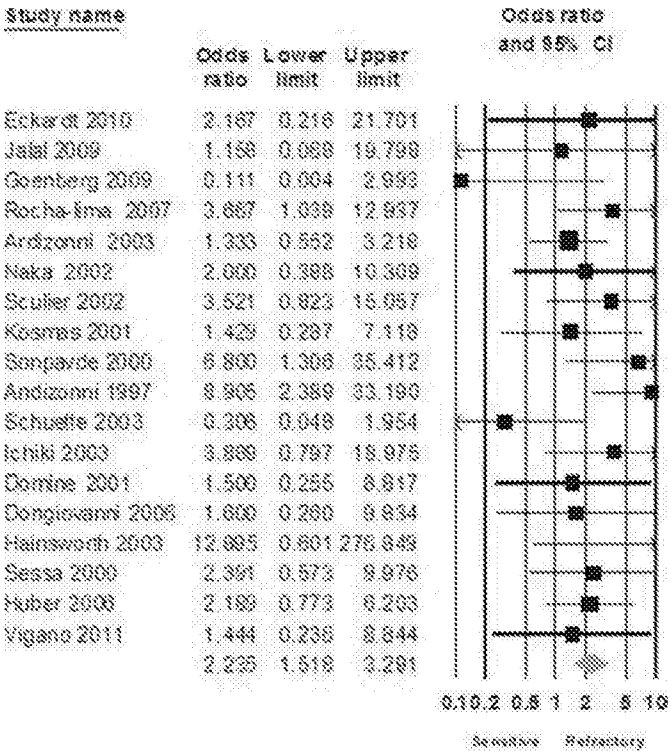

FIGURE 2. Forest plot showing the primary analysis using a random-effect model for odds ratio of response to salvage chemotherapy among patients with sensitive disease or refractory small-cell lung cancer (SCLC) as defined based on response to frontline chemotherapy.

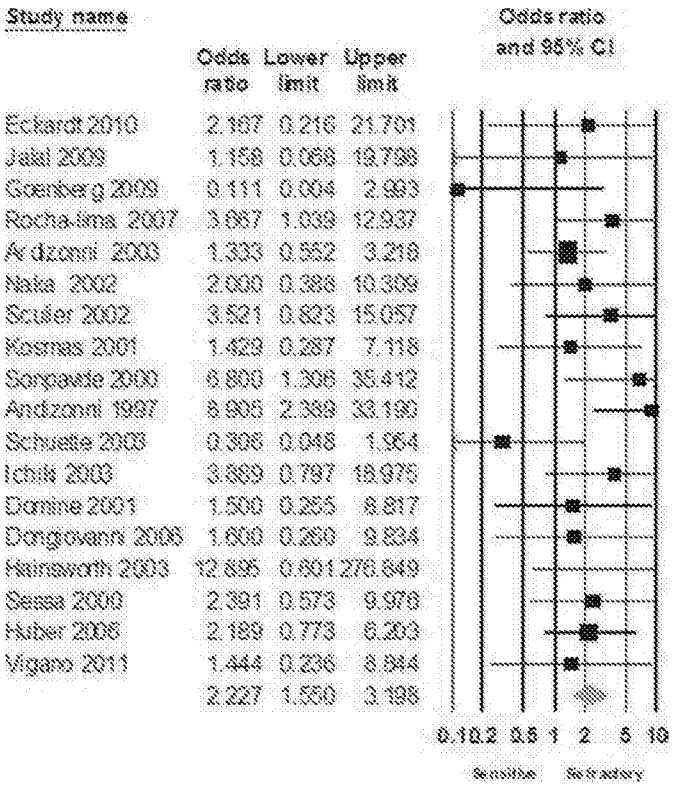

FIGURE 3. Forest plot of analysis using a fixed-effect model for odds ratio of response to salvage chemotherapy among patients with sensitive disease or refractory small-cell lung cancer (SCLC) as defined based on response to frontline chemotherapy.

DISCUSSION

The result of this systematic analysis highlights the poor OS outcome for SCLC patients following progression on frontline therapy. More than 80% of patients enrolled in clinical trials employed for this systematic analysis did not achieve an objective response and a significant proportion of the patients died within 6 months. As previously observed with topotecan,[11–13,15] we observed in this pooled analysis that patients with disease refractory or those resistant to frontline therapy were also less likely to respond to second-line chemotherapy in general, and consequently had a worse survival outcome. Nonetheless, in contrast to historical experience with untreated refractory SCLC where the survival is measured in weeks, our data indicates that patients with resistant/refractory SCLC derive clinical benefit with the receipt of second-line therapy.[6,38–40]

The studies included in our analysis evaluated different types of investigational agents. It is therefore not unexpected that heterogeneity in study design, patient population, and therapeutic agents may confound the result of this analysis. We carefully excluded any such possibility with the extensive sensitivity testing looking at all potential confounders including sample size, the use of topotecan, which is the only approved agent in this setting, and a leave-one-out analysis to examine if any of the included studies had a disproportionate influence on the overall result. Irrespective of the sensitivity test employed, we observed a consistent result of

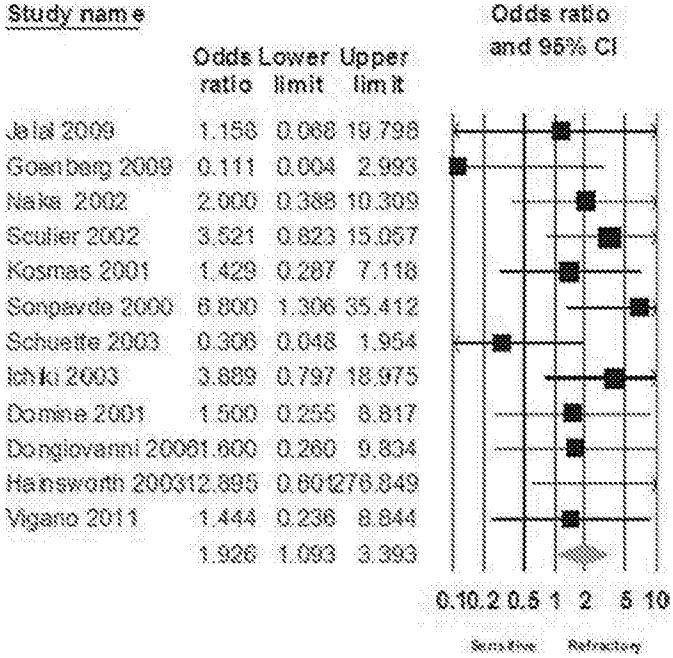

FIGURE 4. Forest plot showing the result of odds-ratio analysis after excluding large studies that enrolled 50 or more patients.

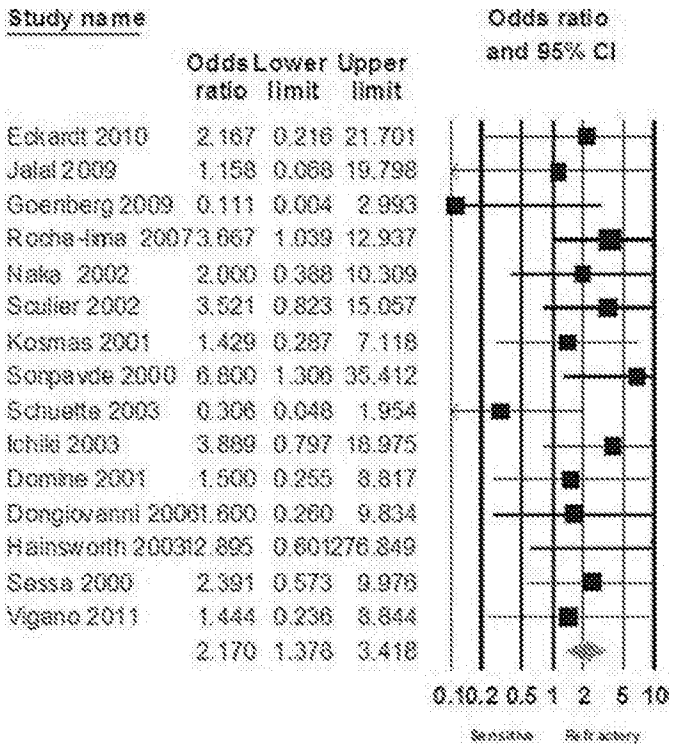

FIGURE 5. Forest plot of the result of systematic analysis for odds ratio of response to salvage chemotherapy after excluding studies that evaluated topotecan.

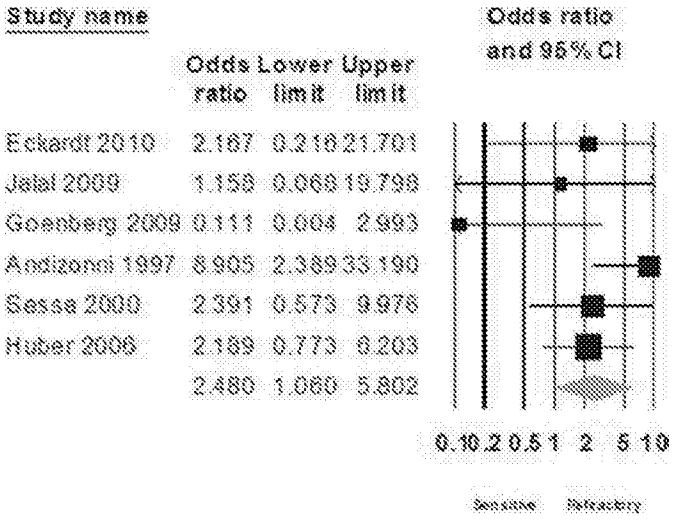

FIGURE 6. Forest plot of the result of systematic analysis for odds ratio of response to salvage chemotherapy after excluding studies that evaluated combination multi-agent therapy.

a worse survival and lower likelihood of response in refractory SCLC. Our result is also consistent with the report by Treat et al.[15] who employed individual patient data from five large randomized studies of topotecan as salvage treatment for SCLC. They reported an overall RR ranging between 14% and 17% with higher responses in chemosensitive disease (range, 18%–24%) than in chemorefractory patients (range, 3%–4%).

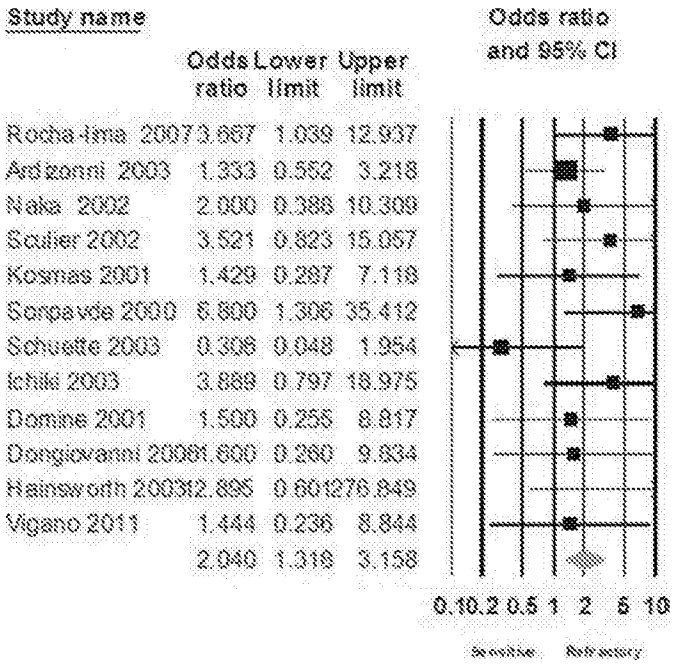

FIGURE 7. Forest plot of the result of systematic analysis for odds ratio of response to salvage chemotherapy after excluding studies that evaluated single-agent treatment regimens.

Moreover, the reported outcome in this analysis is comparable to subset analysis of prospective studies of topotecan in the salvage setting.[12,15] Because the use of intensive multi-agent chemotherapy has been shown to achieve higher RR in SCLC although with heightened toxicities,[41–43] we assessed whether this approach could result in higher likelihood of response in patients with resistant/refractory disease in the second line. However, we did not observe any reversal in the trend of higher odds of response in favor of patients with sensitive SCLC in studies evaluating both single-agent and multi-agent chemotherapy regimens.

To our knowledge, this analysis using pooled data across 21 different prospective studies of second-line chemotherapy is the largest such analysis in this patient population. Our data has now extended the results of previous small retrospective studies using local registry databases that reported superior survival with sensitive SCLC in the second-line setting.[39,44,45] Overgeneralization of the result of this analysis requires some caution because the patient population enrolled in clinical trials represents a select subset with good performance status and preserved organ function that may not accurately represent the general patient population.[46] Indeed, the majority of all patients in this analysis had an Eastern Cooperative Oncology Group performance status of 0 or 1 but we were unable to ascertain whether this is balanced between the two subgroups of patients.

Based on our result and the observation in the frontline setting, we posit that the resistant/refractory-SCLC patient population represents a biologically distinct subgroup of SCLC that requires a uniquely tailored therapeutic approach similar to the different approaches adopted for limited- and extensive-stage SCLC. Given the lack of a highly effective

TABLE 2. Resultant Odds Ratio and *p* Value by *t*-Test When the Indicated Study was Excluded in the Leave-One-Out Analysis for Response and Survival

Leave-One-Out Sensitivity Testing for OR and Survival Comparison			
Excluded Study	**Resultant OR**	**95% CI for OR**	***p* for Median Survival Estimate Comparison**
Eckardt et al.[17]	2.24	1.49–3.36	NR
Jalal et al.[18]	2.26	1.51–3.38	$p \leq 0.02$
Gronberg et al.[19]	2.31	1.60–3.32	$p \leq 0.004$
Rocha-lima et al.[20]	2.14	1.41–3.22	$p \leq 0.008$
Ardizzoni et al.[21]	2.45	1.61–3.70	NR
Naka et al.[22]	2.25	1.48–3.4	$p \leq 0.005$
Soulier et al.[23]	2.16	1.43–3.26	$p \leq 0.005$
Kosmas et al.[24]	2.29	1.52–3.45	NR
Sonpavde et al.[25]	2.10	1.43–3.09	NR
Ardizzoni et al.[26]	1.98	1.36–2.89	$p \leq 0.0017$
Schuette et al.[27]	2.40	1.66–3.48	$p \leq 0.002$
Ichiki et al.[28]	2.16	1.44–3.25	NR
Domine et al.[30]	2.27	1.51–3.42	NR
Dongiovanni et al.[31]	2.27	1.50–3.41	NR
Hainsworth et al.[32]	2.17	1.47–3.2	NR
Sessa et al.[34]	2.22	1.46–3.37	NR
Huber et al.[35]	2.24	1.46–3.44	0.0005
Vigano et al.[37]	2.28	1.51–3.42	NR
Hensing et al.[29]	NR	NR	0.006
Hoang et al.[32]	NR	NR	0.007
Von Pawel et al.[36]			
Amrubicin	NR	NR	$p \leq 0.019$
Topotecan	NR	NR	$p \leq 0.017$

No individual study had a dominant effect on the overall result of this analysis.
OR, odds ratio; CI, confidence interval; OS, overall survival; NR, data required for analysis not reported.

salvage therapy regimen, we agree that patients with sensitive relapse should be re-treated with a platinum/etoposide regimen in line with current management recommendations. In contrast, patient with resistant/refractory disease should be considered for innovative clinical trials, especially studies that are designed to exploit our evolving understanding of tumor biology and drug resistance. One such study is the ESCAPE study, a phase-II study evaluating the efficacy of the combination of standard platinum/etoposide along with amuvatinib in patients with resistant/refractory SCLC [NCT01357395]. Amuvatinib is an oral multitargeted tyrosine kinase inhibitor against mutant forms of c-Kit and PDGFR- and also suppresses DNA-repair capacity by disrupting Rad51 protein activity and consequently homologous recombination, which is central to DNA-damage repair capacity.

Pertinent limitations of our study include the retrospective nature of this analysis and the potential imbalances in important clinical characteristics that may also affect clinical outcome of SCLC patients such as sex, presence of brain metastasis, overall disease burden, and dose intensity.[46–48] However, the large number of patients included in the analysis and the use of tumor biology as defined by response to initial therapy for patient categorization make our result a very important benchmark that could inform prospective clinical and translational research for this greatly understudied patient population.

ACKNOWLEDGMENTS

Supported by NIH P01 CA166999 grant awarded to Fadlo R. Khuri, MD, and P01 grant supplement award to Taofeek K. Owonikoko, MD, and unrestricted research funding to Walter J. Curran, MD, Fadlo R. Khuri, MD, and Suresh S. Ramalingam, MD, from the Georgia Cancer Coalition.

Presented as a poster at the 2010 Chicago Multidisciplinary Symposium in Thoracic Oncology. Chicago December 9–11, 2010.

REFERENCES

1. Jemal A, Siegel R, Xu J, Ward E. Cancer statistics, 2010. *CA Cancer J Clin* 2010;60:277–300.
2. Owonikoko TK, Ragin CC, Belani CP, et al. Lung cancer in elderly patients: an analysis of the surveillance, epidemiology, and end results database. *J Clin Oncol* 2007;25:5570–5577.
3. Owonikoko TK Ramalingam S. Small cell lung cancer in elderly patients: a review. *J Natl Compr Canc Netw* 2008;6:333–344.
4. Lara PN Jr, Natale R, Crowley J, et al. Phase III trial of irinotecan/cisplatin compared with etoposide/cisplatin in extensive-stage small-cell lung cancer: clinical and pharmacogenomic results from SWOG S0124. *J Clin Oncol* 2009;27:2530–2535.
5. Clark R Ihde DC. Small-cell lung cancer: treatment progress and prospects. *Oncology (Williston Park, NY)* 1998;12:647–58; discussion 661.
6. Pelayo Alvarez M, Gallego Rubio O, Bonfill Cosp X, Agra Varela Y. Chemotherapy versus best supportive care for extensive small cell lung cancer. *Cochrane Database Syst Rev* 2009;CD001990.
7. Ardizzoni A, Boni L, Tiseo M, et al.; CISCA (CISplatin versus CArboplatin) Meta-analysis Group. Cisplatin- versus carboplatin-based chemotherapy in first-line treatment of advanced non-small-cell lung cancer: an individual patient data meta-analysis. *J Natl Cancer Inst* 2007;99:847–857.
8. Owonikoko T Ramalingam S. Minimal progress, potential promise in small-cell lung cancer. *Oncology (Williston Park, NY)* 2008;22:1495–1496.
9. Hanna N, Bunn PA, Jr., Langer C, et al: Randomized phase III trial comparing irinotecan/cisplatin with etoposide/cisplatin in patients with previously untreated extensive-stage disease small-cell lung cancer. *J Clin Oncol* 2006;24:2038–2043.
10. Noda K, Nishiwaki Y, Kawahara M, et al: Irinotecan plus cisplatin compared with etoposide plus cisplatin for extensive small-cell lung cancer. *N Engl J Med* 2002;346:85–91.
11. von Pawel J, Schiller JH, Shepherd FA, et al. Topotecan versus cyclophosphamide, doxorubicin, and vincristine for the treatment of recurrent small-cell lung cancer. *J Clin Oncol* 1999;17:658–667.
12. O'Brien ME, Ciuleanu TE, Tsekov H, et al. Phase III trial comparing supportive care alone with supportive care with oral topotecan in patients with relapsed small-cell lung cancer. *J Clin Oncol* 2006;24:5441–5447.
13. Schiller JH, Adak S, Cella D, DeVore RF 3rd, Johnson DH. Topotecan versus observation after cisplatin plus etoposide in extensive-stage small-cell lung cancer: E7593–a phase III trial of the Eastern Cooperative Oncology Group. *J Clin Oncol* 2001;19:2114–2122.
14. Cheng S, Evans WK, Stys-Norman D, Shepherd FA; Lung Cancer Disease Site Group of Cancer Care Ontario's Program in Evidence-based Care. Chemotherapy for relapsed small cell lung cancer: a systematic review and practice guideline. *J Thorac Oncol* 2007;2:348–354.
15. Treat J, Huang CH, Lane SR, Levin J. Topotecan in the treatment of relapsed small cell lung cancer patients with poor performance status. *Oncologist* 2004;9:173–181.
16. Higgins JP, Thompson SG, Deeks JJ, Altman DG. Measuring inconsistency in meta-analyses. *BMJ* 2003;327:557–560.

17. Eckardt JR, Bentsion DL, Lipatov ON, et al. Phase II study of picoplatin as second-line therapy for patients with small-cell lung cancer. *J Clin Oncol* 2009;27:2046–2051.
18. Jalal S, Waterhouse D, Edelman MJ, et al. Pemetrexed plus cetuximab in patients with recurrent non-small cell lung cancer (NSCLC): a phase I/II study from the Hoosier Oncology Group. *J Thorac Oncol* 2009;4:1420–1424.
19. Gronberg BH, Bremnes RM, Aasebø U, et al.; Norwegian Lung Cancer Study Group. A prospective phase II study: high-dose pemetrexed as second-line chemotherapy in small-cell lung cancer. *Lung Cancer* 2009;63:88–93.
20. Rocha-Lima CM, Herndon JE 2nd, Lee ME, et al.; Cancer and Leukemia Group B. Phase II trial of irinotecan/gemcitabine as second-line therapy for relapsed and refractory small-cell lung cancer: Cancer and Leukemia Group B Study 39902. *Ann Oncol* 2007;18:331–337.
21. Ardizzoni A, Manegold C, Debruyne C, et al.; Giuseppe giaccone European organization for research and treatment of cancer (EORTC) lung cancer group. European organization for research and treatment of cancer (EORTC) 08957 phase II study of topotecan in combination with cisplatin as second-line treatment of refractory and sensitive small cell lung cancer. *Clin Cancer Res* 2003;9:143–150.
22. Naka N, Kawahara M, Okishio K, et al. Phase II study of weekly irinotecan and carboplatin for refractory or relapsed small-cell lung cancer. *Lung Cancer* 2002;37:319–323.
23. Scullier JP, Lafitte JJ, Lecomte J, et al.; European lung cancer working party. A phase II randomised trial comparing the cisplatin-etoposide combination chemotherapy with or without carboplatin as second-line therapy for small-cell lung cancer. *Ann Oncol* 2002;13:1454–1459.
24. Kosmas C, Tsavaris NB, Malamos NA, Vadiaka M, Koufos C. Phase II study of paclitaxel, ifosfamide, and cisplatin as second-line treatment in relapsed small-cell lung cancer. *J Clin Oncol* 2001;19:119–126.
25. Soupavde G, Ansari R, Walker P, et al. Phase II study of doxorubicin and paclitaxel as second-line chemotherapy of small-cell lung cancer: a Hoosier Oncology Group Trial. *Am J Clin Oncol* 2000;23:68–70.
26. Ardizzoni A, Hansen H, Dombernowsky P, et al. Topotecan, a new active drug in the second-line treatment of small-cell lung cancer: a phase II study in patients with refractory and sensitive disease. The European Organization for Research and Treatment of Cancer Early Clinical Studies Group and New Drug Development Office, and the Lung Cancer Cooperative Group. *J Clin Oncol* 1997;15:2090–2096.
27. Schuette W, Nagel S, Juergens S, et al. Phase II trial of gemcitabine/irinotecan in refractory or relapsed small-cell lung cancer. *Clin Lung Cancer* 2005;7:133–137.
28. Ichiki M, Gohara R, Rikimaru T, et al. Combination chemotherapy with irinotecan and ifosfamide as second-line treatment of refractory or sensitive relapsed small cell lung cancer: a phase II study. *Chemotherapy* 2003;49:200–205.
29. Hensing TA, Hanna NH, Gillenwater HH, Gabriella Camboni M, Allievi C, Socinski MA. Phase II study of BBR 3464 as treatment in patients with sensitive or refractory small cell lung cancer. *Anticancer Drugs* 2006;17:697–704.
30. Dómine M, Larriba JLG, Morales S, et al: Gemcitabine and Paclitaxel as Second Line Treatment in Small Cell Lung Cancer (SCLC). A Multicentric Phase II Study. *Proc Am Soc Clin Oncol* 2001;20:abstr 1263.
31. Dongiovanni V, Buffoni L, Berruti A, et al. Second-line chemotherapy with weekly paclitaxel and gemcitabine in patients with small-cell lung cancer pretreated with platinum and etoposide: a single institution phase II trial. *Cancer Chemother Pharmacol* 2006;58:203–209.
32. Hoang T, Kim K, Jasiowski A, et al. Phase II study of second-line gemcitabine in sensitive or refractory small cell lung cancer. *Lung Cancer* 2003;42:97–102.
33. Hainsworth JD, Burris HA 3rd, Erland JB, et al., Minnie Pearl Cancer Research Network. Combination chemotherapy with gemcitabine and vinorelbine in the treatment of patients with relapsed or refractory small cell lung cancer: a phase II trial of the Minnie Pearl Cancer Research Network. *Cancer Invest* 2003;21:193–199.
34. Sessa C, Wanders J, Roelvink M, et al. Second-line treatment of small-cell lung cancer with the camptothecin-derivative GI147211: a study of the EORTC Early Clinical Studies Group (ECSG). *Ann Oncol* 2000;11:207–210, 2000
35. Huber RM, Reck M, Gosse H, et al. Efficacy of a toxicity-adjusted topotecan therapy in recurrent small cell lung cancer. *Eur Respir J* 2006;27:1183–1189.
36. von Pawel J, Jotte R, Spigel DR, et al: Randomized phase 3 trial of amrubicin versus topotecan as second-line treatment for small cell lung cancer (SCLC) *J Thorac Oncol* 2011;6:S274; Abstract O
37. Vigano MG, Cavina R, Novello S, et al: Phase II trial of NGR-hTNF and doxorubicin in relapsed small cell lung cancer (SCLC). *J Clin Oncol* 2011; 29 (suppl; abstr 7077) 29:suppl; abstr 7077.
38. Ramalingam SS, Owonikoko TK, Khuri FR. Lung cancer: New biological insights and recent therapeutic advances. *CA Cancer J Clin* 2011;61:91–112.
39. Chute JP, Kelley MJ, Venzon D, Williams J, Roberts A, Johnson BE. Retreatment of patients surviving cancer-free 2 or more years after initial treatment of small cell lung cancer. *Chest* 1996;110:165–171.
40. Agra Y, Pelayo M, Sacristan M, Sacristán A, Serra C, Bonfill X. Chemotherapy versus best supportive care for extensive small cell lung cancer. *Cochrane Database Syst Rev* 2003;CD001990.
41. Ettinger DS, Berkey BA, Abrams RA, et al.; Radiation Therapy Oncology Group 9609. Study of paclitaxel, etoposide, and cisplatin chemotherapy combined with twice-daily thoracic radiotherapy for patients with limited-stage small-cell lung cancer: a Radiation Therapy Oncology Group 9609 phase II study. *J Clin Oncol* 2005;23:4991–4998.
42. Greco FA, Thompson DS, Morrissey LH, et al. Paclitaxel/carboplatin/etoposide versus paclitaxel/topotecan for extensive-stage small cell lung cancer: a Minnie Pearl Cancer Research Network randomized, prospective phase II trial. *Oncologist* 2005;10:728–733.
43. Niell HB, Herndon JE 2nd, Miller AA, et al.; Cancer and Leukemia Group. Randomized phase III intergroup trial of etoposide and cisplatin with or without paclitaxel and granulocyte colony-stimulating factor in patients with extensive-stage small-cell lung cancer: Cancer and Leukemia Group B Trial 9732. *J Clin Oncol* 2005;23:3752–3759.
44. Froeschl S, Nicholas G, Gallant V, Laurie SA. Outcomes of second-line chemotherapy in patients with relapsed extensive small cell lung cancer. *J Thorac Oncol* 2008;3:163–169.
45. Kim YH, Goto K, Yoh K, et al. Performance status and sensitivity to first-line chemotherapy are significant prognostic factors in patients with recurrent small cell lung cancer receiving second-line chemotherapy. *Cancer* 2008;113:2518–2523.
46. Lilenbaum RC, Huber RM, Treat J, et al. Topotecan therapy in patients with relapsed small-cell lung cancer and poor performance status. *Clin Lung Cancer* 2006;8:130–134.
47. Chute JP, Chen T, Feigal E, Simon R, Johnson BE. Twenty years of phase III trials for patients with extensive-stage small-cell lung cancer: perceptible progress. *J Clin Oncol* 1999;17:1794–1801.
48. Chute JP, Venzon DJ, Hankins L, et al. Outcome of patients with small-cell lung cancer during 20 years of clinical research at the US National Cancer Institute. *Mayo Clin Proc* 1997;72:901–912.

Lung Cancer 65 (2009) 187–191

Contents lists available at ScienceDirect

Lung Cancer

journal homepage: www.elsevier.com/locate/lungcan

A multicenter randomized phase II study of the irinotecan/gemcitabine doublet versus irinotecan monotherapy in previously treated patients with extensive stage small-cell lung cancer

Athanasios G. Pallis, Athina Agelidou, Sofia Agelaki, Ioannis Varthalitis, Georgia Pavlakou, Aleka Gerogianni, Pavlos Papakotoulas, Ageliki Rapti, Vassilis Chandrinos, Charalampos Christophyllakis, Vassilis Georgoulias*

Hellenic Oncology Research Group (HORG), Athens, Greece

ARTICLE INFO

Article history:
Received 27 June 2008
Received in revised form 27 October 2008
Accepted 2 November 2008

Keywords:
SCLC
Irinotecan
Gemcitabine
Second-line therapy

ABSTRACT

Objectives: To compare the efficacy and safety profile of irinotecan (I) versus the combination of irinotecan/gemcitabine (IG) as second-line treatment of patients with extensive stage small-cell lung cancer (SCLC).

Treatment: Patients with SCLC who have received at least one chemotherapy regimen were randomized to receive either the IG regimen (gemcitabine 1000 mg/m^2 intravenous (i.v.) on days 1 and 8 and irinotecan 300 mg/m^2 i.v. on day 8) or I monotherapy (300 mg/m^2 i.v. on day 1) both every 3 weeks.

Results: Thirty-eight patients were enrolled in the IG and 31 in the I arm. Due to slow accrual an early closure of the study was decided. Response rate was significantly higher in the IG than in I arm (23.7% vs. 0%; $p = 0.004$). The median time to progression (TTP) was 3.9 months (range: 0.5–14.5 months; 95% CI: 1.4–6.6) and 1.7 months (range: 0.5–9.9 months; 95% CI: 1.2–2.3) ($p = 0.010$) for the IG and I arms, respectively. There was no difference in terms of median overall survival between the two arms (6.8 months and 4.6 months for the IG and I arm, respectively). The most frequent toxicities were grade III/IV neutropenia and grade III/IV diarrhea.

Conclusions: Although the IG regimen seems to be more active than the I monotherapy, the premature closure of the study prevents the drawing of definitive conclusions.

1. Introduction

Small-cell lung cancer (SCLC) accounts for 14% of the new cases of lung carcinomas diagnosed in 2004 in the United States [1]. Combination chemotherapy with etoposide and cisplatin along with chest radiotherapy is the backbone of therapy in patients with limited stage SCLC, while for patients with extensive disease, the combination of etoposide and cisplatin remains the standard treatment [2]. Although SCLC is a quite chemosensitive malignancy, with overall response rates of 80–95% and 60–80% in patients with limited and extensive stage disease, respectively, most patients relapse within a year of starting treatment and almost more than 95% of them eventually die from disease progression [2].

Despite the high response rates observed with first-line treatment, results of second-line treatment for patients with relapsing or progressing disease are generally poor, with a median survival from the time to progression of 4–5 months [3]. The response to second-line therapy depends on the response to first-line therapy and the time between the completion of first-line treatment and recurrence. Patients who did not respond to previous therapy or who relapsed within 3 months of completing therapy are considered refractory, whereas those who had responded to previous treatment and relapsed 3 months or longer after completing such treatment are judged sensitive [2].

In an effort to improve survival rates in this devastating disease, the newer agents that became available during the last 20 years, such as topotecan, docetaxel, paclitaxel, irinotecan, and gemcitabine were introduced in first- and second-line treatment of SCLC [4,5]. Irinotecan, a camptothecin derivative has been reported to be active in pre-treated patients with SCLC [6–9]. A Japanese phase III trial compared the cisplatin/irinotecan doublet with the "standard" doublet of cisplatin/etoposide as first-line treatment in extensive stage SCLC, and produced a statistically significant difference in

* Corresponding author at: Department of Medical Oncology, University General Hospital of Heraklion, P.O. Box: 1352, Heraklion 71110, Crete, Greece. Tel.: +30 2810392783; fax: +30 2810392857.
E-mail address: georgsec@med.uoc.gr (V. Georgoulias).

0169-5002/$ – see front matter © 2008 Elsevier Ireland Ltd. All rights reserved.
doi:10.1016/j.lungcan.2008.11.002

terms of survival in favour of the experimental arm [10]. However, this observation could not be confirmed in a subsequent larger trial [11]. In addition, the administration of single agent gemcitabine in previously untreated patients with extensive stage SCLC resulted in an objective response rate of 27% [12], while when administered to previously treated patients the response rate ranges between 6% and 16% [13,14]. Several phase II studies evaluated the irinotecan/gemcitabine (IG) combination in previously treated patients with extensive stage SCLC and reported an overall response rate of 10–50% [15–20], with a median survival ranging from 3.7 months (for patients with refractory disease) to an impressive 14.4 months [18].

Based on the above-mentioned studies a randomised phase II study was conducted by the Hellenic Oncology Research Group (HORG) in order to compare the efficacy and safety of the irinotecan/gemcitabine doublet versus the irinotecan (I) monotherapy, in previously treated patients with extensive stage small-cell lung cancer.

2. Patients and methods

2.1. Patients

Patients with histologically or cytologically confirmed, SCLC, aged ≥18 years were enrolled in this study. Additionally, eligible patients had to have bidimensionally measurable disease, life expectancy of more than 3 months and a World Health Organization (WHO) performance status of ≤2. All patients previously received at least one prior chemotherapy regimen (patients with extensive stage), or combination of chemotherapy/radiotherapy (patients with limited disease). The etoposide/cisplatin combination was used as front-line treatment in all patients. No previous irinotecan or gemcitabine treatment was allowed. Previous radiotherapy was allowed provided that the measurable lesions were outside the radiation fields. Patients with brain metastases were included, provided that they had been irradiated and had clinical and radiological improvement. Patients had to have adequate liver [serum bilirubin ≤ 1.5 times the upper normal limit (UNL); AST and ALT ≤ 2.5 UNL in the absence of demonstrable liver metastases, or ≤5 UNL in the presence of liver metastases], renal (serum creatinine ≤ 1.5 times the UNL), and bone marrow (neutrophils $\geq 1.5 \times 10^9\ L^{-1}$, and platelets $\geq 100 \times 10^9\ L^{-1}$) function. Other eligibility criteria were: absence of active infection, history of significant cardiac disease (unstable angina, congestive heart failure, myocardial infarction within the previous 6 months, ventricular arrhythmias) or malnutrition (loss of ≥20% of the original body weight). All patients gave written informed consent to participate in the study and the trial was approved by the Ethics and Scientific Committees of the participating centres. The study was conducted according to the Helsinki Declaration and Good Clinical Practice guidelines.

2.2. Patient evaluation

Baseline assessment comprised of a complete medical history, physical examination and vital signs, evaluation of performance status, 12-lead ECG, complete blood cell count with differential and blood biochemistry, chest X-rays and computed tomography scans of the chest, abdomen and brain and a whole-body radionuclide bone scan. Baseline evaluation had to be performed within 2 weeks prior to therapy initiation. All measurable lesions were identified at baseline and were monitored throughout. A complete medical history and a detailed physical examination with complete blood cell count with differential and blood biochemistry, ECG and a chest X-ray were performed before each treatment administration to assess the disease status and treatment toxicity. After completion of study treatment, patients were followed every 2 months.

2.3. Treatment

For the combination arm (IG), treatment consisted of gemcitabine given at a dose of 1000 mg/m^2 as a 30-min intravenous (i.v.) infusion, on days 1 and 8; irinotecan was administered on day 8 as a 90-min i.v. infusion, at a dose of 300 mg/m^2 [15]. For the monotherapy arm (I), treatment consisted of irinotecan administered i.v. on day 1, at a dose of 300 mg/m^2. Treatment was repeated every 3 weeks, for both arms. Treatment was continued until disease progression, the appearance of unacceptable toxicity, or patient's withdrawal of consent.

2.4. Assessment of antitumor activity and toxicity

Response assessment was evaluated every three chemotherapy courses. Objective tumor responses were evaluated according to WHO response criteria [21], with the same method on each occasion; all objective responses were confirmed by repeating the evaluation 4 weeks later. All CT scans were reviewed by an independent radiologist. Toxicity was reported according to National Cancer Institute Common Toxicity Criteria, Version 2 [22].

2.5. Statistical analysis

The primary end-point of the present study was objective response rate (ORR). The sample size estimation was based on ORR. According to chi-square exact test, with a 5% alpha and a beta error of 20%, 89 patients, per arm were required to achieve a clinically relevant response probability of 6% for irinotecan monotherapy and 20% for the irinotecan/gemcitabine combination with a 80% power. All clinical data were centrally collected and analyzed (Clinical Trial Office, Department of Medical Oncology, University Hospital of Heraklion, Crete, Greece) using SPSS Version 10.0 statistical software. Analysis was performed on an intent-to-treat basis. The duration of response was measured from the day of the first documentation of response to chemotherapy until disease progression. The time to tumor progression (TTP) was measured from study entry until the day of the first evidence of disease progression whereas the overall survival (OS) from study entry to death or last contact. The probability of survival was estimated by the method of Kaplan–Meier [23] and tested for differences by using the log-rank test. All tests were two-sided and were considered significant when the resulting p-value was ≤0.05.

3. Results

3.1. Patient characteristics

Thirty-eight patients were enrolled in the IG arm and 36 in the I arm. Five patients in the I arm were not evaluable because did not received the allocated treatment for the following reasons: death within 10 days after randomization ($n = 2$ patients), move to another center where another chemotherapy regimen was initiated and change of treatment plans because of diagnosis of CNS metastases requiring irradiation (1 patient) and pulmonary infection with cardiorespiratory insufficiency (1 patient). Due to slow accrual an early closure of the study was decided. Twenty (52.6%) and 10 (35.7%) patients had sensitive disease in the IG and I arms, respectively ($p = 0.173$). Sixteen patients (42.2%) completed treatment as per protocol in the IG arm and eight patients (25.8%) in the I arm ($p = 0.138$). Early treatment discontinuation occurred in 18 patients (47.4%) in the IG arm and 17 patients (54.8%) in the I arm due to disease progression. Three (7.9%) and six (19.4%) patients

Table 1
Patients' characteristics.

	IG ($n=38$)		I ($n=31$)		p-Value
	N	%	*N*	%	
Age (median, range)	60.5 (39–80)		65 (44–82)		
Sex					
Male	36	94.7	27	87.1	0.263
Female	2	5.3	4	12.9	
PS (ECOG)					
0	12	31.6	10	32.3	0.469
1	20	52.6	19	61.3	
2	6	15.8	2	6.5	
Median time from last chemotherapy (months, range)	3 (0.6–26.8)		2.1 (0.5–15.1)		0.533
Response to previous therapy					
CR + PR	18	47.4	11	35.5	
SD + PD	20	52.6	20	64.5	0.320
Disease					
Refractory	18	47.4	18	64.3	0.173
Sensitive	20	52.6	10	35.7	
No. of prior chemotherapy regimens					
1	26	68.4	26	83.9	0.138
≥2	12	31.6	5	16.1	
No. of organs involved					
1	10	26.3	9	29.0	
2	18	47.4	14	45.2	
3	10	26.3	8	6.1	
Median (min–max)	2	1–4	2	1–4	

IG: irinotecan/gemcitabine; I: irinotecan.

in the combination and monotherapy arms, respectively, discontinued treatment due to adverse events ($p=0.160$). One patient in the IG arm withdrew consent and he was considered as progression in the intention-to-treat analysis. Patients' characteristics are presented in Table 1.

3.2. Treatment compliance

A total of 153 and 86 chemotherapy cycles were administered in the IG and I arm, respectively ($p=0.012$); the median number of cycles received per patient was 3.0 (range 1–9) and 2.0 (range 1–7) for the combination and monotherapy arms, respectively ($p=0.012$). The median interval between cycles was 23 days for the IG combination (range, 21–31 days) and 21 days for the I monotherapy (range 21–25 days). Treatment administration was delayed in 49 (32%) IG and in 12 (14%) I cycles ($p=0.002$). Nineteen (12.4%) IG and four (4.7%) I cycles were delayed due to haematological toxicity; moreover, one (0.6%) IG and one (1.2%) I cycles were delayed because of non-haematological toxicity. All other cycles were delayed for reasons not related to treatment or toxicity (i.e. patient's request for personal reasons, pending imaging studies for response assessment). Dose reductions occurred in 24 (15.7%) IG and in 8 (9.3%) I cycles ($p=0.164$). Dose reductions in both groups were mainly due to haematological toxicity The median dose intensity was: (i) for the IG arm: 76 mg/m^2/week (range: 35.7–100 mg/m^2/week) for irinotecan (76% of planned dose) and 540 mg/m^2/week (range: 249–666.7 mg/m^2/week)) for gemcitabine (81% of planned dose), (ii) for the I arm: 95 mg/m^2/week (range: 67.5–100 mg/m^2/week) for irinotecan (95% of planned dose).

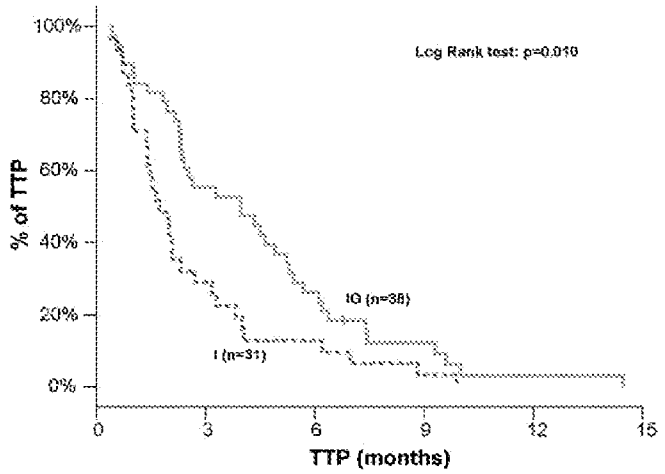

Fig. 1. Kaplan–Meier TTP curve for the two study arms.

3.3. Efficacy results

Responses and survival are based on the intention-to-treat analysis. In the IG arm one (2.6%) patient achieved a complete response (CR) and eight (21.1%) a partial response (PR), for an overall response rate of 23.7% (95% CI: 10.17–37.20%); in the monotherapy arm, no

Table 2
Efficacy results in patients with refractory and sensitive tumors.

	Refractory	Sensitive	p-Value
ORR			
IG	11.1%	16.7%	0.513
I			
TTP			
IG	2.5 months ($n=18$)	4.3 months ($n=20$)	0.128
I	1.9 months ($n=20$)	1.7 months ($n=10$)	0.665
OS			
IG	5.7 months ($n=18$)	8.6 months ($n=20$)	0.381
I	3.8 months ($n=20$)	8.6 months ($n=10$)	0.311

IG: irinotecan/gemcitabine regimen; I: irinotecan monotherapy.

Table 3
Treatment-related toxicity per arm.

	GrI				GrII				GrIII				GrIV				p-Value
	IG		I		IG		I		IG		I		IG		I		
	N	%	N	%	N	%	N	%	N	%	N	%	N	%	N	%	
Neutropenia	8	21.1	4	12.9	8	21.1	3	9.7	3	7.9	3	9.7	6	15.8	4	12.9	0.914*
Anemia	23	60.5	13	41.9	11	28.9	9	29.0	2	5.3	1	3.2	–	–	–	–	0.864**
Thrombocytopenia	11	28.9	6	19.4	5	13.2	–	–	2	5.3	1	3.2	6	15.8	2	6.5	0.199*
Febrile neutropenia	–	–	2	6.5	–	–	–	–	–	–	1	3.2	1	2.6	1	3.2	0.439*
Nausea	2	5.3	2	6.5	–	–	1	3.2	–	–	–	–	–	–	–	–	
Vomiting	7	18.4	2	6.5	–	–	1	3.2	–	–	1	3.2	–	–	–	–	
Diarrhea	3	7.9	3	9.7	3	7.9	1	3.2	2	5.3	4	12.9	–	–	–	–	0.727**
Stomatitis	1	2.6	–	–	–	–	1	3.2	–	–	–	–	–	–	–	–	–
Constipation	–	–	–	–	–	–	1	3.2	–	–	–	–	–	–	–	–	–
Neurotoxicity	2	5.3	–	–	–	–	1	3.2	–	–	–	–	–	–	–	–	0.495**
Allergy	3	7.9	–	–	–	–	–	–	–	–	–	–	–	–	–	–	–
Asthenia	4	10.5	1	3.2	3	7.9	5	16.1	1	2.6	2	6.5	–	–	–	–	0.174**
Edema	1	2.6	–	–	1	2.6	–	–	–	–	–	–	–	–	–	–	
Fever	–	–	2	6.5													

* p-Value for grade III/IV.
** p-Value for grade II/III.

objective clinical response was observed ($p = 0.004$). Additionally, stable disease (SD) was observed in eight (21.1%) patients in the combination arm and eight (25.8%) in the monotherapy arm. Progressive disease (PD) was observed in 21 (55.3%) and 23 (74.2%) patients in the combination and monotherapy arms, respectively. The median duration of response in the IG arm was 4.3 months.

The median follow-up time was 6.8 months (range 0.5–28.3) and 4.6 months (range 0.5–20.9) in the IG and I arm, respectively; the median TTP was 3.9 months (range: 0.5–14.5 months; 95% CI: 1.4–6.6) and 1.7 months (range: 0.5–9.9 months; 95% CI: 1.2–2.3) ($p = 0.010$) for IG and I arms, respectively (Fig. 1). However, median OS was similar between the two study arms: 6.8 months (range: 0.5–28.3 months; 95% CI: 3.6–9.9) and 4.6 months (range: 0.5–20.9 months; 95% CI: 2.3–6.9) for the combination and monotherapy arms ($p = 0.439$), respectively; the 1-year survival rate was 16.7% and 6.5%, respectively.

Table 2 demonstrates that there was no difference in terms of overall response rate (ORR), median TTP and OS in patients with sensitive and refractory disease in the two treatment arms.

3.4. Toxicity

Toxicity was assessed in all chemotherapy cycles and in all patients. Table 3 summarizes all treatment-related toxicities. The most frequent grade III/IV haematologic toxicity was neutropenia which occurred in 23.7% of IG patients and 22.6% of I patients ($p = 0.914$). One patient in the combination arm and two in the monotherapy arm, developed febrile neutropenia necessitating hospitalisation for intravenous administration of wide spectrum antibiotics and rhG-CSF; all patients uneventfully recovered. Thrombocytopenia grade III/IV was also frequent, occurring in 21.1% and 9.7% of IG and I patients, respectively ($p = 0.199$). There was no treatment-related death. The most frequent non-haematologic toxicity was diarrhea (grade III), occurring in 5.3% and 12.9% of combination and monotherapy patients ($p = 0.727$), respectively. All other haematologic and non-haematologic toxicities were relatively infrequent.

4. Discussion

Although SCLC is a chemosensitive disease, the vast majority of patients experience relapse and become candidates for second-line therapy. The results of second-line therapy depend on several factors, such as the time between the administration of first-line treatment and the experience of relapse, the response to first-line treatment, and the drugs administered as first-line therapy. Patients who did not respond to previous therapy or who relapsed within 3 months of completing therapy are considered refractory, and have a poor prognosis, with low probability to respond to second-line treatment, whereas those who had responded to previous treatment and relapsed 3 months or longer after completing such treatment are judged sensitive and are more likely to respond to second-line.

A recent randomized phase III trial demonstrated that second-line chemotherapy with topotecan offers survival benefit to patients with extensive stage SCLC [24]. This trial enrolled 141 patients randomly assigned to best supportive care (BSC) alone ($n = 70$) or oral topotecan (2.3 mg/m^2/day, days 1–5, every 21 days) plus BSC (topotecan; $n = 71$). The authors reported a statistically significant benefit in terms of overall survival and quality of life in favour to the arm with topotecan.

Although our study was prematurely terminated due to slow accrual, the comparison of irinotecan/gemcitabine combination with the irinotecan monotherapy revealed that the combination regimen was significantly more active than irinotecan monotherapy in terms of both response rate (23.7% vs. 0%; $p = 0.004$) and TTP (3.9 months vs. 1.7 months; $p = 0.010$); however, the difference observed, regarding OS, failed to reach statistical significance (6.8 months vs. 4.6 months; $p = 0.439$). This may be attributed to the small number of patients finally included.

The ORR observed with irinotecan monotherapy in our study is considerably lower than that observed by other phase II studies [6–9]. Two Japanese studies [6,7] reported an ORR of 37.1% [6] and 47% [7], respectively. However, in both of these studies, the percentage of refractory patients, which has significant impact on ORR, enrolled in the study was not reported. On the other hand a European study by Le Chevalier et al. [8] administered irinotecan 350 mg/m^2 (every 3 weeks) to 32 sensitive or refractory patients with SCLC and reported an ORR of 16% and median OS of 125 days. A second study by DeVore et al. [9] administered 125 mg/m^2 irinotecan (weekly for 4 weeks, followed by a 2-week rest period) to 44 patients (27 with refractory disease) and reported an ORR of 15.9%. The reasons for these conflicting results concerning the efficacy of irinotecan in second-line setting are not obvious. We cannot exclude that patients' characteristics, genetic heterogeneity as well as disease sensitivity could account for these observations. Indeed, it has been reported that some polymorphisms of the UGT1A1*28 gene, which deactivate the active metabolite of irinotecan, SN-38, may have a significant impact on the irinotecan-mediated toxicity and efficacy in patients with colorectal cancer [25]. In addition, it

has been reported that polymorphisms of the drug target topoisomerase I as well as TDP1 and XRCC1 are significantly associated with irinotecan efficacy and/or tolerance in patients with colorectal cancer [25]. However, the median OS of patients treated with single agent irinotecan was practically similar to that reported in previous phase II studies by other investigators [8].

Phase II studies of the IG combination in terms of ORR, median TTP and OS are conflicting. In a previous phase II study conducted by our group [15] the IG regimen was administered, to 31 SCLC patients (48% of them had refractory disease) resulting in an ORR of 10%, a TTP of 4.5 months and a median OS of 6 months; the lower ORR reported compared to the current study, could be attributed to the fact, that more than 50% of patients, received the IG regimen as third or more line of therapy. Two studies [16,17] used a relatively different regimen in 35 sensitive and 71 refractory SCLC patients (gemcitabine 1000 mg/m^2, days 1 and 8, irinotecan 100 mg/m^2, days 1 and 8; every 21 days) and reported a similar response rate of 17% and 21%, respectively. Median TTP and OS were 3.4 and 5.8 months for the first study [16]. In the second study the reported median TTP and OS was 3.1 months and 7.1 months, respectively in patients with sensitive disease; in patients with refractory disease the median TTP was 1.6 months and the median OS 3.5 months. Finally, three other studies evaluated a biweekly schedule of irinotecan/gemcitabine in patients with refractory or relapsed disease. The ORR was ranged from 27.6% to 50% and the median OS from 8.5 months to 14.4 months [18]. The high response rate (50%) observed in the Castellano's study [19] could be ascribed to the higher doses of both drugs used by this study, and to differences regarding study population (the exact percentage of refractory patients is not reported).

In our study, the irinotecan/gemcitabine combination resulted in a median survival of 8.6 months in sensitive patients and 5.7 months in refractory patients. For irinotecan monotherapy the corresponding survival was 8.6 months and 3.8 months for sensitive and refractory patients, respectively. These differences failed to reach statistical significance, probably due to the small number of patients included in the study. These results are in accordance with these reported by Rocha-Lima et al. [17].

Neutropenia was the most frequent toxicity observed in both arms. Indeed, 23.7% of the patients in the combination arm and 22.6% of the patients in the monotherapy arm developed grade III/IV neutropenia. However, only three patients (one in the combination and two in the monotherapy arm) developed febrile neutropenia, which required hospitalization. All patients were uneventfully recovered. Furthermore, as expected, patients receiving the IG regimen developed to a greater percentage thrombocytopenia, obviously due to gemcitabine. Eight patients (21.1%) in the IG arm and three (9.7%) in the I arm developed grade III/IV thrombocytopenia. However, because of the small number of patients, this difference failed to reach statistical significance. Diarrhea was the most frequent non-haematological toxicity; though in most cases was grade I/II, and easily manageable with administration of loperamide. Only two cases required hospitalization for i.v. administration of fluids.

Although, the results of this study demonstrate a moderately higher activity for the combination arm compared to monotherapy arm, its prematurely closure because of slow accrual prevents the drawing of constant conclusions. However, on the basis of these results, the combination of irinotecan/gemcitabine merits to be further investigated in the second-line setting in a large prospective randomized trial.

Conflict of interest

None declare.

References

[1] Jemal A, Tiwari RC, Murray T, Ghafoor A, Samuels A, Ward E, et al. Cancer statistics. CA Cancer J Clin 2004;54(1):8–29.

[2] Jackman DM, Johnson BE. Small-cell lung cancer. Lancet 2005;366(9494):1385–96.

[3] von PJ, Schiller JH, Shepherd FA, Fields SZ, Kleisbauer JP, Chrysson NG, et al. Topotecan versus cyclophosphamide, doxorubicin, and vincristine for the treatment of recurrent small-cell lung cancer. J Clin Oncol 1999;17(2):658–67.

[4] Ettinger DS. New drugs for chemotherapy-naive patients with extensive-disease small cell lung cancer. Semin Oncol 2001;28(2 Suppl 4):27–9.

[5] Kelly K. New chemotherapy agents for small cell lung cancer. Chest 2000;117(4 Suppl 1):156S–62S.

[6] Negoro S, Fukuoka M, Niitani H, Suzuki A, Nakabayashi T, Kimura M, et al. A phase II study of CPT-11, a camptothecin derivative, in patients with primary lung cancer. CPT-11 Cooperative Study Group. Gan To Kagaku Ryoho 1991;18(6):1013–9.

[7] Masuda N, Fukuoka M, Kusunoki Y, Matsui K, Takifuji N, Kudoh S, et al. CPT-11: a new derivative of camptothecin for the treatment of refractory or relapsed small-cell lung cancer. J Clin Oncol 1992;10(8):1225–9.

[8] Le Chevalier T, Ibrahim N, Chomy P, Riviere A, Monnier A, Magherini E, et al. A phase II study of irinotecan (CPT-11) in patients (pts) with small cell lung cancer (SCLC) progressing after initial response to first-line chemotherapy (CT) (Meeting abstract). Proc Am Soc Clin Oncol 1997;16 (abstr no 1617).

[9] DeVore III RF, Blanke C, Denham C, Hainsworth J, Gralla RJ, Koletsky AJ, et al. Phase II study of Irinotecan (CPT-11) in patients with previously treated small-cell lung cancer (SCLC) (Meeting abstract). Proc Am Soc Clin Oncol 1998;17 (abstr no 1736).

[10] Noda K, Nishiwaki Y, Kawahara M, Negoro S, Sugiura T, Yokoyama A, et al. Irinotecan plus cisplatin compared with etoposide plus cisplatin for extensive small-cell lung cancer. N Engl J Med 2002;346(2):85–91.

[11] Hanna N, Bunn Jr PA, Langer C, Einhorn L, Guthrie Jr T, Beck T, et al. Randomized phase III trial comparing irinotecan/cisplatin with etoposide/cisplatin in patients with previously untreated extensive-stage disease small-cell lung cancer. J Clin Oncol 2006;24(13):2038–43.

[12] Cormier Y, Eisenhauer E, Muldal A, Gregg R, Ayoub J, Goss G, et al. Gemcitabine is an active new agent in previously untreated extensive small cell lung cancer (SCLC). A study of the National Cancer Institute of Canada Clinical Trials Group. Ann Oncol 1994;5(3):283–5.

[13] Masters GA, Declerck L, Blanke C, Sandler A, DeVore R, Miller K, et al. Phase II trial of gemcitabine in refractory or relapsed small-cell lung cancer: Eastern Cooperative Oncology Group Trial 1597. J Clin Oncol 2003;21(8):1550–5.

[14] van dL I, Smit EF, van Putten JW, Groen HJ, Schlosser NJ, Postmus PE, et al. Single-agent gemcitabine in patients with resistant small-cell lung cancer. Ann Oncol 2001;12(4):557–61.

[15] Agelaki S, Syrigos K, Christophylakis C, Boukovinas J, Varthalitis J, Pavlakou G, et al. A multicenter phase II study of the combination of irinotecan and gemcitabine in previously treated patients with small-cell lung cancer. Oncology 2004;66(3):192–6.

[16] Schuette W, Nagel S, Juergens S, Bork I, Wollschlaeger B, Schaedlich S, et al. Phase II trial of gemcitabine/irinotecan in refractory or relapsed small-cell lung cancer. Clin Lung Cancer 2005;7(2):133–7.

[17] Rocha-Lima CM, Herndon JE, Lee ME, Atkins JN, Mauer A, Vokes E, et al. Phase II trial of irinotecan/gemcitabine as second-line therapy for relapsed and refractory small-cell lung cancer: Cancer and Leukemia Group B Study 39902. Ann Oncol 2007;18(2):331–7.

[18] Ohyanagi F, Horiike A, Okano Y, Satoh Y, Okumura S, Ishikawa Y, et al. Phase II trial of gemcitabine and irinotecan in previously treated patients with small-cell lung cancer. Cancer Chemother Pharmacol 2008;61(3):503–8.

[19] Castellano D, Ciruelos E, Garcia-Giron C, Lopez-Martin A, Gerrido P, Jimeno A, et al. Phase II trial of biweekly irinotecan plus gemcitabine combination in refractory or relapsed small cell lung cancer (SCLC). Proc Am Soc Clin Oncol 2003;22 (abstr no 2710).

[20] Domine M, Gonzales-Larriba JL, Garcia Gomez R, Provencio M, Isla D, Terrasa S, et al. CPT-11—gemcitabine for refractory or relapsed small cell lung cancer (SCLC). A Spanish multicentric phase II study. Proc Am Soc Clin Oncol 2003;22 (abstr no 2819).

[21] Miller AB, Hoogstraten B, Staquet M, Winkler A. Reporting results of cancer treatment. Cancer 1981;47(1):207–14.

[22] Cancer Therapy Evaluation Program. Common toxicity criteria. Version 2.0. DCTD, NCI, NIH, DHHS; 1998.

[23] Collet D. Modelling Survival Data in Medical Research. 3rd edn. Oxford: Blackwell Scientific; 1994.

[24] O'Brien ME, Ciuleanu TE, Tsekov H, Shparyk Y, Cucevia B, Juhasz G, et al. Phase III trial comparing supportive care alone with supportive care with oral topotecan in patients with relapsed small-cell lung cancer. J Clin Oncol 2006;24(34):5441–7.

[25] Hoskins JM, Marcuello E, Altes A, Marsh S, Maxwell T, Van Booven DJ, et al. Irinotecan pharmacogenetics: influence of pharmacodynamic genes. Clin Cancer Res 2008;14(6):1788–96.

Anti-HER2 Immunoliposomes: Enhanced Efficacy Attributable to Targeted Delivery[1]

John W. Park,[2] Keelung Hong, Dmitri B. Kirpotin, Gail Colbern,[3] Refaat Shalaby, Jose Baselga,[4] Yvonne Shao, Ulrik B. Nielsen, James D. Marks, Dan Moore, Demetrios Papahadjopoulos, and Christopher C. Benz

Division of Hematology/Oncology [J. W. P., C. C. B.] and Department of Anesthesia [U. B. N., J. D. M.], University of California, San Francisco, San Francisco, California 94143; California Pacific Medical Center Research Institute, San Francisco, California 94115 [K. H., D. B. K., G. C., R. S., Y. S., D. M., D. P.]; Memorial Sloan-Kettering Cancer Center, New York, New York [J. B.]

ABSTRACT

Purpose: **Anti-HER2 immunoliposomes combine the tumor-targeting of certain anti-HER2 monoclonal antibodies (MAbs) with the pharmacokinetic and drug delivery capabilities of sterically stabilized liposomes. We previously showed that anti-HER2 immunoliposomes bind efficiently to and internalize in HER2-overexpressing cells *in vitro*, resulting in intracellular drug delivery.**

Experimental Design: **Here we describe the pharmacokinetics and therapeutic efficacy of anti-HER2 immunoliposomes containing doxorubicin (dox) in a series of animal models.**

Results: **Immunoliposomes displayed long circulation that was identical to that of sterically stabilized liposomes in single- and multiple-dose studies in normal rats. Anti-HER2 immunoliposome-dox produced marked therapeutic results in four different HER2-overexpressing tumor xenograft models, including growth inhibition, regression, and cures. These results demonstrated that encapsulation of dox in anti-HER2 immunoliposomes greatly increased its therapeutic index, both by increasing antitumor efficacy and by reducing systemic toxicity. Immunoliposome-dox was significantly superior to all other treatment conditions tested, including free dox, liposomal dox, and anti-HER2 MAb (trastuzumab). When compared with liposomal dox in eight separate therapy studies in HER2-overexpressing models, immunoliposome delivery produced significantly superior antitumor efficacy in each study ($P < 0.0001$ to 0.04). Anti-HER2 immunoliposome-dox containing either recombinant human MAb HER2-Fab′ or scFv C6.5 yielded comparable therapeutic efficacy. Cure rates for immunoliposome-dox reached 50% (11 of 21) with optimized immunoliposomes and Matrigel-free tumors and overall was 16% (18 of 115) *versus* no cures (0 of 124) with free dox or liposomal dox. Finally, anti-HER2 immunoliposome-dox was also superior to combinations consisting of free MAb plus free dox or free MAb plus liposomal dox.**

Conclusions: **Anti-HER2 immunoliposomes produced enhanced antitumor efficacy via targeted delivery.**

INTRODUCTION

Immunoliposomes represent a novel strategy for tumor-targeted drug delivery (1). Immunoliposomes have become feasible as a result of parallel advances in the areas of liposome research and MAb[5] technology, which in principle can now be combined for tumor-targeted drug delivery.

The development of stable, long-circulating liposomes has led to a new era in liposome drug delivery (2). For example, sterically stabilized liposomes, consisting of small, neutrally charged unilamellar liposomes with a polymeric coating of PEG, display retarded clearance by the RES, resulting in substantially prolonged drug circulation (3). In addition, the long circulation times and small sizes of these liposomes allow preferential extravasation in many solid tumors because of vascular abnormalities associated with tumor angiogenesis (4). However, sterically stabilized liposomes do not interact directly with tumor cells *in vitro* or *in vivo*, and instead release drug for eventual diffusion into tumor cells (5).

Similarly, progress in MAb-based therapy of cancer has finally led to clinical validation after two decades of research (reviewed in Ref. 6). A leading example has been the development of MAbs directed against the $p185^{HER2}$ (HER2; ErbB2) receptor tyrosine kinase, the product of the *HER2* (c-*erb*B2) proto-oncogene. HER2 plays an important role in the pathogenesis of breast and other cancers (reviewed in Ref. (7). HER2 is highly overexpressed in a significant proportion of these can-

Received 6/4/01; revised 1/23/02; accepted 1/30/02.
The costs of publication of this article were defrayed in part by the payment of page charges. This article must therefore be hereby marked *advertisement* in accordance with 18 U.S.C. Section 1734 solely to indicate this fact.
[1] This work was supported by grants from the National Cancer Institute Specialized Programs of Research Excellence (SPORE) in Breast Cancer (Grant P50-CA 58207-01), the Department of Defense Breast Cancer Research Program (Grant DAMD17-94-J-4195), and the American Society of Clinical Oncology Young Investigator Award (to J. W. P.) sponsored by the Don Shula Foundation.
[2] To whom requests for reprints should be addressed, at UCSF Comprehensive Cancer Center, 1600 Sutter Street, 2nd Floor, San Francisco, CA 94115-1710. Phone: (415) 502-3844; Fax: (415) 353-7021; E-mail: jpark@cc.ucsf.edu.
[3] Present address: Alza Corporation, Mountain View, CA 94043.
[4] Present address: Hospital General Universitari Vall D'Hebron, 08035 Barcelona, Spain.

[5] The abbreviations used are: MAb, monoclonal antibody; PEG, polyethylene glycol; RES, reticuloendothelial system; PK, pharmacokinetic; rhuMAb, recombinant human MAb; dox, doxorubicin; Ls, liposome; DTPA, diethylenetriaminepentaacetic acid; IHC, immunohistochemical; MTD, maximum tolerated dose.

cers, and HER2 overexpression is clearly associated with poor prognosis in breast cancer (8, 9). Hence, HER2 is an attractive target for MAb-based therapeutic strategies. rhuMAb HER2 (trastuzumab; Herceptin), a humanized MAb directed against HER2, represents one such therapy (10) and has demonstrated clinical benefit in the treatment of advanced breast cancer. Trastuzumab can induce antitumor responses as a single agent (11, 12), but it is most efficacious when combined with chemotherapy (13).

We have developed anti-HER2 immunoliposomes to combine the tumor-targeting properties of MAbs such as trastuzumab with the drug delivery properties of sterically stabilized liposomes. Anti-HER2 immunoliposomes efficiently bind to and internalize in HER2-overexpressing cells, resulting in intracellular drug delivery (14, 15). Here we show the PK and therapeutic properties of dox-loaded anti-HER2 immunoliposomes in a series of animal models.

MATERIALS AND METHODS

Preparation of MAb Fragments. Immunoliposomes were constructed with several different MAb fragments. Most studies included rhuMAb HER2-Fab′ (Genentech, Inc.), a recombinant Fab′ derived from trastuzumab. Cloned trastuzumab heavy- and light-chain genes were coexpressed in *Escherichia coli*, and Fab′ was recovered as described (16). Later studies included scFv C6.5, an alternative anti-HER2 MAb fragment generated by phage display screening of a human antibody gene library (17). scFv was subsequently modified for immunoliposome conjugation by addition of a cysteine residue near the COOH terminus of the recombinant sequence. The modified scFv C6.5 was expressed in *E. coli* and purified as described (17). Immunoliposomes were also constructed with rhuMAb H52-Fab′, an irrelevant humanized Fab′ that differs from rhuMAb HER2-Fab′ only in the antigen-binding loops and shows no detectable binding to any known antigen (14). Another control consisted of inactivated scFv C6.5, in which the scFv was exposed to additional reduction, resulting in elimination of an internal disulfide bond in the antigen-binding domain essential for binding activity.

Preparation of Liposomes and Immunoliposomes. Liposomes were prepared by a lipid film hydration-extrusion method as small unilamellar vesicles (100 ± 10 nm) containing hydrogenated soy phosphatidylcholine and cholesterol as described (14, 15). Liposomes of this composition have increased rigidity and decreased permeability because of the high transition temperature of hydrogenated soy phosphatidylcholine (T_m = 54°C) at 37°C. PEG (M_r 1900)-derivatized distearoyl-phosphatidylethanolamine was included at 0–7 mol % of total lipid for steric stabilization. dox was encapsulated into liposomes with high efficiency by the ammonium sulfate remote loading method (18). For immunoliposomes, Fab′ or scFv was covalently conjugated to liposomes after drug loading. Conjugation was via a thioether linkages between the free thiol near the COOH terminus of the MAb fragment and terminal maleimide groups at the liposome surface (Ls-MAb linkage) as described (14). Alternatively, the MAb thiol was conjugated to maleimide groups at the termini of PEG chains (PEG-MAb linkage) as described (15).

Animal Studies. PK studies were performed in healthy rats, and therapeutic efficacy studies were performed in tumor xenograft nude mouse models, as described below. Institutional approvals for animal use were obtained at each site at which animal studies were performed (Memorial Sloan-Kettering Cancer Center, University of California, San Francisco, and California Pacific Medical Center Research Institute), and the requirements were followed in each of these studies.

PK Studies. Healthy adult Sprague Dawley rats received single or multiple i.v. injections of immunoliposomes, liposomes, or free drug via indwelling jugular venous catheters. After the injection, blood was serially sampled via catheter up to 48 h postinjection, and plasma was assayed for dox, Fab′, or liposome. Dox concentration was determined by spectrofluorimetry after extraction of plasma with acidified alcohol. For two-component PK studies, plasma samples were divided and analyzed for both dox and rhuMAb HER2-Fab′ concentrations. The Fab′ concentration was determined by ELISA, using wells coated with recombinant HER2 extracellular domain for capture and horseradish peroxidase-linked goat antihuman IgG for detection. For multiple-dose PK studies, rats were given i.v. injections of immunoliposomes every week for 3 weeks as in the therapy studies (see below). The initial two doses consisted of "empty" (no encapsulated agent) immunoliposomes, whereas the final dose consisted of immunoliposomes stably loaded with ^{67}Ga-DTPA chelates. Plasma levels were determined by radioactivity counting.

Tumor Cell Lines. Cell lines BT-474, MDA-MB-453, and MCF-7 were obtained from American Type Culture Collection. These cell lines have been extensively characterized for HER2 expression by flow cytometry, ELISA, and immunohistochemistry (19). MCF-7/HER2 was derived by stable transfection of *HER2* cDNA in MCF-7 cells as described (20). IHC scoring of HER2 expression on a semiquantitative scale (0–3+) was first developed for trastuzumab clinical trials (21) and is now routinely used clinically (22). Recent studies have suggested that the presence of *HER2* gene amplification as detected by fluorescence *in situ* hybridization may be more predictive of response to trastuzumab than IHC assays of HER2 (23, 24).

Tumor Xenograft Models. Highly tumorigenic clones were generated from BT-474, MDA-MB-453, MCF-7, and MCF-7/HER2 lines by *in vivo* selection in nude (athymic) mice. In separate studies, tumorigenic clones of BT-474 were independently derived at Memorial Sloan-Kettering Cancer Center (by J. B.) and California Pacific Medical Center (by G. C.), and the resulting xenograft models were designated BT-474/MSKCC and BT-474/SF, respectively. HER2 expression in tumor xenografts was evaluated by IHC analysis and confirmed to be still overexpressed.[6] Estradiol pellets were also implanted to increase tumorigenicity as described (25). In initial experiments, the BT-474/SF, MDA-MB-453, and MCF-7/HER2 models involved s.c. injection of tumor cells mixed with Matrigel (Collaborative Biomedical Associates, Oxford, MA), a complex

[6] M. R. Shalaby, D. Kirpotin, K. Hong, B-M. Ljung, Z. Meng, and J. W. Park. The use of Matrigel in xenograft models: new implications, submitted for publication.

extracellular matrix substitute. Matrigel was omitted in subsequent studies (see text).

Therapy Studies. For each model, tumor cells were implanted s.c. with or without Matrigel in the dorsum of nude mice. When tumor xenografts had become fully established and tumors were ≥200 mm^3, mice were randomly assigned to different treatment groups (5–15 mice/group). In the nude mice, all i.v. treatments were performed via retro-orbital injection. Anti-HER2 immunoliposomes were administered i.v. at 5.0–7.5 mg dox/kg/dose every week for 3 weeks, for a total dox dose of 15.0–22.5 mg/kg. The corresponding lipid dose was typically 0.6–1.0 μmol of phospholipid per dose and 1.8–3.0 μmol total. Additional treatment groups were included as indicated in the text. Saline (PBS) was administered i.v. at the same injection volume and schedule as immunoliposomes. Free dox (Adriamycin) was administered i.v. at its MTD of 7.5 mg/kg on the same schedule as immunoliposomes. Sterically stabilized liposomal dox was either prepared identically as immunoliposome-dox except for omission of the MAb conjugation step or consisted of commercial PEGylated liposomal dox (Doxil; Alza Pharmaceuticals). Both versions of liposomal dox were administered i.v. at the same dose and schedule as immunoliposomes. Empty immunoliposomes were administered i.v. at the same lipid dose as anti-HER2 immunoliposome-dox and by the same weekly schedule or three times per week. Free trastuzumab (Genentech, Inc.) was administered i.p. at 0.3 mg/kg twice a week for 3 weeks as described (25). Although all other treatments were administered i.v. (retro-orbital injection) weekly, trastuzumab was administered i.p. twice per week based on extensive preclinical optimization with this regimen (21, 25).

Tumors were measured twice a week by caliper, and tumor volumes were calculated using the equation: length × width × depth. Mice with complete tumor regressions by measurement were necropsied at the end of the study and classified as "cured" if no residual tumor cells were detected on histopathological examination of the tumor injection site. Although these xenograft models do not typically support metastatic tumor growth, necropsy also included gross examination of viscera to confirm absence of metastases. Studies were terminated at ~2 months after treatment initiation in these models because of their requirement for estrogen supplementation; estrogen pellets implanted at the time of tumor injection potentially lose potency over extended periods. Mice were also weighed and examined for toxicity twice a week. In most of the studies, the experimenter measuring tumor volumes was blinded to treatment condition.

For MTD studies, nude mice with established tumor xenografts were treated with various doses of free dox, liposomal dox, or anti-HER2 immunoliposome-dox (5–15 mice/group). As in the therapy studies, treatments were administered via retro-orbital i.v. injection over three weekly doses. Total dox administered ranged from 2.5 to 22.5 mg/kg. Mice were monitored for weight and gross toxicity as described over 2 months, the typical duration of the therapy studies. The MTD was defined as the highest tested dose that gave <20% weight loss and no treatment-related deaths.

Statistical Analysis. Tumor growth delay and tumor growth ratio were determined as described in Table 2. Confidence intervals for tumor growth ratios were based on the assumption that the log of the ratios follows a normal distribution, which was consistent with observed data. A separate analysis was performed by fitting a modified Norton-Simon model of tumor growth (26) to the observed data using the method of maximum likelihood to estimate model parameters. In two cases, application of this model to the data did not provide an adequate fit. In these cases, data were analyzed by two-way ANOVA using two factors, treatment group and day. Scheffé *post hoc* comparisons were then used to compare pairs of treatments (Table 2). Cure rates were compared using Fisher's exact test for comparing two proportions.

RESULTS

Preparation of Anti-HER2 Immunoliposomes. Anti-HER2 immunoliposomes were constructed by conjugation of HER2-specific MAb fragments to sterically stabilized liposomes to create a tumor-targeted drug carriers for the treatment of HER2-overexpressing breast cancers. Immunoliposomes were designed to optimize intracellular delivery of encapsulated drug into tumor cells (1). Immunoliposome components included (*a*) a MAb fragment (Fab′ or scFv) to avoid accelerated clearance and immunogenicity associated with intact IgG; (*b*) sterically stabilized liposomes for long circulation and preferential tumor extravasation; (*c*) MAb fragments conjugated to the termini of derivatized PEG chains ("PEG-MAb linkage") to facilitate immunoliposome binding and internalization in target cells; and (*d*) encapsulated anticancer agents (*e.g.*, dox) for which tumor-targeted delivery might enhance the therapeutic index.

dox-loaded anti-HER2 immunoliposomes were initially prepared as described (14), using liposomes containing 0–7 mol % PEG and with rhuMAb HER2-Fab′ conjugated to derivatized head groups of phosphatidylethanolamine on the liposome surface (Ls-MAb linkage). However, immunoliposomes combining the Ls-MAb linkage with a high-density PEG coating showed reduced binding and endocytosis because of steric inhibition (14, 15). This problem was circumvented by use of immunoliposomes with MAb fragments conjugated to the termini of PEG chains (PEG-MAb linkage; Ref. 15). Our optimized construct design therefore consisted of anti-HER2 MAb fragments conjugated via a PEG-MAb linkage to dox-loaded sterically stabilized liposomes containing 6–7 mol % PEG. MAb fragments were either rhuMAb HER2-Fab′ as described (14, 15), or alternatively, scFv C6.5, a fully human anti-HER2 single-chain Fv cloned from a phage antibody library (17). Conjugations were highly efficient, resulting in 30–50 MAb fragments/liposome (70–90% of added MAb fragment).

Pharmacokinetics of Anti-HER2 Immunoliposomes. Although prolonged circulation does not ensure improved efficacy, we sought to construct immunoliposomes with long circulating properties to maximize the effects of tumor targeting. PK studies of anti-HER2 immunoliposome-dox constructs were performed in healthy adult rats. dox-loaded immunoliposomes were prepared with 0–7 mol % PEG and with MAb fragments linked either to the liposome surface (Ls-MAb linkage) or to the termini of PEG chains (PEG-MAb linkage). After a single i.v. dose, all immunoliposome-dox constructs showed a biphasic plasma PK profile for dox (Fig. 1*A*), with terminal $t_{1/2}$ =

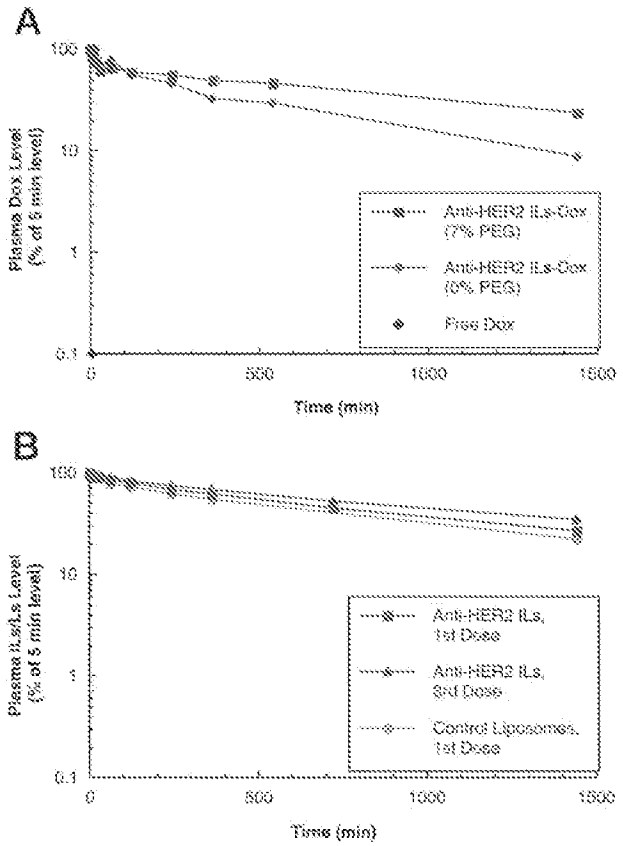

Fig. 1 Plasma pharmacokinetics of anti-HER2 immunoliposomes in rats. *A*, Plasma pharmacokinetics of anti-HER2 immunoliposome-dox *versus* free dox after single i.v. injections in rats. Immunoliposomes containing 0 mol % PEG and Ls-MAb linkage (▨), 7 mol % PEG, PEG-MAb linkage (◈), or free dox (✚) were administered i.v. at time 0. Immunoliposome dose was 5 μmol of total lipid, 0.9 mg of dox; free dox dose was 0.9 mg. Dox levels were determined at the indicated times and expressed as a percentage of the dox concentration at 5 min; dox was undetectable in plasma beyond 5 min after injection of free dox. *B*, Plasma pharmacokinetics of radiolabeled anti-HER2 immunoliposomes after multiple *versus* single i.v. injection in rats. Immunoliposomes (6 mol % PEG, PEG-MAb linkage) were administered i.v. in rats every week for 3 weeks as in the therapy studies. For the third dose, immunoliposomes were loaded with ^{67}Ga-DTPA chelates, and immunoliposome levels were determined at the indicated times by radioactivity counting (△). For comparison, ^{67}Ga-DTPA-loaded immunoliposomes (▨) and sterically stabilized liposomes (○) were also administered to naive rats. Plasma levels of immunoliposomes (*ILs*) or liposomes (*Ls*) are expressed as a percentage of the radioactivity present at 5 min.

11.6–13.6 h, area under the curve of 57,539–93,133 min %, and mean residence time of 15.8–24.3 h (Table 1). In contrast, dox levels were undetectable beyond 5 min after administration of the equivalent dose of free dox. The long circulation times of anti-HER2 immunoliposomes are fully equivalent to previous reports of sterically stabilized liposomal dox and greatly superior to those of "conventional" liposomes (27).

Direct comparison of anti-HER2 immunoliposome-dox *versus* sterically stabilized liposomal dox prepared identically except for omission of MAb fragments showed indistinguishable pharmacokinetics (Table 1). The presence of MAb fragments on immunoliposomes therefore did not measurably alter clearance in normal rats.

Table 1 Plasma pharmacokinetics of anti-HER2 immunoliposome-dox in rats

Anti-HER2 immunoliposomes (0–7 mol % PEG; Ls-MAb or PEG-MAb linkage) were loaded with dox and administered i.v. at a dose of 5.0 μmol of total lipid (0.8–1.0 mg of dox).

Immunoliposome type	Terminal $t_{1/2}$ (h)	AUC[a] (min %)	MRT ± SE (h)
0% PEG, Ls-MAb	11.6	70,954	15.8 ± 1.1
1% PEG, Ls-MAb	13.4	85,695	19.3 ± 3.2
2% PEG, Ls-MAb	12.7	57,539	17.7 ± 3.0
7% PEG, PEG-MAb	16.3	93,133	24.3 ± 0.9
Liposome: 1% PEG, no MAb	13.6	69,882	20.7 ± 1.2

[a] AUC, area under the curve; MRT, mean residual time.

Notably, all anti-HER2 immunoliposome-dox constructs were long circulating. Thus, immunoliposomes of this type (*i.e.*, small unilamellar vesicles, solid bilayer, neutral charge) did not require a polymeric coating such as PEG to achieve long circulation. Nevertheless, PEGylation of immunoliposomes, although not necessary for long circulation, was associated with incremental prolongation of mean residence time (Fig. 1*A* and Table 1).

Stability of Anti-HER2 Immunoliposome-dox *in Vivo*. The stability of dox-loaded anti-HER2 immunoliposomes in circulation was evaluated in two-component PK studies, in which dox and MAb levels were simultaneously assayed to evaluate possible drug leakage or dissociation of MAb fragments from liposomes. For these studies, plasma pharmacokinetics of dox (assayed by spectrofluorimetry) and of rhuMAb HER2-Fab′ fragments (assayed by ELISA) were codetermined from the same plasma samples after single i.v. injection of anti-HER2 immunoliposome-dox. Both the dox and Fab′ components showed concordant plasma PK values after immunoliposome administration, with terminal $t_{1/2}$ = 10 h for both. In contrast, free dox was again undetectable beyond 5 min, whereas free rhuMAb HER2-Fab′ has a terminal $t_{1/2}$ in rats of 1–2 h.[7] These results indicated that immunoliposomes greatly prolonged the circulation of both Fab′ and dox components and suggested that anti-HER2 immunoliposome-dox remained intact in circulation, with negligible drug leakage or MAb dissociation.

Multiple-Dose Pharmacokinetics of Anti-HER2 Immunoliposomes. A major limitation of many immunoconjugate strategies has been the immunogenicity of the construct because the MAb component, the effector/cytotoxic component, or the linker can elicit a host immune response that precludes repeated administrations. To circumvent this problem, anti-HER2 immunoliposomes were designed to have components of minimal immunogenicity: sterically stabilized liposomes and humanized/human MAb fragments. Trastuzumab, a humanized IgG1, induced minimal levels of circulating anti-antibodies in clinical trials (11). MAb fragments rather than intact IgG were used to

[7] D. Maneval, Canji, Inc., San Diego, CA, personal communication.

further reduce the potential for immune recognition associated with Fc sequences. To confirm that repeated administrations of anti-HER2 immunoliposomes do not lead to accelerated clearance, multiple-dose PK studies were performed in normal rats. Radiolabeled anti-HER2 immunoliposomes were administered once a week for three doses, using the same lipid dose and schedule as in the therapy studies (see below). Anti-HER2 immunoliposomes showed equivalent plasma pharmacokinetics in rats after the third and final dose as in naive rats without prior immunoliposome treatment (Fig. 1*B*). Furthermore, anti-HER2 immunoliposomes after one or three doses demonstrated plasma pharmacokinetics that were indistinguishable from those of sterically stabilized liposomes (prepared identically except for omission of Fab′ fragments). Thus, the presence of MAb fragments on immunoliposomes did not result in accelerated clearance over a multiple dose schedule, even when humanized Fab′s were introduced into an immunocompetent rodent host. In humans, immunoliposomes containing humanized Fab′ or fully human scFv are designed to further minimize the potential for immunogenicity.

Antitumor Efficacy of anti-HER2 Immunoliposome-dox against HER2-overexpressing Human Breast Cancer Xenografts. The antitumor efficacy of anti-HER2 immunoliposome-dox constructs was evaluated extensively in four different HER2-overexpressing breast cancer xenograft models: BT474/MSKCC and BT474/SF, independently derived xenograft models from the BT-474 cell line ($\sim 10^6$ HER2 receptors/cell; IHC score, 3+); MCF-7/HER2, MCF-7 cells stably transfected with HER2 ($\sim 10^6$ HER2/cell; IHC score, 3+; Ref. 20); and MDA-MB-453 ($\sim 10^5$ HER2/cell; IHC score, 2+). For each model, tumor cells were implanted in nude mice with or without Matrigel, and treatment was initiated subsequently after tumors had become fully established. Tumor volumes at the start of treatment were 200-1000 mm^3 (0.2–1.0 g) in 20-g mice, thus representing a spectrum from well-established moderate tumors to very large (5% of body weight) tumors.

Anti-HER2 immunoliposomes, prepared with 0–7 mol % PEG and either the Ls-MAb or PEG-MAb linkage, were loaded with dox and administered i.v. at a total dox dose of 15.0–22.5 mg/kg, divided over three weekly doses. Immunoliposomes were directly compared with multiple other treatment conditions, including saline, free dox at its MTD of 7.5 mg/kg, and sterically stabilized liposomal dox at the same dose and schedule as immunoliposome-dox. Additional controls included empty anti-HER2 immunoliposomes (no dox), at the same lipid dose as immunoliposome-dox and free anti-HER2 MAb (trastuzumab) administered at 0.3 mg/kg i.p. twice a week as described (25). Other controls included dox-loaded immunoliposomes containing an irrelevant MAb fragment, rhuMAb H52-Fab′ (14), as well as dox-loaded immunoliposomes containing inactivated anti-HER2 scFv C6.5, in which binding affinity was abrogated by reduction of internal disulfides in the antigen-binding domain before immunoliposome conjugation. Both irrelevant and inactivated immunoliposomes yielded results comparable to those of liposomal dox (data not shown). For this reason, liposomal dox was used as the nontargeted control liposomes for most studies, either by preparing sterically stabilized liposomes identical to anti-HER2 immunoliposome-dox except for omission of MAb fragments or by use of commercial PEGylated liposomal dox (Doxil). The treatment groups are summarized in Table 2.

Each of the anti-HER2 immunoliposome-dox constructs produced marked antitumor effects, including tumor growth inhibition, tumor regression, and cures of mice. These effects were observed in all sizes of tumors. Anti-HER2 immunoliposome-dox consistently showed activity superior to that of all other treatment conditions. For example, initial studies of anti-HER2 immunoliposome-dox containing 1 mol % PEG and Ls-MAb linkage demonstrated suppression of tumor growth that persisted after treatment. Tumor inhibition was clearly superior to that associated with free dox or liposomal dox (Fig. 2 and Table 2).

Comparison of this initial anti-HER2 immunoliposome-dox (1 mol % PEG, Ls-MAb linkage) with the optimized anti-HER2 immunoliposome construct design (6 mol % PEG, PEG-MAb linkage) indicated superior antitumor activity for the latter (data not shown). This result was presumably attributable to the incremental PK advantage associated with the higher PEG concentration (Table 1) and/or the unimpeded internalization associated with the PEG-MAb linkage (15). Subsequent studies therefore evaluated the optimized anti-HER2 immunoliposomes containing 6 mol % PEG and a PEG-Fab′ linkage. In addition, subsequent studies used a Matrigel-free version of the BT-474/SF tumor xenograft model. Matrigel was omitted once tumor localization studies revealed that liposomes and immunoliposomes were nonspecifically trapped in Matrigel deposits.[6] Establishment of tumors without Matrigel coimplantation removed this artifact and produced improved tumor penetration of liposomes and immunoliposomes.

Therapy studies using the optimized anti-HER2 immunoliposome-dox construct in the Matrigel-free BT-474/SF model further demonstrated that targeted delivery of dox was associated with enhanced efficacy (Fig. 3). Anti-HER2 immunoliposome-dox produced substantial tumor regressions in this model, including high rates of cured mice (complete regression of tumor confirmed histopathologically at sacrifice). Indeed, anti-HER2 immunoliposomes containing either rhuMAb HER2-Fab′ or an alternative anti-HER2 antibody fragment, scFv C6.5, produced significantly superior growth inhibition than liposomal dox ($P < 0.0001$ for either anti-HER2 immunoliposome-dox construct *versus* liposomal dox). Furthermore, cure rates in this model reached 50% (5 of 10 mice) for rhuMAb HER2-Fab′ immunoliposomes and 55% (6 of 11 mice) for scFv C6.5 immunoliposomes *versus* 0% (0 of 11 mice) for liposomal dox. These differences were also highly significant, with $P < 0.0001$ for either anti-HER2 immunoliposome-dox construct *versus* liposomal dox.

Treatment with anti-HER2 immunoliposome-dox containing rhuMAb HER2-Fab′ also produced superior efficacy compared with either anti-HER2 MAb (trastuzumab) or empty anti-HER2 immunoliposomes lacking dox (Table 2). In fact, empty anti-HER2 immunoliposomes, administered at the same lipid dose and schedule (once a week) as anti-HER2 immunoliposome-dox, produced no effects on tumor growth (data not shown), indicating that the therapeutic activity of anti-HER2 immunoliposome-dox was attributable to targeted delivery of dox and not to the antiproliferative activity of the rhuMAb HER2-Fab′ fragments on the immunoliposome itself. When

Table 2 Therapeutic efficacy of anti-HER2 immunoliposome-dox

Tumor xenograft-nude mouse model[a]	Cures[b] (*n*)	Tumor growth delay[c] (days)	Tumor growth ratio[d]	*P*, anti-HER2 immunoliposomes-dox *vs.* Lipo-dox[e,f]
BT474/MSKCC				
Study 1				
dox	0/11	3	4.51 ± 2.00	
Lipo-dox	0/9	5	2.62 ± 0.81	
Anti-HER2 ILs-dox	1/7	>40	0.62 ± 0.25	<0.0001
Study 2				
dox	0/8	1	14.95 ± 3.25	
Lipo-dox	0/8	1	4.85 ± 0.78	
Anti-HER2 ILs-dox	0/8	>40	2.63 ± 0.55	<0.0001
BT474/SF				
Study 1 (+Matrigel)				
dox	0/15	1	19.13 ± 1.14	
Lipo-dox	0/15	>40	2.59 ± 0.28	
Anti-HER2 ILs-dox	3/30	>40	0.63 ± 0.12	0.001
Study 2 (+Matrigel)				
Lipo-dox	0/8	>40	1.28 ± 0.25	
Anti-HER2 ILs-dox	0/8	>40	0.60 ± 0.08	0.04
Study 3				
rhuMAb HER2, BIW i.p.	2/8	8	3.61 ± 1.18	
Empty ILs, TIW	0/11	6	8.80 ± 2.02	
Lipo-dox	0/3	9	2.58 ± 0.43	
Anti-HER2 ILs-dox	1/11	>40	1.00 ± 0.24	0.04
Study 4				
Lipo-dox	0/11		2.30 ± 0.70	
Anti-HER2 ILs-dox (Fab′)	6/11	>40	0.74 ± 0.28	<0.0001
Anti-HER2 ILs-dox (scFv)	5/10	>40	0.21 ± 0.06	<0.0001
MCF-7/HER2 (+Matrigel)				
Lipo-dox	0/12	>40	2.14 ± 0.12	
Anti-HER2 ILs-dox	1/12	>40	1.48 ± 0.15	<0.0001
MDA-MB-453 (+Matrigel)				
dox	0/12	17	3.54 ± 0.53	
Lipo-dox	0/12	>40	2.15 ± 0.29	
AntiHER2 ILs-dox	1/18	>40	1.17 ± 0.16	0.004

[a] Tumor xenograft models as described in text, with/without Matrigel as indicated.

[b] Complete regression of established tumor during the study and no evidence of tumor at sacrifice.

[c] Difference in time (days) for treated *vs.* control tumors to increase 3-fold in mean volume. A value >40 indicates mean tumor volume never attained a 3-fold increase during the study.

[d] Ratio of tumor volume at end of study over volume at initiation of treatment, per animal (±SE).

[e] Statistical analysis of the antitumor therapeutic effect of anti-HER2 immunoliposome-dox *vs.* liposomal dox using a modified Norton-Simon model of tumor growth. In BT474/SF studies 3 and 4, statistical analysis was performed by a two-way ANOVA with two factors, treatment and day.

[f] Lipo, liposomal; ILs, immunoliposome; BIW, twice a week; TIW, three times a week.

given three times per week instead of once a week, empty anti-HER2 immunoliposomes containing rhuMAb HER2-Fab′ showed only modest inhibition of tumor growth (Table 2), which again was much less than that of anti-HER2 immunoliposome-dox. These results are consistent with previous studies of trastuzumab, which requires steady-state pharmacokinetics and serum trough concentrations ≥10 μg/ml for tumor inhibition (11, 28). The three weekly doses of anti-HER2 immunoliposome-dox did not lead to steady-state levels.

Taking all of the therapy studies together, in each of four HER2-overexpressing tumor xenograft models (BT474/MSKCC, BT474/SF, MCF-7/HER2, and MDA-MB-453), treatment with anti-HER2 immunoliposome-dox was significantly superior to all other treatment conditions (Table 2). In contrast to free dox, which produced modest tumor growth inhibition in these xenograft models, anti-HER2 immunoliposome-dox showed highly potent antitumor efficacy. In eight separate studies comparing anti-HER2 immunoliposome-dox *versus* liposomal dox, immunoliposome-mediated delivery produced significantly superior therapeutic results ($P < 0.0001$ to 0.04). Furthermore, anti-HER2 immunoliposomes, but not free dox or liposomal dox, produced frequent cures in mice. The total cure rate with immunoliposomes in all studies was 18 of 115 mice (16%), with higher rates of ~50% obtained in later studies using optimized immunoliposomes (PEG-MAb linkage) and non-Matrigel models as described. In contrast, no cures were observed in any of the mice treated with free dox (0 of 46) or liposomal dox (0 of 78). These differences were highly significant ($P < 0.0001$ *versus* free dox or liposomal dox).

Toxicity of Anti-HER2 Immunoliposome-dox. In addition to enhanced efficacy, encapsulation of dox in either liposomes or anti-HER2 immunoliposomes was associated with markedly reduced host toxicity compared with free dox. In studies to determine the MTD in nude mice with tumor xenografts, various doses of free dox, sterically stabilized liposomal dox, or anti-HER2 immunoliposome-dox were administered i.v. once a week for three doses. The MTDs of immunoliposome-dox (≥22.5 mg/kg) and liposomal dox (18.8–

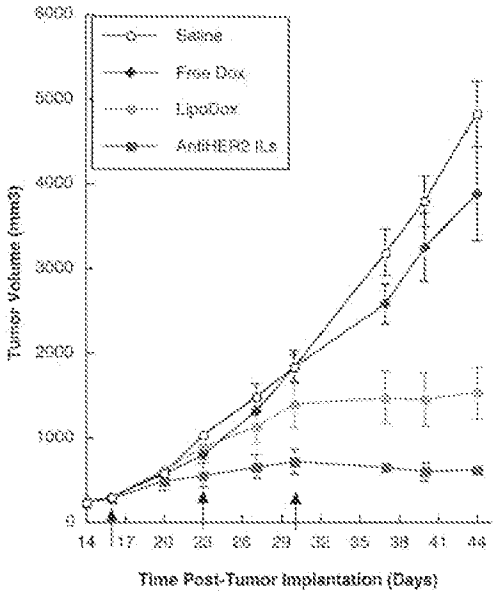

Fig. 2 Efficacy of anti-HER2 immunoliposome-dox in the HER2-overexpressing BT474/MSKCC tumor xenograft model. Anti-HER2 immunoliposome-dox containing 1 mol % PEG/I.s-MAb linkage (▤) was administered by i.v. injection at a total dox dose of 15 mg/kg on the indicated days post-tumor implantation (*arrows*). Other treatment groups included saline (○), free dox (✚) at its MTD of 7.5 mg/kg, and liposomal dox (▨), prepared identically to anti-HER2 immunoliposome-dox but without MAb and given at the same dose and schedule. Anti-HER2 immunoliposome-dox was significantly superior to all other treatment conditions ($P < 0.0001$ *versus* liposomal dox). Data represent mean tumor volumes; *bars*, SE.

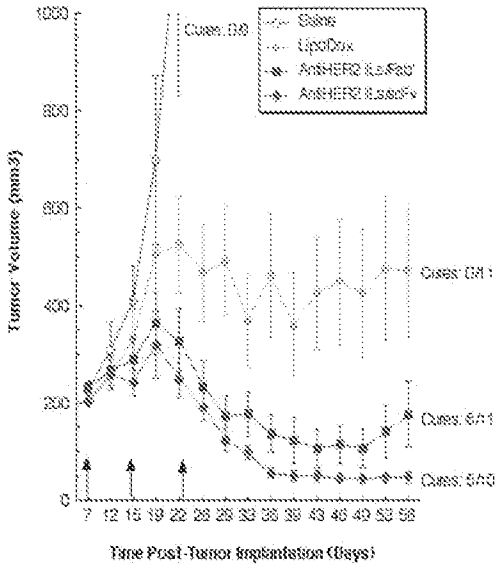

Fig. 3 Efficacy of anti-HER2 immunoliposome-dox in the HER2-overexpressing BT474/SF tumor xenograft model. Anti-HER2 immunoliposome-dox containing 6 mol % PEG/PEG-MAb linkage and either rhuMAb HER2-Fab′ (▤) or C6.5 scFv (◈) were administered i.v. at a total dox dose of 15 mg/kg on the indicated days post-tumor implantation (*arrows*). Other treatment groups included saline (○) and sterically stabilized liposomal dox (▨), prepared identically to anti-HER2 immunoliposome-dox but without MAb and given at the same dose and schedule. Both versions of anti-HER2 immunoliposome-dox were significantly superior to liposomal dox ($P < 0.0001$ for both). Data represent mean tumor volumes; *bars*, SE.

22.5 mg/kg) were 2.5-fold greater than that of free dox (7.5 mg/kg).

Effects of Anti-HER2 Immunoliposome-dox against Non-HER2-overexpressing Tumor Xenografts. As an additional control, anti-HER2 immunoliposome-dox was evaluated in a non-HER2-overexpressing xenograft model. MCF-7 xenografts express low or basal levels of HER2 ($\sim 10^4$ HER2/cell; IHC score, 1+). Previous studies of anti-HER2 immunoliposome binding and internalization in MCF-7 cells *in vitro* showed undetectable uptake by confocal microscopy and quantitative fluorimetry; furthermore, uptake of immunoliposomes was indistinguishable from that of control liposomes lacking MAb fragments (15). To evaluate *in vivo* selectivity, anti-HER2 immunoliposome-dox was administered i.v. in the MCF-7 xenograft model at the same dose and schedule as in the other therapy studies. Equivalent therapeutic effects were obtained for both immunoliposome-dox and nontargeted liposomal dox (Fig. 4). This result confirmed that anti-HER2 immunoliposomes require a threshold HER2 density (or functional activity) to enable appreciable drug delivery *in vivo* as well as *in vitro*.

Antitumor Efficacy of Anti-HER2 Immunoliposome-dox *versus* Combination Therapy. Additional therapy studies in the BT-474/SF model were performed to compare the antitumor efficacy of anti-HER2 immunoliposome-dox *versus* combination therapies consisting of free anti-HER2 MAb (trastuzumab) plus chemotherapy with either free dox or liposomal dox. Trastuzumab has been shown to significantly increase the efficacy of dox-based chemotherapy in both preclinical (25) and clinical studies (13). In a direct comparison of anti-HER2 immunoliposome-dox *versus* the combination of free trastuzumab plus free dox (Fig. 5*A*), anti-HER2 immunoliposome-dox showed efficacy that was significantly superior to that of the combination ($P < 0.0001$). Anti-HER immunoliposome-dox was also directly compared with the combination of free trastuzumab plus liposomal dox, which in this experiment consisted of commercial PEGylated liposomal doxorubicin (Doxil; Fig. 5*B*). Anti-HER2 immunoliposomes again showed significantly superior efficacy than this combination ($P < 0.0001$).

DISCUSSION

Anti-HER2 immunoliposomes combine the tumor-targeting properties of certain anti-HER2 MAbs with the PK and drug delivery properties of long-circulating liposomes. Dox-loaded anti-HER2 immunoliposomes displayed prolonged circulation as stable constructs without drug leakage or MAb dissociation. These results contrast with recent reports of other immunoliposomes constructed with intact IgG, which showed significantly accelerated clearance and reduced circulation times compared with nontargeted liposomes (29, 30). Accelerated clearance of immunoliposomes containing intact IgG may be attributable to recognition of Fc sequences by the RES and/or lability of the IgG conjugation *in vivo*. Immunoliposomes containing covalently conjugated MAb fragments (Fab′ or scFv) have circumvented these limitations.

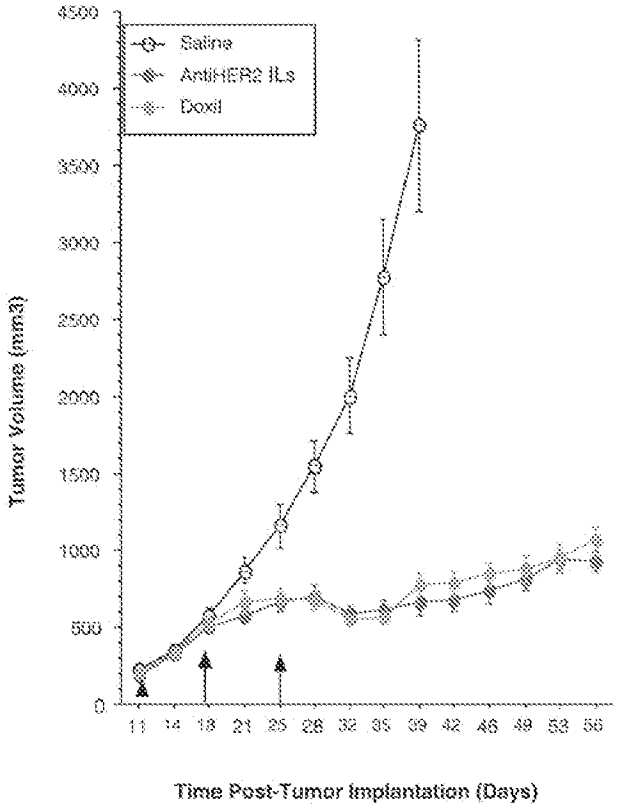

Fig. 4 Lack of enhanced efficacy of anti-HER2 immunoliposome-dox in the non-HER2-overexpressing MCF-7 tumor xenograft model. As a further negative control, therapy studies were performed in nude mice containing xenografted MCF-7 cells, which lack HER2 overexpression (10^4 receptors/cell; IHC score, 1+). Anti-HER2 immunoliposome-dox containing 7 mol % PEG/PEG-MAb linkage and anti-HER2 scFv (●) was administered i.v. at a total dox dose of 15 mg/kg on the indicated days post-tumor implantation (*arrows*). Other treatment groups included saline (○) and sterically stabilized liposomal dox (©), prepared identically to anti-HER2 immunoliposome-dox but without MAb fragment and given at the same dose and schedule. Data represent mean tumor volumes; *bars*, SE.

Therapy studies in four different HER2-overexpressing human tumor xenograft models demonstrated that delivery of dox via anti-HER2 immunoliposomes greatly increased the therapeutic index of dox, both by increasing antitumor efficacy and by reducing systemic toxicity. Furthermore, anti-HER2 immunoliposome-dox was significantly superior to all other relevant treatment conditions, including liposomal dox, free trastuzumab, trastuzumab plus free dox, and trastuzumab plus liposomal dox.

These results indicated that anti-HER2 immunoliposome-dox produced enhanced antitumor efficacy via tumor-targeted drug delivery. An alternative explanation is that rhuMAb HER2-Fab′ fragments provided an independent antiproliferative effect on HER2-overexpressing cancer cells, which in turn acted additively or synergistically with dox therapy. Indeed, we have previously shown that empty anti-HER2 immunoliposomes containing rhuMAb HER2-Fab′, when present continuously *in vitro*, do possess antiproliferative activity approaching that of trastuzumab and greatly exceeding that of rhuMAb HER2-Fab′ alone (14). However, two lines of evidence preclude the possibility that this antiproliferative mechanism contributed to the *in vivo* efficacy of anti-HER2 immunoliposome-dox observed in the present studies. The first consideration is that administration of empty anti-HER2 immunoliposomes at the same lipid dose and schedule as dox-loaded immunoliposomes failed to produce significant antitumor efficacy. This result is consistent with preclinical and clinical studies of trastuzumab, which required steady-state pharmacokinetics with a trough serum concentration ≥10 μg/ml for optimal antitumor activity (11, 28). The dose and schedule for anti-HER2 immunoliposomes-dox were far below this, consisting of just three weekly doses. The second consideration is that immunoliposomes containing either rhuMAb HER2-Fab′ or scFv C6.5 produced comparable therapeutic results, although scFv C6.5 does not possess antiproliferative activity as a monomer or when bivalent as a diabody (31).

We previously showed that anti-HER2 immunoliposomes efficiently bind and internalize in HER2-overexpressing cells *in vitro*, leading to intracellular drug delivery (14, 15). Importantly, we have recently evaluated the mechanism by which anti-HER2 immunoliposomes mediate drug delivery *in vivo*.[8] In the same breast cancer xenograft models described here, tumor xenografts were examined histopathologically after i.v. treatment with either gold-loaded anti-HER2 immunoliposomes or gold-loaded sterically stabilized liposomes. Visualization of liposomes and immunoliposomes via a silver enhancement method revealed striking differences in intratumoral localization and mechanism of delivery. Sterically stabilized liposomes were predominantly observed in extracellular areas of tumor stroma and within tissue macrophages and were not observed within tumor cells, consistent with previous reports (32). In contrast, anti-HER2 immunoliposomes were predominantly found internalized within tumor cells in a broad distribution throughout tumor tissue. These results confirm that anti-HER2 immunoliposomes mediate intracellular drug delivery in HER2-overexpressing tumor cells *in vivo* and suggest that the therapeutic advantage obtained with anti-HER2 immunoliposome-dox derives from this novel mechanism of action.

It is notable that anti-HER2 immunoliposomes constructed using an alternative methodology appear to have properties, including lack of enhanced efficacy, very different from those described here (30). In that report, MAb N-12A5, an intact IgG1 directed against HER2, was conjugated to sterically stabilized liposomal dox. N-12A5 immunoliposomes bound to HER2-overexpressing cells *in vitro*, but were not internalized. Therapy studies showed that these immunoliposomes provided no additional efficacy over sterically stabilized liposomal dox. This result suggests that internalization of anti-HER2 immunoliposome-dox constructs in cancer cells was a critical factor in the enhanced efficacy that we observed.

Targeted delivery of dox by anti-HER2 immunoliposomes may represent a particularly advantageous strategy for the treat-

[8] D. B. Kirpotin, K. Hong, J. W. Park, Y. Shao, R. Shalaby, G. Colbern, C. C. Benz, and D. Papahadjopoulos. Localization of anti-HER2 immunoliposomes in HER2-overexpressing breast cancer xenografts: intracellular delivery via immunotargeting, submitted for publication.

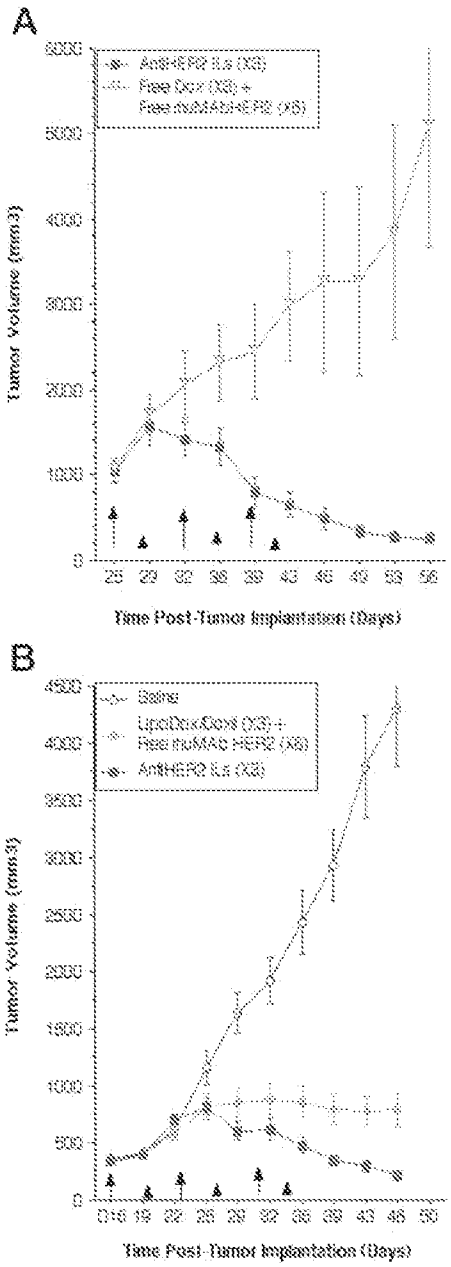

Fig. 5 Efficacy of anti-HER2 immunoliposome-dox *versus* combination therapies in the BT474/SF tumor xenograft model. Data represent mean tumor volumes; *bars*, SE. *A*, dox-loaded anti-HER2 immunoliposomes containing rhuMAb HER2-Fab′ (▨) *versus* combination therapy (▽) of free rhuMAb HER2 (trastuzumab; Herceptin) plus free dox. Anti-HER2 immunoliposomes were administered i.v. at a total dox dose of 15 mg/kg over three doses (*arrows*), free dox was administered i.v. at its MTD of 7.5 mg/kg over three doses (*arrows*), and trastuzumab was administered i.p. at 0.3 mg/kg twice a week over six doses (*arrows* and *arrowheads*). Anti-HER2 immunoliposome-dox was significantly superior to the combination of free MAb plus free drug ($P < 0.0001$). *B*, dox-loaded anti-HER2 immunoliposomes containing rhuMAb HER2-Fab′ (▨) *versus* combination therapy (⊖) of free anti-HER2 MAb (trastuzumab) + commercial PEGylated liposomal dox (Doxil). Immunoliposomes and liposomal dox were each administered i.v. at a total dox dose of 15 mg/kg over three doses (*arrows*), and trastuzumab was administered i.p. over six doses (*arrows* and *arrowheads*). Anti-HER2 immunoliposome-dox was significantly superior to the combination of free MAb plus liposomal drug ($P < 0.0001$).

ment of HER2-overexpressing cancers. Preclinical and clinical studies have raised the possibility that HER2-overexpressing breast cancers may be relatively resistant to hormone therapy and certain types of chemotherapy (reviewed in Ref. (33), but may be especially sensitive to anthracycline-based chemotherapy (34–36). In principle, anti-HER2 immunoliposome-dox can provide maximal anthracycline delivery to HER2-overexpressing cancers while reducing the toxicity of free dox to the myocardium and hematopoietic cells because HER2 expression is extremely low in these cell types (37) and drug delivery by anti-HER2 immunoliposomes is dependent on receptor density (15). Another relevant issue is that trastuzumab therapy is associated with some cardiotoxicity as a single agent (12) and prohibitive cardiotoxicity when used in combination with dox chemotherapy (13). Although the toxicological mechanism remains to be elucidated, it is presumed that trastuzumab-associated cardiotoxicity is related to its therapeutic antiproliferative and/or immunological effects. As discussed, these effects require high steady-state levels of trastuzumab. Hence, immunoliposomes, which can be administered intermittently, should not produce these effects. Consistent with this, empty immunoliposomes containing rhuMAb HER2-Fab′ did not display antiproliferative activity *in vivo* with a weekly schedule. Furthermore, immunoliposomes can be constructed with scFv C6.5, a ligand devoid of antiproliferative activity, and immunoliposomes containing either Fab′ or scFv lack Fc sequences to mediate immunological functions such as antibody-dependent cellular cytotoxicity. Finally, as noted, this delivery system does not accumulate in low-HER2-expressing cells such as MCF-7 (10^4 HER2/cell; Ref. 15); this threshold suggests that significant delivery or accumulation is unlikely in myocardial cells containing $\sim 10^5$ HER2/cell. Hence, we hypothesize that anti-HER2 immunoliposome-dox may represent a particularly apt strategy to deliver dox to HER2-overexpressing cancer cells, resulting in less cardiotoxicity than dox chemotherapy alone and much less than dox chemotherapy plus trastuzumab. Final determination of the safety profile of anti-HER2 immunoliposome-dox will require formal toxicological evaluation and Phase I clinical studies.

We conclude that tumor-targeted drug delivery using anti-HER2 immunoliposomes can enhance the therapeutic index of dox chemotherapy and therefore may provide a particularly potent and useful therapy for cancers that involve HER2 overexpression. In addition, the strategy of immunoliposome delivery may have broad utility for targeted delivery of other anticancer agents, such as those agents with narrow therapeutic indices, PK limitations, or a requirement for intracellular delivery.

ACKNOWLEDGMENTS

We are grateful to Sharon Baughman and I. Craig Henderson for helpful suggestions.

REFERENCES

1. Park, J. W., Hong, K., Kirpotin, D. B., Papahadjopoulos, D., and Benz, C. C. Immunoliposomes for cancer treatment. Adv. Pharmacol., *40:* 399–435, 1997.

2. Lasic, D. D., and Papahadjopoulos, D. Liposomes revisited. Science (Wash. DC), *267:* 1275–1276, 1995.

3. Papahadjopoulos, D., Allen, T. M., Gabizon, A., Mayhew, E., Matthay, K., Huang, S. K., Lee, K. D., Woodle, M. C., Lasic, D. D.,

Redemann, C., *et al.* Sterically stabilized liposomes: improvements in pharmacokinetics and antitumor therapeutic efficacy. Proc. Natl. Acad. Sci. USA, *88:* 11460–11464, 1991.

4. Huang, S. K., Mayhew, E. M., Gilani, S., Lasic, D. D., Martin, F. J., and Papahadjopoulos, D. Pharmacokinetics and therapeutics of sterically stabilized liposomes in mice bearing C-26 colon carcinoma. Cancer Res., *52:* 6774–6781, 1992.

5. Horowitz, A. T., Barenholz, Y., and Gabizon, A. A. *In vitro* cytotoxicity of liposome-encapsulated doxorubicin: dependence on liposome composition and drug release. Biochim. Biophys. Acta, *1109:* 203–209, 1992.

6. Sznol, M., and Holmlund, J. Antigen-specific agents in development. Semin. Oncol., *24:* 173–186, 1997.

7. Olayioye, M. A., Neve, R. M., Lane, H. A., and Hynes, N. E. The ErbB signaling network: receptor heterodimerization in development and cancer. EMBO J., *19:* 3159–3167, 2000.

8. Slamon, D. J., Clark, G. M., Wong, S. G., Levin, W. J., Ullrich, A., and McGuire, W. L. Human breast cancer: correlation of relapse and survival with amplification of HER2/*neu* oncogene. Science (Wash. DC), *235:* 177–182, 1987.

9. Slamon, D. J., Godolphin, W., Jones, L. A., Holt, J. A., Wong, S. G., Keith, D. E., Levin, W. J., Stuart, S. G., Udove, J., Ullrich, A., and Press, M. F. Studies of the HER-2/neu proto-oncogene in human breast and ovarian cancer. Science (Wash. DC), *244:* 707–712, 1989.

10. Carter, P., Presta, L., Gorman, C. M., Ridgway, J. B. B., Henner, D., Wong, W. L. T., Rowland, A. M., Kotts, C., Carver, M. E., and Shepard, H. M. Humanization of an anti-p185HER2 antibody for human cancer therapy. Proc. Natl. Acad. Sci. USA, *89:* 4285–4289, 1992.

11. Baselga, J., Tripathy, D., Mendelsohn, J., Baughman, S., Benz, C. C., Dantis, L., Sklarin, N. T., Seidman, A. D., Hudis, C. A., Moore, J., Rosen, P. P., Twaddell, T., Henderson, I. C., and Norton, L. Phase II study of weekly intravenous recombinant humanized anti-p185^{HER2} monoclonal antibody in patients with HER/*neu*-overexpressing metastatic breast cancer. J. Clin. Oncol., *14:* 737–744, 1996.

12. Cobleigh, M. A., Vogel, C. L., Tripathy, D., Robert, N. J., Scholl, S., Fehrenbacher, L., Wolter, J. M., Paton, V., Shak, S., Lieberman, G., and Slamon, D. J. Multinational study of the efficacy and safety of humanized anti-HER2 monoclonal antibody in women who have HER2-overexpressing metastatic breast cancer that has progressed after chemotherapy for metastatic disease. J. Clin. Oncol., *17:* 2639–2648, 1999.

13. Slamon, D. J., Leyland-Jones, B., Shak, S., Fuchs, H., Paton, V., Bajamonde, A., Fleming, T., Eiermann, W., Wolter, J., Pegram, M., Baselga, J., and Norton, L. Use of chemotherapy plus a monoclonal antibody against HER2 for metastatic breast cancer that overexpresses HER2. N. Engl. J. Med., *344:* 783–792, 2001.

14. Park, J. W., Hong, K., Carter, P., Asgari, H., Guo, L. Y., Keller, G. A., Wirth, C., Shalaby, R., Kotts, C., Wood, W. I., Papahadjopoulos, D., and Benz, C. C. Development of anti-p185HER2 immunoliposomes for cancer therapy. Proc. Natl. Acad. Sci. USA, *92:* 1327–1331, 1995.

15. Kirpotin, D., Park, J. W., Hong, K., Zalipsky, S., Li, W. L., Carter, P., Benz, C. C., and Papahadjopoulos, D. Sterically stabilized anti-HER2 immunoliposomes: design and targeting to human breast cancer cell *in vitro*. Biochemistry, *36:* 66–75, 1997.

16. Carter, P., Rodrigues, M. L., Park, J. W., and Zapata, G. Preparation and uses of Fab′ fragments from *E. coli*. *In:* J. McCafferty, H. R. Hoogenboom, and D. J. Chiswell (eds.), Antibody Engineering: A Practical Approach, pp. 291–308. Oxford: IRL Press, 1996.

17. Schier, R., Marks, J. D., Wolf, E. J., Apell, G., Wong, C., McCartney, J. E., Bookman, M. A., Huston, J. S., Houston, L. L., Weiner, L. M., *et al. In vitro* and *in vivo* characterization of a human anti-c-erbB-2 single-chain Fv isolated from a filamentous phage antibody library. Immunotechnology, *1:* 73–81, 1995.

18. Haran, G., Cohen, R., Bar, L. K., and Barenholz, Y. Transmembrane ammonium sulfate gradients in liposomes produce efficient and stable entrapment of amphipathic weak bases. Biochim. Biophys. Acta, *1151:* 201–215., 1993.

19. Lewis, G. D., Figari, I., Fendly, B., Wong, W. L., Carter, P., Gorman, C., and Shepard, H. M. Differential responses of human tumor cell lines to anti-p185HER2 monoclonal antibodies. Cancer Immunol. Immunother., *37:* 255–263, 1993.

20. Benz, C. C., Scott, G. K., Sarup, J. C., Johnson, R. M., Tripathy, D., Coronado, E., Shepard, H. M., and Osborne, C. K. Estrogen-dependent, tamoxifen-resistant tumorigenic growth of MCF-7 cells transfected with HER2/neu. Breast Cancer Res. Treat., *24:* 85–95, 1993.

21. Park, J. W., Stagg, R., Lewis, G. D., Carter, P., Maneval, D., Slamon, D. J., Jaffe, H., and Shepard, H. M. Anti-p185HER2 monoclonal antibodies: biological properties and potential for immunotherapy. *In:* R. B. Dickson and M. E. Lippman (eds.), Genes, Oncogenes, and Hormones: Advances in Cellular and Molecular Biology of Breast Cancer, pp. 193–211. Boston: Kluwer Academic Publishers, 1992.

22. Park, J. W., Tripathy, D., Campbell, M., and Esserman, L. J. Biological therapy of breast cancer. Biodrugs, *14:* 221–246, 2000.

23. Mass, R. D., Press, M., Anderson, S., Murphy, M., and Slamon, D. Improved survival benefit from Herceptin (trastuzumab) in patients selected by fluorescence *in situ* hybridization. Proc. Amer. Soc. Clin. Oncol., *20:* 22a, 2001.

24. Vogel, C. L., Cobleigh, M., Tripathy, D., Mass, R., Murphy, M., and Stewart, S. J. Superior outcomes with Herceptin (trastuzumab) in fluorescence *in situ* hybridization (FISH)-selected patients. Proc. Am. Soc. Clin. Oncol., *20:* 22a, 2001.

25. Baselga, J., Norton, L., Albanell, J., Kim, Y-M., and Mendelsohn, J. Recombinant humanized anti-HER2 antibody (Herceptin™) enhances the antitumor activity of paclitaxel and doxorubicin against HER2/*neu* overexpressing breast cancer xenografts. Cancer Res., *58:* 2825–2831, 1998.

26. Heitjan, D. F. Generalized Norton-Simon models of tumour growth. Stat. Med., *10:* 1075–1088, 1991.

27. Gabizon, A., Shiota, R., and Papahadjopoulos, D. Pharmacokinetics and tissue distribution of doxorubicin encapsulated in stable liposomes with long circulation times. J. Natl. Cancer Inst. (Bethesda), *81:* 1484–1488, 1989.

28. Pegram, M., Hsu, S., Lewis, G., Pietras, R., Beryt, M., Sliwkowski, M., Coombs, D., Baly, D., Kabbinavar, F., and Slamon, D. Inhibitory effects of combinations of HER-2/neu antibody and chemotherapeutic agents used for treatment of human breast cancers. Oncogene, *18:* 2241–2251, 1999.

29. Zalipsky, S., Hansen, C. B., Menezes, D. L. d., and Allen, T. M. Long-circulating, polyethylene glycol-grafted immunoliposomes. J. Controlled Release, *39:* 153–161, 1996.

30. Goren, D., Horowitz, A. T., Zalipsky, S., Woodle, M. C., Yarden, Y., and Gabizon, A. Targeting of stealth liposomes to erbB-2 (Her/2) receptor: *in vitro* and *in vivo* studies. Br. J. Cancer, *74:* 1749–1756, 1996.

31. Neve, R. M., Nielsen, U. B., Kirpotin, D. B., Poul, M-A., Marks, J. D., and Benz, C. C. Biological effects of anti-ErbB2 single chain antibodies selected for internalizing function. Biochem. Biophys. Res. Commun., *280:* 274–279, 2000.

32. Huang, S. K., Lee, K. D., Hong, K., Friend, D. S., and Papahadjopoulos, D. Microscopic localization of sterically stabilized liposomes in colon carcinoma-bearing mice. Cancer Res., *52:* 5135–5143, 1992.

33. Ravdin, P. M. Should HER2 status be routinely measured for all breast cancer patients? Semin. Oncol., *26:* 117–123, 1999.

34. Muss, H. B., Thor, A. D., Berry, D. A., Kute, T., Liu, E. T., Koerner, F., Cirrincione, C. T., Budman, D. R., Wood, W. C., Barcos, M., and Henderson, I. C. c-*erb*B-2 expression and response to adjuvant chemotherapy in women with node-positive early breast cancer. N. Engl. J. Med., *330:* 1260–1266, 1994.

35. Thor, A. D., Berry, D. A., Budman, D. R., Muss, H. B., Kute, T., Henderson, I. C., Barcos, M., Cirrincione, C., Edgerton, S., Allred, C., Norton, L., and Liu, E. T. erbB-2, p53, and efficacy of adjuvant therapy in lymph node-positive breast cancer. J. Natl. Cancer Inst. (Bethesda), *90:* 1346–1360, 1998.

36. Paik, S., Bryant, J., Park, C., Fisher, B., Tan-Chiu, E., Hyams, D., Fisher, E. R., Lippman, M. E., Wickerham, D. L., and Wolmark, N. erbB-2 and response to doxorubicin in patients with axillary lymph node-positive, hormone receptor-negative breast cancer. J. Natl. Cancer Inst. (Bethesda), *90:* 1998.

37. Press, M. F., Cordon-Cardo, C., and Slamon, D. J. Expression of the HER-2/*neu* proto-oncogene in normal human adult and fetal tissues. Oncogene, *5:* 953–962, 1990.

Clinical Cancer Research

Anti-HER2 Immunoliposomes: Enhanced Efficacy Attributable to Targeted Delivery

John W. Park, Keelung Hong, Dmitri B. Kirpotin, et al.

Clin Cancer Res 2002;8:1172-1181.

ELSEVIER

Journal of Chromatography B, 771 (2002) 3–31

JOURNAL OF CHROMATOGRAPHY B

www.elsevier.com/locate/chromb

Review

Detection technologies in proteome analysis

Wayne F. Patton*

Proteomics Section, Biosciences Department, Molecular Probes, Inc., 4849 Pitchford Avenue, Eugene, OR 97402-9165, USA

Abstract

Common strategies employed for general protein detection include organic dye, silver stain, radiolabeling, reverse stain, fluorescent stain, chemiluminescent stain and mass spectrometry-based approaches. Fluorescence-based protein detection methods have recently surpassed conventional technologies such as colloidal Coomassie blue and silver staining in terms of quantitative accuracy, detection sensitivity, and compatibility with modern downstream protein identification and characterization procedures, such as mass spectrometry. Additionally, specific detection methods suitable for revealing protein post-translational modifications have been devised over the years. These include methods for the detection of glycoproteins, phosphoproteins, proteolytic modifications, *S*-nitrosylation, arginine methylation and ADP-ribosylation. Methods for the detection of a range of reporter enzymes and epitope tags are now available as well, including those for visualizing β-glucuronidase, β-galactosidase, oligohistidine tags and green fluorescent protein. Fluorescence-based and mass spectrometry-based methodologies are just beginning to offer unparalleled new capabilities in the field of proteomics through the performance of multiplexed quantitative analysis. The primary objective of differential display proteomics is to increase the information content and throughput of proteomics studies through multiplexed analysis. Currently, three principal approaches to differential display proteomics are being actively pursued, difference gel electrophoresis (DIGE), multiplexed proteomics (MP) and isotope-coded affinity tagging (ICAT). New multiplexing capabilities should greatly enhance the applicability of the two-dimensional gel electrophoresis technique with respect to addressing fundamental questions related to proteome-wide changes in protein expression and post-translational modification.

Keywords: Reviews; Proteomics; Detection

Contents

*Tel.: +1-541-465-8300; fax: +1-541-344-6504.
E-mail address: wayne.patton@probes.com (W.F. Patton).

1570-0232/02/$ – see front matter
PII: S1570-0232(02)00043-0

1. Introduction

Review articles providing overviews of significant milestones in the development of assorted protein detection techniques, as applied to gel electrophoresis, have already been published in recent years [1–10]. After briefly updating these topics, this review will primarily focus upon current issues in protein visualization as they directly relate to modern proteomics investigations. Since two-dimensional (2D) gel electrophoresis is increasingly being used in the micropreparative isolation of proteins destined for characterization by mass spectrometry, it is now expected that protein visualization methods be validated with respect to their compatibility with this technology. So, in addition to sensitivity, linear dynamic range and reproducibility, visualization methods should be fully capable of interfacing with the modern analysis tools of proteomics. Key issues addressed in this review article include detection methods for determining total protein, protein post-translational modifications and epitope-tagged fusion proteins, as well as strategies for detecting changes in protein profiles by differential display proteomics.

2. General protein detection methods

2.1. Organic dye- and silver stain-based methods

Though a range of organic dyes have been used to visualize proteins in polyacrylamide gels, Coomassie Blue dyes (R and G types) have certainly enjoyed the most popularity due to their low cost, ease of use and unexpectedly good compatibility with downstream microchemical characterization methods, such as mass spectrometry [11]. Typically, Coomassie Blue R-250 dye is used in a regressive staining approach where gels are saturated with dye that has been dissolved in an aqueous solution containing methanol and acetic acid, followed by destaining in a similar solution devoid of dye. Since the proteins have a higher affinity for the dye molecules than the gel matrix, a point is reached where the background staining is minimal but protein bands are well labeled. Gel-to-gel reproducibility in staining is difficult to control, however, as proteins do destain to varying extents along with the gel matrix, albeit with slower kinetics. Later, progressive staining approaches were introduced where proteins are gradually stained to an endpoint, without significant staining of the gel matrix [12]. These methods are

predicated upon the formation of colloidal dye particles. During staining an equilibrium is achieved between colloidal particles and freely dispersed dye in solution. The low concentration of free dye penetrates the gel matrix and preferentially stains the proteins, but the colloidal dye particle is excluded from the gel, thus preventing matrix staining. The limits of detection for conventional Coomassie Blue and colloidal Coomassie Blue stains are 8–10 and 30–100 ng, respectively. Both dyes provide a linear response with protein amount over a 10–30-fold range of concentration. Thus, the principal limitations associated with Coomassie Blue-based staining methods is the poor detection sensitivity and small linear dynamic range obtained with the dyes.

Silver staining techniques are based upon saturating gels with silver ions, washing the less tightly bound metal ions out of the gel matrix and reducing the protein-bound metal ions to form metallic silver [13–15]. Most commonly, silver staining is accomplished using silver nitrate in combination with formaldehyde developer in alkaline carbonate buffer or using an ammonia–silver complex in combination with formaldehyde developer in citrate buffer. Silver stain methods permit detection of as little as a single nanogram of protein, but the linear dynamic range of the stain is restricted to a 10-fold range. Silver staining methods are quite complex, multi-step procedures that must be stopped at some arbitrary time point in order to avoid over development. Consequently, gel-to-gel reproducibility is problematic and variations of 20% in spot intensity have been documented in the literature [16]. Robotic staining devices offer the potential for minimizing the variability of silver staining, but end-point stains provide consistency without investing in expensive machinery [17]. Though the best silver stain methods use aldehyde-based fixatives prior to silver impregnation, this prevents subsequent microchemical analysis by Edman sequencing or mass spectrometry. Thus, alternative silver staining methods must be employed that omit aldehydes in the fixatives [18,19]. Generally, detection sensitivity is poorer and background staining less uniform with the modified staining techniques. Additionally, destaining methods are often employed to improve the compatibility of silver staining with peptide mass profiling methods [20].

2.2. Radioactive labeling methods

Radiolabeling is commonly accomplished by incorporating ^{3}H, ^{14}C, ^{35}S, ^{32}P, ^{33}P, or ^{125}I into proteins [21,22]. After electrophoresis, signal detection may be accomplished using film, by direct autoradiography for the γ-emitting isotopes or by fluorography for the β-emitting isotopes. Fluorography employs fluorescent enhancers impregnated into the gel matrix that improve detection of the radioactive emissions through the generation of light. For certain high-energy isotopes, such as, ^{32}P or ^{125}I, intensifying screens may be used to enhance the signal. These screens absorb the radioactive emissions that pass through the film, fluoresce and generate light that exposes the film. Over the past decade, storage phosphor imagers and microchannel plate analyzers have begun to replace autoradiography film for detecting radiolabeled proteins. The newer technologies offer a wider dynamic range and better detection sensitivity than film.

Radiolabeling has been used extensively for in vivo metabolic experiments. Organic dye or silver stain methods are commonly used in conjunction with radiolabeling techniques to simultaneously assess total protein expression levels along with protein synthesis rates, as well as to provide visual landmarks for the localization of low abundance proteins in 2D gels [23–25]. However, the general utility of radiolabeling as a tool for the assessment of protein synthesis rates has been called into question recently [26–28]. Metabolically incorporating radiolabels such as [^{35}S]methionine, using standard doses and time-courses, has been shown to induce DNA fragmentation, elevate p53 tumor suppressor protein levels, alter cell/nuclear morphology and lead to cell cycle arrest or apoptosis.

Though sensitive detection is readily achieved, radiolabeling is both hazardous and expensive [29,30]. In 1995, the United States National Institutes of Health alone spent more than $4 million disposing of radioactive waste [31]. Additional expenditures were required for monitoring exposure to radioactivity, inventory control and training laboratory personnel. During that same year, a pregnant cancer researcher was deliberately contaminated with at least 600 μCi of ^{32}P in one of the Bethesda, Maryland NIH research laboratories, as detailed in

US National Institutes of Health Case Number 1-96-033; released 09/17/97, entitled "Wrongful administration of P-32". An additional 26 staff members were exposed to lesser amounts of the isotope from a water cooler at this facility. Reducing reliance on radioactivity in biomedical research has become a high priority in many laboratories over the past several years as it makes economic good sense and promotes a better quality of life by providing a safer work environment for laboratory personnel.

2.3. Reverse stain methods

A number of reverse-staining methods for visualizing proteins in SDS–polyacrylamide gels have been described over the years including methods that employ potassium chloride [32], copper chloride [33], zinc chloride [34], cobalt acetate [34], nickel chloride [34] and zinc chloride–imidazole [35,36].

The three reverse stain techniques that have been used most extensively are the potassium chloride, copper chloride and zinc chloride methods. Copper chloride staining is slightly more sensitive, while potassium chloride staining is significantly less sensitive than Coomassie Blue staining [37]. Zinc chloride–imidazole staining is the most sensitive reverse-stain developed to date [38,39]. In the presence of imidazole, free or weakly bound zinc ions are readily precipitated as zinc–imidazole, while tightly bound ions associated with the proteins are refractory to precipitation. This generates clear protein zones on a semi-opaque gel background. Careful attention to the duration of staining is necessary as over-staining of gels can obscure bands and on occasions complex patterns of negative and positive staining are obtained using zinc–imidazole [38]. The limit of detection for the zinc–imidazole stain is roughly 10–20 ng per band for protein separated by SDS–polyacrylamide gel electrophoresis, 40–80 ng per band for protein separated on native polyacrylamide gels, and 100–500 ng per band for proteins separated in carrier ampholyte or immobilized pH gradient isoelectric focusing gels [38,39].

Proteins visualized in zinc–imidazole-stained gels can be evaluated by densitometry, though the linear dynamic range for protein detection is restricted to 10–100 ng [40,41]. Zinc–imidazole-stained gels can be electroblotted or electroeluted by addition of a chelating agent to the transfer buffer [42–45]. Proteins stained with zinc–imidazole are also compatible with Edman-based microsequencing and in-gel tryptic digestion followed by matrix-assisted laser desorption ionization time-of-flight (MALDI-TOF) mass spectrometry for determination of peptide masses and sequences [41,42,46].

2.4. Fluorescence-based staining methods

Fluorescent detection of proteins in electrophoresis gels is gaining popularity, particularly with laboratories engaging in large scale proteomics research. Several recently developed fluorescent stains are suitable for incorporation into integrated proteomics platforms for global analysis of protein regulation. The linear dynamic range of detection using fluorescent stains is usually superior to colorimetric or reverse stains.

Nile Red dye has excitation maxima of about 300 and 540 nm and an emission maximum of roughly 640 nm [47]. The detection sensitivity of 20–100 ng for Nile Red staining is slightly better than detection obtained with Coomassie Blue staining, and the dye is compatible with standard Edman sequencing and immunodetection procedures [48–51]. Nile Red staining is not stable, however, and the dye is prone to precipitation in aqueous solution, consequently making it more difficult to handle than commercialized fluorescent stains. The photolabile nature of Nile Red staining makes quantitation of proteins by image analysis difficult. Nile Red dye can be used to pre-stain gels prior to electroblotting them to polyvinylidene difluoride (PVDF) membrane [50,51].

SYPRO Red, SYPRO Orange and SYPRO Tangerine dyes can detect proteins in SDS–polyacrylamide gels using a simple, one-step staining procedure that requires 30–60 min to complete and does not involve a destaining step [52–55]. As little as 4–8 ng of protein can be detected, rivaling the sensitivity of rapid silver staining techniques and colloidal Coomassie Blue staining methods. Since all three dyes excite at roughly 300 nm, documentation of stained gels can readily be achieved by photography on a standard laboratory UV transilluminator. Alternatively, the dyes may be quantified with commercially available CCD camera-based image analysis workstations or a variety of laser scanners,

providing a linear dynamic range of three orders of magnitude. In addition to their UV excitation peak, SYPRO Orange, Red and Tangerine dyes may be excited by visible light at approximately 470, 550 and 490 nm, respectively. The three dyes emit maximally at 570, 630 and 640 nm, respectively. Thus, SYPRO Orange and Tangerine dyes are well suited for imaging systems with 473 nm second-harmonic generation (SHG) or 488 nm argon-ion (Ar) lasers as well as those that use 470 nm blue-LEDs or 460 nm blue fluorescent light sources. SYPRO Red dye is most suitable for 532-nm frequency-doubled neodymium–yttrium–aluminum–garnet (Nd–YAG) laser sources, 543-nm helium–neon (He–Ne) laser sources or 550-nm green-light transilluminators [56].

Both SYPRO Orange and SYPRO Red dyes require 7% acetic acid in the staining solution, which is problematic when electroblotting, electroeluting or measuring enzyme activity is indicated. SYPRO Tangerine dye is an environmentally benign alternative to conventional protein stains that does not require solvents such as methanol or acetic acid for effective protein visualization [55]. Instead, proteins can be stained in a wide range of buffers, including phosphate-buffered saline or simply 150 m*M* sodium chloride. Since proteins may be stained using SYPRO Tangerine dye without the need for harsh fixatives, they are readily eluted from gels or used in zymographic assays, provided that SDS present during electrophoresis does not inactivate them. SYPRO Tangerine dye is also suitable for staining proteins in gels before they are transferred to membranes by electroblotting. Using a 7% acetic acid staining solution, SYPRO Tangerine dye-stained gels have a slightly higher background fluorescence than SYPRO Orange and SYPRO Red dyes. Thus, the latter dyes are preferred choices for routine staining in a fixative solution.

SYPRO Ruby dye is a proprietary ruthenium-based metal chelate stain, which side-by-side comparisons demonstrate is as sensitive as the best silver stains available (Fig. 1) [57,58]. SYPRO Ruby dye allows one-step, low background staining of proteins in polyacrylamide gels without resorting to lengthy destaining steps. The linear dynamic range of the dye extends over three orders of magnitude, thus surpassing both silver and Coomassie blue stains in performance. The dye can be excited using a standard

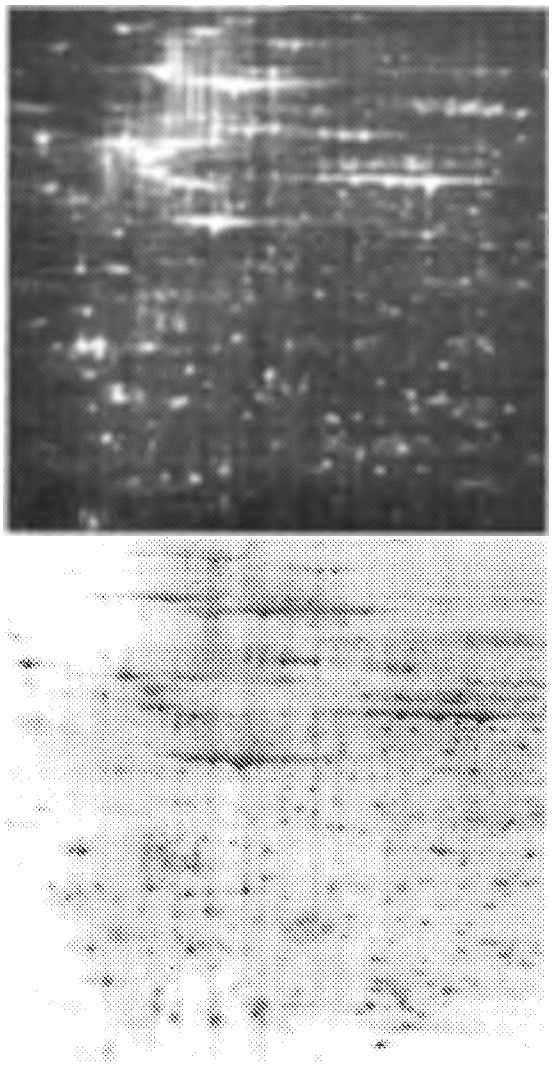

Fig. 1. Fluorescent staining compared with silver staining of two-dimensional gels. Proteins from a cultured fibroblast cell line (Rat-1) were fractionated by 2D gel electrophoresis and then stained using SYPRO Ruby protein gel stain (top image) or silver stain (bottom image), as previously described [9,58]. The comparison demonstrates similar detection sensitivity between these techniques. It should be noted that the silver stain method employed in this comparison is optimized for protein detection, but not compatible with subsequent analysis by mass spectrometry. Mass spectrometry-compatible silver stains are significantly less sensitive than the mass spectrometry-friendly fluorescent stain. In addition, the silver stain provides only qualitative information about the proteins due to its narrow 10-fold linear dynamic range, while the fluorescent stain provides quantitative capabilities extending over 3-logs. Figure courtesy of Drs. Birte Schulenberg and Jill Hendrickson, Molecular Probes.

300-nm UV transilluminator or using imaging systems equipped with 450-, 473-, 488- or even 532-nm lasers. Though more sensitive than SYPRO Orange, SYPRO Red and SYPRO Tangerine dyes, optimal staining is somewhat slower, requiring about 3 h to complete. Similar to colloidal Coomassie Blue stain but unlike silver stain, SYPRO Ruby dye is an end-point stain. Thus, staining times are not critical and staining can be performed over night without gels overdeveloping.

Side-by-side comparisons of silver staining (minus glutaraldehyde) and SYPRO Ruby dye staining have been performed, and SYPRO Ruby stain was found to be superior with respect to possessing a much broader linear dynamic range of quantitation (1000-fold), ability to visualize a 20% greater number of proteins, better reproducibility in quantifying the lowest intensity proteins in a 2D gel profile, and ability to identify lower amounts of protein with higher sequence coverage by peptide mass profiling (75–100 fmol) [57]. This clearly demonstrates that SYPRO Ruby dye is superior to silver staining for modern proteomics applications.

2.5. Chemiluminescence-based staining methods

While commonly employed for the detection of proteins after electroblotting, chemiluminescence had not been used to directly detect proteins in polyacrylamide gels until very recently [59,60]. A chemiluminescent acridan phosphate labeling reagent (maleimide derivative) was used to pre-derivatize bovine serum albumin prior to subjecting the protein to SDS–polyacrylamide gel electrophoresis [59]. Gels were then treated with acidic and basic buffer containing a peroxide, which initiated a rapid generation of light. Roughly 1–650 ng of serum albumin could be detected by the procedure. This should be considered a best-case scenario, however, as serum albumin is unusual in containing a very large number of cysteine residues (35 total) when reduced. Detection sensitivity for proteins with average numbers of cysteine residues would be closer to 10 ng, or the level of sensitivity achieved by colloidal Coomassie Blue stain. Currently, the chemiluminescence detection method has only been validated for feasibility using a single model protein. It remains to be seen whether the labeling technique will permit detection of proteins in complex biological specimens with a detection sensitivity that is competitive with fluorescence stain, reverse-stain or silver stain methods.

The specific detection of an antigen directly in SDS–polyacrylamide gels has also been demonstrated recently, obviating the need to electroblot gels [60]. The method is simply based upon old procedures for immunodetection in gels that were in routine use prior to Towbin's seminal paper on electroblotting [61]. The availability of highly sensitive chemiluminescence methods in recent years has made the in gel technique sensitive enough for certain applications.

2.6. Immobilized pH gradient/MALDI-TOF mass spectrometry and surface-enhanced laser desorption–ionization mass spectrometry (SELDI-MS)

Laser desorption of proteins by direct MALDI-TOF mass spectrometry-based surface scanning of carrier ampholyte isoelectric focusing gels, immobilized pH gradient isoelectric focusing gels, native polyacrylamide gels, and SDS–polyacrylamide gels has been demonstrated, with sub-picomolar detection sensitivities achieved [62–66]. In a preferred embodiment, "virtual" 2D gels may be created by desorbing proteins directly from immobilized pH gradient gels using MALDI-TOF mass spectrometry, in effect substituting mass spectrometry for SDS–polyacrylamide gel electrophoresis [65,66]. Analytical data may be presented as a computer-generated image that is similar to a classical 2D gel in appearance. The "virtual" 2D gel approach appears to detect lower-molecular-mass proteins (<30 kDa) better but higher-molecular-mass proteins (>30 kDa) more poorly than conventional 2D gels [65]. Currently, a number of artifacts must be contended with using the method, including horizontal streaks due to variations in baseline slope, artifacts caused by the presence of protein multimers and matrix adducts on the proteins that generate duplicate or triplicate spots, higher molecular masses than predicted due to difficulty in desorbing proteins from the gel matrix, and difficulty in quantifying the amounts of the proteins due to ion suppression phenomenon, a well-known problem associated with mass spectrometry

[65,66]. The procedure is also currently quite slow, requiring a day to run the gel, 2 days to dry it down and 2 days to acquire spectra [65].

Surface-enhanced laser desorption/ionization (SELDI) involves retaining proteins on a solid-phase chromatographic surface (ProteinChip Array) and direct detection of the retained proteins by time-of-flight mass spectrometry (TOF-MS) [67–69]. Typically, cationic, anionic, hydrophobic, hydrophilic, mixed charge, or immobilized metal ion chemistries are employed on SELDI ProteinChip surfaces, as well as antibodies, DNA, enzymes or receptors. Surfaces are incubated with a crude cell lysate or biological fluid, and then washed at various stringency levels to remove nonspecifically associated components. After this sample purification, the retained components are evaluated by TOF-MS. Quantitation of specifically captured TNF-α over a 100-fold concentration range has been demonstrated, though more complex samples are likely to be susceptible to ion suppression phenomenon [68]. Though excellent for rapid profiling of minute samples, the ability to identify proteins from SELDI profiles remains challenging, and conventional peptide mapping must be employed [69].

3. Specific detection of protein post-translational modifications

Though genomics provides comprehensive databases of sequence information, DNA and mRNA provide no information concerning the activities and post-translational modifications of proteins. The elucidation of protein post-translational modifications is perhaps the most important justification for proteomics as a scientific endeavor. The number of documented protein co- and post-translational modifications now exceeds 400 (http://abrf.org/index.cfm/dm.home). The most common modifications include phosphorylation, glycosylation, lipidation, sulfation and proteolytic modifications. These chemical modifications of proteins are crucial to modulating their function, but are not directly coded for by genes. Even in the simplest self-replicating organism, *Mycoplasma genitalium*, there are 24% more proteins than genes due to post-translational modifications, and in humans there are estimated to be at least three times as many proteins as genes [70]. Post-translational modifications modulate the function of proteins and thus directly impact their capacity to participate in cellular regulatory events.

Mass spectrometry has become a powerful research method for the characterization of protein post-translational modifications, since modifications either increase or decrease the molecular mass of the affected amino acid residue [71]. Generally, some method for the rapid proteome-wide screening of proteins with respect to the presence or absence of a particular modification is required prior to micro-characterization by mass spectrometry. Currently, heavily modified proteins, such as highly glycosylated proteins, can prove difficult to identify by standard mass spectrometry-based methods such as peptide mass profiling, since derivatized proteins cannot be matched to calculated peptide masses derived from genome databases. Finally, the presence of certain post-translational modifications, such as phosphorylation and sialoglycosylation, results in peptide signal suppression, complicating identification of peptides bearing these groups.

The detection of three prominent protein post-translational modifications: glycosylation, phosphorylation and proteolytic modifications are summarized below. In addition, three lesser known post-translational modifications, *S*-nitrosylation, arginine methylation and ADP-ribosylation are discussed. Proteomic investigations regarding certain of these post-translational modifications are only just beginning, as new methodologies allowing their detection have only recently been introduced.

3.1. Glycoprotein detection methods

Protein glycosylation is a key post-translational modification relevant to a range of biological phenomenon. For example, the metastatic spread of tumor cells in malignant progression is known to be a major cause of cancer mortality. Protein glycosylation is increasingly being recognized as one of the most prominent biochemical alterations associated with malignant transformation and tumorigenesis [72–75]. Not only is the total amount of protein-associated carbohydrate of relevance to cancer, but alterations in the branching patterns of the attached glycans also play important roles in malignancy.

Glycosylation changes in human carcinomas appear to contribute to the malignant phenotype observed downstream of certain oncogenic events [72].

Glycoproteins can be detected by autoradiography after incorporation of ^{3}H or ^{14}C sugars into cultured cells or tissues [76–78]. Though sensitive detection is achieved, radiolabeling is slow, hazardous and expensive. Nonradioactive detection of glycoproteins is usually performed using a periodic acid Schiff base procedure that employs the dye, acid fuchsin (pararosanaline) [79,80]. The principal limitation of this colorimetric method is that it has poorer detection sensitivity than Coomassie Blue staining, thus making the technique difficult to implement in the context of modern proteomics research. Similarly, Alcian Blue has been used as a colorimetric stain for glycoproteins [81,82]. Sensitivity of this method is similar to the acid fuchsin dye method and neutral glycoproteins, such as horseradish peroxidase and transferrin, are poorly detected by the staining method.

Dansyl hydrazine is a fluorescent alternative to acid fuchsin dye that can be used for the detection of glycoproteins in polyacrylamide gels [83]. Glycoproteins are subjected to periodate oxidation in gels and the resulting aldehydes are condensed with dansyl hydrazine to form hydrazones. These are in turn reduced to stable hydrazine derivatives with sodium borohydride. The coupling reaction requires incubating gels in acidified dimethylsulfoxide at 60 °C for 2 h and this harsh treatment has undoubtedly prevented widespread adoption of the method. Very high concentrations of dye are required for the dansyl hydrazine labeling procedure (0.5–2.0 g/l) and newer methods offer better specificity and sensitivity of detection.

Three new fluorescence-based methods for detecting glycoproteins have been introduced recently [84–86]. All techniques are based upon periodic acid Schiff base chemistry. Fluorescein semicarbazide hydrazide and 8-aminonaphthalene-1,3,6-trisulfonate have been employed for the detection of glycoproteins electroblotted to PVDF membranes, but the techniques are not suitable for detection of glycoproteins directly in polyacrylamide gels [84,86]. To date, the fluorescein semicarbazide labeling method has not been characterized extensively [86]. However, the method employing ϵ-aminonaphthalene-1,3,6-trisulfonate requires heating at 60 °C for 45–60 min, and limits of detection sensitivity range from 50 to 200 ng [84]. A sensitive green-fluorescent glycoprotein-specific stain, referred to as Pro-Q Emerald 300 dye, was recently reported, that allows detection of glycoproteins on PVDF membranes or directly in polyacrylamide gels [85]. Pro-Q Emerald 300 dye may be conjugated to glycoproteins by a periodic acid Schiff's (PAS) mechanism using very mild reaction conditions at room temperature. Pro-Q Emerald 300 dye-labeled gels may be post-stained with SYPRO Ruby dye, allowing sequential two-color detection of glycosylated and nonglycosylated proteins (Fig. 2). As little as 300 pg of α1-acid glycoprotein (40% carbohydrate) and 1 ng of glucose oxidase (12% carbohydrate) or avidin (7% carbohydrate) are readily detected in gels after staining with Pro-Q Emerald 300 dye, and a 500–1000-fold linear dynamic range of detection is obtained using the labeling method [85]. A UV transilluminator is required to detect the stain, but recently Pro-Q Emerald 488 dye was introduced for detection of glycoproteins using laser-based gel scanners.

A general antibody-based method for detecting glycoproteins involves periodic acid oxidation of the carbohydrate moieties, reaction with digoxigenin hydrazide, and detection with alkaline phosphatase-conjugated anti-digoxigenin antibody [87]. Similar methods have also been devised using biotin hydrazide and alkaline phosphatase-conjugated or horseradish peroxidase-conjugated streptavidin [88,89]. The methods are unsuitable for glycoprotein detection in gels, however, and the introduction of contaminating reporter proteins complicates target identification by peptide mass profiling. Methods for the determination of carbohydrates in proteins after gel electrophoresis by covalent derivatization with fluorophores such as 2-aminobenzoic acid have been introduced, but require band excision and protein hydrolysis in strong acids at high-temperature [90]. Pulsed amperometric detection procedures employing similarly harsh reaction steps have also been devised [91].

3.2. Phosphoprotein detection methods

Though the study of reversible protein phosphorylation reactions has become central to biochemistry

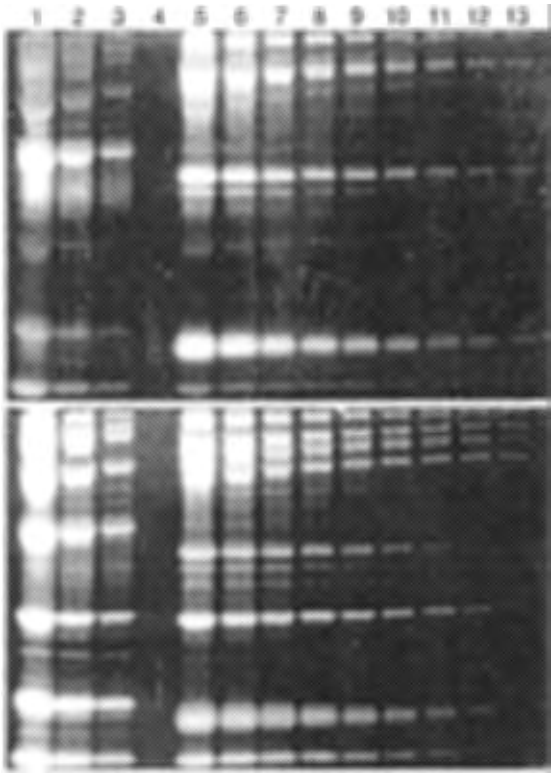

Fig. 2. Serial dichromatic detection of glycosylated and unglycosylated proteins in the same polyacrylamide gel. Detection of glycoproteins using Pro-Q Emerald 488 glycoprotein stain kit (Molecular Probes) (Top image). This PAS-based chemistry generates green fluorescent bands in gels. Detection of total protein profile using SYPRO Ruby protein gel stain (Molecular Probes) (Bottom image). This colloidal metal chelate staining procedure generates orange–red fluorescent bands in gels. Both images were collected using an FLA-3000 laser-based gel scanner (Fuji Film Scientific Imaging). Lanes 1–3: 2-fold serial dilution of broad range molecular mass markers containing the glycoprotein ovalbumin (3% carbohydrate). Lanes 5–13: 2-fold serial dilutions of CandyCane molecular mass markers (Molecular Probes) containing a mixture of glycosylated and unglycosylated proteins. Figure courtesy of Ms. Courtenay Hart, Molecular Probes.

since its discovery in the 1950s, by Nobel Prize winners Drs. Edwin Krebs and Edmond Fischer, phosphoproteomics, the systematic parallel analysis of the phosphorylation status of large sets of proteins involved in the regulatory circuitry of cells and tissues, is a relatively new field destined to drive research in the post-genomics era for many years to come [92,93]. Reversible protein phosphorylation plays a central role in biological regulation, and this is especially true in the context of carcinogenesis. The role of protein phosphorylation cascades in malignant transformation is exceedingly well established. Malignant transformation occurs through successive mutations in specific cellular genes, leading to the activation of oncogenes and the inactivation of tumor suppressor genes [94–96]. The cellular genes that are altered are normally involved in maintaining cellular homeostasis through participation in signaling cascades that are tightly regulated to maintain the functional integrity of the cell [96]. Oncogenic signaling pathways lead to the activation of tyrosine or serine/threonine kinases. Tyrosine kinases that are often found to be mutated in human tumors include the cytoplasmic kinases Src and Abl, as well as the integral plasma membrane kinases EGFR and PDGFR [96]. Serine/threonine kinases that are mutated or activated in human cancer include Raf, Akt and Tpl-2 [96]. These protein kinases are involved in signaling pathways that lead to cell proliferation, or inhibition of apoptosis through activation of transcription factors, inhibition of pro-apoptotic molecules, or deregulation of cell cycle control. A tyrosine phosphatase associated with metastasis in colorectal cancer has recently been identified [97].

Phosphoproteins are most often detected by autoradiography after incorporation of ^{32}P or ^{33}P into cultured cells or after incorporation into subcellular fractions by protein kinases [98]. Such approaches are restricted to a limited range of biological materials, such as tissue culture samples. Needless to say, analysis of clinical samples would require in vivo labeling of patients, which is not feasible. Several alternatives to radiolabeling have also been developed over the years. Phosphoproteins can be detected by immunoblotting [99,100]. Though high quality antibodies to phosphotyrosine are commercially available, antibodies that specifically recognize phosphoserine and phosphothreonine residues have been more problematic, often being sensitive to amino acid sequence context. Immunoblotting is best performed after blocking unoccupied sites on the solid-phase support with protein solutions, which interferes with microchemical analysis. Removal of the antibody and stain require relatively harsh treatments (i.e., heating to 65 °C, incubation with 0.1%

SDS and 1 m*M* DTT). This also poses problems with subsequent use of the protein for sequencing and mass spectrometry.

The cationic carbocyanine dye "Stains-All" (1-ethyl-2-[3-(3-ethylnaphtho[1,2*d*] thiazolin-2-ylidene)-2-methylpropenyl]-naphtho [1,2*d*]thiazolium bromide) stains RNA, DNA, phosphoproteins and calcium-binding proteins blue while unphosphorylated proteins are stained red [101,102]. Stains-All is not routinely used to detect phosphoproteins due to poor specificity and low sensitivity. Stains-All is at least 10 times less sensitive than Coomassie Brilliant Blue and several orders of magnitude less sensitive than ^{32}P autoradiography.

Phosphoproteins may be specifically detected in gels through alkaline hydrolysis of phosphate esters of serine or threonine, precipitation of the released inorganic phosphate with calcium, formation of an insoluble phosphomolybdate complex and then visualization of the complex with a dye such as Methyl Green, Malachite Green or Rhodamine B [103,104]. The Methyl Green dye approach has recently been commercialized as the GelCode Phosphoprotein detection kit (Pierce Chemical, Rockford, IL). The detection sensitivity of the staining method is considerably poorer than Coomassie Blue staining, with 80–160 ng of phosvitin, a protein containing roughly 100 phosphoserine residues, being detectable by the commercialized kit. The staining procedure is fairly complex (involving seven different reagents) and alkaline hydrolysis requires heating gels to 65°C, which causes the gel matrix to hydrolyze and swell considerably. Since phosphotyrosine residues are not hydrolyzed by the alkaline treatment, proteins phosphorylated at this amino acid residue escape detection by the method. Gels may be destained and then post-stained with colloidal Coomassie Blue dye in order to visualize the total protein profile.

Several instrument-based methods are available for the determination of protein phosphorylation such as ^{31}P NMR [105,106], mass spectrometry [71,107–109] and protein sequencing [110]. While these procedures accurately characterize the phosphorylation status of proteins and peptides, they are unsuitable for high-throughput screening of phosphorylated substrates. The techniques are generally used after a phosphoprotein has been identified by autoradiography or immunoblotting with anti-phosphotyrosine antibody. Though methods have recently been introduced to directly quantify the relative abundance of phosphoproteins in two different samples by mass spectrometry through culturing different cell populations in ^{15}N-enriched and ^{14}N-enriched medium, the linear dynamic range of such methods has explicitly been demonstrated over only a 10-fold range [109]. In addition, an isotope-coded affinity tag approach to the differential quantitation of phosphopeptides by β-elimination and subsequent addition of biotinyl-iodoacetamidyl-3,6-dioxaoctanediamine containing either four alkyl hydrogen or four alkyl deuterium atoms has been reported [111]. Ion suppression phenomena associated with mass spectrometry prevents stoichiometric comparison of different phosphoproteins by such techniques.

Recently, two methods for the chemical derivatization and enrichment of phosphopeptides have been described [112,113]. The first method requires proteolytic digestion of the sample, reduction and alkylation of cysteine residues, N-terminal and C-terminal protection of the peptides, formation of phosphoramidate adducts at phosphorylated residues by carbodiimide condensation with cystamine, capture of the phosphopeptides on glass beads coupled to iodoacetate, elution with trifluoroacetic acid and evaluation by mass spectrometry [112]. The second method involves oxidation of cysteine residues with performic acid, alkaline hydrolysis to induce β-elimination of phosphate groups from phosphoserine and phosphothreonine residues, addition of ethanedithiol, coupling of the resulting free sulfhydryl residues with biotin, purification of phosphoproteins by avidin affinity chromatography, proteolytic digestion of the eluted phosphoproteins, a second round of avidin purification and then analysis by mass spectrometry [113]. Both procedures were validated using the phosphoprotein β-casein. Both procedures identified the monophosphorylated trypsin peptide fragment from the test protein, but both failed to detect the tetraphosphorylated peptide fragment [112,113].

Fluorescence detection methods appear to offer the best solution to global protein quantitation in proteomics. However, currently, there is no satisfactory method for the specific and reversible fluorescent detection of gel-separated phosphoproteins from complex samples. Derivatization and fluorophore

labeling of phosphoserine residues by blocking free sulfhydryl groups with iodoacetate or performate, alkaline β-elimination of the phosphate residue, addition of ethanedithiol, and reaction of the resulting free sulfhydryl group with 6-iodoacetamidofluorescein has been demonstrated in capillary electrophoresis using laser-induced fluorescence detection and similar reactions have been performed on protein microsequencing membranes [114,115]. Neither publication demonstrates detection of phosphoproteins directly in gels, but the detection of cysteine residues by similar chemistry is shown, indicating that the pre-derivatization of phosphoproteins by this chemistry should be feasible [115]. One problem with the approach is that a delicate balance must be struck between the base and the ethanedithiol in order to achieve elimination of the phosphate group from the serine residue and addition of the ethane dithiol to the resulting dehydroalanine residue without hydrolysis of the peptide backbone [114]. Though the quest for a Coomassie Blue-like stain allowing the simple and selective detection of phosphoproteins in gels dates back to the 1960s, this holy grail remains lost for the time being.

3.3. Proteolytic modification detection methods

Gel-based methods for the detection of proteolytic activity are too numerous to enumerate in this review article [116,117]. Zymographic assays for serine proteinases, cysteine proteases, aspartate proteases and metalloproteinases have been developed over the years. For example, a fluorescence-based protease assay was recently developed for the detection of different members of the papain family of cysteine proteases within a complex cell lysate [118]. Four different fluorescent BODIPY dye conjugates of the general cysteine protease inhibitor *trans*-epoxysuccinyl-L-leucylamido (4-guanidino)butane were synthesized, allowing multiplexed analysis of papain family proteases. Covalent modification of the proteases through the active site cysteine residue allows analysis of changes in enzyme activity. For example, a specimen can be divided in two, and one sample incubated with the red-fluorescent BODIPY 588/616 conjugate. The other sample can then be incubated with a specific protease inhibitor, along with the blue-fluorescent BODIPY 493/503 conjugate. Next, the samples are combined and the proteins separated on a single 2D gel. Specific inhibition of particular cysteine proteases is readily identified through comparison of the resulting red-fluorescent and blue-fluorescent images. Gels can subsequently be stained with a high sensitivity total protein stain, the protein isoforms of interest excised and then identified by standard mass spectrometry-based techniques.

Tools for the specific proteome-wide detection of natural substrates of proteolytic enzymes are not currently available. Individual proteins can be incubated with specific proteases to determine whether they are potential substrates, but the physiological relevance of such measurements is not assured. Standard immunodetection techniques may be used to monitor the proteolysis of specific proteins after electroblotting, as long as the epitope used for detection is not proteolysed. In the realm of 2D gel electrophoresis, spot-by-spot identification of the majority of proteins resolved in a particular sample generally leads to the identification of subsets of proteins related to one another through proteolytic processing events.

3.4. S-Nitrosylation detection method

Nitric oxide has been implicated in a variety of physiological and pathophysiological conditions, including vasodilation, proliferation, differentiation, NMDA receptor activation, septic shock, atherosclerosis, apoptosis and hypoxia-induced pulmonary hypertension [119,120]. The intracellular reaction of the higher oxides of nitric oxide (NO_2, N_2O_3, $OONO^-$) with reactive cysteine groups leads to the generation of protein *S*-nitrosothiols. Like protein phosphorylation, protein *S*-nitrosylation could potentially represent a fundamental mechanism for the reversible post-translational control of protein activity and by extension cellular functions [119–121].

The difficulty in devising specific gel-based assays for particular post-translational modifications should be readily apparent from the preceding discussion of phosphorylation detection systems. To date, radiolabeling with ^{32}P provides the bulk of the data on protein phosphorylation, with anti-phosphotyrosine antibodies and most recently monitoring 80-Da shifts in peptide mass by mass spectrometry serving as very useful adjunct detection technologies. Until

recently, the evaluation of protein *S*-nitrosylation in biological systems has been hampered by the lack of a detection technology to conveniently monitor this labile post-translational modification. Radioactive isotopes of nitrogen or oxygen, the atoms forming the nitric oxide adduct are not available, and the half life of protein *S*-nitrosylation is in the few second to few minute range. Protein *S*-nitrosylation is not stable enough to survive the rigors of denaturing SDS–polyacrylamide gel electrophoresis, so while anti-*S*-nitrosocysteine antibodies have been generated and applied in immunohistochemistry studies, they are of little use in the context of proteomics investigations.

Recently, the Biotin Switch method was established to allow detection of protein *S*-nitosylation after SDS–polyacrylamide gel electrophoresis and electroblotting [122]. The procedure allows specific biotinylation of *S*-nitrosylated cysteine residues in proteins. First, free thiols are blocked by incubation with a thiol-specific methiolating agent (methyl methanethiosulfonate or MMTS) in the presence of sodium dodecyl sulfate to ensure access to buried cysteine residues. The methiolating agent does not react with nitrosothiols or disulfide bonds under the reaction conditions employed. Excess MMTS is removed using a spin column or by acetone precipitation. Next, nitrosothiol bonds are selectively decomposed to thiols with ascorbate. Finally the free thiol groups are reacted with the sulfhydryl-specific biotinylation reagent, *N*-[6-(biotinamido)hexyl]-3′-(2′-pyridyldithio)propionamide (biotin-HPDP). The labeled proteins may then be separated by SDS–polyacrylamide gel electrophoresis, electroblotted and detected by standard immunoblotting methods using anti-biotin antibodies or streptavidin. Labeled proteins may be selectively enriched using streptavidin affinity chromatography as well. The Biotin Switch method has permitted new proteomic investigations into the fundamental role of protein *S*-nitrosylation in cellular signalling [121,122].

3.5. Arginine methylation detection methods

Arginine methylation was first noted more than 30 years ago, and study of this post-translational modification has benefited from renewed interest due to the completion of several genome sequencing programs [123,124]. A consensus sequence for arginine methylation has been identified, the RGG box RNA-binding motif, allowing identification of numerous proteins as potential substrates of arginine methylation [125]. Other arginine methylation motifs have been identified as well, such as RXR, DRG and GRA [126,127]. Unlike *S*-nitrosylation, arginine methylation is essentially an irreversible post-translational modification, as the generated aminoalkyl bond is quite stable and no dimethylarginine demethylase has been identified to date [126]. Arginine methylation has been noted in proteins involved in signal transduction, nuclear RNA processing, ribosome biogenesis, nucleocytoplasmic transport, and gene silencing [125,128].

As with protein *S*-nitrosylation, investigations into the role of protein arginine methylation have been fettered somewhat by a lack of technologies facilitating the detection of this post-translational modification on a proteome-wide scale [129]. Yeast cells, in contrast to the majority of other cell types, actively import the biological methyl donor *S*-adenosylmethionine, allowing radiolabeling of proteins in intact cells under physiological conditions [128]. Consequently, radiolabelling with [methyl-^{3}H] *S*-adenosyl-L-methionine, followed by electrophoresis and fluorography, is a commonplace approach to the study of arginine methylation in this organism [125,128]. In eukaryotic organisms lacking an active import mechanism, such as mammals and insects, cultured cells are incubated in medium containing protein synthesis inhibitors and then in methionine-free medium containing [methyl-^{3}H] *S*-adenosyl-L-methionine for several hours [130,131]. Conventional gel electrophoresis and fluorography are then employed to detect the modified proteins.

Mass spectrometry is playing an increasingly important role in the characterization of arginine methylation sites [126,127,132–134]. For example, the 24-kDa high-molecular-mass fibroblast growth factor-2 has been demonstrated to contain seven to eight dimethylated arginine residues (28 Da per residue) using a combination of MALDI-TOF mass spectrometry and Edman sequencing [127]. Such studies are performed on a protein by protein basis, with candidates suspected to contain the modification.

An immunological approach to the global de-

tection of arginine methylation has recently been reported that does not require radiolabeling of specimens [129]. At the heart of the procedure are monoclonal antibodies specific for mono- and asymmetric dimethylated arginine residues (Abcam, Cambridge, UK). Proteins are first immunoprecipitated with antibodies to methylarginine, the immunoprecipitated proteins are separated by SDS–polyacrylamide gel electrophoresis, transferred to membranes by electroblotting and specific proteins are then detected by immunoblotting or total protein staining. Unfortunately, while the anti-methylarginine antibodies are suitable for immunoprecipitation, they do not appear to be suitable for Western blot analysis, leaving assignment of the post-translationally modified proteins somewhat tentative. Control experiments are suggested in order to validate the assignment of the post-translational modification [129]. Recombinant protein substrates may be methylated in vitro using *S*-adenosyl-L-methionine and used to monitor the effectiveness of the immunoprecipitation step. Furthermore, preincubation of the antibodies with unmethylated or in vitro methylated protein as competitors can serve as an additional control for the specificity of the immunoprecipitation.

3.6. ADP-ribosylation detection methods

Mono-ADP ribosylation is a reversible post-translational modification of proteins catalyzed by enzymes that transfer the ADP-ribose moiety of NAD to specific amino acid residues, especially arginine residues, on protein substrates [135]. Among the known protein substrates for ADP-ribosyltransferases are small RAS-like membrane GTP-binding proteins. Nonenzymatic ADP ribosylation of cysteine residues in certain proteins, such as nuclear GTP-binding proteins has also been observed [136]. ADP ribosylation is known to regulate membrane trafficking and actin cytoskeleton arrangement [137].

Mono-ADP ribosylation of proteins is typically monitored by incubating cells or membranes with [^{32}P]NAD [138–142]. Protein labeling in the presence of [^{32}P]NAD may arise from several different reactions, however. Two important ones to consider in experiments of this type are poly-ADP ribosylation and nonenzymatic mono-ADP ribosylation [139]. Mono-ADP ribosylation is confirmed if labeled proteins that have been electroblotted and treated with snake venom phosphodiesterase, generate [^{32}P]5′-AMP, as identified by TLC or HPLC analysis. Nonenzymatic mono-ADP ribosylation can be excluded as a possibility if incubation of samples with [^{32}P]ADP ribose does not cause labeling of the proteins.

An alternative approach to detecting ADP ribosylation is the use of anti-ADP ribose antibodies by standard immunoblotting methods [143]. Since ADP ribose-conjugated serum albumin results in 5′-AMP-specific antibodies due to hydrolysis, an ADP ribose analog resistant to enzymatic degradation at the pyrophosphate group was coupled to bovine serum albumin in order to generate an antigen appropriate for the production of anti-ADP ribose antibodies. The antibody is reported to detect as little as 1 pmol of ADP ribosylated proteins. Additionally, 1,6-etheno NAD, a fluorescent analog of NAD, may be employed to measure ADP ribosylation [144–146]. The fluorophore excites maximally at 292 nm and emits maximally at 413 nm.

4. Detection of reporter enzymes and epitope tags

Several recombinant DNA-based strategies for appending affinity tags and reporter enzymes to proteins have been developed as tools for protein purification and detection. These include fusion tags of maltose-binding protein, hemagglutinin, β-galactosidase, β-glucuronidase, green fluorescent protein, glutathione *S*-transferase, c-myc oncoprotein, FLAG peptide or oligohistidine peptide. β-Galactosidase, β-glucuronidase, the oligohistidine peptide tag and green fluorescent protein are discussed in more detail below:

4.1. β-Glucuronidase

The *Escherichia coli* β-glucuronidase-encoded gene, gusA, is commonly used as a reporter gene for nonvertebrate organisms that minimally express endogenous β-glucuronidase activity such as lower and higher plants, most bacteria, yeast, fungi and insects

[147]. As plants express significant amounts of β-galactosidase endogenously, β-glucuronidase is an especially useful reporter enzyme for molecular biology studies focusing upon these organisms. Naturally, β-glucuronidase protein levels can be determined by standard immunoblotting procedures using anti-GUS antibody [148,149]. By measuring β-glucuronidase activity directly in polyacrylamide gels, time-consuming immunoblotting steps and costly antibodies are avoided, however. β-Glucuronidase activity can be detected directly in gels using colorimetric detection systems such as naphthol-AS-BI β-D-glucuronide coupled to Fast Garnet GBC, 6-bromo-2-naphthyl β-D-glucuronide coupled to Fast Blue B or 5-bromoindol-3-yl β-D-glucuronide in combination with nitroblue tetrazolium [116,150]. Gels are incubated in the stain solution until colored bands appear and then fixed in an acidified aqueous solution of 7% acetic acid or 10% trichloroacetic acid. The fluorogenic substrate 4-methylumbelliferyl β-glucuronide is more commonly used to measure β-glucuronidase activity in gels [116]. Typically, the substrate is applied to the gel surface soaked into filter paper. After incubating the gel at 37 °C for 90 min, the filter paper is removed and fluorescent bands are detected using long wavelength ultraviolet (UV-A) illumination in combination with a 420-nm long-pass emission filter. The hydrolytic product of this substrate does not precipitate at the site of enzyme activity, however, making the compound less than ideal for localization studies in polyacrylamide gels due to a tendency to diffuse after a period of time. Additionally, the emission of the product, 4-methylumbelliferone, is maximal at 456 nm, which overlaps with the emission of polyester backings commonly used to support pre-cast polyacrylamide gels. An analogous fluorogenic substrate, fluorescein mono-β-D-glucuronide was recently employed in microchip capillary electrophoresis for rapid enzyme assay [151].

A fluorescent serial staining method based upon detection of total protein after SDS–polyacrylamide gel electrophoresis using SYPRO Tangerine dye in saline solution, followed by enzyme renaturation in 0.1% Triton X-100 and detection of β-glucuronidase activity using ELF 97 β-D-glucuronide was described recently, but unfortunately, simultaneous detection of total protein and enzyme activity was not possible as SYPRO Tangerine dye must intercalate into SDS micelles for protein detection while measuring β-glucuronidase activity requires prior removal of SDS from the gels [55]. Combining ELF 97 β-D-glucuronide with SYPRO Ruby dye does permit convenient dichromatic detection of β-glucuronidase activity and total protein profiles using a single gel, however. Unlike SYPRO Tangerine dye, SYPRO Ruby dye interacts directly with basic amino acids in proteins. This electrostatic binding mechanism allows staining of proteins after renaturation of enzyme activity through removal of SDS from the gels [147].

4.2. β-Galactosidase

The β-galactosidase gene (lacZ) is commonly used as a reporter enzyme for the evaluation of gene regulation, the detection of recombinant fusion genes, monitoring cell transfection efficiencies and the detection of protein–protein interactions by the two-hybrid system [152]. In a parallel manner as with β-glucuronidase, β-galactosidase protein levels may be determined by standard immunoblotting procedures [153]. This enzyme may also be detected directly in gels using a number of assays based upon enzyme activity [116]. Similar to β-glucuronidase, colorimetric and fluorogenic substrates for β-galactosidase, including 5-bromo-4-chloro-3-indolyl β-D-galactopyranoside, alizarin-β-D-galactoside, *p*-naphtholbenzein-β-D-galactoside, cyclohexenosculetin-β-D-galactoside, 4-methylumbelliferyl β-D-galactopyranoside, 3-carboxyumbelliferyl β-D-galactopyranoside, resorufin-β-D-galactopyranoside or fluorescein mono-β-D-galactopyranoside, have been developed for detecting β-galactosidase activity in agar-based colonies or in gel-based zymography [116,154–157]. In an alternate coupled enzyme detection system, gels are incubated in lactose, which is hydrolyzed to D-glucose and D-galactose by β-galactosidase [158]. Galactose dehydrogenase subsequently converts D-galactose to D-galactono-1,4-lactone, utilizing the cofactor NAD. The resulting NADH is coupled to a phenazine methosulfate (PMS)/methyl thiazolyl blue (MTT) chromogenic system to form the colored product formazan. Finally, in yet another method, salicyl β-D-galactoside generates D-galactose and salicylic acid when hydrolyzed by β-galactosidase. Addition of terbium chlo-

ride and EDTA produces a ternary luminescent lanthanide chelate complex with excitation maximum of roughly 280 nm and emission maximum of 515 nm [159].

4.3. Oligohistidine tags

The oligohistidine domain is a transition metal-binding peptide sequence comprising a string of four to 10 histidine residues. Recombinant proteins are often fused to oligohistidine affinity tag sequences to aid in their purification by immobilized nickel-ion affinity chromatography. The detection of oligohistidine-tagged fusion proteins after polyacrylamide gel electrophoresis typically requires many time-consuming steps, including the transfer of the gel to a membrane, the blocking of unoccupied sites on the membrane with protein or detergent solutions, incubation with an oligohistidine-binding agent (primary antibody or biotin-nitrilotriacetic acid), incubation with a secondary detection agent (antibody–reporter enzyme conjugate, streptavidin–reporter enzyme conjugate), and incubation with a visualization reagent (colorimetric, fluorogenic or chemiluminescent reagent). Specifically, biotinylated nitrilotriacetic acid has been used in combination with streptavidin–alkaline phosphatase or streptavidin–horseradish peroxidase conjugates and colorimetric or chemiluminescent substrates to allow detection of the oligohistidine-tagged fusion proteins after electroblotting [160–162]. Additionally, direct reporter enzyme–nitrilotriacetate–nickel conjugates have been used to detect oligohistidine-tagged fusion proteins on electroblots [163,164]. Likewise, colloidal gold–nitrilotriacetic acid conjugates have been used to detect oligohistidine-containing fusion proteins on blots after a silver enhancement step [165]. Lastly, though oligohistidine is not very immunogenic, several high affinity monoclonal antibodies specific to the epitope have been produced that allow detection of fusion proteins by standard immunoblotting techniques [166–168].

Two novel fluorophore–nitrilotriacetic acid conjugates, Pro-Q Sapphire 365 and Pro-Q Sapphire 488 oligohistidine gel stains (Molecular Probes, Eugene, OR), allow for the fluorescence detection of oligohistidine-tagged fusion proteins directly in sodium dodecyl sulfate–polyacrylamide gels, without requiring immunoblotting, reporter enzymes or secondary detection reagents. Pro-Q Sapphire 365 oligohistidine gel stain emits maximally at 450 nm (blue fluorescence) when illuminated with 300–365 nm ultraviolet light. Pro-Q Sapphire 488 oligohistidine gel stain emits maximally at 515 nm (green fluorescence) when illuminated with visible light from a laser-based gel scanner equipped with a 470–488-nm laser source. Roughly 25–65 ng of oligohistidine-tagged fusion protein is detectable using either stain. After recording the fluorescence signal from the Pro-Q Sapphire dyes, gels may be post-stained with the red-fluorescent SYPRO Ruby protein gel stain in order to reveal the total protein profile (Fig. 3).

4.4. Green fluorescent protein

Wild-type green fluorescent protein (GFP) from the jellyfish *Aequorea victoria*, as well as its differently colored variants, are useful tools commonly employed to monitor gene expression and protein localization when expressed as chimeric fusion proteins [169]. Wild type GFP displays excitation maxima of 395 and 475 nm and an emission maximum of 509 nm. Mutants of the GFP protein have been devised with visible excitation maxima of 490 nm, providing excellent compatibility with fluorescein filter sets and argon ion laser sources. From a proteomics perspective, it should be noted that the introduction of a single GFP reporter gene, used to monitor cell metabolism, can profoundly effect a host of cellular processes, including carbon metabolism, protein synthesis and protein translation [170]. Using pH 4–7 isolectric focusing gels and 12% T SDS–polyacrylamide gels, it has been demonstrated that the introduction of GFP into *Escherichia coli* strain JM105 using pBluescript expression vector (Stratagene, La Jolla, CA) leads to the expression of 68 new proteins (including 50S ribosomal protein L9, serine methylase, aerobic glycerol-3-phosphate dehydrogenase and amino acid ABC transporter binding protein) and the loss of 44 others (including sulfate starvation-induced protein 7, histidine-binding periplasmic protein and glucose-permease IIA component) [170]. Numerous quantitative protein changes were observed as well.

Recent studies indicate that GFP may be isolated with high yield and purity employing serial copper

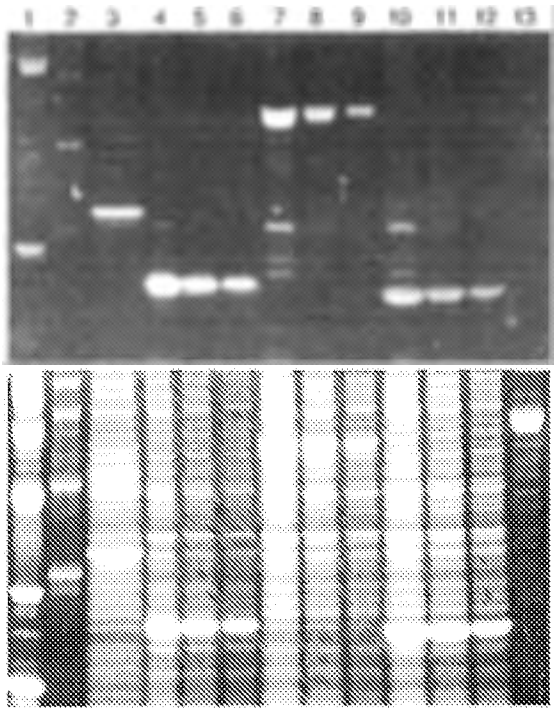

Fig. 3. Serial dichromatic detection of oligohistidine-tagged recombinant proteins and total proteins in the same polyacrylamide gel. Detection of oligohistidine-containing fusion proteins using Pro-Q Sapphire 365 oligohistidine gel stain kit (Molecular Probes) (top image). This nitrilotriacetate-based detection system generates blue fluorescent bands in gels. Detection of total protein profile using SYPRO Ruby protein gel stain (Molecular Probes) (bottom image). This colloidal metal chelate staining procedure generates orange–red fluorescent bands in gels. Lanes: (1) broad range molecular mass markers; (2) 6Xhis protein ladder (Qiagen); (3) protein lysate containing hexahistidine-tagged urate Oxidase (Pierce Corporation), (4–6) serial dilutions of *Escherichia coli* lysate containing the recombinant oligohistidine fusion protein, OSCP; (7–9) serial dilutions of *Escherichia coli* lysate containing the recombinant oligohistidine fusion protein, α-subunit of ATPase; (10–12) serial dilutions of *Escherichia coli* lysate containing the recombinant oligohistidine fusion protein, d subunit of ATPase; (13) bovine serum albumin. Both images were collected using A LumiImager CCD-camera-based gel scanner (Roche Biochemicals). Figure courtesy of Ms. Courtenay Hart, Molecular Probes.

(II) and zinc (II) immobilized metal-ion affinity columns, using diafiltration between the two chromatography steps [171]. Though more complex than the standard nickel (II) immobilized metal-ion affinity column used for isolation of oligohistidine-tagged fusion proteins, the two-step chromatography procedure for GFP is relatively straightforward and likely to be applicable in many instances to GFP-fusion proteins as well. In the context of electrophoretic separations methodologies, the native fluorescence of GFP has had limited utility, as its signal is destroyed by conventional denaturing SDS–polyacrylamide gel electrophoresis. Consequently, overexpressed GFP fusion proteins are typically detected by Coomassie Blue staining, silver staining or by immunoblotting techniques using anti-GFP antibodies [172–175]. GFP may be visualized directly in SDS–polyacrylamide gels if a nonreducing sample buffer is used to prevent complete protein denaturation [176,177].

A GFP-protein A fusion protein has been constructed for use as a single-step detection reagent for Western blotting [178,179]. As with any direct fluorophore conjugate of an antibody, protein A or streptavidin, sensitivity is limited by the overall brightness of the probe, and reporter enzyme constructs employing alkaline phosphatase, horseradish peroxidase or β-galactosidase are generally much more sensitive due to the signal amplification afforded by rapid turnover of large numbers of substrate molecules.

Certain specialized applications of GFP fluorescence in gel electrophoresis have been reported. For instance, a GFP–calmodulin fusion protein has been generated, permitting rapid, nonradioactve detection of interacting proteins in gel overlay assays (Far-Western blots) [176]. Proteins are fractionated by conventional SDS–polyacrylamide gel electrophoresis, electroblotted to poly(vinylidene difluoride) (PVDF) membrane, blocked with 2% nonfat milk protein and incubated with 2–5 μg/ml of the GFP fusion protein over night. After washing the membrane several times, as little as 100 ng of calmodulin-binding proteins may be visualized by UV epi-illumination. Detection sensitivity using biotinylated calmodulin, horseradish peroxidase-conjugated streptavidin and luminol was found to be vastly superior to that obtained by the direct GFP–calmodulin fusion protein, though the conventional detection method required more steps.

In another example, native gel electrophoresis and affinity capillary electrophoresis with laser-induced fluorescence have been employed to monitor the

interaction of a GFP-cyclophilin fusion protein ("bait" protein) with cyclosporin A [177]. The native gel band-shift assay was performed using Tris–borate–EDTA electrophoresis gels and fluorescence signal was visualized using a UV transilluminator/CCD camera system. Roughly 1 μg of purified recombinant protein was required to obtain a band of moderate intensity with the approach. The affinity capillary electrophoresis band-shift assay allowed detection of the protein–protein interaction in phosphate buffer without addition of detergent. Consequently, weak and moderate interactions could be monitored using 60-fold lower amounts of protein and significantly shorter analysis times. Subsequently, both band shift assays were applied to extracts of *Drosophila melanogaster* embryos, and a putative high affinity endogenous ligand of cyclophilin was detected. Since GFP is larger than its fusion partner, it is necessary to establish in control experiments to ensure that any observed interactions arise from the bait component of the fusion protein.

5. Differential display proteomics: approaches and options

Proteomics is often based upon the comparison of different protein profiles. The central objective of differential display proteomics is to increase the information content of proteomics studies through multiplexed analysis. Currently, three principal approaches to differential display proteomics are being actively pursued, difference gel electrophoresis (DIGE), multiplexed proteomics (MP) and isotope-coded affinity tagging (ICAT). The basic principles of these three methods in the context of 2D gel electrophoresis are outlined in Figs. 4, 5 and 7.

5.1. Difference gel electrophoresis (DIGE)

Succinimidyl esters of the cyanine dyes, Cy2, Cy3 and Cy5, may be employed to fluorescently label as many as three different complex protein populations prior to mixing them together and running them simultaneously on the same 2D gel using a method referred to as difference gel electrophoresis (DIGE) (Fig. 4) [180,181]. Recently, a similar procedure utilizing Alexa Fluor dyes has been demonstrated as well [182]. Images of the 2D gels are acquired using as many as three different excitation/emission filters, and the ratio of the differently colored fluorescent signals is used to find protein differences among the samples. DIGE allows two to three samples to be separated under identical electrophoretic conditions, simplifying the process of registering and matching the gel images. Most often, the technology is used to examine differences between two samples (e.g., drug-treated versus control cells or diseased versus healthy tissue). Though seductive in concept, it should be noted that a few problems afflict DIGE technology, especially when endeavoring to perform quantitative proteomics analyses.

One requirement of DIGE is that only ~1–2% of the lysine residues in the proteins be fluorescently modified, so that the solubility of the labeled proteins is maintained during electrophoresis [180]. The solubility of the proteins is decreased considerably when higher degrees of substitution are employed, resulting in the detection of many fewer protein spots on 2D gels. This limited covalent labeling step sets the lower limit for fluorescence detection to 1–2% of its intrinsic limit, given an alternate fluorescence imaging technology that does not have this solubility constraint. In experimental terms, optimized DIGE technology is capable of detecting about half as many proteins as conventional silver staining, or about four times as many proteins as colloidal Coomassie Blue staining [181]. It is almost certain that the proteins missed by DIGE staining represent the lowest abundance species in the sample. DIGE technology is more sensitive than modified silver stain formulations optimized for mass spectrometry, though SYPRO Ruby dye staining detects 40% more protein spots than the Cy dyes [183].

While matched in charge, the dye-labeled proteins produced by DIGE technology migrate with slightly higher mass than the bulk of the unlabeled protein, due to the addition of the fluorophores [180,181]. This produces registration errors between the labeled and unlabeled proteins in 95% of the spots, and consequently complications arise when spots are to be excised and analyzed by mass spectrometry [181]. As a result, gels must be post-stained to aid in protein cutting for spot identification by mass spectrometry [181,183,184]. Regrettably, since colloidal Coomassie Blue staining is less sensitive than the

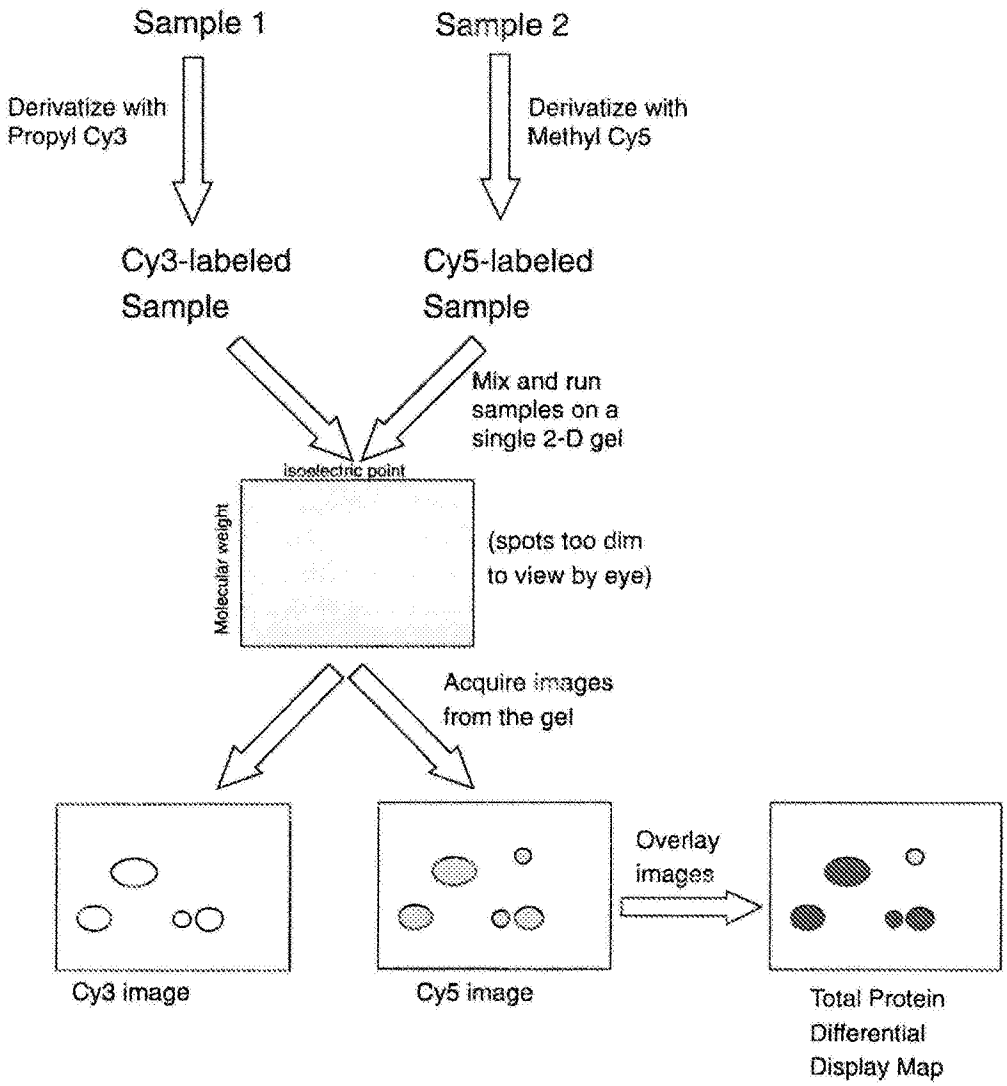

Fig. 4. Schematic illustration of the difference gel electrophoresis (DIGE) technology platform [180]. Two different samples are derivatized with two different fluorophores, combined and then run on a single 2D gel. Proteins are detected using a dual laser scanning device or xenon arc-based instrument equipped with different excitation/emission filters in order to generate two separate images. The images are then matched by a computer-assisted overlay method, signals are normalized, and spots are quantified. Differences in protein expression are identified by evaluation of a pseudo-colored image and data spreadsheet. DIGE technology can maximally evaluate three different samples using Cy2-, Cy3- and Cy5-based chemistries.

DIGE technology, 40% of the proteins of interest cannot be identified directly from the Coomassie Blue-stained gel [181]. Consequently, SYPRO Ruby dye has been adopted as the post-stain dye of choice for DIGE analysis [183,184]. Another issue to be aware of that can effect sensitivity of detection is that fluoresence cross-talk between excitation/emission band-pass filters may cause Cy5-labeled proteins to emit when illuminating at the optimal Cy3 excitation wavelength [185].

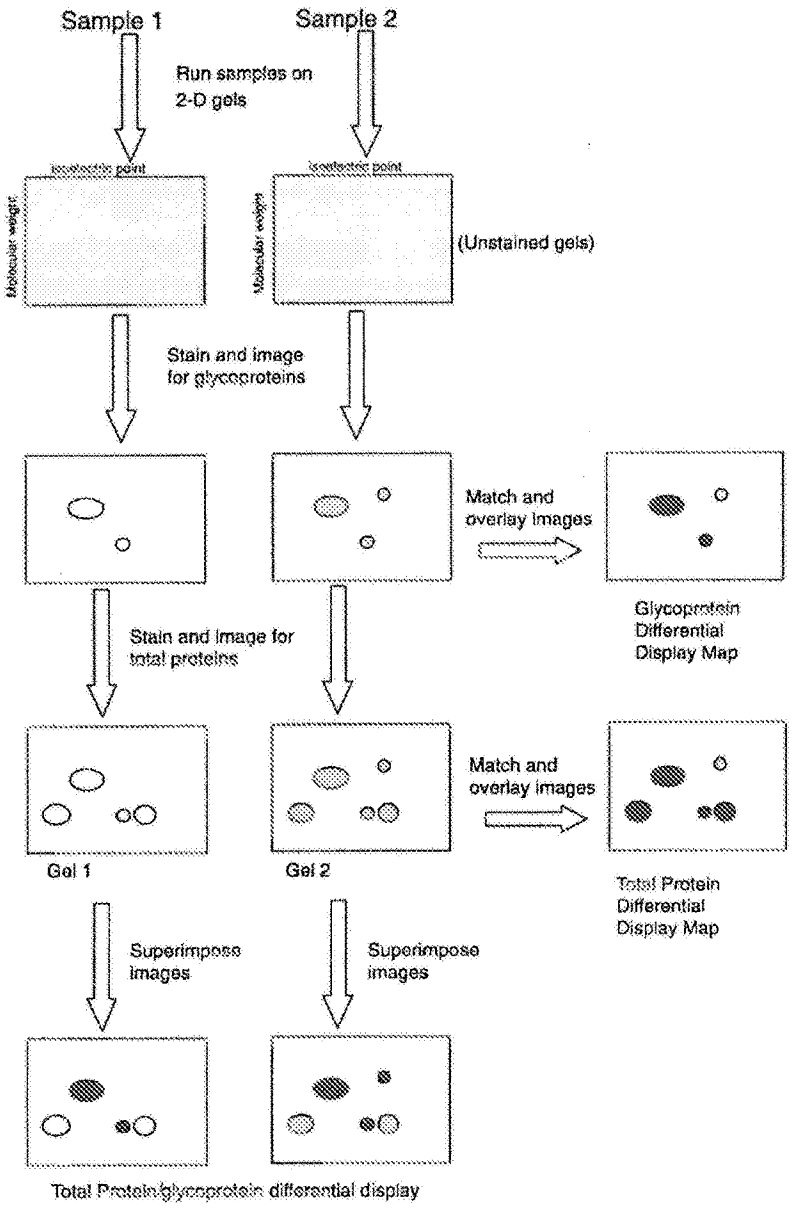

Fig. 5. Schematic illustration of the multiplexed proteomics (MP) technology platform [85]. Two different samples are run on two different 2D gels. Gels are stained for a particular functional attribute, such as glycosylation, and then imaged. Gels are then stained for total protein expression using SYPRO Ruby protein gel stain and imaged again. The images resulting from glycoprotein staining and the images resulting from total protein staining are then matched by computer-assisted rubber sheeting and overlay methods, signals are normalized (if necessary) and spots are quantified. Differences in glycosylation and protein expression are identified by evaluation of pseudo-colored images and data spreadsheets. Registration of total protein profiles with glycosylation patterns is readily accomplished by direct superimposition of images from the same gel. MP technology can evaluate an almost limitless number of 2D gels with respect to two or three different attributes (protein expression, post-translational modification, drug-binding capability, drug-metabolizing capability).

It has been demonstrated recently that 20% changes in very abundant proteins and 800% changes in scarce ones can be quantified reliably at the 90% confidence level using DIGE technology [181]. Thus, though the DIGE technology can be applied to the detection of qualitative changes in protein expression, quantitative changes in lower abundance proteins are likely to be overpowered by dye-dependent photophysical effects. A concrete illustration of the qualitative nature of DIGE technology may be found with regard to the study of protein changes in heart mitochondria of knockout mice lacking sarcomeric mitochondrial creatine kinase [186,187]. Mitochondrial creatine kinase plays a central role in cellular energetics of muscle, catalyzing the reversible transfer of the phosphoryl group between phosphocreatine and ADP [188,189]. Deletion of such a vital enzyme is expected to have proteome-wide repercussions, as cells are forced to adapt to the metabolic crisis. Conventional Western blot analysis has demonstrated loss of the target kinase, as well as 2–4-fold changes in a number of proteins, including mitochondrial cytochrome c oxidase, inorganic phosphate carrier, adenine nucleotide translocator and voltage-dependent anion channel proteins, consistent with the impaired cardiac energetics observed in these animals [187]. Proteome-wide analysis of the mitochondria by DIGE technology confirmed the complete absence of sarcomeric mitochondrial creatine kinase in the knockout mice, as well as a minor difference in the precursor form of aconitase, but surprisingly, no other large-scale changes in heart mitochondrial proteins were revealed by the technique [186]. Presumably, the quantitative changes identified in this model system by Western blotting could not be differentiated from background fluctuations associated with the DIGE labeling methodology.

Recent DIGE studies comparing the difference between normal and cancerous tissue were more successful in demonstrating changes in protein expression levels [183,184]. In a study comparing esophageal carcinoma cells with normal epithelial cells, statistical analysis revealed that 56 proteins were up-regulated by more than 3.5-fold and 39 were down-regulated by more than 4-fold [184]. Two changes, protein gp96 and annexin I, were confirmed by Western blotting. It should be noted that both validated changes were qualitative, with gp96 being absent from normal tissue and annexin I absent from tumor tissue. In a study comparing an ErbB-2-receptor tyrosine kinase transformed luminal epithelial cell line to its untransformed counterpart, 135 proteins with a 1.3-fold average difference in abundance were identified. Though many of these proteins were identified by mass spectrometry, none of the expression changes were confirmed by an independent method, such as Western blotting.

Another important issue with respect to the DIGE technology is that it is predicated upon an overly simplistic tenet that all of the information required in an analysis can be distilled down into a single 2D gel using a simple control versus treated state experimental design. However from a biology perspective, the analysis of drug dose–response curves or the kinetics of changes in tissue/cell proteomes require that multiple 2D gels be quantified. The assessment of different stages of cancer progression and epidemiological studies of global protein expression patterns in populations also require many more than the two to three sample capacity of the DIGE technique. Therefore, multiple 2D gels almost always must be quantified and referenced to one another, regardless of the method employed to detect the proteins. This necessity to quantify multiple 2D gels effectively contradicts the whole premise behind the DIGE detection technology. This shortcoming has been recognized by some, and an innovative method for linking multiple 2D gels generated by DIGE technology has recently been devised [183]. Cy2-labeled proteins are used as internal standards with all Cy3- and Cy5-labeled sample pairs to aid in quantitative comparisons between gels in a database.

Even if the biological problem can realistically be framed as a simple binary experimental/control study, it should be noted that DIGE technology cannot reliably identify differences between two samples using a single 2D gel. In an analysis of six two-color DIGE gels comparing toxin-treated to control liver homogenates, a total of 138 protein changes were identified [181]. Of these 138 differences, however, only 4.4% (eight differences) were observed in all six gels. Thirty percent (41 differences) were finally nominated as real changes in protein abundance, as they occurred in three or more gels. The authenticity of the changes was not corroborated using any independent measurement technique such as Western blotting, however.

Radiolabeling is probably the only method that can compete with fluorescence in terms of linear dynamic range and detection sensitivity. However, radio-imaging procedures for *differential display* such as the $^{125}I/^{131}I$ multi-photon detection (MPD) method devised by BioTraces (Herndon, VA) suffer from the same experimental design limitations as the fluorescence DIGE technology. The inherent slowness of radioactive 2D gel imaging also severely limits this technology. Currently, 2.5 days are required to collect an image with attomole detection sensitivity. Throughput might be improved in a proteomics work environment by employing multiple imaging devices, but the instruments are expensive to manufacture, costing around US $100 000 apiece. By contrast, a typical 2D gel fluorescently labeled with a total-protein dye, such as SYPRO Ruby protein gel stain, may be imaged in 0.1–2 s on a wide range of imaging platforms, approximately 200 000 times faster than radiolabel imaging.

5.2. Multiplexed proteomics (MP)

The multiplexed proteomics (MP) platform is designed to allow the parallel determination of protein expression levels as well as certain functional attributes of the proteins, such as levels of glycosylation, drug-binding capabilities or drug-metabolizing capabilities (Fig. 5). The MP technology platform utilizes the same fluorophore to measure proteins across all gels in the database, and employs additional fluorophores with different excitation and/or emission maxima to accentuate specific functional attributes of the specimen. As stated previously, biological investigations usually require large numbers of 2D gels and methods are required that facilitate the rigorous and reliable matching of proteins across a database. A clear advantage of MP technology over DIGE technology is that it provides a much broader bandwidth of information. A limitless number of gels may be evaluated with respect to a number of distinct attributes.

With the MP platform, a set of 2D gels is fluorescently stained and imaged to reveal some functional attribute of the proteins, such as drug-binding capability, or a particular post-translational modification. Then, protein expression levels are revealed in the same gels using SYPRO Ruby protein gel stain as the foundation staining technology. Differential display comparisons are made by computer, using image analysis software, such as Compugen's Z3 program [190]. All gels are imaged using the same excitation/emission filter sets and resulting images are then automatically matched, with the option of adding some manual anchor points to facilitate the process. Any two images can then be re-displayed as a single pseudo-colored map, permitting the visual inspection of differences in an identical manner as performed with DIGE technology. In addition, quantitative information can readily be obtained in tabular form, with differential expression data calculated. One of the strengths of the platform is that similar profiles, such as total protein patterns, are matched by computer from different gels, while dissimilar ones, such as total protein patterns and glycoprotein patterns, are matched by computer from the same gel. Thus, though few landmarks are shared between total protein profiles and the assayed functional property, the images may be matched by superimposition anyway.

A recently published study demonstrates the feasibility of the MP platform, describing methods to assay for the presence of glycans, followed by the detection of the total protein profile [85]. Pro-Q Emerald 300 dye, a sensitive green-fluorescent glycoprotein-specific stain is employed, having non-overlapping spectral properties with the red-fluorescent total protein stain, SYPRO Ruby dye [85]. This hydrazide dye may be affixed to glycoproteins using a periodic acid Schiff's (PAS) reaction under very mild coupling conditions. Proteins may then be post-stained with SYPRO Ruby dye, allowing sequential two-color detection of glycosylated and non-glycosylated proteins, an unprecedented new capability in proteomics research.

Other functional attributes of protein samples that may be detected in 2D gels with subsequent post-staining by SYPRO Ruby dye include the detection of β-glucuronidase activity using ELF 97 β-D-glucuronide, the detection of penicillin-binding proteins using fluorescent Bocillins, and the detection of oligohistidine-tagged proteins using Pro-Q Sapphire dye [147,191]. These examples illustrate four areas in which the MP platform can find application: analysis of post-translational modifications, enzymatic activity, small ligand binding and epitope tags. Other procedures for detecting hydrolase activi-

ty, and cell surface proteins are actively under development.

5.3. Isotope-coded affinity tagging (ICAT)

Isotope-coded affinity tag (ICAT) peptide labeling is predicated upon distinguishing between two populations of proteins using isotope ratios [192–196]. Isotope-coded affinity tags are reagents consisting of a protein-reactive group, an ethylene glycol linker region and a biotin tag. Currently, the commercialized ICAT reagent employs a reactive functionality specific for the thiol group of cysteine residues in proteins and peptides. Two different isotope tags are generated by using linkers that contain either eight hydrogen atoms (d0, light reagent) or eight deuterium atoms (d8, heavy reagent). A reduced protein mixture from one protein specimen is derivatized with the isotopically light version of the ICAT reagent, while the other reduced protein specimen is derivatized with the isotopically heavy version of the ICAT reagent. Next, the two samples are combined, and proteolytically digested with trypsin or Lys-C to generate peptide fragments. The combined sample is then fractionated by avidin affinity chromatography, thus retrieving only the cysteine-containing peptides. The affinity-purified mixture of peptides contains roughly 10-fold fewer peptides than the original sample, thus simplifying analysis. The peptides may be further separated by microcapillary reversed-phase liquid chromatography, followed by mass spectrometry. The ratio of the isotopic molecular mass peaks that differ by 8 Da, as revealed by mass spectrometry, provides a measure of the relative amounts of each protein from the original samples. Typically, nanoscale liquid chromatography–electrospray ionization mass spectrometry (LC–ESI-MS) provides quantitative information based upon the relative abundances of the heavy and light peptides, while nanoscale liquid chromatography combined with electrospray ionization tandem mass spectrometry (LC–ESI-MS–MS) provides qualitative information based upon the peptide molecular mass and amino acid sequence information [196].

Though quantitation by mass spectrometry is often unreliable, due to ion suppression phenomena, ICAT reagents are chemically identical and differ in mass by only eight neutrons. Nevertheless, it has been suggested that the background of co-eluting peptide pairs does vary in composition and concentration and thus quantification of the peptides occurs in different matrix environments [197]. The deuterated and non-deuterated peptides often separate from each other during liquid chromatography, and are ionized at different times in different matrixes. This can strongly impact the ionization efficiency of peptides across a chromatographic peak, leading to errors in quantitation. In addition, the ICAT tag is a relatively large molecule compared to the size of some small peptides and it has been suggested that the tag may interfere with peptide ionization, leading to complications in the interpretation of mass spectra [198].

One significant obstacle to the routine implementation of ICAT technology in the study of biological systems is that proteolytic digests of cells or tissues are exceedingly complex, with literally hundreds of thousands of peptides generated in a sample [196]. Though isolation of cysteine-containing peptides reduces sample complexity perhaps 10-fold, other fractionation methods are usually required to reduce the number of peptides delivered to the mass spectrometer further. Recently, the microsomal fraction of control versus differentiated HL-60 human myeloid leukemia cells were evaluated by the ICAT method [199]. After labeling with heavy and light ICAT reagents and combining the samples, the peptide mixture was subjected to cation-exchange chromatography, followed by avidin affinity chromatography, a multidimensional chromatographic approach. Finally, peptides were separated and analyzed by LC–ESI-MS. A total of 491 proteins were unambiguously identified and the ratio of each protein between control and differentiated cultures was determined.

One weakness of the current ICAT method is that it requires that the proteins contain cysteine residues flanked by appropriately spaced protease cleavage sites [198]. The problem has recently been highlighted in the study of the multi-subunit membrane protein, *Escherichia coli* F_1–F_0–ATP synthase [200]. This enzyme consists of distinct extramembranous and transmembranous components of known subunit stoichiometry, and thus provides a good model for the combination of hydrophobic and hydrophilic proteins normally encountered in proteomics studies. The membrane-associated F_0 component is composed of three subunits, a, b, and c, polypeptides with five, one and two transmem-

brane domains, respectively. Labeling with the cysteine-reactive fluorophore, monobromobimane, failed to detect four of the eight subunits of ATP synthase (Fig. 6). None of the membrane-embedded proteins in the F_0 complex were visualized. Genome-wide analysis of cysteine distribution in *Escherichia coli* demonstrates that the cysteine-labeling problem does not arise from a peculiar choice of model protein complex. In the *Escherichia coli* genome, the number of proteins containing no cysteine residues is high (~10–15%), obviating the use of any cysteine-specific technology as a total-protein indicator.

This cysteine-labeling problem may be overcome by devising different ICAT reagents, reactive for other amino acid residues in proteins. Indeed, several alternative isotope tags have been devised that label all proteolytic fragments in a sample. A method based upon the growth of cells in either ^{14}N- or ^{15}N-enriched medium has been described for quantifying changes in protein expression by 2D gel electrophoresis and mass spectrometry [199]. Likewise, regular water ($H_2^{16}O$) and heavy water ($H_2^{18}O$) have been employed as the solvent during Glu-C proteolysis of samples, leading to the incorporation of two ^{18}O or two ^{16}O atoms in the C-terminal moiety of each proteolytic fragment [201]. This results in a 4-Da difference in mass between paired peptides. Acetate (d0) and trideuteroacetate (d3) have been employed to acetylate primary amino groups in peptides [202]. Peptide digests are subsequently simplified using copper-immobilized metal affinity chromatography to selectively capture histidine-containing peptides. Alternatively, lectin affinity chromatography is employed to selectively analyze glycoproteins. Similarly, methyl esterification of aspartate and glutamate residues using regular methanol (d0) or trideuteromethanol (d3) has been used as an isotope tagging strategy [203]. Finally, standard 1,2-ethanedithiol (d0) and tetraalkyl deuterated 1,2-ethanedithiol (d4) have been employed to measure differences between *O*-phosphorylation sites in samples using β-elimination chemistry [111]. The pendant sulfhydryl group is then reacted with biotin iodoacetamidyl-3,6-dioxaoctanediamine. Just as with the original cysteine-reactive ICAT reagent, the phosphate-labeling procedure allows enrichment of target peptides using avidin affinity chromatography.

Recently, it has been demonstrated that the advantages of 2D gel electrophoresis and ICAT labeling

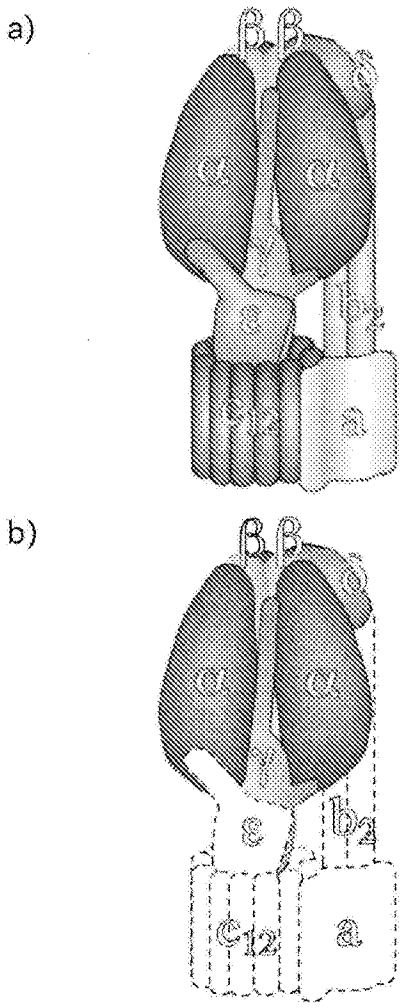

Fig. 6. Subunits of F_1F_0–ATP synthase revealed by two different detection methods [200]. (A) Subunits revealed using a basic amino acid binding dye, SYPRO Ruby protein gel stain. (B) Subunits detected using a thiol-reactive fluorophore, monobromobimane. Thiol-reactive chemistries, such as monobromobimane and ICAT labeling do not globally detect all proteins in a cell or tissue. Roughly 10–15% of the polypeptides escape detection. Secreted proteins and certain plant lectins tend to have a higher than average number of cysteine residues, while polypeptides that are components of multi-subunit protein complexes tend to have lower than average number of cysteine residues. Figure courtesy of Dr. Birte Schulenberg, Molecular Probes.

technology can be combined into a single differential display platform (Fig. 7) [194]. This method closely parallels the DIGE methodology, with some im-

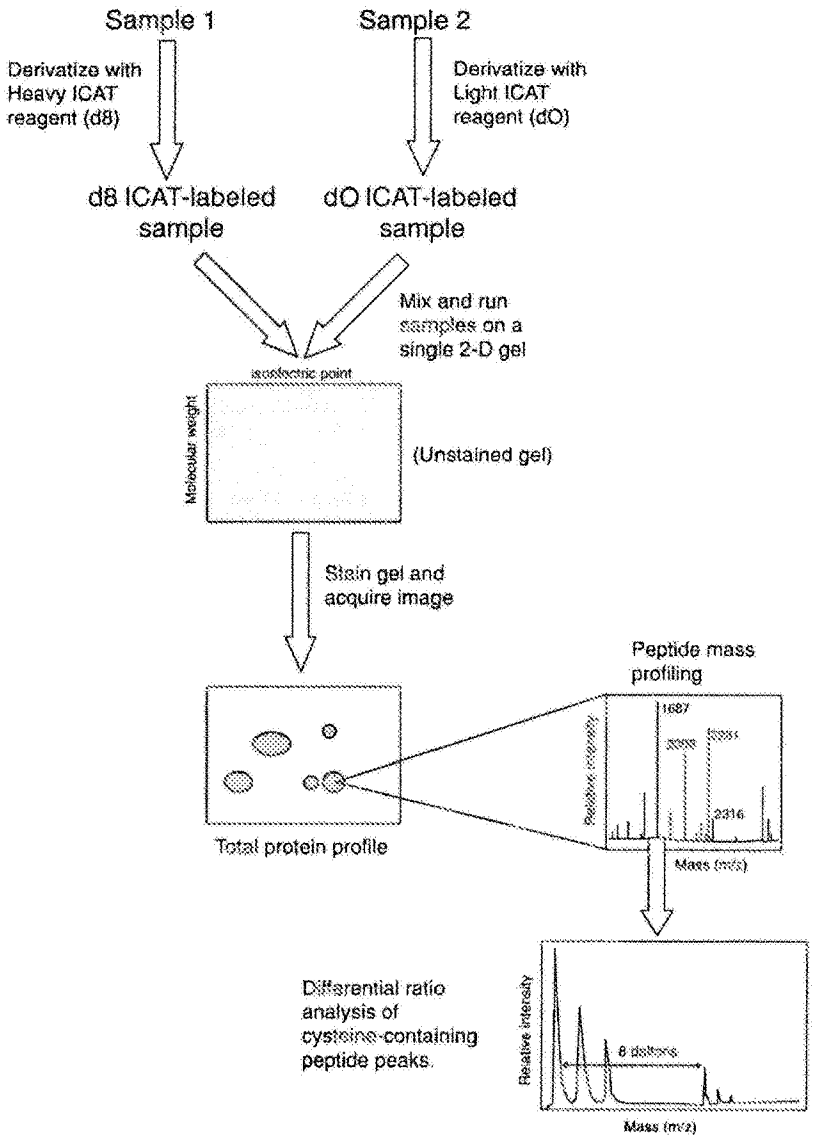

Fig. 7. Schematic illustration of the isotope-coded affinity tagging (ICAT) technology platform [194]. Two different samples are derivatized with two different ICAT reagents; heavy (deuterated) and light (normal). The samples are combined and then run on a single 2D gel. Proteins are detected using a sensitive mass spectrometry-compatible protein stain, such as modified silver stain or SYPRO Ruby protein gel stain. Proteins are excised from the gel, enzymatically digested in the gel matrix, extracted and analyzed by mass spectrometry. Proteins are identified by peptide mass fingerprinting using a single stage mass spectrometer or by collision-induced dissociation of selected peptides and database sequence searching. Differences in protein expression between individual proteins in the two samples are determined by evaluation of the ratio of signal intensities for the isotopically normal and heavy forms of a specifically tagged peptide. As illustrated, every spot in the profile must be evaluated by mass spectrometry and cysteine-containing peptides identified. Alternatively, three gels can be run containing heavy isotope-labeled material, light isotope-labeled material and a mixture of the two. The first two gels are used to generate difference maps using a sensitive protein stain and computer-based matching software. The third gel is then used to excise differences identified from the first two gels.

portant improvements. It is also quite similar to the $^{14}N/^{15}N$ labeling procedure [109]. Unlike the $^{14}N/^{15}N$ labeling scheme, the ICAT method is a post-isolation isotopic labeling approach that does not require cells to be cultured in specialized media. Proteins from two different samples are labeled with heavy and light ICAT reagents, combined and then separated by 2D gel electrophoresis. The gel-separated proteins are detected with a sensitive protein stain, excised, treated with protease and identified by peptide mass profiling. Additionally, selected peptides can be evaluated further using collision-induced dissociation (CID) and sequence database searching. As with DIGE, the ICAT labeling decreases the electrophoretic mobility of proteins, due to addition of 422 Da at every cysteine residue. Since cysteine residues are modified with a neutral ICAT group, the isoelectric point is preserved for all but the most basic proteins. While DIGE requires minimal labeling with the hydrophobic cyanine dyes, ICAT labeling must be performed quantitatively and to completion in order to avoid generating molecular mass ladders of spots with varying degrees of substitution [184,185]. This is readily accomplished using excess labeling reagent and since the ICAT reagent is relatively hydrophilic, migration problems do not arise during electrophoresis. Of course, the biotin component of the tag is superfluous in this application and smaller cysteine-reactive reagents could be employed, as long as a normal and deuterated species are used. One important application of ICAT differential display in 2D gels is for the assessment of the relative abundances of protein isoforms that arise from post-translational modification. This utilizes a similar strategy as originally employed with the $^{14}N/^{15}N$ labeling procedure [109].

6. Conclusions

The pace of technological innovations in protein detection has markedly accelerated in the past 4 years. Undoubtedly, this is partly due to a shift in the focus of the research enterprise from genomics to proteomics, spurred by the completion of the human genome project. Methods for the global analysis of protein abundance, protein post-translational modifications and changes in these two parameters as a function of the biological state of the cell or tissue are being developed utilizing electrophoresis, chromatography, and/or mass spectrometry as key components of the detection platforms. Methods for the differential display analysis of protein populations that parallel the capabilities of mRNA-based approaches are actively under development. Gel electrophoresis remains a formidable analytic tool that has found wide application in a variety of fields, ranging from toxicology, and cancer discovery research to quality control and clinical screening of samples. Though efforts to displace gel-based electrophoretic techniques with alternatives, such as solution-phase, microarray, capillary electrophoresis and microfluidic devices are underway, gel electrophoresis-based technology remains attractive due to its simplicity, reliability, higher information content and ready accessibility to researchers [204].

Acknowledgements

The author thanks Richard Haugland, Joseph Beechem, Tom Steinberg, Kiera Berggren, Courtenay Hart, Birte Schulenberg, Karen Martin, Brad Arnold, Mark Lim, Negin Shojaee and Lily Lam for numerous contributions to the development of metal chelate detection strategies over the past 8 years.

References

[1] M. Dunn, Methods Mol. Biol. 112 (1999) 313.
[2] N. Matsui, D. Smith-Beckerman, L. Epstein, Methods Mol. Biol. 112 (1999) 307.
[3] C. Merril, in: A. Chrambach, M. Dunn, B. Radola (Eds.), Advances in Electrophoresis, Vol. 1, VCH Publishers, New York, NY, 1987, p. 111.
[4] W. Patton, Biotechniques 28 (2000) 944.
[5] W. Patton, Electrophoresis 21 (2000) 1123.
[6] W. Patton, in: S. Pennington, M. Dunn (Eds.), Proteomics: From Protein Sequence To Function, BIOS Scientific Publishing, Oxford, 2001, p. 65.
[7] W. Patton, M. Lim, D. Shepro, Methods Mol. Biol. 112 (1999) 331.
[8] T. Rabilloud, Anal. Chem. 72 (2000) 48A.
[9] T. Rabilloud, Methods Mol. Biol. 112 (1999) 297.
[10] P. Wirth, A. Romano, J. Chromatogr. A 698 (1995) 123.
[11] S. Fazekas de St. Groth, R. Webster, A. Datyner, Biochim. Biophys. Acta 71 (1963) 377.

[12] V. Neuhoff, R. Stamm, H. Eibl, Electrophoresis 6 (1985) 427.
[13] R. Switzer, C. Merril, S. Shifrin, Anal. Biochem. 98 (1979) 231.
[14] B. Oakley, D. Kirsch, N. Morris, Anal. Biochem. 105 (1980) 361.
[15] C. Merril, D. Goldman, S. Sedman, M. Ebert, Science 211 (1981) 1437.
[16] M. Quadroni, P. James, Electrophoresis 20 (1999) 664.
[17] P. Sinha, M. Poland, M. Schnolzer, T. Rabilloud, Proteomics 7 (2001) 835.
[18] A. Shevchenko, M. Wilm, O. Vorm, M. Mann, Anal. Chem. 68 (1996) 850.
[19] J. Yan, R. Wait, T. Berkelman, R. Harry, J. Westbrook, C. Wheeler, M. Dunn, Electrophoresis 21 (2000) 3666.
[20] F. Gharahdaghi, C. Weinberg, D. Meagher, B. Imai, S. Mische, Electrophoresis 20 (1999) 601.
[21] A. Link, Methods Mol. Biol. 112 (1999) 285.
[22] W. Springer, in: J. Walker (Ed.), The Protein Protocols Handbook, Humana Press, Totowa, NJ, 1996, p. 161.
[23] L. Kuhn, J. Kettman, I. Lefkovits, Electrophoresis 10 (1989) 708.
[24] L. Luo, P. Wirth, Electrophoresis 14 (1993) 127.
[25] J. Westbrook, J. Yan, R. Wait, M. Dunn, Proteomics 1 (2001) 370.
[26] J. Yeargin, M. Hass, Curr. Biol. 5 (1995) 423.
[27] V. Hu, D. Heikka, P. Dieffenbach, L. Ha, FASEB J. 15 (2001) 1562.
[28] V. Hu, D. Heikka, FASEB J. 14 (2000) 448.
[29] K. Hofer, W. Hughes, Radiat. Res. 47 (1971) 94.
[30] A. Kassis, S. Adelstein, Radiat. Res. 84 (1980) 407.
[31] J. Steinberg, J. NIH Res. 8 (1996) 30.
[32] D. Hager, R. Burgess, Anal. Biochem. 109 (1980) 76.
[33] C. Lee, A. Levin, D. Branton, Anal. Biochem. 166 (1987) 308.
[34] J. Dzandu, J. Johnson, G. Wise, Anal. Biochem. 174 (1988) 157.
[35] M. Ortiz, M. Calero, C. Fernandez-Patron, C. Patron, L. Castellanos, E. Mendez, FEBS Lett. 296 (1992) 300.
[36] C. Fernandez-Patron, L. Castellanos-Serra, P. Rodriguez, Biotechniques 12 (1992) 564.
[37] L. Adams, K. Weaver, Appl. Theoret. Electrophoresis 1 (1990) 279.
[38] C. Fernandez-Patron, L. Castellanos-Serra, E. Hardy, M. Guerra, E. Estevez, E. Mehl, R. Frank, Electrophoresis 19 (1998) 2398.
[39] L. Castellanos-Serra, E. Hardy, Electrophoresis 22 (2001) 864.
[40] M. Ferreras, J. Gavilanes, J. Garcia-Segura, Anal. Biochem. 213 (1993) 206.
[41] N. Matsui, D. Smith, K. Clausner, J. Fichmann, L. Andrews, C. Sullivan, A. Burlingame, L. Epstein, Electrophoresis 18 (1997) 409.
[42] C. Fernandez-Patron, M. Calero, P. Collazo, J. Garcia, J. Madrazo, A. Musacchio, F. Soriano, R. Estrada, R. Frank, L. Castellanos-Serra, Anal. Biochem. 224 (1995) 203.
[43] E. Hardy, H. Santana, A. Sosa, L. Hernandez, C. Fernandez-Patron, L. Castellanos-Serra, Anal. Biochem. 240 (1996) 150.
[44] L. Castellanos-Serra, C. Fernandez-Patron, E. Hardy, V. Huerta, Electrophoresis 17 (1996) 1564.
[45] L. Castellanos-Serra, C. Fernandez-Patron, E. Hardy, H. Santana, V. Huerta, J. Protein Chem. 16 (1997) 415.
[46] L. Castellanos-Serra, W. Proenza, V. Huerta, R. Moritz, R. Simpson, Electrophoresis 20 (1999) 732.
[47] J. Daban, M. Samso, S. Bartolome, Anal. Biochem. 199 (1991) 162.
[48] J. Daban, S. Bartolome, M. Samso, Anal. Biochem. 199 (1991) 169.
[49] A. Bermudez, J. Daban, J. Garcia, E. Mendez, Biotechniques 16 (1994) 621.
[50] F. Alba, A. Bermudez, J. Daban, Electrophoresis 22 (2001) 399.
[51] F. Alba, J. Daban, Electrophoresis 19 (1998) 2407.
[52] T. Steinberg, L. Jones, R. Haugland, V. Singer, Anal. Biochem. 239 (1996) 223.
[53] T. Steinberg, R. Haugland, V. Singer, Anal. Biochem. 239 (1996) 238.
[54] T. Steinberg, H. White, V. Singer, Anal. Biochem. 248 (1997) 168.
[55] T. Steinberg, W. Lauber, K. Berggren, C. Kemper, S. Yue, W. Patton, Electrophoresis 21 (2000) 497.
[56] F. Alba, A. Bermudez, J. Daban, Electrophoresis 22 (2001) 399.
[57] M. Lopez, K. Berggren, E. Chernokalskaya, A. Lazarev, M. Robinson, W. Patton, Electrophoresis 21 (2000) 3673.
[58] K. Berggren, E. Chernokalskaya, T. Steinberg, C. Kemper, M. Lopez, Z. Diwu, R. Haugland, W. Patton, Electrophoresis 21 (2000) 2509.
[59] H. Akhaven-Tafti, R. DeSilva, K. Sugioka, R. Handley, A. Schaap, Luminescence 16 (2001) 187.
[60] S. Desai, B. Dworecki, E. Cichon, Anal. Biochem. 297 (2001) 94.
[61] H. Towbin, T. Staehelin, J. Gordon, Proc. Natl. Acad. Sci. USA 76 (1979) 4350.
[62] R. Ogorzalek Loo, C. Mitchell, T. Stevenson, S. Martin, W. Hines, P. Juhasz, D. Patterson, J. Peltier, J. Loo, P. Andrews, Electrophoresis 18 (1997) 382.
[63] R. Ogorzalek Loo, J. Loo, P. Andrews, Methods Mol. Biol. 112 (1999) 473.
[64] J. Loo, J. Brown, G. Critchley, C. Mitchell, P. Andrews, R. Ogorzalek Loo, Electrophoresis 20 (1999) 743.
[65] A. Walker, G. Rymar, P. Andrews, Electrophoresis 22 (2001) 933.
[66] R. Ogorzalek Loo, J. Cavalcoli, R. VanBogelon, C. Mitchell, J. Loo, B. Moldover, P. Andrews, Anal Chem. 73 (2001) 4063.
[67] T. Hutchens, T. Yip, Rapid Commun. Mass Spectrom. 7 (1993) 576.
[68] M. Merchant, S. Weinberger, Electrophoresis 21 (2000) 1164.
[69] F. Von Eggeling, K. Junker, W. Fiedler, V. Wollscheid, M. Durst, U. Claussen, G. Ernst, Electrophoresis 22 (2001) 2898.
[70] A. Abbott, Nature 402 (1999) 715.
[71] M. Larsen, P. Roepstorff, Fresenius J. Anal Chem. 366 (2000) 677.

[72] J. Dennis, M. Granovsky, C. Warren, Biochim. Biophys. Acta 1473 (1999) 21.
[73] A. Litynska, M. Przybylo, D. Ksiazek, P. Laidler, Acta Biochim. Pol. 47 (2000) 427.
[74] S. Hakomori, Cancer Res. 56 (1996) 5309.
[75] A. Kobata, Glycoconjugate J. 15 (1998) 323.
[76] D. Ivanov, M. Antonova, J. Stoilov, S. Zacharieva, E. Gavazova, S. Ivanov, Cancer Lett. 125 (1998) 227.
[77] M. Bramwell, J. Cell Sci. 88 (1987) 335.
[78] N. Chandra, M. Spiro, R. Spiro, J. Biol. Chem. 273 (1998) 19715.
[79] R. Zacharius, T. Zell, J. Morrison, J. Woodlock, Anal. Biochem. 30 (1969) 148.
[80] P. Devine, J. Warren, Biotechniques 8 (1990) 493.
[81] A. Wardi, W. Allen, Anal. Biochem. 48 (1972) 621.
[82] A. Wardi, G. Michos, Anal. Biochem. 49 (1972) 607.
[83] A. Eckhardt, C. Hayes, I. Goldstein, Anal. Biochem. 73 (1976) 192.
[84] F. Che, J. Song, L. Yu, K. Wang, Q. Xia, Biotechniques 30 (2001) 1272.
[85] T. Steinberg, K. Pretty On Top, K. Berggren, C. Kemper, L. Jones, Z. Diwu, R. Haugland, W. Patton, Proteomics 1 (2001) 841.
[86] N. Packer, L. Keatinge, in: S. Pennington, M. Dunn (Eds.), Proteomics; From Protein Sequence To Function, BIOS Scientific Publishers, Oxford, 2001, p. 257.
[87] I. Bouchez-Mahiout, C. Doyen, M. Lauriere, Electrophoresis 20 (1999) 1412.
[88] D. O'Shannessy, P. Voorstad, R. Quarles, Anal. Biochem. 163 (1987) 204.
[89] E. Bayer, H. Ben-Hur, M. Wilchek, Anal. Biochem. 161 (1987) 123.
[90] K. Anumula, P. Du, Anal. Biochem. 275 (1999) 236.
[91] E. Zdebska, J. Koscielak, Anal. Biochem. 275 (1999) 171.
[92] D. Stern, Exp. Mol. Pathol. 70 (2001) 327.
[93] N. Ahn, K. Resing, Nat. Biotechnol. 19 (2001) 317.
[94] D. Grander, Med. Oncol. 15 (1998) 20.
[95] R. Weinberg, in: J. Brugge, T. Curran, F. McCormick (Eds.), Origins of Human Cancer; A Comprehensive Review, Cold Spring Harbor Laboratory Press, Cold Spring Harbor, NY, 1991, p. 1.
[96] C. Tsatsanis, D. Spandidos, Int. J. Mol. Med. 5 (2000) 583.
[97] S. Saha, A. Bardelli, P. Buckhaults, V. Velculescu, C. Rago, B. St. Croix, K. Romans, M. Choti, C. Lengauer, K. Kinzler, B. Vogelstein, Science 294 (2001) 1343.
[98] G. Guy, R. Phillip, Y. Tan, Electrophoresis 15 (1994) 417.
[99] D. Moore, B. Sefton, in: Current Protocols in Molecular Biology, Vol. 3, Wiley, New York, 1995, p. 18.0.3.
[100] H. Kaufmann, J. Bailey, M. Fussenegger, Proteomics 1 (2001) 194.
[101] A. Dahlberg, C. Dingman, A. Peacock, J. Mol. Biol. 41 (1969) 139.
[102] M. Green, J. Pastewka, A. Peacock, Anal. Biochem. 56 (1973) 43.
[103] J. Cutting, T. Roth, Anal. Biochem. 54 (1973) 386.
[104] I. Debruyne, Anal. Biochem. 133 (1983) 110.
[105] M. Brauer, B. Sykes, Methods Enzymol. 107 (1984) 36.
[106] K. Swiderek, K. Jaquet, H. Meyer, C. Schachtele, F. Hofmann, L. Heilmeyer, Eur. J. Biochem. 190 (1990) 575.
[107] M. Affolter, J. Watts, D. Krebs, R. Aebersold, Anal. Biochem. 223 (1994) 74.
[108] P. Liao, J. Leykam, P. Andrews, D. Gage, J. Allison, Anal. Biochem. 219 (1994) 9.
[109] Y. Oda, K. Huang, F. Cross, D. Cowburn, B. Chait, Proc. Natl. Acad. Sci. USA 96 (1999) 6591.
[110] R. Aebersold, J. Watts, H. Morrison, E. Bures, Anal. Biochem. 199 (1991) 51.
[111] M. Goshe, T. Conrads, E. Panisko, N. Angell, T. Veenstra, R. Smith, Anal. Chem. 73 (2001) 2578.
[112] H. Zhou, J. Watts, R. Aebersold, Nat. Biotechnol. 19 (2001) 375.
[113] Y. Oda, T. Nagasu, B. Chait, Nat. Biotechnol. 19 (2001) 379.
[114] P. Fadden, T. Haystead, Anal. Biochem. 225 (1995) 81.
[115] K. Hsi, S. O'Neill, D. Dupont, P. Yuan, Anal. Biochem 258 (1998) 38.
[116] G. Manchenko, in: Handbook of Detection of Enzymes On Electrophoretic Gels, CRC Press, Boca Raton, FL, 1994, p. 259.
[117] R. Beynon, J. Bond, in: Proteolytic Enzymes, A Practical Approach, IRL Press, Oxford, England, 1989, p. 25.
[118] D. Greenbaum, A. Baruch, L. Hayrapetian, Z. Darula, A. Burlingame, K. Medzihradszky, M. Bogyo, Molecular and Cellular Proteomics. Papers in Press. Published 11 September 2001 as Manuscript T100003-MCP200.
[119] J. Stamler, O. Jaraki, J. Osborne, D. Simon, J. Keaney, J. Vita, D. Singel, R. Valeri, J. Loscalzo, Proc. Natl. Acad. Sci. USA 89 (1992) 7674.
[120] P. Lane, G. Hao, S. Gross, Science's STKE (2001) http://stke.sciencemag.org/cgi/content/full/OC_sigtrans;2001/86/re1
[121] J. Hoffmann, J. Haendeler, A. Zeiher, S. Dimmeler, J. Biol. Chem. 276 (2001) 41383.
[122] S. Jaffrey, S. Snyder, Science's STKE (2001) http://stke.sciencemag.org/cgi/content/full/OC_sigtrans;2001/86/pl1.5.
[123] W. Paik, S. Kim, J. Biol. Chem. 243 (1968) 2108.
[124] A. Niewmierzycka, S. Clarke, J. Biol. Chem. 274 (1999) 814.
[125] A. McBride, V. Weiss, H. Kim, J. Hogle, P. Silver, J. Biol. Chem. 275 (2000) 3128.
[126] J. Smith, K. Rucknagel, A. Schierhorn, J. Tang, A. Nemeth, M. Linder, H. Herschman, E. Wahle, J. Biol. Chem. 274 (1999) 13229.
[127] S. Klein, J. Carroll, Y. Chen, M. Henry, P. Henry, I Ortonowski, G. Pintucci, R. Beavis, W. Burgess, D. Rifkin, J. Biol. Chem. 275 (2000) 3150.
[128] P. Zobel-Thropp, J. Gary, S. Clarke, J. Biol. Chem. 273 (1998) 29283.
[129] K. Mowen, M. David, Science's STKE 2001 http://stke.sciencemag.org/cgi/content/full/OC_sigtrans;2001/93/pl1
[130] Q. Liu, G. Dreyfuss, Mol. Cell. Biol. 15 (1995) 2800.
[131] R. Desrosiers, R. Tanguay, J. Biol. Chem. 263 (1988) 4686.
[132] L. Belyanskaya, P. Gehrig, H. Gehring, J. Biol. Chem. 276 (2001) 18681.
[133] B. Schurter, S. Koh, D. Chen, G. Bunick, J. Harp, B. Hanson, A. Henschen-Edman, D. Mackay, M. Stallcup, D. Aswad, Biochemistry 40 (2001) 5747.

[134] B. Strahl, S. Briggs, C. Brane, J. Caldwell, S. Koh, H. Ma, R. Cook, J. Shabanowitz, D. Hunt, M. Stallcup, C. Allis, Curr. Biol. 11 (2001) 996.
[135] B. Weng, W. Thompson, H. Kim, R. Levine, J. Moss, J. Biol. Chem. 274 (1999) 31797.
[136] M. Cohen-Armon, I. Hammel, Y. Anis, S. Homburg, D. Noya, J. Biol. Chem. 271 (1996) 26200.
[137] P. Randazzo, Z. Nie, K. Miura, V. Hsu, Science's STKE 2000 http://stke.sciencemag.org/cgi/content/full/OC_sigtrans;2000/59/re1
[138] S. Prasad, J. Walent, A. Dritschilo, Biochem. Biophys. Res. Commun. 204 (1994) 772.
[139] M. Di Gorolamo, M. Silletta, M. De Matteis, A. Braca, A. Colanzi, D. Pawlak, M. Rasenick, A. Luini, D. Corda, Proc. Natl. Acad. Sci. USA 92 (1995) 7065.
[140] L. Ronnov-Jessen, O. Petersen, Electrophoresis 17 (1996) 1776.
[141] H. Phan, C. Boissard, M. Pessah, K. Regnauld, S. Emani, C. Gespach, G. Rosselin, Biochem. Biophys. Res. Commun. 271 (2000) 86.
[142] G. Fritz, I. Just, B. Kaina, Int. J. Cancer 81 (1999) 682.
[143] T. Meyer, H. Hilz, Eur. J. Biochem. 155 (1986) 157.
[144] A. Giovane, C. Balestrieri, L. Quagliuolo, L. Servillo, FEBS Lett. 191 (1985) 191.
[145] V. Hingorani, Y. Ho, J. Biol. Chem. 263 (1988) 19804.
[146] B. Klebl, D. Pette, Anal. Biochem. 239 (1996) 145.
[147] C. Kemper, T. Steinberg, L. Jones, W. Patton, Electrophoresis 22 (2001) 970.
[148] S.-M. Yu, Y.-H. Kuo, G. Sheu, Y.-J. Sheu, L.-F. Liu, J. Biol. Chem. 266 (1991) 21131.
[149] S. Ho, W. Tong, S. Yu, Plant Physiol. 122 (2000) 57.
[150] K. Yoshida, N. Iino, I. Koga, K. Kato, Anal. Biochem. 58 (1974) 77.
[151] D. Starkey, A. Han, J. Bao, C. Ahn, K. Wehmeyer, M. Prenger, H. Halsall, W. Heineman, J. Chromatogr. B. Biomed. Sci. Appl. 762 (2001) 33.
[152] D. Nazarenko, S. Dertinger, T. Gasiewicz, Biotechniques 30 (2001) 776.
[153] R. Duncan, J. Hewitt, P. Weston, Biochem. J. 205 (1982) 219.
[154] B. Burke, F. Regnier, Electrophoresis 22 (2001) 3744.
[155] M. Eggertson, D. Craig, Biomed. Chromatogr. 13 (1999) 516.
[156] A. James, K. Chilvers, J. Perry, L. Armstrong, F. Gould, Appl. Environ. Microbiol. 66 (2000) 5521.
[157] A. James, J. Perry, K. Chilvers, I. Robson, L. Armstrong, K. Orr, Lett. Appl. Microbiol. 30 (2000) 336.
[158] M. Ho, S. Povey, D. Swallow, Am. J. Hum. Genet. 34 (1982) 650.
[159] R. Evangelista, A. Pollak, E. Templeton, Anal. Biochem. 197 (1991) 213.
[160] E. Hochuli, S. Piesecki, Methods 4 (1992) 68.
[161] D. O'Shannessy, K. O'Donnell, J. Martin, M. Brigham-Burke, Anal. Biochem. 229 (1995) 119.
[162] S. McMahan, R. Burgess, Anal. Biochem. 236 (1996) 101.
[163] C. Botting, R. Randall, Biotechniques 19 (1995) 362.
[164] L. Jin, X. Wei, J. Gomez, M. Datta, A. Birkett, D. Peterson, Anal. Biochem. 229 (1995) 54.
[165] J. Hainfeld, W. Liu, C. Halsey, P. Freimuth, R. Powell, J. Struct. Biol. 127 (1999) 185.
[166] H. Zentgraf, M. Frey, S. Schwinn, C. Tessmer, B. Willemann, Y. Samstag, I. Velhagen, Nucleic Acids Res. 23 (1995) 3347.
[167] E. Pogge von Strandmann, C. Zoidl, H. Nakhei, B. Holewa, R. Pogge von Strandmann, P. Lorenz, L. Klein-Hitpass, G. Ryffel, Protein Eng. 8 (1995) 733.
[168] P. Lindner, B. Guth, C. Wulfing, C. Krebber, B. Steipe, F. Muller, A. Pluckthun, Methods 4 (1992) 41.
[169] M. Chalfie, Y. Tu, G. Euskirchen, W. Ward, D. Prasher, Science 263 (1994) 802.
[170] V. Hatzimanikatis, L. Choe, K. Lee, Biotechnol. Prog. 15 (1999) 312.
[171] Y. Li, A. Agrawal, J. Sakon, R. Beitle, J. Chromatogr. A 909 (2001) 183.
[172] S. Ericksson, E. Raivio, J. Kukkonen, K. Eriksson, C. Lindqvist, J. Virol. Methods 59 (1996) 127.
[173] D. Richards, C. Stathakis, R. Polakowski, H. Ahmadzadeh, N. Dovichi, J. Chromatogr. A 853 (1999) 21.
[174] C. Gordon, V. Khalaj, A. Ram, D. Archer, J. Brookman, A. Trinci, D. Jeenes, J. Doonan, B. Wells, P. Punt, C. van den Hondel, G. Robson, Microbiology 146 (2000) 415.
[175] C. Nemetz, R. Reichhuber, R. Schweizer, P. Hloch, M. Watzele, Electrophoresis 22 (2001) 966.
[176] N. Garameszegi, Z. Garameszegi, M. Rogers, S. DeMarco, E. Strehler, Biotechniques 23 (1997) 864.
[177] S. Kiessig, J. Reissmann, C. Rascher, G. Kullertz, A. Fischer, F. Thunecke, Electrophoresis 22 (2001) 1428.
[178] T. Aoki, Y. Takahashi, K. Koch, H. Leffert, H. Watanabe, FEBS Lett. 384 (1996) 193.
[179] T. Aoki, M. Miyashita, H. Fujino, H. Watanabe, Biosci. Biotechnol. Biochem. 64 (2000) 1547.
[180] M. Unlu, M. Morgan, J. Minden, Electrophoresis 18 (1997) 2071.
[181] R. Tonge, J. Shaw, B. Middleton, R. Rowlinson, S. Rayner, J. Young, F. Pognan, E. Hawkins, I. Currie, M. Davison, Proteomics 1 (2001) 377.
[182] F. Von Eggeling, A. Gawriljuk, W. Fiedler, G. Ernst, U. Claussen, J. Klose, I. Romer, Int. J. Mol. Med. 8 (2001) 373.
[183] S. Gharbi, P. Gaffney, A. Yang, M. Zvelebil, R. Cramer, M. Waterfield, J. Timms, Mol. Cell. Prot. (2002) in press.
[184] G. Zhou, H. Li, D. DeCamp, S. Chen, H. Shu, Y. Gong, M. Flaig, J. Gillespie, N. Hu, P. Taylor, M. Emmert-Buck, L. Liotta, E. Petricoin, Y. Zhao, Mol. Cell. Prot. (2002) in press.
[185] J. Minden, A. Waggoner (2000), US patent 6,043,025.
[186] F. Kernec, M. Unlu, W. Labeikovsky, J. Minden, A. Koretsky, Physiol. Genomics 6 (2001) 117.
[187] A. de Groof, F. Oerlemans, C. Jost, B. Wieringa, Muscle Nerve 24 (2001) 1188.
[188] K. Saupe, M. Spindler, J. Hopkins, W. Shen, J. Ingwall, J. Biol. Chem 275 (2000) 19742.
[189] V. Veksler, A. Kuznetsov, K. Anflous, P. Mateo, J. van Deursen, B. Wieringa, R. Ventura-Clapier, J. Biol. Chem. 270 (1995) 19921.

[190] Z. Smilansky, Electrophoresis 22 (2001) 1616.
[191] K. Gee, H. Kang, T. Meier, G. Zhao, L. Blaszcak, Electrophoresis 22 (2001) 960.
[192] S. Gygi, B. Rist, S. Gerber, F. Turecek, M. Gelb, R. Aebersold, Nat. Biotechnol. 17 (1999) 994.
[193] R. Aebersold, B. Rist, S. Gygi, Ann. NY Acad. Sci. 919 (2000) 33.
[194] M. Smolka, H. Zhou, R. Aebersold, Mol. Cell. Proteomics. (2002) in press.
[195] M. Smolka, H. Zhou, S. Purkayastha, R. Aebersold, Anal. Biochem. 297 (2001) 25.
[196] M. Moseley, Trends Biotechnol. 19 (2001) S10.
[197] R. Zhang, C. Sioma, S. Wang, F. Regnier, Anal. Chem. 73 (2001) 5142.
[198] P. Haynes, J. Yates, Yeast 17 (2000) 81.
[199] D. Han, J. Eng, H. Zhou, R. Aebersold, Nat. Biotechnol. 19 (2001) 946.
[200] K. Berggren, E. Chernokalskaya, M. Lopez, J. Beechem, W. Patton, Proteomics 1 (2001) 54.
[201] C. Henry, Chem. Eng. News 2 (2001) 47.
[202] J. Ji, A. Chakraborty, M. Geng, X. Zhang, A. Amini, M. Bina, F. Regnier, J. Chromatogr. B 745 (2000) 197.
[203] D. Goodlett, A. Keller, J. Watts, R. Newitt, E. Yi, S. Purvine, J. Eng, P. von Haller, R. Aebersold, E. Kolker, Rapid Commun. Mass. Spectrom. 15 (2001) 1214.
[204] J. Hille, A. Freed, H. Watzig, Electrophoresis 22 (2001) 4035.

Liposomal irinotecan vs topotecan in patients with small cell lung cancer who have progressed on/after platinum-based therapy

Luis G. Paz-Ares,[1] James Chih-Hsin Yang,[2] Christoph Zielinski,[3] Silvia Novello,[4] Gilberto Schwartsmann,[5] David Spigel,[6] Frank Griesinger,[7] Afshin Dowlati,[8] Tania Small,[9] Floris A. de Jong,[10] Bin Zhang,[9] Natalya Nazarenko,[9] Paul Bunn[11]

[1]Hospital Universitario 12 de Octubre, Madrid, Spain; [2]National Taiwan University Hospital and National Taiwan University Cancer Center, Taipei, Republic of China; [3]Comprehensive Cancer Centre, Medical University Vienna - General Hospital, Vienna, Austria; [4]Oncology Department, University of Turin, AOU San Luigi, Orbassano, Italy; [5]Hospital de Clínicas de Porto Alegre, Porto Alegre, Brazil; [6]Sarah Cannon Research Institute, Nashville, TN, United States; [7]Lung Cancer Network NOWEL, Oldenburg, Germany; Pius Hospital, Medical Campus, University of Oldenburg, Oldenburg, Germany; [8]University Hospitals Cleveland Medical Center, Cleveland, OH, United States; [9]Ipsen Bioscience, Boston, MA, United States; [10]Servier, Zürich, Switzerland; [11]University of Colorado, Cancer Center and Department of Medicine, Denver, CO, United States

BACKGROUND

- Small cell lung cancer (SCLC) is an aggressive disease marked by rapid growth and early metastasis and accounts for some 15% of all lung cancers worldwide.[1,2]
- In the United States, Europe, and Asia, first-line therapy for extensive-stage SCLC is typically a combination of a platinum-based therapy (carboplatin or cisplatin) plus etoposide.[3,4]
  - Patients usually demonstrate initial sensitivity to chemotherapy and radiotherapy, followed by rapid relapse and development of drug resistance.[4,5]
- Topoisomerase I (TOP1) is a validated drug target in SCLC and is the target of topotecan, which is approved for second-line treatment of SCLC in the United States, Europe, and Asia.[3,4,6-8]
- Liposomal irinotecan (nal-IRI) is a TOP1 inhibitor approved for the treatment of mPDAC following gemcitabine-based therapy and is currently being investigated for the treatment of other solid tumors (Figure 1).
  - SN-38, the active metabolite of nal-IRI, is known to target TOP1.
  - nal-IRI was designed to utilize the enhanced permeability and retention effect to achieve liposomal deposition in tumor tissue followed by local irinotecan release and subsequent conversion to the active metabolite SN-38 mediated by macrophage carboxylesterases.[9,10]

Presented at the 19th World Conference on Lung Cancer | Toronto, Canada | September 23-26, 2018

Figure 1. Liposomal structure of nal-IRI

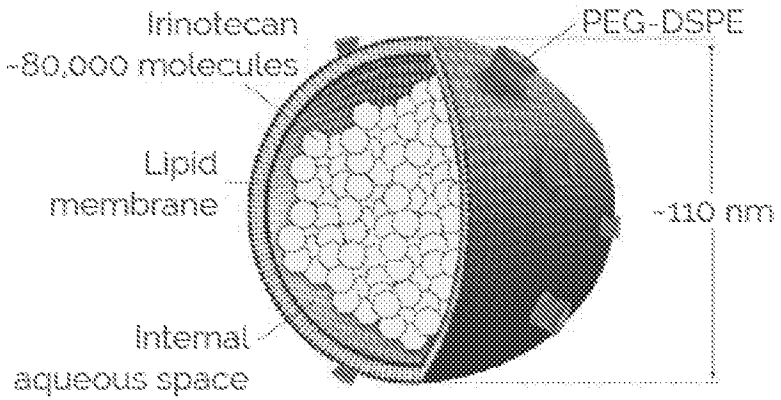

Mechanism of action/delivery: liposomal irinotecan

- The mechanism of action of nal-IRI comprises extended plasma circulation of irinotecan while remaining encapsulated in the stable liposome, deposition into tumor tissue via the vasculature, uptake by phagocytic cells, release of irinotecan and subsequent conversion to the active metabolite SN-38 mediated by macrophage carboxylesterases.[11]
  - Pharmacokinetic analyses have demonstrated prolonged circulation of the irinotecan-containing liposome and sustained TOP1 inhibition.[10,12,13]
  - Sustained tumor-derived SN-38 delivery by nal-IRI injection leads to sustained TOP1 inhibition, resulting in subsequent DNA damage and tumor cell death.[11,13]

Rationale for evaluating nal-IRI in SCLC

- The rationale for testing nal-IRI in patients with SCLC is based on:
  - Identification of a valid SCLC drug target (TOP1) for therapeutic intervention
  - Supportive nonclinical data
  - The concordance between SCLC biology and the proposed nal-IRI mechanism of action
  - Prior clinical data for irinotecan HCl in SCLC and other indications

- Based on these factors, nal-IRI has the potential to improve upon the clinical activity of both topotecan and irinotecan HCl.
  - In SCLC models, nal-IRI was deposited in tumors and delivered irinotecan to tumors to a similar or greater extent than other tumor types and resulted in therapeutically relevant levels of tumor SN-38.[13,14]
  - nal-IRI demonstrated anti-tumor activity in multiple xenograft models of SCLC at clinically relevant dose levels and, importantly, demonstrated greater anti-tumor activity than irinotecan HCl and topotecan.[14]
  - nal-IRI demonstrated greater anti-tumor activity than irinotecan HCl and topotecan in a model of second-line SCLC following tumor progression on prior carboplatin plus etoposide (Figure 2).[14]

Figure 2. Anti-tumor activity of nal-IRI, irinotecan HCl, and topotecan in a preclinical model of second-line SCLC[14]

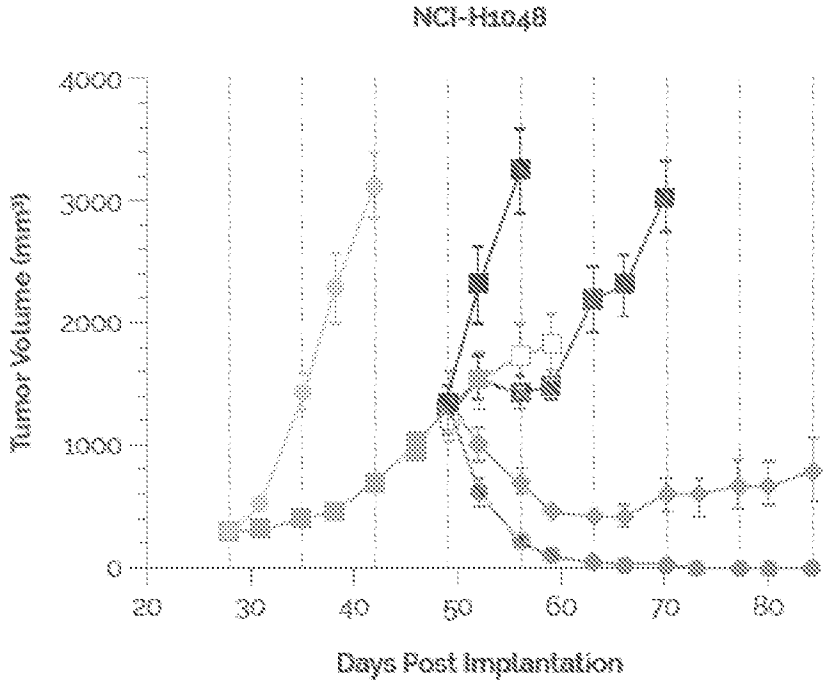

NOD/SCID mice with NCI-H1048 SCLC xenograft tumors were treated weekly with the combination of 30 mg/kg carboplatin plus 25 mg/kg etoposide. When tumors reached approximately 1200 mm³, mice were randomized to receive weekly treatment with topotecan (1.66 mg/kg/wk administered IP in equal fractions on days 1 and 2), irinotecan HCl (33 mg/kg/wk administered IV on day 1), nal-IRI (16 mg/kg/wk administered IV on day 1), or continue treatment with carboplatin plus etoposide or vehicle control. Vertical dotted lines indicate start of weekly dosing. nal-IRI dose is shown on irinotecan HCl basis. After tumors progressed on first-line treatment with carboplatin plus etoposide, nal-IRI displayed significant anti-tumor activity compared to topotecan and irinotecan HCl ($p<0.0002$ on day 70 and $p<0.0002$ on day 84 for topotecan and irinotecan HCl, respectively). NOD/SCID, non-obese diabetic/severe combined immunodeficiency; SCLC, small cell lung cancer.

STUDY OBJECTIVES

- The current trial (RESILIENT; *ClinicalTrials.gov* identifier: NCT03088813) is being undertaken to investigate the safety and efficacy of nal-IRI versus topotecan in patients with SCLC who have progressed on or after platinum-based first-line therapy.

STUDY DESIGN

- There are 2 parts to the RESILIENT study (Figure 3).
  - Part 1: open-label, single-arm, safety run-in phase
    - Safety Run-in Objectives
      - Describe the safety, tolerability, and preliminary efficacy of nal-IRI monotherapy administered every 2 weeks (Q2W)
      - Determine the nal-IRI monotherapy dose for Part 2 of this study
  - Part 2: randomized, active-controlled, efficacy-assessment phase
    - Main Study Objectives
      - Compare the efficacy and safety profiles following treatment with either nal-IRI or topotecan

Figure 3. Study design for RESILIENT parts 1 and 2

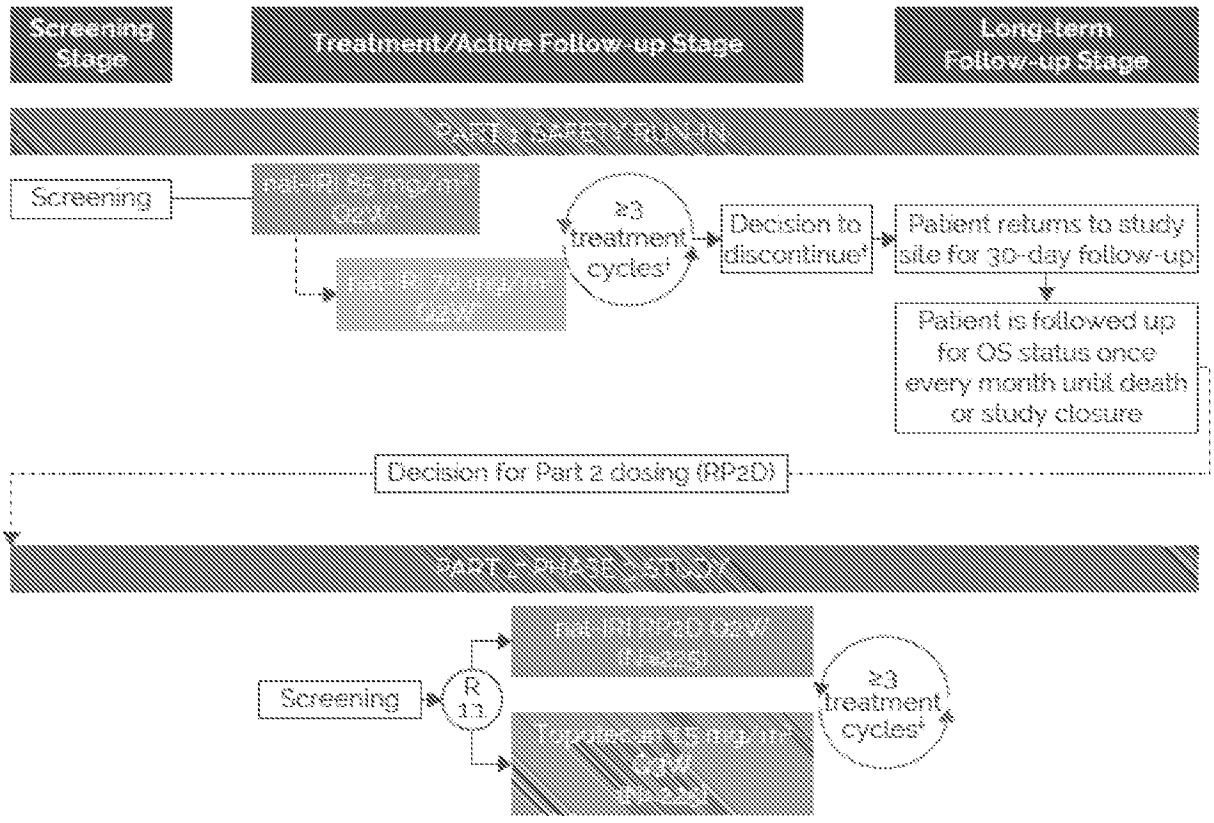

[1]Up to 12 patients per dose level of liposomal irinotecan may be treated at either 85 mg/m² or 70 mg/m², one of these two dose levels will subsequently be expanded to a total of 24 patients. [1]1 cycle = 6 weeks. [2]Decision to discontinue may occur earlier in case of toxicity.
nal-IRI, liposomal irinotecan; OS, overall survival; Q2W, every 2 weeks; Q3W, every 3 weeks; R, randomization; RP2D, recommended Part 2 dosing. All dosing based on free base dose expression.

- Part 1 is the safety run-in phase, during which patients will be treated with different doses of nal-IRI to identify a tolerable dose level (Figure 4).
  - nal-IRI will be administered intravenously at a dose of 85 mg/m² (free base; 100 mg/m² HCl salt) over 90 minutes every 2 weeks in a 6-week cycle.
  - A dose level of 70 mg/m² (free base; 80 mg/m² HCl salt) over 90 minutes every 2 weeks in a 6-week cycle will be utilized as a low-dose cohort contingency should nal-IRI 85 mg/m² be deemed to have unacceptable toxicity.
  - The safety assessment and the corresponding expansion will be conducted according to a "6+6" design followed by enrollment of an additional 12 patients.

Figure 4. Part 1 safety run-in treatment cohorts

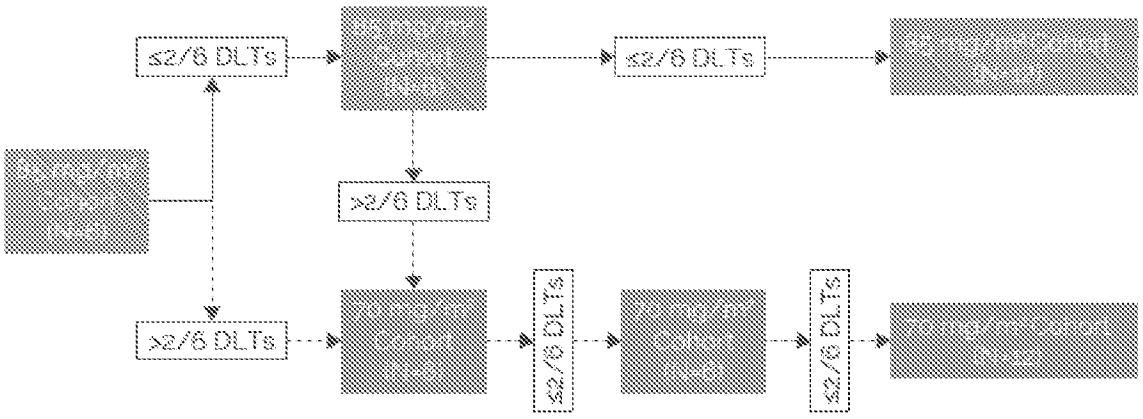

DLT, dose-limiting toxicity.

- In Part 2, ~450 patients will be randomized in a 1:1 ratio between nal-IRI and topotecan.
  - nal-IRI will be administered intravenously at the dose determined from Part 1.
  - Topotecan will be administered intravenously at an initial dose of 1.5 mg/m² over 30 minutes daily for 5 consecutive days, every 3 weeks (Q3W) in a 6-week cycle.
  - Follow-up will continue until at least 350 OS events are observed across the 2 treatment arms, providing at least 85% power to detect a true hazard ratio of HR ≤0.714 (median OS: 7.5 vs 10.5 months) using a stratified log-rank test with overall 1-sided significance level of 0.025.
- For both parts, patients will be treated for a minimum of 3 cycles (1 cycle = 6 weeks) or until progressive disease or unacceptable toxicity.
  - Up to 2 dose reductions of nal-IRI or topotecan per patient are permitted to manage treatment-associated toxicities.
  - Dose delays are permitted to allow recovery from treatment-associated toxicities.
  - 1 cycle = 6 weeks and includes 2 administrations of topotecan or 3 administrations of nal-IRI. In the event of dose delay, the cycle may extend beyond 6 weeks.
  - Tumor assessment will occur every 6 weeks after the first dose of study drug regardless if the subsequent dose is delayed or interrupted.

PATIENT ELIGIBILITY CRITERIA

- Key inclusion criteria:
  - Adults (≥18 years)
  - Eastern Cooperative Oncology Group performance status of 0 or 1
  - Life expectancy ≥12 weeks
  - Histopathologically/cytologically confirmed SCLC
  - Evaluable disease (RECIST v1.1)
  - Adequate bone marrow reserves and renal/hepatic function
  - *Prior exposure to immuno-oncology therapies is allowed*
- Key exclusion criteria:
  - Diagnosis of large cell neuroendocrine lung carcinoma
  - Prior treatment regimens with TOP1 inhibitors
  - Re-treatment with platinum-based regimens after relapse of first-line platinum-containing therapy.

STUDY ENDPOINTS

	Part 1: Safety Run-in	Part 2: Phase 3 Study
Primary Endpoint	Safety and tolerability	Overall survival
Secondary Endpoints	Objective response rate* Progression-free survival* Overall survival	Objective response rate* Progression-free survival* Patient-reported outcomes Safety
Exploratory Endpoints	Biomarker assessments Pharmacokinetics Patient-reported outcomes	Biomarker assessments Pharmacokinetics Additional patient-reported outcomes

*Tumor assessment will occur at screening and every 6 weeks (± 1 week) from the first day of cycle 1 according to Response Evaluation Criteria In Solid Tumors (RECIST) version 1.1, as assessed by the investigator.

Current status of enrollment

- Enrollment for the RESILIENT trial Part 1 (safety run-in) opened in April 2018.
- Recruitment is ongoing in the United States, Australia, France, Spain, and Taiwan, with additional countries to be added for part 2 (Phase 3); ~137 sites are expected to participate.
- Target enrollment is ~486 patients, with an overall duration of the entire study anticipated to be ~5 years.

References

1. van Meerbeeck JP. *Lancet*. 2011. 2. Govindan R. *J Clin Oncol*. 2006. 3. Morabito A. *Crit Rev Oncol Hematol*. 2014. 4. Fruh M. *Ann Oncol*. 2013. 5. Simon GR. *Chest*. 2007. 6. Ardizzoni A. *J Clin Oncol*. 1997. 7. von Pawel J. *J Clin Oncol*. 1999. 8. O'Brien ME. *J Clin Oncol*. 2006. 9. Bertrand N. *Adv Drug Deliv Rev*. 2014. 10. Drummond DC. *Cancer Res*. 2006. 11. Kalra AV. *Cancer Res*. 2014. 12. Roy AC. *Ann Oncol*. 2013. 13. Ramanathan RK. *Clin Cancer Res*. 2017. 14. Leonard SC. *Anticancer Drugs*. 2017.

Author Contributions

LGPA, JCHY, CZ, SN, GS, DS, FG, AD, TS, FAdJ, BZ, NN, PB: made substantial contributions to study conception/design, drafting of the abstract and poster, or revising it critically for important intellectual content, and provided final approval of this poster presentation.

Disclosures

LGPA: Holder Honoraria: AstraZeneca, Boehringer Ingelheim, Bristol-Myers Squibb, Lilly, MSD, Roche. **JCHY:** Speakers/Advisory Board: Boehringer Ingelheim, Eli Lilly, Bayer, Roche/Genentech/Chugai, Astellas, MSD, Merck Serono, Pfizer, Novartis, Clovis Oncology, Celgene, Merrimack, Yuhan Pharmaceuticals, BMS, Ono Pharmaceutical, Daiichi Sankyo, AstraZeneca, Hansoh Pharmaceuticals. Honoraria: Boehringer Ingelheim, Eli Lilly, Bayer, Roche/Genentech/Chugai, Astellas, MSD, Merck Serono, Pfizer, Novartis, Clovis Oncology, Celgene, Merrimack, Yuhan Pharmaceuticals, BMS, Ono Pharmaceutical, Daiichi Sankyo, AstraZeneca, Hansoh Pharmaceuticals. **CZ:** Speakers/Advisory Board: Roche, Novartis, MSD, BMS, Merck KgA, ARIAD, Boehringer Ingelheim, Imugene, Fibrogen, AstraZeneca. **SN:** Speakers Bureau: AstraZeneca, MSD, Bristol-Myers Squibb, Roche, Pfizer, Eli Lilly. **GS:** Nothing to disclose. **DS:** Consultant: Genentech/Roche, Celgene, Bristol-Myers Squibb, Lilly, AstraZeneca, Pfizer, Clovis Oncology, Novartis, Boehringer Ingelheim. Grants/Research Support: Genentech/Roche, Novartis, Celgene, Bristol-Myers Squibb, Lilly, AstraZeneca, Pfizer, Clovis Oncology, Boehringer Ingelheim, Peregrine Pharmaceuticals, Oncogenex, OncoMed, Amgen, Veraclem, Daiichi Sankyo, University of Texas Southwestern Medical Center- Simmons Cancer Center, Merck. Other: Bristol-Myers Squibb. **FG:** Consultant: ARIAD, AstraZeneca, Boehringer Ingelheim, Bristol-Myers Squibb, Celgene, Clovis, Lilly, MSD, Novartis, Pfizer, Roche Pharma AG. Other: Roche, AstraZeneca, Lilly, BMS, MSD, Celgene, Boehringer, Pfizer, Novartis, Clovis. Grants/Research Support: Roche, AstraZeneca, Lilly, BMS, MSD, Celgene, Boehringer, Pfizer, Novartis. **AD:** Consulting or Advisory Role: Abbvie/Stemcentrx, ARIAD. Research Funding: Amgen (Inst), Bristol-Myers Squibb (Inst), EMD Serono (Inst), Lilly/ImClone (Inst), MedImmune (Inst), OncoMed (Inst). **TS:** Employment: Novartis. Stock/Other ownership interests: Novartis. Research funding: Novartis. Travel, Accommodations, Expenses: Novartis. **FdJ:** Employment: Servier. Stock/Other ownership interests: Amgen, Shire. **BZ and NN:** Employment: Ipsen. **PB:** Consultant: AZ, BMS, Genentech, Lilly, Pfizer, Merck, Novartis, Merrimack, Daiichi. Other: AstraZeneca, Bristol-Myers Squibb, Genentech, Merck, Pfizer.

Medical Writing Support

The authors thank Susan Martin, PhD, of The Medicine Group, New Hope, PA, US, for providing medical writing support, which was funded by Ipsen Biopharmaceuticals, Inc., Basking Ridge, NJ, US, in accordance with Good Publication Practice guidelines.

Acknowledgements

The authors thank all patients involved in the study, as well as their caregivers, care teams, investigators, and research staff in participating institutions.

RESILIENT: study of irinotecan liposome injection (nal-IRI) in patients with small cell lung cancer: preliminary findings from part 1 dose-defining phase

Luis G Paz-Ares,[1] David R Spigel,[2] Christoph Zielinski,[3] Yuanbin Chen,[4] Maria Jove,[5] Oscar Juan-Vidal,[6] David Chu,[7] Patricia Rich,[8] Theresa Hayes,[9] Vanesa Gutierrez Calderon,[10] Reyes Bernabe Caro,[11] Alejandro Navarro Mendivil,[12] Afshin Dowlati,[13] Bin Zhang,[14] Yan Moore,[14] Tiffany Wang,[14] Natalya Nazarenko,[14] Paul Bunn[15]

[1]Hospital Universitario 12 de Octubre, Madrid, Spain; [2]Sarah Cannon Research Institute, Tennessee Oncology, Nashville, TN, USA; [3]Vienna Cancer Center and Central European Cooperative Oncology Group, Vienna, Austria; [4]Cancer & Hematology Centers of Western Michigan, Grand Rapids, MI, USA; [5]Institut Català d'Oncologia, Hospital Duran i Reynals, Barcelona, Spain; [6]Hospital Universitari i Politecnic La Fe, Valencia, Spain; [7]North Shore Hematology Oncology Associates, PC, Bay Shore, NY, USA; [8]Cancer Treatment Centers of America, Atlanta, GA, USA; [9]South West Healthcare, VIC, Australia; [10]Hospital Regional Universitario de Malaga, Malaga, Spain; [11]Hospital Universitario Virgen del Rocio, Seville, Spain; [12]Vall d'Hebron Barcelona Hospital, Barcelona, Spain; [13]Case Western Reserve University, Cleveland, OH, USA; [14]Ipsen Bioscience, Cambridge, MA, USA; [15]Cancer Center and Department of Medicine, University of Colorado, Denver, CO, USA

Abstract 8562

BACKGROUND

- In the treatment of small cell lung cancer (SCLC), the mainstay first-line (1L) treatment is combination chemotherapy, typically involving platinum-based therapy (carboplatin or cisplatin) plus etoposide.[1,2]
  - Although SCLC is often sensitive to chemotherapy and radiotherapy, many patients relapse and develop drug resistance.[2,3]
- Irinotecan is an inhibitor of topoisomerase 1, a validated drug target in SCLC.
- Liposomal irinotecan (nal-IRI) is a liposomal formulation of irinotecan, designed to use the enhanced permeability and retention effect to achieve liposomal deposition in tumor tissue followed by local irinotecan release and subsequent conversion to the active metabolite SN-38.
- nal-IRI in combination with fluorouracil and leucovorin is approved for the treatment of patients with metastatic adenocarcinoma of the pancreas after disease progression following gemcitabine-based therapy.[4]
- RESILIENT is an ongoing phase II/III trial assessing the safety, tolerability and efficacy of nal-IRI injection in patients with SCLC, comprising part 1 (dose-finding and dose-expansion phases) and part 2 (randomized controlled trial).
- Here, we report data from the dose-finding phase of part 1 of the RESILIENT trial.

Presented at ASCO 2019 | Chicago, IL USA | May 31- June 4, 2019
This study was sponsored by Ipsen

METHODS

Study design

- RESILIENT (NCT03088813) is a two-part phase II/III study (Figure 1).
- Part 1 of the study consists of open-label, single-arm, dose-finding and dose-expansion phases with the aim of:
  - determining the recommended nal-IRI monotherapy dose for part 2 of the study
  - defining the safety and tolerability of nal-IRI and demonstrating the preliminary efficacy of nal-IRI monotherapy administered every 2 weeks.
- Part 2 is a randomized, controlled, efficacy-assessment phase with the aim of comparing efficacy and safety profiles of nal-IRI monotherapy and topotecan monotherapy.

Figure 1. RESILIENT study design

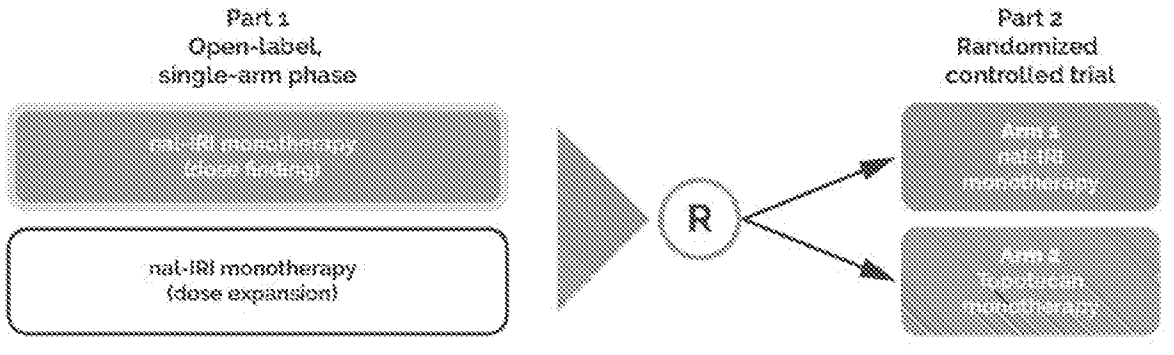

Patients

- Adults (≥ 18 years old) with SCLC who progressed on or after 1L platinum-based chemotherapy (carboplatin or cisplatin), immunotherapy or chemoradiation, including platinum-based chemotherapy for treatment of limited or extensive-stage SCLC.
- Additional inclusion criteria:
  - Eastern Cooperative Oncology Group performance status of 0 or 1 and adequate organ function.
  - Prior exposure to immunotherapy is allowed.
  - Asymptomatic central nervous system metastases are allowed.

Treatment during the dose-finding phase of RESILIENT part 1

- nal-IRI at a dose of 85 mg/m^2 (free base) is administered intravenously over 90 minutes every 2 weeks (cohort 1 (C-1)).
- If nal-IRI 85 mg/m^2 is deemed to have unacceptable toxicity, a dose of 70 mg/m^2 (free base) administered over 90 minutes every 2 weeks is recommended as a low-dose cohort contingency (cohort 2 (C-2)).

Endpoints of the dose-finding phase of RESILIENT part 1

- Primary endpoints are safety and tolerability at the 85 mg/m^2 and 70 mg/m^2 dose levels.
- Secondary endpoints are objective response rate (ORR), progression-free survival (PFS) and overall survival (OS).
- For efficacy endpoints, tumor assessment (by the investigator) is performed at screening and every 6 weeks (± 1 week) from cycle 1, day 1, and in accordance with Response Evaluation Criteria in Solid Tumors (RECIST) v1.1.

RESULTS OF THE DOSE-FINDING PHASE OF RESILIENT PART 1

Patient disposition and baseline characteristics

- As of December 24, 2018, 12 patients had received at least one dose of nal-IRI in part 1: four patients in C-1 (85 mg/m^2) and eight patients in C-2 (70 mg/m^2).
- Baseline characteristics are summarized in Table 1.

Table 1. Baseline characteristics

Characteristic	nal-IRI		
	Cohort 1 85 mg/m^2 (n = 4)	Cohort 2 70 mg/m^2 (n = 8)	Total (N = 12)
Sex, n (%)			
Male	2 (50.0)	3 (37.5)	5 (41.7)
Female	2 (50.0)	5 (62.5)	7 (58.3)
Age, years			
Median	61.5	58.0	60.0
Range	59–63	49–73	49–73
Race, n (%)			
White	4 (100.0)	8 (100.0)	12 (100.0)
ECOG performance status, n (%)			
0	1 (25.0)	1 (12.5)	2 (16.7)
1	3 (75.0)	7 (87.5)	10 (83.3)
Prior to chemotherapy cycles, n (%)			
4	0	1 (12.5)	1 (8.3)
≥ 6	4 (100.0)	7 (87.5)	11 (91.7)
Best response to prior therapy, n (%)			
CR	0	1 (12.5)	1 (8.3)
PR	2 (50.0)	4 (50.0)	6 (50.0)
SD	1 (25.0)	1 (12.5)	2 (16.7)
PD	1 (25.0)	2 (25.0)	3 (25.0)

*Only categories for which non-zero values were recorded are shown.
CR, complete response; ECOG, Eastern Cooperative Oncology Group; nal-IRI, liposomal irinotecan; PD, progressive disease; PR, partial response; SD, stable disease

- The 12 patients were followed up for at least 6 weeks.
- All four patients in C-1 discontinued study treatment (two owing to disease progression, one owing to a study drug-related adverse event [AE] and one owing to death due to reasons unrelated to study treatment).
- Two patients in C-2 discontinued study treatment (both owing to disease progression).
- One patient in each cohort died before completion of the dose-finding phase of the study.
- As of December 24, 2018, eight patients continued on the study (one in C-1 and seven in C-2).

Safety and tolerability

- Mean (standard deviation) of the total actual dose received was 459.8 mg (278.7 mg) and 714.8 mg (331.3 mg) in C-1 and C-2, respectively.
- The most commonly reported treatment-emergent AEs of any grade were diarrhea (91.7%), nausea (66.7%), decreased appetite (58.3%), fatigue (41.7%) and vomiting (41.7%) (Table 2).
- Serious AEs occurred in 3 of 4 patients in C-1 and 1 of 8 patients in C-2.
  - Serious AEs considered to be related to study treatment occurred in two patients (both in C-1, one report each of diarrhea, nausea, vomiting, hepatotoxicity and abnormal liver function test).
- Four patients in C-1 had dose-limiting toxicities (diarrhea, n = 3; abnormal liver function test, n = 1; hyponatremia, n = 1); there were no dose-limiting toxicities in C-2.

Table 2. Treatment-emergent adverse events occurring in > 1 patient in total

Preferred term	nal-IRI		
	Cohort 1 85 mg/m² (n = 4)	Cohort 2 70 mg/m² (n = 8)	Total (N = 12)
Diarrhea	4 (100.0)	7 (87.5)	11 (91.7)
Nausea	3 (75.0)	5 (62.5)	8 (66.7)
Decreased appetite	4 (100.0)	3 (37.5)	7 (58.3)
Fatigue	2 (50.0)	3 (37.5)	5 (41.7)
Vomiting	1 (25.0)	4 (50.0)	5 (41.7)
Abdominal pain	1 (25.0)	3 (37.5)	4 (33.3)
Hypokalemia	1 (25.0)	3 (37.5)	4 (33.3)
Asthenia	1 (25.0)	2 (25.0)	3 (25.0)
Constipation	2 (50.0)	1 (12.5)	3 (25.0)
Hypomagnesemia	1 (25.0)	2 (25.0)	3 (25.0)
Anemia	2 (50.0)	0	2 (16.7)
Arthralgia	2 (50.0)	0	2 (16.7)
Dehydration	0	2 (25.0)	2 (16.7)
Edema peripheral	1 (25.0)	1 (12.5)	2 (16.7)
Headache	1 (25.0)	1 (12.5)	2 (16.7)
Hypocalcemia	1 (25.0)	1 (12.5)	2 (16.7)
Neutropenia	2 (50.0)	0	2 (16.7)
Weight decreased	1 (25.0)	1 (12.5)	2 (16.7)

Data are number (%) of patients. Treatment-emergent AEs are AEs that occurred or worsened on or after the day of the first dose of study medication and in the 30 days after discontinuation of the study drug. Patients with multiple AEs within a system organ class or preferred term were only counted once under each category.
AE, adverse event; nal-IRI, liposomal irinotecan

Efficacy

- The ORR for the total study population was 33.3% (Table 3).
  - The ORR was 37.5% with the 70 mg/m^2 dose and 25.0% with the 85 mg/m^2 dose.

Table 3. Objective response rates

Category	nal-IRI		
	Cohort 1 85 mg/m^2 (n = 4)	Cohort 2 70 mg/m^2 (n = 8)	Total (n = 12)
Best objective response, n (%)			
CR	0	0	0
PR	1 (25.0)	3 (37.5)	4 (33.3)
SD	1 (25.0)	2 (25.0)	3 (25.0)
PD	1 (25.0)	1 (12.5)	2 (16.7)
Non-evaluable	1 (25.0)	2 (25.0)	3 (25.0)
ORR, n (%)			
CR+PR	1 (25.0)	3 (37.5)	4 (33.3)
Non-responder (censored)	3 (75.0)	5 (62.5)	8 (66.7)

CR, complete response; nal-IRI, liposomal irinotecan; ORR, objective response rate; PD, progressive disease; PR, partial response; SD, stable disease

CONCLUSION

- Initial assessment suggests that nal-IRI at a dose of 70 mg/m^2 administered every 2 weeks is well tolerated and has promising antitumor activity in patients with SCLC who progressed on or after a platinum-based regimen.
- The part 1 dose-expansion phase is ongoing.

References

1. Horvitz A et al. Cell Oncol (Dordr). 2018;41(5):491-501.
2. Roth M et al. Ann Oncol. 2015;26(Suppl 5):v126-132.
3. Sehdev S et al. Oncol Rev. 2017;11(Suppl 1):319-328.
4. ClinicalTrials.gov. A phase 1/2 study of nal-IRI in combination with 5-fluorouracil, leucovorin and oxaliplatin in patients with metastatic pancreatic cancer. https://clinicaltrials.gov/ct2/show/NCT03086616. Accessed May 2019.

Disclosures

LDW – Advisory/consulting: AstraZeneca, Boehringer Ingelheim, Bristol-Myers Squibb, Lilly, Merck Sharp & Dohme and Roche.
CMS – Consultant/advisory: AstraZeneca, Boehringer Ingelheim, Bristol-Myers Squibb, Celgene, Clovis Oncology, Genentech/Roche, Lilly, Novartis and Pfizer; grants/research support: Amgen, AstraZeneca, Boehringer Ingelheim, Bristol-Myers Squibb, Celgene, Clovis Oncology, Exelixis, Genentech/Roche, Lilly, Merck, Peloton, Oncothyreon, Sanofi/aventis Pharmaceuticals, Seragon Pharmaceuticals, Pfizer, University of Texas Southwestern Medical Center – Simmons Comprehensive Cancer Center and Parkinson's Foundation; other: Bristol-Myers Squibb.
CT – Consultant/advisory: Ipsen, Merck, Pharmacyclics, AstraZeneca, Boehringer Ingelheim, Bristol-Myers Squibb, Pfizer/Sanofi, Celgene, Merck, Roche, Merck Sharp & Dohme, Novartis and Roche.
KL – Immediate family: Employee: AstraZeneca, Bristol-Myers Squibb, Genentech/Roche, Celgene, Merck, Sharp & Dohme, Novartis and Roche.
AS – Consultant/advisory: AstraZeneca, Bristol-Myers Squibb, Genentech/Roche, Merck, Sharp & Dohme, Novartis and Roche; grants/research support: AstraZeneca, Bristol-Myers Squibb, Genentech, Merck, Sharp & Dohme, Novartis, Roche, Lilly, Merck, Pfizer and Sanofi; travel and lodging: AstraZeneca, Bristol-Myers Squibb, Celgene, Genentech, Roche, Lilly, Merck, Pfizer and Sanofi; other: Bristol-Myers Squibb, Celgene, Genentech, Roche, Lilly, Merck, Pfizer and Sanofi; research funding: AstraZeneca, Bristol-Myers Squibb, Celgene, Genentech, Roche, Lilly, Merck, Pfizer and Sanofi.
MJ – advisory role: Boehringer Ingelheim.
CW – consultant/advisory role: Incyte, AstraZeneca/MedImmune, Boehringer Ingelheim, Bristol-Myers Squibb, Genentech/Roche, Merck, Sharp & Dohme and Pfizer; research funding: Incyte, AstraZeneca, Merck and Bristol-Myers Squibb.
DK – research funding: Celgene/Receptos, Daiichi Sankyo, Ipsen and Pfizer.
RR – nothing to disclose.
TK – nothing to disclose.
MGK – nothing to disclose.
RSC – consultant/advisory role: AstraZeneca, Bristol-Myers Squibb and Roche.
AJVH – consultant/advisory role: Boehringer Ingelheim, Bristol-Myers Squibb, Celgene and Roche; expert testimony: Dr. Oyer; Dr. Gerber.
AG – consultant/advisory role: Abbvie, Genentech and Abbvie, Pharmacyclics; policy research funding: Amgen, Bristol-Myers Squibb, BMS Servier, Lilly, Medivation, Novartis and Sanofi/Aventis.
RP, TM, TVE and MH – employment: Ipsen.
RK – consultant: AstraZeneca, Bristol-Myers Squibb, Daiichi Sankyo, Genentech, Lilly, Merck, Novartis Pharmaceuticals, Novocure and Pfizer; other: AstraZeneca, Bristol-Myers Squibb, Genentech, Merck and Pfizer.

Acknowledgments

The authors thank all patients involved in this study, as well as their caregivers, site staff, investigators, and research staff at participating institutions.
This study was sponsored by Ipsen.
The authors thank Isabelle Kaufmann of Oxford PharmaGenesis, Oxford, UK, for providing medical writing support, which was sponsored by Ipsen in accordance with Good Publication Practice guidelines.
Contact: study.inquiries@ipsen.com

Journal of Clinical Oncology®
An American Society of Clinical Oncology Journal

Article Tools

LUNG CANCER—NON-SMALL CELL LOCAL-REGIONAL/SMALL CELL/OTHER THORACIC CANCERS

RESILIENT: Study of irinotecan liposome injection (nal-IRI) in patients with small cell lung cancer—Preliminary findings from part 1 dose-defining phase.

Luis G. Paz-Ares, David R. Spigel, Christoph Zielinski, Yuanbin Chen, Maria Jove, Oscar Juan Vidal, David Chu, Patricia Rich, Theresa M. Hayes, M Vanesa Gutierrez Calderon, Reyes Bermabe Cano, Alejandro Navarro, Afshin Dowlati, Bin Zhang, Yan Moore, Haofei Tiffany Wang, Natalya Nazarenko, Santiago Ponce Aix, Paul A. Bunn

Hospital Universitario 12 de Octubre, CiberOnc, Universidad Complutense and CNIO, Madrid, Spain; Sarah Cannon Research Institute and Tennessee Oncology, Nashville, TN; Vienne Cancer Center and Central European Cooperative Oncology Group, Vienna, Austria; Natl Cancer Inst, Ada, MI; Institut Català d'Oncologia, L'Hospitalet, Barcelona, Spain; Hospital Universitario La Fé, València, Spain; North Shore Hematology Oncology Associates, East Setauket, NY; Cancer Treatment Centers of America, Southeastern Regional Medical Center, Newnan, GA; St. John of God Health Care, Warrnambool, VIC, Australia; Regional University Hospital Carlos Haya, Málaga, Spain; Hospital Virgen Del Rocio, Sevilla, Spain; Hospital Universitari Vall d'Hebron, D'hebron, Spain; Case Western Reserve University and University Hospitals Case Medical Center, Cleveland, OH; Ipsen Bioscience, Boston, MA; Ipsen Bioscience, Cambridge, MA; Hospital 12 de Octubre, Madrid, Spain; University of Colorado Denver, Aurora, CO

Show Less

Abstract Disclosures

Abstract

8562

Background: Nal-IRI is investigated as monotherapy in patients with SCLC who progressed on or after platinum regimen. The RESILIENT study is a Part 1 study of a Phase 2/3 trial to assess safety, tolerability, and efficacy of Irinotecan Liposome Injection in patients with SCLC. Methods: Nal-IRI is evaluated in patients ≥18 yrs with advanced SCLC with an ECOG performance status ≤1 and adequate organ function;

ARTICLE CITATION

DOI: 10.1200/JCO.2019.37.15_suppl.8562
Journal of Clinical Oncology 37, no. 15_suppl (May 20, 2019) 8562-8562.

Published online May 26, 2019.

prior exposure to immunotherapy is allowed. Safety and tolerability at dose levels of 85 mg/m^2 and 70 mg/m^2 are the primary endpoints, with assessment of exploratory efficacy signal. Results: At 24 Dec 2018 safety cutoff 12 patients in Part 1 received ≥1 dose of nal-IRI (Cohort 1 [C-1] at 85 mg/m^2 dose n=4; Cohort 2 [C-2] at 70 mg/m^2 dose n=8; median age 60.0 yrs; range 49–73 yrs). Three patients experienced ≥1 DLT (Cohort 1 n=3/4; Cohort 2 n=0/8). Most frequent treatment-emergent adverse events (TEAE) were gastrointestinal (GI) disorders (any grade): diarrhea (91.7%), nausea (58.3%), vomiting (41.7%), decreased appetite (58%), abdominal pain (33%) manageable by antidiarrheal regimen and antiemetics; as well as fatigue (50%) and asthenia (37.5%). Overall, hematologic toxicity was neutropenia (any grade) at 16.7% and anemia (any grade) at 16.7%. At 11 Dec 2018 efficacy cutoff the best objective response was partial response (PR) at 33.3% in 4/12 patients (C-1 n=1/4; C-2 n=3/8), median time to response was 6 wks. Overall disease control rate (DCR) was 58.3%; progressive disease (PD) was observed in 2 patients (16.7%), and 3 patients were non-evaluable (25%). Conclusions: Initial assessment suggests that nal-IRI at 70 mg/m^2 dose given bi-weekly is well-tolerated and has promising antitumor activity in patients with SCLC who progressed on or after platinum regimen. Part 1 dose expansion is ongoing. Clinical trial information: NCTN03088813.

Best Objective Response (BOR).

Best Objective Response (BOR)	Nal-IRI 85 mg/m^2 (n=4)	Nal-IRI 70 mg/m^2 (n=8)	Nal-IRI Overall dosing (N=12)
Complete response (CR)	0	0	0
Partial response (PR)	1 (25%)	3 (37.5%)	4 (33.3)
Stable disease (SD)	1 (25%)	2 (25%)	3 (25%)
Progressive disease (PD)	1 (25%)	1 (12.5%)	2 (16.7%)
Non-evaluable	1 (25%)	2 (25%)	3 (25%)

Outpatient Management of Fever and Neutropenia in Adults Treated for Malignancy: American Society of Clinical Oncology and Infectious Diseases Society of America Clinical Practice Guideline Update
Taplitz et al.

Antiemetics: American Society of Clinical Oncology Clinical Practice Guideline Update
Hesketh et al.

Minimal Residual Disease Assessed by Multiparameter Flow Cytometry in Multiple Myeloma: Impact on Outcome in the Medical Research Council Myeloma IX Study
Rawstron et al.

Comparison of an Oral Factor Xa Inhibitor With Low Molecular Weight Heparin in Patients With Cancer With Venous Thromboembolism: Results of a Randomized Trial (SELECT-D)
Young et al.

PATENT COOPERATION TREATY

PCT

INTERNATIONAL PRELIMINARY REPORT ON PATENTABILITY
(Chapter I of the Patent Cooperation Treaty)

(PCT Rule 44*bis*)

Applicant's or agent's file reference P070787WO:ECO/SJD	**FOR FURTHER ACTION**	See item 4 below
International application No. PCT/IB2017/000681	International filing date *(day/month/year)* 17 May 2017 (17.05.2017)	Priority date *(day/month/year)* 18 May 2016 (18.05.2016)
International Patent Classification (8th edition unless older edition indicated) See relevant information in Form PCT/ISA/237		
Applicant IPSEN BIOPHARM LTD.		

1. This international preliminary report on patentability (Chapter I) is issued by the International Bureau on behalf of the International Searching Authority under Rule 44 *bis*.1(a).

2. This REPORT consists of a total of 6 sheets, including this cover sheet.

   In the attached sheets, any reference to the written opinion of the International Searching Authority should be read as a reference to the international preliminary report on patentability (Chapter I) instead.

3. This report contains indications relating to the following items:

☒	Box No. I	Basis of the report
☐	Box No. II	Priority
☐	Box No. III	Non-establishment of opinion with regard to novelty, inventive step and industrial applicability
☐	Box No. IV	Lack of unity of invention
☒	Box No. V	Reasoned statement under Article 35(2) with regard to novelty, inventive step or industrial applicability; citations and explanations supporting such statement
☐	Box No. VI	Certain documents cited
☐	Box No. VII	Certain defects in the international application
☐	Box No. VIII	Certain observations on the international application

4. The International Bureau will communicate this report to designated Offices in accordance with Rules 44*bis*.3(c) and 93*bis*.1 but not, except where the applicant makes an express request under Article 23(2), before the expiration of 30 months from the priority date (Rule 44*bis* .2).

	Date of issuance of this report 20 November 2018 (20.11.2018)
The International Bureau of WIPO 34, chemin des Colombettes 1211 Geneva 20, Switzerland Facsimile No. +41 22 338 82 70	Authorized officer Cécile Chatel e-mail: ro.ib@wipo.int

Form PCT/IB/373 (January 2004)

PATENT COOPERATION TREATY

From the
INTERNATIONAL SEARCHING AUTHORITY

To:

see form PCT/ISA/220

PCT

WRITTEN OPINION OF THE INTERNATIONAL SEARCHING AUTHORITY

(PCT Rule 43*bis*.1)

Date of mailing
(day/month/year) see form PCT/ISA/210 (second sheet)

Applicant's or agent's file reference
see form PCT/ISA/220

FOR FURTHER ACTION
See paragraph 2 below

International application No.	International filing date *(day/month/year)*	Priority date *(day/month/year)*
PCT/IB2017/000681	17.05.2017	18.05.2016

International Patent Classification (IPC) or both national classification and IPC
INV. A61K31/4745 A61P35/00 A61K9/127

Applicant
IPSEN BIOPHARM LTD

1. This opinion contains indications relating to the following items:

- ☒ Box No. I Basis of the opinion
- ☐ Box No. II Priority
- ☐ Box No. III Non-establishment of opinion with regard to novelty, inventive step and industrial applicability
- ☐ Box No. IV Lack of unity of invention
- ☒ Box No. V Reasoned statement under Rule 43*bis*.1(a)(i) with regard to novelty, inventive step and industrial applicability; citations and explanations supporting such statement
- ☐ Box No. VI Certain documents cited
- ☐ Box No. VII Certain defects in the international application
- ☐ Box No. VIII Certain observations on the international application

2. **FURTHER ACTION**

If a demand for international preliminary examination is made, this opinion will usually be considered to be a written opinion of the International Preliminary Examining Authority ("IPEA") except that this does not apply where the applicant chooses an Authority other than this one to be the IPEA and the chosen IPEA has notifed the International Bureau under Rule 66.1*bis*(b) that written opinions of this International Searching Authority will not be so considered.

If this opinion is, as provided above, considered to be a written opinion of the IPEA, the applicant is invited to submit to the IPEA a written reply together, where appropriate, with amendments, before the expiration of 3 months from the date of mailing of Form PCT/ISA/220 or before the expiration of 22 months from the priority date, whichever expires later.

For further options, see Form PCT/ISA/220.

Name and mailing address of the ISA:	Date of completion of this opinion	Authorized Officer
European Patent Office D-80298 Munich Tel. +49 89 2399 - 0 Fax: +49 89 2399 - 4465	see form PCT/ISA/210	Baurand, Petra Telephone No. +49 89 2399-0

Box No. I Basis of the opinion

1. With regard to the **language**, this opinion has been established on the basis of:

   ☒ the international application in the language in which it was filed.

   ☐ a translation of the international application into , which is the language of a translation furnished for the purposes of international search (Rules 12.3(a) and 23.1 (b)).

2. ☐ This opinion has been established taking into account the **rectification of an obvious mistake** authorized by or notified to this Authority under Rule 91 (Rule 43*bis*.1(a))

3. ☐ With regard to any **nucleotide and/or amino acid sequence** disclosed in the international application, this opinion has been established on the basis of a sequence listing:

   a. ☐ forming part of the international application as filed:

      ☐ in the form of an Annex C/ST.25 text file.

      ☐ on paper or in the form of an image file.

   b. ☐ furnished together with the international application under PCT Rule 13*ter*.1(a) for the purposes of international search only in the form of an Annex C/ST.25 text file.

   c. ☐ furnished subsequent to the international filing date for the purposes of international search only:

      ☐ in the form of an Annex C/ST.25 text file (Rule 13*ter*.1(a)).

      ☐ on paper or in the form of an image file (Rule 13*ter*.1(b) and Administrative Instructions, Section 713).

4. ☐ In addition, in the case that more than one version or copy of a sequence listing has been filed or furnished, the required statements that the information in the subsequent or additional copies is identical to that forming part of the application as filed or does not go beyond the application as filed, as appropriate, were furnished.

5. Additional comments:

Box No. V Reasoned statement under Rule 43*bis*.1(a)(i) with regard to novelty, inventive step or industrial applicability; citations and explanations supporting such statement

1. Statement

Novelty (N)	Yes:	Claims	1-20
	No:	Claims	
Inventive step (IS)	Yes:	Claims	
	No:	Claims	1-20
Industrial applicability (IA)	Yes:	Claims	1-20
	No:	Claims	

2. Citations and explanations

see separate sheet

Re Item V

Reasoned statement with regard to novelty, inventive step or industrial applicability; citations and explanations supporting such statement

5.1 Reference is made to the following documents:

D1 CHAN DANIEL C ET AL: "Evaluating the pharmacodynamics and pharmacokinetic effects of MM-398, a nanoliposomal irinotecan (nal-IRI) in subcutaneous xenograft tumor models of human squamous cell carcinoma and small cell lung cancers", CANCER RESEARCH, vol. 74, no. 19, Suppl. S, October 2014 (2014-10), page 4626,
& 105TH ANNUAL MEETING OF THE AMERICAN-ASSOCIATION-FOR-CANCER-RESEARCH (AACR); SAN DIEGO, CA, USA; APRIL 05 -09, 2014

D2 KALRA ASHISH V ET AL: "Preclinical Activity of Nanoliposomal Irinotecan Is Governed by Tumor Deposition and Intratumor Prodrug Conversion", CANCER RESEARCH, vol. 74, no. 23, December 2014 (2014-12), pages 7003-7013, ISSN: 0008-5472

D3 Anonymous: "Merrimack Pharmaceuticals Initiates Cross-Tumor Study to Investigate Potential Predictive Response Markers for a Developmental Nanotherapeutic Chemotherapy", Internet, 19 December 2012 (2012-12-19), Retrieved from the Internet: URL:http://files.shareholder.com [retrieved on 2017-07-31]

D4 TARDI PAUL G ET AL: "Drug ratio-dependent antitumor activity of irinotecan and cisplatin combinations in vitro and in vivo", MOLECULAR CANCER THERAPEUTICS, vol. 8, no. 8, August 2009 (2009-08), pages 2266-2275, ISSN: 1535-7163

5.2 The present application does not meet the criteria of Article 33(3) PCT, because the subject-matter of claims 1 - 20 does not involve an inventive step.

The document **D1** is regarded as being the prior art closest to the subject-matter of independent claims 1, 11 and 18, and discloses inhibition of tumor growth induced by MM-398 (30 or 50 mg/kg/week) in a xenograft model of small cell lung cancer (abstract).

The subject-matter of claims 1, 11 and 18 therefore differs from this known document in that MM-398 liposomal irinotecan is administered at a dose of 90 mg/m^2 once every two weeks (corresponding to 16 mg/kg/week according to Example 11).

The problem to be solved by the present invention may therefore be regarded as provision of an alternative dosage regimen for liposomal irinotecan.

The solution proposed by the present application cannot be considered as involving an inventive step (Article 33(3) PCT) for the following reasons: The only technical feature distinguishing the presently claimed subject-matter over the cited

prior art appears to be the dosage regimen (16 mg/kg/week as claimed (see also Example 11) compared to 30 or 50 mg/kg/week according to D1). In order to meet the requirements of Article 33(3) PCT, the Applicant is expected to demonstrate the presence of an unexpected special technical effect linked to the claimed dosage regimen compared to the known therapy either in the form of in vivo tests or of clinical trials. It is pointed out that the skilled person would always try to lower the dosage to the minimum required for obtaining the desired effect, to reduce side effects and to lower costs. Therefore, if the same effect is obtained with the new dosage regimen (as it is the case here), this feature is to be considered obvious.

5.3 Dependent claims 2 - 10, 12 - 17, 19 and 20 do not contain any features which, in combination with the features of any claim to which they refer, meet the requirements of the PCT in respect of inventive step.

5.4 Claims 1 - 20 relate to subject-matter considered by this Authority to be covered by the provisions of Rule 39.1(iv) / 67.1(iv) PCT. The patentability can be dependent upon the formulation of the claims. The EPO, for example, does not recognise as patentable claims to the use of a compound in medical treatment, but may allow claims to a product, in particular substances or compositions for use in a first or further medical treatment.

PATENT COOPERATION TREATY

PCT

INTERNATIONAL SEARCH REPORT

(PCT Article 18 and Rules 43 and 44)

Applicant's or agent's file reference	**FOR FURTHER ACTION**	see Form PCT/ISA/220 as well as, where applicable, item 5 below.
P070787WO:ECO/SJD		
International application No.	International filing date *(day/month/year)*	(Earliest) Priority Date *(day/month/year)*
PCT/IB2017/000681	17 May 2017 (17-05-2017)	18 May 2016 (18-05-2016)
Applicant		
IPSEN BIOPHARM LTD		

This international search report has been prepared by this International Searching Authority and is transmitted to the applicant according to Article 18. A copy is being transmitted to the International Bureau.

This international search report consists of a total of 3 sheets.

[X] It is also accompanied by a copy of each prior art document cited in this report.

1. **Basis of the report**
   a. With regard to the **language,** the international search was carried out on the basis of:
      [X] the international application in the language in which it was filed
      [ ] a translation of the international application into _____, which is the language of a translation furnished for the purposes of international search (Rules 12.3(a) and 23.1(b))
   b. [ ] This international search report has been established taking into account the **rectification of an obvious mistake** authorized by or notified to this Authority under Rule 91 (Rule 43.6*bis*(a)).
   c. [ ] With regard to any **nucleotide and/or amino acid sequence** disclosed in the international application, see Box No. I.

2. [ ] **Certain claims were found unsearchable** (See Box No. II)

3. [ ] **Unity of invention is lacking** (see Box No III)

4. With regard to the **title,**
   [ ] the text is approved as submitted by the applicant
   [X] the text has been established by this Authority to read as follows:

   NANOLIPOSOMAL IRINOTECAN FOR USE IN TREATING SMALL CELL LUNG CANCER

5. With regard to the **abstract,**
   [X] the text is approved as submitted by the applicant
   [ ] the text has been established, according to Rule 38.2, by this Authority as it appears in Box No. IV. The applicant may, within one month from the date of mailing of this international search report, submit comments to this Authority

6. With regard to the **drawings,**
   a. the figure of the **drawings** to be published with the abstract is Figure No. 1
      [X] as suggested by the applicant
      [ ] as selected by this Authority, because the applicant failed to suggest a figure
      [ ] as selected by this Authority, because this figure better characterizes the invention
   b. [ ] none of the figures is to be published with the abstract

INTERNATIONAL SEARCH REPORT

International application No
PCT/IB2017/000681

A. CLASSIFICATION OF SUBJECT MATTER
INV. A61K31/4745 A61P35/00 A61K9/127
ADD.

According to International Patent Classification (IPC) or to both national classification and IPC

B. FIELDS SEARCHED

Minimum documentation searched (classification system followed by classification symbols)
A61K

Documentation searched other than minimum documentation to the extent that such documents are included in the fields searched

Electronic data base consulted during the international search (name of data base and, where practicable, search terms used)
EPO-Internal, BIOSIS, EMBASE, FSTA, INSPEC, WPI Data

C. DOCUMENTS CONSIDERED TO BE RELEVANT

Category*	Citation of document, with indication, where appropriate, of the relevant passages	Relevant to claim No.
Y	CHAN DANIEL C ET AL: "Abstract 4626: Evaluating the pharmacodynamics and pharmacokinetic effects of MM-398, a nanoliposomal irinotecan (nal-IRI) in subcutaneous xenograft tumor models of human squamous cell carcinoma and small cell lung cancers", CANCER RESEARCH , vol. 74 1 October 2014 (2014-10-01), XP002772684, & 105TH ANNUAL MEETING OF THE AMERICAN-ASSOCIATION-FOR-CANCER-RESEARCH (AACR); SAN DIEGO, CA, USA; APRIL 05 -09, 2014 DOI: 10.1158/1538-7445.AM2014-4626 Retrieved from the Internet: URL:http://cancerres.aacrjournals.org/content/74/19_Supplement/4626 -/--	1-20

[X] Further documents are listed in the continuation of Box C. [ ] See patent family annex.

* Special categories of cited documents :

"A" document defining the general state of the art which is not considered to be of particular relevance

"E" earlier application or patent but published on or after the international filing date

"L" document which may throw doubts on priority claim(s) or which is cited to establish the publication date of another citation or other special reason (as specified)

"O" document referring to an oral disclosure, use, exhibition or other means

"P" document published prior to the international filing date but later than the priority date claimed

"T" later document published after the international filing date or priority date and not in conflict with the application but cited to understand the principle or theory underlying the invention

"X" document of particular relevance; the claimed invention cannot be considered novel or cannot be considered to involve an inventive step when the document is taken alone

"Y" document of particular relevance; the claimed invention cannot be considered to involve an inventive step when the document is combined with one or more other such documents, such combination being obvious to a person skilled in the art

"&" document member of the same patent family

Date of the actual completion of the international search	Date of mailing of the international search report
2 August 2017	25/08/2017

Name and mailing address of the ISA/	Authorized officer
European Patent Office, P.B. 5818 Patentlaan 2 NL - 2280 HV Rijswijk Tel. (+31-70) 340-2040, Fax: (+31-70) 340-3016	Baurand, Petra

2

Form PCT/ISA/210 (second sheet) (April 2005)

C(Continuation). DOCUMENTS CONSIDERED TO BE RELEVANT

Category*	Citation of document, with indication, where appropriate, of the relevant passages	Relevant to claim No.
	[retrieved on 2017-07-31] abstract -----	
Y	KALRA ASHISH V ET AL: "Preclinical Activity of Nanoliposomal Irinotecan Is Governed by Tumor Deposition and Intratumor Prodrug Conversion", CANCER RESEARCH, vol. 74, no. 23, December 2014 (2014-12), pages 7003-7013, XP002772685, ISSN: 0008-5472 page 7004, right-hand column, "Antitumor activity studies" page 7004, right-hand column, "Characterizing tumors" figure 6C -----	1-20
Y	Anonymous: "Merrimack Pharmaceuticals Initiates Cross-Tumor Study to Investigate Potential Predictive Response Markers for a Developmental Nanotherapeutic Chemotherapy", Internet , 19 December 2012 (2012-12-19), XP002772686, Retrieved from the Internet: URL:http://files.shareholder.com [retrieved on 2017-07-31] page 1, paragraph 4 - paragraph 5 -----	1-20
Y	TARDI PAUL G ET AL: "Drug ratio-dependent antitumor activity of irinotecan and cisplatin combinations in vitro and in vivo", MOLECULAR CANCER THERAPEUTICS, vol. 8, no. 8, August 2009 (2009-08), pages 2266-2275, XP002772687, ISSN: 1535-7163 figure 2A page 2266, abstract -----	1-20

PATENT COOPERATION TREATY

From the
INTERNATIONAL SEARCHING AUTHORITY

To:

see form PCT/ISA/220

PCT

WRITTEN OPINION OF THE INTERNATIONAL SEARCHING AUTHORITY

(PCT Rule 43*bis*.1)

Date of mailing
(day/month/year) see form PCT/ISA/210 (second sheet)

Applicant's or agent's file reference
see form PCT/ISA/220

FOR FURTHER ACTION
See paragraph 2 below

International application No.	International filing date *(day/month/year)*	Priority date *(day/month/year)*
PCT/IB2017/000681	17.05.2017	18.05.2016

International Patent Classification (IPC) or both national classification and IPC
INV. A61K31/4745 A61P35/00 A61K9/127

Applicant
IPSEN BIOPHARM LTD

1. This opinion contains indications relating to the following items:

- ☒ Box No. I Basis of the opinion
- ☐ Box No. II Priority
- ☐ Box No. III Non-establishment of opinion with regard to novelty, inventive step and industrial applicability
- ☐ Box No. IV Lack of unity of invention
- ☒ Box No. V Reasoned statement under Rule 43*bis*.1(a)(i) with regard to novelty, inventive step and industrial applicability; citations and explanations supporting such statement
- ☐ Box No. VI Certain documents cited
- ☐ Box No. VII Certain defects in the international application
- ☐ Box No. VIII Certain observations on the international application

2. **FURTHER ACTION**

If a demand for international preliminary examination is made, this opinion will usually be considered to be a written opinion of the International Preliminary Examining Authority ("IPEA") except that this does not apply where the applicant chooses an Authority other than this one to be the IPEA and the chosen IPEA has notifed the International Bureau under Rule 66.1*bis*(b) that written opinions of this International Searching Authority will not be so considered.

If this opinion is, as provided above, considered to be a written opinion of the IPEA, the applicant is invited to submit to the IPEA a written reply together, where appropriate, with amendments, before the expiration of 3 months from the date of mailing of Form PCT/ISA/220 or before the expiration of 22 months from the priority date, whichever expires later.

For further options, see Form PCT/ISA/220.

Name and mailing address of the ISA:	Date of completion of this opinion	Authorized Officer
European Patent Office D-80298 Munich Tel. +49 89 2399 - 0 Fax: +49 89 2399 - 4465	see form PCT/ISA/210	Baurand, Petra Telephone No. +49 89 2399-0

Box No. I Basis of the opinion

1. With regard to the **language**, this opinion has been established on the basis of:

   ☒ the international application in the language in which it was filed.

   ☐ a translation of the international application into , which is the language of a translation furnished for the purposes of international search (Rules 12.3(a) and 23.1 (b)).

2. ☐ This opinion has been established taking into account the **rectification of an obvious mistake** authorized by or notified to this Authority under Rule 91 (Rule 43*bis*.1(a))

3. ☐ With regard to any **nucleotide and/or amino acid sequence** disclosed in the international application, this opinion has been established on the basis of a sequence listing:

   a. ☐ forming part of the international application as filed:

      ☐ in the form of an Annex C/ST.25 text file.

      ☐ on paper or in the form of an image file.

   b. ☐ furnished together with the international application under PCT Rule 13*ter*.1(a) for the purposes of international search only in the form of an Annex C/ST.25 text file.

   c. ☐ furnished subsequent to the international filing date for the purposes of international search only:

      ☐ in the form of an Annex C/ST.25 text file (Rule 13*ter*.1(a)).

      ☐ on paper or in the form of an image file (Rule 13*ter*.1(b) and Administrative Instructions, Section 713).

4. ☐ In addition, in the case that more than one version or copy of a sequence listing has been filed or furnished, the required statements that the information in the subsequent or additional copies is identical to that forming part of the application as filed or does not go beyond the application as filed, as appropriate, were furnished.

5. Additional comments:

Box No. V Reasoned statement under Rule 43*bis*.1(a)(i) with regard to novelty, inventive step or industrial applicability; citations and explanations supporting such statement

1. Statement

Novelty (N)	Yes:	Claims	1-20
	No:	Claims	
Inventive step (IS)	Yes:	Claims	
	No:	Claims	1-20
Industrial applicability (IA)	Yes:	Claims	1-20
	No:	Claims	

2. Citations and explanations

see separate sheet

Re Item V

Reasoned statement with regard to novelty, inventive step or industrial applicability; citations and explanations supporting such statement

5.1 Reference is made to the following documents:

D1 CHAN DANIEL C ET AL: "Evaluating the pharmacodynamics and pharmacokinetic effects of MM-398, a nanoliposomal irinotecan (nal-IRI) in subcutaneous xenograft tumor models of human squamous cell carcinoma and small cell lung cancers", CANCER RESEARCH, vol. 74, no. 19, Suppl. S, October 2014 (2014-10), page 4626,
& 105TH ANNUAL MEETING OF THE AMERICAN-ASSOCIATION-FOR-CANCER-RESEARCH (AACR); SAN DIEGO, CA, USA; APRIL 05 -09, 2014

D2 KALRA ASHISH V ET AL: "Preclinical Activity of Nanoliposomal Irinotecan Is Governed by Tumor Deposition and Intratumor Prodrug Conversion", CANCER RESEARCH, vol. 74, no. 23, December 2014 (2014-12), pages 7003-7013, ISSN: 0008-5472

D3 Anonymous: "Merrimack Pharmaceuticals Initiates Cross-Tumor Study to Investigate Potential Predictive Response Markers for a Developmental Nanotherapeutic Chemotherapy", Internet, 19 December 2012 (2012-12-19), Retrieved from the Internet: URL:http://files.shareholder.com [retrieved on 2017-07-31]

D4 TARDI PAUL G ET AL: "Drug ratio-dependent antitumor activity of irinotecan and cisplatin combinations in vitro and in vivo", MOLECULAR CANCER THERAPEUTICS, vol. 8, no. 8, August 2009 (2009-08), pages 2266-2275, ISSN: 1535-7163

5.2 The present application does not meet the criteria of Article 33(3) PCT, because the subject-matter of claims 1 - 20 does not involve an inventive step.

The document **D1** is regarded as being the prior art closest to the subject-matter of independent claims 1, 11 and 18, and discloses inhibition of tumor growth induced by MM-398 (30 or 50 mg/kg/week) in a xenograft model of small cell lung cancer (abstract).

The subject-matter of claims 1, 11 and 18 therefore differs from this known document in that MM-398 liposomal irinotecan is administered at a dose of 90 mg/m^2 once every two weeks (corresponding to 16 mg/kg/week according to Example 11).

The problem to be solved by the present invention may therefore be regarded as provision of an alternative dosage regimen for liposomal irinotecan.

The solution proposed by the present application cannot be considered as involving an inventive step (Article 33(3) PCT) for the following reasons: The only technical feature distinguishing the presently claimed subject-matter over the cited

prior art appears to be the dosage regimen (16 mg/kg/week as claimed (see also Example 11) compared to 30 or 50 mg/kg/week according to D1). In order to meet the requirements of Article 33(3) PCT, the Applicant is expected to demonstrate the presence of an unexpected special technical effect linked to the claimed dosage regimen compared to the known therapy either in the form of in vivo tests or of clinical trials. It is pointed out that the skilled person would always try to lower the dosage to the minimum required for obtaining the desired effect, to reduce side effects and to lower costs. Therefore, if the same effect is obtained with the new dosage regimen (as it is the case here), this feature is to be considered obvious.

5.3 Dependent claims 2 - 10, 12 - 17, 19 and 20 do not contain any features which, in combination with the features of any claim to which they refer, meet the requirements of the PCT in respect of inventive step.

5.4 Claims 1 - 20 relate to subject-matter considered by this Authority to be covered by the provisions of Rule 39.1(iv) / 67.1(iv) PCT. The patentability can be dependent upon the formulation of the claims. The EPO, for example, does not recognise as patentable claims to the use of a compound in medical treatment, but may allow claims to a product, in particular substances or compositions for use in a first or further medical treatment.

Electronic Acknowledgement Receipt

EFS ID:	38237264
Application Number:	15809815
International Application Number:	
Confirmation Number:	5137
Title of Invention:	Methods for Treating Metastatic Pancreatic Cancer Using Combination Therapies Comprising Liposomal Irinotecan and Oxaliplatin
First Named Inventor/Applicant Name:	Eliel Bayever
Customer Number:	153749
Filer:	Mary Rucker Henninger/Richard King
Filer Authorized By:	Mary Rucker Henninger
Attorney Docket Number:	263266-421428
Receipt Date:	09-JAN-2020
Filing Date:	10-NOV-2017
Time Stamp:	10:57:46
Application Type:	Utility under 35 USC 111(a)

Payment information:

Submitted with Payment	no

File Listing:

Document Number	Document Description	File Name	File Size(Bytes)/ Message Digest	Multi Part /.zip	Pages (if appl.)
1	Non Patent Literature	Hycamtin_PI_2014.pdf	1165825 de596c6167ad1d5f29e3c1dc772aa63a44abaa94	no	23

Warnings:

Information:					
2	Non Patent Literature	Hycamtin_PI_2015.pdf	979245 27527d725065dd8fb13c50bc51a4eed43c98bf03	no	21
Warnings:					
Information:					
3	Non Patent Literature	Kalra_2014_7003-13.pdf	424533 3c7df4ef520b4afd3f9a5203373ef818304fc2aa	no	12
Warnings:					
Information:					
4	Non Patent Literature	Kalra_2014_poster_V2pdf.pdf	918097 a0eb8a8359a7c977de25f4ab3788a7b61bd34224	no	5
Warnings:					
Information:					
5	Non Patent Literature	Kalra_2014_presentation.pdf	3186740 9e33c66b1a98ddc71b660ab28c20e43901d82a17	no	32
Warnings:					
Information:					
6	Non Patent Literature	Kang_2015_V2pdf.pdf	749229 b7445ad17b529c33ac213f0b1c45e3224f295852	no	13
Warnings:					
Information:					
7	Non Patent Literature	Kim_2014_poster_V2pdf.pdf	1351197 328aba69af0c39ad472f7f0c84c3cef21c4e03fc	no	10
Warnings:					
Information:					
8	Non Patent Literature	Kirpotin_2006.pdf	1349888 7f5463a7c16cb1616b258145649bce458424b5a1	no	10
Warnings:					
Information:					

9	Non Patent Literature	Klinz_2011_abst_C207.pdf	114573 cb509b85ebc7d616202d2e2987ee1831d6debf6e	no	2
Warnings:					
Information:					
10	Non Patent Literature	Klinz_2016_poster_V3pdf.pdf	1008844 b2e512dcb6c491f0d60a3c3dbb204e6fc28d3916	no	10
Warnings:					
Information:					
11	Non Patent Literature	Klinz_2013_poster_V2pdf.pdf	1013659 1a20ada8fbb31aa4ebefc8aa3b91a46635c39463	no	7
Warnings:					
Information:					
12	Non Patent Literature	Klinz_2011_abst_3637.pdf	54862 3fad4b0b727792e6b7f0c77f626e4496de34dabd	no	1
Warnings:					
Information:					
13	Non Patent Literature	Korn_2014.pdf	5167513 fb2e309ecddb818c68942374b746dd16d773f197	no	23
Warnings:					
Information:					
14	Non Patent Literature	Koshkaryev_2016_poster_V2.pdf	825366 1f1d7695ba4a614dfdf8665a8e738b3f0b14341d	no	5
Warnings:					
Information:					
15	Non Patent Literature	Krauze_2007.pdf	916028 e954cbe19c52088ba1da10f15d3308c3eef8b729	no	11
Warnings:					
Information:					

16	Non Patent Literature	Kummar_2011.pdf	1195754 89d9299d742968077de0dfe4bc131e0077b05322	no	10
Warnings:					
Information:					
17	Non Patent Literature	Landry_2005.pdf	1649680 f04e36ab44e16729ee7103a3e0d72d0f78825a8a	no	11
Warnings:					
Information:					
18	Non Patent Literature	Lee_2012_abstract.pdf	131187 d62edf65e2b840b3b60e576762eaebfa5ef89c49	no	2
Warnings:					
Information:					
19	Non Patent Literature	Lee_2012_poster_V3pdf.pdf	929703 7fb11e45f311e56ed4ff93f774f008822335ac60	no	13
Warnings:					
Information:					
20	Non Patent Literature	Lee_2016_poster_V2pdf.pdf	1031764 0d94f9a137a92ab31385ac127b378f3ce57fef2c	no	8
Warnings:					
Information:					
21	Non Patent Literature	Leonard_2017.pdf	672310 8137c94ef8b13cc07f61954565600a2df4af7964	no	11
Warnings:					
Information:					
22	Non Patent Literature	Leonard__2017_poster.pdf	583517 2b66ef365e5c49f3d7f548a55dbe065a815f5fe5	no	6
Warnings:					
Information:					

23	Non Patent Literature	Leonard_2016_abstract.pdf	116936 64520d659cd472e8e78374298cc7b7e51c0c5df5	no	1
Warnings:					
Information:					
24	Non Patent Literature	Leonard__2016_poster.pdf	801025 12383598520f6f30ff51d23acb7696552c1d9c9b	no	5
Warnings:					
Information:					
25	Non Patent Literature	LoRusso_2016_V2.pdf	508074 7ab789e47be4e0bd68526f3d6cb70cd817d4a2b5	no	12
Warnings:					
Information:					
26	Non Patent Literature	LoRusso_2011_abst.pdf	62694 b111de8eac8c997d9a647492ec268d824773488b	no	1
Warnings:					
Information:					
27	Non Patent Literature	LoRusso_2011_slides.pdf	13720868 b3d56fd567e18d8918d027c84c046be737487200	no	37
Warnings:					
Information:					
28	Non Patent Literature	Lynparza_PI_2014.pdf	598399 061ce254f541a3c274b26571f408c534854746a4	no	6
Warnings:					
Information:					
29	Non Patent Literature	Mamot_2005.pdf	1388937 3c947c35e98d9ba03e45a7dbbd48f254b82a4d4f	no	9
Warnings:					
Information:					

30	Non Patent Literature	Mamot_2004_V2pdf.pdf	181894 d868935448aefd5cda74d92e99d94069dc8d22da	no	10
Warnings:					
Information:					
31	Non Patent Literature	Masuda_1992.pdf	486740 6bd3b97936348dc083c71f92206e9175321fb864	no	5
Warnings:					
Information:					
32	Non Patent Literature	Merrimack_2012.pdf	13677 d85d12708c1d18af79e47c4caf76cea7a209830f	no	2
Warnings:					
Information:					
33	Non Patent Literature	Messerer_2004.pdf	1264876 2aa57d725dc9887ff9893ba2a1ff30f55b22c119	no	12
Warnings:					
Information:					
34	Non Patent Literature	Miles_2002.pdf	658776 7b078a13c618631f5650952ec999de433dfe50be	no	9
Warnings:					
Information:					
35	Non Patent Literature	Miller_2015b.pdf	4119957 5a7183190eb805bda02dbafea8bc3f00709c96e3	no	37
Warnings:					
Information:					
36	Non Patent Literature	Miller_2015.pdf	2926963 dcb8682b98c6413f18d8b208e285a82f56f4de72	no	24
Warnings:					
Information:					

37	Non Patent Literature	Mohammad_2018.pdf	2244388 58298e7b8028d3965b99d4a6ab4177c6dd161e32	no	10
Warnings:					
Information:					
38	Non Patent Literature	Mukhtar_2011.pdf	993058 14b7b61363a6c01659e97b37c6e0b81c6789434d	no	10
Warnings:					
Information:					
39	Non Patent Literature	Murai_2014b_V2.pdf	341784 4f58af239c081fc1a8b876a7cc83577799ff3ce4	no	13
Warnings:					
Information:					
40	Non Patent Literature	Murai_2014.pdf	1094460 e5055e1d4a54b0a8a5073d9eba0de231a8188fc1	no	9
Warnings:					
Information:					
41	Non Patent Literature	Noble_2006.pdf	355566 eddf47088dd3f2649044a36c28f5268158553feb	no	6
Warnings:					
Information:					
42	Non Patent Literature	Noble_2014.pdf	4066131 17306ff3d125609197f01f7a882dea33e1ee6d65	no	10
Warnings:					
Information:					
43	Non Patent Literature	O_Brien_2006.pdf	109378 805c185177bac2a35c2911b771c344bc4e445293	no	7
Warnings:					
Information:					

44	Non Patent Literature	Owonikoko___2012.pdf	1210351 07d1e905bab42e07237a1c002065046e176ce46c	no	7
Warnings:					
Information:					
45	Non Patent Literature	Pallis_2008.pdf	173866 a280ae3af37c64dad5266507dab0c5c81db6ffb2	no	5
Warnings:					
Information:					
46	Non Patent Literature	Park_2002.pdf	1454318 ee074a180529badb65fea6a80104e0e271a3a492	no	11
Warnings:					
Information:					
47	Non Patent Literature	Patton_2002.pdf	3859234 fc8301d3c76e563c2124dc54632a94e7db41720e	no	29
Warnings:					
Information:					
48	Non Patent Literature	Paz-Ares__2018_poster.pdf	699352 fc245f56583bebfb64545fb4c0c6f8de9203ac6e	no	9
Warnings:					
Information:					
49	Non Patent Literature	Paz-Arez_2019__poster.pdf	1265847 e85e80f5ea092a58c7db862ebf25259e648cc022	no	6
Warnings:					
Information:					
50	Non Patent Literature	Paz-Ares_2019_abstract.pdf	1585761 dd52e56896b3e75911dcdf915f466039f1b3091a	no	3
Warnings:					
Information:					

51	Other Reference-Patent/App/Search documents	PCTIB2017000681_IPRP.pdf	207847 3111eb5ba5e7584ac9fbf2cf2b9887a036e68039	no	6
Warnings:					
Information:					
52	Other Reference-Patent/App/Search documents	PCTIB2017000681_ISR_WO.pdf	292884 031c0ff18c12c6f89d28a0f0405b9814c08fb48e	no	8
Warnings:					
Information:					
		Total Files Size (in bytes):	72223555		

This Acknowledgement Receipt evidences receipt on the noted date by the USPTO of the indicated documents, characterized by the applicant, and including page counts, where applicable. It serves as evidence of receipt similar to a Post Card, as described in MPEP 503.

New Applications Under 35 U.S.C. 111

If a new application is being filed and the application includes the necessary components for a filing date (see 37 CFR 1.53(b)-(d) and MPEP 506), a Filing Receipt (37 CFR 1.54) will be issued in due course and the date shown on this Acknowledgement Receipt will establish the filing date of the application.

National Stage of an International Application under 35 U.S.C. 371

If a timely submission to enter the national stage of an international application is compliant with the conditions of 35 U.S.C. 371 and other applicable requirements a Form PCT/DO/EO/903 indicating acceptance of the application as a national stage submission under 35 U.S.C. 371 will be issued in addition to the Filing Receipt, in due course.

New International Application Filed with the USPTO as a Receiving Office

If a new international application is being filed and the international application includes the necessary components for an international filing date (see PCT Article 11 and MPEP 1810), a Notification of the International Application Number and of the International Filing Date (Form PCT/RO/105) will be issued in due course, subject to prescriptions concerning national security, and the date shown on this Acknowledgement Receipt will establish the international filing date of the application.

PATENT COOPERATION TREATY

PCT

INTERNATIONAL PRELIMINARY REPORT ON PATENTABILITY
(Chapter I of the Patent Cooperation Treaty)

(PCT Rule 44*bis*)

Applicant's or agent's file reference 156363.00003	**FOR FURTHER ACTION**	See item 4 below
International application No. PCT/US2013/046914	International filing date *(day/month/year)* 20 June 2013 (20.06.2013)	Priority date *(day/month/year)* 20 June 2012 (20.06.2012)
International Patent Classification (8th edition unless older edition indicated) See relevant information in Form PCT/ISA/237		
Applicant MERRIMACK PHARMACEUTICALS, INC.		

1. This international preliminary report on patentability (Chapter I) is issued by the International Bureau on behalf of the International Searching Authority under Rule 44 *bis*.1(a).

2. This REPORT consists of a total of 7 sheets, including this cover sheet.

   In the attached sheets, any reference to the written opinion of the International Searching Authority should be read as a reference to the international preliminary report on patentability (Chapter I) instead.

3. This report contains indications relating to the following items:

☒	Box No. I	Basis of the report
☐	Box No. II	Priority
☐	Box No. III	Non-establishment of opinion with regard to novelty, inventive step and industrial applicability
☐	Box No. IV	Lack of unity of invention
☒	Box No. V	Reasoned statement under Article 35(2) with regard to novelty, inventive step or industrial applicability; citations and explanations supporting such statement
☐	Box No. VI	Certain documents cited
☐	Box No. VII	Certain defects in the international application
☐	Box No. VIII	Certain observations on the international application

4. The International Bureau will communicate this report to designated Offices in accordance with Rules 44*bis*.3(c) and 93*bis*.1 but not, except where the applicant makes an express request under Article 23(2), before the expiration of 30 months from the priority date (Rule 44*bis* .2).

	Date of issuance of this report 23 December 2014 (23.12.2014)
The International Bureau of WIPO 34, chemin des Colombettes 1211 Geneva 20, Switzerland Facsimile No. +41 22 338 82 70	Authorized officer Yukari Nakamura e-mail: pt07.pct@wipo.int

Form PCT/IB/373 (January 2004)

PATENT COOPERATION TREATY

From the
INTERNATIONAL SEARCHING AUTHORITY

To:
RUSSETT, MARK D.

EDWARDS WILDMAN PALMER LLP P.O. BOX 55874
BOSTON, MASSACHUSETTS 02205 USA

PCT

WRITTEN OPINION OF THE INTERNATIONAL SEARCHING AUTHORITY

(PCT Rule 43bis.1)

Date of mailing *(day/month/year)* **02 September 2013 (02.09.2013)**

Applicant's or agent's file reference
93445WO(309768)

FOR FURTHER ACTION
See paragraph 2 below

International application No.	International filing date *(day/month/year)*	Priority date *(day/month/year)*
PCT/US2013/046914	**20 June 2013 (20.06.2013)**	20 June 2012 (20.06.2012)

International Patent Classification (IPC) or both national classification and IPC
G01N 33/68(2006.01)i, G01N 33/53(2006.01)i, G01N 33/48(2006.01)i, G01N 33/574(2006.01)i

Applicant
MERRIMACK PHARMACEUTICALS, INC.

1. This opinion contains indications relating to the following items:

- [x] Box No. I Basis of the opinion
- [ ] Box No. II Priority
- [ ] Box No. III Non-establishment of opinion with regard to novelty, inventive step and industrial applicability
- [ ] Box No. IV Lack of unity of invention
- [x] Box No. V Reasoned statement under Rule 43bis.1(a)(i) with regard to novelty, inventive step or industrial applicability; citations and explanations supporting such statement
- [ ] Box No. VI Certain documents cited
- [ ] Box No. VII Certain defects in the international application
- [ ] Box No. VIII Certain observations on the international application

2. **FURTHER ACTION**

If a demand for international preliminary examination is made, this opinion will be considered to be a written opinion of the International Preliminary Examining Authority ("IPEA") except that this does not apply where the applicant chooses an Authority other than this one to be the IPEA and the chosen IPEA has notified the International Bureau under Rule 66.1bis(b) that written opinions of this International Searching Authority will not be so considered.

If this opinion is, as provided above, considered to be a written opinion of the IPEA, the applicant is invited to submit to the IPEA a written reply together, where appropriate, with amendments, before the expiration of 3 months from the date of mailing of Form PCT/ISA/220 or before the expiration of 22 months from the priority date, whichever expires later.
For further options, see Form PCT/ISA/220.

Name and mailing address of the ISA/KR	Date of completion of this opinion	Authorized officer
Korean Intellectual Property Office 189 Cheongsa-ro, Seo-gu, Daejeon Metropolitan City, 302-701, Republic of Korea Facsimile No. +82-42-472-7140	29 August 2013 (29.08.2013)	KIM Seung Beom Telephone No. +82-42-481-3371

WRITTEN OPINION OF THE INTERNATIONAL SEARCHING AUTHORITY

International application No.
PCT/US2013/046914

Box No. I Basis of this opinion

1. With regard to the **language**, this opinion has been established on the basis of :

   ☒ the international application in the language in which it was filed

   ☐ a translation of the international application into _____ , which is the language of a translation furnished for the purposes of international search (Rules 12.3(a) and 23.1(b))

2. ☐ This opinion has been established taking into account the **rectification of an obvious mistake** authorized by or notified to this Authority under Rule 91 (Rule 43*bis*.1(a))

3. With regard to any **nucleotide and/or amino acid sequence** disclosed in the international application, this opinion has been established on the basis of:

   a. a sequence listing filed or furnished
      ☐ on paper
      ☐ in electronic form

   b. time of filing or furnishing
      ☐ contained in the international application as filed.
      ☐ filed together with the international application in electronic form.
      ☐ furnished subsequently to this Authority for the purposes of search.

4. ☐ In addition, in the case that more than one version or copy of a sequence listing has been filed or furnished, the required statements that the information in the subsequent or additioanl copies is identical to that in the application as filed or does not go beyond the application as filed, as appropriate, were furnished.

5. Additional comments:

WRITTEN OPINION OF THE INTERNATIONAL SEARCHING AUTHORITY

International application No.
PCT/US2013/046914

Box No. V Reasoned statement under Rule 43bis.1(a)(i) with regard to novelty, inventive step or industrial applicability; citations and explanations supporting such statement

1. Statement

Novelty (N)	Claims	7-8,11-14	YES
	Claims	1-6,9-10,15-20	NO
Inventive step (IS)	Claims	NONE	YES
	Claims	1-20	NO
Industrial applicability (IA)	Claims	1-20	YES
	Claims	NONE	NO

2. Citations and explanations :

Reference is made to the following document:
D1: US 7219016 B2 (RIMM et al.) 15 May 2007

D1 relates to systems and methods for rapidly analyzing cell containing samples.

1. Novelty and Inventive Step
1.1. Claim 1
Claim 1 relates to a method of quantitatively measuring levels of a cellular protein comprising steps of: (a) preparing a section from a tissue sample; (b) staining the section with a first stain specific to the cellular protein, a second stain specific to cell nuclei, and a third stain allowing the discrimination of target cells from non-target cells; (c) obtaining one or more microscopic images of the section; (d) identifying target cells with the one or more images based upon staining with the second and third stains; (e) measuring the intensity of staining with the first stain and recording cell location coordinate data; (f) ascertaining a level of stained cellular protein that is detected in each identified target cell by comparing stain intensity of the cellular protein; and (g) creating a map of quantity distribution of the cellular protein in each of the target cells within a region of the section.

D1, which is considered to be the closest prior art to the subject matter of claim 1, discloses a computer implemented method for localizing and quantitating a particular biomarker of subcellular compartments present in individual cells of interest contained in a tissue sample comprising: (a' and b') incubating the tissue sample with a first stain that specifically labels a first marker defined subcellular compartment, a second stain that specifically labels a second marker defined subcellular compartment, and a third stain that specifically labels the biomarker; (c') obtaining a high resolution image of each of the first, the second, and the third stain in the tissue sample using an upright or inverted optical microscope; (d' and e') determining the first and second stain intensity in each of the pixel locations in the first and the second image and assigning those pixel locations having an intensity; and (f" and g') analyzing in the third image the pixel locations assigned to the first subcellular compartment or the second subcellular compartment so as to thereby localize and quantitate the biomarker in the first subcellular compartment relative to the second subcellular compartment (See claim 1). D1 further describes that the subcellular compartment is selected from the group consisting of a cell nucleus, a

Continued on Supplemental Box

Supplemental Box

In case **the space in any of the preceding boxes is not sufficient.**
Continuation of : Box No. V

cytoplasm, a nuclear membrane, a cellular membrane, a mitochondria, an endoplasmic reticulum, a peroxisome and a lysosome (See claim 2).

Although the names of the some components are slightly different, the main features of the inventions are substantially the same or they are very easily anticipated by D1 or well-known arts.
Therefore, claim 1 lacks novelty under PCT Article 33(2) and does not involve an inventive step under PCT Article 33(3).

1.2. Claim 2
Claim 2, dependent on claim 1, further defines that a) the tissue sample is a tumor sample; that b) the target cells are malignant cells; and that c) the non-target cells are stromal cells.
D1 further discloses monochromatic images of a colon carcinoma taken after staining with fluorescently-tagged markers and combined into a single color image as follows: DAPI (to visualize nuclei, blue), anti-cytokeratin (to distinguish tumor from non-tumor elements, green), and anti-alpha-catenin (to visualize cell membranes, red) (See figures 1A-1D). Accordingly, claim 2 is substantially the same as D1.
Therefore, claim 2 lacks novelty under PCT Article 33(2) and does not involve an inventive step under PCT Article 33(3).

1.3. Claims 3-6
Claims 3-6, dependent on claims 1 and 3-5 respectively, further define that the cellular protein is a cell surface receptor (claim 3) comprising a growth factor receptor (claim 4) such as an EGFR family receptor (claim 5), specifically HER2, HER3 or EGFR (claim 6).
D1 further discloses a construction of tissue microarrays for a survival analysis of the Estroge Receptor (ER) and HER2/neu and for analysis of nuclear associated bata-catenin and D1 further describes that membrane-localized signal is analyzed for HER2/neu (See column 18, lines 29-67, column 19, lines 1-58). Accordingly, claims 3-6 are substantially the same as D1.
Therefore, claims 3-6 lack novelty under PCT Article 33(2) and do not involve an inventive step under PCT Article 33(3).

1.4. Claims 7 and 8
Claims 7 and 8, dependent on claim 1, further define that the quantity distribution of the cellular protein is a continuous distribution (claim 7) and that the first stain comprises an antibody specific to the cellular protein (claim 8).
D1 further discloses a redistribution of the pixel intensities by the computer (See column 5, lines 31-41) and D1 describes that the first subcellular compartment stained by the first stain is a cellular membrane (See claim 8).
Claims 7 and 8 differ from D1 in the continuous distribution and the antibody. However, the features of claims 7 and 8 are merely one of several straightforward possibilities from which a

Continued on The Next Page

Supplemental Box

In case **the space in any of the preceding boxes is not sufficient.**
Continuation of : Previous Page

skilled person in the art would select in accordance with circumstances, without the exercise of inventive skill, in order to solve the problem posed.
Therefore, claims 7 and 8 are novel under PCT Article 33(2), but lack an inventive step under PCT Article 33(3).

1.5. Claims 9 and 10
Claims 9 and 10, dependent on claims 1 and 9 respectively, further define that the second stain is a DNA stain (claim 9) and that the second stain comprises either or both of DAPI and a Hoechst stain (claim 10).
D1 further describes that the second stain comprises a fluorophore selected from the group consisting of 4′,6-diamidino-2-phenylindole (DAPI) (See claim 11). Accordingly, claims 9 and 10 are substantially the same as D1.
Therefore, claims 9 and 10 lack novelty under PCT Article 33(2) and do not involve an inventive step under PCT Article 33(3).

1.6. Claims 11 and 12
Claims 11 and 12, dependent on claims 1 and 11 respectively, further define that the third stain comprises an antibody (claim 11) and that the antibody comprised by the third stain is specific to a cytokeratin (claim 12).
The technical feature of the third stain comprising a cytokerain antibody is not explicitly disclosed in D1. However, said feature is virtually suggested by the same document considering the third stain that specifically labels the biomarker and the biomarker selected from the group comprising anti-cytokeratines (See claim 1 and column 15, lines 19-24, 64-65). Therefore, a person skilled in the art would easily conceive the idea of employing the feature of the third stain comprising a cytokerain antibody.
Therefore, claims 11 and 12 are novel under PCT Article 33(2), but lack an inventive step under PCT Article 33(3).

1.7. Claims 13 and 14
Claims 13 and 14, dependent on claim 1, further define that the map is in the form of a complementary cumulative distribution (claim 13) and that the identifying and measuring and ascertaing are done by automated image analysis (claim 14).
As described in points 1.1. and 1.4., D1 further discloses a redistribution of the pixel intensities by the computer.
Claims 13 and 14 differ from D1 in a cumulative distribution and ascertaining. However, the features of claims 13 and 14 are merely one of several straightforward possibilities from which a skilled person in the art would select in accordance with circumstances, without the exercise of inventive skill, in order to solve the problem posed.
Therefore, claims 13 and 14 novel under PCT Article 33(2), but lack an inventive step under PCT Article 33(3).

Continued on The Next Page

Supplemental Box

In case **the space in any of the preceding boxes is not sufficient.**
Continuation of : Previous Page

1.8. Claims 15-18
Claims 15-17, dependent on claim 1, further define that the plurality of identified target cells comprise at least 500 (claim 15), 1000 (claim 16), or 2000 (claim 17) cells. Claim 18, dependent on claim 1, further defines that the plurality of standard cell preparations are in the form of an array of stained standard cells.
D1 further discloses a tissue microarray which may include any number of histospots (corresponding to target cells), typically on the order of several hundred to a few thousand (See column 10, lines 53-55). Accordingly, claims 15-18 are substantially the same as D1.
Therefore, claims 15-18 lack novelty under PCT Article 33(2), and do not involve an inventive step under PCT Article 33(3).

1.9. Claims 19 and 20
Claims 19 and 20, dependent on claims 8 or 11, further define that the antibody is a labeled antibody (claim 19) and that the antibody is an unlabeled antibody that is subsequently labeled with a labeled secondary antibody specific to an antibody type characteristic of the first antibody (claim 20).
D1 further describes that one effectively builds a sandwich of binding members, where the first binding member binds to the cellular component and serves to provide for secondary binding, where the secondary binding member may or may not include a label, which may further provide for tertiary binding where the tertiary binding member will provide a label (See column 16, lines 32-46). Accordingly, claims 19 and 20 are substantially the same as D1.
Therefore, claims 19 and 20 lack novelty under PCT Article 33(2), and do not involve an inventive step under PCT Article 33(3).

2. Industrial Applicability
Claims 1-20 are industrially applicable under PCT Article 33(4).

PATENT COOPERATION TREATY

PCT

INTERNATIONAL SEARCH REPORT

(PCT Article 18 and Rules 43 and 44)

Applicant's or agent's file reference 93445WO(309768)	**FOR FURTHER ACTION**	see Form PCT/ISA/220 as well as, where applicable, item 5 below.
International application No. **PCT/US2013/046914**	International filing date *(day/month/year)* **20 June 2013 (20.06.2013)**	(Earliest) Priority Date *(day/month/year)* 20 June 2012 (20.06.2012)

Applicant

MERRIMACK PHARMACEUTICALS, INC.

This International search report has been prepared by this International Searching Authority and is transmitted to the applicant according to Article 18. A copy is being transmitted to the International Bureau.

This international search report consists of a total of **3** sheets.

☐ It is also accompanied by a copy of each prior art document cited in this report.

1. **Basis of the report**
   a. With regard to the **language**, the international search was carried out on the basis of :
      ☒ the international application in the language in which it was filed
      ☐ a translation of the international application into _____ , which is the language of a translation furnished for the purposes of international search (Rules 12.3(a) and 23.1(b))
   b. ☐ This international search report has been established taking into account the **rectification of an obvious mistake** authorized by or notified to this Authority under Rule 91 (Rule 43.6*bis*(a)).
   c. ☐ With regard to any **nucleotide and/or amino acid sequence** disclosed in the international application, see Box No. I.
2. ☐ **Certain claims were found unsearchable** (See Box No. II)
3. ☐ **Unity of invention is lacking** (See Box No. III)
4. With regard to the **title,**
   ☒ the text is approved as submitted by the applicant.
   ☐ the text has been established by this Authority to read as follows:
5. With regard to the **abstract,**
   ☒ the text is approved as submitted by the applicant.
   ☐ the text has been established, according to Rule 38.2, by this Authority as it appears in Box No. IV. The applicant may, within one month from the date of mailing of this international search report, submit comments to this Authority.
6. With regard to the drawings,
   a. the figure of the **drawings** to be published with the abstract is Figure No. _____
      ☐ as suggested by the applicant.
      ☐ as selected by this Authority, because the applicant failed to suggest a figure.
      ☐ as selected by this Authority, because this figure better characterizes the invention.
   b. ☒ none of the figure is to be published with the abstract.

INTERNATIONAL SEARCH REPORT

International application No.
PCT/US2013/046914

A. CLASSIFICATION OF SUBJECT MATTER

G01N 33/68(2006.01)i, G01N 33/53(2006.01)i, G01N 33/48(2006.01)i, G01N 33/574(2006.01)i

According to International Patent Classification (IPC) or to both national classification and IPC

B. FIELDS SEARCHED

Minimum documentation searched (classification system followed by classification symbols)
G01N 33/68; G01N 33/48; G01N 33/53; G01N 33/574

Documentation searched other than minimum documentation to the extent that such documents are included in the fields searched
Korean utility models and applications for utility models
Japanese utility models and applications for utility models

Electronic data base consulted during the international search (name of data base and, where practicable, search terms used)
eKOMPASS(KIPO internal) & Keywords:quantitative, measurement, cellular protein, staining, tissue, section, and mapping

C. DOCUMENTS CONSIDERED TO BE RELEVANT

Category*	Citation of document, with indication, where appropriate, of the relevant passages	Relevant to claim No.
X	US 7219016 B2 (RIMM et al.) 15 May 2007 See abstract; columns 5,10,13,15-16,18-19; and claims 1-3, 8-12.	1-20
A	WAHLBY et al., `Sequential immunofluorescence staining and image analysis for detection of large numbers of antigens in individual cell nuclei` Cytometry, Vol.47, No.1, pp.32-41 (2002) See the whole document.	1-20
A	PATTON, `Detection technologies in proteome analysis` Journal of Chromatography B, Vol.771, No.1, pp.3-31 (2002) See the whole document.	1-20
A	ALFERT et al., `A selective staining method for the basic proteins of cell nuclei` PNAS, No.39, Vol.10, pp.991-999 (1953) See the whole document.	1-20
A	BUTT et al., `Postfractionation for enhanced proteomic analyses: routine electrophoretic methods increase the resolution of standard 2D-PAGE` Journal of Proteome Research, Vol.4, No.3, pp.982-991 (2005) See the whole document.	1-20

☐ Further documents are listed in the continuation of Box C.

☒ See patent family annex.

* Special categories of cited documents:
"A" document defining the general state of the art which is not considered to be of particular relevance
"E" earlier application or patent but published on or after the international filing date
"L" document which may throw doubts on priority claim(s) or which is cited to establish the publication date of citation or other special reason (as specified)
"O" document referring to an oral disclosure, use, exhibition or other means
"P" document published prior to the international filing date but later than the priority date claimed
"T" later document published after the international filing date or priority date and not in conflict with the application but cited to understand the principle or theory underlying the invention
"X" document of particular relevance; the claimed invention cannot be considered novel or cannot be considered to involve an inventive step when the document is taken alone
"Y" document of particular relevance; the claimed invention cannot be considered to involve an inventive step when the document is combined with one or more other such documents,such combination being obvious to a person skilled in the art
"&" document member of the same patent family

Date of the actual completion of the international search	Date of mailing of the international search report
29 August 2013 (29.08.2013)	**02 September 2013 (02.09.2013)**

Name and mailing address of the ISA/KR
Korean Intellectual Property Office
189 Cheongsa-ro, Seo-gu, Daejeon Metropolitan City, 302-701, Republic of Korea
Facsimile No. +82-42-472-7140

Authorized officer
KIM Seung Beom
Telephone No. +82-42-481-3371

INTERNATIONAL SEARCH REPORT

Information on patent family members

International application No.
PCT/US2013/046914

Patent document cited in search report	Publication date	Patent family member(s)	Publication date
US 7219016 B2	15/05/2007	AU 2002311827 B2	14/08/2008
		AU 2002311827 B9	12/03/2009
		CA 2442604 A1	31/10/2002
		CA 2442604 C	07/06/2011
		EP 1390747 A1	25/02/2004
		EP 1390747 A4	08/07/2009
		JP 2004-532410 A	21/10/2004
		JP 2008-139322 A	19/06/2008
		JP 2011-117978 A	16/06/2011
		JP 2013-092540 A	16/05/2013
		JP 4433674 B2	08/01/2010
		JP 4873574 B2	02/12/2011
		US 2002-0177149 A1	28/11/2002
		US 2008-0013816 A1	17/01/2008
		US 2008-0026420 A1	31/01/2008
		US 2008-0046190 A1	21/02/2008
		US 2008-0056553 A1	06/03/2008
		US 2012-0329665 A1	27/12/2012
		US 7873480 B2	18/01/2011
		US 8036833 B2	11/10/2011
		US 8121794 B2	21/02/2012
		US 8185320 B2	22/05/2012
		WO 02-086498 A1	31/10/2002
		WO 02-086498 A8	12/12/2002

PATENT COOPERATION TREATY

PCT

INTERNATIONAL PRELIMINARY REPORT ON PATENTABILITY
(Chapter I of the Patent Cooperation Treaty)

(PCT Rule 44*bis*)

Applicant's or agent's file reference 156363.00004	**FOR FURTHER ACTION**	See item 4 below
International application No. PCT/US2013/075513	International filing date *(day/month/year)* 17 December 2013 (17.12.2013)	Priority date *(day/month/year)* 14 December 2012 (14.12.2012)
International Patent Classification (8th edition unless older edition indicated) See relevant information in Form PCT/ISA/237		
Applicant MERRIMACK PHARMACEUTICALS, INC.		

1. This international preliminary report on patentability (Chapter I) is issued by the International Bureau on behalf of the International Searching Authority under Rule 44 *bis*.1(a).

2. This REPORT consists of a total of 7 sheets, including this cover sheet.

   In the attached sheets, any reference to the written opinion of the International Searching Authority should be read as a reference to the international preliminary report on patentability (Chapter I) instead.

3. This report contains indications relating to the following items:

☒	Box No. I	Basis of the report
☐	Box No. II	Priority
☐	Box No. III	Non-establishment of opinion with regard to novelty, inventive step and industrial applicability
☐	Box No. IV	Lack of unity of invention
☒	Box No. V	Reasoned statement under Article 35(2) with regard to novelty, inventive step or industrial applicability; citations and explanations supporting such statement
☐	Box No. VI	Certain documents cited
☐	Box No. VII	Certain defects in the international application
☐	Box No. VIII	Certain observations on the international application

4. The International Bureau will communicate this report to designated Offices in accordance with Rules 44*bis*.3(c) and 93*bis*.1 but not, except where the applicant makes an express request under Article 23(2), before the expiration of 30 months from the priority date (Rule 44*bis* .2).

	Date of issuance of this report 16 June 2015 (16.06.2015)
The International Bureau of WIPO 34, chemin des Colombettes 1211 Geneva 20, Switzerland Facsimile No. +41 22 338 82 70	Authorized officer Yukari Nakamura e-mail: pt07.pct@wipo.int

Form PCT/IB/373 (January 2004)

PATENT COOPERATION TREATY

From the
INTERNATIONAL SEARCHING AUTHORITY

To: MARK D. RUSSETT
EDWARDS WILDMAN PALMER LLP
P.O. BOX 55874
BOSTON, MA 02205

PCT

WRITTEN OPINION OF THE
INTERNATIONAL SEARCHING AUTHORITY

(PCT Rule 43*bis*.1)

Date of mailing *(day/month/year)*	06 JUN 2014
Applicant's or agent's file reference 94489WO(309768)	**FOR FURTHER ACTION** See paragraph 2 below

International application No.	International filing date *(day/month/year)*	Priority date *(day/month/year)*
PCT/US 13/75513	17 December 2013 (17.12.2013)	14 December 2012 (14.12.2012)

International Patent Classification (IPC) or both national classification and IPC
IPC(8) - A61B 5/055, A61K 49/06, A61P 35/00 (2014.01)
USPC - 424/9.321, 514/19.3, 600/410

Applicant MERRIMACK PHARMACEUTICALS, INC.

1. This opinion contains indications relating to the following items:

- ☒ Box No. I Basis of the opinion
- ☐ Box No. II Priority
- ☐ Box No. III Non-establishment of opinion with regard to novelty, inventive step and industrial applicability
- ☐ Box No. IV Lack of unity of invention
- ☒ Box No. V Reasoned statement under Rule 43*bis*.1(a)(i) with regard to novelty, inventive step or industrial applicability; citations and explanations supporting such statement
- ☐ Box No. VI Certain documents cited
- ☐ Box No. VII Certain defects in the international application
- ☐ Box No. VIII Certain observations on the international application

2. **FURTHER ACTION**

If a demand for international preliminary examination is made, this opinion will be considered to be a written opinion of the International Preliminary Examining Authority ("IPEA") except that this does not apply where the applicant chooses an Authority other than this one to be the IPEA and the chosen IPEA has notified the International Bureau under Rule 66.1 *bis*(b) that written opinions of this International Searching Authority will not be so considered.

If this opinion is, as provided above, considered to be a written opinion of the IPEA, the applicant is invited to submit to the IPEA a written reply together, where appropriate, with amendments, before the expiration of 3 months from the date of mailing of Fom PCT/ISA/220 or before the expiration of 22 months from the priority date, whichever expires later.

For further options, see Form PCT/ISA/220.

Name and mailing address of the ISA/US	Date of completion of this opinion	Authorized officer:
Mail Stop PCT, Attn: ISA/US Commissioner for Patents P.O. Box 1450, Alexandria, Virginia 22313-1450 Facsimile No. 571-273-3201	19 May 2014 (19.05.2014)	Lee W. Young PCT Helpdesk: 571-272-4300 PCT OSP: 571-272-7774

Form PCT/ISA/237 (cover sheet) (July 2011)

WRITTEN OPINION OF THE INTERNATIONAL SEARCHING AUTHORITY

International application No.
PCT/US 13/75513

Box No. I Basis of this opinion

1. With regard to the **language**, this opinion has been established on the basis of:

   ☒ the international application in the language in which it was filed.

   ☐ a translation of the international application into _____ which is the language of a translation furnished for the purposes of international search (Rules 12.3(a) and 23.1(b)).

2. ☐ This opinion has been established taking into account the **rectification of an obvious mistake** authorized by or notified to this Authority under Rule 91 (Rule 43*bis*.1(a))

3. With regard to any **nucleotide and/or amino acid sequence** disclosed in the international application, this opinion has been established on the basis of a sequence listing filed or furnished:

   a. (means)

      ☐ on paper

      ☐ in electronic form

   b. (time)

      ☐ in the international application as filed

      ☐ together with the international application in electronic form

      ☐ subsequently to this Authority for the purposes of search

4. ☐ In addition, in the case that more than one version or copy of a sequence listing has been filed or furnished, the required statements that the information in the subsequent or additional copies is identical to that in the application as filed or does not go beyond the application as filed, as appropriate, were furnished.

5. Additional comments:

WRITTEN OPINION OF THE INTERNATIONAL SEARCHING AUTHORITY

International application No.
PCT/US 13/75513

Box No. V **Reasoned statement under Rule 43*bis*.1(a)(i) with regard to novelty, inventive step or industrial applicability; citations and explanations supporting such statement**

1. Statement

Novelty (N)	Claims	1-19	YES
	Claims	None	NO
Inventive step (IS)	Claims	None	YES
	Claims	1-19	NO
Industrial applicability (IA)	Claims	1-19	YES
	Claims	None	NO

2. Citations and explanations:

Claims 1-12 and 14-16 lack an inventive step under PCT Article 33(3) as being obvious over US 2012/0003160 A1 to Wolf et al. (hereinafter 'Wolf') in view of the abstract entitled "Identifying differential mechanisms of action for MM-398/PEP02, a novel nanotherapeutic encapsulation of irinotecan" by Klinz et al. (hereinafter 'Klinz 'MM398').

Regarding claim 1, Wolf discloses a method for selecting and providing pharmaceutical treatment to a patient for a neoplastic condition (para [0020] - "method of assessing a stage of cancer"; para [0042] - "assessing stage of cancer refers to providing any type of information, including ... information useful in selecting an appropriate treatment"; para [0075] staging cancer for a variety of tumor types), the method comprising:

diagnosing a localized neoplastic condition in a patient and identifying one or more locations of neoplasia in the patient (para [0115] - "Once diagnosis of the primary tumor is made, whole-body MRI is appropriate. If a whole-body MEMRI is performed, identification of soft tissues where there is excessive macrophage density will identify where metastasis may be present"), and subsequently, obtaining a contrast-enhanced MRI image of a first location of the one or more locations (para [0020] - "The method comprises administering a macrophage enhancing contrast agent to the subject during an administration session; allowing passage of time sufficient for accumulation of the agent in macrophages of the subject; acquiring a first magnetic resonance image of regions of the subject's body at risk of cancer; using the image to assess macrophage density and displacement associated with any primary cancer or metastatic cancer in the subject, such density and displacement being indicative of neoplasia"; para [0075] - "Using macrophage-seeking contrast agents and whole-body MRI to perform a MEMRI evaluation ... (b) determine the degree of metastasis that may have already begun, (c) identify the location of the metastatic tumors"), and subsequently, selecting an anti-neoplastic pharmaceutical agent and treating the patient with the selected pharmaceutical agent (para [0075] - "(d) customize the anticancer treatment based on the characteristics and metastatic extent of the primary tumor (or metastatic tumors already present), and (e) assess the efficacy of such treatment"); and

wherein, the contrast-enhanced MRI image is obtained following administration of an MRI contrast agent (para [0020]) comprising an MRI contrast-enhancing amount of superparamagnetic iron oxide nanoparticles of about 15-30 nm in diameter (para [0020] - "In a particular embodiment, the macrophage enhancing contrast agent is ferumoxytol"; para [0062] ultrasmall superparamagnetic iron oxides such as ferumoxytol; para [0059] - "10 .micro.m to about 10 nm in diameter).

Wolf does not specifically teach that if the contrast-enhanced MRI image shows contrast enhancement within the first location, the selected pharmaceutical agent is an agent that is formulated as nanoparticles or nanoliposomes of about 70 to about 200 nm in diameter, but if the contrast-enhanced MRI image does not show contrast enhancement at first location, the selected pharmaceutical agent is an agent that is not formulated as nanoparticles or nanoliposomes of about 70 to about 200 nm in diameter. However, Wolf does teach that its method is used to visualize the presence of tumor-associated macrophages (para [0050] - "embodiments of the present invention utilize macrophage-enhancing contrast agents within tumor-associated macrophages ("TAMs") to provide contrast around, and hence visualization of, primary or metastatic tumors"; para [0075] - "any tissue or organ in the entire body that has become surrounded by or associated with macrophages--a marker of the tumorigenic capabilities of that tumor--will be visualized by the whole-body MEMRI performed with any of the macrophage-seeking contrast agents") and that the selected therapy can be liposomal drug delivery (para [0129]). Klinz 'MM398 discloses a pharmaceutical agent formulated as nanoparticles or nanoliposomes of about 70 to about 200 nm in diameter for the treatment of cancer (box entitled "Abstract" - "MM-398 (aka PEP02) is a stable, nanotherapeutic encapsulation of the pro-drug CPT-11 (irinotecan)" that is a "relatively large (100nm) liposomal nanotherapeutic"). Klinz 'MM398 further teaches that MM-398 liposomes are preferentially internalized by macrophages, and especially tumor-associated macrophages (box entitled "Abstract" - "Through cellular uptake studies, we demonstrated in vitro that MM-398 was preferentially internalized by phagocytic macrophage/monocyte cell lines and, to a far lesser extent, by tumor cell lines. Furthermore, tumor microdistribution studies by flow cytometry and IHC showed uptake of MM-398 liposomes in both tumor cells and tumor-associated macrophages with more liposomal material being present in the macrophages.").

One of ordinary skill in the art would have found it obvious that the presence of contrast enhancement within the first location would indicate the presence of tumor-associated macrophages, as taught by Wolf, and that the presence of these tumor-associated macrophages would indicate that treatment with the tumor-associated macrophage-targeting nanoliposomes of Klinz 'MM398 would be appropriate. Likewise, a lack of contrast enhancement within the first location would indicate a lack of tumor-associated macrophages for the nanoliposomes to target, and that treatment with the tumor-associated macrophage targeting nanoliposomes would not be appropriate.

Regarding claim 2, Wolf and Klinz 'MM398 disclose the method of claim 1, and Wolf further teaches wherein the MRI contrast agent is ferumoxytol (para [0020] - " In a particular embodiment, the macrophage enhancing contrast agent is ferumoxytol"; para [0070] - "ferumoxytol and ferumoxtran-10, contrast agents that are particularly suited for use in embodiments of the presently claimed invention. Ferumoxytol and ferumoxtran-10 are MRI agents that are superparamagnetic and USPIOs").

---------Please see continuation in supplemental box---------

WRITTEN OPINION OF THE INTERNATIONAL SEARCHING AUTHORITY

International application No.
PCT/US 13/75513

Supplemental Box

In case the space in any of the preceding boxes is not sufficient.
Continuation of:
Box No. V2 Citations and Explanations

Regarding claim 3, Wolf and Klinz 'MM398 disclose the method of claim 2, and Wolf further teaches wherein the ferumoxytol is administered at 5 mg iron per kg (para [0139] - "On a first visit, she is given 5 mg/kg ferumoxytol and scheduled for an MRI at a second visit 4 days later").

Regarding claim 4, Wolf and Klinz 'MM398 disclose the method of claim 2, and Wolf further teaches wherein the patient is an adult (para [0139] - "A woman with a high risk history and a palpable lump in the right breast"). Although Wolf does not specifically teach that 100 - 1000 milligrams (iron) of ferumoxytol are administered to the patient, Wolf does teach that 5 mg/kg of ferumoxytol are administered to the patient (para [0139] - "she is given 5 mg/kg ferumoxytol"). Given that an average adult woman weighs at least 45 kg (i.e. 100 lbs), a dose as disclosed by Wolf would be at least 225 milligrams (i.e. 5 x 45 = 225) for an adult woman, and thus, a dose in the range of 100 - 1000 milligrams would have been obvious in view of Wolf.

Regarding claim 5, Wolf and Klinz 'MM398 disclose the method of claim 2, and Wolf further teaches wherein the patient is an adult (para [0139] - "A woman with a high risk history and a palpable lump in the right breast"). Although Wolf does not specifically teach that 510 milligrams of ferumoxytol are administered to the patient, Wolf does teach that the patient is administered ferumoxytol in an amount of 5 mg/kg (para [0139] - "she is given 5 mg/kg ferumoxytol"). Thus in view of the dosage guideline taught by Wolf, one of ordinary skill in the art would have found it obvious that an adult woman who weighs 102 kg (i.e. 225 lbs) would be administered 510 milligrams (i.e. 5 x 102 = 510) of ferumoxytol.

Regarding claim 6, Wolf and Klinz 'MM398 disclose the method of claim 1, and Wolf further teaches wherein the contrast-enhanced MRI image is obtained no more than 72, 96, 120, 144 or 168 hours after administration of the superparamagnetic iron oxide nanoparticles (para [0122] - "the USPIO is administered to the patient at a dose of at least 2 mg/kg or up to the maximal safe dose, and a MRI is scheduled for 48-144 hours later"; para [0051] - "ultrasmall superparamagnetic iron oxide particle (USPIO)").

Regarding claim 7, Wolf and Klinz 'MM398 disclose the method of claim 1, and Wolf further teaches wherein the contrast-enhanced MRI image is obtained from 72-96, 96-120, 120-144, or 144 to 168 hours after administration of the superparamagnetic iron oxide nanoparticles (para [0122] - "the USPIO is administered to the patient at a dose of at least 2 mg/kg or up to the maximal safe dose, and a MRI is scheduled for 48-144 hours later"; para [0051] - "ultrasmall superparamagnetic iron oxide particle (USPIO)").

Regarding claim 8, Wolf discloses a method for selecting and providing pharmaceutical treatment to a patient for a neoplastic condition (para [0020] - "method of assessing a stage of cancer"; para [0042] - "assessing stage of cancer refers to providing any type of information, including ... information useful in selecting an appropriate treatment"; para [0075] staging cancer for a variety of tumor types), the method comprising:
diagnosing a localized neoplastic condition in a patient and identifying one or more locations of neoplasia in the patient (para [0115] - "Once diagnosis of the primary tumor is made, whole-body MRI is appropriate. If a whole-body MEMRI is performed, identification of soft tissues where there is excessive macrophage density will identify where metastasis may be present"), and subsequently, obtaining a first contrast-enhanced MRI image of a first location of the one or more locations, obtaining a second contrast-enhanced MRI image of a second location of the one or more locations (para [0020] - "The method comprises administering a macrophage enhancing contrast agent to the subject during an administration session; ... acquiring a first magnetic resonance image of regions of the subject's body at risk of cancer; ... acquiring a second magnetic resonance image of the regions of the subject's body indicating neoplasia "; para [0075] - "Using macrophage-seeking contrast agents and whole-body MRI to perform a MEMRI evaluation ... (b) determine the degree of metastasis that may have already begun, (c) identify the location of the metastatic tumors"), and subsequently, selecting an anti-infective, anti-inflammatory, or anti-neoplastic pharmaceutical agent and treating the patient with the selected pharmaceutical agent (para [0075] - "(d) customize the anticancer treatment based on the characteristics and metastatic extent of the primary tumor (or metastatic tumors already present), and (e) assess the efficacy of such treatment");
wherein, the first and second contrast-enhanced MRI images are obtained following administration of an MRI contrast agent (para [0020]) comprising an MRI contrast-enhancing amount of superparamagnetic iron oxide nanoparticles of about 15-30 nm in diameter (para [0020] - "In a particular embodiment, the macrophage enhancing contrast agent is ferumoxytol"; para [0062] ultrasmall superparamagnetic iron oxides such as ferumoxytol; para [0059] - "10 .micro.m to about 10 nm in diameter).
Wolf does not specifically teach that if both the first and the second contrast-enhanced MRI images show contrast enhancement within both the first location and second location, the selected pharmaceutical agent is an agent that is formulated as nanoparticles or nanoliposomes of about 70 to about 200 nm in diameter, but if both the first and the second contrast-enhanced MRI images do not show contrast enhancement within both the first location and second location, the selected pharmaceutical agent is an agent that is not formulated as nanoparticles or nanoliposomes of about 70 to about 200 nm in diameter. However, Wolf does teach that its method is used to visualize the presence of tumor-associated macrophages (para [0050] - "embodiments of the present invention utilize macrophage-enhancing contrast agents within tumor-associated macrophages ("TAMs") to provide contrast around, and hence visualization of, primary or metastatic tumors"; para [0075] - "any tissue or organ in the entire body that has become surrounded by or associated with macrophages--a marker of the tumorigenic capabilities of that tumor--will be visualized by the whole-body MEMRI performed with any of the macrophage-seeking contrast agents") and that the selected therapy can be liposomal drug delivery (para [0129]). Klinz 'MM398 discloses a pharmaceutical agent formulated as nanoparticles or nanoliposomes of about 70 to about 200 nm in diameter for the treatment of cancer (box entitled "Abstract" - "MM-398 (aka PEP02) is a stable, nanotherapeutic encapsulation of the pro-drug CPT-11 (irinotecan)" that is a "relatively large (100nm) liposomal nanotherapeutic"). Klinz 'MM398 further teaches that MM-398 liposomes are preferentially internalized by macrophages, and especially tumor-associated macrophages (box entitled "Abstract" - "Through cellular uptake studies, we demonstrated in vitro that MM-398 was preferentially internalized by phagocytic macrophage/monocyte cell lines and, to a far lesser extent, by tumor cell lines. Furthermore, tumor microdistribution studies by flow cytometry and IHC showed uptake of MM-398 liposomes in both tumor cells and tumor-associated macrophages with more liposomal material being present in the macrophages."). [claim 8 is continued on next supplemental box]

--------Please see continuation in next supplemental box--------

WRITTEN OPINION OF THE INTERNATIONAL SEARCHING AUTHORITY

International application No.
PCT/US 13/75513

Supplemental Box

In case the space in any of the preceding boxes is not sufficient.
Continuation of:
Box No. V2 Citations and Explanations

[continuation of claim 8] One of ordinary skill in the art would have found it obvious that the presence of contrast enhancement within the first and second images would indicate the presence of tumor-associated macrophages around a tumor, as taught by Wolf, and that the presence of these tumor-associated macrophages would indicate that treatment with the tumor-associated macrophage targeting nanoliposomes of Klinz 'MM398 would be appropriate. Likewise, a lack of contrast enhancement within the first location would indicate a lack of tumor-associated macrophages for the nanoliposomes to target, and that treatment with the tumor-associated macrophage targeting nanoliposomes would not be appropriate.

Regarding claim 9, Wolf and Klinz 'MM398 disclose the method of claim 8, and Wolf further teaches wherein the contrast agent is ferumoxytol (para [0020], [0070]) and 1) is administered at 5 mg/kg, (para [0139] - "On a first visit, she is given 5 mg/kg ferumoxytol and scheduled for an MRI at a second visit 4 days later").

Regarding claim 10, Wolf and Klinz 'MM398 disclose the method of any one of claims 1-9. Although neither specifically teaches wherein the MRI image is obtained using a magnetic field strength of 1-10 Tesla or about 1.5 Tesla, or about 3 Tesla, this would have been obvious in view of Wolf, which teaches that traditional magnet systems used in MRI scanners for human subjects can employ superconducting magnet systems in high field systems that have magnetic field strength of greater than 1 Tesla (para [0067] - "superconducting magnet systems in high field systems (>10,000 gauss; >1T)").

Regarding claim 11, Wolf and Klinz 'MM398 disclose the method of any one of claims 1-9, and Klinz 'MM398 further teaches wherein the liposomal therapeutic agent comprises liposomes of an average size of about 100 nm in diameter (box entitled "Abstract" - "relatively large (100nm) liposomal nanotherapeutic").

Regarding claim 12, Wolf and Klinz 'MM398 disclose the method of any one of claims 1-9, and Klinz 'MM398 further teaches wherein the liposomal therapeutic agent is MM-398 (box entitled "Abstract" - "MM-398 (aka PEP02) is a stable, nanotherapeutic encapsulation of the pro-drug CPT-11 (irinotecan)").

Regarding claim 14, Wolf and Klinz 'MM398 disclose the method of any one of claims 1-9, and Wolf further teaches wherein the first contrast-enhanced MRI image shows contrast enhancement within the first location, the neoplastic condition comprises at least one tumor (para [0050] - "embodiments of the present invention utilize macrophage-enhancing contrast agents within tumor-associated macrophages ("TAMs") to provide contrast around, and hence visualization of, primary or metastatic tumors"; para [0075] - "any tissue or organ in the entire body that has become surrounded by or associated with macrophages--a marker of the tumorigenic capabilities of that tumor--will be visualized by the whole-body MEMRI performed with any of the macrophage-seeking contrast agents"), and Klinz 'MM398 further teaches the pharmaceutical agent is a liposomal antineoplastic agent (box entitled "Abstract").

Regarding claim 15, Wolf and Klinz 'MM398 disclose the method of claim 14, and Wolf further teaches wherein the tumor is a non-small cell lung cancer (NSCLC) tumor, a colorectal cancer (CRC) tumor, a pancreatic cancer tumor, an ovarian cancer tumor, a small cell lung cancer tumor, a gastric cancer tumor, a head and neck cancer tumor, a cervical cancer tumor (para [0036]-[0037]), and Klinz 'MM398 further teaches wherein the selected pharmaceutical agent is a liposomal formulation of irinotecan (box entitled "Abstract" - "MM-398 (aka PEP02) is a stable, nanotherapeutic encapsulation of the pro-drug CPT-11 (irinotecan)").

Regarding claim 16, Wolf and Klinz 'MM398 disclose the method of claim 15, and Klinz 'MM398 further teaches wherein the liposomal formulation of irinotecan is MM-398 (irinotecan sucrosofate liposome injection) (box entitled "Abstract" - "MM-398 (aka PEP02) is a stable, nanotherapeutic encapsulation of the pro-drug CPT-11 (irinotecan)").

Claims 13 and 17-19 lack an inventive step under PCT Article 33(3) as being obvious over Wolf in view of Klinz 'MM398 and further in view of the abstract entitled "MM-302, a HER2-targeted liposomal doxorubicin, shows binding/uptake and efficacy in HER2 2+ cells and xenograft models" by Klinz et al. (hereinafter 'Klinz 'MM302').

Regarding claim 13, Wolf and Klinz 'MM398 disclose the method of any one of claims 1-9, but do not teach wherein the liposomal therapeutic agent is MM-302. However, Klinz 'MM302 discloses that MM-302 is an ErbB2/HER2-targeted liposomal doxorubicin formulation designed to target doxorubicin to HER2-overexpressing cancer cells (box entitled "Abstract"). Klinz 'MM302 further teaches that MM-302 was shown to have improved anti-tumor efficacy while limiting uptake into non-target cells, and is a valuable tool for against HER2 2+ tumors (box entitled "Abstract"). One of ordinary skill in the art would have found it obvious that the liposomal therapeutic agent of the method of Wolf and Klinz 'MM398 may be the MM-302 of Klinz 'MM302, because the liposomal therapeutic agent of Klinz 'MM302 would be able to enhance the treatment of metastatic tumors by preferentially targeting HER2 tumor cells for destruction while minimizing damage to healthy non-cancerous cells.

Regarding claim 17, Wolf and Klinz 'MM398 disclose the method of claim 14, but do not teach wherein the liposomal anti-neoplastic agent is liposomal doxorubicin. However, Klinz 'MM302 discloses that MM-302 is an ErbB2/HER2-targeted liposomal doxorubicin formulation designed to target doxorubicin to HER2-overexpressing cancer cells (box entitled "Abstract"). Klinz 'MM302 further teaches that MM-302 was shown to have improved anti-tumor efficacy while limiting uptake into non-target cells, and would be a valuable tool for treating HER2 2+ tumors (box entitled "Abstract"). One of ordinary skill in the art would have found it obvious that the liposomal therapeutic agent of the method of Wolf and Klinz 'MM398 may be the MM-302 of Klinz 'MM302, because the liposomal therapeutic agent of Klinz 'MM302 would be able to enhance the treatment of metastatic tumors by preferentially targeting HER2 tumor cells for destruction while minimizing damage to healthy non-cancerous cells.

---------Please see continuation in next supplemental box---------

WRITTEN OPINION OF THE
INTERNATIONAL SEARCHING AUTHORITY

International application No.
PCT/US 13/75513

Supplemental Box

In case the space in any of the preceding boxes is not sufficient.
Continuation of:
Box No. V2 Citations and Explanations

Regarding claim 18, Wolf, Klinz 'MM398, and Klinz 'MM302 disclose the method of claim 17, and Klinz 'MM302 further teaches wherein the liposomal doxorubicin comprises antibody-targeted doxorubicin liposomes (box entitled "Abstract" - "MM-302 is an ErbB2/HER2-targeted liposomal doxorubicin formulation", with illustration showing anti-HER2 scFv as part of the liposomal targeting moiety).

Regarding claim 19, Wolf, Klinz 'MM398, and Klinz 'MM302 disclose the method of claim 18, and Klinz 'MM302 further teaches wherein the antibody-targeted doxorubicin liposomes are targeted with an anti-HER2 antibody (box entitled "Abstract" - illustration showing anti-HER2 scFv as part of the liposomal targeting moiety).

Claims 1-19 have industrial applicability as defined by PCT Article 33(4) because the subject matter can be made or used in industry.

PATENT COOPERATION TREATY

PCT

INTERNATIONAL SEARCH REPORT

(PCT Article 18 and Rules 43 and 44)

Applicant's or agent's file reference 94489WO(309768)	**FOR FURTHER ACTION**	see Form PCT/ISA/220 as well as, where applicable, item 5 below.
International application No. PCT/US 13/75513	International filing date *(day/month/year)* 17 December 2013 (17.12.2013)	(Earliest) Priority Date *(day/month/year)* 14 December 2012 (14.12.2012)
Applicant MERRIMACK PHARMACEUTICALS, INC.		

This international search report has been prepared by this International Searching Authority and is transmitted to the applicant according to Article 18. A copy is being transmitted to the International Bureau.

This international search report consists of a total of 2 sheets.

☐ It is also accompanied by a copy of each prior art document cited in this report.

1. **Basis of the report**

a. With regard to the **language**, the international search was carried out on the basis of:

☒ the international application in the language in which it was filed.

☐ a translation of the international application into _____ which is the language of a translation furnished for the purposes of international search (Rules 12.3(a) and 23.1(b)).

b. ☐ This international search report has been established taking into account the **rectification of an obvious mistake** authorized by or notified to this Authority under Rule 91 (Rule 43.6*bis*(a)).

c. ☐ With regard to any **nucleotide and/or amino acid sequence** disclosed in the international application, see Box No. I.

2. ☐ **Certain claims were found unsearchable** (see Box No. II).

3. ☐ **Unity of invention is lacking** (see Box No. III).

4. With regard to the **title**,

☒ the text is approved as submitted by the applicant.

☐ the text has been established by this Authority to read as follows:

5. With regard to the **abstract**,

☒ the text is approved as submitted by the applicant.

☐ the text has been established, according to Rule 38.2, by this Authority as it appears in Box No. IV. The applicant may, within one month from the date of mailing of this international search report, submit comments to this Authority.

6. With regard to the **drawings**,

a. the figure of the **drawings** to be published with the abstract is Figure No. _____

☐ as suggested by the applicant.

☐ as selected by this Authority, because the applicant failed to suggest a figure.

☐ as selected by this Authority, because this figure better characterizes the invention.

b. ☒ none of the figures is to be published with the abstract.

INTERNATIONAL SEARCH REPORT PCT/US2013/075513 06.06.2014

International application No.
PCT/US 13/75513

A. CLASSIFICATION OF SUBJECT MATTER
IPC(8) - A61B 5/055, A61K 49/06, A61P 35/00 (2014.01)
USPC - 424/9.321, 514/19.3, 600/410
According to International Patent Classification (IPC) or to both national classification and IPC

B. FIELDS SEARCHED

Minimum documentation searched (classification system followed by classification symbols)
IPC(8) - A61B 5/055, A61K 49/06, A61P 35/00 (2014.01)
USPC - 424/9.321, 514/19.3, 600/410

Documentation searched other than minimum documentation to the extent that such documents are included in the fields searched
USPC - 424/9.3, 424/9.32, 424/9.323, 424/450, 514/19.2, 600/411
(keyword limited; terms below)

Electronic data base consulted during the international search (name of data base and, where practicable, search terms used)
PatBase, PubWEST(USPT,PGPB,EPAB,JPAB), Google Scholar, Google Web
Search terms: MRI, magnetic resonance imaging, ferumoxytol, cancer, tumor, neoplasm, malignancy, contrast enhancement, liposome, nanoliposome, nanoparticle, MM-398, irinotecan, sucrosofate, MM-302, doxorubicin, Her2, tumor-associated macrophages, TAM

C. DOCUMENTS CONSIDERED TO BE RELEVANT

Category*	Citation of document, with indication, where appropriate, of the relevant passages	Relevant to claim No.
Y	US 2012/0003160 A1 (WOLF et al.) 5 January 2012 (05.01.2012) para [0020], [0042], [0050], [0051], [0059], [0062], [0075], [0115], [0122], [0129], [0139]	1-19
Y	KLINZ et al., Identifying differential mechanisms of action for MM-398/PEP02, a novel nanotherapeutic encapsulation of irinotecan. AACR/EORTC 2011, Abstract C207, 2011 [online]. [Retrieved on 16 May 2014]. Retrieved from the Internet <URL: http://www.merrimackpharma.com/sites/default/files/documents/AACR%20EORTC%20MM-398%20MOA%20SKlinz%20November%202011%20FINAL.pdf> Especially box entitled "Abstract"	1-19
Y	KLINZ et al., MM-302, a HER2-targeted liposomal doxorubicin, shows binding/uptake and efficacy in HER2 2+ cells and xenograft models. AACR 2011, Abstract 3637, 2011 [online]. [Retrieved on 16 May 2014]. Retrieved from the Internet <URL: http://www.merrimackpharma.com/sites/default/files/documents/10.%20AACR%202011%20MM-302%20HER2%20Threshold%20Klintz.pdf> Especially box entitled "Abstract"	13, 17-19

☐ Further documents are listed in the continuation of Box C. ☐

* Special categories of cited documents:
"A" document defining the general state of the art which is not considered to be of particular relevance
"E" earlier application or patent but published on or after the international filing date
"L" document which may throw doubts on priority claim(s) or which is cited to establish the publication date of another citation or other special reason (as specified)
"O" document referring to an oral disclosure, use, exhibition or other means
"P" document published prior to the international filing date but later than the priority date claimed
"T" later document published after the international filing date or priority date and not in conflict with the application but cited to understand the principle or theory underlying the invention
"X" document of particular relevance; the claimed invention cannot be considered novel or cannot be considered to involve an inventive step when the document is taken alone
"Y" document of particular relevance; the claimed invention cannot be considered to involve an inventive step when the document is combined with one or more other such documents, such combination being obvious to a person skilled in the art
"&" document member of the same patent family

Date of the actual completion of the international search	Date of mailing of the international search report
19 May 2014 (19.05.2014)	06 JUN 2014
Name and mailing address of the ISA/US Mail Stop PCT, Attn: ISA/US, Commissioner for Patents P.O. Box 1450, Alexandria, Virginia 22313-1450 Facsimile No. 571-273-3201	Authorized officer: Lee W. Young PCT Helpdesk: 571-272-4300 PCT OSP: 571-272-7774

PATENT COOPERATION TREATY

PCT

INTERNATIONAL PRELIMINARY REPORT ON PATENTABILITY
(Chapter I of the Patent Cooperation Treaty)

(PCT Rule 44*bis*)

Applicant's or agent's file reference 94153WO(309768)	**FOR FURTHER ACTION**	See item 4 below
International application No. PCT/US2014/062007	International filing date *(day/month/year)* 23 October 2014 (23.10.2014)	Priority date *(day/month/year)* 23 October 2013 (23.10.2013)
International Patent Classification (8th edition unless older edition indicated) See relevant information in Form PCT/ISA/237		
Applicant MERRIMACK PHARMACEUTICALS, INC.		

1. This international preliminary report on patentability (Chapter I) is issued by the International Bureau on behalf of the International Searching Authority under Rule 44 *bis*.1(a).

2. This REPORT consists of a total of 10 sheets, including this cover sheet.

   In the attached sheets, any reference to the written opinion of the International Searching Authority should be read as a reference to the international preliminary report on patentability (Chapter I) instead.

3. This report contains indications relating to the following items:

☒	Box No. I	Basis of the report
☐	Box No. II	Priority
☒	Box No. III	Non-establishment of opinion with regard to novelty, inventive step and industrial applicability
☐	Box No. IV	Lack of unity of invention
☒	Box No. V	Reasoned statement under Article 35(2) with regard to novelty, inventive step or industrial applicability; citations and explanations supporting such statement
☐	Box No. VI	Certain documents cited
☐	Box No. VII	Certain defects in the international application
☐	Box No. VIII	Certain observations on the international application

4. The International Bureau will communicate this report to designated Offices in accordance with Rules 44*bis*.3(c) and 93*bis*.1 but not, except where the applicant makes an express request under Article 23(2), before the expiration of 30 months from the priority date (Rule 44*bis* .2).

	Date of issuance of this report 26 April 2016 (26.04.2016)
The International Bureau of WIPO 34, chemin des Colombettes 1211 Geneva 20, Switzerland Facsimile No. +41 22 338 82 70	Authorized officer Lingfei Bai e-mail: pt02.pct@wipo.int

Form PCT/IB/373 (January 2004)

From the
INTERNATIONAL SEARCHING AUTHORITY

To: Mark D. Russett
Edwards Wildman Palmer LLP
P.O. Box 55874
Boston, Massachusetts 02205
United States of America

PCT

WRITTEN OPINION OF THE
INTERNATIONAL SEARCHING AUTHORITY

(PCT Rule 43*bis*.1)

Date of mailing *(day/month/year)*	09 JAN 2015
Applicant's or agent's file reference 94153WO(309768)	**FOR FURTHER ACTION** See paragraph 2 below

International application No.	International filing date *(day/month/year)*	Priority date *(day/month/year)*
PCT/US14/62007	23 October 2014 (23.10.2014)	23 October 2013 (23.10.2013)

International Patent Classification (IPC) or both national classification and IPC
IPC(8) - A61K 9/127, 51/00, 51/12; A61M 36/00 (2014.01)
CPC - A61K 9/127, 9/1271, 49/0084, 51/1234

Applicant MERRIMACK PHARMACEUTICALS, INC.

1. This opinion contains indications relating to the following items:

- ☒ Box No. I Basis of the opinion
- ☐ Box No. II Priority
- ☒ Box No. III Non-establishment of opinion with regard to novelty, inventive step and industrial applicability
- ☐ Box No. IV Lack of unity of invention
- ☒ Box No. V Reasoned statement under Rule 43*bis*.1(a)(i) with regard to novelty, inventive step or industrial applicability; citations and explanations supporting such statement
- ☐ Box No. VI Certain documents cited
- ☐ Box No. VII Certain defects in the international application
- ☐ Box No. VIII Certain observations on the international application

2. **FURTHER ACTION**

If a demand for international preliminary examination is made, this opinion will be considered to be a written opinion of the International Preliminary Examining Authority ("IPEA") except that this does not apply where the applicant chooses an Authority other than this one to be the IPEA and the chosen IPEA has notified the International Bureau under Rule 66.1 *bis*(b) that written opinions of this International Searching Authority will not be so considered.

If this opinion is, as provided above, considered to be a written opinion of the IPEA, the applicant is invited to submit to the IPEA a written reply together, where appropriate, with amendments, before the expiration of 3 months from the date of mailing of Form PCT/ISA/220 or before the expiration of 22 months from the priority date, whichever expires later.

For further options, see Form PCT/ISA/220.

Name and mailing address of the ISA/US	Date of completion of this opinion	Authorized officer:
Mail Stop PCT, Attn: ISA/US Commissioner for Patents P.O. Box 1450, Alexandria, Virginia 22313-1450 Facsimile No. 571-273-3201	23 December 2014 (23.12.2014)	Shane Thomas PCT Helpdesk: 571-272-4300 PCT OSP: 571-272-7774

Form PCT/ISA/237 (cover sheet) (July 2011)

WRITTEN OPINION OF THE
INTERNATIONAL SEARCHING AUTHORITY

International application No.
PCT/US14/62007

Box No. I Basis of this opinion

1. With regard to the **language**, this opinion has been established on the basis of:

   ☒ the international application in the language in which it was filed.

   ☐ a translation of the international application into _____ which is the language of a translation furnished for the purposes of international search (Rules 12.3(a) and 23.1(b)).

2. ☐ This opinion has been established taking into account the **rectification of an obvious mistake** authorized by or notified to this Authority under Rule 91 (Rule 43*bis*.1(a))

3. With regard to any **nucleotide and/or amino acid sequence** disclosed in the international application, this opinion has been established on the basis of a sequence listing filed or furnished:

   a. (means)

      ☐ on paper

      ☐ in electronic form

   b. (time)

      ☐ in the international application as filed

      ☐ together with the international application in electronic form

      ☐ subsequently to this Authority for the purposes of search

4. ☐ In addition, in the case that more than one version or copy of a sequence listing has been filed or furnished, the required statements that the information in the subsequent or additional copies is identical to that in the application as filed or does not go beyond the application as filed, as appropriate, were furnished.

5. Additional comments:

WRITTEN OPINION OF THE INTERNATIONAL SEARCHING AUTHORITY

International application No.
PCT/US14/62007

Box No. III Non-establishment of opinion with regard to novelty, inventive step and industrial applicability

The questions whether the claimed invention appears to be novel, to involve an inventive step (to be non obvious), or to be industrially applicable have not been examined in respect of:

☐ the entire international application.

☒ claims Nos. 4-8 and 17-24

because:

☐ the said international application, or the said claims Nos. _____ relate to the following subject matter which does not require an international search *(specify)*:

☒ the description, claims or drawings *(indicate particular elements below)* or said claims Nos. 4-8 and 17-24 are so unclear that no meaningful opinion could be formed *(specify)*:

because they are dependent claims and are not drafted in accordance with the second and third sentences of Rule 6.4(a).

☐ the claims, or said claims Nos. _____ are so inadequately supported by the description that no meaningful opinion could be formed *(specify)*:

☒ no international search report has been established for said claims Nos. 4-8 and 17-24

☐ a meaningful opinion could not be formed without the sequence listing; the applicant did not, within the prescribed time limit

- ☐ furnish a sequence listing on paper complying with the standard provided for in Annex C of the Administrative Instructions, and such listing was not available to the International Searching Authority in a form and mannacceptable to it.
- ☐ furnish a sequence listing in electronic form complying with the standard provided for in Annex C of the Administrative Instructions, and such listing was not available to the International Searching Authority in a form and mannacceptable to it.
- ☐ pay the required late furnishing fee for the furnishing of a sequence listing in response to an invitation under Rule 13*ter*.1(a) or (b).

☐ See Supplemental Box for further details.

WRITTEN OPINION OF THE INTERNATIONAL SEARCHING AUTHORITY

International application No.: PCT/US14/62007

Box No. V **Reasoned statement under Rule 43*bis*.1(a)(i) with regard to novelty, inventive step or industrial applicability; citations and explanations supporting such statement**

1. Statement

Novelty (N)	Claims	*** Please See Box Below****	YES
	Claims	13, 15/13, 16/15/13, 28	NO
Inventive step (IS)	Claims	*** Please See Box Below****	YES
	Claims	*** Please See Box Below****	NO
Industrial applicability (IA)	Claims	*** Please See Box Below****	YES
	Claims	NONE	NO

2. Citations and explanations:

-Continued from Box No. V: 1.:

Novelty (N): YES; 1-2, 3/1-2, 9-11, 12/9-11, 14, 15/14, 16/15/14, 25-27, 29-30, 31/28-30, 32/31/28-30, 33/32/31/28-30, 34/33/32/31/28-30, 35/34/33/32/31/28-30, 36/35/34/33/32/31/28-30 .

Inventive step (IS): YES; 25-27, 33/32/31/28-30, 34/33/32/31/28-30, 35/34/33/32/31/28-30, 36/35/34/33/32/31/28-30

Inventive step (IS): NO; 1-2, 3/1-2, 9-11, 12/9-11, 13-14, 15/13-14, 16/15/13-14, 28-30, 31/28-30, 32/31/28-30

Industrial applicabiliy (IA): YES; 1-2, 3/1-2, 9-11, 12/9-11, 13-14, 15/13-14, 16/15/13-14, 25-30, 31/28-30, 32/31/28-30, 33/32/31/28-30, 34/33/32/31/28-30, 35/34/33/32/31/28-30, 36/35/34/33/32/31/28-30

Claims 13, 15/13, 16/15/13 and 28 lack novelty under PCT Article 33(2) as being anticipated by WO 2003/101474 A1 to Transmolecular, Inc. (hereinafter 'Transmolecular').

As per claim 13, Transmolecular discloses a method of imaging a lesion in a patient (method of PET imaging in a patient of abnormal cells including tumors; page 26, line 34; page 27, lines 1-3, lines 10-12), the method comprising: (a) administering to the patient an injection (administration to the patient by intravenous; page 29, lines 5-6) comprising a preparation of 64Cu-loaded liposomes (liposome composition containing preferred 64Cu; page 26, lines 7-8; page 28, lines 29-30), the injection administered at a dose of 10.8 mCi of 64Cu (+/- 15 percent) (intravenous dose of 64Cu is less than 20 mCi; page 29, lines 5-6; page 33, lines 7-10); and (b) within 48 hours following the injection (imagining after administration by intravenous between thirty minutes to forty-eight hours; page 29, lines 5-6, lines 9-12),, obtaining a PET scan of a region of the patient (obtaining a PET scan of the area of a subject; page 29, lines 10-12), the region comprising the location of the lesion (area of subject under investigation; page 29, lines 9-19).

As per claim 15/13, Transmolecular discloses the method of claim 13, and Transmolecular further discloses the method wherein the PET scan is obtained within 3 hours following the injection (PET scan is obtained in patient after intravenous administration between 30 minutes and forty-eight hours; page 29, lines 5-6, lines 9-12).

As per claim 16/15/13, Transmolecular discloses the method of claims 15/13-14, and Transmolecular further discloses the method wherein the within 3 hours is within 2 hours or within 1 hour(PET scan is obtained in patient after intravenous administration between 30 minutes and forty-eight hours; page 29, lines 5-6, lines 9-12)..

As per claim 28, Transmolecular discloses a composition comprising 64Cu-loaded liposomes (liposome composition containing preferred 64Cu; page 26, lines 7-8; page 28, lines 29-30) containing doxorubicin (liposomal composition includes doxorubicin; page 24, lines 10-25; page 30, table 3; claim 6).

-***-Continued Within the Next Supplemental Box-***-

Supplemental Box

In case **the space in any of the preceding boxes is not sufficient.**
Continuation of:

-***-Continued from Box V: Citations and Explanations-***-

Claims 1-2, 3/1-2, 9-11, 12/9-11, 14, 15/14, 16/15/14, 29, and 31/28-29 lack an inventive step under PCT Article 33(3) as being obvious over Transmolecular in view of WO 2012/078695 A2 to Merrimack Pharmaceutical (hereinafter 'Merrimack').

As per claim 1, Transmolecular discloses a method of preparing a patient for PET imaging of a lesion in the patient (method of PET imaging in a patient of abnormal cells including tumors; page 26, line 34; page 27, lines 1-3, lines 10-12), the method comprising: administering to the patient an injection (parenteral administration to subject; page 21, lines 22-23) comprising a dose of a preparation of 64Cu-loaded liposomal (liposome composition containing preferred 64Cu; page 26, lines 7-8; page 28, lines 29-30) doxorubicin (liposomal composition includes doxorubicin; page 24, lines 10-25; page 30, table 3; claim 6), the liposomes comprised by the preparation having an average diameter of 75-110 nm, wherein the dose comprises 3-5 mg/m2 doxorubicin and is formulated to deliver 10.8 (+/-15 percent) mCi of 64Cu (dose of 64Cu is less than 20 mCi; page 33, lines 7-10) when administered to the patient (parenteral administration to subject; page 21, lines 22-23). Transmolecular does not disclose the method comprised by the preparation having an average diameter of 75-110 nm, wherein the dose comprises 3-5 mg/m2 doxorubicin. However, Merrimack discloses a method comprised by the preparation having an average diameter of 75-110 nm (liposomes of preparation have diameter of approximately 75-110 nm; page 9, lines 2-3), wherein the dose comprises 3-5 mg/m2 doxorubicin (doxorubicin dose can be 3, 4, or 5 mg/m2; page 9, lines 23-24). It would have been obvious to one skilled in the art at the time of the invention to have modified the method, as disclosed by Transmolecular, to provide the method comprised by the preparation having an average diameter of 75-110 nm, wherein the dose comprises 3-5 mg/m2 doxorubicin, as disclosed by Merrimack, to provide a method of targeting tumor tissue and treating cancer without increasing the risk of cardiotoxicity (Merrimack; page 4, lines 23-26).

As per claim 2, Transmolecular and Merrimack, in combination, disclose the method of claim 1, and Transmolecular further discloses the method wherein the lesion is a benign tumor or a malignant tumor (treatment of cancers that are malignant; page 5, lines 9-21), optionally a brain tumor.

As per claims 3/1-2, Transmolecular and Merrimack, in combination, disclose the method of claims 1 and 2, and Transmolecular further discloses the method wherein the injection comprises 10.8 mCi of 64Cu +/- 10 percent (dose of 64Cu is less than 20 mCi; page 33, lines 7-10).

As per claim 9, Transmolecular discloses a method of imaging a lesion in a patient (method of PET imaging in a patient of abnormal cells including tumors; page 26, line 34; page 27, lines 1-3, lines 10-12), the method comprising: (a) administering to the patient an injection comprising a preparation of 64Cu-loaded liposomal (liposome composition containing preferred 64Cu; page 26, lines 7-8; page 28, lines 29-30) doxorubicin (liposomal composition includes doxorubicin; page 24, lines 10-25; page 30, table 3; claim 6); (b) within 48 hours following the injection (administration by intravenous image obtained between thirty minutes to forty-eight hours; page 29, lines 5-6, lines 9-12), obtaining a PET scan of a region of the patient (obtaining a PET scan of the area of a subject; page 29, lines 10-12), the region comprising the location of the lesion (area of subject under investigation; page 29, lines 9-19). Transmolecular does not disclose the method comprising: (a) the liposomes comprised by the preparation having an average diameter of 75-110 nm, at a dose of 3-5 mg/m2 doxorubicin. However, Merrimack discloses a method comprising; (a) the liposomes comprised by the preparation having an average diameter of 75-110 nm (liposomes of preparation have diameter of approximately 75-110 nm; page 9, lines 2-3), at a dose of 3-5 mg/m2 doxorubicin (doxorubicin dose can be 3, 4, or 5 mg/m2; page 9, lines 23-24). It would have been obvious to one skilled in the art at the time of the invention to have modified the method, as disclosed by Transmolecular, to provide the method comprised by the preparation having an average diameter of 75-110 nm, at a dose of 3-5 mg/m2 doxorubicin, as disclosed by Merrimack, to provide a method of targeting tumor tissue and treating cancer without increasing the risk of cardiotoxicity (Merrimack; page 4, lines 23-26).

As per claim 10, Transmolecular and Merrimack, in combination, disclose the method of claim 9, and Transmolecular further discloses the method wherein the lesion is a site of inflammation, a site of infection, a benign tumor or a malignant tumor (treatment of cancers that are malignant; page 5, lines 9-21), optionally a malignant brain tumor.

As per claim 11, Transmolecular and Merrimack, in combination, disclose the method of claim 10, and Transmolecular further discloses the method wherein the dose of liposomal doxorubicin (liposomal composition includes doxorubicin; page 24, lines 10-25; page 30, table 3; claim 6) is formulated to deliver to the patient (liposome composition for delivery to patient; page 21, lines 20-21; page 24, lines 29-31; page 29, lines 5-6), when administered, 10.8 (+/- 15 percent, optionally+/- 10 percent) mCi of 64Cu) (dose of 64Cu is less than 20 mCi; page 33, lines 7-10).

As per claim 12/9-11, Transmolecular and Merrimack, in combination, disclose the method of claims 9-11, and Transmolecular further discloses the method wherein the PET scan is obtained within 24 hours, within 12 hours, within six hours, within 3 hours, within 2 hours, or within 1 hour following the injection (PET scan is obtained in patient after intravenous administration between 30 minutes and forty-eight hours; page 29, lines 5-6, lines 9-12).

As per claim 14, Transmolecular discloses the method of claim 13, and Transmolecular further discloses wherein the preparation comprises liposomes (liposome composition; page 21, lines 20-21). Transmolecular does not disclose the method with an average diameter of 75-110 nm. However, Merrimack discloses a method with an average diameter of 75-110 nm (liposomes of preparation have diameter of approximately 75-110 nm; page 9, lines 2-3). It would have been obvious to one skilled in the art at the time of the invention to have modified the method, as disclosed by Transmolecular, to provide the method with an average diameter of 75-110 nm , as disclosed by Merrimack, to provide a liposomal dosage form for dosing tumors (Merrimack; page 9, lines 2-3, lines 20-27).

-***-Continued Within the Next Supplemental Box-***-

WRITTEN OPINION OF THE INTERNATIONAL SEARCHING AUTHORITY

International application No.
PCT/US14/62007

Supplemental Box

In case **the space in any of the preceding boxes is not sufficient.**
Continuation of:

-***-Continued from Previous Supplemental Box-***-

As per claim 15/14, Transmolecular and Merrimack, in combination, disclose the method of claim 14, and Transmolecular further discloses the method wherein the PET scan is obtained within 3 hours following the injection (PET scan is obtained in patient after intravenous administration between 30 minutes and forty-eight hours; page 29, lines 5-6, lines 9-12).

As per claim 16/15/13-14, Transmolecular and Merrimack, in combination, disclose the method of claim 15/13-14, and Transmolecular further discloses the method wherein the within 3 hours is within 2 hours or within 1 hour(PET scan is obtained in patient after intravenous administration between 30 minutes and forty-eight hours; page 29, lines 5-6, lines 9-12).

As per claim 29, Transmolecular discloses the composition of claim 28, but Transmolecular does not disclose the composition wherein the liposomes are HER2-targeted immunoliposomes. However, Merrimack discloses a composition wherein the liposomes are HER2-targeted immunoliposomes (immunoliposomes target HER2-expression cancers; page 4, lines 23-26). It would have been obvious to one skilled in the art at the time of the invention to have modified the composition, as disclosed by Transmolecular, to provide the composition wherein the liposomes are HER2-targeted immunoliposomes, as disclosed by Merrimack, to provide a imaging and targeting tumor tissue without increasing the risk of cardiotoxicity (Merrimack; page 4, lines 23-35).

As per claim 31/28, Transmolecular discloses the composition of claim 28, but Transmolecular does not disclose the composition wherein the composition is adapted for administration to a human patient at a dose of at least 0.028, at least 3, at least 4, at least 5, at least 6, or 7 mg/m2 of doxorubicin. However, Merrimack discloses a composition wherein the composition is adapted for administration to a human patient (composition is administered to human cancer patient; page 5, lines 1-4) at a dose of at least 0.028, at least 3, at least 4, at least 5, at least 6, or 7 mg/m2 of doxorubicin (doxorubicin dose can be 3, 4, or 5 mg/m2; page 9, lines 23-24). It would have been obvious to one skilled in the art at the time of the invention to have modified the composition, as disclosed by Transmolecular, to provide the composition wherein the composition is adapted for administration to a human patient at a dose of at least 0.028, at least 3, at least 4, at least 5, at least 6, or 7 mg/m2 of doxorubicin, as disclosed by Merrimack, to provide targeting of tumor tissue without increasing the risk of cardiotoxicity (Merrimack; page 5, lines 5-15).

As per claim 31/29, Transmolecular and Merrimack, in combination discloses the composition of claim 29, but Transmolecular does not disclose the composition wherein the composition is adapted for administration to a human patient at a dose of at least 0.028, at least 3, at least 4, at least 5, at least 6, or 7 mg/m2 of doxorubicin. However, Merrimack discloses a composition wherein the composition is adapted for administration to a human patient (composition is administered to human cancer patient; page 5, lines 1-4) at a dose of at least 0.028, at least 3, at least 4, at least 5, at least 6, or 7 mg/m2 of doxorubicin (doxorubicin dose can be 3, 4, or 5 mg/m2; page 9, lines 23-24). It would have been obvious to one skilled in the art at the time of the invention to have modified the composition, as disclosed by Transmolecular, to provide the composition wherein the composition is adapted for administration to a human patient at a dose of at least 0.028, at least 3, at least 4, at least 5, at least 6, or 7 mg/m2 of doxorubicin, as disclosed by Merrimack, to provide targeting of tumor tissue without increasing the risk of cardiotoxicity (Merrimack; page 5, lines 5-15).

Claims 30 lacks an inventive step under PCT Article 33(3) as being obvious over Transmolecular in view of US 2013/0209481 A1 to Zhou, et al. (hereinafter 'Zhou').

As per claim 30, Transmolecular discloses the composition of claim 28, but Transmolecular does not disclose the composition wherein the liposomes are EphA2-targeted immunoliposomes. However, Zhou discloses a composition wherein the liposomes are EphA2-targeted immunoliposomes (liposomes are conjugated, immunoliposomes, and can be used to target EphA2 overexpressing cancer cells; paragraphs [0212], [0215]). It would have been obvious to one skilled in the art at the time of the invention to have modified the composition, as disclosed by Transmolecular, to provide the composition wherein the liposomes are EphA2-targeted immunoliposomes, as disclosed by Zhou, to provide targeting of EphA2 overexpressing cancer cells for treatment (Zhou; paragraph [0212]).

Claim 31/30 lacks an inventive step under PCT Article 33(3) as being obvious over Transmolecular in view of Zhou in further view of Merrimack.

As per claim 31/30, Transmolecular and Zhou, in combination, disclose the composition of claim 30, and Transmolecular further discloses wherein the composition is adapted for administration to a human patient (administration to the patient; page 29, lines 5-6). Transmolecular does not disclose wherein the composition at a dose of at least 0.028, at least 3, at least 4, at least 5, at least 6, or 7 mg/m2 of doxorubicin. However, Merrimack discloses a composition wherein the composition at a dose of at least 0.028, at least 3, at least 4, at least 5, at least 6, or 7 mg/m2 of doxorubicin (doxorubicin dose can be 3, 4, or 5 mg/m2; page 9, lines 23-24). It would have been obvious to one skilled in the art at the time of the invention to have modified the composition, as disclosed by Transmolecular, to provide the composition wherein the composition at a dose of at least 0.028, at least 3, at least 4, at least 5, at least 6, or 7 mg/m2 of doxorubicin, as disclosed by Merrimack, to provide targeting of tumor tissue without increasing the risk of cardiotoxicity (Merrimack; page 5, lines 5-15).

-***-Continued Within the Next Supplemental Box-***-

WRITTEN OPINION OF THE INTERNATIONAL SEARCHING AUTHORITY

International application No.
PCT/US14/62007

Supplemental Box

In case **the space in any of the preceding boxes is not sufficient.**
Continuation of:

-***-Continued from Previous Supplemental Box-***-

Claims 32/31/28-29 lack an inventive step under PCT Article 33(3) as being obvious over Transmolecular in view of Merrimack and in further view of WO 2012/079582 A1 to Tech University of Denmark (hereinafter 'DENMARK').

As per claim 32/31/28-29, Transmolecular and Merrimack, in combination, disclose the composition of claim 31/28-29, but Transmolecular does not disclose the composition wherein the liposomes comprise a gradient-loadable chelator. However, Denmark discloses a composition wherein the liposomes comprise a gradient-loadable chelator (liposomes composition contains chelators that load or entrap in liposomes to form gradient; page 8, lines 4-10). It would have been obvious to one skilled in the art at the time of the invention to have modified the composition, as disclosed by Transmolecular, to provide the composition wherein the liposomes comprise a gradient-loadable chelator, as disclosed by Denmark, to provide a method of entrapping 64Cu radiolabeled into liposomes and preventing linkage (Denmark; page 7, lines 1-3, lines 13-14; page 8, lines 17-22).

Claims 32/31/30 lacks an inventive step under PCT Article 33(3) as being obvious over Transmolecular in view of Zhou and in further view of Merrimack and in further view of Denmark.

As per claim 32/31/30, Transmolecular, Zhou and Merrimack, in combination, disclose the composition of claim 31/30, but Transmolecular does not disclose the composition wherein the liposomes comprise a gradient-loadable chelator. However, Denmark discloses a composition wherein the liposomes comprise a gradient-loadable chelator (liposomes composition contains chelators that load or entrap in liposomes to form gradient; page 8, lines 4-10). It would have been obvious to one skilled in the art at the time of the invention to have modified the composition, as disclosed by Transmolecular, to provide the composition wherein the liposomes comprise a gradient-loadable chelator, as disclosed by Denmark, to provide a method of entrapping 64Cu radiolabeled into liposomes and preventing linkage (Denmark; page 7, lines 1-3, lines 13-14; page 8, lines 17-22).

Claims 25-27, 33/32/31/28-30, 34/33/32/31/28-30, 35/34/33/32/31/28-30, 36/35/34/33/32/31/28-30 meet the criteria set out in PCT Article 33(2)-(3).

Claim 25 meets the criteria set out in PCT Article 33(2)-(3), because the prior art does not teach or fairly suggest a method of treating and imaging a patient, the method comprising:(a) administering to the patient a first injection comprising immunoliposomal doxorubicin that does not comprise detectable levels of 64Cu, the injection administered at a dose of at least 25, at least 30, at least 35, at least 40, or at least 45, or 50 mg/m2 of doxorubicin; (b) at between one and 6 hours following the first injection, administering to the patient a second injection comprising 64Cu-loaded immunoliposomal doxorubicin, the doxorubicin comprised by the second injection consisting of a dose of at least 3, at least 4, at least 5, at least 6, or 7 mg/m2 of doxorubicin, said dose comprising at 10.8 mCi of 64Cu +/- 15 percent; and (c) obtaining at least two PET/CT scans of a region of pathology in the patient, wherein each scan is obtained at a different time point, and wherein time elapsed from the injection of(a) until a final scan of the at least two scans is obtained is no more than three days.

Merrimack discloses a method of treating and imaging a patient (method of treating a patient; claim 1), the method comprising:(a) administering to the patient a first injection comprising immunoliposomal doxorubicin that does not comprise detectable levels of 64Cu (first administration is injection of immunoliposome comprising doxorubicin without 64Cu in first dosage; page 5, lines 27-31), the injection administered at a dose of at least 25, at least 30, at least 35, at least 40, or at least 45, or 50 mg/m2 of doxorubicin (first injection is 50 mg/m2; page 5, lines 27-31); but Merrimack does not disclose a method comprising (b) at between one and 6 hours following the first injection, administering to the patient a second injection comprising 64Cu-loaded immunoliposomal doxorubicin, the doxorubicin comprised by the second injection consisting of a dose of at least 3, at least 4, at least 5, at least 6, or 7 mg/m2 of doxorubicin, said dose comprising at 10.8 mCi of 64Cu +/- 15 percent; and (c) obtaining at least two PET/CT scans of a region of pathology in the patient, wherein each scan is obtained at a different time point, and wherein time elapsed from the injection of(a) until a final scan of the at least two scans is obtained is no more than three days.

US 8,329,213 B2 to Hong, et al. (hereinafter 'Hong') discloses a method of treating and imaging a patient (method of treating and imaging a patient; column 2, lines 10-18), the method comprising:(a) administering to the patient a first injection comprising immunoliposomal doxorubicin that does not comprise detectable levels of 64Cu (first administration is injection of immunoliposome comprising doxorubicin and without 64Cu in first dosage; column 8, lines 59-61; column 23, line 1), but Hong does not disclose the method comprising the injection administered at a dose of at least 25, at least 30, at least 35, at least 40, or at least 45, or 50 mg/m2 of doxorubicin; (b) at between one and 6 hours following the first injection, administering to the patient a second injection comprising 64Cu-loaded immunoliposomal doxorubicin, the doxorubicin comprised by the second injection consisting of a dose of at least 3, at least 4, at least 5, at least 6, or 7 mg/m2 of doxorubicin, said dose comprising at 10.8 mCi of 64Cu +/- 15 percent; and (c) obtaining at least two PET/CT scans of a region of pathology in the patient, wherein each scan is obtained at a different time point, and wherein time elapsed from the injection of(a) until a final scan of the at least two scans is obtained is no more than three days.

-***-Continued Within the Next Supplemental Box-***-

WRITTEN OPINION OF THE INTERNATIONAL SEARCHING AUTHORITY

International application No.
PCT/US14/62007

Supplemental Box

In case **the space in any of the preceding boxes is not sufficient.**
Continuation of:

-***-Continued from Previous Supplemental Box-***-

WO 2012/079582 A1 to Technical University Of Denmark (hereinafter 'Denmark') discloses a method of treating and imaging a patient (method of treating and imaging a patient; page 1, lines 4-11), and Denmark further discloses a method comprising administration 64Cu containing liposomes for PET imagining (page 1, lines 4-14). But, Denmark does not disclose the method comprising:(a) administering to the patient a first injection comprising immunoliposomal doxorubicin that does not comprise detectable levels of 64Cu comprising the injection administered at a dose of at least 25, at least 30, at least 35, at least 40, or at least 45, or 50 mg/m2 of doxorubicin; b) at between one and 6 hours following the first injection, administering to the patient a second injection comprising 64Cu-loaded immunoliposomal doxorubicin, the doxorubicin comprised by the second injection consisting of a dose of at least 3, at least 4, at least 5, at least 6, or 7 mg/m2 of doxorubicin, said dose comprising at 10.8 mCi of 64Cu +/- 15 percent; and (c) obtaining at least two PET/CT scans of a region of pathology in the patient, wherein each scan is obtained at a different time point, and wherein time elapsed from the injection of(a) until a final scan of the at least two scans is obtained is no more than three days.

Transmolecular discloses a method of treating and imaging a patient (method of treating and imaging a patient; page 24, lines 1-5; page 26, lines 31-34), and Transmolecular further discloses a 64Cu-loaded liposome said dose comprising 10.8 mCi of 64Cu +/- 15 percent (liposome composition containing preferred 64Cu at a dose of less than 20 mCi; page 26, lines 7-8; page 28, lines 29-30; page 29, lines 5-6; page 33, lines 7-10). But, Transmolecular does not disclose the method comprising:(a) administering to the patient a first injection comprising immunoliposomal doxorubicin that does not comprise detectable levels of 64Cu comprising the injection administered at a dose of at least 25, at least 30, at least 35, at least 40, or at least 45, or 50 mg/m2 of doxorubicin; b) at between one and 6 hours following the first injection, administering to the patient a second injection comprising 64Cu-loaded immunoliposomal doxorubicin, the doxorubicin comprised by the second injection consisting of a dose of at least 3, at least 4, at least 5, at least 6, or 7 mg/m2 of doxorubicin, said dose comprising at 10.8 mCi of 64Cu +/- 15 percent; and (c) obtaining at least two PET/CT scans of a region of pathology in the patient, wherein each scan is obtained at a different time point, and wherein time elapsed from the injection of(a) until a final scan of the at least two scans is obtained is no more than three days.

The prior art does not disclose a method of treating and imaging a patient, the method comprising:(a) administering to the patient a first injection comprising immunoliposomal doxorubicin that does not comprise detectable levels of 64Cu, the injection administered at a dose of at least 25, at least 30, at least 35, at least 40, or at least 45, or 50 mg/m2 of doxorubicin; (b) at between one and 6 hours following the first injection, administering to the patient a second injection comprising 64Cu-loaded immunoliposomal doxorubicin, the doxorubicin comprised by the second injection consisting of a dose of at least 3, at least 4, at least 5, at least 6, or 7 mg/m2 of doxorubicin, said dose comprising at 10.8 mCi of 64Cu +/- 15 percent; and (c) obtaining at least two PET/CT scans of a region of pathology in the patient, wherein each scan is obtained at a different time point, and wherein time elapsed from the injection of(a) until a final scan of the at least two scans is obtained is no more than three days

Claims 26-27 meet the criteria set out in PCT Article 33(2)-(3), based on their dependency on positive claim 25.

Claim 33/32/31/28-29 meets the criteria set out in PCT Article 33(2)-(3), because the prior art does not teach or fairly suggest a method the composition of claims 32/31/28-30, wherein the chelator is 4-DEAP-ATSC.

Transmolecular and Merrimack, in combination, disclose the composition of claims 32/31/30, but Transmolecular does not disclose the composition wherein the chelator is 4-DEAP-ATSC.

Denmark discloses a composition comprising a chelator selected from a group of chelators (page 8; lines 4-10), but Denmark does not disclose a chelator is 4-DEAP-ATSC.

The publication "A Novel 64Cu-Liposome PET Agent (MM-DX-929) Predicts Response to Liposomal Chemotherapeutics in Preclinical Breast Cancer Models" to Lee, e al. (hereinafter 'Lee') discloses a chelator (figure 3), but Lee does not disclose a chelator is 4-DEAP-ATSC.

Merrimack discloses a method of imaging a patient (method of treating a patient; claim 1), but Merrimack does not disclose a chelator is 4-DEAP-ATSC.

The prior art does not disclose a liposomal composition comprising a chelator 4-DEAP-ATSC.

Claims 34/33/32/31/28-29, 35/34/33/32/31/28-29, and 36/35/34/33/32/31/28-29 meet the criteria set out in PCT Article 33(2)-(3), based on their dependency on positive claim 33/32/31/28-29.

-***-Continued Within the Next Supplemental Box-***-

WRITTEN OPINION OF THE INTERNATIONAL SEARCHING AUTHORITY

International application No.
PCT/US14/62007

Supplemental Box

In case **the space in any of the preceding boxes is not sufficient.**
Continuation of:
-***-Continued from Previous Supplemental Box-***-

Claim 33/32/31/30 meets the criteria set out in PCT Article 33(2)-(3), because the prior art does not teach or fairly suggest a method the composition of claims 32/31/28-30, wherein the chelator is 4-DEAP-ATSC.

Transmolecular, Merrimack, and Zhou, in combination, disclose the composition of claims 32/31/30, but Transmolecular does not disclose the composition wherein the chelator is 4-DEAP-ATSC.

Denmark discloses a composition comprising a chelator selected from a group of chelators (page 8; lines 4-10), but Denmark does not disclose a chelator is 4-DEAP-ATSC.

Lee discloses a chelator (figure 3), but Lee does not disclose a chelator is 4-DEAP-ATSC.

Merrimack discloses a method of imaging a patient (method of treating a patient; claim 1), but Merrimack does not disclose a chelator is 4-DEAP-ATSC.

The prior art does not disclose a liposomal composition comprising a chelator 4-DEAP-ATSC.

Claims 34/33/32/31/30, 35/34/33/32/31/30, and 36/35/34/33/32/31/30 meet the criteria set out in PCT Article 33(2)-(3), based on their dependency on positive claim 33/32/31/30.

Claims 1-2, 3/1-2, 9-11, 12/9-11, 13-14, 15/13-14, 16/15/13-14, 25-30, 31/28-30, 32/31/28-30, 33/32/31/28-30, 34/33/32/31/28-30, 35/34/33/32/31/28-30, and 36/35/34/33/32/31/28-30 have industrial applicability as defined by PCT Article 33(4) because the subject matter can be made or used in industry.

PATENT COOPERATION TREATY

PCT

INTERNATIONAL SEARCH REPORT

(PCT Article 18 and Rules 43 and 44)

Applicant's or agent's file reference 94153WO(309768)	FOR FURTHER ACTION	see Form PCT/ISA/220 as well as, where applicable, item 5 below.
International application No. PCT/US14/62007	International filing date *(day/month/year)* 23 October 2014 (23.10.2014)	(Earliest) Priority Date *(day/month/year)* 23 October 2013 (23.10.2013)
Applicant MERRIMACK PHARMACEUTICALS, INC.		

This international search report has been prepared by this International Searching Authority and is transmitted to the applicant according to Article 18. A copy is being transmitted to the International Bureau.

This international search report consists of a total of 3 sheets.

☒ It is also accompanied by a copy of each prior art document cited in this report.

1. **Basis of the report**

   a. With regard to the **language**, the international search was carried out on the basis of:

   ☒ the international application in the language in which it was filed.

   ☐ a translation of the international application into _____ which is the language of a translation furnished for the purposes of international search (Rules 12.3(a) and 23.1(b)).

   b. ☐ This international search report has been established taking into account the **rectification of an obvious mistake** authorized by or notified to this Authority under Rule 91 (Rule 43.6*bis*(a)).

   c. ☐ With regard to any **nucleotide and/or amino acid sequence** disclosed in the international application, see Box No. I.

2. ☒ **Certain claims were found unsearchable** (see Box No. II).

3. ☐ **Unity of invention is lacking** (see Box No. III).

4. With regard to the **title**,

   ☐ the text is approved as submitted by the applicant.

   ☒ the text has been established by this Authority to read as follows:

LIPOSOMES FOR NON-INVASIVE IMAGING AND DRUG DELIVERY

5. With regard to the **abstract**,

   ☒ the text is approved as submitted by the applicant.

   ☐ the text has been established, according to Rule 38.2, by this Authority as it appears in Box No. IV. The applicant may, within one month from the date of mailing of this international search report, submit comments to this Authority.

6. With regard to the **drawings**,

   a. the figure of the **drawings** to be published with the abstract is Figure No. 1

   ☒ as suggested by the applicant.

   ☐ as selected by this Authority, because the applicant failed to suggest a figure.

   ☐ as selected by this Authority, because this figure better characterizes the invention.

   b. ☐ none of the figures is to be published with the abstract.

International application No.
PCT/US14/62007

Box No. II Observations where certain claims were found unsearchable (Continuation of item 2 of first sheet)

This international search report has not been established in respect of certain claims under Article 17(2)(a) for the following reasons:

1. ☐ Claims Nos.:
because they relate to subject matter not required to be searched by this Authority, namely:

2. ☐ Claims Nos.:
because they relate to parts of the international application that do not comply with the prescribed requirements to such an extent that no meaningful international search can be carried out, specifically:

3. ☒ Claims Nos.: 4-8 and 17-24
because they are dependent claims and are not drafted in accordance with the second and third sentences of Rule 6.4(a).

Box No. III Observations where unity of invention is lacking (Continuation of item 3 of first sheet)

This International Searching Authority found multiple inventions in this international application, as follows:

1. ☐ As all required additional search fees were timely paid by the applicant, this international search report covers all searchable claims.

2. ☐ As all searchable claims could be searched without effort justifying additional fees, this Authority did not invite payment of additional fees.

3. ☐ As only some of the required additional search fees were timely paid by the applicant, this international search report covers only those claims for which fees were paid, specifically claims Nos.:

4. ☐ No required additional search fees were timely paid by the applicant. Consequently, this international search report is restricted to the invention first mentioned in the claims; it is covered by claims Nos.:

Remark on Protest

☐ The additional search fees were accompanied by the applicant's protest and, where applicable, the payment of a protest fee.

☐ The additional search fees were accompanied by the applicant's protest but the applicable protest fee was not paid within the time limit specified in the invitation.

☐ No protest accompanied the payment of additional search fees.

INTERNATIONAL SEARCH REPORT

International application No.
PCT/US14/62007

A. CLASSIFICATION OF SUBJECT MATTER

IPC(8) - A61K 9/127, 51/00, 51/12; A61M 36/00 (2014.01)
CPC - A61K 9/127, 9/1271, 49/0084, 51/1234

According to International Patent Classification (IPC) or to both national classification and IPC

B. FIELDS SEARCHED

Minimum documentation searched (classification system followed by classification symbols)

IPC(8)- A61K 9/127, 47/28, 47/42, 51/00, 51/08, 51/12; A61M 36/00 (2014.01); CPC - A61K 9/0019, 9/127, 9/1271, 9/1277, 49/0084, 51/1234; USPC - 424/9.321, 450, 812; 514/26, 34, 449, 558

Documentation searched other than minimum documentation to the extent that such documents are included in the fields searched

Electronic data base consulted during the international search (name of data base and, where practicable, search terms used)

MicroPatent (US-G, US-A, EP-A, EP-B, WO, JP-bib, DE-C,B, DE-A, DE-T, DE-U, GB-A, FR-A); Patseer, Google Scholar; PubMed; ClinicalTrials.gov; IP.com; ProQuest; Liposome, immunoliposome, positron emission, PET, imaging, doxorubicin, anthracycline, Adriamycin, doxil, hydroxydaunorubicin, lesion, tumor, 64Cu, copper64, HER-2, ERBB2, EphA2, gradient chelator, 4-DEAP-ATSC, mCi, millicurie,

C. DOCUMENTS CONSIDERED TO BE RELEVANT

Category*	Citation of document, with indication, where appropriate, of the relevant passages	Relevant to claim No.
X --- Y	WO 2003/101474 A1 (TRANSMOLECULAR, INC) December 11, 2003; claim 6; page 5, lines 9-21; page 21, lines 20-23; page 24, lines 10-31; page 26, lines 7-34; page 27, lines 1-12; page 28, lines 29-30; page 29, lines 5-6; page 30, table 3; page 33, lines 7-10	13, 15/13, 16/15/13, 28 ---- 1-2, 3/1-2, 9-11, 12/9-11, 14, 15/14, 16/15/14, 29-30, 31/28-30, 32/31/28-20
Y	WO 2012/078695 A2 (MERRIMACK PHARMACEUTICALS, INC.) June 14, 2012; page 4, lines 23-35; page 5, lines 5-15; page 9, lines 2-27	1-2, 3/1-2, 9-11, 12/9-11, 14, 15/14, 16/15/14, 29, 31/28-30, 32/31/28-30
Y	WO 2012/079582 A1 (TECHNICAL UNIVERSITY OF DENMARK) June 21, 2012; page 1, lines 4-14; page 8, lines 4-10	32/31/28-30
Y	US 2013/0209481 A1 (ZHOU, Y et al.) August 15, 2013; paragraphs [0212], [0215]	30, 31/30, 32/31/30
A	US 8,329,213 B2 (HONG, K et al.) December 11, 2012; column 2, lines 10-18; column 18, lines 59-61; column 23, line 1	25-27
A	LEE, H et al. "A Novel 64Cu-Liposome PET Agent (MM-DX-929) Predicts Response to Liposomal Chemotherapeutics in Preclinical Breast Cancer Models" December 4-8, 2012. Retrieved from internet <http://origin-qps.onstreammedia.com/origin/multivu_archive/ENR/FX-20121210-DC26113-01.pdf> [Retrieved 13.12.2014]; figure 3	33/32/31/28-30, 34/33/32/31/28-30, 35/34/33/32/31/28-30, 36/35/34/33/32/31/28-30

☐ Further documents are listed in the continuation of Box C. ☐

* Special categories of cited documents:

"A" document defining the general state of the art which is not considered to be of particular relevance

"E" earlier application or patent but published on or after the international filing date

"L" document which may throw doubts on priority claim(s) or which is cited to establish the publication date of another citation or other special reason (as specified)

"O" document referring to an oral disclosure, use, exhibition or other means

"P" document published prior to the international filing date but later than the priority date claimed

"T" later document published after the international filing date or priority date and not in conflict with the application but cited to understand the principle or theory underlying the invention

"X" document of particular relevance; the claimed invention cannot be considered novel or cannot be considered to involve an inventive step when the document is taken alone

"Y" document of particular relevance; the claimed invention cannot be considered to involve an inventive step when the document is combined with one or more other such documents, such combination being obvious to a person skilled in the art

"&" document member of the same patent family

Date of the actual completion of the international search	Date of mailing of the international search report
23 December 2014 (23.12.2014)	09 JAN 2015

Name and mailing address of the ISA/US	Authorized officer:
Mail Stop PCT, Attn: ISA/US, Commissioner for Patents P.O. Box 1450, Alexandria, Virginia 22313-1450 Facsimile No. 571-273-3201	Shane Thomas PCT Helpdesk: 571-272-4300 PCT OSP: 571-272-7774

PATENT COOPERATION TREATY

PCT

INTERNATIONAL PRELIMINARY REPORT ON PATENTABILITY
(Chapter I of the Patent Cooperation Treaty)

(PCT Rule 44*bis*)

Applicant's or agent's file reference 239669-381051	**FOR FURTHER ACTION**	See item 4 below
International application No. PCT/US2015/064491	International filing date *(day/month/year)* 08 December 2015 (08.12.2015)	Priority date *(day/month/year)* 09 December 2014 (09.12.2014)
International Patent Classification (8th edition unless older edition indicated) See relevant information in Form PCT/ISA/237		
Applicant IPSEN BIOPHARM LTD.		

1. This international preliminary report on patentability (Chapter I) is issued by the International Bureau on behalf of the International Searching Authority under Rule 44 *bis*.1(a).

2. This REPORT consists of a total of 7 sheets, including this cover sheet.

   In the attached sheets, any reference to the written opinion of the International Searching Authority should be read as a reference to the international preliminary report on patentability (Chapter I) instead.

3. This report contains indications relating to the following items:

☒	Box No. I	Basis of the report
☒	Box No. II	Priority
☐	Box No. III	Non-establishment of opinion with regard to novelty, inventive step and industrial applicability
☐	Box No. IV	Lack of unity of invention
☒	Box No. V	Reasoned statement under Article 35(2) with regard to novelty, inventive step or industrial applicability; citations and explanations supporting such statement
☒	Box No. VI	Certain documents cited
☐	Box No. VII	Certain defects in the international application
☒	Box No. VIII	Certain observations on the international application

4. The International Bureau will communicate this report to designated Offices in accordance with Rules 44*bis*.3(c) and 93*bis*.1 but not, except where the applicant makes an express request under Article 23(2), before the expiration of 30 months from the priority date (Rule 44*bis* .2).

	Date of issuance of this report 13 June 2017 (13.06.2017)
The International Bureau of WIPO 34, chemin des Colombettes 1211 Geneva 20, Switzerland Facsimile No. +41 22 338 82 70	Authorized officer Athina Nickitas-Etienne e-mail: pct.team4@wipo.int

Form PCT/IB/373 (January 2004)

PATENT COOPERATION TREATY

From the
INTERNATIONAL SEARCHING AUTHORITY

To:

see form PCT/ISA/220

PCT

WRITTEN OPINION OF THE INTERNATIONAL SEARCHING AUTHORITY

(PCT Rule 43*bis*.1)

Date of mailing
(day/month/year) see form PCT/ISA/210 (second sheet)

Applicant's or agent's file reference
see form PCT/ISA/220

FOR FURTHER ACTION
See paragraph 2 below

International application No.	International filing date *(day/month/year)*	Priority date *(day/month/year)*
PCT/US2015/064491	08.12.2015	09.12.2014

International Patent Classification (IPC) or both national classification and IPC
INV. A61K31/436 A61K9/127 A61K35/04

Applicant
MERRIMACK PHARMACEUTICALS, INC.

1. This opinion contains indications relating to the following items:

- ☒ Box No. I Basis of the opinion
- ☒ Box No. II Priority
- ☐ Box No. III Non-establishment of opinion with regard to novelty, inventive step and industrial applicability
- ☐ Box No. IV Lack of unity of invention
- ☒ Box No. V Reasoned statement under Rule 43*bis*.1(a)(i) with regard to novelty, inventive step and industrial applicability; citations and explanations supporting such statement
- ☒ Box No. VI Certain documents cited
- ☐ Box No. VII Certain defects in the international application
- ☒ Box No. VIII Certain observations on the international application

2. **FURTHER ACTION**

If a demand for international preliminary examination is made, this opinion will usually be considered to be a written opinion of the International Preliminary Examining Authority ("IPEA") except that this does not apply where the applicant chooses an Authority other than this one to be the IPEA and the chosen IPEA has notifed the International Bureau under Rule 66.1*bis*(b) that written opinions of this International Searching Authority will not be so considered.

If this opinion is, as provided above, considered to be a written opinion of the IPEA, the applicant is invited to submit to the IPEA a written reply together, where appropriate, with amendments, before the expiration of 3 months from the date of mailing of Form PCT/ISA/220 or before the expiration of 22 months from the priority date, whichever expires later.

For further options, see Form PCT/ISA/220.

Name and mailing address of the ISA:	Date of completion of this opinion	Authorized Officer
European Patent Office D-80298 Munich Tel. +49 89 2399 - 0 Fax: +49 89 2399 - 4465	see form PCT/ISA/210	Steendijk, Martin Telephone No. +49 89 2399-0

Box No. I Basis of the opinion

1. With regard to the **language**, this opinion has been established on the basis of:

   ☒ the international application in the language in which it was filed.

   ☐ a translation of the international application into , which is the language of a translation furnished for the purposes of international search (Rules 12.3(a) and 23.1 (b)).

2. ☐ This opinion has been established taking into account the **rectification of an obvious mistake** authorized by or notified to this Authority under Rule 91 (Rule 43*bis*.1(a))

3. ☐ With regard to any **nucleotide and/or amino acid sequence** disclosed in the international application, this opinion has been established on the basis of a sequence listing:

   a. ☐ forming part of the international application as filed:

      ☐ in the form of an Annex C/ST.25 text file.

      ☐ on paper or in the form of an image file.

   b. ☐ furnished together with the international application under PCT Rule 13*ter*.1(a) for the purposes of international search only in the form of an Annex C/ST.25 text file.

   c. ☐ furnished subsequent to the international filing date for the purposes of international search only:

      ☐ in the form of an Annex C/ST.25 text file (Rule 13*ter*.1(a)).

      ☐ on paper or in the form of an image file (Rule 13*ter*.1(b) and Administrative Instructions, Section 713).

4. ☐ In addition, in the case that more than one version or copy of a sequence listing has been filed or furnished, the required statements that the information in the subsequent or additional copies is identical to that forming part of the application as filed or does not go beyond the application as filed, as appropriate, were furnished.

5. Additional comments:

Box No. II Priority

1. ☒ The validity of the priority claim has not been considered because the International Searching Authority does not have in its possession a copy of the earlier application whose priority has been claimed or, where required, a translation of that earlier application. This opinion has nevertheless been established on the assumption that the relevant date (Rules 43*bis*.1 and 64.1) is the claimed priority date.

2. ☐ This opinion has been established as if no priority had been claimed due to the fact that the priority claim has been found invalid (Rules 43*bis*.1 and 64.1). Thus for the purposes of this opinion, the international filing date indicated above is considered to be the relevant date.

3. Additional observations, if necessary:

Box No. V Reasoned statement under Rule 43*bis*.1(a)(i) with regard to novelty, inventive step or industrial applicability; citations and explanations supporting such statement

1. Statement

Novelty (N)	Yes:	Claims	1-19
	No:	Claims	20, 21
Inventive step (IS)	Yes:	Claims	
	No:	Claims	1-21
Industrial applicability (IA)	Yes:	Claims	1-21
	No:	Claims	

2. Citations and explanations

see separate sheet

Box No. VI Certain documents cited

1. Certain published documents (Rules 43*bis*.1 and 70.10)

and / or

2. Non-written disclosures (Rules 43*bis*.1 and 70.9)

see form 210

Box No. VIII Certain observations on the international application

The following observations on the clarity of the claims, description, and drawings or on the question whether the claims are fully supported by the description, are made:

see separate sheet

item V

Item VIII

1) The present application relates to the utility of liposomal irinotacan in treatment of metastatic breast cancer (MBC), in particular HER2 negative MBC and HER2 positive or negative MBC with brain lesions.

2) Cited documents

D1 JEFFREY R INFANTE ET AL: "Phase I and pharmacokinetic study of IHL-305 (PEGylated liposomal irinotecan) in patients with advanced solid tumors",
CANCER CHEMOTHERAPY AND PHARMACOLOGY, SPRINGER, BERLIN, DE,
vol. 70, no. 5, 2 September 2012 (2012-09-02), pages 699-705, XP035132528,
ISSN: 1432-0843, DOI: 10.1007/S00280-012-1960-5

D2 WO 2014/113167 A1 (MERRIMACK PHARMACEUTICALS INC [US]) 24 July 2014 (2014-07-24)

D3 WO 03/030864 A1 (NEOPHARM INC [US]; RAHMAN AQUILUR [US]; AHMAD IMRAN [US]) 17 April 2003 (2003-04-17)

D4 US 2007/110798 A1 (DRUMMOND DARYL C [US] ET AL) 17 May 2007 (2007-05-17)

D5 HIDETOSHI HAYASHI ET AL: "Phase II study of bi-weekly irinotecan for patients with previously treated HER2-negative metastatic breast cancer: KMBOG0610B",
BREAST CANCER,
vol. 20, no. 2, 29 November 2011 (2011-11-29), pages 131-136, XP055246819,
JP
ISSN: 1340-6868, DOI: 10.1007/s12282-011-0316-z

D6 WO 2012/012454 A1 (BIPAR SCIENCES INC [US]; BRADLEY CHARLES [US]) 26 January 2012 (2012-01-26)

D7 WO 2013/188586 A1 (MERRIMACK PHARMACEUTICALS INC [US]) 19 December 2013 (2013-12-19)

D8 Anonymous: "Abstract P5-01-06: Characterization of metastatic breast cancer lesions with ferumoxytol MRI and treatment response to MM-398, nanoliposomal irinotecan (nal-IRI)",
, 1 May 2015 (2015-05-01), XP55245815,
Retrieved from the Internet:
URL:http://cancerres.aacrjournals.org/content/75/9_Supplement/P5-01-06
[retrieved on 2016-01-28]

Document D8 was published after the claimed priority. On the presumption that the priority is valid for the claimed subject-matter this document is not considered as prior art.

3) Novelty

3.1 Document D1 describes the positive effect (partial response) of treatment of a metastatic breast cancer patient with PEGylated liposomal irinotecan. The document does not specify HER2 status nor brain lesions.

Documents D2 and D3 refer to liposomal irinotecan, including MM-398, as effective in treatment of breast cancer; document D2 further indicates FMX-MRI as valuable for prediction of efficacy. These documents do not refer specifically to MBC, HER2 status or brain lesions.

Document D4 indicates liposomal formulation as suitable for increasing residence of a camptothecin compound such as irinotecan in brain tissue (see claim 1); the document further indicates antitumor efficacy of liposomal irinotecan against breast cancer xenografts. The document does not specifically adress treatment of MCB.

The disclosure of liposomal irinotecan, including MM-398, in documents D1-D4 is however considered to anticipate claims 20-21, which merely refer to a kit comprising instructions, which is not regarded as limiting the subject-matter in technical terms to the intended indications.

3.2 Documents D5 and D6 describe the known utility of irinotecan in treatment of MCB. The documents do not specifically refer to liposomal irinotecan.

Document D7 refers to the utility of liposomal irinotecan in treatment of pancreatic cancer, mentioning treatment of metastatic pancreatic cancer and relevance of UGT1A1*28 status on suitable dosage regimen. The document does not refer to MBC.

4) Inventive step

Documents D5 and D6 may be regarded as closest prior art, in view of which the problem to be solved may be seen in the provision of further, possibly improved treatment of relevant MBC. As solution the use of liposomal irinotecan (e.g. MM-398) would seem obvious to the skilled person in the light of any of documents D1-D4, which already indicate that liposomal irinotecan may indeed be effective in against breast cancer (D2-D4), including MBC (D1) and may in fact be particular effective in brain tissue (D4). In fact, that liposomal formulation was actually known for preferential deposition in tumors with favourable toxicity characteristics (D2, D3). In this context it is noted that the present application does not seem to substantiate an unexpected favourable effect supportive of any inventive merit.

5) Further observations

Claims 1-19 relate to subject-matter considered by this Authority to be covered by the provisions of Rule 39.1(iv) / 67.1(iv) PCT.

The patentability can be dependent upon the formulation of the claims. The EPO, for example, does not recognise as patentable claims to the use of a compound in medical treatment, but may allow claims to a product, in particular substances or compositions for use in a first or further medical treatment.

PATENT COOPERATION TREATY

PCT

INTERNATIONAL SEARCH REPORT

(PCT Article 18 and Rules 43 and 44)

Applicant's or agent's file reference	**FOR FURTHER ACTION**	see Form PCT/ISA/220 as well as, where applicable, item 5 below.
239669-381051		
International application No.	International filing date *(day/month/year)*	(Earliest) Priority Date *(day/month/year)*
PCT/US2015/064491	8 December 2015 (08-12-2015)	9 December 2014 (09-12-2014)
Applicant		
MERRIMACK PHARMACEUTICALS, INC.		

This international search report has been prepared by this International Searching Authority and is transmitted to the applicant according to Article 18. A copy is being transmitted to the International Bureau.

This international search report consists of a total of 4 sheets.

[X] It is also accompanied by a copy of each prior art document cited in this report.

1. **Basis of the report**
   a. With regard to the **language,** the international search was carried out on the basis of:
      [X] the international application in the language in which it was filed
      [ ] a translation of the international application into _____, which is the language of a translation furnished for the purposes of international search (Rules 12.3(a) and 23.1(b))
   b. [ ] This international search report has been established taking into account the **rectification of an obvious mistake** authorized by or notified to this Authority under Rule 91 (Rule 43.6*bis*(a)).
   c. [ ] With regard to any **nucleotide and/or amino acid sequence** disclosed in the international application, see Box No. I.

2. [ ] **Certain claims were found unsearchable** (See Box No. II)

3. [ ] **Unity of invention is lacking** (see Box No III)

4. With regard to the **title,**
   [X] the text is approved as submitted by the applicant
   [ ] the text has been established by this Authority to read as follows:

5. With regard to the **abstract,**
   [X] the text is approved as submitted by the applicant
   [ ] the text has been established, according to Rule 38.2, by this Authority as it appears in Box No. IV. The applicant may, within one month from the date of mailing of this international search report, submit comments to this Authority

6. With regard to the **drawings,**
   a. the figure of the **drawings** to be published with the abstract is Figure No. _____
      [ ] as suggested by the applicant
      [ ] as selected by this Authority, because the applicant failed to suggest a figure
      [ ] as selected by this Authority, because this figure better characterizes the invention
   b. [ ] none of the figures is to be published with the abstract

INTERNATIONAL SEARCH REPORT

International application No
PCT/US2015/064491

A. CLASSIFICATION OF SUBJECT MATTER
INV. A61K31/436 A61K9/127 A61K35/04
ADD.

According to International Patent Classification (IPC) or to both national classification and IPC

B. FIELDS SEARCHED

Minimum documentation searched (classification system followed by classification symbols)
A61K

Documentation searched other than minimum documentation to the extent that such documents are included in the fields searched

Electronic data base consulted during the international search (name of data base and, where practicable, search terms used)
EPO-Internal, BIOSIS, CHEM ABS Data, EMBASE, WPI Data

C. DOCUMENTS CONSIDERED TO BE RELEVANT

Category*	Citation of document, with indication, where appropriate, of the relevant passages	Relevant to claim No.
X	JEFFREY R INFANTE ET AL: "Phase I and pharmacokinetic study of IHL-305 (PEGylated liposomal irinotecan) in patients with advanced solid tumors", CANCER CHEMOTHERAPY AND PHARMACOLOGY, SPRINGER, BERLIN, DE, vol. 70, no. 5, 2 September 2012 (2012-09-02), pages 699-705, XP035132528, ISSN: 1432-0843, DOI: 10.1007/S00280-012-1960-5	20
Y	page 702	1-21

X	WO 2014/113167 A1 (MERRIMACK PHARMACEUTICALS INC [US]) 24 July 2014 (2014-07-24)	20,21
Y	claim 15	1-21

	-/--	

[X] Further documents are listed in the continuation of Box C.

[X] See patent family annex.

* Special categories of cited documents :

"A" document defining the general state of the art which is not considered to be of particular relevance

"E" earlier application or patent but published on or after the international filing date

"L" document which may throw doubts on priority claim(s) or which is cited to establish the publication date of another citation or other special reason (as specified)

"O" document referring to an oral disclosure, use, exhibition or other means

"P" document published prior to the international filing date but later than the priority date claimed

"T" later document published after the international filing date or priority date and not in conflict with the application but cited to understand the principle or theory underlying the invention

"X" document of particular relevance; the claimed invention cannot be considered novel or cannot be considered to involve an inventive step when the document is taken alone

"Y" document of particular relevance; the claimed invention cannot be considered to involve an inventive step when the document is combined with one or more other such documents, such combination being obvious to a person skilled in the art

"&" document member of the same patent family

Date of the actual completion of the international search	Date of mailing of the international search report
2 February 2016	19/02/2016

Name and mailing address of the ISA/	Authorized officer
European Patent Office, P.B. 5818 Patentlaan 2 NL - 2280 HV Rijswijk Tel. (+31-70) 340-2040, Fax: (+31-70) 340-3016	Steendijk, Martin

1

Form PCT/ISA/210 (second sheet) (April 2005)

INTERNATIONAL SEARCH REPORT

International application No
PCT/US2015/064491

C(Continuation). DOCUMENTS CONSIDERED TO BE RELEVANT

Category*	Citation of document, with indication, where appropriate, of the relevant passages	Relevant to claim No.
X	WO 03/030864 A1 (NEOPHARM INC [US]; RAHMAN AQUILUR [US]; AHMAD IMRAN [US]) 17 April 2003 (2003-04-17)	20,21
Y	page 6; claim 1	1-21
X	US 2007/110798 A1 (DRUMMOND DARYL C [US] ET AL) 17 May 2007 (2007-05-17)	20,21
Y	page 25; claims; example 10	1-21
Y	HIDETOSHI HAYASHI ET AL: "Phase II study of bi-weekly irinotecan for patients with previously treated HER2-negative metastatic breast cancer: KMBOG0610B", BREAST CANCER, vol. 20, no. 2, 29 November 2011 (2011-11-29), pages 131-136, XP055246819, JP ISSN: 1340-6868, DOI: 10.1007/s12282-011-0316-z abstract	1-21
Y	WO 2012/012454 A1 (BIPAR SCIENCES INC [US]; BRADLEY CHARLES [US]) 26 January 2012 (2012-01-26) claims	1-21
A	WO 2013/188586 A1 (MERRIMACK PHARMACEUTICALS INC [US]) 19 December 2013 (2013-12-19) claims	1-21
X,P	Anonymous: "Abstract P5-01-06: Characterization of metastatic breast cancer lesions with ferumoxytol MRI and treatment response to MM-398, nanoliposomal irinotecan (nal-IRI)", , 1 May 2015 (2015-05-01), XP55245815, Retrieved from the Internet: URL:http://cancerres.aacrjournals.org/content/75/9_Supplement/P5-01-06 [retrieved on 2016-01-28] abstract	1-21

1

INTERNATIONAL SEARCH REPORT

Information on patent family members

International application No
PCT/US2015/064491

Patent document cited in search report	Publication date	Patent family member(s)	Publication date
WO 2014113167 A1	24-07-2014	AU 2013374248 A1	11-06-2015
		US 2014170075 A1	19-06-2014
		WO 2014113167 A1	24-07-2014
WO 03030864 A1	17-04-2003	US 2005019387 A1	27-01-2005
		WO 03030864 A1	17-04-2003
US 2007110798 A1	17-05-2007	US 2007110798 A1	17-05-2007
		US 2014127136 A1	08-05-2014
WO 2012012454 A1	26-01-2012	AU 2011282223 A1	07-03-2013
		CA 2805774 A1	26-01-2012
		EP 2595618 A1	29-05-2013
		EP 2595619 A1	29-05-2013
		JP 2013531068 A	01-08-2013
		JP 2013531069 A	01-08-2013
		US 2013274281 A1	17-10-2013
		WO 2012012448 A1	26-01-2012
		WO 2012012454 A1	26-01-2012
WO 2013188586 A1	19-12-2013	AU 2013202947 A1	16-01-2014
		AU 2013274287 A1	29-01-2015
		CA 2875824 A1	19-12-2013
		CN 104717961 A	17-06-2015
		EP 2861210 A1	22-04-2015
		JP 2015523355 A	13-08-2015
		KR 20150021565 A	02-03-2015
		US 2015182521 A1	02-07-2015
		US 2015328156 A1	19-11-2015
		US 2015374682 A1	31-12-2015
		WO 2013188586 A1	19-12-2013

PATENT COOPERATION TREATY

PCT

INTERNATIONAL PRELIMINARY REPORT ON PATENTABILITY
(Chapter I of the Patent Cooperation Treaty)

(PCT Rule 44*bis*)

Applicant's or agent's file reference 239669-401612	**FOR FURTHER ACTION**	See item 4 below
International application No. PCT/US2016/047814	International filing date *(day/month/year)* 19 August 2016 (19.08.2016)	Priority date *(day/month/year)* 20 August 2015 (20.08.2015)
International Patent Classification (8th edition unless older edition indicated) See relevant information in Form PCT/ISA/237		
Applicant IPSEN BIOPHARM LTD.		

1. This international preliminary report on patentability (Chapter I) is issued by the International Bureau on behalf of the International Searching Authority under Rule 44 *bis*.1(a).

2. This REPORT consists of a total of 6 sheets, including this cover sheet.

   In the attached sheets, any reference to the written opinion of the International Searching Authority should be read as a reference to the international preliminary report on patentability (Chapter I) instead.

3. This report contains indications relating to the following items:

☒	Box No. I	Basis of the report
☐	Box No. II	Priority
☐	Box No. III	Non-establishment of opinion with regard to novelty, inventive step and industrial applicability
☐	Box No. IV	Lack of unity of invention
☒	Box No. V	Reasoned statement under Article 35(2) with regard to novelty, inventive step or industrial applicability; citations and explanations supporting such statement
☐	Box No. VI	Certain documents cited
☐	Box No. VII	Certain defects in the international application
☐	Box No. VIII	Certain observations on the international application

4. The International Bureau will communicate this report to designated Offices in accordance with Rules 44*bis*.3(c) and 93*bis*.1 but not, except where the applicant makes an express request under Article 23(2), before the expiration of 30 months from the priority date (Rule 44*bis* .2).

	Date of issuance of this report 20 February 2018 (20.02.2018)
The International Bureau of WIPO 34, chemin des Colombettes 1211 Geneva 20, Switzerland Facsimile No. +41 22 338 82 70	Authorized officer Agnès Wittmann-Regis e-mail: pct.team6@wipo.int

Form PCT/IB/373 (January 2004)

PATENT COOPERATION TREATY

From the
INTERNATIONAL SEARCHING AUTHORITY

To:

see form PCT/ISA/220

PCT

WRITTEN OPINION OF THE INTERNATIONAL SEARCHING AUTHORITY

(PCT Rule 43*bis*.1)

Date of mailing
(day/month/year) see form PCT/ISA/210 (second sheet)

Applicant's or agent's file reference
see form PCT/ISA/220

FOR FURTHER ACTION
See paragraph 2 below

International application No.	International filing date *(day/month/year)*	Priority date *(day/month/year)*
PCT/US2016/047814	19.08.2016	20.08.2015

International Patent Classification (IPC) or both national classification and IPC
INV. A61K31/04 A61K31/166 A61K31/416 A61K31/4184 A61K31/436 A61K31/4745 A61K31/475 A61K31/502 A61K31/55 A61K9/127 A61K47/06 A61P35/00

Applicant
MERRIMACK PHARMACEUTICALS, INC.

1. This opinion contains indications relating to the following items:

- ☒ Box No. I Basis of the opinion
- ☐ Box No. II Priority
- ☐ Box No. III Non-establishment of opinion with regard to novelty, inventive step and industrial applicability
- ☐ Box No. IV Lack of unity of invention
- ☒ Box No. V Reasoned statement under Rule 43*bis*.1(a)(i) with regard to novelty, inventive step and industrial applicability; citations and explanations supporting such statement
- ☐ Box No. VI Certain documents cited
- ☐ Box No. VII Certain defects in the international application
- ☐ Box No. VIII Certain observations on the international application

2. **FURTHER ACTION**

If a demand for international preliminary examination is made, this opinion will usually be considered to be a written opinion of the International Preliminary Examining Authority ("IPEA") except that this does not apply where the applicant chooses an Authority other than this one to be the IPEA and the chosen IPEA has notifed the International Bureau under Rule 66.1*bis*(b) that written opinions of this International Searching Authority will not be so considered.

If this opinion is, as provided above, considered to be a written opinion of the IPEA, the applicant is invited to submit to the IPEA a written reply together, where appropriate, with amendments, before the expiration of 3 months from the date of mailing of Form PCT/ISA/220 or before the expiration of 22 months from the priority date, whichever expires later.

For further options, see Form PCT/ISA/220.

Name and mailing address of the ISA:	Date of completion of this opinion	Authorized Officer
European Patent Office D-80298 Munich Tel. +49 89 2399 - 0 Fax: +49 89 2399 - 4465	see form PCT/ISA/210	Engl, Brigitte Telephone No. +49 89 2399-0

Box No. I Basis of the opinion

1. With regard to the **language**, this opinion has been established on the basis of:

   ☒ the international application in the language in which it was filed.

   ☐ a translation of the international application into , which is the language of a translation furnished for the purposes of international search (Rules 12.3(a) and 23.1 (b)).

2. ☐ This opinion has been established taking into account the **rectification of an obvious mistake** authorized by or notified to this Authority under Rule 91 (Rule 43*bis*.1(a))

3. ☐ With regard to any **nucleotide and/or amino acid sequence** disclosed in the international application, this opinion has been established on the basis of a sequence listing:

   a. ☐ forming part of the international application as filed:

      ☐ in the form of an Annex C/ST.25 text file.

      ☐ on paper or in the form of an image file.

   b. ☐ furnished together with the international application under PCT Rule 13*ter*.1(a) for the purposes of international search only in the form of an Annex C/ST.25 text file.

   c. ☐ furnished subsequent to the international filing date for the purposes of international search only:

      ☐ in the form of an Annex C/ST.25 text file (Rule 13*ter*.1(a)).

      ☐ on paper or in the form of an image file (Rule 13*ter*.1(b) and Administrative Instructions, Section 713).

4. ☐ In addition, in the case that more than one version or copy of a sequence listing has been filed or furnished, the required statements that the information in the subsequent or additional copies is identical to that forming part of the application as filed or does not go beyond the application as filed, as appropriate, were furnished.

5. Additional comments:

Box No. V Reasoned statement under Rule 43*bis*.1(a)(i) with regard to novelty, inventive step or industrial applicability; citations and explanations supporting such statement

1. Statement

Novelty (N)	Yes:	Claims	1-20
	No:	Claims	
Inventive step (IS)	Yes:	Claims	
	No:	Claims	1-20
Industrial applicability (IA)	Yes:	Claims	1-20
	No:	Claims	

2. Citations and explanations

see separate sheet

Box V:

1 Prior Art

The following prior art is cited from the International Search Report:

D1 MESSERER CORRIE LYNN ET AL: "Liposomal irinotecan: formulation development and therapeutic assessment in murine xenograft models of colorectal cancer", CLINICAL CANCER RESEARCH : AN OFFICIAL JOURNAL OF THE AMERICAN ASSOCIATION FOR CANCER RESEARCH 1 OCT 2004, vol. 10, no. 19, 1 October 2004 (2004-10-01), pages 6638-6649, XP002763354, ISSN: 1078-0432

D2 SYBIL M GENTHER WILLIAMS ET AL: "Treatment with the PARP inhibitor, niraparib, sensitizes colorectal cancer cell lines to irinotecan regardless of MSI/MSS status", CANCER CELL INTERNATIONAL, BIOMED CENTRAL, LONDON, GB, vol. 15, no. 1, 4 February 2015 (2015-02-04), page 14, XP021213062, ISSN: 1475-2867, DOI: 10.1186/S12935-015-0162-8

D3 DAVIDSON DAVID ET AL: "The PARP inhibitor ABT-888 synergizes irinotecan treatment of colon cancer cell lines", INVESTIGATIONAL NEW DRUGS APR 2013, vol. 31, no. 2, April 2013 (2013-04), pages 461-468, XP002763355, ISSN: 1573-0646

D4 DOUILLARD J ET AL: "Irinotecan combined with fluorouracil compared with fluorouracil alone as first-line treatment for metastatic colorectal cancer: a multicentre randomised trial", THE LANCET, THE LANCET PUBLISHING GROUP, GB, vol. 355, no. 9209, 25 March 2000 (2000-03-25), pages 1041-1047, XP004814762, ISSN: 0140-6736, DOI: 10.1016/S0140-6736(00)02034-1

D5 HARE JENNIFER I ET AL: "Treatment of colorectal cancer using a combination of liposomal irinotecan (Irinophore C(TM)) and 5-fluorouracil", PLOS ONE 2013, vol. 8, no. 4, 2013, page e62349, XP002763356, ISSN: 1932-6203

D1 reports that liposomal irinotecan has an enhanced therapeutic activity compared to irinotecan.

D2 teaches that the PARP inhibitor niraparib potentiates the effect of irinotecan on colorectal cancer cells.

D3 shows significant synergy between irinotecan and the PARP inhibitor ABT-888 (= veliparib) and suggests an increase in the therapeutic index with the said combination in the treatment of patients with metastatic colon cancer.

D4 shows that the addition of irinotecan to weekly or 2-weekly regimens of fluorouracil and calcium folinate brings clear clinical benefit over the use of fluorouracil and calcium folinate alone in the treatment of metastatic colorectal cancer.

D5 discloses the use of a combination of liposomal irinotecan and 5-fluorouracil in the treatment of colorectal cancer.

2 Novelty

Liposomal irinotecan in combination with a PARP inhibitor has not been disclosed in the available prior art. Novelty (Article 33(2) PCT) is therefore acknowledged for the claims.

3 Inventive Step

3.1 The underlying problem was the provision of a composition for treating a solid tumour.

3.2 The claimed solution is a combination of liposomal irinotecan and a PARP inhibitor according to the schedule specified in the claims.

3.3 The claimed solution appears to have been rendered obvious by the prior art: It is known from **D1** that liposomal irinotecan has a greater therapeutic activity than irinotecan and from **D2** or **D3** that irinotecan synergises with the PARP inhibitors niraparib and veliparib. The anti-cancer activity of a combination of liposomal irinotecan with a PARP inhibitor was therefore to be expected in the light of the prior art. In the absence of an unexpected effect shown for the claimed subject-matter, inventive step (Article 33(3) PCT) cannot be acknowledged.

4 Industrial Applicability

The claimed subject-matter is industrially applicable (Article 33(4) PCT) in medicine/ pharmacy. The wording of the claims might be found objectionable.

PATENT COOPERATION TREATY

PCT

INTERNATIONAL SEARCH REPORT

(PCT Article 18 and Rules 43 and 44)

Applicant's or agent's file reference	**FOR FURTHER ACTION**	see Form PCT/ISA/220 as well as, where applicable, item 5 below.
239669-401612		
International application No.	International filing date *(day/month/year)*	(Earliest) Priority Date *(day/month/year)*
PCT/US2016/047814	19 August 2016 (19-08-2016)	20 August 2015 (20-08-2015)
Applicant		
MERRIMACK PHARMACEUTICALS, INC.		

This international search report has been prepared by this International Searching Authority and is transmitted to the applicant according to Article 18. A copy is being transmitted to the International Bureau.

This international search report consists of a total of 3 sheets.

[X] It is also accompanied by a copy of each prior art document cited in this report.

1. **Basis of the report**
   a. With regard to the **language,** the international search was carried out on the basis of:
      [X] the international application in the language in which it was filed
      [ ] a translation of the international application into _____, which is the language of a translation furnished for the purposes of international search (Rules 12.3(a) and 23.1(b))
   b. [ ] This international search report has been established taking into account the **rectification of an obvious mistake** authorized by or notified to this Authority under Rule 91 (Rule 43.6*bis*(a)).
   c. [ ] With regard to any **nucleotide and/or amino acid sequence** disclosed in the international application, see Box No. I.

2. [ ] **Certain claims were found unsearchable** (See Box No. II)

3. [ ] **Unity of invention is lacking** (see Box No III)

4. With regard to the **title,**
   [ ] the text is approved as submitted by the applicant
   [X] the text has been established by this Authority to read as follows:

   COMBINATION THERAPY USING LIPOSOMAL IRINOTECAN AND A PARP INHIBITOR FOR CANCER TREATMENT

5. With regard to the **abstract,**
   [X] the text is approved as submitted by the applicant
   [ ] the text has been established, according to Rule 38.2, by this Authority as it appears in Box No. IV. The applicant may, within one month from the date of mailing of this international search report, submit comments to this Authority

6. With regard to the **drawings,**
   a. the figure of the **drawings** to be published with the abstract is Figure No. _____
      [ ] as suggested by the applicant
      [ ] as selected by this Authority, because the applicant failed to suggest a figure
      [ ] as selected by this Authority, because this figure better characterizes the invention
   b. [X] none of the figures is to be published with the abstract

INTERNATIONAL SEARCH REPORT

International application No
PCT/US2016/047814

A. CLASSIFICATION OF SUBJECT MATTER
INV. A61K31/04 A61K31/166 A61K31/416 A61K31/4184 A61K31/436
A61K31/4745 A61K31/475 A61K31/502 A61K31/55 A61K9/127
A61K47/06 A61P35/00

According to International Patent Classification (IPC) or to both national classification and IPC

B. FIELDS SEARCHED

Minimum documentation searched (classification system followed by classification symbols)
A61K

Documentation searched other than minimum documentation to the extent that such documents are included in the fields searched

Electronic data base consulted during the international search (name of data base and, where practicable, search terms used)
EPO-Internal

C. DOCUMENTS CONSIDERED TO BE RELEVANT

Category*	Citation of document, with indication, where appropriate, of the relevant passages	Relevant to claim No.
Y	MESSERER CORRIE LYNN ET AL: "Liposomal irinotecan: formulation development and therapeutic assessment in murine xenograft models of colorectal cancer", CLINICAL CANCER RESEARCH : AN OFFICIAL JOURNAL OF THE AMERICAN ASSOCIATION FOR CANCER RESEARCH, vol. 10, no. 19, 1 October 2004 (2004-10-01), pages 6638-6649, XP002763354, ISSN: 1078-0432 the whole document ----- -/--	1-20

[X] Further documents are listed in the continuation of Box C. [ ] See patent family annex.

* Special categories of cited documents :

"A" document defining the general state of the art which is not considered to be of particular relevance

"E" earlier application or patent but published on or after the international filing date

"L" document which may throw doubts on priority claim(s) or which is cited to establish the publication date of another citation or other special reason (as specified)

"O" document referring to an oral disclosure, use, exhibition or other means

"P" document published prior to the international filing date but later than the priority date claimed

"T" later document published after the international filing date or priority date and not in conflict with the application but cited to understand the principle or theory underlying the invention

"X" document of particular relevance; the claimed invention cannot be considered novel or cannot be considered to involve an inventive step when the document is taken alone

"Y" document of particular relevance; the claimed invention cannot be considered to involve an inventive step when the document is combined with one or more other such documents, such combination being obvious to a person skilled in the art

"&" document member of the same patent family

Date of the actual completion of the international search	Date of mailing of the international search report
27 October 2016	17/11/2016

Name and mailing address of the ISA/	Authorized officer
European Patent Office, P.B. 5818 Patentlaan 2 NL - 2280 HV Rijswijk Tel. (+31-70) 340-2040, Fax: (+31-70) 340-3016	Engl, Brigitte

2

Form PCT/ISA/210 (second sheet) (April 2005)

C(Continuation). DOCUMENTS CONSIDERED TO BE RELEVANT

Category*	Citation of document, with indication, where appropriate, of the relevant passages	Relevant to claim No.
Y	SYBIL M GENTHER WILLIAMS ET AL: "Treatment with the PARP inhibitor, niraparib, sensitizes colorectal cancer cell lines to irinotecan regardless of MSI/MSS status", CANCER CELL INTERNATIONAL, vol. 15, no. 1, 4 February 2015 (2015-02-04), page 14, XP021213062, BIOMED CENTRAL, LONDON, GB ISSN: 1475-2867, DOI: 10.1186/S12935-015-0162-8 the whole document	1-20
Y	DAVIDSON DAVID ET AL: "The PARP inhibitor ABT-888 synergizes irinotecan treatment of colon cancer cell lines", INVESTIGATIONAL NEW DRUGS, vol. 31, no. 2, April 2013 (2013-04), pages 461-468, XP002763355, ISSN: 1573-0646 the whole document	1-20
Y	DOUILLARD J ET AL: "Irinotecan combined with fluorouracil compared with fluorouracil alone as first-line treatment for metastatic colorectal cancer: a multicentre randomised trial", THE LANCET, vol. 355, no. 9209, 25 March 2000 (2000-03-25), pages 1041-1047, XP004814762, THE LANCET PUBLISHING GROUP, GB ISSN: 0140-6736, DOI: 10.1016/S0140-6736(00)02034-1 the whole document	1-20
Y	HARE JENNIFER I ET AL: "Treatment of colorectal cancer using a combination of liposomal irinotecan (Irinophore C(TM)) and 5-fluorouracil", PLOS ONE, vol. 8, no. 4, E623491, 23 April 2013 (2013-04-23), pages 1-12, XP002763356, ISSN: 1932-6203, DOI: 10.1371/journal.pone.0062349 the whole document	1-20

PATENT COOPERATION TREATY

PCT

INTERNATIONAL PRELIMINARY REPORT ON PATENTABILITY
(Chapter I of the Patent Cooperation Treaty)

(PCT Rule 44*bis*)

Applicant's or agent's file reference 239669-395864	**FOR FURTHER ACTION**	See item 4 below
International application No. PCT/US2016/047827	International filing date *(day/month/year)* 19 August 2016 (19.08.2016)	Priority date *(day/month/year)* 20 August 2015 (20.08.2015)
International Patent Classification (8th edition unless older edition indicated) See relevant information in Form PCT/ISA/237		
Applicant IPSEN BIOPHARM LTD.		

1. This international preliminary report on patentability (Chapter I) is issued by the International Bureau on behalf of the International Searching Authority under Rule 44 *bis*.1(a).

2. This REPORT consists of a total of 6 sheets, including this cover sheet.

   In the attached sheets, any reference to the written opinion of the International Searching Authority should be read as a reference to the international preliminary report on patentability (Chapter I) instead.

3. This report contains indications relating to the following items:

☒	Box No. I	Basis of the report
☐	Box No. II	Priority
☐	Box No. III	Non-establishment of opinion with regard to novelty, inventive step and industrial applicability
☐	Box No. IV	Lack of unity of invention
☒	Box No. V	Reasoned statement under Article 35(2) with regard to novelty, inventive step or industrial applicability; citations and explanations supporting such statement
☐	Box No. VI	Certain documents cited
☐	Box No. VII	Certain defects in the international application
☐	Box No. VIII	Certain observations on the international application

4. The International Bureau will communicate this report to designated Offices in accordance with Rules 44*bis*.3(c) and 93*bis*.1 but not, except where the applicant makes an express request under Article 23(2), before the expiration of 30 months from the priority date (Rule 44*bis* .2).

	Date of issuance of this report 20 February 2018 (20.02.2018)
The International Bureau of WIPO 34, chemin des Colombettes 1211 Geneva 20, Switzerland Facsimile No. +41 22 338 82 70	Authorized officer Agnès Wittmann-Regis e-mail: pct.team6@wipo.int

Form PCT/IB/373 (January 2004)

PATENT COOPERATION TREATY

From the
INTERNATIONAL SEARCHING AUTHORITY

To:

see form PCT/ISA/220

PCT

WRITTEN OPINION OF THE INTERNATIONAL SEARCHING AUTHORITY

(PCT Rule 43*bis*.1)

Date of mailing
(day/month/year) see form PCT/ISA/210 (second sheet)

Applicant's or agent's file reference
see form PCT/ISA/220

FOR FURTHER ACTION
See paragraph 2 below

International application No.	International filing date *(day/month/year)*	Priority date *(day/month/year)*
PCT/US2016/047827	19.08.2016	20.08.2015

International Patent Classification (IPC) or both national classification and IPC
INV. A61K31/04 A61K31/166 A61K31/416 A61K31/4184 A61K31/436 A61K31/4745 A61K31/475 A61K31/502 A61K31/55 A61K9/127 A61K47/06 A61P35/00

Applicant
MERRIMACK PHARMACEUTICALS, INC.

1. This opinion contains indications relating to the following items:

- ☒ Box No. I Basis of the opinion
- ☐ Box No. II Priority
- ☐ Box No. III Non-establishment of opinion with regard to novelty, inventive step and industrial applicability
- ☐ Box No. IV Lack of unity of invention
- ☒ Box No. V Reasoned statement under Rule 43*bis*.1(a)(i) with regard to novelty, inventive step and industrial applicability; citations and explanations supporting such statement
- ☐ Box No. VI Certain documents cited
- ☐ Box No. VII Certain defects in the international application
- ☐ Box No. VIII Certain observations on the international application

2. **FURTHER ACTION**

If a demand for international preliminary examination is made, this opinion will usually be considered to be a written opinion of the International Preliminary Examining Authority ("IPEA") except that this does not apply where the applicant chooses an Authority other than this one to be the IPEA and the chosen IPEA has notifed the International Bureau under Rule 66.1*bis*(b) that written opinions of this International Searching Authority will not be so considered.

If this opinion is, as provided above, considered to be a written opinion of the IPEA, the applicant is invited to submit to the IPEA a written reply together, where appropriate, with amendments, before the expiration of 3 months from the date of mailing of Form PCT/ISA/220 or before the expiration of 22 months from the priority date, whichever expires later.

For further options, see Form PCT/ISA/220.

Name and mailing address of the ISA:	Date of completion of this opinion	Authorized Officer
European Patent Office D-80298 Munich Tel. +49 89 2399 - 0 Fax: +49 89 2399 - 4465	see form PCT/ISA/210	Engl, Brigitte Telephone No. +49 89 2399-0

Box No. I Basis of the opinion

1. With regard to the **language**, this opinion has been established on the basis of:

   ☒ the international application in the language in which it was filed.

   ☐ a translation of the international application into , which is the language of a translation furnished for the purposes of international search (Rules 12.3(a) and 23.1 (b)).

2. ☐ This opinion has been established taking into account the **rectification of an obvious mistake** authorized by or notified to this Authority under Rule 91 (Rule 43*bis*.1(a))

3. ☐ With regard to any **nucleotide and/or amino acid sequence** disclosed in the international application, this opinion has been established on the basis of a sequence listing:

   a. ☐ forming part of the international application as filed:

      ☐ in the form of an Annex C/ST.25 text file.

      ☐ on paper or in the form of an image file.

   b. ☐ furnished together with the international application under PCT Rule 13*ter*.1(a) for the purposes of international search only in the form of an Annex C/ST.25 text file.

   c. ☐ furnished subsequent to the international filing date for the purposes of international search only:

      ☐ in the form of an Annex C/ST.25 text file (Rule 13*ter*.1(a)).

      ☐ on paper or in the form of an image file (Rule 13*ter*.1(b) and Administrative Instructions, Section 713).

4. ☐ In addition, in the case that more than one version or copy of a sequence listing has been filed or furnished, the required statements that the information in the subsequent or additional copies is identical to that forming part of the application as filed or does not go beyond the application as filed, as appropriate, were furnished.

5. Additional comments:

Box No. V Reasoned statement under Rule 43*bis*.1(a)(i) with regard to novelty, inventive step or industrial applicability; citations and explanations supporting such statement

1. Statement

Novelty (N)	Yes:	Claims	1-20
	No:	Claims	
Inventive step (IS)	Yes:	Claims	
	No:	Claims	1-20
Industrial applicability (IA)	Yes:	Claims	1-20
	No:	Claims	

2. Citations and explanations

see separate sheet

Box V:

1 Prior Art

The following prior art is cited from the International Search Report:

D1 MESSERER CORRIE LYNN ET AL: "Liposomal irinotecan: formulation development and therapeutic assessment in murine xenograft models of colorectal cancer", CLINICAL CANCER RESEARCH : AN OFFICIAL JOURNAL OF THE AMERICAN ASSOCIATION FOR CANCER RESEARCH 1 OCT 2004, vol. 10, no. 19, 1 October 2004 (2004-10-01), pages 6638-6649, XP002763354, ISSN: 1078-0432

D2 SYBIL M GENTHER WILLIAMS ET AL: "Treatment with the PARP inhibitor, niraparib, sensitizes colorectal cancer cell lines to irinotecan regardless of MSI/MSS status", CANCER CELL INTERNATIONAL, BIOMED CENTRAL, LONDON, GB, vol. 15, no. 1, 4 February 2015 (2015-02-04), page 14, XP021213062, ISSN: 1475-2867, DOI: 10.1186/S12935-015-0162-8

D3 DAVIDSON DAVID ET AL: "The PARP inhibitor ABT-888 synergizes irinotecan treatment of colon cancer cell lines", INVESTIGATIONAL NEW DRUGS APR 2013, vol. 31, no. 2, April 2013 (2013-04), pages 461-468, XP002763355, ISSN: 1573-0646

D4 DOUILLARD J ET AL: "Irinotecan combined with fluorouracil compared with fluorouracil alone as first-line treatment for metastatic colorectal cancer: a multicentre randomised trial", THE LANCET, THE LANCET PUBLISHING GROUP, GB, vol. 355, no. 9209, 25 March 2000 (2000-03-25), pages 1041-1047, XP004814762, ISSN: 0140-6736, DOI: 10.1016/S0140-6736(00)02034-1

D5 HARE JENNIFER I ET AL: "Treatment of colorectal cancer using a combination of liposomal irinotecan (Irinophore C(TM)) and 5-fluorouracil", PLOS ONE 2013, vol. 8, no. 4, 2013, page e62349, XP002763356, ISSN: 1932-6203

D1 reports that liposomal irinotecan has an enhanced therapeutic activity compared to irinotecan.

D2 teaches that the PARP inhibitor niraparib potentiates the effect of irinotecan on colorectal cancer cells.

D3 shows significant synergy between irinotecan and the PARP inhibitor ABT-888 (= veliparib) and suggests an increase in the therapeutic index with the said combination in the treatment of patients with metastatic colon cancer.

D4 shows that the addition of irinotecan to weekly or 2-weekly regimens of fluorouracil and calcium folinate brings clear clinical benefit over the use of fluorouracil and calcium folinate alone in the treatment of metastatic colorectal cancer.

D5 discloses the use of a combination of liposomal irinotecan and 5-fluorouracil in the treatment of colorectal cancer.

2 Novelty

Liposomal irinotecan in combination with a PARP inhibitor has not been disclosed in the available prior art. Novelty (Article 33(2) PCT) is therefore acknowledged for the claims.

3 Inventive Step

3.1 The underlying problem was the provision of a composition for treating a solid tumour.

3.2 The claimed solution is a combination of liposomal irinotecan and a PARP inhibitor according to the schedule specified in the claims.

3.3 The claimed solution appears to have been rendered obvious by the prior art: It is known from **D1** that liposomal irinotecan has a greater therapeutic activity than irinotecan and from **D2** or **D3** that irinotecan synergises with the PARP inhibitors niraparib and veliparib. The anti-cancer activity of a combination of liposomal irinotecan with a PARP inhibitor was therefore to be expected in the light of the prior art. In the absence of an unexpected effect shown for the claimed subject-matter, inventive step (Article 33(3) PCT) cannot be acknowledged.

4 Industrial Applicability

The claimed subject-matter is industrially applicable (Article 33(4) PCT) in medicine/ pharmacy. The wording of the claims might be found objectionable.

PATENT COOPERATION TREATY

PCT

INTERNATIONAL SEARCH REPORT

(PCT Article 18 and Rules 43 and 44)

Applicant's or agent's file reference	**FOR FURTHER ACTION**	see Form PCT/ISA/220 as well as, where applicable, item 5 below.
239669-395864		
International application No.	International filing date *(day/month/year)*	(Earliest) Priority Date *(day/month/year)*
PCT/US2016/047827	19 August 2016 (19-08-2016)	20 August 2015 (20-08-2015)
Applicant		
MERRIMACK PHARMACEUTICALS, INC.		

This international search report has been prepared by this International Searching Authority and is transmitted to the applicant according to Article 18. A copy is being transmitted to the International Bureau.

This international search report consists of a total of 3 sheets.

[X] It is also accompanied by a copy of each prior art document cited in this report.

1. **Basis of the report**
   a. With regard to the **language,** the international search was carried out on the basis of:
      [X] the international application in the language in which it was filed
      [ ] a translation of the international application into _____, which is the language of a translation furnished for the purposes of international search (Rules 12.3(a) and 23.1(b))
   b. [ ] This international search report has been established taking into account the **rectification of an obvious mistake** authorized by or notified to this Authority under Rule 91 (Rule 43.6*bis*(a)).
   c. [ ] With regard to any **nucleotide and/or amino acid sequence** disclosed in the international application, see Box No. I.

2. [ ] **Certain claims were found unsearchable** (See Box No. II)

3. [ ] **Unity of invention is lacking** (see Box No III)

4. With regard to the **title,**
   [X] the text is approved as submitted by the applicant
   [ ] the text has been established by this Authority to read as follows:

5. With regard to the **abstract,**
   [X] the text is approved as submitted by the applicant
   [ ] the text has been established, according to Rule 38.2, by this Authority as it appears in Box No. IV. The applicant may, within one month from the date of mailing of this international search report, submit comments to this Authority

6. With regard to the **drawings,**
   a. the figure of the **drawings** to be published with the abstract is Figure No. _____
      [ ] as suggested by the applicant
      [ ] as selected by this Authority, because the applicant failed to suggest a figure
      [ ] as selected by this Authority, because this figure better characterizes the invention
   b. [X] none of the figures is to be published with the abstract

INTERNATIONAL SEARCH REPORT

International application No
PCT/US2016/047827

A. CLASSIFICATION OF SUBJECT MATTER
INV. A61K31/04 A61K31/166 A61K31/416 A61K31/4184 A61K31/436
A61K31/4745 A61K31/475 A61K31/502 A61K31/55 A61K9/127
A61K47/06 A61P35/00

According to International Patent Classification (IPC) or to both national classification and IPC

B. FIELDS SEARCHED

Minimum documentation searched (classification system followed by classification symbols)
A61K

Documentation searched other than minimum documentation to the extent that such documents are included in the fields searched

Electronic data base consulted during the international search (name of data base and, where practicable, search terms used)
EPO-Internal

C. DOCUMENTS CONSIDERED TO BE RELEVANT

Category*	Citation of document, with indication, where appropriate, of the relevant passages	Relevant to claim No.
Y	MESSERER CORRIE LYNN ET AL: "Liposomal irinotecan: formulation development and therapeutic assessment in murine xenograft models of colorectal cancer", CLINICAL CANCER RESEARCH : AN OFFICIAL JOURNAL OF THE AMERICAN ASSOCIATION FOR CANCER RESEARCH, vol. 10, no. 19, 1 October 2004 (2004-10-01), pages 6638-6649, XP002763354, ISSN: 1078-0432 the whole document ----- -/--	1-20

[X] Further documents are listed in the continuation of Box C. [ ] See patent family annex.

* Special categories of cited documents :

"A" document defining the general state of the art which is not considered to be of particular relevance

"E" earlier application or patent but published on or after the international filing date

"L" document which may throw doubts on priority claim(s) or which is cited to establish the publication date of another citation or other special reason (as specified)

"O" document referring to an oral disclosure, use, exhibition or other means

"P" document published prior to the international filing date but later than the priority date claimed

"T" later document published after the international filing date or priority date and not in conflict with the application but cited to understand the principle or theory underlying the invention

"X" document of particular relevance; the claimed invention cannot be considered novel or cannot be considered to involve an inventive step when the document is taken alone

"Y" document of particular relevance; the claimed invention cannot be considered to involve an inventive step when the document is combined with one or more other such documents, such combination being obvious to a person skilled in the art

"&" document member of the same patent family

Date of the actual completion of the international search	Date of mailing of the international search report
25 October 2016	17/11/2016

Name and mailing address of the ISA/	Authorized officer
European Patent Office, P.B. 5818 Patentlaan 2 NL - 2280 HV Rijswijk Tel. (+31-70) 340-2040, Fax: (+31-70) 340-3016	Engl, Brigitte

2

Form PCT/ISA/210 (second sheet) (April 2005)

C(Continuation). DOCUMENTS CONSIDERED TO BE RELEVANT

Category*	Citation of document, with indication, where appropriate, of the relevant passages	Relevant to claim No.
Y	SYBIL M GENTHER WILLIAMS ET AL: "Treatment with the PARP inhibitor, niraparib, sensitizes colorectal cancer cell lines to irinotecan regardless of MSI/MSS status", CANCER CELL INTERNATIONAL, vol. 15, no. 1, 14, 4 February 2015 (2015-02-04), pages 1-11, XP021213062, BIOMED CENTRAL, LONDON, GB ISSN: 1475-2867, DOI: 10.1186/S12935-015-0162-8 the whole document	1-20
Y	DAVIDSON DAVID ET AL: "The PARP inhibitor ABT-888 synergizes irinotecan treatment of colon cancer cell lines", INVESTIGATIONAL NEW DRUGS, vol. 31, no. 2, April 2013 (2013-04), pages 461-468, XP002763355, ISSN: 1573-0646 the whole document	1-20
Y	DOUILLARD J ET AL: "Irinotecan combined with fluorouracil compared with fluorouracil alone as first-line treatment for metastatic colorectal cancer: a multicentre randomised trial", THE LANCET, vol. 355, no. 9209, 25 March 2000 (2000-03-25), pages 1041-1047, XP004814762, THE LANCET PUBLISHING GROUP, GB ISSN: 0140-6736, DOI: 10.1016/S0140-6736(00)02034-1 the whole document	1-20
Y	HARE JENNIFER I ET AL: "Treatment of colorectal cancer using a combination of liposomal irinotecan (Irinophore C(TM)) and 5-fluorouracil", PLOS ONE, vol. 8, no. 4, E62349, 23 April 2013 (2013-04-23), pages 1-12, XP002763356, ISSN: 1932-6203, DOI: 10.1371/journal.pone.0062349 the whole document	1-20

Background Document on the UGT1A1 Polymorphisms and Irinotecan Toxicity: ACPS November 3, 2004 Advisory Committee Meeting

AVAILABLE FOR PUBLIC DISCLOSURE WITHOUT REDACTION

October 4, 2004

Table of Contents

Background Document on the UGT1A1 Polymorphisms and Irinotecan Toxicity: ACPS November 3, 2004 Advisory Committee Meeting

1. Introduction

Pfizer is strongly committed to fully investigate and understand the potential value of genotyping in improving the safety and efficacy of irinotecan.

Several recent publications suggest an association between the UGT1A1 7/7 genotype and irinotecan toxicities. This background document is a review of the published literature examining the clinical impact of UGT1A1 polymorphisms. Clinical studies currently underway that contain a pharmacogenomics component examining UGT1A1 and other factors involved in the metabolism, distribution, and transport of irinotecan and its active metabolite, SN-38, are summarized. In the near future, as studies better define the population at risk and diagnostic tests become readily available, healthcare providers and patients can be provided important information that will allow for better benefit/risk evaluation in the use of irinotecan as a chemotherapeutic agent.

2. Summary

The disposition of irinotecan is quite complex and involves numerous metabolic enzymes and transport proteins. SN-38, the active metabolite of irinotecan, is principally eliminated via UGT1A1-mediated metabolism to SN-38G, a biologically inactive glucuronide conjugate, which is then cleared via biliary excretion.

The natural function of UGT1A1 is the catalysis of bilirubin glucuronidation. A genetic polymorphism in the UGT1A1 promoter (UGT1A1*28) results in enzyme underexpression, causing an impairment of bilirubin metabolism (reduced glucuronidation), clinically recognized as Gilbert's syndrome (UGT1A1 7/7 genotype). Case reports describing severe neutropenia in Gilbert's patients receiving standard starting doses of irinotecan suggested a link between this UGT1A1 polymorphism and irinotecan toxicity. The current Camptosar label indicates that patients with abnormal glucoronidation of bilirubin, such as those with Gilbert's syndrome, may also be at greater risk of myelosuppression when receiving therapy with Camptosar (PRECAUTIONS: *Patients at Particular Risk*).

Results from several recently published trials suggest that patients who are homozygous for the UGT1A1*28 allele (known as the "7/7" genotype) are at greater risk for irinotecan-induced severe diarrhea or neutropenia. A trend for lower ratios of [SN-38G plasma AUC/SN-38 plasma AUC] has been observed in patients who are homozygous for UGT1A1*28. These findings are consistent with the hypothesis of reduced SN-38 to SN-38G metabolism in patients with this UGT1A1 polymorphism.

Although these results are intriguing, it is important to note that the individual trials were small (sample sizes ranging from 20-118), with only 3 to 20% of the patients having the 7/7 genotype. The studies utilized a variety of irinotecan dosing schedules and combination regimens that are known to have an impact on the degree and severity of diarrhea and/or neutropenia. The small sample sizes and trial design issues make estimation of the risk to 7/7 genotype patients difficult. For example, some trials found a significant association between UGT1A1 genotype and neutropenia but not for diarrhea. Other trials reported a genotype association with diarrhea but found no association with neutropenia. In all studies, a substantial proportion of 7/7 patients did not experience severe toxicity. Thus the precise, quantitative implications of UGT1A1 genotype on the safety, efficacy, and development of individualized patient dosing of irinotecan are not yet clear.

Based on the pharmacology of irinotecan, it might be expected that pre-treatment serum bilirubin concentrations could guide irinotecan starting doses. In fact, reduced, safe starting doses have been defined for hepatically compromised patients based on bilirubin and/or AST/ALT values exceeding institutional upper normal limit (hepatic dysfunction label supplement submitted June 25, 2004). However, in patients with serum bilirubin values within the normal range, the association between baseline bilirubin and toxicity, while statistically significant, is not strong enough to guide starting-dose selection.

Reports from the initial irinotecan pharmacogenomic trials prompted the pharmacogenomic component of NCCTG's N9741, phase III, metastatic colorectal cancer study of several irinotecan- and oxaliplatin-based regimens. Pharmacogenomic and clinical data from N9741 are currently being analyzed collaboratively with investigators and Pfizer clinicians and scientists. In addition, Pfizer is conducting pharmacogenomic correlative studies in a companion study to its sponsored, phase III, metastatic colorectal cancer trial (known as the BICC-C trial) as well as several other company-sponsored and large cooperative-group trials. These trials will look for associations between toxicity, efficacy, and genotype. These activities underscore Pfizer's strong commitment to fully investigate and understand the potential value of genotyping in improving the safety and efficacy of irinotecan.

3. Clinical and Regulatory Overview

Irinotecan hydrochloride injection (CPT-11, CAMPTOSAR® Injection) is an antineoplastic topoisomerase-I inhibitor with broad activity in colorectal cancer and other tumors. Irinotecan was originally developed in Japan by the Yakult Honsha Company. Licensing rights for clinical development in the US were granted to Pharmacia, whereas similar rights in Europe were granted to Aventis.

Irinotecan was first approved in the US for the treatment of metastatic colorectal cancer after failure of first-line treatment with 5-FU. This initial approval was based on tumor response rate data from phase II, uncontrolled studies. Conditional marketing authorization in the US was granted in 1996 under FDA regulations designed to accelerate approval of new and promising drugs for serious or life-threatening illnesses.

Subsequently, Aventis completed two European randomized, phase III studies comparing second-line irinotecan therapy with best supportive care or with infusional 5-FU-based therapy and provided the data from these trials to Pharmacia. The survival advantages associated with irinotecan use in each of these trials were the basis for full FDA approval for irinotecan as second-line therapy for patients with metastatic colorectal cancer in September 1998.

In the first-line therapy of colorectal cancer, two phase III, randomized, controlled, multicenter, multinational, clinical trials were conducted to evaluate whether the combination of irinotecan with 5-FU/LV would improve tumor control and survival relative to standard 5-FU/LV alone in patients with previously untreated metastatic colorectal cancer. The results of these trials were the basis for approval of irinotecan in combination with 5-FU/LV as first-line therapy of metastatic colorectal cancer in April 2000.

4. Human Safety Overview

Virtually all studies of irinotecan have reported neutropenia and/or delayed diarrhea (diarrhea generally occurring more than 8 hours after irinotecan administration) as the dose-limiting toxicities. The frequency of neutropenic fever has been low (usually 3-8%). Clinically significant thrombocytopenia or severe anemia is uncommon. Occurrences of ileus and/or colitis (sometimes with gastrointestinal bleeding) have been observed, but have been rare.

Patients may have transient cholinergic symptoms of rhinitis, increased salvation, miosis, lacrimation, diaphoresis, flushing, and intestinal hyperperistalsis that can cause abdominal cramping and diarrhea (early diarrhea). If they occur, cholinergic symptoms manifest during or shortly after drug infusion and are most commonly mild or moderate in severity.

Other adverse events have included nausea/vomiting, anorexia, delayed abdominal cramping, alopecia, and asthenia. Elevations in serum creatinine have sometimes occurred in association with dehydration as a consequence of diarrhea or severe vomiting, or due to occasional tumor lysis syndrome. Elevations in hepatic enzymes have been noted, but almost all of these patients have had progressive liver involvement with tumor and a relationship to irinotecan has not clearly been established.

Based on this toxicity profile, recommendations for supportive care include immediate initiation of loperamide therapy for delayed diarrhea, IV or subcutaneous atropine as prophylaxis or therapy of cholinergic symptoms, and antiemetics for prevention of nausea and vomiting. Consistent with American Society of Clinical Oncology guidelines, routine prophylactic use of a colony-stimulating factor is not advised, given the low rate of neutropenic fever generally associated with irinotecan use.

Subsequent to the NDA filing for irinotecan as a single agent, further analysis of baseline variables that might predict neutropenia was performed. Univariate and multiple regression analyses showed that in addition to prior pelvic/abdominal irradiation, mild elevations in bilirubin above the normal range can result in variable but significant increases in the likelihood of grade 3+ neutropenia during the first cycle of treatment. This led to filing a label revision stating, in PRECAUTIONS: *Patients at Particular Risk*, the following text:

"In clinical trials of the weekly dosage schedule, it has been noted that patients with modestly elevated baseline serum total bilirubin levels (1.0 to 2.0 mg/dL) have had a significantly greater likelihood of experiencing first-course grade 3 or 4 neutropenia than those with bilirubin levels that were less than 1.0 mg/dL (50.0% [19/38] versus 17.7% [47/226]; p<0.001). Patients with abnormal glucuronidation of bilirubin, such as those with Gilbert's syndrome, may also be at greater risk of myelosuppression when receiving therapy with CAMPTOSAR. An association between baseline bilirubin elevations and an increased risk of late diarrhea has not been observed in studies of the weekly dosage schedule."

The predictive value of baseline serum bilirubin levels up to 1.5 mg/dl for chemotherapy-induced toxicity or efficacy in patients receiving single-agent irinotecan for metastatic colorectal cancer was recently evaluated [Meyerhardt 2004]. The median follow-up of 287 patients was 15.8 months. It was concluded that "*baseline serum bilirubin levels does not reliably predict overall irinotecan-related toxicity or efficacy.*"

5. Irinotecan Pharmacokinetic/Pharmacodynamic and Pharmacogenomic Overview

The complex disposition pathways and plasma pharmacokinetics (PK) of irinotecan have been well-characterized [Slatter 2000; reviewed in Mathijssen 2001]. In aqueous environments, camptothecin and its derivatives exist as two interconvertible species: a biologically active, lactone form in a pH-dependent equilibrium with a biologically inactive, carboxylate (or hydroxyacid anion) form. Lower pH promotes the formation of the lactone while higher pH favors the carboxylate. In the case of SN-38 circulating in the bloodstream, this equilibrium is also affected by preferential binding of SN-38 lactone to serum albumin. While only the lactone form of camptothecin and its derivatives is cytotoxic, "total" (lactone + carboxylate) concentrations showed a strong correlation within individual patients between the AUC values for lactone and total species [e.g., Rivory 1994]. Thus, PK parameters computed from analysis of total (lactone + carboxylate) concentrations accurately reflect the PK of the bioactive lactone species.

Key features of irinotecan metabolism include carboxylesterase cleavage of the water-solubilizing dipiperidino moiety to yield the potent topoisomerase-I inhibitor SN-38 and CYP3A4-mediated oxidation of irinotecan to the biologically inactive APC metabolite. SN-38 is excreted in bile but its principal elimination route appears to be via glucuronidation carried out by UDP-glucuronosyltransferases, principally UGT1A1 and UGT1A7 [Tukey 2002]. SN-38 also may be formed within the gastrointestinal lumen via β-glucuronidase-mediated hydrolysis of SN-38G excreted in bile. In cancer patients with relatively normal organ function, irinotecan and metabolite PK parameters exhibit marked interpatient variability but fall within reproducible ranges and, in most trials, appear to be dose-proportional [Rowinsky 1994; de Forni 1994]. Relative SN-38 exposure is greater in patients with hepatic dysfunction, correlating with a lower MTD in such patients [Raymond 2002].

Based on the pharmacology of irinotecan, it might be expected that pre-treatment serum bilirubin concentrations could guide irinotecan starting doses. In fact, reduced, safe starting doses have been defined for hepatically compromised patients based on bilirubin and/or AST/ALT values exceeding institutional upper normal limit (proposed label revision has been submitted to the agency). However, in patients with serum bilirubin values within the normal range, the association between baseline bilirubin and toxicity, while statistically significant, is not strong enough to guide starting dose selection.

With regard to PK/pharmacodynamic relationships, weak yet statistically significant associations have been found between PK parameters and toxicities (neutropenia and diarrhea) in patients with uncompromised organ function. For example, in a pivotal phase II trial supporting registration of single-agent irinotecan in 2nd-line colorectal cancer [Study M/6475/0006], the variability in the severity of neutropenia or diarrhea was poorly associated with SN-38 exposure (Figues 1-3 and Table 1). Several published studies, which analyzed the association between PK parameters and neutropenia, or diarrhea reached conflicting conclusions [Mathijssen 2001]. Promising initial results suggested that a "biliary index" computed from the plasma AUCs of irinotecan, SN-38, and SN-38G might be predictive of severe diarrhea [Gupta 1994] but this finding has not been confirmed in several subsequent trials [Mathijssen 2001]. These results may be indicative of a poor correlation between plasma irinotecan and SN-38 levels and those at the relevant sites of action for efficacy and toxicity (bone marrow, gastrointestinal epithelium, tumors). This theoretical disconnect in plasma and local CPT-11, SN-38, and SN-38G concentrations could be due to variable expression of the enzyme systems responsible for irinotecan activation (carboxylesterases) and those that facilitate SN-38 detoxification/elimination (i.e., UGT1A and the ABC transporter family) [Mathijssen 2001]. There is currently an incomplete understanding of the complex relationships between the PK of the various systems that control irinotecan and metabolite disposition and the probability of toxicity in an individual patient. Thus, the use of traditional dose modification approaches based on the achievement of target plasma exposures of irinotecan or its metabolites is not likely to succeed as an approach to optimize dosing.

Results obtained in several recently conducted trials (sample sizes ranging from 20-118) suggest that genetic factors may contribute to interpatient variability in irinotecan disposition and toxicity. In particular, the homozygous "7/7" promoter genotype causing UGT1A1 underexpression has been associated with an increased severity of irinotecan-induced diarrhea or leucopenia/neutropenia and decreased conversion of SN-38 to SN-38G [Ando 2000; Iyer 2002; Innocenti 2004; Mathijssen 2003; Sai 2004]. It is interesting to note that the association between the adverse event severity (neutropenia and diarrhea) and genotype appears to be stronger than between systemic exposure (CPT-11, SN-38, and SN-38G) and genotype. These findings may be consequences of the complex factors, discussed above, that potentially affect the disposition of these compounds.

There is considerable interest in further exploring the proposed associations between irinotecan-induced toxicities and polymorphisms in genes that affect target tissue exposures to irinotecan and SN-38 in clinical trials that are larger than those conducted to date. In addition to UGT1A1, other genes of interest

include UGT1A7 as well as several members of the ABC transport protein family that are reported to play key roles in cellular efflux of irinotecan [e.g., BCRP; Zamber 2003]. The findings from such studies may lead to a better understanding of factors that predict toxicity and efficacy and may ultimately play some role in the development of genotype-based dosing recommendations.

Figure 1. Scatter plots of Cycle-1 diarrhea severity vs Cycle-1, Day-1 irinotecan $AUC_{0\text{-}24}$ (upper) and SN-38 $AUC_{0\text{-}24}$ (lower) in Study M/6475/0006

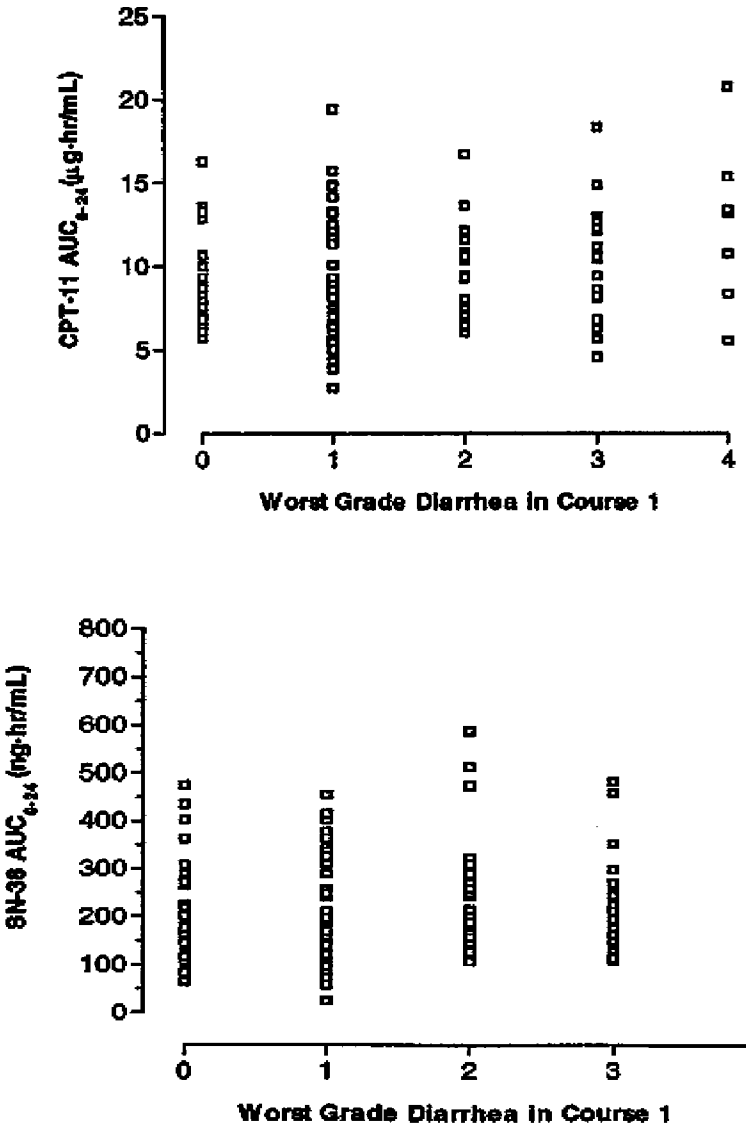

Figure 2. Scatter plots of Cycle-1 neutropenia severity vs Cycle-1, Day-1 irinotecan AUC_{0-24} (upper) and SN-38 AUC_{0-24} (lower) in Study M/6475/0006

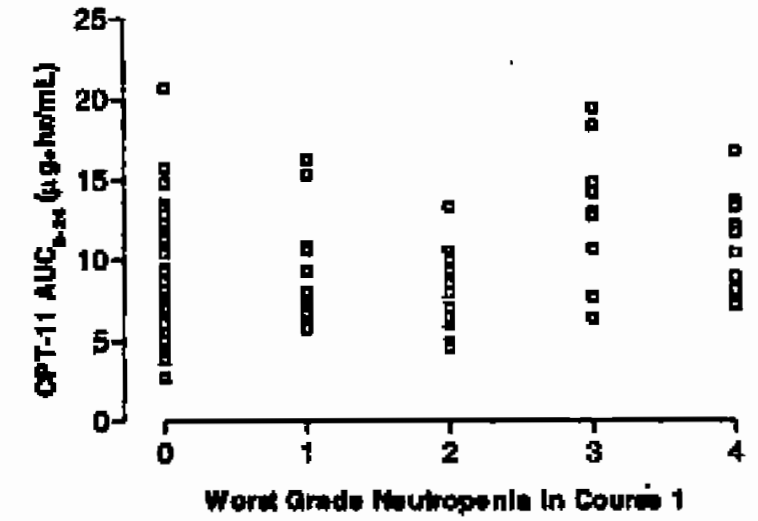

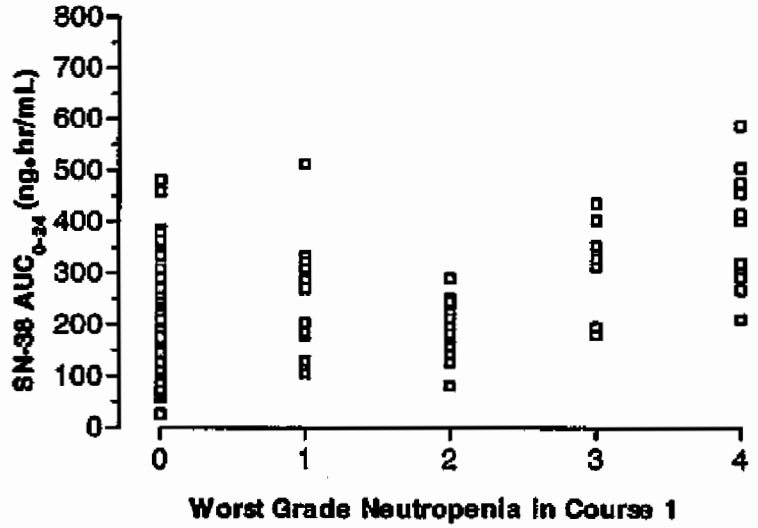

Table 1. Relationships between irinotecan and SN-38 PK parameters and diarrhea or neutropenia in Study M/6475/0006

PK Parameter	Late Diarrhea		Neutropenia	
	r[a]	p value[b]	r[a]	p value[b]
Irinotecan C_{max}, µg/mL	0.09	0.2501	0.12	0.1436
Irinotecan AUC_{0-24}, µg·h/mL	0.21	0.0086	0.26	0.0013
SN-38 C_{max}, ng/mL	0.13	0.1069	0.38	0.0001
SN-38 AUC_{0-24}, ng·h/mL	0.14	0.0799	0.43	0.0001

[a] Spearman correlation coeffecient.
[b] Spearman rank order correlation test.

Figure 3. Relationship between Cycle-1, Day-1 irinotecan (upper) and SN-38 (lower) AUC_{0-24} and % ANC decrease in Study M/6475/0006. Dashed lines represent the fit to an E_{max} model

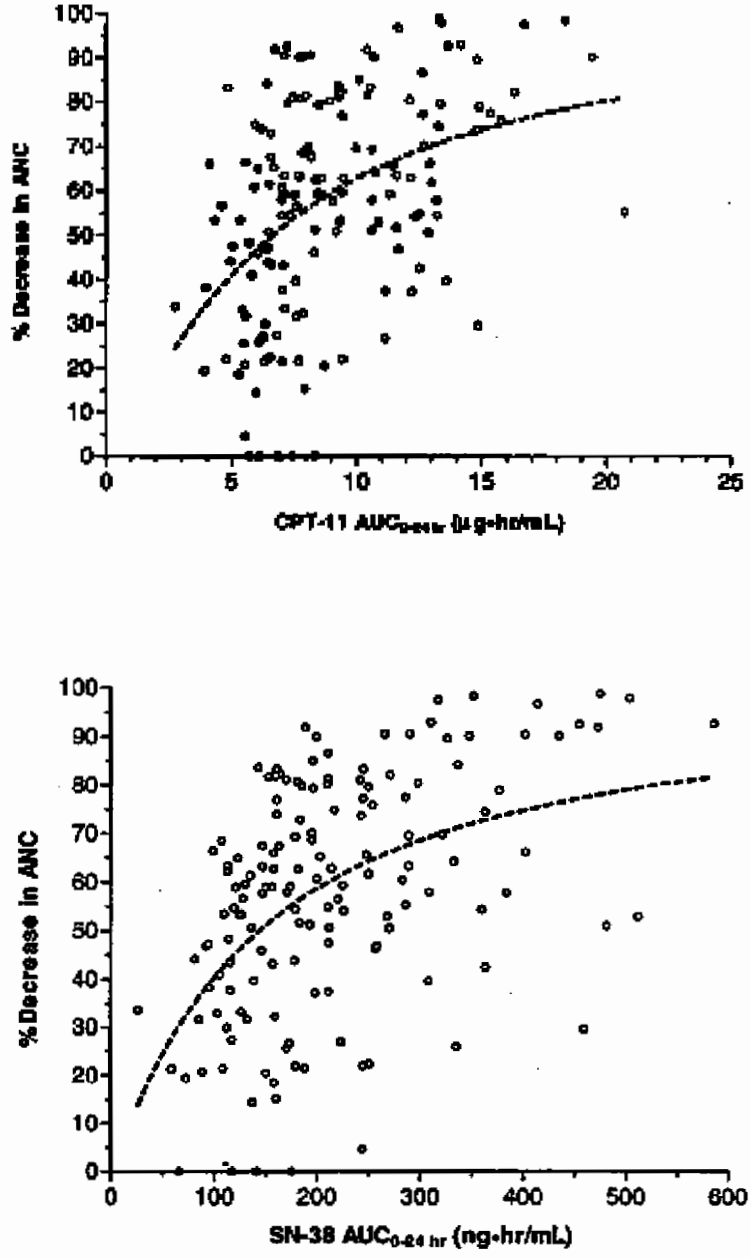

6. The UGT1 Gene and UGT1A1 Isoform

The UGT1 gene is located on chromosome 2 and contains at least 13 different promoters/first exons which are spliced to common exons 2 thorough 5, resulting in separate isoforms with unique N-termini and conserved C-terminal domains [Ritter 1992; Gong 2001]. In terms of nucleotide sequence, exons 1 for UGT1A1 and UGT1A6 are unique, sharing only ~50% of identity with all other exon 1 regions. The other exon 1s can be clustered in two groups of high sequence identity. Each exon 1 determines substrate specificity while the N-terminal interacts with UDP-glucuronic acid.

Although there is some selectivity in substrate specificity between different UGTs, there is also remarkable redundancy to accept similar compounds as substrates [Tukey 2000]. The number of compounds that can serve as substrates for UGTs range in the thousands, and since few glucuronides retain biological activity, glucuronidation is a major detoxification mechanism [Dutton 1975].

It is not surprising that the UGTs are specifically regulated and distributed in critical tissues which come into xenobiotic contact [Strassburg 1998; Strassburg 2000]. Although the liver is a major site for glucuronidation, there is also a significant contribution from extrahepatic tissues, primarily the gastrointestinal tract. The mRNAs for UGT1A isoforms are differentially expressed in hepatic and extrahepatic tissues [Tukey 2001] with different tissues showing different levels of expression. The glucuronidation activity in the most proximal (esophagus) and most distal (colon) gastrointestinal tract is clearly reduced compared to the jejunum and liver. Interindividual polymorphic regulation of the expression of UGTs in the small intestine is in contrast to the total absence of polymorphic variation in liver [Strassburg 2000].

UGT1A1 is the only isoform that contributes in a biologically relevant way to bilirubin glucuronidation [Bosma 2003]. Mutations in the UGT1A1 gene are responsible for severe (Crigler-Najjar syndrome) and mild (Gilbert syndrome) forms of hyperbilirubinemia [Kadakol 2000]. The reduced glucuronidating activity of these mutated forms contributes to lower biliribin excretion by the liver. In addition to these mutations, the UGT1A1 gene shows great sequence variation among individuals in the form of insertion/deletion and single nucleotide polymorphisms (SNPs). Table 2 lists some of the polymorphic alleles of the UGT1A1 gene [Tukey 2000].

Table 2. Polymorphic alleles of the UGT1A1 gene				
Allele	**Nucleotide Changes**	**Protein Changes**	**Type**	**Exon**
UGT1A1*1	Wild type	—	—	—
UGT1A1*2	879 del 13	Truncation	Deletion	2
UGT1A1*3	1124 C→T	S375F	Missense	4
UGT1A1*4	1069 C→T	Q357X	Nonsense	3
UGT1A1*5	991 C→T	Q331 del 44	132 nt deletion	2
UGT1A1*6	221G→A	G71R	Missense	1
UGT1A1*7	145 T→G	Y486D	Missense	5
UGT1A1*8	625 C→T	R209W	Missense	1
UGT1A1*9	992 A→G	Q331R	Missense	2
UGT1A1*10	1021 C→T	R341X	Nonsense	3
UGT1A1*11	923 G→A	G308E	Missense	2
UGT1A1*12	524 T→A	L175Q	Missense	1
UGT1A1*13	508 del 3	F170del	Deletion	1
UGT1A1*14	826 G→C	G276R	Missense	1
UGT1A1*15	529 T→C	C177R	Missense	1
UGT1A1*16	1070 A→G	O357R	Missense	3
UGT1A1*17	1143 C→G	S381R	Missense	4
UGT1A1*18	1201 G→C	A401P	Missense	4
UGT1A1*19	1005 G→A	W335X	Missense	3
UGT1A1*20	1102 G→A	A368T	Missense	4
UGT1A1*21	1223 ins G	Frameshift	Frameshift	4
UGT1A1*22	875 C→T	A292V	Missense	2
UGT1A1*23	1282 A→G	K426E	Missense	4
UGT1A1*24	1309 A→T	K437X	Missense	5
UGT1A1*25	840 C→A	C280X	Missense	1
UGT1A1*26	973 del G	Frameshift	Frameshift	2
UGT1A1*27	686 C→A	P229Q	Missense	1
UGT1A1*28	***TAATA7***	***Transcription***	***Insertion***	***Promotor***
UGT1A1*29	1099 C→G	R367G	Missense	4
UGT1A1*30	44 T→G	L15R	Missense	1
UGT1A1*31	11609 CC→GT	P387R	2nt miss.	4
UGT1A1*32	1006 C→T	R336W	Missense	3
UGT1A1*33	881 T→C	I294T	Missense	2

Of the 33 reported variable positions, the most extensively studied is a variation of the TATA box. The most common form is UGT1A1*1(wild type), which contains 6 TA repeats in the TATA box. The UGT1A1*28 variant allele contains 7 TA repeats. There are also variant alleles containing 5 or 8 TA repeats. Individuals may have any combination of two alleles. Individuals having 2 wild-type alleles (6 TA repeats) are classified as having a 6/6 homozygous genotype; 2 UGT1A1*28 alleles as a 7/7 homozygous genotype; and one wild-type allele and one UGT1A1*28 allele as a 6/7 heterozygous genotype. The number of TA repeats in the TATA box is associated with enhanced [$(TA)_5$] or reduced [$(TA)_{7,8}$] UGT1A1 expression [Beutler 1998]. There are additional SNPs causing reduced enzymatic activity (-3279T>G, 211G>A, and 686C>A) [Jinno 2003].

Multiple polymorphic positions along the gene can be inherited as a single block (the haplotype). Haplotypes are a more comprehensive representation of sequence variation in the whole gene. The haplotype structure of the promoter region of UGT1A1 gene has been studied in Caucasian and African-American populations [Innocenti 2002]. In addition, the haplotype structure for the whole gene was recently reported for the Japanese population [Sai 2004]. The Japanese study demonstrated that there are two independent haplotype blocks and that variants in the 3′-terminal end of the gene (3′-UTR) may modulate mRNA stability contributing to the modulation of UGT1A1 expression.

Recent discoveries have contributed to a greater understanding of the extent and significance of variation in the UGT1A1 gene. Ultimately, the field will need to define the frequency of haplotypes in the different populations, their biological function, and their potential association with clinical phenotypes.

7. UGT1A1 and Irinotecan Toxicity

The association of UGT1A1 with the glucuronidation of bilirubin and SN-38 [Iyer 1998], along with the knowledge of polymorphic variation affecting the activity of UGT1A1, suggested the investigation of the association of these variants with pharmacokinetic values (SN38/SN38 AUC) and/or toxicity endpoints (primarily diarrhea and neutropenia). Most studies have focused on the UGT1A1*28 variant (a common polymorphism in the UGT1A1 promoter TATA box). A list of published papers and meeting abstracts reports is presented in Table 3.

Results from these trials suggest that patients who are homozygous for the UGT1A1*28 allele (known as the "7/7" genotype) are at greater risk for irinotecan-induced severe diarrhea or neutropenia. A trend for lower ratios of [SN-38G plasma AUC/SN-38 plasma AUC] has been observed in patients who are homozygous for UGT1A1*28. These findings are consistent with the hypothesis of reduced SN-38 to SN-38G metabolism in patients with this UGT1A1 polymorphism.

Although these results are intriguing, it is important to note that the individual trials were small (sample sizes ranging from 20-118), with only 3 to 20% of the patients having the 7/7 genotype. The studies utilized a variety of irinotecan dosing schedules and combination regimens that are known to have an impact on the degree and severity of diarrhea and/or neutropenia. The small sample sizes and trial design issues make estimation of the risk to 7/7 genotype patients difficult. For example, some trials found a significant association between UGT1A1 genotype and neutropenia but not for diarrhea [e.g., Innocenti 2004]. Other trials reported a genotype association with diarrhea but found no association with neutropenia [e.g., Marcuello 2004]. In all studies, a substantial proportion of 7/7 patients did not experience severe toxicity, and in one study there was no significant association between the polymorphism and toxicity whatsoever [Carlini 2004]. In addition, some studies were based on Japanese populations, which differ from the Caucasian population in haplotypes and varying genotype frequencies. Thus, the precise implications of UGT1A1 genotype on the safety, efficacy, and development of individualized patient dosing of irinotecan are not yet clear.

Table 3. Summary of Published Studies on Association between UGT1A1*28 Genotypes and Irinotecan Toxicity and PK					
Reference	**Irinotecan Dosage & Schedule**	**Study Design**	**Sample Size**	**PK Relationship**	**Toxicity Relationship**
Full Papers					
Ando, Cancer Res 2000	Variety of doses, schedules, and combos	Retrospective	118 Japanese pts; 7/118 pts were 7/7	Not evaluated	7/7 genotype had 5.2-fold risk of gr 4 leukopenia and/or diarrhea (P<0.001) compared to pooled 6/7 and 6/6
Ando, Ther Drug Monitor 2002	Variety of doses, schedules, and combos	Retrospective	100 Japanese pts for PK; 14/100 were genotyped for UGT1A1 and 4/14 were 7/7 or 6/7	7/7 or 6/7 genotype SN-38G/SN-38 AUC ratio <25th percentile of 100 PK patients	Not evaluated
Iyer, Pharmacogenom J 2002	300 mg/m^2, single dose every 3-weeks	Prospective	20; 9/20 were 6/6, 7/20 were 6/7, and 4 were 7/7	7/7 genotype SN-38G/SN-38 AUC ratio was 3.9-fold lower than 6/6 genotype (P=0.001)	7/7 genotype had 2.5-fold lower ANC nadir than 6/6 pts (P=0.04)
Font, Invest New Drugs 2003	Irino, 70 mg/m^2/day + docetaxel, 25 mg/m^2/ day, days 1, 8 & 15 every 28 days	Prospective	51 2nd-line NSCLC patients; 25/51 were 6/6, 19/51 were 6/7, and 7/51 were 7/7	Not evaluated	No genotype-dependent differences in toxicity. Non-significant trend to improved time-to-tumor progression and survival in 6/7 and 7/7 relative to 6/6.
Mathijssen, Clin Cancer Res 2003	200-350 mg/m^2, single dose every 3-weeks	Prospective	58 genotyped (majority EU Caucasian); 2/58 were 7/7, 22/58 were 6/7, and 34/58 were 6/6	Non-significant trend for genotype-dependent decrease in SN-38G/SN-38 AUC ratio (6/6 vs 6/7 vs 7/7)	Not evaluated
Innocenti, JCO 2004	350 mg/m^2, single dose every 3-weeks	Prospective	66; 30/66 were 6/6, 25/66 were 6/7, and 6/66 were 7/7; remainder were 6/8, 5/6, or 7/8	7/7 genotype SN-38G/SN-38 AUC ratio was 1.8-fold lower than 6/6 genotype (P=0.03)	7/7 genotype had 9.3-fold higher risk of gr 4 leukopenia (P=0.001)

Table 3 (Continued)					
Reference	**Irinotecan Dosage & Schedule**	**Study Design**	**Sample Size**	**PK Relationship**	**Toxicity Relationship**
Full Papers					
Sai, Clin Pharmacol Ther 2004		Retrospective	41 Japanese pts genotyped; 15/41 were 6/7 and 3/41 were 7/7	Significant genotype-dependent decrease in SN-38G/SN-38 AUC ratio (6/6 vs 6/7 vs 7/7; P=0.0014) Significant genotype-dependent pre-treatment bilirubin (6/6 vs 6/7 vs 7/7; P=0.0007)	Not evaluated
Marcuello, Brit J Cancer 2004	Variety of doses, schedules, and combos	Unspecified	95; 45/95 were 6/7 and 10/95 were 7/7	Not evaluated	Severe diarrhea in 7/10 7/7, 15/45 6/7, and 7/40 6/6 (P=0.005). Severe myelosuppression increased in 6/7 and 7/7 but did not reach statistical significance.
Rouits, Clin Cancer Res 2004	Two irinotecan/FU regimens	Retrospective	75; 7/95 7/7, 35/95 6/7, 31/95 6/6, and 2/95 5/6 or 5/7	Not evaluated	7/7 group at greater risk of severe neutropenia compared to 6/7 and 6/6 (P=0.02 and 0.003, respect). No significant difference for severe diarrhea.

Table 3 (Continued)					
Reference	**Irinotecan Dosage & Schedule**	**Study Design**	**Sample Size**	**PK Relationship**	**Toxicity Relationship**
Abstracts/Presentations					
Ando, Proc ASCO 2003	Unspecified	Unspecified	119 Japanese genotyped for UGT1A1*28 and UGT1A1 T3263G	Not evaluated	Severe tox 6.2-fold more likely in pts with both UGT1A1*28 and T3263G than in pts with wild-type UGT1A1
Chowbay, Proc ASCO 2003	100 mg/m^2, weekly	Prospective	20 Chinese pts genotyped; 12 6/6, 6 6/7, and 2 7/7	No significant genotype-dependent differences in irino, SN-38, or SN-38G AUC	Not evaluated
Carlini, Proc ASCO, 2004	Irino, 100-125 mg/m^2/day, days 1 & 8 every 21 days + capecitabine, 900-1000 mg/m^2 bid, days 2-25 every 21 days	Prospective	67 chemonaive metastatic CRC genotyped for UGT1A1*28 as well as UGT1A6 & UGT1A7 polymorphisms	Not evaluated	No significant associations between UGT1A1 genotypes and toxicity or efficacy. UGT1A7 genotypes conferring lower activity were significantly associated with higher response rate and lack of toxicity.
Grem, Proc ASCO 2004	Irino, 70-140 mg/m^2/24 h + LV, 500 mg/m^2/30 min + FU 2000-3900 mg/m^2/48 h, days 1 & 15 every 4 weeks	Prospective	30 GI cancer pts genotyped; 9/30 were 6/6 & 21/30 were 6/7 or 7/7	End-of-infusion SN-38G/SN-38 plasma level ratio was lower in 6/6 than in 6/7 or 7/7 genotypes (P=0.037)	Not reported
Massacesi, Proc ASCO 2004	Irino, 80 mg/m^2/day, days 1, 8, 15, 22 every 5 weeks + raltitrexed, 3 mg/m^2, single dose every 3 weeks	Prospective	56 pre-treated CRC patients genotyped; genotype frequencies not reported	Not evaluated	6/6 protective for diarrhea (P<0.00005), emesis (P<0.0001, and asthenia (P=0.006)
Singh, Proc ASCO 2004	Irino, 600 mg fixed dose	Prospective	86 adult pts genotyped; 44/86 were 6/6, 37 were 6/7, and 5 were 7/7	Significant genotype-dependent trend to SN-38G/SN-38 AUC ratio (P=0.022)	Not evaluated

8. Ongoing Studies

Preliminary reports from these trials prompted the pharmacogenomic component of NCCTG's N9741, a phase III metastatic colorectal cancer study of several irinotecan- and oxaliplatin-based regimens. Pharmacogenomic and clinical data from N9741 are currently being analyzed collaboratively by investigators and Pfizer clinicians and scientists. In addition, Pfizer is conducting pharmacogenomic correlative studies in a companion study to its sponsored, phase III metastatic colorectal cancer trial (known as the BICC-C trial) as well as several other company sponsored and large cooperative group trials (Table 4). These trials will look for associations between toxicity, efficacy, and genotype for numerous genes in addition to UGT1A1. These activities underscore Pfizer's strong commitment to fully

investigate and understand the potential value of genotyping in improving the safety and efficacy of irinotecan.

Table 4. Irinotecan Clinical Trials with a Pharmacogenomic Component[1]

Protocol	Enrollment Goal	Correlative Studies
Aventis V307 (PETACC3)	>1000 (1 of 2 arms with irinotecan)	LOH, MSI, SMAD-4 Immunopath: TS, DPD, TP, telomerase,
NCCTG N9741[2]	520[3]	ABCB1, ABCG2, CYP3A4/5, DYPD, ERCC2, GSTM1/GSTP1, MTHFR, TS, UGTA1A, XRCC1
SWOG 0124	620 (1 of 2 arms with irinotecan)	UGT1A1, ERCC-1, XRCC1
NCCTG N0147	4800 (2 of 3 arms with irinotecan)	UGT1A1, TS, MTHFR, excision repair cross complementation Immunopath: TS, DYPD, carboylesterase-2, EGFR, topo I MSI
440E-ONC-0020-366 (Pfizer)	>250	Carboxylesterase family, UGT1A family, c-MOAT, CYP3A4/5, DYPD, topo I, BCRP/ABCG2, TS, β-glucuronidase family, COX-2
CALGB 80203[4]	2200 (1 of 2 arms with irinotecan)	TYMS, DYPD, MTHFR, UGT1A1, CYP3A4/5, ABCB1, GSTP1, XRCC1, ERCC2, EGFR
E3301[4]	72	UGT1A1 Immunopath: VEGF, COX-2

[1] Trials are in progress unless otherwise specified.
[2] Trial completed; pharmacogenomic analysis is in progress.
[3] Number of patients for whom genomic analyses were performed.
[4] Not a Pfizer-sponsored study.

The inability to replicate many results from association studies for detection of genetic variants contributing to common complex traits may be due to several factors, including confounding from population structure, variability of phenotype, and allelic heterogeneity (multiple alleles contributing to same phenotype). In addition to these factors, publication bias, failure to attribute results to chance, and inadequate sample sizes, can contribute to the lack of replication [Colhoun 2003; Cardon 2001].

In order to avoid some of the limitations of small pharmacogenomic studies investigating the association of genetic variants with safety and efficacy end points with irinotecan treatment, Pfizer sponsors and actively participates in several large ongoing trials.

It is clear that the body of evidence is growing rapidly and warrants further monitoring. Pfizer hopes to place this literature into context with data from the phase III studies in the near future and will continue to work with the medical and scientific community and the Agency to address this important question.

9. References

Ando M, Kitagawa C, Ando Y, Sekido Y, Wakai K, Suzuki R et al. Genetic polymorphisms in the phenobarbital-responsive enhancer module of the UDP-glucuronosyltransferase (UGT) 1A1 gene and irinotecan toxicity in Japanese patients. Proc Amerc Soc Clin Oncol 2003;22:abst #496.

Ando Y, Saka H, Ando M, Sawa T, Muro K, Ueoka H et al. Polymorphisms of UDP-glucuronosyltranserase gene and irinotecan toxicity: A pharmacogenetic analysis. Cancer Res 2000;60:6921-6.

Ando Y, Ueoka H, Sugiyama T, Ichiki M, Shimokata K, Hasegawa Y. Polymorphisms of UDP-glucuronosyltransferase and pharmacokinetics of irinotecan. Ther Drug Monitor 2002;24:111-6.

Beutler E, Gelbert T, Demina A. Racial variability in the UDP-glucuronosyltransferase 1 (UGT1A1) promoter: A balanced polymorphism for regulation of bilirubin metabolism? Proc Natl Acad Sci USA 1998;95:8170-4.

Bosma PJ. Inherited disorders of bilirubin metabolism. J Hepatol 2003;38:107-17.

Cardon LR, Bell JI. Association Study Designs for Complex Diseases. Nature Rev 2001;2:91-9.

Carlini LE, Meropol NJ, Chen Y-M, McGarry C, Hill T, Gold P et al. Pharmacogenetic analysis of UGT1A1, UGT1A6, UGT1A7 and thymidylate synthase in a phase II study of capecitabine plus irinotecan in patients with metastatic colorectal cancer. Proc Amer Soc Clin Oncol 2004;23:abst #3623.

Chowbay B, Zhou Q, Kibat C, Leong SS, Tan EH. Pharmacogenetics of UGT1A1 and ABCG2 in relation to irinotecan (CPT-11) disposition in Chinese nasopharyngeal carcinoma patients. Proc Amer Soc Clin Oncol 2003;22:abst #568.

Colhoun HM, McKeigue PM, Smith GD. Problems of reporting genetic associations with complex outcomes. Lancet 2003;361:865-72.

de Forni M, Bugat R, Chabot GG, Culine S, Extra JM, Gouyette A, et al. Phase I and pharmacokinetic study of the camptothecin derivative irinotecan, administered on a weekly schedule in cancer patients. Cancer Res 1994;54(16):4347-54.

Dutton, GJ. Control of UDP-glucuronyltransferase activity. Biochem Pharmacol 1975;24:1835-41.

Font A, Sánchez JM, Tarón M, Martinez-Balibrea ER, Sánchez JJ et al. Weekly regimen of irinotecan docetaxel in previously treated non-small cell lung cancer and correlation with uridine diphosphate glucuronysyltransferase 1A1 (UGT1A1) polymorphism. Invest New Drugs 2003;21:435-43.

Gong QH, Cho JW, Huang T, Potter C, Gholami N, Basu N et al. Thirteen UDPglucuronosyltransferase genes are encoded at the human UGT1 gene complex locus. Pharmacogenetics 2001;11:357-68.

Grem JL, Wright M, Morrison G, Lin P-X, Leonard G, Nguyen D et al. Phase I pharmacokinetic & pharmacogenetic study of sequential infusional irinotecan and fluorouracil. Proc Amer Soc Clin Oncol 2004;23:abst #2075.

Gupta E, Lestingi TM, Mick R, et al. Metabolic fate of irinotecan in humans: Correlation of glucuronidation with diarrhea. Cancer Research 1994;54:3723-3725.

Innocenti F, Grimsley C, Das S, Ramirez J, Cheng C, Kuttab-Boulos H et al. Haplotype structure of the UDP-glucuronosyltransferase 1A1 promoter in different ethnic groups. Pharmacogenetics 2002;12:725-33.

Innocenti F, Undevia SD, Iyer L, Chen PX, Das S, Kocherginsky M et al. Genetic variants in the UDP-glucuronasyltransferase 1A1 gene predict the risk of severe neutropenia of irinotecan. J Clin Oncol 2004;22(8);1382-8.

Iyer L, King CD, Whitington PF, Green MD, Roy SK, Tephly TR et al. Genetic predisposition to the metabolism of Irinotecan (CPT-11). J Clin Invest 1998;101(4):847-54.

Iyer L, Das S, Janisch L, Wen M, Ramírez J, Karrison T et al. UGT1A1*28 polymorphisms as a determinant of irinotecan disposition and toxicity. Pharmacogenom J 2002;2:43-7.

Jinno H, Tanaka-Kagawa T, Hanioka N, Saeki M, Ishida S, Nishimura T et al. Glucuronidation of 7-ethyl-10-hydroxycamptothecin (SN-38), an active metabolite of Irinotecan (CPT-11), by human UGT1A1 variants, G71R, P229Q, and Y486D. Drug Metabolism and Disposition 2003;31(01):108-13.

Kadakol A, Ghosh SS, Sappal BS, Sharma G, Chowdhury JR, Chowdhury NR. Genetic lesions of bilirubin uridine-diphosphoglucuronate glucuronosyltransferase (UGT1A1) causing Crigler-Najjar and Gilbert syndromes: correlation of genotype to phenotype. Human Mutation 2000;16:297-306.

Marcuello E, Altés A, Menoyo A, del Rio E, Gómez-Pardo M, Baiget M. UGT1A1 gene variations and irinotecan treatment in patients with metastatic colorectal cancer. British J Cancer 2004:1-5.

Massacesi C, Terrazzino S, Maracucci F, Rocchi MBL, Cappalletti C, Giustini L et al. Role of UGT1A1, MTHFR and TS gene polymorphisms in the prediction of irinotecan and raltitrexed gastrointestinal toxicity in pre-treated patients with metastatic colorectal cancer. Proc Amer Soc Clin Oncol 2004;23:abst 2064.

Mathijssen RJH, van Alphen RJ, Verweij J, et al. Clinical pharmacokinetics and metabolism of irinotecan (CPT-11). Clin Cancer Res 2001;7:2182-94.

Mathijssen RHJ, Marsh S, Karlsson MO, Xie R, Baker SD, Verweij J et al. Irinotecan pathway genotype analysis to predict pharmacokinetics. Clin Cancer Res 2003;9:3246-53.

Meyerhardt JA, Kwok A, Ratain MJ, McGovren P, Fuchs CS. Relationship of baseline serum bilirubin to efficacy and toxicity of single-agent irinotecan in patients with metastatic colorectal cancer. J Clin Oncol 2004;22(8):1439-46

Raymond E, Boige V, Faivre S, Sanderink GJ, Rixe O, Vernillet L et al. Dosage adjustment and pharmacokinetic profile of irinotecan in cancer patients with hepatic dysfunction. J Clinl Oncol 2002;20 (21):4303-12.

Ritter JK, Chen F, Sheen YY, Tran HM, Kimura S, Yeatman MT, Owens IS. A novel complex locus UGT1 encodes human bilirubin, phenol, and other UDP-glucuronosyltransferase isozymes with identical carboxyl termini. J Biological Chem 1992;267(5):3257-61.

Rivory LP, Chatelut E, Canal P, et al. Kinetics of the in vivo interconversion of the carboxylate and lactone forms of irinotecan (CPT-11) and of its metabolite SN-38 in patients. Cancer Res 1994;54:6330-3.

Rouits E, Boisdron-Celle M, Dumont A, Guérin O, Morel A, Gamelin E. Relevance of different UGT1A1 polymorphisms in irinotecan-induced toxicity: a molecular and clinical study of 75 patients. Clin Cancer Res 2004;10:5151-9

Rowinsky EK, Grochow LB, Ettinger DS, Sartorius SE, Lubejko BG, Chen TL, et al. Phase I and pharmacological study of the novel topoisomerase I inhibitor 7-ethyl-10-[4-(1-piperidino)-1-piperidino]-carbonyloxycamptothecin (CPT-11) administered as a ninety-minute infusion every 3 weeks. Cancer Res 1994;54:427-36.

Sai K, Saeki M, Saito Y, Ozawa S, Katori N, Jinno H et al. UGT1A1 haplotypes associated with reduced glucuronidation and increased serum bilirubin in irinotecan-administered Japanese patients with cancer. Clin Pharmacol Ther 2004;75(6):501-15.

Singh A, Paoluzzi L, Price D, Danesi R, Mathijssen RH, Verweij J, et al. Influence of genetic variants in UGT1A1 and UGT1A9 on the in vivo glucuronidation of SN-38. Proc Amer Soc Clin Oncol 2004;23:abst #2072.

Slatter JG, Schaaf LJ, Sams JP, Feenstra KL, Johnson MG, Bombardt PA, et al. Pharmacokinetics, metabolism, and excretion of irinotecan (CPT-11) following I.V. infusion of [^{14}C]CPT-11 in cancer patients. Drug Metabolism and Disposition 2000;28(4):423-33.

Strassburg CP, Manns MP, Tukey RH. Expression of the UDP-glucuronosyltransferase 1A locus in human colon. J Biological Chem 1998:273(15):8719-26.

Strassburg CP, Kneip S, Topp J, Obermayer-Straub P, Barut A, Tukey RH, Manns MP. Polymorphic gene regulation and interindividual variation of UDP-glucuronosyltransferase activity in human small intestine. J Biological Chem 2000:275(46):36164-71.

Tukey RH, Strassburg CP. Human UDP-glucuronosyltransferases: metabolism, expression, and disease. Annu Rev Pharmacol Toxicol. 2000;40:581-616.

Tukey RH, Strassburg CP. Genetic multiplicity of the human UDP-glucuronosyltransferases and regulation in the gastrointestinal tract. Molecular Pharmacol 2001;59(3):405-14.

Tukey RH, Strassburg CP, MacKenzie PI. Pharmacogenomics of human UDP-glucuronosyltransferases and irinotecan toxicity. Molec Pharmacol 2002;62:446-50.

Zamber CP, Jatinder K, et al. Natural allelic variants of breast cancer resistance protein (BCRP) and their relationship to BCRP expression in human intestine. Pharmacogenetics 2003;13:19-28.

Published OnlineFirst February 3, 2017; DOI: 10.1158/1078-0432.CCR-16-1990

Personalized Medicine and Imaging

Clinical Cancer Research

Correlation between Ferumoxytol Uptake in Tumor Lesions by MRI and Response to Nanoliposomal Irinotecan in Patients with Advanced Solid Tumors: A Pilot Study

Ramesh K. Ramanathan[1,2], Ronald L. Korn[1,3], Natarajan Raghunand[4], Jasgit C. Sachdev[1], Ronald G. Newbold[1,3], Gayle Jameson[1], Gerald J. Fetterly[5], Joshua Prey[5], Stephan G. Klinz[6], Jaeyeon Kim[6], Jason Cain[6], Bart S. Hendriks[6], Daryl C. Drummond[6], Eliel Bayever[6], and Jonathan B. Fitzgerald[6]

Abstract

Purpose: To determine whether deposition characteristics of ferumoxytol (FMX) iron nanoparticles in tumors, identified by quantitative MRI, may predict tumor lesion response to nanoliposomal irinotecan (nal-IRI).

Experimental Design: Eligible patients with previously treated solid tumors had FMX-MRI scans before and following (1, 24, and 72 hours) FMX injection. After MRI acquisition, $R2^*$ signal was used to calculate FMX levels in plasma, reference tissue, and tumor lesions by comparison with a phantom-based standard curve. Patients then received nal-IRI (70 mg/m^2 free base strength) biweekly until progression. Two percutaneous core biopsies were collected from selected tumor lesions 72 hours after FMX or nal-IRI.

Results: Iron particle levels were quantified by FMX-MRI in plasma, reference tissues, and tumor lesions in 13 of 15 eligible patients. On the basis of a mechanistic pharmacokinetic model, tissue permeability to FMX correlated with early FMX-MRI signals at 1 and 24 hours, while FMX tissue binding contributed at 72 hours. Higher FMX levels (ranked relative to median value of multiple evaluable lesions from 9 patients) were significantly associated with reduction in lesion size by RECIST v1.1 at early time points ($P < 0.001$ at 1 hour and $P < 0.003$ at 24 hours FMX-MRI, one-way ANOVA). No association was observed with post-FMX levels at 72 hours. Irinotecan drug levels in lesions correlated with patient's time on treatment (Spearman $\rho = 0.7824$, $P = 0.0016$).

Conclusions: Correlation between FMX levels in tumor lesions and nal-IRI activity suggests that lesion permeability to FMX and subsequent tumor uptake may be a useful noninvasive and predictive biomarker for nal-IRI response in patients with solid tumors. *Clin Cancer Res; 23(14); 3638–48. ©2017 AACR.*

Introduction

Liposomal drug delivery carriers can enhance utility of existing anticancer drugs by shielding the encapsulated drug from rapid clearance and metabolism, and extending mean residence time in plasma and tumor tissue (1, 2). Aberrant characteristics in the tumor neovasculature and microenvironment lead to passive accumulation of nanomedicines and macromolecular drugs in tumor lesions, which is known as the enhanced permeability and retention (EPR) effect (3, 4). The extent to which the EPR effect occurs in humans is controversial and subject to debate. Existing data suggest the EPR effect is highly variable across tumor lesions (5) and may be heavily influenced by the tumor microenvironment (6). Rationales for noninvasive imaging aimed toward selection of patients with a sufficiently high level of lesion-specific nanotherapeutic accumulation have been proposed (7, 8); however, clinical implementation has been limited (4, 9).

Nanoliposomal irinotecan (nal-IRI; Onivyde, irinotecan liposome injection, MM-398, PEP02, BAX2398) comprises irinotecan encapsulated in a nanoparticle drug delivery system in the form of the irinotecan sucrose octasulfate salt with an average particle size of 110 nm (10, 11). Nal-IRI in combination with 5-fluorouracil/leucovorin (5-FU/LV) is approved for use in the United States, European Union, and Taiwan Health Authorities for the treatment of patients with metastatic pancreatic cancer after disease progression following gemcitabine-based therapy (11, 12). The liposomal payload, irinotecan, is a member of the camptothecin class of topoisomerase I (TOP1) inhibitors and causes cell death through DNA damage after replication-fork collisions with transiently trapped drug–TOP1–DNA cleavage complexes, thus highlighting length of drug exposure as an important driver for

[1]Virginia G Piper Cancer Center, Honor Healthcare, Scottsdale, Arizona. [2]Translational Genomics Research Institute, Phoenix, Arizona. [3]Imaging Endpoints, Scottsdale, Arizona. [4]Moffitt Cancer Center, Tampa, Florida. [5]Roswell Park Cancer Institute, Buffalo, New York. [6]Merrimack Pharmaceuticals, Inc., Cambridge, Massachusetts.

Note: Supplementary data for this article are available at Clinical Cancer Research Online (http://clincancerres.aacrjournals.org/).

R.K. Ramanathan and R.L. Korn contributed equally to this article.

Current address for G.J. Fetterly: Athenex, Buffalo, New York; current address for E. Bayever: Glenmark Pharmaceuticals Inc., Mahwah, New Jersey; and current address for R. Ramanathan: Mayo Clinic Hospital, Phoenix, Arizona.

Corresponding Authors: Ramesh K. Ramanathan, Mayo Clinic Hospital, 5777 East Mayo Boulevard, Phoenix, AZ 85054. Phone: 480-302-6185; Fax: 480-323-1359; E-mail: Ramanathan.ramesh@mayo.edu; and Stephan G. Klinz, Merrimack Pharmaceuticals, One Kendall Square, Suite B7201, Cambridge, MA 02139. Phone: 617-441-7434; Fax: 617-491-1386; E-mail: Sklinz@merrimack.com

doi: 10.1158/1078-0432.CCR-16-1990

Published OnlineFirst February 3, 2017; DOI: 10.1158/1078-0432.CCR-16-1990

Translational Relevance

Liposomal or nanoparticle-based drug delivery partly depends on enhanced tumor permeability and retention (EPR) properties. Nanoparticle permeability rates are highly variable and differ from small drug molecules that readily diffuse across tumor vasculature. Therefore, standard DCE-MRI pharmacokinetic analysis using low-molecular weight contrast may not be suitable for evaluating tumor lesion permeability to nanoparticles. The ferumoxytol (FMX) iron oxide nanoparticle has pharmacokinetic properties similar to nal-IRI and may be appropriate for estimating EPR effects given its close particle size and longer retention in the blood compared with standard gadolinium-based contrast agents. Using a quantitative MRI approach, we estimated FMX levels in tumor lesions and demonstrated marked heterogeneity of tumor EPR effect. Higher FMX levels were associated with greater reduction in lesion size after nal-IRI treatment. This study suggests that quantitative FMX-MRI may serve as a predictive biomarker for nanoparticle-based drug delivery and may enable patient stratification according to comparatively high tumor uptake of such therapies.

cytotoxicity (13). Compared with pharmacokinetic data of nonliposomal irinotecan (14), nal-IRI is characterized by a higher exposure, lower clearance, and smaller volume of distribution.

Preclinical experiments (15) have demonstrated that nal-IRI greatly increased availability of the active metabolite of irinotecan, SN-38, in the tumor and showed dose-dependent antitumor efficacy at much lower doses than nonliposomal irinotecan. A semimechanistic pharmacokinetic model identified the duration of prolonged SN-38 levels above an intratumoral threshold as a major pharmacologic determinant for *in vivo* activity of irinotecan in mice. A sensitivity analysis found that pharmacokinetic properties and permeability of the tumor vasculature to nal-IRI positively affected duration of SN-38 in tumors. Liposomal deposition in tumors was also found to be a rate-limiting step for drug delivery to cells for other long-circulating liposomes (16). It has previously been shown that tumor deposition of a liposomal contrast agent correlated with treatment outcome to a liposomal drug in a rat xenograft model (17).

CT or MRI modalities have been used in clinical settings to assess tissue perfusion and permeability, particularly with small-molecule and macromolecular contrast media (18, 19). These studies demonstrated that permeability rates depended on molecular or particle properties such as hydrodynamic diameter and shape (4). Liposomal imaging agents based on single-photon emission computed tomographic (SPECT) or positron emission tomographic (PET) imaging have been examined as well (20–22). A widely studied class of imaging agents is superparamagnetic iron oxide nanoparticles, which have excellent MRI contrast characteristics and demonstrate concentration-related negative contrast on T2- and T2*-weighted sequences. Variable coatings applied to these particles can modulate their pharmacokinetic behavior. Longer-circulating iron oxide nanoparticles exhibit delayed enhancement and uptake into reactive cells within lesions (23, 24) and mirror pharmacokinetic and distribution characteristics seen for liposomes (25, 26) and similarly sized nanotherapeutics (27).

Ferumoxytol (FMX) is an approximately 750-kDa superparamagnetic iron oxide nanoparticle with an average colloidal particle size of 23 nm and a narrow particle size distribution ranging from 10 to 70 nm (28). FMX is approved to treat iron deficiency anemia in patients with chronic renal failure (29). FMX is composed of a nonstoichiometric magnetite core covered by a semisynthetic carbohydrate coating of polyglucose sorbitol carboxymethyl ether. FMX has slower clearance and delayed enhancement properties compared with gadolinium-based contrast agents and also allows after tissue deposition visualization of inflammatory cells in vessel walls and tissue because of uptake of the nanoparticles by macrophages (24, 30). In preclinical studies, FMX did not interfere with the pharmacokinetics, biodistribution, or cellular distribution of liposomes within tumors (25). Broad colocalization of liposomes and FMX was observed in perivascular stromal areas, and correlation between the FMX-MRI signal and tumor drug uptake was seen particularly in tumors with high liposomal drug delivery (25). Comparable results were reported with PLGA-PEG–based polymeric therapeutic nanoparticles (27). We hypothesized that FMX-MRI could be used as a clinical imaging approach for predicting delivery to tumor lesions and subsequent antitumor activity of nanotherapeutics. Here we measure the deposition characteristics of FMX in tumor lesions using a quantitative MRI approach and compare them with tumor lesion responses after treatment with nal-IRI.

Materials and Methods

Study design

This publication describes the pilot phase of an ongoing institutional review board–approved clinical study (31) that was conducted at the Virginia G Piper Cancer Center in Scottsdale, AZ. The primary objective was to assess the feasibility of quantitative MRI to determine FMX levels in tumor lesions and to assess lesion biopsies for macrophage content and metabolite levels. A secondary endpoint was tumor response assessed by RECIST v1.1 every 8 weeks. Plasma samples to assess the PK of FMX and nal-IRI were collected. Data cut-off date for the pilot phase was February 20, 2015. For study procedures, see Supplementary Information and Supplementary Fig. S1.

Study criteria

Eligible patients were 18 years of age or older and had advanced solid tumors that had progressed while on ≥1 prior regimen. Eastern Cooperative Oncology Group performance status of 0, 1, or 2, and acceptable kidney, bone marrow, and liver function. All patients had metastatic disease with 2 lesions ≥2 cm in diameter, accessible for a percutaneous biopsy. Exclusion criteria included prior irinotecan or bevacizumab therapy within the preceding 6 months. Additional inclusion and exclusion criteria are available (31).

FMX and MRI phantom

Patients received FMX (AMAG Pharmaceuticals) intravenously at a dose of 5 mg/kg, delivered as a bolus injection (29) at 1 mg/second and capped at 510 mg. All FMX concentrations are expressed as amounts of elemental iron. After injection, patients were kept under observation for 30 minutes with continuous vital sign monitoring for possible signs of hypersensitivity reactions. Administration by bolus injection was consistent with FDA-approved labeling at the time of the study (29). Since the

completion of this pilot study, the original package insert for Feraheme (ferumoxytol injection) was changed in March 2015 from a bolus injection to an intravenous infusion over at least 15 minutes. Patients are to be observed for signs or symptoms of hypersensitivity reactions during and for at least 30 minutes following FMX infusion, including monitoring of blood pressure and pulse during and after FMX administration. These changes will be reflected in the design of all our ongoing and future clinical studies with FMX (29).

A FMX phantom was assembled consisting of 15-mL tubes with FMX at concentrations of 0, 10, 20, 30, 40, 50, 100, 150, or 200 μg/mL elemental iron in 2% agarose containing 5 mmol/L sodium azide. Agarose gel provides tissue equivalent phantom material for measuring contrast agent relaxivity (32). This phantom was included in all MRI scans of either patients or isolated plasma samples.

FMX-MRI acquisition

MRI for FMX relaxometry was acquired on a GE 1.5-T instrument with a series of 6 coregistered fat-suppressed fast spoiled gradient echo (FSPGR) scans with echo times (TE) of 1.5, 3.0, 4.5, 6.0, 9.0, and 13.2 milliseconds using a phased-array torso body coil (Supplementary Table S1). The FSPGR sequences started on average at 69 min after FMX injection [95% confidence interval (CI) 54–85 minutes], and TE acquisition averaged approximately 18 minutes. Slice thickness and spacing were 6 mm × 1 mm, using a 256 × 256 matrix with a field of view to match the size of the body part being imaged. $T2^*$ and $R2^*$ maps were fitted by linear regression of the log-transformed signal intensities at each echo. Mean $T2^*$ and $R2^*$ values were determined from operator-defined 2D regions of interest (ROI) circumscribing tumor lesions and select organ sites (liver, spleen, muscle) that were traced around the tissue–tumor interface of selected FMX-MRI target lesions on each FSGPR echo sequence. A FMX phantom was placed under the patient and included in the scan field of view.

For determination of FMX concentrations in plasma, samples of patient plasma were placed next to the FMX phantom and scanned using the same MRI acquisition series as for study patients.

FMX-MRI analysis

From each scan, the $T2^*$ relaxation time was extrapolated from the decay in signal intensity with increasing echo times for a given image slice and displayed as the relaxation rate $R2^*$, the inverse of the relaxation time $T2^*$ (Fig. 1A). ROIs were manually drawn on a reference image of the cross-sections of each phantom tube to include all pixels without visible susceptibility artifacts. $R2^*$ values for each phantom concentration were calculated by linear regression of the log-transformed average ROI signal for each slice. For each tube, the slice with the highest R^2 (goodness of fit) was selected for plotting the linear relationship between $R_2^* = 1/T_2^*$ and FMX concentrations (Fig. 1B) as given in Eq. 1, with $R2^*_0$ representing the intrinsic relaxation rate of plasma without FMX and $r2^*$ representing a relaxivity constant. Plasma control samples into which a known amount of FMX had been added served as

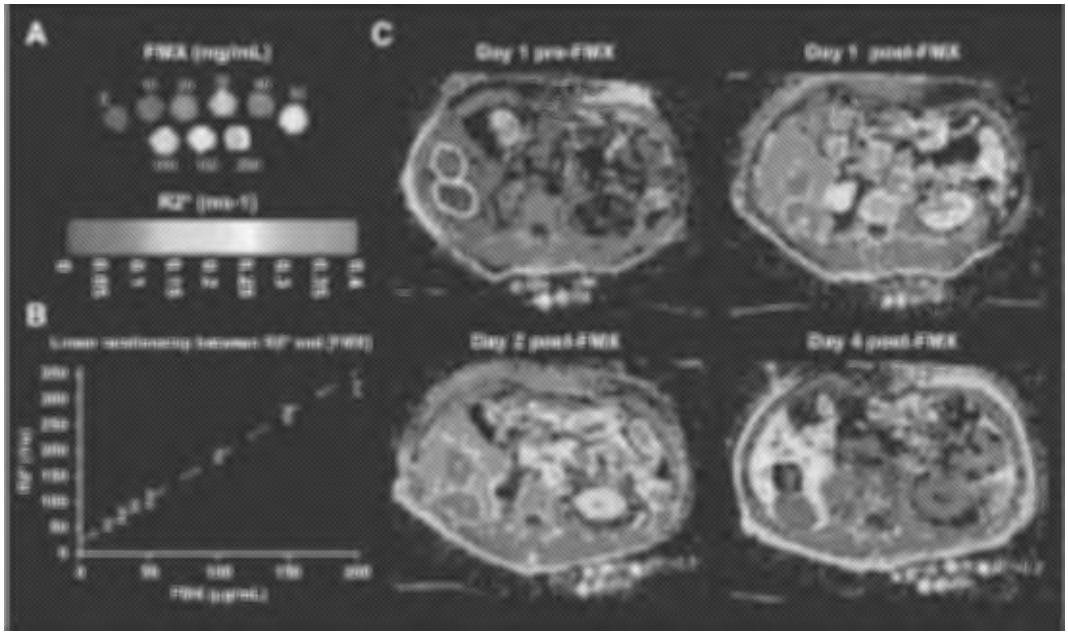

Figure 1.

FMX distribution kinetics assessed by MRI $R2^*$ maps. **A,** Enlarged view of the FMX phantom, with tubes containing FMX concentrations from 0–200 μg/mL. A pixel-by-pixel view of $R2^*$ is shown for illustration purposes only, as $R2^*$ values for each phantom concentration were actually calculated by linear regression of the log-transformed mean ROI signal for each slice. **B,** Linearity of relationship between FMX concentration and the relaxation rate $R2^*$ across 37 measurements of the FMX phantom during plasma FMX measurements (mean ± SD). The 200-μg/mL FMX tube was not included in the trend line. **C,** Representative pseudocolored relaxometric $R2^*$ maps derived from patient images before FMX dosing, immediately after (1–2 hours), 24 hours, and 72 hours after dosing with 5 mg/kg FMX. Approximate lesion locations are indicated by dashed lines in the image before FMX dosing.

Published OnlineFirst February 3, 2017; DOI: 10.1158/1078-0432.CCR-16-1990

additional process validation (not shown).

$$R2^* = R2^*_0 + r2^* \times [FMX] \quad (1)$$

Similarly, FMX concentrations in lesions, tissues, or other regions of interest were extrapolated from the pre- and postinjection relaxation rates using the nominal relationship observed for the FMX phantom [Eq. 2].

$$[FMX] = \frac{\left(R2^*_{post} - R2^*_{0,post}\right)}{r2^*} - \frac{\left(R2^*_{pre} - R2^*_{0,pre}\right)}{r2^*} \quad (2)$$

$FMX_{0\to72}$ tumor exposure parameters were estimated from FMX values derived from MRI using a simple linear piecewise function (33). We made the assumption that the difference in the contribution of local field inhomogeneities to $R2^*$ on the different scan days (captured in the difference between $R2^*_{0,post}$ and $R2^*_{0,pre}$) is negligible relative to the change in $R2^*$ produced by FMX (captured in the difference between $R2^*_{post}$ and $R2^*_{pre}$).

Response analysis

Patient response assessment was performed by local investigators per RECIST 1.1. For further analysis of lesion responses in correlation to FMX-MRI, a central radiology review was performed in a blinded, independent manner. Details regarding central radiology review can be found in Supplementary Materials.

Plasma and tumor pharmacokinetic modeling of FMX

Pharmacokinetic profiles of FMX in plasma were described by a one-compartment model, which was then connected to the tumor pharmacokinetic model with tumor capillary and tissue compartments (Fig. 2A; Supplementary Information). As the volume of distribution for FMX (Supplementary Table S2) suggests a low transvascular flux compared with small-molecule contrast agents, it was assumed that FMX transport to the tumor tissue compartment is permeability limited. The levels of FMX in tumor capillary thus correspond to the central blood compartment, hence making the volume transfer constant K^{trans} equal to the inward permeability surface area product, PeS_{in} (34). The tissue deposition of FMX depends on tissue

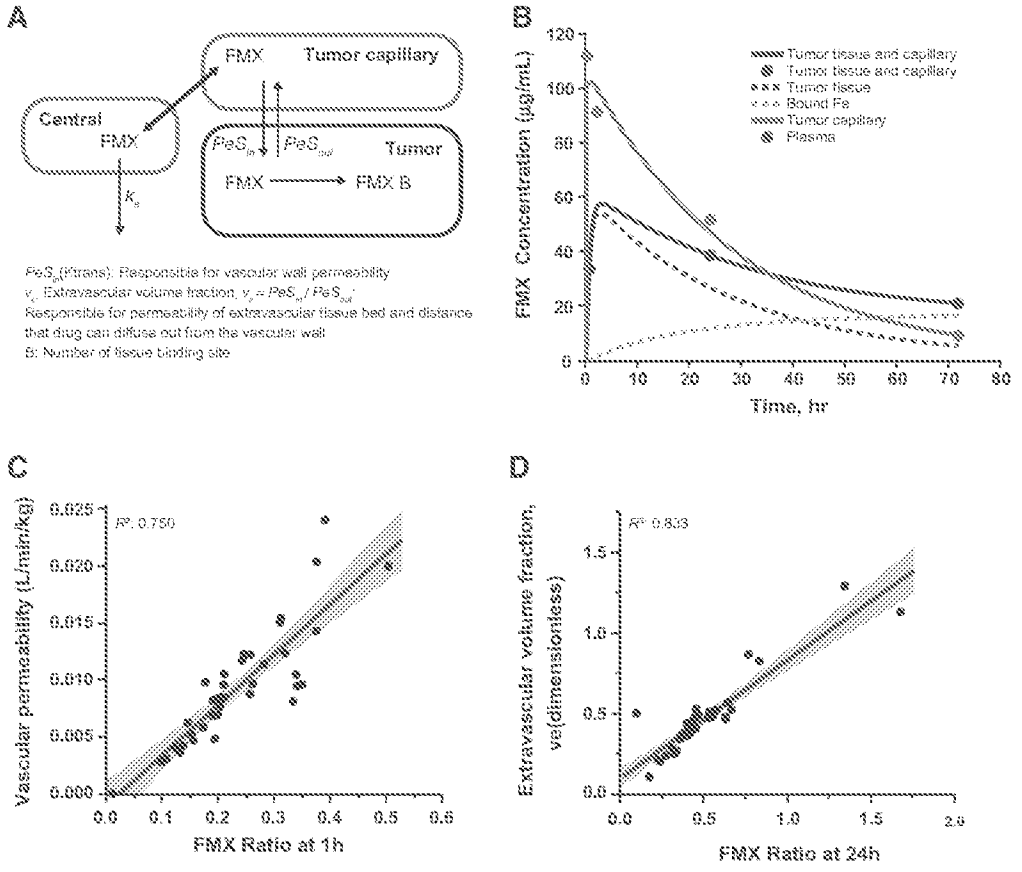

Figure 2.

Pharmacokinetic model of FMX. **A,** Schematic of multicompartment model for FMX distribution between plasma, tumor capillaries, and tumor compartments. Retention of FMX in the tumor compartment is mimicked by tissue binding sites. **B,** Mechanistic pharmacokinetic model for tumor deposition of FMX driven by permeability and binding parameters; an example of lesion fits for high-permeability/high-signal retention is shown. **C** and **D,** Permeability-based parameters for tumor deposition in pharmacokinetic model correlate strongly with FMX signal measured at 1 hour (PeS_{in}; **C**) and 24 hours (**D**; PeS_{in}/PeS_{out}). The normalized FMX ratio between tumor and plasma values is shown to account for plasma FMX pharmacokinetic variability.

permeability (PeS_m or K^{trans}) and extravascular volume fraction (v_e). In the tumor tissue compartment, it is assumed that FMX can also bind to the tissue-binding sites (B), which is intended to capture macrophage uptake of FMX (Fig. 2A). Model equations and additional information are summarized in Supplementary Information. Estimated model parameters are summarized in Supplementary Table S3.

Statistical analysis

Pearson pairwise correlation analysis was performed between FMX levels, lesion size changes, and pharmacokinetic model parameter. Spearman rank correlation analysis was performed between individual lesion averages of irinotecan levels and the patient's time on treatment. One-way ANOVA was used to assess the relationship between lesion size change and FMX groups below and above the median. ROC for lesion classification were calculated by using two different thresholds for lesion size change to define responding patients: either lesion shrinkage (any decrease from baseline) or partial response (≥30% decrease from baseline). All statistical analyses were implemented in JMP v11 (SAS).

See Supplementary information for additional Materials and Methods.

Results

Clinical observations

Between December 12, 2012 and March 3, 2014, 21 patients with metastatic solid tumors were screened, of whom 15 met eligibility criteria and enrolled on the FMX-MRI portion of the protocol. Data acquisition for image analysis was successfully completed in all but two patients. Thirteen patients continued to nal-IRI treatment and received between 1 and 31 doses (median, 4 doses). Patient demographics are given in Table 1. On average, patients received 95% of the intended dose. Nine (69%) patients underwent FMX imaging, biopsy collection, nal-IRI treatment, and at least one posttreatment CT scan for RECIST response assessment and were therefore evaluable for detailed analyses of FMX deposition characteristics and tumor lesion responses, while 4 patients discontinued nal-IRI without acquisition of a scan because of clinical deterioration and/or serious adverse events. We observed 1 partial response (breast cancer), 5 stable disease, and 5 progressive disease responses; 2 patients were not clinically evaluated. Median time on treatment was 57 days (range, 29–434 days), with 4 patients [breast (2), duodenal, and mesothelioma] on treatment for >110 days.

Table 1. Demographic and baseline characteristics

	FMX $n = 15$	nal-IRI $n = 13$
Age, years, median (range)	60 (28–80)	58 (28–80)
Sex, *n* (%)		
Male	4 (27)	4 (31)
Female	11 (73)	9 (69)
Race, *n* (%)		
White	14 (93)	12 (92)
American-Indian/American-Native	1 (7)	1 (8)
ECOG, *n* (%)		
0	7 (47)	7 (54)
1	8 (53)	6 (46)
Prior lines of therapy, median (range)	4 (1–10)	4 (1–10)

No adverse effects such as hypersensitivity, other allergic reactions, or dizziness were observed during the FMX administration and during a 30-minute observation phase before the first post-injection MRI. Adverse events with nal-IRI were consistent with those previously reported, including diarrhea, nausea, vomiting, and neutropenia (11, 35).

FMX-MRI imaging and quantitation

Calibration curves for the dependence of R2* on FMX concentration yielded consistent values, with an average r2* relaxivity of 1.661 mL/s/μg (92.8 1/s/mmol/L) (Fig. 1B). The R2* values for the 150-μg/mL FMX phantom tube were comparable with the maximally observed R2* values in either plasma or tissues.

Baseline relaxation rates were 21.8 ± 12.8/s, 33.5 ± 17.6/s, 39.0 ± 42.0/s, and 28.4 ± 3.1/s for tumor lesions, liver, spleen, and muscle, respectively. FMX led to rapid R2* increases in the blood, liver, and spleen (Fig. 1C). FMX accumulation in tumor lesions was detectable and heterogeneous within lesions, but generally at levels lower than the liver and spleen. Liver lesions were also well demarcated from the surrounding tissue in the presence of FMX (see Supplementary Fig. S2A as example). The R2* signal had not returned to baseline in select tissues and most tumor lesions at 72 hours (Fig. 1C, day 4 following FMX). For lesions evaluated by FMX-MRI, lesion sizes at baseline measured on average 32.1 ± 15.62 mm in diameter. No correlations between lesion sizes and uptake were observed.

FMX levels in background tissues or tumor lesions ($n = 46$) were calculated on the basis of phantom measurements. Maximal tumor lesion FMX concentrations were observed at the 1- or 24-hour imaging time points after FMX injection (Fig. 3A). Median (with median absolute deviation) FMX levels for all measured lesions were 32.7 (6.2) μg/mL measured at 1 hour after FMX injection, 34.5 (10.4) μg/mL after 24 hours, and 11.4 (4.5) μg/mL after 72 hours. Lesion uptake for individual patients is shown in Fig. 3B. Heterogeneity of uptake across lesions was observed within patients as well as across patients. Lesion levels reached 2.5%–30% of the injected dose per kilogram of tissue at 24 hours. The 24-hour FMX levels correlated linearly with overall FMX exposure AUC_{0-72h} ($R^2 = 0.9502$; slope 95% CI, 42.9–49.4); exposures differed by 8.3× between all imaged lesions, while interlesional ranges of 1.03× to 4.22× were observed for individual patients. Intralesion heterogeneity showed median exposure differences of 1.56×, although >10× higher differences were also observed.

FMX uptake was minimal in normal muscle, a tissue with small endothelial fenestrations, and returned to baseline levels within 72 hours (Fig. 3C). In liver and spleen, the FMX concentration was initially comparable with plasma levels at 0.5–2 hours, but the FMX concentration decreased much more rapidly in plasma than in these tissues. After 72 hours, FMX levels in liver and spleen were 6× and 4× higher, respectively, than in plasma. In plasma, the elimination half-life of FMX was 22.1 hours ($n = 14$; 95% CI, 19.7–24.5; Fig. 3C), consistent with previously published data in healthy subjects (36, 37) and comparable with the reported half-life of nal-IRI (11, 35). Plasma exposure ($AUC_{0-\infty}$) for FMX and nal-IRI were correlated ($r = 0.7528$; $P = 0.0030$). Other pharmacokinetic parameters for FMX are summarized in Supplementary Table S2. Metabolic turnover of FMX resulted in elevated plasma ferritin levels as described previously (29, 36). Ferritin

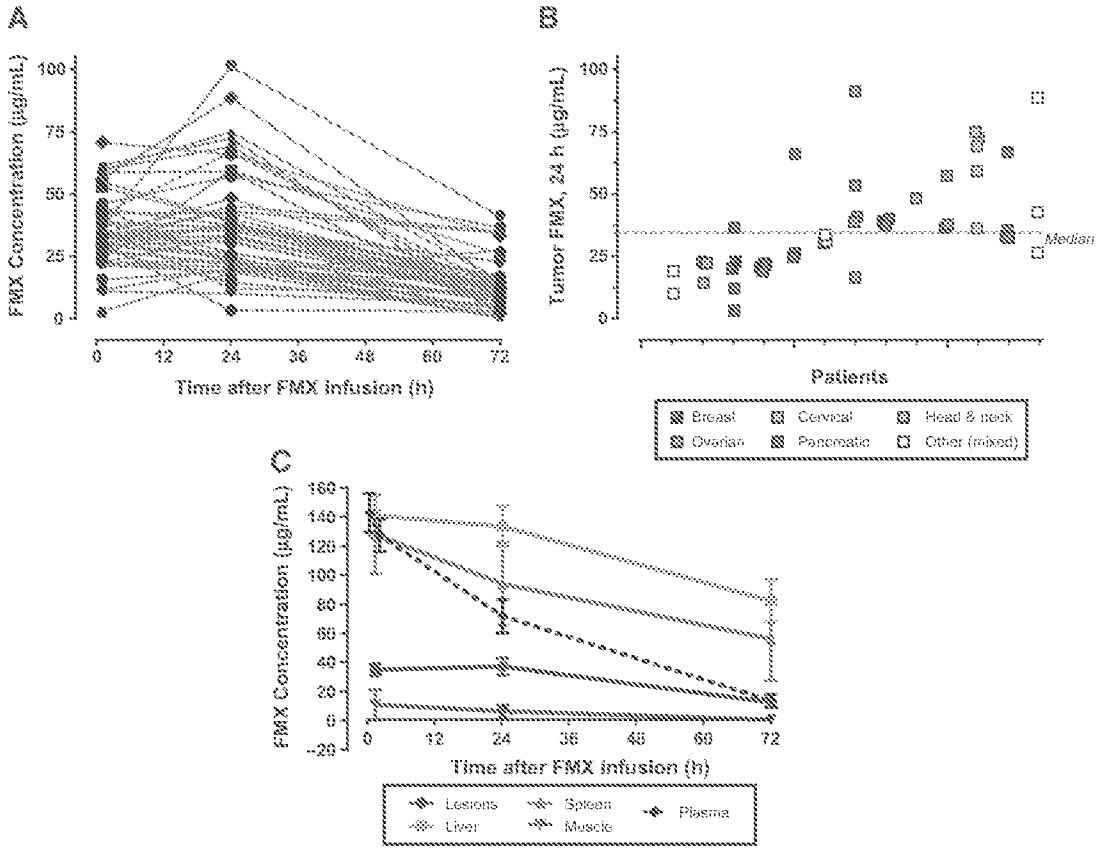

Figure 3.

FMX concentration in lesions. **A,** Time-course of FMX concentration in tumor lesions 1 hour, 24 hours, and 72 hours after FMX injection. **B,** Extrapolated tumor FMX concentrations per individual patient data at 24 hours. **C,** Average FMX kinetics in tumor lesions ($n = 46$) and comparison with liver and spleen clearance organs ($n = 11$) and normal tissue ($n = 13$) as well as plasma pharmacokinetics ($n = 14$). Error bars, 95%CI.

levels in plasma increased from a median concentration of 267 ng/mL (range, 45–1,481 ng/mL) during patient screening to 691 ng/mL (range, 430–1,730 ng/mL) at day 4 after FMX injection. One month later, levels declined to the previously observed baseline with median concentrations of 238 ng/mL (range, 115–775 ng/mL).

Pharmacokinetic modeling of FMX

The multicompartmental pharmacokinetic model described lesion-specific data well, with the exception of a single patient, and captured signal characteristics from regions of interest for either whole lesions or lesion subregions chosen to represent areas of high permeability/high retention (Fig. 2B) or low permeability/low retention (Supplementary Fig. S3A). The FMX lesion values measured at 1 hour following injection correlated best with the permeability parameter (PS_m or K^{trans}) with $R^2 = 0.750$ (Fig. 2C). The extravascular volume fraction (ratio between the inward and outward permeability-surface products) correlated best with FMX lesion values measured at 24 hours following injection ($R^2 = 0.833$; Fig. 2D). In contrast, permeability-related parameters did not correlate with FMX lesion values measured after 72 hours. However, the tissue binding site parameter contributed weakly to the FMX lesion levels at 72 hours ($R^2 = 0.425$; Supplementary Fig. S3B) but showed no correlation ($R^2 = 0.000$) to the 1-hour and 24-hour FMX lesion signals. The estimated K^{trans} values of FMX, averaged for each of the 13 evaluable patients, were greater than those of liposomes, consistent with the expectation of greater permeability of the smaller FMX nanoparticle relative to nal-IRI (18, 38).

FMX distribution and irinotecan levels in biopsies

Staining of serial tumor sections demonstrated deposition of FMX in macrophage-rich regions of vascular-accessible stromal areas located around tumor nests (Fig. 4A). This was particularly evident in liver lesions in which the regular pattern of Kupffer cells was replaced by a higher density of CD68-positive cells in the stromal area around tumor nests. Prussian blue staining of iron was seen in Kupffer cells, which provides an indirect assessment of FMX deposition. The strongest staining overlapped with accumulation of CD68-positive cells in stromal areas (Fig. 4B; Supplementary Fig. S4). Prussian blue signals were observed in biopsies at both 72 hours and 168 hours after FMX administration.

Irinotecan levels, averaged from 2 separate biopsy locations in the same tumor lesion, showed a statistically nonsignificant correlation to the corresponding permeability associated FMX signals at 1 hour (Fig. 4C) and 24 hours (Fig. 4D), respectively

Published OnlineFirst February 3, 2017; DOI: 10.1158/1078-0432.CCR-16-1990

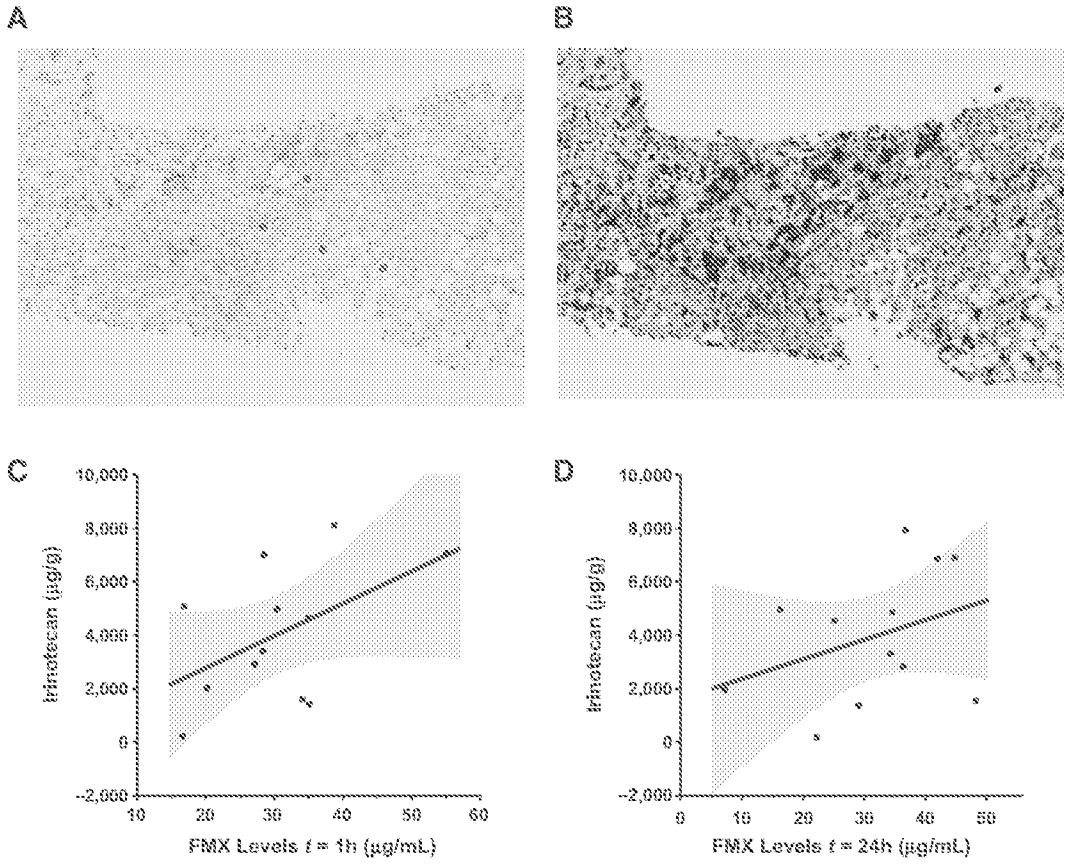

Figure 4.

Macrophage and iron staining in tumor biopsies. **A** and **B**, Serial tumor sections from FFPE biopsies of liver lesions were stained for FMX (Prussian blue; **A**) and macrophages (CD68; **B**). FMX deposition is detectable primarily in vascular-accessible macrophages in stromal areas surrounding tumor lesions. **C** and **D**, Relationship between lesion FMX concentrations measured at 1 hour (**C**) or 24 hours (**D**) with the average irinotecan concentrations measured in the biopsies.

[Spearman $\rho = 0.4266$ ($P = 0.1667$) at 1 hour; 0.3706 ($P = 0.2356$) at 24 hours; 0.1608 ($P = 0.6175$) at 72 hours]. Irinotecan levels in biopsies showed median differences of 2.22× (range, 1.01–9.06; $n = 13$) between different biopsy locations for each patient, and 2.29× differences (range, 1.10–5.71, $n = 6$) for consecutive passes in the same lesion. Average biopsy pass levels of irinotecan in tumor lesions represented 0.14%–6.07% of the injected dose of nal-IRI per kilogram of tissue at 72 hours and were 21.1% lower than the corresponding plasma levels.

Lesion response

Lesion averages of irinotecan levels showed a strong and significant correlation to the time on treatment for each patient (Supplementary Fig. S5; Spearman's $\rho = 0.7824$, $P = 0.0016$). There was also a positive trend between FMX lesion values and irinotecan levels. We therefore evaluated if FMX lesion values also correlated with response characteristics at the lesion level.

Response assessments from CT imaging (see Supplementary Fig. S2B as example) were available from 9 patients for at least 1 evaluation at 8 weeks after the start of treatment. For 4 patients more than 1 assessment was available. Six of 33 lesions were classified as responders as assessed by a decrease of the longest diameter of 30% or more, and 10 lesions were classified as responders as assessed by volume decreases of 50% or more. Fourteen lesions (42%) had decreased in diameter during at least 1 assessment interval. CT image density changes did not correlate with changes in diameter or volume of lesions.

For the subset of CT-evaluable lesions for which FMX-MRI was available ($n = 31$), the median FMX levels were 34.1 µg/mL measured approximately 1 hour after FMX injection, 33.6 µg/mL after 24 hours, and 9.8 µg/mL after 72 hours. Individual lesions were classified on the basis of FMX levels as either below or above the median of all lesion values at that time point. FMX levels at 1 hour (Fig. 5A) and 24 hours (Fig. 5B) after FMX injection were significantly associated with better lesion responses as measured by best change in lesion size ($P < 0.0001$ at 1 hour; $P < 0.003$ at 24 hours); no relationship was observed at 72 hours ($P = 0.83$; data not shown). Lesion responses measured at the earliest available posttreatment CT imaging at 8 weeks showed a similar statistical significance for this association ($P = 0.0001$ at 1 hour; $P < 0.003$ at 24 hours; data not shown). Receiver operating characteristics for lesion classification according to 2 separate thresholds for lesion size reduction, namely lesion shrinkage (best lesion size change

Published OnlineFirst February 3, 2017; DOI: 10.1158/1078-0432.CCR-16-1990

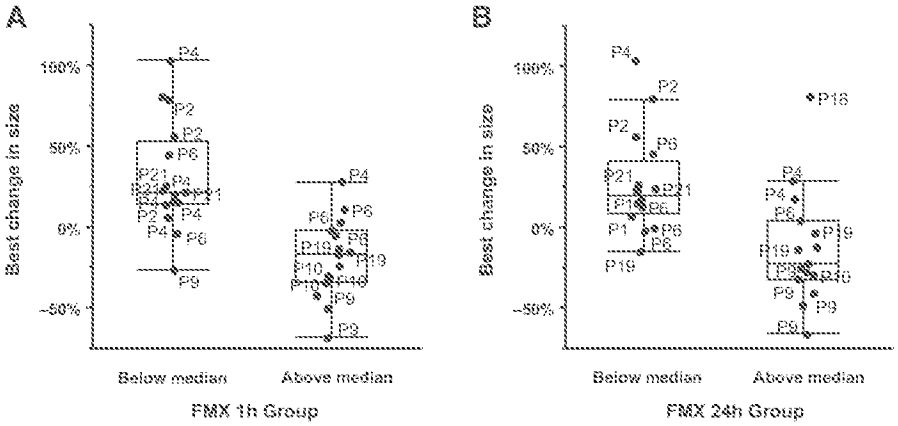

Figure 5.
FMX signal in lesion correlates with lesion size change. FMX signals at 1 hour (**A**) or 24 hours (**B**) are grouped relative to the median value observed in the evaluable lesions (9 patients, 31 lesions) and compared with the best change in lesion size seen with RECIST CT.

<0%) and partial response (best lesion size change ≤−30%), had an AUC ≥0.8 for early FMX measurements (i.e., 1 hour and 24 hours; Supplementary Fig. S6). This classification approach also performed slightly better with data from the 1-hour time point that correlated best with the inward permeability-surface product (PS_{in} or K^{trans}) parameter of FMX.

Discussion

This study provides a first clinical evaluation of using noninvasive imaging of a potential nanodiagnostic to evaluate lesion permeability characteristics as a surrogate measure for the effectiveness of a subsequently dosed nanotherapeutic. In particular, we demonstrate the feasibility of an MRI method using the superparamagnetic iron oxide particle FMX to quantitatively assess tumor permeability properties in patients and relate it with lesion response to treatment with nal-IRI. Our results indicate that lesion FMX measurements at up to 24 hours strongly correlated with lesion-specific permeability parameters from a FMX mechanistic pharmacokinetic model. Lesion FMX levels at 72 hours correlated more with late binding events, likely corresponding to the observed Prussian blue staining overlapping with CD68 signals in stromal areas of tumor biopsies. This FMX-based evaluation can be implemented with a minimum of 2 imaging sessions, and its timing can be selected to emphasize distinct lesion characteristics of interest depending on the nanotherapeutic under investigation.

We analyzed the relationship between FMX levels in tumor lesions and nal-IRI activity, and found a statistically significant correlation between changes in lesion diameters and lesion-specific uptake of FMX at 1 and 24 hours after FMX administration. This suggests that lesion permeability to FMX may be a useful biomarker for tumor response to nal-IRI in patients with solid tumors and also indicates that EPR-driven initial deposition effects may correlate across different nanoparticle types. FMX and nal-IRI both displayed extended plasma circulation and are thought to share plasma clearance mechanisms such as interaction with the monocyte phagocytic system. Although patient-specific differences in the interaction of plasma proteins with these nanoparticles (39) may add confounding factors, this feasibility study was not powered to evaluate the effect of patient covariates, including ethnicity, sex, and age. Our results were based on data obtained from a small number of patients with multiple cancer types. If this relationship holds true in a larger population, it would suggest that deposition may be a dominant factor for response to nal-IRI in certain tumor types. The importance of lesion permeability for liposomal delivery has been shown in preclinical tumor models (15, 16).

We had also hypothesized that imaging of macrophage levels in tumor lesions may yield information about the drug retention of nal-IRI and associated drug conversion activities. This hypothesis was based on observations in preclinical models (25) that showed broad colocalization of FMX with liposomes in perivascular stromal areas as well as enrichment of both liposomes and FMX in host cells such as tumor-associated macrophages (TAM). For example, experiments in murine syngeneic or xenogeneic models have demonstrated that myeloid cells, particularly TAMs, accumulate the largest share (78%–94% depending on tumor model at 24 hours) of nal-IRI (40). Miller and colleagues (27) noted similar patterns of colocalization and predominant accumulation of FMX and nanoparticles in host cells, driven by the comparable extended circulating half-life of both nanoparticles and the EPR effect. Both nanoparticles take advantage of overlapping microvascular accessibility, even if deposition kinetics for FMX are faster and the distribution of the two nanoparticles within the perivascular space of the tumor can be more divergent on the cellular level. Notably, colocalization of FMX and a therapeutic nanoparticle improved at the lower spatial resolution found in clinical MRI (27). A surprising observation in this study is that late binding events identifiable by FMX-MRI at 72 hours did not correlate with lesion response in patients treated with nal-IRI. This is reminiscent of a previous report (26) in which liposomal deposition into tumors was shown to be independent of liposomal binding characteristics, whereas subsequent intratumoral biodistribution and cellular retention was affected. FMX measurements at 72 hours also had a lower signal-to-noise ratio, thus making stratification more difficult at that time point. For clinical evaluation of binding events by FMX-MRI, imaging times between 24 and 72 hours may have to be explored.

Miller and colleagues (27) had suggested that when payload release from a nanocarrier is more rapid, its intratumoral distribution may be more dependent on vascular permeability and extracellular volume fraction. Nanoliposomal carriers are thought to release their payload either interstitially, possibly modulated by ammonia levels (41), or from cells after liposomal uptake and intracellular processing by target cells following ligand-mediated endocytosis or phagocytic cells such as macrophages in the case of passively-targeted liposomes such as nal-IRI (2, 4). In addition,

cellular release is likely to be affected by payload and/or metabolite physicochemical properties, including their polar surface area or interaction with cellular components. Preclinical results with nal-IRI indicated that bioavailability of the liposomal payload is likely not restricted to TAMs. Although liposomal deposition is nonuniform and perivascular, primarily in stromal areas, γH2AX staining at 24–72 hours after liposome dosing in a pancreatic orthotopic model was broadly seen across all tumor areas but not the stroma (42). Nanoliposomal carriers may thus exhibit comparably faster drug release rates than therapeutic nanoparticles with a more erosive, slower release mechanism (27, 43), which could possibly explain the lack of correlation between lesion response to nal-IRI and late binding events of FMX in this study.

R2 and R2* mapping are accepted clinical tools for evaluating tissue iron concentrations, both for iron overload disorders (44, 45) and for tracking of ultrasmall superparamagnetic iron oxide particles (18, 24, 46). To enable accurate lesion FMX assessments, baseline MRI signals were subtracted from later time points, and FMX phantom reference was used with all scans. Our R2* values for reference tissues at baseline and at 72 hours compared well with published values (44), despite differences in MRI acquisition parameters such as flip angle, repetition time, and slice thickness. The metabolism of FMX and compartmentalization within cells are potential confounding factors that may influence accurate quantitation of FMX levels in tumor lesions. Findings by Storey and colleagues (44) suggest that the magnetite core of FMX remains largely intact over 72 hours, the time scale of our study. Therefore, FMX metabolism is not expected to greatly influence measurements with tumor lesions. FMX degradation (44, 47) will result in a corresponding decrease in the R2* signal, as the magnetic moment of ferritin is far smaller than that of FMX. Compartmentalization of iron oxide particles after phagocytic uptake into macrophages can double R2* (48, 49) and may thus counteract any loss of signal due to partial degradation of FMX particles during the imaging period (36, 44, 47). The effects of compartmentalization may also lead to an overestimation of FMX levels particularly at late time points, although this error contribution is thought to be relatively uniform across a patient population. Subtraction of baseline MRI signal proved to be important: baseline R2* values were variable, and the correlation with response to nal-IRI was not significant without correcting for baseline signal in this patient population. Inclusion of a FMX phantom reference allowed transformation of R2* values to FMX concentrations and also served as an MRI quality control. Furthermore, the inclusion of a phantom reference is potentially important for expanding to multiple sites and MRI scanners that have capabilities of acquiring T2* sensitive sequences by a variety of methods including FSPGR acquisition series and multiecho multislice gradient-echo (mGRE) sequences. The now recommended extended infusion schedule of FMX (29) is not expected to affect current strategies of image data analysis because the duration of administration is still small relative to the extended half-life and, thus, deposition time frame of FMX.

Lesion response is dependent not only on sufficient deposition and distribution of the payload but also on appropriate conversion to SN-38 and chemosensitivity of tumor cells, confounding factors adding to response variability in patients and not interrogated with this FMX imaging approach. This study did not address whether treatment with nal-IRI may potentially modify delivery characteristics for later treatment cycles. However, initial response characteristics of tumor lesions appear sufficiently representative of the overall treatment response in the current study. We observed a strong and significant correlation between average irinotecan levels in lesions and the time on treatment for each patient. Furthermore, the concentrations of irinotecan measured in biopsies at 72 hours after administration of nal-IRI were far higher than could be accounted for by microcirculatory levels for total irinotecan and its liposomal encapsulation (15, 50), consistent with intratumoral deposition of nal-IRI. The composition of nal-IRI precluded any direct IHC-based analysis of the liposomal distribution in post-treatment FFPE samples from our patients. Preclinical findings (15) had suggested that irinotecan levels at 72 hours may be used as a surrogate measure for nal-IRI permeability. The limited correlation between irinotecan and FMX levels in tumor biopsies is likely due to the fact that biopsy location and region selection on MRI and CT images could only be approximated in this study and that the biopsy needle with an inner diameter of 0.838 mm was 1/7th of the MRI slice thickness. Punch biopsies may be better suited for evaluating liposome and FMX deposition, but this is only amenable to a surgical setting.

This study demonstrated that the EPR effect, as measured by FMX-MRI, is highly variable in a diverse patient cohort with solid tumors. Furthermore, variability was observed not only across patients, but also across individual lesions within a patient. The observation that FMX delivery correlated with response to treatment with nal-IRI at the lesion level suggests the potential significance of this finding. However, individual lesion responses may not directly translate into patient-specific outcomes, and the integration of permeability characteristics across multiple patient lesions requires further investigation. Presumably, sufficient delivery is required to most, if not all, lesions within a patient to successfully treat disease. This variability highlights a key challenge in successful therapy with nanotherapeutic agents. FMX-MRI is a promising, novel noninvasive biomarker that may predict responsiveness to therapeutic nanoparticles in general and nal-IRI therapy as indicated in this study. Further development using this approach continues in the expansion phase of a study in patients with metastatic breast cancer (31).

Disclosure of Potential Conflicts of Interest

R. Korn is a consultant/advisory board member for ImaginAB. J.C. Sachdev reports receiving commercial research grants from Celgene and Pfizer Inc, and is a consultant/advisory board member for Celgene. D.C. Drummond and J.B. Fitzgerald hold ownership interest (including patents) in Merrimack Pharmaceuticals. No potential conflicts of interest were disclosed by the other authors.

Authors' Contributions

Conception and design: R.K. Ramanathan, R. Korn, S.G. Klinz, D.C. Drummond, E. Bayever, J.B. Fitzgerald

Development of methodology: R.K. Ramanathan, R. Korn, N. Raghunand, J. Prey, S.G. Klinz, J. Kim, E. Bayever

Acquisition of data (provided animals, acquired and managed patients, provided facilities, etc.): R.K. Ramanathan, R. Korn, J.C. Sachdev, R.C. Newbold, C. Jameson, J. Cain, E. Bayever

Analysis and interpretation of data (e.g., statistical analysis, biostatistics, computational analysis): R.K. Ramanathan, R. Korn, N. Raghunand, J.C. Sachdev, C.J. Fetterly, S.G. Klinz, J. Kim, J. Cain, B.S. Hendriks, E. Bayever, J.B. Fitzgerald

Writing, review, and/or revision of the manuscript: R.K. Ramanathan, R. Korn, N. Raghunand, J.C. Sachdev, C. Jameson, C.J. Fetterly, S.G. Klinz, J. Kim, J. Cain, B.S. Hendriks, D.C. Drummond, E. Bayever, J.B. Fitzgerald

Administrative, technical, or material support (i.e., reporting or organizing data, constructing databases): J. Kim

Study supervision: R.K. Ramanathan, E. Bayever, J.B. Fitzgerald

Acknowledgments

We thank the patients and their families for their incredible help. We thank Daniel D. Von Hoff for his support of nal-IRI and his interest in this study. We thank all clinical staff who assisted with the study, especially Katie Marceau, Vickie Marsh, and Sam Ejadi, of the Virginia G. Piper Cancer Center, Scottsdale, Arizona, and radiologists John M. Neil and Gavin P. Stetbaug, of Imaging Endpoints. Brynne Crowell, Linda Vocila, and Linda Bavisotto of TGen Drug Development provided study support. Kimberly Clark, of Roswell Park Cancer Institute, Buffalo, New York, supported the biopsy metabolite studies. Among the supporting staff at Merrimack Pharmaceuticals, Aurelie Bouzelmat and Sarah Blanchette managed the study, Jon Tate and Victor Moyo provided additional study support, and Ashish Kalra, Nancy Paz, Helen Lee, Omid Ghasemi, and Walid Kamoun participated in reviews, brainstorming, and discussions. We thank Ulrik B. Nielsen for his vision and support of nal-IRI and this study. Editorial assistance was provided by Payal Gandhi of ApotheCom.

Grant Support

This work was supported by Merrimack Pharmaceuticals, Inc. The LC/MS-MS analysis was conducted by the Bioanalytics, Metabolomics and Pharmacokinetics (BMPK) Shared Resource of Roswell Park Cancer Institute, which is partially supported by National Cancer Institute (NCI) grant P30CA016056.

The costs of publication of this article were defrayed in part by the payment of page charges. This article must therefore be hereby marked *advertisement* in accordance with 18 U.S.C. Section 1734 solely to indicate this fact.

Received August 11, 2016; revised January 19, 2017; accepted January 20, 2017; published OnlineFirst February 3, 2017.

References

1. Drummond DC, Meyer O, Hong K, Kirpotin DB, Papahadjopoulos D. Optimizing liposomes for delivery of chemotherapeutic agents to solid tumors. Pharmacol Rev 1999;51:691–743.
2. Drummond DC, Noble CO, Hayes ME, Park JW, Kirpotin DB. Pharmacokinetics and in vivo drug release rates in liposomal nanocarrier development. J Pharm Sci 2008;97:4696–740.
3. Maeda H, Wu J, Sawa T, Matsumura Y, Hori K. Tumor vascular permeability and the EPR effect in macromolecular therapeutics: a review. J Control Release 2000;65:271–84.
4. Bertrand N, Wu J, Xu X, Kamaly N, Farokhzad OC. Cancer nanotechnology: the impact of passive and active targeting in the era of modern cancer biology. Adv Drug Deliv Rev 2013;66:2–25.
5. Harrington KJ, Mohammadtaghi S, Uster PS, Glass D, Peters AM, Vile RG, et al. Effective targeting of solid tumors in patients with locally advanced cancers by radiolabeled pegylated liposomes. Clin Cancer Res 2001;7:243–54.
6. Hobbs SK, Monsky WL, Yuan F, Roberts WG, Griffith L, Torchilin VP, et al. Regulation of transport pathways in tumor vessels: role of tumor type and microenvironment. Proc Natl Acad Sci U S A 1998;95:4607–12.
7. Lammers T, Kiesse LY, Storm G, Kiessling F. Personalized nanomedicine. Clin Cancer Res 2012;18:4889–94
8. Baetke SC, Lammers T, Kiessling F. Applications of nanoparticles for diagnosis and therapy of cancer. Br J Radiol 2015;88:20150207.
9. Shields AF, Siegel BA, Miller KD, Munster PN, Ma C, Lee H, et al. Quantification of 64Cu-MM-302 liposome biodistribution and lesion deposition kinetics using PET/CT imaging in advanced breast cancer patients. WMIC 2014;13–88 109.
10. Drummond DC, Noble CO, Guo Z, Hong K, Park JW, Kirpotin DB. Development of a highly active nanoliposomal irinotecan using a novel intraliposomal stabilization strategy. Cancer Res 2006;66:3271–7.
11. Onivyde [package insert]. Cambridge, MA: Merrimack Pharmaceuticals, Inc; 2015.
12. Wang-Gillam A, Li C, Bodoky G, Dean A, Shan YS, Jameson G, et al. Nanoliposomal irinotecan with fluorouracil and folinic acid in metastatic pancreatic cancer after previous gemcitabine-based therapy (NAPOLI-1): a global, randomised, open-label, phase 3 trial. Lancet 2016;387:545–57
13. Pommier Y. Topoisomerase I inhibitors: camptothecins and beyond. Nat Rev Cancer 2006;6:789–802.
14. Chabot GG. Clinical pharmacokinetics of irinotecan. Clin Pharmacokinet 1997;33:245–59.
15. Kalra AV, Kim J, Klinz SG, Paz N, Cain J, Drummond DC, et al. Preclinical activity of nanoliposomal irinotecan is governed by tumor deposition and intratumor pro-drug conversion. Cancer Res 2014;74:7003–13.
16. Hendriks BS, Reynolds JG, Klinz SG, Cetetti E, Lee H, Leonard SC, et al. Multiscale kinetic modeling of liposomal doxorubicin delivery quantifies the role of tumor and drug-specific parameters in local delivery to tumors. CPT Pharmacometrics Syst Pharmacol 2012;1:e15.
17. Karathanasis E, Chan L, Karumbaiah L, McNeeley K, D'Orsi CJ, Annapragada AV, et al. Tumor vascular permeability to a nanoprobe correlates to tumor-specific expression levels of angiogenic markers. PLoS One 2009;4:e5843
18. Daldrup-Link HE, Shames DM, Wendland M, Okuhata Y, Link TM, Rosenau W, et al. Correlation of dynamic contrast-enhanced magnetic resonance imaging with histologic tumor grade: comparison of macromolecular and small-molecular contrast media. Pediatr Radiol 1998; 28:67–78.
19. Turetschek K, Preda A, Novikov V, Brasch RC, Weinmann HJ, Wunderbaldinger P, et al. Tumor microvascular changes in antiangiogenic treatment: Assessment by magnetic resonance contrast media of different molecular weights. J Magn Reson Imaging 2004;20:138–44.
20. Jensen GM, Bunch PB. Conventional liposome performance and evaluation: lessons from the development of Vescan. J Liposome Res 2007; 17:121–37.
21. Lee H, Zheng J, Gaddy D, Ozturk KD, Leonard S, Ceretti E, et al. A gradient-loadable ^{64}Cu-chelator for quantifying tumor deposition kinetics of nanoliposomal therapeutics by positron emission tomography. Nanomedicine 2015;11:155–65.
22. Izaguirre EW, Sun M, Drummond DC, Kirpotin DB, Funk T, Thompson S, et al. SPECT-CT study of directed drug delivery using In-111 labeled liposomes in a murine mammary carcinoma model. IEEE Nuclear Science Symposium Conference Record 2005;4:1965–8.
23. Neuwelt EA, Hamilton BE, Varallyay CG, Rooney WR, Edelman RD, Jacobs PM, et al. Ultrasmall superparamagnetic iron oxides (USPIOs): a future alternative magnetic resonance (MR) contrast agent for patients at risk for nephrogenic systemic fibrosis (NSF)? Kidney Int 2009; 75:465–74.
24. Hamilton BE, Nesbit GM, Dosa E, Gahramanov S, Rooney B, Nesbit EG, et al. Comparative analysis of ferumoxytol and gadoteridol enhancement using T1- and T2-weighted MRI in neuroimaging. AJR Am J Roentgenol 2011;197:981–8.
25. Kalra A, Spetnyak J, Kim J, Kamoun W, Sengooba A, Klinz SG, et al. Magnetic resonance imaging with an iron oxide nanoparticle demonstrates preclinically the feasibility of predicting intratumoral uptake and activity of MM-398, a nanoliposomal irinotecan (nal-IRI). Cancer Res 2014;74(19 suppl):2065.
26. Kirpotin DB, Drummond DC, Shao Y, Shalaby MR, Hong K, Nielsen UB, et al. Antibody targeting of long-circulating lipidic nanoparticles does not increase tumor localization but does increase internalization in animal models. Cancer Res 2006;66:6732–40.
27. Miller MA, Gadde S, Pfirschke C, Engblom C, Sprachman MM, Kohler RH, et al. Predicting therapeutic nanomedicine efficacy using a companion magnetic resonance imaging nanoparticle. Sci Transl Med 2015;7: 314ra183.
28. Pohlmann A, Kaczewski P, Ku M-C, Dietinger B, Waiczies H, Wisbrun N, et al. Cerebral blood volume estimation by ferumoxytol-enhanced steady-state MRI at 9.4 T reveals microvascular impact of α1-adrenergic receptor antibodies. NMR Biomed 2014;27:1085–93.
29. Feraheme (ferumoxytol injection) [package insert]. Waltham, MA: AMAG Pharmaceuticals, Inc.; 2009–2015.
30. Daldrup-Link HE, Golovko D, Ruffel B, Denardo DG, Castaneda R, Ansari C, et al. MRI of Tumor-associated macrophages with clinically applicable iron oxide nanoparticles. Clin Cancer Res 2011;17: 5695–704.

31. Merrimack Pharmaceuticals. Pilot study to determine biodistribution of MM-398 and feasibility of ferumoxytol as a tumor imaging agent. In: ClinicalTrials.gov [Internet]. Bethesda (MD): National Library of Medicine (US); 2000[cited 2016 Nov 01]. Available from: http://www.clinicaltrials.gov/ct2/show/NCT01770353.
32. Mitchell MD, Kundel HL, Axel L, Joseph PM. Agarose as a tissue equivalent phantom material for NMR imaging. Magn Reson Imaging 1986;4:263–6.
33. Koay EJ, Truty MJ, Cristini V, Thomas RM, Chen R, Chatterjee D, et al. Transport properties of pancreatic cancer describe gemcitabine delivery and response. J Clin Invest 2014;124:1525–36.
34. Miller JC, Pien HH, Sahani D, Sorensen AG, Thrall JH. Imaging angiogenesis: applications and potential for drug development. J Natl Cancer Inst 2005;97:172–87.
35. Roy AC, Park SR, Cunningham D, Kang YK, Chao Y, Chen LT, et al. A randomized phase II study of PEP02 (MM-398), irinotecan or docetaxel as a second-line therapy in patients with locally advanced or metastatic gastric or gastro-oesophageal junction adenocarcinoma. Ann Oncol 2013;24:1567–73.
36. Landry R, Jacobs PM, Davis R, Shenouda M, Bolton WK. Pharmacokinetic study of ferumoxytol: a new iron replacement therapy in normal subjects and hemodialysis patients. Am J Nephrol 2005;25:408–10.
37. Pai AB, Nielsen JC, Kausz A, Miller P, Owen IS. Plasma pharmacokinetics of two consecutive doses of ferumoxytol in healthy subjects. Clin Pharmacol Ther 2010;88:237–42.
38. Schmidt MM, Wittrup KD. A modeling analysis of the effects of molecular size and binding affinity on tumor targeting. Mol Cancer Ther 2009;8:2861–71.
39. Caracciolo G, Farokhzad OC, Mahmoudi M. Biological identity of nanoparticles in vivo: clinical implications of the protein corona. Trends Biotechnol. 2016Sep 20. [Epub ahead of print]
40. Kalra AV, Kim J, Klinz SG, Paz N, Peutt J, Patel J, et al. The tumor microenvironment modulates the delivery and activation of liposomal encapsulated irinotecan, MM-398. Cancer Res 2013;73(8 suppl):5622.
41. Silverman L, Barenholz Y. In vitro experiments showing enhanced release of doxorubicin from Doxil® in the presence of ammonia may explain drug release at tumor site. Nanomedicine 2015;11:1841–50.
42. Klinz S, Zheng J, De Souza R, Ventura M, Paz N, Hedley D, et al. Nanoliposomal irinotecan (nal-IRI) is an active treatment and reduces hypoxia as measured through longitudinal imaging using [18F] FAZA-PET in an orthotopic patient-derived tumorgraft model of pancreatic cancer. Poster #B47, presented at: Pancreatic Cancer: Advances in Science and Clinical Care; May 12–15, 2016; Orlando, FL.
43. Miller MA, Zheng Y-R, Gadde S, Pfirschke C, Zope H, Engblom C, et al. Tumour-associated macrophages act as a slow-release reservoir of nano-therapeutic Pt(IV) pro-drug. Nat Commun 2015;6:8692.
44. Storey P, Lim RP, Chandarana H, Rosenkrantz AB, Kim D, Stoffel DR, et al. MRI assessment of hepatic iron clearance rates after USPIO administration in healthy adults. Invest Radiol 2012;47:717–24.
45. Hernando D, Levin YS, Sirlin CB, Reeder SB. Quantification of liver iron with MRI: state of the art and remaining challenges. J Magn Reson Imaging 2014;29:997–1003.
46. Hedgire SS, Mino-Kenudson M, Elmi A, Thayer S, Fernandez-Del Castillo C, Harisinghani MG. Enhanced primary tumor delineation in pancreatic adenocarcinoma using ultrasmall super paramagnetic iron oxide nanoparticle-ferumoxytol: an initial experience with histopathologic correlation. Int J Nanomedicine 2014;9:1891–6.
47. Briley-Saebo KC, Johansson LO, Hustvedt SO, Haldorsen AG, Bjerkerud A, Fayad ZA, et al. Clearance of iron oxide particles in rat liver: effect of hydrated particle size and coating material on liver metabolism. Invest Radiol 2006;41:560–71.
48. Kuhlpeter R, Dahnke H, Matuszewski L, Persigehl T, von Wallbrunn A, Allkemper T, et al. R2 and R2' mapping for sensing cell-bound superparamagnetic nanoparticles: in vitro and murine in vivo testing. Radiology 2007;245:449–57.
49. Girard OM, Ramirez R, McCarty S, Mattrey RF. Toward absolute quantification of iron oxide nanoparticles as well as cell internalized fraction using multiparametric MRI. Contrast Media Mol Imaging 2012;7:411–7.
50. Chang TC, Shiah HS, Yang CH, Yeh KH, Cheng AL, Shen BN, et al. Phase I study of nanoliposomal irinotecan (PEP02) in advanced solid tumor patients. Cancer Chemother Pharmacol 2015;75:579–86.

AACR American Association for Cancer Research

Clinical Cancer Research

Correlation between Ferumoxytol Uptake in Tumor Lesions by MRI and Response to Nanoliposomal Irinotecan in Patients with Advanced Solid Tumors: A Pilot Study

Ramesh K. Ramanathan, Ronald L. Korn, Natarajan Raghunand, et al.

Clin Cancer Res 2017;23:3638-3648. Published OnlineFirst February 3, 2017.

Lesion characterization with ferumoxytol MRI in patients with advanced solid tumors and correlation with treatment response to MM-398, nanoliposomal irinotecan (nal-IRI)

Ramesh K. Ramanathan[1], Ronald L. Korn[2], Jasgit C. Sachdev[1], Gerald J. Fetterly[3], Gayle Jameson[1], Katie Marceau[1], Vickie Marsh[1], Natarajan Raghunand[4], Joshua Prey[3], Stephan G. Klinz[5], Jaeyeon Kim[5], Eliel Bayever[5], Jonathan B. Fitzgerald[5]

[1]Virginia G Piper Cancer Center, Scottsdale [1]Virginia G Piper Cancer Center, Scottsdale Healthcare, Scottsdale, AZ; [2]Imaging Endpoints, Scottsdale, AZ; [3]Roswell Park Cancer Institute, Buffalo, NY;
[4]Translational Cancer Imaging, Arizona Cancer Center, Tucson, AZ; [5]Merrimack Pharmaceuticals, Inc., Cambridge, MA

Introduction

Purpose: Drug delivery of nanoliposomal irinotecan (nal-IRI) is dependent on deposition characteristics of the tumor lesion. We hypothesized that deposition characteristics of ferumoxytol (FMX) iron nanoparticles identified by quantitative MRI could define deposition of nal-IRI in tumor which would be related to its efficacy.

Experimental Design: Eligible patients (n=15) with previously treated solid tumors with progressive disease had MRI scans prior to and following (1, 24, 72 h) FMX infusion. Patients then received nal-IRI (80 mg/m2 q2w) until progression. After MRI acquisition, the R2* = 1/T2* signal was used to calculate FMX levels in plasma and tumor lesions by comparison to a standard curve. Tumor core biopsies were collected 72hr after ferumoxytol injection and again 72h after nal-IRI infusion, yielding two biopsies/lesion for each collection point.

Results: Ferumoxytol MRI was able to robustly quantify ferumoxytol levels in plasma as well as normal tissues and tumors. A mechanistic PK model built on these values indicated that tissue permeability to FMX contributed to early FMX MRI signals at 1 h and 24 h, while FMX binding contributed at 72 h. Higher FMX levels, when ranked relative to the median value observed in multiple evaluable lesions from 9 patients, were significantly associated with better lesion responses as measured FMX levels at early time points ($p<0.001$ at 1 h post-FMX; $p<0.003$ at 24 h post-FMX); no relationship was observed at with post-FMX levels at 72 h. Average CPT-11 drug levels in lesions correlated with patient's time on study ($\rho=0.7824$; $p=0.0016$).

Conclusions: The relationship between FMX levels in tumor lesions and nal-IRI activity suggests that lesion permeability to FMX may be a useful biomarker for tumor response to nal-IRI in patients with solid tumors.

CITS – Cross Indication Translational Study

Eligible patients with refractory solid tumors were recruited. PK samples for FMX were collected at 0.5h, 2h, 24h and 72h. PK samples for nal-IRI were collected at 1.5h, 3.5h, 72h and 168h. RECIST v1.1 evaluation was done every 8 weeks. 13 Patients received MM-398 q2w at 80mg/m^2. CT images at time of RECIST evaluation demonstrate reduction in tumor burden.

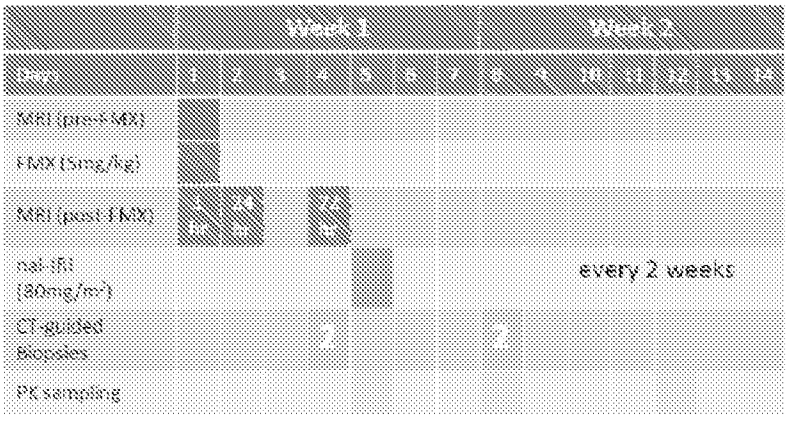

	All patients (n=13)
Age (median, range)	60 (28-80)
Gender: Male	4 (27%)
Gender: Female	11 (73%)
Race: Caucasian	14 (93%)
Race: African American	1 (7%)
Prior Gem	7 (47%)
Prior Oxa	8 (53%)
Prior Lines on Therapy (Median/Range)	4 (1-10)

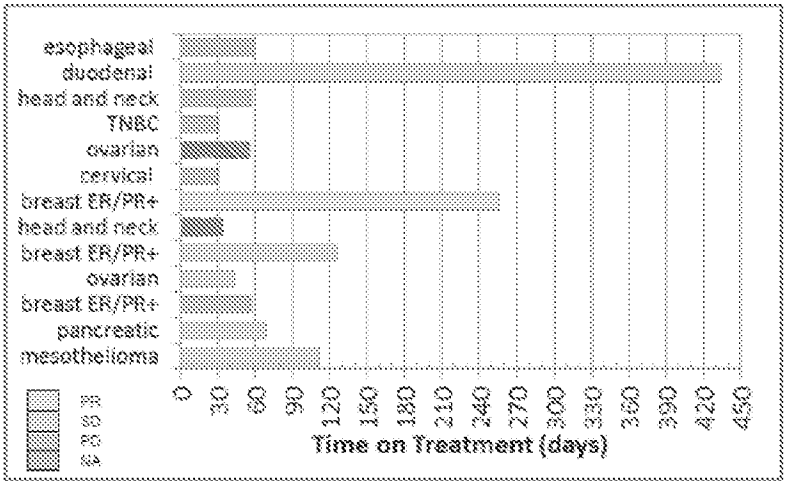

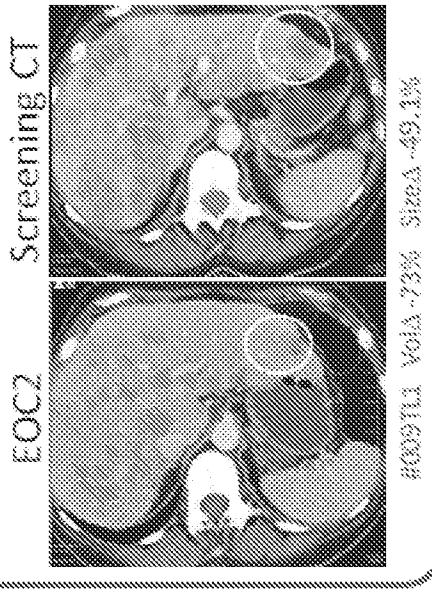

Ferumoxytol (FMX) is a slow-clearing ~~17-31~~ 23 nm size superparamagnetic iron oxide nanoparticle. FMX is approved for iron supplement in patients with chronic kidney disease and recently has been used as an MRI contrast agent (off-label).

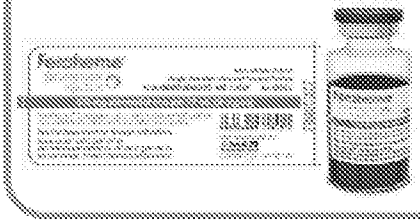

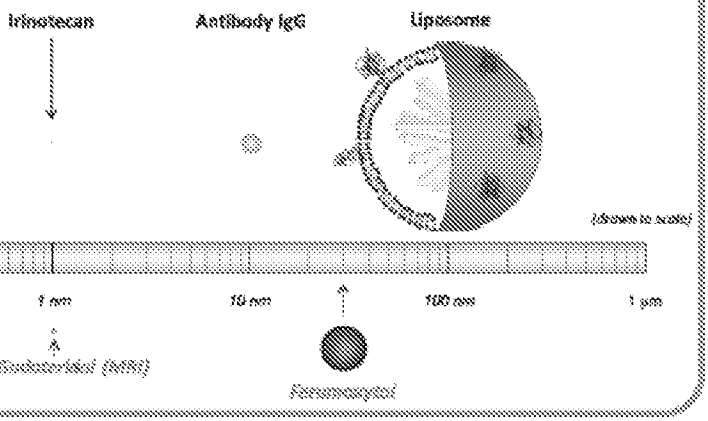

Ferumoxytol Imaging and Quantitation

MRI images were acquired on a GE 1.5T MRI instrument with a T1 FSPGR series with echo delay times from 1.5 – 13.2ms. Slice thickness and spacing was 6mmx1mm using a 256x256 matrix. T2* values were extrapolated from each image series by exponential fit of signal intensities. A phantom containing known FMX concentrations from 10 – 200µg/ml (A) was included during each MRI session and demonstrated a linear relationship between R2*=1/T2* and FMX levels (B). For each imaging series an R2* map was constructed (C). FMX levels were calculated for each post-injection time point (postFMX) after subtraction of baseline values (preFMX).

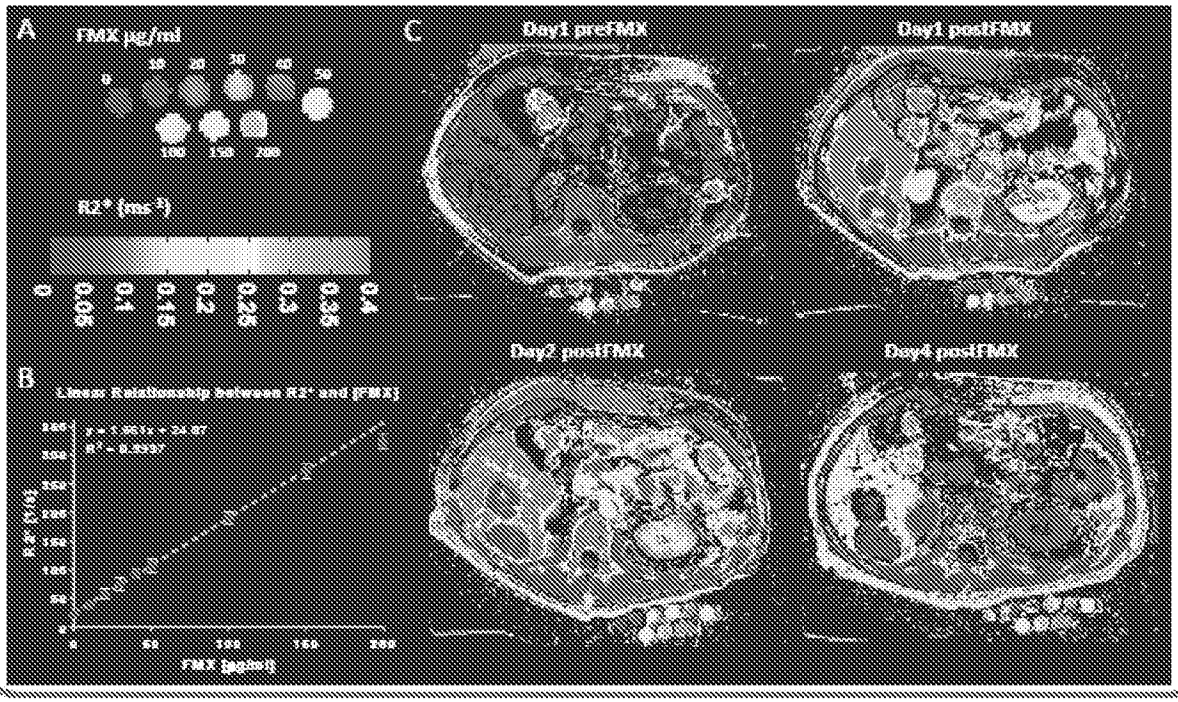

Ferumoxytol Lesion Concentration and Kinetics

(A) FMX levels were measured in individual lesions from all patients. Lesions within a patient often showed a similar range of uptake levels at 24h, and patients could also be ranked according to tumor FMX levels. Error bars are estimated. Median of all lesions (m) is indicated. (B) Average FMX kinetics in tumor lesions (n=46) and comparison to RES clearance organs (n=11) and normal tissue (n=13) as well as plasma samples (n=14).

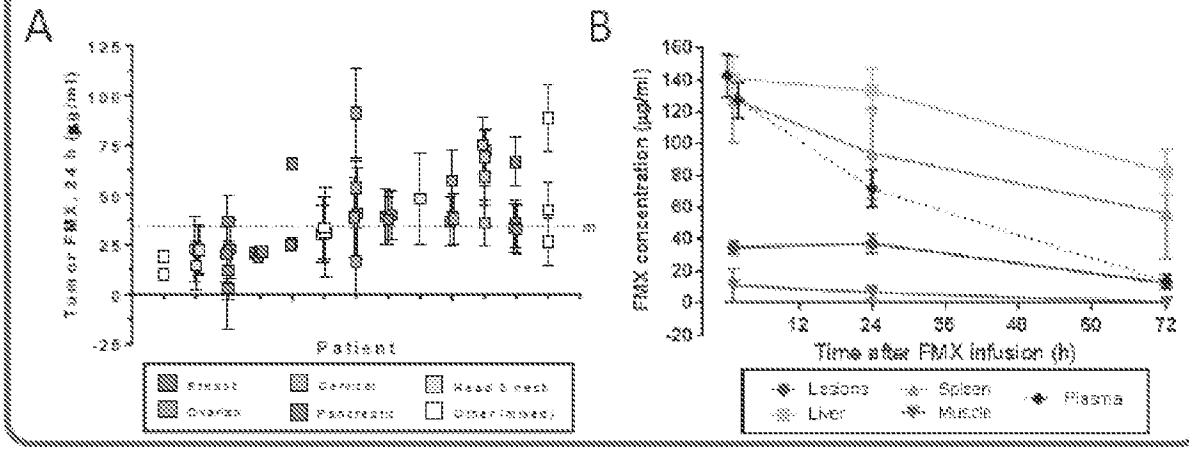

Pharmacokinetic Model of Ferumoxytol

A) FMX tumor PK model was developed by using SimBiology® toolbox in MATLAB®. B) FMX tumor PK model could quantify the degree of tissue permeability and FMX binding activity across all tumor lesions. C, D) Earlier FMX signals (1h and 24h) were explained by the model parameters related to vascular permeability.

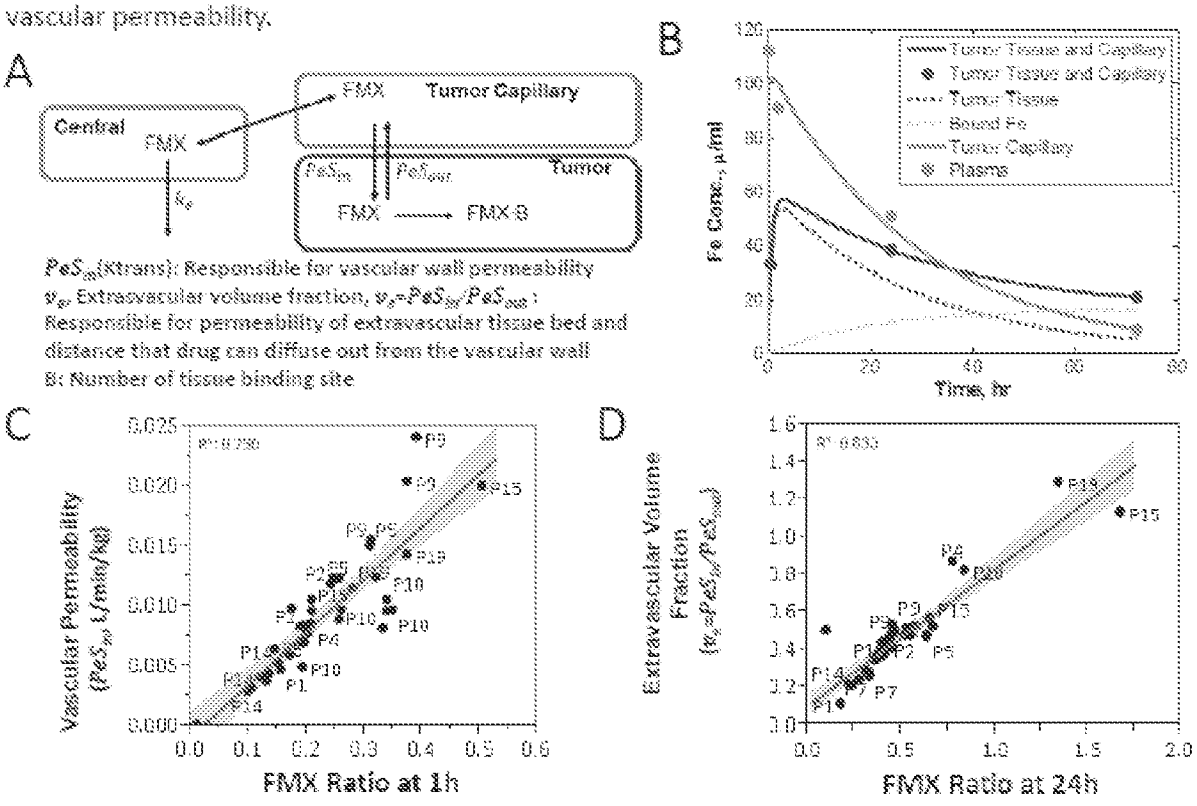

PeS_{in}(Ktrans): Responsible for vascular wall permeability

v_e: Extravascular volume fraction, $v_e = PeS_{in}/PeS_{out}$: Responsible for permeability of extravascular tissue bed and distance that drug can diffuse out from the vascular wall

B: Number of tissue binding site

Macrophage and Iron Signals in Tumor Biopsies

A, B) Serial tumor sections from FFPE biopsies of liver lesions were stained for FMX (Prussian Blue, PrB) (A) and Macrophages (CD68) (B). FMX deposition is detectable primarily in vascular-accessible macrophages in stromal areas surrounding lesions. C) The CPT-11 levels averaged from two separate biopsies only showed a moderate correlation to the corresponding FMX signals at 1h ($\rho = 0.4266$ $p = 0.1667$)

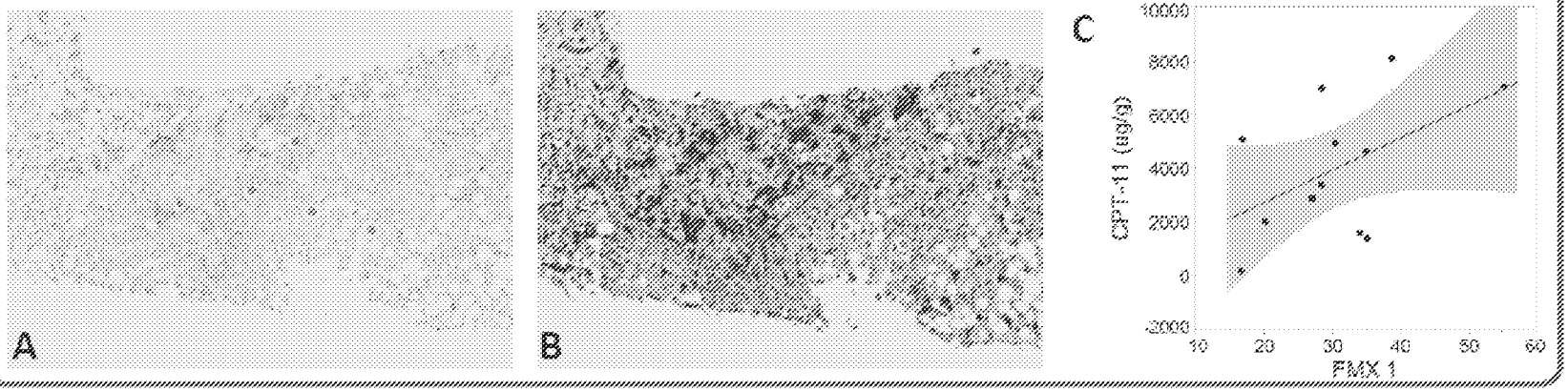

FMX Signal and Lesion Response Relationships

A) Correlation between patient's time on study and the average irinotecan concentration of the biopsied lesion of that patient (Spearman's r=0.7824; p=0.0016). Biopsies are obtained 72h after MM-398 infusion. Time on study is measured from the time of first MM-398 dose. B) FMX signal correlates with lesion size change. FMX signals at each respective time point are grouped relative to the median value observed in the evaluable lesions (9 patients, 31 lesions) and compared to the best change in lesion size seen with RECIST CT. Lesions with FMX levels (in µg/ml) above the population median showed a statistically significant reduction in individual lesion size at early timepoints (1h and 24h). No significant lesion response relationship was observed at 72h. Lesions from each patient were treated as independent samples.

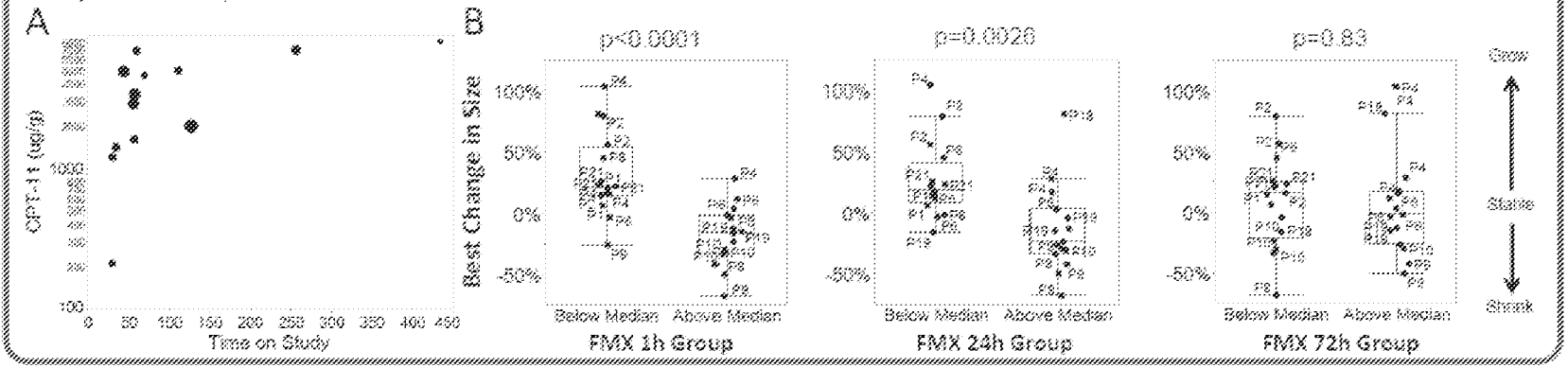

FMX Deposition and Plasma Clearance

Lesion FMX levels measured 72h after FMX injection correlate significantly with MM-398 plasma levels at 72 h ($\rho = 0.7133$; $p = 0.0092$) and also with FMX plasma levels at 72h ($\rho = 0.6154$; $p = 0.0332$; data not shown). This may indicate some overlap in the respective clearance processes for FMX and MM-398.

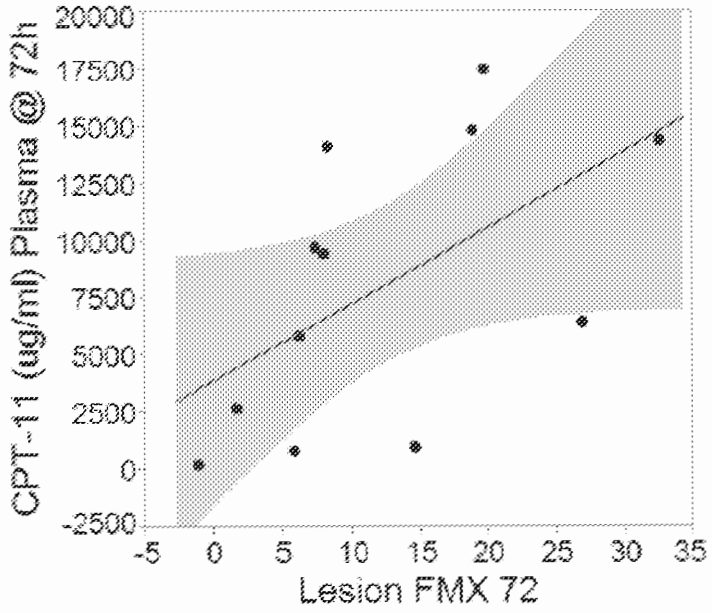

Summary and Conclusions

- This phase I study demonstrated the feasibility of incorporating ferumoxytol MRI into a clinical workflow
- Phantom evaluation shows that accurate estimates of tumor/tissue Fe concentrations can be obtained with T2* MRI based sequences
- FMX tumor PK model suggested that tumor permeability to FMX contributed to early FMX MRI signals at 1 h and 24 h, while FMX binding contributed at 72 h
- Significantly higher SN-38 levels in tumor suggested strong local conversion activity of nal-IRI. Drug and metabolite levels found in the tumor mass concur with pharmacokinetic modeling expectations [Not Shown Today]
- Prussian Blue staining of ferumoxytol is predominately observed at the stroma-tumor interface and coincides with vascular accessible macrophages
- Early FMX signals showed a significant relationship with lesion size change response suggesting the potential use as a diagnostic tool
- FMX and MM-398 may share clearance and deposition characteristics

Acknowledgements

We thank the patients and their families for their incredible support

Imaging Endpoints
Scottsdale, AZ
John M Hoi
Gavin P Gladney
Ronald G Newbold

Clinical Drug Development
Scottsdale, AZ
Vicky Baumschlag
Dayane Crowell
Linda Vocila
Lloyd Swisher

Merrimack
Cambridge, MA
Karen Campbell
Sarah Deschenes
Nancy M Gold
Chad Glowney
Kristi Kennedy
Nancy Lee
Yvette Rose
Aurelie Salvemini
Daryl Sampenzo
Ashish Sethi
Craig A Stevens
Jun Tan

Lesion characterization with ferumoxytol MRI in patients with advanced solid tumors and correlation with treatment response to MM-398, nanoliposomal irinotecan (nal-IRI)

Ramesh K. Ramanathan[1], Ronald L. Korn[2], Jasgit C. Sachdev[3], Gerald J. Fetterly[3], Gayle Jamieson[4], Katie Marceau[4], Vickie Marsh[4], Nataraj an Raghunand[4], Joshua Prey[2], Stephan G. Kunz[2], Jaeyeon Kim[2], Eliel Bayever[2], Jonathan B. Fitzgerald[2]

[1]Virginia G Piper Cancer Center, Scottsdale Healthcare, Scottsdale, AZ; [2]Imaging Endpoints, Scottsdale, AZ; [3]Roswell Park Cancer Institute, Buffalo, NY; [4]Translational Cancer Imaging, Arizona Cancer Center, Tucson, AZ; [5]Merrimack Pharmaceuticals, Inc., Cambridge, MA

260 POSTER

Hsp90 Inhibitor Drug Conjugates (HDC): Payloads and possibilities

D. Chimmanamada[1], W. Ying[2], J. Zhang[2], D. Proia[3], T. Przewloka[1], J. Jiang[1], D. Vutukuri[1], G. Lu[1], S. Osman[1], S. Chen[1], J. Chu[3], P. Rao[3], D. Zhou[3], T. Inoue[4], L. Shin Ogawa[4], R. Singh[4], N. Tatsuta[4], A. Sonderfan[4], C. Cortis[5]. [1]*Synta Pharmaceuticals, Chemistry, Lexington MA, USA;* [2]*Synta Pharmaceuticals, Chemistry, Lexington MA, USA;* [3]*Synta Pharmaceuticals, Biology, Lexington MA, USA;* [4]*Synta Pharmaceuticals, DMPK, Lexington MA, USA;* [5]*Synta Pharmaceuticals, Business Development, Lexington MA, USA*

Background: Despite the emergence of various therapies, chemotherapy still plays a significant role in the treatment of cancer. Though toxic, the potency and broad applicability of chemotherapeutic drugs make compelling rationale for using them as payloads in drug delivery systems. Several recent technologies, especially antibody drug conjugates (ADC) have been very successful, however for narrow sets of indications. We have recently disclosed the HSP90 inhibitor Drug Conjugate (HDC) platform, which utilizes the unique pharmacokinetic property of HSP90 inhibitors, where the drug is selectively retained in tumor in high concentrations while clearing from plasma and normal tissues relatively quickly. By combining the overexpression of HSP90 and longer residency of its inhibitors in tumor, we conceived an idea to conjugate small molecule anticancer drugs (payload) to HSP90 inhibitor in such a way that the payload is released selectively and gradually in tumor having a prolonged exposure.
Results: In this presentation, the rationale for payload selection, their applicability and preliminary assessments will be discussed. Though virtually any small molecule anticancer agent qualifies as payload for HDC technology, the expensive drug development paradigm calls for a strong rationale every time. It has been shown by multiple groups including us that a combination therapy of an HSP90 inhibitor with a suitable drug, such as docetaxel is superior compared to the single agent. Hence, the HDC of taxanes make sense. Other categories include but not limited to, are the drugs that have poor solid tumor penetration such as proteasome inhibitors, drugs that have poor pharmacokinetics (highly metabolized) such as gemcitabine and other antimetabolites, drugs that develop resistance due to efflux (e.g., pgp) from cancer cells such as camptothecins all make good payloads. Several cell cycle inhibitors, such as pan-CDK inhibitors and pan-PI3K inhibitors (such as staurorporine) are also considered.
A lead SN-38 conjugate for which detailed evaluations has been done showed that the payload is released in tumor for a prolonged period of time (0.22uM and 0.38uM at 24 h and72 h respectively in tumor against 30nM at 24 h and no drug quantified at 72 h for Irinotecan, at their maximum tolerated doses (MTDs). In vivo efficacy in multiple tumor models also exhibited remarkable activity for the HDC compared to Irinotecan. Toxicological evaluations also revealed that the HDC is safer than Irinotecan at their efficacious doses.
Conclusion: The HDC platform has the potential to utilize a number of commonly used small molecule anticancer agents as payloads; expanding applicability through improved efficacy and toxicity profiles. It also has the potential to resuscitate the development of drugs that were abandoned due to toxicity.

261 POSTER

Lesion characterization with ferumoxytol MRI in patients with advanced solid tumors and correlation with treatment response to MM-398, nanoliposomal irinotecan (nal-IRI)

R.K. Ramanathan[1], R.L. Korn[2], J.C. Sachdev[1], G.J. Fetterly[3], G. Jameson[1], K. Marceau[1], V. Marsh[1], N. Raghunand[4], J. Prey[3], S.G. Klinz[5], J. Kim[5], E. Bayever[5], J.B. Fitzgerald[5]. [1]*Scottsdale HealthcarelTGen, Virginia Piper Cancer Center, Scottsdale AZ, USA;* [2]*Imaging Endpoints, Scottsdale AZ, USA;* [3]*Roswell Park Cancer Institute, Buffalo NY, USA;* [4]*Arizona Cancer Center, Translational Cancer Imaging, Tucson AZ, USA;* [5]*Merrimack Pharmaceuticals, Inc., Cambridge MA, USA*

Introduction: MM-398, a nanoliposomal irinotecan (nal-IRI), is designed to exploit leaky vasculature for enhanced drug delivery to tumors. Deposition of nal-IRI and subsequent conversion to SN-38 in both neoplastic cells and tumor associated macrophages (TAM) may positively correlate with activity. Predictive biomarkers to measure tumor deposition could identify patients likely to benefit from nal-IRI. Ferumoxytol (FMX), a 30 nm iron-oxide nanoparticle with MRI contrast properties, is taken up by TAMs and has similar biodistribution patterns to nal-IRI in preclinical models. We have shown the feasibility of quantitative FMX MRI of tumor lesions and report here the correlation of FMX levels with nal-IRI activity in the study population.
Patients and Methods: Eligible patients (n = 15; 4M, 11F; median age 58 [28–80] years) with refractory solid tumors had FMX MRI scans prior to and following (1, 24, 72 h) FMX infusion. T2* signal was used to calculate FMX levels in plasma and lesions by comparison to a standard curve. A mechanistic PK model built on these values indicated that tissue permeability to FMX contributed to early FMX MRI signals at 1 h and 24 h, while FMX binding contributed at 72 h. Patients continued on nal-IRI at 80 mg/m^2 q2w until progression. Core biopsies were obtained 72 h after both FMX and nal-IRI infusions. RECIST v1.1 evaluation was done by CT every 8 weeks.
Results: 13/15 (87%) patients received nal-IRI, and 11/13 (85%) were evaluated for response with 1 (7%) partial response (PR), 5 (38%) stable disease and 5 (38%) progressive disease. FMX levels were measured in 31 lesions from 9 patients and compared to lesion size changes after nal-IRI treatment. Median FMX levels in tumor lesions at 1 h and 24 h were 34.1 and 33.6 mcg/mL, respectively. FMX levels above the median were significantly associated with better lesion responses as measured by change in lesion size ($p < 0.001$ at 1 h; $p < 0.003$ at 24 h); no relationship was observed at 72 h. Receiver operating characteristics for lesion classification according to PR or lesion size reduction had an AUC$\geqslant$ 0.8 for early FMX measurements. Levels of irinotecan and SN-38 averaged 3.73 mcg/g [0.13–12.75 mcg/g] and 14.67 ng/g [1.2–64.0 ng/g], respectively, at 72 h. SN-38 levels in biopsies were 5-fold higher than in plasma at 72 h ($p = 0.013$). Prussian Blue staining of ferumoxytol in biopsies was predominately observed at the stroma-tumor interface where it colocalized with TAMs.
Conclusions: Clinical activity of nal-IRI was observed in refractory solid tumors. Our findings are consistent with local activation of MM-398 in the tumor. The relationship between FMX levels in tumor lesions and nal-IRI activity suggests that lesion permeability to FMX may be a useful biomarker for tumor response to nal-IRI in patients with solid tumors.

262 POSTER

Improved cytotoxic activity of Nor-β-lapachone-loaded PLGA microcapsules in PC3M prostate cancer cell line

C. Pessoa[1], A.C.S. Feitosa[1], M.P. Costa[1], F.C. Evangelista[1], F.A.M. Sales[1], I.S. Bomfim[1], E.N. Silva Júnior[2], G.G. Dias[2], V.N. Freire[3], W.S. Caetano[4]. [1]*Ceara Federal University, Pharmacology and Physiology, Fortaleza, Brazil;* [2]*Minas Gerais Federal University, Chemistry, Fortaleza, Brazil;* [3]*Ceara Federal University, Physics, Fortaleza, Brazil;* [4]*Instituto Federal do Ceará, Physics, Fortaleza, Brazil*

Background: β-lapachone is one of the most widely studied naphtho-quinones. However, several efforts have been made to find new lapachone analogues, more potent and less toxic. Nor-β-lapachone (NβL), a semisynthetic naphthoquinone derivative from b-Lapachone, is a cytotoxic agent against several cancer cell lines.
Material and Methods: To overcome its liposolubility and non-specific toxicity, this drug was formulated in Poly(d,l)-lactide-co-glycolide (PLGA) microparticles by the emulsion-solvent evaporation technique. Surface morphology, particle size distribution, zeta potential, Raman spectroscopy, Fourier transform infrared (FT-IR) spectroscopy, drug encapsulation efficiency, drug release kinetics and *in vitro* cytotoxicity of the drug-loaded microcapsules were determined.
Results: Spherical microcapsules with a size range of 1.03±0.46 μm were obtained. The drug encapsulation efficiency was approximately 19%. The NβL-loaded PLGA microcapsules exhibited a pronounced initial burst release. After the *in vitro* treatment with the NβL-loaded PLGA microcapsules, a clearly phagocytosis of the spheres was observed in a few minutes. The cytotoxic activity of NβL against PC3M cells was greater when delivered by PLGA microcapsules compared to the free drug. After incubation for 72 h, the IC_{50} values of the free and encapsulated forms of NβL were 2.045 (1.97–2.12) and 1.046 (0.82–1.34) $\mu g \cdot mL^{-1}$, respectively. We suggest that PLGA microcapsules containing NβL could be a promising drug delivery system to be studied using *in vivo* models of prostate cancer.
Conclusions: The results suggest that NβL-loaded PLGA microcapsules could be used as a promising delivery system for NβL administration in *in vivo* tests of prostate cancer.

263 POSTER

Controlled release of cisplatin using hyaluronic oligosaccharides-coated gold nanoparticles as an efficient delivery system applied to the treatment of pancreatic tumors

H. Parkkola[1], L. Sobrevals Amieva[1], L. Vivero[2], R. Miñana[2], J. Sendra[3]. [1]*Endor Nanotechnologies, Preclinical, Barcelona, Spain;* [2]*Endor Nanotechnologies, Nanomaterials, Barcelona, Spain;* [3]*Endor Nanotechnologies, R&d Director, Barcelona, Spain*

Many chemotherapeutic agents currently used in oncology can produce toxicity inducing many side effects, even at the optimal therapeutic doses.

Pilot study in patients with advanced solid tumors to evaluate feasibility of ferumoxytol (FMX) as a tumor imaging agent prior to MM-398, a nanoliposomal irinotecan (nal-IRI)

Ramesh K. Ramanathan[1], Ronald L. Korn[2], Jasgit C. Sachdev[1], Gerald J. Fetterly[3], Katie Marceau[1], Vickie Marsh[1], Natarajan Raghunand[4], Stephan G. Klinz[5], Eliel Bayever[5], Jonathan B. Fitzgerald[5]

[1]Virginia G Piper Cancer Center, Scottsdale Healthcare, Scottsdale, AZ; [2]Imaging Endpoints, Scottsdale, AZ; [3]Roswell Park Cancer Institute, Buffalo, NY; [4]Translational Cancer Imaging, Arizona Cancer Center, Tucson, AZ; [5]Merrimack Pharmaceuticals, Inc., Cambridge, MA

CT224

Abstract

Introduction

MM-398, a stable nanoliposomal irinotecan (nal-IRI), is designed to exploit leaky tumor vasculature for enhanced drug delivery to tumors. Tumor deposition of nal-IRI and subsequent irinotecan conversion by CES enzymes in both neoplastic cells and tumor associated macrophages (TAM) may positively correlate with activity. Predictive biomarkers to measure tumor deposition could identify patients likely to benefit from nal-IRI. FMX is a 30nm iron-oxide, superparamagnetic nanoparticle with MRI contrast properties. The particle size, its propensity for uptake by TAMs and similar distribution patterns to nal-IRI in preclinical models led to the design of a clinical study to evaluate the feasibility of correlating FMX-based MRI (Fe-MRI) acquisition with tissue drug metabolite levels and other biomarkers to estimate drug delivery to tumors.

Patients and methods

Eligible patients (n=12) with refractory solid tumors with at least two metastatic lesions >2cm accessible for a percutaneous biopsy were enrolled from one institution. Fe-MRI scans were performed on a 1.5T MRI using T2* iron sensitive sequences prior to and following FMX infusion (1h, 24h, 72h). MR images were used to direct biopsies at 72h to FMX high or low regions, permitting intra- and inter-patient comparisons of FMX and nal-IRI tumor levels. Patients continued on nal-IRI at 80mg/m^2 q2w until progression. Tissue iron and TAM distribution were assessed by IHC, tissue-bound metabolite levels by mass-spectrometry. T2* signal was used to calculate FMX levels in total lesions along with FMX estimates on biopsy images derived from fused MRI-CT biopsy images. The first 9 patients (2M 7F; median age 57 years, range 28-71 years) are reported here.

Results

There were no safety-related or other potential interactions observed with nal-IRI and FMX. Adverse events of nal-IRI were consistent with previous studies. FMX levels, quantified in 36 tumor lesions from the first 9 subjects, showed mean FMX accumulation of 37.9 mcg/mL [3.3-101.2 mcg/mL] and 13.2 mcg/mL [0.1-41.0 mcg/mL] at 24h and 72h, respectively. Lesions were localized mostly in liver (67%) and lymph nodes/peritoneal sites (25%). A mechanistic PK model indicated that tissue permeability to FMX contributed to Fe-MRI signals at 24h, while FMX binding contributed at 72h. Levels of irinotecan and SN-38 were 3.59mcg/g [2.29-4.89mcg/g] and 11.43ng/g [4.04-18.8ng/g], respectively, at 72h in biopsies from the first 6 patients.

Conclusions

This study is one of the first to measure active metabolite SN-38 levels in patient tumors. FMX was safely used as a tumor contrast agent prior to nal-IRI treatment. T2* MRI sequences allowed for quantitation of FMX concentrations in tumor and reference tissue. A mechanistic model provided an estimation of FMX tumor tissue permeability and binding that may be useful as a predictive biomarker of nanotherapeutics such as nal-IRI.

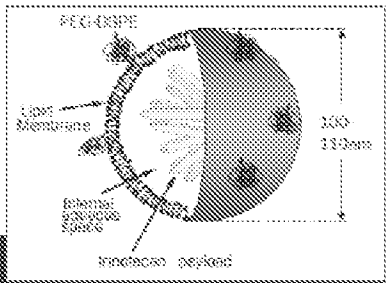

Cross Indication Translational Study Design

Cross Indication Translational Study Design

Timing of Study Components

	Week 1							Week 2						
Days	-4	-2	-1	1	3	6	7	8	9	10	11	12	13	14
MRI (pre-FMX)														
FMX (5mg/kg)														
MRI (post-FMX)	1 hr	24 hr		72 hr										
nal-IRI (80mg/m²)								every 2 weeks						
CT guided Biopsies					2				2					
PK sampling														

Collection of Translational Samples

Phase	Samples		Site Action
Screening Phase	Archival Tumor		prepare sections or block according to Biomarker
Pharmacodynamic Phase	Hi Biopsy	Pass 1	Biobank
		Pass 2	Freeze
		Pass 3	soak in RNALater and freeze
	Lo Biopsy	Pass 1	Biobank
		Pass 2	Freeze
		Pass 3	soak in RNALater and freeze
	PK sample (pre enrollment)	Aliquot 1	Pharmacy Assay
		Aliquot 2	Freeze

Phase	Samples		Site Action
MM-398 Treatment Phase	Hi Biopsy	Pass 1	freeze
		Pass 2	Biobank
		Pass 3	soak in RNALater and freeze
	Lo Biopsy	Pass 1	freeze
		Pass 2	Biobank
		Pass 3	soak in RNALater and freeze
	PK sample (pre enrollment)	Aliquot 1	freeze
		Aliquot 2	freeze
	Blood samples	Plasma	freeze
		Whole Blood/Per Cells	freeze
	Urine		freeze

- Eligible patients with refractory solid tumors in the following indications:
  - NSCLC, CRC, TNBC,
  - ER/PR positive breast cancer,
  - pancreatic cancer,
  - ovarian cancer,
  - gastric cancer,
  - gastro-esophageal junction adenocarcinoma,
  - head and neck cancer
- FMX dosed at 5mg/kg not to exceed 510mg total
- PK samples for FMX collected at 0.5h, 2h, 24h and 72h
- nal-IRI dosed at 80mg/m² q2w
- PK samples for nal-IRI collected at 1.5h, 3.5h, 72h and 168h
- Biopsies are targeted towards two separate areas of a lesion. Three passes are collected
- Biopsies are obtained 72h after dosing with either FMX or nal-IRI from separate lesions
- RECIST v1.1 evaluation every 8 weeks

NCT01770353

Study Objectives and Eligibility Criteria

Primary Objectives:

- Evaluate the feasibility of Fe-MRI to identify TAMs
- Measure tumor levels of irinotecan and SN-38

Secondary Objectives

- Correlations between Fe-MRI, TAM levels, and tumor levels of irinotecan and SN-38 with administration of nal-IRI
- Value of Fe-MRI in directing tissue biopsy
- Safety profile of nal-IRI in the presence of Ferumoxytol
- Assess tumor response to nal-IRI using RECIST 1.1 criteria and volumetric tumor change on CT
- Characterize the PK of nal-IRI

Major Inclusion Criteria :

- At least two metastatic lesions >2cm
- Amenable to multiple pass percutaneous biopsies
- ECOG performance status 0 - 2
- Bone marrow reserves as evidenced by:
  - ANC > 1,500 cells/μl without the use of hematopoietic growth factors
  - Platelet count > 100,000 cells/μl
  - Hemoglobin > 9 g/dL
- Adequate hepatic function as evidenced by:
  - Normal serum total bilirubin
  - AST and ALT ≤ 2.5 x ULN (≤ 5 x ULN acceptable if liver metastases present)

Major Exclusion Criteria :

- Having received irinotecan or anti-VEGF therapy within the last six months
- Unable to undergo MRI imaging due to presence of errant metal, cardiac pacemakers, pain pumps or other MRI incompatible devices.
- A history of allergic reactions to compounds similar to ferumoxytol
- Evidence of Iron overload

Patient Demographics & Safety

Patient demographics

		All patients n=14
Age (median/range)		60 (28-80)
Gender	Male	3 (21%)
	Female	11 (79%)
Race	Caucasian	13 (93%)
	Other	1 (7%)
ECOG	0	7 (50%)
	1	7 (50%)
Prior Lines of Therapy (med/range)		3.5 (1-10)

Patient disposition

Treatment Termination Reason	FUFIRINOX n=14	nal-IRI n=12
Progressive Disease (RECIST)		6 (50%)
Clinical Deterioration	2 (14%)	2 (17%)
Adverse Event		1 (8%)
Withdrawal of Consent		1 (8%)
Ongoing		2 (17%)

MRI lesions/patient

# of MRI lesions	# of patients
0	1
1	1
2	1
3	2
4	4
5	3

nal-IRI doses/patient

# of doses	# of patients
2	4
3	1
5	2
6	1
7	1
>7	3*

*** 2 of these are ongoing**

Adverse Events of at least Grade 3

FUFIRINOX phase (n=14)

	# of AE	
Adverse Event	Total	Study drug related
Anaemia	2	0
Hypokalaemia	1	0
Hypotension	1	0
Sepsis	1	0

nal-IRI phase (n=12)

	# of AE	
Adverse Event	Total	Study drug related
Diarrhoea	3	3 (25%)
Hypokalaemia	3	1 (8%)
Abdominal pain	2	2 (17%)
Anaemia	2	1 (8%)
Nausea	2	2 (17%)
Neutropenia	2	2 (17%)
Colitis	1	1 (8%)
Dehydration	1	1 (8%)
Enterocolitis infectious	1	1 (8%)
Hyperglycaemia	1	1 (8%)
Vomiting	1	1 (8%)
Urinary tract infection	2	0
Hypertension	1	0
Hyponatraemia	1	0
Hypophosphataemia	1	0
Thrombocytopenia	1	0
Urinary tract infection (enterococcal)	1	0

Tables reflects data cutoff date of 10MAR2014

Time on Treatment and Best Overall Response

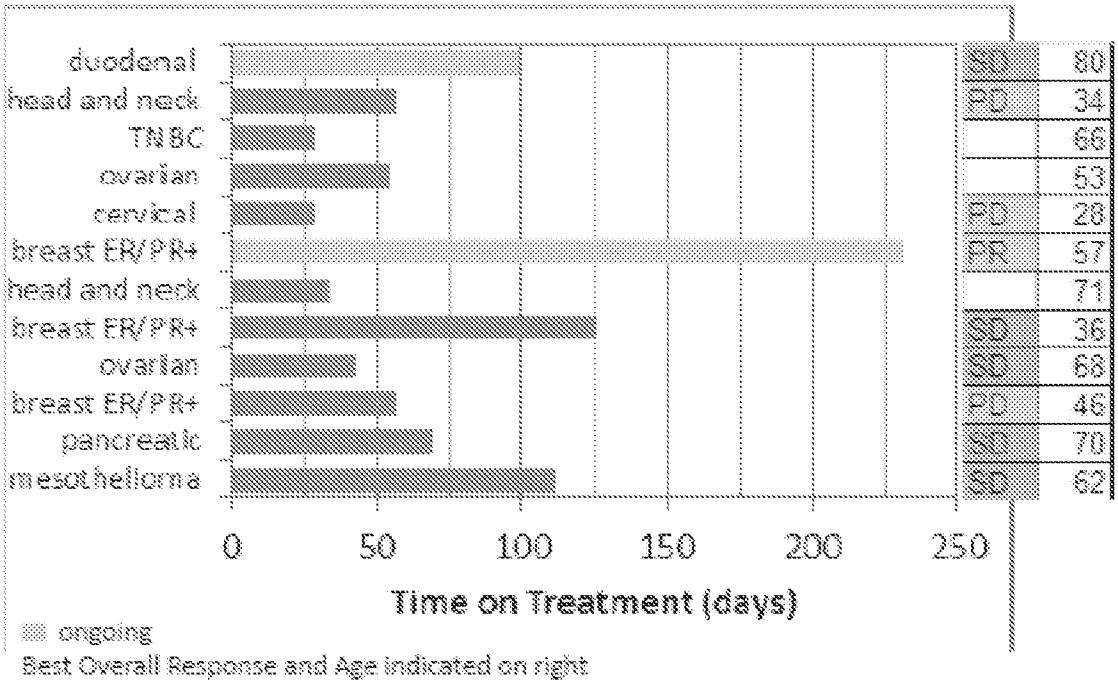

Evaluation after 2 cycles of MM-398 (CHOI, RECIST = PR)

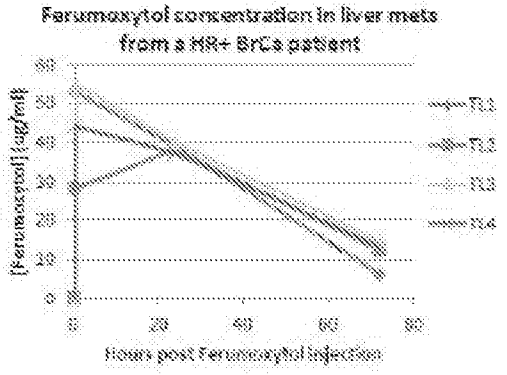

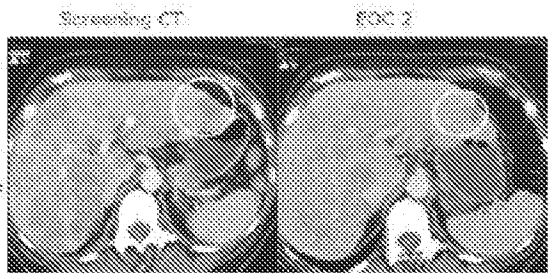

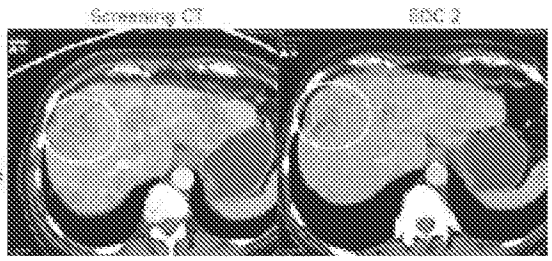

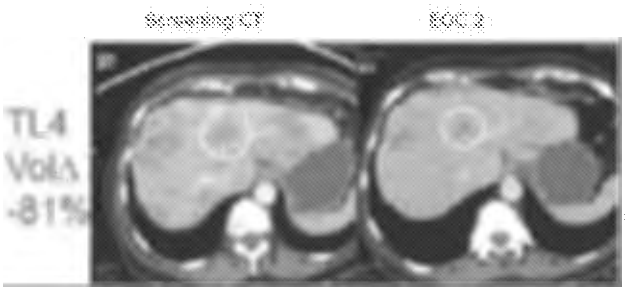

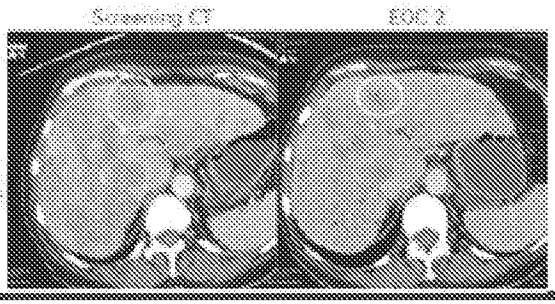

Ferumoxytol Imaging and Quantitation

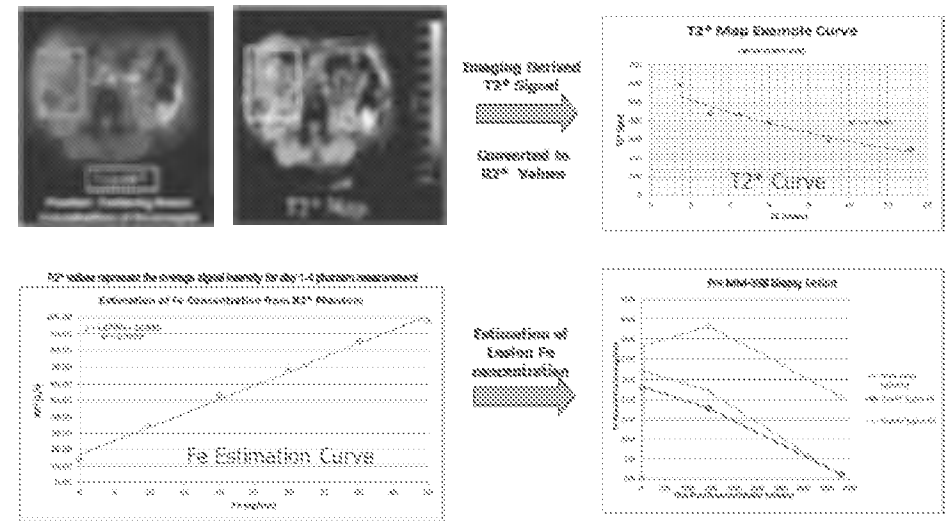

MRI FSPGR FatSat TE 13.2 ms Breathhold Images

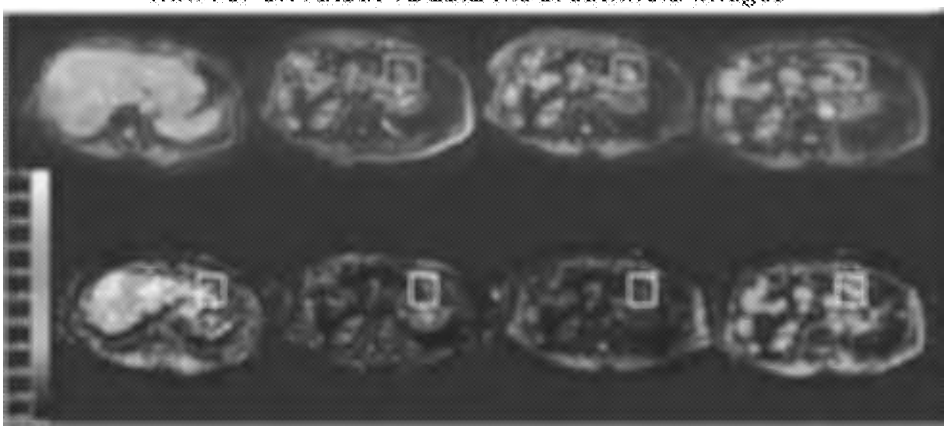

Day 1 Pre-Fe | Day 1 Post-Fe | Day 2 Post-Fe | Day 4 Post-Fe

Figure 1. MRI images were acquired on a GE 1.5T MRI instrument with a T1 FSPGR series with echo delay times from 1.5 – 13.2ms. Slice thickness and spacing was 6mm×1mm using a 256x256 matrix. T2* values were extrapolated from each image series to construct a T2* map. A phantom containing known FMX concentrations from 10 – 200μg/ml was included during each MRI session and demonstrated a linear relationship between R2*=1/T2* and FMX levels.

MRI images were taken prior to FMX injection and at 1h, 24h and 72h after injection. FMX levels were calculated for each post-injection time point (Post-Fe) after subtraction of baseline values (Pre-Fe). Calculation was done for the complete lesion and for select sub-lesion areas corresponding to biopsy locations.

To measure plasma FMX levels the plasma tubes were placed next to the phantom and imaged in the same instrument (not shown).

Ferumoxytol Levels in Lesions and PK Model Building

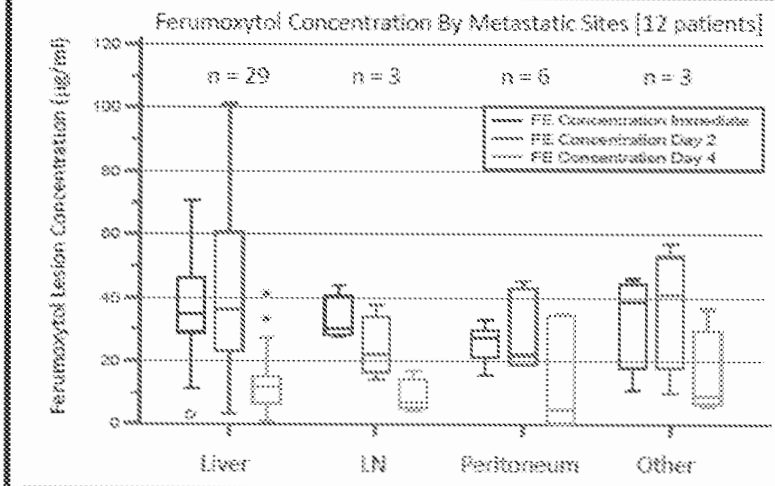

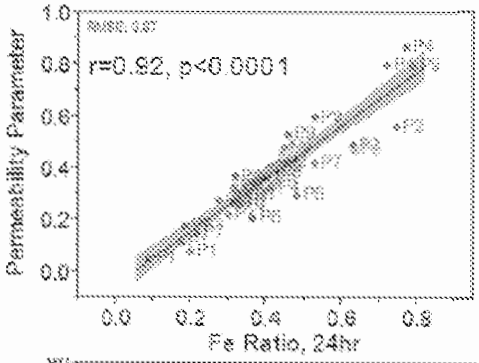

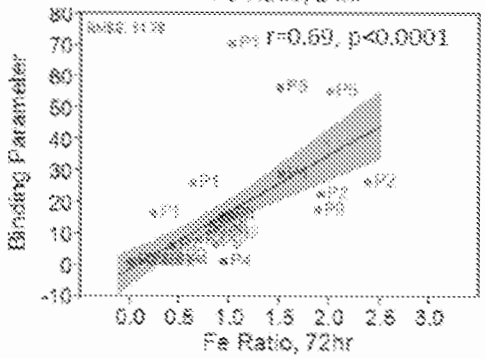

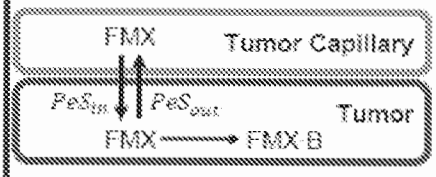

High permeability and high signal retention model

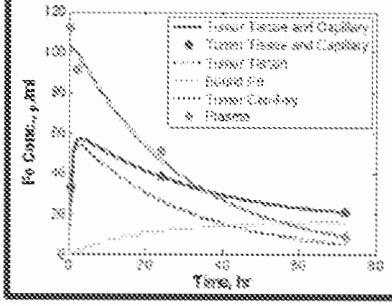

Changes in Lesion size categorized by 24h FMX lesion levels

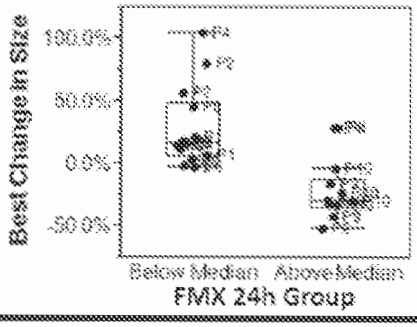

Figure 2. FMX levels in lesions and sub-lesion ROIs are fitted into a PK deposition model that links plasma and lesion values to permeability-surface products (K_{trans}, $k_{washout}$) and its ratio (Permeability) as well as a binding/retention parameter. Different lesions or sub-lesion areas show distinct PK characteristics. The FMX plasma/lesion ratios show time-dependent parameter correlations. In a preliminary analysis evaluable lesion size changes (CT) from 6 patients are categorized relative to the median of the FMX lesion levels measured at 24hr.

Co-localization of CD68+ Macrophages and FMX at Stromal Interfaces

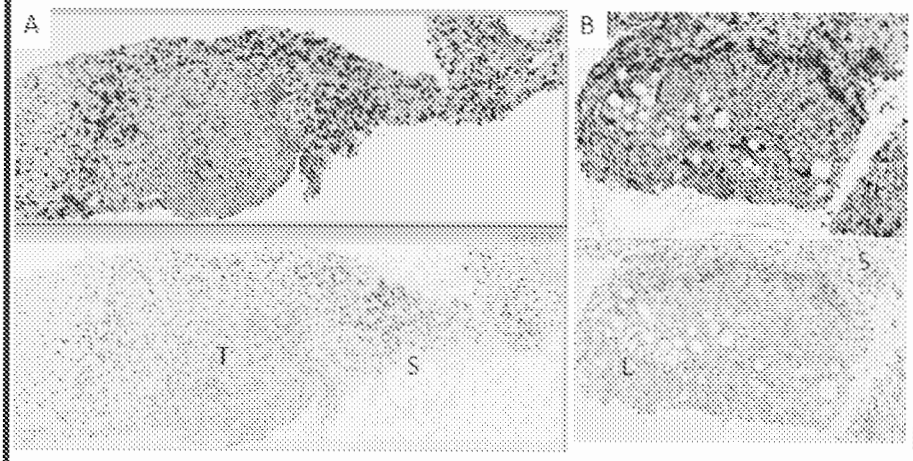

Figure 3. Serial tumor sections from FFPE biopsies of liver (L) lesions were assessed by staining with anti-CD68 antibody (clone PG-M1, DAKO) for macrophages and by Prussian Blue staining for FMX. FMX deposition was detectable primarily in stromal areas (S) around tumor nests (T). The staining pattern suggests intracellular accumulation and is co-localized with macrophages stained in adjacent sections. This association was observed in biopsies obtained at 72h (A) and 168h (B) and suggests that FMX deposition can identify vascular-accessible macrophages within tumor lesions.

Drug Metabolite Quantitation in Tumor Biopsies and Plasma

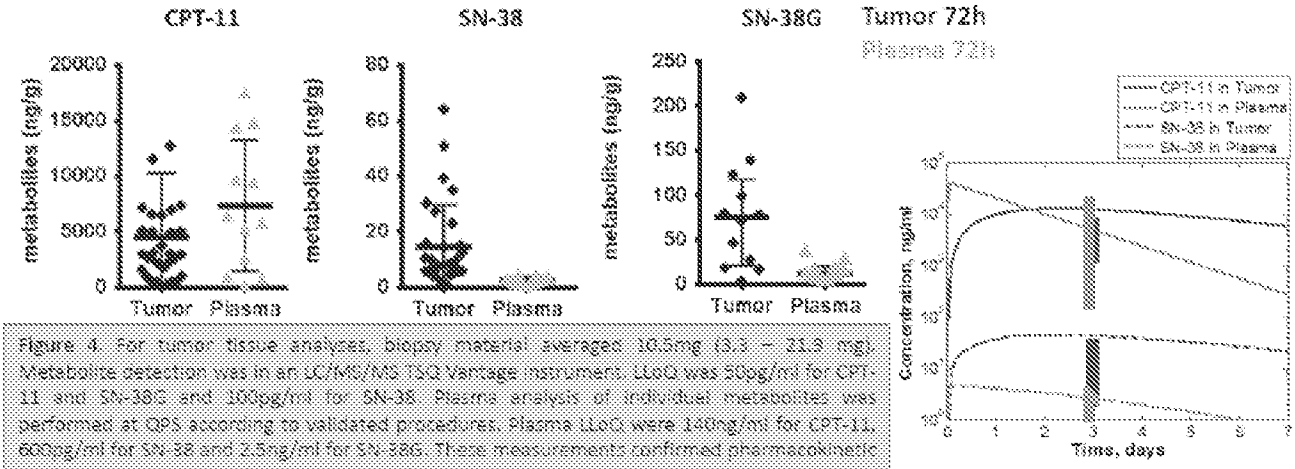

Figure 4. For tumor tissue analyses, biopsy material averaged 10.5mg (3.3 – 21.3 mg). Metabolite detection was in an LC/MS/MS TSQ Vantage instrument. LLoQ was 50pg/ml for CPT-11 and SN-38G and 100pg/ml for SN-38. Plasma analysis of individual metabolites was performed at QPS according to validated procedures. Plasma LLoQ were 140ng/ml for CPT-11, 600pg/ml for SN-38 and 2.5ng/ml for SN-38G. These measurements confirmed pharmacokinetic modeling of drug metabolites in plasma and tumor compartments based on prior preclinical and clinical (plasma PK only) observations. Measurement ranges are represented by vertical bars.

Conclusions

- This phase I study demonstrated the feasibility of incorporating ferumoxytol MRI into a clinical workflow
- No adverse events were attributable to FMX
- Phantom evaluation shows that accurate estimates of tumor/tissue Fe concentrations can be obtained with T2* MRI based sequences
- FMX tumor PK model successfully described FMX MR signals for each lesion characterizing the information from different time points
- Drug and metabolites are found in the tumor mass and concur with pharmacokinetic modeling expectations
- Prussian Blue staining of ferumoxytol is predominately observed at the stroma-tumor interface and coincides with vascular accessible macrophages
- The correlation between the FMX MRI tumor signal and lesion size change was limited by the small sample size of evaluable patients (n=6 at time of data cutoff); if confirmatory, the FMX MRI may be a useful imaging predictive biomarker for liposomal therapies

Acknowledgements

We thank the patients and their families for their incredible support

Virginia G. Piper Cancer Center
Scottsdale, AZ
Gustavo A. Cardenes
Jennifer Hoffman
Kelly Maxwell
Jennifer Moore
Gail Roboz

Roswell Park Cancer Institute
Buffalo, NY
Gerald J. Fetterly
Thomas Kelly
Kimberly Clark

Imaging Endpoints
Scottsdale, AZ
Gregg Jones
Jessica Faulhaber
Kevin Haworth
Charles Kroger
Mahesh Patel

TGen Drug Development
Scottsdale, AZ
Brynna Grunwald
Linda Vahdat
Lance Pohlmann

Tufts Medical Pharmacometrics
Cambridge, MA
Joseph D. Gardinier
Lang Li
Xiaoyan Deng
Sandra Kim
Donald E. Mager

SCOTTSDALE HEALTHCARE
Pilot study in patients with advanced solid tumors to evaluate feasibility of ferumoxytol (FMX) as a tumor imaging agent prior to MM-398, a nanoliposomal irinotecan (nal-IRI)
CT24
Ramesh K. Ramanathan[1], Ronald L. Korn[2], Jasgit C. Sachdev[3], Gerald I. Fetterly[3], Katie Marcom[3], Vickie Marsh[3], Natarajan Raghunand[4], Stephan G. Kiniz[5], Eliel Bayever[6], Jonathan B. Fitzgerald[6]
[1]Virginia G. Piper Cancer Center, Scottsdale Healthcare, Scottsdale, AZ; [2]Imaging Endpoints, Scottsdale, AZ; [3]Roswell Park Cancer Institute, Buffalo, NY; [4]Translational Cancer Imaging, Arizona Cancer Center, Tucson, AZ; [5]Merrimack Pharmaceuticals, Inc., Cambridge, MA
MERRIMACK®

OT3-02-14

A Phase 1 Study in Patients with Metastatic Breast Cancer to Evaluate the Feasibility of Magnetic Resonance Imaging with Ferumoxytol as a Potential Biomarker for Response to Treatment with Irinotecan Liposome Injection (nal-IRI, MM-398)

Jasgit C. Sachdev[1], Natarajan Raghunand[2], Carey Anders[3], Pamela Munster[3], Susan Minton[3], Don Northfelt[3], Ramesh K Ramanathan[3], Sarah Blanchette[4], Karen Campbell[4], Iga Stanczyto[4], Helen Lee[4], Stephan G. Klinz[5], Bart S. Hendriks[6], Victor Moyo[6], Eliel Bayever[6], Jonathan E. Fitzgerald[6], Ronald L. Korn[7]

[1]Virginia G. Piper Cancer Center, Scottsdale Healthcare, Scottsdale, AZ; [2]Mayo Clinic, Scottsdale, AZ; [3]Moffitt Cancer Center, Tampa, FL; [4]University of North Carolina Lineberger Cancer Center, Chapel Hill, NC; [5]Helen Diller Family Comprehensive Cancer Center, San Francisco, CA; [6]Merrimack Pharmaceuticals, Inc., Cambridge, MA; [7]Imaging Endpoints, Scottsdale, AZ

Abstract

Background: Irinotecan liposome injection (Nal-IRI, MM-398), is designed to extend circulation of liposomal irinotecan relative to free irinotecan and to exploit leaky tumor vasculature to enhance drug delivery to tumors. Tumor deposition of MM-398 and subsequent conversion to SN-38 in both neoplastic cells and tumor associated macrophages (TAM) may positively correlate with response to therapy. In phase I studies activity has been shown in metastatic breast cancer (MBC), pancreatic and colorectal cancer. Ferumoxytol (FMX) is an iron-oxide superparamagnetic nanoparticle that has been used off-label for its MRI contrast properties. FMX has long-circulating pharmacokinetics and is taken up by TAMs with similar distribution patterns to MM-398 in preclinical models. A single site pilot study established the feasibility of performing quantitative FMX MRI. Thirteen patients with advanced cancer (3 with ER/PR+ MBC) were imaged with FMX MRI and treated with MM-398. Median tumor lesion FMX uptake in the pilot study was 32.6 and 34.5 µg/mL at 1 h and 24 h, respectively. Lesions with FMX uptake above the median were associated with greater reductions in tumor size following treatment with MM-398 as determined by CT lesion measurements. The relationship between FMX levels in tumor lesions and MM-398 activity may serve as a potential biomarker for MM-398 deposition and response in solid tumors. This study has been expanded to include additional MBC patients to further evaluate the technical feasibility of FMX MRI at multiple study sites, and to evaluate activity of MM-398 in patients with MBC.

Trial Design: Three cohorts of 10 patients with MBC in the following categories will be enrolled: ER and/or PR positive/HER2-negative, triple negative (TNBC) and MBC with brain metastases. An imaging phase will be followed by a treatment phase. The imaging phase consists of a baseline MRI scan, FMX infusion, and follow-up MRI scans at 1-4 and 24 h after infusion. The treatment phase begins 1-6 days after imaging and consists of biweekly MM-398 70 mg/m^2 (irinotecan as the free base; dose equivalent to 80 mg/m^2 irinotecan hydrochloride trihydrate). A pretreatment biopsy is required for correlative studies.

Study Objectives: The primary objective of this multisite expansion is to investigate the feasibility of FMX quantitation in tumor lesions at multiple lesion sites in breast cancer. The secondary objective is to characterize the efficacy of MM-398 in patients with metastatic breast cancer.

Eligibility Criteria: The key inclusion criteria include patients with MBC, ECOG 0 or 1 with adequate bone marrow reserve and no prior topoisomerase 1 inhibitor or anti-VEGF treatment. ER and/or PR positive/HER2-negative and TNBC patients must have had no more than 5 prior lines of chemotherapy in the metastatic setting and have at least 2 measurable lesions. Patients with brain metastasis must be neurologically stable and have new or progressive brain metastases after prior radiation therapy with at least one lesion measuring ≥ 1 cm in longest diameter on gadolinium-enhanced MRI.

Status: This trial is currently recruiting patients.

Irinotecan Liposome Injection (ONIVYDE™, MM-398, Nal-IRI)

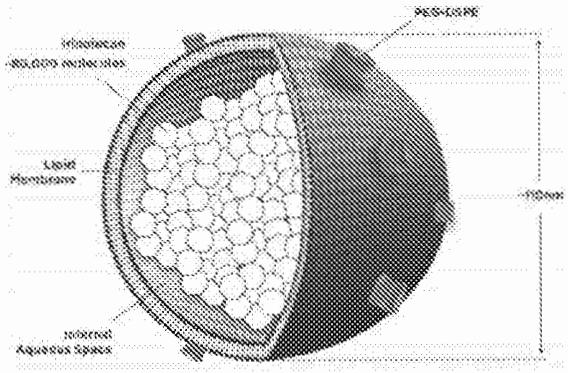

- In mice bearing human tumor xenografts, irinotecan liposome administered at irinotecan HCl-equivalent doses 5-fold lower than irinotecan HCl achieved similar intratumoral doses.
- The half-life of total irinotecan and total SN-38 following administration of MM-398, 70 mg/m^2 free base (equivalent to 80mg/m^2 of irinotecan as the hydrochloride trihydrate) was 25.8 and 67.8 hours, respectively.
- Metabolite profiling of tumor biopsies 72 h post MM-398 administration indicated 5-fold higher SN-38 levels in tumor than plasma. (Ramanathan, et al. EORTC-NCI-AACR Symposium on Molecular Targets and Cancer Therapeutics 2014 #261)

- Recently approved in US in combination with fluorouracil and leucovorin, for the treatment of patients with metastatic adenocarcinoma of the pancreas after disease progression following gemcitabine-based therapy. Limitation of Use: ONIVYDE is not indicated as a single agent for the treatment of patients with metastatic adenocarcinoma of the pancreas.

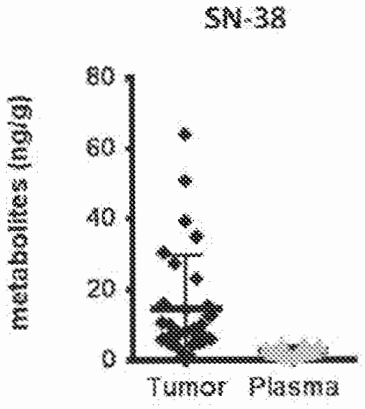

Nanoparticle Deposition Hypothesis

Ferumoxytol pharmacokinetics and biodistribution has similarities to MM-398:

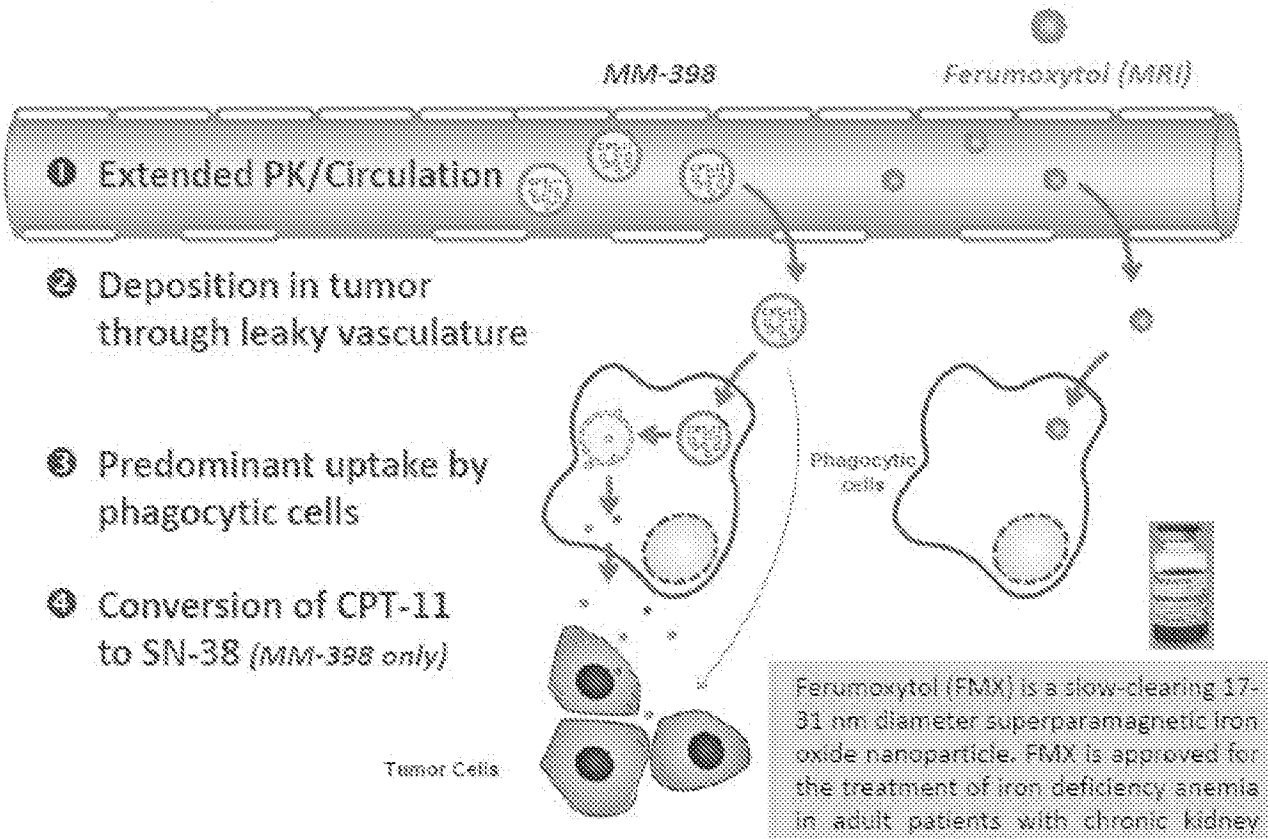

Ferumoxytol (FMX) is a slow-clearing 17-31 nm diameter superparamagnetic iron oxide nanoparticle. FMX is approved for the treatment of iron deficiency anemia in adult patients with chronic kidney disease and has been used as an MRI contrast agent (off-label).

We hypothesize that local tumor delivery of MM-398 to solid tumors is potentially rate-limiting for effective delivery and response to therapy.

Ferumoxytol tumor lesion delivery, as determined by quantitative MR imaging, may serve as a surrogate measure for MM-398 delivery and may be predictive of the likelihood of response to treatment with MM-398.

Ferumoxytol Quantification

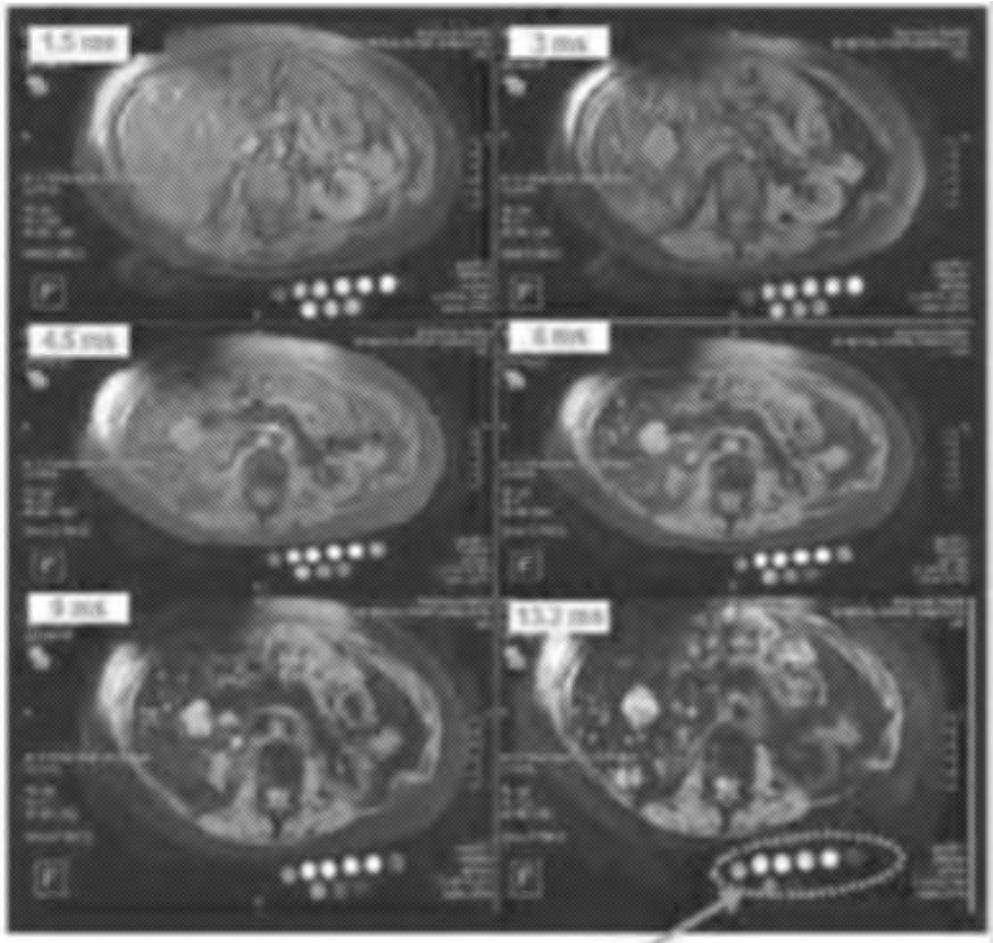

- 6 images (different echo times) acquired
- Repeated for each slice
- Images from 6 echo times are combined to enable quantitation (relaxometry).
- FMX standard curve (phantom) imaged directly with patient

MM-398 Activity in Breast Cancer

Experience with MM-398 in patients with metastatic breast cancer:

Trial	n=	Treatment*	Breast Cancer**	Best Response	
PEP0201	11	104 mg/m^2 (120)	IDC	PD	q3w
		104 mg/m^2 (120)	IDC	SD	
PEP0203 (+5-FU/LV)	16	52 mg/m^2 (60)	IDC	PD	
		87 mg/m^2 (100)	BC	PR	
		87 mg/m^2 (100)	BC	NA	
		104 mg/m^2 (120)	BC	SD	
CITS Pilot	13	70 mg/m^2 (80)	HR+	PD	q2w
		70 mg/m^2 (80)	HR+	SD	
		70 -> 43 (80 -> 50) mg/m^2	HR+	PR	
		70 mg/m^2 (80)	TNBC	PD	

** Doses are listed based on irinotecan free base. Equivalent dosing based on irinotecan hydrochloride trihydrate is shown in parentheses.*

*** IDC, infiltrating ductal carcinoma; BC, breast cancer; HR+, hormone receptor positive; TNBC, triple negative breast cancer.*

In previous trials 10 patients with metastatic breast cancer received MM-398 (alone or in combination with 5-FU/LV). Two patients achieved a partial response and 3 patients had stable disease.

Breast Cancer Expansion: Study Design

Indication

- Metastatic breast cancer
- 3 cohorts of 10 patients each
  - ER/PR+, HER2-
  - TNBC
  - Brain metastases (allows all sub-types, including HER2+)

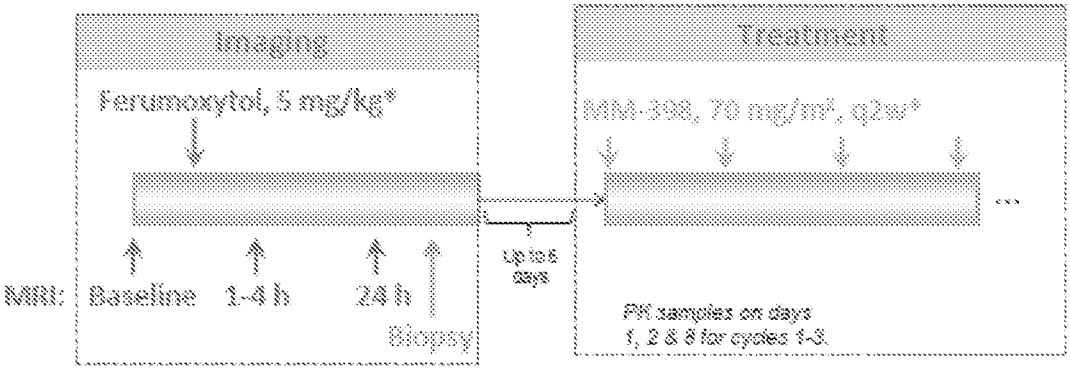

Ferumoxytol is used off-label in this study.

*Dosing based on irinotecan free base (rounded from 69.3 mg/m²). Converting a dose based on irinotecan free base to a dose based on irinotecan hydrochloride trihydrate is accomplished by substituting the molecular weight of irinotecan free base (586.68 g/mole) with the molecular weight of irinotecan hydrochloride trihydrate (677.19 g/mole), resulting in a conversion factor of 1.155. The 70 mg/m² dose based on irinotecan free base (rounded from 69.3 mg/m²) is equivalent to 80 mg/m² based on irinotecan hydrochloride trihydrate.

Inclusion criteria:

- ≤ 5 prior lines of chemotherapy in the metastatic setting (no limit to prior lines of hormonal therapy in ER/PR+ cohort)
- Topo1 inhibitor (irinotecan-derived and topotecan) naïve
- At least 1 measurable lesions

Primary objectives:

- To further investigate the feasibility of FMX quantitation in tumor lesions
- To characterize the relationship between FMX tumor uptake and response

Secondary objectives:

- Characterize efficacy in this patient population
- Assess analytical performance of ferumoxytol MRI measurements and optimize ferumoxytol MRI parameterization

This study is open and currently recruiting patients.

Results from Pilot Study

(Sachdev, et al. SABCS 2014 PS-01-06; Romanathan, et al. EORTC 2014 #251)

Anecdotal Examples from Pilot Study:

ER+ Breast Cancer Patient

Pre-FMX

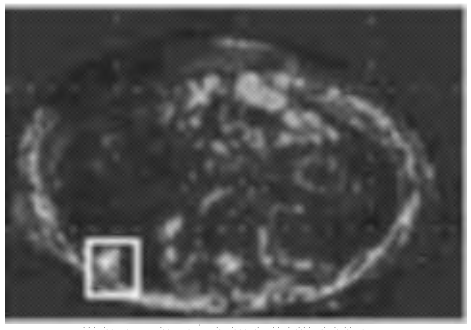

24 hours post FMX

Lesion did not go dark
→ Low [ferumoxytol]

Lesion size ↑ 45% following treatment with MM-398.

ER+ Breast Cancer Patient w/ partial response

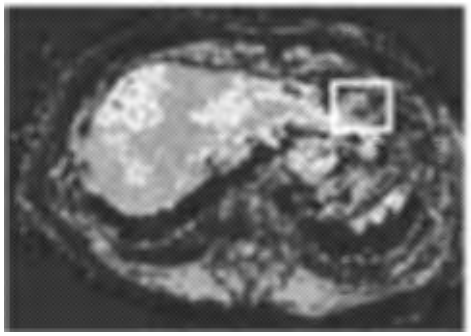

Pre-FMX

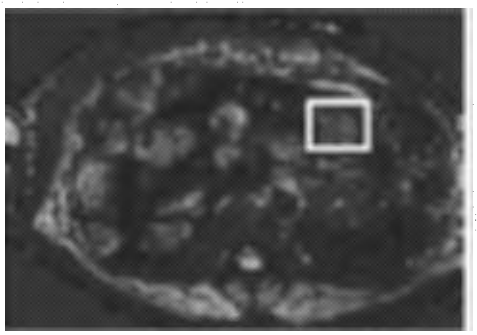

24 hours post FMX

Lesion went dark
→ High [ferumoxytol]

Lesion size ↓ 49% following treatment with MM-398.

----- T2* weighted images -----

(darker = more FMX)

Lesion Uptake:

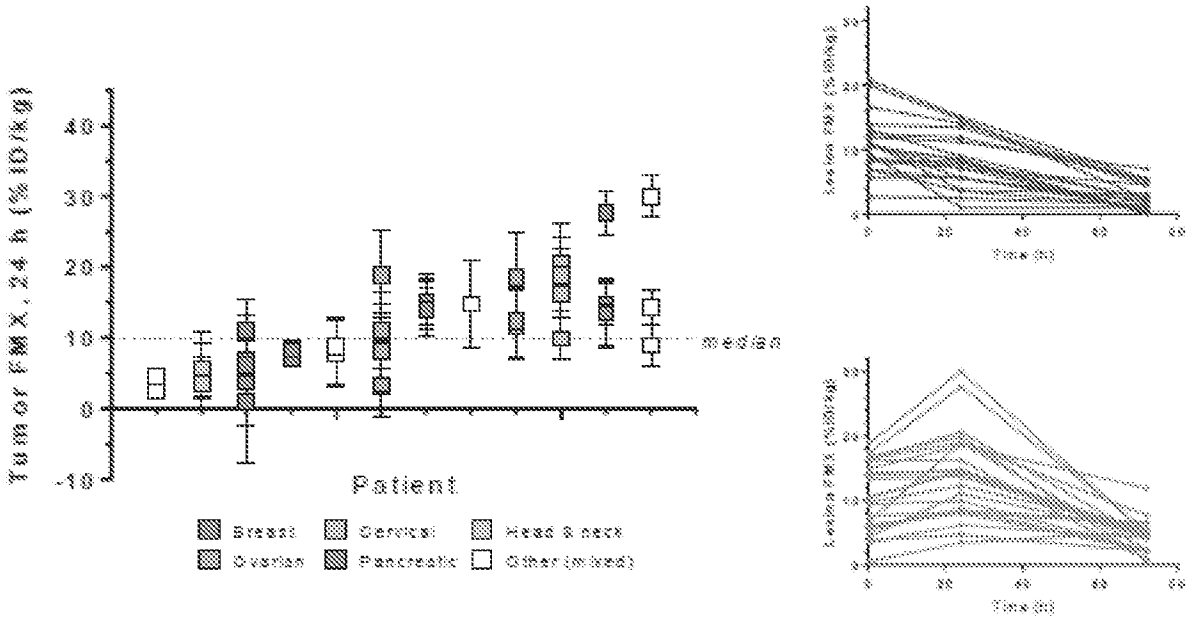

MRI images were acquired on a GE 1.5T MRI instrument with a T1 FSPGR series with echo delay times from 1.5 – 13.2 ms. Slice thickness and spacing was 6 mmx1 mm using a 256x256 matrix. T2* values were extrapolated from each image series by exponential fit of signal intensities to construct a T2* map. A phantom containing known FMX concentrations from 10 – 200 mg/mL was included during each MRI session. FMX levels were calculated for each post-injection time point (post-FMX) after subtraction of baseline values (pre-FMX) and converted to concentrations using the standard curve; data for 24 h, organized by patient is shown on the left. Individual lesion ferumoxytol uptake dynamics are shown to the right, organized by shape (decreasing lesions in blue, peaking and increasing lesions in red).

Lesion Response:

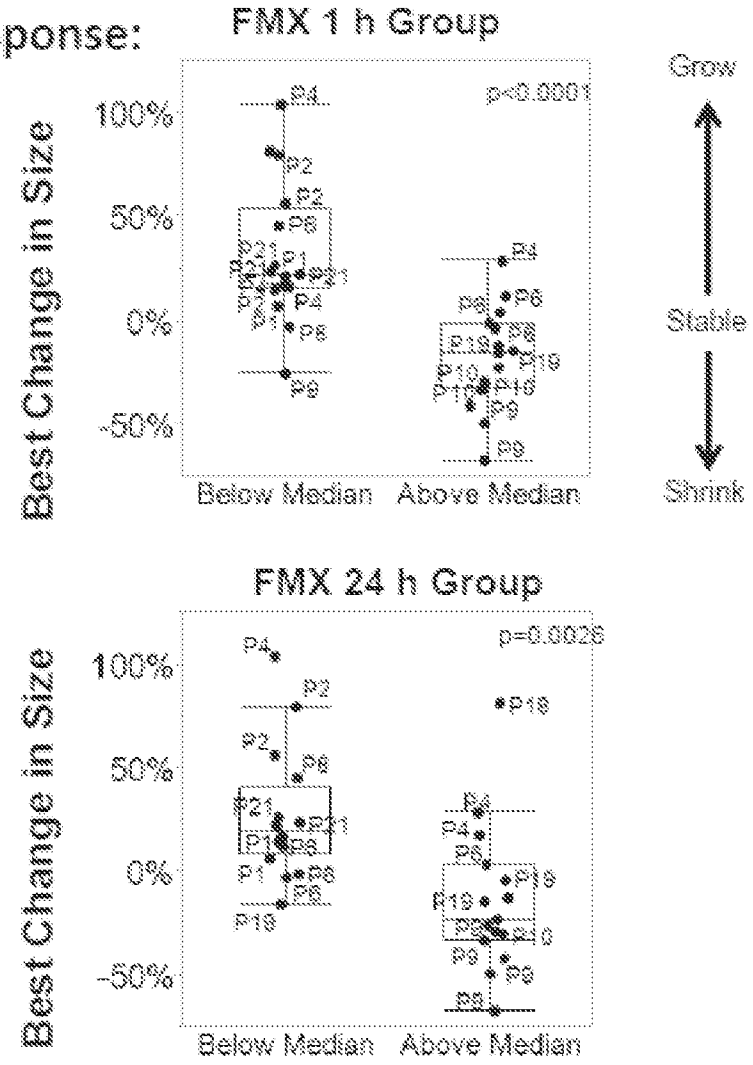

Lesions with FMX levels (in mg/mL) above the population median at early MRI timepoints (1 h and 24 h) showed a statistically significant reduction in individual lesion size. Lesions from each patient were treated as independent samples.

Acknowledgements

We thank the patients and their families for their incredible support. We also would like to acknowledge clinical trial staff, TD2 and Imaging Endpoints.

A Phase 1 Study of Patritumab Deruxtecan (U3-1402) in Patients with Unresectable and/or Metastatic Breast Cancer for Whom Prior Systemic Therapy Including HER3-Directed Therapy Is Indicated

Rebecca Dent, MD, PhD[1]; Sara A. Hurvitz, MD[2]; Hope S. Rugo, MD[3]; Sung-Bae Kim, MD, PhD[4]; Wolfgang Eberhardt, MD[5]; Fabrice Andre, MD, PhD[6]; Yasuhiro Fujiwara, MD, PhD[7]; Kenji Tamura, MD, PhD[8]; Ana Maria Wilson, MD[9]; Jing Zhang, MD, PhD[9]; Ken Takeshita, MD, PhD[10]; Yoshinori Iwata, MD, PhD[10]; Shunsuke Kagawa, MD, PhD[10]; Yoshiaki Nakamura, MD, PhD[11]; Hiroji Iwata, MD, PhD[12]

[1]National Cancer Centre Singapore, Singapore; [2]David Geffen School of Medicine at UCLA, Los Angeles, CA; [3]University of California San Francisco Comprehensive Cancer Center, San Francisco, CA; [4]Asan Medical Center, University of Ulsan College of Medicine, Seoul, Republic of Korea; [5]Evangelische Kliniken Essen-Mitte, Essen, Germany; [6]Institut Gustave Roussy, Villejuif, France; [7]National Cancer Center Hospital East, Kashiwa, Japan; [8]Shizuoka Cancer Center, Shizuoka, Japan; [9]Daiichi Sankyo, Inc., Basking Ridge, NJ; [10]Daiichi Sankyo Co., Ltd., Tokyo, Japan; [11]Aichi Cancer Center Hospital, Nagoya, Japan; [12]Aichi Medical University, Nagakute, Japan

Poster presented at the 2019 San Antonio Breast Cancer Symposium; December 10-14, 2019; San Antonio, TX

Abstract

Background: Patritumab deruxtecan (U3-1402) is a HER3-directed antibody drug conjugate (ADC) consisting of a fully human anti-HER3 IgG1 monoclonal antibody conjugated to a topoisomerase I inhibitor via a stable tetrapeptide-based cleavable linker. HER3 is a member of the HER family of receptor tyrosine kinases and is frequently overexpressed in breast cancer. This first-in-human study evaluated the safety, tolerability, pharmacokinetics, and preliminary antitumor activity of U3-1402 in patients with HER3-expressing unresectable and/or metastatic breast cancer.

Methods: Patients received U3-1402 intravenously every 3 weeks (Q3W) in dose escalation (5.4 mg/kg to 8.0 mg/kg) and dose expansion (6.4 mg/kg) cohorts. Primary objectives were to assess safety and tolerability and to determine the recommended dose for expansion (RDE). Secondary objectives included pharmacokinetics, immunogenicity, and preliminary antitumor activity. Exploratory objectives included evaluation of HER3 expression in archival tumor tissue by immunohistochemistry (IHC).

Results: As of the data cutoff (July 31, 2019), 57 patients had received U3-1402 at 5.4 mg/kg (n=3), 6.4 mg/kg (n=41), or 8.0 mg/kg (n=13). Patients had received a median of 5 (range 1-14) prior lines of therapy, including prior HER3-directed therapy in 14 patients (25%). Dose-limiting toxicities were observed in 1 patient each at 5.4 mg/kg (Grade 3 interstitial lung disease) and 8.0 mg/kg (Grade 3 stomatitis). The RDE was established as 6.4 mg/kg Q3W. Treatment-related adverse events (TRAEs) occurred in 96% of patients; the most common were nausea (61%), alopecia (54%), and fatigue (46%). Grade ≥3 TRAEs occurred in 39% of patients. Interstitial lung disease (ILD) occurred in 5 patients (9%), including 1 Grade 5 event. Pharmacokinetic analysis showed dose-proportional exposure. Immunogenicity was low. Among 49 patients with evaluable tumor tissue, HER3 IHC H-score ranged from 0 to 300. Objective responses were observed in patients with HER3 IHC H-score ≥100 and in those with lower HER3 expression.

Conclusions: U3-1402 demonstrated a manageable safety profile and encouraging antitumor activity in heavily pretreated patients with unresectable and/or metastatic breast cancer. The RDE was established as 6.4 mg/kg Q3W. ILD was the most clinically significant TRAE and required careful monitoring. Enrollment in the dose-expansion cohort is ongoing.

Introduction

- Metastatic breast cancer
- Expression of HER3 in breast cancer
  - ~70-90%
  - ~50%
- HER3 expression is not routinely tested in clinical practice

Methods

Study Design and Patients

Dose Escalation and Dose Expansion

Assessments

Results

Patient Disposition and Baseline Characteristics

Safety

Pharmacokinetics

Immunogenicity

Antitumor Activity

Exploratory Biomarker Analysis

Conclusions

References

Characterization of metastatic breast cancer lesions with ferumoxytol MRI and clinical response to MM-398, nanoliposomal irinotecan (nal-IRI), in 3 subjects

Jasgit C. Sachdev[1], Ramesh K. Ramanathan[1], Natarajan Raghunand[2], Jaeyeon Kim[3], Stephan G. Klinz[3], Eliel Bayever[3], Jonathan B. Fitzgerald[3], Ronald L. Korn[4]

[1] Virginia G Piper Cancer Center, Scottsdale Healthcare, Scottsdale, AZ; [2]Translational Cancer Imaging, Arizona Cancer Center, Tucson, AZ; [3]Merrimack Pharmaceuticals, Inc., Cambridge, MA; [4]Imaging Endpoints, Scottsdale, AZ

#563

Abstract

Introduction

Irinotecan has known activity in metastatic breast cancer (MBC). MM-398, nanoliposomal irinotecan (nal-IRI), is designed to exploit leaky tumor vasculature for enhanced drug delivery to tumors. Tumor deposition of nal-IRI and subsequent conversion to SN-38 in both neoplastic cells and tumor associated macrophages (TAM) may positively correlate with activity. Predictive biomarkers to measure tumor deposition could identify patients likely to benefit from nal-IRI. Ferumoxytol (FMX), an iron-oxide superparamagnetic nanoparticle with MRI contrast properties, is taken up by TAMs with similar distribution patterns to nal-IRI in preclinical models. Our previous work has shown the feasibility of quantitative FMX MRI (Fe-MRI) of tumor lesions and development of a quantitative mechanistic PK model (AACR 2014, abstract #CT224). Here we report nal-IRI activity and FMX levels in MBC patients on the study.

Patients and methods

Patients (n=15) with refractory solid tumors and at least two metastatic lesions >2 cm accessible for percutaneous biopsy were enrolled in a Phase 1 study. Fe-MRI scans were performed using T2* iron sensitive sequences prior to and following FMX infusion (1 h, 24 h, 72 h). T2* signal was used to calculate FMX levels in total lesions by comparison to a standard curve. Comparison of quantified FMX lesion uptake with a mechanistic PK model previously indicated that tissue permeability to FMX contributed to early Fe-MRI signals at 1 h and 24 h, while FMX binding contributed at 72 h. Patients then received nal-IRI (80 mg/m2 q2w) until progression. Core biopsies were obtained 72 h after both FMX and nal-IRI infusions. RECIST evaluation was done by CT every 8 weeks.

Results

FMX was well tolerated, and adverse events to nal-IRI were consistent with previous studies. Three of the 13 patients receiving nal-IRI had ER/PR+ MBC (median # of prior Rx: 8 compared to 4 for all study patients). Thirteen liver lesions (4-5/pt) were evaluated by FMX-MRI and CT for these 3 patients. Average lesion size: 26.9±11.2 mm diameter and 8.1±11.3 cm3 (median 4.7 cm3). Time on treatment for the 3 patients was 57, 126 and 256 days (study median 57 days). Best overall response was 1 stable disease (SD) and 1 partial response (PR) in these 3 patients. The patient with a PR had an average lesion size reduction of 44.5%, while the patient with SD had an average lesion size increase of 12.5% at final evaluation. Lesions that shrank after nal-IRI showed higher early levels of FMX compared to the study median (median 39.6 vs. 32.6 mcg/mL at 1 h; median 37.7 vs. 34.5 mcg/mL at 24 h). This relationship between lesion response and FMX levels was consistent with the lesion behavior in the full data set (n=31 lesions/9 patients across 7 indications) of the study.

Conclusions

Clinical activity of nal-IRI was observed in a subset of heavily treated ER/PR+ MBC patients. The relationship between FMX levels in tumor lesions and nal-IRI activity suggests that lesion permeability to FMX may be a useful biomarker for nal-IRI deposition and tumor response in MBC and potentially other indications. A multi-institution expansion of this study in HER2-negative MBC is planned to confirm these findings.

Nanoliposomal Deposition – a Critical Process for nal-IRI

A mechanistic PK model showed that longer duration of SN-38 in tumor differentiates nal-IRI from free drug for *in vivo* activity. Critical processes to influence SN-38 tumor duration were predicted by sensitivity analysis on the model parameters to be deposition into tumors and local conversion to SN-38.

Ferumoxytol* (FMX) is a slow-clearing 17-31 nm size superparamagnetic iron oxide nanoparticle. FMX is approved for the treatment of iron deficiency anemia in adult patients with chronic kidney disease and recently has been used as an MRI contrast agent (off-label).

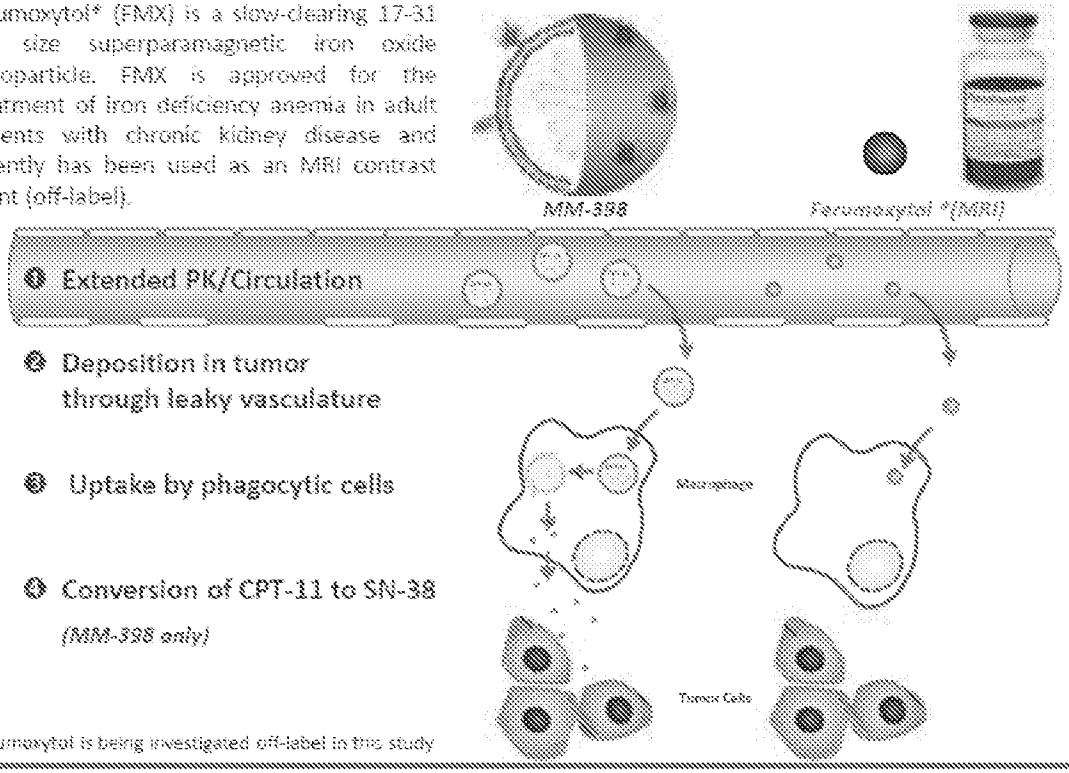

*Ferumoxytol is being investigated off-label in this study

CITS – Cross-Indication Translational Study

Eligible patients with refractory solid tumors were recruited. PK samples for FMX were collected at 0.5h, 2h, 24h and 72h. PK samples for nal-IRI were collected at 1.5h, 3.5h, 72h and 168h. 15 patients received FMX, and 13 patients received FMX + nal-IRI q2w at 80mg/m². RECIST v1.1 evaluation was done every 8 weeks, with best response shown below. No adverse events were attributable to FMX.

		All (n=15)	ER/PR (n=8)
Age, median (range)		60 (28-80)	46 (36-57)
Gender	Male	4 (27%)	
	Female	11 (73%)	x
Race	Caucasian	14 (93%)	x
	AA/AA	1 (7%)	
ECOG	0	7 (47%)	2
	1	8 (53%)	1
Prior Lines, median (range)		4 (1-10)	8 (5-10)

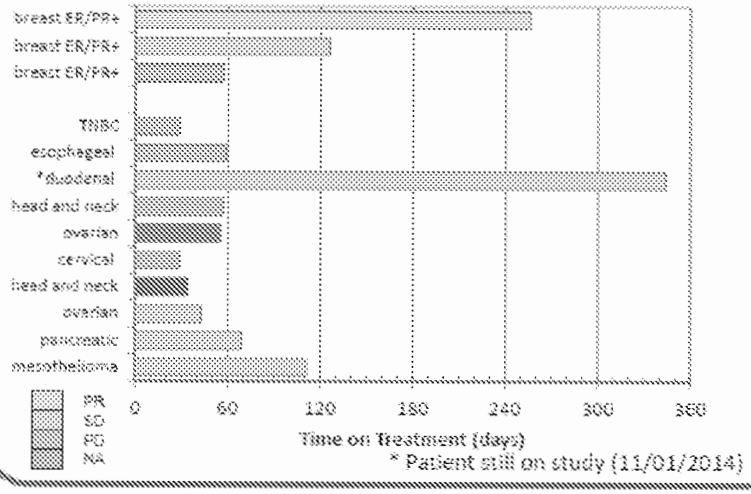

Adverse Events ≥ Grade 3	
	FMX + nal-IRI (N=13) n (%)
DIARRHOEA	4 (30.8)
HYPOKALAEMIA	3 (23.1)
ABDOMINAL PAIN	2 (15.4)
ANAEMIA	2 (15.4)
NAUSEA	2 (15.4)
NEUTROPENIA	2 (15.4)

Ferumoxytol Imaging and Quantitation

MRI images (here PM004) were acquired on a GE 1.5T MRI instrument with a T1 FSPGR series with echo delay times from 1.5 – 13.2ms. Slice thickness and spacing was 6mm×1mm using a 256x256 matrix. T2* values were extrapolated from each image series by exponential fit of signal intensities to construct a T2* map. A phantom containing known FMX concentrations from 10 – 200μg/ml was included during each MRI session and demonstrated a linear relationship between R2*=1/T2* and FMX levels. FMX levels were calculated for each post-injection time point (postFMX) after subtraction of baseline values (preFMX).

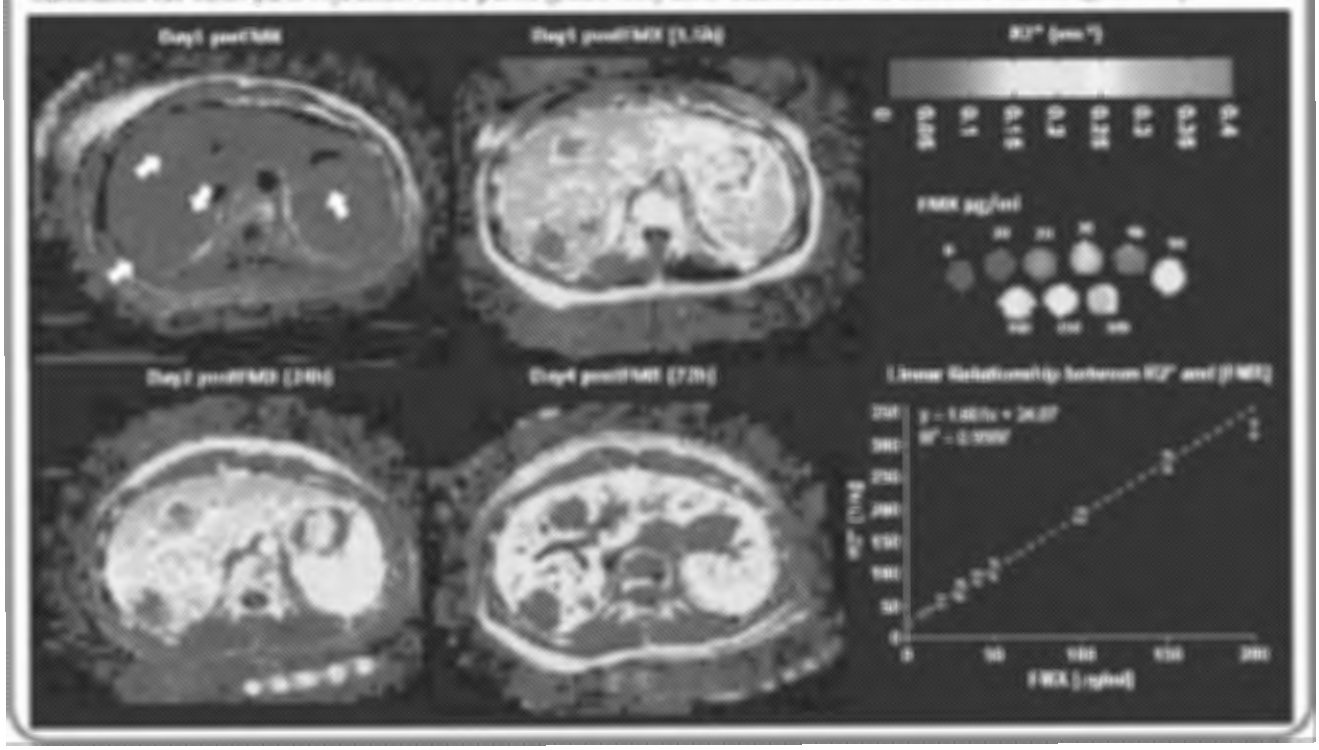

FMX levels measured in all patients

FMX levels were measured in individual lesions from all patients, however an indication-specific pattern was not seen. The change in FMX levels over time also varies by patient (ER/PR+ breast cancer patients are shown in blue, right panel). CT images show reduction in tumor burden during the treatment period for ER/PR+ BC patient #0009. RECIST evaluation demonstrated a partial response following nal-IRI treatment.

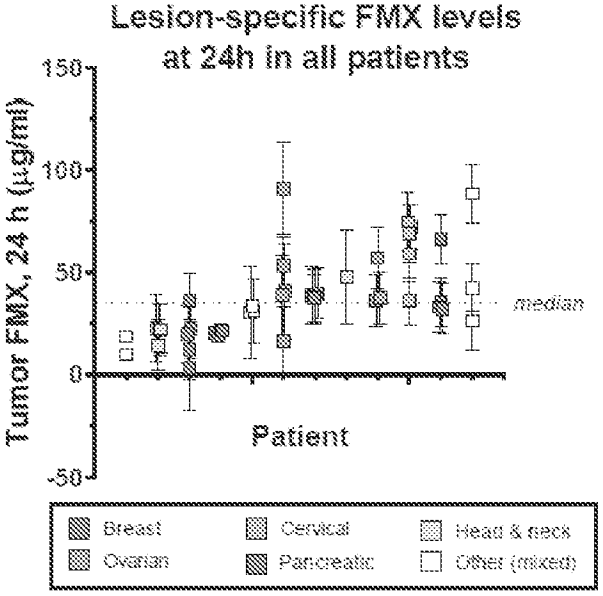

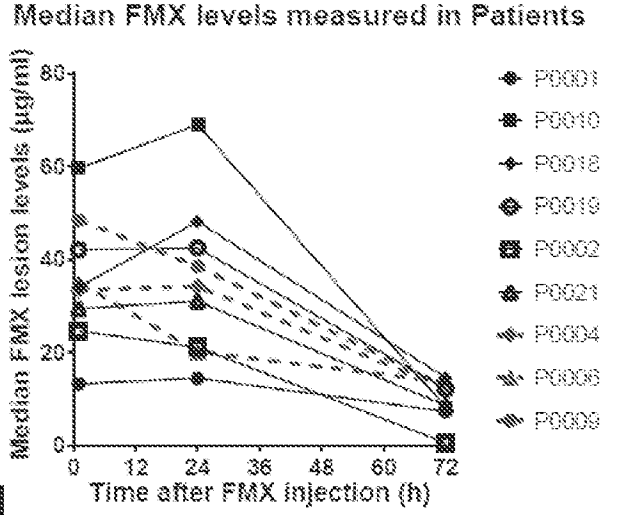

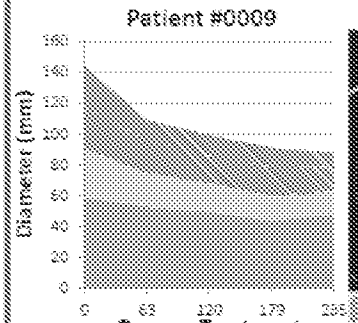

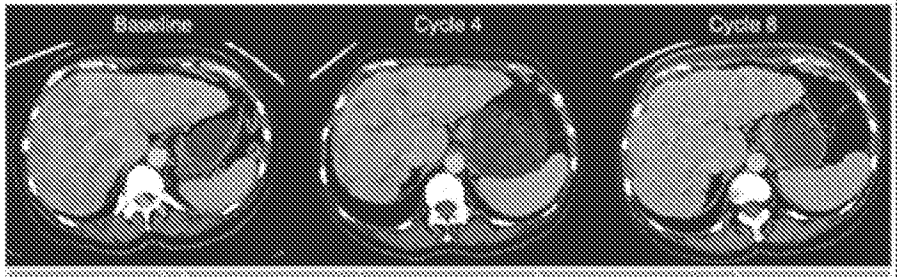

Response Criteria	Baseline	Cycle 4	Cycle 8	% Change from Baseline
RECIST 1.1	144.0mm	99.0 mm	62.7 mm	-56.5
Tumor Volume	67.5 cc	22.3 cc	22.0 cc	-67.4

FMX Signal and Lesion Response Relationships

Best change in size of individual lesions from MBC patients (right panel) and the overall study population (bottom panel) shows a relationship with FMX levels. Lesions with FMX levels (in μg/ml) above the population median at early MRI timepoints (1h and 24h) showed a statistically significant reduction in individual lesion size. Lesions from each patient were treated as independent samples.

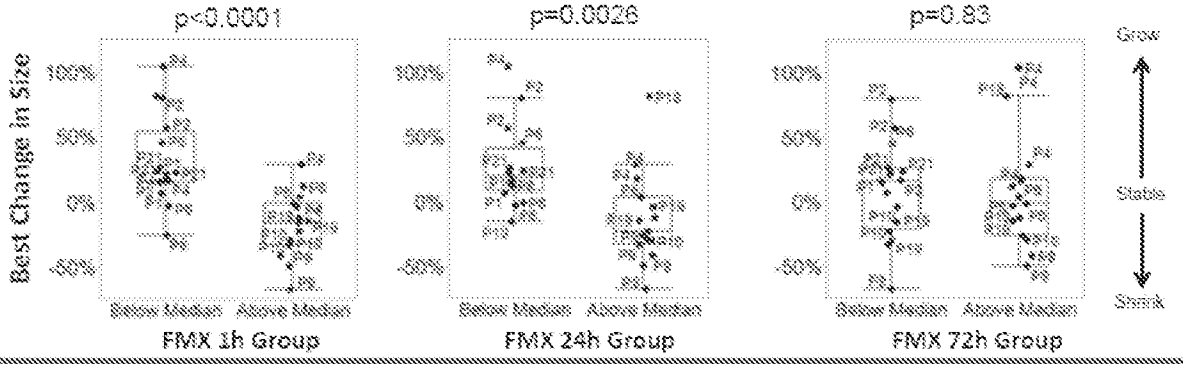

Study expansion in breast cancer patients

A multi-site expansion in metastatic breast cancer is underway.

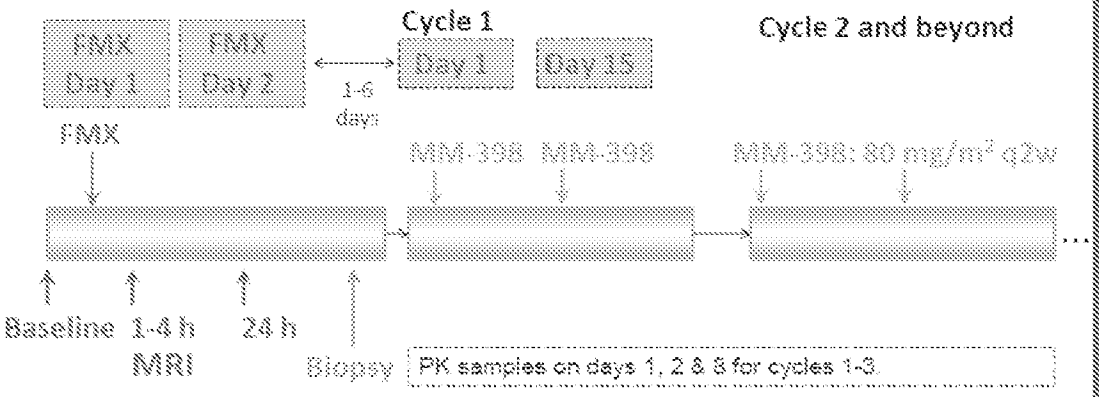

Indication
- Metastatic breast cancer
- 3 cohorts of 10 pts/each
  - ER/PR+, HER2-
  - TNBC
  - Brain metastases*

*allows all sub-types including HER2+

Primary objectives:
- To further investigate the feasibility of FMX quantitation in tumor lesions
- To characterize the relationship between FMX tumor uptake and response

Secondary objectives:
- Characterize efficacy in MBC
- Assess analytical performance of Fe-MRI measurements and optimize Fe-MRI parameterization

Inclusion criteria:
- ≤ 3 prior lines of chemotherapy in the metastatic setting (no limit to prior lines of hormonal therapy in Cohort 1)
- Topo1 inhibitor (irinotecan-derived and topotecan) naïve
- At least 2 measurable lesions

Conclusions

- Ferumoxytol MRI can be incorporated into a clinical workflow prior to nal-IRI treatment in several cancer indications, including metastatic breast cancer
- Treatment with nal-IRI resulted in disease control (stable disease, n=1; and partial response, n=1) in 2 of 3 patients with hormone receptor-positive metastatic breast cancer
- Metastatic lesions can be characterized using quantitative ferumoxytol MRI
- Early FMX signals showed a significant relationship with tumor response to treatment, suggesting further investigation is warranted for the potential use of FMX imaging as a predictive diagnostic tool
- Lesion permeability to FMX may be a useful biomarker for nal-IRI deposition and tumor response
- Further exploration of nal-IRI response, and the relationship with tumor FMX levels, in a larger population of breast cancer patients is warranted

Acknowledgements

We thank the patients and their families for their incredible support

This study was supported by Merrimack Pharmaceuticals, Inc. and Merrimack Pharmaceuticals GmbH, Basel, Switzerland

Translational Breast Cancer Research Consortium
Scottsdale, AZ
Jason Boyd
Kelly Comstock
Kelly Conlon
Kristen Kurland

Imaging Endpoints
Scottsdale, AZ
Anne C. Hall
Jennifer Stringfield
Christine O'Connell

Tesaro Drug Development
Scottsdale, AZ
Vicki Goldschmidt
Brianna Maxwell
Linda Wood
Brent Reynolds

Merrimack Pharmaceuticals
Cambridge, MA
Mark Gaschuk
Kristin Gronemeyer
Robert Hall
Kathy Hall
Kelly Hall
Kathy Hall
Kelly Hall
Jeff Hall

#5633
Characterization of metastatic breast cancer lesions with ferumoxytol MRI and clinical response to MM-398, nanoliposomal irinotecan (nal-IRI), in 3 subjects
Jasgit C. Sachdev[1], Ramesh K. Ramanathan[2], Kalarajan Raghunand[3], Jaeyeon Kim[3], Stephan G. Klimt[3], Ellel Bayever[3], Jonathan B. Fitzgerald[3], Ronald L. Korn[4]
[1]Virginia G Piper Cancer Center, Scottsdale Healthcare, Scottsdale, AZ; [2]Translational Cancer Imaging, Arizona Cancer Center, Tucson, AZ; [3]Merrimack Pharmaceuticals, Inc, Cambridge, MA; [4]Imaging Endpoints, Scottsdale, AZ
SCOTTSDALE HEALTHCARE
MERRIMACK

Cancer Research

Poster Session Abstracts

Abstract P5-01-06: Characterization of metastatic breast cancer lesions with ferumoxytol MRI and treatment response to MM-398, nanoliposomal irinotecan (nal-IRI)

Jasgit C Sachdev, Ramesh K Ramanathan, Natarajan Raghunand, Jaeyeon Kim, Stephan G Klinz, Eliel Bayever, Jonathan B Fitzgerald, and Ronald L Korn

DOI: 10.1158/1538-7445.SABCS14-P5-01-06 Published May 2015

Thirty-Seventh Annual CTRC-AACR San Antonio Breast Cancer Symposium; December 9-13, 2014; San Antonio, TX

Abstract

Introduction

Irinotecan has known activity in metastatic breast cancer (MBC). MM-398, nanoliposomal irinotecan (nal-IRI), is designed to exploit leaky tumor vasculature for enhanced drug delivery to tumors. Tumor deposition of nal-IRI and subsequent conversion to SN-38 in both neoplastic cells and tumor associated macrophages (TAM) may positively correlate with activity. Predictive biomarkers to measure tumor deposition could identify patients likely to benefit from nal-IRI. Ferumoxytol (FMX), an iron-oxide superparamagnetic nanoparticle with MRI contrast properties, is taken up by TAMs with similar distribution patterns to nal-IRI in preclinical models. Our previous work has shown the feasibility of quantitative FMX MRI (Fe-MRI) of tumor lesions, and we developed a quantitative mechanistic PK model of FMX deposition (AACR 2014, abstract #CT224). Here we report nal-IRI activity and FMX levels in MBC patients on the study.

Patients and methods

Patients (n=15) with refractory solid tumors and at least two metastatic lesions >2 cm accessible for percutaneous biopsy were enrolled in a Phase 1 study. Fe-MRI scans were performed using T2* iron sensitive sequences prior to and following FMX infusion (1 h, 24 h, 72 h). T2* signal was used to calculate FMX levels in total lesions by comparison to a standard curve. Comparison of quantified FMX lesion uptake with a mechanistic PK model previously indicated that tissue permeability to FMX contributed to early Fe-MRI signals at 1 h and 24 h, while FMX binding contributed at 72 h. Patients then received nal-IRI (80 mg/m^2 q2w) until progression. Core biopsies were obtained 72 h after both FMX and nal-IRI infusions. RECIST evaluation was done by CT every 8 weeks.

Results

FMX was well tolerated, and adverse events to nal-IRI were consistent with previous studies. Three of the 13 patients receiving nal-IRI had ER/PR+ MBC (median # of prior Rx: 8 compared to 4 for all study patients). Thirteen liver lesions (4-5/pt) were evaluated by FMX-MRI and CT for these 3 patients. Average lesion size: 26.9±11.2 mm diameter and 8.1±11.3 cm^3 (median 4.7 cm^3). Time on treatment for the 3 patients was 57, 126 and 256 days (study median 57 days). Best overall response was 1 stable disease (SD) and 1 partial response (PR) in these 3 patients. The patient with a PR had an average lesion size reduction of 44.5%, while the patient with SD had an average lesion size increase of 12.5% at final evaluation. Lesions that shrank after nal-IRI showed higher early levels of FMX compared to the study median (median 39.6 vs. 32.6 mcg/mL at 1 h; median 37.7 vs. 34.5 mcg/mL at 24 h). This relationship between lesion response and FMX levels was consistent with the lesion behavior in the full data set (n=31 lesions/9 patients across 7 indications) of the study.

Conclusions

Clinical activity of nal-IRI was observed in a subset of heavily treated ER/PR+ MBC patients. The relationship between FMX levels in tumor lesions and nal-IRI activity suggests that lesion permeability to FMX may be a useful biomarker for nal-IRI deposition and tumor response in MBC and potentially other indications. A multi-institution expansion of this study in HER2-negative MBC is planned to confirm these findings.

Citation Format: Jasgit C Sachdev, Ramesh K Ramanathan, Natarajan Raghunand, Jaeyeon Kim, Stephan G Klinz, Eliel Bayever, Jonathan B Fitzgerald, Ronald L Korn. Characterization of metastatic breast cancer lesions with ferumoxytol MRI and treatment response to MM-398, nanoliposomal irinotecan (nal-IRI) [abstract]. In: Proceedings of the Thirty-Seventh Annual CTRC-AACR San Antonio Breast Cancer Symposium: 2014 Dec 9-13; San Antonio, TX. Philadelphia (PA): AACR; Cancer Res 2015;75(9 Suppl):Abstract nr P5-01-06.

Previous

Back to top

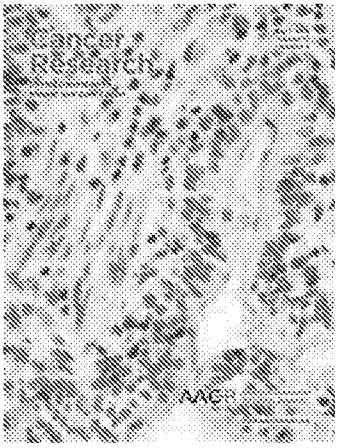

May 2015
Volume 75, Issue 9 Supplement
Table of Contents
Index by Author

Search this issue

Sign up for alerts

[CANCER RESEARCH 64, 2572–2579, April 1, 2004]

Distribution of Liposomes into Brain and Rat Brain Tumor Models by Convection-Enhanced Delivery Monitored with Magnetic Resonance Imaging

Ryuta Saito,[1] John R. Bringas,[1] Tracy R. McKnight,[3] Michael F. Wendland,[3] Christoph Mamot,[2] Daryl C. Drummond,[4,5] Dmitri B. Kirpotin,[4,5] John W. Park,[2,5] Mitchel S. Berger,[1] and Krys S. Bankiewicz[1]

[1]Department of Neurological Surgery, Brain Tumor Research Center, [2]Division of Hematology-Oncology, and [3]Department of Radiology, University of California, San Francisco, San Francisco, California; [4]California Pacific Medical Center Research Institute, Liposome Research Laboratory, San Francisco, California; and [5]Hermes Biosciences, Inc., South San Francisco, California

ABSTRACT

Although liposomes have been used as a vehicle for delivery of therapeutic agents in oncology, their efficacy in targeting brain tumors has been limited due to poor penetration through the blood-brain barrier. Because convection-enhanced delivery (CED) of liposomes may improve the therapeutic index for targeting brain tumors, we conducted a three-stage study: stage 1 established the feasibility of using *in vivo* magnetic resonance imaging (MRI) to confirm adequate liposomal distribution within targeted regions in normal rat brain. Liposomes colabeled with gadolinium (Gd) and a fluorescent indicator, 1,1′-dioctadecyl-3,3,3′,3′-tetramethylindocarbocyanine-5,5′-disulfonic acid [DiI-DS; formally $DiIC_{18}(3)$-DS], were administered by CED into striatal regions. The minimum concentration of Gd needed for monitoring, correlation of infused volume with distribution volume, clearance of infused liposome containing Gd and DiI-DS (Lip/Gd/DiI-DS), and potential local toxicity were evaluated. After determination of adequate conditions for MRI detection in normal brain, stage 2 evaluated the feasibility of *in vivo* MRI monitoring of liposomal distribution in C6 and 9L-2 rat glioma models. In both models, the distribution of Lip/Gd/DiI-DS covering the tumor mass was well defined and monitored with MRI. Stage 3 was designed to develop a clinically relevant treatment strategy in the 9L-2 model by infusing liposome containing Gd (Lip/Gd), prepared in the same size as Lip/Gd/DiI-DS, with Doxil, a liposomal drug of similar size used to treat several cancers. MRI detection of Lip/Gd coadministered with Doxil provided optimum CED parameters for complete coverage of 9L-2 tumors. By permitting *in vivo* monitoring of therapeutic distribution in brain tumors, this technique optimizes local drug delivery and may provide a basis for clinical applications in the treatment of malignant glioma.

INTRODUCTION

Liposomes (phospholipid bilayers formed into spheres in the presence of water that can be made to incorporate a variety of agents) are a vehicle for administering therapeutic agents, including drugs and genes, to areas of the body afflicted with cancer (1, 2). Recently, efforts have been made to increase the vehicular efficiency of liposomes and to direct therapeutic agents to specific target sites (3, 4). Preclinical studies using drug-encapsulated liposomes have shown improvement in the sustained release of the drug, prolongation of the drug's half-life, and an increase in the therapeutic index of corresponding drugs (5). Although immunoliposomes using antibody fragments for molecular targeting have shown promising results (6, 7), the potential effectiveness of such immunoliposomes in targeting tumors of the central nervous system (CNS) has not been established. Systemic administration may not achieve satisfactory penetration of the blood-brain barrier, and local injection cannot achieve optimum distribution.

Convection-enhanced delivery (CED) is a direct intracranial drug delivery technique that utilizes a bulk-flow mechanism to deliver and distribute macromolecules to clinically significant volumes of solid tissues (8, 9). This approach offers a greater volume of distribution than simple diffusion and is designed to direct a drug to a specific target site. As compared with systemic delivery, the CED of liposomes carrying chemotherapeutic drugs bypasses the blood-brain barrier (8), provides a larger distribution of liposomes within the target site, allows for a locally sustained release of drugs, and minimizes systemic exposure, thereby producing fewer side effects.

Despite advances in neurosurgical techniques and in radiation and drug therapies, the mean survival for patients who have a malignant glioma is less than 12 months, and only 20% of patients survive for more than 2 years. More than 80% of patients with this disease experience local recurrence of tumor, which leads to their death (10, 11). Therefore, development of new local management strategies such as the CED of therapeutic liposomes may provide a therapeutic advantage in the adjuvant medical management of gliomas.

To develop a CED method for the administration of liposomal therapeutics in the treatment of malignant glioma, our study was designed in three stages. Stage 1 studies were designed to establish the feasibility of using direct *in vivo* magnetic resonance imaging (MRI) of liposomal delivery to confirm adequate drug distribution within targeted CNS regions. MRI was used to visualize liposomes incorporating the contrast agent gadodiamide [a stable gadolinium (Gd) chelate], which were dispensed by CED to obtain robust distribution in the CNS. The following issues related to the successful application of this technology were assessed in normal brain parenchyma of intact rats: (*a*) monitoring of the CED infusion of liposomes containing Gd and a fluorescent indicator, 1,1′-dioctadecyl-3,3,3′,3′-tetramethylindocarbocyanine-5,5′-disulfonic acid [DiI-DS; formally $DiIC_{18}(3)$-DS], into rat brain hemispheres to evaluate its feasibility and determination of the lowest concentration of contrast agent required to show the targeted distribution area; (*b*) evaluation of the liposome containing Gd and DiI-DS (Lip/Gd/DiI-DS) distribution when infusing a defined volume at intervals from 5 to 40 μl using MRI monitoring and histological detection of the fluorescence; (*c*) a time-course evaluation to determine retention of Gd-containing liposomes in the brain after infusion by CED as represented by the liposomal clearance of the magnetic resonance (MR) signal generated by Lip/Gd/DiI-DS; and (*d*) possible adverse effects of Lip/Gd/DiI-DS infused into the CNS by CED.

After several conditions for MRI detection of Lip/Gd/DiI-DS were established in normal brain parenchyma of intact rats, stage 2 studies evaluated the feasibility of *in vivo* MRI of liposomal distribution in two morphologically dissimilar rat brain tumor models, C6 and 9L-2. These studies addressed the following issues: (*a*) comparison of Lip/Gd/DiI-DS distribution in normal brain and brain tumor tissues to assess the feasibility of using CED administration of liposomes for the treatment of malignant glioma; and (*b*) determination of the distribu-

Received 11/19/03; revised 1/7/04; accepted 1/28/04.

Grant support: National Cancer Institute Specialized Programs of Research Excellence grant (M. Berger, K. Bankiewicz, and J. Park) and Accelerate Brain Cancer Cure (K. Bankiewicz).

The costs of publication of this article were defrayed in part by the payment of page charges. This article must therefore be hereby marked *advertisement* in accordance with 18 U.S.C. Section 1734 solely to indicate this fact.

Requests for reprints: Krys S. Bankiewicz, Department of Neurological Surgery, University of California at San Francisco, 1855 Folsom Street, Mission Center Building Room 230, San Francisco, California 94103. Phone: (415) 502-3132; Fax: (415) 514-2177; E-mail: kbank@itsa.ucsf.edu.

tion of Lip/Gd/DiI-DS in brain tumors using MRI and correlated with the volume infused.

Stage 3 was designed to develop a clinically relevant treatment strategy in the 9L-2 rat brain tumor model by infusing liposome containing Gd (Lip/Gd), prepared as the same size liposome as Lip/Gd/DiI-DS, together with Doxil, a commercially available liposomal drug of similar size that is used clinically in the treatment of cancers other than malignant glioma. The goal of this experiment was to provide a basis for future applications coupling real-time MRI techniques during CED to the direct delivery of therapeutic liposomal agents into brain tumors.

MATERIALS AND METHODS

Liposome Preparation

Liposomes were prepared to contain a MR contrast agent, a fluorescent marker to visualize liposomal distribution histologically, or both of those agents. The paramagnetic contrast agent Gd diethylenetriaminepentaacetatediamide (gadodiamide) was in the form of a commercial United States Pharmacopoeia preparation of Omniscan (Amersham Health, Buckinghamshire, United Kingdom) that contains 0.5 M gadodiamide in water. The fluorescent indicator DiI-DS was obtained from Molecular Probes (Eugene, OR); 1–2-dioleoyl-3-*sn*-glycerophosphocholine and *N*-methoxy-poly(ethylene glycol)-1,2-distearoyl-3-*sn*-phosphoethanolamine (M_r 2000) were obtained from Avanti Polar Lipids (Alabaster, AL); and cholesterol (Chol) was obtained from Calbiochem (San Diego, CA).

For all liposomal preparations, 1–2-dioleoyl-3-*sn*-glycerophosphocholine and cholesterol (molar ratio, 3:2) and *N*-methoxy-poly(ethylene glycol)-1,2-distearoyl-3-sn-phosphoethanolamine (5 mol%) were codiluted in chloroform and brought to dryness in a vacuum by rotary evaporation to form a lipid film. For the preparations to be used in histological studies, DiI-DS (0.2 mol%) was added to the lipid solution. For the MRI studies, liposomes were passively loaded with Gd. The lipid film was hydrated by gentle shaking in 250 mM aqueous solution of gadodiamide and then underwent six successive cycles of freezing at −80°C and thawing at 37°C. The resulting multilamellar liposomes were extruded through polycarbonate membrane filters with defined pore sizes (5 × 0.2 and 5 × 0.05 μm; Ref. 12), yielding liposomes of 77.1 ± 6.6 nm in diameter as determined by dynamic light scattering. The removal of unencapsulated Gd chelate by using a Sephadex G-75 size exclusion column (Pharmacia, Piscataway, NJ) was followed by extensive dialysis against HEPES-buffered saline (pH 6.5). Control liposomes lacking Gd were similarly prepared, except that the lipid film was rehydrated in HEPES-buffered saline (pH 6.5) rather than the Gd solution. Liposome concentration was measured by using a standard phosphate assay (13) and adjusted to 20 mM phospholipid for all experiments. Doxil (doxorubicin hydrochloride liposome i.v. injection; ALZA Pharmaceuticals, Mountain View, CA), used in the Stage 3 experiment, was obtained commercially; in Europe, Japan, and Israel, Doxil is distributed as Caelyx by Schering-Plough (Baulkham Hills, New South Wales, Australia).

Quantification of Liposome-Entrapped Gadodiamide by MR

The concentration of gadodiamide entrapped in the liposomes was determined from nuclear MR relaxivity measurements. The relationship between the change in the intrinsic relaxation rate imposed by a paramagnetic agent (ΔR), also known as "T_1 shortening," and the concentration of the agent is defined by the following equation:

$$\Delta R = r[\text{agent}]$$

in which r = relaxivity of the paramagnetic agent, and $\Delta R = (1/T_{1\,\text{observed}} - 1/T_{1\,\text{intrinsic}})$ [Ref. 14]. Because gadodiamide was encapsulated within the liposome together with DiI-DS, we corrected for the change in the observed T_1 imposed by the lipid and DiI-DS by measuring the T_1 of solubilized liposome containing DiI-DS (Lip/DiI-DS) with and without gadodiamide by using an iterative inversion recovery MRI sequence on a 2 Tesla Brucker Omega scanner (Brucker Medical, Karlsruhe, Germany). The relaxivity of gadodiamide had been empirically derived previously on the same system and was known to have a value of 4.07 $mM^{-1}s^{-1}$. The concentration of the encapsulated gadodiamide was then calculated with the following equation:

$$[\text{gadodiamide}] = [(1/T_{1\,\text{wGado}}) - (1/T_{1\text{w/oGado}})]/4.07$$

Animals

Male Sprague Dawley rats weighing 300–350 g (Charles River Laboratories, Wilmington, MA) and male Fisher 344 rats weighing 200–250 g (Harlan, Indianapolis, IN) were housed under aseptic conditions, which included filtered air and sterilized food, water, bedding, and cages. The protocol used in these studies was approved by the Institutional Animal Care and Use Committee of the University of California, San Francisco.

Surgery and the CED Procedure

While under deep isofluorane anesthesia, rats were placed in a small animal stereotactic frame (David Kopf Instruments, Tujunga, CA). A sagittal incision was made through the skin to expose the cranium, and a burr hole was made in the skull at 0.5 mm anteriorly and 3 mm laterally from the bregma with a small dental drill (15). Infusions were performed at the depth of 4.5 mm from brain surface by using the CED method described previously (16, 17). Briefly, an infusion cannula connected to the Hamilton syringe (Hamilton, Reno, NV) was attached to a rate-controllable microinfusion pump (Bioanalytical Systems, Lafayette, IN). Slow-infusion CED was performed by controlling the infusion rate. For the volume determinations, we evaluated 5-, 10-, 20-, and 40-μl infusions of Lip/Gd/DiI-DS at the original concentration (20 mM phospholipid). The following ascending infusion rates were applied throughout the study to achieve the appropriate target volumes: (*a*) for a 5-μl volume, 0.2 μl/min (15 min) and 0.5 μl/min (4 min); (*b*) for a 10-μl volume, 0.2 μl/min (15 min), 0.5 μl/min (10 min), and 0.8 μl/min (2.5 min); (*c*) for a 20-μl volume, 0.2 μl/min (15 min), 0.5 μl/min (10 min), and 0.8 μl/min (15 min); and (*d*) for a 40 μl volume, 0.2 μl/min (15 min), 0.5 μl/min (10 min), and 0.8 μl/min (40 min).

MRI Methods

Distribution of liposomes was visualized on coronal T_1-weighted spoiled-gradient echo images acquired on a 1.5 Tesla Signa LX scanner (GE Medical Systems, Waukesha, WI) with a pelvic phased array surface coil. The imaging parameters varied according to the number of rats scanned [Repetition Time (TR)/Echo Time (TE)/flip angle = 40 ms/6 ms/30°, 2 number of excitations (NEX), matrix = 256 × 256 or 384 × 256, field of view (FOV) = 18–22 cm, slice thickness = 1.0 mm]. These parameters resulted in nominal voxel sizes that ranged from 0.33 to 0.74 mm^3. Images were acquired approximately 2–4 h after surgery or, for the time-course study, at the indicated intervals. During the MRI examination, rats were anesthetized with an i.p. injection of sodium pentobarbital (50 mg/kg). Three to four rats were scanned during each MRI session.

Stage 1: Determination of Optimal Parameters for MRI Detection of Lip/Gd/DiI-DS in Normal Brain Parenchyma of Intact Sprague Dawley Rats

MRI Detection of Lip/Gd/DiI-DS after Slow-Infusion CED. Four rats were given 20-μl infusions of Lip/Gd/DiI-DS into the right hemisphere and of Lip/DiI-DS (control liposomes) into the left hemisphere. Two rats received, in each hemisphere, 20-μl infusions of gadodiamide solution in a vehicle (HEPES-buffered saline) containing the same concentration of Gd as Lip/Gd/DiI-DS. MR images were acquired approximately 2 h after the infusion. To address the detection limits of Gd when using MRI and to determine the lowest concentration of Gd required to show the targeted distribution area, the original 100% Lip/Gd/DiI-DS mixture was diluted with the vehicle to achieve concentrations of 10%, 20%, and 50%. The diluted mixture was infused into the striatum at a fixed volume of 20 μl/site (9 rats, 18 hemispheres; n = 6 for 100% and 20%; n = 3 for 10% and 50%).

Correlation between Volume of Administration and Volume of Distribution as Measured by MRI and Histological Analysis. To address the relationship between infused volume and volume of distribution inside the normal brain, 20 hemispheres (10 rats) each received 5, 10, 20, or 40 μl of Lip/Gd/DiI-DS by CED infusion; that is, 5 hemispheres received each volume.

MRI was performed about 2 h after surgery, and the MR image-based volume of Lip/Gd/DiI-DS distribution in the right and left hemispheres of each rat was quantified by using image analysis software developed at University of California, San Francisco. A subregion containing only one hemisphere and the surrounding skull from one rat was masked out from the main image. An automated contouring routine that outlines image regions with intensities greater than a specified threshold was used to generate a region of interest (ROI) that corresponded to the liposome distribution in each brain. To control for variations in image intensity arising from the position of each rat within the phased-array MRI coil, we used slightly different threshold intensities for liposome presence based on the mean background signal intensity in each rat. The background signal intensity was determined by averaging the intensity in circular ROIs placed in muscle regions outside of the skull on the same image slices that contained liposomes (Fig. 2*B*). The threshold for liposome presence was the mean background signal intensity + 4 SD. All ROIs generated automatically by the software were visually inspected to confirm accuracy. In some instances, multiple ROIs highlighting liposomes in different brain regions (*e.g.,* white matter and cortex) were combined into a single ROI representing the total volume in one hemisphere. Small (<0.003 cm^3) spurious ROIs located more than 1 mm distant from the primary ROI or in regions outside of the brain parenchyma were excluded from analysis.

For the histological evaluation of Lip/Gd/DiI-DS distribution, the rats were euthanized immediately after each MRI session. The brains were harvested, freshly frozen by using ice-cold isopentane, and cut into serial coronal sections (25 μm) with a cryostat. The fluorescent signal generated by DiI-DS was visualized with a fluorescence microscope, and a charged-coupled device camera with a fixed aperture was used to capture the image. The volume of Lip/Gd/DiI-DS distribution was analyzed by using a Macintosh-based image analysis system (NIH Image 1.62; NIH Bethesda, MD) as described previously (18). The volume of DiI-DS distribution, as determined by the fluorescent microscopy images, was compared with the volume of Gd distribution as detected with 1.5 Tesla MRI.

Liposomal Time-Course Study. Clearance of the MR signal generated by Lip/Gd/DiI-DS when infused by CED into the intact brain was analyzed in the hemispheres of six rats ($n = 12$). MR images were acquired every day [*i.e.,* from 2 to 72 h after CED infusions of Lip/Gd/DiI-DS (20 μl/site)], and the signal intensity was analyzed. In addition, the hemispheres of two rats ($n = 4$) received the infusion by CED with gadodiamide solution (20 μl/hemisphere) in the same vehicle and at the same concentration (4.7 mM) as the Lip/Gd/DiI-DS preparation.

Evaluation of Liposomal Toxicity. To evaluate possible adverse effects of Lip/Gd/DiI-DS on normal brain parenchyma, five Sprague Dawley rats were given 20-μl infusions of the original 100% Lip/Gd/DiI-DS concentration into their right hemisphere and Lip/DiI-DS into their left hemisphere by CED. Body weight was measured before the CED procedure and on day 7 and day 14 after the procedure. Two rats were euthanized on day 7 after the CED procedure for histological evaluation, and three rats were euthanized on day 14 after the CED procedure for histological evaluation. The rats were perfused with 10% formalin, and the brains were processed for histological examination with H&E staining.

Stage 2: *In Vivo* MRI of Liposome Distribution in Brain Tumor Models

Brain Tumor Models. Two established rat glioma cell lines (C6 and 9L-2) were obtained from the Department of Neurological Surgery Tissue Bank at University of California, San Francisco. Cells were seeded into tissue culture flasks approximately 2–3 days before they were implanted into the brains of rats and maintained as monolayers in a complete medium consisting of Eagle's MEM supplemented with 10% FCS and nonessential amino acids. Cells were cultured at 37°C in a humidified atmosphere containing 95% air and 5% CO_2. For the tumor models, cells were harvested by trypsinization, washed once with HBSS without Ca^{2+} and Mg^{2+}, and resuspended in HBSS for implantation.

The C6 glioma cells were implanted into the CNS of three Sprague Dawley rats. The 9L-2 glioma cells were implanted into the CNS of nine Fisher 344 rats. For both tumor models, 5×10^5 cells were stereotactically implanted into the right hemisphere of each rat by using the following coordinates: 0.5 mm anterior and 3 mm lateral from the bregma; and 4.5 mm deep from the brain surface.

CED of liposomal agents was performed on day 16 after tumor implantation for the C6 glioma model and on day 10 after tumor implantation for the 9L-2 glioma model.

Liposome Infusion in a C6 Glioma Brain Tumor Model. To evaluate the feasibility of this method for treating brain tumors, liposomal agents containing Gd/DiI-DS were slowly infused by CED into the C6 glioma brain tumor model in three Sprague Dawley rats. On day 16 after implantation of the tumor cells, 20 μl of Lip/Gd/DiI-DS were administered via intratumoral CED infusion, and a T_1-weighted coronal MR image was taken. Rats were euthanized after the MRI session, and the brains were processed for histological detection of fluorescent signal generated by DiI-DS.

Liposome Infusion in a 9L-2 Rat Brain Tumor Model. CED infusion of Lip/Gd/DiI-DS was evaluated in a 9L-2 tumor model in nine Fisher 344 rats. To test the effect of liposomes on the 9L-2 infiltrative brain tumor model, CED infusions were performed on day 10 after tumor implantation. Because this tumor was invisible without contrast enhancement, a baseline MR image was obtained with the i.p. administration of gadopentetate dimeglumine (Magnevist; Berlex Laboratories, Montreal, Canada) on day 9, before the administration of liposomes, to visualize the tumor size (Fig. 6*B*; Ref. 19). To maximize the signal:noise ratio for better visualization of the tumor volume, we used a T_1-weighted spin echo sequence (TR/TE = 500 ms/20 ms, 4 NEX, 256 × 256 matrix, 18 cm FOV, 1-mm slice thickness) instead of the gradient echo sequence used in the other experiments. On the next day, CED infusion of Lip/Gd/DiI-DS was performed in nine rats; of those rats, three received 20-μl infusions, and six received 40-μl infusions. Similarly to the study with the C6 glioma model, rats were euthanized after the MRI session, and the brains were processed.

Stage 3: Administration of Lip/Gd Together with Doxil

To develop a clinically relevant treatment strategy, a separate experiment addressed the feasibility of coinfusing Lip/Gd, using the same size liposome as Lip/Gd/DiI-DS, with Doxil. Because Doxil (97.8 ± 30.3 nm) and Lip/Gd (77.1 ± 6.6 nm) share similar size characteristics, we hypothesized a similar distribution pattern. To verify this hypothesis, three intact Fisher 344 rats were given a 20-μl infusion of Lip/Gd/DiI-DS by CED into the left hemisphere ($n = 3$) and given the same dose of Doxil into the right hemisphere ($n = 3$). Because Doxil is a liposomal drug containing doxorubicin, which generates fluorescence with UV illumination, the distribution volume was calculated as the fluorescence area generated from Doxil and similarly from Lip/Gd/DiI-DS. Thereafter, 40 μl of a liposome mixture consisting of 20% Lip/Gd (without DiI-DS) and 80% Doxil were infused by CED into the 9L-2 brain tumor in three Fisher 344 rats on day 10 after tumor implantation. MRI was followed by histological examination including H&E staining. The volume of distribution was calculated from the fluorescence generated from Doxil in the 9L-2 tumor model and compared with area of distribution measure using MRI.

RESULTS

Stage 1: Determination of Parameters for MRI Detection of Lip/Gd/DiI-DS in Normal Brain Parenchyma of Intact Rats

MRI Detection of Lip/Gd/DiI-DS after Slow-Infusion CED. Using MRI, the gadodiamide concentration in Lip/Gd/DiI-DS was determined to be 4.7 mM. Infused into a rat brain, this Lip/Gd/DiI-DS (20 μl) generated a clear signal that was detected by MRI and could be monitored at 2 h after infusion. In contrast, Lip/DiI-DS, which contained no Gd, generated no MRI-detectable signal (Fig. 1*A, ii*). Distribution of the gadodiamide solution (4.7 mM) after CED (Fig. 1*A, iii*) differed substantially from that of Lip/Gd/DiI-DS. Whereas the MR signal generated from the Lip/Gd/DiI-DS-treated hemisphere was well defined and confined to regions near the infusion site (Fig. 1*A, ii*), the tissue distribution pattern of gadodiamide solution within the striatum was more diffuse (Fig. 1*A, iii*). Because of the robust MR signal generated by Lip/Gd/DiI-DS containing 4.7 mM Gd, serial dilutions of Lip/Gd/DiI-DS were made to evaluate the sensitivity of the imaging system after CED. Fig. 1*B* shows the signal generated from the stock 100%

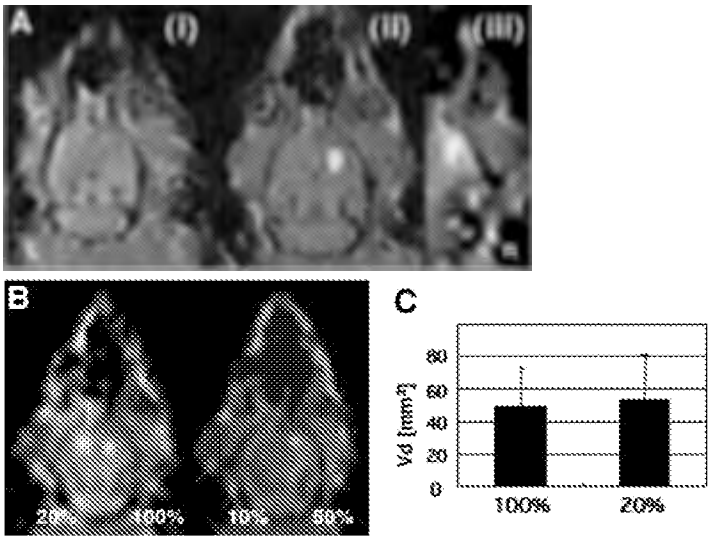

Fig. 1. *A*, T_1-weighted axial magnetic resonance image of an intact normal rat (*i*), a rat given a convection-enhanced delivery infusion of Lip/Gd/DiI-DS into the right hemisphere and a convection-enhanced delivery infusion of Lip/DiI-DS into the left hemisphere (*ii*), and a rat given gadodiamide solution at the same concentration as that for Lip/Gd/DiI-DS into the right hemisphere [20-μl vehicle containing 4.7 mM Gd (*iii*)]. Magnetic resonance imaging (MRI) was performed 2 h after infusion. The signal from Gd-containing liposomes was detected, whereas Lip/DiI-DS could not be detected. The signal from the gadodiamide solution revealed more diffuse distribution. *B*, the concentration of Lip/Gd/DiI-DS detectable with MRI was estimated. Dilutions down to 20% were detectable with a similar distribution volume; however, the signal intensity from 10% Lip/Gd/DiI-DS was insufficient. Lip/Gd/DiI-DS containing 4.7 mM Gd was used for the study. *C*, the volume of distribution as calculated from MRI of the rats receiving a 20% concentration of Lip/Gd./DiI-DS ($n = 6$) was almost the same as that of the rats receiving a 100% concentration ($n = 11$).

Lip/Gd/DiI-DS solution and the 10%, 20%, and 50% dilutions. Signal intensity was observed with the 50% and 20% diluted mixtures of Lip/Gd/DiI-DS, but signal intensity from the 10% Lip/Gd/DiI-DS dilution was insufficient to generate a consistent MRI signal. On the MR images, comparisons showed a similar volume of distribution between the rats receiving the 20% solution and those receiving the Lip/Gd/DiI-DS stock 100% solution (Fig. 1*C*).

Correlation between Volume of Administration and Volume of Distribution as Measured by MRI and Histological Analysis. The volume of liposomal distribution in normal brain was estimated by using histological detection of fluorescence generated from DiI-DS and MR signals. Fig. 2*A* shows representative sections from rats given 10 μl of Lip/Gd/DiI-DS into the left hemisphere and 20 μl of Lip/Gd/DiI-DS into the right hemisphere by CED infusion. Areas of fluorescence were delineated using the NIH Image analysis system, and the volume of distribution was calculated. Correlations between the volume of distribution and the infused dose were made and confirmed by T_1-weighted MR images (Fig. 2*B*). Not surprisingly, the volume of Lip/Gd/DiI-DS distribution as measured by histological techniques was greater than that obtained with MRI, probably due to increased levels of sensitivity. Both methods, however, detected a strong correlation between the volume of Lip/Gd/DiI-DS administration and the volume of distribution (Fig. 2).

Liposomal Time-Course Study. Representative images of Lip/Gd/DiI-DS distribution at 2, 24, 48, and 72 h after CED are shown in Fig. 3*A*. Fig. 3*B* shows the distribution of gadodiamide solution, dispensed at the same concentration as in the Lip/Gd/DiI-DS preparation, at 2 and 24 h after CED. Evaluation of the change of MR signal over time for the gadodiamide solution infusion and Lip/Gd/DiI-DS preparations showed that the gadodiamide solution started to distribute rapidly and also washed out earlier. For the gadodiamide solution, MR signals were diffuse as early as 2 h after CED, and they appeared to disappear at 24 h after infusion. In contrast, the MR signal generated from Lip/Gd/DiI-DS was robust at 2 h and was slightly to moderately diffuse at the infused loci at the 24 and 48 h time points. Even after 72 h, the signal from infused Lip/Gd/DiI-DS was clearly observed. Fig. 3*C* shows the change of MR signal over time after Lip/Gd/DiI-DS infusion, standardized by background MR signal intensity. A correlation between the MR signal intensity and time elapsed was observed.

Evaluation of Liposomal Toxicity. Sprague Dawley rats receiving 20-μl CED infusions of Lip/Gd/DiI-DS into their right hemisphere and the same infusion of Lip/DiI-DS into their left hemisphere showed no substantial evidence of adverse effects over a 14-day period. Daily observations revealed no clinical deficits during the study. The rats appeared healthy and gained or maintained body weight at the same rate as did normal intact rats (Fig. 4*D*). Histological evaluation from two rats euthanized on day 7 after infusion revealed some evidence of tissue inflammation in striatal regions proximal to the needle track on the site infused with Lip/DiI-DS (Fig. 4*A*). The contralateral hemisphere, infused with Lip/Gd/DiI-DS, showed a similar but slightly more intense reaction at the same site (Fig. 4*B*). This tissue reaction was observed only adjacent to the

Fig. 2. *A*, volume of liposome distribution was estimated by using histological detection of fluorescence generated from DiI-DS as compared with that detected from the magnetic resonance (MR) signal. Histological estimations were made from the fluorescent microscopy image detecting the DiI-DS. Representative sections from rat brain receiving a 20-μl infusion into the right hemisphere and a 10-μl infusion into the left hemisphere are shown. Regions generating fluorescence were delineated, and those areas were estimated by using the NIH Image analysis system. Tissue distribution in the normal striatum of rat brain correlated well with the infusion volume. *B*, estimation for volume of liposome distribution was also made from MR images. Representative T_1-weighted axial MR images of rat brain receiving a 20-μl infusion into the right hemisphere (*red-highlighted area*) and a 10-μl infusion into left hemisphere (*green-highlighted area*) are shown. The *yellow-circled area* shows the extra-brain region used for evaluation of background signal intensity. Tissue distribution calculated with MR imaging also showed a good correlation to the infused volume.

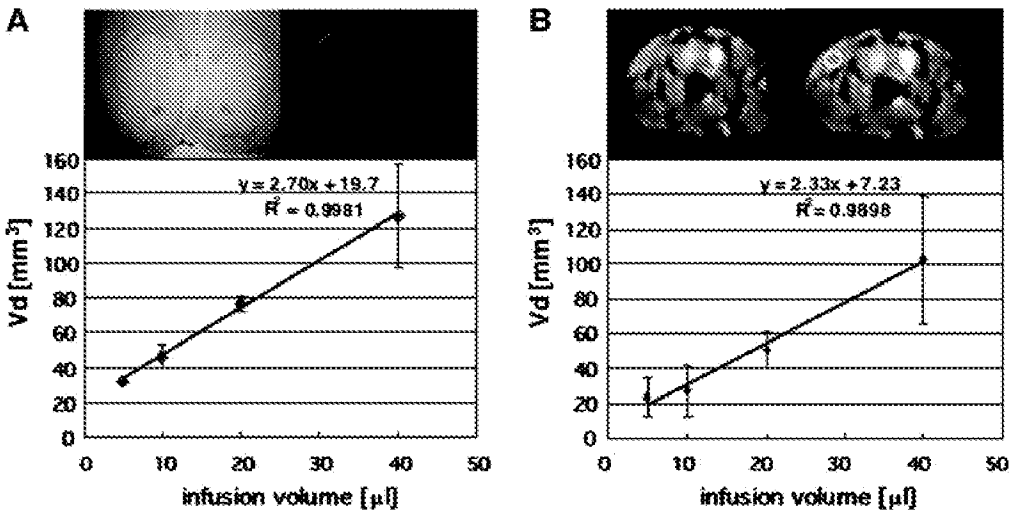

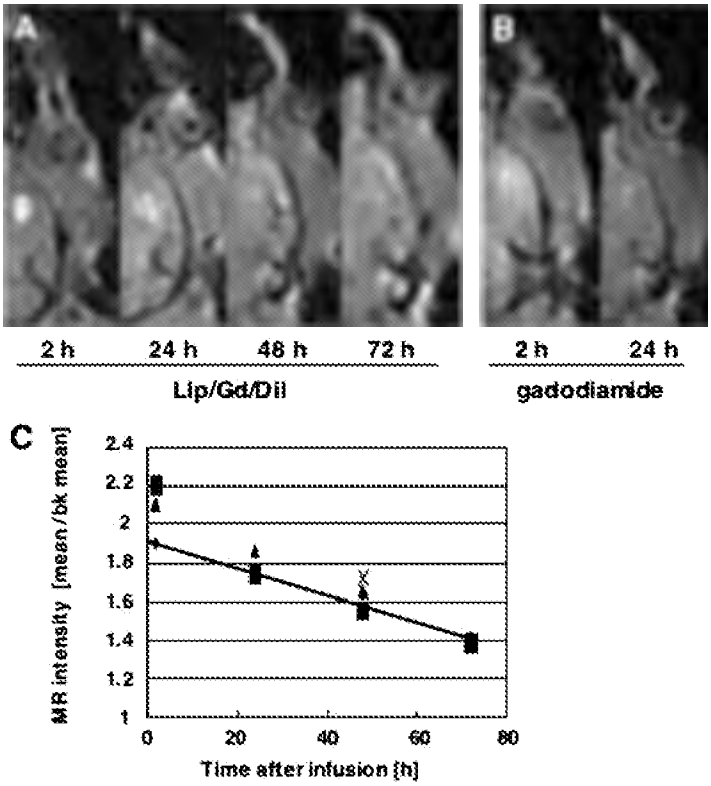

Fig. 3. *A*, T_1-weighted axial magnetic resonance (MR) image showing time-course changes after convection-enhanced delivery infusion of 20 μl of Lip/Gd/DiI-DS. Gd signals were detected even after 72 h of infusion. *B*, T_1-weighted axial MR image showing time-course changes after infusion of gadodiamide solution. As compared with the Lip/Gd/DiI-DS, gadodiamide solution distributed rapidly initially and washed out earlier. *C*, change in MR signals after Lip/Gd/DiI-DS infusion. Mean MR intensity of the distributed area was standardized with the background (*bk*) mean MR signal intensity and plotted against the time after infusion. *Line*, regression line; $R^2 = 0.9905$.

needle tract and had resolved on day 14 (in every three rats euthanized on day 14; Fig. 4*C*).

Stage 2: *In Vivo* MRI of Liposome Distribution in Brain Tumor Models

Two rat brain tumor models with quite different characteristics were used in this study.

C6 Rat Glioma Model. Histological evaluation of the C6 brain tumor model used in our studies showed a heterogeneous tumor with multiple necrosis sites inside and a relatively clearly encapsulated border (Fig. 5*A*; Ref. 20). Liposomes, when infused into this heterogeneous tumor, became distributed in an irregular shape and leaked into the encapsulated tumor margin (Fig. 5, *B* and *C*). This finding was consistent in all three rats we tested. After infusion (Fig. 5*D*), the distribution pattern of fluorescence generated from Lip/Gd/DiI-DS was the same as that observed with MRI (Fig. 5*E*). The volume of liposomal distribution, calculated by histological analysis, achieved within the brain tumor mass was almost the same as that achieved in normal brain (Fig. 5*F*).

9L-2 Rat Gliosarcoma Model. Histological evaluation of the 9L-2 rat brain tumor model used showed a relatively homogeneous tumor with invasive chracteristics (Fig. 6*A*). T_1-weighted MRI with contrast enhancement obtained a day before liposome infusion detected a tumor mass (Fig. 6*B*). After CED infusion of Lip/Gd/DiI-DS, almost the whole tumor mass was covered with Lip/Gd/DiI-DS (Fig. 6*C*). Histological evaluation of the tumor after the infusion showed the tumor mass (Fig. 6*D*), and the whole brain tumor together with surrounding normal brain was covered with Lip/Gd/DiI-DS (Fig. 6*E*). MRI showed a similar volume of distribution in the 9L-2 tumor model (Fig. 6*F*) and in normal brain (Fig. 2*B*).

Stage 3: Administration of Lip/Gd Together with Doxil

In assessing the potential clinical relevance of a treatment strategy based on these studies, we found that Lip/Gd/DiI-DS had a distribution pattern similar to that of the drug Doxil after CED infusion in normal brain (Fig. 7*A*). After CED infusion of Lip/Gd (in liposomes the same size as Lip/Gd/DiI-DS) and Doxil into rats with a 9L-2 brain tumor (Fig. 7*B*), MRI showed that almost the entire tumor mass was covered with the liposome mixture (Fig. 7*C*). The representative histological tumor section from the same rat obtained immediately after the MRI session (Fig. 7*D*) and the fluorescent signal generated from Doxil in the same section (Fig. 7*E*) correlated with MRI. Heterogeneous pattern of Doxil distribution was attributed to different tissue density in the tumor and surrounding area; however, both structures contained Doxil (Fig. 7, *E* and *F*). The volume of distribution calculated from the fluorescent signal generated from Doxil in the 9L-2 tumor model was in the same range as expected from the data presented in Fig. 2*A* (histological data for Doxil not shown).

DISCUSSION

The blood-brain barrier, while otherwise protecting the brain, restricts the delivery of systemically administered agents for treating brain tumors. Although partial disruption of blood-brain barrier is noted in brain tumors, efficient systemic drug delivery throughout the tumor is very difficult. In addition, infiltrating cells that are often outside of main tumor mass could not be targeted via systemic delivery. Therefore, CED techniques, introduced in 1994, as a method to circumvent the blood-brain barrier and enhance distribution of

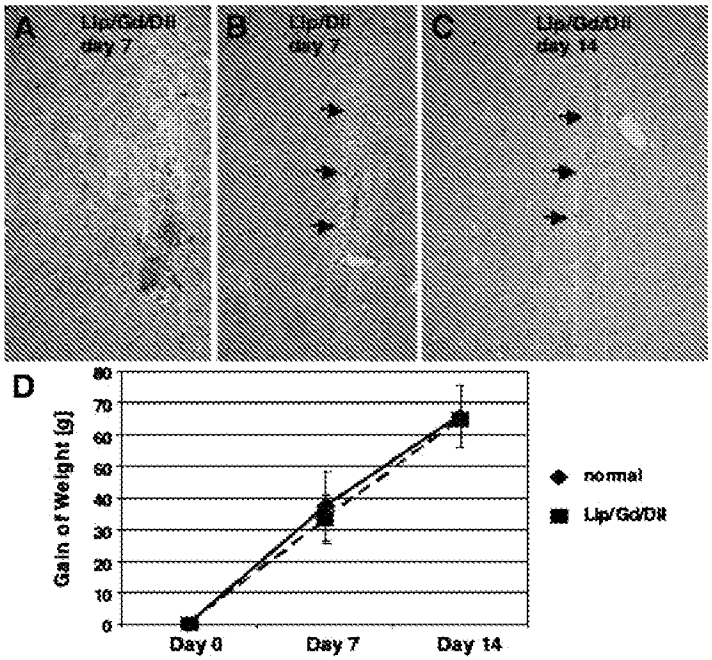

Fig. 4. Toxicity analysis. *A*–*C*, H&E stainings of paraffin sections (magnification, ×50). Five rats received a 20-μl infusion of Lip/Gd/DiI-DS into the right hemisphere and a 20-μl infusion of Lip/DiI-DS into the left hemisphere. After 7 days of infusion, inflammation noted in the brain receiving Lip/Gd/DiI-DS (*A*) was a little greater than inflammation of the brain receiving Lip/DiI-DS (*B*); however, the only inflamed tissue was adjacent to the needle tract and was resolving after 14 days (*C*). *Arrow* shows the needle tract found in these sections. *D*, gain in body weight of the rats receiving Lip/Gd/DiI-DS and Lip/DiI-DS infusions was compared with that of intact normal rats (data point: $n = 5$ for day 7; $n = 3$ for day 14).

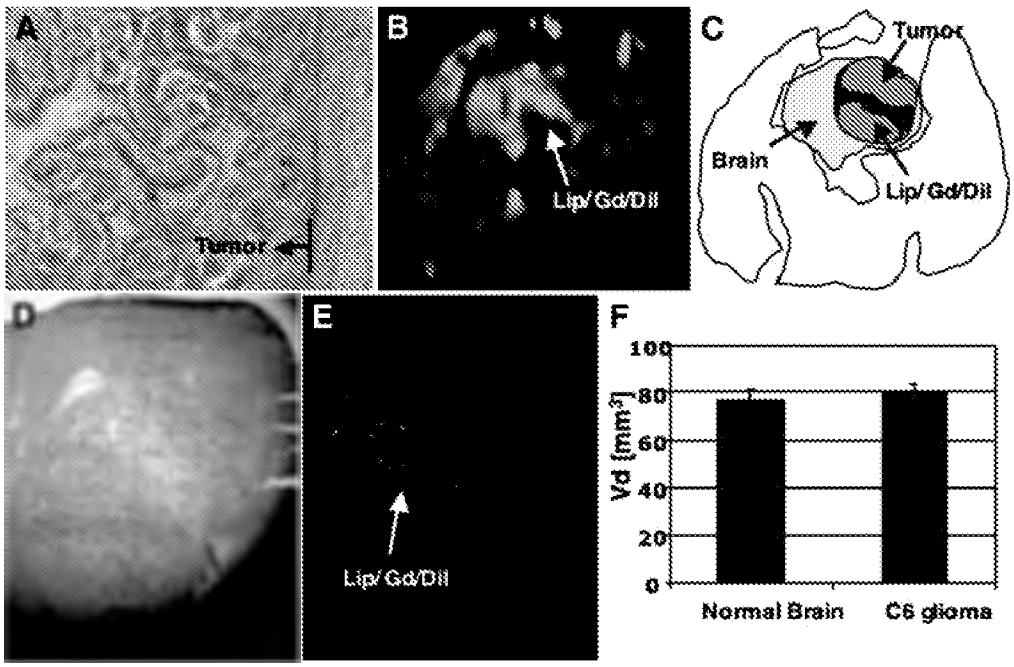

Fig. 5. Convection-enhanced delivery infusion of Lip/Gd/DiI-DS in the C6 glioma rat brain tumor model. *A*, histological image of a C6 glioma implanted into the brain of Sprague Dawley rat shows a heterogeneous tumor with necrosis inside and a relatively clearly encapsulated border (H&E staining). *B*, T_1-weighted coronal magnetic resonance image after the infusion of 20 μl of Lip/Gd/DiI-DS into a C6 glioma on day 16 after implantation. *C*, illustration depicting *B*: the brain is the *light blue area*; the C6 glioma tumor is *gray*; and the infused liposome is shown as the *black region*. Liposomes, when infused into this heterogeneous C6 glioma tumor, became distributed in an irregular shape and leaked into the encapsulated tumor margin. *D*, histological image (H&E staining) made after infusion shows a large tumor. *E*, fluorescence generated from DiI-DS in the same section. The distribution pattern and shape were comparable with that observed in *B*. *F*, the volume of distribution in the tumor mass, as calculated from histological analysis and compared with that achieved in normal brain, showed almost the same volume of distribution in tumor and normal brain.

therapeutic agents by local administration (8), represent promising technique for brain tumor therapy, and the safety and feasibility of CED have been well established (16, 17, 21). However, to deliver cytotoxic agents as therapy for brain tumors, which often reside in such critical regions of the brain as the motor cortex, CED administration must meet several requirements. The anticancer agent must be distributed as completely as possible within the tumor and the tumor margins to achieve maximum therapeutic response, but if the agent does not specifically target tumor cells, its distribution has to be restricted to the target tissue to limit nonspecific toxicity. In addition, as shown in our result with infusion in C6 glioma model, tissue distribution can be heterogenic, with therapeutic agent leaking into an undesirable area. Tissue distribution after CED can be significantly reduced when the catheter tip is placed in the proximity of a large blood vessel, white matter tracts, or a resection cavity due to fluid escape along path of less resistance. Moreover, receptor distribution in the brain tumor and resident cells also will limit tissue penetration of the compounds that possess affinity to these receptors (18, 22). Thus, the only way to ensure efficient delivery of therapeutic agents with CED is to use a vehicle for the compound that will permit visualization of its tissue distribution by using real-time imaging (23). Liposomes have been extensively studied as a carrier of drugs for cancer therapy, including surrogate markers for visualization, and are a good candidate to fill this role (24).

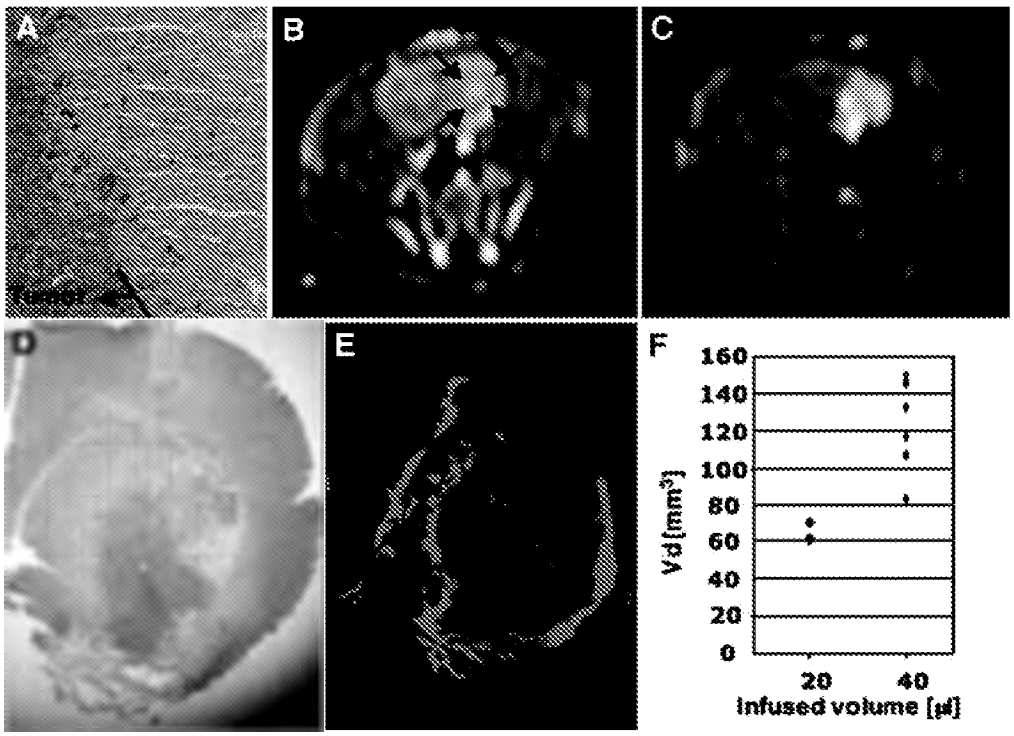

Fig. 6. Convection-enhanced delivery infusion of Lip/Gd/DiI-DS into a 9L-2 glioma rat brain tumor model. *A*, histological image of a 9L-2 glioma grown in the brain of Fisher 344 rat shows a relatively homogeneous tumor with invasive characteristics (H&E staining). *B*, on day 9, this T_1-weighted spin echo magnetic resonance image was obtained after i.p. injection of a contrast agent. *C*, on day 10, 40 μl of Lip/Gd/DiI-DS were infused by convection-enhanced delivery. Almost the whole tumor mass was covered with Lip/Gd/DiI-DS. *D*, histological image of the tumor after infusion of liposomes (H&E staining). *E*, DiI-DS distribution was detected in this section. Almost the whole brain tumor and the surrounding normal brain were covered with Lip/Gd/DiI-DS. *F*, the volume of distribution detected by magnetic resonance imaging in the 9L-2 tumor-bearing rat brain. Three rats received a 20-μl infusion, and 9 rats received a 40-μl infusion. The distribution was similar to that in normal brain, as shown in Fig. 2*B*.

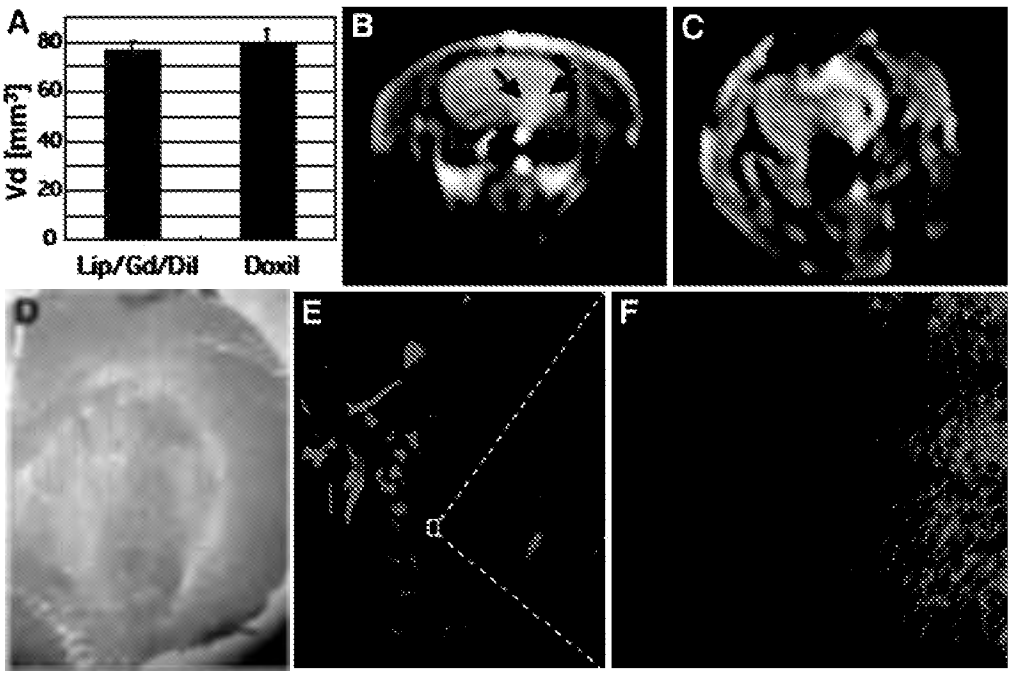

Fig. 7. Infusion of Gd-loaded liposomes mixed with Doxil for convection-enhanced delivery. *A*, Lip/Gd/DiI-DS (20 μl) and Doxil (20 μl) were infused in normal intact Sprague Dawley rats (n = 3 for each group). The volume of distribution was calculated by histological detection of the fluorescence generated from DiI-DS in the Lip/Gd/DiI-DS and the fluorescence generated from Doxil itself. The volume of distribution was almost the same for Lip/Gd/DiI-DS and Doxil. *B*, T_1-weighted coronal magnetic resonance image of a 9L-2 rat brain tumor made with contrast enhancement on day 9 after tumor implantation. *C*, a mixture of Lip/Gd (20%) and Doxil (80%) was infused with convection-enhanced delivery in three rats on day 10. The total volume infused was 40 μl. *D*, histological image (H&E staining) made after infusion. *E*, fluorescence generated by Doxil in the same slice covers almost the whole tumor mass. *F*, higher magnification of *highlighted area* of *E* (×100).

In this study, to develop an effective method of liposomal brain tumor therapy administered with CED, we established a method for using MRI to monitor the CED of liposomes in the brain. Although there were small differences between the volumes calculated from fluorescent images and MR images, they could be attributed to the greater sensitivity of the histological methods as compared with evaluation of MR images, and monitoring with MRI gave precise information about distribution pattern. MRI monitoring also enabled us to monitor the difference of distribution between different tumor models, *i.e.*, C6 gliomas and 9L-2 gliomas, which suggests the importance of real-time imaging when clinical application is considered. The tumor model with 9L-2 cells, which is a subline derived from commonly used 9L gliosarcoma cells, used in this study has invasive properties, thus it can be considered as a proper model for drug delivery. CED effectively distributed the liposomes in the tumor and the surrounding normal brain tissue that contained isolated invasive tumor cells, implying the potential of a valuable therapeutic advantage in using CED for the treatment of human glioblastoma. In addition, the correlation between the infused volume and the distribution of liposomes in the brain tumor models was almost identical to that observed in normal brain tissue, a finding that could be important in predicting the distribution volume after infusion. One more finding was that the distribution of Doxil infused into the 9L-2 brain tumor model could be monitored using MRI by mixing Doxil with Lip/Gd (marker liposome), which also implies potential anticancer effects of this type of drug administration.

On the other hand, liposome-encapsulated cytotoxic drugs have several potential advantages over corresponding unencapsulated agents (2, 25, 26). When infused systemically, the liposome prolongs the half-life of the drugs in circulation and alters the biodistribution pattern, such that drug deposition is increased in tumor tissue. Taking this advantage, many liposome-encapsulated cytotoxic agents are currently undergoing clinical evaluation, including doxorubicin (27, 28), vincristine (29), and cisplatin (30), and some of them have shown efficacy in patients with solid cancers. After CED of liposomes containing pharmaceutical agents, the majority of the drug is contained within the region of infusion. We believe that drugs may slowly leak into the interstitium after nonspecific intracellular endocytosis (31), thus prolonging exposure of the targeted tissue to the drug. Our recent data after CED of Doxil into rodent brain tumors suggest that doxorubicin is present in the tissue several weeks after a single administration.[6] In addition, greater therapeutic response was detected after CED of Doxil than after systemic administration,[6] further demonstrating therapeutic advantage of local administration of liposomes.

Our findings provide a foundation for real-time MRI monitoring of therapy delivered by liposomal administration through CED into the CNS. They indicate that liposomes containing an anticancer drug could be either loaded with gadodiamide or administered simultaneously with gadodiamide liposomes to provide direct evidence of the volume of distribution of the drug in tissues during CED. Several parameters of CED, such as precise placement of the cannula and control of the rate of infusion and volume of agent delivered, could be adjusted during the infusion to ensure the most safe and efficient local administration of the medication. Several key issues must be addressed, however, before clinical application of this method could be considered. Development of real-time MRI monitoring of liposome distribution during CED is now being developed in our laboratory using nonhuman primates. As for the liposomes, the best therapeutic drug for encapsulation must be identified; liposome constructs, including lipid composition and surface pegylation, must be evaluated, and there must be further development of immunoliposomes for targeting tumor cells. Nonetheless, we believe that the MRI-monitored *in vivo* detection of liposomes after CED is a first step toward successful clinical application of this technology.

ACKNOWLEDGMENTS

We thank Pamela Jackson (Department of Radiology, University of California, San Francisco) for technical assistance, Dr. David Newitt (Magnetic Resonance Science Center, University of California, San Francisco) for providing the software to measure distribution volume with MRI, and Susan Eastwood (Department of Neurological Surgery, University of California, San Francisco) for editorial advice.

[6] Unpublished data.

REFERENCES

1. Gregoriadis G, Wills EJ, Swain CP, Tavill AS. Drug-carrier potential of liposomes in cancer chemotherapy. Lancet 1974;29:1313–6.
2. Harrington KJ. Liposomal cancer chemotherapy: current clinical applications and future prospects. Exp Opin Investig Drugs 2001;10:1045–61.
3. Voinea M, Simionescu M. Designing of "intelligent" liposomes for efficient delivery of drugs. J Cell Mol Med 2002;6:465–74.
4. Maruyama K. In vivo targeting by liposomes. Biol Pharm Bull 2000;23:791–9.
5. Moog R, Burger AM, Brandl M, et al. Change in pharmacokinetics and pharmacodynamic behavior of gemcitabine in human tumor xenografts upon entrapment in vesicular phospholipid gels. Cancer Chemother Pharmacol 2002;49:356–66.
6. Park JW, Hong K, Kirpotin DB, et al. Anti-HER2 immunoliposomes for targeted therapy of human tumors. Cancer Lett 1997;118:153–60.
7. Park JW, Hong K, Kirpotin DB, Papahadjopoulos D, Benz CC. Immunoliposomes for cancer treatment. In: August JT, Coyle, JT, editors. Gene Therapy, Advances in Pharmacology, Vol. 40. San Diego, CA: Academic Press; 1997. p. 399–435.
8. Bobo RH, Laske DW, Akbasak A, et al. Convection-enhanced delivery of macromolecules in the brain. Proc Natl Acad Sci USA 1994;91:2076–80.
9. Morrison PF, Laske DW, Bobo H, Oldfield EH, Dedrick RL. High-flow microinfusion: tissue penetration and pharmacodynamics. Am J Physiol 1994;266:R292–305.
10. Behin A, Hoang-Xuan K, Carpentier AF, Delettre, JY. Primary brain tumors in adults. Lancet 2003;361:323–31.
11. Gupta T, Sarin R. Poor-prognosis high-grade gliomas: evolving an evidence-based standard of care. Lancet Oncol 2002;3:557–64.
12. Szoka F, Olson F, Heath T, et al. Preparation of unilamellar liposomes of intermediate size (0.1–0.2 μm) by a combination of reverse phase evaporation and extrusion through polycarbonate membranes. Biochim Biophys Acta 1980;601:559–71.
13. Bartlett GR. Phosphorus assay in column chromatography. J Biol Chem 1959;234: 466–8.
14. Caravan P, Ellison JJ, McMurry TJ, Lauffer RB. Gadolinium(III) chelates as MRI contrast agents: structure, dynamics, and applications. Chem Rev 1999;99:2293–352.
15. Paxinos G, Watson C. The rat brain in stereotactic coordinates, 3rd ed. Orlando, FL: Academic Press; 1997.
16. Lieberman DM, Laske DW, Morrison PF, Bankiewicz KS, Oldfield EH. Convection-enhanced distribution of large molecules in gray matter during interstitial drug infusion. J Neurosurg 1995;82:1021–9.
17. Bankiewicz KS, Eberling JL, Kohutnicka M, et al. Convection-enhanced delivery of AAV vector in parkinsonian monkeys; in vivo detection of gene expression and restoration of dopaminergic function using pro-drug approach. Exp Neurol 2000;164: 2–14.
18. Hamilton JF, Morrison PF, Chen MY, et al. Heparin coinfusion during convection-enhanced delivery (CED) increases the distribution of the glial-derived neurotrophic factor (GDNF) ligand family in rat striatum and enhances the pharmacological activity of neurturin. Exp Neurol 2001;168:155–61.
19. Wilkins DE, Raaphorst GP, Saunders JK, Sutherland GR, Smith IC. Correlation between Gd-enhanced MR imaging and histopathology in treated and untreated 9L rat brain tumors. Magn Reson Imaging 1995;13:89–96.
20. Grobben B, De Deyn PP, Slegers H. Rat C6 glioma as experimental model system for the study of glioblastoma growth and invasion. Cell Tissue Res 2002;310:257–70.
21. Bruce JN, Falavigna A, Johnson JP, et al. Intracerebral clysis in a rat glioma model. Neurosurgery 2000;46:683–91.
22. Nguyen JB, Sanchez-Pernaute R, Cunningham J, Bankiewicz KS. Convection-enhanced delivery of AAV-2 combined with heparin increases TK gene transfer in the rat brain. Neuroreport 2001;12:1961–4.
23. Lonser RR, Walbridge S, Garmestani K, et al. Successful and safe perfusion of the primate brainstem: in vivo magnetic resonance imaging of macromolecular distribution during infusion. J Neurosurg 2002;97:905–13.
24. Rubesova E, Berger F, Wendland MF, et al. Gd-labeled liposomes for monitoring liposome-encapsulated chemotherapy: quantification of regional uptake in tumor and effect on drug delivery. Acad Radiol 2002;9(Suppl. 2):S525–7.
25. Harrington KJ, Lewanski CR, Stewart JS. Liposomes as vehicles for targeted therapy of cancer. Part 1: preclinical development. Clin Oncol 2000;12:2–15.
26. Drummond DC, Meyer O, Hong K, Kirpotin DB, Papahadjopoulos D. Optimizing liposomes for delivery of chemotherapeutic agents to solid tumors. Pharmacol Rev 1999;51:691–743.
27. Cowens JW, Creaven PJ, Greco WR, et al. Initial clinical (Phase I) trial of TLC D-99 (doxorubicin encapsulated in liposomes). Cancer Res 1993;53:2796–802.
28. Perez AT, Domenech GH, Frankel C, Vogel CL. Pegylated liposomal doxorubicin (Doxil) for metastatic breast cancer: the Cancer Research Network, Inc., experience. Cancer Investig 2002;20 (Suppl. 2):22–9.
29. Sarris AH, Hagemeister F, Romaguera J, et al. Liposomal vincristine in relapsed non-Hodgikin's lymphomas: early results of an ongoing Phase II trial. Ann Oncol 2000;11:69–72.
30. Harrington KJ, Lewanski CR, Northcote AD, et al. Phase I-II study of pegylated liposomal cisplatin (SPI-077) in patients with inoperable head and neck cancer. Ann Oncol 2001;12:493–6.
31. Forssen EA, Male-Brune R, Adler-Moore JP, et al. Fluorescence imaging studies for the disposition of daunorubicin liposomes (DaunoXome) within tumor tissue. Cancer Res 1996;56:2066–75.

Available online at www.sciencedirect.com
SCIENCE DIRECT
ELSEVIER
Experimental Neurology 196 (2005) 381–389
Experimental Neurology
www.elsevier.com/locate/yexnr

Regular Article

Gadolinium-loaded liposomes allow for real-time magnetic resonance imaging of convection-enhanced delivery in the primate brain

Ryuta Saito [a], Michal T. Krauze [a], John R. Bringas [a], Charles Noble [b], Tracy R. McKnight [c], Pamela Jackson [c], Michael F. Wendland [c], Christoph Mamot [b], Daryl C. Drummond [d], Dimitri B. Kirpotin [d], Keelung Hong [d], Mitchel S. Berger [a], John W. Park [b], Krystof S. Bankiewicz [a,*]

[a] *Department of Neurological Surgery, Brain Tumor Research Center, University of California, San Francisco, 1855 Folsom Street, Room 226, San Francisco, CA 94103, USA*
[b] *Division of Hematology-Oncology, University of California, San Francisco, 1855 Folsom Street, Room 226, San Francisco, CA 94103, USA*
[c] *Department of Radiology, University of California, San Francisco, 1855 Folsom Street, Room 226, San Francisco, CA 94103, USA*
[d] *Hermes Biosciences, Inc., 65 Airport Blvd. Suite B, South San Francisco, CA 94080, USA*

Received 9 April 2005; revised 18 July 2005; accepted 23 August 2005
Available online 28 September 2005

Abstract

Drug delivery to brain tumors has long posed a major challenge. Convection-enhanced delivery (CED) has been developed as a drug delivery strategy to overcome this difficulty. Ideally, direct visualization of the tissue distribution of drugs infused by CED would assure successful delivery of therapeutic agents to the brain tumor while minimizing exposure of the normal brain. We previously developed a magnetic resonance imaging (MRI)-based method to visualize the distribution of liposomal agents after CED in rodent brains. In the present study, CED of liposomes was further examined in the non-human primate brain ($n = 6$). Liposomes containing Gadoteridol, DiI-DS, and rhodamine were infused in corona radiata, putamen nucleus, and brain stem. Volume of distribution was analyzed for all delivery locations by histology and MR imaging. Real-time MRI monitoring of liposomes containing gadolinium allowed direct visualization of a robust distribution. MRI of liposomal gadolinium was highly accurate at determining tissue distribution, as confirmed by comparison with histological results from concomitant administration of fluorescent liposomes. Linear correlation for liposomal infusions between infusion volume and distribution volume was established in all targeted locations. We conclude that an integrated strategy combining liposome/nanoparticle technology, CED, and MRI may provide new opportunities for the treatment of brain tumors. Our ability to directly monitor and to control local delivery of liposomal drugs will most likely result in greater clinical efficacy when using CED in management of patients.

Keywords: Convection-enhanced delivery; MRI; Primate; Liposomes; CNS

Introduction

Despite recent advances in drug delivery techniques, effective drug delivery to the central nervous system (CNS) still remains a challenge. Several randomized trials of systemic chemotherapy for malignant glioma, performed over a period of almost 30 years, have provided disappointing results (Stewart, 2002). The blood–brain barrier (BBB), though compromised to some extent in tumor tissue, can limit the effective distribution of systemically administered agents. Although direct local injection methods bypass the BBB, the effect of the injected drug is limited by poor tissue penetration in the brain parenchyma as well as in tumor tissue. Several newer drug delivery systems, including drug polymers (Guerin et al., 2004), have shown promise, although the extent of tissue penetration and distribution of these therapeutic agents remains suboptimal.

Several investigators (Bobo et al., 1994) have recently demonstrated the efficacy of convection-enhanced delivery (CED) as an alternative therapeutic strategy for treating focal CNS diseases such as brain tumors. This local infusion technique, utilizing bulk flow, enables the delivery of small

* Corresponding author. Fax: +1 415 514 2177.
E-mail address: kbank@itsa.ucsf.edu (K.S. Bankiewicz).

0014-4886/$ - see front matter © 2005 Elsevier Inc. All rights reserved.
doi:10.1016/j.expneurol.2005.08.016

and large molecules to clinically significant volumes of targeted tissues, offering an improved volume of distribution (Vd) compared to simple diffusion. Clinically, CED techniques have mainly been explored for the treatment of brain tumors (Lidar et al., 2004). However, CED-mediated strategies are now being actively studied for the treatment of Parkinson's disease (Bankiewicz et al., 2000), peripheral nerve injury (Ratliff and Oldfield, 2001), and other CNS disorders (Levy et al., 2001). CED of therapeutic agents bypasses the BBB, and provides a high concentration of the therapeutic agent within the injection site and a larger distribution of therapeutic agents within the target site. The net result is minimal systemic exposure and a change in the toxicity profile of the infused agents. When applying CED techniques to treating brain tumors, at least two issues need to be addressed: (1) how to deliver the therapeutic agents to cover the entire brain tumor mass, and (2) how to protect adjacent and surrounding normal brain tissue. With the hypothesis that visualization of drug distribution during CED administration will be the first step toward this goal, and with the aid of recent advances in liposome nanotechnology, we have focused on liposomes that carry chemotherapeutic drugs and a surrogate marker for MRI detection (Rubesova et al., 2002). In these studies, we demonstrated the effective distribution of liposomes using CED techniques in the brains of rodents (Mamot et al., 2004; Saito et al., 2004). We also validated MRI monitoring of liposome distribution during CED in a rodent intracranial tumor model (Saito et al., 2004).

To further develop this nanotechnology-based strategy toward clinical application, we evaluated the feasibility of performing real-time MRI monitoring of liposomes during CED infusion in the brains of non-human primates. For MRI studies, liposomes loaded with a gadolinium (Gd) chelate–Gadoteridol–(liposomal Gd) were constructed and imaged in real-time during CED to assess distribution, retention, and safety in the primate CNS. By using liposomes loaded with fluorescent markers, the correlation between infused volume and distribution volume was studied by careful histological analysis. Liposomal Gd and liposomes with fluorescent markers were co-infused during real-time MR imaging, and co-registration of MR images, with histological images acquired after necropsies, was performed.

Methods

Liposome preparation

Separate liposomes were prepared for detection by MRI and by histological examination. Liposomes containing the MRI contrast agent were composed of 1,2-dioleoyl-*sn*-glycero-3-phosphocholine (DOPC)/cholesterol/1,2-distearoyl-*sn*-glycero-3-[methoxy(polyethylene glycol)-2000 (PEG-DSG) with a molar ratio of 3:2:0.3. DOPC was purchased from Avanti Polar Lipids (Alabaster, AL), PEG-DSG was purchased from NOF Corporation (Tokyo, Japan), and cholesterol was purchased from Calbiochem (San Diego, CA). The lipids were dissolved in chloroform/methanol (90:10, vol/vol), and then the solvent was removed by rotary evaporation, resulting in a thin lipid film. The lipid film was dissolved in ethanol and heated to 60°C. A commercial United States Pharmacopeia solution of 0.5 M Gadoteridol (10-(2-hydroxy-propyl)-1,4,7,10-tetraazacyclododecane-1,4,7-triacetic acid (Prohance; Bracco Diagnostics, Princeton, NJ) was heated to 60°C and injected rapidly into the ethanol/lipid solution. Unilamellar liposomes were formed by extrusion (Lipex; Northern Lipids, Vancouver, Canada) with 15 passes through double-stacked polycarbonate membranes (Whatman Nucleopore, Clifton, NJ) with a pore size of 100 nm, resulting in a liposome diameter of 124 ± 24.4 nm as determined by quasi-elastic light scattering (N4Plus particle size analyzer, Beckman Coulter, Fullerton, LA). Unencapsulated Gadoteridol was removed with a Sephadex G-75 (Sigma, St. Louis, MO) size-exclusion column eluted with pH 6.5 HEPES-buffered saline (5 mM HEPES, 135 mM NaCl, pH adjusted with NaOH). Liposomes loaded with rhodamine for histological studies were formulated using the same lipid composition and preparation method as the Gadoteridol-containing liposomes, except that the lipids were hydrated directly with 20 mM sulforhodamine B (Sigma) in pH 6.5 HEPES-buffered saline by six successive cycles of rapid freezing and thawing rather than by ethanol injection. The sulforhodamine B liposomes had a diameter of 90±30 nm (used alone for histological analysis) or 115±40.1 nm (used for co-infusion with the Gadoteridol-containing liposomes in the MRI-monitoring study). For the preparation of liposomes containing a DiI-DS fluorescent probe, 1,1′-dioctadecyl-3,3,3′,3′-tetramethylindocarbocyanine-5,5′-disulfonic acid ($DiIC_{18}(3)$-DS) (DiI-DS; Molecular Probes, Eugene, OR) was added to the lipid solution at a concentration of 0.2 mol% of the total lipid. DiI-DS liposomes had a diameter of 110 ± 40 nm.

Quantification of liposome-entrapped Gadoteridol by magnetic resonance imaging

In order to determine the total concentration of Gadoteridol infused into the brain, we first calculated the concentration of Gadoteridol entrapped in the liposomes using nuclear MR relaxivity measurements. The relationship between the change in the intrinsic relaxation rate imposed by a paramagnetic agent ($\Delta R1$), also known as "T1 shortening," and the concentration of the agent is defined by the equation:

$$\Delta R1 = r[\text{agent}]$$

in which r = relaxivity of the paramagnetic agent and $\Delta R1 = (1/T1_{observed} - 1/T1_{intrinsic})$. As Gadoteridol was encapsulated within the liposome, we corrected for the change in the observed T1 imposed by the lipid by measuring the T1 of solubilized liposomes with and without Gadoteridol by using an iterative inversion-recovery MRI sequence on a 2-T Brucker Omega scanner (Brucker Medical, Karlsruhe, Germany). The relaxivity of Gadoteridol had been empirically derived previously on the same system and was known to have a value of 4.07 $mM^{-1}\,s^{-1}$. The concentration of Gadoteridol encapsulated

within the liposomes was then calculated with the following equation:

$$[\text{Gadoteridol}] = \left[\left(1/T1_{\text{wGado}}\right) - \left(1/T1_{\text{w/oGado}}\right)\right]/4.07$$

where $T1_{\text{wGado}}$ was the T1 of the Gadoteridol-filled liposomes and $T1_{\text{w/oGado}}$ was the T1 of empty liposomes (with no Gadoteridol).

The total Gadoteridol dose delivered could then be determined directly from the concentration of liposomes infused into each brain region.

In this study, we did not attempt to determine the local dose distribution within the tissue using the T1 relaxivity changes observed before and after infusion, primarily because the effect of the brain micro-environment on the permeability of the liposomes is unknown. Gadoteridol shortens the T1 of water with which it interacts, thus, local enzymatic and/or thermal processes that alter the permeability or size of the liposomes may cause a T1 change that is independent of the local concentration of liposomes. Additional experiments with co-infused liposomes containing a quantitative histologic indicator are needed to determine the accuracy of using T1 measurements to determine local dose.

Experimental subjects

The protocol was reviewed and approved by the Institutional Animal Care and Use Committees at the University of California San Francisco (San Francisco, CA) and at Sierra Biomedical (Reno, NV). Adult male cynomolgus monkeys (*Macaca fasicularis*, $n = 6$, 3–10 kg, imported from China) were individually housed in stainless steel cages. Each animal room was maintained on a 12-h light/dark cycle and room temperature ranged between 64°F and 84°F. Purina Primate Diet was provided on a daily basis in amounts appropriate for the size and age of the animals. This diet was supplemented with fruit or vegetables daily. Also, small bits of fruit, cereal, or other treats were provided as part of the environmental enrichment program. Tap water was available ad libitum to each animal through an automatic watering device or an attached water bottle. Prior to assignment to the study, all animals underwent at least a 31-day quarantine period as mandated by the Centers for Disease Control and Prevention (Atlanta, GA).

Liposome infusion procedures

Acute infusion of rhodamine or DiI-DS liposomes

Animals ($n = 3$) received intracranial infusions of either rhodamine liposomes (90 ± 30 nm) or DiI-DS liposomes (110 ± 40 nm) into the corona radiata and putamen. In a separate study, we confirmed that liposomal size difference (90 nm–110 nm) and difference in loaded fluorescent dye (rhodamine or DiI-DS) did not have any impact on distribution (data submitted for publication). Twelve target sites were chosen: the corona radiata and putamen of both hemispheres in three monkeys. Infusion volume was 33 μl for 2 monkeys and 99 μl for the third monkey. Infusions were performed by previously established CED techniques for non-human primates (Bankiewicz et al., 2000). Briefly, the infusion system consisted of a fused-silica cannula that was connected to a loading line (containing either rhodamine liposomes or DiI-DS liposomes) and an oil-infusion line. A 1-ml syringe (filled with oil) mounted onto a micro-infusion pump (BeeHive; Bioanalytical Systems, West Lafayette, IN) regulated the flow of fluid through the system. A micro-infusion pump was placed outside the scanner for proper operation and precision of infused volume. Based on MRI coordinates, each needle cannula was mounted onto stereotactic holders and manually guided to targeted regions of the brain through burr-holes made in the skull. An initial infusion rate of 0.1 μl/min was applied, and increased at 10-min intervals to 0.2, 0.5, 0.8, and 1.0 μl/min, and then to a maximum of 1.5 μl/min. The concentration of liposomes injected corresponded to a concentration 20 mM of phospholipids. Approximately 15 min after infusion, the cannula was raised out of the brain, the cortex was rinsed with saline, and the wound site was closed in anatomical layers. Immediately after the intracranial CED procedure, the animal was euthanized with an overdose of pentobarbital, and the brain was harvested and coronally sectioned into 3- to 6- mm blocks. Each brain slice was immediately frozen in isopentane cooled in dry ice and processed for histological analysis.

Repeated infusion of Gadoteridol-loaded liposomes during real-time magnetic resonance imaging monitoring

Monkeys ($n = 2$, 3–5 kg) received a baseline MRI scan and underwent neurosurgical procedures to position MRI-compatible guide cannulas in the right corona radiata, left putamen, and left brain stem. Each customized cannula was cut to a specified length and stereotactically guided to its target through a burr-hole created in the skull. The guide cannulas were secured to the skull with dental acrylic, and the tops of the guide cannula assemblies were capped with stylet screws for simple access during the infusion procedure. Two to 4 weeks after surgical recovery, CED procedures were performed to infuse liposomal Gd into each target site during MRI procedures. Briefly, under isoflurane anesthesia, the animal's head was placed in an MRI-compatible stereotactic frame and a baseline MRI scan was performed. Vital signs including heart rate and PO_2 were monitored during the procedure. Three non-ferromagnetic needle cannulas connected aseptically to micro-infusion pumps were introduced into the brain using the implanted guides. The length of each infusion cannula was measured to ensure that the distal tip extended approximately 3 to 4 mm beyond the length of the respective guide. This created a "step" design at the tip of the cannula to maximize fluid distribution during CED procedures. Following secure placement of the needle cannula, the animal's head was repositioned in the MRI gantry and CED procedures were initiated while MRI data were continuously acquired. An initial infusion rate of 0.2 μl/min was applied and was increased at 10-min intervals to a maximum of 1.5 μl/min, as described for the fluorescent liposomes. The total infusion volumes for the first monkey were 99 μl for the corona radiata and putamen, and 66 μl for the brain stem. The second monkey received a total

infusion volume of 113.5 μl for the corona radiata and putamen, and 66 μl for the brain stem. The total infusion time ranged from 67 min 20 s (to deliver 66 μl) to 99 min (to deliver 113.5 μl). The approximate concentration of liposomes injected corresponded to a concentration of 5 mM of phospholipids and 5 mM of Gadoteridol, for a final injected Gadoteridol dose of 0.33 and 0.50 μmol/infusion site, respectively, for the 66 and 99 μl infusion volumes. The final injected Gadoteridol dose for 113.5 μl infusion volume was 0.57 μmol/infusion site. Following completion of the CED/MRI procedure, each needle cannula was removed from the brain and the respective guide-cannula entry site was cleansed with alcohol. The animal was removed from the MRI scanner and monitored for full recovery from anesthesia.

During the first infusion, each animal received liposomal Gd, which was monitored by MRI. MRI was also acquired 48 h after the first infusion to evaluate the retention of Gd at the infused sites. During the second infusion procedure, which took place 3 months after the first infusion, each animal received a mixture of liposomal Gd and rhodamine liposomes (10 mM phospholipids, 5 mM Gadoteridol). Immediately after the second infusion session, the animals were euthanized and the brains were processed for histological examination. Volume of distribution was compared between MRI observations and histological analysis. These animals were also carefully monitored for any potential side effects during the entire study period, and local toxicity of the liposomal Gd was evaluated by staining the histological sections acquired at necropsy with hematoxylin and eosin.

Extended infusion of Gadoteridol-loaded liposomes during real-time magnetic resonance imaging monitoring

Additionally, one monkey was prepared in the same manner as described above for the infusion during MRI. Under isoflurane anesthesia, the animal's head was placed in an MRI-compatible stereotactic frame and a CED of liposomal Gd was performed at three target sites (i.e. corona radiata, putamen, and brain stem). MR-images were acquired every 10 min during the infusion. An initial infusion rate of 0.2 μl/min was applied and was increased at 10-min intervals to a maximum of 3.0 μl/min (0.2 μl/min → 0.5 → 0.8 → 1.0 → 1.5 → 2.0 → 2.5 → 3.0). Infusion was continued at the rate of 3.0 μl/min until the infusion volume for the monkey brain reached a maximum. Three-dimensional reconstruction of the acquired MR images was performed using software provided by Brain Lab (Brain LAB, Westchester, IL).

MRI acquisition

T1-weighted images of the primates' brains were acquired on a 1.5-T Signa LX scanner (GE Medical Systems, Waukesha, WI) with a 5″ surface coil. Prior to inserting infusion catheters, baseline spoiled gradient echo (SPGR) images were taken: repetition time (TR)/echo time (TE)/flip angle = 28 ms/8 ms/40°, number of excitations (NEX) = 4, matrix = 256 × 192, field of view (FOV) = 16 cm × 12 cm, slice thickness = 1 mm. These parameters resulted in a 0.391 mm^3 voxel volume. Once the catheters were inserted and the infusion commenced, SPGR scans were taken consecutively throughout the infusion. The scan time was dependent on the number of slices needed to cover the extent of infusion and ranged from 9 min 44 s to 11 min 53 s.

Volume quantification from fluorescent images

After necropsy, brains were sectioned with a cryostat. Sequential sections with 40 μm thickness and 400 μm interval were obtained. Fluorescence generated from rhodamine or DiI-DS was visualized with an ultra-violet light source, and a charged-coupled device camera with a fixed aperture was used to capture the images. The volume of fluorescent liposome distribution was analyzed with a Macintosh-based image analysis system (NIH Image 1.62; NIH, Bethesda, MD) as described previously (Hamilton et al., 2001).

Volume quantification from MR images

The volume of liposomal distribution within each brain region was quantified from the final set of images acquired after the infusion was completed. The infusion baseline images were subtracted from the final infusion images to remove the background intensities in the brain. The standard deviation (σ) for the background corrected image was calculated over the range of slices that included liposomes. The image was segmented for liposomal distributions by a contouring function that created a region of interest (ROI) around contiguous voxels with a minimum intensity of 5σ. The ROIs were visually inspected and edited for accuracy before being included in the calculation of Vd.

Results

Distribution of liposomes after convection-enhanced delivery detected by fluorescent labeling

In order to test the feasibility of CED of liposomes in the non-human primate brain, liposomes (20 mM phospholipids) loaded with fluorescent dye (either rhodamine or DiI-DS, as described in the Methods section; the difference in fluorescent dye had no impact on liposomal distribution) were infused by CED at a volume of either 33 μl or 99 μl into the corona radiata or putamen of both hemispheres in 3 non-human primates. The animals were euthanized immediately after infusion. A robust distribution of liposomes was achieved and was detected at necropsy (Fig. 1A). Six data points were acquired [$n = 4$ for the 33 μl infusions (3 corona radiata and 1 putamen) and $n = 2$ for the 99 μl infusion (2 putamen)] out of 12 attempted infusion sites [2 infusion sites (corona radiata and putamen) per hemisphere in 3 monkeys]; the data from the other 6 infusion sites were not usable due to infusion problems, including errors in targeting or pump malfunction. The distribution volume was calculated and plotted against the infused volume (Fig. 1B; black circles). Two additional data points for a 99 μl infusion were taken from the

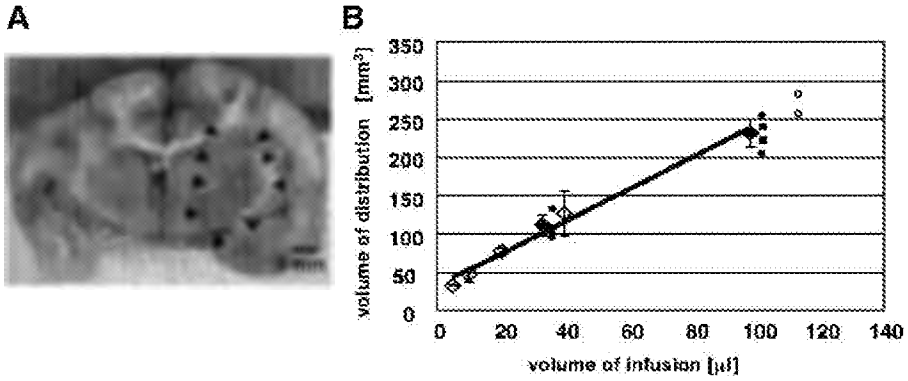

Fig. 1. Correlation between infusion volume and distribution volume after CED infusion of fluorescent liposomes. Liposomes (20 mM phospholipids) loaded with fluorescent dye (either rhodamine or DiI-DS) at a volume of 33 µl or 99 µl were infused by CED into the corona radiata or putamen of 3 non-human primates. Animals were euthanized immediately post-infusion. (A) Representative images from the putamen infusion (99 µl; DiI-DS liposomes). Brains were sectioned and distribution of the liposomes was detected by fluorescence microscopy. (B) Volume of distribution (Vd) was calculated and plotted against volume of infusion (Vi) (black circles = data points). Data acquired from histological evaluation of the brains used for real-time MR monitoring were also plotted (black boxes = data points for 99 µl infusion volume, white circles = data points for 113.5 µl infusion volume; black diamonds = mean, bars = SD). Data from our previous study using rodent brains and a Vi of 5, 10, 20, and 40 µl were plotted with the primate data (white diamonds = mean; bars = SD) and the correlation between Vi and Vd was evaluated [trend line; Vd = 2.09 Vi + 31, R^2 = 0.983].

histological evaluation of the monkey brain used for the real-time MR monitoring study (Fig. 1B; black boxes). Data from our previous study (Saito et al., 2004) of CED infusion volumes (Vi) of 5, 10, 20, and 40 µl in the rodent brain were plotted together with the primate data, and the correlation between Vi and Vd was calculated. A linear trend line revealed a strong correlation between Vi and Vd (R^2 = 0.95). According to these findings, a Vd twice as large as the Vi would be expected with Vi ranging from 5 to 99 µl. During real-time MR monitoring (see below), we evaluated the volume of distribution of a 113.5 µl infusion (Vi) in two infusion sites in 1 monkey. The calculated volume (Vd) from histological sections

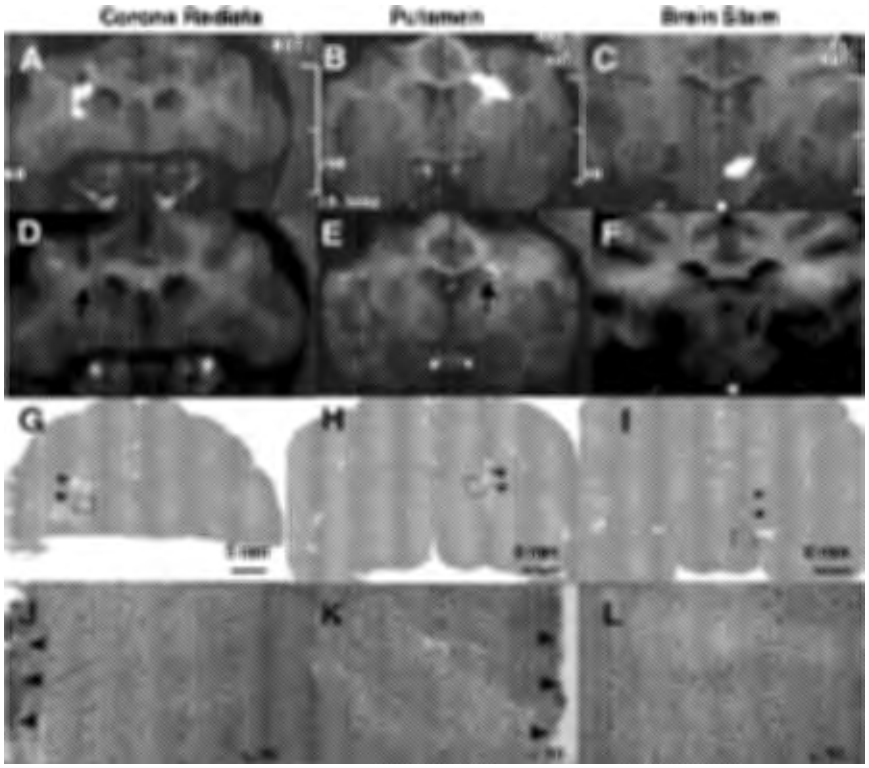

Fig. 2. MR imaging after CED infusion of liposomal Gd, and toxicity evaluation. Liposomal Gd (approximately 5 mM phospholipids, 5 mM Gadoteridol) was infused by CED in one non-human primate to test feasibility. Infusion volume was 99 µl for the corona radiata (A, D, G, J) and the putamen (B, E, H, K), and 66 µl for the brain stem (C, F, I, L). MR images clearly detected the distribution in all three sites (A, B, C). MR images acquired after 48 h of infusion (D, E, F) revealed retention of liposomes with no adverse effects. The animal was euthanized 3 months after infusion. This animal developed no abnormal symptoms during the observation period. Postmortem H&E staining (G, H, I) revealed tissue damage due to cannula placement; however, this tissue damage was limited to the cannula tract (arrows) despite the large distribution of liposomes. Figures J, K, and L are the higher magnification (×50) of highlighted regions (box) in figures G, H, and I, respectively.

(289 mm^3 and 260 mm^3) still stayed on the linear trend line (Fig. 1B; white circles), suggesting the accuracy of this acquired trend line.

Detection of liposomal gadolinium after convection-enhanced delivery in primates, and evaluation of toxicity

To assess the feasibility of using MRI to monitor liposome distribution in the brain of non-human primates during CED and to confirm the safety of CED for drug distribution, CED of liposomal Gd was performed in 2 non-human primates. Targeted infusion sites were the right corona radiata, the left putamen, and the left brain stem. Infusion volumes consisted of 99 μl or 113.5 μl for the corona radiata and putamen, and 66 μl for the brain stem. Robust and clearly delineable distributions of liposomal Gd were observed at each infusion site in the T1-weighted MR images obtained immediately after infusion (Figs. 2A–C). MR images acquired 48 h after infusion (Figs. 2D–F) revealed retention of the liposomes at each infusion site with no adverse effects. The animals proceeded to a second infusion approximately 3 months later and were euthanized immediately following the second infusion. The animals developed no abnormal symptoms during the observation period. Postmortem hematoxylin and eosin staining showed some tissue damage due to the cannula (Figs. 2G–L). This damage was likely a consequence of long-term cannula placement, as the outer "guide" cannula was placed at the infusion site for more than 3 months. However, the tissue damage was limited to the cannula track despite the large distribution of liposomes. Throughout the study, there were no adverse clinical effects observed in any of the animals at any time points following CED of liposomal Gd.

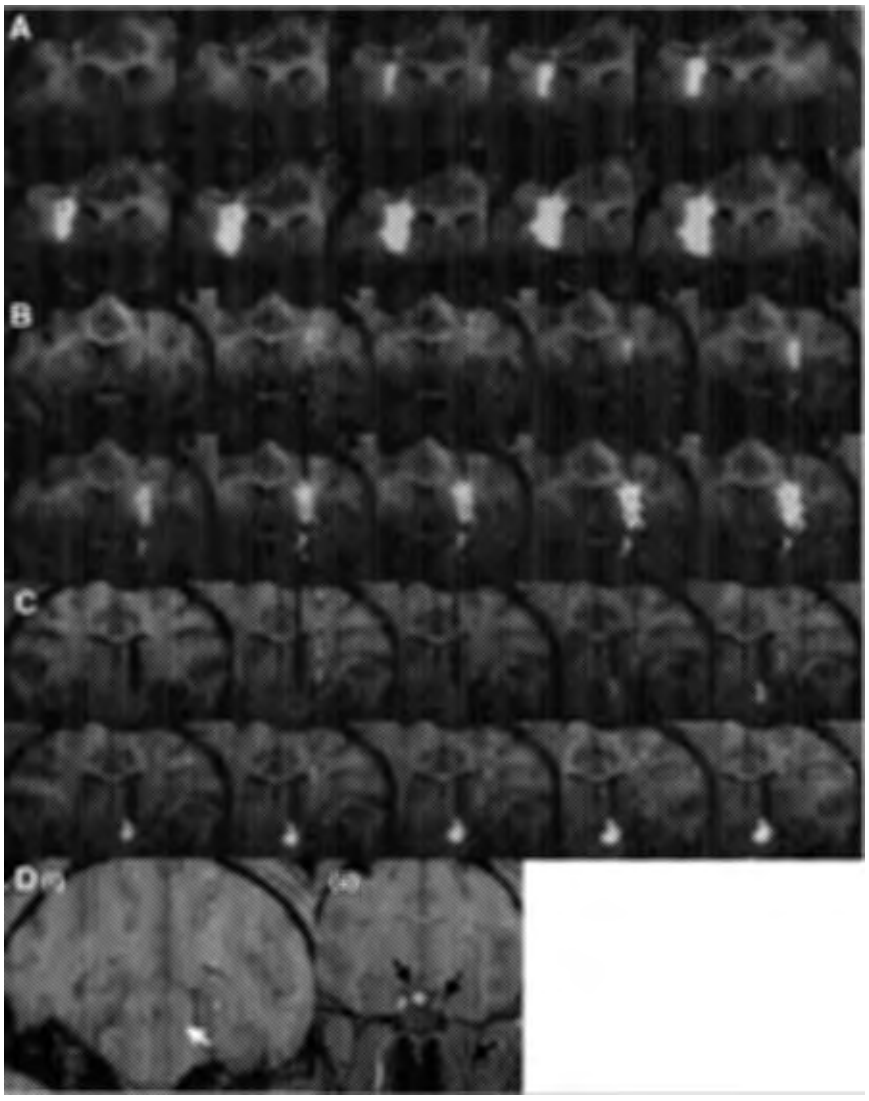

Fig. 3. Real-time monitoring of the CED infusion of liposomal Gd. Liposome distribution was successfully monitored using MRI at three infusion sites; the corona radiata (A), the putamen (B), and the brain stem (C). T1-weighted MR images were obtained sequentially at approximately 10-min intervals. Too-close placement of the infusion cannula (white arrow) to the fourth ventricle in one monkey caused an unsuccessful infusion into the brain stem [D(i)]. No clear distribution was detectable throughout the procedure at the infusion site. However, in the images more caudal to the targeted site [D(ii)], Gd signal (black arrows) was detected in the cerebrospinal fluid.

Real-time magnetic resonance imaging of liposomal gadolinium in primates

Real-time monitoring of liposome distribution was obtained in the corona radiata, putamen, and brain stem (Figs. 3A–C). MR images were obtained at approximately 10-min intervals during the infusions. These real-time images detected liposomal distribution from approximately 10 to 20 min after initiation of infusion and clearly detected the enlargement of distribution area during infusion. The distribution areas were all well delineated from non-distributed brain tissue, again suggesting the feasibility of this strategy. During the brain-stem infusion of one non-human primate, unsuccessful infusion was also monitored with our real-time system. Fig. 3D(i) depicts the placement of the infusion cannula too close to the fourth ventricle. No clear distribution was detectable throughout the procedure at the infusion site. However, in the images more caudal to the targeted site, Gd signal was detected in the cerebrospinal fluid (CSF) [Fig. 3D(ii)], suggesting a leak of infusate into the CSF.

Confirmation of distribution volume by histological detection using fluorescence

Both animals used for real-time MR imaging of liposomal gadolinium received concomitant administration of fluorescent liposomes. One animal received real-time infusion of 99 μl of a liposomal mixture (liposomal Gd and rhodamine liposome) into the corona radiata and putamen, and 66 μl into the brain stem, was euthanized immediately after MR imaging, and was processed for histological detection of fluorescence generated from the rhodamine liposomes that were co-infused with liposomal Gd. When compared with the MR image, the fluorescent area completely overlapped with the liposome distribution detected by MRI (Figs. 4A–C). Volume calculations performed with MRI and histological fluorescence data were 259 mm^3 and 240.7 mm^3 for the corona radiata, 210 mm^3 and 223.5 mm^3 for the putamen, and 83 mm^3 and 77.8 mm^3 for brain stem, respectively, which further confirmed that real-time MRI gives an accurate measurement of distribution volume (Fig. 4D, black diamonds). The second animal received a real-time infusion of 113.5 μl of the liposomal mixture in both hemispheres, and was euthanized and processed in the same manner. The volume of distribution calculations performed with MRI and histological fluorescence data were 305 mm^3 and 289 mm^3 for the left hemisphere and 290 mm^3 and 259.8 mm^3 for the right hemisphere, respectively (Fig. 4D, white diamonds).

Robust distribution of Gadoteridol-loaded liposomes and three-dimensional real-time magnetic resonance imaging monitoring

When volume of infusion (Vi) reached 300 μl, some leakage of the liposomal Gd was found in the subarachnoid space. Thus, the infusion was stopped at this point. Although it was unclear where this leakage originated, robust distribution was found at all three sites and almost an entire striatum was covered with liposomal Gd at this point (Fig. 5A). Therefore, this volume of infusion might be the maximum for the monkey brain. Volume of distribution was plotted against time elapsed from initiation of infusion (Fig. 5B). It took 141 min and 40 s to infuse total volume of 300 μl. Three-dimensional reconstruction of acquired images was also performed at the end of infusion (Fig. 5C).

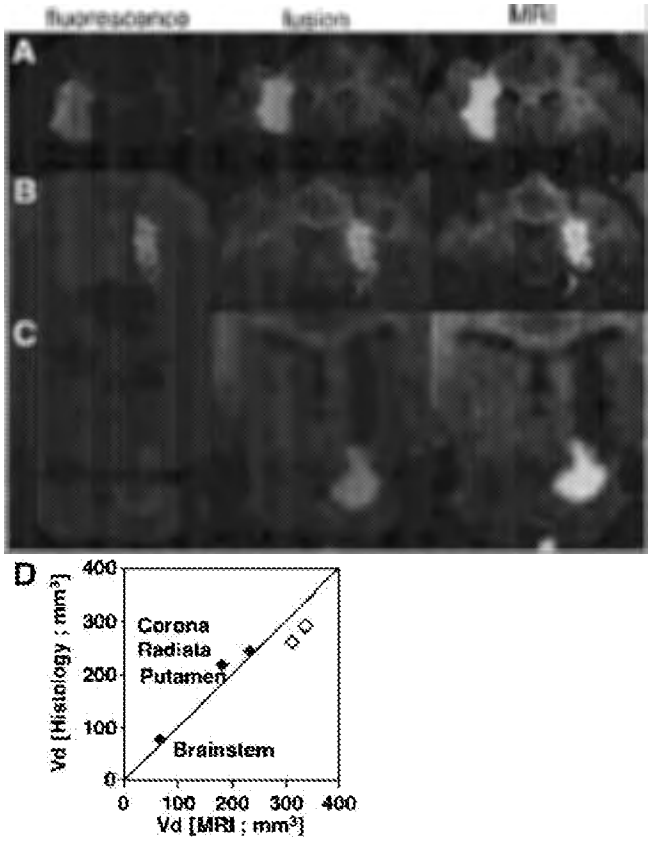

Fig. 4. Overlayed fluorescent and MRI images of liposomal probes delivered to the brain of a monkey using CED. Correlation of MR images and histological fluorescence images showed the accuracy of the MRI monitoring. Animals euthanized immediately after real-time MR imaging were processed for histological detection of fluorescence generated from rhodamine liposomes that were co-infused with liposomal Gd. When compared to the MR images, the fluorescent areas successfully overlapped with liposome distribution detected by MRI (A–C). Volume calculations done with MRI and histological fluorescence data further confirmed this finding (D).

Discussion

Development of an accurate and effective monitoring system for CED is of considerable interest. Previously, we reported the feasibility of MRI detection of Gd-loaded nanoparticle liposomes following CED infusion into the central nervous system of rodents, as well as into intracranial brain tumor xenografts (Saito et al., 2004). However, the robust distribution of liposomes obtained in small rodent brains did not guarantee similar results in the much larger primate CNS. Therefore, several key factors were further explored in the present study. These included correlating the volume of infusion and volume of distribution in larger brains, developing a real-time imaging system, and evaluating the accuracy of MRI monitoring for detection of liposome distribution.

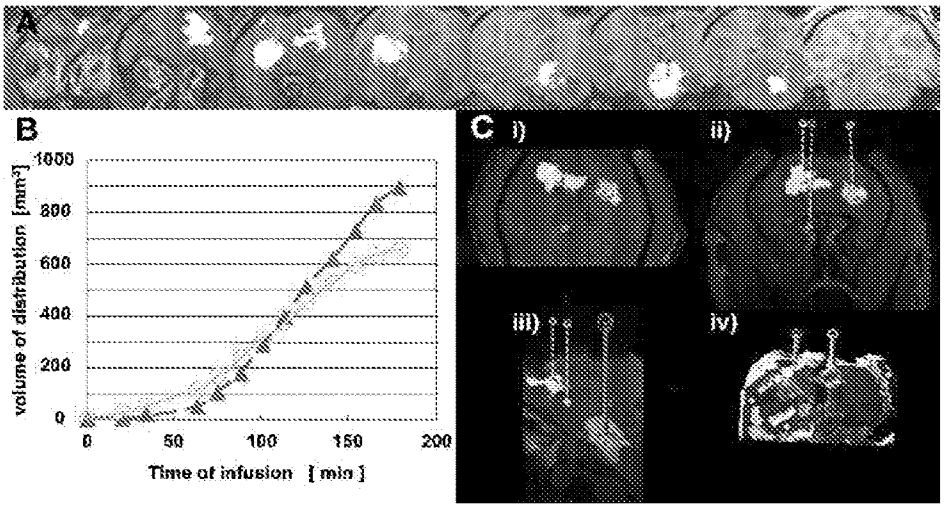

Fig. 5. Serial coronal MR images with 5 mm interval obtained at the end of infusion (A; left, rostral; right, caudal). Total of 300 μl for each site was infused to corona radiata, putamen, and brain stem using CED. Volumes of distribution (mm^3) were plotted against time elapsed (min) from the beginning of infusion (B; yellow, corona radiata; green, putamen; red, brain stem). Three-dimensional reconstruction of the acquired MR images after 300 μl CED infusion into each targeted sites (C; i, axial image; ii, coronal image; iii, sagittal image; iv, three dimensional reconstructed image). Lines depict the cannula tracts.

To evaluate this approach, we initially performed CED procedures fluorescent liposomes into the brains of non-human primates. Defined injection volumes of 33 μl and 99 μl resulted in robust distribution within the target sites. When the calculated volume of distribution was plotted against the volume of infusion from this study and previously acquired data from the rodent study (Vi = 5 μl, 10 μl, 20 μl, and 40 μl) (Saito et al., 2004), a definite correlation between infusion volume and distribution volume was found. Based on these data, a 2:1 ratio between the volume of distribution to the volume of liposomes infused can be expected, which will be helpful for surgical planning when considering clinical application of this technology.

Subsequently, we tested the methodology for obtaining real-time MRI monitoring of CED of liposomes in non-human primates. The use of Gd chelate-albumin conjugates was previously reported as a means for MRI guidance of infusates during CED of macromolecular drugs (Lonser et al., 2002). In a related approach, Rubesova et al. (2002) suggested the use of Gd chelate-loaded liposomes to monitor the delivery of liposomal drugs to tumors following systemic administration. We have previously shown the feasibility of this approach to monitoring of liposomal CED in rodents (Mamot et al., 2004). In this study, non-ferromagnetic cannulas were fabricated based on our previous "step" design system that makes the cannulas reflux resistant (Krauze et al., in press). The distribution was successfully monitored in 3 different target sites as demonstrated in Fig. 2. Liposomal Gd was still detectable 48 h post-infusion, confirming our previous finding in rats that indicated prolonged retention of Gd by means of liposomal encapsulation (Saito et al., 2004). Histological sections taken 3 months after infusion revealed tissue damage at the needle track, which was attributed to cannula placement. Even with enhanced distribution, the toxicity of liposomal Gd was almost negligible. These studies confirmed the feasibility of using an MRI-guided strategy for monitoring CED of liposomes.

Real-time monitoring of CED was performed on 2 monkeys (Fig. 3). In one animal, attempts to infuse the brain stem were unsuccessful. Real-time MRI revealed almost no tissue distribution of liposomal Gd in the target site. This apparent lack of distribution was due to "escape" of liposomal Gd into the CSF due to close proximity of the cannula tip to the fourth ventricle. Clearly, lack of successful delivery of liposomal Gd in this region was realized only because CED was performed with real-time imaging. This example highlights the need for a detection strategy during drug delivery into the brain. In the second animal, histological detection of co-infused rhodamine liposomes was performed to address any differences between distribution areas observed with MRI versus histological examination. Complete overlap of the MR image and the histological image proved the accuracy of MRI monitoring, which is critical for accurate detection of drug distribution during clinical application of this technology.

Delivery of liposomal drugs directly into brain tissue offers a number of potential advantages for the treatment of brain tumors. For example, liposomes are capable of providing slow and sustained release of a drug when distributed within a tumor. Furthermore, immunoliposomes and other targeted liposomes can provide tumor-cell directed drug delivery via tumor-associated markers such as epidermal growth factor receptor (Mamot et al., 2003). In this study, we show that liposomal drug delivery to tumor tissue can be effectively monitored in real time by the use of a liposomally encapsulated, pharmaceutically acceptable Gd chelate. This provides additional rationale for the use of liposomes as drug delivery carriers for CED into the brain. Regardless of whether the encapsulated material was an MRI probe or a fluorescent marker, liposomes of similar size and lipid composition yielded practically identical distribution (Saito et al., 2004). Thus,

therapeutic liposomes can be co-infused with liposomal Gd to monitor the distribution of the drug carrier. From this point of view, liposomal Gd is superior to the formerly proposed Gd chelate–albumin conjugates (Lonser et al., 2002), because albumin and therapeutic molecules will likely possess different tissue-binding and diffusion properties, and thus will distribute differently, reducing the predictive value of the probe distribution with regard to the distribution of the drug (Nguyen et al., 2001). The current study used co-infusion of liposomes loaded with different detectable agents, and provides the basis for a clinical strategy in which liposomal drugs are co-infused with an otherwise identical liposome containing Gd as a marker of distribution.

In summary, we have developed and evaluated a strategy for real-time MRI monitoring of liposomes after CED infusion into the brain of non-human primates. These primate studies verified the ability of CED to extensively and safely distribute liposomes, and determined that the procedure could be accurately monitored by MRI. Real-time imaging based on MRI and other modalities may also lead to strategies to measure the concentration and tissue half-lives of administered drugs within target tissues. Since liposome- and nanoparticle-based technologies are generating novel and promising therapeutic constructs, an integrated strategy for administration of these agents by using CED under MRI guidance may bring us closer toward an effective therapy for treating brain tumors.

Acknowledgments

This work was supported in part by a National Cancer Institute Specialized Programs of Research Excellence (SPORE) grant (MSB, KSB, and JWP), Accelerate Brain Cancer Cure (KSB), NIH/NCI grant U54 CA90788 (JWP, DBK), NIH/NCI contract N01-CO-27031-16 to Hermes Biosciences, Inc, and CBCRP grant 7KB-0066 (DCD). We thank Ms. Sharon Reynolds of the Department of Neurological Surgery, University of California, San Francisco for editorial assistance. Special thanks to Dr. Christoph Pedain for assistance with BrainLab software.

References

Bankiewicz, K.S., Eberling, J.L., Kohutnicka, M., Jagust, W., Pivirotto, P., Bringas, J., Cunningham, J., Budinger, T.F., Harvey-White, J., 2000. Convection-enhanced delivery of AAV vector in parkinsonian monkeys; in vivo detection of gene expression and restoration of dopaminergic function using pro-drug approach. Exp. Neurol. 164, 2–14.

Bobo, R.H., Laske, D.W., Akbasak, A., Morrison, P.F., Dedrick, R.L., Oldfield, E.H., 1994. Convection-enhanced delivery of macromolecules in the brain. Proc. Natl. Acad. Sci. U. S. A. 91, 2076–2080.

Guerin, C., Olivi, A., Weingart, J.D., Lawson, H.C., Brem, H., 2004. Recent advances in brain tumor therapy: local intracerebral drug delivery by polymers. Invest. New Drugs 22, 27–37.

Hamilton, J.F., Morrison, P.F., Chen, M.Y., Harvey-White, J., Pernaute, R.S., Phillips, H., Oldfield, E., Bankiewicz, K.S., 2001. Heparin coinfusion during convection-enhanced delivery (CED) increases the distribution of the glial-derived neurotrophic factor (GDNF) ligand family in rat striatum and enhances the pharmacological activity of neurturin. Exp. Neurol. 168, 155–161.

Krauze, M.T., Saito, R., Noble, Ch., Tamas, M., Bringas, J., Park, J.W., Berger, M.S., Bankiewicz, K.S., in press. Reflux-free cannula for convection-enhanced delivery permitting high-speed delivery of therapeutic agents. J. Neurosurg.

Levy, R.M., Major, E., Ali, M.J., Cohen, B., Groothius, D., 2001. Convection-enhanced intraparenchymal delivery (CED) of cytosine arabinoside (AraC) for the treatment of HIV-related progressive multifocal leukoencephalopathy (PML). J. Neurovirol. 7, 382–385.

Lidar, Z., Mardor, Y., Jonas, T., Pfeffer, R., Faibel, M., Nass, D., Hadani, M., Ram, Z., 2004. Convection-enhanced delivery of paclitaxel for the treatment of recurrent malignant glioma: a phase I/II clinical study. J. Neurosurg. 100, 472–479.

Lonser, R.R., Walbridge, S., Garmestani, K., Butman, J.A., Walters, H.A., Vortmeyer, A.O., Morrison, P.F., Brechbiel, M.W., Oldfield, E.H., 2002. Successful and safe perfusion of the primate brainstem: in vivo magnetic resonance imaging of macromolecular distribution during infusion. J. Neurosurg. 97, 905–913.

Mamot, C., Drummond, D.C., Greiser, U., Hong, K., Kirpotin, D.B., Marks, J.D., Park, J.W., 2003. Epidermal growth factor receptor (EGFR)-targeted immunoliposomes mediate specific and efficient drug delivery to EGFR- and EGFRvIII-overexpressing tumor cells. Cancer Res. 63, 3154–3161.

Mamot, C., Nguyen, J.B., Pourdehnad, M., Hadaczek, P., Saito, R., Bringas, J.R., Drummond, D.C., Hong, K., Kirpotin, D.B., McKnight, T., Berger, M.S., Park, J.W., Bankiewicz, K.S., 2004. Extensive distribution of liposomes in rodent brains and brain tumors following convection-enhanced delivery. J. Neurooncol. 68, 1–9.

Nguyen, J.B., Sanchez-Pernaute, R., Cunningham, J., Bankiewicz, K.S., 2001. Convection-enhanced delivery of AAV-2 combined with heparin increases TK gene transfer in the rat brain. NeuroReport 12, 1961–1964.

Ratliff, J.K., Oldfield, E.H., 2001. Convection-enhanced delivery in intact and lesioned peripheral nerve. J. Neurosurg. 95, 1001–1011.

Rubesova, E., Berger, F., Wendland, M.F., Hong, K., Stevens, K.J., Gooding, C.A., Lang, P., 2002. Gd-labeled liposomes for monitoring liposome-encapsulated chemotherapy: quantification of regional uptake in tumor and effect on drug delivery. Acad. Radiol. 9 (Suppl. 2), S525–S527.

Saito, R., Bringas, J.R., McKnight, T.R., Wendland, M.F., Mamot, C., Drummond, D.C., Kirpotin, D.B., Park, J.W., Berger, M.S., Bankiewicz, K.S., 2004. Distribution of liposomes into brain and rat brain tumor models by convection-enhanced delivery monitored with magnetic resonance imaging. Cancer Res. 64, 2572–2579.

Stewart, L.A., 2002. Chemotherapy in adult high-grade glioma: a systematic review and meta-analysis of individual patient data from 12 randomised trials. Lancet 359, 1011–1018.

ELSEVIER

Journal of Neuroscience Methods 154 (2006) 225–232

JOURNAL OF NEUROSCIENCE METHODS

www.elsevier.com/locate/jneumeth

Tissue affinity of the infusate affects the distribution volume during convection-enhanced delivery into rodent brains: Implications for local drug delivery

Ryuta Saito[a,1], Michal T. Krauze[a], Charles O. Noble[b], Matyas Tamas[a], Daryl C. Drummond[c], Dimitri B. Kirpotin[c], Mitchel S. Berger[a], John W. Park[b], Krystof S. Bankiewicz[a,*]

[a] *Department of Neurological Surgery, Brain Tumor Research Center, University of California San Francisco, 1855 Folsom Street, Mission Center Building, Room 226, San Francisco, CA 94103, USA*

[b] *Division of Hematology-Oncology, University of California San Francisco, San Francisco, CA, USA*

[c] *Hermes Biosciences Inc., South San Francisco, CA, USA*

Received 6 June 2005; received in revised form 16 December 2005; accepted 22 December 2005

Abstract

Convection-enhanced delivery (CED) is a recently developed technique for local delivery of agents to a large volume of tissue in the central nervous system (CNS). We have previously reported that this technique can be applied to CNS delivery of nanoparticles including viruses and liposomes. In this paper, we describe the impact of key physical and chemical properties of infused molecules on the extent of CED-mediated delivery. For simple infusates, CED distribution was significantly increased if the infusate was more hydrophilic or had less tissue affinity. Encapsulation of tissue-affinitive molecules by neutral liposomes significantly increased their tissue distribution. The poorer brain distribution observed with cationic liposomes, due to their greater tissue affinity, was completely overcome by PEGylation, which provides steric stabilization and reduced surface charge. Finally, liposomal encapsulation of doxorubicin reduced its tissue affinity and substantially increased its distribution within brain tumor tissue. Taken together, the physical and chemical properties of drugs, small molecules and macromolecular carriers determine the tissue affinity of the infusate and strongly affect the distribution of locally applied agents. Thus, an increased and more predictable tissue distribution can be achieved by reducing the tissue affinity of the infusate using appropriately engineered liposomes or other nanoparticles.

Keywords: Convection-enhanced delivery; Volume of distribution; Liposome; CNS; Brain tumor

1. Introduction

While a number of drugs have been identified that have excellent therapeutic activity against brain tumors, effective delivery to the brain has been a challenge. Many systemically administered agents fail to reach therapeutic levels in the brain, limited by the blood–brain barrier (BBB) and by the systemic toxicity caused by the high doses required to cross it. This has led to investigation of local drug-delivery techniques that bypass the BBB and can maintain therapeutic drug levels in the brain for extended periods of time, potentially achieving a high therapeutic index (Walter et al., 1995). However, many such local-delivery strategies face a major difficulty: poor diffusion of the applied agent (Fleming and Saltzman, 2002). In 1994, Bobo et al. (1994) introduced convection-enhanced delivery (CED) as a strategy to overcome this difficulty. Since then, CED has shown considerable promise for the treatment of brain tumors (Lidar et al., 2004). Utilizing bulk flow, CED allows the direct delivery of small and large molecules to targeted sites in clinically significant volumes of tissue, offering an improved volume of distribution (V_d) over simple diffusion techniques. Since CED is believed to be a highly effective method for the delivery of micro- or macromolecules to brain tissue, in many in vivo drug-delivery studies, the anti-tumor effects were evaluated without confirmation of the drug distribution (Bruce et al., 2000; Heimberger et al., 2000). It is apparent, however, that even using the same method (CED), the volumes of distribution for different compounds are not consistent. Previous studies have investigated

* Corresponding author. Tel.: +1 415 502 3132; fax: +1 415 514 2177.
E-mail address: kbank@itsa.ucsf.edu (K.S. Bankiewicz).
[1] Present address: Department of Neurosurgery, Tohoku University School of Medicine, Sendai, Japan.

0165-0270/$ – see front matter © 2006 Elsevier B.V. All rights reserved.
doi:10.1016/j.jneumeth.2005.12.027

distribution of liposomes in brain after convection-enhanced delivery (MacKay et al., 2005). Results show important differences in distribution for various liposome formulations that warrant further investigation for clinical applications. In this study, we demonstrate differences in distributions for molecules displaying varying physical and chemical properties. In previous reports (Mamot et al., 2004; Saito et al., 2004a), we demonstrated the detection of gadolinium-loaded liposomes in brain tumors after CED, using magnetic resonance imaging (MRI). Because our present focus is to develop a CED strategy for the delivery of liposomes encapsulating various agents, including chemotherapeutic drugs or therapeutic genes, we evaluated the effect of size, surface charge and steric stabilization of liposomes on delivery by using CED. Based on our findings, we conclude that in order to obtain the maximum benefits of CED, the tissue affinity of the delivered material must be carefully characterized. Our results have several important implications for local drug delivery in the treatment of brain tumors.

2. Materials and methods

2.1. Dyes and liposome components

1,1′-Dioctadecyl-3,3,3′,3′-tetramethylindocarbocyanine-perchlorate ($DiIC_{18}$, 934 g/mol)) and rhodamine (sulforhodamine B, 581 g/mol) were purchased from Sigma (St. Louis, MO). A stock solution of $DiIC_{18}$ was prepared in dimethylsulfoxide (Sigma) at a concentration of 2 mg/ml. Both $DiIC_{18}$ and rhodamine were diluted in phospate buffered saline (PBS) to a concentration of 100 μM. Trypan blue (961 g/mol) was obtained from Sigma, and coomassie brilliant blue R-250 854 g/mol) was obtained from BioRad (Richmond, CA). Both trypan blue and coomassie blue were diluted with PBS to a concentration of 4 mM. Doxorubicin (doxorubicin HCl, 580 g/mol) and Doxil (liposomal doxorubicin HCl, Alza Pharmaceuticals Inc.) were obtained from the UCSF pharmacy. 1,2-Distearoyl-*sn*-glycero-3-phosphocholine (DSPC), 1,2-dioleoyl-*sn*-glycero-3-phosphocholine (DOPC), 1,2-dioleoyl-3-(trimethylammonium) propane (DOTAP) and 1,2-distearoyl-*sn*-glycero-3-phosphoethanolamine-*N*-[methoxy(polyethylene glycol)-2000] (PEG-DSPE) were all purchased from Avanti Polar Lipids (Alabaster, AL). Cholesterol was obtained from Calbiochem (San Diego, CA).

2.2. Liposome preparation

All liposomes were prepared by lipid-film hydration (Szoka and Papahadjopoulos, 1980) using HEPES-buffered saline (pH 6.5) as the hydration buffer. Each sample was hydrated by six successive cycles of freezing (−80 °C) and thawing (60 °C). Unilamellar liposomes were formed by extrusion using a 10 ml-capacity thermostatted extruder (Northern Lipids, Vancouver, Canada). Extrusion was performed through polycarbonate membranes using the appropriate pore size and number of extrusions required to reach the desired liposome size, which was determined by light scattering (Beckman Coulter, Fullerton, CA). All liposomes were composed of a 3:2 (mol:mol) phospholipid/cholesterol mixture. In all formulations, DSPC or DOPC was used as the phospholipid component. "PEGylated" refers to liposomes having 10% (mol/mol) of the phospholipids consisting of PEG-DSPE. PEGylated neutral and PEGylated cationic liposomes are used in this manuscript. In the case of cationic liposomes, 10% (mol/mol) of the phospholipid content was composed of DOTAP. All fluorescent liposomes were labeled with membrane-bound $DiIC_{18}$ (Sigma, St. Louis) or 3,3′-dioctadecyloxacarbocyanine perchlorate ($DiOC_{18}$; Sigma) dyes, each having two C_{18} chains. The dye composition in all formulations was 1% (mol/mol) of the total phospholipids. For all infusion studies, liposomes were infused at a phospholipid concentration of 100 μM.

2.3. Animals

Male Sprague–Dawley rats weighing 300–350 g (Charles River Laboratories, Wilmington, MA) and male Fisher 344 rats weighing 200–250 g (Harlan, Indianapolis, IN) were housed under aseptic conditions that included filtered air and sterilized food, water, bedding and cages. The protocol used in these studies was approved by the Institutional Animal Care and Use Committee of the University of California, San Francisco (UCSF).

2.4. Surgery and the convection-enhanced delivery procedure

While under deep isoflurane anesthesia, rats were placed in a small-animal stereotactic frame (David Kopf Instruments, Tujunga, CA). A sagittal incision was made through the skin to expose the cranium, and a burr hole was made in the skull 0.5 mm anterior and 3 mm lateral to the bregma with a small dental drill. Infusions were performed at a depth of 4.5 mm from the brain surface, using the CED method described in our previous studies (Saito et al., 2004a; Lieberman et al., 1995). Briefly, an infusion cannula connected to a Hamilton syringe (Hamilton, Reno, NV) was attached to a rate-controllable microinfusion pump (Bioanalytical Systems, Lafayette, IN). Slow-infusion CED was performed using an ascending schedule of infusion rates to achieve a total volume of 20 μl (0.2 μl/min for 15 min, 0.5 μl/min for 10 min and 0.8 μl/min for 15 min). All infusion studies except the study using doxorubicin were performed using Sprague–Dawley rats. Dyes (rhodamine, $DiIC_{18}$, trypan blue, coomassie blue) and neutral 10% (mol/mol) PEGylated liposomes containing $DiIC_{18}$ or rhodamine were infused separately. In contrast, mixtures of different liposomal constructs were infused to evaluate the difference in distribution between various liposomes (differing in size, charge and PEGylation). Free doxorubicin or liposomal doxorubicin were infused separately into Fischer 344 rats bearing 9L-2 intracranial xenograft tumors. Animals used in our study were either infused in both hemispheres ($n = x$ hemispheres) or infused in only one hemisphere ($n = x$ animals).

2.5. Brain-tumor model

An established rat glioma cell line (9L-2) was obtained from the Department of Neurological Surgery Tissue Bank at UCSF.

Cells were seeded into tissue-culture flasks approximately 2–3 days before they were implanted, and were maintained as monolayers in a complete medium consisting of Eagle's minimal essential medium supplemented with 10% fetal calf serum and non-essential amino acids. Cells were cultured at 37 °C in a humidified atmosphere containing 95% air and 5% CO_2. Cells were harvested for use by trypsinization, washed once with Hanks' balanced salt solution (HBSS) without Ca^{2+} and Mg^{2+}, and resuspended in HBSS for implantation. Cells were implanted into the brain of six Fisher 344 rats; 5×10^5 cells were stereotaxically implanted into the right hemisphere of each rat by using the following coordinates: 0.5 mm anterior and 3 mm lateral to the bregma, and at a depth of 4.5 mm from the brain surface. CED infusion of doxorubicin or Doxil was performed 10 days after tumor implantation using the same methods as other infusions.

2.6. Evaluation of volume of distribution after convection-enhanced delivery

Rats that received dyes or liposomes were euthanized no later than 1 h after infusion. The brains were harvested, frozen using −20 °C isopentane and cut into serial coronal sections (25 μm) with a cryostat. Fluorescent signal was visualized with a fluorescence microscope (Axioskop; Carl Zeiss, Jena, Germany) with a FITC filter (#31001; Chroma Technology Corp., Rockingham, VT) and a TRITC filter (#31002; Chroma Technology Corp.), and a charged coupled device (CCD) camera with a fixed aperture was used to capture the images. In the study using liposomal mixture infusion, pilot study determining conditions for data analysis were performed to visualize fluorescence from $DiIC_{18}$ and that from $DiOC_{18}$ separately. The tissue distributions were evaluated using the same camera settings determined in this pilot study. The distribution margin of fluorescent liposome distribution after CED, as seen in high magnification of Fig. 4C, is very clear and was used for delineation. Previous experiments comparing distribution of co-infused fluorescent liposomes on histology with distribution of gadolinium-loaded liposomes on MRI validated this method (Saito et al., 2004a, submitted for publication). Sections from brains injected with coomassie blue or trypan blue were scanned using a scanner (Perfection 1660 photo; Epson, Long Beach, CA). The area of distribution of infused coomassie blue or trypan blue in each tissue section was automatically determined using a threshold of 50% of the maximal stained optical density. The volume of distribution in all studies was analyzed using a Macintosh-based image analysis system (NIH Image 1.62, Bethesda, MD) as described previously (Hamilton et al., 2001). All statistical analyses were performed using a non-parametric test (Mann–Whitney *U*-test).

3. Results

3.1. Different volumes of distribution between dyes

Tissue distributions of hydrophilic fluorescent dye (rhodamine, $n = 4$ hemispheres) and lipophilic fluorescent dye ($DiIC_{18}$, $n = 4$ hemispheres) were compared after CED delivery into the striatum. A significant difference in tissue distribution was observed between these dyes ($p = 0.021$, Fig. 1A). Hydrophilic rhodamine distributed much more widely than lipophilic $DiIC_{18}$. Subsequently, tissue distributions of two different hydrophilic dyes – trypan blue and coomassie blue – were compared. Both dyes distributed much more widely than $DiIC_{18}$; however, there was also a significant difference between the distributions of trypan blue and coomassie blue ($p = 0.021$). The distribution of coomassie blue, which is known to have an affinity for proteins, was less extensive than that of trypan blue (Fig. 1B).

3.2. Liposome encapsulation allows consistent volume of distribution

Based on the above observations, differences in tissue distribution appear to be related to the tissue affinity of the compound that is being delivered. We next investigated if distribution volume could be increased by neutralizing the affinity of the infusate for the surrounding tissue. Since liposomes can mask the affinity of enclosed agents for surrounding tissue, $DiIC_{18}$ ($n = 4$ hemispheres) and rhodamine ($n = 4$ hemispheres) were loaded into liposomes and their distributions after CED were assessed. Neutral, PEGylated liposomes were used to create drug-delivery systems with very low affinity for surrounding tissues. Infusion of both $DiIC_{18}$ liposomes and rhodamine liposomes resulted in similar, extensive volumes of distribution after CED of 20 μl (Fig. 2). When distribution of rhodamine encapsulated in the liposomes was compared with free rhodamine, distribution of the former was slightly diminished, most likely due to its larger size when compared to free rhodamine. On the other hand, encapsulation of the $DiIC_{18}$ in the liposomes, which reduced tissue affinity of lipophilic $DiIC_{18}$, resulted in significantly improved distribution of $DiIC_{18}$ liposomes over free $DiIC_{18}$.

3.3. Charge and surface PEGylation rather than size affects volume of distribution of liposomes following convection-enhanced delivery

Because consistent tissue distribution was observed following CED of neutral PEGylated liposomes regardless of the loaded material, we evaluated several physical characteristics of the liposomal carrier itself, including particle size, PEGylation and surface charge. We used a co-infusion strategy to determine the volume of distribution when characterizing these variables. First, several sizes of liposomes were compared. CED was used to infuse a mixture of $DiIC_{18}$ liposomes (84.1 nm diameter, $n = 6$ animals) and $DiOC_{18}$ liposomes (130.2 nm diameter, $n = 6$ animals), and serial sections were compared (Fig. 3A). Identical tissue distributions were observed for both liposomes, indicating that sizes between 85 and 130 nm have no effect on distribution. Subsequently, a mixture of PEGylated neutral liposomal $DiOC_{18}$ ($n = 4$ animals) and non-PEGylated cationic liposomal $DiIC_{18}$ ($n = 6$ animals) was infused by CED (Fig. 3B). A significant difference ($p = 0.008$) is observed in distribution of cationic liposomal $DiIC_{18}$, which was restricted to a small area near the site

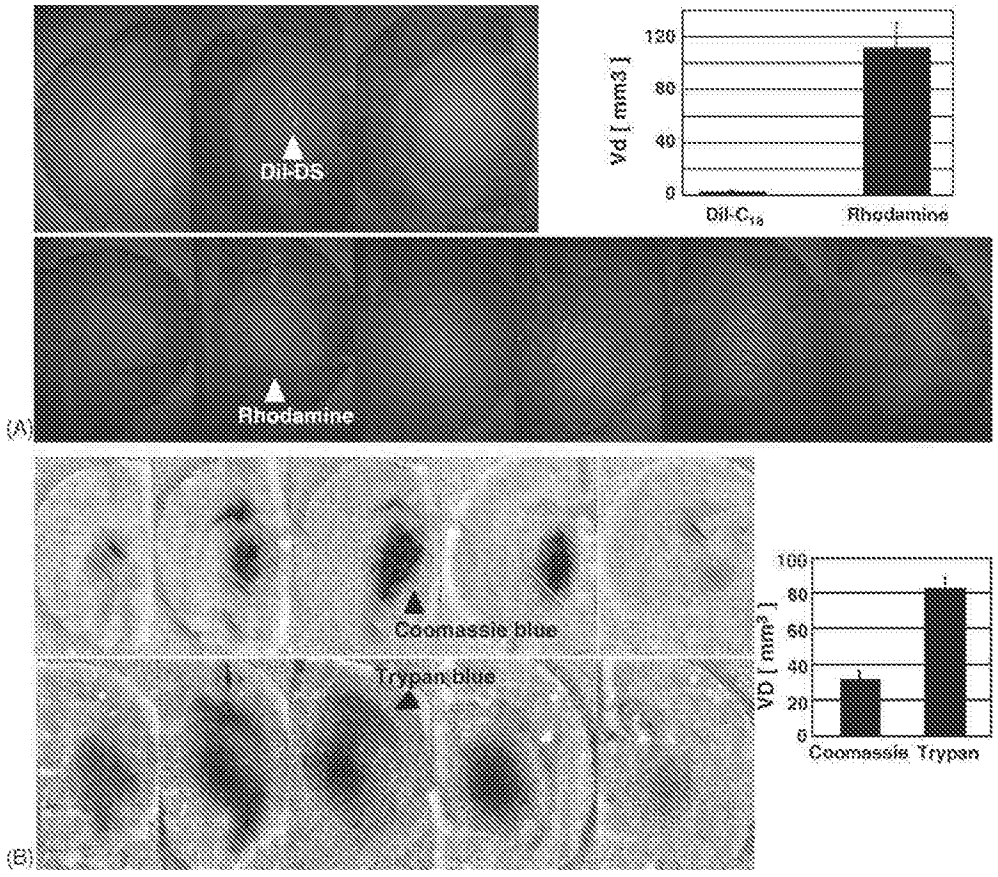

Fig. 1. Distribution of lipophilic dye, $DiIC_{18}$ (A, upper left) and water-soluble dye, rhodamine (A, lower), and distribution of water-soluble dyes coomassie blue (B, upper left) and trypan blue (B, lower left). Dyes (20 μl) were infused locally into the striatum of rodent brains by CED. Animals were euthanized immediately after infusion and sequential sections were obtained by using a cryostat (25 μm thickness; 1 mm interval). The column graph shows the calculated volume of distribution ($n = 4$ hemispheres for each dye; bar = standard deviation).

of infusion, and the extensively distributed neutral PEGylated liposomal $DiOC_{18}$. Binding of cationic liposomes to negatively charged cellular membranes likely restricted the distribution to a small area of the brain. Distributions of PEGylated cationic liposomal $DiOC_{18}$ ($n = 3$ animals) and non-PEGylated cationic liposomal $DiIC_{18}$ ($n = 6$ animals) were also compared using same method (Fig. 3C). Highly PEGylated [10%, mol/mol] cationic liposomes had the same distribution as neutral liposomes (Fig. 3D). Distributions of PEGylated neutral liposomes and non-PEGylated neutral liposomes were identical (Fig. 3D).

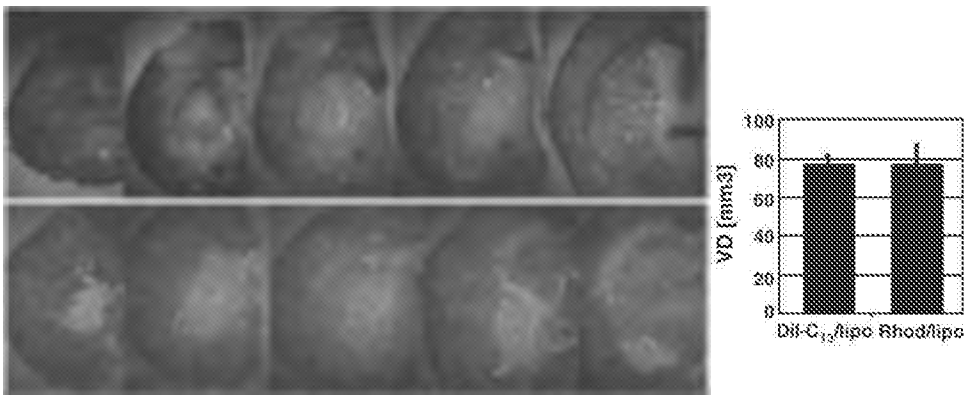

Fig. 2. Distribution of $DiIC_{18}$ liposomes (upper), and rhodamine liposomes (lower). Both dyes were loaded into PEGylated (10%, mol/mol) neutral liposomes and infused (20 μl) into the striatum of rodent brains by CED. Animals were euthanized immediately after infusion and sequential sections were obtained by using a cryostat (25 μm thickness; 1 mm interval). The column graph shows the calculated volume of distribution ($n = 4$ hemispheres for each type of liposome; bar = standard deviation).

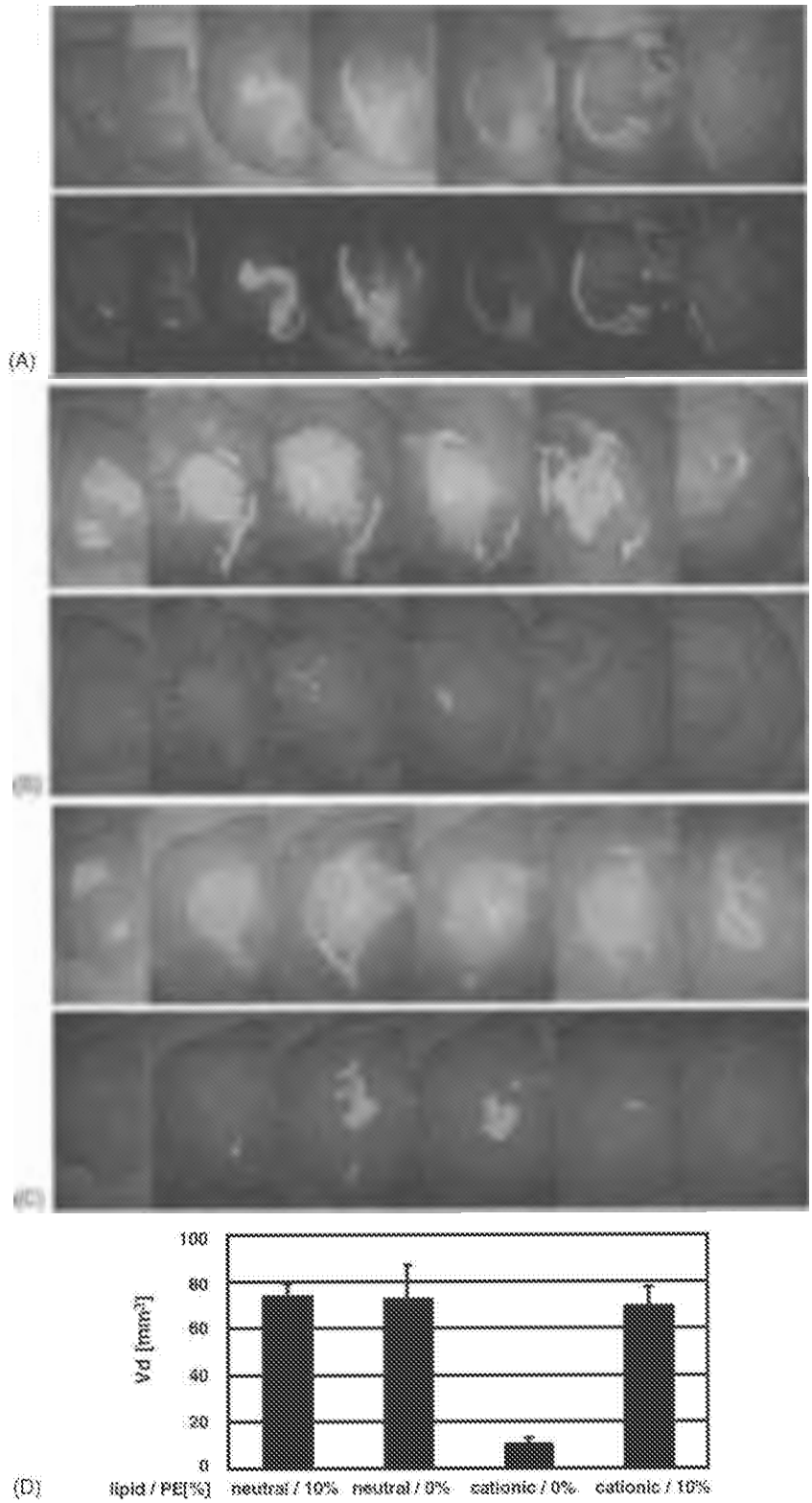

Fig. 3. Differences in volumes of distribution between liposomes with different compositions: size difference (A), charge (B), and surface PEGylation (C and D) were compared. (A) A mixture of PEGylated (10%, mol/mol) neutral liposomes with either a diameter of 84.1 nm and $DiOC_{18}$ fluorescence (A, upper) or a diameter of 130.2 nm and $DiIC_{18}$ fluorescence (A, lower). (B) A mixture of PEGylated (10%, mol/mol) neutral liposomes with a diameter of 84.1 nm and $DiOC_{18}$ fluorescence (B, upper) and non-PEGylated cationic liposome with a diameter of 86.8 nm and $DiIC_{18}$ fluorescence (B, lower). (C) A mixture of PEGylated (10%, mol/mol) cationic liposomes with a diameter of 71.7 nm and $DiOC_{18}$ fluorescence (C, upper) and non-PEGylated cationic liposomes with a diameter of 86.8 nm and $DiIC_{18}$ fluorescence (C, lower). For all infusates, 20 μl of the mixture was infused into the striatum of the rat brains. Calculated volumes of distributions are shown in the column graph [D; PEGylated (10%, mol/mol) neutral, $n = 6$; non-PEGylated neutral, $n = 4$; non-PEGylated cationic, $n = 6$; PEGylated (10%, mol/mol) cationic, $n = 3$; bar = standard deviation].

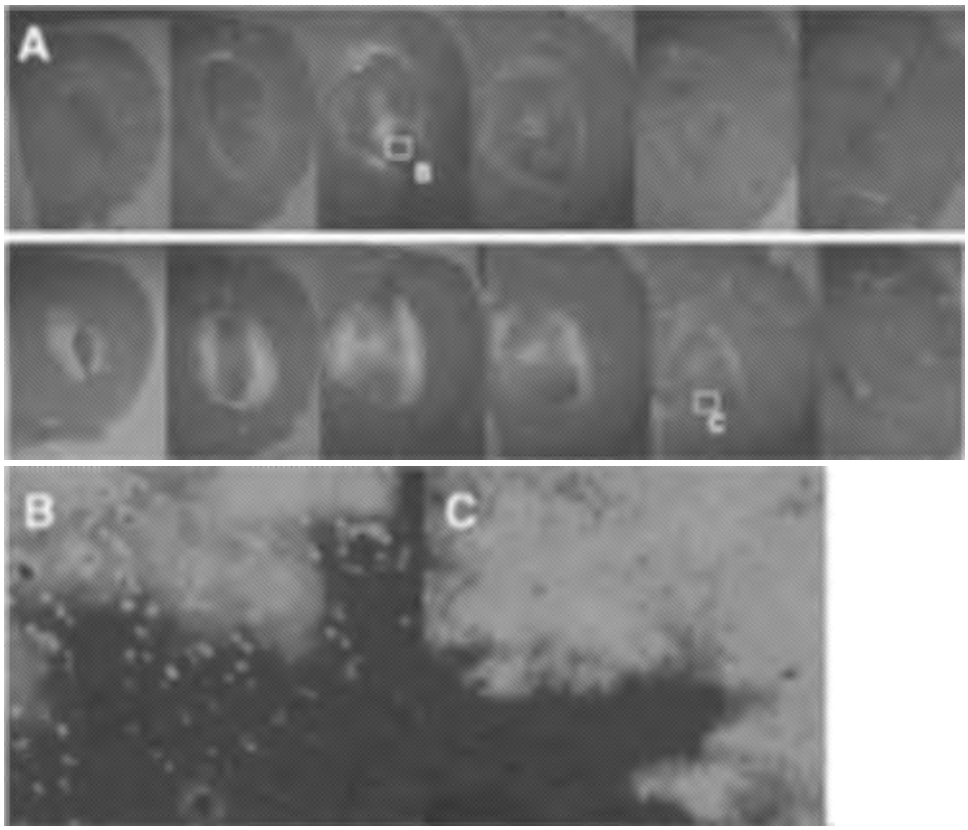

Fig. 4. CED of doxorubicin (2 mg/ml, A, upper) or Doxil (2 mg/ml liposomal doxorubicin, A, lower) were infused in an attempt to cover 9L-2 intracranial xenograft rodent brain-tumor models (A). Ten days after tumor implantation, 20 μl of either agent was infused by CED. Animals were euthanized immediately and sequential sections were obtained by using a cryostat (25 μm thickness; 1 mm interval). Fluorescence generated from doxorubicin was visualized with a fluorescent microscope. Fluorescent images were superimposed on hematoxylin and eosin stainings. B and C show a higher magnification (×200) at the margin of the distribution area (boxed region in A) for both free doxorubicin (B) and Doxil (C).

3.4. Liposomal drug encapsulation provides coverage of almost the entire tumor mass in a rodent intracranial xenograft model

The apparent capability of neutral liposomes to reduce the tissue affinity of an infusate, resulting in enhanced tissue distribution, was tested in a 9L-2 rat brain-tumor model. Ten days after tumor inoculation, doxorubicin ($n = 6$ animals) or PEGylated liposomal doxorubicin ($n = 6$ animals, Doxil, Alza Pharmaceuticals Inc.; Caelyx, Schering-Plough Inc.), was infused using CED, and fluorescence generated by doxorubicin was detected with a fluorescent microscope (Fig. 4A). Doxorubicin by itself had poor tissue distribution, probably because of its affinity to cell components such as nucleic acids. In contrast, Doxil distributed widely over the tumor mass, almost covering it entirely. Higher-power observation at the edge of the distribution revealed the likely reason for the difference in distribution patterns for the two agents—doxorubicin was accumulating in cellular nuclei (Fig. 4B), whereas Doxil was found in the intercellular spaces (Fig. 4C).

4. Discussion

Recently, our group demonstrated methods to increase the volume of distribution of proteins (Hamilton et al., 2001) and genes (Nguyen et al., 2001; Hadaczek et al., 2004) using CED. Heparin co-infusion reduced the binding of growth factors to heparin-binding sites in the extracellular matrix and increased the distribution of glial-derived neurotrophic factor ligand family proteins (Hamilton et al., 2001). Distribution of adeno-associated virus type 2 (AAV-2) was also increased by heparin co-infusion, likely as a result of reduced viral binding to heparin-sulfate proteoglycans (Nguyen et al., 2001). Co-infusion of basic fibroblast growth factor also enhanced the viral transduction volume mediated by AAV-2, seemingly by reducing AAV-2-binding sites (Hadaczek et al., 2004). These findings suggest the importance of considering the tissue affinity of the infusate when delivering therapeutic agents locally into the brain.

In this report, we have demonstrated the difference in tissue distribution of several dyes after CED. Lipophilic dyes did not distribute well upon injection compared to hydrophilic dyes, and were found at the cannula site only. Even among hydrophilic dyes, distribution was not identical due to differences in tissue affinity. These findings have several implications for local drug delivery. In the treatment of malignant gliomas, a drug polymer containing 1,3-bis (2-chloroethyl)-1-nitrosourea (BCNU) showed some efficacy in clinical trials (Brem et al., 1995); however, due to limited diffusion of the drug, the clinical outcome was limited (Fleming and Saltzman, 2002). Poor distribution of BCNU could be at least partially explained by the lipophilic

characteristics of the drug. Although numerous preclinical animal studies have demonstrated the efficacy of CED-based local chemotherapy without monitoring or confirming the drug distribution (Bruce et al., 2000; Heimberger et al., 2000), our results suggest the importance of characterizing drug distribution within the targeted tissue even when a very promising delivery technique is used.

An important point raised by our results is that neutral liposomes can mask the tissue affinity of a variety of agents and enhance the volume of distribution of lipophilic agents. Moreover, distribution was identical regardless of the agent encapsulated within the liposomes, supporting the use of neutral liposomes as a drug carrier for predictable and highly efficient local delivery. In a previous report, we demonstrated a strategy for monitoring liposomal distribution using MRI (Saito et al., 2004a). Considering the identical distribution of neutral liposomes, this monitoring system can be used for rapid screening of tissue distribution by co-infusing a liposome-encapsulated compound of interest and liposomes containing gadolinium. In addition, the size of the neutral liposomes (ranging from 85 to 130 nm) did not affect the tissue distribution, which has practical implications when considering the co-infusion of marker liposomes (gadolinium/liposome) with drug-loaded liposomes sized between 85 and 130 nm.

The tissue distribution of cationic liposomes was also addressed in this study. Cationic liposomes or cationic/lipid based nucleic acid particles are important because they are often used as vectors for gene delivery (Gao and Huang, 1995). Several studies have been proposed, including clinical evaluation using local injection of gene-loaded cationic liposomes (Yoshida et al., 2004). However, cationic liposomes result in very limited gene delivery to the area immediately adjacent to the needle tract (Natsume et al., 1999). Our findings with cationic liposomes were similar to those previous findings. However, we demonstrated that surface PEGylation of the cationic liposomes significantly reduced their tissue affinity and helped to distribute the cationic liposomes. This may be a result of steric stabilization of the particles, which prevents access for surface groups on cellular membranes, or a result of the titration of cationic groups with the negatively charged phosphate of PEG-DSPE, resulting in an essentially neutral liposome. A more careful characterization of these effects will help further refine the mechanism for increased tissue penetration using highly PEGylated cationic liposomes. Although other design constraints need to be explored prior to identifying an effective lipid-based gene-delivery vector for use with CED (MacKay et al., 2005), our findings offer one possibility for increasing the volume of gene delivery using liposomes.

Since CED is one of the most promising drug-delivery methods for brain tumor treatment, we confirmed our findings on tissue affinity in experimental brain tumors. Using the 9L-2 intracranial tumor model, which has an infiltrative tumor margin and can therefore better mimic human gliomas (Saito et al., 2004b), we compared the distribution of doxorubicin infused by CED to that of liposomal doxorubicin (Doxil). Due to the affinity of free doxorubicin for cellular components, primarily nucleic acids, doxorubicin failed to cover a large volume of the brain tumors. Liposomal encapsulation, on the other hand, reduced cellular affinity and increased the distribution to allow coverage of almost the entire tumor mass. Observation with higher magnification supported this difference in tissue affinity; accumulation of doxorubicin was found in cellular nuclei, whereas most of the Doxil was found in the intercellular space. The difference in distribution between free doxorubicin and Doxil verifies that liposomes remain intact during the CED infusion process. Liposome infusion stability is further demonstrated by CED of sulforhodamine B (Mamot et al., 2004) and gadodiamide (Saito et al., submitted for publication, 2004a) because each exhibit distribution behavior dissimilar to that when encapsulated in liposomes. The intracellular fate of Doxil and doxorubicin after CED is driven by two main parameters: peak tissue concentration of drug and the area of distribution within brain and tumor tissue. Because of the narrow therapeutic window of free doxorubicin and the poor distribution, it is much less efficacious than is Doxil, even though the peak tissue concentration of the liposomal doxorubicin (Doxil) is much lower (Yamashita et al., in press). Encapsulation of the drug within the liposome affords us a method of ensuring quantitative distribution of drug such that very prolonged tissue exposure is also attained. In addition, the avoidance of unnecessarily high concentrations of drug that trigger non-specific toxicity can be avoided while at the same time extending efficacy as demonstrated in our work. The use of liposomes as drug carriers in focal CNS disorders may help to overcome the important limiting factor of variable tissue affinity in successful local drug delivery.

Stability of the small molecule/liposome construct is the predominant influence on the distribution of encapsulated agents over time. This manuscript focuses on the distribution of free and liposomal agents during CED rather than time resolved factors such as post-CED diffusion and clearance. Most agents in this work are surrogate markers chosen for characteristics exemplifying a particular infusion behavior and suitability in detection. Validation of detection techniques was confirmed previously by comparing co-infused liposomal and free markers using multible detections schemes including MRI, fluorescence, histology and visual inspection (Saito et al., submitted for publication; Mamot et al., 2004; Krauze et al., 2005a,b).

In summary, our results clearly identify the tissue affinity of locally delivered agents as a limiting factor in successful local distribution within the brain. The tissue distribution of agents following local delivery cannot be assumed based on the co-administration of marked compounds that have different tissue affinity. In addition, our results suggest that using liposomes as drug carriers may help in both monitoring drug distribution and reducing tissue affinity of the drugs. Since liposomes can carry various agents including drugs, genes and oligonucleotides, our finding may have an impact on improving local treatment methods for brain tumors.

Acknowledgments

The authors thank Sharon Reynolds of the Department of Neurological Surgery, University of California, San Francisco for editorial assistance. This work was supported by grants from

National Cancer Institute Specialized Programs of Research Excellence grant (to M.S. Berger, K.S. Bankiewicz, J.W. Park) and Accelerate Brain Cancer Cure (to K.S. Bankiewicz).

References

Bobo RH, Laske DW, Akbasak A, Morrison PF, Dedrick RL, Oldfield EH. Convection-enhanced delivery of macromolecules in the brain. Proc Natl Acad Sci USA 1994;91:2076–80.

Brem H, Piantadosi S, Burger PC, Walker M, Selker R, Vick NA, et al., The Polymer-brain Tumor Treatment Group. Placebo-controlled trial of safety and efficacy of intraoperative controlled delivery by biodegradable polymers of chemotherapy for recurrent gliomas. Lancet 1995;345:1008–12.

Bruce JN, Falavigna A, Johnson JP, Hall JS, Birch BD, Yoon JT, et al. Intracerebral clysis in a rat glioma model. Neurosurgery 2000;46:683–91.

Fleming AB, Saltzman WM. Pharmacokinetics of the carmustine implant. Clin Pharmacokinet 2002;41:403–19.

Gao X, Huang L. Cationic liposome-mediated gene transfer. Gene Ther 1995;2:710–22.

Hadaczek P, Mirek H, Bringas J, Cunningham J, Bankiewicz K. Basic fibroblast growth factor enhances transduction, distribution, and axonal transport of adeno-associated virus type 2 vector in rat brain. Hum Gene Ther 2004;15:469–79.

Hamilton JF, Morrison PF, Chen MY, Harvey-White J, Pernaute RS, Phillips H, et al. Heparin coinfusion during convection-enhanced delivery (CED) increases the distribution of the glial-derived neurotrophic factor (GDNF) ligand family in rat striatum and enhances the pharmacological activity of neurturin. Exp Neurol 2001;168:155–61.

Heimberger AB, Archer GE, McLendon RE, Hulette C, Friedman AH, Friedman HS, et al. Temozolomide delivered by intracerebral microinfusion is safe and efficacious against malignant gliomas in rats. Clin Cancer Res 2000;6:4148–53.

Krauze MT, Saito R, Noble Ch, Tamas M, Bringas J, Park JW, et al. Reflux-free cannula for convection-enhanced delivery permitting high-speed delivery of therapeutic agents. JNS 2005a;103(5):923–9.

Krauze MT, McKnight TR, Yamashita Y, Bringas J, Noble CO, Saito R, et al. Real time visualization and characterization of liposomal delivery into the monkey brain by magnetic resonance imaging. Brain Res Brain Res Protoc 2005b;16(1–3):20–6.

Lidar Z, Mardor Y, Jonas T, Pfeffer R, Faibel M, Nass D, et al. Convection-enhanced delivery of paclitaxel for the treatment of recurrent malignant glioma: a phase I/II clinical study. J Neurosurg 2004;100:472–9.

Lieberman DM, Laske DW, Morrison PF, Bankiewicz KS, Oldfield EH. Convection-enhanced distribution of large molecules in gray matter during interstitial drug infusion. J Neurosurg 1995;82:1021–9.

MacKay JA, Deen DF, Szoka Jr FC. Distribution in brain of liposomes after convection enhanced delivery; modulation by particle charge, particle diameter, and presence of steric coating. Brain Res 2005;1035:139–53.

Mamot C, Nguyen JB, Pourdehnad M, Hadaczek P, Saito R, Bringas JR, et al. Extensive distribution of liposomes in rodent brains and brain tumors following convection-enhanced delivery. J Neurooncol 2004;68:1–9.

Natsume A, Mizuno M, Ryuke Y, Yoshida J. Antitumor effect and cellular immunity activation by murine interferon-beta gene transfer against intracerebral glioma in mouse. Gene Ther 1999;6:1626–33.

Nguyen JB, Sanchez-Pernaute R, Cunningham J, Bankiewicz KS. Convection-enhanced delivery of AAV-2 combined with heparin increases TK gene transfer in the rat brain. Neuroreport 2001;12:1961–4.

Saito R, Bringas J, Mirek H, Berger MS, Bankiewicz KS. Invasive phenotype observed in 1,3-bis(2-chloroethyl)-1-nitrosourea-resistant sublines of 9L rat glioma cells: a tumor model mimicking a recurrent malignant glioma. J Neurosurg 2004a;101:826–31.

Saito R, Bringas JR, McKnight TR, Wendland MF, Mamot C, Drummond DC, et al. Distribution of liposomes into brain and rat brain tumor models by convection-enhanced delivery monitored with magnetic resonance imaging. Cancer Res 2004b;64:2572–9.

Saito R, Krauze MT, Bringas JR, Noble C, McKnight TR, Jackson P, et al. Gadolinium-loaded liposomes allow for real-time magnetic resonance imaging of convection-enhanced delivery in the primate brain. Exp Neurol, submitted for publication.

Szoka Jr F, Papahadjopoulos D. Comparative properties and methods of preparation of lipid vesicles (liposomes). Annu Rev Biophys Bioeng 1980;9:467–508.

Walter KA, Tamargo RJ, Olivi A, Burger PC, Brem H. Intratumoral chemotherapy. Neurosurgery 1995;37:1128–45.

Yamashita R, Ryuta S, Krauze MT, Noble CO, Kawaguchi T, Bankiewicz KS. Convection-enhanced delivery of liposomal doxorubicin in intracranial brain tumor xenografts. Targeted-Oncology, in press.

Yoshida J, Mizuno M, Fujii M, Kajita Y, Nakahara N, Hatano M, et al. Human gene therapy for malignant gliomas (glioblastoma multiforme and anaplastic astrocytoma) by in vivo transduction with human interferon beta gene using cationic liposomes. Hum Gene Ther 2004;15:77–86.

Molecular Cancer Therapeutics

The Use of Olaparib (AZD2281) Potentiates SN-38 Cytotoxicity in Colon Cancer Cells by Indirect Inhibition of Rad51-Mediated Repair of DNA Double-Strand Breaks

Makiko Tahara[1,3], Takeshi Inoue[1], Futoshi Sato[1], Yasuyuki Miyakura[3], Hisanaga Horie[3], Yoshikazu Yasuda[3], Hirofumi Fujii[4], Kenjiro Kotake[2], and Kokichi Sugano[1]

Abstract

Potent application of topoisomerase I inhibitor plus PARP inhibitor has been suggested to be an effective strategy for cancer therapy. Reportedly, mismatch repair (MMR)–deficient colon cancer cells are sensitive to topoisomerase I inhibitor, presumably due to microsatellite instability (MSI) of the *MRE11* locus. We examined the synergy of SN-38, an active metabolite of irinotecan, in combination with the PARP inhibitor olaparib in colon cancer cells showing different MMR status, such as MSI or microsatellite stable (MSS) phenotype. Treatment with SN-38 and olaparib in combination almost halved the IC_{50} of SN-38 for a broad spectrum of colon cancer cells independent of the MMR status. Furthermore, olaparib potentiated S-phase–specific double-strand DNA breaks (DSB) induced by SN-38, which is followed by Rad51 recruitment. siRNA-mediated knockdown of Rad51, but not Mre11 or Rad50, increased the sensitivity to olaparib and/or SN-38 treatment in colon cancer cells. *In vivo* study using mouse xenograft demonstrated that olaparib was effective to potentiate the antitumor effect of irinotecan. In conclusion, olaparib shows a synergistic effect in colon cancer cells in combination with SN-38 or irinotecan, potentiated by the Rad51-mediated HR pathway, irrespective of the Mre11-mediated failure of the MRN complex. These results may contribute to future clinical trials using PARP inhibitor plus topoisomerase I inhibitor in combination. Furthermore, the synergistic effect comprising topoisomerase I-mediated DNA breakage–reunion reaction, PARP and Rad51-mediated HR pathway suggests the triple synthetic lethal pathways contribute to this event and are applicable as a potential target for future chemotherapy. *Mol Cancer Ther; 13(5); 1170–80. ©2014 AACR.*

Introduction

Colorectal cancer is the third most common cancer in men and the second in women worldwide, while almost 60% of the cases occur in developed countries. Colorectal cancer is estimated to be the cause of about 8% of all cancer-related deaths, making it the fourth most common cause (1).

The incidence of distant metastasis (stage IV) is reported to be 18% to 25%, with differences depending on ethnicity, and the 5-year relative survival rate for stage IV disease is as low as 12% (2), which shows the need for developing novel systemic chemotherapy. Conventionally, 5-fluorouracil (5-FU) and its analogs were employed as the first-line or adjuvant chemotherapy for colon cancer, while cases relapsing after 5-FU–based adjuvant chemotherapy were mostly resistant to 5-FU–based systemic chemotherapy. Irinotecan (CPT-11) was introduced as a drug effective for 5-FU–resistant colorectal cancer, the molecular target of which is type I topoisomerase. At present, either FOLFOX (5-FU + leucovorin + oxaliplatin) or FOLFIRI (5-FU + leucovorin + irinotecan) is recommended as the first-line regimen for stage IV colorectal cancer.

DNA repair systems have drawn attention as molecular targets of cancer therapy. Cancers with DNA repair deficiency could be more sensitive to certain therapeutic agents. One of the well-known syndromes is hereditary breast/ovarian cancer (HBOC) harboring a mutated *BRCA1* or *BRCA2* gene, which is involved in double-strand DNA break (DSB) repair. PARP inhibitors showed synthetic lethality to HBOC-related tumors (3, 4) and clinical trials on cases with HBOC have been ongoing worldwide. PARP inhibitors mainly target PARP-1 and PARP-2, which synthesize poly(ADP-ribose) (PAR) and are involved in DNA repair, cell differentiation, regulation of chromatin structure, and gene regulation (5–7).

Authors' Affiliations: [1]Oncogene Research Unit/Cancer Prevention Unit, Tochigi Cancer Center Research Institute, [2]Department of Surgery, Tochigi Cancer Center, Utsunomiya; and [3]Department of Gastrointestinal Surgery and [4]Division of Clinical Oncology, Jichi Medical University, Shimotsuke, Tochigi, Japan

Note: Supplementary data for this article are available at Molecular Cancer Therapeutics Online (http://mct.aacrjournals.org/).

Corresponding Author: Kokichi Sugano, Oncogene Research Unit/Cancer Prevention Unit, Tochigi Cancer Center Research Institute, 4-9-13 Yohnan, Utsunomiya, Tochigi 320-0834, Japan. Phone: 812-8658-5151; Fax: 812-8684-5756; E-mail: ksugano@tcc.pref.tochigi.lg.jp

doi: 10.1158/1535-7163.MCT-13-0683

PARP-1 has an important role in single-strand DNA break (SSB) repair and base excision repair (8). Recently, PARP has been reported to participate in the DSB repair pathway by nonhomologous end joining (NHEJ; refs. 9, 10) or homologous recombination (HR; ref. 11). The mechanism of PARP in DSB repair has been elucidated.

On the other hand, mismatch repair (MMR) deficiency showing microsatellite instability (MSI) due to aberration of mismatch repair genes such as *MSH2*, *MLH1*, *MSH6*, or *PMS2* could be a novel target for cancer treatment because such cases often show frameshift mutation in *MRE11* and/or *RAD50* genes, of which the gene products form a heterotrimer with Nbs1 and are associated with DSB repair (12–15). Reportedly, MMR deficiencies in colorectal cancer could be available as a surrogate marker for various chemotherapeutic agents. MMR-deficient cells were sensitive to topoisomerase I inhibitors (16–19), such as irinotecan and camptothecin, which form a covalent bond with topoisomerase I and inhibit the breakage–reunion reaction in DNA replication or translation; they are now available as the major chemotherapeutic drugs for colorectal cancer (20, 21). *In vivo*, irinotecan is converted to its active metabolite, SN-38, in the presence of carboxylesterase (22, 23).

The combinational treatment of PARP inhibitor and topoisomerase I inhibitor has been considered as a potent strategy for cancer therapeutics, especially for colorectal cancer cells (24–30). However, the mechanisms of inducing topoisomerase I inhibitor hypersensitivity using PARP inhibitor remain unclear and the correlation of the MMR status with the sensitivity to topoisomerase I inhibitor treatment in combination with PARP inhibitor has not been elucidated yet.

Olaparib (AZD2281) is a PARP inhibitor that has been used in clinical trials targeting breast or ovarian cancers. In this study, first, we investigated the sensitivity to SN-38 plus olaparib combinational treatment in colon cancer cell lines characterized by their MMR status, using the ^{3}H-thymidine incorporation assay, the cell counting assay and the clonogenic assay. Second, we investigated the intracellular response of treated cells by using cell diameter measurements as a surrogate marker of G_2–M arrest and apoptosis. Third, we examined the expression of DSB repair-related proteins and the incorporation of 5-bromo-2′-deoxyuridine (BrdUrd), that is, a S-phase–specific cell-cycle marker, using immunofluorescence microscopy to elucidate the mechanisms of enhanced chemosensitivity evoked by olaparib. Finally, we examined the antitumor effect of irinotecan plus olaparib in mouse xenograft models to confirm the results of *in vitro* study as the final stage of the preclinical setting.

Materials and Methods

Reagents

SN-38 and irinotecan (CPT-11) were purchased from Sigma-Aldrich and SANDOZ, respectively. Olaparib (AZD2281) was kindly provided by AstraZeneca K.K. SN-38 and olaparib were dissolved in dimethyl sulfoxide at a concentration of 10 mmol/L and stored at −20°C until the *in vitro* experiment. Irinotecan (20 mg/mL) was stored at room temperature for the *in vivo* experiment.

Cell lines and culturing

SW48, RKO, HCT116, and HT29 were purchased from American Type Culture Collection (ATCC; Summit Pharmaceutical International) from January 2010 through March 2011, which had been characterized using short tandem repeat polymorphism analysis by ATCC. LoVo was purchased from Health Science Research Resources Bank (HSRRB) in January 2011, which had been verified using isoenzyme analysis by HSRRB. These cell lines were passaged for less than 6 months after receipt. HCT-15 was kindly provided by Cell Resource Center for Biomedical Research, Institute of Development, Aging and Cancer (Tohoku University, Sendai, Japan) in January 2011. SW1116, C-1, and colo320HSR were provided by the National Cancer Center (Tokyo, Japan) in 1999. These four cell lines had not been authenticated in our laboratory.

All of these human colon cancer cell lines were cultured in RPMI-1640 medium (Life Technologies Japan) supplemented with 10% FBS (Thermo Fisher Scientific Japan) and 100 μg/mL kanamycin (Sigma-Aldrich) at 37°C in a humidified atmosphere containing 5% CO_2.

SW48 and RKO lack *MLH1* expression due to promoter hypermethylation, causing MSI (31). HC116, LoVo, and HCT-15 have mutated MMR genes, *MLH1* (p.S252X), *MSH2* (p.R359fsX8), and *MSH6* (p.L290fsX1 and p.D1171fsX4), respectively (Supplementary Table S1).

Cell proliferation assay

The procedures for the ^{3}H-thymidine incorporation assay and the cell counting assay using the Scepter 2.0 cell counter were as described previously in detail (32) and are described in the Supplementary Methods.

Western blot analysis

The procedures for Western blot analysis were described in the Supplementary Methods. The primary antibodies used were as follows: anti-PAR (10H) mouse monoclonal antibody (1:500; GeneTex), anti–PARP-1 mouse monoclonal antibody (1:2,000, Santa Cruz Biotechnology), anti–PARP-2 mouse monoclonal antibody (1:1,000, Merck Millipore), anti-Mre11 rabbit polyclonal antibody (1:2,000, Cell Signaling Technology), anti-Rad50 mouse monoclonal antibody (1:1,000, GeneTex), anti-Nbs1 rabbit polyclonal antibody (1:1,000, Novus Biologicals), and anti-Rad51 rabbit polyclonal antibody (1:2,000, Santa Cruz). Anti–β-actin mouse monoclonal antibody (1:200, Santa Cruz Biotechnology) was used as an internal control.

Immunofluorescence microscopy

The detail of the procedures for the immunofluorescence staining is described in the Supplementary Methods. The primary antibodies were as follows: anti-53BP1 rabbit polyclonal antibody (1:500, Abcam), anti-Rad51 rabbit polyclonal antibody (1:50, Santa Cruz

Biotechnology), anti–γ-H2AX mouse monoclonal antibody (1:500, Merck Millipore) and anti-BrdUrd mouse monoclonal antibody (1:500, Sigma-Aldrich). Fluorescence images were recorded with a BZ-9000 fluorescence microscope (KEYENCE) and analyzed using BZ-II Analyzer (KEYENCE). For quantification of 53BP1, Rad51, and γ-H2AX foci, haze-reduced images of about 100 to 200 nuclei from at least 4 fields were observed and the number of foci per nucleus was counted. For counting nuclei with BrdUrd incorporation, at least 6 fields (about 200–1,300 nuclei/field) were observed.

RNA interference

siRNAs directed to Mre11, Rad50, and Rad51 as well as a negative control were purchased from Life Technologies Japan. As commercially available negative control siRNA was cytotoxic for transfection with HCT116, we synthesized nontargeted siRNA using the Silencer siRNA Construction Kit (Life Technologies Japan). The nontarget siRNA sequences were designed as the scrambled sequences of the siRNA directed to RAD51: ACGTATGGATCTAAGATGGtt (sense) and CCATCTCGATCCATACGTat (antisense).

A total of 1–3 × 10^4 cells were plated in 24-well culture plates (500 μL/well). After 24 hours, the cells were transfected with 10 nmol/L siRNA using Lipofectamine RNAiMAX transfection reagent (Life Technologies Japan) in accordance with the manufacturer's recommended protocol. After 24 hours, the medium was replaced with fresh growth medium and exposed to SN-38 and/or olaparib for 48 hours, and then cells were harvested for the cell counting assay. For Western blot analysis, cells were plated in 100 mm dishes (10 mL/dish) and harvested 24 hours after transfection.

In vivo growth inhibitory assay

Five-week-old SCID hairless outbred (SHO) mice (Crl:SHO-Prkdc^{scid}Hr^{hr}) were purchased from Charles River Japan, Inc.. Xenograft models were established by injecting HT29 or SW1116 cells (5 × 10^6) subcutaneously into the left flank of mice. When the tumors reached a size of 100 mm^3, xenografted mice were divided into four groups as follows: control, olaparib alone, irinotecan alone, and olaparib plus irinotecan, and treatment was initiated (day 0). Olaparib (50 mg/kg) was dissolved in 9% β-cyclodextrin (33) and administered orally (*per os*) once a day for 5 days followed by an intermission of two days. In the no treatment group, 9% cyclodextrin alone was administered. Irinotecan (10 mg/kg) was administered intraperitoneally twice weekly. In the no treatment group, PBS alone was administered. In the combinational treatment group, olaparib was administered 1 hour before irinotecan treatment. The tumor diameters were measured with calipers and the tumor volumes were calculated using the following formula: length (mm) × width $(mm)^2/2$. The mice were killed on day 18 for HT29 and on day 30 for SW1116. The tumor sizes and body weights were measured three times weekly. In the study of SW1116 xenografted mice, blood sampling was carried out for analysis of hematologic toxicity and liver dysfunction. The blood samples were analyzed by SRL. Relative tumor volume was determined using the value relative to that on day 0. The data of the relative tumor volume are shown as mean ± SEMs.

Statistical analysis

The data of the *in vitro* study are presented as means ± SDs and that of the *in vivo* study are presented as mean ± SEMs. Statistical significance of *in vitro* study was either analyzed by the Student *t* test (between 2 groups) or one-way ANOVA with the Tukey test or Tukey–Kramer method (between 4 groups). In *in vivo* study, a linear trend test was performed as a utility of one-way ANOVA in each group, and statistical significance between four groups was analyzed by one-way ANOVA with the Tukey–Kramer method. All statistics were calculated using the GraphPad Prism V5.0 software (GraphPad Software, Inc.).

Results

Molecular profiles of the colon cancer cell lines

The molecular profiles of the cell lines used for the assay were examined and summarized as regards MSI status, genetic or epigenetic alterations of the MMR genes, and mutational status of *TP53*, *MRE11*, and *RAD50* (Supplementary Table S1). Of the 9 cell lines examined, 5 cell lines (SW48, RKO, HCT116, LoVo, and HCT-15) showed MSI, whereas 4 cell lines (C-1, colo320HSR, HT29, and SW1116) had a MSS phenotype. MMR-deficient cell lines also had MSI in the genes responsible for HR, such as *MRE11* and *RAD50*. SW48, RKO, HCT116, and LoVo had biallelic MSI in the poly(T)11 tract of *MRE11*, whereas HCT-15 had monoallelic MSI. As for *RAD50* poly(A)8 mutations, RKO, HCT116, and LoVo were heterozygous while SW48 and HCT-15 showed the wild-type phenotype. *TP53* gene mutations were detected in 1 MMR-deficient cell line (HCT-15) and 3 MMR-proficient cell lines (colo320HR, HT29, and SW1116).

Olaparib potentiates SN-38 sensitivity by inhibiting the synthesis of PAR polymer

To assess the effect of olaparib, we first evaluated the cell growth inhibitory effects of olaparib alone by using the ^{3}H-thymidine incorporation assay (Fig. 1A). Of all the cell lines examined, HCT116 was the most sensitive to olaparib, the IC_{50} of which was 2.5 μmol/L and SW1116 was the most resistant, with the IC_{50} of more than 100 μmol/L. We also evaluated the expression of PAR, PARP-1, and PARP-2 in HCT116 cells treated with various concentrations of olaparib. Poly (ADP-ribosyl)ation (PARylation) induced by 1 nmol/L SN-38 in HCT116 was inhibited by olaparib in a dose-dependent manner without affecting the expression levels of PARP-1 and PARP-2 (Fig. 1B).

Next, we evaluated the cell growth inhibitory effects of SN-38 with various concentrations of olaparib in HCT116 and HT29, which have different MMR status and sensitivities to SN-38 (17, 32, 34). In the presence of 0.5 nmol/L SN-38, cell growth was inhibited with 10 nmol/L ($P < 0.01$) or

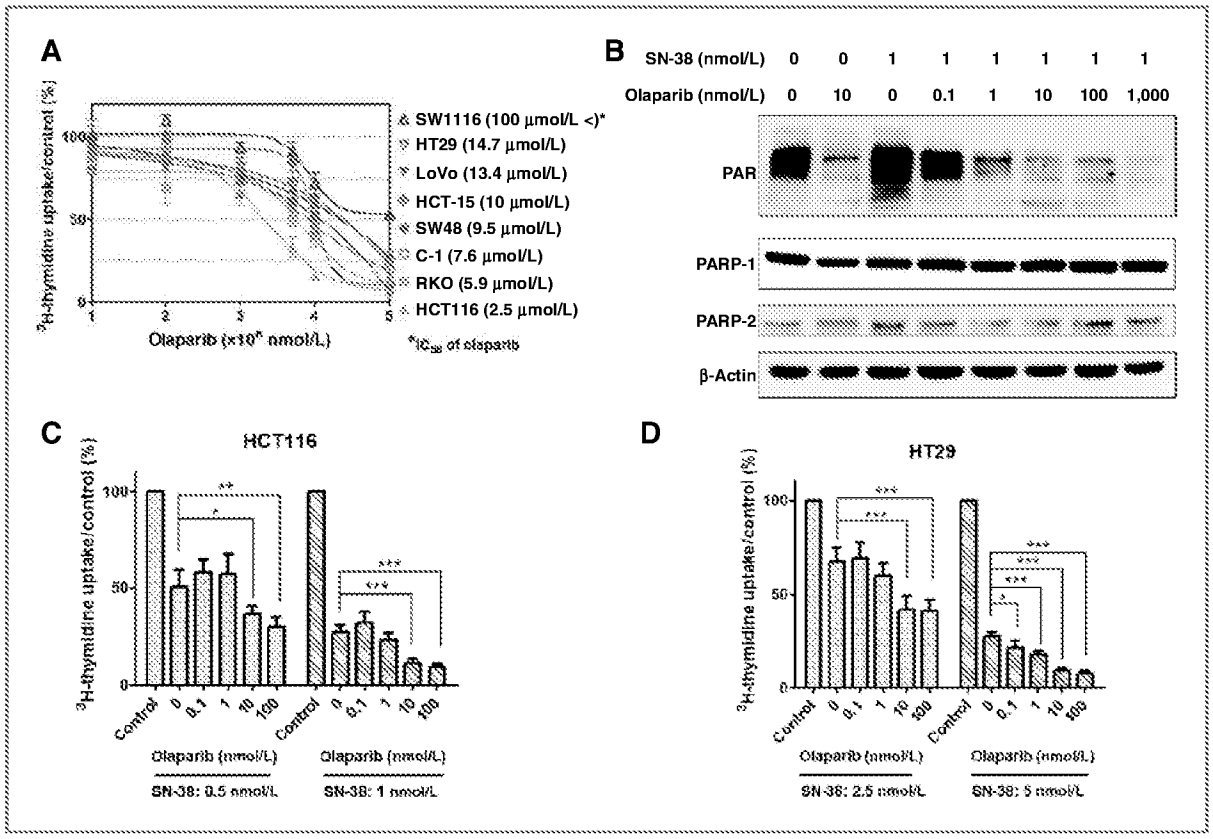

Figure 1. Effects of olaparib in the presence or absence of SN-38 on colon cancer cell lines. A, cell growth inhibition curves of colon cancer cell lines exposed to various concentrations of olaparib were determined using ^{3}H-thymidine incorporation assay. For each cell line, cell growth inhibition (%) was calculated as follows: (^{3}H-thymidine uptake of treated cells − background) × 100/(^{3}H-thymidine uptake of untreated cells − background). Error bars, SDs from replicate experiments ($n = 6$). Each number in parentheses shows the IC_{50} of olaparib analyzed using the cell growth inhibition curves. B, Western blot analysis of PAR, PARP-1, PARP-2, and β-actin (internal control) of HCT116 exposed to various concentrations of olaparib in the presence or absence of 1 nmol/L SN-38. C, cell growth inhibition (%) of HCT116 exposed to various concentrations of olaparib with SN-38 (0.5 or 1 nmol/L). D, cell growth inhibition (%) of HT29 exposed to various concentrations of olaparib with SN-38 (2.5 and 5 nmol/L). Each value is expressed as mean ± SD ($n = 6$). Control, nontreated cells. The Student t test was performed between cells exposed to SN-38 alone and cells exposed to SN-38 plus each concentration of olaparib in HCT116 and HT29 (*, $P < 0.01$; **, $P < 0.001$; ***, $P < 0.0001$).

100 nmol/L ($P < 0.001$) olaparib, and these effects were enhanced when cells were treated with 1 nmol/L SN-38 ($P < 0.0001$ for 10 nmol/L and $P < 0.0001$ for 100 nmol/L olaparib) in HCT116. Concentrations of olaparib less than 1 nmol/L had no inhibitory effect on cell growth in HCT116 treated with 0.5 nmol/L or 1 nmol/L SN-38 (Fig. 1C). Likewise, olaparib also potentiated SN-38 sensitivity at concentrations above 10 nmol/L in HT29 (Fig. 1D). Olaparib concentrations less than 1 μmol/L did not show cell cytotoxicity (Fig. 1A). Considering these results, we determined the concentration of olaparib as 10 nmol/L in the subsequent *in vitro* experiments.

Olaparib potentiates SN-38 cytotoxicity irrespective of MMR status

To assess whether the potentiating effects of olaparib on SN-38 sensitivity were correlated with MMR status or not, we evaluated the SN-38 sensitivity in the presence or absence of olaparib by a variety of assays using colon cancer cell lines showing either MMR-deficient or -proficient phenotypes.

First, we evaluated the IC_{50} of SN-38 in the presence or absence of olaparib by the ^{3}H-thymidine incorporation assay (Fig. 2). Each cell line was treated with SN-38 and/or olaparib for 48 hours. Olaparib significantly potentiated the sensitivity to SN-38 for all cell lines except HCT-15 (Fig. 2 and Supplementary Table S2). SN-38 in combination with olaparib almost halved the IC_{50} of SN-38 in each cell line.

In four cell lines (HCT116, RKO, HT29, and SW1116) showing different MMR status, the results of the ^{3}H-thymidine incorporation assay were reproducible with those measured by the Scepter 2.0 cell counter (Supplementary Fig. S1).

We previously reported that cell diameter changes measured by the Scepter 2.0 cell counter could be used as a marker of G_2–M arrest and apoptosis evoked by SN-38 (32). The increase of the mean cell diameter evoked by SN-

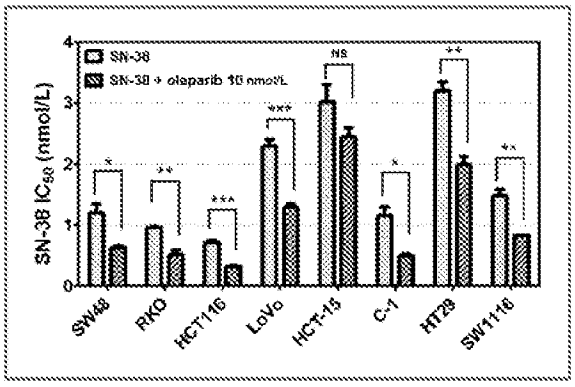

Figure 2. Comparison of SN-38 IC_{50} in the presence or absence of 10 nmol/L olaparib. ^{3}H-thymidine incorporation assay was carried out to calculate the IC_{50} values by cell growth inhibition curves. Each cell line was exposed to either SN-38 alone or SN-38 plus 10 nmol/L olaparib for 48 hours. Data of IC_{50}, mean ± SD of three independent experiments. In each cell line, the Student *t* test was performed between the IC_{50} of cells exposed to SN-38 alone and those exposed to SN-38 plus olaparib in combination (*, $P < 0.05$; **, $P < 0.01$; ***, $P < 0.001$; NS, not significant).

38 plus olaparib was greater than that of SN-38 alone in each cell line (Supplementary Table S3). These results indicate that olaparib enhanced G_2–M arrest induced by SN-38, together with the increase of the apoptotic cell fraction shown by the appearance of small-sized particles. These results show that olaparib potentiates SN-38 sensitivity in various colon cancer cell lines by inducing G_2–M arrest and apoptosis, irrespective of MMR status.

To assess the efficacy of the treatments with shorter duration of treatment, we performed robust colony assays. Two cell lines (HCT116 and HT29) were exposed to SN-38 and/or olaparib for 6, 12, 24, and 48 hours and subjected to colony formation. Olaparib potentiated the inhibitory effect of colony formation by SN-38, while these effects were not observed in the treatment using SN-38 alone after 12 hours of exposure in both cell lines (Supplementary Fig. S2). Colony formation was suppressed significantly after 24 hours in both cell lines treated with SN-38 alone or SN-38 plus olaparib. These results were well correlated with the data obtained by the ^{3}H-thymidine incorporation assay or the cell counting assay in which cells were treated for 48 hours as described above.

Olaparib increases DNA double-strand breaks induced by SN-38

Reportedly, SN-38 induces DSBs and PARP inhibitor is involved in the inhibition of SSB repair and PARylation of the proteins involved in DNA repair (5–8, 35). To elucidate whether olaparib increases DSBs induced by SN-38, we examined the formation of the 53BP1 nuclear foci, for example, a DSB marker in HCT116 and HT29 exposed to SN-38 and/or olaparib for 12 hours (Fig. 3).

The formation of 53BP1 nuclear foci did not increase by the treatment with olaparib alone, while they increased significantly in the groups treated with SN-38 or SN-38 plus olaparib (Fig. 3A and B). In analysis using one-way ANOVA, numbers of foci were significantly increased in the group treated with SN-38 plus olaparib as compared with SN-38 alone in both cell lines ($P < 0.001$; Fig. 3C and D).

We compared the results of the 53BP1 foci formation with those of ^{3}H-thymidine incorporation assay, using immunofluorescence double staining for BrdUrd and 53BP1 in HCT116 cells exposed to SN-38 and/or olaparib for different periods ranging from 6, 12, 24, and 48 hours (Supplementary Fig. S3). Exposed to SN-38 plus olaparib for 48 hours, BrdUrd incorporation decreased significantly as compared with SN-38 alone (Supplementary Fig. S3A). As BrdUrd incorporation is a surrogate marker of the S-phase, this was compatible with the data of ^{3}H-thymidine incorporation assay shown in Fig. 1C. When exposed to SN-38 plus olaparib for 6 hours, 53BP1 foci seemed to increase in the nuclei with BrdUrd incorporation (Supplementary Fig. S3B). This finding lasted until 12 hours of treatment, but BrdUrd-stained cell decreased markedly when they were exposed over 24 hours, leaving 53BP1 foci in the nuclei without BrdUrd incorporation (Supplementary Fig. S3B).

Olaparib increases Rad51 recruitment to the DSB sites induced by SN-38

As the major DSB repair pathway is mediated by HR (36–38), we examined formation of the Rad51 and γ-H2AX foci and their colocalization in HT29 cells. As antibodies directed against 53BP1 and Rad51 were both rabbit polyclonal antibodies and unsuitable for double staining, we used mouse anti–γ-H2AX monoclonal antibody as a DSB marker and examined its colocalization with Rad51 foci using double staining. Numbers of γ-H2AX foci and Rad51 foci showed a significant increase between SN-38 versus SN-38 plus olaparib and a part of γ-H2AX foci colocalized with Rad51 foci (Fig. 4). These data indicate that olaparib potentiates the recruitment of Rad51 to the DSB site in SN-38–treated cells.

Baseline levels of the DNA repair–related protein expression in cell lines were examined by Western blot analysis (Supplementary Fig. S4). It was found that the potentiating effects of olaparib on SN-38 sensitivity might not be correlated with the baseline levels of PARP-1, PARP-2, Mre11, Rad50, Nbs1, and Rad51 expressions. Furthermore, Rad51 expression by Western blot analysis did not differ between cells treated with SN-38 alone and SN-38 plus olaparib in RKO, HCT116, HT29, and SW1116 (data not shown).

Rad51 knockdown increases sensitivity to SN-38 and/or olaparib

To elucidate an effector molecule concerned with the potentiating effects of olaparib on SN-38 sensitivity, we performed a siRNA-mediated knockdown experiment of HR-related molecules, including Mre11, Rad50, and Rad51. SW1116 cells harboring wild-type *MRE11* and *RAD50* were used for the assay in that it is suitable for siRNA transfection. Drug sensitivities were evaluated by the cell counting assay. SW1116 cells transfected with

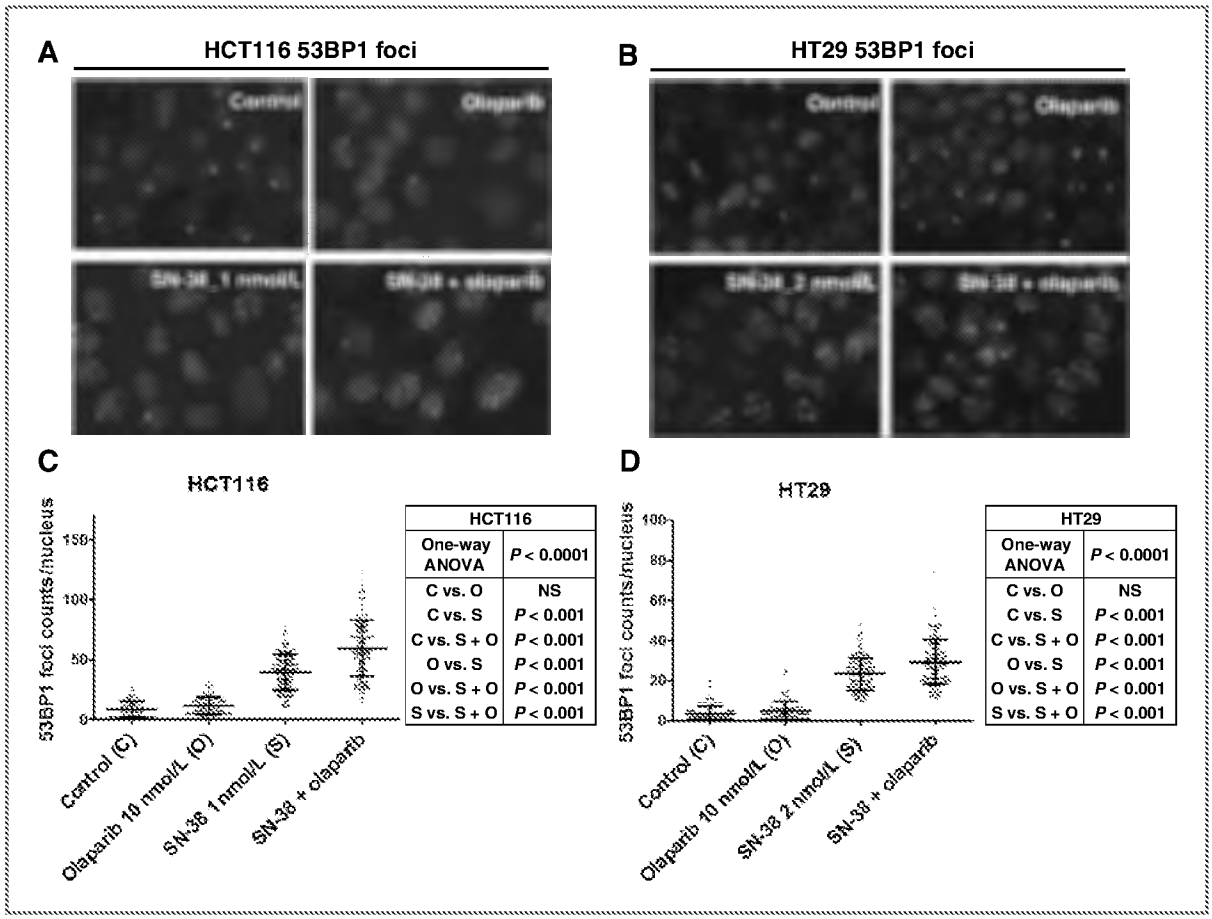

Figure 3. Olaparib potentiates DNA DSBs induced by SN-38. The formation of 53BP1 foci was examined by immunofluorescence microscopy upon counterstaining with 4′, 6-diamidino-2-phenylindole (DAPI) in HCT116 (A) and HT29 (B) exposed to SN-38 (1 nmol/L for HCT116 and 2 nmol/L for HT29) in the presence or absence of 10 nmol/L olaparib for 12 hours. Counts of 53BP1 foci per nucleus were performed for HCT116 (C) and HT29 (D). Error bars, mean ± SD. The significance of differences between the four groups was analyzed using one-way ANOVA with the Tukey–Kramer method (NS, not significant).

Rad51 siRNA became significantly sensitive in all conditions, that is, with SN-38, SN-38 plus olaparib, and even with olaparib alone, as compared with the cells transfected with control siRNA (Fig. 5A, Supplementary Fig. S5). In cells transfected with Mre11 or Rad50 siRNA, there were no changes in the sensitivities to the olaparib or SN-38 treatments. Cell diameters of the transfectant with Rad51 siRNA increased according to the order of the treatments, namely, control < olaparib < SN-38 < SN-38 plus olaparib, indicating that G_2–M arrest occurred preferentially for SN-38 or SN-38 plus olaparib compared with olaparib alone (Fig. 5B and Supplementary Table S4). Furthermore, the increase of small particles indicated the increase of cell apoptosis in each treatment (Fig. 5B and Supplementary Table S4). Knockdown effects of these cells were confirmed by Western blot analysis, in which the protein expressions of Mre11, Rad50, and Rad51 were diminished 24 hours after transfection with each targeted siRNA (Fig. 5C–E). In addition, we observed the formation of Rad51 foci in cells transfected with Rad51 or control siRNA after SN-38 treatment by immunofluorescence microscopy and confirmed that the formation of Rad51 foci was inhibited in cells transfected with Rad51 siRNA compared with control siRNA (Fig. 5F).

We also evaluated the effects of Rad51 knockdown in HCT116 cells, which have biallelic *MRE11* mutations. HCT116 cells have endogenously weak expression of Mre11 and Rad50 (Supplementary Fig. S4). In cells transfected with Rad51 siRNA, the sensitivities to olaparib, SN-38, and combinational treatment increased significantly more than in cells transfected with control siRNA (Supplementary Fig. S6A). Moreover, the cell diameter changes indicated the increase of G_2–M arrest and apoptosis in cells transfected with Rad51 siRNA and subsequently treated with SN-38 and/or olaparib (Supplementary Fig. S6B and Supplementary Table S5). The expression of Rad51 protein was markedly diminished 24 hours after transfection with Rad51-targeted siRNA (Supplementary Fig. S6C). These results suggest that Rad51 may play an important role in DSB repair upon SN-38 and/or

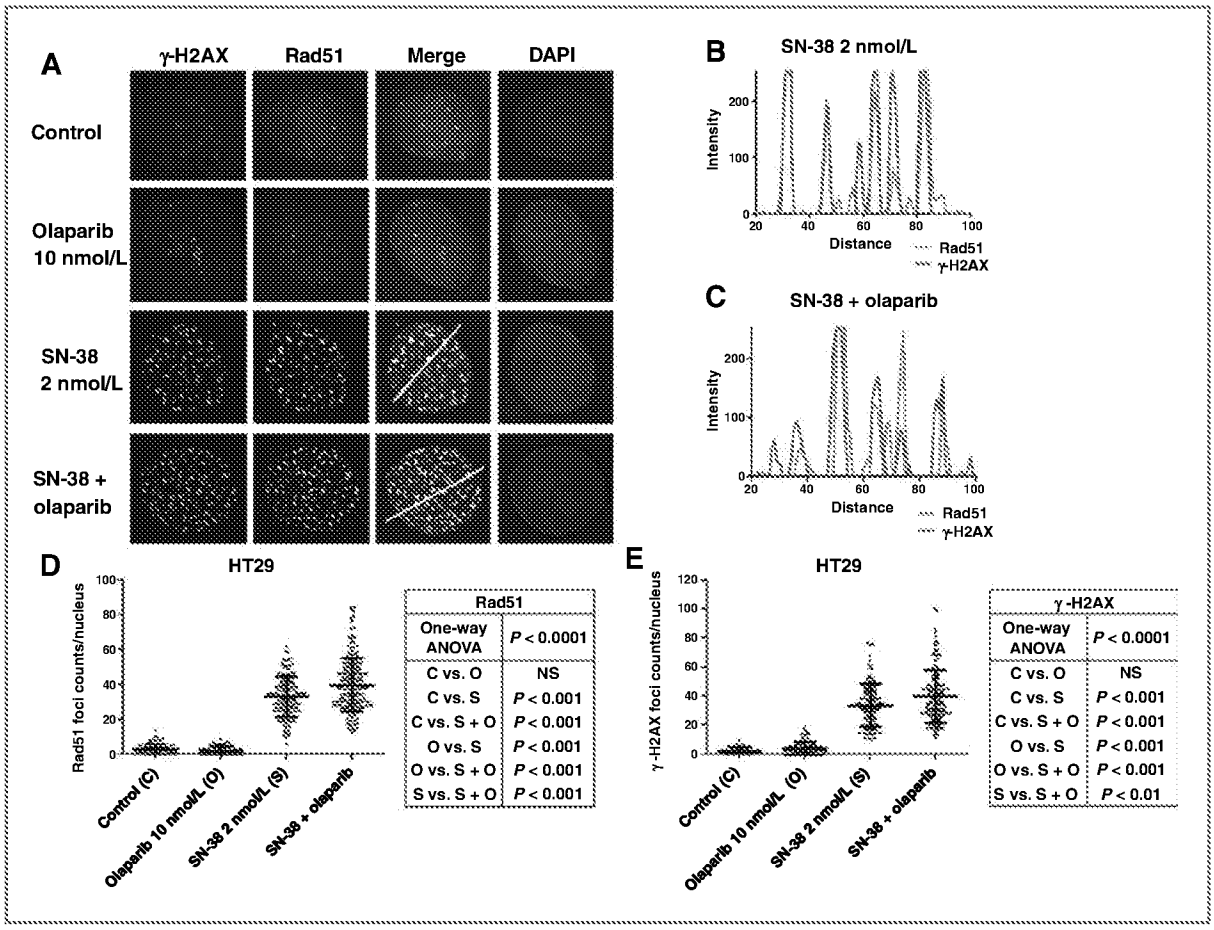

Figure 5. Olaparib potentiates Rad51 recruitment for double-strand break sites induced by SN-38. A, the formation of Rad51 and γ-H2AX foci was examined by immunofluorescence microscopy in HT29 exposed to 2 nmol/L SN-38 and/or 10 nmol/L olaparib for 12 hours. For analysis of the colocalization of Rad51 and γ-H2AX, fluorescence intensity of Rad51 (green) and γ-H2AX (red) above the white line in the merged image was measured and we adopted two-color line plots to overlay the two-color histograms as shown in graphs B (SN-38-treated cell) and C (SN-38 plus olaparib-treated cell). Counts of Rad51 foci (D) and γ-H2AX foci (E) per nucleus in HT29 were carried out. Error bars, mean ± SD. The significance of differences between the four groups was analyzed using one-way ANOVA with the Tukey–Kramer method (NS, not significant).

olaparib treatment, irrespective of the Mre11 or Rad50 pathway.

Olaparib potentiates the antitumor effect of irinotecan in mouse xenograft models

To confirm whether the treatment with irinotecan plus olaparib in combination has an antitumor effect compared with irinotecan alone in *in vivo* experiment, we established two mouse xenograft models using HT29 and SW1116, of which the *in vitro* sensitivities to SN-38 were different. In HT29 xenografts, tumor growth in the irinotecan-treated group was not significantly suppressed compared with that in the control group. However, the group treated with irinotecan plus olaparib showed a significant decrease of the tumor volumes compared with the control group and the irinotecan-treated group ($P < 0.01$ for control vs. combination and olaparib vs. combination, $P < 0.05$ for irinotecan vs. combination; Fig. 6A). In SW1116 xenografts, tumor growth in the irinotecan-treated group was significantly suppressed compared with that in the control group. In the combinational treatment group, antitumor effects also increased significantly compared with those in the control group and the olaparib-treated group ($P < 0.001$ for control vs. irinotecan or combination and olaparib vs. irinotecan or combination; Fig. 6B). There was no significant change between irinotecan- and combinational-treated group, due to high sensitivity of SW1116 to irinotecan; however, the result of the trend test showed decrease of the slope in the irinotecan plus olaparib-treated group compared with the irinotecan alone (0.008 vs. 0.04; $P < 0.0001$; Fig. 6B). No significant body weight loss was observed in the treated groups compared with the control group (data not shown). In the experiment using SW1116 mouse xenograft, clinical blood chemistry was examined to analyze hematologic toxicity and liver dysfunction. In each treated group, neither

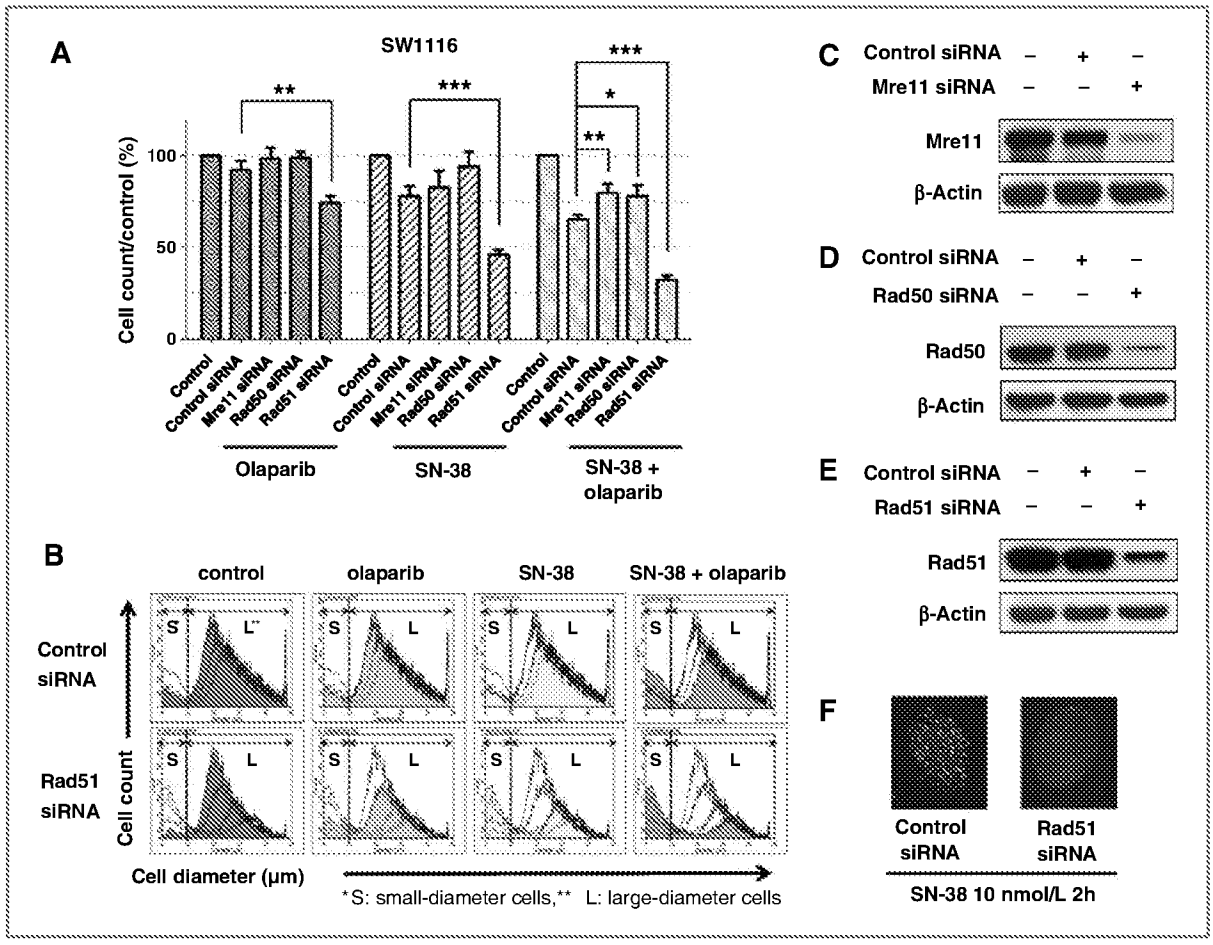

Figure 5. The siRNA-mediated knockdown targeting Rad51 potentiates the sensitivity to SN-38 and/or olaparib in SW1116. A, cell counting assay of SW1116 exposed to 1 nmol/L SN-38 and/or 10 nmol/L olaparib for 48 hours after transfection with control siRNA, Mre11 siRNA, Rad50 siRNA, or Rad51 siRNA. Data, mean ± SD of triplicate experiments. Control means nontreated cells. The Student *t* test was performed between cells transfected with control siRNA and those with the other siRNA (*, $P < 0.05$; **, $P < 0.01$; ***, $P < 0.0001$). B, measurement of the cell diameter and cell count was performed using the Scepter 2.0 cell counter. The *x*-axis of each graph represents the cell diameter (μm) and the *y*-axis represents the cell count (demonstrated in the inset of Supplementary Fig. S5). Experiments were performed in triplicate in each condition and each graph of cells transfected with control siRNA and Rad51 siRNA represents the result of a single run in triplicate experiments. The mean ± SD of the cell diameters and the proportion of the cells with small diameter in each condition are shown in Supplementary Table S4. Graphs of cells transfected with Mre11 siRNA and RAD50 siRNA are shown in Supplementary Fig. S5. Effects of knockdown were confirmed by Western blot analysis 24 hours after siRNA-mediated transfection targeting Mre11 (C), Rad50 (D), or Rad51 (E). F, formation of the Rad51 foci 24 hours after transfection was examined by immunofluorescence microscopy. Cells were exposed to 10 nmol/L SN-38 for 2 hours before PFA fixation to induce double-strand DNA breaks.

hematocytopenia nor liver dysfunction was observed at the doses of irinotecan and olaparib used in this study, and the regimen was well tolerable in the mouse experiments (Supplementary Table S6).

Discussion

In this study, we assessed the effect of olaparib on potentiating the tumor cytotoxicity of SN-38 in colon cancer cell lines and whether the administration of olaparib in combination with irinotecan had suppressed the tumor growth in mouse xenograft models. As reported previously, the IC_{50s} of SN-38 were lower in MMR-deficient cells harboring homozygous mutations in *MRE11* and genetic or epigenetic alterations of *MLH1* as compared with the MMR-proficient cells, suggesting that Mre11 deficiency brought about the sensitization of the MMR-deficient cells to the topoisomerase I inhibitor (19, 34, 39). In analysis using ^{3}H-thymidine incorporation assay, olaparib almost halved the IC_{50} of SN-38 in each cell lines, irrespective of MMR status (Fig. 2 and Supplementary Table S2).

We counted the number of the 53BP1 foci formation in 2 cell lines, HCT116 and HT29 exposed to SN-38 or SN-38 plus olaparib for 12 hours: the former as a SN-38–sensitive cell line and the latter as a SN-38–resistant one. There was a significant increase in the number of 53BP1 foci in cells treated with SN-38 plus olaparib as compared with those treated with SN-38 alone, irrespective of the original sensitivity in each cell line (Fig. 3).

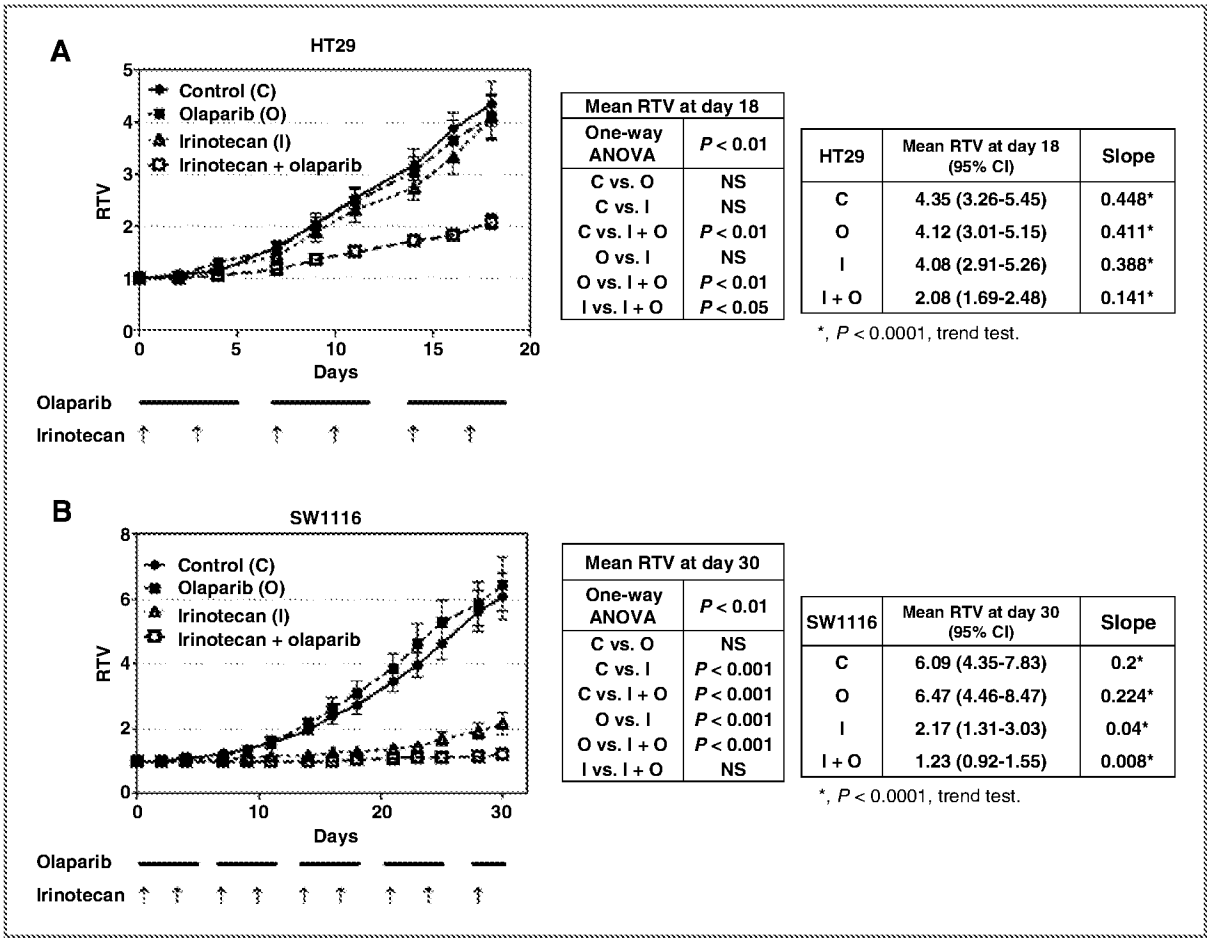

Mean RTV at day 18	
One-way ANOVA	$P < 0.01$
C vs. O	NS
C vs. I	NS
C vs. I + O	$P < 0.01$
O vs. I	NS
O vs. I + O	$P < 0.01$
I vs. I + O	$P < 0.05$

HT29	Mean RTV at day 18 (95% CI)	Slope
C	4.35 (3.26-5.45)	0.448*
O	4.12 (3.01-5.15)	0.411*
I	4.08 (2.91-5.26)	0.388*
I + O	2.08 (1.69-2.48)	0.141*

*, $P < 0.0001$, trend test.

Mean RTV at day 30	
One-way ANOVA	$P < 0.01$
C vs. O	NS
C vs. I	$P < 0.001$
C vs. I + O	$P < 0.001$
O vs. I	$P < 0.001$
O vs. I + O	$P < 0.001$
I vs. I + O	NS

SW1116	Mean RTV at day 30 (95% CI)	Slope
C	6.09 (4.35-7.83)	0.2*
O	6.47 (4.46-8.47)	0.224*
I	2.17 (1.31-3.03)	0.04*
I + O	1.23 (0.92-1.55)	0.008*

*, $P < 0.0001$, trend test.

Figure 8. Olaparib increases the antitumor effects of irinotecan in mouse xenograft models. Tumor xenografts of HT29 and SW1116 were treated with olaparib (50 mg/kg, *per os*, every day consecutively for 5 days with intermission for 2 days per week) and/or irinotecan (10 mg/kg i.p., twice a week). A, relative tumor volumes (RTV) were measured in HT29 xenograft models (control, $n = 6$; olaparib, $n = 7$; irinotecan, $n = 5$; irinotecan plus olaparib, $n = 5$). B, relative tumor volumes were measured in SW1116 xenograft models (control, $n = 7$; olaparib, $n = 7$; irinotecan, $n = 6$; irinotecan plus olaparib, $n = 7$). Data, mean ± SEM. A linear trend test was performed in each group, and statistical significance between four groups was analyzed by one-way ANOVA with the Tukey–Kramer method (NS, not significant).

Results of the ^{3}H-thymidine incorporation assay and the correlation with the formation of 53BP1 foci were further analyzed by immunofluorescence double staining using antibodies directed to BrdUrd and 53BP1. Accumulation of nuclear BrdUrd incorporation persisted at 12 hours and decreased after 24 hours of exposure to SN-38 with or without olaparib (Supplementary Fig. S3A), while the formation of 53BP1 foci was consistent with positive BrdUrd nuclear staining in cells exposed to SN-38 or SN-38 plus olaparib for 12 hours, while in cells exposed for over 24 hours, 53BP1 foci was observed in the nuclei without BrdUrd incorporation (Supplementary Fig. S3B). Furthermore, results of the clonogenic assay showed that colony formation was suppressed significantly when cells were exposed to SN-38 or SN-38 plus olaparib over 24 hours as compared with the control or olaparib alone, whereas those exposed to SN-38 or SN-38 plus olaparib for less than 12 hours did not show reduced colony formation (Supplementary Fig. S2). Wu and colleagues reported that DSBs induced by SN-38 were biphasic events: an immediate phase was S-phase specific and inhibited by aphidicolin, a DNA polymerase inhibitor and a lagging phase, associated with apoptotic cell death (35). The data of BrdUrd and 53BP1 double staining indicated that DSBs at 12 hours after exposure to SN-38 or SN-38 plus olaparib seemed to be S-phase–specific immediate phase, and the cytotoxic effects observed at 48 hours exposure correspond to the lagging phase. The data of ^{3}H-thymidine incorporation assay were well compatible with those of the clonogenic assay (Fig. 2 and Supplementary Fig. S2).

IC_{50}s of olaparib were more than 2.5 μmol/L in all cell lines and 10 nmol/L olaparib used in *in vitro* experiments seemed to have the least cytotoxic effect (Fig. 1). At this concentration, olaparib alone did not increase DSBs and there were no differences in cell counts, cell cycle, and apoptotic change between control and olaparib-treated cells

(Fig. 3 and Supplementary Fig. S1). Nonetheless, olaparib in combination with SN-38 increased DSBs and potentiated SN-38 sensitivity, leading to G_2–M arrest and apoptosis.

SN-38 plus olaparib treatment in HT29 cells increased the number of Rad51 foci colocalized with γ-H2AX, another marker of DSB, implying that DSBs induced by SN-38 would be repaired by the Rad51-mediated DNA repair pathway (Fig. 4). On the other hand, Mre11-Rad50-Nbs1 complex forms a MRN trimmer, which has 3′ to 5′ exonuclease activity and acts as a sensor molecule in the initiating process of DSB repair with the activation the checkpoint kinase ATM (40–45). If the hypersensitivity to SN-38 is caused by *MRE11* mutations resulting in disruption of the MRN complex, does it arise independent of the Rad51-mediated HR or not? To address this, we performed a knockdown experiment using Mre11, Rad50, and Rad51 siRNAs for SW1116 cells, a cell line with MMR-proficient phenotype without MSI in the *MRE11* locus. As a result, cell proliferation was suppressed significantly in the absence of Rad51, but not MRE11 nor RAD50 (Fig. 5).

A series of experiments denoted that single-strand DNA breaks caused by treating cells with SN-38 proceeds to S-phase–specific DSBs, which is repaired through HR-mediated DNA repair. The addition of olaparib in combination with SN-38 increased the number of Rad51 foci, which is colocalized with γ-H2AX foci, indicating the DSBs repaired by the HR-mediated DNA repair pathway (Figs. 3 and 4). Suppression of PARylation enhanced the sensitivity to SN-38, leading to G_2–M arrest and apoptosis in most of the colon cancer cell lines used in this study (Fig. 1 and Supplementary Fig. S1). The use of olaparib in combination with SN-38 may indirectly inhibit HR-mediated DNA repair through suppressing PARylation. This effect was also reproducible in the experiment using HCT116, an MMR-deficient cell line harboring biallelic *MRE11* mutations (Supplementary Fig. S6). SiRNA-mediated Rad51 knockdown increases the sensitivity of HCT116 cells to SN-38 and olaparib, indicating that PARP plays an indirect role for this synthetic lethality mediated by Rad51, irrespective of neither MMR deficiency nor *MRE11* inactivation.

In the experiment using the mouse xenograft models, combination of irinotecan and olaparib suppressed tumor growth significantly, without critical systemic or hematologic toxicity (Fig. 6 and Supplementary Table S6). The results of the *in vivo* study well confirmed the synergistic effect observed in the *in vitro* study. Dose of irinotecan employed in this study seems to be lower than LD_{50} reported in the nude mouse (177 mg/kg, i.p.), although LD_{50} of irinontecan in SHO mouse was not reported elsewhere (46). Tentori and colleagues reported that PARP inhibitor prevents irinotecan-induced intestinal damage in *in vivo* study using rat models (29). In the clinical settings, topoisomerase I inhibitor has adverse effects such as gastrointestinal symptoms, hematologic toxicity, and liver dysfunction, while olaparib was reported to be less toxic than irinotecan and its combined use may improve chemotherapeutic compliance by reducing the dose or frequency of irinotecan administration.

In summary, we found that SN-38 or irinotecan plus olaparib in combination could be applicable as a useful approach in a broad spectrum of colon cancer cells, regardless of the MMR status. *In vivo* study demonstrated that olaparib would be effective to potentiate the antitumor effect of irinotecan without serious adverse effects. Results of this preclinical study endorse further approaches to be pursued in clinical settings. Furthermore, triple synthetic lethality comprising topoisomerase I-mediated DNA breakage–reunion reaction, PARylation, and Rad51-mediated HR pathway may contribute as a potential target for future chemotherapy.

Disclosure of Potential Conflicts of Interest

No potential conflicts of interest were disclosed.

Authors' Contributions

Conception and design: M. Tahara, T. Inoue, K. Sugano
Development of methodology: M. Tahara, T. Inoue
Acquisition of data (provided animals, acquired and managed patients, provided facilities, etc.): M. Tahara, F. Sato, K. Kotake
Analysis and interpretation of data (e.g., statistical analysis, biostatistics, computational analysis): M. Tahara, K. Sugano
Writing, review, and/or revision of the manuscript: M. Tahara, Y. Miyakura, Y. Yasuda, K. Sugano
Administrative, technical, or material support (i.e., reporting or organizing data, constructing databases): M. Tahara, H. Horie, Y. Yasuda, H. Fujii, K. Sugano
Study supervision: Y. Miyakura, Y. Yasuda, K. Kotake, K. Sugano

Grant Support

This study was supported, in part, by Grants-in-Aid for Cancer Research and for the Third Term Comprehensive Control Research for Cancer from the Ministry of Health, Labor, and Welfare, Japan, as well as by the National Cancer Center Research and Development Fund (21bunshi-9-②, 23-A-2 and 23-A-7;to K. Sugano).

The costs of publication of this article were defrayed in part by the payment of page charges. This article must therefore be hereby marked *advertisement* in accordance with 18 U.S.C. Section 1734 solely to indicate this fact.

Received August 30, 2013; revised January 26, 2014; accepted February 17, 2014; published OnlineFirst February 27, 2014.

References

1. Ferlay J, Soerjomataram I, Ervik M, Dikshit R, Eser S, Mathers C, et al. GLOBOCAN 2012 v1.0, Cancer Incidence and Mortality Worldwide: IARC CancerBase No. 11 [Internet]. Lyon, France: International Agency for Research on Cancer; 2013 [updated Oct 2012; cited 2013 Jul 10]. Available from: http://globocan.iarc.fr/Pages/fact_sheets_population.aspx.
2. American Cancer Society. Colorectal Cancer Facts & Figures 2011-2013 [Internet]. Atlanta, GA: American Cancer Society; 2011 [cited 2013 Jul 10]. Available from: http://www.cancer.org/research/cancerfactsstatistics/colorectal-cancer-facts-figures.
3. Farmer H, McCabe N, Lord CJ, Tutt AN, Johnson DA, Richardson TB, et al. Targeting the DNA repair defect in BRCA mutant cells as a therapeutic strategy. Nature 2005;434:917–21.
4. Helleday T, Bryant HE, Schultz N. Poly(ADP-ribose) polymerase (PARP-1) in homologous recombination and as a target for cancer therapy. Cell Cycle 2005;4:1176–8.
5. Sallmann FR, Vodenicharov MD, Wang ZQ, Poirier GG. Characterization of sPARP-1. An alternative product of PARP-1 gene with poly (ADP-ribose) polymerase activity independent of DNA strand breaks. J Biol Chem 2000;275:15504–11.

6. Mortusewicz O, Ame JC, Schreiber V, Leonhardt H. Feedback-regulated poly(ADP-ribosyl)ation by PARP-1 is required for rapid response to DNA damage in living cells. Nucleic Acids Res 2007;35:7665–75.
7. Meyer-Ficca ML, Lonchar JD, Ihara M, Meistrich ML, Austin CA, Meyer RG. Poly(ADP-ribose) polymerases PARP1 and PARP2 modulate topoisomerase II beta (TOP2B) function during chromatin condensation in mouse spermiogenesis. Biol Reprod 2011;84:900–9.
8. Dantzer F, Schreiber V, Niedergang C, Trucco C, Flatter E, De La Rubia G, et al. Involvement of poly(ADP-ribose) polymerase in base excision repair. Biochimie 1999;81:69–75.
9. Miwa M, Masutani M. PolyADP-ribosylation and cancer. Cancer Sci 2007;98:1528–35.
10. Wang M, Wu W, Wu W, Rosidi B, Zhang L, Wang H, et al. PARP-1 and Ku compete for repair of DNA double strand breaks by distinct NHEJ pathways. Nucleic Acids Res 2006;34:6170–82.
11. Hegan DC, Lu Y, Stachelek GC, Crosby ME, Bindra RS, Glazer PM. Inhibition of poly(ADP-ribose) polymerase down-regulates BRCA1 and RAD51 in a pathway mediated by E2F4 and p130. Proc Natl Acad Sci U S A 2010;107:2201–6.
12. Giannini G, Ristori E, Cerignoli F, Rinaldi C, Zani M, Viel A, et al. Human MRE11 is inactivated in mismatch repair-deficient cancers. EMBO Rep 2002;3:248–54.
13. Giannini G, Rinaldi C, Ristori E, Ambrosini MI, Cerignoli F, Viel A, et al. Mutations of an intronic repeat induce impaired MRE11 expression in primary human cancer with microsatellite instability. Oncogene 2004;23:2640–7.
14. Miquel C, Jacob S, Grandjouan S, Aime A, Viguier J, Sabourin JC, et al. Frequent alteration of DNA damage signalling and repair pathways in human colorectal cancers with microsatellite instability. Oncogene 2007;26:5919–26.
15. Kim NG, Choi YR, Baek MJ, Kim YH, Kang H, Kim NK, et al. Frameshift mutations at coding mononucleotide repeats of the hRAD50 gene in gastrointestinal carcinomas with microsatellite instability. Cancer Res 2001;61:36–8.
16. Bras-Goncalves RA, Rosty C, Laurent-Puig P, Soulie P, Dutrillaux B, Poupon MF. Sensitivity to CPT-11 of xenografted human colorectal cancers as a function of microsatellite instability and p53 status. Br J Cancer 2000;82:913–23.
17. Jacob S, Aguado M, Fallik D, Praz F. The role of the DNA mismatch repair system in the cytotoxicity of the topoisomerase inhibitors camptothecin and etoposide to human colorectal cancer cells. Cancer Res 2001;61:6555–62.
18. Magrini R, Bhonde MR, Hanski ML, Notter M, Scherubl H, Boland CR, et al. Cellular effects of CPT-11 on colon carcinoma cells: dependence on p53 and hMLH1 status. Int J Cancer 2002;101:23–31.
19. Fallik D, Borrini F, Boige V, Viguier J, Jacob S, Miquel C, et al. Microsatellite instability is a predictive factor of the tumor response to irinotecan in patients with advanced colorectal cancer. Cancer Res 2003;63:5738–44.
20. Pommier Y, Redon C, Rao VA, Seiler JA, Sordet O, Takemura H, et al. Repair of and checkpoint response to topoisomerase I-mediated DNA damage. Mutat Res 2003;532:173–203.
21. Shimada Y, Yoshino M, Wakui A, Nakao I, Futatsuki K, Sakata Y, et al. Phase II study of CPT-11, a new camptothecin derivative, in metastatic colorectal cancer. CPT-11 Gastrointestinal Cancer Study Group. J Clin Oncol 1993;11:909–13.
22. Kaneda N, Nagata H, Furuta T, Yokokura T. Metabolism and pharmacokinetics of the camptothecin analogue CPT-11 in the mouse. Cancer Res 1990;50:1715–20.
23. Satoh T, Hosokawa M, Atsumi R, Suzuki W, Hakusui H, Nagai E. Metabolic activation of CPT-11, 7-ethyl-10-[4-(1-piperidino)-1- piperidino]carbonyloxycamptothecin, a novel antitumor agent, by carboxylesterase. Biol Pharm Bull 1994;17:662–4.
24. Bowman KJ, Newell DR, Calvert AH, Curtin NJ. Differential effects of the poly (ADP-ribose) polymerase (PARP) inhibitor NU1025 on topoisomerase I and II inhibitor cytotoxicity in L1210 cells in vitro. Br J Cancer 2001;84:106–12.
25. Miknyoczki S, Chang H, Grobelny J, Pritchard S, Worrell C, McGann N, et al. The selective poly(ADP-ribose) polymerase-1(2) inhibitor, CEP-8983, increases the sensitivity of chemoresistant tumor cells to temozolomide and irinotecan but does not potentiate myelotoxicity. Mol Cancer Ther 2007;6:2290–302.
26. Miknyoczki SJ, Jones-Bolin S, Pritchard S, Hunter K, Zhao H, Wan W, et al. Chemopotentiation of temozolomide, irinotecan, and cisplatin activity by CEP-6800, a poly(ADP-ribose) polymerase inhibitor. Mol Cancer Ther 2003;2:371–82.
27. Calabrese CR, Almassy R, Barton S, Batey MA, Calvert AH, Canan-Koch S, et al. Anticancer chemosensitization and radiosensitization by the novel poly(ADP-ribose) polymerase-1 inhibitor AG14361. J Natl Cancer Inst 2004;96:56–67.
28. Smith LM, Willmore E, Austin CA, Curtin NJ. The novel poly(ADP-Ribose) polymerase inhibitor, AG14361, sensitizes cells to topoisomerase I poisons by increasing the persistence of DNA strand breaks. Clin Cancer Res 2005;11:8449–57.
29. Tentori L, Leonetti C, Scarsella M, Muzi A, Mazzon E, Vergati M, et al. Inhibition of poly(ADP-ribose) polymerase prevents irinotecan-induced intestinal damage and enhances irinotecan/temozolomide efficacy against colon carcinoma. FASEB J 2006;20:1709–11.
30. Miura K, Sakata K, Someya M, Matsumoto Y, Matsumoto H, Takahashi A, et al. The combination of olaparib and camptothecin for effective radiosensitization. Radiat Oncol 2012;7:62.
31. Deng G, Chen A, Hong J, Chae HS, Kim YS. Methylation of CpG in a small region of the hMLH1 promoter invariably correlates with the absence of gene expression. Cancer Res 1999;59:2029–33.
32. Tahara M, Inoue T, Miyakura Y, Horie H, Yasuda Y, Fujii H, et al. Cell diameter measurements obtained with a handheld cell counter could be used as a surrogate marker of G2/M arrest and apoptosis in colon cancer cell lines exposed to SN-38. Biochem Biophys Res Commun 2013;434:753–9.
33. Rottenberg S, Jaspers JE, Kersbergen A, van der Burg E, Nygren AO, Zander SA, et al. High sensitivity of BRCA1-deficient mammary tumors to the PARP inhibitor AZD2281 alone and in combination with platinum drugs. Proc Natl Acad Sci U S A 2008;105:17079–84.
34. Vilar E, Scaltriti M, Balmana J, Saura C, Guzman M, Arribas J, et al. Microsatellite instability due to hMLH1 deficiency is associated with increased cytotoxicity to irinotecan in human colorectal cancer cell lines. Br J Cancer 2008;99:1607–12.
35. Wu J, Yin MB, Hapke G, Toth K, Rustum YM. Induction of biphasic DNA double strand breaks and activation of multiple repair protein complexes by DNA topoisomerase I drug 7-ethyl-10-hydroxy-camptothecin. Mol Pharmacol 2002;61:742–8.
36. Valerie K, Povirk LF. Regulation and mechanisms of mammalian double-strand break repair. Oncogene 2003;22:5792–812.
37. Li X, Heyer WD. Homologous recombination in DNA repair and DNA damage tolerance. Cell Res 2008;18:99–113.
38. San Filippo J, Sung P, Klein H. Mechanism of eukaryotic homologous recombination. Annu Rev Biochem 2008;77:229–57.
39. Jacob S, Miquel C, Sarasin A, Praz F. Effects of camptothecin on double-strand break repair by non-homologous end-joining in DNA mismatch repair-deficient human colorectal cancer cell lines. Nucleic Acids Res 2005;33:106–13.
40. Kanaar R, Hoeijmakers JH, van Gent DC. Molecular mechanisms of DNA double strand break repair. Trends Cell Biol 1998;8:483–9.
41. Haber JE. The many interfaces of Mre11. Cell 1998;95:583–6.
42. Khanna KK, Jackson SP. DNA double-strand breaks: signaling, repair and the cancer connection. Nat Genet 2001;27:247–54.
43. Lee AC, Fernandez-Capetillo O, Pisupati V, Jackson SP, Nussenzweig A. Specific association of mouse MDC1/NFBD1 with NBS1 at sites of DNA-damage. Cell Cycle 2005;4:177–82.
44. Lee JH, Paull TT. Direct activation of the ATM protein kinase by the Mre11/Rad50/Nbs1 complex. Science 2004;304:93–6.
45. Takemura H, Rao VA, Sordet O, Furuta T, Miao ZH, Meng L, et al. Defective Mre11-dependent activation of Chk2 by ataxia telangiectasia mutated in colorectal carcinoma cells in response to replication-dependent DNA double strand breaks. J Biol Chem 2006;281:30814–23.
46. Choi SH, Tsuchida Y, Yang HW. Oral versus intraperitoneal administration of irinotecan in the treatment of human neuroblastoma in nude mice. Cancer Lett 1998;124:15–21.

Published OnlineFirst August 11, 2009; DOI: 10.1158/1535-7163.MCT-09-0243

XP-002772687

Drug ratio–dependent antitumor activity of irinotecan and cisplatin combinations *in vitro* and *in vivo*

Paul G. Tardi, Nancy Dos Santos, Troy O. Harasym, Sharon A. Johnstone, Natalia Zisman, Alan W. Tsang, David G. Bermudes, and Lawrence D. Mayer

Celator Pharmaceuticals Corp., Vancouver, British Columbia, Canada

Abstract

Irinotecan and cisplatin are two established anticancer drugs, which together constitute an effective combination for treating small-cell lung cancer. We investigated whether the efficacy of this combination could be improved by controlling drug ratios following *in vivo* administration. Irinotecan and cisplatin combinations were evaluated systematically for drug ratio–dependent synergy *in vitro* using a panel of 20 tumor cell lines. *In vitro* screening informatics on drug ratio–dependent cytotoxicity identified a consistently antagonistic region between irinotecan/cisplatin molar ratios of 1:2 to 4:1, which was bordered by two synergistic regions. Liposomal co-formulations of these two agents were developed that exhibited plasma drug half-lives of 6 hours and maintained a fixed drug ratio for more than 24 hours. Drug ratio–dependent antitumor activity was shown *in vivo* for these liposome formulations, and irinotecan/cisplatin ratios between 5:1 and 10:1 were identified as therapeutically optimal. The relationship between irinotecan/cisplatin ratio and *in vivo* efficacy was consistent with *in vitro* drug ratio dependency results. Superior antitumor activity was observed for the liposome-encapsulated 7:1 molar ratio of irinotecan/cisplatin (designated CPX-571) compared with the free-drug cocktail in all models tested. Further efficacy studies in a range of human tumor xenografts, including an irinotecan-resistant model, showed that both liposomal agents contributed to the overall efficacy in a manner consistent with *in vivo* synergy. These results show the ability of drug delivery technology to enhance the therapeutic activity of irinotecan/cisplatin combination treatment by maintaining synergistic ratios *in vivo*. CPX-571, a fixed-ratio formulation of irinotecan and cisplatin, is a promising candidate for clinical development. [Mol Cancer Ther 2009;8(8):2266–75]

Introduction

Small-cell lung cancer (SCLC) is characterized by rapid disease progression, low cure rates, and a high incidence of mortality. There are an estimated 32,000 new cases per year in the United States, representing 15% of all lung cancers (1). Patients receive multimodality treatment including a chemotherapy regimen of etoposide/cisplatin (EP) and chest radiation therapy, which has remained the standard of care for 25 years (2). SCLC is initially responsive to both chemotherapy and radiotherapy; however, the vast majority of patients relapse. Although the current standard of care represents the most effective drug therapy for patients, novel treatments are warranted to improve survival rates.

Irinotecan has emerged as a promising drug candidate in the treatment of SCLC. Phase II clinical evaluation of irinotecan in SCLC patients showed a 50% objective response rate in chemotherapy-naïve patients and a 47% objective response rate in patients previously treated with cisplatin (3). These values are higher than the 35% response rate observed for patients receiving etoposide monotherapy (4). Based on these studies, it was anticipated that a combination of irinotecan and cisplatin may be superior to etoposide/cisplatin chemotherapy, the standard of care for extensive-stage SCLC.

The combination of irinotecan and cisplatin has shown synergy or supra-additive effects when exposed to cultured human tumor cells (5, 6), human xenograft tumor models (5, 7), and cancer cells freshly isolated from colorectal patients (8). This information provided the scientific rationale for testing this combination in a clinical setting. A phase III study by the Japan Clinical Oncology Group in 2002 showed that the irinotecan and cisplatin chemotherapy regimen (IP) in SCLC patients was significantly more efficacious than the etoposide and cisplatin chemotherapy regimen (EP), leading to the adoption of IP as standard of care in Japan and other Asian countries (9). In 2006, a North American follow-up study compared IP and EP protocols and showed that IP was equally effective and potentially less toxic (10). A recent phase III trial by the Southwest Oncology Group was designed to confirm the Japanese results by using the same dose and schedule; however, this trial concluded that IP had the same response rate, progression-free survival, and overall survival profiles as EP (11). The lack of survival benefit with the irinotecan/cisplatin combination is somewhat surprising considering

Received 3/16/09; revised 5/21/09; accepted 6/2/09; published OnlineFirst 8/11/09.

The costs of publication of this article were defrayed in part by the payment of page charges. This article must therefore be hereby marked *advertisement* in accordance with 18 U.S.C. Section 1734 solely to indicate this fact.

Note: Supplementary material for this article is available at Molecular Cancer Therapeutics Online (http://mct.aacrjournals.org/).

Requests for reprints: Paul G. Tardi, Celator Pharmaceuticals Corp., 1779 West 75th Avenue, Vancouver, British Columbia, Canada V6P 6P2. Phone: 604-675-2105; Fax: 604-708-5883. E-mail: ptardi@celatorpharma.com

doi:10.1158/1535-7163.MCT-09-0243

Published OnlineFirst August 11, 2009; DOI: 10.1158/1535-7163.MCT-09-0243

the superiority of irinotecan over etoposide as a monotherapy in SCLC patients.

We hypothesized that the failure to show a therapeutic benefit with irinotecan/cisplatin over the etoposide/cisplatin combination may be attributed, in part, to the occurrence of drug ratio dependency in one or both combinations. Recent studies by our laboratory and others have shown that the therapeutic activity of drug combinations is often drug ratio dependent, where synergistic or antagonistic interactions occur when tumors are exposed to different drug/drug ratios (12–15). Thus, the full benefit of combination chemotherapy may not be realized *in vivo* unless the ratios of the drugs are carefully controlled and maintained to avoid exposure of tumor cells to antagonistic drug ratios. In the studies presented here, we evaluated the combination of irinotecan/cisplatin for drug ratio–dependent synergy *in vitro* and used liposome nanotechnology to maintain drug ratios *in vivo* and deliver synergistic ratios to tumor sites (13, 16). The efficacy of this dual-drug liposome formulation was compared with the free-drug cocktail as well as individual liposome-encapsulated drugs in a variety of human xenograft tumor models.

Materials and Methods

Reagents

Phospholipids were purchased from Lipoid LLC. [^{3}H] Cholesteryl hexadecyl ether was purchased from Perkin-Elmer Life Sciences. Lyophilized cisplatin was purchased from Polymed, and irinotecan hydrochloride trihydrate was obtained from ScinoPharm. 3-(4,5-Dimethylthiazol-2-yl)-2,5-diphenyltetrazolium bromide (MTT) and all other chemicals were obtained from Sigma Chemical Company.

Cell Culture

All tumor cell lines used in the study were purchased from American Type Culture Collection. An irinotecan-resistant HCT-116 human colon carcinoma line with 10-fold resistance compared with the parental strain was obtained by exposing cells to 1.0 μmol/L irinotecan, followed by clonal selection and confirmation of resistance by IC_{50} analysis as described below. Cells were propagated in their recommended tissue culture media supplemented with 10% FCS and 2 mmol/L L-glutamine at 37°C in a humidified atmosphere with 5% CO_2.

Cell Proliferation Assays

The sensitivity of a panel of tumor cells to individual drugs and the drug combination was determined using a cytotoxicity assay previously described (13, 14). Briefly, cells were plated in triplicate in 96-well, flat-bottomed microplates and incubated for 24 h in medium, followed by addition of the test agents. Following a 72-h incubation, the relative effect on the presence of viable cells was determined by MTT assay (17). Due to the wide range of ratios analyzed and differences in IC_{50} values, the data sets were truncated at the two ends of the sigmoidal curve where the MTT assay is unresponsive at low drug concentrations and again at high cytotoxicity where there is a low MTT signal. Synergy of the two drugs over a range of drug ratios and concentrations was analyzed by the median-effect algorithm (18, 19). The occurrence of ratio-dependent synergy was determined by plotting the combination index (CI < 1, synergy; CI ~ 1, additivity; and CI > 1, antagonism) versus the fraction of cells affected (Fa), which indirectly reflects the drug concentration.

Liposome Preparation

The required amount of 1,2-distearoyl-*sn*-glycero-3-phosphatidylcholine/1,2-dipalmitoyl-*sn*-glycero-3-phosphatidylcholine/1,2-distearoyl-*sn*-glycero-3-phosphatidylglycerol/cholesterol (35:35:20:10 molar ratio) was dissolved in dichloromethane/methanol/water (93:5:2, v/v/v). Radiolabeled liposomes were prepared by adding [^{3}H]cholesteryl hexadecyl ether, a nonexchangeable, nonmetabolizable liposome tracer. Liposome preparation details are described in Supplementary Data. For cisplatin encapsulation, the drug was dissolved at a concentration of 7.5 mg/mL in 150 mmol/L NaCl and mixed with the liposome solution for 1 h at 60°C in the presence of ethanol to enhance drug uptake. Subsequently, the cisplatin liposomes were buffer exchanged against 150 mmol/L NaCl to remove ethanol and unencapsulated drug. For irinotecan encapsulation, liposomes and irinotecan were mixed at a 0.22:1 drug-to-lipid molar ratio at 41°C for 1 h. The liposomes were subsequently buffer exchanged against 300 mmol/L sucrose, 20 mmol/L phosphate (pH 7). To generate CPX-571, liposomal cisplatin and liposomal irinotecan formulations were mixed together at a 7:1 molar drug ratio and stored at −20°C. Following storage, the drug encapsulation was ~98%. Liposome pharmacokinetics and tumor accumulation data are included in Supplementary Data.

Experimental Tumor Models

Female CD-1 nude (Charles River) and *Foxn1* nude mice (Harlan) were used in these studies. All procedures involving experimental mice were conducted according to the guidelines of the Canadian Council of Animal Care. Maximum tolerated dose (MTD) values were defined as survival in the absence of significant tumor burden with ≤15% body weight loss nadir lasting ≤2 d. Animals were terminated (CO_2 asphyxiation) when signs of toxicity or tumor-related illness were observed. Tumor cells, consisting of human SCLC cell line H69 (1×10^7 in 50% growth factor–reduced Matrigel; BD Bioscience), human non–small cell lung cancer (NSCLC) H460 (2×10^6), human NSCLC H1299 (2×10^6), human colon carcinoma HT29 (2×10^6), or human pancreatic carcinoma Capan-1 (2×10^6), were implanted s.c. in the right flank of mice. Tumor volumes were measured using calipers, and the values calculated according to the equation $L \times W^2/2$.

Statistical Analysis

A standard one-way ANOVA was used to determine statistically significant differences from the mean. Survival curves were computed using the Kaplan-Meier method. Treatment groups were analyzed by Microsoft Excel statistics software and compared using a two-sample log-rank test. $P < 0.05$ was considered significant for all statistical tests.

Published OnlineFirst August 11, 2009; DOI: 10.1158/1535-7163.MCT-09-0243

Results

In vitro Examination of Irinotecan/Cisplatin Combinations for Drug Ratio–Dependent Synergy

High-throughput screening using MTT cytotoxicity assays was done for multiple fixed-ratio combinations of irinotecan and cisplatin diluted over a range of concentrations within the complete cell viability dose-response curve for 20 tumor cell lines. We chose to focus our *in vitro* evaluations on irinotecan, rather than its potent metabolite 7-ethyl-10-hydroxy-camptothecin (SN-38), because this reflects the situation experienced for liposomal delivery of irinotecan *in vivo* where extravasation and accumulation of liposomes in tumors provide a local infusion reservoir of irinotecan. In addition, in contrast to irinotecan, SN-38 is extremely membrane permeable and was not amenable to stable retention in liposomal delivery systems after injection.

Median-effect analysis of dose-response curves was used to calculate the combination index (CI) for each tested irinotecan/cisplatin ratio at a 0.8 fraction of affected cells (80% cell growth inhibition) to determine whether synergy depended on the drug ratio (18, 19). This mathematical algorithm generates CI values <0.9 when drug-drug interactions are synergistic, 0.9–1.1 when additive, and >1.1 when antagonistic. The results are presented as a synergy "heat map" (Table 1) where CI values reflecting synergy, additivity, and antagonism are color coded as green, yellow, and red, respectively. The results identify two distinct regions of synergy separated by a zone of antagonism between irinotecan/cisplatin molar ratios of 1:2 and 4:1. This transition between synergy and antagonism was striking given that an irinotecan/cisplatin molar ratio of 2:1 produced antagonism in 12 of 20 cell lines (maximum CI value of 2.57), whereas increasing the ratio to 8:1 resulted in synergy in 17 of 20 cell lines (minimum CI value of 0.18; see Table 1) and no antagonism. Synergy also predominated at irinotecan/cisplatin molar ratios <1:2. For example, 13 of 20 cell lines exhibited synergy at a drug ratio of 1:4 and antagonism was observed in only 4 of 20 tumor lines. It should be noted that similar relationships were obtained for other therapeutically relevant fraction of affected cell levels (e.g., Fa = 0.5).

Irinotecan and Cisplatin Liposome Formulations That Maintain Drug Ratios *In vivo*

We next investigated whether the drug ratio–dependent synergy observed *in vitro* could be manifested *in vivo* by delivering irinotecan/cisplatin as a fixed-ratio formulation using nanoscale liposomal delivery vehicles. Irinotecan and cisplatin were formulated into individual liposomes with identical membrane compositions to alleviate drug instability when the two agents were co-encapsulated. By combining individual liposomal agents, the internal buffer composition was tailored for each individual drug, thereby increasing drug stability and providing additional flexibility in coordinating drug release kinetics. In a recent study

Table 1. ***In vitro*** **synergy heat map of irinotecan/cisplatin ratios for a panel of 20 human tumor cell lines for CI values at Fa = 0.8**

Cell lines screened	Tumor	CI at Fa = 0.8											
		1:64	1:32	1:16	1:8	1:4	1:2	1:1	2:1	4:1	8:1	16:1	32:1	64:1
LCC6	Breast	0.69	0.58	0.71	0.89	0.83	1.01	1.57	1.03	0.85	0.63	0.52	0.54	0.76
MCF-7	Breast	0.71	0.67	0.86	0.88	0.95	1.05	0.71	0.82	0.70	1.00	0.87	0.83	0.88
MB 231	Breast	1.02	1.01	0.90	0.90	0.70	0.87	1.54	1.34	0.90	1.10	0.76	1.40	0.61
HCT-116	Colon	0.38	0.36	0.37	0.33	0.62	0.84	1.50	1.73	2.40	0.71	0.76	0.82	1.06
Colon-26	Colon	1.22	1.67	1.40	1.16	1.00	1.21	1.04	1.38	1.10	1.03	1.31	1.25	0.82
HT-29	Colon	1.05	0.88	0.90	0.86	1.21	1.09	1.57	1.17	0.90	0.76	0.82	0.97	1.05
A549	Lung	0.67	0.61	0.67	0.56	0.44	0.39	0.44	1.65	1.31	0.49	0.37	0.41	0.49
H460	Lung	0.92	0.81	0.84	0.80	0.75	0.73	0.94	1.14	2.03	0.53	0.36	0.80	0.48
H322	Lung	0.47	0.52	0.68	0.96	0.57	1.28	1.29	0.95	0.73	0.54	0.44	0.52	0.54
H1299	Lung	1.07	1.08	1.02	1.09	0.76	0.98	3.01	2.57	1.88	0.65	0.64	1.49	0.82
H522	Lung	1.05	0.62	1.09	0.84	0.82	0.92	2.26	1.80	0.89	0.48	0.39	0.73	0.47
Ovcar-3	Ovarian	1.83	1.85	1.08	1.10	0.80	0.78	0.89	0.89	1.84	0.58	0.28	0.38	0.35
Ovcar-5	Ovarian	1.29	1.64	1.55	1.34	1.30	1.42	1.51	1.30	1.08	0.80	1.05	0.99	1.07
SK-OV-3	Ovarian	1.38	1.26	1.30	1.51	1.45	1.70	1.75	1.28	1.17	0.55	0.70	0.79	0.76
IGROV-1	Ovarian	1.16	1.16	1.16	1.00	0.95	0.95	1.23	1.20	1.16	0.77	0.78	0.71	0.75
A2780	Ovarian	0.93	0.94	0.81	0.75	0.80	0.81	0.87	0.70	0.81	0.81	1.20	1.03	1.25
Capan-1	Pancreatic	1.46	1.22	1.10	1.25	0.86	0.89	1.12	1.17	0.69	0.89	0.83	0.71	0.99
BXPC-3	Pancreatic	1.00	1.02	0.91	1.10	0.81	0.99	1.04	0.88	0.70	0.60	0.49	0.64	0.61
N87	Gastric	1.76	1.87	1.85	1.55	1.65	1.09	1.05	0.68	0.51	0.18	0.11	0.06	0.04
A253	H&N	0.85	0.84	0.81	0.92	0.76	0.63	0.79	0.78	0.86	0.83	0.90	0.82	0.84

NOTE: Irinotecan and cisplatin were simultaneously exposed to cells for 72 h at indicated molar ratios, and the dose-response curve for each cell line was determined by an MTT cytotoxicity assay. The dose-response curves were subsequently evaluated by the Chou and Talalay median-effect method to calculate the CI at ED_{80} (Fa = 0.8) and summarized in a heat map. Two areas of synergy are observed at <1:2 and >4:1 irinotecan/cisplatin ratios. Green indicates synergy (CI < 1); yellow indicates additivity (CI ~ 1); and red indicates antagonism (CI > 1). Results reflect compiled results from multiple experiments.
Abbreviation: H&N, head and neck.

Published OnlineFirst August 11, 2009; DOI: 10.1158/1535-7163.MCT-09-0243

Table 2. Tumor growth delay and LCK values for mice given synergistic (7:1) and antagonistic (3:1) irinotecan/cisplatin ratios in an H460 NSCLC xenograft model

Treatment	Irino/Cis ratio	Dose (mg/kg; Irino/Cis)	TGD	%TGD	LCK*
CPX-5	7:1	40/2.5	23.3	131	2.06
Lipo-irinotecan		40	13.8	78	1.22
Lipo-cisplatin		2.5	2.8	16	0.24
Predicted additive value†	7:1		16.6		1.46
CPX-5	3:1	20/3	13.5	76	1.20
Lipo-irinotecan		20	6	34	0.53
Lipo-cisplatin		3	7.3	41	0.64
Predicted additive value†	3:1		13.3		1.17

Abbreviations: TGD, tumor growth delay; Cis, cisplatin; Irino, irinotecan.
*LCK = $[T - C] / (3.32 \times T_d)$, where $T - C$ is the treatment-induced delay for tumors to reach 400 mg and T_d is the tumor doubling time of the control group.
†Value determined from adding the sum of TGD or LCK values for individual liposomal drugs.

examining the effect of bilayer composition on the *in vivo* activity of liposomal cisplatin, we identified the formulation of 1,2-distearoyl-*sn*-glycero-3-phosphatidylcholine/1,2-dipalmitoyl-*sn*-glycero-3-phosphatidylcholine/1,2-distearoyl-*sn*-glycero-3-phosphatidylglycerol/cholesterol (35:35:20:10, mole ratio) to be the most efficacious (20). As a result, formulation efforts focused on this membrane composition to coordinate the release rates of irinotecan and cisplatin while maintaining the therapeutic activity of the cisplatin. Coordinated pharmacokinetics were achieved for a range of different irinotecan/cisplatin ratios *in vivo* (Supplementary Fig. S1).

Drug Ratio–Dependent Activity of Liposomal Irinotecan:Cisplatin Formulations *In vivo*

In vitro screening studies of irinotecan/cisplatin drug ratios in a panel of 20 tumor cell lines discerned two areas of synergy: <1:2 and >4:1 irinotecan/cisplatin molar ratios. Identifying which of these irinotecan/cisplatin molar ratios would yield the most efficacious combination for preclinical studies was pertinent. In addition, we wanted to examine drug ratio–dependent efficacy *in vivo* by comparing synergistic and antagonistic irinotecan/cisplatin ratios encapsulated in liposomes. One of the challenges in comparing the molar ratios of liposome-encapsulated irinotecan/cisplatin *in vivo* was the low MTD of liposomal cisplatin (~3 mg/kg). Because of this, high irinotecan/cisplatin molar ratio combinations could bias efficacy results to favor the synergistic ratio based on dose intensity rather than drug ratio–dependent synergy. Therefore, we selected irinotecan/cisplatin molar ratios of 1:5 and 2:1 for drug ratio–dependent efficacy comparisons, which represented ratios found *in vitro* to be synergistic and antagonistic, respectively. For the efficacy comparison of these two formulations, the cisplatin dose could be maintained at 3.3 mg/kg while the irinotecan dose differed 10-fold between the 1:5 (1.5 mg/kg) and 2:1 (15 mg/kg) irinotecan/cisplatin molar ratios. Consequently, an increase in efficacy for the synergistic 1:5 ratio formulation over the 2:1 ratio would clearly reflect drug ratio–dependent efficacy given that increased antitumor activity would be associated with a reduced drug dose.

We examined the therapeutic activity of fixed molar ratios of 1:5 and 2:1 in the H1299 NSCLC model (Supplementary Fig. S2). This model was chosen based on the strong antagonism obtained at the 2:1 irinotecan/cisplatin ratio for this cell line *in vitro* (CI, 2.57) as well as the large absolute difference in CI value observed for these two drug ratios (see Table 1). We compared the degree of antitumor activity for the different treatment groups based on the treatment-induced delay for tumors to reach a size of 400 mg. We correlated the degree of tumor growth delay to a more quantifiable measure of antitumor activity using the established relationship (21) of:

$$\log_{10} \text{cell kill} = (T-C)/(3.32 \times T_d)$$

where: (T–C) = tumor growth delay

T_d = tumor doubling time

The liposome-encapsulated irinotecan:cisplatin formulation containing the drugs at a 1:5 molar ratio, identified as synergistic *in vitro*, exhibited a tumor growth delay of 26 days and a corresponding log cell kill (LCK) of 1.11 (Supplementary Fig. S2). Increasing the irinotecan dose 10-fold to 15 mg/kg while maintaining the cisplatin dose at 3.3 mg/kg (reflecting a 2:1 irinotecan/cisplatin molar ratio, identified as antagonistic *in vitro*) resulted in a reduced tumor growth delay of 16 days and a LCK of only 0.68. Liposomal cisplatin administered alone provided a tumor growth delay of 10.5 days and LCK of 0.44. Consequently, the addition of 1.5 mg/kg liposomal irinotecan at the synergistic 1:5 ratio increased the LCK by 0.67, whereas the addition of 15 mg/kg liposomal irinotecan at the antagonistic 2:1 ratio increased the LCK by only 0.24. Strikingly, the 1:5 molar ratio formulation of irinotecan/cisplatin provided comparable therapeutic activity to liposomal irinotecan administered at a 27-fold higher dose of 40 mg/kg, for which a LCK of 1.2 was observed (data not shown). These results highlight the *in vivo* importance of drug ratios and indicate that higher irinotecan doses may not necessarily result in higher therapeutic activity if antagonistic drug ratios ensue.

Published OnlineFirst August 11, 2009; DOI: 10.1158/1535-7163.MCT-09-0243

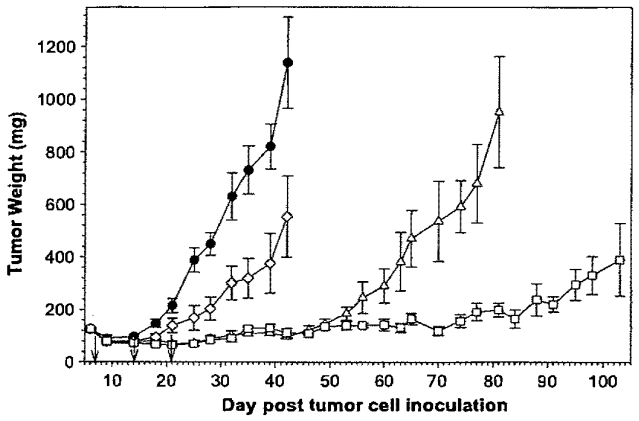

Figure 1. Antitumor efficacy of individual and combined irinotecan/cisplatin liposomal drugs. Tumor growth delay was assessed in the H69 SCLC human tumor xenograft model using a q7d×3 dosing schedule. Mice received injections of saline (●), liposomal cisplatin at 2.5 mg/kg (◊), liposomal irinotecan at 39 mg/kg (△), or liposomal irinotecan/cisplatin (7:1 molar ratio) at 39:2.5 mg/kg (□). *Downward arrows,* injection days.

To assess the *in vivo* drug ratio dependency at high irinotecan/cisplatin molar ratios, we conducted two efficacy comparisons using the H460 human NSCLC xenograft tumor model. *In vitro,* this tumor cell line displayed a very sharp transition from antagonism at an irinotecan/cisplatin molar ratio of 4:1 (CI, 2.03) to synergy at a molar drug ratio of 8:1 (CI, 0.53) and higher (Table 1). Assessing the degree of synergy or antagonism for these two formulations required the comparison of the liposomal combination with matched doses of the individual liposome-encapsulated agents rather than comparisons between the two fixed-ratio formulations. This is due to the fact that increasing irinotecan/cisplatin ratios in this range also increased total drug doses because the cisplatin component predominated toxicity effects, and thus increased efficacy at higher irinotecan/cisplatin ratios could not be attributed solely to drug ratio–dependent synergy.

We evaluated the efficacy of fixed-ratio liposome formulations of irinotecan/cisplatin encapsulated below (3:1 molar ratio) and above (7:1 molar ratio) the *in vitro* transition point between antagonism and synergy. As shown in Table 2, administering liposome-encapsulated irinotecan/cisplatin with a 7:1 molar ratio at its MTD of 40:2.5 mg/kg yielded a LCK of 2.06. The LCK values of the individual liposomal drugs at matched doses were 1.22 for irinotecan and 0.24 for cisplatin, which would predict a LCK of 1.46 for the liposome-encapsulated combination if the two drugs combined in an additive fashion. The observed LCK of 2.06 for the 7:1 molar ratio formulation is ~4-fold greater antitumor activity than predicted for additivity based on the

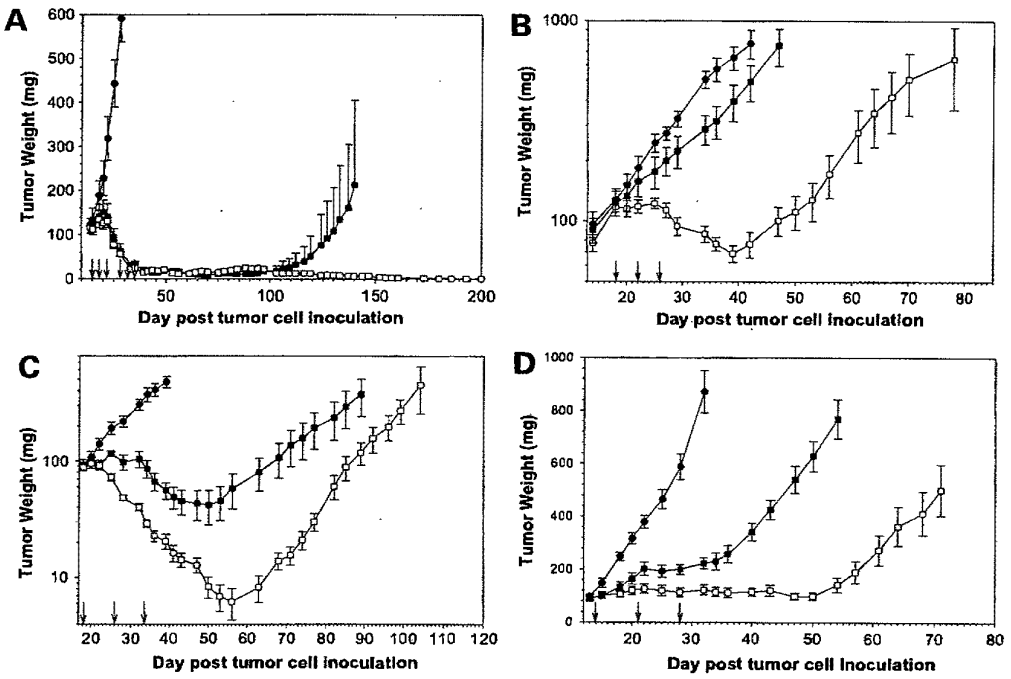

Figure 2. Antitumor efficacy of CPX-571 compared with free-drug cocktail in SCLC, colon, and pancreatic human xenograft models. **A,** H69 human SCLC xenograft growth curves using a (q4d×3)×2 dosing schedule. Mice received injections of saline (●), free-drug cocktail (7:1 molar ratio) at 34:2.1 mg/kg (■), or liposomal irinotecan/cisplatin (7:1 molar ratio) at 34:2.1 mg/kg (□). **B,** HT29 human colon xenograft growth curves using a q4d×3 dosing schedule. Mice received injections of saline (●), free-drug cocktail of irinotecan/cisplatin (7:1 molar ratio) at 47:3 mg/kg (■), or liposomal irinotecan/cisplatin (7:1 molar ratio) at 47:3 mg/kg (□). **C** and **D,** Capan-1 human pancreatic xenograft growth curves (**C**) and HCT-116 human colon xenograft growth curves (**D**) both used a q7d×3 dosing schedule. For both, mice received injections of saline (●), free-drug cocktail of irinotecan/cisplatin at 47:3 mg/kg (■), or liposomal irinotecan/cisplatin at 47:3 mg/kg (□). *Downward arrows,* injection days.

Published OnlineFirst August 11, 2009; DOI: 10.1158/1535-7163.MCT-09-0243

individual liposomal drugs, consistent with *in vivo* synergy. In contrast, when irinotecan and cisplatin were formulated in liposomes at a 3:1 molar ratio and administered at MTD to tumor-bearing mice, the degree of antitumor activity was consistent with additivity, where the observed LCK value for the combination of 1.20 was comparable to the predicted LCK value of 1.17 based on the additive activities of the dose-matched individual liposomal agents (Table 2).

Further studies investigated the therapeutic activity of synergistic irinotecan/cisplatin molar ratios of 5:1, 7:1, and 10:1 in the H460 NSCLC tumor xenograft model to determine which ratio may provide optimal therapeutic activity when administered at MTD. Although synergistic activity may be obtained for all three irinotecan/cisplatin ratios, absolute drug doses of the two agents vary when the fixed-ratio liposomal formulations are administered at their MTDs (47:2.1, 40:2.5, and 34:3.0 mg/kg for liposome formulations containing irinotecan/cisplatin molar ratios of 10:1, 7:1, and 5:1, respectively). Over this range of irinotecan/cisplatin ratios delivered in liposomes, equivalent LCK values of 2.00, 1.93, and 2.05, respectively, were obtained (data not shown).

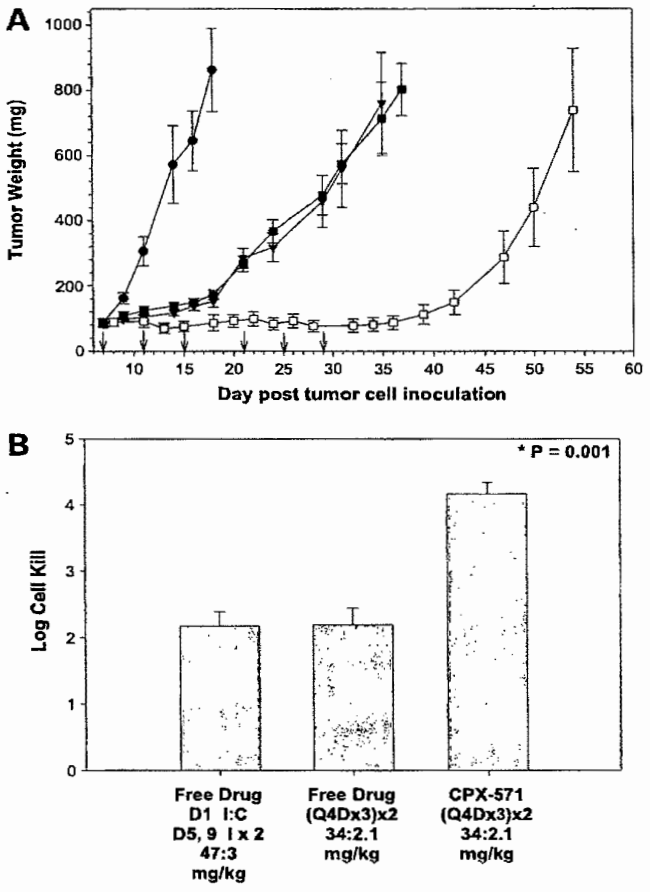

Figure 3. Antitumor efficacy of CPX-571 compared with optimized free-drug cocktail schedules. Two free-drug dosing schedules were compared directly with CPX-571 on a (q4d×3)×2 schedule in the human H460 NSCLC xenograft model. **A**, mice received injections of saline (●); two courses of free-drug cocktail containing irinotecan and cisplatin at a 7:1 molar ratio (47:3 mg/kg dose; *I:C*) on day 1 and 47 mg/kg irinotecan only (*I*) on days 5 and 9 (▼); free-drug cocktail of irinotecan and cisplatin at a 7:1 molar ratio (34:2.1 mg/kg) dosed on a (q4d×3)×2 schedule (■); or CPX-571 dosed at 34:2.1 mg/kg on a (q4d×3)×2 schedule (□). *Downward arrows*, injection days. **B**, LCK achieved by the different free-drug and liposomal irinotecan/cisplatin combinations. *, *P* value of CPX-571 compared with both of the free-drug cocktail dosing schedules.

Expanded Efficacy Evaluations of Irinotecan/Cisplatin Formulated at a 7:1 Molar Ratio

The liposomal formulation of irinotecan/cisplatin at a 7:1 molar ratio (hereafter referred to as CPX-571) was selected for further efficacy testing based on the fact that it delivered intermediate doses of both agents and may provide more consistent activity against tumor types that exhibit a range of sensitivities to irinotecan and/or cisplatin. Based on the established clinical activity of irinotecan/cisplatin combination therapy in SCLC, we evaluated the efficacy of CPX-571 in the H69 SCLC human solid tumor xenograft model (Fig. 1). We compared the efficacy of CPX-571 to that of the individual liposome-encapsulated drugs to elucidate the contribution of each agent to the overall therapeutic effect. Treatment with liposomal cisplatin at a dose of 2.5 mg/kg resulted in a modest tumor growth delay of 15 days (LCK, 0.72) relative to the saline control group, whereas liposomal irinotecan at a dose of 39 mg/kg resulted in a tumor growth delay value of 39 days (LCK, 1.95). Treatment with a dose-matched CPX-571 resulted in a significantly higher tumor growth delay of 76 days (LCK, 4.58). Not only did both liposome-encapsulated agents contribute significantly to the overall therapeutic effect but also the degree of antitumor activity observed reflected nearly 100 fold greater tumor growth inhibition than predicted for additivity based on the LCK values of the individual liposomal drugs (e.g., LCK values of 0.72 + 1.95 predict LCK value of 2.67 for additivity), consistent with strong *in vivo* synergy.

We expanded the efficacy evaluation of CPX-571 to compare its activity to that of the free-drug cocktail in several additional tumor xenograft models. In the case of the free-drug cocktail, the molar ratio of irinotecan/cisplatin reflecting both agents pushed to their respective MTDs was 7:1, equivalent to the optimal ratio when delivered in liposomes. In addition, the MTD of the free-drug cocktail was equivalent to that exhibited by CPX-571 when examined across a panel of tumor models (irinotecan/cisplatin doses ranging from 34:2.1 to 47:3 mg/kg, depending on the tumor model; see Fig. 2). These two features simplified direct efficacy comparisons between CPX-571 and free irinotecan/cisplatin cocktail groups because multiple comparisons based on matched ratios versus MTDs or relative potencies were not necessary.

In H69 human SCLC tumor xenograft studies, administration of CPX-571 on a (q4d×3)×2 schedule significantly enhanced survival of treated mice, resulting in 100% long-term tumor elimination and survival (>300 days after treatment) shown in Fig. 2A. Preclinical studies in the HT29 colon xenograft model showed that CPX-571 had substantially

Published OnlineFirst August 11, 2009; DOI: 10.1158/1535-7163.MCT-09-0243

greater tumor growth inhibition including tumor regression (Fig. 2B). The mean tumor volume regressed from 150 to 60 mg following completion of treatment with CPX-571. The free-drug combination counterpart did not cause any regression and tumor growth delay was minimal. Similarly, CPX-571 caused greater tumor regression than its free-drug counterpart against the Capan-1 pancreatic xenograft model (Fig. 2C). In this model, treatment with the CPX-571 resulted in a 60-day regression of all tumors, with the mean tumor size reduced to a low of 6 mg. During the same 60-day period in this experiment, the unencapsulated drugs caused minimal tumor regression followed by tumor progression. The effects of CPX-571 on tumor growth inhibition were also tested in the HCT-116 human colon xenograft model, and although no tumor regression was observed, CPX-571 treatment resulted in tumor growth delay of 44.5 days, compared with 19.5 days for free-drug cocktail (Fig. 2D).

CPX-571 was also compared with free-drug cocktail administered at varying dosing schedules, including a dosing schedule that mimics the clinical regimen where both cisplatin and irinotecan are administered on day 1 followed by irinotecan administered independently for the following two doses per cycle (22). This study was undertaken to ensure that the efficacy improvements observed above for CPX-571 were not biased due to suboptimal dosing of the free-drug cocktail. We observed that the absolute therapeutic activity of the free-drug cocktail could be increased by administering two courses of treatment with each course, consisting of three injections on a q4d schedule (Fig. 3). Alterations to the dosing schedule to mimic the clinical regimen provided equivalent efficacy. Administering CPX-571 on the (q4d×3)×2 schedule also increased the degree of tumor growth inhibition over single-course CPX-571 treatment with a LCK value of 4.2 (and 1 complete regression), a value markedly higher than that obtained with free-drug cocktail and one considered highly active for antitumor agents (23).

Efficacy of CPX-571 in an Irinotecan-Resistant Tumor Xenograft Model

One of the primary hurdles to successful treatments for SCLC is the emergence of resistant disease. Consequently, we examined the efficacy of free-drug cocktail and CPX-571 in an irinotecan-resistant variant of the HCT-116 solid tumor model (HCT-116IR, Fig. 4) to determine if controlling drug ratios *in vivo* may enhance the activity of this combination in resistant tumors. Mice were given saline, individual free drugs or free cocktail (Fig. 4A), or individual liposomal drugs or CPX-571 (Fig. 4B). In Fig. 4A, the tumor growth delay, based on the time for tumors to reach 400 mg, was determined for free-drug comparisons. The tumor growth delay was 7 days for cisplatin (LCK, 0.35), 14.5 days for irinotecan (LCK, 0.73), and 19 days for the combination of irinotecan and cisplatin (LCK, 0.95). The free-drug cocktail LCK value of 0.95 was less than the predicted additive value of 1.08 for the individual free cisplatin (LCK, 0.35) and free irinotecan (LCK, 0.73). Tumor growth delays for liposomal cisplatin, liposomal irinotecan, and CPX-571 were 10 days (LCK, 0.5), 26 days (LCK, 1.31), and 48 days (LCK, 2.41), respectively. Not only was the absolute extent of antitumor activity for CPX-571 increased compared with free-drug cocktail but also the LCK value of 2.41 for CPX-571 was greater than the predicted additive value of 1.81 based on liposomal cisplatin (LCK, 0.50) and liposomal irinotecan (LCK, 1.31).

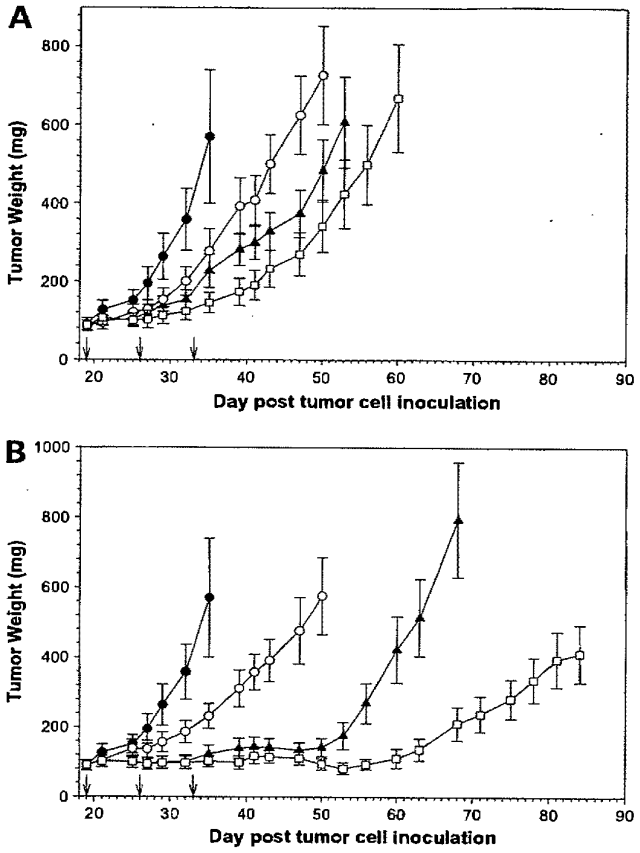

Figure 4. Antitumor efficacy of free-drug cocktail and CPX-571 in the irinotecan-resistant HCT-116IR colon tumor xenograft model. Tumor growth delay was assessed in this model using a q7d×3 schedule. **A,** mice received injections of saline (●), free cisplatin at 3 mg/kg (○), free irinotecan at 47 mg/kg (▲), or free-drug cocktail of irinotecan/cisplatin (7:1 molar ratio) at 47:3 mg/kg (□). **B,** mice received injections of saline (●), liposomal cisplatin at 3 mg/kg (○), liposomal irinotecan at 47 mg/kg (▲), or liposomal irinotecan/cisplatin (7:1 molar ratio) at 47:3 mg/kg (□). *Downward arrows,* injection days.

Discussion

Human clinical studies have shown that combination treatment with irinotecan and cisplatin is efficacious in a wide range of cancer types including SCLC (9–11, 24–26), NSCLC (27–29), ovarian cancer (30), upper gastrointestinal cancers (31–35), and other less prevalent tumor types (36–38). Based on phase III randomized trials, this combination remains a prospective treatment for extensive-stage SCLC, with response and survival end points comparable to that

Published OnlineFirst August 11, 2009; DOI: 10.1158/1535-7163.MCT-09-0243

of etoposide/cisplatin in the presence of reduced myelosuppression. However, these results have been somewhat disappointing in view of the promising synergy shown preclinically (5, 6), the broad-spectrum activity, and the historical clinical superiority of irinotecan over etoposide in a monotherapy setting (3), which together would suggest that irinotecan/cisplatin therapy should be therapeutically superior. In view of these apparent discrepancies, we investigated whether this drug combination exhibited drug ratio–dependent synergy and if ratiometric dosing using liposome delivery vehicles could significantly augment therapeutic activity.

Ratiometric dosing is an approach to develop drug combinations based on drug ratio–dependent synergy using nanoscale drug carriers *in vivo*. If the degree of synergy (and/or antagonism) depends on the molar ratio of irinotecan/cisplatin, then it may be expected that the differing distribution and elimination kinetics of the two individual agents administered in conventional aqueous formulations could lead to rapid changes in circulating and tissue-associated drug ratios resulting in the exposure of tumor cells to antagonistic drug ratios. This is relevant given that the treatment of SCLC cancer patients typically uses a regimen of irinotecan at 60 mg/m^2 i.v. on days 1, 8, and 15 and cisplatin at 60 mg/m^2 i.v. on day 1 of a 28-day cycle (22), resulting in constantly changing irinotecan/cisplatin ratios during the entire course of treatment. Controlling drug pharmacokinetics through liposome delivery provides an avenue whereby synergistic irinotecan/cisplatin ratios identified *in vitro* can be maintained for extended times after administration *in vivo* and antagonistic drug ratios can be avoided, with the potential benefit of improved efficacy for the combination.

Individual irinotecan and cisplatin liposomes were developed and evaluated for their ability to maintain coordinated pharmacokinetics. A liposome formulation was identified that coordinated the release of irinotecan and cisplatin such that the administered drug ratio was maintained within the plasma for more than 24 hours following injection, independent of the encapsulated drug ratio (Supplementary Fig. S1). The plasma half-life of the liposomes was ~16 hours, with drug half-lives of 6 hours. The decreased drug half life relative to the liposome half life reflected that the drugs were being made bioavailable in a time course commensurate with the accumulation of liposomes in solid tumors via the enhanced penetration and retention effect (39). These features allowed drug ratio dependency to be evaluated *in vivo* by comparing the efficacy of liposome formulations containing synergistic and antagonistic irinotecan/cisplatin ratios.

Irinotecan/cisplatin combinations were systematically screened against a panel of 20 tumor cell lines, which identified trends in synergy and antagonism. Unlike the combination of irinotecan and floxuridine investigated previously (13, 14), a 1:1 molar ratio of irinotecan/cisplatin was strongly antagonistic, consistent with previously published results (40). In the case of irinotecan/cisplatin, either high irinotecan concentrations (>4:1 irinotecan/cisplatin) or high cisplatin concentrations (≤1:4 irinotecan/cisplatin) were synergistic. With this knowledge, liposome irinotecan:cisplatin formulations were tested against a variety of human tumor xenograft models at synergistic and antagonistic ratios. Liposome-encapsulated irinotecan/cisplatin molar ratios above 4:1 could be administered at high relative dose intensities and were more efficacious than molar ratios of 1:4 and below where low irinotecan doses resulted. Consistent with the *in vitro* studies, drug ratios identified as antagonistic provided inferior therapeutic activity *in vivo* compared with a synergistic drug ratio despite using 10-fold greater doses of irinotecan (with the same cisplatin dose). These results confirm that the enhanced efficacy observed for the synergistic ratio liposome formulations was not simply due to a general liposome effect on drug pharmacokinetic properties but rather showed the ability to translate *in vitro* informatics on drug ratio–dependent synergy to *in vivo* efficacy using drug delivery technology.

We found that fixed irinotecan/cisplatin molar ratios ranging from 5:1 to 10:1 were highly active in tumor xenograft models, resulting in greater antitumor activity than with the free-drug cocktail or either of the individual liposomal drugs at their respective MTDs. Because the 7:1 ratio was highly active, intermediate between the 5:1 and 10:1 ratios and further away from the antagonistic region, the 7:1 ratio formulation (CPX-571) became the lead candidate for further study. CPX-571 was markedly superior to the unencapsulated drugs using all dosing regimens tested. The superior therapeutic activity attained by CPX-571 compared with unencapsulated irinotecan and cisplatin may partially be explained by our results showing that administration of CPX-571 in H460 tumor–bearing mice leads to tumor accumulation of irinotecan/cisplatin molar ratios that were in the synergistic range (Supplementary Fig. S3), which was not observed for unencapsulated drugs. One of the main obstacles in the treatment of SCLC is recurrent disease and the emergence of drug-resistant tumor cells. Therefore, we evaluated CPX-571 compared with the irinotecan/cisplatin free-drug cocktail in the HCT-116 irinotecan-resistant tumor model. In these studies, the magnitude of CPX-571 therapeutic activity was maintained and evidence of synergy preserved as it was in the parental drug-sensitive tumor xenograft. These results indicate that CPX-571 may be a promising treatment for recurrent disease where response rates with currently available agents are 2- to 3-fold lower than for first-line treatment, presumably reflecting an increased resistance to chemotherapy.

The *in vitro* synergy from concomitant administration of irinotecan and cisplatin may arise through reciprocal effects whereby the drugs enhance each other's activity. Specifically, irinotecan/SN-38 inhibition of the topoisomerase I DNA repair activity may augment the persistence of DNA adducts following their initial formation (41) and enhance cisplatin accumulation (42). Conversely, cisplatin has been shown to down-regulate topoisomerase I activity, which correlates with increased irinotecan sensitivity (42, 43). Topoisomerase inhibitors also down-regulate the antiapoptotic protein Bcl-2 thereby sensitizing the cells to apoptosis (44). Thus, it is apparent that both drugs have the potential to

Published OnlineFirst August 11, 2009; DOI: 10.1158/1535-7163.MCT-09-0243

improve each other's relative efficacy by enhancing sensitivity to the other drug.

Based on the above putative interactions, however, one can also envisage conditions under which certain irinotecan/cisplatin ratios may be rendered antagonistic rather than synergistic. For example, exposure of irinotecan and cisplatin to cells results in single- and double-strand breaks and, ultimately, G_2 cell cycle arrest. It is known that irinotecan is most active during the S phase of the cell cycle and more cytotoxic with increasing time of drug exposure. Therefore, drug interactions that result in G_2 arrest but not sufficient for inducing apoptosis could result in antagonistic interactions. We observed a high degree of synergy at higher irinotecan/cisplatin ratios, which is consistent with previous findings where high drug concentrations increase the number of cells in G_1-S phases (45) and also exhibit cytotoxic activity against cells that are not in S phase (46). Such mechanisms could render either synergistic or antagonistic interactions between irinotecan and cisplatin depending on the drug/drug ratios, consistent with our observations here for both *in vitro* and *in vivo* systems.

The application of ratiometric screening data to identify synergistic drug combinations and deliver them within liposomal formulations has led to two ongoing clinical programs, one in colorectal cancer patients (CPX-1, a liposomal combination of floxuridine and irinotecan; see ref. 47) and one in acute myeloid leukemia patients (CPX-351, a liposomal combination of cytarabine and daunorubicin; see ref. 48), with encouraging early signs of antitumor activity in both cases. CPX-571, a fixed-ratio drug combination of irinotecan and cisplatin at a 7:1 molar ratio, optimizes enhanced synergy and improved efficacy with potential for clinical applications in the treatment of a range of solid tumors.

Disclosure of Potential Conflicts of Interest

All authors are employees of Celator Pharmaceuticals Corp. and have no other conflicts of interest with other companies to declare.

References

1. Jemal A, Siegel R, Ward E, Murray T, Xu J, Thun M. Cancer statistics, 2008. CA Cancer J Clin 2008;58:71–96.

2. Evans WK, Shepherd FA, Feld R, Osoba D, Dang P, Deboer G. VP-16 and cisplatin as first-line therapy for small-cell lung cancer. J Clin Oncol 1985;3:1471–7.

3. Rothenberg ML. CPT-11: an original spectrum of clinical activity. Semin Oncol 1996;23:21–6.

4. Matsui Y, Oshima S, Kado M, et al. Phase II study of oral VP-16-213 in small cell lung cancer. Cancer 1987;60:2882–5.

5. Takada M, Fukuoka M, Kudoh S, Masuda N, Nakagawa K, Kishimoto S. Synergistic effects of CPT-11 and cisplatin or etoposide on human lung cancer cell lines and xenografts in nude mice. Proc Amer Assoc Cancer Res 1992;33:226.

6. Kano Y, Suzuki K, Akutsu M, et al. Effects of CPT-11 in combination with other anti-cancer agents in culture. Int J Cancer 1992;50:604–10.

7. Kudoh S, Takada M, Masuda N, et al. Enhanced antitumor efficacy of a combination of CPT-11, a new derivative of camptothecin, and cisplatin against human lung tumor xenografts. Jpn J Cancer Res 1993;84:203–7.

8. Tsunoda T, Tanimura H, Hotta T, et al. *In vitro* augmentation of antitumor effect in combination with CPT-11 and CDDP for human colorectal cancer. J Surg Oncol 2000;73:6–11.

9. Noda K, Nishiwaki Y, Kawahara M, et al. Irinotecan plus cisplatin compared with etoposide plus cisplatin for extensive small-cell lung cancer. N Engl J Med 2002;346:85–91.

10. Hanna N, Bunn PA, Jr., Langer C, et al. Randomized phase III trial comparing irinotecan/cisplatin with etoposide/cisplatin in patients with previously untreated extensive-stage disease small-cell lung cancer. J Clin Oncol 2006;24:2038–43.

11. Natale R. S0124: a randomized phase III trial comparing irinotecan/cisplatin (IP) with etoposide/cisplatin (EP) in patients with previously untreated extensive stage small cell lung cancer (E-SCLC). ASCO Meeting 2008; abstract 7512.

12. Adams DJ, Sandvold ML, Myhren F, Jacobsen TF, Giles F, Rizzieri DA. Anti proliferative activity of ELACYT™ (CP-4055) in combination with cloretazine (VNP40101M) idarubicin, gemcitabine, irinotecan and topotecan in human leukemia and lymphoma cells. Leuk Lymphoma 2008;49:786–97.

13. Mayer LD, Harasym TO, Tardi PG, et al. Ratiometric dosing of anticancer drug combinations: controlling drug ratios after systemic administration regulates therapeutic activity in tumor-bearing mice. Mol Cancer Ther 2006;5:1854–63.

14. Harasym TO, Tardi PG, Johnstone SA, Bally MB, Janoff AS, Mayer LD. Fixed drug ratio liposome formulations of combination cancer therapeutics. In: Gregoriadis G, editor. Liposome technology. 3rd ed. Volume III. Interactions of liposomes with the biological milieu. 2006. p 25–48.

15. Harasym TC, Tardi PG, Harasym NL, Harvie P, Johnstone SA, Mayer LD. Increased preclinical efficacy of irinotecan and floxuridine coencapsulated inside liposomes is associated with tumor delivery of synergistic drug ratios. Oncol Res 2007;16:361–74.

16. Tardi PG, Gallagher RC, Johnstone S, et al. Coencapsulation of irinotecan and floxuridine into low cholesterol-containing liposomes that coordinate drug release *in vivo*. Biochim Biophys Acta 2007;1768:678–87.

17. Mosmann T. Rapid colorimetric assay for cellular growth and survival: application to proliferation and cytotoxicity assays. J Immunol Methods 1983;65:55–63.

18. Chou T-C, Talalay P. Quantitative analysis of dose effect relationships: the combined effects of multiple drugs or enzyme inhibitors. Adv Enzyme Regul 1984;22:27–55.

19. Chou TC, Hayball MP. CalcuSyn: Windows software for dose effects analysis. Cambridge(MA): Biosoft; 1996. p. 1–56.

20. Tardi P, Harasym T, Johnstone S, Zisman N, Mayer L, Bermudes D. Drug ratio-dependent antitumor activity of irinotecan and cisplatin combination *in vitro* and *in vivo*. AACR Meeting 2007; abstract C114.

21. Corbett T, Valeriote F, LoRusso P, et al. *In vivo* methods for screening and preclinical testing. In: Teicher BA, editor. Anticancer drug development guide: preclinical screening, clinical trials, and approval. New Jersey: Humana Press; 1997. p. 75–99.

22. Chu E, DeVita V, Jr. Physicians' cancer chemotherapy drug manual 2006. Sudbury (MA): Jones and Bartlett Publishers; 2006. p. 546.

23. Corbett TH, Polin L, Roberts BJ, et al. Transplantable syngeneic rodent tumors: solid tumors in mice. Tumor models in cancer research. In: Teicher BA, editor. Totowa (NJ): Humana Press, Inc.; 2002. p. 41–71.

24. Kurup A, Hanna NH. Treatment of small cell lung cancer. Crit Rev Oncol Hematol 2004;52:117–26.

25. Hong YS, Lee HR, Park S, et al. Three-week schedule of irinotecan plus cisplatin in patients with previously untreated extensive-stage small-cell lung cancer. Br J Cancer 2006;95:1648–52.

26. Sohn JH, Moon YW, Lee CG, et al. Phase II trial of irinotecan and cisplatin with early concurrent radiotherapy in limited-disease small-cell lung cancer. Cancer 2007;109:1845–950.

27. Hino M, Kobayashi K, Yoshimura A, et al. East Japan Chesters Group. Weekly administration of irinotecan (CPT-11) plus cisplatin for non-small cell lung cancer. Anticancer Res 2006;26:4697–703.

28. Kim HT, Han JY, Lee DH, et al. A phase II study of irinotecan plus cisplatin for patients with advanced stage IIIB or IV NSCLC previously treated with nonplatinum-based chemotherapy. Cancer 2006;107:799–805.

29. Rinaldi M, Cauchi C, Gridelli C. First line chemotherapy in advanced or metastatic NSCLC. Ann Oncol 2006;17:64–7.

30. Sugiyama T, Yakushiji M, Kamura T, et al. Irinotecan (CPT-11) and cisplatin as first-line chemotherapy for advanced ovarian cancer. Oncology 2002;63:16–22.

Published OnlineFirst August 11, 2009; DOI: 10.1158/1535-7163.MCT-09-0243

31. Imamura H, Ikeda M, Furukawa H, et al. Phase II study of protracted irinotecan infusion and a low dose cisplatin for metastatic gastric cancer. World J Gastroenterol 2006;12:6522–6.

32. Shah MA, Ramanathan RK, Ilson DH, et al. Multicenter phase II study of irinotecan, cisplatin, and bevacizumab in patients with metastatic gastric or gastroesophageal junction adenocarcinoma. J Clin Oncol 2006;24:5201–6.

33. Michel P, Adenis A, Di Fiore F, et al. Induction cisplatin-irinotecan followed by concurrent cisplatin-irinotecan and radiotherapy without surgery in esophageal cancer: multicenter phase II FFCD trial. Br J Cancer 2006;95:705–9.

34. Jeung HC, Rha SY, Noh SH, Roh JK, Chung HC. A phase II trial of weekly fractionated irinotecan and cisplatin for advanced gastric cancer. Cancer Chemother Pharmacol 2007;59:313–20.

35. Lee DH, Kim HT, Han JY, et al. A phase II trial of modified weekly irinotecan and cisplatin for chemotherapy-naive patients with metastatic or recurrent squamous cell carcinoma of the esophagus. Cancer Chemother Pharmacol 2008;61:83–8.

36. Sugita H, Hirota M, Ichihara A, Furuhashi S, Kihara S, Shimada S. Combined chemotherapy of irinotecan and low-dose cisplatin (I/low-P) against metastatic biliary tract cancer. J Hepatobiliary Pancreat Surg 2006;13:463–7.

37. Kulke MH, Wu B, Ryan DP, et al. A phase II trial of irinotecan and cisplatin in patients with metastatic neuroendocrine tumors. Dig Dis Sci 2006;51:1033–8.

38. Markham C, Stocken DD, Hassan AB. A phase II irinotecan-cisplatin combination in advanced pancreatic cancer. Br J Cancer 2003;89:1860–4.

39. Matsumura Y, Maeda H. A new concept for macromolecular therapeutics in cancer chemotherapy: mechanism of tumoritropic accumulation of the antitumor agent smancs. Cancer Res 1986;46:6387–92.

40. Zastre J, Anantha M, Ramsay E, Bally M. Irinotecan-cisplatin interactions assessed in cell-based screening assays: cytotoxicity, drug accumulation and DNA adduct formation in an NSCLC cell line. Cancer Chemother Pharmacol 2007;60:91–102.

41. Masumoto N, Nakano S, Esaki T, Fujishima H, Tatsumoto T, Niho Y. Inhibition of *cis*-diamminedichloroplatinum (II)-induced DNA interstrand cross-link removal by 7-ethyl-10-hydroxy-camptothecin in HST-1 human squamous-carcinoma cells. Int J Cancer 1995;62:70–5.

42. Matsumura T, Takigawa N, Kiura K, et al. Determinants of cisplatin and irinotecan activities in human lung adenocarcinoma cells: evidence of cisplatin accumulation and topoisomerase I activity. In Vivo 2005;19:717–21.

43. Aoe K, Kiura K, Ueoka H, et al. Cisplatin down-regulates topoisomerase I activity in lung cancer cell lines. Anticancer Res 2004;24:3893–7.

44. Oizumi S, Isobe H, Ogura S, et al. Topoisomerase inhibitor-induced apoptosis accompanied by down-regulation of Bcl-2 in human lung cancer cells. Anticancer Res 2002;22:4029–37.

45. Ma J, Maliepaard M, Nooter K, et al. Synergistic cytotoxicity of cisplatin and topotecan or SN-38 in a panel of eight solid-tumor cell lines *in vitro*. Cancer Chemother Pharmacol 1998;41:307–16.

46. Morris EJ, Geller HM. Induction of neural apoptosis by camptothecin, an inhibitor of DNA topoisomerase-I: evidence for cell cycle-independent toxicity. J Cell Biol 1996;134:757–70.

47. Batist G, Chi K, Miller W, et al. Phase 1 study of CPX-1, a fixed ratio formulation of irinotecan (IRI) and floxuridine (FLOX), in patients with advanced solid tumors (abstract 18S). J Clin Oncol 2006 ASCO Annual Meeting Proceedings;24:2014.

48. Feldman E, Lancet J, Kolitz JE, et al. Phase I study of a liposomal carrier (CPX-351) containing an optimized, synergistic, fixed molar ratio of cytarabine and daunorubicin in advanced leukemias and myelodysplastic syndromes. American Society for Hematology (abstract 2984). Blood 2007;112:1025.

Published OnlineFirst August 11, 2009; DOI: 10.1158/1535-7163.MCT-09-0243

AACR American Association for Cancer Research

Molecular Cancer Therapeutics

Drug ratio–dependent antitumor activity of irinotecan and cisplatin combinations *in vitro* and *in vivo*

Paul G. Tardi, Nancy Dos Santos, Troy O. Harasym, et al.

Mol Cancer Ther 2009;8:2266-2275. Published OnlineFirst August 11, 2009.

Influence of MLH1 on colon cancer sensitivity to poly(ADP-ribose) polymerase inhibitor combined with irinotecan

LUCIO TENTORI[1*], CARLO LEONETTI[4*], ALESSIA MUZI[1], ANNALISA SUSANNA DORIO[1], MANUELA PORRU[4], SUSANNA DOLCI[2], FEDERICA CAMPOLO[2], PATRIZIA VERNOLE[3], PEDRO MIGUEL LACAL[5], FRANÇOISE PRAZ[6,7] and GRAZIA GRAZIANI[1]

Departments of [1]System Medicine, [2]Biomedicine and [3]Science and Technology of Education, University of Rome 'Tor Vergata', I-00133 Rome; [4]Experimental Preclinical Laboratory, Regina Elena National Cancer Institute, I-00158 Rome; [5]Laboratory of Molecular Oncology, Istituto Dermopatico Dell'Immacolata (IDI), Istituto di Recovero e Cura a Carattere Scientifico (IRCCS)', I-00167 Rome, Italy; [6]INSERM, UMR_S 938, Saint-Antoine Research Centre, F-75012 Paris; [7]UPMC Univ Paris 06, UMR_S 938, Saint-Antoine Research Centre, F-75012 Paris, France

Received January 16, 2013; Accepted March 1, 2013

DOI: 10.3892/ijo.2013.1932

Abstract. Poly(ADP-ribose) polymerase inhibitors (PARPi) are currently evaluated in clinical trials in combination with topoisomerase I (Top1) inhibitors against a variety of cancers, including colon carcinoma. Since the mismatch repair component MLH1 is defective in 10-15% of colorectal cancers we have investigated whether MLH1 affects response to the Top1 inhibitor irinotecan, alone or in combination with PARPi. To this end, the colon cancer cell lines HCT116, carrying MLH1 mutations on chromosome 3 and HCT116 in which the wild-type MLH1 gene was replaced via chromosomal transfer (HCT116+3) or by transfection of the corresponding MLH1 cDNA (HCT116 1-2) were used. HCT116 cells or HCT116+3 cells stably silenced for PARP-1 expression were also analysed. The results of *in vitro* and *in vivo* experiments indicated that MLH1, together with low levels of Top1, contributed to colon cancer resistance to irinotecan. In the MLH1-proficient cells SN-38, the active metabolite of irinotecan, induced lower levels of DNA damage than in MLH1-deficient cells, as shown by the weaker induction of γ-H2AX and p53 phosphorylation. The presence of MLH1 contributed to induce of prompt Chk1 phosphorylation, restoring G2/M cell cycle checkpoint and repair of DNA damage. On the contrary, in the absence of MLH1, HCT116 cells showed minor Chk1 phosphorylation and underwent apoptosis. Remarkably, inhibition of PARP function by PARPi or by PARP-1 gene silencing always increased the antitumor activity of irinotecan, even in the presence of low PARP-1 expression.

Correspondence to: Dr Grazia Graziani, Department of System Medicine, University of Rome 'Tor Vergata', Via Montpellier 1, I-00133 Rome, Italy
E-mail: graziani@uniroma2.it

*Contributed equally

Key words: colon cancer, chemotherapy, drug resistance, DNA repair, poly(ADP-ribose) polymerase, mismatch repair

Introduction

Colorectal cancer (CRC) is the second most common cause of cancer-related death in many industrialized countries. Although the addition of oxaliplatin or of the topoisomerase I (Top1) inhibitor irinotecan to 5-fluorouracil (5-FU)/leucovorin regimen has greatly improved survival (1), treatment failure frequently occurs. Resistance to Top1 poisons has been generally attributed to overexpression of efflux pumps and low expression or mutations of Top1 (2). Strategies to counteract resistance to Top1 poisons include their combination with poly(ADP-ribose) polymerase (PARP) inhibitors (PARPi) (3-7). PARP-1 is the oldest member of a family of enzymes that synthesizes and transfers ADP-ribose polymers to acceptor proteins (including PARP-1 itself) using NAD^+ as a substrate. PARP-1 has a key role in the surveillance and maintenance of genome integrity, sensing DNA breaks and signalling damage to DNA repair pathways (8). The interaction of poly(ADP-ribosyl)ated PARP-1 with specific domains of Top1 results in disjoining of Top1-DNA cleavable complex and favours resealing of strand breaks by the ligase activity of Top1 (9). Thus, PARPi would remove the antagonistic effect exerted by poly(ADP-ribose) on the mechanism of action of Top1 poisons, contributing to the formation of persistent DNA breaks (10). Another explanation for the synergism between PARPi and irinotecan implies the intervention of the base excision repair (BER) in the repair of the DNA damage induced by the Top1 poison (5).

The MMR that eliminates replication errors and maintains genomic stability can be defective in familial or sporadic CRC and contributes to drug resistance/sensitivity (11). MMR is composed of several proteins forming different heterodimers: MutSα (MSH2/MSH6) recognizes single base mismatches, as

well as 1-bp insertion-deletion loops, whereas MutSβ (MSH2/MSH3) primarily recognizes 2-4-bp insertion-deletion loops; MutLα, (MLH1/PMS2), forms a ternary complex with a MutS heterodimer that binds to mismatches during replication, recruiting other proteins to complete the repair process (11). MutSα and MutLα also contribute to signal transduction pathways which lead to growth arrest or cell death induced by the methylating agent temozolomide (TMZ) (12,13).

While the influence of MutSα and MutLα function in TMZ-induced sensitivity is known, the role of MLH1 in CRC susceptibility to irinotecan is controversial (6,14-19). On the other hand, MLH1-deficiency confers resistance to cisplatin or carboplatin, but not to oxaliplatin (20).

Aims of the present study were to clarify whether MLH1 loss of function affects colon cancer sensitivity to irinotecan and whether lack of PARP-1 expression/activity has different outcome depending on MLH1 status.

Materials and methods

Cell lines and transfection. The colon cancer HCT116 cell line has a hemizygous nonsense mutation in the MLH1 gene located on chromosome 3 (21). The MLH1-proficient HCT116/3-6 cell line (HCT116+3) was created by microcell chromosome transfer of a single normal human chromosome (22) and kindly provided by Dr Giancarlo Marra (Institute of Molecular Cancer Research, University of Zürich, Switzerland). The HCT116 1-2 and HCT116 0-1 cells were generated by transfection with the full-length wild-type MLH1 cDNA cloned into the pcDNA3.1/Hygro vector or with the empty control vector, respectively (15). Cell lines were cultured in DMEM (Sigma-Aldrich, Milan, Italy), supplemented with 10% fetal calf serum, 2 mM L-glutamine and antibiotics. The HCT116+3 cells were cultured in the presence of 400 μg/ml geneticin (Sigma-Aldrich), the HCT116 1-2 and HCT116 0-1 cells in the presence of 100 μg/ml hygromycin (Sigma-Aldrich).

Stable silencing of PARP-1 in HCT116+3 cells (HCT116+3 SiP) was obtained by co-transfection of the pBS-U6-SiP912 vector and the pBabe vector, carrying the puromycin resistance gene. HCT116+3 cells, transfected with pBabe vector only, were used as control (HCT116+3 Babe). The HCT116 SiP and Babe cell lines were previously described (23). Cells were maintained in the presence of 1 μg/ml puromycin (Sigma-Aldrich).

Drugs for in vitro studies. SN-38 (2.5 mM, Alexis), TMZ (100 mM, Sigma-Aldrich) and 7-hydroxystaurosporine (UCN-01, 100 nM, Sigma-Aldrich) stock solutions were prepared by dissolving the drugs in dimethyl sulfoxide. The final concentration of dimethyl sulfoxide was always <0.5% (v/v) and did not contribute to toxicity. The PARP inhibitor GPI 15427 [10-(4-methyl-piperazin-1-ylmethyl)-2H-7-oxa-1,2-diazabenzo[de]anthracen-3-one, Eisai, Baltimore, MD, USA] stock solution (1 mM) was prepared by dissolving GPI 15427 in 70 mM PBS without potassium (24).

Cell growth assays. Cell proliferation of colon cancer cell lines was evaluated by colony formation assay. Cells were seeded in triplicate into 6-well plates ($2x10^2$/well) and, after overnight incubation, treated with SN-38, TMZ or GPI 15427. Cells were cultured to allow colony-formation; after 10 days colonies were fixed, stained with 2% methylene blue in 95% ethanol and counted. Only colonies comprising >50 cells were scored as survival colonies. Chemosensitivity was evaluated in terms of IC_{50}, i.e., the concentration of the drug capable of inhibiting cell growth by 50%.

Flow cytometry analysis. Apoptosis and cell cycle perturbations induced by the drugs were evaluated by flow cytometry analysis of the DNA content. Untreated or drug treated cells ($1x10^6$) were washed with PBS and fixed in 70% ethanol at -20°C for ≥18 h. Cells were then centrifuged, suspended in 1 ml of a solution containing 0.1% (w/v) sodium citrate, 0.1% Triton-X (v/v), 50 μg/ml propidium iodide, 10 μg/ml RNase and incubated in the dark at 37°C for 15 min. The fluorescence was measured on a linear scale using a FACScan flow cytometer and the CellQuest software. Data collection was gated using forward light scatter and side scatter to exclude cell debris and aggregates. Apoptotic cells were represented by a broad hypodiploid peak easily distinguishable from the diploid DNA content in the red fluorescence channel. For cell cycle analysis, the Mod-Fit software version 3.0 was used (Becton-Dickinson, San Jose, CA, USA).

Western blot analysis. For immunoblot analysis the following primary antibodies were used: rabbit polyclonal anti-human phosphorylated p53 (Ser15) (Cell Signaling Technology; Beverly, MA, USA; 1:1,000 dilution); rabbit polyclonal anti-human phosphorylated Chk2 (Thr68) (Cell Signaling Technology; 1:1,000); rabbit polyclonal anti-human β-tubulin (clone H-235; Santa Cruz Biotechnology Inc., Santa Cruz, CA, USA; 1:400); rabbit polyclonal anti-human γ-H2AX (phospho-S139) (Abcam, Cambridge, UK; 1:1,000); mouse monoclonal antibody anti-human Chk1 (G4, Santa Cruz Biotechnology Inc; 1:500); rabbit monoclonal anti-human phosphorylated Chk1 (Ser345) (133D3, Cell Signaling Technology; 1:1,000); mouse monoclonal anti-human MLH1 (clone G168-15, BD Biosciences, San Jose, CA, USA; 1/500); mouse monoclonal anti-calf PARP-1 (clone C2-10; Trevigen, Gaithersburg, MD, USA; 1:2,000 dilution); mouse monoclonal anti-human Top1 (clone C-21 BD Biosciences; 1:500). Anti-rabbit and anti-mouse secondary antibodies (Sigma-Aldrich) were used at the appropriate dilutions. Signals were quantified using a Kodak densitometer (Rochester, NY, USA).

PARP activity assay. Cells ($5x10^6$) were lysed in 0.5 ml of a buffer containing 0.1% Triton X-100, 50 mM Tris-HCl pH 8.0, 0.6 mM EDTA, 14 mM β-mercaptoethanol, 10 mM $MgCl_2$ and protease inhibitors. Proteins (25 μg) were incubated with 2 μCi ^{32}P-NAD$^+$ (GE Healthcare, Milan, Italy), 100 μM NAD$^+$, 50 mM Tris-HCl, 10 mM $MgCl_2$, 14 mM β-mercaptoethanol, in the presence (maximally stimulated activity) or absence (basal activity) of 10 μg nuclease-treated salmon testes DNA. After 15 min at 30°C the reaction was stopped adding ice-cold trichloroacetic acid 20% (v/v). The radioactivity associated with the acid-insoluble material, corresponding to poly (ADP-ribosyl)ated proteins, was counted on a liquid scintillation counter. PARP activity was evaluated as fmol of ^{32}P-NAD$^+$/μg of protein and data were presented as the ratio between maximally stimulated and basal activity.

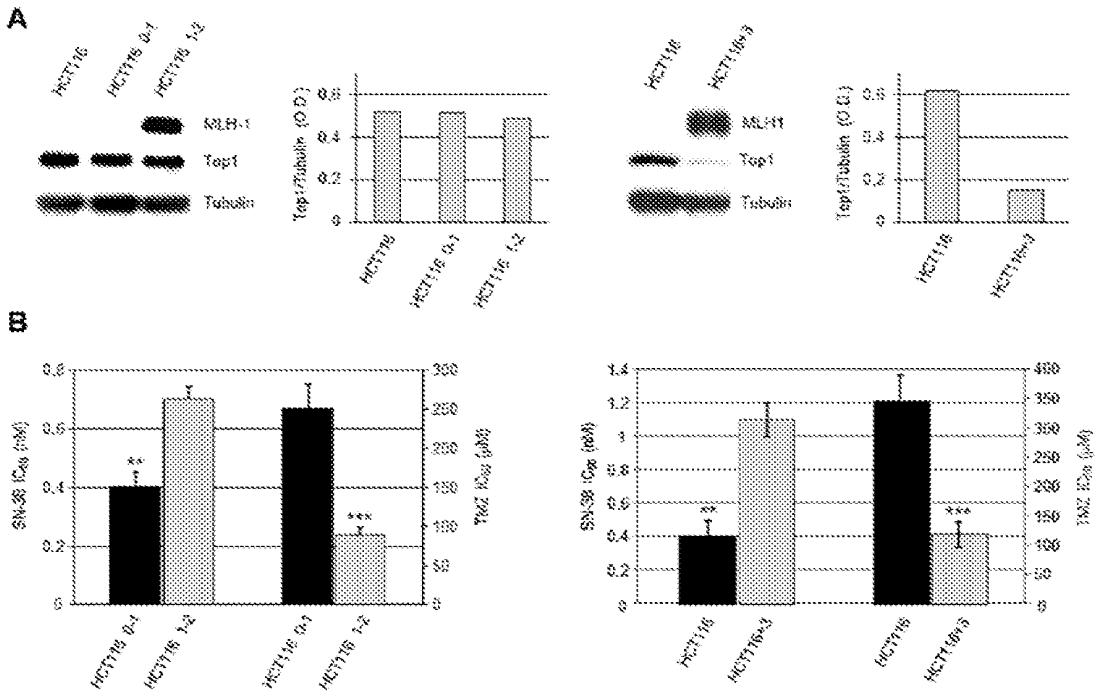

Figure 1. Analysis of MLH1 or Top1 expression and of sensitivity to SN-38 in HCT116 derived cell lines. (A) Analysis of MLH1 and Top1 expression. Cell lysates from parental HCT116 cells, HCT116 1-2 cells, transfected with MLH1 cDNA, and HCT116 0-1 cells, transfected with the empty control vector, or HCT116+3 cells, in which MLH1 had been introduced by chromosome transfer, were electrophoresed and analysed for the expression of MLH1, Top1 and tubulin. Histograms represent the ratios between the optical densities (OD) of Top1 and those of tubulin. The results are representative of one out of two experiments with similar results. (B) *In vitro* chemosensitivity. Tumor cell susceptibility to SN-38 or TMZ was assessed by colony-formation assay and the results were expressed as IC_{50}. Only colonies comprising >50 cells were scored as survival colonies. Data are means [± standard deviation (SD)] from three independent experiments. The results of statistical analysis by Student's *t*-test of the differences in sensitivity are as follows: SN-38, HCT116 0-1 vs. HCT116 1-2, $^{**}P=0.003$; TMZ, HCT116 0-1 vs. HCT116 1-2, $^{***}P<0.0001$; SN-38, HCT116 vs. HCT116+3, $^{**}P=0.002$; TMZ, HT116 vs. HCT116+3, $^{***}P<0.0001$.

Immunofluorescence microscopy of γ-H2AX. Cells were grown on poly-L-lysine coated glass coverslips and treated with SN-38. After 24 h, slides were washed twice with PBS and fixed in 4% (w/v) paraformaldehyde in PBS for 30 min. Cells were permeabilised with 0.1% Triton X-100 in PBS for 2 min, incubated in 2.5% goat serum-PBS for 20 min and with rabbit anti-γ-H2AX polyclonal antibody for 2 h (Abcam, 1:250 in 2.5% goat serum-PBS). After washing in PBS, cells were incubated with goat anti-rabbit-Alexa 488 secondary antibody (Molecular Probes, Eugene, OR, USA; 1:2,000) for 1 h. Slides were counterstained by vectashield antifade solution containing 4,6 diamidino-2-phenylindole (DAPI, Vector Laboratories, Burlingame, CA, USA) and examined with a fluorescent microscope (Nikon Eclipse, E600, Yokohama, Japan). Images were analysed with the Arkon FISH program (Nikon). For quantitative analysis, foci were counted by eye during the microscopic and imaging process using a x100 objective. Cells with ≥5 foci were considered positive for γ-H2AX expression (28).

In vivo studies. The intramuscular transplantation procedure was performed as previously described (6). Tumor cells ($3x10^6$) were inoculated intramuscularly (i.m.) in male athymic CD-1 mice (nu/nu genotype, 6/group; Charles River, Calco, Milan, Italy). Xenograft growth was monitored by measuring tumor nodules with calliper every 2-3 days for 3 weeks and volumes were calculated according to the following formula: $[(width)^2 \times length]/2$. Irinotecan (Campto®, Aventis, Milan, Italy) was administered intraperitoneally (i.p) at 5 mg/kg/dx5d; treatment started when nodules reached 300 mm^3. The animals were euthanized when their tumors reached a volume of ~1500 mm^3. All procedures involving mice and care were performed in compliance with our institutional animal care guidelines and with international directives (directive 2010/63/EU of the European parliament and of the council; Guide for the Care and Use of Laboratory Animals, United States National Research Council, 2011). The study was approved by the ethics committee of the University of Rome 'Tor Vergata'.

Results

Analysis of MLH1 and Top1 expression and of sensitivity to Top1 inhibitor in HCT116 colon cancer cells transfected with the wild-type MLH1 cDNA or with chromosome 3. In order to evaluate the influence of MLH1 and Top1 or both in the susceptibility to the Top1 poison we initially performed immunoblot analysis of Top1 in the parental HCT116 cell line (devoid of MLH1 protein as a result of mutation in the MLH1 gene located on chromosome 3), in an HCT116 clone transfected with a control vector (HCT116 0-1) or with a vector expressing the wild-type MLH1 cDNA (HCT116 1-2) and in HCT116 cells in which MLH1 was introduced by transfer of chromosome 3 (HCT116+3). Our results indicated that HCT116, HCT116 0-1 and HCT116 1-2 expressed high and comparable levels of Top1 protein. On the other hand, HCT116+3 cells showed very low Top1 expression (Fig. 1A). Then we analysed the sensitivity

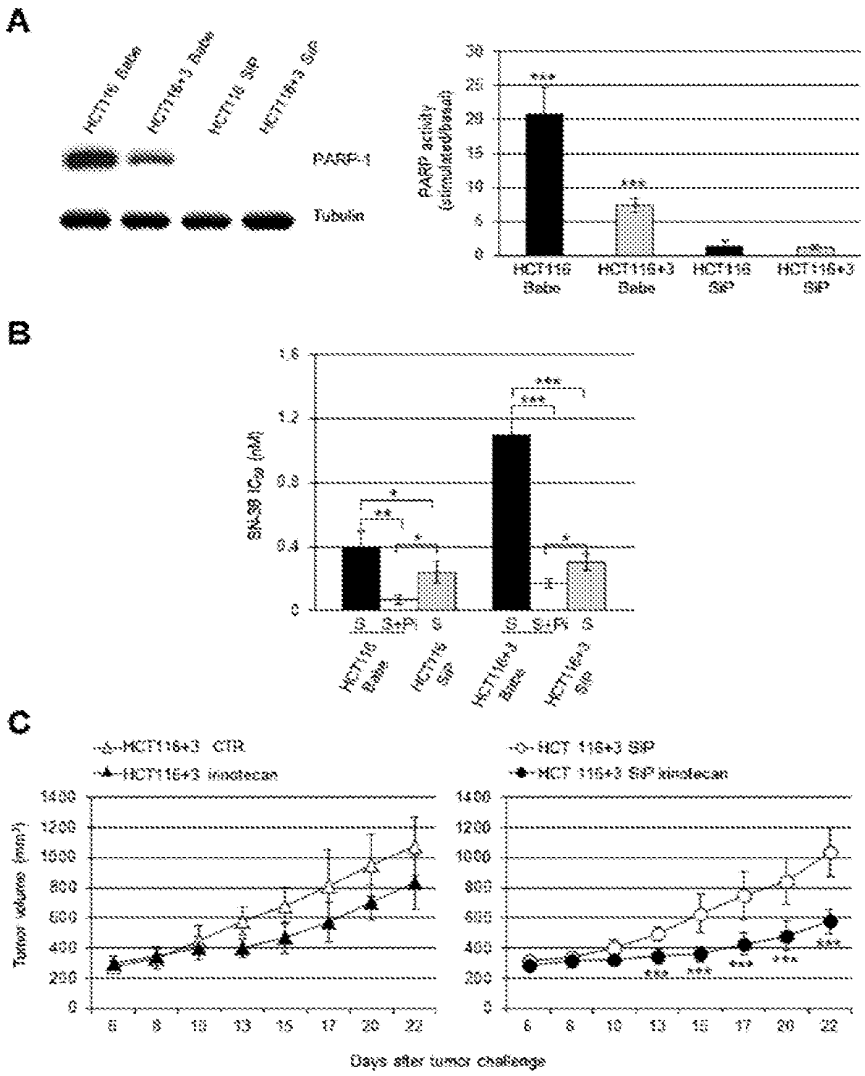

Figure 2. Sensitivity to SN-38 of HCT116 or HCT116+3 cells treated with a PARPi or stably silenced for PARP-1 expression. (A) Analysis of PARP-1 expression (left) and activity (right). Immunoblot analysis was performed in HCT116 or HCT116+3 clones transfected with the pBabe vector (HCT-116 Babe or HCT116+3 Babe) or with the pBabe and pBS-U6-SiP912 vectors (HCT-116 SiP or HCT116+3 SiP). Cellular extracts were electrophoresed and analysed for the expression of PARP-1 or tubulin. Total cellular PARP activity was measured in cell extracts, in the absence (basal activity) or in the presence of nuclease-treated DNA (maximally stimulated activity) and ^{32}P-NAD$^+$. The results were expressed as means (± SD) of stimulated and basal activity ratios of three independent experiments. The results of statistical analysis by Student's *t*-test of the differences in PARP activity ratios are as follows: HCT116 Babe vs. HCT116+3 Babe, ***P<0.0001; HCT116 Babe vs. HCT116 SiP, ***P<0.0001; HCT116+3 Babe vs. HCT116+3 SiP, ***P<0.0001; HCT116 SiP vs. HCT116+3 SiP; NS, not significant. (B) Comparison of HCT116 or HCT116+3 sensitivity to SN-38, as single agent or in combination with a PARPi, with that of PARP-1 silenced HCT116 or HCT116+3 cells. Control HCT116 or HCT116+3 (Babe) or PARP-1 silenced (SiP) cells were exposed to graded concentrations of SN-38 (S) and analysed by colony-formation assay. In the case of Babe cells SN-38 was also combined with the PARPi GPI 15427 (Pi), at a concentration (0.3 μM) capable of significantly inhibiting cellular PARP activity (70-75% inhibition of the synthesis of ADP-ribose polymers) and devoid of a significant growth inhibitory effect (<15%). The results were expressed as IC_{50}. Data are means (± SD) from three independent experiments. The results of statistical analysis by Student's *t*-test of the differences in sensitivity are as follows: HCT116 Babe treated with SN-38 vs. HCT116 Babe treated with SN-38+PARPi, **P=0.004; HCT116 Babe treated with SN-38 vs. HCT116 SiP treated with SN-38, *P=0.04; HCT116 Babe treated with SN-38+PARPi vs. HCT116 SiP treated with SN-38, *P=0.01; HCT116+3 Babe treated with SN-38 vs. HCT116+3 Babe treated with SN-38+PARPi, ***P<0.0001; HCT116+3 Babe treated with SN-38 vs. HCT116+3 SiP treated with SN-38, ***P<0.0001; HCT116+3 Babe treated with SN-38+PARPi vs. HCT116+3 SiP treated with SN-38, *P=0.02; HCT116 SiP treated with SN-38 vs. HCT116+3 SiP treated with SN-38; NS, not significant. (C) Analysis of *in vivo* chemosensitivity of HCT116+3 Babe and SiP cells in mice treated with irinotecan. Mice were inoculated i.m. with Babe (n=6) or SiP (n=6) HCT116+3 cells and treated with irinotecan (as indicated in Materials and methods). Statistical analysis by Student's *t*-test indicated that the growth of SiP grafts is significantly inhibited by irinotecan compared with untreated control grafts (***P<0.001 from day 13 onward); differences between the volumes of tumor nodules of untreated or drug treated mice injected with HCT116+3, NS, not significant.

of MLH1-deficient and -proficient cells to SN-38, the active metabolite of irinotecan and to the methylating agent TMZ, as a control for MLH1 functional proficiency. In fact, MLH1 is required for the processing and cytotoxicity of O^{6}MethylG/T mispairs generated by TMZ. The results, expressed as IC_{50}, indicated that the MLH1-deficient HCT116 0-1 and HCT116 cells were more sensitive to SN-38 as compared to MLH1-proficient HCT116 1-2 and HCT116+3 cells (Fig. 1B). The lower constitutive expression of Top1 might contribute to the higher SN-38 resistance of HCT116+3 cells compared with HCT116 1-2 cells (Fig. 1A). In HCT116 and HCTT116+3 cells the breast cancer resistance protein (BCRP), an ATP binding

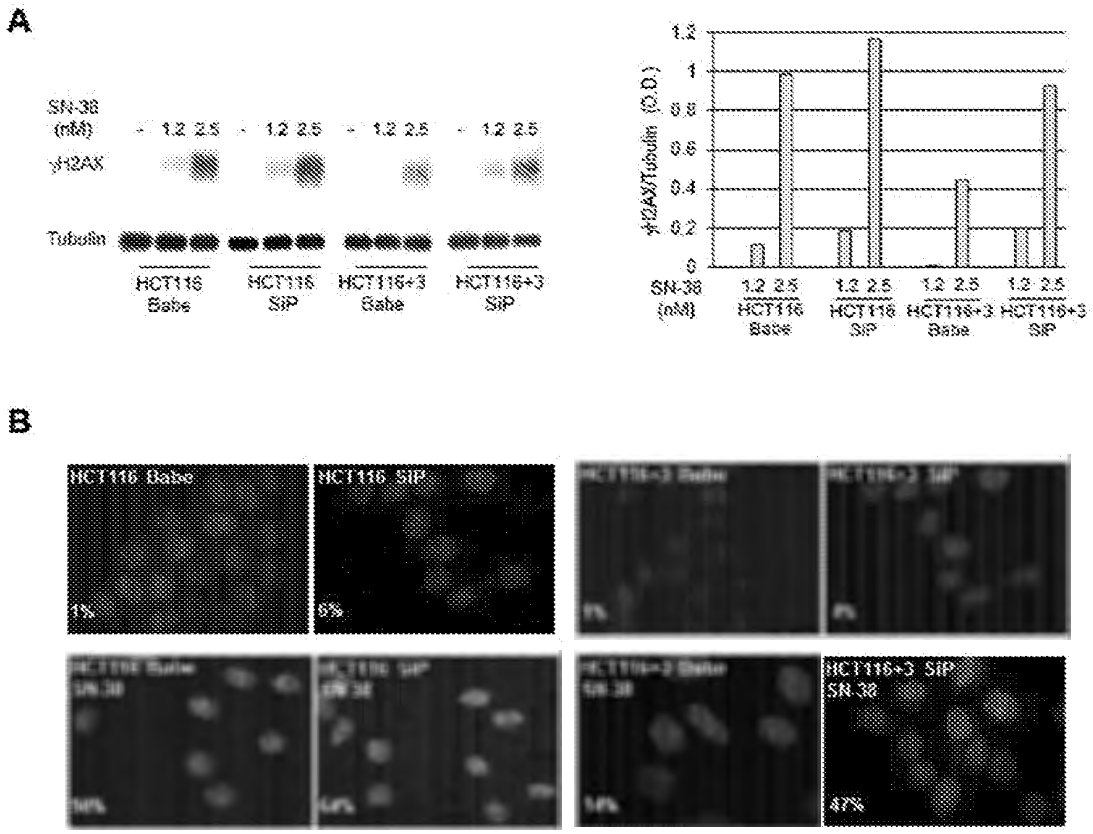

Figure 3. Analysis of DNA damage induced by SN-38 in HCT116 or HCT116+3 cells control or stably silenced for PARP-1 expression. (A) Immunoblot analysis of γ-H2AX expression in SN-38 treated cells. Cells were treated with SN-38 (1.2 and 2.5 nM) for 24 h and analysed for the expression of γ-H2AX or tubulin. Histograms represent the ratios between the OD of γ-H2AX in SN-38 treated groups and tubulin. The results are representative of one out of two experiments with similar results. (B) Immunofluorescence analysis of γ-H2AX foci (green) in untreated or SN-38 treated cells. Nuclei were stained with DAPI (blue). The percentage of cells with ≥5 γ-H2AX foci of one representative out of two experiments is presented (50 cells counted for each experiment).

cassette transporter, which is regarded as an important determinant of resistance to camptothecins, was, instead, equally expressed (6). On the contrary, MLH1 proficiency conferred sensitivity to TMZ to a similar extent in both cellular models (Fig. 1B).

Lack of PARP-1 activity increases the sensitivity to irinotecan in MLH1-proficient and -deficient HCT116 cells. We then evaluated the influence on tumor sensitivity to SN-38 of down-regulation of PARP function by PARP-1 gene silencing and by pharmacological inhibition of poly(ADP-ribose) synthesis using PARPi. To this end HCT116 and HCT116+3 were stably silenced for PARP-1 expression (SiP clones) by transfection of a siRNA vector targeting specific sequences of PARP-1, which is responsible for >90% of the cellular poly(ADP-ribosyl) ating activity. Control clones were obtained by transfection of the pBabe vector only (Babe clones). Immunoblot analysis and PARP activity assay (Fig. 2A) revealed lack of PARP-1 expression and negligible synthesis of poly(ADP-ribose) in SiP clones. Moreover, HCT116 Babe cells showed significantly higher levels of PARP-1 expression and activity compared with HCT116+3 Babe cells.

Then, control Babe clones were tested for their susceptibility to the anti-proliferative effects of SN-38 in combination with a PARPi and the results compared to those obtained in their SiP counterparts. Pharmacological inhibition of PARP activity by GPI 15427 significantly increased sensitivity to SN-38 both in MLH1-deficient and in MLH1-proficient cells, as indicated by the IC_{50} values of SN-38 in the presence of PARPi that were ~6-fold lower than those of SN-38 used as single agent (Fig. 2B). PARP-1 silenced clones were ~2-4-fold more susceptible to the Top1 poison than control clones (Fig. 2B). The enhancing effect mediated by PARPi or PARP-1 gene silencing was more pronounced in the less sensitive HCT116+3 cells (Fig. 2B). Noteworthy, *in vivo* studies showed that lack of PARP-1 expression in HCT116+3 SiP cells resulted in a higher tumor growth inhibition induced by irinotecan compared with HCT116+3 Babe cells (Fig. 2C). Analysis of the doubling times, evaluated on the basis of the growth kinetics of each clone, indicated that SiP clones possessed doubling times in the same range of those observed in PARP-1 proficient clones (22-26 h). Therefore, the distinct chemosensitivity profiles of Babe and SiP clones did not depend on different proliferation rates.

According to the results of colony formation assay, immunoblot analysis of histone H2AX phosphorylation (γ-H2AX), as an indicator of DSB, showed that treatment with SN-38 induced histone phosphorylation at higher level in HCT116 Babe than in HCT116+3 Babe cells and in PARP-1 silenced clones with respect to their PARP-1 proficient controls (Fig. 3A). Immunofluorescence analysis of γ-H2AX foci in cells treated with SN-38 confirmed the results of immunon-

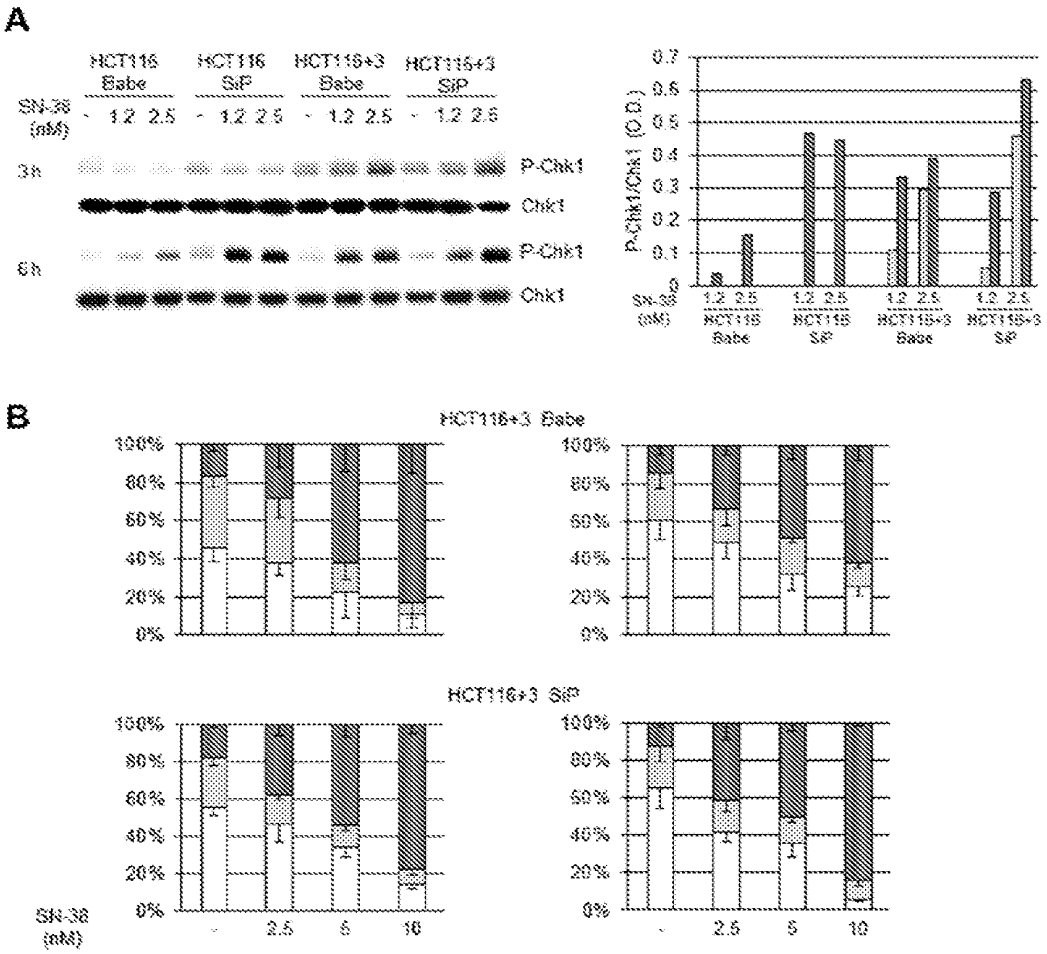

Figure 4. Analysis of Chk1 phosphorylation and cell cycle in Babe and SiP HCT116 and HCT116+3 cells treated with SN-38. (A) Immunoblot analysis of Chk1 phosphorylation. HCT116 and HCT116+3 Babe or SiP cells were treated with SN-38 (1.2 and 2.5 nM) for 3 and 6 h; cell lysates were electrophoresed and analysed for the expression of phosphorylated Chk1 (P-Chk1) or Chk1. Histograms represent the ratios between the OD of phosphorylated Chk1 (after subtraction of OD values of untreated controls) and Chk1 in SN-38 treated groups (3 h, light grey columns; 6 h, dark grey columns). The results are representative of one out of two experiments with comparable results.(B) Cell cycle analysis. HCT116+3 Babe or SiP cells were treated with SN-38 (2.5-10 nM) and analysed by flow cytometry. The results are indicated as percentages of cells in the different phases of cell cycle at 24 h (left) and 72 h (right) after treatment and are the means (- SD) from three independent experiments. G1 phase, white columns; S phase, light grey columns; M phase, dark grey columns.

oblot analysis of γ-H2AX expression (Fig. 3B). The data also showed that the increment of γ-H2AX expression and foci formation resulting from the comparison of HCT116+3 SiP with HCT116+3 Babe cells was higher than that deriving from HCT116 SiP and HCT116 Babe comparison (Fig. 3).

Since MLH1 is known to be involved in DNA damage-induced checkpoint, signalling the control of G2/M arrest by methylating agents like TMZ through phosphorylation of Chk1 (25-27), we have investigated whether treatment with SN-38 might induce different kinetics of induction of Chk1 phosphorylation and cell cycle perturbations depending on the presence of MLH1 and/or PARP-1. The results of immunoblot analysis of Chk1 phosphorylation revealed that SN-38 treatment induced an earlier Chk1 phosphorylation (3 h) in MLH1-proficient cells than in MLH1-deficient cells (Fig. 4A). At a later time-point (6 h) the highest level of Chk1 phosphorylation was detected in cells silenced for PARP-1, regardless of MLH1 expression (Fig. 4A). Cell treatment with SN-38 did not result in Chk2 phosphorylation (data not shown). Cell cycle analysis at 24 h after treatment showed a dose-dependent cell accumulation at the G2/M phase (Fig. 4B for HCT116+3 Babe and Sip cells; data not shown for HCT116 Babe and Sip cells). At 72 h after treatment the percentage of cells in the G2/M phase decreased in both Babe cell lines, whereas both PARP-1 silenced cells underwent G2/M arrest (Fig. 4B for HCT116+3 Babe and SiP cells; data not shown for HCT116 Babe and SiP cells).

In HCT116 MLH1-deficient Babe and SiP clones treatment with SN-38 induced a dose-dependent and marked increase of p53 phosphorylation and of the percentage of apoptotic cells; this effect was more pronounced in PARP-1 silenced cells (Fig. 5). On the other hand, in HCT116+3 Babe and SiP cells only marginal level of p53 phosphorylation and apoptosis were detected (Fig. 5). Treatment of HCT116+3 Babe and SiP cells with a non-toxic concentration of the Chk1 inhibitor UCN-01 reduced the G2/M cell accumulation (data not shown) favouring apoptosis induction by SN-38 in both cell lines (Fig. 5B).

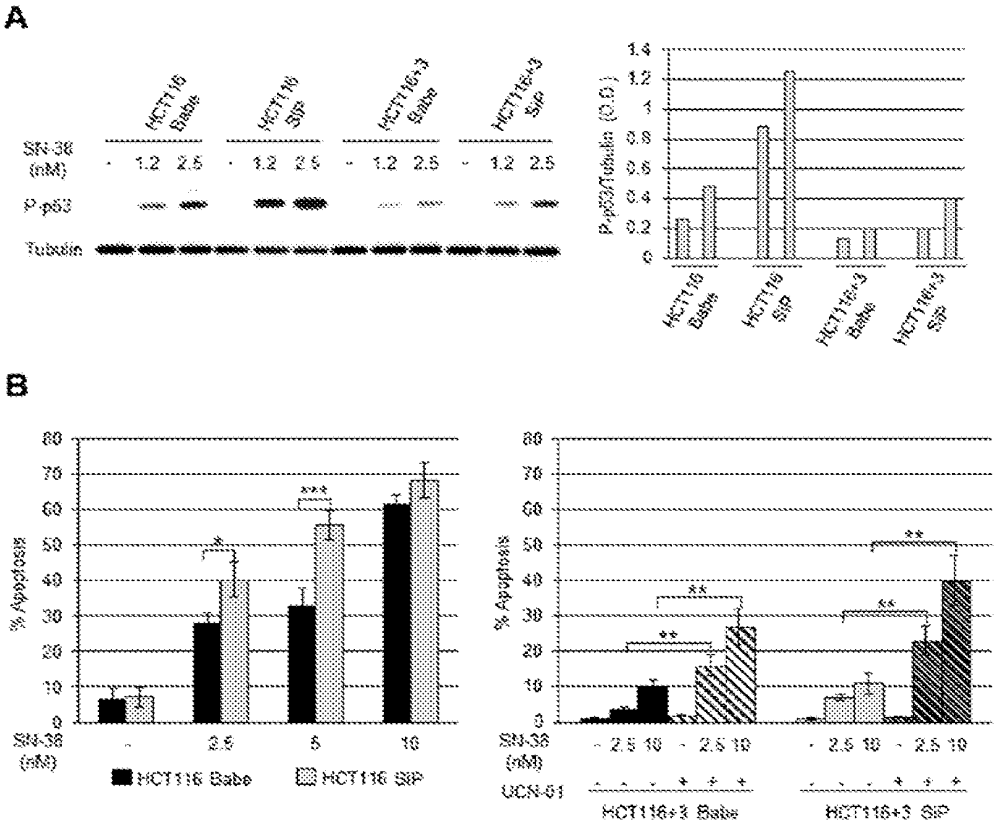

Figure 5. Analysis of p53 activation (A) and apoptosis induction (B) in MLH1-deficient HCT116 Babe and SiP cells treated with SN-38. (A) HCT116 and HCT116+3 Babe or SiP cells were treated with the indicated concentrations of SN-38 for 6 h; cell lysates were electrophoresed and analysed for the expression of phosphorylated p53 (P-p53) or tubulin. Histograms represent the ratios between the OD of phospho-p53 in SN-38 treated groups and tubulin. The results are representative of one out of two experiments with similar results. (B) Apoptosis was analysed by flow cytometry in HCT116 and HCT116+3 Babe or SiP cells at 72 h after treatment with SN-38. In the case of HCT116+3 Babe and SiP cells SN-38 was also tested in combination with 100 nM UCN-01 (striped columns). Histograms represent the mean percentage values (± SD) of apoptotic cells from three independent experiments. The results of statistical analysis by Student's *t*-test of the differences in sensitivity to apoptosis induction are as follows: left histogram, 2.5 nM SN-38 HCT116 Babe vs. HCT116 SiP, *P=0.02; 5 nM SN-38, HCT116 Babe vs. HCT116 SiP, ***P=0.004; 10 nM SN-38 HCT116 Babe vs. HCT116 SiP; NS, not significant; right histogram, HCT116+3 Babe, 2.5 nM SN-38 vs. 2.5 nM SN-38+UCN-01, **P=0.002; 10 nM SN-38 vs. 10 nM SN-38+UCN-01, **P=0.005; HCT116+3 SiP, 2.5 nM SN-38 vs. 2.5 nM SN-38+UCN-01, **P=0.002; 10 nM SN-38 vs. 10 nM SN-38+UCN-01, **P=0.003.

Discussion

Germline mutations of MMR genes or epigenetic inactivation of MLH1 may be present in CRC and influence the clinical behavior (28,29). While the lack of function of MLH1 and the presence of microsatellite instability have been associated with lower response to 5-FU (30), the predictive impact of the MLH1 functional status for irinotecan, as single agent or in combination with PARPi, needs to be clarified. Using a panel of human colon cancer cell lines derived from HCT116 and characterized by different patterns of MLH1, Top1 and PARP-1 expression, we investigated the influence of these proteins on colon cancer cell response to irinotecan, as single agent or in combination with PARPi. To study the impact of MLH1 expression on colon cancer cell chemosensitivity we used cell lines in which the defective gene product was restored by chromosome transfer or by transfection of the corresponding wild-type cDNA. The results indicated that MLH1-proficiency and low Top1 expression resulted in reduced sensitivity to irinotecan, but pharmacological inhibition of PARP activity or silencing of PARP-1 gene increased the susceptibility of colon cancer cells to the Top1 poison. Interestingly, cells with lower levels of PARP-1 protein could still be sensitized to irinotecan by PARPi.

DNA damage consequent to Top1 poisoning derives from stabilization of the cleavable complex formed by Top1 and DNA, with formation of a transient single strand DNA nick. When the stabilized drug-DNA-Top1 complex collides with replication or transcription machineries, it leads to replication fork stalling and eventually DSB. Before DSB generation, the repair of DNA damage induced by Top1 inhibitors includes proteasomal degradation of Top1, hydrolysis of the phosphodiester bond, between the 3'-end of DNA and a tyrosine residue of Top1, by the tyrosyl DNA phosphodiesterase-1 and removal of Top1-cleavable complex by the endonucleases XPF-ERCC1 (2). In MLH1-proficient cells SN-38 induced a lower level of DNA damage with respect to MLH1-deficient cells, as evidenced by the weak induction of γ-H2AX and p53 phosphorylation. The presence of MLH1 contributed to induce prompt Chk1 phosphorylation, restoring G2/M cell cycle checkpoint and repair of DNA damage. On the contrary, in the absence of MLH1, HCT116 cells showed minor Chk1

phosphorylation and underwent apoptosis. Actually, inhibition of Chk1 by UCN-01 decreased G2/M cell accumulation induced by the Top1 poison in MLH1-proficient cells and triggered apoptosis. Treatment with SN-38 did not result in Chk2 phosphorylation (data not shown) likely for the presence of mutations in the Mre11 gene. The consequent lack of Mre11 protein (31) and very low expression of RAD50 cause destabilization of the MRN complex, which is required for Chk2 phosphorylation by ATM in response to DSB (32).

Low levels of Top1 protein are known to confer a moderate level of resistance to camptothecins due to the formation of a small amount of DNA-Top1 cleavable complexes (2). Since HCT116+3 cells expressed lower level of Top1 protein with respect to HCT116 cells, this might have contributed to the poorer response of HCT116+3 cells to irinotecan. In fact, the sensitivity to SN-38 of HCT116 1-2 cells transfected with the MLH1 cDNA differed to a lesser extent from that of HCT116 control cells, which showed comparable Top1 expression. Our data indicated that when a defective gene product is replaced by chromosome transfer the expression of other proteins involved in tumor drug response may change and influence tumor chemosensitivity.

Pharmacological inhibition or stable gene silencing of PARP-1 increased sensitivity to SN-38 both in MLH1-proficient and -deficient cells. Notably, the enhancing effect deriving from abrogation of PARP-1 function was particularly evident in the HCT116+3 derived line and translated into an increased *in vivo* response of HCT116+3 SiP to irinotecan. Tumor chemosensitization mediated by lack of function of PARP-1 is likely due to the decrease of DNA repair mediated by the BER system. PARP-1 contributes to the repair of Top1 mediated damage promoting the recruitment of XRRC1 and tyrosyl DNA phosphodiesterase-1 with removal of Top1 from DNA (5). These results are consistent with the reported higher toxicity of Top1 poisons in cervical cancer or in melanoma cells stably silenced for PARP-1 (33,34). On the other hand, the transient silencing of PARP-1 in an ovarian cancer cell line did not result in chemosensitisation to Top1 poisons (35). During the preparation of this study, a report was published indicating that the PARPi veliparib synergized with irinotecan *in vitro* in HCT116 cells (36). In our study we showed, for the first time, that the chemosensitising effect induced by pharmacological inhibition of PARP or by PARP-1 gene silencing can be achieved even in the presence of low Top1 levels and in the case of both MLH1-proficient and MLH1-deficient tumors.

In PARP-1 silenced cells devoid also of MLH1 expression SN-38 induced more DNA damage than in MLH1-proficient SiP cells, causing a remarkable p53 phosphorylation and apoptosis induction. In MLH1-deficient SiP cells the Top1 poison also induced a delayed (compared with MLH1-proficient SiP) but robust Chk1 phosphorylation, suggesting that MLH1 might influence the kinetics of induction rather than the extent of Chk1 post-translational modifications.

Interestingly, the low levels of PARP-1 expression in HCT116+3 cells did not hamper the chemosensitising effect mediated by the PARPi GPI 15427 in combination with SN-38. These results are different from those obtained in MEF lines derived from PARP-1$^{-/-}$ mice that could not be sensitized to topotecan by the PARPi veliparib (35). However, in MEF cells PARP-1 was totally lacking, whereas in HCT116+3 cells PARP-1, even though expressed at lower levels than in HCT116 cells, was sufficient to allow the chemosensitising effect by GPI 15427.

In conclusion, these data indicated that MLH1, together with low levels of Top1, contributes to colon cancer resistance to Top1 poisons. Remarkably, inhibition of PARP-1 function always increases the antitumor activity of irinotecan even in the presence of low PARP-1 expression.

Acknowledgements

This study was supported by a grant from the Italian Ministry of Education and Research, 'Programmi di ricerca scientifica di Rilevante Interesse Nazionale' (PRIN) project to L.T. A.M. is recipient of a fellowship from 'Regione Lazio-Filas'.

References

1. Davies JM and Goldberg RM: Treatment of metastatic colorectal cancer. Semin Oncol 38: 552-560, 2011.
2. Alagoz M, Gilbert DC, El-Khamisy S and Chalmers AJ: DNA repair and resistance to topoisomerase I inhibitors: mechanisms, biomarkers and therapeutic targets. Curr Med Chem 19: 3874-3885, 2012.
3. Miknyoczki SJ, Jones-Bolin S, Pritchard S, Hunter K, Zhao H, Wan W, Ator M, *et al*: Chemopotentiation of temozolomide, irinotecan and cisplatin activity by CEP-6800, a poly(ADP-ribose) polymerase inhibitor. Mol Cancer Ther 2: 371-382, 2003.
4. Calabrese CR, Almassy R, Barton S, Batey MA, Calvert AH, Canan-Koch S, Durkacz BW, *et al*: Anticancer chemosensitization and radiosensitization by the novel poly(ADP-ribose) polymerase-1 inhibitor AG14361. J Natl Cancer Inst 96: 56-67, 2004.
5. Smith LM, Willmore E, Austin CA and Curtin NJ: The novel poly(ADP-Ribose) polymerase inhibitor, AG14361, sensitizes cells to topoisomerase I poisons by increasing the persistence of DNA strand breaks. Clin Cancer Res 11: 8449-8457, 2005.
6. Tentori L, Leonetti C, Scarsella M, Muzi A, Mazzon E, Vergati M, Forini O, *et al*: Inhibition of poly(ADP-ribose) polymerase prevents irinotecan-induced intestinal damage and enhances irinotecan/temozolomide efficacy against colon carcinoma. FASEB J 20: 1709-1711, 2006.
7. Daniel RA, Rozanska AL, Thomas HD, Mulligan EA, Drew Y, Castelbuono DJ, Hostomsky Z, *et al*: Inhibition of poly(ADP-ribose) polymerase-1 enhances temozolomide and topotecan activity against childhood neuroblastoma. Clin Cancer Res 15: 1241-1249, 2009.
8. Schreiber V, Dantzer F, Ame JC and de Murcia G: Poly(ADP-ribose): novel functions for an old molecule. Nat Rev Mol Cell Biol 7: 517-528, 2006.
9. Malanga M and Althaus FR: Poly(ADP-ribose) reactivates stalled DNA topoisomerase I, induces DNA strand break resealing. J Biol Chem 279: 5244-5248, 2004.
10. Leonetti C, Biroccio A, Graziani G and Tentori L: Targeted therapy for brain tumours: role of PARP inhibitors. Curr Cancer Drug Targets 12: 218-236, 2012.
11. Martin SA, Lord CJ and Ashworth A: Therapeutic targeting of the DNA mismatch repair pathway. Clin Cancer Res 16: 5107-5113, 2010.
12. D'Atri S, Tentori L, Lacal PM, Graziani G, Pagani E, Benincasa E, Zambruno G, *et al*: Involvement of the mismatch repair system in temozolomide-induced apoptosis. Mol Pharmacol 54: 334-341, 1998.
13. Tentori L and Graziani G: Recent approaches to improve the antitumor efficacy of temozolomide. Curr Med Chem 16: 245-257, 2009.
14. Fedier A, Schwarz VA, Walt H, Carpini RD, Haller U and Fink D: Resistance to topoisomerase poisons due to loss of DNA mismatch repair. Int J Cancer 93: 571-576, 2001.
15. Jacob S, Aguado M, Fallik D and Praz F: The role of the DNA mismatch repair system in the cytotoxicity of the topoisomerase inhibitors camptothecin and etoposide to human colorectal cancer cells. Cancer Res 61: 6555-6562, 2001.

16. Magrini R, Bhonde MR, Hanski ML, Notter M, Scherübl H, Boland CR, Zeitz M and Hanski C: Cellular effects of CPT-11 on colon carcinoma cells: dependence on p53 and hMLH1 status. Int J Cancer 101: 23-31, 2002.
17. Fallik D, Borrini F, Boige V, Viguier J, Jacob S, Miquel C, Sabourin JC, *et al*: Microsatellite instability is a predictive factor of the tumor response to irinotecan in patients with advanced colorectal cancer. Cancer Res 63: 5738-5744, 2003.
18. Papouli E, Cejka P and Jiricny J: Dependence of the cytotoxicity of DNA-damaging agents on the mismatch repair status of human cells. Cancer Res 64: 3391-3394, 2004.
19. Bhonde MR, Hanski ML, Stehr J, Jebautzke B, Peiró-Jordán R, Fechner H, Yokoyama KK, *et al*: Mismatch repair system decreases cell survival by stabilizing the tetraploid G1 arrest in response to SN-38. Int J Cancer 126: 2813-2825, 2010.
20. Martin LP, Hamilton TC and Schilder RJ: Platinum resistance: the role of DNA repair pathways. Clin Cancer Res 14: 1291-1295, 2008.
21. Papadopoulos N, Nicolaides NC, Wei YF, Ruben SM, Carter KC, Rosen CA, Haseltine WA, *et al*: Mutation of a mutL homolog in hereditary colon cancer. Science 263: 1625-1629, 1994.
22. Koi M, Umar A, Chauhan DP, Cherian SP, Carethers JM, Kunkel TA and Boland CR: Human chromosome 3 corrects mismatch repair deficiency and microsatellite instability and reduces N-methyl-N'-nitro-N-nitrosoguanidine tolerance in colon tumor cells with homozygous hMLH1 mutation. Cancer Res 54: 4308-4312, 1994.
23. Vernole P, Muzi A, Volpi A, Terrinoni A, Dorio AS, Tentori L, Shah GM and Graziani G: Common fragile sites in colon cancer cell lines: role of mismatch repair, RAD51 and poly(ADP-ribose) polymerase-1. Mutat Res 712: 40-48, 2011.
24. Tentori L, Leonetti C, Scarsella M, D'Amati G, Vergati M, Portarena I, Xu W, *et al*: Systemic administration of GPI 15427, a novel poly(ADP-ribose) polymerase-1 inhibitor, increases the antitumor activity of temozolomide against intracranial melanoma, glioma, lymphoma. Clin Cancer Res 9: 5370-5379, 2003.
25. Yamane K, Taylor K and Kinsella TJ: Mismatch repair-mediated G2/M arrest by 6-thioguanine involves the ATR-Chk1 pathway. Biochem Biophys Res Commun 318: 297-302, 2004.
26. Yoshioka K, Yoshioka Y and Hsieh P: ATR kinase activation mediated by MutSalpha and MutLalpha in response to cytotoxic O6-methylguanine adducts. Mol Cell 22: 501-510, 2006.
27. Adamson AW, Beardsley DI, Kim WJ, Gao Y, Baskaran R and Brown KD: Methylator-induced, mismatch repair-dependent G2 arrest is activated through Chk1 and Chk2. Mol Biol Cell 16: 1513-1526, 2005.
28. Marra G and Jiricny J: DNA mismatch repair and colon cancer. Adv Exp Med Biol 570: 85-123, 2005.
29. Damia G and D'Incalci M: Genetic instability influences drug response in cancer cells. Curr Drug Targets 11: 1317-1324, 2010.
30. Sinicrope FA, Foster NR, Thibodeau SN, Marsoni S, Monges G, Labianca R, Kim GP, *et al*: DNA mismatch repair status and colon cancer recurrence and survival in clinical trials of 5-fluorouracil-based adjuvant therapy. J Natl Cancer Inst 103: 863-875, 2011.
31. Garner KM and Eastman A: Variations in Mre11/Rad50/Nbs1 status and DNA damage-induced S-phase arrest in the cell lines of the NCI60 panel. BMC Cancer 206: 1-13, 2011.
32. Takemura H, Rao VA, Sordet O, Furuta T, Miao ZH, Meng L, Zhang H and Pommier Y: Defective Mre11-dependent activation of Chk2 by ataxia telangiectasia mutated in colorectal carcinoma cells in response to replication-dependent DNA double strand breaks. J Biol Chem 281: 30814-30823, 2006.
33. Tentori L, Muzi A, Dorio AS, Scarsella M, Leonetti C, Shah GM, Xu W, *et al*: Pharmacological inhibition of poly(ADP-ribose) polymerase (PARP) activity in PARP-1 silenced tumour cells increases chemosensitivity to temozolomide and to a N3-adenine selective methylating agent. Curr Cancer Drug Targets 10: 368-383, 2010.
34. D'Onofrio G, Tramontano F, Dorio AS, Muzi A, Maselli V, Fulgione D, Graziani G, *et al*: Poly(ADP-ribose) polymerase signaling of topoisomerase 1-dependent DNA damage in carcinoma cells. Biochem Pharmacol 81: 194-202, 2011.
35. Patel AG, Flatten KS, Schneider PA, Dai NT, McDonald JS, Poirier GG and Kaufmann SH: Enhanced killing of cancer cells by poly(ADP-ribose) polymerase inhibitors and topoisomerase I inhibitors reflects poisoning of both enzymes. J Biol Chem 287: 4198-4210, 2012.
36. Davidson D, Wang Y, Aloyz R and Panasci L: The PARP inhibitor ABT-888 synergizes irinotecan treatment of colon cancer cell lines. Invest New Drugs 31: 461-468, 2013.

UNITED STATES PATENT AND TRADEMARK OFFICE

UNITED STATES DEPARTMENT OF COMMERCE
United States Patent and Trademark Office
Address: COMMISSIONER FOR PATENTS
P.O. Box 1450
Alexandria, Virginia 22313-1450
www.uspto.gov

APPLICATION NO.	FILING DATE	FIRST NAMED INVENTOR	ATTORNEY DOCKET NO.	CONFIRMATION NO.
14/964,571	12/09/2015	ELIEL BAYEVER	263266-411575	1063

153749 7590 06/12/2019

McNeill Baur PLLC/Ipsen
Ipsen Bioscience, Inc.
125 Cambridge Park Drive
Suite 301
Cambridge, MA 02140

EXAMINER	
BAEK, BONG-SOOK	

ART UNIT	PAPER NUMBER
1611	

NOTIFICATION DATE	DELIVERY MODE
06/12/2019	ELECTRONIC

Please find below and/or attached an Office communication concerning this application or proceeding.

The time period for reply, if any, is set in the attached communication.

Notice of the Office communication was sent electronically on above-indicated "Notification Date" to the following e-mail address(es):

docketing@mcneillbaur.com
eofficeaction@appcoll.com
patents.us@ipsen.com

Office Action Summary	Application No. 14/964,571	Applicant(s) BAYEVER et al.	
	Examiner BONG-SOOK BAEK	Art Unit 1611	AIA (FITF) Status Yes

-- The MAILING DATE of this communication appears on the cover sheet with the correspondence address --

Period for Reply

A SHORTENED STATUTORY PERIOD FOR REPLY IS SET TO EXPIRE 3 MONTHS FROM THE MAILING DATE OF THIS COMMUNICATION.

- Extensions of time may be available under the provisions of 37 CFR 1.136(a). In no event, however, may a reply be timely filed after SIX (6) MONTHS from the mailing date of this communication.
- If NO period for reply is specified above, the maximum statutory period will apply and will expire SIX (6) MONTHS from the mailing date of this communication.
- Failure to reply within the set or extended period for reply will, by statute, cause the application to become ABANDONED (35 U.S.C. § 133). Any reply received by the Office later than three months after the mailing date of this communication, even if timely filed, may reduce any earned patent term adjustment. See 37 CFR 1.704(b).

Status

1)☑ Responsive to communication(s) filed on 01 May 2018.

☐ A declaration(s)/affidavit(s) under **37 CFR 1.130(b)** was/were filed on _____.

2a)☑ This action is **FINAL.** 2b) ☐ This action is non-final.

3)☐ An election was made by the applicant in response to a restriction requirement set forth during the interview on _____; the restriction requirement and election have been incorporated into this action.

4)☐ Since this application is in condition for allowance except for formal matters, prosecution as to the merits is closed in accordance with the practice under *Ex parte Quayle*, 1935 C.D. 11, 453 O.G. 213.

Disposition of Claims*

5) ☑ Claim(s) 1,8,10 and 15-31 is/are pending in the application.

5a) Of the above claim(s) _____ is/are withdrawn from consideration.

6) ☐ Claim(s) _____ is/are allowed.

7) ☑ Claim(s) 1,8,10 and 15-31 is/are rejected.

8) ☐ Claim(s) _____ is/are objected to.

9) ☐ Claim(s) _____ are subject to restriction and/or election requirement

* If any claims have been determined allowable, you may be eligible to benefit from the **Patent Prosecution Highway** program at a participating intellectual property office for the corresponding application. For more information, please see http://www.uspto.gov/patents/init_events/pph/index.jsp or send an inquiry to **PPHfeedback@uspto.gov.**

Application Papers

10)☐ The specification is objected to by the Examiner.

11)☐ The drawing(s) filed on _____ is/are: a)☐ accepted or b)☐ objected to by the Examiner.

Applicant may not request that any objection to the drawing(s) be held in abeyance. See 37 CFR 1.85(a).

Replacement drawing sheet(s) including the correction is required if the drawing(s) is objected to. See 37 CFR 1.121(d).

Priority under 35 U.S.C. § 119

12)☐ Acknowledgment is made of a claim for foreign priority under 35 U.S.C. § 119(a)-(d) or (f).

Certified copies:

a)☐ All b)☐ Some** c)☐ None of the:

1.☐ Certified copies of the priority documents have been received.

2.☐ Certified copies of the priority documents have been received in Application No. _____.

3.☐ Copies of the certified copies of the priority documents have been received in this National Stage application from the International Bureau (PCT Rule 17.2(a)).

** See the attached detailed Office action for a list of the certified copies not received.

Attachment(s)

1) ☑ Notice of References Cited (PTO-892)

2) ☑ Information Disclosure Statement(s) (PTO/SB/08a and/or PTO/SB/08b) Paper No(s)/Mail Date _____.

3) ☐ Interview Summary (PTO-413) Paper No(s)/Mail Date _____.

4) ☐ Other: _____.

Notice of Pre-AIA or AIA Status

The present application, filed on or after March 16, 2013, is being examined under the first inventor to file provisions of the AIA.

DETAILED ACTION

Status of claims

The amendment filed on Feb. 25 2019 is acknowledged. Claims 2-7, 9, and 11-14 have been canceled and new claims 15-31 have been added. Claims 1, 8, 10, and 15-31 are under examination in the instant office action.

Applicants' arguments, filed on Feb. 25 2019, have been fully considered but they are moot in view of new grounds of rejection necessitated by the amendments (i.e., deleted limitations which change the scope of the patent and new claims). Also, Applicant's submission of an information disclosure statement under 37 CFR 1.97(c) with the fee set forth in 37 CFR 1.17(p) on Feb. 25, 2019 prompted the new ground(s) of rejection presented in this Office action. Rejections and/or objections not reiterated from previous office actions are hereby withdrawn. The following rejections and/or objections are either reiterated or newly applied. They constitute the complete set presently being applied to the instant application.

Claim Rejections - 35 USC § 112 (b)

(N***ew grounds of rejection necessitated by new claim)***

The following is a quotation of 35 U.S.C. 112(b):

> (B) CONCLUSION.—The specification shall conclude with one or more claims particularly pointing out and distinctly claiming the subject matter which the inventor or a joint inventor regards as the invention.

The following is a quotation of 35 U.S.C. 112 (pre-AIA), second paragraph:

> The specification shall conclude with one or more claims particularly pointing out and distinctly claiming the subject matter which the applicant regards as his invention.

Claim 20 is rejected under 35 U.S.C. 112(b) or 35 U.S.C. 112 (pre-AIA), second paragraph, as being indefinite for failing to particularly point out and distinctly claim the subject matter which the inventor or a joint inventor, or for pre-AIA the applicant regards as the invention.

New Claim 20 recites the limitation "the sucrose octasulfate salt" in line 3. There is insufficient antecedent basis for this limitation in the claim.

Claim Rejections - 35 USC § 112 (d)

(N***ew grounds of rejection necessitated by new claims)***

The following is a quotation of 35 U.S.C. 112(d):

> (d) REFERENCE IN DEPENDENT FORMS.—Subject to subsection (e), a claim in dependent form shall contain a reference to a claim previously set forth and then specify a further limitation of the subject matter claimed. A claim in dependent form shall be construed to incorporate by reference all the limitations of the claim to which it refers.

The following is a quotation of 35 U.S.C. 112 (pre-AIA), fourth paragraph:

> Subject to the [fifth paragraph of 35 U.S.C. 112 (pre-AIA)], a claim in dependent form shall contain a reference to a claim previously set forth and then specify a further limitation of the subject matter claimed. A claim in dependent form shall be construed to incorporate by reference all the limitations of the claim to which it refers.

Claims 23 and 30-31 are rejected under 35 U.S.C. 112(d) or 35 U.S.C. 112 (pre-AIA), 4th paragraph, as being of improper dependent form for failing to further limit the subject matter of the claim upon which it depends, or for failing to include all the limitations of the claim upon which it depends.

New claims 23 and 30-31 recite "a first dose of liposomal irinotecan to the patient on day 1 of a first 2-week cycle and administering subsequent doses on the first day of each subsequent cycle ± 2 days". When the first day of the second 2-week cycle is 15th day from day 1 of the first 2-week cycle, 15th day ± 2 days encompasses 13th, 14th, 16th, and 17th day. However, administering the subsequent dose of the second cycle on 13th, 14th, 16th, or 17th day does not meet once every two week as recited in claim 1, 8, and 10 from which they depend. As such, claims 23 and 30-31 fail to further limit the subject matter of the claims from which they depend.

Applicant may cancel the claim, amend the claim to place the claim in proper dependent form, rewrite the claim in independent form, or present a sufficient showing that the dependent claim complies with the statutory requirements.

Claim Rejections - 35 USC § 103

(N***ew grounds of rejection necessitated by the amendments and IDS)***

The following is a quotation of 35 U.S.C. 103 which forms the basis for all obviousness rejections set forth in this Office action:

> A patent for a claimed invention may not be obtained, notwithstanding that the claimed invention is not identically disclosed as set forth in section 102 of this title, if the differences between the claimed invention and the prior art are such that the claimed invention as a whole would have been obvious before the effective filing date of the claimed invention to a person having ordinary skill in the art to which the claimed invention pertains. Patentability shall not be negated by the manner in which the invention was made.

The factual inquiries set forth in *Graham v. John Deere Co.*, 383 U.S. 1, 148 USPQ 459 (1966), that are applied for establishing a background for determining obviousness under 35 U.S.C. 103 are summarized as follows:

1. Determining the scope and contents of the prior art.

2. Ascertaining the differences between the prior art and the claims at issue.

3. Resolving the level of ordinary skill in the pertinent art.

4. Considering objective evidence present in the application indicating obviousness or nonobviousness.

Claims 1, 8, 10, 17-21, 23-27, and 30-31 are rejected under 35 U.S.C. 103 as being unpatentable over US 20070110798 (cited in the IDS filed on 2/25/2019) in view of Hayashi *et al.* (Breast Cancer, 20:131-136, 2013, Epub, Nov. 29, 2011, cited in the IDS filed on 2/25/2019) in further view of Chen *et al.* (Journal of Clinical Oncology 26, no. 15_suppl, May 20 2008) 2565-2565).

US 20070110798 discloses unilamellar liposomes (lipid bilayer vesicles) loaded with CPT-11 (irinotecan as a hydrochloride trihydrate salt) in a gelated or precipitated state , yielding a final diameter of 95-110 nm and the drug/lipid ratio of about 500 mg/mmol phospholipid, wherein liposomes with entrapped triethylammonium sucrose octasulfate (0.65 M TEA, pH 6.4, osmolality 485 mmol/kg) and lipid composition of 1,2-Distearoyl-SN-phosphatidylcholine (DSPC), Cholesterol, and N-(omega-methoxy-poly(ethylene glycol)-oxycarbonyl)-1,2-distearoylphosphatidyl ethanolamine (PEG-DSPE) in a molar ratio of 3:2:0.015 were prepared (abstract, [0003], [0081], [0172], [0178], [0313], and [0327]).

US 20070110798 further discloses that the liposome composition of the present invention can be administered in any way which is medically acceptable which may depend on the condition or injury being treated and possible administration routes include injections, by parenteral routes such as intramuscular, subcutaneous, intravenous, intraarterial, intraperitoneal, intraarticular, intraepidural, intrathecal, or others ([0134]).

US 20070110798 also discloses that the liposomal composition comprising a camptothecin compound such as irinotecan (CPT-11) has an anticancer activity at least two times, four times, or

ten times higher than the camptothecin compound similarly administered in the absence of the composition, while the toxicity of the composition does not exceed, is at least two times, or at least four times lower than the toxicity of the camptothecin compound similarly administered in the absence of the composition ([0010]). US 20070110798 further discloses antitumor efficacy of CPT-11 liposomes (drug/phospholipid ratio 192 mg/mmol; average liposome size 86.8 nm) in the model of human breast carcinoma BT-474 and U87 tumors implanted within brain wherein greater anti-tumor activity with CPT-11 liposomes treatment were shown compared with free CPT-11 ([0184], [0185], [0330] and Fig. 3 and 49). US 20070110798 further discloses the liposome formulation of CPT-11 showed extended blood life, sustained release characteristics, and increased antitumor activity in the studied tumor model without an appreciable increase in toxicity ([0187] and Fig, 4).

In addition, US 20070110798 discloses that the mean residence time of the liposomal drug in the healthy brain was at comparable infusate concentration (3 mg/mL) 24 times higher than that of the free CPT-11 (as a hydrochloride trihydrate salt, dissolved) and the mean residence time of the drug in the tumor tisse, at equal drug concentration in the infusate, was 4 times higher than in the normal brain ([0327]).

While US 20070110798 discloses antitumor activity of liposomal irinotecan in the model of human breast carcinoma and brain tumor, the reference does not specifically disclose administering one every two weeks at a dose of 60 mg/m^2 for the treatment of breast cancer with active brain metastasis or HER2 negative metastatic breast cancer.

Hyashi *et al.* disclose phase II study of bi-weekly irinotecan for patients with previously treated HER2-negative metastatic breast cancer (MBC) wherein eligible patients were HER2-negative, had a performance status of 0 to 2, and had been treated previously with either

anthracyclines or taxanes for MBC (title and abstract). Hyashi *et al.* further disclose that patients received irinotecan intravenously at 150 mg/ m^2 on days 1 and 15 every 4 weeks (once every two weeks) and biweekly administration of 150 mg/ m^2 irinotecan was feasible for patients with MBC treated previously with anthracyclines or taxanes (abstract).

Chen *et al*. discloses phase I study of liposome encapsulated irinotecan (PEP02), which is a novel nanoparticle liposome formulation of irinotecan aiming to enhance tumor localization and improve pharmacokinetic properties of irinotecan and its active metabolite-SN38, in advanced refractory solid tumor patients wherein PEP02 was given as 90 mins i.v. infusion, repeated every 3 weeks and the doses would have been escalated from 60, 120, 180 to 240 mg/m2 in a single-patient cohort accelerated titration design (Title, Methods, and Results).

It would have been prima facie obvious to one of ordinary skill in the art before the effective filing date of the claimed invention to use liposomal irinotecan taught by US 20070110798 for treating breast cancer with active brain metastasis or HER2 negative metastatic breast cancer because anti-tumor efficacies of liposomal irinotecan in both breast and brain cancer models are already disclosed by US 20070110798 and irinotecan was taught to be effective for treating metastatic breast cancer such as HER2-negative metastatic breast cancer as evidenced by Hyashi *et al.* Also, US 20070110798 teaches that liposomal irinotecan has extended blood life, sustained release characteristics, increased antitumor activity in breast cancer model, and higher residence time in brain without an appreciable increase in toxicity compared with free irinotecan. Thus, one of ordinary skill in the art would have been motivated to use the liposomal irinotecan taught by US 20070110798 in the treatment of HER2-negative metastatic breast cancer or breast cancer with active brain metastasis on the reasonable expectation that it would be more effective in the treatment of both cancers than free irinotecan.

With regard to the step of identifying a tumor lesion in the patient recited in the claim 10, implicitly in any disclosure of giving a treatment to a patient with a cancer is first determining that the patient has the tumor lesion. Therefore, the subject under treatment should have been identified prior to applying the cancer treatment. A person of ordinary skill in the art is a healthcare provider which first identify patients with a tumor lesion and then treats them with an appropriate drug. This is what a person of ordinary skill in the corresponding art normally does.

As to the dose of 60 mg/m^2, Hyashi *et al.* already disclose intravenously administering free irinotecan at 150 mg/m^2 once every two weeks in the treatment of HER2-negative metastatic breast cancer and US 20070110798 discloses that the liposomal composition comprising irinotecan (CPT-11) has an anticancer activity at least two times, four times, or ten times higher than free irinotecan (not in liposomal formulation). Thus, one of ordinary skill in the art would have been motivated to use liposomal irinotecan at a dose less than half the dose of free irinotecan taught by Hyashi *et al.* (e.g., less than 75 mg/ m^2) on the reasonable expectation that liposomal irinotecan at a dose less than half the dose of free irinotecan would provide anticancer activity comparable to free irinotecan. In addition, Chen *et al.* teaches titration of the dose of liposomal irinotecan (PEP02) from 60, 120, 180 to 240 mg/ m^2. Thus, it would have been prima facie obvious to one of ordinary skill in the art before the effective filing date of the claimed invention to optimize the dose of the liposomal irinotecan for getting desired effects based on the effective dosing ranges disclosed in the prior art in combination. Also, the claimed range falls within the range disclose in the prior art in combination. In the case where the claimed ranges "overlap or lie inside ranges disclosed by the prior art" a prima facie case of obviousness exists. *In re Wertheim*, 541 F.2d 257, 191 USPQ 90 (CCPA 1976). Furthermore, "[A] prior art reference that discloses a range encompassing a somewhat narrower claimed range

is sufficient to establish a prima facie case of obviousness." *In re Peterson*, 315 F.3d 1325, 1330, 65 USPQ2d 1379, 1382-83 (Fed. Cir. 2003). In addition, it is well-established that merely selecting proportions and ranges is not patentable absent a showing of criticality. *In re Becket*, 33 USPQ 33; *In re Russell*, 169 USPQ 426. "[W]here the general conditions of a claim are disclosed in the prior art, it is not inventive to discover the optimum or workable ranges by routine experimentation." *In re Aller*, 220 F.2d 454, 456, 105 USPQ 233, 235 (CCPA 1955); see also Peterson, 315 F.3d at 1330, 65 USPQ2d at 1382 ("The normal desire of scientists or artisans to improve upon what is already generally known provides the motivation to determine where in a disclosed set of percentage ranges is the optimum combination of percentages.")

As to new claims 24-25, US 20070110798 does not specifically disclose that the patient has failed at least one prior platinum- based chemotherapy regimen, has failed prior treatment with gemcitabine, and/or has become resistant to gemcitabine. However, Hyashi *et al.* disclose that irinotecan was effective for patients previously treated with other chemotherapeutic agents such as anthracyclines or taxanes for MBC. Thus, one of ordinary skill in the art would have been motivated to use the liposomal irinotecan taught by US 20070110798 as an alternative treatment for patients who failed at least one prior platinum-based chemotherapy regimen or gemcitabine, and/or has become resistant to gemcitabine. It would have obvious to use alternative cancer treatment for MBC such as liposomal irinotecan taught by US 20070110798 and Hyashi *et al.* when the other existing anticancer therapy was not working because irunotecan was taught to be effective for those cancers. This is what a person of ordinary skill in the corresponding art normally does.

Claims 15-16 are rejected under 35 U.S.C. 103 as being unpatentable over US 20070110798 (cited in the IDS filed on 2/25/2019) in view of Hayashi *et al.* (Breast Cancer, 20:131-136, 2013, Epub, Nov. 29, 2011, cited in the IDS filed on 2/25/2019) and Chen *et al.* (Journal of Clinical Oncology 26, no. 15_suppl, May 20 2008, 2565-2565), in further view of US 2007/0219268.

US 20070110798, Hayashi *et al. and* Chen *et al.* as applied *supra* are herein applied for the same teachings in their entirety.

US 20070110798 does not specifically teach pre-medicating with at least one anti-emetic such as 5-HT3 antagonist as recited in new claims 15-16.

However, it was well known in the art that at least one anti-emetic such as 5-HT3 antagonist is pre-medicated before the treatment with a chemotherapeutic agent including irinotecan for preventing vomiting (abstract, [0119] and [0142]). Thus, it would have been prima facie obvious to one of ordinary skill in the art before the effective filing date of the claimed invention to pre-medicate with at least one anti-emetic such as 5-HT3 antagonist prior to administering liposomal irinotecan as taught by US 20070110798 in the treatment of breast cancer with active brain metastasis or HER2 positive breast cancer because it was well known practice in the chemotherapy as evidenced by US 20070110798 and vomiting is a known adverse event related with irinotecan treatment as evidenced by Hayashi *et al.* (see p134, Toxicity section and Table 2). One of ordinary skill in the art would have been motivated to do so for preventing vomiting caused by anti-cancer treatment.

Claims 22 and 28-29 are rejected under 35 U.S.C. 103 as being unpatentable over US 20070110798 (cited in the IDS filed on 2/25/2019) in view of Hayashi *et al.* (Breast Cancer,

20:131-136, 2013, Epub, Nov. 29, 2011, cited in the IDS filed on 2/25/2019) and Chen *et al.* (Journal of Clinical Oncology 26, no. 15_suppl, May 20 2008, 2565-2565), in further view of US 2014/0170075 (prior art of record).

US 20070110798, Hayashi *et al. and* Chen *et al.* as applied *supra* are herein applied for the same teachings in their entirety.

US 20070110798 does not specifically teach administering a ferumoxytol infusion followed by an MRI scan prior to treatment with the liposomal irinotecan as recited in claims 22 and 28-29.

US 2014/0170075 teaches a method for selecting and providing pharmaceutical treatment to a patient for a localized infectious, inflammatory, or neoplastic condition, the method comprising identifying one or more locations of infection, inflammation or neoplasia in a patient, and subsequently, obtaining at least one contrast-enhanced MRI image of a first location of the one or more locations, and subsequently, selecting an anti-infective, anti-inflammatory, or anti-neoplastic pharmaceutical agent and treating the patient with the selected pharmaceutical agent, wherein the contrast agent is ferumoxytol (FMX) which is intravenously administered at 5 mg/kg up to 510 mg/kg and wherein the pharmaceutical agent is a liposomal anti-neoplastic agent (abstract, [0019], [0020]claims 8-13). US 2014/0170075 also teaches that the liposomal therapeutic agent is MM-398 (irinotecan sucroseoctasulfate liposome injection) and the tumor is a non-small cell lung cancer (NSCLC) tumor, a triple negative breast cancer (TNBC) tumor, a colorectal cancer (CRC) tumor, a pancreatic cancer tumor, a small cell lung cancer tumor, a gastric cancer tumor, a cervical cancer tumor, or Ewing's sarcoma ([0068] and claims 14-16). US 2014/0170075 teaches that as FMX has been demonstrated to be safe for intravenous administration to patients and is shown herein not to interfere with nanoliposome therapies if

used as an imaging agent, even within 1-4 hours prior to administration of nanoliposomal therapeutics, these results indicate that FMX MRI allows for selection patients who will (or will not) benefit from nanoliposomal therapy ([0105]). US 2014/0170075 further teaches that patients identified as having sites of pathology that are predicted to exhibit nanoparticle accumulation would be considered more likely to respond to nanoparticulate therapeutic agents and patients identified as having sites of pathology that are predicted not to exhibit nanoparticle accumulation would be considered less likely to respond to nanoparticulate therapeutic agents and treating patients in accordance with such identifications would avoid the administration of sub-optimal therapeutic treatments to patients in need of therapy ([0011]). The reference specifically discloses a human clinical trial (ClinicalTrials.gov Identifier: NCT01770353) wherein patients with advanced solid tumors and multiple metastases were injected with FMX at 5 mg/kg and then were infused with 80 mg/m^2 MM-398 and shows that the patents have tumor lesion with FMX uptake (see[0135], [0139], and Examples 9-10 and Figs. 6-8).

It would have been prima facie obvious to one of ordinary skill in the art before the effective filing date of the claimed invention to administer ferumoxytol infusion followed by an MRI scan prior to treatment with the liposomal irinotecan because US 2014/0170075 teaches that treatment with FMX followed by MRI prior to administration of nanoliposomal therapeutics such as liposomal irinotecan allows for selection patients who will (or will not) benefit from nanoliposomal therapy and identifies as having sites of pathology that are predicted to exhibit nanoparticle accumulation. Thus, one of ordinary skill in the art would have been motivated to do so on the reasonable expectation that treating patients in accordance with such identifications would avoid the administration of sub-optimal therapeutic treatments to patients in need of therapy as taught by US 2014/0170075.

Conclusion

No claims are allowed.

Applicant's amendment necessitated the new ground(s) of rejection presented in this Office action. Also, Applicant's submission of an information disclosure statement under 37 CFR 1.97(c) with the fee set forth in 37 CFR 1.17(p) on May 30, 2013 prompted the new ground(s) of rejection presented in this Office action. Accordingly, **THIS ACTION IS MADE FINAL**. See MPEP § 706.07(a). Applicant is reminded of the extension of time policy as set forth in 37 CFR 1.136(a).

A shortened statutory period for reply to this final action is set to expire THREE MONTHS from the mailing date of this action. In the event a first reply is filed within TWO MONTHS of the mailing date of this final action and the advisory action is not mailed until after the end of the THREE-MONTH shortened statutory period, then the shortened statutory period will expire on the date the advisory action is mailed, and any extension fee pursuant to 37 CFR 1.136(a) will be calculated from the mailing date of the advisory action. In no event, however, will the statutory period for reply expire later than SIX MONTHS from the date of this final action.

Any inquiry concerning this communication or earlier communications from the examiner should be directed to BONG-SOOK BAEK whose telephone number is 571-270-5863. The examiner can normally be reached 9:00AM-6:00PM Monday-Friday.

If attempts to reach the examiner by telephone are unsuccessful, the examiner's supervisor, Bethany Barham can be reached on 571-272-6175. The fax phone number for the organization where this application or proceeding is assigned is (571) 273-8300.

Information regarding the status of an application may be obtained from the Patent Application Information Retrieval (PAIR) system. Status information for published applications may be obtained from either Private PAIR or Public PAIR. Status information for unpublished applications is available through Private PAIR only. For more information about the PAIR system, see http://pair-direct.uspto.gov. Should you have questions on access to the Private PAIR system, contact the Electronic Business Center (EBC) at 866-217-9197 (toll-free). If you would like assistance from a USPTO Customer Service Representative or access to the automated information system, call 800-786-9199 (IN USA OR CANADA) or 571-272-1000.

/BONG-SOOK BAEK/
Primary Examiner, Art Unit 1611

UNITED STATES PATENT AND TRADEMARK OFFICE

UNITED STATES DEPARTMENT OF COMMERCE
United States Patent and Trademark Office
Address: COMMISSIONER FOR PATENTS
P.O. Box 1450
Alexandria, Virginia 22313-1450
www.uspto.gov

APPLICATION NO.	FILING DATE	FIRST NAMED INVENTOR	ATTORNEY DOCKET NO.	CONFIRMATION NO.
15/664,976	07/31/2017	Keelung Hong	263266-416123	4323

153749 7590 05/21/2019

McNeill Baur PLLC/Ipsen
Ipsen Bioscience, Inc.
125 Cambridge Park Drive
Suite 301
Cambridge, MA 02140

EXAMINER	
SHOMER, ISAAC	

ART UNIT	PAPER NUMBER
1612	

NOTIFICATION DATE	DELIVERY MODE
05/21/2019	ELECTRONIC

Please find below and/or attached an Office communication concerning this application or proceeding.

The time period for reply, if any, is set in the attached communication.

Notice of the Office communication was sent electronically on above-indicated "Notification Date" to the following e-mail address(es):

docketing@mcneillbaur.com
eofficeaction@appcoll.com
patents.us@ipsen.com

Office Action Summary	Application No. 15/664,976	Applicant(s) Hong et al.	
	Examiner ISAAC SHOMER	Art Unit 1612	AIA (FITF) Status No

-- The MAILING DATE of this communication appears on the cover sheet with the correspondence address --

Period for Reply

A SHORTENED STATUTORY PERIOD FOR REPLY IS SET TO EXPIRE 3 MONTHS FROM THE MAILING DATE OF THIS COMMUNICATION.

- Extensions of time may be available under the provisions of 37 CFR 1.136(a). In no event, however, may a reply be timely filed after SIX (6) MONTHS from the mailing date of this communication.
- If NO period for reply is specified above, the maximum statutory period will apply and will expire SIX (6) MONTHS from the mailing date of this communication.
- Failure to reply within the set or extended period for reply will, by statute, cause the application to become ABANDONED (35 U.S.C. § 133). Any reply received by the Office later than three months after the mailing date of this communication, even if timely filed, may reduce any earned patent term adjustment. See 37 CFR 1.704(b).

Status

1)☑ Responsive to communication(s) filed on 08 March 2019.

☐ A declaration(s)/affidavit(s) under **37 CFR 1.130(b)** was/were filed on _____.

2a)☐ This action is **FINAL.** 2b) ☑ This action is non-final.

3)☐ An election was made by the applicant in response to a restriction requirement set forth during the interview on _____; the restriction requirement and election have been incorporated into this action.

4)☐ Since this application is in condition for allowance except for formal matters, prosecution as to the merits is closed in accordance with the practice under *Ex parte Quayle*, 1935 C.D. 11, 453 O.G. 213.

Disposition of Claims*

5) ☑ Claim(s) 173-182 is/are pending in the application.

5a) Of the above claim(s) _____ is/are withdrawn from consideration.

6) ☐ Claim(s) _____ is/are allowed.

7) ☑ Claim(s) 173-175 and 177-178 is/are rejected.

8) ☑ Claim(s) 176 and 179-182 is/are objected to.

9) ☐ Claim(s) _____ are subject to restriction and/or election requirement

* If any claims have been determined allowable, you may be eligible to benefit from the **Patent Prosecution Highway** program at a participating intellectual property office for the corresponding application. For more information, please see http://www.uspto.gov/patents/init_events/pph/index.jsp or send an inquiry to **PPHfeedback@uspto.gov.**

Application Papers

10)☐ The specification is objected to by the Examiner.

11)☐ The drawing(s) filed on _____ is/are: a)☐ accepted or b)☐ objected to by the Examiner.

Applicant may not request that any objection to the drawing(s) be held in abeyance. See 37 CFR 1.85(a).

Replacement drawing sheet(s) including the correction is required if the drawing(s) is objected to. See 37 CFR 1.121(d).

Priority under 35 U.S.C. § 119

12)☐ Acknowledgment is made of a claim for foreign priority under 35 U.S.C. § 119(a)-(d) or (f).

Certified copies:

a)☐ All b)☐ Some** c)☐ None of the:

1.☐ Certified copies of the priority documents have been received.

2.☐ Certified copies of the priority documents have been received in Application No. _____.

3.☐ Copies of the certified copies of the priority documents have been received in this National Stage application from the International Bureau (PCT Rule 17.2(a)).

** See the attached detailed Office action for a list of the certified copies not received.

Attachment(s)

1) ☑ Notice of References Cited (PTO-892)

2) ☑ Information Disclosure Statement(s) (PTO/SB/08a and/or PTO/SB/08b) Paper No(s)/Mail Date _____.

3) ☐ Interview Summary (PTO-413) Paper No(s)/Mail Date _____.

4) ☐ Other: _____.

DETAILED ACTION

Applicants' arguments, filed 8 March 2019, have been fully considered. Rejections and/or objections not reiterated from previous office actions are hereby withdrawn. The following rejections and/or objections are either reiterated or newly applied. They constitute the complete set presently being applied to the instant application.

The present application is being examined under the pre-AIA first to invent provisions.

Reopening of Prosecution

In the previous office action, the examiner erred by not rejecting the instant claims under 35 U.S.C. 103. This error is corrected in this office action. In view of this error made by the examiner, this office action is made NON-FINAL.

Support for Newly Added Claims

Newly added claims 180-182 recite that there is less than 5% leakage of irinotecan at 6 months of storage at 4-8 degrees Celsius, as of Example 17, paragraph 0189 of the instant specification. As such, more than 95% of the irinotecan would have remained encapsulated under these conditions. While the instant specification discloses 4-8 degrees Celsius rather than 2-8 degrees Celsius on page 69 of the specification, the skilled artisan would have expected that at 2-4 degrees Celsius, there would have been less leakage than at 4-8 degrees Celsius. This is because at lower temperatures, there

is less Brownian and otherwise random motion of molecules, and chemical reactions are slower at lower temperatures. As such, the skilled artisan would have expected that if there is less than 5% leakage at 4-8 degrees Celsius, which would also have applied to 2-4 degrees Celsius. See MPEP 2163.07(a).

Claim Rejections - 35 USC § 103 – Obviousness

The following is a quotation of pre-AIA 35 U.S.C. 103(a) which forms the basis for all obviousness rejections set forth in this Office action:

> (a) A patent may not be obtained though the invention is not identically disclosed or described as set forth in section 102, if the differences between the subject matter sought to be patented and the prior art are such that the subject matter as a whole would have been obvious at the time the invention was made to a person having ordinary skill in the art to which said subject matter pertains. Patentability shall not be negatived by the manner in which the invention was made.

The factual inquiries set forth in *Graham v. John Deere Co.*, 383 U.S. 1, 148 USPQ 459 (1966), that are applied for establishing a background for determining obviousness under pre-AIA 35 U.S.C. 103(a) are summarized as follows:

1. Determining the scope and contents of the prior art.

2. Ascertaining the differences between the prior art and the claims at issue.

3. Resolving the level of ordinary skill in the pertinent art.

4. Considering objective evidence present in the application indicating obviousness or nonobviousness.

This application currently names joint inventors. In considering patentability of the claims under pre-AIA 35 U.S.C. 103(a), the examiner presumes that the subject matter of the various claims was commonly owned at the time any inventions covered therein

were made absent any evidence to the contrary. Applicant is advised of the obligation under 37 CFR 1.56 to point out the inventor and invention dates of each claim that was not commonly owned at the time a later invention was made in order for the examiner to consider the applicability of pre-AIA 35 U.S.C. 103(c) and potential pre-AIA 35 U.S.C. 102(e), (f) or (g) prior art under pre-AIA 35 U.S.C. 103(a).

Claims 173-175 and 177-178 is/are rejected under pre-AIA 35 U.S.C. 103(a) as being unpatentable over Chou et al. (Journal of Bioscience and Bioengineering, Vol. 95 No. 4, 2003, pages 405-408) in view of Schlessinger et al. (US Patent 5,783,568).

Chou et al. (hereafter referred to as Chou) is drawn to liposomal irinotecan, as of Chou, page 405, title and abstract.

Chou does not teach sucrose octasulfate.

Schlessinger et al. (hereafter referred to as Schlessinger) is drawn to treatment of cancer or other proliferative diseases. Schlessinger teaches administration of a salt of sucrose octasulfate for treating cancer or abnormal angiogenic cell proliferation, as of Schlessinger, column 27 line 19 to column 28 line 2.

Schlessinger does not teach a liposome comprising irinotecan.

It would have been prima facie obvious for one of ordinary skill in the art to have combined sucrose octasulfate, as of Schlessinger, with the liposome of Chou. The liposome of Chou comprises irinotecan, and is intended for the treatment of cancer. Sucrose octasulfate is also useful for the treatment of cancer, as taught by

Schlessinger. As such, it would have been prima facie obvious for one of ordinary skill in the art to have combined sucrose octasulfate, as of Schlessinger, with the irinotecan containing liposome of Chou for predictable treatment of cancer with a reasonable expectation of success. Combining prior art elements (e.g. the irinotecan liposome of Chou and sucrose octasulfate, as of Schlessinger) according to known methods to yield predictable results is prima facie obvious. See MPEP 2143, Exemplary Rationale A.

As to claim 173, the skilled artisan would have expected that this combination would have resulted in irinotecan in a gelated or precipitated state as the sucrose octasulfate salt. This is at least because the mixture of chemicals in the prior art is the same as that in the instantly claimed invention, and as such, the skilled artisan would have expected the physical state of the composition of the prior art to have been the same as in the claimed invention. See MPEP 2112.

As to claim 174, Chou teaches a liposome size of between 80 nm and 140 nm, as of Chou, page 405, right column, end of last full paragraph. While the prior art does not disclose the exact claimed values, but does overlap: in such instances even a slight overlap in range establishes a *prima facie* case of obviousness. See MPEP 2144.05(I).

As to claim 175, Chou teaches cholesterol, DSPC, and DSPE-PEG2000, as of Chou, page 405, right column, first full paragraph. In another embodiment, Chou teaches DSPE/Chol/PEG2000 liposomes at a ratio of 100:30:5, as of Chou, page 406, figure 1, reproduced below.

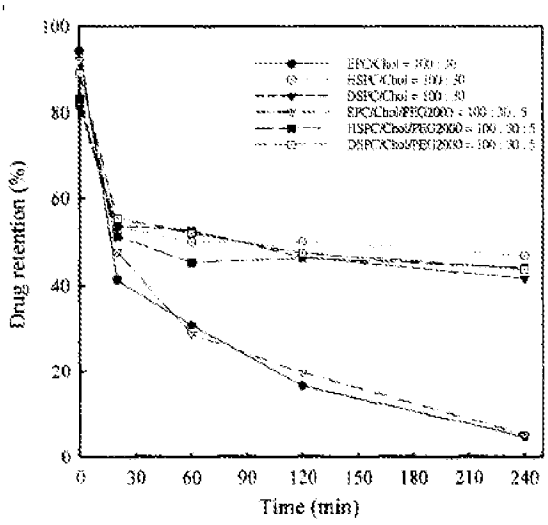

While the amounts of the lipids are not exactly the same as those recited by the instant claims, the skilled artisan would have been motivated to have optimized the amount of each lipid in the liposome. Where the general conditions of a claim are disclosed in the prior art, it is not inventive to discover the optimum or workable ranges by routine experimentation. See MPEP 2144.05(II)(A). In this case, the general conditions of the claim are understood to be taught by the prior art because a liposome comprising irinotecan, DSPC, cholesterol, and DSPE-PEG is taught by Chou. As such, the skilled artisan would have been motivated to have optimized the amount of each lipid ingredient. Additionally, there is a motivation to optimize result effective variables. See MPEP 2144.05(II)(B). In this case, the DSPC and cholesterol have the result of forming the structure of a membrane of a liposome, and the DSPE-PEG has the result of protecting such a liposome from early clearance by the reticuloendothelial system. As such, the concentrations of these lipids are understood to be result-effective variables.

As to claim 177, the claim requires a ratio of 0.15 to 1.5 moles of irinotecan per mole of lipid. Chou teaches an amount of drug (irinotecan) of 0.254 mg drug per mg lipid, as of Chou, page 407, right column, last full paragraph. Assuming a molecular

weight of phospholipid of about 790 grams per mole (which is the molecular weight of distearoyl phosphatidylcholine), this is a concentration of

$$\frac{0.254\ mg\ irinotecan}{1\ mg\ lipid} \times \frac{790\ mg\ lipid}{1\ mmol\ lipid} \times \frac{1\ mmol\ irinotecan}{586\ mg\ irinotecan} \approx 0.342\ \frac{mmol\ irinotean}{mmol\ lipid}$$

This concentration is understood to be within the claimed range.

As to claim 178, the examiner notes that the calculation of claim 177 also applies to this claim. The amount of 0.342 mol of irinotecan per mol of lipid is less than what is recited by the instant claims. Nevertheless, the skilled artisan would have been motivated to have optimized the amount of irinotecan to have been within the claimed range. Where the general conditions of a claim are disclosed in the prior art, it is not inventive to discover the optimum or workable ranges by routine experimentation. See MPEP 2144.05(II)(A). In this case, the general condition of an irinotecan containing liposome is taught by Chou, as such, it would have been prima facie obvious for the skilled artisan to have optimized the molar ratio of irinotecan to lipids.

Terminal Disclaimers

The terminal disclaimer filed on 8 March 2019 disclaiming the terminal portion of any patent granted on this application which would extend beyond the expiration date of

US Patent 8,147,867

US Patent 8,329,213

US Patent 8,703,181

US Patent 8,992,970

US Patent 8,658,203

US Patent 9,717,723

US Patent 9,717,349

US Patent 9,737,528

US Patent 9,724,303 and

US Patent 9,703,891

has been reviewed and is accepted. The terminal disclaimer has been recorded.

The terminal disclaimer filed on 8 March 2019 disclaiming the terminal portion of any patent granted on this application which would extend beyond the expiration date of

US application 15/227,561

US application 15/227,631

US application 15/896,389; and

US application 15/896,436

has been reviewed and is accepted. The terminal disclaimer has been recorded.

Allowable Subject Matter

Claims 176 and 179-182 are objected to as being dependent upon a rejected base claim, but would be allowable if rewritten in independent form including all of the limitations of the base claim and any intervening claims.

As close prior art, the examiner cites Chou et al. (Journal of Bioscience and Bioengineering, Vol. 95 No. 4, 2003, pages 405-408) and Schlessinger et al. (US Patent

5,783,568). Chou is drawn to a liposome comprising irinotecan, and Schlessinger is drawn to sucrose octasulfate. See the rejection above over Chou in view of Schlessinger. Nevertheless, the above rejection does not apply to claims 176 and 179-182. This is because there is insufficient evidence for the examiner to make the determination that the requirements regarding stability during storage would have been met by the prior art. The fact that a certain result or characteristic (the recited stability during storage) may occur or be present in the prior art is not sufficient to establish the inherency of that result or characteristic. See MPEP 2112(IV). In addition, there does not appear to be a reasonable expectation that the composition of the prior art could have been successfully optimized to have the storage stability recited by claims 176 and 179-182.

Conclusion

Any inquiry concerning this communication or earlier communications from the examiner should be directed to ISAAC SHOMER whose telephone number is (571)270-7671. The examiner can normally be reached on 7:30 AM to 5:00 PM Monday Through Friday.

Examiner interviews are available via telephone, in-person, and video conferencing using a USPTO supplied web-based collaboration tool. To schedule an interview, applicant is encouraged to use the USPTO Automated Interview Request (AIR) at http://www.uspto.gov/interviewpractice.

If attempts to reach the examiner by telephone are unsuccessful, the examiner's supervisor, Frederick F Krass can be reached on (571)272-0580. The fax phone number for the organization where this application or proceeding is assigned is 571-273-8300.

Information regarding the status of an application may be obtained from the Patent Application Information Retrieval (PAIR) system. Status information for published applications may be obtained from either Private PAIR or Public PAIR. Status information for unpublished applications is available through Private PAIR only. For more information about the PAIR system, see https://ppair-my.uspto.gov/pair/PrivatePair. Should you have questions on access to the Private PAIR system, contact the Electronic Business Center (EBC) at 866-217-9197 (toll-free). If you would like assistance from a USPTO Customer Service Representative or access to the automated information system, call 800-786-9199 (IN USA OR CANADA) or 571-272-1000.

ISAAC . SHOMER
Primary Examiner
Art Unit 1612

/ISAAC SHOMER/
Primary Examiner, Art Unit 1612

UNITED STATES PATENT AND TRADEMARK OFFICE

UNITED STATES DEPARTMENT OF COMMERCE
United States Patent and Trademark Office
Address: COMMISSIONER FOR PATENTS
P.O. Box 1450
Alexandria, Virginia 22313-1450
www.uspto.gov

APPLICATION NO.	FILING DATE	FIRST NAMED INVENTOR	ATTORNEY DOCKET NO.	CONFIRMATION NO.
15/768,352	04/13/2018	Daryl C. Drummond	01208-0010-07US	2349

153749 7590 02/14/2019

McNeill Baur PLLC/Ipsen
Ipsen Bioscience, Inc.
125 Cambridge Park Drive
Suite 301
Cambridge, MA 02140

EXAMINER	
SHOMER, ISAAC	

ART UNIT	PAPER NUMBER
1612	

NOTIFICATION DATE	DELIVERY MODE
02/14/2019	ELECTRONIC

Please find below and/or attached an Office communication concerning this application or proceeding.

The time period for reply, if any, is set in the attached communication.

Notice of the Office communication was sent electronically on above-indicated "Notification Date" to the following e-mail address(es):

docketing@mcneillbaur.com
eofficeaction@appcoll.com
patents.us@ipsen.com

Office Action Summary	Application No. 15/768,352	Applicant(s) Drummond et al.	
	Examiner ISAAC SHOMER	Art Unit 1612	AIA Status Yes

-- The MAILING DATE of this communication appears on the cover sheet with the correspondence address --

Period for Reply

A SHORTENED STATUTORY PERIOD FOR REPLY IS SET TO EXPIRE 3 MONTHS FROM THE MAILING DATE OF THIS COMMUNICATION.

- Extensions of time may be available under the provisions of 37 CFR 1.136(a). In no event, however, may a reply be timely filed after SIX (6) MONTHS from the mailing date of this communication.
- If NO period for reply is specified above, the maximum statutory period will apply and will expire SIX (6) MONTHS from the mailing date of this communication.
- Failure to reply within the set or extended period for reply will, by statute, cause the application to become ABANDONED (35 U.S.C. § 133). Any reply received by the Office later than three months after the mailing date of this communication, even if timely filed, may reduce any earned patent term adjustment. See 37 CFR 1.704(b).

Status

1)☑ Responsive to communication(s) filed on 28 November 2018.

☐ A declaration(s)/affidavit(s) under **37 CFR 1.130(b)** was/were filed on _____.

2a)☐ This action is **FINAL.** 2b) ☑ This action is non-final.

3)☐ An election was made by the applicant in response to a restriction requirement set forth during the interview on _____; the restriction requirement and election have been incorporated into this action.

4)☐ Since this application is in condition for allowance except for formal matters, prosecution as to the merits is closed in accordance with the practice under *Ex parte Quayle*, 1935 C.D. 11, 453 O.G. 213.

Disposition of Claims*

5) ☑ Claim(s) 24-49 is/are pending in the application.

5a) Of the above claim(s) _____ is/are withdrawn from consideration.

6) ☐ Claim(s) _____ is/are allowed.

7) ☑ Claim(s) 24-49 is/are rejected.

8) ☐ Claim(s) _____ is/are objected to.

9) ☐ Claim(s) _____ are subject to restriction and/or election requirement

* If any claims have been determined allowable, you may be eligible to benefit from the **Patent Prosecution Highway** program at a participating intellectual property office for the corresponding application. For more information, please see http://www.uspto.gov/patents/init_events/pph/index.jsp or send an inquiry to **PPHfeedback@uspto.gov.**

Application Papers

10)☐ The specification is objected to by the Examiner.

11)☐ The drawing(s) filed on _____ is/are: a)☐ accepted or b)☐ objected to by the Examiner.

Applicant may not request that any objection to the drawing(s) be held in abeyance. See 37 CFR 1.85(a).

Replacement drawing sheet(s) including the correction is required if the drawing(s) is objected to. See 37 CFR 1.121(d).

Priority under 35 U.S.C. § 119

12)☐ Acknowledgment is made of a claim for foreign priority under 35 U.S.C. § 119(a)-(d) or (f).

Certified copies:

a)☐ All b)☐ Some** c)☐ None of the:

1.☐ Certified copies of the priority documents have been received.

2.☐ Certified copies of the priority documents have been received in Application No. _____.

3.☐ Copies of the certified copies of the priority documents have been received in this National Stage application from the International Bureau (PCT Rule 17.2(a)).

** See the attached detailed Office action for a list of the certified copies not received.

Attachment(s)

1) ☑ Notice of References Cited (PTO-892)

2) ☐ Information Disclosure Statement(s) (PTO/SB/08a and/or PTO/SB/08b) Paper No(s)/Mail Date _____.

3) ☐ Interview Summary (PTO-413) Paper No(s)/Mail Date _____.

4) ☐ Other: _____.

DETAILED ACTION

Notice of Pre-AIA or AIA Status

The present application, filed on or after March 16, 2013, is being examined under the first inventor to file provisions of the AIA.

Claim Rejections - 35 USC § 112(b) – Indefiniteness

The following is a quotation of 35 U.S.C. 112(b):
(b) CONCLUSION.—The specification shall conclude with one or more claims particularly pointing out and distinctly claiming the subject matter which the inventor or a joint inventor regards as the invention.

The following is a quotation of 35 U.S.C. 112 (pre-AIA), second paragraph:
The specification shall conclude with one or more claims particularly pointing out and distinctly claiming the subject matter which the applicant regards as his invention.

Claims 24-49 are rejected under 35 U.S.C. 112(b) or 35 U.S.C. 112 (pre-AIA), second paragraph, as being indefinite for failing to particularly point out and distinctly claim the subject matter which the inventor or a joint inventor, or for pre-AIA the applicant regards as the invention.

Claim 24 includes various claim recitations in parentheses. While some of these recitations appear to be defining acronyms, other recitations appear to be reciting claim limitations (e.g. that reciting ±10% by weight). With regard to the claim limitations in parentheses, it is unclear to the examiner whether these limitations are required or are optional.

For the purposes of examination under prior art, these limitations in parentheses will be understood to be required.

The examiner suggests that applicant respond to this rejection by removing parentheses with the exception of those used to define acronyms.

Claim Interpretation

Claim 27 recites a specific concentration of irinotecan measured as an equivalent to 4.3 mg/mL irinotecan free base anhydrous. However, claim 27 depends upon claim 24, which recites an irinotecan liposome at pH 7.25-7.50. As best understood by the examiner, at this pH range, irinotecan is protonated and in the form of a salt (e.g. a hydrochloride salt). However, despite this, claim 27 is not considered indefinite. This is because claim 27 is not understood to recite that irinotecan is present as a free base. In contrast, claim 27 is understood to recite the concentration of irinotecan would have been had the irinotecan been present as a free base.

Non-Statutory Double Patenting

The nonstatutory double patenting rejection is based on a judicially created doctrine grounded in public policy (a policy reflected in the statute) so as to prevent the unjustified or improper timewise extension of the "right to exclude" granted by a patent and to prevent possible harassment by multiple assignees. A nonstatutory double patenting rejection is appropriate where the conflicting claims are not identical, but at least one examined application claim is not patentably distinct from the reference claim(s) because the examined application claim is either anticipated by, or would have been obvious over, the reference claim(s). See, e.g., *In re Berg*, 140 F.3d 1428, 46

USPQ2d 1226 (Fed. Cir. 1998); *In re Goodman*, 11 F.3d 1046, 29 USPQ2d 2010 (Fed. Cir. 1993); *In re Longi*, 759 F.2d 887, 225 USPQ 645 (Fed. Cir. 1985); *In re Van Ornum*, 686 F.2d 937, 214 USPQ 761 (CCPA 1982); *In re Vogel*, 422 F.2d 438, 164 USPQ 619 (CCPA 1970); *In re Thorington*, 418 F.2d 528, 163 USPQ 644 (CCPA 1969).

A timely filed terminal disclaimer in compliance with 37 CFR 1.321(c) or 1.321(d) may be used to overcome an actual or provisional rejection based on nonstatutory double patenting provided the reference application or patent either is shown to be commonly owned with the examined application, or claims an invention made as a result of activities undertaken within the scope of a joint research agreement. See MPEP § 717.02 for applications subject to examination under the first inventor to file provisions of the AIA as explained in MPEP § 2159. See MPEP §§ 706.02(l)(1) - 706.02(l)(3) for applications not subject to examination under the first inventor to file provisions of the AIA. A terminal disclaimer must be signed in compliance with 37 CFR 1.321(b).

The USPTO Internet website contains terminal disclaimer forms which may be used. Please visit www.uspto.gov/patent/patents-forms. The filing date of the application in which the form is filed determines what form (e.g., PTO/SB/25, PTO/SB/26, PTO/AIA/25, or PTO/AIA/26) should be used. A web-based eTerminal Disclaimer may be filled out completely online using web-screens. An eTerminal Disclaimer that meets all requirements is auto-processed and approved immediately upon submission. For more information about eTerminal Disclaimers, refer to www.uspto.gov/patents/process/file/efs/guidance/eTD-info-I.jsp.

Claims 24-49 are provisionally rejected on the ground of nonstatutory double patenting as being unpatentable over claim 1 of copending Application No. 15/967,638 (reference application). Although the claims at issue are not identical, they are not patentably distinct from each other because of the following reasons:

Instant claim 24 is drawn to a liposomal irinotecan composition comprising sucrose octasulfate. The composition was made by a particular process, and has an explicit storage stability that results in less than 20 mol% of double-chain phosphatidylcholine disintegrating to lysophosphatidylcholine after 6 months in storage. The claimed composition recites a pH range of 7.25 to 7.50.

Copending claim 1 is drawn to a storage stabilized liposome comprising irinotecan and sucrose octasulfate. The liposome has an explicit storage stability that results in less than 20 mol% of double-chain phosphatidylcholine disintegrating to lysophosphatidylcholine after 6 months in storage. The composition reictes a pH range of 7.25 to 7.50.

The instant and copending claims differ because the instant claims recite that the liposome was prepared by a specific process, which was not recited by the copending claims. Nevertheless, the skilled artisan would have expected the instant and copending claims to have had the same structural elements of liposome lipids, irinotecan, and sucrose octasulfate. The skilled artisan would have also expected the composition of the copending claims to have had the same stability as that of the instant claims. As such, in view of overlapping ranges, the skilled artisan would have expected the composition of the copending claim to have rendered the subject matter of the instant

claims prima facie obvious. As such, this appears to be a case of obviousness-type non-statutory double patenting.

This is a provisional nonstatutory double patenting rejection because the patentably indistinct claims have not in fact been patented.

The examiner further notes here that both the instant and copending claims appear to have the same effective filing date of 15 October 2016, excluding priority to provisional applications. As such, even if the double patenting rejection is the only remaining rejection, the examiner should not withdraw this rejection until the rejection has been overcome. See MPEP 804(I)(b)(ii).

Close Prior Art and Non-Rejection of Instant Claims as Prima Facie Obvious

The instant claims have not been rejected under 35 U.S.C. 102 or 103 as anticipated or obvious. The following rationale has been provided by the examiner for the non-rejection of the instant claims. The examiner notes that the rationale is similar to the reasons for allowance provided by the examiner in prior cases such as 15/331,318 and 15/661,868.

The instant claims are drawn to a liposomal composition comprising irinotecan and sucrose octasulfate. As close and relevant prior art, the examiner cites Drummond et al. (US 2007/0110798 A1) and Hong et al. (US 2007/0116753 A1), which are also drawn to liposomes comprising sucrose octasulfate and irinotecan.

The following reasons are provided by the examiner explaining why the instant claims have not been rejected as anticipated by these references or obvious over these

references. Also cited by the examiner is Saetern et al. (International Journal of Pharmaceutics, Vol. 288, 2005, pages 73-80).

Liposomes are known to suffer from degradation when in storage. One such form of degradation involves the hydrolysis of phosphatidylcholine, which is a phospholipid molecule with two chains that makes up the structural of the bilayer of the liposome, to lysophosphatidylcholine. Such lysophosphatidylcholine is understood to have poor stability in the liposome bilayer, and a bilayer comprising lysophosphatidylcholine is subject to degradation. The instantly claimed invention is drawn to a liposome that has unexpectedly greater storage stability than the liposomes of the Drummond and Hong prior art references cited above. As such, the instantly claimed invention differs from the composition of the prior art for the following reasons:

A) pH Range: First, the instantly claimed liposome is stored in a medium wherein the pH is 7.25 to 7.50 (as in instant claim 24). Hong teaches that the liposome should be stored at a pH of between 6.0 and 7.5, with a pH of 6.5 as most optimal, as of Hong, paragraph 0115. However, additional relevant prior art shows that storage of a liposome in a pH of about 6.25 to 6.5 has the greatest storage stability, and that deviation from pH 6.25-6.5 results in more degradation during storage as compared to storage at pH 6.5. In support of this position, the examiner cites Saetern et al. (International Journal of Pharmaceutics, Vol. 288, 2005, pages 73-80). Saetern et al. (hereafter referred to as Saetern), teaches the following graph regarding degradation of phosphatidylcholine to lysophosphatidylcholine, as of page 77, right column, Figure 5, which is reproduced below.

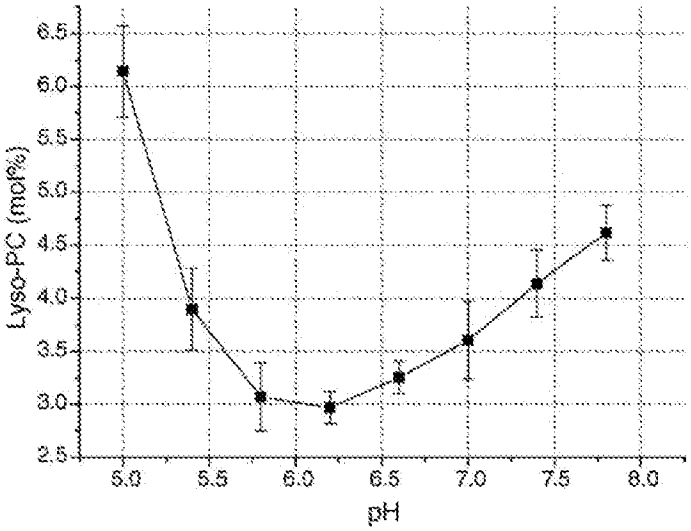

As such, the data of Saetern indicates that a pH of about 6.25 provides the greatest stability of a phosphatidylcholine containing liposome. The examiner also notes that the Saetern publication is especially relevant here because Saetern is drawn to encapsulating camptothecin as a drug, and the instant claims are drawn to a liposome that encapsulates irinotecan as a drug, wherein irinotecan is a derivative of camptothecin.

However, in the instant specification, applicant has presented data showing that a pH range of 7.25 to 7.50 unexpectedly provides increased stability as compared to a pH of about 6.5. In support of this position, the examiner cites table 1B on page 26 of the instant specification, which is reproduced below.

Table 1B: *Irinotecan Liposome Stability Ratio and Lyso-PC (after 6 months at 4 °C)*[b]

Sample	Molar (M) concentration of sulfate groups in the sucrosofate entrapped in the liposomes	Stability Ratio	pH	[mol% Lyso-PC] at 6 mos.
1	0.45	1047	6.5	19.5
2	0.475	992	6.5	17
3	0.5	942	6.5	26.5
4	0.6	785	6.5	30.2
5	0.45	1047	7.25	7.1
6	0.45	1047	6.5	14.6
7	0.45	1047	7.25	7.4
8	0.45	1047	7.5	5.4
9	0.6	785	6.5	29.8
10	0.6	785	7.25	24.1
11	0.6	785	7.5	22.8
13	0.45	1047	7.25	9.72

[b] Measured according to Method B, as described herein.

Instant table 1B discloses that a liposome at a pH of 6.5 and a sulfate group concentration of 0.45 M (Sample #1) shows 14.6 mol% or 19.5 mol% of lysophosphatidylcholine after 6 months, as of samples #6 and #1 respectively. In contrast, a sample with a pH of 7.25 and an identical sucrose octasulfate concentration of 0.45 M (Samples #5 and #7) shows only about 7.1 mol% or 7.4 mol% of lyosphosphatidylcholine after 6 months of storage. As a greater percentage of lysophosphatidylcholine indicates a less stable liposome, the data presented in Table 1 show an increase in stability when the pH of a sucrose octasulfate containing irinotecan liposome is raised from 6.5 to 7.25.

This increase in stability with increase in pH is at odds with the teachings of the prior art, which indicate that a lower pH of 6.25 to 6.5 is optimal for achieving stability of the liposome. As applicant has shown that the claimed pH range is critical for achieving increased stability, this is understood to be evidence of non-obviousness. See MPEP 2144.05(III)(A).

B) Sucrose Octasulfate Loading Concentration: In the instantly claimed product-by-process, sucrose octasulfate was loaded in a concentration such that the sulfate groups are present in a concentration of 0.4 to 0.5 M, as of part (a) of claim 1. This appears to be a sucrose octasulfate concentration of 0.05 to 0.0625 M. This value was value calculated by the examiner by dividing the range of 0.4 to 0.5 by 8 as there are 8 sulfate groups per sucrose octasulfate molecule. In contrast, in the examples of the prior art, the concentration of either sucrose octasulfate or sulfate groups inside the liposome was at minimum 0.65 M to about 1.0 M, e.g. as of Hong, page 11, end of paragraph 0104.

Data in the instant application show that loading with a lower level of sucrose octasulfate with a sulfate group concentration of 0.4 M to 0.5 M appears to provide a liposome with increased stability as compared with a liposome loaded at 0.60 to 0.65 M. In support of this position, the examiner cites table 1B on page 26 of the instant specification, which is reproduced above. Sample 10 of the instant specification shows loading at 0.60 M sucrose octasulfate and pH 7.25. In this example, there was 24.1 mol% lysophosphatidylcholine after 6 months of storage. In contrast, samples 5 and 7 are drawn to a liposome loaded with 0.45 M sucrose octasulfate and also a pH of 7.25, and these show 7.1% and 7.4% of lysophosphatidylcholine respectively after 6 months of storage.

As a greater percentage of lysophosphatidylcholine indicates a less stable liposome, the data presented in Table 1 show an increase in stability when the concentration of sulfate groups from sucrose octasulfate is decreased from the prior art amount of 0.65 M to a lower amount of 0.4 M to 0.5 M. This would not have been

expected by the skilled artisan, and this also indicates that the concentration of sucrose octasulfate used in loading the liposome is critical to the liposome stability. This showing regarding the criticality of the claimed loading concentration of sucrose octasulfate is evidence of non-obviousness, and applicant's data show that the claimed range of sucrose octasulfate is critical with regard to the stability of the liposome that is ultimately formed. See MPEP 2144.05(III)(A).

C) Lack of Inherency Regarding Lysophosphatidylcholine Content After 6 Months of Storage: Additionally, the instant claims recite that the composition is stabilized such that after 6 months of storage at the recited conditions, there is less than 20 mol% of lysophosphatidylcholine. The cited prior art references Drummond and Hong do not provide any teachings with regard to the amount of lysophosphatidylcholine after 6 months of storage, and are silent with respect to this issue.

In order to reject such a claim limitation in the absence of an explicit teaching, the examiner must provide rationale or evidence tending to show inherency. See the heading of MPEP 2112(IV). In this case, the evidence appears to tend against inherency. This is because inherency must be based on what is necessarily present in the prior art (e.g. a composition with a pH of 6.5 and between 0.65 M to 1.0 M sulfate groups from sucrose octasulfate), and should not be based on optimization of conditions. See MPEP 2112(IV), first paragraph. In this case, the examiner takes the position that with regard to the composition that is necessarily present in the prior art, this composition would not have been expected to have had the slow rate of

degradation such that the percentage of lyso-phosphatidylcholine would have been less than 20% after 6 months of storage.

The prior art examples appear to include a sulfate concentration of between 0.65 M to 1.0 M, as of Hong, paragraph 0104, and a pH of 6.5, as of Hong, end of paragraph 0105. However, the examples in table 1B of the instant specification on page 26 of the instant specification that most resemble the prior art examples (e.g. 0.65 M sucrose octasulfate and pH 6.5) appear to show a greater level of lysophosphatidylcholine after 6 months of storage. The example in the instant specification which appear to be most similar to the prior art are samples 4, and 9, which utilizes a pH of 6.5 and a concentration of sulfate groups of 0.60 M in samples. These liposomes show that the percentage of phosphatidylcholine after 6 months is 29.8% in sample 9 and 30.2%.

As such, the data in the instant specification show that the compositions that are necessarily present in the prior art would have been expected to have degraded to an extent that there would have been more than 20 mol% of lyso-phosphatidylcholine after 6 months of storage. As such, the claimed requirement that there be less than 20 mol% of lyso-phosphatidylcholine after 6 months of storage does not appear to be inherent in the teachings of the prior art.

Conclusion

No claim is allowed.

Any inquiry concerning this communication or earlier communications from the examiner should be directed to ISAAC SHOMER whose telephone number is (571)270-

7671. The examiner can normally be reached on 7:30 AM to 5:00 PM Monday Through Friday.

Examiner interviews are available via telephone, in-person, and video conferencing using a USPTO supplied web-based collaboration tool. To schedule an interview, applicant is encouraged to use the USPTO Automated Interview Request (AIR) at http://www.uspto.gov/interviewpractice.

If attempts to reach the examiner by telephone are unsuccessful, the examiner's supervisor, Frederick F Krass can be reached on (571)272-0580. The fax phone number for the organization where this application or proceeding is assigned is 571-273-8300.

Information regarding the status of an application may be obtained from the Patent Application Information Retrieval (PAIR) system. Status information for published applications may be obtained from either Private PAIR or Public PAIR. Status information for unpublished applications is available through Private PAIR only. For more information about the PAIR system, see http://pair-direct.uspto.gov. Should you have questions on access to the Private PAIR system, contact the Electronic Business Center (EBC) at 866-217-9197 (toll-free). If you would like assistance from a USPTO Customer Service Representative or access to the automated information system, call 800-786-9199 (IN USA OR CANADA) or 571-272-1000.

ISAAC . SHOMER
Primary Examiner
Art Unit 1612

/ISAAC SHOMER/
Primary Examiner, Art Unit 1612

UNITED STATES PATENT AND TRADEMARK OFFICE

UNITED STATES DEPARTMENT OF COMMERCE
United States Patent and Trademark Office
Address: COMMISSIONER FOR PATENTS
P.O. Box 1450
Alexandria, Virginia 22313-1450
www.uspto.gov

APPLICATION NO.	FILING DATE	FIRST NAMED INVENTOR	ATTORNEY DOCKET NO.	CONFIRMATION NO.
15/768,352	04/13/2018	Daryl C. Drummond	01208-0010-07US	2349

153749 7590 06/03/2019

McNeill Baur PLLC/Ipsen
Ipsen Bioscience, Inc.
125 Cambridge Park Drive
Suite 301
Cambridge, MA 02140

EXAMINER	
SHOMER, ISAAC	

ART UNIT	PAPER NUMBER
1612	

NOTIFICATION DATE	DELIVERY MODE
06/03/2019	ELECTRONIC

Please find below and/or attached an Office communication concerning this application or proceeding.

The time period for reply, if any, is set in the attached communication.

Notice of the Office communication was sent electronically on above-indicated "Notification Date" to the following e-mail address(es):

docketing@mcneillbaur.com
eofficeaction@appcoll.com
patents.us@ipsen.com

Examiner-Initiated Interview Summary	Application No. 15/768,352	Applicant(s) Drummond et al.		
	Examiner ISAAC SHOMER	Art Unit 1612	AIA (First Inventor to File) Status Yes	Page 1 of 2

All participants (applicant, applicants representative, PTO personnel):

1. ISAAC SHOMER (Primary Examiner); Telephonic 2. Deborah M. Herzfeld (Attomey of Record); Telephonic

Date of Interview: 28 May 2019

Claims Discussed: 24-47, 50-55 and proposed new claim 56

Amendment proposed: See attached proposed amendments. It is clarified here that the proposed amendments were proposed by the examiner.

Brief Description of the main topic(s) of discussion: Examiner verbally proposed examiner's amendments. These examiner's amendments are provided as an attachment to this interview summary. Representative of applicant will review the proposed examiner's amendments with applicant. No agreement has been reached as of the date which the examiner prepared this interview summary.

Issues Discussed:

Proposed Amendments:
Examiner verbally proposed examiner's amendments. One such amendment was to claim 26, in which the examiner proposed deleting the term "essentially."

Representative of applicant questioned examiner as to why this change is needed. The examiner explained that it is unclear how the term "essentially" limits the phrase "unilamellar", and as such the relevant issue is under 35 U.S.C. 112(b). This is because a liposome either has one lamella (unilamellar) or multiple lamellae (multilamellar), and as such it is not clear how a liposome can be "essentially unilamellar." Examiner also explained that a claim that recites that the composition comprises unilamellar would be interpreted by examiner for the purposes of examination as requiring that at least some of the liposomes are unilamellar. This interpretation is made in view of the fact that
a) the term "comprising" does not exclude additional unrecited elements (MPEP 2111.03(I)), and
b) claims must be given their broadest reasonable interpretation during examination.

As of the preparation of this interview summary, no agreement has been reached as to whether the proposed changes are acceptable to applicant.

Attachment(s): Proposed Amendments,

/ISAAC SHOMER/ Primary Examiner, Art Unit 1612	

Applicant is reminded that a complete written statement as to the substance of the interview must be made of record in the application file. It is the applicants responsibility to provide the written statement, unless the interview was initiated by the Examiner and the Examiner has indicated that a written summary will be provided. See MPEP 713.04
Please further see:
MPEP 713.04
Title 37 Code of Federal Regulations (CFR) § 1.133 Interviews, paragraph (b)
37 CFR § 1.2 Business to be transacted in writing

Applicant recordation instructions: It is not necessary for applicant to provide a separate record of the substance of interview.

Examiner recordation instructions: Examiners must summarize the substance of any interview of record. A complete and proper recordation of the substance of an interview should include the items listed in MPEP 713.04 for complete and proper recordation including the identification of the general thrust of each argument or issue discussed, a general indication of any other pertinent matters discussed regarding patentability and the general results or outcome of the interview, to include an indication as to whether or not agreement was reached on the issues raised.

X) Claim 26 is proposed to be amended in the following manner:

Claim 26 (Proposed Amended): The storage stabilized liposomal irinotecan composition of claim 25, wherein the composition comprises **[[** ~~essentially~~ **]]** unilamellar liposomes.

X) Claim 29 is proposed to be amended in the following manner:

Claim 29 (Proposed Amended): The storage stabilized liposomal irinotecan composition of claim 24, wherein at least 98% of the irinotecan **[[** ~~is~~ **]]** **remains** encapsulated within the liposomes after 6 months, at a storage temperature of from 2 to 8°C.

X) Claim 31 is proposed to be amended in the following manner:

Claim 31 (Proposed Amendment): The storage stabilized liposomal irinotecan composition of claim 24, **further** comprising sodium chloride present at a concentration of from 130 to 160 mM.

X) Claim 34 is proposed to be amended in the following manner:

Claim 34 (Proposed Amendment): The storage stabilized liposomal irinotecan composition of claim 33, wherein the liposomes are **[[** ~~essentially~~ **]]** unilamellar.

X) Claim 37 is proposed to be amended in the following manner:

Claim 37 (Proposed Amendment): The storage stabilized liposomal irinotecan composition of claim 36, wherein the composition comprises **[[** ~~essentially~~ **]]** unilamellar liposomes.

X) Claim 41 is proposed to be amended in the following manner:

Claim 41 (Proposed Amendment): The storage stabilized liposomal irinotecan composition of claim 40, comprising **triethylammonium (**TEA**)** or **diethylammonium (**DEA**)** in a total amount of less than 100 ppm.

X) Claim 47 is proposed to be amended in the following manner:

Claim 47 (Proposed Amendment): The storage stabilized liposomal irinotecan composition of claim **[[** ~~27,~~ **]] 46,** wherein the time is about 30 minutes.

X) Claim 51 is proposed to be amended in the following manner:

Claim 51 (Proposed Amendment): The storage stabilized liposomal irinotecan composition of claim 24, wherein the composition comprises **[[** ~~essentially~~ **]]** unilamellar liposomes.

X) The following new claim is proposed to be added:

Claim 56 (Proposed New): The storage stabilized liposomal irinotecan composition of claim **[[** ~~24,~~ **]] 27,** wherein the time the liposomes are contacted with the solution comprising irinotecan above the transition temperature in step (b) is about 30 minutes.

UNITED STATES PATENT AND TRADEMARK OFFICE

UNITED STATES DEPARTMENT OF COMMERCE
United States Patent and Trademark Office
Address: COMMISSIONER FOR PATENTS
P.O. Box 1450
Alexandria, Virginia 22313-1450
www.uspto.gov

NOTICE OF ALLOWANCE AND FEE(S) DUE

153749 7590 06/12/2019

McNeill Baur PLLC/Ipsen
Ipsen Bioscience, Inc.
125 Cambridge Park Drive
Suite 301
Cambridge, MA 02140

EXAMINER
SHOMER, ISAAC

ART UNIT	PAPER NUMBER
1612	

DATE MAILED: 06/12/2019

APPLICATION NO.	FILING DATE	FIRST NAMED INVENTOR	ATTORNEY DOCKET NO.	CONFIRMATION NO.
15/768,352	04/13/2018	Daryl C. Drummond	01208-0010-07US	2349

TITLE OF INVENTION: Stabilizing Camptothecin Pharmaceutical Compositions

APPLN. TYPE	ENTITY STATUS	ISSUE FEE DUE	PUBLICATION FEE DUE	PREV. PAID ISSUE FEE	TOTAL FEE(S) DUE	DATE DUE
nonprovisional	UNDISCOUNTED	$1000	$0.00	$0.00	$1000	09/12/2019

THE APPLICATION IDENTIFIED ABOVE HAS BEEN EXAMINED AND IS ALLOWED FOR ISSUANCE AS A PATENT. PROSECUTION ON THE MERITS IS CLOSED. THIS NOTICE OF ALLOWANCE IS NOT A GRANT OF PATENT RIGHTS. THIS APPLICATION IS SUBJECT TO WITHDRAWAL FROM ISSUE AT THE INITIATIVE OF THE OFFICE OR UPON PETITION BY THE APPLICANT. SEE 37 CFR 1.313 AND MPEP 1308.

THE ISSUE FEE AND PUBLICATION FEE (IF REQUIRED) MUST BE PAID WITHIN THREE MONTHS FROM THE MAILING DATE OF THIS NOTICE OR THIS APPLICATION SHALL BE REGARDED AS ABANDONED. THIS STATUTORY PERIOD CANNOT BE EXTENDED. SEE 35 U.S.C. 151. THE ISSUE FEE DUE INDICATED ABOVE DOES NOT REFLECT A CREDIT FOR ANY PREVIOUSLY PAID ISSUE FEE IN THIS APPLICATION. IF AN ISSUE FEE HAS PREVIOUSLY BEEN PAID IN THIS APPLICATION (AS SHOWN ABOVE), THE RETURN OF PART B OF THIS FORM WILL BE CONSIDERED A REQUEST TO REAPPLY THE PREVIOUSLY PAID ISSUE FEE TOWARD THE ISSUE FEE NOW DUE.

HOW TO REPLY TO THIS NOTICE:

I. Review the ENTITY STATUS shown above. If the ENTITY STATUS is shown as SMALL or MICRO, verify whether entitlement to that entity status still applies.

If the ENTITY STATUS is the same as shown above, pay the TOTAL FEE(S) DUE shown above.

If the ENTITY STATUS is changed from that shown above, on PART B - FEE(S) TRANSMITTAL, complete section number 5 titled "Change in Entity Status (from status indicated above)".

For purposes of this notice, small entity fees are 1/2 the amount of undiscounted fees, and micro entity fees are 1/2 the amount of small entity fees.

II. PART B - FEE(S) TRANSMITTAL, or its equivalent, must be completed and returned to the United States Patent and Trademark Office (USPTO) with your ISSUE FEE and PUBLICATION FEE (if required). If you are charging the fee(s) to your deposit account, section "4b" of Part B - Fee(s) Transmittal should be completed and an extra copy of the form should be submitted. If an equivalent of Part B is filed, a request to reapply a previously paid issue fee must be clearly made, and delays in processing may occur due to the difficulty in recognizing the paper as an equivalent of Part B.

III. All communications regarding this application must give the application number. Please direct all communications prior to issuance to Mail Stop ISSUE FEE unless advised to the contrary.

IMPORTANT REMINDER: Maintenance fees are due in utility patents issuing on applications filed on or after Dec. 12, 1980. It is patentee's responsibility to ensure timely payment of maintenance fees when due. More information is available at www.uspto.gov/PatentMaintenanceFees.

PART B - FEE(S) TRANSMITTAL

Complete and send this form, together with applicable fee(s), by mail or fax, or via EFS-Web.

By mail, send to: Mail Stop ISSUE FEE
Commissioner for Patents
P.O. Box 1450
Alexandria, Virginia 22313-1450

By fax, send to: (571)-273-2885

INSTRUCTIONS: This form should be used for transmitting the ISSUE FEE and PUBLICATION FEE (if required). Blocks 1 through 5 should be completed where appropriate. All further correspondence including the Patent, advance orders and notification of maintenance fees will be mailed to the current correspondence address as indicated unless corrected below or directed otherwise in Block 1, by (a) specifying a new correspondence address; and/or (b) indicating a separate "FEE ADDRESS" for maintenance fee notifications.

CURRENT CORRESPONDENCE ADDRESS (Note: Use Block 1 for any change of address)

153749 7590 06/12/2019

McNeill Baur PLLC/Ipsen
Ipsen Bioscience, Inc.
125 Cambridge Park Drive
Suite 301
Cambridge, MA 02140

Note: A certificate of mailing can only be used for domestic mailings of the Fee(s) Transmittal. This certificate cannot be used for any other accompanying papers. Each additional paper, such as an assignment or formal drawing, must have its own certificate of mailing or transmission.

Certificate of Mailing or Transmission

I hereby certify that this Fee(s) Transmittal is being deposited with the United States Postal Service with sufficient postage for first class mail in an envelope addressed to the Mail Stop ISSUE FEE address above, or being transmitted to the USPTO via EFS-Web or by facsimile to (571) 273-2885, on the date below.

(Typed or printed name)
(Signature)
(Date)

APPLICATION NO.	FILING DATE	FIRST NAMED INVENTOR	ATTORNEY DOCKET NO.	CONFIRMATION NO.
15/768,352	04/13/2018	Daryl C. Drummond	01208-0010-07US	2349

TITLE OF INVENTION: Stabilizing Camptothecin Pharmaceutical Compositions

APPLN. TYPE	ENTITY STATUS	ISSUE FEE DUE	PUBLICATION FEE DUE	PREV. PAID ISSUE FEE	TOTAL FEE(S) DUE	DATE DUE
nonprovisional	UNDISCOUNTED	$1000	$0.00	$0.00	$1000	09/12/2019

EXAMINER	ART UNIT	CLASS-SUBCLASS
SHOMER, ISAAC	1612	424-450000

1. Change of correspondence address or indication of "Fee Address" (37 CFR 1.363).

❑ Change of correspondence address (or Change of Correspondence Address form PTO/SB/122) attached.

❑ "Fee Address" indication (or "Fee Address" Indication form PTO/SB/47; Rev 03-09 or more recent) attached. **Use of a Customer Number is required.**

2. For printing on the patent front page, list
(1) The names of up to 3 registered patent attorneys or agents OR, alternatively,
(2) The name of a single firm (having as a member a registered attorney or agent) and the names of up to 2 registered patent attorneys or agents. If no name is listed, no name will be printed.

1 _____
2 _____
3 _____

3. ASSIGNEE NAME AND RESIDENCE DATA TO BE PRINTED ON THE PATENT (print or type)

PLEASE NOTE: Unless an assignee is identified below, no assignee data will appear on the patent. If an assignee is identified below, the document must have been previously recorded, or filed for recordation, as set forth in 37 CFR 3.11 and 37 CFR 3.81(a). Completion of this form is NOT a substitute for filing an assignment.

(A) NAME OF ASSIGNEE (B) RESIDENCE: (CITY and STATE OR COUNTRY)

Please check the appropriate assignee category or categories (will not be printed on the patent) : ❑ Individual ❑ Corporation or other private group entity ❑ Government

4a. Fees submitted: ❑ Issue Fee ❑ Publication Fee (if required) ❑ Advance Order - # of Copies _____

4b. Method of Payment: *(Please first reapply any previously paid fee shown above)*

❑ Electronic Payment via EFS-Web ❑ Enclosed check ❑ Non-electronic payment by credit card (Attach form PTO-2038)

❑ The Director is hereby authorized to charge the required fee(s), any deficiency, or credit any overpayment to Deposit Account No. _____

5. **Change in Entity Status** (from status indicated above)

❑ Applicant certifying micro entity status. See 37 CFR 1.29

❑ Applicant asserting small entity status. See 37 CFR 1.27

❑ Applicant changing to regular undiscounted fee status.

NOTE: Absent a valid certification of Micro Entity Status (see forms PTO/SB/15A and 15B), issue fee payment in the micro entity amount will not be accepted at the risk of application abandonment.
NOTE: If the application was previously under micro entity status, checking this box will be taken to be a notification of loss of entitlement to micro entity status.
NOTE: Checking this box will be taken to be a notification of loss of entitlement to small or micro entity status, as applicable.

NOTE: This form must be signed in accordance with 37 CFR 1.31 and 1.33. See 37 CFR 1.4 for signature requirements and certifications.

Authorized Signature _____ Date _____

Typed or printed name _____ Registration No. _____

UNITED STATES PATENT AND TRADEMARK OFFICE

UNITED STATES DEPARTMENT OF COMMERCE
United States Patent and Trademark Office
Address: COMMISSIONER FOR PATENTS
P.O. Box 1450
Alexandria, Virginia 22313-1450
www.uspto.gov

APPLICATION NO.	FILING DATE	FIRST NAMED INVENTOR	ATTORNEY DOCKET NO.	CONFIRMATION NO.
15/768,352	04/13/2018	Daryl C. Drummond	01208-0010-07US	2349

153749 7590 06/12/2019

McNeill Baur PLLC/Ipsen
Ipsen Bioscience, Inc.
125 Cambridge Park Drive
Suite 301
Cambridge, MA 02140

EXAMINER	
SHOMER, ISAAC	
ART UNIT	PAPER NUMBER
1612	

DATE MAILED: 06/12/2019

Determination of Patent Term Adjustment under 35 U.S.C. 154 (b)
(Applications filed on or after May 29, 2000)

The Office has discontinued providing a Patent Term Adjustment (PTA) calculation with the Notice of Allowance.

Section 1(h)(2) of the AIA Technical Corrections Act amended 35 U.S.C. 154(b)(3)(B)(i) to eliminate the requirement that the Office provide a patent term adjustment determination with the notice of allowance. See Revisions to Patent Term Adjustment, 78 Fed. Reg. 19416, 19417 (Apr. 1, 2013). Therefore, the Office is no longer providing an initial patent term adjustment determination with the notice of allowance. The Office will continue to provide a patent term adjustment determination with the Issue Notification Letter that is mailed to applicant approximately three weeks prior to the issue date of the patent, and will include the patent term adjustment on the patent. Any request for reconsideration of the patent term adjustment determination (or reinstatement of patent term adjustment) should follow the process outlined in 37 CFR 1.705.

Any questions regarding the Patent Term Extension or Adjustment determination should be directed to the Office of Patent Legal Administration at (571)-272-7702. Questions relating to issue and publication fee payments should be directed to the Customer Service Center of the Office of Patent Publication at 1-(888)-786-0101 or (571)-272-4200.

OMB Clearance and PRA Burden Statement for PTOL-85 Part B

The Paperwork Reduction Act (PRA) of 1995 requires Federal agencies to obtain Office of Management and Budget approval before requesting most types of information from the public. When OMB approves an agency request to collect information from the public, OMB (i) provides a valid OMB Control Number and expiration date for the agency to display on the instrument that will be used to collect the information and (ii) requires the agency to inform the public about the OMB Control Number's legal significance in accordance with 5 CFR 1320.5(b).

The information collected by PTOL-85 Part B is required by 37 CFR 1.311. The information is required to obtain or retain a benefit by the public which is to file (and by the USPTO to process) an application. Confidentiality is governed by 35 U.S.C. 122 and 37 CFR 1.14. This collection is estimated to take 30 minutes to complete, including gathering, preparing, and submitting the completed application form to the USPTO. Time will vary depending upon the individual case. Any comments on the amount of time you require to complete this form and/or suggestions for reducing this burden, should be sent to the Chief Information Officer, U.S. Patent and Trademark Office, U.S. Department of Commerce, P.O. Box 1450, Alexandria, Virginia 22313-1450. DO NOT SEND FEES OR COMPLETED FORMS TO THIS ADDRESS. SEND TO: Commissioner for Patents, P.O. Box 1450, Alexandria, Virginia 22313-1450. Under the Paperwork Reduction Act of 1995, no persons are required to respond to a collection of information unless it displays a valid OMB control number.

Privacy Act Statement

The Privacy Act of 1974 (P.L. 93-579) requires that you be given certain information in connection with your submission of the attached form related to a patent application or patent. Accordingly, pursuant to the requirements of the Act, please be advised that: (1) the general authority for the collection of this information is 35 U.S.C. 2(b)(2); (2) furnishing of the information solicited is voluntary; and (3) the principal purpose for which the information is used by the U.S. Patent and Trademark Office is to process and/or examine your submission related to a patent application or patent. If you do not furnish the requested information, the U.S. Patent and Trademark Office may not be able to process and/or examine your submission, which may result in termination of proceedings or abandonment of the application or expiration of the patent.

The information provided by you in this form will be subject to the following routine uses:

1. The information on this form will be treated confidentially to the extent allowed under the Freedom of Information Act (5 U.S.C. 552) and the Privacy Act (5 U.S.C 552a). Records from this system of records may be disclosed to the Department of Justice to determine whether disclosure of these records is required by the Freedom of Information Act.
2. A record from this system of records may be disclosed, as a routine use, in the course of presenting evidence to a court, magistrate, or administrative tribunal, including disclosures to opposing counsel in the course of settlement negotiations.
3. A record in this system of records may be disclosed, as a routine use, to a Member of Congress submitting a request involving an individual, to whom the record pertains, when the individual has requested assistance from the Member with respect to the subject matter of the record.
4. A record in this system of records may be disclosed, as a routine use, to a contractor of the Agency having need for the information in order to perform a contract. Recipients of information shall be required to comply with the requirements of the Privacy Act of 1974, as amended, pursuant to 5 U.S.C. 552a(m).
5. A record related to an International Application filed under the Patent Cooperation Treaty in this system of records may be disclosed, as a routine use, to the International Bureau of the World Intellectual Property Organization, pursuant to the Patent Cooperation Treaty.
6. A record in this system of records may be disclosed, as a routine use, to another federal agency for purposes of National Security review (35 U.S.C. 181) and for review pursuant to the Atomic Energy Act (42 U.S.C. 218(c)).
7. A record from this system of records may be disclosed, as a routine use, to the Administrator, General Services, or his/her designee, during an inspection of records conducted by GSA as part of that agency's responsibility to recommend improvements in records management practices and programs, under authority of 44 U.S.C. 2904 and 2906. Such disclosure shall be made in accordance with the GSA regulations governing inspection of records for this purpose, and any other relevant (i.e., GSA or Commerce) directive. Such disclosure shall not be used to make determinations about individuals.
8. A record from this system of records may be disclosed, as a routine use, to the public after either publication of the application pursuant to 35 U.S.C. 122(b) or issuance of a patent pursuant to 35 U.S.C. 151. Further, a record may be disclosed, subject to the limitations of 37 CFR 1.14, as a routine use, to the public if the record was filed in an application which became abandoned or in which the proceedings were terminated and which application is referenced by either a published application, an application open to public inspection or an issued patent.
9. A record from this system of records may be disclosed, as a routine use, to a Federal, State, or local law enforcement agency, if the USPTO becomes aware of a violation or potential violation of law or regulation.

Notice of Allowability	Application No. 15/768,352	Applicant(s) Drummond et al.	
	Examiner ISAAC SHOMER	Art Unit 1612	AIA (FITF) Status Yes

-- The MAILING DATE of this communication appears on the cover sheet with the correspondence address--

All claims being allowable, PROSECUTION ON THE MERITS IS (OR REMAINS) CLOSED in this application. If not included herewith (or previously mailed), a Notice of Allowance (PTOL-85) or other appropriate communication will be mailed in due course. **THIS NOTICE OF ALLOWABILITY IS NOT A GRANT OF PATENT RIGHTS.** This application is subject to withdrawal from issue at the initiative of the Office or upon petition by the applicant. See 37 CFR 1.313 and MPEP 1308.

1. ☑ This communication is responsive to Amendment on 14 May 2019.
   ☐ A declaration(s)/affidavit(s) under **37 CFR 1.130(b)** was/were filed on _____.

2. ☐ An election was made by the applicant in response to a restriction requirement set forth during the interview on _____; the restriction requirement and election have been incorporated into this action.

3. ☑ The allowed claim(s) is/are 24-47 and 50-56 . As a result of the allowed claim(s), you may be eligible to benefit from the **Patent Prosecution Highway** program at a participating intellectual property office for the corresponding application. For more information , please see **http://www.uspto.gov/patents/init_events/pph/index.jsp** or send an inquiry to **PPHfeedback@uspto.gov.**

4. ☐ Acknowledgment is made of a claim for foreign priority under 35 U.S.C. § 119(a)-(d) or (f).

   Certified copies:

   a) ☐ All b) ☐ Some *c) ☐ None of the:

   1. ☐ Certified copies of the priority documents have been received.
   2. ☐ Certified copies of the priority documents have been received in Application No. _____ .
   3. ☐ Copies of the certified copies of the priority documents have been received in this national stage application from the International Bureau (PCT Rule 17.2(a)).

   * Certified copies not received: _____ .

Applicant has THREE MONTHS FROM THE "MAILING DATE" of this communication to file areply complying with the requirements noted below. Failure to timely comply will result in ABANDONMENT of this application.
THIS THREE-MONTH PERIOD IS NOT EXTENDABLE.

5. ☐ CORRECTED DRAWINGS (as "replacement sheets") must be submitted.
   ☐ including changes required by the attached Examiner's Amendment / Comment or in the Office action of Paper No./Mail Date _____ .

   Identifying indicia such as the application number (see 37 CFR 1.84(c)) should be written on the drawings in the front (not the back) of each sheet. Replacement sheet(s) should be labeled as such in the header according to 37 CFR 1.121(d).

6. ☐ DEPOSIT OF and/or INFORMATION about the deposit of BIOLOGICAL MATERIAL must be submitted. Note the attached Examiner's comment regarding REQUIREMENT FOR THE DEPOSIT OF BIOLOGICAL MATERIAL.

Attachment(s)

1. ☐ Notice of References Cited (PTO-892)
2. ☑ Information Disclosure Statements (PTO/SB/08), Paper No./Mail Date _____.
3. ☐ Examiner's Comment Regarding Requirement for Deposit of Biological Material _____.
4. ☑ Interview Summary (PTO-413), Paper No./Mail Date. _____.
5. ☑ Examiner's Amendment/Comment
6. ☑ Examiner's Statement of Reasons for Allowance
7. ☑ Other Interview email attachment.

/ISAAC SHOMER/
Primary Examiner, Art Unit 1612

EXAMINER'S AMENDMENT

An examiner's amendment to the record appears below. Should the changes and/or additions be unacceptable to applicant, an amendment may be filed as provided by 37 CFR 1.312. To ensure consideration of such an amendment, it MUST be submitted no later than the payment of the issue fee.

Authorization for this examiner's amendment was given in an interview with Deborah Herzfeld on 4 June 2019.

The application has been amended as follows:

A) Claims 1-23 have been cancelled without prejudice or disclaimer.

B) Claim 24 has been allowed without further amendment.

C) Claim 25 has been allowed without further amendment.

D) Claim 26 has been amended in the following manner:

Claim 26 (Amended): The storage stabilized liposomal irinotecan composition of claim 25, wherein the composition comprises **[[** ~~essentially~~ **]]** unilamellar liposomes.

E) Claim 27 has been allowed without further amendment.

F) Claim 28 has been amended in the following manner:

Claim 28 (Amended): The storage stabilized liposomal irinotecan composition of claim 24, having less than 20 mol%**,** **[[** ~~(with respect to total phospholipids)~~ **]]** **with respect to total phospholipids,** of lyso-PC after a storage time from 9 to 12 months, at a storage temperature ranging of from 2 to 8 °C.

G) Claim 29 has been amended in the following manner:

Claim 29 (Amended): The storage stabilized liposomal irinotecan composition of claim 24, **[[** ~~wherein~~ **]]** **having** at least 98% of the irinotecan **[[** ~~is~~ **]]** encapsulated within the liposomes after 6 **[[** ~~months,~~ **]]** **months** at a storage temperature of from 2 to 8°C.

H) Claim 30 has been allowed without further amendment.

I) Claim 31 has been amended in the following manner:

Claim 31 (Amended): The storage stabilized liposomal irinotecan composition of claim 24, **further** comprising sodium chloride present at a concentration of from 130 to 160 mM.

J) Claim 32 has been allowed without further amendment.

K) Claim 33 has been allowed without further amendment.

L) Claim 34 has been amended in the following manner:

Claim 34 (Amended): The storage stabilized liposomal irinotecan composition of claim 33, wherein the liposomes are **[[** ~~essentially~~ **]]** unilamellar.

M) Claim 35 has been allowed without further amendment.

N) Claim 36 has been allowed without further amendment.

O) Claim 37 has been amended in the following manner:

Claim 37 (Amended): The storage stabilized liposomal irinotecan composition of claim 36, wherein the composition comprises **[[** ~~essentially~~ **]]** unilamellar liposomes.

P) Claim 38 has been allowed without further amendment.

Q) Claim 39 has been allowed without further amendment.

R) Claim 40 has been allowed without further amendment.

S) Claim 41 has been amended in the following manner:

Claim 41 (Amended): The storage stabilized liposomal irinotecan composition of claim 40, comprising **triethylammonium [[** ~~TEA~~ **]]** or **diethylammonium [[** ~~DEA~~ **]]** in a total amount of less than 100 ppm.

T) Claim 42 has been amended in the following manner:

Claim 42 (Amended): The storage stabilized liposomal irinotecan composition of claim 41, comprising **[[** ~~TEA~~ **]]** **triethylammonium** or **[[** ~~DEA~~ **]]** **diethylammonium** in a total amount of from 30 to 100 ppm.

U) Claim 43 has been amended in the following manner:

Claim 43 (Amended): The storage stabilized liposomal irinotecan composition of claim 40, having a total irinotecan moiety content equivalent to 4.3 mg/mL irinotecan free base, wherein **[[** ~~TEA~~ **]]** **triethylammonium** or **[[** ~~DEA~~ **]]** **diethylammonium** is present in a total amount of less than 100 ppm, and wherein the liposomes have an average diameter of about 110 nm, as measured by quasi-elastic light scattering.

V) Claim 44 has been allowed without further amendment.

W) Claim 45 has been allowed without further amendment.

X) Claim 46 has been allowed without further amendment.

Y) Claim 47 has been amended in the following manner:

Claim 47 (Amended): The storage stabilized liposomal irinotecan composition of claim **[[** ~~27,~~ **]]** **46,** wherein the time is about 30 minutes.

Z) Claim 48 has been cancelled without prejudice or disclaimer.

AA) Claim 49 has been cancelled without prejudice or disclaimer.

AB) Claim 50 has been allowed without further amendment.

AC) Claim 51 has been amended in the following manner:

Claim 51 (Amended): The storage stabilized liposomal irinotecan composition of claim 24, wherein the composition comprises **[[** ~~essentially~~ **]]** unilamellar liposomes.

AD) Claim 52 has been allowed without further amendment

AE) Claim 53 has been allowed without further amendment.

AF) Claim 54 has been allowed without further amendment.

AG) Claim 55 has been allowed without further amendment.

AH) The following new claim is added:

Claim 56 (New): The storage stabilized liposomal irinotecan composition of claim 27, wherein the time the liposomes are contacted with the solution comprising irinotecan above the transition temperature in step (b) is about 30 minutes.

REASONS FOR ALLOWANCE

The following is an examiner's statement of reasons for allowance:

A reasons for allowance is presented. The examiner notes that the rationale is similar to the reasons for allowance provided by the examiner in prior cases such as 15/331,318 and 15/661,868, and is mostly the same as the reasons for non-rejection of the claims under prior art submitted with the office action on 14 February 2019. The art cited here has been previously cited in the file record.

The instant claims are drawn to a liposomal composition comprising irinotecan and sucrose octasulfate. As close and relevant prior art, the examiner cites Drummond et al. (US 2007/0110798 A1) and Hong et al. (US 2007/0116753 A1), which are also drawn to liposomes comprising sucrose octasulfate and irinotecan.

The following reasons are provided by the examiner explaining why the instant claims have not been rejected as anticipated by these references or obvious over these references. Also cited by the examiner is Saetern et al. (International Journal of Pharmaceutics, Vol. 288, 2005, pages 73-80).

Liposomes are known to suffer from degradation when in storage. One such form of degradation involves the hydrolysis of phosphatidylcholine, which is a phospholipid molecule with two hydrocarbon chains that makes up the structural of the bilayer of the liposome, to lysophosphatidylcholine, which has only one hydrocarbon chain. Such lysophosphatidylcholine is understood to have poor stability in the liposome bilayer, and a bilayer comprising lysophosphatidylcholine is subject to degradation. The instantly claimed invention is drawn to a liposome that has unexpectedly greater storage stability

than the liposomes of the Drummond and Hong prior art references cited above. As such, the instantly claimed invention differs from the composition of the prior art for the following reasons:

A) pH Range: First, the instantly claimed liposome is stored in a medium wherein the pH is 7.25 to 7.50 (as in instant claim 24). Hong teaches that the liposome should be stored at a pH of between 6.0 and 7.5, with a pH of 6.5 as most optimal, as of Hong, paragraph 0115. However, additional relevant prior art shows that storage of a liposome in a pH of about 6.25 to 6.5 has the greatest storage stability, and that deviation from pH 6.25-6.5 results in more degradation during storage as compared to storage at pH 6.5. In support of this position, the examiner cites Saetern et al. (International Journal of Pharmaceutics, Vol. 288, 2005, pages 73-80). Saetern et al. (hereafter referred to as Saetern), teaches the following graph regarding degradation of phosphatidylcholine to lysophosphatidylcholine, as of page 77, right column, Figure 5, which is reproduced below.

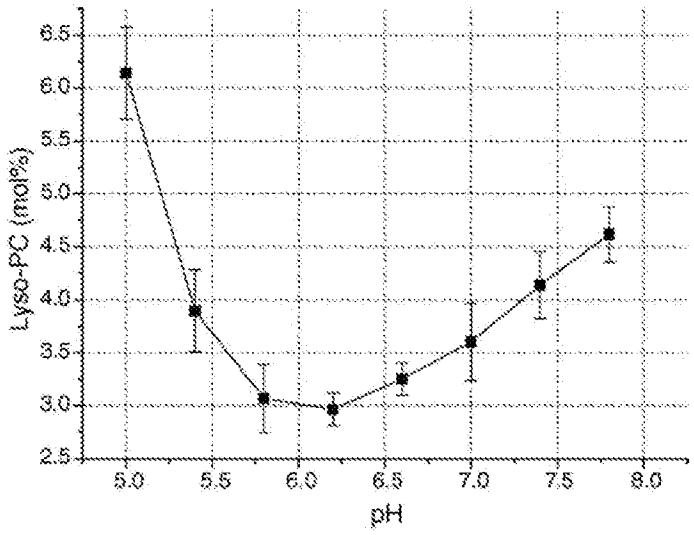

As such, the data of Saetern indicates that a pH of about 6.25 provides the greatest stability of a phosphatidylcholine containing liposome. The examiner also notes that the Saetern publication is especially relevant here because Saetern is drawn to encapsulating camptothecin as a drug, and the instant claims are drawn to a liposome that encapsulates irinotecan as a drug, wherein irinotecan is a derivative of camptothecin.

However, in the instant specification, applicant has presented data showing that a pH range of 7.25 to 7.50 unexpectedly provides increased stability as compared to a pH of about 6.5. In support of this position, the examiner cites table 1B on page 26 of the instant specification, which is reproduced below.

Table 1B: *Irinotecan Liposome Stability Ratio and Lyso-PC (after 6 months at 4 °C)*[b]

Sample	Molar (M) concentration of sulfate groups in the sucrosofate entrapped in the liposomes	Stability Ratio	pH	[mol% Lyso-PC] at 6 mos.
1	0.45	1047	6.5	19.5
2	0.475	992	6.5	17
3	0.5	942	6.5	26.5
4	0.6	785	6.5	30.2
5	0.45	1047	7.25	7.1
6	0.45	1047	6.5	14.6
7	0.45	1047	7.25	7.4
8	0.45	1047	7.5	5.4
9	0.6	785	6.5	29.8
10	0.6	785	7.25	24.1
11	0.6	785	7.5	22.8
13	0.45	1047	7.25	9.72

[b] Measured according to Method B, as described herein.

Instant table 1B discloses that a liposome at a pH of 6.5 and a sulfate group concentration of 0.45 M (Sample #1) shows 14.6 mol% or 19.5 mol% of lysophosphatidylcholine after 6 months, as of samples #6 and #1 respectively. In contrast, a sample with a pH of 7.25 and an identical sucrose octasulfate concentration

of 0.45 M (Samples #5 and #7) shows only about 7.1 mol% or 7.4 mol% of lyosphosphatidylcholine after 6 months of storage. As a greater percentage of lysophosphatidylcholine indicates a less stable liposome, the data presented in Table 1 show an increase in stability when the pH of a sucrose octasulfate containing irinotecan liposome is raised from 6.5 to 7.25.

This increase in stability with increase in pH is at odds with the teachings of the prior art, which indicate that a lower pH of 6.25 to 6.5 is optimal for achieving stability of the liposome. As applicant has shown that the claimed pH range is critical for achieving increased stability, this is understood to be evidence of non-obviousness. See MPEP 2144.05(III)(A). Additionally, proceeding contrary to accepted wisdom is evidence of nonobviousness. See MPEP 2145(X)(D)(3), citing In re Hedges, 783 F.2d 1038, 228 USPQ 685 (Fed. Cir. 1986).

B) Sucrose Octasulfate Loading Concentration: In the instantly claimed product-by-process, sucrose octasulfate was loaded in a concentration such that the sulfate groups are present in a concentration of 0.4 to 0.5 M, as of part (a) of claim 1. This appears to be a sucrose octasulfate concentration of 0.05 to 0.0625 M. This value was value calculated by the examiner by dividing the range of 0.4 to 0.5 by 8 as there are 8 sulfate groups per sucrose octasulfate molecule. In contrast, in the examples of the prior art, the concentration of either sucrose octasulfate or sulfate groups inside the liposome was at minimum 0.65 M to about 1.0 M, e.g. as of Hong, page 11, end of paragraph 0104.

Data in the instant application show that loading with a lower level of sucrose octasulfate with a sulfate group concentration of 0.4 M to 0.5 M appears to provide a

liposome with increased stability as compared with a liposome loaded at 0.60 to 0.65 M. In support of this position, the examiner cites table 1B on page 26 of the instant specification, which is reproduced above. Sample 10 of the instant specification shows loading at 0.60 M sucrose octasulfate and pH 7.25. In this example, there was 24.1 mol% lysophosphatidylcholine after 6 months of storage. In contrast, samples 5 and 7 are drawn to a liposome loaded with 0.45 M sucrose octasulfate and also a pH of 7.25, and these show 7.1% and 7.4% of lyosphosphatidylcholine respectively after 6 months of storage.

As a greater percentage of lysophosphatidylcholine indicates a less stable liposome, the data presented in Table 1 show an increase in stability when the concentration of sulfate groups from sucrose octasulfate is decreased from the prior art amount of 0.65 M to a lower amount of 0.4 M to 0.5 M. This would not have been expected by the skilled artisan, and this also indicates that the concentration of sucrose octasulfate used in loading the liposome is critical to the liposome stability. This showing regarding the criticality of the claimed loading concentration of sucrose octasulfate is evidence of non-obviousness, and applicant's data show that the claimed range of sucrose octasulfate is critical with regard to the stability of the liposome that is ultimately formed. See MPEP 2144.05(III)(A).

C) Lack of Inherency Regarding Lysophosphatidylcholine Content After 6 Months of Storage: Additionally, the instant claims recite that the composition is stabilized such that after 6 months of storage at the recited conditions, there is less than 20 mol% of lysophosphatidylcholine. The cited prior art references Drummond and Hong do not provide any teachings with regard to the amount of

lysophosphatidylcholine after 6 months of storage, and are silent with respect to this issue.

In order to reject such a claim limitation in the absence of an explicit teaching, the examiner must provide rationale or evidence tending to show inherency. See the heading of MPEP 2112(IV). In this case, the evidence appears to tend against inherency. This is because inherency must be based on what is necessarily present in the prior art (e.g. a composition with a pH of 6.5 and between 0.65 M to 1.0 M sulfate groups from sucrose octasulfate), and should not be based on optimization of conditions. See MPEP 2112(IV), first paragraph. Additionally, inherency may not be established by probabilities or possibilities. The mere fact that a certain thing may result from a given set of circumstances is not sufficient. See MPEP 2163.07(a), citing In re Robertson, 169 F.3d 743, 745, 49 USPQ2d 1949, 1950-51 (Fed. Cir. 1999). In this case, the examiner takes the position that with regard to the composition that is necessarily present in the prior art, this composition would not have been expected to have had the slow rate of degradation such that the percentage of lyso-phosphatidylcholine would have been less than 20% after 6 months of storage.

The prior art examples appear to include a sulfate concentration of between 0.65 M to 1.0 M, as of Hong, paragraph 0104, and a pH of 6.5, as of Hong, end of paragraph 0105. However, the examples in table 1B of the instant specification on page 26 of the instant specification that most resemble the prior art examples (e.g. 0.65 M sucrose octasulfate and pH 6.5) appear to show a greater level of lysophosphatidylcholine after 6 months of storage. The example in the instant specification which appear to be most similar to the prior art are samples 4, and 9, which utilizes a pH of 6.5 and a

concentration of sulfate groups of 0.60 M in samples. These liposomes show that the percentage of phosphatidylcholine after 6 months is 29.8% in sample 9 and 30.2%.

As such, the data in the instant specification show that the compositions that are necessarily present in the prior art would have been expected to have degraded to an extent that there would have been more than 20 mol% of lyso-phosphatidylcholine after 6 months of storage. As such, the claimed requirement that there be less than 20 mol% of lyso-phosphatidylcholine after 6 months of storage does not appear to be inherent in the teachings of the prior art.

D) Additional Note Regarding Claim 29: With regard to claim 29, the examiner clarifies that what is being recited by this claim is that the liposome is stored under specific conditions for a specific period of time, and after said period of storage, at least 98% of the irinotecan initially encapsulated is remaining in the liposome. This indicates that only up to 2% of the irinotecan leaked out of the liposome during the recited storage period. This claim helps distinguish over the prior art in that in the composition of the prior art, more irinotecan than 2% would have been expected to have leaked out in the recited storage period. This is because, as the lipid bilayer in the prior art is more prone to degradation as compared with the claimed lipid bilayer by degradation of phosphatidylcholine to lysophosphatidylcholine, as explained above. This would have been expected to have resulted in a less structurally stable liposome. Said less structurally stable liposome would have been expected to have suffered more leakage of its contents (i.e. irinotecan) as compared with the claimed liposome.

Any comments considered necessary by applicant must be submitted no later than the payment of the issue fee and, to avoid processing delays, should preferably

accompany the issue fee. Such submissions should be clearly labeled "Comments on Statement of Reasons for Allowance."

Terminal Disclaimer

The terminal disclaimer filed on 14 May 2019 disclaiming the terminal portion of any patent granted on this application which would extend beyond the expiration date of **US application 15/967,638** has been reviewed and is accepted. The terminal disclaimer has been recorded.

Conclusion

Any inquiry concerning this communication or earlier communications from the examiner should be directed to ISAAC SHOMER whose telephone number is (571)270-7671. The examiner can normally be reached on 7:30 AM to 5:00 PM Monday Through Friday.

Examiner interviews are available via telephone, in-person, and video conferencing using a USPTO supplied web-based collaboration tool. To schedule an interview, applicant is encouraged to use the USPTO Automated Interview Request (AIR) at http://www.uspto.gov/interviewpractice.

If attempts to reach the examiner by telephone are unsuccessful, the examiner's supervisor, Frederick F Krass can be reached on (571)272-0580. The fax phone number for the organization where this application or proceeding is assigned is 571-273-8300.

Information regarding the status of an application may be obtained from the Patent Application Information Retrieval (PAIR) system. Status information for published applications may be obtained from either Private PAIR or Public PAIR. Status information for unpublished applications is available through Private PAIR only. For more information about the PAIR system, see https://ppair-my.uspto.gov/pair/PrivatePair. Should you have questions on access to the Private PAIR system, contact the Electronic Business Center (EBC) at 866-217-9197 (toll-free). If you would like assistance from a USPTO Customer Service Representative or access to the automated information system, call 800-786-9199 (IN USA OR CANADA) or 571-272-1000.

ISAAC . SHOMER
Primary Examiner
Art Unit 1612

/ISAAC SHOMER/
Primary Examiner, Art Unit 1612

Applicant-Initiated Interview Summary	Application No. 15/768,352	Applicant(s) Drummond et al.		
	Examiner ISAAC SHOMER	Art Unit 1612	AIA (First Inventor to File) Status Yes	Page 1 of 2

All participants (applicant, applicants representative, PTO personnel):

1. ISAAC SHOMER (Primary Examiner); Telephonic 2. Deborah Herzfeld (Attorney of Record); Telephonic

Date of Interview: 04 June 2019

Claims Discussed: 24-47, 50-56

Amendment proposed: See attached document, which comprises a proposed amendment emailed from representative of applicant to examiner.

Brief Description of the main topic(s) of discussion: Representative of applicant provided counter-proposal regarding examiner's proposed amendments. Examiner agreed with the counter-proposal. As such, agreement was reached and this interview summary is attached to a notice of allowance.

Issues Discussed:

Proposed Amendments:
The examiner had previously proposed examiner's amendments in this case, as of the interview summary added to the file record on 3 June 2019. In response, representative of applicant sent an email on 4 June 2019 with a counter-proposal of proposed amendments. These proposed amendments are in response to examiner's proposal attached with the interview summary added to the file record on 3 June 2019.

Examiner agreed that the amendments proposed by representative of applicant in the email on 4 June 2019 are in condition for allowance. As such, this interview summary is attached to a notice of allowance. The documents emailed from representative of applicant with the proposed claim amendments emailed to the examiner are attached along with this interview summary.

Attachment(s): Proposed Amendments, Other Attachment
{Email Record, Notice of Allowance.}

/ISAAC SHOMER/ Primary Examiner, Art Unit 1612	

Applicant is reminded that a complete written statement as to the substance of the interview must be made of record in the application file. It is the applicants responsibility to provide the written statement, unless the interview was initiated by the Examiner and the Examiner has indicated that a written summary will be provided. See MPEP 713.04
Please further see:
MPEP 713.04
Title 37 Code of Federal Regulations (CFR) § 1.133 Interviews, paragraph (b)
37 CFR § 1.2 Business to be transacted in writing

Applicant recordation instructions: The formal written reply to the last Office action must include the substance of the interview. (See MPEP section 713.04). If a reply to the last Office action has already been filed, applicant is given a non-extendable period of the longer of one month or thirty days from this interview date, or the mailing date of this interview summary form, whichever is later, to file a statement of the substance of the interview.

Examiner recordation instructions: Examiners must summarize the substance of any interview of record. A complete and proper recordation of the substance of an interview should include the items listed in MPEP 713.04 for complete and proper recordation including the identification of the general thrust of each argument or issue discussed, a general indication of any other pertinent matters discussed regarding patentability and the general results or outcome of the interview, to include an indication as to whether or not agreement was reached on the issues raised.

UNITED STATES PATENT AND TRADEMARK OFFICE

UNITED STATES DEPARTMENT OF COMMERCE
United States Patent and Trademark Office
Address: COMMISSIONER FOR PATENTS
P.O. Box 1450
Alexandria, Virginia 22313-1450
www.uspto.gov

APPLICATION NO.	FILING DATE	FIRST NAMED INVENTOR	ATTORNEY DOCKET NO.	CONFIRMATION NO.
15/768,352	04/13/2018	Daryl C. Drummond	01208-0010-07US	2349

153749 7590 07/12/2019

McNeill Baur PLLC/Ipsen
Ipsen Bioscience, Inc.
125 Cambridge Park Drive
Suite 301
Cambridge, MA 02140

EXAMINER	
SHOMER, ISAAC	

ART UNIT	PAPER NUMBER
1612	

NOTIFICATION DATE	DELIVERY MODE
07/12/2019	ELECTRONIC

Please find below and/or attached an Office communication concerning this application or proceeding.

The time period for reply, if any, is set in the attached communication.

Notice of the Office communication was sent electronically on above-indicated "Notification Date" to the following e-mail address(es):

docketing@mcneillbaur.com
eofficeaction@appcoll.com
patents.us@ipsen.com

Applicant-Initiated Interview Summary	Application No. 15/768,352	Applicant(s) Drummond et al.		
	Examiner ISAAC SHOMER	Art Unit 1612	AIA (First Inventor to File) Status Yes	Page 1 of 3

All participants (applicant, applicants representative, PTO personnel):

1. ISAAC SHOMER (Primary Examiner); Telephonic 2. Deborah M. Herzfeld (Attomey of Record); Telephonic

Date of Interview: 09 July 2019

Claims Discussed: 28

Prior Art Discussed: Hong et al. (US 2007/0116753 A1) of record

Amendment proposed: Brief changes to claim 28 were discussed.

Brief Description of the main topic(s) of discussion: An error made by the examiner regarding claim 28 was discussed. Examiner agrees that an error was made, and representative of applicant will submit an amendment after allowance to correct this error. Also discussed was page 10, last full paragraph of the reasons for allowance. After review after the interview, the examiner takes the position that there was an error made by the examiner in the reasons for allowance, but the claims are still allowable.

Issues Discussed:

Correction of Information:
A) Claim 28: Representative of applicant pointed to an error in instant claim 28 as of the examiner's amendment mailed on 12 June 2019. The examiner does not dispute that an error was made by the examiner in the examiner's amendment in that examiner failed to accurately represent the claim prior to amendment. To correct this, representative of applicant took the position that applicant intends to file an amendment after allowance.

B) Reasons for Allowance: Representative of applicant specifically questioned page 10, last full paragraph of the notice of allowance (which is part of the reasons for allowance). Representative of applicant took the position that Hong, page 11, end of paragraph 0104 does not actually teach sucrose octasulfate. As such, representative of applicant took the position that the examiner's position that Hong teaches the concentration of sucrose of octasulfate in this paragraph is incorrect.

In response, examiner noted that paragraph 0104 of Hong teaches a polyanion salt. Sucrose octasulfate is a polyanion (as it includes multiple ionic groups), and a salt of sucrose octasulfate is therefore a polyanion salt. Sucrose octasulfate is taught elsewhere in the Hong reference, e.g. as of at least Examples 6 and 11 of Hong. As such, sucrose octasulfate is understood by the examiner to be a polyanion to which Hong was referring in paragraph 0104.

After the interview was over, the examiner further reviewed paragraph 0104 of Hong and page 10, last full paragraph , of the notice of allowance on 12 June 2019. The examiner noted that the molarity of polyanion salt, which is taught as ranging from 10 mM to 1.0 M is calculated based on the substituted ammonium salt. The substituted ammonium salt is best understood to be a monovalent cation (e.g. triethylammonium, in paragraph 0038 of Hong). As such, the concentrations of Hong, paragraph 0104, are directly comparable to the concentrations recited in the instant claims. Therefore, the examiner now takes the position that the mathematical calculation performed by the examiner on page 10, last full paragraph of the notice of allowance on 12 June 2019 is incorrect. Therefore, the teachings of a polyanion concentration of 0.2 M and 0.5 M, as of Hong, paragraph 0104, (which is being read by the examiner as 0.2 M to 0.5 M) does overlap with the claimed range of 0.4 M to 0.5 M.

Nevertheless, the claimed range of 0.4 M to 0.5 M is below Hong's preferred range of about 0.65 M to about 1.0 M as of the last sentence of Hong, paragraph 0104. As explained on the paragraph bridging pages 10-11 and page 11, second paragraph of the notice of allowance, there are unexpected results in terms of greater stability in storage associated with the claimed range of sucrose octasulfate concentration that are not evident in the higher concentrations of polyanion preferred by Hong. As such, the examiner takes the position that these unexpected results still support a finding of allowability.

In view of representative of applicant's comments, the examiner also reviewed the file wrappers of related cases. The examiner notes that this issue regarding sucrose octasulfate concentration was discussed in the interview summary in case 15/331648 added to the file record on 17 March 2017 in that case. This interview summary summarizes an interview that took place on 13 March 2017 in case 15/331648. The issue regarding sucrose octasulfate concentration was discussed specifically as of item "2)" in the section of the interview summary drawn to items under 35 U.S.C. 103. The examiner notes here that case 15/331648 is in the same family tree as the instant case, has the same inventors as the instant case and appears to have the same assignee as the instant case, and is drawn to similar subject matter as the instant case. As such, the rationale provided in the interview summary in the ' 648 case is believed to be relevant in the instant case.

/ISAAC SHOMER/ Primary Examiner, Art Unit 1612	

Applicant is reminded that a complete written statement as to the substance of the interview must be made of record in the application file. It is the applicants responsibility to provide the written statement, unless the interview was initiated by the Examiner and the Examiner has indicated that a written summary will be provided. See MPEP 713.04
Please further see:
MPEP 713.04
Title 37 Code of Federal Regulations (CFR) § 1.133 Interviews, paragraph (b)
37 CFR § 1.2 Business to be transacted in writing

Applicant recordation instructions: The formal written reply to the last Office action must include the substance of the interview. (See MPEP section 713.04). If a reply to the last Office action has already been filed, applicant is given a non-extendable period of the longer of one month or thirty days from this interview date, or the mailing date of this interview summary form, whichever is later, to file a statement of the substance of the interview.

Examiner recordation instructions: Examiners must summarize the substance of any interview of record. A complete and proper recordation of the substance of an interview should include the items listed in MPEP 713.04 for complete and proper recordation including the identification of the general thrust of each argument or issue discussed, a general indication of any other pertinent matters discussed regarding patentability and the general results or outcome of the interview, to include an indication as to whether or not agreement was reached on the issues raised.

UNITED STATES PATENT AND TRADEMARK OFFICE

UNITED STATES DEPARTMENT OF COMMERCE
United States Patent and Trademark Office
Address: COMMISSIONER FOR PATENTS
P.O. Box 1450
Alexandria, Virginia 22313-1450
www.uspto.gov

APPLICATION NO.	FILING DATE	FIRST NAMED INVENTOR	ATTORNEY DOCKET NO.	CONFIRMATION NO.
15/768,352	04/13/2018	Daryl C. Drummond	01208-0010-07US	2349

153749 7590 08/28/2019

McNeill Baur PLLC/Ipsen
Ipsen Bioscience, Inc.
125 Cambridge Park Drive
Suite 301
Cambridge, MA 02140

EXAMINER	
SHOMER, ISAAC	

ART UNIT	PAPER NUMBER
1612	

NOTIFICATION DATE	DELIVERY MODE
08/28/2019	ELECTRONIC

Please find below and/or attached an Office communication concerning this application or proceeding.

The time period for reply, if any, is set in the attached communication.

Notice of the Office communication was sent electronically on above-indicated "Notification Date" to the following e-mail address(es):

docketing@mcneillbaur.com
eofficeaction@appcoll.com
patents.us@ipsen.com

Supplemental ***Notice of Allowability***	**Application No.** 15/768,352	**Applicant(s)** Drummond et al.	
	Examiner ISAAC SHOMER	**Art Unit** 1612	**AIA (FITF) Status** Yes

-- The MAILING DATE of this communication appears on the cover sheet with the correspondence address--

All claims being allowable, PROSECUTION ON THE MERITS IS (OR REMAINS) CLOSED in this application. If not included herewith (or previously mailed), a Notice of Allowance (PTOL-85) or other appropriate communication will be mailed in due course. **THIS NOTICE OF ALLOWABILITY IS NOT A GRANT OF PATENT RIGHTS.** This application is subject to withdrawal from issue at the initiative of the Office or upon petition by the applicant. See 37 CFR 1.313 and MPEP 1308.

1. ☑ This communication is responsive to Amendment on 12 August 2019.
   ☐ A declaration(s)/affidavit(s) under **37 CFR 1.130(b)** was/were filed on _____.

2. ☐ An election was made by the applicant in response to a restriction requirement set forth during the interview on _____; the restriction requirement and election have been incorporated into this action.

3. ☑ The allowed claim(s) is/are 24-47 and 50-56 . As a result of the allowed claim(s), you may be eligible to benefit from the **Patent Prosecution Highway** program at a participating intellectual property office for the corresponding application. For more information , please see **http://www.uspto.gov/patents/init_events/pph/index.jsp** or send an inquiry to **PPHfeedback@uspto.gov.**

4. ☐ Acknowledgment is made of a claim for foreign priority under 35 U.S.C. § 119(a)-(d) or (f).

   Certified copies:

   a) ☐ All b) ☐ Some *c) ☐ None of the:

   1. ☐ Certified copies of the priority documents have been received.
   2. ☐ Certified copies of the priority documents have been received in Application No. _____ .
   3. ☐ Copies of the certified copies of the priority documents have been received in this national stage application from the International Bureau (PCT Rule 17.2(a)).

   * Certified copies not received: _____ .

Applicant has THREE MONTHS FROM THE "MAILING DATE" of this communication to file a reply complying with the requirements noted below. Failure to timely comply will result in ABANDONMENT of this application.
THIS THREE-MONTH PERIOD IS NOT EXTENDABLE.

5. ☐ CORRECTED DRAWINGS (as "replacement sheets") must be submitted.
   ☐ including changes required by the attached Examiner's Amendment / Comment or in the Office action of Paper No./Mail Date _____ .

   Identifying indicia such as the application number (see 37 CFR 1.84(c)) should be written on the drawings in the front (not the back) of each sheet. Replacement sheet(s) should be labeled as such in the header according to 37 CFR 1.121(d).

6. ☐ DEPOSIT OF and/or INFORMATION about the deposit of BIOLOGICAL MATERIAL must be submitted. Note the attached Examiner's comment regarding REQUIREMENT FOR THE DEPOSIT OF BIOLOGICAL MATERIAL.

Attachment(s)

1. ☐ Notice of References Cited (PTO-892)
2. ☐ Information Disclosure Statements (PTO/SB/08), Paper No./Mail Date _____.
3. ☐ Examiner's Comment Regarding Requirement for Deposit of Biological Material _____.
4. ☑ Interview Summary (PTO-413), Paper No./Mail Date. _____.
5. ☐ Examiner's Amendment/Comment
6. ☑ Examiner's Statement of Reasons for Allowance
7. ☐ Other _____.

/ISAAC SHOMER/
Primary Examiner, Art Unit 1612

Corrected/Supplemental Reasons For Allowance

The following is an examiner's statement of reasons for allowance:

The notice of allowance on 12 June 2019 included a reasons for allowance. After an interview with applicant (see the interview summary mailed on 12 July 2019 summarizing an interview on 9 July 2019) and further consideration by the examiner, the examiner takes the position that various statements made by the examiner in the previous reasons for allowance were either unclear or incorrect. The examiner has set forth the following reasons for allowance below in an attempt to correct the record and to make examiner's reasons more clear. This reasons for allowance supersedes the reasons for allowance set forth in the notice of allowance on 12 June 2019.

The instant claims are drawn to a liposomal composition comprising irinotecan and sucrose octasulfate. As close and relevant prior art, the examiner cites Drummond et al. (US 2007/0110798 A1) and Hong et al. (US 2007/0116753 A1), which are also drawn to liposomes comprising sucrose octasulfate and irinotecan. Also cited by the examiner is Saetern et al. (International Journal of Pharmaceutics, Vol. 288, 2005, pages 73-80).

The following reasons are provided by the examiner explaining why the instant claims have not been rejected as anticipated by these references or obvious over these references.

Summary of Examiner's Position: Liposomes are known to suffer from degradation when in storage. One such form of degradation involves the hydrolysis of phosphatidylcholine, which is a phospholipid molecule with two hydrocarbon chains that makes up the structural of the bilayer of the liposome, to lysophosphatidylcholine, which

has only one hydrocarbon chain. Such lysophosphatidylcholine is understood to have poor stability in the liposome bilayer, and a bilayer comprising lysophosphatidylcholine is subject to degradation. The instantly claimed invention is drawn to a liposome that has unexpectedly greater storage stability in that there is less degradation of phosphatidylcholine to lysophosphatidylcholine as compared with the liposomes of the Drummond and Hong prior art references cited above. The following reasons are presented by the examiner in support of this position.

A) pH Range: First, the instantly claimed liposome is stored in a medium wherein the pH is about 7.25 to about 7.50 (as in instant claim 24). Hong teaches that the liposome should be stored at a pH of between 6.0 and 7.5, with a pH of 6.5 as most optimal, as of Hong, paragraph 0115. However, additional relevant prior art shows that storage of a liposome in a pH of about 6.25 to 6.5 has the greatest storage stability, and that deviation from pH 6.25-6.5 results in more degradation during storage as compared to storage at pH 6.5. In support of this position, the examiner cites Saetern et al. (International Journal of Pharmaceutics, Vol. 288, 2005, pages 73-80). Saetern et al. (hereafter referred to as Saetern), teaches the following graph regarding degradation of phosphatidylcholine to lysophosphatidylcholine, as of page 77, right column, Figure 5, which is reproduced below.

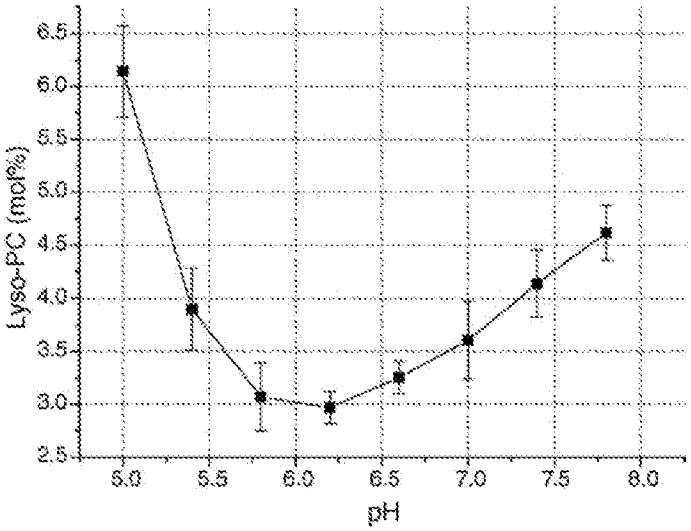

As such, the data of Saetern indicates that a pH of about 6.25 provides the greatest stability of a phosphatidylcholine containing liposome. The examiner also notes that the Saetern publication is especially relevant here because Saetern is drawn to encapsulating camptothecin as a drug, and the instant claims are drawn to a liposome that encapsulates irinotecan as a drug, wherein irinotecan is a derivative of camptothecin.

However, in the instant specification, applicant has presented data showing that a pH range of about 7.25 to about 7.50 unexpectedly provides increased stability as compared to a pH of about 6.5. In support of this position, the examiner cites table 1B on page 26 of the instant specification, which is reproduced below.

Table 1B: *Irinotecan Liposome Stability Ratio and Lyso-PC (after 6 months at 4 °C)*[b]

Sample	Molar (M) concentration of sulfate groups in the sucrosofate entrapped in the liposomes	Stability Ratio	pH	[mol% Lyso-PC] at 6 mos.
1	0.45	1047	6.5	19.5
2	0.475	992	6.5	17
3	0.5	942	6.5	26.5
4	0.6	785	6.5	30.2
5	0.45	1047	7.25	7.1
6	0.45	1047	6.5	14.6
7	0.45	1047	7.25	7.4
8	0.45	1047	7.5	5.4
9	0.6	785	6.5	29.8
10	0.6	785	7.25	24.1
11	0.6	785	7.5	22.8
13	0.45	1047	7.25	9.72

[b] Measured according to Method B, as described herein.

Instant table 1B discloses that a liposome at a pH of 6.5 and a sulfate group concentration of 0.45 M (Sample #1) shows 14.6 mol% or 19.5 mol% of lysophosphatidylcholine after 6 months, as of samples #6 and #1 respectively. In contrast, a sample with a pH of 7.25 and an identical sucrose octasulfate concentration of 0.45 M (Samples #5 and #7) shows only about 7.1 mol% or 7.4 mol% of lysophosphatidylcholine after 6 months of storage. As a greater percentage of lysophosphatidylcholine indicates a less stable liposome, the data presented in Table 1 show an increase in stability when the pH of a sucrose octasulfate containing irinotecan liposome is raised from 6.5 to 7.25.

This increase in stability with increase in pH is at odds with the teachings of the prior art, which indicate that a lower pH of 6.25 to 6.5 is optimal for achieving stability of the liposome. As applicant has shown that the claimed pH range is critical for achieving increased stability, this is understood to be evidence of non-obviousness. See MPEP 2144.05(III)(A). Additionally, proceeding contrary to accepted wisdom is evidence of

nonobviousness. See MPEP 2145(X)(D)(3), citing In re Hedges, 783 F.2d 1038, 228 USPQ 685 (Fed. Cir. 1986). In this case, applicant has proceeded contrary to the expected wisdom of the Saetern reference and has achieved beneficial results of increased stability.

B) Sucrose Octasulfate Loading Concentration: As an initial matter, the examiner notes that this section of the reasons for allowance is significantly rewritten as compared with the corresponding section B on the notice of allowance on 12 June 2019. The examiner notes that the issue of unexpected results and comparison with the closest prior art, as of MPEP 716.02(e), is an important feature of the examiner's reasoning.

B1 – Explanation of Teachings of Hong Regarding Sucrose Octasulfate Concentration: In the instantly claimed product-by-process, sucrose octasulfate was loaded in a concentration such that the sulfate groups are present in a concentration of 0.4 to 0.5 M based on sulfate groups, as of part (a) of claim 1.

Hong teaches that the substituted ammonium and/or polyanion salt inside the liposome is in a concentration ranging from 10 mM to 1.0 M, with a preferred concentration range of about 0.65 M to about 1.0 M, as of Hong, paragraph 0104.

The examiner provides the following explanation of paragraph 0104 of Hong: Sucrose octasulfate is a polyanion (as it includes multiple sulfate anionic groups), and a salt of sucrose octasulfate is therefore a polyanion salt. Sucrose octasulfate as a substituted ammonium salt is taught in the examples of the Hong reference, e.g. as of paragraph 0138 in Example 7 of Hong and paragraph 0161 of Hong in Example 11.

Paragraph 0161 of Hong teaches TEA-SOS, which is triethylammonium sucrose octasulfate.

As such, it is the examiner's best understanding that the "substituted ammonium and/or polyanion salt" in paragraph 0104 of Hong is a salt such as triethylammonium sucrose octasulfate (wherein triethylammonium is a substituted ammonium).

The examiner makes the following note regarding the chemistry of sucrose octasulfate. Sucrose octasulfate is a molecule comprising sucrose substituted with eight sulfate groups covalently attached thereto. Each sulfate group carries a formal charge of -1. As such, cations are needed to balance the negative formal charge in sucrose octasulfate. In the teachings of Hong, the most preferred cation is a substituted ammonium cation such as tetraethylammonium. The tetraethylammonium cation has a formal charge of +1, e.g. as of paragraph 0161 of Hong. As such, eight tetraethylammonium cations are needed to balance the charge of one sucrose octasulfate anion.

The instant claims recites sucrose octasulfate concentration in terms of the sulfate concentration. Hong, in paragraph 0104, expresses polyanion (e.g. sucrose octasulfate) concentration in terms of the molarity of the substituted ammonium ion. These are equivalent concentrations, as one substituted ammonium ion is needed to balance the charge of one sulfate group.

As such, the value of 0.5 M in paragraph 0104 of Hong is the same as the recited value of 0.5 M. Nevertheless, any *prima facie* case of obviousness is overcome by unexpected results, as explained below.

B2 – Summary of Unexpected Results: In this case, any prima facie case of obviousness that may be present is overcome with unexpected results. See MPEP 716.01 and 716.02.

Data in the instant application show that loading with a level of sucrose octasulfate with a sulfate group concentration of 0.4 M to 0.5 M appears to provide a liposome with increased stability as compared with a liposome loaded at 0.60 to 0.65 M. In support of this position, the examiner cites table 1B on page 26 of the instant specification, which is reproduced above in section A of the reasons for allowance. Sample 10 of the instant specification shows loading at 0.60 M sucrose octasulfate and pH 7.25. In this example, there was 24.1 mol% lysophosphatidylcholine after 6 months of storage. In contrast, samples 5 and 7 are drawn to a liposome loaded with 0.45 M sucrose octasulfate and also a pH of 7.25, and these show 7.1% and 7.4% of lyosphosphatidylcholine respectively after 6 months of storage.

As a greater percentage of lysophosphatidylcholine indicates a less stable liposome, the data presented in Table 1 show an increase in stability when the concentration of sulfate groups from sucrose octasulfate is decreased from the preferred concentration in the prior art of 0.65 M to a lower concentration of 0.4 M to 0.5 M. This would not have been expected by the skilled artisan, and this also indicates that the concentration of sucrose octasulfate used in loading the liposome is critical to the liposome stability. This showing regarding the criticality of the claimed loading concentration of sucrose octasulfate is evidence of non-obviousness, and applicant's data show that the claimed range of sucrose octasulfate is critical with regard to the stability of the liposome that is ultimately formed. See MPEP 2144.05(III)(A).

B3 – Examiner's Statement Regarding MPEP 716.02(e) and the Prior Art: The examiner has included this section of the reasons for allowance to make the case that applicant successfully compared the claimed invention to a comparative example that is at least as close as what is actually present in the prior art. See MPEP 716.02(e), especially 716.02(e)(II) and 716.02(e)(III). The following reasoning is presented by the examiner in support of this position.

The examiner notes here that while paragraph 0104 of Hong may teach sucrose octasulfate in amounts that overlap with the claimed amounts, most of the examples of Hong teach sucrose octasulfate in amounts that are greater than the claimed amount or that differ from the claimed invention in other ways. For example, Hong, paragraph 072, Example 13, teaches sucrose octasulfate in an amount of 0.643 N. The same teaching is present on Hong, Example 15, paragraph 0176. Example 16, paragraph 0183 of Hong teaches sucrose octasulfate at 0.65 M based upon triethylammonium. Hong teaches a higher concentration of 1.05 N sucrose octasulfate in Example 24, paragraph 0295.

The closest example in Hong appears to be a teaching of a liposome comprising 0.47 M triethylammonium sucrose octasulfate in Example 23, paragraph 0204 of Hong. However, this example is for the drug topotecan, which differs from the claimed irinotecan. Also, this example has a pH that of 6.27, which differs as compared with the claimed pH range of about 7.25 to about 7.50.

As such, Hong does not appear to teach an example comprising a liposome with irinotecan and sucrose octasulfate in a concentration of 0.4 M to 0.5 M.

In the case of determination of a prima facie case of obviousness, whether sucrose octasulfate in a concentration of 0.4 M to 0.5 M is taught in the examples or in the broad disclosure of Hong is not particularly relevant. This is because, regardless of whether the teaching is in the examples or in the broad disclosure, there is a prima facie case of obviousness. See MPEP 2123. However, in this case, the relevant issue being discussed in this section of the reasons for allowance is in regards to unexpected results rather than a prima facie case of obviousness. For the relevant analysis regarding unexpected results, the examiner cites MPEP 716.02(e), which states that the claimed invention must be compared with the closest prior art.

Crucially, MPEP 716.02(e)(III) states that [a]lthough evidence of unexpected results must compare the claimed invention with the closest prior art, applicant is not required to compare the claimed invention with subject matter that does not exist in the prior art. In this case, the examiner understands that an irinotecan liposome comprising 0.4-0.5 M sucrose octasulfate and a pH of about 7.25 to about 7.50, thought potentially suggested by Hong through teachings at disparate portions of the reference, does not actually exist in Hong because it is not present in the examples of Hong.

As such, applicant's comparison of the claimed invention vs. a comparative example comprising 0.6 M sucrose octasulfate, as of Table 1B of the instant specification, which is reproduced above, is understood to successfully compare the claimed invention against a comparative example that is closer than the subject matter which actually exists in the prior art.

C) Combination of pH and Sucrose Octasulfate Concentration: The data shown above appear to indicate that it is not only the pH and the sucrose octasulfate

concentration, but the combination of the pH and sucrose octasulfate concentration that lead to greater stability as compared with the prior art. For that matter, the only embodiments in Figure 1B, reproduced above, that form less than 10 mol% lysophosphatidylcholine after 6 months storage at 4°C have a pH of 7.25 or 7.5 and a sucrose octasulfate concentration of 0.45 M. Examples that differ by either pH, sucrose octasulfate concentration, or both, form a higher mol% of lysophosphatidylcholine after storage, which indicates lower stability.

D) Additional Note Regarding Claim 29: With regard to claim 29, the examiner clarifies that what is being recited by this claim is that the liposome is stored under specific conditions for a specific period of time, and after said period of storage, at least 98% of the irinotecan initially encapsulated is remaining in the liposome. This indicates that only up to 2% of the irinotecan leaked out of the liposome during the recited storage period. This claim helps distinguish over the prior art in that in the composition of the prior art, more irinotecan than 2% would have been expected to have leaked out in the recited storage period. This is because, as the lipid bilayer in the prior art is more prone to degradation as compared with the claimed lipid bilayer by degradation of phosphatidylcholine to lysophosphatidylcholine, as explained above. This would have been expected to have resulted in a less structurally stable liposome. Said less structurally stable liposome would have been expected to have suffered more leakage of its contents (i.e. irinotecan) as compared with the claimed liposome.

E) Additional Note Regarding Volume Weighting: The term “volume weighted” is disclosed on page 68, bottom line, in paragraph 00199 in the instant specification. As best understood by the examiner, all of the sizes in Table 7 on pages 69-70 of the

instant specification are volume weighted. As such, applicant's amendments reciting that the sizes are volume weighted is not new matter.

Any comments considered necessary by applicant must be submitted no later than the payment of the issue fee and, to avoid processing delays, should preferably accompany the issue fee. Such submissions should be clearly labeled "Comments on Statement of Reasons for Allowance."

Conclusion

Any inquiry concerning this communication or earlier communications from the examiner should be directed to ISAAC SHOMER whose telephone number is (571)270-7671. The examiner can normally be reached on 7:30 AM to 5:00 PM Monday Through Friday.

Examiner interviews are available via telephone, in-person, and video conferencing using a USPTO supplied web-based collaboration tool. To schedule an interview, applicant is encouraged to use the USPTO Automated Interview Request (AIR) at http://www.uspto.gov/interviewpractice.

If attempts to reach the examiner by telephone are unsuccessful, the examiner's supervisor, Frederick F Krass can be reached on (571)272-0580. The fax phone number for the organization where this application or proceeding is assigned is 571-273-8300.

Information regarding the status of an application may be obtained from the Patent Application Information Retrieval (PAIR) system. Status information for

published applications may be obtained from either Private PAIR or Public PAIR. Status information for unpublished applications is available through Private PAIR only. For more information about the PAIR system, see https://ppair-my.uspto.gov/pair/PrivatePair. Should you have questions on access to the Private PAIR system, contact the Electronic Business Center (EBC) at 866-217-9197 (toll-free). If you would like assistance from a USPTO Customer Service Representative or access to the automated information system, call 800-786-9199 (IN USA OR CANADA) or 571-272-1000.

ISAAC . SHOMER
Primary Examiner
Art Unit 1612

/ISAAC SHOMER/
Primary Examiner, Art Unit 1612

Examiner-Initiated Interview Summary	Application No. 15/768,352	Applicant(s) Drummond et al.		
	Examiner ISAAC SHOMER	Art Unit 1612	AIA (First Inventor to File) Status Yes	Page 1 of 2

All participants (applicant, applicants representative, PTO personnel):

1. ISAAC SHOMER (Primary Examiner); Telephonic 2. Deborah M. Herzfeld (Attomey of Record); Telephonic

Date of Interview: 26 August 2019

Claims Discussed: 24

Prior Art Discussed: all references of record

Amendment proposed: Examiner proposed the addition of an additional claim. The proposed dependent claim was to modify claim 24 by reciting that the liposomal irinotecan is stabilized to have less than 10 mol%, with respect to total phospholipids, of lyso-phosphatidylcholine during the first 6 months of storage of the liposomal irinotecan composition at a temperature ranging from 2 to 8 degrees Celsius. This amendment was proposed verbally by the examiner.

Brief Description of the main topic(s) of discussion: The examiner proposed amending the instant claims to add a new dependent claim. The proposed new dependent claim was not agreed to by applicant.

Issues Discussed:

Proposed Amendments:
The examiner suggests that applicant add a dependent claim modifying independent claim 24 by reciting that the liposomal irinotecan composition is stabilized to have less than 10 mol%, with respect to total phospholipids, of lyso-phosphatidylcholine during the first 6 months of storage at a temperature ranging from 2 to 8°C. The proposed new claim is supported as of page 38, paragraph 00125 of the instant specification. The proposed new claim would further limit instant claim 24 because it would exclude compositions that are relatively less stable and form 10-20% lysophosphatidylcholine after storage at the recited time and temperature, but would not exclude compositions that are relatively more stable and form less than 10% lysophosphatidylcholine after storage at the recited time and temperature.

After consideration, representative of applicant communicated to examiner that representative of applicant did not agree to the addition of the proposed new claim.

Attachment(s): Other Attachment
{Corrected notice of allowability}

/ISAAC SHOMER/ Primary Examiner, Art Unit 1612	

Applicant is reminded that a complete written statement as to the substance of the interview must be made of record in the application file. It is the applicants responsibility to provide the written statement, unless the interview was initiated by the Examiner and the Examiner has indicated that a written summary will be provided. See MPEP 713.04
Please further see:
MPEP 713.04
Title 37 Code of Federal Regulations (CFR) § 1.133 Interviews, paragraph (b)
37 CFR § 1.2 Business to be transacted in writing

Applicant recordation instructions: It is not necessary for applicant to provide a separate record of the substance of interview.

Examiner recordation instructions: Examiners must summarize the substance of any interview of record. A complete and proper recordation of the substance of an interview should include the items listed in MPEP 713.04 for complete and proper recordation including the identification of the general thrust of each argument or issue discussed, a general indication of any other pertinent matters discussed regarding patentability and the general results or outcome of the interview, to include an indication as to whether or not agreement was reached on the issues raised.

UNITED STATES PATENT AND TRADEMARK OFFICE

UNITED STATES DEPARTMENT OF COMMERCE
United States Patent and Trademark Office
Address: COMMISSIONER FOR PATENTS
P.O. Box 1450
Alexandria, Virginia 22313-1450
www.uspto.gov

APPLICATION NO.	FILING DATE	FIRST NAMED INVENTOR	ATTORNEY DOCKET NO.	CONFIRMATION NO.
15/809,815	11/10/2017	Eliel Bayever	263266-421428	5137

153749 7590 07/08/2019

McNeill Baur PLLC/Ipsen
Ipsen Bioscience, Inc.
125 Cambridge Park Drive
Suite 301
Cambridge, MA 02140

EXAMINER	
RONEY, CELESTE A	

ART UNIT	PAPER NUMBER
1612	

NOTIFICATION DATE	DELIVERY MODE
07/08/2019	ELECTRONIC

Please find below and/or attached an Office communication concerning this application or proceeding.

The time period for reply, if any, is set in the attached communication.

Notice of the Office communication was sent electronically on above-indicated "Notification Date" to the following e-mail address(es):

docketing@mcneillbaur.com
eofficeaction@appcoll.com
patents.us@ipsen.com

Office Action Summary	Application No. 15/809,815	Applicant(s) Bayever et al.	
	Examiner CELESTE A RONEY	Art Unit 1612	AIA (FITF) Status Yes

-- The MAILING DATE of this communication appears on the cover sheet with the correspondence address --

Period for Reply

A SHORTENED STATUTORY PERIOD FOR REPLY IS SET TO EXPIRE 3 MONTHS FROM THE MAILING DATE OF THIS COMMUNICATION.

- Extensions of time may be available under the provisions of 37 CFR 1.136(a). In no event, however, may a reply be timely filed after SIX (6) MONTHS from the mailing date of this communication.
- If NO period for reply is specified above, the maximum statutory period will apply and will expire SIX (6) MONTHS from the mailing date of this communication.
- Failure to reply within the set or extended period for reply will, by statute, cause the application to become ABANDONED (35 U.S.C. § 133). Any reply received by the Office later than three months after the mailing date of this communication, even if timely filed, may reduce any earned patent term adjustment. See 37 CFR 1.704(b).

Status

1)☑ Responsive to communication(s) filed on 11 February 2019.

☐ A declaration(s)/affidavit(s) under **37 CFR 1.130(b)** was/were filed on _____.

2a)☐ This action is **FINAL.** 2b) ☑ This action is non-final.

3)☐ An election was made by the applicant in response to a restriction requirement set forth during the interview on _____; the restriction requirement and election have been incorporated into this action.

4)☐ Since this application is in condition for allowance except for formal matters, prosecution as to the merits is closed in accordance with the practice under *Ex parte Quayle*, 1935 C.D. 11, 453 O.G. 213.

Disposition of Claims*

5) ☑ Claim(s) 1,4-15,18-19 and 21-23 is/are pending in the application.

5a) Of the above claim(s) _____ is/are withdrawn from consideration.

6) ☐ Claim(s) _____ is/are allowed.

7) ☑ Claim(s) 1,4-15,18-19 and 21-23 is/are rejected.

8) ☐ Claim(s) _____ is/are objected to.

9) ☐ Claim(s) _____ are subject to restriction and/or election requirement

* If any claims have been determined allowable, you may be eligible to benefit from the **Patent Prosecution Highway** program at a participating intellectual property office for the corresponding application. For more information, please see http://www.uspto.gov/patents/init_events/pph/index.jsp or send an inquiry to **PPHfeedback@uspto.gov.**

Application Papers

10)☐ The specification is objected to by the Examiner.

11)☐ The drawing(s) filed on _____ is/are: a)☐ accepted or b)☐ objected to by the Examiner.

Applicant may not request that any objection to the drawing(s) be held in abeyance. See 37 CFR 1.85(a).

Replacement drawing sheet(s) including the correction is required if the drawing(s) is objected to. See 37 CFR 1.121(d).

Priority under 35 U.S.C. § 119

12)☐ Acknowledgment is made of a claim for foreign priority under 35 U.S.C. § 119(a)-(d) or (f).

Certified copies:

a)☐ All b)☐ Some** c)☐ None of the:

1.☐ Certified copies of the priority documents have been received.

2.☐ Certified copies of the priority documents have been received in Application No. _____.

3.☐ Copies of the certified copies of the priority documents have been received in this National Stage application from the International Bureau (PCT Rule 17.2(a)).

** See the attached detailed Office action for a list of the certified copies not received.

Attachment(s)

1) ☑ Notice of References Cited (PTO-892)

2) ☑ Information Disclosure Statement(s) (PTO/SB/08a and/or PTO/SB/08b) Paper No(s)/Mail Date 8/6/18; 2/11/19 (2); 2/13/19 (4).

3) ☐ Interview Summary (PTO-413) Paper No(s)/Mail Date _____.

4) ☐ Other: _____.